

**Proceedings of MENU 2007**  
**11th International Conference on**  
**Meson-Nucleon Physics**  
**and the Structure of the Nucleon**

IKP, Forschungszentrum Jülich

Germany

September 10-14, 2007

Editors

H. Machner and S. Krewald

Volume I  
Invited Talks



## Foreword

The 11th International Conference on Meson-Nucleon Physics and the Structure of the Nucleon - MENU 2007 - was organized by the Institut für Kernphysik, Forschungszentrum Jülich, Jülich, Germany. It took place from September 10-14, 2007, when approximately 350 participants came together. Conferences in this series take place now in a three year interval. Previous conferences were held in Karlsruhe, Germany (1983), Los Alamos, USA (1987), Gatchina (Leningrad), Russia (1989), Bad Honnef, Germany (1991), Boulder, USA (1993), Blaubeuren, Germany (1995), Vancouver, Canada (1997), Zuz, Switzerland (1999), Washington, DC, USA (2001), and Beijing, China (2004).

The aim of the Conference was to bring together the experts of both meson physics and baryon spectroscopy because of the great overlap of the physics questions in both fields. The progress in symmetry studies and its possible relevance for other fields was discussed. A critical review of the methods for resonance extractions was done and the role of final state interactions in modifying resonance properties has been addressed. Important questions for the future development of the field with regard to common aspects of the charmed quark sector and the light quark sector were worked out.

The aim of the Conference is to bring together the experts of both meson physics and baryon spectroscopy because of the great overlap of the physics questions in both fields. The progress in symmetry studies and its possible relevance for other fields will be discussed. A critical review of the methods for resonance extractions will be done and the role of final state interactions in modifying resonance properties has to be addressed. An important question for the future development of the field is to work out common aspects of the charmed quark sector and the light quark sector. A few overview talks which focus on the basic open questions of the field and possible applications in neighboring fields will be included.

Hadron physics investigates an open frontier of the Standard Model: the strong interaction for large gauge couplings. Experimentally, there two major strategies currently pursued:

- Precision experiments study symmetries and their violations with the aim to extract fundamental quantities of Quantum Chromodynamics, such as the quark masses,
- Studies of the excited states and their decays try to establish the ordering principles of the hadronic spectra in order to shed light on the problem of the confinement of the quarks.

On the theoretical side, the scientific paradigm has shifted within the last two decades to effective field theories. The basic idea is to characterize a physical system by its energy or length scales. Within a given energy range, the important symmetries have to be identified and only the relevant degrees of freedom have to be treated explicitly, while physics at higher energy scales can be summarized by a finite set of low-energy constants. The number of those constants is limited by a systematic counting scheme and depends on the precision one aims for. The effective field theory of Quantum Chromodynamics is called Chiral Perturbation Theory. By now, it is a standard tool for hadron physics in the threshold region. For larger energies, chiral perturbation theory has to be unitarized. Nuclear effective field theory is an extension of chiral perturbation theory based on Weinberg's suggestions. In this field, there has been considerable progress. The two-nucleon potential obtained within nuclear effective field theory has been developed to a precision which is as high as the one of the best phenomenological potentials. Moreover, it allows a systematic inclusion of few-body forces. The few-body forces derived in effective field theory are closely linked to experimental data, such as pion-nucleon scattering and few-body reactions with polarized partners. Since the isospin dependence of those three-body interactions is determined mainly by data, one gains predictive power for theoretical studies of nuclear matter and eventually neutron-rich finite nuclei. These new developments start to bring together previously separated communities which makes them an interesting topic for the MENU conference. Presently, there is a wealth of new data for physics involving the strange quarks. Polarized electron scattering finds that the strangeness content of the nucleon is small. The recent experimental results for exotic atoms obtained by DEAR and at KEK are of high precision and have significantly increased the data base for antikaon-nucleon scattering. These new results start to impact on the discussion concerning the structure of the  $\Lambda(1405)$  which is notoriously difficult to obtain in quark models. Kaon production both with the electromagnetic probe and hadronic probes has been investigated and evidence for some new resonances has been claimed.

We hope that the programm achieved these goals. The next conference of this series will be held 2010 when Jefferson Lab. is the host. We wish it great success with exciting new results.

The proceedings consist of two volumes. In Volume I all submitted invited talks are compiled while Volume II contains all submitted contributions, presented orally or as posters.

Siegfried Krewald and Hartmut Machner  
Chairpersons, Organizing Committee



## Acknowledgements

Many people must be thanked for contributing to the success of the MENU 2007 Conference. There are the members of the International Advisory Committee, the Organizing Committee, the Editorial Committee and the conference secretary Mrs. Y. Abdel-Fattah. The help of a lot of young people, graduate students as well as postdocs, was essential in order to have a smooth running conference. The advice given by the Editorial Committee and the referees is gratefully acknowledged by the editors. Finally we thank the exhibitors and our sponsors for making this meeting possible.

Siegfried Krewald and Hartmut Machner  
Chairpersons, Organizing Committee

## International Advisory Committee

- Marco Battaglieri (INFN Genoa)
- Veronique Bernard (ULP Strasbourg, France)
- Stan Brodsky (SLAC, Stanford, USA)
- David V. Bugg (Queen Mary, U of London, England)
- Volker Burkert (JLAB, Newport News, VA, USA)
- Avraham Gal (HUJI, Jerusalem, Israel)
- Haiyan Gao (TUNL, Durham, NC, USA)
- Jürg Gasser (University of Bern, Switzerland)
- Carlo Guaraldo (LN Frascati, Italy)
- Hans-Werner Hammer (Univ. Bonn, Germany)
- Muhsin N. Harakeh (KVI, Groningen, The Netherlands)
- Bo Hoistad (TSL, Uppsala, Sweden)
- Bernd Krusche (University of Basel, Switzerland)
- Volker Metag (Univ. Giessen, Germany)
- Takashi Nakano (Osaka U, Japan)
- B.M.K. Nefkens (UCLA, CA, USA)
- Eulogio Oset (University of Valencia, Spain)
- Dan-Olof Riska (University of Helsinki, Finland)
- Craig D. Roberts (ANL, Argonne, IL, USA)
- Andreas Schäfer (Univ. Regensburg, Germany)
- Madeleine Soyeur (DAPHNIA/SPhN-CEA, Saclay, France)
- Ulrike Thoma (Univ. Bonn, Germany)

- Anthony Thomas (JLAB, Newport News, VA, USA)
- Hiroshi Toki (Osaka U, Japan)
- Willem T.H. van Oers (University of Manitoba, Winnipeg, Canada)
- Eberhard Widmann (Austrian Academy of Sciences, Vienna, Austria)
- Frank Wilczek (MIT, Boston, MA, USA)
- Bingsong Zou (Institute of High Energy Physics, Beijing, China)

### **Organizing Committee**

- A. Gillitzer, Jülich
- Detlev Gotta, Jülich
- Christoph Hanhart, Jülich
- Siegfried Krewald, Jülich (Co-Chair)
- Hartmut Machner, Jülich (Co-Chair)
- Rudolf Mayer, Jülich
- Ulf-G. Meißner, Jülich
- James Ritman, Jülich
- Susan Schadmand, Jülich (Scientific Secretary)
- Hans Ströher, Jülich

### **Editorial Committee**

- Albrecht Gillitzer, Jülich
- Detlev Gotta, Jülich
- Christoph Hanhart, Jülich

- Siegfried Krewald, Jülich
- Hartmut Machner, Jülich
- Susan Schadmand, Jülich

## **Sponsors**

- Forschungszentrum Jülich
- Deutsche Forschungsgemeinschaft
- International Union of Pure and Applied Physics
- Jefferson Laboratory
- European Community-Research Infrastructure Activity under the FP6 "Structuring the European Research Area" programme (HadronPhysics, contract number RII3-CT-2004-506078)

## **Industrial Exhibitors**

- CAEN ([www.caen-de.com](http://www.caen-de.com))
- Iseg High Voltage ([www.iseg-hv.de](http://www.iseg-hv.de))
- CalPlus ([www.calplus.de](http://www.calplus.de))
- Oerlikon ([www.oerlikon.com](http://www.oerlikon.com))
- Pfeiffer-Vacuum ([www.pfeiffer-vacuum.de](http://www.pfeiffer-vacuum.de))
- Struck Innovative Systems ([www.struck.de](http://www.struck.de))
- Tektronix ([www.tek.com](http://www.tek.com))
- Wiener ([www.wiener-d.com](http://www.wiener-d.com))



# Contents

<b>1</b>	<b>EFFECTIVE QUANTUM FIELD THEORIES</b>	<b>2</b>
	<i>J. Gasser</i>	
<b>2</b>	<b>KAONIC ATOMS EXPERIMENTAL STUDIES AT DAΦNE</b>	<b>12</b>
	<i>C. Curceanu et al.</i>	
<b>3</b>	<b>WIGNER-CUSP IN KAON DECAYS AND DETERMINATION OF <math>\pi\pi</math> SCATTERING LENGTHS</b>	<b>22</b>
	<i>R. Wanke</i>	
<b>4</b>	<b>ETA AND ETA' PHYSICS</b>	<b>33</b>
	<i>J. Bijnens</i>	
<b>5</b>	<b>RECENT KLOE RESULTS ON HADRON PHYSICS</b>	<b>44</b>
	<i>C. Bini</i>	
<b>6</b>	<b>STRUCTURE OF THE SCALARS</b>	<b>54</b>
	<i>M. R. Pennington</i>	
<b>7</b>	<b>SCALAR MESONS FROM AN EFFECTIVE LAGRANGIAN APPROACH</b>	<b>66</b>
	<i>A. H. Fariborz et al.</i>	
<b>8</b>	<b>PHYSICS PROGRAM AT COSY</b>	<b>76</b>
	<i>K.-Th. Brinkmann</i>	
<b>9</b>	<b>HADRON-HADRON AND HADRON-HADRON-HADRON PROPERTIES FROM LATTICE QCD</b>	<b>88</b>
	<i>Silas R. Beane</i>	
<b>10</b>	<b>HADRON STRUCTURE FROM LATTICE QCD</b>	<b>98</b>
	<i>A. Schäfer</i>	

<b>11 THE PHYSICS PROGRAM AT MAMI-C</b>	<b>111</b>
<i>P. Achenbach</i>	
<b>12 BARYON RESONANCES OBSERVED AT BES</b>	<b>121</b>
<i>B. S. Zou</i>	
<b>13 <math>K^+</math> PHOTOPRODUCTION AND <math>\pi^0</math> PHOTOPRODUCTION BY LINEARLY POLARIZED PHOTONS AT SPring-8/LEPS</b>	<b>134</b>
<i>M. Sumihama et al.</i>	
<b>14 BARYON SPECTROSCOPY WITH INELASTIC CHANNELS</b>	<b>144</b>
<i>A. Starostin and S. Prakhov</i>	
<b>15 CHARGED PION PHOTOPRODUCTION AND SCALING</b>	<b>155</b>
<i>H. Gao</i>	
<b>16 HADRONIC B DECAYS INTO NEW CHARMONIUM LIKE STATES</b>	<b>166</b>
<i>W. Toki</i>	
<b>17 ON THE BRINK OF MAJOR DISCOVERIES IN WEAK CHARM DECAYS – A BISMARCKIAN CHANCE TO MAKE HISTORY</b>	<b>177</b>
<i>I. Bigi</i>	
<b>18 THREE NUCLEON SYSTEM DYNAMICS STUDIED VIA <math>d</math>-<math>p</math> BREAKUP</b>	<b>190</b>
<i>St. Kistryn et al.</i>	
<b>19 THREE NUCLEON SCATTERING EXPERIMENTS FROM RIKEN</b>	<b>200</b>
<i>Kimiko Sekiguchi</i>	
<b>20 ELECTROMAGNETIC REACTIONS ON LIGHT NUCLEI USING CHIRAL EFFECTIVE THEORY</b>	<b>210</b>
<i>D. R. Phillips</i>	
<b>21 HADRONS IN MEDIUM – THEORY MEETS EXPERIMENT</b>	<b>221</b>

*U. Mosel*

<b>22 TOWARDS POLARIZED ANTIPROTONS AT FAIR</b>	<b>231</b>
<i>P. Lenisa and F. Rathmann</i>	
<b>23 HADRON PHYSICS WITH ANTI-PROTONS: The <math>\bar{\text{P}}\text{ANDA}</math> EXPERIMENT AT FAIR</b>	<b>241</b>
<i>J. Messchendorp</i>	
<b>24 FUTURE SCIENTIFIC OPPORTUNITIES AT JEFFERSON LAB</b>	<b>251</b>
<i>A. W. Thomas</i>	
<b>25 DYNAMICS, SYMMETRIES AND HADRON PROPERTIES</b>	<b>262</b>
<i>I.C. Cloët et al.</i>	
<b>26 CONCLUDING REMARKS</b>	<b>273</b>
<i>B. Nefkens and A. Starostin</i>	
<b>27 PION-DEUTERON SCATTERING LENGTH IN CHIRAL PERTURBATION THEORY UP TO ORDER <math>\chi^{3/2}</math></b>	<b>286</b>
<i>V. Baru et al.</i>	
<b>28 PROGRESS IN <math>NN \rightarrow NN\pi</math></b>	<b>297</b>
<i>V. Baru et al.</i>	
<b>29 <math>\sigma</math> CHANNEL LOW-MASS ENHANCEMENT IN DOUBLE- PIONIC FUSION – IS A DIBARYON RESONANCE THE REASON FOR THE ABC EFFECT?</b>	<b>307</b>
<i>M. Bashkanov et al.</i>	
<b>30 HOW WE DISCOVERED THE NONET OF LIGHT SCALAR MESONS</b>	<b>317</b>
<i>E. van Beveren and G. Rupp</i>	
<b>31 THE HEXAQUARK-FLAVOURED ANTIK-N-N STATE COMPUTED MICROSCOPICALLY WITH A CLUSTER- IZED OCTOQUARK</b>	<b>328</b>
<i>P. Bicudo</i>	

<b>32 THREE-BODY FORCE EFFECTS IN NEUTRON-DEUTERON SCATTERING AT 95 MeV</b>	<b>332</b>
<i>J. Blomgren et al.</i>	
<b>33 DECAYS OF <math>\eta</math> AND <math>\eta'</math></b>	<b>348</b>
<i>B. Borasoy</i>	
<b>34 GENERALIZED PARTON DISTRIBUTIONS AND DEEPLY VIRTUAL COMPTON SCATTERING AT CLAS</b>	<b>358</b>
<i>R. De Masi</i>	
<b>35 THE NATURE OF THE <math>N^*(1535)</math></b>	<b>363</b>
<i>M. Döring et al.</i>	
<b>36 PHOTOPRODUCTION OF <math>\eta</math> AND <math>\eta'</math> MESONS FROM THE PROTON</b>	<b>373</b>
<i>M. Dugger</i>	
<b>37 DELTA-RESONANCE CONTRIBUTIONS TO THE NUCLEAR FORCE</b>	<b>383</b>
<i>E. Epelbaum</i>	
<b>38 COULOMB EFFECTS IN FEW-NUCLEON SYSTEMS</b>	<b>393</b>
<i>A. C. Fonseca</i>	
<b>39 PRECISION EXTRACTION OF <math>a_{nn}</math> FROM <math>\pi^-d \rightarrow nn\gamma</math> USING CHIRAL PERTURBATION THEORY</b>	<b>403</b>
<i>A. Gårdestig and D. R. Phillips</i>	
<b>40 QCD SYMMETRIES IN EXCITED HADRONS</b>	<b>414</b>
<i>L. Ya. Glozman</i>	
<b>41 NEUTRON POLARIZABILITIES FROM DEUTERON COMPTON SCATTERING IN <math>\chi</math>EFT</b>	<b>424</b>
<i>H. W. Griesshammer</i>	
<b>42 RECENT BES RESULTS AND THE BESIII UPGRADE</b>	<b>435</b>
<i>F. A. Harris</i>	
<b>43 KAON-NUCLEON AND ANTI-KAON-NUCLEON INTERACTIONS IN A CONSTITUENT QUARK MODEL</b>	<b>445</b>
<i>F. Huang</i>	

<b>44</b>	<b>DYNAMICAL COUPLED-CHANNEL MODEL ANALYSIS OF <math>\pi</math>-N SCATTERING AND ELECTROMAGNETIC PION PRODUCTION REACTIONS</b>	<b>455</b>
	<i>B. Julia-Diaz</i>	
<b>45</b>	<b>VECTOR AND TENSOR ANALYZING POWERS OF THE <math>^1\text{H}(d,\gamma^3\text{He})</math> CAPTURE REACTION</b>	<b>466</b>
	<i>D. Kiselev et al.</i>	
<b>46</b>	<b>ISOSPIN VIOLATING NUCLEON FORM FACTORS</b>	<b>478</b>
	<i>B. Kubis</i>	
<b>47</b>	<b>PION SCALAR FORM FACTORS FROM <math>J/\psi</math> DECAYS</b>	<b>483</b>
	<i>T.A. Lähde</i>	
<b>48</b>	<b>HERMES RESULTS ON HARD-EXCLUSIVE PROCESSES AND PROSPECTS USING THE NEW RECOIL DETECTOR</b>	<b>493</b>
	<i>I. Lehmann</i>	
<b>49</b>	<b>ILLUMINATING THE <math>1/x</math> MOMENT OF PARTON DISTRIBUTION FUNCTIONS</b>	<b>502</b>
	<i>F.J. Llanes-Estrade et al.</i>	
<b>50</b>	<b>STUDIES OF CHARGE SYMMETRY BREAKING REACTIONS AT COSY</b>	<b>513</b>
	<i>A. Magiera</i>	
<b>51</b>	<b>LATTICE APPROACH TO LIGHT SCALARS</b>	<b>523</b>
	<i>C. McNeile</i>	
<b>52</b>	<b>LOCAL QUARK-HADRON DUALITY IN ELECTRON SCATTERING</b>	<b>533</b>
	<i>W. Melnitchouk</i>	
<b>53</b>	<b>TWO-PION-EXCHANGE EFFECTS IN <math>pp \rightarrow pp\pi^0</math> REACTION</b>	<b>542</b>
	<i>F. Myhrer</i>	
<b>54</b>	<b>MESON PRODUCTION IN NN COLLISIONS</b>	<b>550</b>
	<i>K. Nakayama et al.</i>	

<b>55 THE NATURE OF THE LIGHT SCALAR MESONS FROM THEIR RADIATIVE DECAYS</b>	<b>558</b>
<i>A. Nefediev</i>	
<b>56 SCALAR RADIUS OF THE PION AND TWO PHOTONS INTO TWO PIONS. STRONG S-WAVE FINAL STATE INTERACTIONS</b>	<b>563</b>
<i>J. A. Oller et al.</i>	
<b>57 PHOTOPRODUCTION OF <math>\omega</math> AND <math>\omega</math> IN THE NUCLEAR MEDIUM</b>	<b>573</b>
<i>E. Oset et al.</i>	
<b>58 SCALAR MESONS FROM UNITARIZED CHIRAL PERTURBATION THEORY: <math>N_c</math> AND QUARK MASS DEPENDENCES</b>	<b>583</b>
<i>J. Peláez et al.</i>	
<b>59 RECENT RESULTS FROM THE COMPASS EXPERIMENT AT CERN</b>	<b>593</b>
<i>S. Platchkov</i>	
<b>60 NEW RESULTS ON THE RARE DECAY <math>\eta \rightarrow \pi^0 \gamma \gamma</math></b>	<b>598</b>
<i>S. Prakhov</i>	
<b>61 SPIN PHYSICS WITH CLAS AT JEFFERSON LABORATORY</b>	<b>609</b>
<i>Y. Prok</i>	
<b>62 RENORMALIZING THE SCHRÖDINGER EQUATION FOR NN SCATTERING</b>	<b>617</b>
<i>E. Ruiz Arriola et al.</i>	
<b>63 EFFECTIVE FIELD THEORY FRAMEWORK FOR <math>\bar{K}d</math> SCATTERING</b>	<b>627</b>
<i>A. Rusetsky et al.</i>	
<b>64 TETRAQUARK SPECTROSCOPY</b>	<b>631</b>
<i>E. Santopinto et al.</i>	
<b>65 POSITIVE AND NEGATIVE PARITY CHARMED MESONS</b>	

<b>IN HEAVY HADRON CHIRAL PERTURBATION THEORY</b>	<b>641</b>
<i>R. P. Springer</i>	
<b>66 QUARK MODEL: RECENT ISSUES</b>	<b>649</b>
<i>Fl. Stancu</i>	
<b>67 PARTIAL-WAVE ANALYSIS AND SPECTROSCOPY: FROM <math>\pi</math>-N SCATTERING TO PION-ELECTROPRODUCTION</b>	<b>659</b>
<i>R. Arndt et al.</i>	
<b>68 ON AMBIGUITIES AND UNCERTAINTIES IN PWA</b>	<b>663</b>
<i>A. Švarc et al.</i>	
<b>69 NUCLEON AND PION-NUCLEON FORM FACTORS FROM LATTICE QCD</b>	<b>673</b>
<i>A. Tsapalis</i>	



# Plenary Session I

Welcome

Welcome to the Research Center

Opening Remarks on IUPAP

*Hartmut Machner*

*U. Samm*

*Willem van Oers*

**Session Chair:**

Chiral Effective Field Theory

Kaonic Atoms Experimental Studies at DAPHNE

Siegfried Krewald

*Jürg Gasser*

*Catalina Curceanu*

**Session Chair:**

Wigner-Cusp in Kaon Decays and Determination  
of  $\pi$ - $\pi$  Scattering Lengths

$\eta$  and  $\eta'$  Physics

$\eta$  Meson Decays with WASA-at-COSY

Jim Ritman

*Rainer Wanke*

*Johan Bijnens*

*Magnus Wolke*

MENU 2007  
11th International Conference  
on Meson-Nucleon Physics and  
the Structure of the Nucleon  
September 10-14, 2007  
IKP, Forschungszentrum Jülich, Germany

# EFFECTIVE QUANTUM FIELD THEORIES

*Jürg Gasser*  
Institute for Theoretical Physics  
University of Bern  
Sidlerstrasse 5  
CH 3012 Bern, Switzerland

## Abstract

After a short introduction to effective field theory, I concentrated in my talk on a recent application of the method: previous analyses of  $K_{e4}$  data neglected an important isospin breaking effect, generated by the pion mass difference and by  $\pi^0 - \eta$  mixing. Once it is taken into account, the previous discrepancy between NA48/2 data on  $K_{e4}$  decays and the prediction of  $\pi\pi$  scattering lengths in the framework of chiral perturbation theory disappears.

## 1 Introduction

In my talk, I provided a short introduction to effective quantum field theories. It is not necessary to provide here yet another introduction to the method, because there are many excellent reviews available on the market. A selected list of recent work is given in the bibliography [1], see also the contribution of Bijmans to this conference [2].

However, there is a point which is worth elaborating here. Chiral perturbation theory (ChPT) [3], combined with Roy equations, allows one to make very precise predictions for the values of the threshold parameters in elastic  $\pi\pi$  scattering [4] – see Colangelo’s contribution at KAON07 for a status report [5]. Several experiments allow one to confront these predictions with experimental data: i)  $K^+ \rightarrow \pi^+\pi^-e^+\nu_e$  decays [6, 7], ii) the pionium lifetime, measured by the DIRAC collaboration [8], and iii) the cusp effect in  $K \rightarrow 3\pi$  decays, investigated by the NA48/2 collaboration [9–11].

The experiments performed by the NA48/2 collaboration have generated an impressive data basis, as a result of which the matrix elements of  $K_{e4}$  and

$K \rightarrow 3\pi$  decays can be determined with an unprecedented accuracy [7, 9, 11]. The interpretation of these measurements was the main topic of my talk. In particular, I pointed out that the theoretical predictions and the measurements are performed in two different settings: the predictions concern pure QCD, in the isospin symmetry limit  $m_u = m_d$ , with photons absent. To be more precise, the convention is to choose the quark masses and the renormalization group invariant scale of QCD such that the pion and the kaon masses coincide with the values of the charged ones, and the pion decay constant is  $F_\pi = 92.4$  MeV. [I do not specify the masses of the heavy quarks, because in the present context, their precise values do not matter.] I refer to this framework as a *paradise world*.

On the other hand, experiments are all carried out in the presence of isospin breaking effects, generated by real and virtual photons, and by the mass difference of the up and down quarks: this is the *real world*, described by the Standard Model. We are thus faced with the problem to find the relation between quantities measured in the real world, where isospin breaking effects are always present, and the predictions made in the paradise world. I discuss the relevant points here for the case of  $K_{e4}$  decays. See also Ref. [12], and section 6 in the recent review Ref. [13].

## 2 $K_{e4}$ decays

### 2.1 General

In the NA48/2 experiment, the general purpose Monte Carlo program PHOTOS [14] is used to calculate electromagnetic corrections. In addition, the Sommerfeld factor is applied, to account for the Coulomb interaction between charged particles [15].

In my talk, I pointed out that in these prescriptions to perform radiative corrections, one specific mechanism is not included. Namely, the kaon may decay first into a neutral pion pair, that then annihilates into two charged pions, or first decay into a charged pion pair, that then re-scatters. In the real world, the neutral pion mass is smaller than the charged one by about 4.6 MeV<sup>1</sup>. As a result of this, the two contributions to the decay matrix element have a different holomorphic structure: the neutral (charged) pion loop generates a branch point at  $s_\pi = 4M_{\pi^0}^2$  (at  $s = 4M_\pi^2$ ), and the *phase* of the relevant form factor is affected with a cusp, and does not vanish at the threshold  $s = 4M_\pi^2$ .

---

<sup>1</sup>Throughout the text, I use the symbols  $M_\pi$  ( $M_{\pi^0}$ ) for the charged (neutral) pion mass.

## 2.2 Partial wave expansion: isospin symmetry limit

The matrix element for  $K^+(p) \rightarrow \pi^+(p_1)\pi^-(p_2)e^+(p_e)\nu_e(p_\nu)$  is

$$T = \frac{G_F}{\sqrt{2}} V_{us}^* \bar{u}(p_\nu) \gamma^\mu (1 - \gamma_5) v(p_e) (V_\mu - A_\mu), \quad (1)$$

where the last factor denotes hadronic matrix elements of the strangeness changing (vector and axial vector) currents,

$$V_\mu - A_\mu = \langle \pi^+(p_1)\pi^-(p_2) \text{ out} | (\bar{s}\gamma_\mu u - \bar{s}\gamma_\mu\gamma_5 u) | K^+(p) \rangle. \quad (2)$$

In the following, I concentrate on the matrix element of the axial vector current, because it carries information on the  $\pi\pi$  final state interactions and, in particular, on the  $\pi\pi$  phases. One decomposes  $A_\mu$  into Lorentz scalars,

$$A_\mu = -i \frac{1}{M_K} [(p_1 + p_2)_\mu F + (p_1 - p_2)_\mu G + (p_e + p_\nu)_\mu K]. \quad (3)$$

The form factors  $F, G, K$  are holomorphic functions of the three variables

$$s_\pi = (p_1 + p_2)^2, \quad t = (p_1 - p)^2, \quad u = (p_2 - p)^2. \quad (4)$$

Sometimes, it is useful to use instead

$$s_\pi = (p_1 + p_2)^2, \quad s_\ell = (p_e + p_\nu)^2, \quad \cos \theta_\pi, \quad (5)$$

where  $\theta_\pi$  is the angle of the  $\pi^+$  in the CM system of the two charged pions, with respect to the dipion line of flight in the rest system of the kaon [7, 16]. In the isospin symmetry limit, one identifies the  $\pi\pi$  phases in the matrix element in a standard manner, by performing a partial wave expansion, and using unitarity and analyticity, although, in the present case, this is a slightly intricate endeavor [17]. It is useful to introduce a particular combination of form factors,

$$F_1 = F + \frac{(M_K^2 - s_\pi - s_\ell)\sigma}{\lambda(M_K^2, s_\pi, s_\ell)^{1/2}} \cos \theta_\pi G. \quad (6)$$

Here,  $\sigma = \sqrt{1 - 4M_\pi^2/s_\pi}$ , and  $\lambda(x, y, z)$  is the triangle function. The form factor  $F_1$  has a simple partial wave expansion,

$$F_1 = f(s_\pi, s_\ell) + \sum_{k \geq 1} P_k(\cos \theta_\pi) f_k(s_\pi, s_\ell). \quad (7)$$

In the low-energy region  $s_\pi \leq 16M_\pi^2$ ,  $f_k$  carry the  $\pi\pi$  phases [17] in the pertinent isospin channel. In the following, I consider the lowest partial

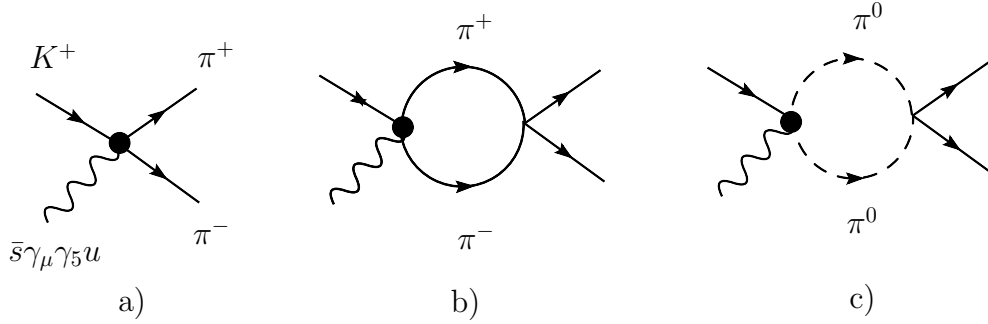


Figure 1: Some of the graphs that contribute to the matrix element of the axial current at tree and one-loop order. The filled vertex indicates that the axial current also couples to a single kaon line. That graph contributes to the form factor  $K$ . There are many additional graphs at one-loop order, not displayed in the figure.

wave  $f(s_\pi, s_\ell)$ . In the interval  $4M_\pi^2 \leq s_\pi \leq 16M_\pi^2$ , its phase coincides with the isospin zero  $S$ -wave phase  $\delta_0^0$  in elastic  $\pi\pi$  scattering,

$$f_+ = e^{2i\delta_0^0} f_-, \quad f_\pm = f(s_\pi \pm i\epsilon, s_\ell). \quad (8)$$

It is instructive to calculate the form factors in chiral perturbation theory and to verify that  $F_1$  indeed has the behaviour just discussed. For this, it is sufficient to consider the effective Lagrangian

$$\mathcal{L}_2 = \frac{F_0^2}{4} \langle D_\mu U D^\mu U^\dagger + 2B_0 \mathcal{M}(U + U^\dagger) \rangle, \quad (9)$$

where the covariant derivative  $D_\mu U$  contains the external vector and axial vector currents, and  $\mathcal{M} = \text{diag}(\hat{m}, \hat{m}, m_s)$ . Some of the graphs that contribute at tree level and at one loop are displayed in Figure 1. The result is [18]

$$f(s_\pi, s_\ell) = \frac{M_K}{\sqrt{2}F_0} \left\{ 1 + \Delta(s_\pi) + H(s_\pi, s_\ell) + O(p^4) \right\}, \quad (10)$$

with

$$\begin{aligned} \Delta(s_\pi) &= \frac{1}{2F_0^2} (2s_\pi - M_\pi^2) \bar{J}(s_\pi), \\ 16\pi^2 \bar{J}(s_\pi) &= \sigma \left( \ln \frac{1-\sigma}{1+\sigma} + i\pi \right) + 2, \quad s_\pi \geq 4M_\pi^2. \end{aligned} \quad (11)$$

Here,  $M_\pi (F_0)$  denotes the pion mass (pion decay constant), at leading order in the chiral expansion. The quantity  $H(s_\pi, s_\ell)$  is real in the interval of elastic  $\pi\pi$  scattering. It is now seen that  $f$  indeed has the property Eq. (8) at this order in the low-energy expansion, with

$$\delta_0^0 = \frac{(2s_\pi - M_\pi^2)}{32\pi F_0^2} \sigma. \quad (12)$$

This is the phase of the isospin zero  $S$ -wave, in tree approximation.

### 2.3 Partial wave expansion: the real world

In reality, experiments are not carried out in the paradise world of the previous subsection: we have not included so far photons, nor did we consider isospin breaking effects generated by different up and down quark masses. Here, I investigate these effects in several steps [19]:

- i) I assume that the manner in which real and virtual photons are treated in the analysis of the NA48/2 experiment (PHOTOS + Sommerfeld factor) is a decent approximation to the effects generated by soft photons.
- ii) This procedure misses the effects generated by the pion and kaon mass differences, and by the quark mass difference  $m_d - m_u$ . These must therefore be taken into account separately.
- iii) ChPT is the appropriate tool to evaluate these contributions.
- iv) I assume that PHOTOS+Sommerfeld factor + mass effects provide a good approximation to the full isospin breaking contributions.

Remark: One may envisage a more ambitious procedure [20], by working out the relevant matrix elements in the framework of ChPT including photons and leptons [21], and then constructing a new event generator, to be used in the analysis of  $K_{e4}$  decays. [A one-loop calculation was already performed in Ref. [22]. It needs to be checked, and brought into a form which is suitable for the present purpose.] Eventually, such an analysis might lead to an improved algorithm, but I consider it a long term project. End of remark.

According to iii), we simply need to perform a ChPT calculation of the effects generated by the mass differences. This is rather easy to achieve at one-loop order: one adapts the quark mass matrix,  $\mathcal{M} \rightarrow \text{diag}(m_u, m_d, m_s)$ , and enlarges the Lagrangian  $\mathcal{L}_2$  [23],

$$\mathcal{L}_2 \rightarrow \mathcal{L}_2 + C \langle QUQU^\dagger \rangle, \quad Q = \frac{e}{3} \text{diag}(2, -1, -1), \quad (13)$$

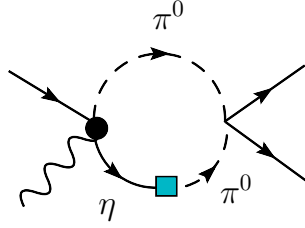


Figure 2: The contribution from  $\pi^0 - \eta$  mixing, at leading order in  $m_d - m_u$ . The filled square denotes the vertex from  $\pi^0 - \eta$  mixing. Otherwise, the notation is the same as in Figure 1.

where  $C$  is a new low-energy constant, that breaks the isospin symmetry of the meson masses:  $M_\pi \neq M_{\pi^0}$ ,  $M_K \neq M_{K^0}$ .

The effect of the replacement Eq. (13) is twofold [19]: first, as just mentioned, the meson masses split. As a result of this, the loop contributions in Fig. 1b),c) have a different threshold, and the phase of the form factor  $f$  generates a cusp. Second, in addition to the graphs displayed in Figure 1, there is a new contribution shown in Figure 2: the kaon interacts with the axial current to generate a  $\pi^0\eta$  intermediate state. Because  $m_u \neq m_d$ , the  $\eta$  can transform back into a neutral pion, that then re-scatters with the second neutral pion into a charged pion pair.

Working out the relevant diagrams, one finds [24, 25] that the phase Eq. (12) becomes in the elastic region

$$\delta_0^0 \rightarrow \delta = \frac{1}{32\pi F_0^2} \left\{ (4\Delta_\pi + s_\pi)\sigma + (s_\pi - M_{\pi^0}^2) \left( 1 + \frac{3}{2R} \right) \sigma_0 \right\}, \quad (14)$$

with

$$\Delta_\pi = M_\pi^2 - M_{\pi^0}^2, \quad \sigma_0 = \sqrt{1 - 4M_{\pi^0}^2/s_\pi}, \quad R = \frac{m_s - \hat{m}}{m_d - m_u}. \quad (15)$$

The one-loop expressions for the form factors  $F, G$  given in Refs. [22] contain the effects considered here, up to terms of order  $\alpha_{QED}(m_d - m_u)$ .

I consider the result Eq. (14) to be very interesting, for the following reasons. First, due to the presence of the phase space factor  $\sigma_0$ , the phase  $\delta$  does not vanish at the threshold  $s_\pi = 4M_\pi^2$ . This unexpected behavior of the phase is the cusp effect already experienced in  $K \rightarrow 3\pi$  decays, with the role of neutral and charged pions interchanged. Second, the difference  $\delta - \delta_0^0$  is positive for  $s_\pi$  above the threshold, and even *increases* at large  $s_\pi$ ,

$$\delta - \delta_0^0 = \frac{3s_\pi}{64\pi F_0^2} \frac{1}{R} + O(1), \quad s_\pi/M_\pi^2 \gg 1. \quad (16)$$

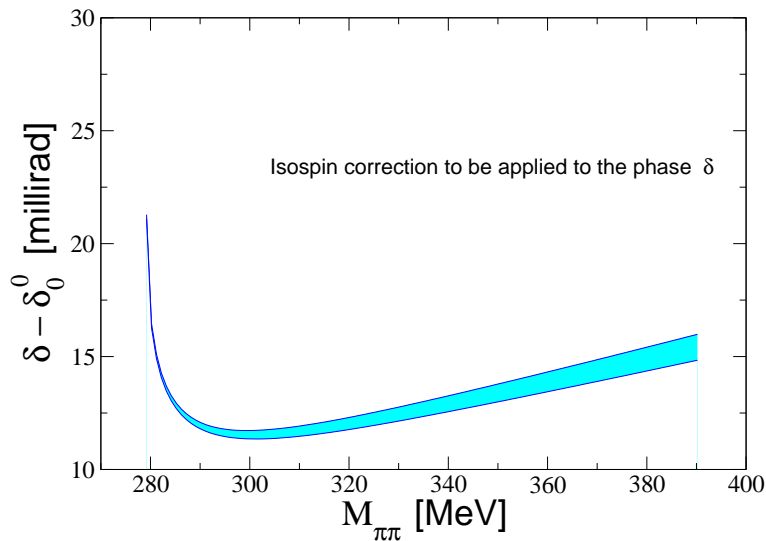


Figure 3: The isospin breaking correction that must be subtracted from the phase  $\delta$  measured in  $K_{e4}$  decays. The width of the band reflects the uncertainty in the ratio  $R$ .

We now come to the main point. According to point iv) above, it is the phase  $\delta$  that is measured in  $K_{e4}$  decays (up to contributions from higher orders in the chiral expansion). Therefore, before comparing the phase so determined with ChPT predictions, one has to subtract from the measured phase the (positive) difference  $\delta - \delta_0^0$ , because  $\delta_0^0 = \delta - (\delta - \delta_0^0)$ . In Figure 3 we display this difference in the relevant decay region, for  $R = 37 \pm 4^2$ . The width of the band reflects the uncertainty in  $R$ . [Two-loop contributions are modest in the analogous case of the scalar form factor of the pion [25].] It is seen that the isospin correction is quite substantial – well above the uncertainties quoted for the measured phase [7]. [In Ref. [26], the cusp in  $K_{e4}$  decays was investigated as well. The expressions presented there do not agree with Eq. (14), because these authors do not take into account derivative couplings of the  $\pi\pi$  amplitude, as is dictated by chiral symmetry.]

Colangelo has performed fits to  $K_{e4}$  data, with and without isospin breaking corrections applied. It turns out that the former discrepancy [27] of the NA48/2 data with the prediction [4] disappears, once isospin breaking effects are taken into account in the manner just described, see Refs. [5, 7]. Colan-

<sup>2</sup>This value for  $R$  should be considered as preliminary – it was used in my talk for illustrative purposes. A more refined estimate will be provided in Ref. [25]. Of course, the conclusions to be drawn from the isospin breaking effects considered here will not change.

gelo also shows that the former agreement between the chiral prediction and the E865 data [6] becomes marginal. This is an issue that should be understood, because it is independent of the special effects considered here. On the other hand, since the NA48/2 data are so precise, they will dominate the E865 result, in any case.

### Acknowledgments

It is a pleasure to thank the organizers for the invitation to give this talk, and for the excellent organization of this exciting conference. I thank M. Bissegger, G. Colangelo, A. Fuhrer, B. Kubis, H. Leutwyler and A. Rusetsky for a most enjoyable collaboration, B. Bloch–Devaux for explaining to me with patience details of the data analysis of  $K_{e4}$  decays, and Z. Was for discussions on PHOTOS.

## References

- [1] S. Scherer, *Adv. Nucl. Phys.* **27** (2003) 277 [arXiv:hep-ph/0210398]; B. Ananthanarayan, *Pramana* **61**, 911 (2003) [arXiv:hep-ph/0304061]; B. Moussallam, arXiv:hep-ph/0407246; J. L. Goity, *Czech. J. Phys.* **51** (2004) B35; J. Bijnens, *Prog. Part. Nucl. Phys.* **58**, 521 (2007) [arXiv:hep-ph/0604043]; V. Bernard and U. G. Meissner, *Ann. Rev. Nucl. Part. Sci.* **57** (2007) 33 [arXiv:hep-ph/0611231]; B. Kubis, arXiv:hep-ph/0703274; V. Bernard, *Prog. Part. Nucl. Phys.* **60** (2008) 82 [arXiv:0706.0312 [hep-ph]]; C. P. Burgess, arXiv:hep-th/0701053; B. Borasoy, arXiv:hep-ph/0703297.
- [2] J. Bijnens, *Eta and Eta' physics*, talk given at this conference, arXiv:0710.4017 [nucl-th].
- [3] S. Weinberg, *Physica A* **96** (1979) 327.
- [4] G. Colangelo, J. Gasser and H. Leutwyler, *Nucl. Phys. B* **603** (2001) 125 [arXiv:hep-ph/0103088].
- [5] G. Colangelo, *Theoretical progress on  $\pi\pi$  scattering lengths and phases*, talk given at KAON'07 [28], PoS(KAON)038 [arXiv:0710.3050 [hep-ph]].
- [6] L. Rossetet *et al.*, *Phys. Rev. D* **15** (1977) 574; S. Pislak *et al.* [BNL-E865 Collaboration], *Phys. Rev. Lett.* **87** (2001) 221801 [arXiv:hep-ex/0106071]; S. Pislak *et al.* [BNL-E865 Collaboration], *Phys. Rev. D* **67** (2003) 072004 [arXiv:hep-ex/0301040].

- [7] B. Bloch-Devaux, *Recent results from NA48/2 on  $Ke_4$  decays and interpretation in term of  $\pi\pi$  scattering lengths*, talk given at KAON'07 [28], PoS (KAON) 035.
- [8] B. Adeva *et al.* [DIRAC Collaboration], Phys. Lett. B **619** (2005) 50 [arXiv:hep-ex/0504044]; L. Tauscher, *An update of the DIRAC result on the  $\pi\pi |a_0 - a_2|$  scattering length*, talk given at KAON'07 [28].
- [9] J. R. Batley *et al.* [NA48/2 Collaboration], Phys. Lett. B **633** (2006) 173 [arXiv:hep-ex/0511056]; L. Di Lella, *Review of  $\pi\pi$  scattering measurements in  $K$  decays*, talk given at KAON'07 [28]; E. Goudzovski, *Precision study of  $K^\pm \rightarrow \pi^\pm\pi^0\pi^0$  and  $K^\pm \rightarrow \pi^\pm\pi^+\pi^-$  Dalitz plot distributions by NA48/2*, talk given at KAON'07 [28], PoS (KAON) 034 [arXiv:0706.4059 [hep-ex]].
- [10] N. Cabibbo, Phys. Rev. Lett. **93** (2004) 121801 [arXiv:hep-ph/0405001]; N. Cabibbo and G. Isidori, JHEP **0503** (2005) 021 [arXiv:hep-ph/0502130]; G. Colangelo, J. Gasser, B. Kubis and A. Rusetsky, Phys. Lett. B **638** (2006) 187 [arXiv:hep-ph/0604084]; M. Bissegger, A. Fuhrer, J. Gasser, B. Kubis and A. Rusetsky, arXiv:0710.4456 [hep-ph].
- [11] R. Wanke, *Wigner-Cusp in Kaon Decays and Determination of  $\pi\pi$  Scattering Lengths*, talk given at this conference.
- [12] J. Gasser, A. Rusetsky and I. Scimemi, Eur. Phys. J. C **32** (2003) 97 [arXiv:hep-ph/0305260].
- [13] J. Gasser, V. E. Lyubovitskij and A. Rusetsky, arXiv:0711.3522 [hep-ph].
- [14] E. Barberio and Z. Was, Comput. Phys. Commun. **79** (1994) 291; G. Nanava and Z. Was, Eur. Phys. J. C **51** (2007) 569 [arXiv:hep-ph/0607019].
- [15] B. Bloch-Devaux and Z. Was, private communications.
- [16] N. Cabibbo and A. Maksymovicz, Phys. Rev. **137** (1965) B438; erratum Phys. Rev. **168** (1968) 1926.
- [17] F. A. Berends, A. Donnachie and G. C. Oades, Phys. Lett. **26B** (1967) 109; Phys. Rev. **171** (1968) 1457.
- [18] J. Bijnens, Nucl. Phys. B **337** (1990) 635 ; C. Riggensbach, J. Gasser, J. F. Donoghue and B. R. Holstein, Phys. Rev. D **43** (1991) 127.

- [19] J. Gasser and A. Rusetsky, internal note, March 2007.
- [20] M. Knecht, private communication, and internal note, June 2007.
- [21] M. Knecht, H. Neufeld, H. Rupertsberger and P. Talavera, Eur. Phys. J. C **12** (2000) 469 [arXiv:hep-ph/9909284].
- [22] V. Cuplov and A. Nehme, arXiv:hep-ph/0311274; A. Nehme, Phys. Rev. D **69** (2004) 094012 [arXiv:hep-ph/0402007]; A. Nehme, Eur. Phys. J. C **40** (2005) 367 [arXiv:hep-ph/0408104].
- [23] R. Urech, Nucl. Phys. B **433** (1995) 234 [arXiv:hep-ph/9405341]; H. Neufeld and H. Rupertsberger, Z. Phys. C **71** (1996) 131 [arXiv:hep-ph/9506448].
- [24] J. Gasser, *Theoretical progress on cusp effect and  $K_{l4}$  decays*, talk given at KAON'07 [28], PoS (KAON) 033 [arXiv:0710.3048 [hep-ph]].
- [25] G. Colangelo, J. Gasser and A. Rusetsky, to appear.
- [26] S. R. Gevorkyan, A. N. Sissakian, A. V. Tarasov, H. T. Torosyan and O. O. Voskresenskaya, arXiv:0704.2675 [hep-ph].
- [27] B. Bloch-Devauux, *Recent results from NA48/2 on  $K_{e4}$  and  $K_{3\pi}$  decays - Interpretation in terms of  $\pi\pi$  scattering lengths*, talk given at: QCD 2006, Montpellier, France, 3-7 July 2006, Nucl. Phys. B (Proceedings Supplements), volume **174C**, pp. 91-96 (in press); B. Bloch-Devauux, *Recent results from NA48/2 on  $K_{e4}$  and  $K_{3\pi}$  decays - Interpretation in terms of  $\pi\pi$  scattering lengths*, talk given at: XLII<sup>nd</sup> Rencontres de Moriond QCD 2007, La Thuile, Italy, 17-24 March 2007, in: QCD PROCEEDINGS [[http://events.lal.in2p3.fr/Moriond/QCD\\_PROC.html](http://events.lal.in2p3.fr/Moriond/QCD_PROC.html)].
- [28] Kaon International Conference (KAON'07), Frascati, Italy, May 21 – 25, 2007.

## KAONIC ATOMS EXPERIMENTAL STUDIES AT DAΦNE

C. Curceanu (Petrascu)<sup>1,2</sup>, M. Bazzi<sup>2</sup>, G. Beer<sup>3</sup>, L. Bombelli<sup>4</sup>,  
A.M. Bragadireanu<sup>2,5</sup>, M. Cargnelli<sup>6</sup>, M. Catitti<sup>2</sup>, C. Fiorini<sup>4</sup>, T. Frizzi<sup>4</sup>,  
F. Ghio<sup>7</sup>, B. Girolami<sup>7</sup>, C. Guaraldo<sup>2</sup>, R. Hayano<sup>8</sup>, M. Iliescu<sup>2,5</sup>,  
T. Ishiwatari<sup>6</sup>, M. Iwasaki<sup>9</sup>, P. Kienle<sup>6,10</sup>, P. Lechner<sup>11</sup>, P. Levi Sandri<sup>2</sup>,  
A. Longoni<sup>4</sup>, V. Lucherini<sup>2</sup>, J. Marton<sup>6</sup>, D. Pietreanu<sup>2</sup>, T. Ponta<sup>5</sup>,  
D.L. Sirghi<sup>2,5</sup>, F. Sirghi<sup>2,5</sup>, H. Soltau<sup>11</sup>, L. Struder<sup>12</sup>, H. Tatsuno<sup>8</sup>,  
O. Vazquez Doce<sup>2</sup>, E. Widmann<sup>6</sup>, J. Zmeskal<sup>6</sup>

<sup>2</sup>INFN, Laboratori Nazionali di Frascati, Frascati (Roma), Italy

<sup>3</sup>Department of Physics and Astronomy, University of Victoria, Victoria  
B.C., Canada

<sup>4</sup>Politecnico di Milano, Dip. di Elettronica, Milano, Italy

<sup>5</sup>IFIN-HH, Magurele, Bucharest, Romania

<sup>6</sup>Stefan Meyer Institut für subatomare Physik, Vienna, Austria

<sup>7</sup>INFN Sezione di Roma I and Istituto Superiore di Sanita', Roma, Italy

<sup>8</sup>Univ. of Tokyo, Tokyo, Japan

<sup>9</sup>RIKEN, The Institute of Physical and chemical research, Muon Science  
Laboratory, Saitama, Japan

<sup>10</sup>Technische Universität München, Physik Department, Garching, Germany

<sup>11</sup>PNSensors GmbH, München, Germany

<sup>12</sup>MPI for Extraterrestrial Physics, Garching, Germany

### Abstract

The DAΦNE electron-positron collider at the Frascati National Laboratories has made available a unique “beam” of negative kaons. The DEAR (DAΦNE Exotic Atom Research) experiment at DAΦNE and its successor SIDDHARTA (Silicon Drift Detector for Hadronic Atom Research by Timing Application) aim at a precision measurement of the strong interaction energy shift and width of the  $1s$  level, via the measurement of the X-ray transitions to this level, for kaonic hydrogen and kaonic deuterium. The final aim is to extract the isospin dependent antikaon-nucleon scattering lengths which contribute to the understanding of aspects of non-perturbative QCD in the strangeness sector. Other hadronic atoms transition measurements possible at DAΦNE are under study.

---

<sup>1</sup>E-mail address: catalina.petrascu@lnf.infn.it

# 1 Introduction

The DAΦNE [1] electron-positron collider at the Frascati National Laboratories produces the  $\phi$ -resonance, which decays with a probability of about 50% in  $K^+K^-$ , providing low energy kaons (16 MeV of kinetic energy) which can be used for the study of the low-energy kaon-nucleon interaction, a field still largely unexplored. By making use of the  $K^-$  from DAΦNE, the DEAR (DAΦNE Exotic Atom Research) experiment [2] at DAΦNE and its successor SIDDHARTA (Silicon Drift Detector for Hadronic Atom Research by Timing Application) [3] aim at eV precision measurement of the strong interaction energy shifts and widths of the  $1s$  level, via the measurement of the X-ray transitions to this level, for kaonic hydrogen and kaonic deuterium. The final goal is to extract, for the first time, the isospin dependent antikaon-nucleon scattering lengths, fundamental quantities for the understanding of aspects of chiral symmetry breaking in the strangeness sector.

In practice, in studying kaonic hydrogen (deuterium) in order to measure the strong interaction component of the kaon-nucleon force, one measures the energy shift  $\epsilon$  of the  $K_\alpha$  line ( $2p \rightarrow 1s$  transition) from the one calculated from a purely electromagnetic interaction:

$$\epsilon = |E_{2p \rightarrow 1s}^{measured}| - |E_{2p \rightarrow 1s}^{e.m.}| \quad (1)$$

and the width (broadening)  $\Gamma$  of the  $1s$  level given by the strong interaction.

The electromagnetic transition energy in kaonic hydrogen is calculated with 1 eV precision by solving the corresponding Klein-Gordon equation and applying the corrections for finite size and vacuum polarization. The resulting value is:

$$E_{2p \rightarrow 1s}^{e.m.} = (6480 \pm 1) \text{ eV} \quad (2)$$

where the 1 eV error is dominated by the uncertainty of the kaon mass [4].

Until the advent of DAΦNE, the kaonic hydrogen parameters were measured at KEK [5], where the following results were found:

$$\epsilon = -323 \pm 63(stat.) \pm 11(syst.) \text{ eV} \quad (3)$$

$$\Gamma = 407 \pm 208(stat.) \pm 100(syst.) \text{ eV} \quad (4)$$

This measurement, which solved the so-called “kaonic hydrogen puzzle”, showed clearly that the antikaon-nucleon interaction is of repulsive type, but cannot be considered a precision measurement. The challenging aim of the DEAR/SIDDHARTA experiment is, therefore, to measure the kaonic hydrogen transition with a precision at the eV level. The kaonic deuterium,

fundamental to determine the two antikaon-nucleon isospin dependent scattering lengths (as will be shown in the next Section), will be measured for the first time. These results will represent a breakthrough in the study of the low-energy antikaon-nucleon interaction.

In Section 2, the DEAR/SIDDHARTA scientific case will be discussed. Section 3 contains the presentation of the SIDDHARTA setup, while the paper ends with Section 4, dedicated to Conclusions.

## 2 The DEAR/SIDDHARTA scientific case

The aim of the experiment is a precise determination of the isospin dependent antikaon-nucleon scattering lengths, through an eV measurement of the  $K_\alpha$  line shift and width in kaonic hydrogen, and, for the first time, a similar measurement of kaonic deuterium. SIDDHARTA measures the X-ray transitions occurring in the cascade processes of kaonic atoms. A kaonic atom is formed when a negative kaon (from the decays of  $\phi$ s, produced at DAΦNE) enters a target, loses its kinetic energy through the ionization and excitation of the atoms and molecules of the medium, and is eventually captured, replacing the electron, in an excited orbit. Via different cascade processes (Auger effect, Coulomb deexcitation, scattering, electromagnetic transitions) the kaonic atom deexcites to lower states. Whenever a small angular momentum state is reached, the strong interaction with the nucleus comes into play. This strong interaction is the reason for a shift in energy of the lowest-lying level from the purely electromagnetic value and for a finite lifetime of the state, due to nuclear reaction of the kaon.

For kaonic hydrogen and deuterium the K-series transitions are of primary experimental interest since they are the ones mostly affected by the strong interaction (the shift of the energy due to the presence of strong interaction is at the level of hundred(s) of eV). The  $K_\alpha$  lines are clearly separated from the higher K transitions. The shift  $\epsilon$  and the width  $\Gamma$  of the 1s state of kaonic hydrogen are related in a fairly model-independent way to the real and imaginary part of the complex s-wave scattering length,  $a_{K-p}$  :

$$\epsilon + i\Gamma/2 = 412a_{K-p} \text{ eV fm}^{-1} \quad (5)$$

This expression is known as the Deser-Trueman formula [6]. A similar relation applies to the case of kaonic deuterium and to its corresponding scattering length,  $a_{K-d}$ .

The observable scattering lengths  $a_{K-p}$  and  $a_{K-d}$  can be expressed in terms of the  $\bar{K}N$  isospin dependent scattering lengths  $a_0$  (I=0) and  $a_1$  (I=1). The kaonic hydrogen scattering length is simply the average of the two:

$$a_{K^-p} = 1/2(a_0 + a_1) \quad (6)$$

while the kaonic deuterium scattering length  $a_{K^-d}$  is related to  $a_0$  and  $a_1$  in the following way:

$$a_{K^-d} = 2\left(\frac{m_N + m_K}{m_N + m_K/2}\right)a^{(0)} + C \quad (7)$$

where

$$a^{(0)} = \frac{1}{2}(a_{K^-p} + a_{K^-n}) = \frac{1}{4}(3a_1 + a_0) \quad (8)$$

corresponds to the isoscalar  $\overline{K}N$  scattering length. The first term in eq. (8) represents the lowest-order impulse approximation, i.e.  $K^-$  scattering from each (free) nucleon. The second term,  $C$ , includes all higher contributions related to the physics associated to the  $K^-d$  three-body interaction.

The determination of the  $\overline{K}N$  scattering lengths requires the calculation of  $C$ . This is a well-known three-body problem, solvable by the use of Faddeev equations, when the two-body interactions are specified. The  $K^-d$  three-body problem includes the complication that the  $K^-p$  and  $K^-n$  interactions involve significant inelastic channels. The  $K^-p$  and  $K^-n$  scattering lengths are thus complex and so is the  $K^-d$  scattering length. Incorporating  $\overline{K}N$  scattering data and its sub-threshold behavior, the two-body potentials are determined in a coupled-channel formalism including both elastic and inelastic channels. Three-body Faddeev equations are then solved by the use of the potentials, taking into account the coupling among the multi-channel interactions.

An accurate determination of the  $K^-N$  isospin dependent scattering lengths will place strong constraints on the low-energy  $K^-N$  dynamics, which in turn constrains the SU(3) description of chiral symmetry breaking [7].

In 2002, the DEAR experiment performed the most precise measurement to date of kaonic hydrogen X-ray transitions to the 1s level [8]:

$$\epsilon = -193 \pm 37(stat.) \pm 6(syst.) eV \quad (9)$$

$$\Gamma = 249 \pm 111(stat.) \pm 30(syst.) eV \quad (10)$$

This measurement has triggered new interest from the theoretical groups working in the low-energy kaon-nucleon interaction field, and as well it is related to non-perturbative QCD tests [9–13].

The new experiment, SIDDHARTA, aims to improve the precision obtained by DEAR by an order of magnitude and to perform the first measurement ever of kaonic deuterium. Other measurements (kaonic helium, sigmonic atoms, precise determination of the charged kaon mass) are also considered in the scientific program.

### 3 The SIDDHARTA experiment

SIDDHARTA represents a new phase in the study of kaonic atoms at DAΦNE. The DEAR precision was limited by a signal/background ratio of about 1/70. To significantly improve this ratio, a breakthrough is necessary. An accurate study of the background sources present at DAΦNE was redone. The background includes two main sources: synchronous background, coming together with the kaons – related to  $K^-$  interactions in the setup materials and also to the  $\phi$ -decay processes; it can be defined as hadronic background; asynchronous background, final products of electromagnetic showers in the machine pipe and in the setup materials originating from particles lost from primary circulating beams either due to the interaction of particles in the same bunch (Touschek effect) or due to the interaction with the residual gas. Accurate studies performed by DEAR showed that the main background source in DAΦNE is of the second type, which shows the way to reduce it. A fast trigger correlated to a kaon entering into the target would cut the main part of the asynchronous background.

X rays were detected by DEAR using CCDs (Charge-Coupled Devices) [14], which are excellent X-ray detectors, with very good energy resolution (about 140 eV FWHM at 6 keV), but having the drawback of being non-triggerable devices (since the read-out time per device is at the level of 10 s). A recently developed device, which preserves all good features of CCDs (energy resolution, stability and linearity), but additionally is triggerable - i.e. fast (at the level of  $1\mu\text{s}$ ), was implemented. This new detector is a large area Silicon Drift Detector (SDD), specially designed for spectroscopic application. The development of the new  $1\text{ cm}^2$  SDD device is partially performed under the Joint Research Activity JRA10 of the I3 project "Study of strongly interacting matter (HadronPhysics)" within FP6 of the EU.

The trigger in SIDDHARTA will be given by a system of scintillators which will recognize a kaon entering the target making use of the back-to-back production mechanism of the charged kaons at DAΦNE from  $\phi$  decay: of the type:  $e^+e^- \rightarrow \phi \rightarrow K^+K^-$ .

Monte Carlo simulations, together with tests on the Beam Test Facility (BTF) of LNF-INFN extrapolated to SIDDHARTA conditions, showed that the S/B ratio in the region of interest for kaonic hydrogen is about 20/1 for the asynchronous background, which is mainly due to the Touschek effect. Taking into account the synchronous background contribution as well, we can estimate a total S/B ratio of about 4/1.

The SIDDHARTA setup will contain 216 SDD chips of  $1\text{ cm}^2$  each, grouped in chips containing 3 SDDs (Fig. 1), organized in units containing  $18\text{ cm}^2$  SDDs (Fig. 2). The SDDs are placed around a cryogenic cylindrical

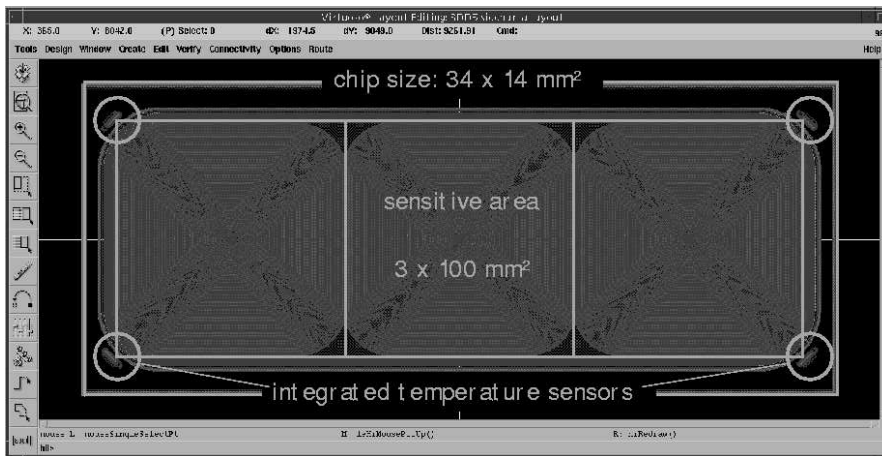


Figure 1: SDD layout on the readout side: 3 SDD cells, read independently, each of  $1 \text{ cm}^2$  area, monolithically integrated on one chip.

target, containing high density gaseous hydrogen (deuterium). The target is going to be made of kapton,  $75 \mu\text{m}$  thick, reinforced with an aluminium grid.

SDDs together with the readout electronics were intensively tested. The tests proved a very good experimental resolution, Figure 3, and a stability of the order of 2-3 eV at 6 keV (by using a 1 mV stabilized power supply developed in the framework of SIDDHARTA). 12 SDD  $18 \text{ cm}^2$  units will be placed all around the target cell, as shown in Figure 4. The setup will be installed above the beam pipe; in Figure 5 there is a drawing of the final setup in the DAΦNE interaction region.

SIDDHARTA is being assembled and it's going to be installed at DAΦNE by the end of 2007; a period of DAQ will follow in 2008, with the plan to collect  $400 \text{ pb}^{-1}$  integrated luminosity for kaonic hydrogen and about  $600 \text{ pb}^{-1}$  for kaonic deuterium, such as to obtain few eV precision for the parameters  $\epsilon$  and  $\Gamma$ .

## 4 Conclusions

DAΦNE has unique features as a kaon source which is intrinsically clean and of low momentum – a situation unattainable with fixed target machines – especially suitable for kaonic atom research.

The SIDDHARTA experiment combines the newly available techniques of large area triggerable SDD detectors with the good kaon beam quality to initiate a renaissance in the investigation of the low-energy kaon-nucleon

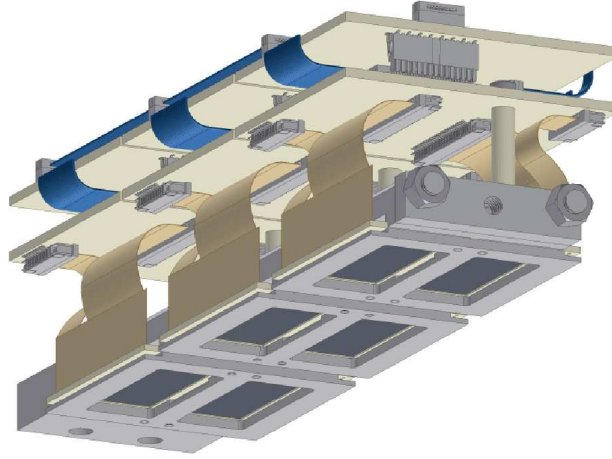


Figure 2: An 18 cm<sup>2</sup> SDD unit, containing 18 SDD individual chips.

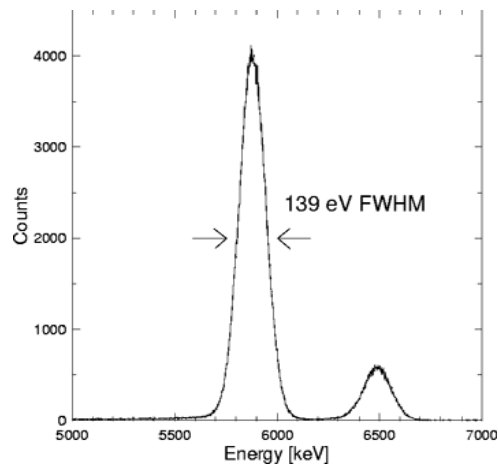


Figure 3: The X-ray spectrum from an Iron source as measured in the laboratory with a 1cm<sup>2</sup> SDD chip prototype. The experimental resolution, FWHM (Full Width Half Maximum) at 5.9 keV is 139 eV.

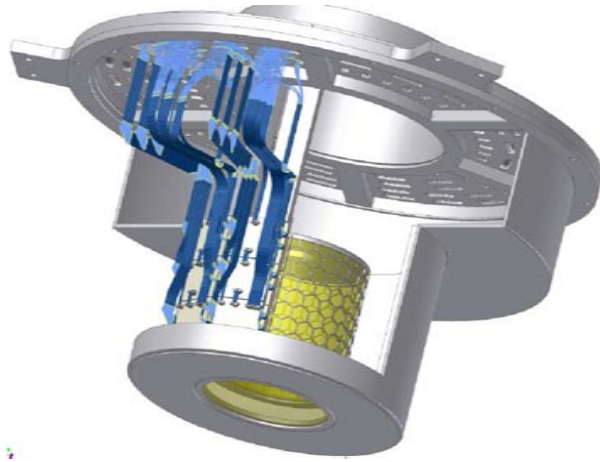


Figure 4: The SIDDHARTA target cell surrounded by SDD units (detail).

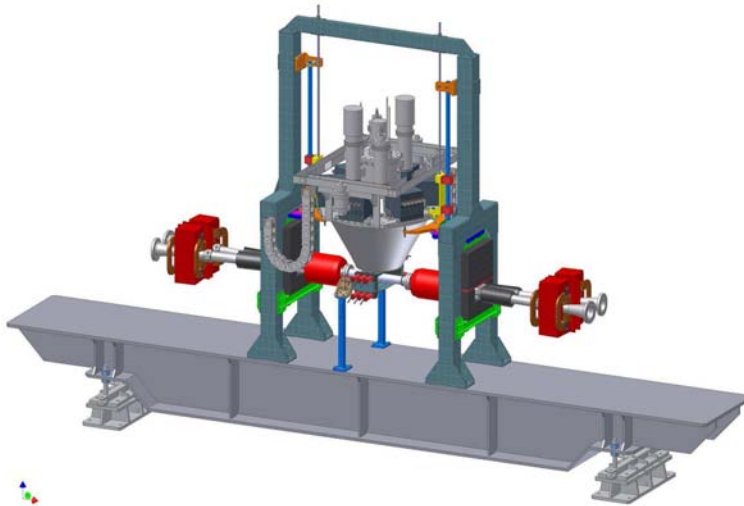


Figure 5: The schematic drawing of the SIDDHARTA setup in the Interaction Region of DAΦNE.

interaction. DEAR has performed the most precise measurement of kaonic hydrogen; the eV precision measurement of the strong interaction shift and width of the ground state in kaonic hydrogen will be performed by SIDDHARTA. The first measurement of kaonic deuterium is also planned. It will be then possible to extract the isospin dependent antikaon-nucleon scattering lengths, which will open new windows in the study of the kaon-nucleon

interaction.

The measurement of kaonic helium (with  $^3\text{He}$  and  $^4\text{He}$ ), feasible in SIDDHARTA, allows to study of the behaviour of the subthreshold resonance  $\Lambda(1405)$  in nuclei. Such measurements are of utmost importance, considering the recent KEK precision measurement on kaonic helium ( $^4\text{He}$ ) [15], consistent with the optical model calculations (see contributions to the present conference). Other light kaonic atoms can be studied in SIDDHARTA as well.

The precision measurement of the charged kaon mass by using kaonic nitrogen transitions, proved to be possible by DEAR, is as well under study.

DAΦNE proves to be a real and ideal “kaonic atom” factory.

### Acknowledgements

We thank Giovanni Corradi (LNF) and Diego Tagnani (LNF) for their fundamental contribution in designing and building part of the electronics and the highly stabilized power supply for the experiment. Part of this work was supported by HadronPhysics I3 FP6 European Community programme, Contract No. RII3-CT-2004-506078.

## References

- [1] G. Vignola, Proc. of the “5th European Particle Accelerator Conference”, Sitges (Barcelona), Eds. S. Myres *et al.*, (1996) 22.
- [2] S. Bianco *et al.*, Rivista del Nuovo Cimento **22**, No. 11 (1999) 1.
- [3] C. Curceanu *et al.*, Eur. Phys. J. **A31** (2007) 537.
- [4] C. Guaraldo *et al.*, Nucl. Phys. **A623** (1997) 311c.
- [5] M. Iwasaki *et al.*, Phys. Rev. Lett **78** (1997) 3067; T.M. Ito *et al.*, Phys. Rev. **A58** (1998) 2366.
- [6] S. Deser *et al.*, Phys. Rev. **96** (1954) 774; T.L. Truemann, Nucl. Phys. **26** (1961) 57; A. Deloff, Phys. Rev. **C13** (1976) 730.
- [7] C. Guaraldo, Physics and detectors for DAΦNE, Frascati Physics Series **16** (1999) 643.
- [8] G. Beer *et al.*, Phys. Rev. Lett. **94** (2005), 212302.
- [9] U.-G. Meissner, U. Raha and A. Rusetsky, E. Phys. J. **C35** (2004) 349.

- [10] J. Gasser, Mini-proceedings of the 4th International Workshop on *Chiral Dynamics 2003: Theory and Experiment*, Bonn 2003, edited by U.-G. Meissner, H.-W. Hammer and A. Wirzba, p.126.
- [11] B. Borasoy, R. Nissler and W. Weise, Phys. Rev. Lett. **94** (2005) 213401;  
B. Borasoy, R. Nissler and W. Weise, Phys. Rev. Lett. **96** (2006) 199201.
- [12] J. A. Oller, J. Prades and M. Verbeni, Phys. Rev. Lett. **95** (2005) 172502;  
J. A. Oller, J. Prades and M. Verbeni, Phys. Rev. Lett. **96** (2006) 199202.
- [13] J. Mares, E. Friedman and A. Gal, Nucl. Phys. **A770** (2006); J. Mares,  
E. Friedman and A. Gal, Phys. Lett. **B606** (2005) 295.
- [14] J.-P. Egger, D. Chatellard, E. Jeannet, Part. World. **3** (1993) 139.
- [15] S. Okada *et al.*, Phys. Lett. **B653** (2007) 387.

# WIGNER-CUSP IN KAON DECAYS AND DETERMINATION OF $\pi\pi$ SCATTERING LENGTHS

*R. Wanke*  
Institut für Physik  
Universität Mainz  
D-55099 Mainz, Germany

## Abstract

In the last few years it has become possible to study low energy  $\pi\pi$  scattering in kaon decays to three pions, thanks to the high statistics measurement of  $K^\pm \rightarrow \pi^\pm \pi^0 \pi^0$  decays performed by the NA48/2 experiment at the CERN SPS. At the  $\pi^+ \pi^-$  threshold, the  $\pi^0 \pi^0$  mass spectrum exhibits a Wigner-cusp, from which the  $S$ -wave  $\pi\pi$  scattering lengths are extracted with high precision. This measurement is complementary to the extraction of the scattering lengths from  $K_{e4}$  decays, which is also performed by the NA48/2 experiment.

## 1 Introduction

In the low-energy regime, the perturbative description of the strong interaction breaks down, as the strong coupling constant becomes of  $\mathcal{O}(1)$ . Chiral Perturbation Theory (ChPT) is an effective theory, which circumvents this problem by making use of the chiral symmetry of the theory in the limit of vanishing quark masses. Spontaneous breaking of the chiral symmetry generates 8 pseudo-scalar Goldstone bosons, among them pions and kaons. They obtain their small but non-zero masses by the additional symmetry breaking of non-vanishing quark masses. In the framework of ChPT, the values of the iso-spin 0 and 2  $S$ -wave  $\pi\pi$  scattering lengths  $a_0$  and  $a_2$  are directly connected with the size of the chiral condensate and the pion mass [1]. The scattering lengths can accurately be predicted to  $a_0 m_{\pi^+} = 0.220 \pm 0.005$  and  $a_2 m_{\pi^+} = -0.044 \pm 0.010$  [2]. Thus, precise measurements of the  $\pi\pi$  scattering lengths are a crucial test of ChPT.

Previous measurements have traditionally been performed in the semileptonic decay  $K^\pm \rightarrow \pi^+ \pi^- e^\pm \nu(\bar{\nu})$  ( $K_{e4}$ ). An early measurement by the Geneva-Saclay experiment analyzed 30000 events [3]. More recently, the BNL experiment E865 has measured  $(a_0 - a_2) m_{\pi^+} = 0.258 \pm 0.013$  from about 400000

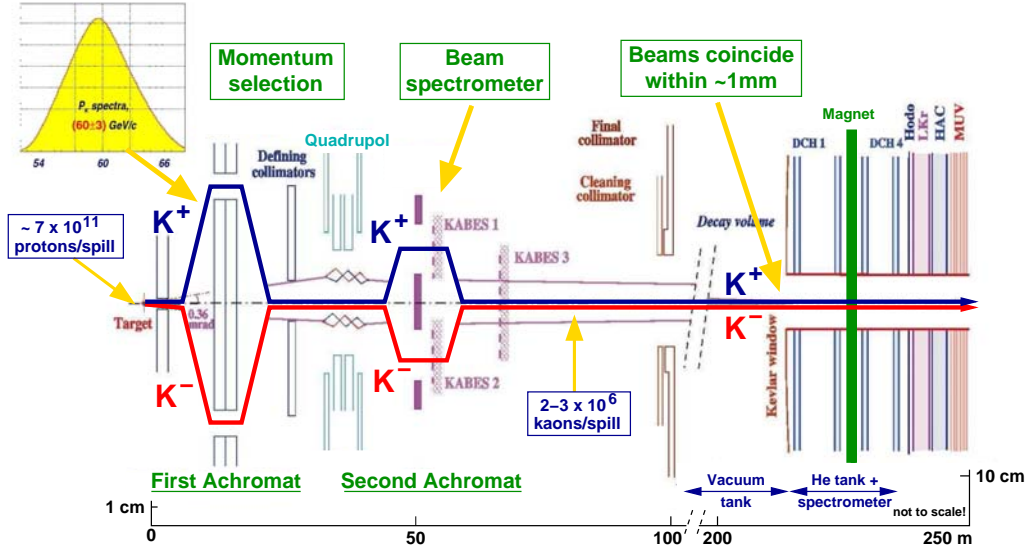


Figure 1: Set-up of the NA48/2 experiment.

$K_{e4}$  events [4]. Another recent determination of the scattering lengths has been carried out by the DIRAC experiment at CERN from the lifetime of pionium atoms. They obtain  $(a_0 - a_2)m_{\pi^+} = 0.264^{+0.020}_{-0.011}$  from an analysis of a part of their data [5].

Here, new measurements of the NA48/2 Collaboration are reported. In  $K^\pm \rightarrow \pi^\pm \pi^0 \pi^0$  decays, a Wigner-cusp from  $\pi\pi$  rescattering in the decay amplitude was discovered at  $m(\pi^0 \pi^0) = 2m_{\pi^+}$ . This allows a very precise determination of  $a_0$  and  $a_2$  with a completely new method. In addition, the NA48/2 Collaboration has also determined  $a_0$  and  $a_2$  in  $K_{e4}$  decays, with a greatly improved precision with respect to previous measurements.

The NA48/2 experiment has been taking data in the years 2003 and 2004. From a 400 GeV/c proton beam, positive and negative kaons with a momentum bite of  $p_K = (60 \pm 3)$  GeV/c were simultaneously selected by a system of achromats (see Fig. 1). A detailed detector description can be found in [6]. The main aim of the experiment was the search for direct CP violation in decays of charged kaons into three pions. The trigger therefore was designed to efficiently select events with three charged tracks as well as  $K^\pm \rightarrow \pi^\pm \pi^0 \pi^0$  events. In total, about  $2 \times 10^9$  three-track events and about  $90 \times 10^6$   $K^\pm \rightarrow \pi^\pm \pi^0 \pi^0$  events were recorded in the two years of data-taking.

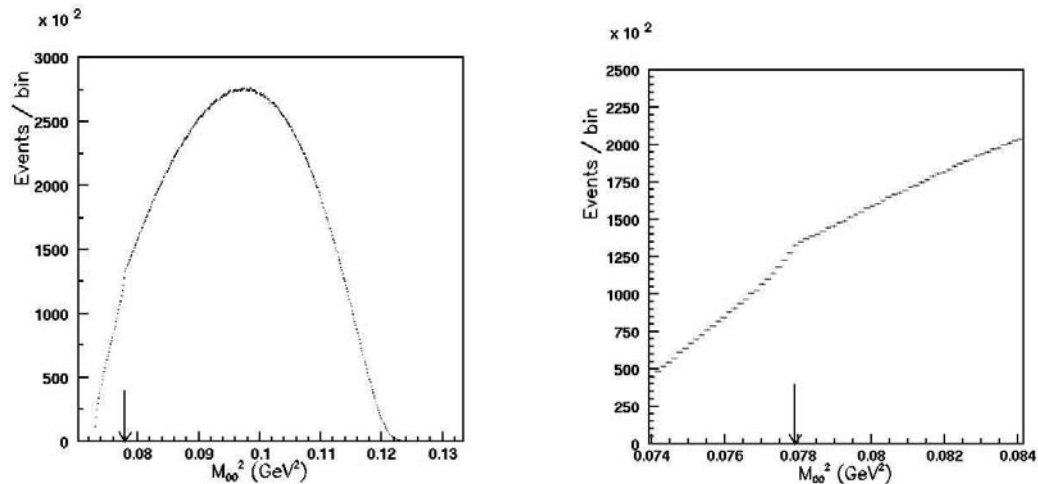


Figure 2: Distribution of  $m_{\pi^0\pi^0}^2$  of the NA48/2  $K^\pm \rightarrow \pi^\pm\pi^0\pi^0$  data. Left: Full kinematic region. Right: Zoom into the cusp region. The arrow marks the  $(2m_{\pi^+})^2$  threshold.

## 2 Wigner-Cusp and $\pi\pi$ Rescattering in $K^\pm \rightarrow \pi^\pm\pi^0\pi^0$ Decays

With the unprecedented statistics collected in the channel  $K^\pm \rightarrow \pi^\pm\pi^0\pi^0$ , it was possible for NA48/2 to precisely measure the distribution of the  $\pi^0\pi^0$  invariant mass. The original aim of this analysis was the search for the decay  $K^\pm \rightarrow \pi^\pm(\pi^+\pi^-)_{\text{atom}}$  with the subsequent decay of the pionium atom  $(\pi^+\pi^-)_{\text{atom}}$  into  $\pi^0\pi^0$ . It came as a surprise, that the  $\pi^0\pi^0$  invariant mass distribution exhibited a distinct and clearly visible cusp at the  $\pi^+\pi^-$  mass threshold (see Figure 2).

After its discovery, the effect was explained by N. Cabibbo [7] as Wigner cusp, arising from  $\pi^+\pi^- \rightarrow \pi^0\pi^0$  rescattering from the decay  $K^\pm \rightarrow \pi^\pm\pi^+\pi^-$ <sup>1</sup>. As consequence, a rescattering amplitude  $\mathcal{M}_1$  from  $K^\pm \rightarrow \pi^\pm\pi^+\pi^-$  has to be added to the unperturbed  $K^\pm \rightarrow \pi^\pm\pi^0\pi^0$  amplitude  $\mathcal{M}_0$ . Below the cusp point  $m_{\pi^0\pi^0} = 2m_{\pi^+}$ ,  $\mathcal{M}_1$  is real and negative, thus explaining the observed deficit of events. In the one-loop approximation,  $\mathcal{M}_1$  turns imaginary above the cusp. In this region, the effect on  $m_{\pi^0\pi^0}$  is much smaller and less visible. The cusp strength is proportional to  $(a_0 - a_2)m_{\pi^+}$ , the effect therefore allows the extraction of the  $\pi\pi$  scattering lengths.

<sup>1</sup>Independently, the effect had already been predicted in  $\pi\pi$  scattering much earlier by U.-G. Meißner and collaborators [8].

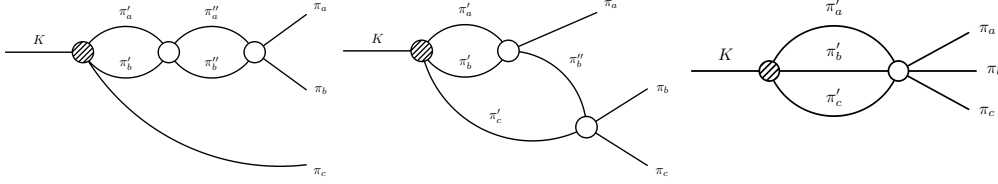


Figure 3: Diagrams of two-loop  $\mathcal{O}(a_i^2)$  corrections (from ref. [9]).

Second order calculations were performed by Cabibbo and Isidori [9]. These include two-loop level  $\mathcal{O}(a_i^2)$  corrections (Fig. 3), which allow the separate determination of the scattering length  $a_2$ . Also other rescattering processes as  $\pi^0\pi^0 \rightarrow \pi^0\pi^0$ ,  $\pi^+\pi^0 \rightarrow \pi^+\pi^0$ , etc. are considered, and all  $K \rightarrow 3\pi$  decays as e.g.  $K_L \rightarrow \pi^0\pi^0\pi^0$  are covered. From this, the theoretical error on the extraction of  $a_0 - a_2$  is about 5%. To reach a higher level of precision,  $\mathcal{O}(a_i^3)$  and radiative corrections have to be taken into account.

Using the Cabibbo-Isidori model, the NA48/2 collaboration has performed a fit to the  $m_{\pi^0\pi^0}^2$  distribution seen in  $K^\pm \rightarrow \pi^\pm\pi^0\pi^0$  [10], following a previous analysis on a fraction of the data [11]. Free fit parameters were the scattering lengths  $a_0 - a_2$ ,  $a_2$ , the linear and quadratic slopes  $g$  and  $h$  of the Dalitz plot  $u$  distribution, and the normalisation. The region around the cusp point at  $m_{\pi^0\pi^0}^2 = (2m_{\pi^+})^2$  was excluded from the fit to avoid an influence of possible pionium formation. The result of the fit is

$$\begin{aligned} (a_0 - a_2) m_{\pi^+} &= 0.261 \pm 0.006_{\text{stat}} \pm 0.003_{\text{syst}} \pm 0.001_{\text{ext}} \pm 0.013_{\text{theory}} \\ a_2 m_{\pi^+} &= -0.037 \pm 0.013_{\text{stat}} \pm 0.009_{\text{syst}} \pm 0.002_{\text{ext}}. \end{aligned} \quad (1)$$

The result is still preliminary. The residuals of the fit are shown in Fig. 4. When the correlation of  $\rho = -0.92$  between both values are taken into account, the result on the scattering length  $a_0$  is

$$a_0 m_{\pi^+} = 0.224 \pm 0.008_{\text{stat}} \pm 0.006_{\text{syst}} \pm 0.003_{\text{ext}} \pm 0.013_{\text{theory}}. \quad (2)$$

The main contributions to the systematic uncertainty come from the shower simulation in the calorimeter, the trigger efficiency, and the dependence of the Dalitz plot  $v$  parameter. The external error comprises the ratio between the  $K^+ \rightarrow \pi^+\pi^+\pi^-$  and  $K^+ \rightarrow \pi^+\pi^0\pi^0$  decay widths [13]. The theoretical uncertainty is estimated due to the neglected  $\mathcal{O}(a_i^3)$  and radiative corrections, as mentioned above.

Using analyticity and chiral symmetry,  $a_0$  and  $a_2$  are directly related with each other [14]. With this constraint, the experimental error is reduced sig-

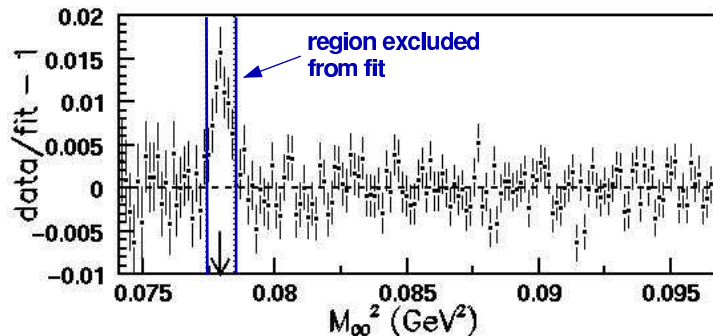


Figure 4: Pulls of the fit to the  $m_{\pi^0\pi^0}^2$  distribution. The region between the vertical lines was excluded from the fit.

nificantly and the NA48/2 result becomes  $(a_0 - a_2) m_{\pi^+} = 0.263 \pm 0.003_{\text{stat}} \pm 0.001_{\text{syst}} \pm 0.001_{\text{ext}} \pm 0.013_{\text{theory}}$ .

When including the region around the cusp into the fit and allowing for an additional pionium component in the fit, NA48/2 observed an excess of  $(1.8 \pm 0.2) \times 10^{-5}$  events per  $K^\pm \rightarrow \pi^\pm \pi^+ \pi^-$  decay at the cusp point (see Fig. 4). This is a factor of  $2.3 \pm 0.3$  larger than the predicted rate of  $0.8 \times 10^{-5}$  for pionium formation in  $K^\pm \rightarrow \pi^\pm \pi^+ \pi^-$  [15]. However, it has recently pointed out [16], that electromagnetic corrections to final state interactions have to be taken into account, which might explain the observed excess over the prediction.

### 3 Rescattering in $K_L \rightarrow \pi^0 \pi^0 \pi^0$ decays

In  $K_L \rightarrow \pi^0 \pi^0 \pi^0$  events, a similar cusp at  $m_{\pi^0\pi^0} = 2 m_{\pi^+}$  is expected [12]. By computing the matrix elements for  $K^+/K_L \rightarrow 3\pi$  at the cusp point from the measured partial widths and Dalitz plot slopes [13], the visibility is expected to be about 13 times smaller in  $K_L \rightarrow \pi^0 \pi^0 \pi^0$  compared to  $K^\pm \rightarrow \pi^\pm \pi^0 \pi^0$ .

The NA48 collaboration has analyzed about 88 million  $K_L \rightarrow \pi^0 \pi^0 \pi^0$  events, recorded in a special data-taking period in 2000 with no material in front of the electro-magnetic calorimeter. The data are practically background-free. The distribution of squared  $\pi^0 \pi^0$  invariant mass is shown in Fig. 5 (left). It should be noted, that in the region of low invariant mass around the  $\pi^+ \pi^-$  threshold the plot contains at maximum one entry per event, and therefore no double-counting occurs. When dividing the data with events from a Monte Carlo simulation without  $\pi\pi$  rescattering, clear evidence for a change of slope near the cusp point is observed (Fig. 5 (right)).

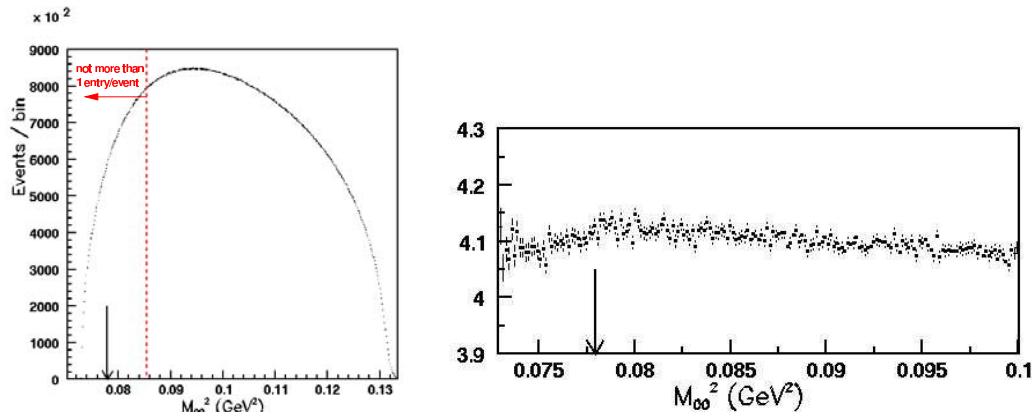


Figure 5: Distribution of  $m_{\pi^0\pi^0}^2$  of the NA48  $K_L \rightarrow \pi^0\pi^0\pi^0$  data. Left: Full region. Right: Data divided by Monte Carlo simulated events without rescattering (arbitrary normalisation). The arrow marks the  $(2m_{\pi^+})^2$  threshold.

## 4 Rescattering in $K^\pm \rightarrow \pi^\pm\pi^+\pi^-$ decays

Effects from  $\pi\pi$  rescattering should also occur in decays to charged pions as in  $K^\pm \rightarrow \pi^\pm\pi^+\pi^-$ . In this case,  $\pi^+\pi^- \rightarrow \pi^+\pi^-$  and  $\pi^\pm\pi^\pm \rightarrow \pi^\pm\pi^\pm$  contribute. Here no cusp is possible inside the physical region, but the Dalitz plot distribution is modified. The  $K \rightarrow 3\pi$  matrix element, as a function of the Dalitz plot variables  $u = (s_3 - s_0)/m_{\pi^+}^2$  and  $v = (s_1 - s_2)/m_{\pi^+}^2$ , is given by [13]

$$|\mathcal{M}|^2 = 1 + gu + hu^2 + kv^2 + \dots, \quad (3)$$

with the slope parameters  $g$ ,  $h$ , and  $k$ .

NA48/2 has performed a combined fit to their  $K^\pm \rightarrow \pi^\pm\pi^0\pi^0$  and  $K^\pm \rightarrow \pi^\pm\pi^+\pi^-$  data, using the non-relativistic effective field theory of the Bern-Bonn group [17]. Free parameters in the fit were the normalisations,  $a_0 - a_2$ , and the slope parameters  $g$ ,  $h$ , and  $k$  of  $K^\pm \rightarrow \pi^\pm\pi^+\pi^-$  and  $g_0$  and  $h_0$  of  $K^\pm \rightarrow \pi^\pm\pi^0\pi^0$ . The fit had a nearly perfect  $\chi^2$  of 757.1/757 d.o.f. and resulted in significantly shifted values of the slope parameters  $g$ ,  $h$ , and  $k$  with respect to a fit with no rescattering taken into account. However, in the latter fit the  $\chi^2$  value was equally good (516.9/517). This means, that on the one hand  $\pi\pi$  rescattering has a significant impact on the values of the Dalitz plot slopes. On the other hand, there is practically no possibility to extract the scattering lengths from the  $K^\pm \rightarrow \pi^\pm\pi^+\pi^-$  Dalitz plot slopes alone.

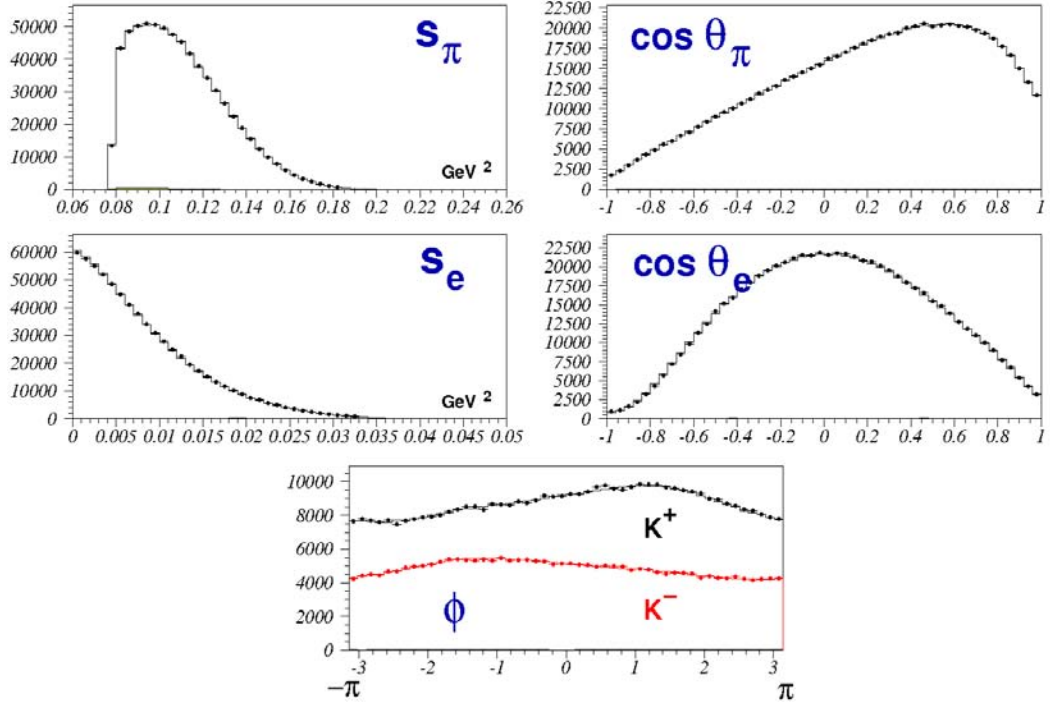


Figure 6: Distributions of the five Cabibbo-Maksymowicz variables in the NA48/2 2003  $K_{e4}$  data.

## 5 Measurement of $\pi\pi$ Scattering Lengths in $K_{e4}$ Decays

An independent and complementary method for the determination of  $\pi\pi$  scattering lengths is the analysis of  $K^\pm \rightarrow \pi^+\pi^-e^\pm\nu(\bar{\nu})$  ( $K_{e4}$ ) decays. The  $K_{e4}$  decay is a rare decay with a branching fraction of about  $4 \times 10^{-5}$  [13]. Its amplitude depends on the two complex phases  $\delta_0$  and  $\delta_1$ , which are the  $S$  and  $P$  wave  $\pi\pi$  scattering phase shifts for isospin  $I = 0$ . In  $K_{e4}$  decays, their difference  $\delta = \delta_0 - \delta_1$  can be measured as a function of  $m_{\pi\pi}$ .

In the 2003 data-taking period, the NA48/2 collaboration has collected 677510  $K_{e4}$  decays with very small background contamination of only about 0.5% [18]. An analysis was carried out in the five independent Cabibbo-Maksymowicz variables: these are the squared invariant dipion and dilepton masses  $s_\pi$  and  $s_e$ , the angles  $\theta_\pi$  and  $\theta_e$  of  $\pi^+$  and  $e^+$  with respect to the  $\pi\pi$  and  $e\nu$  directions in the  $\pi\pi$  and  $e\nu$  rest frames, respectively, and the angle  $\phi$  between the  $\pi\pi$  and  $e\nu$  decay planes. The distributions of these variables are shown in Fig. 6.

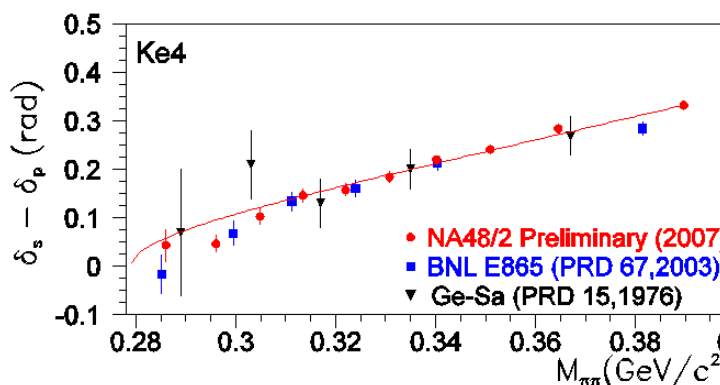


Figure 7: Measurements of the phase difference  $\delta_s - \delta_p$  as function of  $m_{\pi\pi}$  in  $K_{e4}$  decays. The line shows the best fit to  $a_0$  and  $a_2$  of NA48/2.

NA48/2 has performed a combined fit to the decay form factors and the phase shift difference  $\delta$  as a function of  $m_{\pi\pi}$ . The results are shown in Fig. 7 together with the earlier measurements of the Geneva-Saclay [3] and BNL E865 [4] experiments. The results are in good agreement with each other (except perhaps the highest data point of E865). From the phase shift measurements, the  $\pi\pi$  scattering lengths can be extracted. Using dispersion relations (Roy equations) and data above 800 MeV,  $a_2$  is related to  $a_0$  (the so-called Universal Band). From a one-parameter fit, NA48/2 obtained

$$a_0 m_{\pi^+} = 0.256 \pm 0.006_{\text{stat}} \pm 0.002_{\text{syst}} \begin{matrix} +0.018 \\ -0.017_{\text{theo}} \end{matrix}, \quad (4)$$

where the theoretical error corresponds to the width of the universal band, which is given by the experimental uncertainties of the measurements above 800 MeV. This result implies  $a_2 m_{\pi^+} = -0.031 \pm 0.001_{\text{exp}} \pm \begin{matrix} +0.013 \\ -0.012_{\text{theo}} \end{matrix}$ . When both  $a_0$  and  $a_2$  are left free in the fit, the results are

$$\begin{aligned} a_0 m_{\pi^+} &= 0.233 \pm 0.016_{\text{stat}} \pm 0.007_{\text{syst}}, \\ a_2 m_{\pi^+} &= -0.047 \pm 0.011_{\text{stat}} \pm 0.004_{\text{syst}}. \end{aligned} \quad (5)$$

It has recently been realized, that effects from isospin symmetry breaking ( $m_d \neq m_u$ ) are not negligible and do have a significant impact on the value of the phase shift difference  $\delta$ . A preliminary ChPT calculation gives a shift of  $\delta$  between 12 and 15 mrad for  $m_{\pi\pi} > 300$  MeV/ $c^2$  [19]. Taking into account these corrections, the value of  $a_0$  shifts by  $\sim -0.02$ . Note, that these corrections also have to be applied on the data of the previous  $K_{e4}$  measurements.

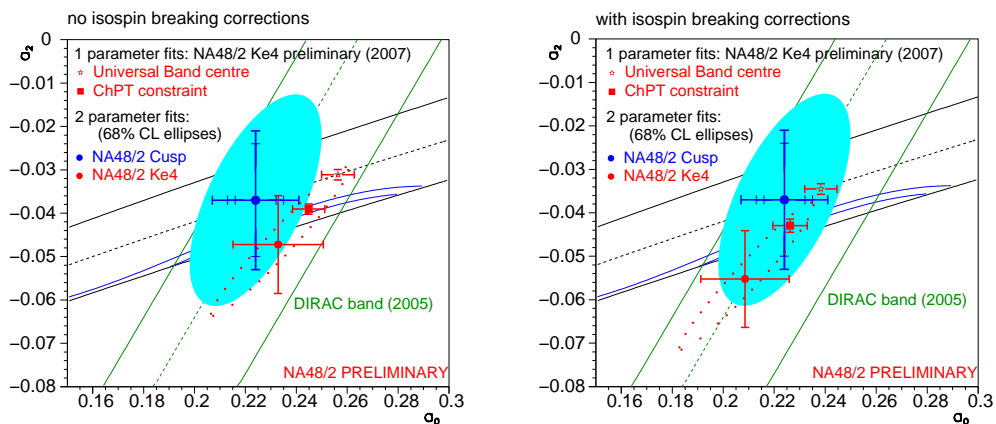


Figure 8: Comparison of results on the scattering lengths  $a_0$  and  $a_2$  from the NA48/2 and DIRAC experiments without (left) and with (right) isospin breaking corrections applied to  $K_{e4}$ . Shown are also the universal band (black band), predicted using the Roy equations and higher energy data, and the ChPT prediction (narrow blue band).

## 6 Conclusions

In the past year, there has been significant progress in the extraction of  $\pi\pi$  scattering lengths from kaon decays. The NA48/2 experiment has discovered a Wigner-cusp in the  $m_{\pi^0\pi^0}$  distribution of  $K^\pm \rightarrow \pi^\pm\pi^0\pi^0$  decays, arising from  $\pi\pi$  rescattering in this channel and thus allowing the precise extraction of the scattering lengths  $a_0$  and  $a_2$ . At the moment, the uncertainty is dominated by the neglect of radiative corrections and higher order terms. Given the on-going theoretical work, this is expected to improve in the near future. In addition, evidence for  $\pi\pi$  rescattering in  $K_L \rightarrow \pi^0\pi^0\pi^0$  events from  $K_L \rightarrow \pi^+\pi^-\pi^0$  has been found, using NA48 data from a  $K_L$  run period. The more traditional method for determination of  $a_0$  and  $a_2$  is the angular analysis of  $K_{e4}$  decays, where the NA48/2 collaboration has presented a new analysis with much larger precision than previous experiments.

The constraints on  $a_0$  and  $a_2$  from the NA48/2 measurements, together with the recent  $a_0 - a_2$  determination from pionium lifetime by DIRAC [5], are shown in Fig. 8. When taking into account the corrections for isospin symmetry breaking in  $K_{e4}$ , there is very good agreement within the results and with the ChPT prediction. Further improvements are expected in the near future from the analysis of the complete NA48/2  $K_{e4}$  and DIRAC data sets, as well as from a better theoretical understanding on the extraction of scattering lengths from  $K^\pm \rightarrow \pi^\pm\pi^0\pi^0$  and  $K_{e4}$ .

## References

- [1] J. Gasser and H. Leutwyler, *Annals Phys.* **158**, 142 (1984).
- [2] G. Colangelo, J. Gasser, H. Leutwyler, *Nucl. Phys.* **B 603**, 125 (2001).
- [3] L. Rosselet *et al.* [Geneva-Saclay Collab.], *Phys. Rev. D* **15**, 574 (1977).
- [4] S. Pislak *et al.* [E865 Collab.], *Phys. Rev. Lett.* **87**, 221801 (2001); *Phys. Rev. D* **67**, 072004 (2003).
- [5] B. Adeva *et al.* [DIRAC Collab.], *Phys. Lett.* **B 619**, 50 (2005).
- [6] V. Fanti *et al.* [NA48 Collab.] *Nucl. Instrum. Methods A* **574**, 433 (2007).
- [7] N. Cabibbo, *Phys. Rev. Lett.* **93**, 12181 (2004).
- [8] U.-G. Meißner, G. Müller, S. Steininger, *Phys. Lett.* **B 406**, 154 (1997); Erratum *ibid.* **407**, 454 (1997).
- [9] N. Cabibbo, G. Isidori, *JHEP* **0503**, 021 (2005).
- [10] E. Goudzovski, to appear in *Proc. KAON07 Conference*, Frascati, May 2007 (hep-ph/0706.4059).
- [11] J.R. Batley *et al.* [NA48/2 Collab.], *Phys. Lett.* **B 633**, 173 (2006).
- [12] M. Bissegger, A. Fuhrer, J. Gasser, B. Kubis, and A. Rusetsky, *Phys. Lett.* **B 659**, 576 (2008).
- [13] W.-M. Yao *et al.* [Particle Data Group], *J. Phys.* **G 33**, 1 (2006).
- [14] G. Colangelo, J. Gasser, H. Leutwyler, *Phys. Rev. Lett.* **86**, 5008 (2001).
- [15] Z.K. Silagadze, *JETP Lett.* **60**, 689 (1994).
- [16] S.R. Gevorkian, A.V. Tarasov, O.O. Voskresenskaya, *Phys. Lett.* **B 649**, 159 (2007).
- [17] G. Colangelo, J. Gasser, B. Kubis, A. Rusetsky, *Phys. Lett.* **B 638**, 187 (2006).
- [18] J.R. Batley *et al.* [NA48/2 Collab.], CERN-PH-EP/2007-035, submitted to *Eur. Phys. J. C*.

- [19] J. Gasser, to appear in *Proc. KAON07 Conference*, Frascati, May 2007 (hep-ph/0710.3048); to appear in *Proc. MENU 2007 Conference*, Jülich, September 2007.

# ETA AND ETA' PHYSICS

*Johan Bijnens*

Department of Theoretical Physics  
Lund University  
Sölvegatan 14A  
SE 22362 Lund, Sweden

## Abstract

This talk describes the reasons why  $\eta$  and  $\eta'$  decays are an interesting topic of study for both theory and experiment. The main part discusses the results of the recent calculation of  $\eta \rightarrow 3\pi$  at two-loop order in ChPT. Some puzzling aspects of the results compared to earlier dispersive calculations are highlighted. I also like to remind the reader of the use of  $\eta$  and  $\eta'$  decays for studying the anomaly.

## 1 Introduction

This conference has a lot of talks related to  $\eta$  and  $\eta'$ , both on decays, production and in a hadronic medium. The production is treated in a plenary talk by Krusche and decays experimentally in the talk by Wolke. There were also a lot of talks for both production and decay in the parallel sessions. In this talk I will concentrate on decays and in particular mainly on  $\eta \rightarrow 3\pi$ . There are lots of references treating  $\eta$  and  $\eta'$  physics. Many of them can be found in the proceedings of two recent conferences devoted to them [1, 2]. There have also been more recent workshops in Jülich (ETA06) and Peniscola (ETA07).

This talk first discusses why  $\eta$  and  $\eta'$  are interesting, then reminds the reader of some of the aspects of Chiral Perturbation Theory (ChPT) after which the main part, devoted to  $\eta \rightarrow 3\pi$  comes. I close by pointing out some properties of  $\eta' \rightarrow \eta\pi\pi, \pi\pi\pi$  decays and the anomaly. Earlier reviews covering similar material are Refs. [3, 4].

## 2 Why are $\eta$ and $\eta'$ Interesting?

The  $\eta$  and  $\eta'$  are particles that decay strongly but all their decays are suppressed. That means that they are good laboratories to study non-dominant

strong interaction effects. Weak decays can happen but do occur at branching ratios of order  $10^{-11}$  or lower. So, if charge conjugation violation would be discovered it would be very important. On the other hand, most standard extensions of the standard model do not predict such effects at an observable level in  $\eta$  or  $\eta'$  decays.

But let us first see why pseudo-scalars are special. The QCD Lagrangian is

$$\mathcal{L}_{QCD} = \sum_{q=u,d,s} [i\bar{q}_L \not{D} q_L + i\bar{q}_R \not{D} q_R - m_q (\bar{q}_R q_L + \bar{q}_L q_R)] \quad (1)$$

So if  $m_q = 0$  then the left and right handed quarks are decoupled and they can be interchanged freely among themselves leading to a global symmetry  $G = U(3)_L \times U(3)_R$ . This symmetry is clearly broken in the hadron spectrum, the proton and the  $S_{11}$ , as well as the  $\rho$  and the  $a_1$  have very different masses<sup>1</sup>. The chiral symmetry group  $G$  must thus be spontaneously broken, only the vector part of the group is clearly visible in the spectrum.

As a consequence there must be a set of light particles, the pseudo-Goldstone boson, whose interactions vanish at zero momentum as follows from Goldstone's theorem. There are eight fairly light particles around with the right quantum number,  $\pi^0$ ,  $\pi^\pm$ ,  $K^\pm$ ,  $K^0$ ,  $\bar{K}^0$  and  $\eta$ . But the next candidate with the correct quantum numbers, the  $\eta'$ , is heavy. We write the group  $G$  in terms of simple groups,

$$G = U(3)_L \times U(3)_R = SU(3)_L \times SU(3)_R \times U(1)_V \times U(1)_A, \quad (2)$$

and notice that the breaking pattern of  $G = SU(3)_L \times SU(3)_R \longrightarrow H = SU(3)_V$  gives eight light particles as observed. The reason is that the  $U(1)_A$  part of  $G$  is a good symmetry of the classical action but not of the full quantum theory. The divergence of its current has a part coming from the anomaly which couples to gluons via

$$\partial_\mu A^{0\mu} = 2\sqrt{N_f}\omega \quad \text{with} \quad \omega = \frac{1}{16\pi^2} \varepsilon^{\mu\nu\alpha\beta} \text{tr} G_{\mu\nu} G_{\alpha\beta}. \quad (3)$$

$\omega$  is strongly interacting thus the divergence of the singlet axial-current cannot be treated as zero. So the  $\eta'$  can be heavy as is seen experimentally. Quantum effects break thus the  $U(1)_A$ , however the r.h.s. of (3) is a total divergence, so how can it have an effect? The answer was found by 't Hooft [7]. Gauge field configurations with non-zero winding number, instantons, can produce an effect. This in turn led to the so-called strong CP problem *but*

<sup>1</sup>There is a discussion at present whether chiral symmetry is restored for higher hadron masses. This is not relevant for this talk. Recent references can be traced from [5, 6].

solved the  $\eta'$  mass problem. A conclusion is thus that the  $\eta'$  has potentially large and very interesting non-perturbative effects and interactions with gluonic degrees of freedom that differ from other hadrons. Since  $\hat{m} \neq m_s$  this also affects  $\eta$  physics via mixing.

### 3 Chiral Perturbation Theory

The chiral symmetry of QCD and its spontaneous breaking has many consequences. The best method to exploit these is Chiral Perturbation Theory (ChPT) which is best defined via

ChPT  $\equiv$  “Exploring the consequences of the chiral symmetry of QCD and its spontaneous breaking using effective field theory techniques.”

A derivation which clearly brings out all the assumptions involved is [8]. Lectures and review articles can be found in my Lattice07 talk [9] or on the webpage [10]. The original modern references are [11, 12].

ChPT uses as power-counting essentially dimensional counting in terms of a generic momentum  $p$ . Momenta and meson masses are counted as order  $p$ . Because of the Gell-Mann-Oakes-Renner relation,  $m_M^2 \propto m_q$ , quark masses and external scalar and pseudo-scalar fields are counted as order  $p^2$  and the covariant derivative requires external vector and axial-vector field to be counted as order  $p$ . With this counting there is no term of order  $p^0$  in the chiral Lagrangian. The lowest order Lagrangian is given by

$$\mathcal{L}_2 = \frac{F_0^2}{4} \{ \langle D_\mu U^\dagger D^\mu U \rangle + \langle \chi^\dagger U + \chi U^\dagger \rangle \}, \quad (4)$$

with  $U$  parameterizing the Goldstone Boson manifold  $G/H$  with

$$U(\phi) = \exp(i\sqrt{2}\Phi/F_0), \quad \Phi(x) = \begin{pmatrix} \frac{\pi^0}{\sqrt{2}} + \frac{\eta_8}{\sqrt{6}} & \pi^+ & K^+ \\ \pi^- & -\frac{\pi^0}{\sqrt{2}} + \frac{\eta_8}{\sqrt{6}} & K^0 \\ K^- & \bar{K}^0 & -\frac{2\eta_8}{\sqrt{6}} \end{pmatrix}. \quad (5)$$

The external fields are in the covariant derivative,  $D_\mu U = \partial_\mu U - ir_\mu U + iUl_\mu$  for the left and right external currents:  $r(l)_\mu = v_\mu + (-)a_\mu$  and the external scalar and pseudo-scalar external densities are in  $\chi = 2B_0(s + ip)$ . Quark masses come via the scalar density  $s = \mathcal{M} + \dots$  and traces are over (quark) flavors  $\langle A \rangle = Tr_F(A)$ . The number of parameters increases fast at higher orders, there are 10+2 at order  $p^4$  [13] and 90+4 at order  $p^6$  [14] for three-flavor mesonic ChPT.

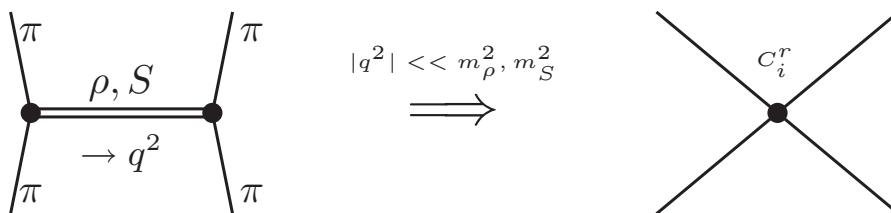


Figure 1: Resonance saturation of the order  $p^6$  low-energy-constants  $C_i^r$  via resonance exchange for  $\pi\pi$ -scattering.

The main uses of ChPT are that it contains all the  $SU(3)_V$  relations automatically and in addition relates processes with different numbers of pseudo-scalars and it includes the nonanalytic dependencies on masses and kinematical quantities, often referred to as chiral logarithms. As an example, the pion mass in two-flavor ChPT is given by [12]

$$m_\pi^2 = 2B\hat{m} + \left(\frac{2B\hat{m}}{F}\right)^2 \left[ \frac{1}{32\pi^2} \log \frac{(2B\hat{m})}{\mu^2} + 2l_3^r(\mu) \right] + \dots, \quad (6)$$

with  $M^2 = 2B\hat{m}$  and  $B \neq B_0$ ,  $F \neq F_0$  because of two versus three-flavor ChPT. In (6) we see the logarithm and the occurrence of the higher order parameter  $l_3^r(\mu)$ . Eq. (6) also shows some of the choices that need to be made when performing higher order ChPT calculations: Which subtraction scale  $\mu$  and which quantities should be used to express the results. Lowest order masses or physical meson masses and dito for the decay constants and other kinematical quantities as  $s, t, u$  in  $\pi\pi$ -scattering. There is clearly no unique choice and the choice can influence the *apparent* convergence of the ChPT series quite strongly. Another problem is that typically, not all the higher order parameters that show up in the calculations are known experimentally. Thus one needs to make estimates of these, usually via a version of resonance saturation originally introduced in ChPT in [15]. This is schematically depicted in Fig. 1. More recent references on resonance saturation and possible pitfalls are [16, 17]. Discussions on this problem can also be found in the papers on order  $p^6$  ChPT and the review [18].

## 4 $\eta \rightarrow 3\pi$

In the limit of conserved isospin, i.e. we turn off electromagnetism and set  $m_u = m_d$ , the  $\eta$  is stable. Direct electromagnetic effects have been known

to be small since long ago [19, 20]. It should thus proceed mainly through the quark-mass difference  $m_u - m_d$ . The lowest order was done in [21, 22], order  $p^4$  in [23] and recently the full order  $p^6$  has been evaluated [24]. In this section I will mainly present the new results of [24].

The momenta for the decay  $\eta \rightarrow \pi^+\pi^-\pi^0$  are labeled as  $p_\eta, p_+, p_-$  and  $p_0$  respectively and we introduce the kinematical Mandelstam variables

$$s = (p_+ + p_-)^2, t = (p_+ + p_0)^2, u = (p_- + p_0)^2. \quad (7)$$

These are linearly dependent,  $s + t + u = m_{\pi^0}^2 + m_{\pi^-}^2 + m_{\pi^+}^2 + m_\eta^2 \equiv 3s_0$ . The amplitude is for the charged and neutral decay

$$\begin{aligned} \langle \pi^0 \pi^+ \pi^- \text{out} | \eta \rangle &= i (2\pi)^4 \delta^4(p_\eta - p_{\pi^+} - p_{\pi^-} - p_{\pi^0}) A(s, t, u), \\ \langle \pi^0 \pi^0 \pi^0 \text{out} | \eta \rangle &= i (2\pi)^4 \delta^4(p_\eta - p_1 - p_2 - p_3) \bar{A}(s_1, s_2, s_3), \\ \bar{A}(s_1, s_2, s_3) &= A(s_1, s_2, s_3) + A(s_2, s_3, s_1) + A(s_3, s_1, s_2). \end{aligned} \quad (8)$$

The relation in the last line of (8) is only valid to first order in  $m_u - m_d$ . The factor of  $m_u - m_d$  can be pulled out in various ways. Two common ones are

$$A(s, t, u) = \frac{\sqrt{3}}{4R} M(s, t, u) \quad \text{or} \quad A(s, t, u) = \frac{1}{Q^2} \frac{m_K^2}{m_\pi^2} (m_\pi^2 - m_K^2) \frac{\mathcal{M}(s, t, u)}{3\sqrt{3}F_\pi^2}, \quad (9)$$

with quark-mass ratios  $R = (m_s - \hat{m})/(m_d - m_u)$  and  $Q^2 = R(m_s + m_d)/(2\hat{m})$ . The lowest order result corresponds to

$$M(s, t, u)_{LO} = ((4/3) m_\pi^2 - s) / F_\pi^2. \quad (10)$$

The tree level determination of  $R$  in terms of meson masses gives with (10) a decay rate of 66 eV which should be compared with the experimental results of  $295 \pm 17$  eV [25]. In principle, since the decay rate is proportional to  $1/R^2$  or  $1/Q^4$ , this should allow for a precise determination of  $R$  and  $Q$ . However, the change required seems somewhat large. The order  $p^4$  calculation [23] increased the predicted decay rate to 150 eV albeit with a large error. About half of the enhancement in the amplitude came from  $\pi\pi$  rescattering and the other half from other effects like the chiral logarithms [23]. The rescattering effects have been studied at higher orders using dispersive methods in [26] and [27]. Both calculations found a similar enhancement in the decay rate bringing it to about 220 eV but differ in the way the Dalitz plot distributions look. This can be seen in Fig. 2 where I show the real part of the amplitude as a function of  $s$  along the line  $s = u$ . The calculations use a very different formalism but make similar approximations, they mainly differ in the way the subtraction constants are determined. That discrepancy and the facts that in

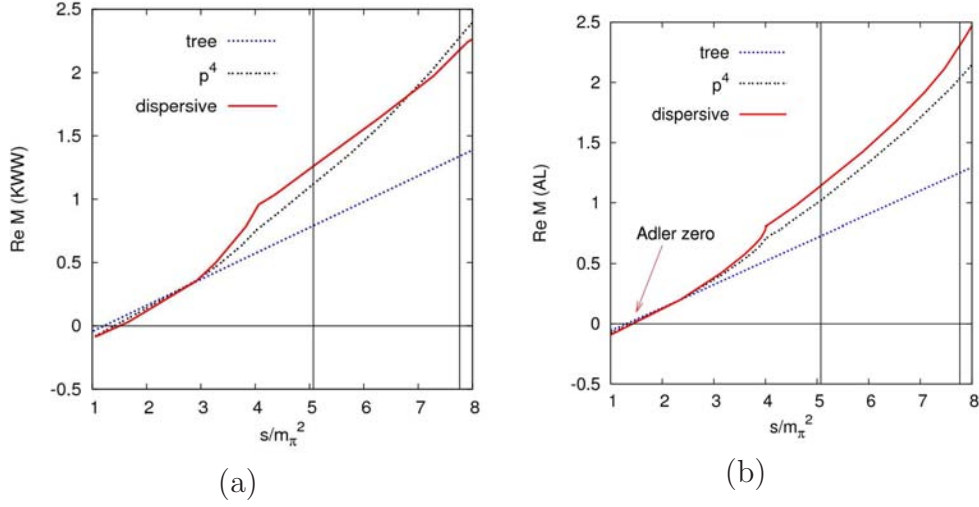


Figure 2: (a) Decay amplitude obtained by use of extended Khuri-Treiman equations [26] along the line  $s = u$ . (b) Alternative dispersive analysis for the decay amplitude [27]. Figs. from [4], adapted from [26, 27].

$K_{\ell 4}$  the dispersive estimate [28] was about half the full ChPT calculation [29] and at order  $p^4$  the dispersive effect was about half of the correction for  $\eta \rightarrow 3\pi$  makes it clear that also for this process a full order  $p^6$  calculation is desirable. This has been done recently in [24].

Ref. [24] generalizes the methods of [30] to deal with  $\pi^0$ - $\eta$  mixing to processes with mixing on more than one external leg. The input parameters are from the main order  $p^6$  fit, called fit 10, of [30] and the needed order  $p^6$  constants are determined by resonance exchange as discussed earlier. Details can be found in [24]. In Fig. 3 I show the numerical result for the amplitude along two lines in the Dalitz plot,  $t = u$  and  $s = u$ . The latter can be compared directly with the dispersive result of Fig. 2. The correction found in [24] at order  $p^6$  is 20-30% in amplitude, larger in magnitude than the dispersive estimates [26, 27] but with a shape similar to [27].

The Dalitz plot in  $\eta \rightarrow 3\pi$  is parameterized in terms of  $x$  and  $y$  defined in terms of the kinetic energies of the pions  $T_i$  and  $Q_\eta = m_\eta - 2m_{\pi^+} - m_{\pi^0}$  for the charged decay and  $z$  defined in terms of the pion energies  $E_i$ . The amplitudes are expanded in  $x, y, z$ .

$$\begin{aligned}
 x &= \sqrt{3} \frac{T_+ - T_-}{Q_\eta}, & y &= \frac{3T_0}{Q_\eta} - 1, & z &= \frac{2}{3} \sum_{i=1,3} \left( \frac{3E_i - m_\eta}{m_\eta - 3m_{\pi^0}} \right)^2, \\
 |M(s, t, u)|^2 &= A_0^2 (1 + ay + by^2 + dx^2 + fy^3 + \dots), \\
 |\overline{M}(s, t, u)|^2 &= \overline{A}_0^2 (1 + 2\alpha_2 + \dots).
 \end{aligned} \tag{11}$$

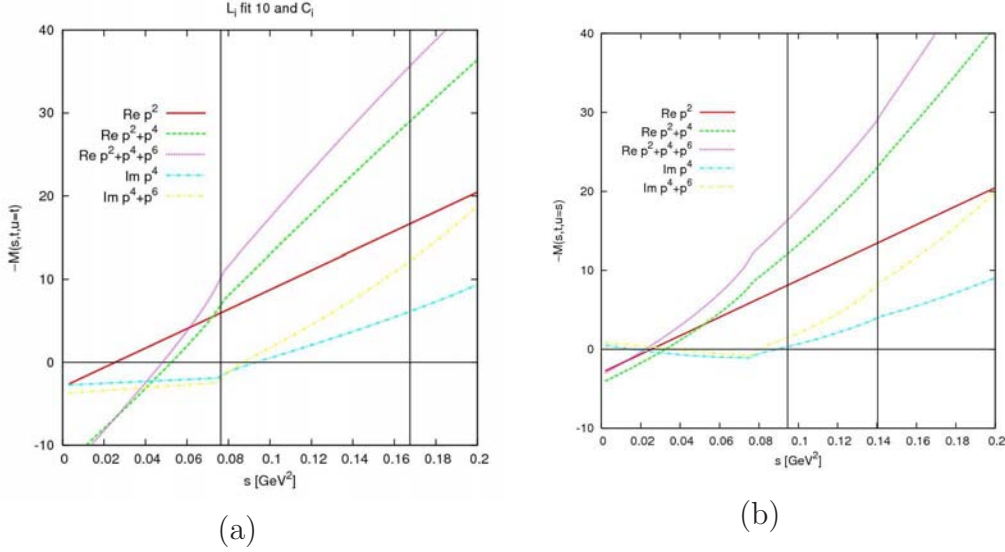


Figure 3: (a) The amplitude  $M(s, t, u)$  along the line  $t = u$ . The vertical lines indicate the physical region. Shown are the real and imaginary parts with all parts summed up to the given order. (b) Similar plot but along the line  $s = u$ . Figs. from [24].

Table 1: Measurements of the Dalitz plot distributions in  $\eta \rightarrow \pi^+ \pi^- \pi^0$ . The KLOE result [31] for  $f$  is  $f = 0.14 \pm 0.01 \pm 0.02$ .

Exp.	a	b	d
KLOE [31]	$-1.090 \pm 0.005^{+0.008}_{-0.019}$	$0.124 \pm 0.006 \pm 0.010$	$0.057 \pm 0.006^{+0.007}_{-0.016}$
CB [32]	$-1.22 \pm 0.07$	$0.22 \pm 0.11$	$0.06 \pm 0.04$ (input)
[33]	$-1.08 \pm 0.014$	$0.034 \pm 0.027$	$0.046 \pm 0.031$
[34]	$-1.17 \pm 0.02$	$0.21 \pm 0.03$	$0.06 \pm 0.04$

Recent experimental results for these parameters are shown in Tabs. 1 and 2. There are discrepancies among the experiments but the two latest precision experimental measurements of  $\alpha$  agree. The predictions from ChPT to order  $p^6$  with the input parameters fixed as described earlier are give in Tabs. 3 and 4. The predictions from the dispersive analysis as well as [38] have not been included. The different lines corresponds to variations on the input and the order of ChPT. The lines labelled NNLO are the central results. The agreement with experiment is not too good and clearly needs further study. Especially puzzling is the  $\alpha$  is consistently positive while the dispersive calculations as well as [38] give a negative value. The inequality  $\alpha \leq (d + b - a^2/4)/4$  derived in [24] shows that  $\alpha$  has rather large cancellations inherent in its prediction and that the overestimate of  $b$  is a likely

Table 2: Measurements of the Dalitz plot distribution in  $\eta \rightarrow \pi^0\pi^0\pi^0$ .

Exp.	$\alpha$
KLOE [35]	$-0.027 \pm 0.004_{-0.006}^{+0.004}$
Crystal Ball [36]	$-0.031 \pm 0.004$
WASA/CELSIUS [37]	$-0.026 \pm 0.010 \pm 0.010$

Table 3: Theoretical estimate of the Dalitz plot distributions in  $\eta \rightarrow \pi^+\pi^-\pi^0$ .

	$A_0^2$	a	b	d	f
LO	120	-1.039	0.270	0.000	0.000
NLO	314	-1.371	0.452	0.053	0.027
NLO ( $L_i^r = 0$ )	235	-1.263	0.407	0.050	0.015
NNLO	538	-1.271	0.394	0.055	0.025
NNLO ( $\mu = 0.6$ GeV)	543	-1.300	0.415	0.055	0.024
NNLO ( $\mu = 0.9$ GeV)	548	-1.241	0.374	0.054	0.025
NNLO ( $C_i^r = 0$ )	465	-1.297	0.404	0.058	0.032
NNLO ( $L_i^r = C_i^r = 0$ )	251	-1.241	0.424	0.050	0.007

cause of the wrong sign obtained for  $\alpha$ . In addition, the fairly large correction obtained gives in the end somewhat larger values of  $Q$  compared to those derived from the masses [24].

## 5 Other Remarks

I would simply like to repeat here some remarks made earlier, see e.g. [4]. The hadronic decays of the  $\eta'$  are interesting, they are predicted to be small at lowest order.  $\eta' \rightarrow 3\pi$  agrees reasonably well with expectations but  $\eta' \rightarrow \eta\pi\pi$  has very large higher order corrections since the lowest order is suppressed by a factor of  $m_\pi^2$ . I would also like to emphasize once more that the decay

Table 4: Theoretical estimates of the Dalitz plot distribution in  $\eta \rightarrow \pi^0\pi^0\pi^0$ .

	$\overline{A_0^2}$	$\alpha$
LO	1090	0.000
NLO	2810	0.013
NLO ( $L_i^r = 0$ )	2100	0.016
NNLO	4790	0.013
NNLO ( $C_i^r = 0$ )	4140	0.011
NNLO ( $L_i^r = C_i^r = 0$ )	2220	0.016

of  $\eta$  and  $\eta'$  allow many tests of the triangle, quadrangle, . . . anomaly.

## Acknowledgments

This work is supported in part by the European Commission RTN network, Contract MRTN-CT-2006-035482 (FLAVIANet), the European Community-Research Infrastructure Activity Contract RII3-CT-2004-506078 (Hadron-Physics) and the Swedish Research Council.

## References

- [1] J. Bijnens, G. Faldt and B.M.K. Nefkens (eds.) *Phys. Scripta* **T99**, 1-282 (2002).
- [2] B. Höistad and P. Moskal (eds.), *Acta Phys. Slov.* **56** 193-409 (2005).
- [3] J. Bijnens and J. Gasser, *Phys. Scripta* **T99**, 24 (2002) [hep-ph/0202242].
- [4] J. Bijnens, *Acta Phys. Slov.* **56**, 305 (2005) [hep-ph/0511076].
- [5] L. Y. Glozman, arXiv:0710.0978 [hep-ph].
- [6] M. Shifman and A. Vainshtein, arXiv:0710.0863 [hep-ph].
- [7] G. 't Hooft, *Phys. Rev.* **D14**, 3432 (1976) [Erratum **D18**, 2199 (1978)].
- [8] H. Leutwyler, *Ann. Phys.* **235**, 165 (1994) [hep-ph/9311274].
- [9] J. Bijnens, *PoS LATTICE 2007* (2007) 004 [arXiv:0708.1377 [hep-lat]].
- [10] <http://www.thep.lu.se/~bijnens/chpt.html>.
- [11] S. Weinberg, *Physica* **A96**, 327 (1979).
- [12] J. Gasser and H. Leutwyler, *Annals Phys.* **158**, 142 (1984).
- [13] J. Gasser and H. Leutwyler, *Nucl. Phys.* **B250**, 465 (1985).
- [14] J. Bijnens *et al.*, *JHEP* **9902** (1999) 020 [hep-ph/9902437].
- [15] G. Ecker *et al.*, *Nucl. Phys.* **B321** 311 (1989).
- [16] V. Cirigliano *et al.*, *Nucl. Phys.* **B753**, 139 (2006) [hep-ph/0603205].

- [17] J. Bijnens *et al.*, *JHEP* **0304** (2003) 055 [hep-ph/0304222].
- [18] J. Bijnens, *Prog. Part. Nucl. Phys.* **58**, 521 (2007) [hep-ph/0604043].
- [19] D. G. Sutherland *Phys. Lett.* **23**, 384 (1966).
- [20] J. S. Bell and D. G. Sutherland, *Nucl. Phys.* **B4**, 315 (1968).
- [21] J. A. Cronin, *Phys. Rev.* **161**, 1483 (1967).
- [22] H. Osborn and D. J. Wallace, *Nucl. Phys.* **B20**, 23 (1970).
- [23] J. Gasser and H. Leutwyler, *Nucl. Phys.* **B250**, 539 (1985).
- [24] J. Bijnens and K. Ghorbani, arXiv:0709.0230 [hep-ph].
- [25] W. M. Yao *et al.* [Particle Data Group], *J. Phys.* **G33**, 1 (2006).
- [26] J. Kambor *et al.*, *Nucl. Phys.* **B465**, 215 (1996) [hep-ph/9509374].
- [27] A. V. Anisovich and H. Leutwyler, *Phys. Lett.* **B375**, 335 (1996) [hep-ph/9601237].
- [28] J. Bijnens *et al.*, *Nucl. Phys.* **B427**, 427 (1994) [hep-ph/9403390].
- [29] G. Amorós *et al.*, *Nucl. Phys.* **B585**, 293 (2000) [hep-ph/0003258].
- [30] G. Amorós *et al.*, *Nucl. Phys.* **B602**, 87 (2001) [hep-ph/0101127].
- [31] F. Ambrosino *et al.* arXiv:0707.2355 [hep-ex].
- [32] A. Abele *et al.* *Phys. Lett.* **B417**, 197 (1998).
- [33] J. G. Layter *et al.*, *Phys. Rev.* **D7**, 2565 (1973).
- [34] M. Gormley *et al.*, *Phys. Rev.* **D2**, 501 (1970).
- [35] F. Ambrosino *et al.* arXiv:0707.4137 [hep-ex].
- [36] W. B. Tippens *et al.* *Phys. Rev. Lett.* **87**, 192001 (2001).
- [37] M. Bashkanov *et al.*, arXiv:0708.2014 [nucl-ex].
- [38] B. Borasoy and R. Nissler, *Eur. Phys. J.* **A26**, 383 (2005) [hep-ph/0510384].

# Plenary Session II

**Session Chair:**

Andreas Schäfer

KLOE Results on Hadron Physics

*Cesare Bini*

Structure of Light Scalar Mesons

*Michael R. Pennington*

Scalar Mesons from an Effective Lagrangian Approach

*Joseph Schechter*

Physics Program at COSY

*Kai Brinkmann*

**Session Chair:**

Haiyan Gao

Hadron-Hadron and Hadron-Hadron-Hadron

*Silas Beane*

Properties from Lattice QCD

*Uwe-Jens Wiese*

Chiral Symmetry on the Lattice

*Andreas Schäfer*

Hadron Structure from Lattice QCD

# RECENT KLOE RESULTS ON HADRON PHYSICS

*C. Bini*<sup>1</sup>

Dipartimento di Fisica<sup>2</sup>

Sapienza Università di Roma and INFN Roma

## Abstract

The KLOE experiment at the  $e^+e^-$  collider DAFNE of the Frascati Laboratories has collected about  $8 \times 10^9$  decays of the  $\phi$  meson. From the study of the radiative decays in non-strange pseudoscalar and scalar mesons several information have been obtained concerning the structure of the lowest mass mesons. A review of the most significant results is presented.

## 1 Introduction

The main physics motivation of an  $e^+e^-$  collider centered at the  $\phi$  meson mass, a  $\phi$ -factory, is the study of kaon physics, 83% of  $\phi$  decays being in kaon pairs. However a  $\phi$ -factory is also a copious source of other low mass mesons, essentially through the radiative decays in one or more pseudoscalar mesons. Hence it is a laboratory for the study of the properties of all the lowest mass mesons.

Along the years KLOE has published several results concerning the properties of the low mass mesons. Here a review of the most recent results is given. After a brief description of the KLOE experiment (sect.2) the results are presented in Sect.3 and 4.

---

<sup>1</sup>on behalf of the KLOE collaboration: F. Ambrosino, A. Antonelli, M. Antonelli, F. Archilli, C. Bacci, P. Beltrame, G. Bencivenni, S. Bertolucci, C. Bini, C. Bloise, S. Bocchetta, F. Bossi, P. Branchini, R. Caloi, P. Campana, G. Capon, T. Capussela, F. Ceradini, S. Chi, G. Chiefari, P. Ciambrone, E. De Lucia, A. De Santis, P. De Simone, G. De Zorzi, A. Denig, A. Di Domenico, C. Di Donato, S. Di Falco, B. Di Micco, A. Doria, M. Dreucci, G. Felici, A. Ferrari, M. L. Ferrer, G. Finocchiaro, S. Fiore, C. Forti, P. Franzini, C. Gatti, P. Gauzzi, S. Giovannella, E. Gorini, E. Graziani, M. Incagli, W. Kluge, V. Kulikov, F. Lacava, G. Lanfranchi, J. Lee-Franzini, D. Leone, M. Martini, P. Massarotti, W. Mei, S. Meola, S. Miscetti, M. Moulson, S. Müller, F. Murtas, M. Napolitano, F. Nguyen, M. Palutan, E. Pasqualucci, A. Passeri, V. Patera, F. Perfetto, M. Primavera, P. Santangelo, G. Saracino, B. Sciascia, A. Sciubba, F. Scuri, I. Sfiligoi, T. Spadaro, M. Testa, L. Tortora, P. Valente, G. Venanzoni, R. Versaci, G. Xu

<sup>2</sup>P.le A.Moro 5, 00185 Roma, Italy, e-mail, [cesare.bini@roma1.infn.it](mailto:cesare.bini@roma1.infn.it)

## 2 The KLOE experiment

DAFNE is an  $e^+e^-$  collider running at a center of mass energy of 1.02 GeV at the Frascati Laboratories of INFN with a luminosity that has reached a peak value of  $1.5 \times 10^{32} \text{cm}^{-2}\text{s}^{-1}$ , the maximum luminosity ever reached at this energy. KLOE has taken data in 4 years up to 2006 and has collected about  $2.7 \text{fb}^{-1}$  total integrated luminosity. Most of these data ( $2.5 \text{fb}^{-1}$  corresponding to about  $8 \times 10^9$   $\phi$  decays) have been taken at the  $\phi$  peak, the others have been taken off-peak.

The KLOE detector is conceptually very simple. It consists of a large volume drift chamber [2] in full stereo geometry filled with a He-IsoButane gas mixture, for the measurement of charged tracks, and a lead scintillating fibers calorimeter [3] surrounding it for the measurement of neutral particles (essentially photons and  $K_L$ ) and for the identification of the charged particles through time of flight. A superconducting coil provides a 0.52 T solenoidal magnetic field. The KLOE physics program includes kaon physics [4], hadron physics (see next sections) and the measurement of the  $e^+e^- \rightarrow \pi^+\pi^-$  cross-section [5] for the hadronic corrections to  $g_\mu - 2$ . The prospects for a possible KLOE continuation are discussed in Ref. [6].

## 3 Results on Pseudoscalar mesons

The lowest mass pseudoscalar meson nonet consists of the pions, the kaons, the  $\eta$  and the  $\eta'$ . All these particles are well established since long time. However the high statistics of  $\eta$  and  $\eta'$  accumulated by KLOE allows to perform precision measurements of the properties of these particles (some are still controversial) and to improve the knowledge of some decays. In the following I review the main KLOE results on  $\eta$  and  $\eta'$ .

### 3.1 Precision measurement of the $\eta$ mass

In the last years the precision on the measurement of the  $\eta$  mass has significantly improved. Few experiments, based on completely different experimental methods have pushed the uncertainty well below 100 keV. GEM at Juelich [7] and NA48 at CERN [8] reported 2 measurements in bad disagreement between each other. More recently CLEO has reported a further measurement [9] in agreement with the NA48 value and in disagreement with the GEM value.

In KLOE the  $\eta$  mass is measured using the decay channel  $\phi \rightarrow \eta\gamma$  with the subsequent decay  $\eta \rightarrow \gamma\gamma$ , resulting in a fully neutral 3-photon final state.

The excellent space and time resolutions of the calorimeter allow, through a kinematic fit constrained, to obtain a background free  $\eta$  sample with a well defined mass peak. The absolute calibration of the mass scale is provided by the measurement of the center of mass energy that, in turn, is normalised to the  $\phi$  mass precisely measured by CMD-2 [10]. The result is:

$$m(\eta) = 547.873 \pm 0.007 \pm 0.048 \text{ MeV} \quad (1)$$

and is compared to the other measurements in fig.1.

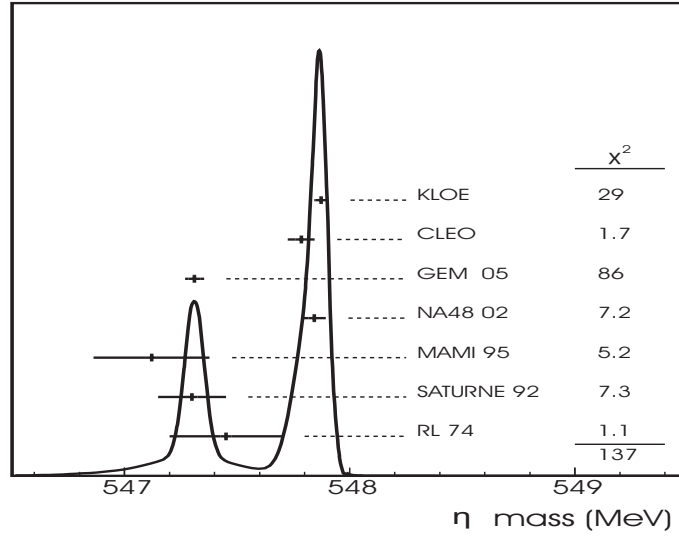


Figure 1: Review of all the measurements of the  $\eta$  mass available now. The curve shown and the  $\chi^2$  values are obtained according to the prescriptions of PDG [1].

### 3.2 $\eta$ - $\eta'$ mixing and the gluon content of the $\eta'$

Since the  $\phi$  meson is essentially a pure  $s\bar{s}$  state, the ratio of branching ratios

$$R = \frac{B.R.(\phi \rightarrow \eta'\gamma)}{B.R.(\phi \rightarrow \eta\gamma)} \quad (2)$$

is directly related to the pseudoscalar mixing angle  $\phi_P$  in the flavour basis, assuming no gluonium contribution in the  $\eta$  and  $\eta'$  wave-functions [11].

KLOE has measured the ratio  $R$  using 2 different data sets and 2 different final states [12,13]. The results are in agreement between each other and the best estimate of the mixing angle is:

$$\phi_P = (41.4 \pm 0.3 \pm 0.9)^\circ \quad (3)$$

where the systematic uncertainty is dominated by the knowledge of the intermediate  $\eta$  and  $\eta'$  branching ratios entering in the evaluation of  $R$ .

If we allow a gluonium contribution in the  $\eta'$  wave function, the ratio  $R$  gives a band in the  $\phi_P$ - $Z_{\eta'}^2$  plane,  $Z_{\eta'}$  being the size normalized to 1 of the gluonium content. The band is shown in fig.2. Other bands can be put in the same plot following the analyses of refs. [14–16]. The intersection between the bands define the allowed region. According to the KLOE analysis [13] the allowed region is about 3 standard deviation away from  $Z_{\eta'} = 0$ . More recently a different analysis [17] using different constraints and also a different set of free parameters obtain a result compatible with 0.

Notice that a significant improvement for this combined analysis can be obtained by pushing the measurements of  $\eta$  and  $\eta'$  widths and branching ratios down to 1% level.

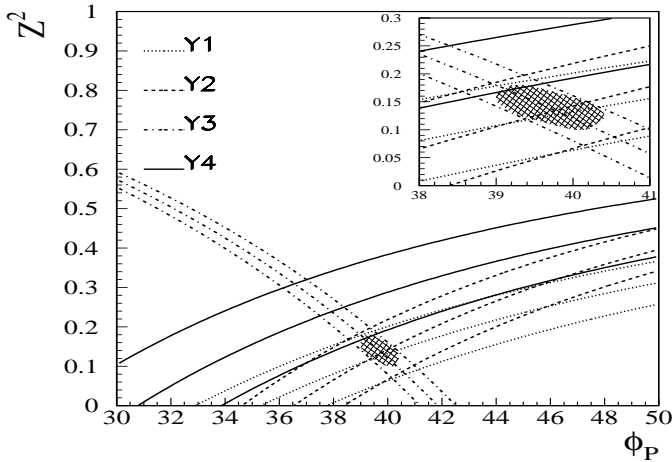


Figure 2: Analysis of the  $\eta'$  gluonium content. The four bands shown in the  $Z_{\eta'}^2$ - $\phi_P$  plane are: (Y1) from  $\Gamma(\eta' \rightarrow \gamma\gamma)/\Gamma(\pi^0 \rightarrow \gamma\gamma)$ , (Y2) from  $\Gamma(\eta' \rightarrow \rho\gamma)/\Gamma(\omega \rightarrow \pi^0\gamma)$ , (Y3) from the KLOE result (see text) and finally (Y4) from  $\Gamma(\eta' \rightarrow \omega\gamma)/\Gamma(\omega \rightarrow \pi^0\gamma)$ . A detailed view of the intersection region is shown in the box.

### 3.3 Dynamic of the decay $\eta \rightarrow 3\pi$

The  $\eta$  decays in 3 pions are isospin violating decays. In fact a 3 pion system with 0 angular momentum can be only in a I=0 isospin state. Since the  $\eta$  meson cannot decay to 2 pions due to P and CP invariance in strong interactions, the  $\eta$  in 3 pion is the most frequent hadronic  $\eta$  decay with a very small electromagnetic contribution. Models inspired to chiral perturbation theory allow to evaluate the decay widths and the dynamics [18] of both  $\eta \rightarrow \pi^+\pi^-\pi^0$  and  $\eta \rightarrow \pi^0\pi^0\pi^0$ .

KLOE detects both decays with a large statistics and a completely negligible background. We give here the final result for the study of  $\eta \rightarrow \pi^+\pi^-\pi^0$  and a preliminary result concerning  $\eta \rightarrow \pi^0\pi^0\pi^0$ .

Table 1: In each line the result of a fit is reported with a different set of free parameters. Empty cells means that in that particular fit the parameter has been fixed to 0.

dof	p( $\chi^2$ )	$10^3a$	$10^3b$	$10^3c$	$10^3d$	$10^3e$	$10^3f$
147	73%	-1090±5	124±6	2±3	57±6	-6±7	140±10
149	74%	-1090±5	124±6		57±6		140±10
150	$10^{-6}$	-1069±5	104±5				130±10
150	$10^{-8}$	-1041±3	145±6		50±6		
151	$10^{-6}$	-1026±3	125±6				

The  $\eta \rightarrow \pi^+\pi^-\pi^0$  Dalitz plot has been fit using the following expansion of the amplitude  $A$ :

$$|A(X, Y)|^2 = 1 + aY + bY^2 + cX + dX^2 + eXY + fY^3 \quad (4)$$

where the Dalitz plot variables are defined as usual:

$$X = \frac{\sqrt{3}T_+ - T_- Q_\eta}{Q_\eta}; \quad Y = \frac{3T_0}{Q_\eta} \quad (5)$$

with  $T_{+,-,0}$  the kinetic energies of the three pions and  $Q_\eta = m_\eta - 2m_{\pi^\pm} - m_{\pi^0}$ . The results of the fit, based on a sample of 1.34 million of events are shown in Tab.1. The following comments can be made on these results:

- the odd terms in X ( $c$  and  $e$ ) are compatible with 0, so that no C violation is observed;
- the quadratic term in X ( $d$ ) is unambiguously different from 0;

- the cubic term in  $Y(f)$  is needed to get an acceptable fit;
- the  $b = a^2/2$  rule expected based on current algebra is largely violated.

KLOE has also analysed a sample of  $0.6 \times 10^6$   $\eta \rightarrow \pi^0 \pi^0 \pi^0$ . In this case the fit is done on the 1-dimensional  $Z$  distribution:

$$|A(Z)|^2 = 1 + 2\alpha Z \quad (6)$$

where  $Z$  is

$$Z = \frac{2}{3} \sum_{i=1}^3 \left( \frac{3E_i - m_\eta}{m_\eta - 3m_{\pi^0}} \right)^2 \quad (7)$$

The fit of the  $Z$  spectrum divided by the simulated spectrum with a pure phase-space distribution gives the value of the slope  $\alpha$ :

$$\alpha = -0.027 \pm 0.004 \pm 0.005 \quad (8)$$

in good agreement with Crystal Ball result [19]

## 4 Results on Scalar mesons

The lowest mass scalar nonet is not well established. On one side the two lowest mass states, the  $I=0$   $\sigma(600)$  and the  $I=1/2$   $\kappa(800)$  are both controversial; on the other side for what concern the two highest mass states, the  $I=0$   $f_0(980)$  and the  $I=1$   $a_0(980)$ , although they are firmly established states, several different interpretations of their structure have been proposed.

KLOE contributes in the understanding of the scalar mesons in two ways: in the assessment of the  $\sigma(600)$  looking at the  $\pi\pi$  low energy mass spectra and by measuring the couplings of the  $f_0(980)$  and the  $a_0(980)$  to the  $\phi$  and to the  $KK$ ,  $\pi\pi$  and  $\eta\pi$  final states. The analysis of the radiative  $\phi$  decays in  $\pi\pi\gamma$ ,  $\eta\pi\gamma$  and  $K\bar{K}\gamma$  allows to carry on this program. In the following I give the most recent results concerning the analysis of these decay channels.

### 4.1 Analysis of $\pi\pi\gamma$ : the $f_0(980)$ and the $\sigma(600)$ .

The final states  $\pi^+\pi^-\gamma$  and  $\pi^0\pi^0\gamma$  receives contributions from the radiative decays  $\phi \rightarrow f_0(980)\gamma$  and  $\phi \rightarrow \sigma(600)\gamma$ , but also from other processes that give rise to large unreducible backgrounds. By fitting the mass spectra of  $\pi^+\pi^-\gamma$  [21] and  $\pi^0\pi^0\gamma$  [22, 23] final states KLOE has extracted the scalar part of the amplitude and has obtained relevant informations on the isoscalar scalar low mass  $\pi\pi$  amplitude concerning in particular the couplings. Summarising the fit results the following statements can be done:

- the Kaon-Loop prescription [20] for the coupling of the  $\phi$  meson to the scalar provides a good description of the data;
- the  $f_0(980)$  meson is strongly coupled to the  $\phi$  and coupled to the  $KK$  system more than to the  $\pi\pi$  system;
- the scalar amplitude has a low mass tail ( $m_{\pi\pi}$  lower than 600 MeV) that can be interpreted as due to the  $\sigma$  meson.

A combined fit of the two spectra with an improved parametrisation of the scalar amplitude is in progress and will be presented soon.

## 4.2 Analysis of $\eta\pi\gamma$ : the $a_0(980)$

The  $\eta\pi$  system is a  $I=1$  state, so that is dominated by the radiative decay  $\pi \rightarrow a_0(980)\gamma$ . In this case the possible irreducible backgrounds are much less than in the case of the  $\pi\pi$  state.

KLOE has selected these final states in two ways: looking for  $\eta\pi\gamma$  with  $\eta \rightarrow \gamma\gamma$  (decay 1 in the following) and looking for the same final state but with  $\eta \rightarrow \pi^+\pi^-\pi^0$  (decay 2). The two decay channels are characterized by different systematic effects and reducible backgrounds that can affect the measurement. Two branching ratios are obtained independently:

$$BR(\phi \rightarrow \eta\pi\gamma)(1) = (6.92 \pm 0.10_{stat} \pm 0.20_{syst}) \times 10^{-5}$$

$$BR(\phi \rightarrow \eta\pi\gamma)(2) = (7.19 \pm 0.17_{stat} \pm 0.24_{syst}) \times 10^{-5}$$

in good agreement between each other. The uncertainty is improved from 9% of the previous KLOE measurement [24] to 3%.

The two mass spectra are fitted simultaneously with the Kaon-Loop model. The result for the parameters are given in tab.2.

Table 2: Result of the  $\eta\pi\gamma$  combined fit using the Kaon-Loop parametrisation for the scalar amplitude. Apart from the  $a_0$  mass, free parameters are the couplings and the ratio  $R$  between the  $\eta$  branching ratios that is left free in the fit and results in agreement with the PDG value.

dof	$p(\chi^2)$	$M_{a_0}$ (MeV)	$g_{a_0K^+K^-}$ (GeV)	$g_{a_0\eta\pi}$ (GeV)	$R$
136	11%	$983 \pm 1$	$2.16 \pm 0.04$	$2.8 \pm 0.1$	$1.69 \pm 0.04$

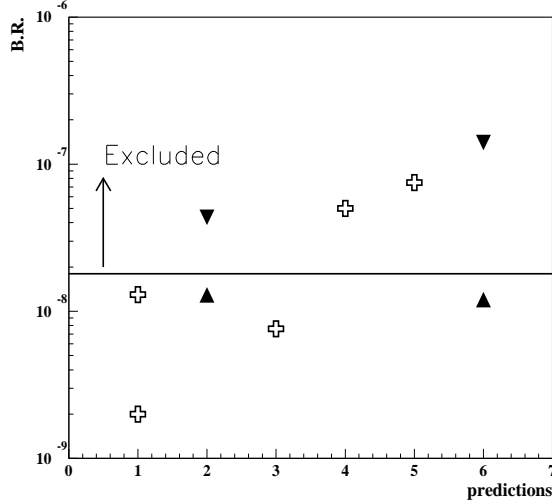


Figure 3: Published predictions on the branching ratio of the process  $\phi \rightarrow K^0 \bar{K}^0 \gamma$  (abscissas 1-6 corresponds to refs. [20, 25–29]). The models above the horizontal line are excluded by the data.

### 4.3 Search for the decay $\phi \rightarrow K^0 \bar{K}^0 \gamma$

In the decay  $\phi \rightarrow K^0 \bar{K}^0 \gamma$  the KK pair is produced in a symmetric state with 0 angular momentum, so that either  $K_S K_S$  or  $K_L K_L$  pairs can be obtained with equal probability. KLOE has searched for the decay  $\phi \rightarrow K_S K_S \gamma$  with both  $K_S$  decaying to the most frequent final state  $\pi^+ \pi^-$ . The predictions for the branching ratio of this decay depend on the model used to describe the intermediate scalar states: the  $f_0(980)$  for the I=0 part of the amplitude and the  $a_0(980)$  for the I=1 part. Due to the very small available phase-space, very small branching ratios are predicted, all in the region between  $10^{-9}$  and  $10^{-7}$  as shown in fig.3. Notice that no experimental measurements are available for this decay.

KLOE has searched for this decays requiring: (i) 2 vertices both connected to 2 charged tracks near the  $e^+ e^-$  interaction point (ii) kaon invariant masses for both vertices (iii) a combined two-kaon invariant mass well below the  $\phi$  mass and finally (iv) a low energy photon. In the end only 1 event survives the selection while the estimate of the background based on the Montecarlo sample with the same luminosity of the data gives 0 expected events. Based on the numbers we set the upper limit:

$$B.R.(\phi \rightarrow K^0 \bar{K}^0 \gamma) < 1.8 \times 10^{-8} \quad (90\% C.L.) \quad (9)$$

that allows to exclude several among the proposed models (see fig.3).

## References

- [1] W.M.Yao et al., (Particle Data Group), Journ. of Phys. **G33** (2006) 1.
- [2] M.Adinolfi et al., Nucl. Instr. and Meth. **A488**, (2002) 1.
- [3] M.Adinolfi et al., Nucl. Instr. and Meth. **A482**, (2002) 364.
- [4] M.Antonelli et al. (KLOE collaboration), talk given at Lepton-Photon 2007, Seoul;
- [5] A.Aloisio et al. (KLOE collaboration), Phys. Lett. **B606**, (2005) 12.
- [6] F.Ambrosino et al., Eur.Phys.J. **C50** (2007) 729;
- [7] M.Abdel-Bary et al. (GEM collaboration), Phys. Lett. **B619** (2005) 281.
- [8] A.Lai et al. (NA48 collaboration), Phys. Lett. **B533** (2002) 196.
- [9] D.H.Miller et al. (CLEO collaboration), arXiv:0707.1810, submitted to Phys.Rev.Lett.;
- [10] A.Akhmetshin et al., (CMD-2 collaboration), Phys. Lett.**B578** (2004) 285.
- [11] A.Bramon et al., Eur. Phys. J. **C7** (1999) 24.
- [12] A.Aloisio et al. (KLOE collaboration), Phys. Lett. **B541**, (2002) 45.
- [13] F.Ambrosino et al. (KLOE collaboration), Phys. Lett. **B648**, (2007) 267.
- [14] J.L.Rosner, Phys. Rev. **D27** (1983) 1101;
- [15] A.Bramon et al., Phys. Lett. **B503**, (2001) 271.
- [16] E.Kou, Phys. Rev. **D63** (2001) 54027;
- [17] R.Escribano, J.Nadal, JHEP 0705 (2007) 006;
- [18] B.Borasoy, R.Nissler, AIP Conf.Proc.796 (2005) 150;
- [19] W.B.Tippens et al., (Crystal Ball collaboration), Phys. Rev. Lett. **87** (2001) 192001;

- [20] N.N.Achasov and V.N.Ivanchenko, Nucl. Phys. **B315** (1989) 465.
- [21] F.Ambrosino et al. (KLOE collaboration), Phys. Lett. **B634**, (2006) 148.
- [22] A.Aloisio et al., (KLOE collaboration), Phys. Lett. **B537** (2002) 21.
- [23] F.Ambrosino et al., (KLOE collaboration), Eur. Phys. J. **C49** (2006) 433;
- [24] A.Aloisio et al. (KLOE collaboration), Phys. Lett. **B536**, (2002) 209.
- [25] N.N.Achasov, V.V.Gubin, Phys.Rev.**D64** (2001) 094016;
- [26] A.Bramon, A.Grau, G.Pancheri, Phys. Lett. **B289** (1992) 97;
- [27] J.A.Oller, Phys. Lett. **B426**(1998) 7;
- [28] R.Escribano, Eur. Phys. J. **A31** (2007) 454;
- [29] A.Gokalp, C.S.Korkmaz, O.Yilmaz hep-ph/0702214.

# STRUCTURE OF THE SCALARS

*M. R. Pennington*

Institute for Particle Physics Phenomenology  
Durham University  
Durham DH1 3LE, U.K.

## Abstract

The PDG Tables list more scalar mesons than can fit into one quark model nonet: indeed, even more than can belong to two multiplets. Consequently, some of these must be states beyond the quark model. So which of these is  $\bar{q}q$  or  $\bar{q}q\bar{q}q$  or multi-meson molecule or largely glue? How experiment can help us distinguish between these possibilities is discussed.

## 1 Why scalars?

This meeting has a plenary session and three parallel sessions devoted to the *Scalar Mesons*, and still that is not enough to accommodate all the many contributions to this subject. Others appear under the Heavy Flavour label. All these speakers [1] have something to say about the “Structure of the light scalars”. Here I will address this topic by first explaining why scalars are interesting, for those who do not think about scalars every day of the week. Then I will discuss when experiment can distinguish between a  $\bar{q}q$  meson, a tetraquark state, a  $\bar{K}K$  molecule or a glueball.

So why are the light scalars interesting? This is because they are fundamental. They constitute the Higgs sector of the strong interaction. It is these scalar fields, which have a non-zero vacuum expectation value that breaks chiral symmetry and ensures pions are very light, while giving mass to all other light flavored hadrons [2]. In terms of QCD, quarks interact weakly over short distances and they propagate freely. In contrast, over distances of the order of a fermi, the interactions between quarks, antiquarks and gluons are so strong that they generate long range correlations that polarize the vacuum. It is through this medium that quarks have to propagate across a hadron. The mass of the *up* and *down* quarks, which is only a few MeV over short distances, becomes 3-400 MeV over the size of a hadron. This change in the behavior of the quark mass is largely produced by a  $\bar{q}q$  condensate of the size of  $-(240 \text{ MeV})^3$  for *up* and *down* quarks. This “large”  $\bar{q}q$

condensate accords with standard Chiral Perturbation Theory [3]. Indeed, with its ferromagnetic analogy this supports Nambu's original picture of chiral symmetry breaking at the hadron level [2]. But then what is the scalar field that is the chiral partner of the pion? In the Nambu-Jona-Lasinio [4] and Gell-Mann-Levy [5] models it is a single  $\sigma$  field. It is the exchange of this particle that was thought to generate the long range isoscalar force between nucleons. However, if we check the PDG tables [6], there is not just the  $f_0(600)$ , which is referred to as the  $\sigma$ , but a multitude of other isoscalar scalar states:  $f_0(980)$ ,  $f_0(1370)$ ,  $f_0(1500)$ ,  $f_0(1710)$ , and the more recently discovered  $f_0(1830)$  [7]. These appear to have isodoublet and isotriplet companions:  $\kappa$ ,  $K_0^*(1430)$ ,  $a_0(980)$  and  $a_0(1450)$  below 1.9 GeV. It is tempting to regard these as the partners of the  $f_0$ 's, but which? Different modellers, many represented at this meeting [1], claim to know the answer.

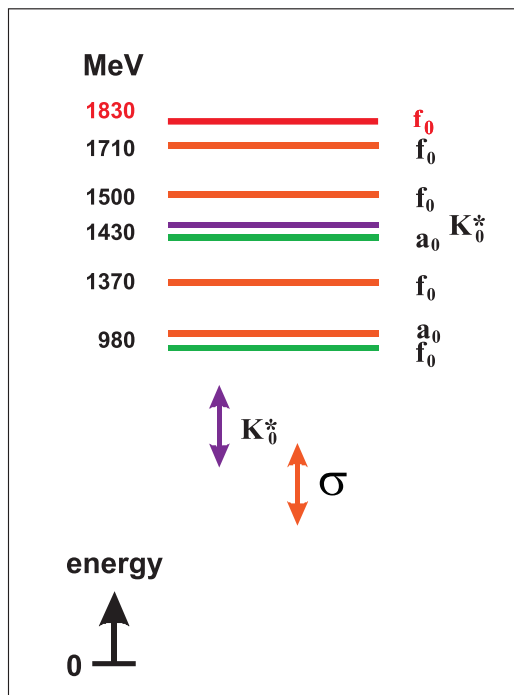


Figure 1: Spectrum of  $J^{PC} = 0^{++}$  states in the Particle Data Tables [6].

We expect there to be a simple quark model  $^3P_0$  multiplet. We have long known [8] this cannot be readily identified with the nine lightest scalars in Fig. 1 — formed from the isotriplet  $a_0$ , an isodoublet  $K_0^*$  and two  $f_0$ 's. The argument goes: how can the  $a_0(980)$  and  $f_0(980)$  be degenerate in mass with strong couplings to  $\bar{K}K$ , when a simple nonet would have just one  $\bar{s}s$  system? Jaffe [9] has long predicted the existence of multi-quark mesons, which in the

case of the scalars would form a nonet with lower mass than the simple  $\bar{q}q$  multiplet. Many have identified this tetraquark,  $\bar{q}\bar{q}qq$ , system with the nine lightest scalars. In this nonet the  $a_0, f_0(980)$  are the two heaviest states. Both built from an  $[sn]$  diquark and  $[\bar{s}\bar{n}]$  anti-diquark, with  $n = u, d$ , they are naturally degenerate in mass. In the non-relativistic potential model of Weinstein and Isgur [10], however, it is only these tetraquark states with their  $\bar{K}K$  configurations that bind. The nonet would be reduced to a quartet. In either picture the heavier  $a_0$  at 1450 MeV defines the isotriplet central line of the  $\bar{q}q$  nonet. Of course,  $\bar{q}q$  and tetraquark mesons are not orthogonal. They inevitably mix, through their common decay channels, like  $\pi\pi, \bar{K}K$ .

Almost by definition the simple quark model considers only the simplest components in a hadron's Fock space. For the well-known vector and tensor mesons, like the  $\rho^+$  and  $a_2^+$ , this is just  $u\bar{d}$ . For, the  $\phi$ , it is  $\bar{s}s$ . Of course, the Fock space of each is really more complicated. The  $\phi$  has  $\bar{K}K$  components, the  $\rho$  has  $\pi\pi$ , the  $a_2$  has  $\rho\pi$ . It is through these that the  $\phi$ ,  $\rho$  and  $a_2$ , respectively, decay. Though present these "multi-quark" components have a relatively small effect on the structure of these mesons. The  $\bar{q}q$  components dominate, and the picture of the simple quark model works. In contrast for scalars, the channels to which they decay are crucial. While they, like the vectors and tensors, have dominant two pseudoscalar decays, they have couplings that are not only intrinsically larger but  $S$ -wave. This means the decay channels have a dramatic effect. With scalars seeded by  $\bar{q}q$  configurations, new states are generated dynamically. The isotriplet and an isosinglet appear close to  $\bar{K}K$  threshold as first found by van Beveren and collaborators [11]. These then have sizeable ( $\sim 40\%$ )  $\bar{K}K$  components in their wavefunctions [12]. The quark model works where decay channels are unimportant, but for scalars they are an intrinsic part of their make-up.

A further complication is that lattice calculations universally predict that even in a world without quarks there would be a spectrum of colorless hadrons made of glue. Of these the scalar is always the lightest [13]. Predictions, by UKQCD [13], by Weingarten and by Morningstar and Peardon [14], range from 1500 to 1750 MeV. Experiment reveals states at 1500 MeV largely explored by Crystal Barrel [15], at 1710 MeV first found by Crystal Ball and confirmed by Mark III [16] at SLAC (initially as a tensor, but then revised to be a scalar [6]), and most recently at 1830 MeV by BES as an  $\omega\phi$  enhancement in  $J/\psi$  radiative decay [7]. Each of these is claimed to be the glueball, or at least largely gluish. Each has their protagonists [17–19]. No argument is yet conclusive. Scalars with a significant mixture of glue may well exist, but which states have this mixture is still a matter of debate.

## 2 $f_0(980)$ : a $\bar{q}q$ or $\bar{s}qsq$ scalar or $\bar{K}K$ molecule?

Is the deuteron a six quark state, or is it a bound state of two baryons? If the distinction is that a six quark state is generated by short range inter-quark forces, while a bound state of a proton and a neutron is formed by longer range inter-hadron interactions, then Weinberg [20] showed that this question can be answered. This is closely related to the issue of whether a CDD pole is needed in an  $N/D$  description of the relevant scattering amplitudes [21]: an argument Dalitz [22] applied to the nature of the  $\Lambda(1405)$ . Morgan [23] showed that this same idea can in principle decide whether the  $f_0$  and  $a_0(980)$  mesons are intrinsically quark states or  $\bar{K}K$  molecules [10, 24]. Data from heavy meson decays are now accumulating significant statistics on channels like  $\pi\pi$ ,  $\pi\eta$  and  $\bar{K}K$  where the  $f_0$  and  $a_0$  appear, with sufficient precision and detail to address this.

The method relies on established notions of  $S$ -matrix theory. The partial waves of scattering and production amplitudes are analytic functions of c.m. energy. At each threshold the sheets of the energy plane bifurcate. A typical resonance has poles on a whole series of sheets. It is the pole on the nearest unphysical sheet that normally controls experiment. The reflections on other sheets are further away and rather like a series of reflections in parallel mirrors the more distant have less and less impact. However, a Breit-Wigner resonance with a position close to a threshold to which it strongly couples (as exemplified by a Flatté form [25]) will have poles on sheets that are equally nearby and **both** will be required to shape the features seen in experiment. For the  $f_0(980)$  the relevant sheets are four in number being defined by the  $\pi\pi$  and  $\bar{K}K$  channels. These sheets can be unfolded in the neighborhood of  $\bar{K}K$  threshold, by considering the  $k_2$ -plane, where  $k_2$  is the centre-of-mass 3-momentum in the  $\bar{K}K$  channel, as shown in Fig. 2. Experiment is performed on the edge of sheet I, moving down the imaginary axis up to  $K^+K^-$  threshold, then round to  $\bar{K}^0K^0$  threshold, and then along the real axis as the energy increases. A resonance with a conventional Breit-Wigner shape, coupling largely to  $\pi\pi$ , would have poles on sheets II and III equidistant from the axes where experiment is performed. Such a resonance is generated by short range forces. Crudely speaking, each pole causes the phase-shift to rise by  $\sim 90^\circ$  [26]. In contrast a state generated by longer range hadronic forces only has a pole on the 2nd sheet [23]. If there were no coupling to  $\pi\pi$ , this would be a bound state with a pole on the imaginary axis. Its coupling to  $\pi\pi$  moves this away into sheet II. In some rough sense, it is “half” a Breit-Wigner resonance. Precision data on the  $f_0$  and  $a_0(980)$  in this region can in principle differentiate between the need for one pole or two [26, 27].

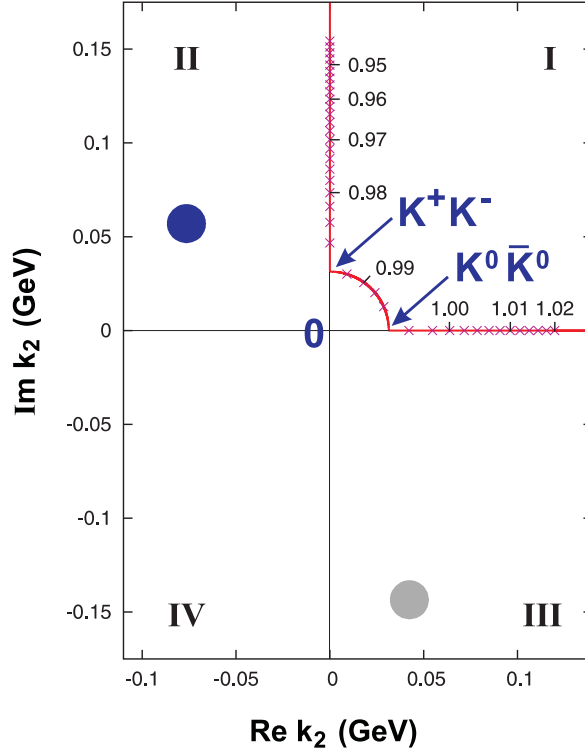


Figure 2: The complex  $k_2$ -plane in the neighborhood of the two  $\bar{K}K$  thresholds, where  $k_2$  is the c.m. 3-momentum of the  $\bar{K}K$  channel. The c.m. energy is marked ( $\times$ ) every 20 MeV, with the energy in GeV enumerated every 100 MeV. The circles illustrate the position of poles on Sheets II and III.

Ever since its discovery, the  $f_0(980)$  has been known to have a distorted shape, as seen in Fig. 3. Indeed, this is well described by the Flatté variation [25] of a Breit-Wigner form. By representing the  $S$ -matrix elements as quotients of Jost functions, the number of poles in the neighborhood of  $\bar{K}K$  threshold can then be controlled [26]. The  $\pi\pi$  phase-shift from the classic CERN-Munich experiment [28], the corresponding behavior of the inelasticity and the phase in  $\pi\pi \rightarrow \bar{K}K$  [26, 29] allow equally good descriptions with both one or two nearby poles. However, these data are in rather wide bins. Fortunately, heavy flavor decays studied in  $e^+e^-$  colliders add key information. We have from Mark III [30], DM2 [31] and BES [32] results on  $J/\psi \rightarrow \phi(MM)$  decay with  $M = \pi$  and  $K$ . Though the more recent BES data have the highest statistics, they have been binned in 30 MeV intervals. So it is the older results from Mark III in 10 MeV bins that are the most constraining. Nevertheless, they too allow both one pole and two pole descriptions of equal accuracy [33].

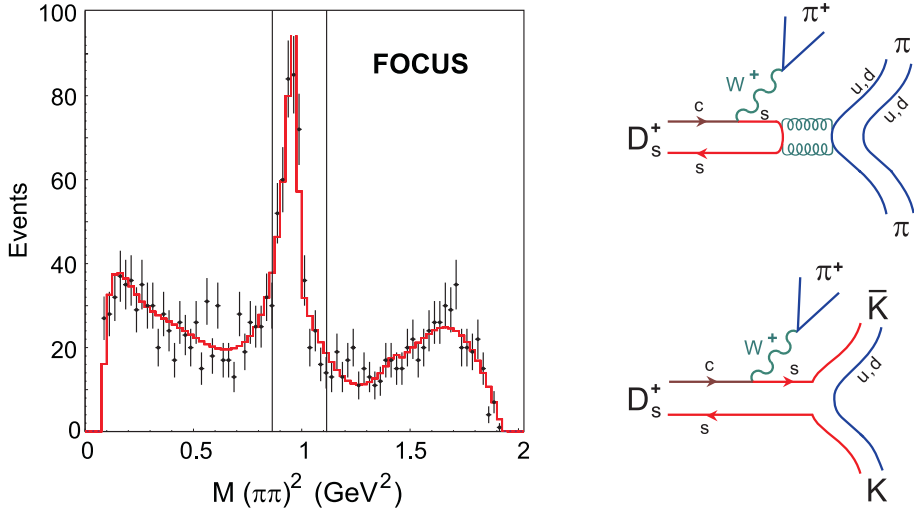


Figure 3:  $D_s^+ \rightarrow (MM)\pi^+$  decay. On the left is an illustration of the  $\pi^+\pi^-$  mass spectrum as observed by the FOCUS experiment [34] — the vertical lines around the  $f_0(980)$  peak delineate the region employed in the Jost function analysis of Ref. [33]. On the right are the corresponding quark line graphs appropriate to  $\pi\pi$  and  $\bar{K}K$  final states.

What we need are precision results in small energy bites. Fortunately, these are provided by  $D_s \rightarrow \pi(MM)$  decays. To see the quality we show in Fig. 3, the  $\pi\pi$  mass spectrum for this decay from the FOCUS collaboration [34]. The region close to  $\bar{K}K$  threshold used in this analysis is indicated by the vertical lines around the  $f_0(980)$  peak in Fig. 3. What makes the most difference are data from BaBar, as these have been partial wave analysed in both the  $\pi^+\pi^-$  and  $K^+K^-$  channels [35]. While these results are *under wraps* and cannot be displayed, the  $\bar{K}K$  data are in 4 MeV bins. When the  $S$ -wave is fitted together with the data on classic meson scattering experiments and  $J/\psi$  decay, discussed above, these  $D_s$  amplitudes constrain the position of the poles rather well. Still fits with both one and two nearby poles are equally likely. Seemingly we cannot distinguish between a molecule and an intrinsically quark state. The pole on Sheet II (indicated in Fig. 2) is at essentially the same location in both solutions. How can it be that fits that are so different in structure in the nearby complex plane can describe data nearly identically on the real axis? Since the presence of the Sheet III pole is the difference, exploration of the amplitudes reveals that the fit positions its Sheet III pole just where its residues in both the  $\pi\pi$  and  $\bar{K}K$  channels are vanishingly small [33]. Thus, the two pole fit is really just pretending to be the single pole fit, and so a structure for the  $f_0(980)$  generated by longer range inter-hadron forces dominates. This would be exciting, if it were the

definitive conclusion. However these are only preliminary conclusions [33] of an analysis based on preliminary results from BaBar. Definitive conclusions will have to wait till BaBar have finalised their partial wave analysis.

### 3 Radiative width of the low mass scalars

Another way to learn about the constitution of a hadron is to measure its coupling to photons. For instance the coupling of vector mesons to  $e^+e^-$  is readily predicted in the simple quark model, and experiment confirms this to be correct. For scalars (as with tensors) the coupling is to two photons, Fig. 4. The quark model predicts that the radiative width of each is determined by the square of the mean charge squared of their constituents, Fig. 4. For the tensors the ratio of radiative widths accords with the expectation for an ideally mixed quark model multiplet. The corresponding predictions exist for the light spinless mesons. For a  $(\bar{u}u + \bar{d}d)$  scalar the two photon width is 5-10 keV at a mass of 700 MeV, reducing to 2-4 keV if the mass is down at 500 MeV [36], while for an  $\bar{s}s$  state it is predicted to be  $\sim 0.2 - 0.4$  keV [37,38]. Calculations for a  $\bar{K}K$  molecule are  $\sim 0.2 - 0.6$  keV [39–41]. However one should treat these with some care. Experience with the pseudoscalars  $\pi^0, \eta$

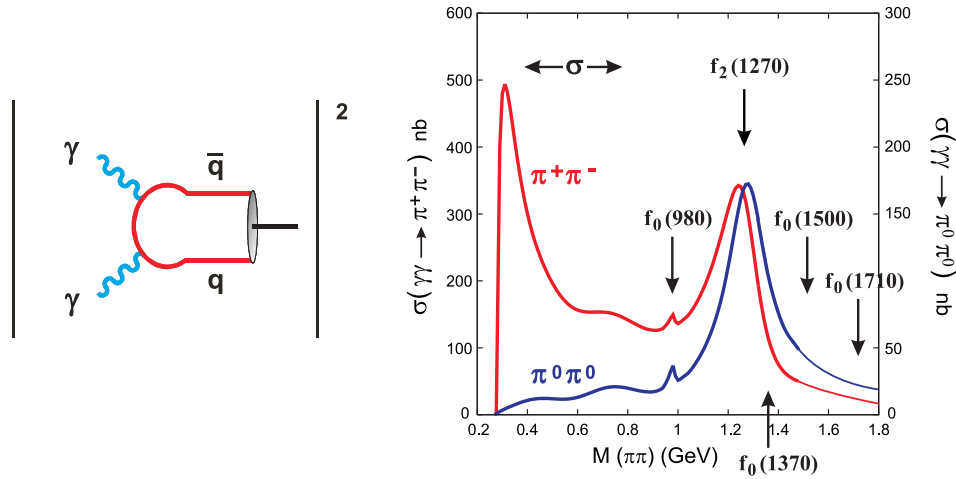


Figure 4: Two photon process: on the left a graph depicting the radiative width of a  $\bar{q}q$  bound state. On the right is a sketch of the integrated cross-section for  $\gamma\gamma \rightarrow \pi^+\pi^-$  and  $\pi^0\pi^0$  with different scales. Below 1.5 GeV this sketch is based on data from Mark II [42], CELLO [43], Belle [44] and Crystal Ball [45]. The positions of key resonances are indicated. There is as yet no evidence for the sharp peaking near 1 GeV in the  $\pi^0\pi^0$  channel, or for any structures above 1.5 GeV to associate with the higher scalars.

and  $\eta'$ , shows that agreement with experiment only comes if the quark model prediction is assumed to be bolted on to a factor of  $mass^3$  [46]. That such an *ad hoc* correction is required illustrates that for light hadrons, including the scalars, a truly relativistic strong coupling calculation is essential.

How do we extract the two photon widths from experiment? The two channels  $\gamma\gamma \rightarrow \pi^+\pi^-$  and  $\pi^0\pi^0$  are those with the most data. The charged and neutral pion results are starkly different close to threshold as sketched in Fig. 4. The charged channel is dominated by the one-pion exchange Born term, while that in the neutral case is very small (a factor of 40 or 50 less). It might appear that it is in the  $\pi^0\pi^0$  channel that one should look for the  $\sigma$  and extract its two photon coupling. Simply given a cross-section of  $\sim 10$  nb, this might suggest a glueball character. This is the idea of the *red dragon* of Minkowski and Ochs [47], but for them this scalar is at higher mass away from threshold. In contrast, the  $\sigma$  with a pole at  $E = 441 - i272$  MeV [48] is crouching at much lower mass: see Fig. 5. Its two photon coupling is controlled by final state interactions. Despite the neutral cross-section being small the “effective” radiative width of the  $\sigma$  is not  $\sim 0.1$  keV but several keV [49] : telling us that quarks are an essential part of the  $\sigma$ ’s make-up.

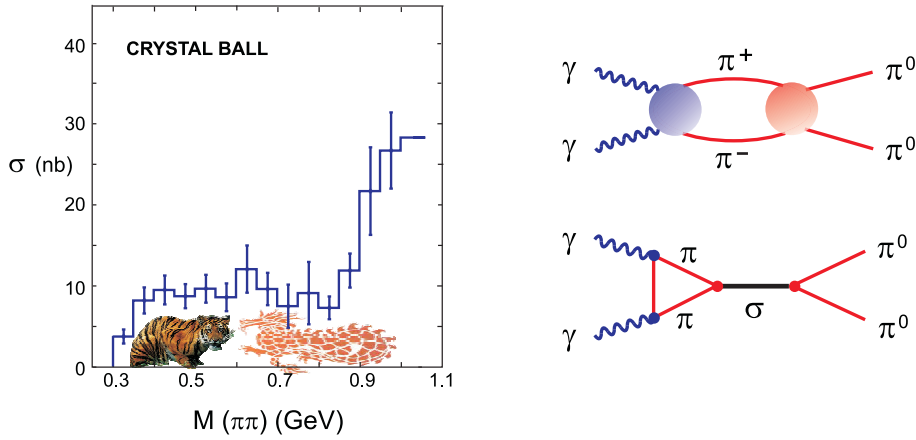


Figure 5: Cross-section for  $\gamma\gamma \rightarrow \pi^0\pi^0$ , integrated over the angular range  $|\cos\theta^*| \leq 0.8$  from Crystal Ball [45]. The dominant mechanism for generating the  $\pi^0\pi^0$  final state is through the process  $\gamma\gamma \rightarrow \pi^+\pi^-$  by one-pion-exchange, followed by  $\pi^+\pi^- \rightarrow \pi^0\pi^0$ : the  $\sigma$  is one component of this, as shown in the graphs on the right. Though the  $\sigma$  has an effective two photon width of several keV, the final state interactions in this channel mean that it is hidden, as indicated by the “crouching tiger”. At slightly higher mass Minkowski and Ochs [47] have claimed a scalar – the *red dragon* – is there.

Now let us turn to the  $f_0(980)$ . Though earlier results from Mark II [42] and CELLO [43] hinted at a shoulder in the  $\gamma\gamma \rightarrow \pi^+\pi^-$  cross-section around 1 GeV, Belle with data in 5 MeV bins in  $\pi\pi$  mass is the first experiment to reveal a clear peak, sketched in Fig. 4. However, extracting the radiative width for this narrow state is still not easy. Belle fit their integrated cross-section and find  $\Gamma(f_0(980) \rightarrow \gamma\gamma) = (0.205 \pm 0.089 \pm 0.132)$  keV [44]. The errors reflect the marked systematic sensitivity to the assumed non-resonant background and the presumption of pure helicity two for the  $f_2(1270)$ . The way to proceed is to perform an Amplitude Analysis using all the available data on charged and neutral channels and all the angular information to separate out the  $I = 0$   $S$ -wave signal. This is non-trivial given that the charged pion data cover no more than 60% of the angular range and the contributions of individual partial waves are then not orthogonal. Preliminary results of the Amplitude Analysis from the Belle group and myself [50] show that solutions with a radiative width for the  $f_0(980)$  from 0.1 to 0.4 keV are equally possible. These solutions differ in the amount  $S$ -wave and helicity zero  $D$ -wave. This is not better determined because Belle has difficulty in separating the background  $\mu^+\mu^-$  pairs. This results in a rather poor angular distribution in the key 0.80 and 1.05 GeV region. Finer  $\pi^0\pi^0$  differential cross-sections covering a bigger angular range, perhaps 80%, are promised soon from Belle and these will hopefully allow a cleaner amplitude separation and a more precise width for the  $f_0(980)$ . Exactly how many tenths of a keV will be critical in confirming its sizeable  $\overline{K}K$  composition. Once this is settled we can go on and study the higher mass scalar states, like the  $f_0(1370)$ ,  $f_0(1500)$  and  $f_0(1710)$  as indicated in Fig. 4. That is for the future.

## 4 Conclusions

The structure of the scalars is far from simple. The isoscalar members couple to the vacuum of QCD and reflect its structure. The fact that there is not just one scalar, but many, may be echoed as GeV scales give way to TeV and we learn, as the LHC has its first collisions, about the scalar(s) that break electroweak symmetry.

## Acknowledgments

It is a pleasure to thank the organisers for the invitation to give this talk. The work presented here was partially supported by the EU-RTN Programme, Contract No. MRTN-CT-2006-035482, “FLAVIANet”.

## References

- [1] These proceedings.
- [2] Y. Nambu, *Phys. Rev. Lett.* **4**, 380 (1960).
- [3] J. Gasser and H. Leutwyler, *Ann. Phys. (NY)* **158**, 142 (1984).
- [4] Y. Nambu and G. Jona-Lasinio, *Phys. Rev.* **122**, 345 (1961), *ibid.* **124**, 246 (1961).
- [5] M. Gell-Mann and M. Levy, *Nuovo Cim.* **16**, 705 (1960).
- [6] W.-M. Yao *et al.* [Particle Data Group], *J. Phys.* **G33**, 1 (2006).
- [7] M. Ablikim *et al.*, *Phys. Rev. Lett.* **96**:162002 (2006) [hep-ex/0602031].
- [8] D. Morgan, *Phys. Lett.* **B51** (1974) 71.
- [9] R. L. Jaffe, *Phys. Rev.* **D15**, 267 (1977).
- [10] J. D. Weinstein and N. Isgur, *Phys. Rev. Lett.* **48**, 659 (1982), *Phys. Rev.* **D27**, 588 (1983), **D41**, 2236 (1990).
- [11] E. Van Beveren, T. A. Rijken, K. Metzger, C. Dullemond, G. Rupp and J. E. Ribeiro, *Z. Phys.* **C30**, 615 (1986); E. Van Beveren and G. Rupp, (these proceedings) [arXiv:0710.3056]
- [12] N. A. Tornqvist, *Z. Phys.* **C68**, 647 (1995).
- [13] G.S. Bali *et al.* [UKQCD], *Phys. Lett.* **B309**, 378 (1993).
- [14] J. Sexton, A. Vaccarino and D. Weingarten, *Phys. Rev. Lett.* **75**, 4563 (1995); C. Morningstar and M. Peardon, *Nucl. Phys. Proc. Suppl.* **53**, 917 (1997).
- [15] C. Amsler *et al.* [Crystal Barrel], *Phys. Lett.* **B342**, 433 (1995), *ibid.* **B353**, 571 (1995).
- [16] C. Edwards *et al.* [Crystal Ball/SLAC], *Phys. Rev. Lett.* **48**, 458 (1982); R. M. Baltrusaitis *et al.* [Mark III], *Phys. Rev.* **D35**, 2077 (1987).
- [17] W. Lee and D. Weingarten, *Nucl. Phys. B, Proc Suppl.* **53**, 236 (1997), *ibid* **63**, 194 (1998).
- [18] C. Amsler and F. E. Close, *Phys. Lett.* **B353**, 385 (1995), *Phys. Rev.* **D53**, 295 (1996).

- [19] P. Bicudo, S. R. Cotanch, F. J. Llanes-Estrada and D. G. Robertson, *Eur. Phys. J.* **C52**, 363 (2007).
- [20] S. Weinberg, *Phys. Rev.* **130**, 776 (1963), *ibid.* **131**, 440 (1963), *ibid.* **137** (1965) B672.
- [21] L. Castellejo, R.H. Dalitz and F.J. Dyson, *Phys. Rev.* **101**, 453 (1956).
- [22] R. H. Dalitz and J. G. McGinley, *Low and intermediate energy kaon-nucleon physics*, ed. E. Ferrari and G. Violini (pub. Reidel, 1981) p. 381; R. H. Dalitz, J. G. McGinley, C. Belyea and S. Anthony, *Proc. Int. Conf. on hypernuclear and kaon physics*, Heidelberg, June 1982, ed. B. Povh (pub. MPI, Heidelberg, 1982, p. 201.
- [23] D. Morgan, *Nucl. Phys. A* **543**, 632 (1992).
- [24] N. N. Achasov, S. A. Devyanin and G. N. Shestakov, *Sov. J. Nucl. Phys.*, **32**, 566 (1980).
- [25] S. M. Flatté, *Phys. Lett.* **B63**, 224 (1976).
- [26] D. Morgan and M R. Pennington, *Phys. Lett.* **B258**, 444 (1991), *Phys. Rev.* **D48**, 1185 (1993).
- [27] V. Baru *et al.*, *Phys. Lett.* **B586**, 53 (2004) [hep-ph/0308129].
- [28] B. Hyams *et al.* [CERN-Munich], *Nucl. Phys.* **B64**, 134 (1973); G. Grayer *et al.* [CERN-Munich], *Nucl. Phys.* **B75**, 189 (1974). W. Ochs, Ph.D. thesis submitted to the University of Munich (1973).
- [29] A. Etkin *et al.*, *Phys. Rev.* **D25**, 1786 (1982); D. M. Cohen *et al.*, *Phys. Rev.* **D22**, 2595 (1980).
- [30] U. Mallik [Mark III], in *Strong Interactions and Gauge Theories*, Proc XXXI Rencontre de Moriond, Les Arcs, France, 1986, (ed. J. Tran Thanh Vanh) Editions Frontières, Gif-sur-Yvette, 1986, Vol. 2, p. 431; W. Lockman [Mark III], *Hadron '89*, Proc. 3rd Int. Conf. on Hadron Spectroscopy, Ajaccio, France 1989 (ed. F. Binon *et al*), Editions Frontières, Gif-sur-Yvette, 1989) p. 709.
- [31] A. Falvard *et al.* [DM2], *Phys. Rev.* **D38**, 2706 (1988).
- [32] M. Ablikim *et al.* [BES], *Phys. Lett.* **B607**, 243 (2005) [hep-ex/0411001].
- [33] M. R. Pennington and D. J. Wilson, (work in progress).

- 
- [34] P. L. Frabetti *et al.* [FOCUS], *Phys. Lett.* **B407**, 79 (1997);  
J. M. Link *et al.* [FOCUS], *Phys. Lett.* **B585**, 200 (2004).
- [35] M. Pappagallo [BaBar], (work in progress).
- [36] M. S. Chanowitz, *Proc. VIIIth Int. Workshop on Photon-Photon Collisions* (Shoresh, 1988), ed. U. Karshon (World Scientific, 1988), p. 205.
- [37] T. Barnes, *Phys. Lett.* **165B**, 434 (1985).
- [38] A. V. Anisovich, V. V. Anisovich, D. V. Bugg and V. A. Nikonov, *Phys. Lett.* **B456**, 80 (1999) [hep-ph/9903396]; A. V. Anisovich *et al.*, (hep-ph/0508260).
- [39] N. N. Achasov, S. A. Devyanin and G. N. Shestakov, *Z. Phys.* **C16**, 55 (1982).
- [40] T. Barnes, *Proc. IXth Int. Workshop on Photon-Photon Collisions* (San Diego, 1992), ed. D. Caldwell and H. P. Paar (World Sci., 1992), p. 263.
- [41] C. Hanhart, Yu. S. Kalashnikova, A. E. Kudryavtsev and A. V. Nefediev, *Phys. Rev.* **D75**: 074015 (2007) [hep-ph/0701214].
- [42] J. Boyer *et al.* [Mark II], *Phys. Rev.* **D42**, 1350 (1990).
- [43] J. Harjes, Ph.D. Thesis, submitted to the University of Hamburg; H.J. Behrend *et al.* [CELLO], *Z. Phys.* **C56**, 381 (1992).
- [44] K. Abe *et al.* [Belle], *Phys. Rev.* **D75**, 051101 (2007) [hep-ex/0610038].
- [45] H. Marsiske *et al.* [Crystal Ball], *Phys. Rev.* **D41**, 3324 (1990).
- [46] C. Hayne and N. Isgur, *Phys. Rev.* **D25**, 1944 (1982).
- [47] P. Minkowski and W. Ochs, *Eur. Phys. J.* **C9**, 283 (1999) [hep-ph/9811518]; W. Ochs, *Proc. Hadron '03*, AIP Conf. Proc. **717**, 295 (2004).
- [48] I. Caprini, G. Colangelo and H. Leutwyler, *Phys. Rev. Lett.* **96** (2006) 132001 (2006) [hep-ph/0512364].
- [49] M. R. Pennington, *Phys. Rev. Lett.* **97**, 011601 (2006) [hep-ph/0604212], *Mod. Phys. Lett.* **A22**, 1439 (2007) [arXiv:0705.3314].
- [50] T. Mori, Y. Watanabe, S. Uehara and M.R. Pennington, (work in progress).

MENU 2007  
11th International Conference  
on Meson-Nucleon Physics and  
the Structure of the Nucleon  
September 10-14, 2007  
IKP, Forschungszentrum Jülich, Germany

# SCALAR MESONS FROM AN EFFECTIVE LAGRANGIAN APPROACH

*A.H. Fariborz*<sup>1</sup>

Department of Mathematics/Physics  
State University of New York Institute of Technology  
P.O. Box 3050, Utica, New York 13504-3050, USA.

*R. Jora*<sup>2</sup>

Physics Department  
Syracuse University, Syracuse, New York 13244-1130, USA.

*J. Schechter*<sup>3</sup>

Physics Department  
Syracuse University, Syracuse, New York 13244-1130, USA.

## Abstract

A brief discussion of the recent interest in light scalar mesons motivates the study of a generalized linear sigma model. In an  $SU(3)$  flavor invariant version of the model there is a prediction that the lighter scalars have sizeable “four quark” content. It is further predicted that one of the singlet scalars should be exceptionally light. Due to the presence of scalar mesons, the model gives “controlled” corrections to the current algebra formula for threshold pion pion scattering. These corrections act in the direction to improve agreement with current experiments.

## 1 Introduction

A linear sigma model with both fields representing quark-antiquark type composites and fields representing (in an unspecified configuration) two quarks and two antiquarks, seems useful for understanding the light scalar spectrum of QCD. To see this, note that, at present, the scalars below 1 GeV appear

---

<sup>1</sup>email:fariboa@sunyit.edu

<sup>2</sup>email:cjora@phy.syr.edu

<sup>3</sup>Speaker;email:schechte@phy.syr.edu

to fit into a nonet as:

$$\begin{aligned}
I = 0 : m[f_0(600)] &\approx 500 \text{ MeV} \\
I = 1/2 : m[\kappa] &\approx 800 \text{ MeV} \\
I = 0 : m[f_0(980)] &\approx 980 \text{ MeV} \\
I = 1 : m[a_0(980)] &\approx 980 \text{ MeV}
\end{aligned} \tag{1}$$

This level ordering may be compared with that of the most conventional meson nonet- the low lying vector mesons. In fact it is completely flipped compared to that one; the almost degenerate  $I=0$  and  $I=1$  vector states lie lowest rather than highest and the other  $I=0$  state lies highest. The ordering for vectors is conventionally understood as due to the strange quark being heavier than the up and down quarks and the vectors being quark anti-quark composites. The ordering is gotten just by counting the number of strange quarks in each state. It was pointed out a long time ago in Ref. [1], using the same reasoning, that the level order is automatically flipped when the mesons are made of two quarks and two antiquarks instead. That argument was given for a diquark- anti diquark structure but is easily seen to also hold for the meson- anti meson structure which was advocated for example in Ref. [2]. Thus, on empirical grounds a four quark structure for the light scalars seems very suggestive and well worth investigating.

Now one expects higher mass scalars related to p wave quark antiquark composites to also exist. It is natural to expect mixing between states with the same quantum numbers and there is some phenomenological evidence for this as noted in Refs [3] and [4]. Considering the importance of spontaneously broken chiral symmetry in low energy QCD, it seems interesting to investigate packaging the whole scheme in an effective chiral Lagrangian containing a “two quark” *chiral* nonet (with both scalars and pseudoscalars) as well as a “four quark” *chiral* nonet.

We employ the  $3 \times 3$  matrix chiral nonet fields;

$$M = S + i\phi, \quad M' = S' + i\phi'. \tag{2}$$

Here  $M$  represents scalar,  $S$  and pseudoscalar,  $\phi$  quark-antiquark type states, while  $M'$  represents states which are made of two quarks and two antiquarks. The transformation properties under  $SU(3)_L \times SU(3)_R \times U(1)_A$  are

$$M \rightarrow e^{2i\nu} U_L M U_R^\dagger, \quad M' \rightarrow e^{-4i\nu} U_L M' U_R^\dagger, \tag{3}$$

where  $U_L$  and  $U_R$  are unitary unimodular matrices, and the phase  $\nu$  is associated with the  $U(1)_A$  transformation, which also distinguishes the two quark type from the four quark type fields. However, together with our model,

it does not distinguish between different types of four quark configurations. That question is discussed in more detail in ref. [5]. The general Lagrangian density which defines our model is

$$\mathcal{L} = -\frac{1}{2}\text{Tr}(\partial_\mu M \partial_\mu M^\dagger) - \frac{1}{2}\text{Tr}(\partial_\mu M' \partial_\mu M'^\dagger) - V_0(M, M') - V_{SB}, \quad (4)$$

where  $V_0(M, M')$  stands for a function made from  $SU(3)_L \times SU(3)_R$  (but not necessarily  $U(1)_A$ ) invariants formed out of  $M$  and  $M'$ . The quantity  $V_{SB}$  stands for chiral symmetry breaking terms which transform in the same way as the quark mass terms in the fundamental QCD Lagrangian. The model was proposed in section V of ref. [6] and followed up in refs. [7], [8], [9], [10] and [11], the last two of which will be briefly described here. Related models for thermodynamic properties of QCD are discussed in refs. [13]. In [10], we focused on general properties which continued to hold when  $V_{SB}$  was set to zero while in [11] we included the  $SU(3)$  symmetric mass term:

$$V_{SB} = -2A \text{Tr}(S) \quad (5)$$

where  $A$  is a real parameter.

A characteristic feature of the model is the presence of “two-quark” and “four-quark” condensates:

$$\langle S_a^b \rangle = \alpha_a \delta_a^b, \quad \langle S'^b_a \rangle = \beta_a \delta_a^b. \quad (6)$$

We shall assume the vacuum to be  $SU(3)_V$  invariant, which implies

$$\alpha_1 = \alpha_2 = \alpha_3 \equiv \alpha, \quad \beta_1 = \beta_2 = \beta_3 \equiv \beta. \quad (7)$$

The  $SU(3)$  particle content of the model consists of two pseudoscalar octets, two pseudoscalar singlets, two scalar octets and two scalar singlets. This gives us eight different masses and four mixing angles.

Note that the transformation between the diagonal fields ( $\pi^+$  and  $\pi'^+$ ) and the original pion fields is given as:

$$\begin{bmatrix} \pi^+ \\ \pi'^+ \end{bmatrix} = \begin{bmatrix} \cos \theta_\pi & -\sin \theta_\pi \\ \sin \theta_\pi & \cos \theta_\pi \end{bmatrix} \begin{bmatrix} \phi_1^2 \\ \phi_1'^2 \end{bmatrix}.$$

Thus  $100 \sin^2 \theta_\pi$  represents the four quark percentage of the ordinary pion while  $100 \cos^2 \theta_\pi$  represents the four quark percentage of the “heavy” pion in the model. Also of relevance is the one particle piece of the isovector axial vector current,

$$(J_\mu^{axial})_1^2 = F_\pi \partial_\mu \pi^+ + F_{\pi'} \partial_\mu \pi'^+ + \dots, \quad (8)$$

where,

$$\begin{aligned} F_\pi &= 2\alpha \cos \theta_\pi - 2\beta \sin \theta_\pi, \\ F_{\pi'} &= 2\alpha \sin \theta_\pi + 2\beta \cos \theta_\pi. \end{aligned} \quad (9)$$

Note that  $\tan \theta_\pi = -\beta/\alpha$  when the pion is massless.

## 2 Specific Lagrangian

As discussed in ref. [10] one may obtain certain general results from tree level Ward identities without restrictions on the form of the potential  $V_0$ . For a complete description however, a specific form must be furnished. The leading choice of terms corresponding to eight or fewer quark plus antiquark lines at each effective underlying vertex reads [10]:

$$\begin{aligned} V_0 = & -c_2 \text{Tr}(MM^\dagger) + c_4^a \text{Tr}(MM^\dagger MM^\dagger) \\ & + d_2 \text{Tr}(M'M'^\dagger) + e_3^a (\epsilon_{abc} \epsilon^{def} M_d^a M_e^b M_f^{c'} + h.c.) \\ & + c_3 \left[ \gamma_1 \ln \left( \frac{\det M}{\det M^\dagger} \right) + (1 - \gamma_1) \frac{\text{Tr}(MM^\dagger)}{\text{Tr}(M'M'^\dagger)} \right]^2. \end{aligned} \quad (10)$$

All the terms except the last two have been chosen to also possess the  $U(1)_A$  invariance. Further details of the  $U(1)_A$  aspect are given in ref. [10].

As the corresponding experimental inputs [12] we take the non-strange quantities:

$$\begin{aligned} m(0^+ \text{ octet}) &= m[a_0(980)] = 984.7 \pm 1.2 \text{ MeV} \\ m(0^+ \text{ octet}') &= m[a_0(1450)] = 1474 \pm 19 \text{ MeV} \\ m(0^- \text{ octet}') &= m[\pi(1300)] = 1300 \pm 100 \text{ MeV} \\ m(0^- \text{ octet}) &= m_\pi = 137 \text{ MeV} \\ F_\pi &= 131 \text{ MeV} \end{aligned} \quad (11)$$

Clearly  $m[\pi(1300)]$  has a large uncertainty and will essentially be regarded as a free parameter.

Predictions for the two unspecified  $0^+$  masses are shown in Fig.1. The lighter of these clearly invites us to identify it as the sigma. Predictions for the four quark contents of the lightest four  $SU(3)$  multiplets are shown in Fig.2. Clearly the lighter  $0^-$  octet is primarily two quark and the lighter  $0^-$  singlet has a primarily two quark solution. On the other hand, both the lighter  $0^+$  octet and singlet have large four quark content!

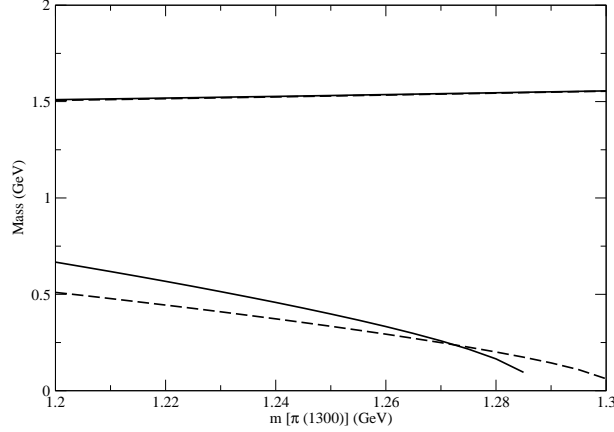


Figure 1: The predictions for the masses of the two SU(3) singlet scalars vs.  $m[\pi(1300)]$ . The solid lines correspond to the massive pion case while the dashed lines correspond to the massless pion case.

### 3 Pion pion scattering

The tree level form for the conventional Mandelstam amplitude in the present model is:

$$A(s, t, u) = -\frac{g}{2} + \sum_i \frac{g_i^2}{m_i^2 - s}, \quad (12)$$

where  $g$  is the four pion coupling constant, the four  $g_i$ 's are the three-point coupling constants of two pions with each of the four scalar isosinglets and the  $m_i$  represent the masses of the four scalar isosinglets. To really understand what is happening we should expand in powers of  $(s - m_\pi^2)$ :

$$\begin{aligned} A(s, t, u) &= -\frac{g}{2} + \sum_i \frac{g_i^2}{m_i^2 - m_\pi^2} \left[ 1 + \frac{s - m_\pi^2}{m_i^2 - m_\pi^2} + \left( \frac{s - m_\pi^2}{m_i^2 - m_\pi^2} \right)^2 + \dots \right] \\ &\approx (s - m_\pi^2) \left[ \frac{2}{F_\pi^2} + (s - m_\pi^2) \sum_i \frac{g_i^2}{(m_i^2 - m_\pi^2)^3} + \dots \right]. \end{aligned} \quad (13)$$

The exact first equation contains, for each  $m_i$ , a geometrical expansion in the quantity  $(s - m_\pi^2)/(m_i^2 - m_\pi^2)$ . Thus the radius of convergence in  $s$  for this expression is the squared mass of the lightest scalar isosinglet. To apply this expression in the resonance region we must, of course, unitarize the formula in some way. Here we will look at the threshold region. In going from the first

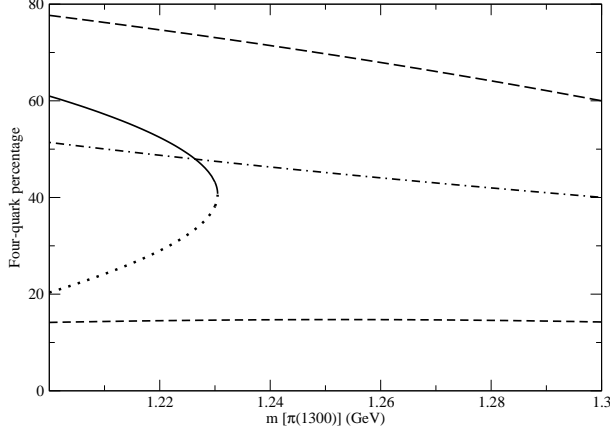


Figure 2: Four quark percentages of the pion (dashed line), the  $a_0(980)$  (top long-dashed line), the very light  $0^+$  singlet (dotted-dashed line) and the  $\eta(958)$  in the scenario where the higher state is identified as the  $\eta(1475)$  (curve containing both solid and dotted pieces) as functions of the undetermined input parameter,  $m[\pi(1300)]$ . Note that there are two solutions for the  $\eta(958)$ : the dotted curve choice gives it a predominant two quark structure and the solid curve choice, a larger four quark content.

to the second equation of Eq.(13) we used the facts established in ref. [10] for the  $m_\pi = 0$  case and in ref. [11] (in the very good approximation where  $F_{\pi'} = 0$ ) for the massive pion case that: 1) the sum of the first two terms of the first equation vanishes and 2) the third term of the first equation simplifies to become the first, current algebra, term of the second equation. These results hold for any chiral symmetric choice of the potential. The third term of the second equation represents the model dependent leading correction to the usual current algebra formula. It depends on the masses of the scalar mesons and would vanish in a hypothetical limit (often used) in which the scalar meson masses are taken to infinity. At low energies the third term is seen to be suppressed by order  $(m_\pi/m_i)^2$  compared to the current algebra term.

For comparison, we give the usual current algebra results [14] for the two

s-wave scattering lengths:

$$\begin{aligned} m_\pi a_0^0 &= \frac{7m_\pi^2}{16\pi F_\pi^2} \approx 0.15, \\ m_\pi a_0^2 &= \frac{-2m_\pi^2}{16\pi F_\pi^2} \approx -0.04. \end{aligned} \quad (14)$$

Recent experimental data on the s-wave scattering lengths  $a_0^0$  and  $a_0^2$  include the following,

NA48/2 collaboration [15]:

$$m_{\pi^+}(a_0^0 - a_0^2) = 0.264 \pm 0.015 \quad (15)$$

$$m_{\pi^+} a_0^0 = 0.256 \pm 0.011 \quad (16)$$

E865 Collaboration [16]:

$$m_{\pi^+} a_0^0 = 0.216 \pm 0.015 \quad (17)$$

DIRAC Collaboration [17]

$$m_{\pi^+} a_0^0 = 0.264_{-0.020}^{+0.038} \quad (18)$$

Clearly, the current algebra value of  $a_0^0$  is lower than experiment. Including the corrections from non-infinite scalar meson masses with the choice of  $V_0$  in Eq.(10), yields the results shown in Fig.3. The corresponding lightest scalar mass for each value of  $m[\pi(1300)]$  can be read from Fig. 1. The value of  $a_0^2$  for the non resonant channel is not altered much but it can be seen that the prediction for  $a_0^0$  is definitely improved.

## 4 Further discussion

1. A criticism of linear sigma models is that they obtain the current algebra result as an almost complete cancellation of large quantities. This may be seen in the left panel of Fig. 4 which shows the five different terms in Eq.(12) appearing to almost cancel in a haphazard pattern. On the other hand, once we make the Taylor expansion in Eq.(13), the corrections to the current algebra result are seen in the right panel to be completely dominated by the lightest scalar; this contribution is suppressed, as noted above, by  $(m_\pi/m_\sigma)^2$ .

2. We plan to increase the accuracy of our model by including SU(3) breaking effects and also by unitarizing the model so that it would be suitable also in the energy region around the scalar resonances. The simplest

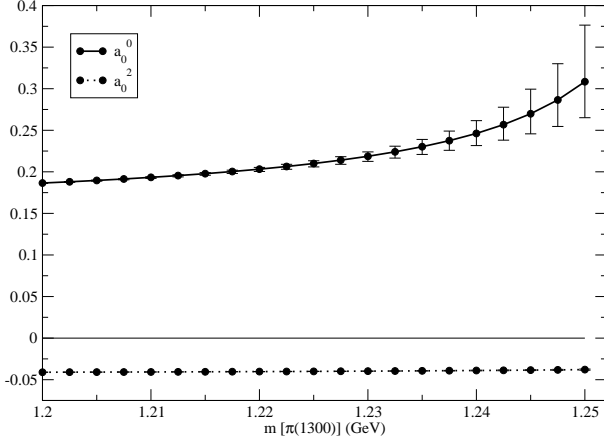


Figure 3: Top curve:  $I = J = 0$  scattering length,  $m_\pi a_0^0$  vs.  $m[\pi(1300)]$ . Bottom curve:  $I = 2, J = 0$  scattering length,  $m_\pi a_0^2$  vs.  $m[\pi(1300)]$ . The error bars reflect the uncertainty of  $m[a_0(1450)]$ .

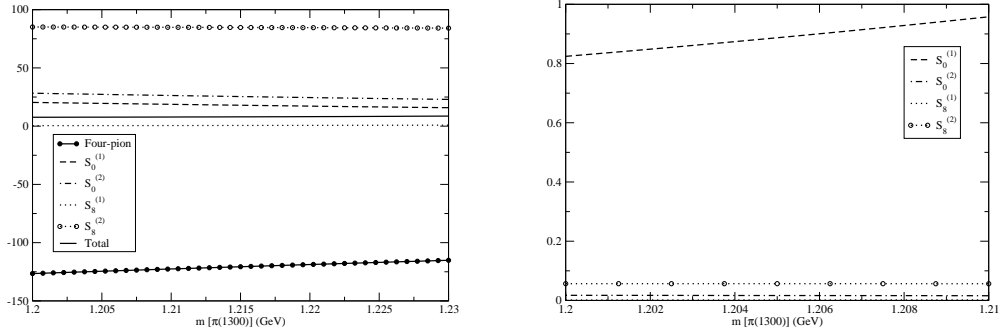


Figure 4: Left: Individual contributions in Eq.(12) to  $A(s, t, u)$  at threshold. Right: Individual contributions to the second of Eq.(13) to  $A(s, t, u)$  at threshold.

unitarization is the K-matrix type. It was carried out for the two flavor linear sigma model in ref. [18]. We expect the results for the present model to be generally similar to the ones obtained in ref. [6] for the single  $M$  three flavor linear model.

3. A possible general question about the present model is that it introduces both states made of a quark and an antiquark as well as states with two quarks and two antiquarks. According to the usual 't Hooft large  $N_c$  extrapolation [19] of QCD the “four quark” states are expected to be suppressed. However, it was recently pointed out [20] that the alternative, mathematically allowed, Corrigan Ramond [21] extrapolation does not suppress the multi-quark states. This kind of extrapolation may be relevant for understanding the physics of the light scalar mesons.

## Acknowledgments

We are happy to thank A. Abdel-Rehim, D. Black, M. Harada, S. Moussa, S. Nasri and F. Sannino for many helpful related discussions. The work of A.H.F. has been partially supported by the NSF Award 0652853. The work of R.J. and J.S. is supported in part by the U. S. DOE under Contract no. DE-FG-02-85ER 40231.

## References

- [1] R.L. Jaffe, Phys. Rev. D **15**, 267 (1997).
- [2] J.D. Weinstein and N. Isgur, Phys. Rev. Lett. **48**, 659 (1982).
- [3] D. Black, A. H. Fariborz and J. Schechter, Phys. Rev. D **61** 074001 (2000).
- [4] T. Teshima, I. Kitamura and N. Morisita, J. Phys. G **28**, 1391 (2002); *ibid* **30**, 663 (2004); F. Close and N. Tornqvist, *ibid.* **28**, R249 (2002); A.H. Fariborz, Int. J. Mod. Phys. A **19**, 2095 (2004); 5417 (2004); Phys. Rev. D **74**, 054030 (2006); F. Giacosa, Th. Gutsche, V.E. Lyubovitskij and A. Faessler, Phys. Lett. B **622**, 277 (2005); J. Vijande, A. Valcarce, F. Fernandez and B. Silvestre-Brac, Phys. Rev. D **72**, 034025 (2005); S. Narison, Phys. Rev. D **73**, 114024 (2006); L. Maiani, F. Piccinini, A.D. Polosa and V. Riquer, hep-ph/0604018.
- [5] Y. S. Kalashnikova, A. E. Kudryavtsev, A. V. Nefediev, C. Hanhart and J. Haidenbauer, Eur. Phys. J. A **24** (2005) 437.

- 
- [6] D. Black, A.H. Fariborz, S. Moussa, S. Nasri and J. Schechter, Phys. Rev. D **64**, 014031 (2001).
  - [7] M. Napsuciale and S. Rodriguez, Phys. Rev. D **70**, 094043 (2004).
  - [8] A.H. Fariborz, R. Jora and J. Schechter, Phys. Rev. D **72**, 034001 (2005).
  - [9] A.H. Fariborz, R. Jora and J. Schechter, Phys. Rev. D **76**, 014011 (2007).
  - [10] A.H. Fariborz, R. Jora and J. Schechter, arXiv:0707.0843 [hep-ph].
  - [11] A.H. Fariborz, R. Jora and J. Schechter, arXiv:0708.3402 [hep-ph].
  - [12] W-M Yao et al, J. Phys. G: Nucl. Part. Phys. **33**, 1 (2006).
  - [13] N. Yamamoto, M. Tachibana, T. Hatsuda and G. Baym, Phys. Rev. D **76**, 074001 (2007), arXiv:0704.2654 [hep-ph]; A.A. Andrianov and D. Espriu, arXiv:0709.0049 [hep-ph].
  - [14] S. Weinberg, Phys. Rev. Lett. **17**, 616 (1966).
  - [15] J.R. Betley et al [NA48/2 Collaboration], Phys. Lett. B **633**, 173 (2006) [arXiv:hep-ex/0511056].
  - [16] S. Pislak et al [E865 Collaboration], Phys. Rev. D **67**, 072004 (2003) [arXiv: hep-ex/0301040].
  - [17] B. Adeva et al [DIRAC Collaboration], Phys. Lett. B **619**, 50 (2005) [arXiv:hep-ex/0504044].
  - [18] N.N. Achasov and G.N. Shestakov, Phys. Rev. D **49**, 5779 (1994).
  - [19] G.'t Hooft, Nucl. Phys. B **72**, 461 (1974).
  - [20] F. Sannino and J. Schechter, Phys. Rev. D **76**, 014014 (2007), arXiv:0704.0602 [hep-ph].
  - [21] E. Corrigan and P. Ramond, Phys. Lett. B **87**, 73 (1979).

# PHYSICS PROGRAM AT COSY

*K.-Th. Brinkmann*

Technische Universität Dresden  
Institut für Kern- und Teilchenphysik  
D-01062 Dresden, Germany

## Abstract

The COoler SYnchrotron COSY at the Forschungszentrum Jülich accelerates protons and deuterons to momenta of up to  $3.7\text{ GeV}/c$ . Experiments in the ring use the coasting beam, which can be produced with transverse polarization in excess of 80%. These experiments center around the production, interaction and decay of hadrons, mesons as well as baryons. This contribution summarizes the ongoing physics program at the COSY facility, highlighting recent results and detailing future developments and plans.

## 1 Introduction

Hadron physics with hadronic probes provides insight into the production, interaction and decay of hadrons. The search for missing states predicted in the scheme of constructing hadrons from elementary building blocks can shed light on quark interactions and selection rules. The symmetries expected in strong interactions, such as chiral symmetry and isospin, and their breaking are a matter of ongoing research. Mass modifications of mesons embedded in the nuclear medium may allow to understand chiral restoration and, thus, deepen the insight into the chiral symmetry concept.

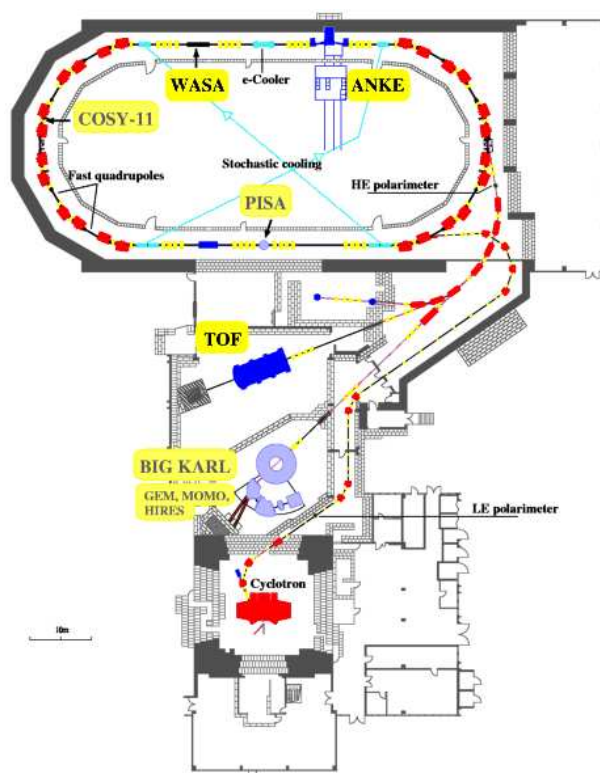
The COoler SYnchrotron *COSY* [1] is designed for experimental research in this field of physics. It accelerates protons and deuterons to momenta of  $3.7\text{ GeV}/c$ . Vector polarization of up to 80% can be achieved. Deuterons can also be tensor-polarized. In the past, a number of experiments addressed a broad range of topics at *COSY*. Results include the most complete set of observables in elastic proton-proton interactions between 500 and 2500 *MeV* beam energy [2] and many measurements on production of a variety of mesons in the pseudoscalar, vector and scalar sector very close to threshold and at higher excess energies (for a recent review, see [3]). Experiments at *COSY* have access to the production of strangeness degrees of freedom, most commonly through associated production of hyperons and kaons.

The large experience gained in these studies has recently mounted in the formulation of a physics program that centers around three big experimental installations, the internal *ANKE* magnetic spectrometer, the external  $4\pi$  *TOF* spectrometer and the *WASA* detector, which was successfully transferred from TSL in Uppsala to Jülich and has commenced operation recently after a period of refurbishing and upgrades to match the higher energies accessible at *COSY*. With *WASA*, explicit searches for isospin-violating processes have become feasible. Rare decays of  $\eta$  and  $\eta'$  will be investigated. These studies will be complemented by polarization physics using polarized beams and targets, and hyperon production experiments, which give access to the hyperon-nucleon interaction and baryon resonances. *COSY* research also provides a window into the *FAIR* future with studies on spin manipulation and polarization build-up of protons in polarized targets.

## 2 The COSY Facility

Figure 1 shows a schematic view of the experimental facility. Negative ions are accelerated to  $40\text{ MeV}$  in the cyclotron and injected into *COSY* where electron cooling can be used to improve the phase space distribution of the beam before acceleration to the appropriate energy for a given experiment. At a circumference of  $184\text{ m}$  *COSY* can store  $10^{11}$  protons or deuterons. The coasting beam after acceleration has a typical momentum spread of  $\Delta p/p \approx 10^{-4}$  and an emittance of better than  $\pi\text{ mm mrad}$ . When the beam is used at one of the internal target stations its emittance can be continuously controlled with stochastic cooling, which guarantees constant beam properties for an extended duration of beam-target interaction. In addition, *COSY* features slow extraction of beams with momenta up to  $3.3\text{ GeV}/c$  for external experiments. This features provides continuous beams of  $10^5$  to  $10^9$  particles per second on target for up to  $100\text{ s}$  or more depending on beam current. These beams can be polarized as well.

The figure also shows the experiments at *COSY*, some of which are phasing out (shaded entries) to be replaced by recent additions and massive upgrades of other detectors also shown. *PISA* was an experiment designed to study the interaction of high-energy protons with heavy targets and measure fragment isotopic distributions and differential cross sections. [4]. *EDDA* has been mentioned before. Here, an extensive data base of pp elastic scattering over the full *COSY* energy range was collected with very high statistics and precision. Both polarized beam and polarized beam and target in combination were used to measure all differential observables that can be obtained

Figure 1: Schematic view of the *COSY* accelerator.

with polarization degrees of freedom in the entrance channel [2]. These measurements have then been introduced into the SAID database and phase shift analysis [5] and caused a dramatic improvement of the reliability of this analysis. *EDDA* is still in use as a reliable polarization monitor for *COSY* beams, e.g. in the spin manipulation program of the "Spin at *COSY*" collaboration. *COSY - 11* used one of the *COSY* accelerator dipoles as an analyzing magnet by placing a gas jet target in front of the magnet. Reaction products have a smaller magnetic rigidity than the beam. Particles of positive charge therefore get deflected inward into the ring and can be detected with tracking and time-of-flight devices to determine particle species and velocity. Because of the limited acceptance *COSY - 11* was best suited for measurements only slightly above threshold. *COSY - 11* has produced detailed excitation functions for a number of reaction channels, in particular in the production of single mesons, e.g.  $pp \rightarrow pp\eta$ ,  $pp \rightarrow pp\eta'$  [6] and in  $dp$  interactions [7] and channels involving open strangeness such as  $pp \rightarrow pKY$  [8] and also double-kaon production,  $pp \rightarrow ppKK$  [9].

*WASA* at *COSY*, the *ANKE* magnetic spectrometer and the Time-of-flight experiment *COSY – TOF* will be described in some more detail later. The magnetic spectrometer *BIGKARL*, located at an external beam line, concludes the list of experiments in hadron physics at *COSY*. The large acceptance of the *BIGKARL* spectrometer and its excellent resolution has been used in a number of meson-production reactions where usually the mesons were detected in additional detectors that covered large solid angles, such as *MOMO*, a tracking detector covering polar angles up to  $45^\circ$  degrees and the *GEM* germanium wall that measured particle energies and energy loss in addition to the spatial information. Here, high-precision mass measurements for the  $\eta$  [10] and double-meson production in proton-deuteron fusion ( $\pi^+\pi^-$  as well as  $K^+K^-$  [11], [12]) are among the highlights of the program.

### 3 Experiments at COSY

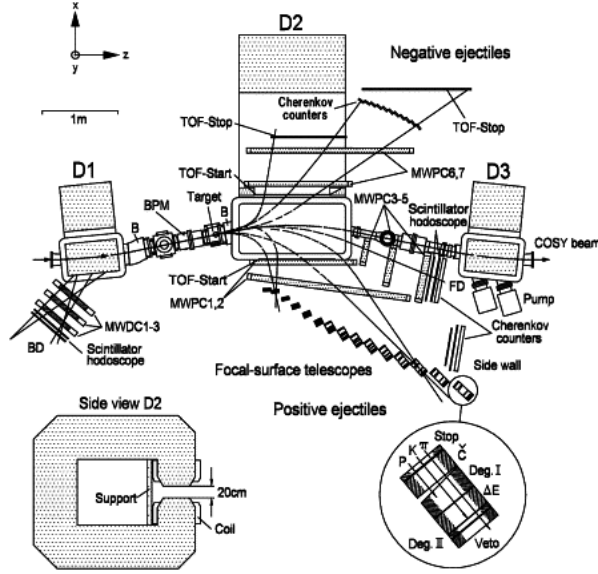
The ongoing physics program at *COSY* centers around three large experiments. These setups are complementary in their layout. Each of these will be discussed in some detail in the following.

#### The ANKE spectrometer

The *ANKE* magnetic spectrometer (cf. Fig. 2, from [13]) is a rather large-acceptance spectrometer featuring excellent momentum resolution. It is optimized for kaon identification. To this end, detectors inside the yoke allow detection of negatively charged particles. The detectors in the focal surface on the positive bending side are of  $\Delta E - E$  type with absorbers inserted in order to identify kaons over a wide momentum range. The measurement of forward-going high-momentum particles is augmented by an array of silicon telescopes in the target region to measure recoil protons. This telescope can identify recoil protons from deuteron targets with good resolution, facilitating measurements on the neutron through recoil tagging. Apart from heavy foil targets, a cluster jet target and a polarized atomic beam target for protons and deuterons are available at *ANKE*. Exploiting these features, the *ANKE* collaboration performs experiments on three-body final states using polarized beams and targets. The focus here is on polarized nucleon-nucleon scattering also including  $np$  interactions and on investigations of meson-baryon and baryon-baryon final state interactions.

#### WASA at COSY

The *WASA* setup at *COSY* (cf. Fig. 3, see [14]) has a much larger geometrical acceptance than the devices discussed so far. A very thin superconducting solenoid surrounding the target generates a magnetic field in which the

Figure 2: Schematic view of the *ANKE* spectrometer.

momenta of charged particles are measured using a cylindrical tracker surrounded by a plastic scintillator barrel. In forward direction, a calorimeter with differential energy measurement and a set of tracking devices allows to measure particle ID and total energy as well as direction of charged particles with high accuracy. The central barrel of *WASA* is surrounded by a photon spectrometer with high granularity, which allows to measure photons from  $\pi$  and  $\eta$  decay as well as electrons with good spatial as well as energy resolution. The *WASA* setup is equipped with a hydrogen pellet target which permits operation at very high luminosity. Because of the large geometrical acceptance of *WASA*, rare final states can be searched for efficiently. The physics focus of *WASA* is the investigation of violation and breaking of basic symmetries through the measurement of exclusive final states. With the *WASA* detector, *COSY* becomes a factory for  $\eta$  and  $\eta'$  mesons, whose successive decay into a variety of channels can be studied.

### COSY-TOF

The Time-of-Flight detector *COSY – TOF* (cf. Fig. 4) takes a very different approach which is optimized for the measurement of produced particles that subsequently decay in the region behind the target. The *COSY-TOF* spectrometer is located at an external *COSY* beamline. A small target cell with a length of 4 mm only and a beam extension of less than 1 mm guarantee a very good definition of the primary reaction vertex. Reaction products

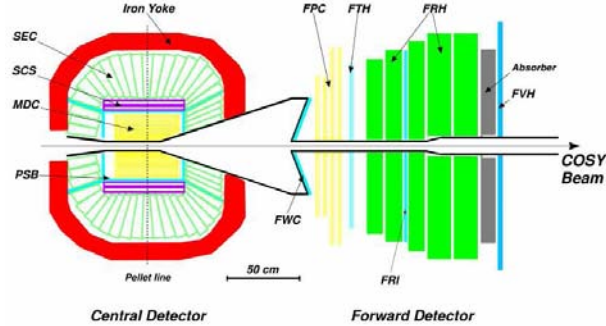


Figure 3: Schematic view of the *WASA* setup at *COSY*. (SEC: electromagnetic calorimeter; SCS, PSB, MDC: tracking and time-of-flight; FWC: forward window counter; FPC, FTH: tracking; FRH: range hodoscope; FVH: forward veto hodoscope).

are then detected in a series of position-sensitive detectors that define the particle tracks. (See inlay of 4, which shows the enlarged target region. The distance of the last two tracking layers is  $10\text{ cm}$ .) Delayed decays in particular of neutral particles, e.g.  $\Lambda \rightarrow \pi^+ p$  or  $K_s \rightarrow \pi^+ \pi^-$ , can be resolved by appropriate combinations of detector hits. The outer detector consists of a scintillator barrel and forward part. The barrel section with a length and diameter of about  $3\text{ m}$ , respectively, is covered with 96 scintillator bars of  $100\text{ mm}$  width and  $15\text{ mm}$  thickness with double-sided photomultiplier readout that allows a position resolution of  $\approx 3\text{ cm}$  using mean timing and signal intensities on both sides. The forward part is made from two annular detectors consisting of three scintillator layers, one cut into wedges, one left- and one right-wound Archimedian spiral layer. The geometrical overlap of these three layers as seen from the target forms roughly triangular-shaped "pixels". Thus, a total of about 5000 individual subdetectors in the forward region is obtained, again yielding very good spatial and time-of-flight resolution of  $\sigma_{ToF} \leq 250\text{ ps}$ . The strength of this high-acceptance spectrometer with particle tracking and secondary-vertex recognition is the measurement of reactions involving strangeness production and reaction channels such as  $pp \rightarrow pp\eta$  and  $pp \rightarrow pp\omega, \omega \rightarrow \pi^+\pi^-\pi^0$  where the number of charged particles in the exit channel allows efficient triggering and the complete exit channel kinematics can be reconstructed from the velocity vectors of the charged ejectiles.

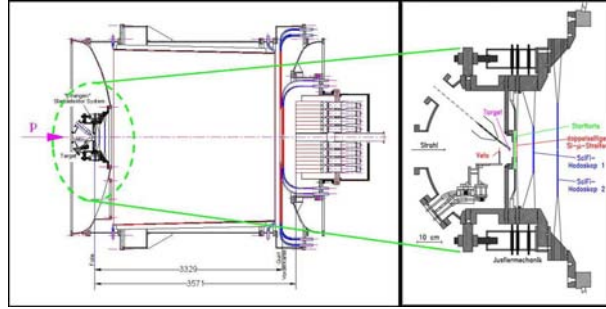


Figure 4: Schematic view of the *TOF* spectrometer at *COSY*.

## 4 Physics at *COSY*

Using hadronic probes, *COSY* experiments can help to shed light on open questions on the structure of hadrons and their interaction as well as the symmetries of nature and their breaking involved in the formation of hadrons from more fundamental building blocks, whose individual properties get lost in the process of making hadrons. This chapter will highlight some of the recent experiments that address specific questions in this context.

In 2003, a number of experiments claimed to have seen evidence for a manifestly exotic baryon resonance, the so-called  $\Theta^+$  with a quark structure  $uudd\bar{s}$ , a surprisingly low mass of  $1540 \text{ MeV}/c^2$  and a width of less than  $20 \text{ MeV}$  in reactions involving very different beam-target combinations. The signal was seen in  $\Theta^+ \rightarrow K^+n$  and  $\Theta^+ \rightarrow K^0p$  decay; for a summary see [15]. Such a state had been predicted theoretically shortly before [16]. *COSY – TOF* was among the experiments reporting evidence. At *TOF* an indication for a signal was seen in exclusively reconstructed  $pp \rightarrow pK_s\Sigma^+$  events at a beam momentum of  $pc = 2.95 \text{ GeV}$  [17]. As in all other experiments, the indication was rather weak with only a few tens of events over significant "background", in this case meaning non-resonant reactions leading to the same exit channel. *COSY – TOF* has meanwhile repeated the measurement at  $pc = 3.06 \text{ GeV}$  with an improved detector setup with increased detection efficiency, increase of the luminosity by a factor of five and exploitation of three independent strains of analysis which differ significantly in the weighting of employed observables and methods. The result of this analysis as published in [18] is summarized in Figure 5. The left column of the figure shows invariant mass spectra in the  $Kp$  two-body subsystem. The region of interest for the  $\Theta^+$  is shown by the overlaid shaded bar. The right column in the figure shows the average cross section deter-

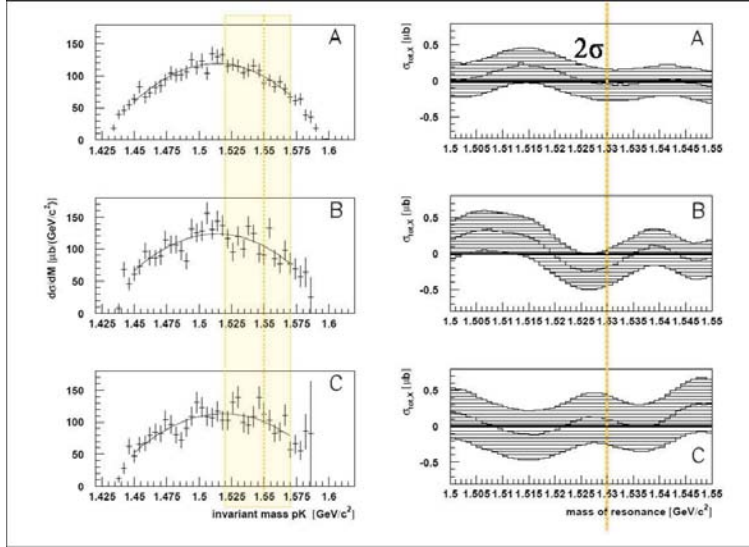


Figure 5: *COSY – TOF* result on the question of the existence of a  $\Theta^+$  resonance decaying into  $K^0p$ . The left column shows invariant mass spectra in the relevant two-body subsystem in the exit channel. The region of interest is shown by the overlaid shaded bar. The right column shows the average cross section determined for a possible structure in each invariant mass spectrum based on a smooth background parametrization over the full spectral range, and the shaded bar is the  $2\sigma$  confidence interval from which an upper limit can be derived for each of the three analyses.

mined for a possible narrow structure in each invariant mass spectrum based on a smooth background parametrization over the full spectral range, and the shaded bar is the  $2\sigma$  confidence interval from which an upper limit can be derived for each of the three analyses. In total, the upper cross section limit for a possible structure with a width compatible with the detector resolution was determined to be  $150 \text{ nb}$  ( $2\sigma$ ). An additional upper cross section limit for  $\Theta^+$  production in  $pp \rightarrow \Theta^+\pi^+\Lambda$  of  $\sigma \leq 58 \text{ nb}$  was established at a beam momentum of  $3.65 \text{ GeV}/c$  by *ANKE* [19].

*ANKE* has observed the much discussed  $\Lambda(1405)$  [20] resonance via its decay into  $\Sigma^0\pi^0$  [21]. Careful analysis of missing momenta and invariant masses in subsystems allowed discrimination of background from the  $\Sigma(1385) \rightarrow \Lambda\pi^0$  channel which interferes with  $\Lambda(1405)$  production in the charged decay channels ( $\Sigma(1385)/\Lambda(1405) \rightarrow \Sigma^{+/-}\pi^{-/+}$ ) so that the line shape is distorted. The data show a rather symmetric Breit-Wigner-like shape compatible with old data [22] and a genuine resonance interpretation within the limited statis-

tics available.

Apart from the search for exotics at *COSY – TOF*, a series of experiments has addressed hyperon production in various exit channels in *pp* collisions, also employing polarized beams. These measurements clearly indicate the contributions of decays of nucleon resonances with masses of around  $1700 \text{ MeV}/c^2$  to the Dalitz plot, which due to the high acceptance of *TOF* is uniformly covered [23].  $\omega$  meson production in *pp* at the same energies also appears to involve resonances decaying to  $p\omega$ . Here, further data are needed to establish resonance excitation and discriminate contributions from different meson exchange currents [24]. *COSY – TOF* is currently undergoing a major upgrade in equipment. A straw tube tracker will replace the layered fiber hodoscopes in the start region, greatly increasing collection and reconstruction efficiency for strange decays. A new silicon detector will be used as a start and first tracking device [25].

Regular operation of *WASA* has commenced. A wealth of data on the decay of  $\eta$  and  $\eta'$  is to be expected in the near future [26]. First runs have been performed at the  $pp \rightarrow pp\eta$  as well as the  $pp \rightarrow pp\eta'$  reactions. A high-statistics sample on the decay  $\eta \rightarrow 3\pi^0$  is already under investigation and compares favorably with data taken previously on the same channel with *WASA* at *CELSIUS* [27]. In the near future, investigations shall address the  $\eta \rightarrow \pi^+\pi^-e^+e^-$  decay. The branching ratio of this decay has not been measured very precisely yet [28], but the decay allows a test of CP violation. *WASA* at *COSY* will surpass the statistics of previous samples by orders of magnitude. Experiments on  $dd \rightarrow \alpha\pi\pi, {}^3\text{He}n\pi^0$  as background to the very rare isospin violating  $dd \rightarrow \alpha\pi^0$  process and on  $pd \rightarrow {}^3\text{He}a_0/f_0$  in order to study the radiative decay of the scalar mesons will be performed in 2007.

The spin physics program at *ANKE* strives to provide detailed exclusive data on *NN* scattering, in particular *np* scattering, over the full *COSY* energy range. Data on  $\mathbf{d}p \rightarrow (pp)_{1S_0}$  have recently been published [30], further measurements also using the polarized atomic beam target and the spectator detector are under preparation [31]. These double-polarization experiments together with detailed investigations on spin manipulation in *COSY* [32] have implications in the extended program of the facility for antiprotons and ion research *FAIR* at *GSI*, Darmstadt [33]. Here, an extension of the high-energy antiproton program at the *HESR* antiproton storage ring was proposed by the *PAX* collaboration [34] based on experience collected at *COSY* and other storage rings. *COSY* is also used for preparatory studies for the *HESR* and the *PANDA* experiment [35]. This includes conceptual studies for accelerator items such as stochastic cooling, a  $2 \text{ MeV}$  electron cooler, cavities and RF structures, magnets and diagnostics.

## 5 Summary and Conclusions

The ongoing physics program at *COSY* holds the potential to significantly contribute to our understanding of hadron physics in the light quark sector. With the commissioning of *WASA* at *COSY* a tool has become available that allows high-statistics studies aiming at very rare decays of  $\eta$  and  $\eta'$ , effectively turning *COSY* into a meson factory. These experiments touch upon fundamental questions such as symmetries and symmetry violation within and outside of the standard model.

Experiments on the structure and interaction of baryons and mesons will continue at *ANKE* and *COSY-TOF*. A quantitative analysis of the observed baryon states and an extension of the investigations toward polarization degrees of freedom and neutron interactions using deuteron beams or targets and spectator detection where applicable is envisaged. These experiments have a clear and direct perspective into the *FAIR* future.

## References

- [1] R. Maier, *Nucl. Inst. Meth.* **A390**, 1 (1997).
- [2] D. Albers *et al.* (EDDA collaboration), *Eur. Phys. J.* **A22**, 125 (2004); M. Altmeier *et al.* (EDDA collaboration), *Eur. Phys. J.* **A23**, 351 (2005); F. Bauer *et al.* (EDDA collaboration), *Phys. Rev.* **C71**, 054002 (2005).
- [3] Annual Report of the IKP, Forschungszentrum Jülich GmbH (2007), available at:  
[http : //www.fz - juelich.de/ikp/en/publications.shtml](http://www.fz-juelich.de/ikp/en/publications.shtml) (as of Oct. 2007).
- [4] R. Barna *et al.*, *Nucl. Inst. Meth.* **A519**, 610 (2004) and A. Bubak *et al.*, *Phys. Rev.* **C76**, 014618 (2007).
- [5] A. Arndt *et al.*, *Phys. Rev.* **C62**, 034005 (2000); current solution retrieved from: [http : //gwdac.phys.gwu.edu](http://gwdac.phys.gwu.edu) (as of Sept. 2007).
- [6] R. Czyzykiewicz *et al.*, *Phys. Rev. Lett.* **98**, 122003 (2007).
- [7] J. Smyrzki *et al.*, accepted for publication in *Phys. Lett. B*, available at: [arXiv : nucl - ex/0702043v1](http://arXiv:nucl-ex/0702043v1).
- [8] T. Rozek *et al.*, *Phys. Lett. B* **643**, 251 (2006).
- [9] P. Winter *et al.*, *Phys. Lett. B* **635**, 23 (2006).

- 
- [10] M. Abdel-Bary *et al.* (GEM Collaboration), *Phys. Lett. B* **619**, 281 (2005).
- [11] F. Bellemann *et al.* (MOMO Collaboration), *Phys. Rev. C* **60**, 061002 (1999).
- [12] F. Bellemann *et al.* (MOMO Collaboration), *Phys. Rev. C* **75**, 015204 (2007).
- [13] S. Barsov *et al.* (ANKE Collaboration) *Nucl. Inst. Meth. A* **462**, 364 (2001).
- [14] WASA-at-COSY Collaboration, B. Hoistad, J. Ritman *et al.*, Proposal for WASA at COSY (2004), *available as: arXiv : nucl - ex/0411038v1*.
- [15] Q. Zhao and F.E. Close, *J. Phys. G* **31**, L1 (2005).
- [16] D. Diakonov, V. Petrov and M. Polyakov, *Z. Phys. A* **359**, 305 (1997); M.V. Polyakov *et al.*, *Eur. Phys. Jour. A* **9**, 115 (2000); D. Diakonov, V. Petrov, *Phys. Rev. D* **72**, 074009 (2005).
- [17] COSY-TOF collaboration, *Phys. Lett.*, **B595**, 27 (2004).
- [18] COSY-TOF collaboration, *Phys. Lett.*, **B649**, 252 (2007).
- [19] M. Nikipelov *et al.* (ANKE collaboration), *J. Phys. G: Nucl. Part. Phys.* **34**, 627 (2007).
- [20] E. Oset, L.S. Geng, M. Döring, *arXiv : 0710.5925*.
- [21] I. Zychor *et al.* (ANKE collaboration), *available as: arXiv : 0705.1039v1* [nucl-ex], submitted for publication in *Phys. Rev. Lett.*.
- [22] R.J. Hemingway, *Nucl. Phys. B* **253**, 742 (1984); D.W. Thomas *et al.*, *Nucl. Phys. B* **56**, 15 (1973).
- [23] COSY-TOF collaboration, *Phys. Lett. B* **632**, 27 (2006).
- [24] W. Ullrich, this conference.
- [25] COSY-TOF collaboration, Strangeness Physics at COSY-TOF, *available at:*  
[http : //www.kfa - juelich.de/ikp/publications/PAC34/TOF\\_perspectives\\_final.pdf](http://www.kfa-juelich.de/ikp/publications/PAC34/TOF_perspectives_final.pdf)  
(as of Nov. 2007).
- [26] M. Wolke, this conference.

- [27] C. Pauly, this conference.
- [28] C. Bargholtz *et al.*, *Phys. Lett.* **B644**, 299 (2007).
- [29] ANKE collaboration, Spin Physics from COSY to FAIR, it available at:  
[http : //www.fz – juelich.de/ikp/anke/en/proposal/spin\\_proposal.pdf](http://www.fz-juelich.de/ikp/anke/en/proposal/spin_proposal.pdf)  
(as of Nov. 2007).
- [30] D. Chiladze *et al.*, *Phys. Lett.* **B637**, 170 (2006).
- [31] F. Rathmann, A. Kacharava, this conference.
- [32] A. Krisch *et al.*, SPIN COSY: Spin-Manipulating Polarized Deuterons and Protons, it available at:  
[http : //www.kfa – juelich.de/ikp/publications/PAC32/SPIN\\_at\\_COSY – Proposal.3oct06.pdf](http://www.kfa-juelich.de/ikp/publications/PAC32/SPIN_at_COSY-Proposal.3oct06.pdf) (as of Nov. 2007).
- [33] FAIR baseline technical report, GSI (2006), *available at*:  
<http://www.gsi.de/fair/reports/btr.html> (as of Oct. 2007).
- [34] PAX Technical Proposal, Spokespersons P. Lenisa and F. Rathmann, hep-ex/0505054,  
*available at*:  
[http : //www.fz – juelich.de/ikp/pax](http://www.fz-juelich.de/ikp/pax) (as of Oct. 2007).
- [35] K.-Th. Brinkmann, Paola Gianotti, I. Lehmann, *Nucl. Phys. News* **16**, 15 (2006), *see also*:  
[http : //www – panda.gsi.de/](http://www-panda.gsi.de/) (as of Oct. 2007).

# HADRON-HADRON AND HADRON-HADRON-HADRON PROPERTIES FROM LATTICE QCD

*Silas R. Beane*  
Department of Physics  
University of New Hampshire  
Durham, NH 03824-3568

## Abstract

While lattice QCD is able to compute some single-hadron properties to few-percent accuracy, only very recently has it become possible to extract precise information about the interactions among hadrons. I will review the methodology for extracting scattering and many-body information from lattice QCD correlation functions in a finite volume, and I will discuss recent progress in computing the  $\pi^+\pi^+$  ( $I = 2$ ) scattering length and the  $\pi^+\pi^+\pi^+$  interaction using fully-dynamical lattice QCD calculations.

## 1 Introduction

One of the grand challenges of strong-interaction physics is to make quantitative predictions for the properties and interactions of nuclei directly from Quantum ChromoDynamics (QCD). Recently, Moore's Law, coupled with algorithmic breakthroughs, have allowed pioneering preliminary studies of low-energy nucleon-nucleon (NN) [1] and hyperon-nucleon (YN) [2] scattering in fully dynamical-lattice QCD. While in the context of nuclear physics one may be tempted to focus attention on potentials and wavefunctions rather than on S-matrix elements, these are not fundamental objects in QCD, and they are therefore useful tools only to the extent that they are able to encode information about low-energy scattering [3].

In order to make contact between nuclear physics and lattice QCD, it is essential to understand the mapping between the finite-volume energy levels that one measures in a lattice calculation and the hadronic interactions that give rise to nuclei. The first step in this direction was taken by Lüscher [4, 5] who noted that the two-body elastic S-matrix can be directly related to the energy levels of two particles interacting in a space-time lattice. Analogous

relations for the interaction of  $n$  particles in the weakly-interacting limit were derived long ago by Huang and Yang and others [6–8]. Only very recently have these relations been extended to include the presence of three-body forces [9, 10].

Current lattice QCD calculations of the interactions among baryons are severely impeded by the exponential decay of the signal/noise ratio [11], and it is clear that, barring theoretical or algorithmic developments that will alleviate the signal problem, significantly more computer power than is now available will have to be brought to bear on nuclear physics before real nuclei can be studied in a quantitative way using lattice QCD. However, it is important to develop and test the technology necessary to extract hadronic interactions from lattice QCD calculations using tractable hadronic systems. In this respect, pions provide the ideal theoretical laboratory for such a study as correlation functions of pions—even arbitrary numbers of them—do not suffer from an exponential decay of the signal/noise ratio. Pions have several additional advantages; they are bosons, and they are guaranteed by the chiral symmetry of QCD to interact weakly.

After we introduce the basic methodology, we will discuss two examples of recent fully-dynamical lattice QCD calculations of pion properties. First we will discuss a lattice measurement of the  $I = 2$   $\pi\pi$  scattering length which is now at 1% precision. We will then present recent pioneering work which aims to extract a signal for 3-pion interactions from lattice QCD. Finally we will make some comments about baryons; specifically, why they are difficult.

## 2 $n$ bosons in a box

The ground-state energy of an  $n$ -boson system [9] is calculated with an interaction of the form

$$V(\mathbf{r}_1, \dots, \mathbf{r}_n) = \eta \sum_{i < j}^n \delta^{(3)}(\mathbf{r}_i - \mathbf{r}_j) + \eta_3 \sum_{i < j < k}^n \delta^{(3)}(\mathbf{r}_i - \mathbf{r}_k) \delta^{(3)}(\mathbf{r}_j - \mathbf{r}_k) + \dots, \quad (1)$$

where the ellipsis denote higher-body interactions that do not contribute at the order to which we work (in general,  $m$ -body interactions will enter at  $\mathcal{O}(L^{3(1-m)})$ ). For an  $s$ -wave scattering phase shift,  $\delta(p)$ , the two-body contribution to the pseudo-potential is given by  $\eta = -\frac{4\pi}{M} p^{-1} \tan \delta(p) = \frac{4\pi}{M} a + \frac{2\pi}{M} a^2 r p^2 + \dots$ , keeping only the contributions from the scattering length and effective range,  $a$  and  $r$ , respectively. At  $\mathcal{O}(L^{-6})$  the coefficient of the three-body potential,  $\eta_3$ , is momentum independent.

As an example, consider the 2-boson energy. The volume dependence of the energy is easily built up using Rayleigh-Schrödinger time-independent

perturbation theory. The leading contribution to the perturbative expansion of the energy is given by

$$\Delta E_2^{(1)} = \langle -\mathbf{k}, \mathbf{k} | V(\mathbf{r}_1, \mathbf{r}_2) | -\mathbf{p}, \mathbf{p} \rangle, \quad (2)$$

where  $|-\mathbf{p}, \mathbf{p}\rangle$  are the two-body momentum eigenstates in the center-of-mass system. The single-particle wavefunctions in the finite volume are given by:  $\langle \mathbf{r} | \mathbf{p} \rangle = \exp(i\mathbf{k} \cdot \mathbf{r})/L^{3/2}$ . Inserting two complete sets of position eigenstates in Eq. (2), one easily finds  $\Delta E_2^{(1)} = \eta/L^3 = 4\pi a/M L^3$ . It is straightforward to calculate higher-order  $1/L$  corrections in this manner.

The volume dependence of the energy of the  $n$ -boson (of mass  $M$ ) ground state in a periodic cubic spatial volume of periodicity  $L$  up to  $\mathcal{O}(1/L^6)$  is known to be [4–10]

$$\begin{aligned} \Delta E_n = & \frac{4\pi a}{M L^3} \binom{n}{2} \left\{ 1 - \frac{a\mathcal{I}}{\pi L} + \left(\frac{a}{\pi L}\right)^2 [\mathcal{I}^2 + (2n-5)\mathcal{J}] \right. \\ & \left. - \left(\frac{a}{\pi L}\right)^3 [\mathcal{I}^3 + (2n-7)\mathcal{I}\mathcal{J} + (5n^2 - 41n + 63)\mathcal{K}] \right\} \\ & + \binom{n}{2} \frac{8\pi^2 a^3}{M L^6} r + \binom{n}{3} \frac{\bar{\eta}_3^L}{L^6} + \mathcal{O}(1/L^7), \end{aligned} \quad (3)$$

where the geometric constants are  $\mathcal{I} = -8.9136329$ ,  $\mathcal{J} = 16.532316$  and  $\mathcal{K} = 8.4019240$ , and

$$\bar{\eta}_3^L = \eta_3(\mu) + \frac{64\pi a^4}{M} (3\sqrt{3} - 4\pi) \log(\mu L) - \frac{96 a^4}{\pi^2 M} [2\mathcal{Q} + \mathcal{R}] \quad (4)$$

is the renormalization-scheme and scale independent three-boson interaction [9]. Note the logarithmic dependence on  $L$ . At this order in the  $1/L$  expansion, the energy is only sensitive to a combination of the effective range and scattering length,  $\bar{a} = a + \frac{2\pi}{L^3} a^3 r$  and in what follows we will sometimes replace  $a \rightarrow \bar{a}$ , eliminating  $r$ .

While the calculation of ground-state energies described here has been derived in a non-relativistic framework, the results remain valid relativistically. In the two-body case, this has been shown by Lüscher [5]. In the higher-body case, the non-relativistic calculation will not correctly recover a field-theoretic calculation, due to relativistic effects in multiple, two-body interactions involving three or more particles. At  $\mathcal{O}(L^{-4})$ , only two-particle interactions contribute to the  $n$ -body ground-state energy and the results of Ref. [5] follow without modification. Since the interaction of three particles due to the two-body interaction first enters at  $L^{-5}$ , and relativistic effects in such interactions are suppressed by  $(ML)^{-2}$ , the first relativistic effects will occur at  $\mathcal{O}(L^{-7})$  [9].

### 3 Hadron-hadron interactions

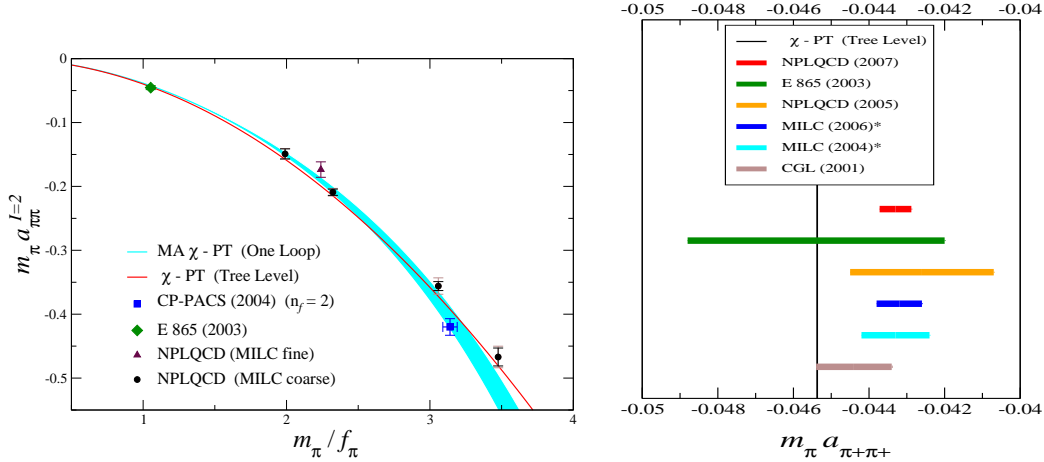


Figure 1: Left panel:  $m_\pi a_{\pi\pi}^{I=2}$  vs.  $m_\pi/f_\pi$  (ovals) with statistical (dark bars) and systematic (light bars) uncertainties. Also shown are the experimental value from Ref. [19] (diamond) and the lowest quark mass result of the  $n_f = 2$  dynamical calculation of CP-PACS [20] (square). The blue band corresponds to a weighted fit to the lightest three data points (fit B) using the one-loop MA $\chi$ -PT formula in Eq. (9) (the shaded region corresponds only to the statistical error). The red line is the tree-level  $\chi$ -PT result. Right panel: A compilation of the various measurements and predictions for the  $I = 2$   $\pi\pi$  scattering length. The prediction made in this paper is labeled NPLQCD (2007), and the Roy equation determination of Ref. [14] is labeled CGL (2001).

As the simplest application of Eq. (3), let us consider recent results for the  $\pi\pi$  interaction [12]. Due to the chiral symmetry of QCD, pion-pion ( $\pi\pi$ ) scattering at low energies is the simplest and best-understood hadron-hadron scattering process. The scattering lengths for  $\pi\pi$  scattering in the s-wave are uniquely predicted at leading order (LO) in chiral perturbation theory ( $\chi$ -PT) [13]:

$$m_\pi a_{\pi\pi}^{I=0} = 0.1588 \quad ; \quad m_\pi a_{\pi\pi}^{I=2} = -0.04537 \quad , \quad (5)$$

at the charged pion mass. While experiments do not provide stringent constraints on the scattering lengths, a theoretical determination of s-wave  $\pi\pi$  scattering lengths which makes use of experimental data has reached a remarkable level of precision [14, 15]:

$$m_\pi a_{\pi\pi}^{I=0} = 0.220 \pm 0.005 \quad ; \quad m_\pi a_{\pi\pi}^{I=2} = -0.0444 \pm 0.0010 \quad . \quad (6)$$

These values result from the Roy equations [16–18], which use dispersion theory to relate scattering data at high energies to the scattering amplitude near threshold. At present lattice QCD can compute  $\pi\pi$  scattering only in the  $I = 2$  channel as the  $I = 0$  channel contains disconnected diagrams. It is of course of great interest to compare the precise Roy equation predictions with lattice QCD calculations.

The lattice calculations that are described in this paper involve a mixed-action lattice QCD scheme of domain-wall valence quarks on a rooted staggered sea. Details of the lattice calculation can be found in Ref. [12]. A  $\pi^+\pi^+$  ( $I = 2$ ) correlation function that projects onto the s-wave state in the continuum limit is

$$C_{\pi^+\pi^+}(p, t) = \sum_{|\mathbf{p}|=p} \sum_{\mathbf{x}, \mathbf{y}} e^{i\mathbf{p}\cdot(\mathbf{x}-\mathbf{y})} \langle \pi^-(t, \mathbf{x}) \pi^-(t, \mathbf{y}) \pi^+(0, \mathbf{0}) \pi^+(0, \mathbf{0}) \rangle, \quad (7)$$

where  $\pi^+(t, \mathbf{x}) = \bar{u}(t, \mathbf{x})\gamma_5 d(t, \mathbf{x})$  is an interpolating field for the  $\pi^+$ . In order to extract the energy difference one forms the ratio of correlation functions,  $G_{\pi^+\pi^+}(p, t)$ , where

$$G_{\pi^+\pi^+}(p, t) \equiv \frac{C_{\pi^+\pi^+}(p, t)}{C_{\pi^+}(t)C_{\pi^+}(t)} \rightarrow \sum_{n=0}^{\infty} \mathcal{A}_n e^{-\Delta E_n t}, \quad (8)$$

and  $C_{\pi^+}(t)$  is the single-pion correlation function. The arrow in Eq. (8) denotes the large-time behavior of  $G_{\pi^+\pi^+}$  in the absence of boundaries on the lattice and becomes an equality in the limit of an infinite number of gauge configurations.

We have computed the energy difference  $\Delta E_n$  (and via Eq. (3) the scattering length) at pion masses,  $m_\pi \sim 290$  MeV, 350 MeV, 490 MeV and 590 MeV, and at a single lattice spacing,  $b \sim 0.125$  fm and lattice size  $L \sim 2.5$  fm [12]. In order to obtain the physical value of the scattering length, one must extrapolate. In two-flavor mixed-action  $\chi$ -PT (MA $\chi$ -PT) (i.e. including finite lattice-spacing corrections) the chiral expansion of the scattering length at NLO takes the form [21]

$$m_\pi a_{\pi\pi}^{I=2} = -\frac{m_\pi^2}{8\pi f_\pi^2} \left\{ 1 + \frac{m_\pi^2}{16\pi^2 f_\pi^2} \left[ 3 \log\left(\frac{m_\pi^2}{\mu^2}\right) - 1 - l_{\pi\pi}^{I=2}(\mu) - \frac{\tilde{\Delta}_{ju}^4}{6m_\pi^4} \right] \right\}, \quad (9)$$

where it is understood that  $m_\pi$  and  $f_\pi$  are the lattice-physical parameters [21] and

$$\tilde{\Delta}_{ju}^2 = b^2 \Delta_I + \dots \quad (10)$$

where the dots denote higher-order corrections to the meson masses. With domain-wall fermion masses tuned to match the staggered Goldstone pion, one finds (in lattice units)  $\tilde{\Delta}_{ju}^2 = b^2 \Delta_I = 0.0769(22)$  [22] on the coarse MILC lattices (with  $b \sim 0.125$  fm and  $L \sim 2.5$  fm). Eq. (9), which contains all  $\mathcal{O}(m_\pi^2 b^2)$  and  $\mathcal{O}(b^4)$  lattice artifacts, reduces to the continuum expression for the scattering length in the QCD limit where  $\tilde{\Delta}_{ju}^2 \rightarrow 0$ . Figure 1 (left panel) is a plot of  $m_\pi a_{\pi\pi}^{I=2}$  vs.  $m_\pi/f_\pi$  with the lattice results and the fit curves from MA $\chi$ -PT.

The final result is:

$$m_\pi a_{\pi\pi}^{I=2} = -0.04330 \pm 0.00042 \quad , \quad (11)$$

where the statistical and systematic uncertainties have been combined in quadrature. Notice that 1% precision is claimed in this result. This result is consistent with all previous determinations within uncertainties (see Figure 1 (right panel)).

## 4 Hadron-hadron-hadron interactions

It is straightforward to generalize the two-pion correlation function of Eq. (7) to  $n$  pions. A non-trivial test of Eq. (3) then results from extracting the two-body scattering length from the  $n$  pion correlators. In this respect, one particularly useful combination of the energy differences defined in Eq. (3) is:

$$\begin{aligned} & \frac{L^3 M(\Delta E_n m(m^2 - 3m + 2) - \Delta E_m n(n^2 - 3n + 2))}{2(m-1)m(m-n)(n-1)n\pi} \\ &= \bar{a} \left\{ 1 - \frac{\bar{a}}{\pi L} \mathcal{I} + \left( \frac{\bar{a}}{\pi L} \right)^2 [\mathcal{I}^2 - \mathcal{J}] + \left( \frac{\bar{a}}{\pi L} \right)^3 \right. \\ & \quad \left. \times [-\mathcal{I}^3 + 3\mathcal{I}\mathcal{J} + (19 + 5mn - 10(n+m))\mathcal{K}] \right\} , \quad (12) \end{aligned}$$

(for  $n, m > 2$ ) which is independent of  $\bar{\eta}_3^L$  and allows a determination of  $\bar{a}$  up to  $\mathcal{O}(1/L^4)$  corrections (combinations achieving the same result using all of the  $n = 3, 4, 5$  energies can also be constructed).

Figure 2 (left panel) presents extractions of the scattering length at all four orders in the  $1/L$  expansion in Eq. (3) for  $m_\pi \sim 350$  MeV. For  $n > 2$ , the N<sup>3</sup>LO ( $1/L^6$ ) extraction is performed using Eq. (12) with the point at  $n = 3$  arising from the energy shifts  $\Delta E_4$  and  $\Delta E_5$ , and so on. Significant dependence on  $n$  in the lower-order extractions (LO, NLO and NNLO) is

observed, indicating the presence of residual finite-volume effects. However the most accurate extractions using Eq. (12), which eliminate the three- $\pi^+$  interaction (Eq. (3) for  $n=2$ ), are in close agreement for all  $n$ . This provides a non-trivial check of the  $n$ -dependence of Eq. (3), particularly the presence of a term that scales as  $\binom{n}{3}$ , which can be identified as the three-pion interaction.

To isolate the three-body interaction, we can form a second useful combination of the energy differences defined in Eq. (3):

$$\begin{aligned} \bar{\eta}_3^L &= L^6 \binom{n}{3}^{-1} \left\{ \Delta E_n - \binom{n}{2} \Delta E_2 - 6 \binom{n}{3} M^2 \Delta E_2^3 \right. \\ &\quad \left. \times \left( \frac{L}{2\pi} \right)^4 \left[ \mathcal{J} + \frac{L^2 M \Delta E_2}{2\pi^2} (\mathcal{I}\mathcal{J} - (5n - 31)\mathcal{K}) \right] \right\}, \end{aligned} \quad (13)$$

( $n > 2$ ) with corrections arising at  $\mathcal{O}(1/L)$ . To avoid uncertainties arising from scale setting, we focus on the dimensionless quantity  $m_\pi f_\pi^4 \bar{\eta}_3^L$  ( $\bar{\eta}_3^L$  is expected to scale as  $m_\pi^{-1} f_\pi^{-4}$  by naive dimensional analysis (NDA)). A nonzero value of  $m_\pi f_\pi^4 \bar{\eta}_3^L$  is found for  $m_\pi \sim 290$  and 350 MeV. Figure 2 (right panel) summarizes the results for the three- $\pi^+$ -interaction,  $m_\pi f_\pi^4 \bar{\eta}_3^L$ , at  $L = 2.5$  fm. The magnitude of the result is consistent with NDA.

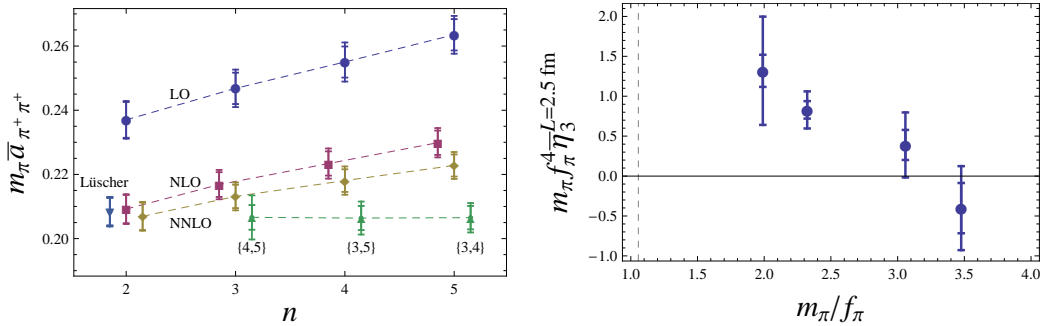


Figure 2: Left panel: extracted values of  $m_\pi \bar{a}_{\pi^+\pi^+}$  at  $m_\pi \sim 350$  MeV. LO, NLO and NNLO correspond to extractions of  $\bar{a}$  at  $\mathcal{O}(1/L^3, 1/L^4, 1/L^5)$  from Eq. (3), respectively. The N<sup>3</sup>LO results for  $\{n, m\} = \{3, 4\}, \{3, 5\}$ , and  $\{4, 5\}$  are determined from Eq. (12). For  $n = 2$ , the exact solution of the eigenvalue equation [4] is denoted by “Lüscher”. Right panel: Effective  $m_\pi f_\pi^4 \bar{\eta}_3^L$  plots extracted from the  $n = 3, 4$ , and 5  $\pi^+$  energy shifts. The fits shown correspond to the  $n = 5$  calculation. The statistical and systematic uncertainties have been combined in quadrature.

Further lattice QCD calculations are required before a definitive statement about the physical value of the three-pion interaction,  $m_\pi f_\pi^4 \bar{\eta}_3^L$ , can be made. While at lighter pion masses, there is evidence for a contribution to the various  $n$ -pion energies beyond two body scattering that scales as the three-body contribution in Eq. (3), a number of systematic effects must be further investigated. The extraction of this quantity has corrections that are formally suppressed by  $\bar{a}/L$ , however, the coefficient of the higher order term(s) may be large, and the next order term in the volume expansion needs to be computed (for  $n = 3$ , this result is known [10]).

Future calculations will extend these results to larger  $n$  and to systems involving multiple kaons and pions. Further, calculations must be performed in different spatial volumes to determine the leading correction ( $\mathcal{O}(1/L)$ ) to the three- $\pi^+$  interaction, and at different lattice spacings in order to eliminate finite-lattice spacing effects, which are expected to be small.

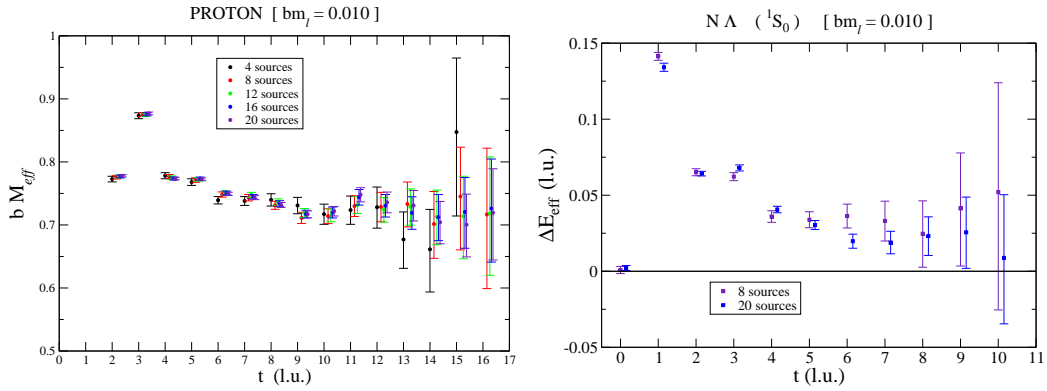


Figure 3: Left panel: effective mass plot for the proton at a pion mass of 350 MeV, with increasing statistics. Right panel: effective mass plot for the  $^1S_0$  neutron-lambda ground state energy at a pion mass of 350 MeV with increasing statistics.

## 5 Baryons

As the lattice QCD study of nuclei is the underlying motivation for this work, it is worth considering difficulties that will be encountered in generalizing the result described here to baryonic systems. The ratio of signal-to-noise scales very poorly for baryonic observables [11], requiring an exponentially-large number of configurations to extract a precise result. Several examples are

shown in Figure 3. the left panel is an effective mass plot for the proton mass and the right panel is an effective mass plot for the  $^1S_0$  neutron-lambda ground state energy. The number of sources indicates the number of light (and strange) propagators computed per lattice configuration. While the error bars do decrease more or less as expected, the signal certainly does not improve as it does for the pions. For instance, for the proton, the signal/noise ratio is expected to die exponentially as  $\exp(-(M_N - 3m_\pi/2)t)$ . And too, the factorial growth of the combinatoric factors involved in forming the correlators for large systems of bosons and fermions and the high powers to which propagators are raised (*e.g.*, for the  $12\text{-}\pi^+$  correlator, there is a term  $43545600 \text{tr}[\Pi^{11}]\text{tr}[\Pi]$ ) implies that the propagators used to form the correlation functions must be known to increasingly high precision.

While recent pioneering studies of low-energy NN and YN scattering [1, 2] are clearly plagued by the signal/noise problem discussed above, it is remarkable that the NN s-wave scattering lengths evaluated at pion masses in the range  $m_\pi \sim 350 - 600$  MeV are all of natural size,  $\sim \Lambda_{QCD}^{-1}$ , in sharp contrast with the physical values.

## 6 Conclusions

Lattice QCD calculations of 2-body pion (and kaon) interactions are now a precision science (for those channels that do not involve disconnected diagrams). The study of multi-pion systems has led to the first lattice QCD evidence of many-body forces. While this result provides an important test of the basic methodology for extracting many-body physics from lattice QCD, it is, of course, somewhat somewhat academic as pions are weakly interacting bosons. The holy grail for this area of research is to see a definitive signal for nuclear physics. Given the current state of lattice QCD calculations involving baryons, it is clear that there is much room for theoretical advances in this area.

## Acknowledgments

I thank W. Detmold, T.C. Luu, K. Orginos, A. Parreño, M.J. Savage, A. Torok and A. Walker-Loud for fruitful collaboration. This work was supported by NSF CAREER Grant No. PHY-0645570.

## References

- [1] S. R. Beane, *et al.*, Phys. Rev. Lett. **97**, 012001 (2006).
- [2] S. R. Beane, *et al.*, Nucl. Phys. A **794**, 62 (2007).
- [3] W. Detmold, K. Orginos and M. J. Savage, arXiv:hep-lat/0703009.
- [4] M. Lüscher, Commun. Math. Phys. **105**, 153 (1986).
- [5] M. Lüscher, Nucl. Phys. B **354**, 531 (1991).
- [6] K. Huang and C. N. Yang, Phys. Rev. **105**, 767 (1957).
- [7] T. T. Wu, Phys. Rev. **155**, 1390 (1959).
- [8] T. D. Lee, K. Huang, and C. N. Yang, Phys. Rev. **106**, 1135 (1957)
- [9] S. R. Beane, W. Detmold and M. J. Savage, Phys. Rev. D **76**, 074507 (2007).
- [10] S. Tan, arXiv:0709.2530 [cond-mat.stat-mech].
- [11] G. P. Lepage, in *From Actions to Answers: Proceedings of the TASI 1989*, Degrand, T., & Toussaint, D. (1990), Singapore, World Scientific.
- [12] S. R. Beane, *et al.*, arXiv:0706.3026 [hep-lat].
- [13] S. Weinberg, Phys. Rev. Lett. **17**, 616 (1966).
- [14] G. Colangelo, J. Gasser and H. Leutwyler, Nucl. Phys. B **603**, 125 (2001).
- [15] H. Leutwyler, arXiv:hep-ph/0612112.
- [16] S. M. Roy, Phys. Lett. B **36**, 353 (1971).
- [17] J. L. Basdevant, C. D. Froggatt and J. L. Petersen, Nucl. Phys. B **72**, 413 (1974).
- [18] B. Ananthanarayan, *et al.*, Phys. Rept. **353**, 207 (2001).
- [19] S. Pislak *et al.*, Phys. Rev. D **67**, 072004 (2003).
- [20] T. Yamazaki *et al.* [CP-PACS], Phys. Rev. D **70**, 074513 (2004).
- [21] J. W. Chen, D. O'Connell and A. Walker-Loud, Phys. Rev. D **75**, 054501 (2007).
- [22] C. Aubin *et al.* [MILC], Phys. Rev. D **70**, 114501 (2004).

# HADRON STRUCTURE FROM LATTICE QCD

*A. Schäfer*  
Institute of Theoretical Physics  
University of Regensburg  
93047 Regensburg  
Germany

## Abstract

Some elements and current developments of lattice QCD are reviewed, with special emphasis on hadron structure observables. In principle, high precision experimental and lattice data provide nowadays a very detailed picture of the internal structure of hadrons. However, to relate both, a very good control of perturbative QCD is needed in many cases. Finally chiral perturbation theory is extremely helpful to boost the precision of lattice calculations. The mutual need and benefit of all four elements: experiment, lattice QCD, perturbative QCD and chiral perturbation theory is the main topic of this review.

## 1 Elements of lattice QCD

All information on hadron structure is, in principle, contained in the generating functional of QCD

$$Z[J_\mu^a, \bar{\eta}^i, \eta^i] = \int \mathcal{D}[A^{\mu}, \bar{\psi}^i, \psi^i] \exp \left( i \int d^4x \left[ \mathcal{L}_{\text{QCD}} - J_\mu^a A_\mu^a - \bar{\psi}^i \eta^i - \bar{\eta}^i \psi^i \right] \right) \quad (1)$$

The tasks to be performed are:

- i.) to classify this information in a suitable manner, namely in terms of specific correlators
- ii.) to calculate these from Eq.(1), which is done numerically by lattice QCD after analytic continuation to Euclidean space-time,
- iii.) and to relate them to experimental observables, which is done by Operator Product Expansion and perturbative QCD.

i.) Let us illustrate the physical content of specific correlators with a few typical examples:

$\langle P(p) | \bar{q}(x) \gamma_\mu D_{\mu_1} \dots D_{\mu_n} q(x) | P(p) \rangle$ : Here  $D_{\mu_j}$  is the gauge invariant derivative. For a suitable symmetrization of the Lorentz indices these operators are of twist-2 and thus have a simple probabilistic interpretation in terms of moments of the momentum distribution of a quark species  $q$  in a hadron  $P$ , e.g. a proton,  $\int_0^1 dx x^n (q(x) \pm \bar{q}(x))$ . For mixed symmetry combinations these correlators describe, e.g., specific correlations between the quark and gluon fields. (One should remember that the commutator  $[D_{\mu_i}, D_{\mu_j}]$  gives the gluon field strength tensor.)

$$\langle P(p) | \bar{q}(x) \Gamma_\mu q(x) \bar{q}'(x) \Gamma'_\mu q'(x) | P(p) \rangle:$$

This quantity describes diquark correlations within a proton.

$\langle P(p') | \bar{q}(x) \gamma_\mu q(x) | P(p) \rangle$ : This quantity provides the form factors of a proton.

$\langle 0 | \bar{d}(-z) \not{z} [-z, z] u(z) | \rho^+(p, s) \rangle$ : This expression provides information on the  $\rho$  distribution amplitude. While distribution functions correspond to the squares of a wave functions, integrated over  $k_\perp$ , distribution amplitudes correspond to the wave functions themselves, integrated over  $k_\perp$ .

$\langle 0 | \bar{u}(z) u(z) | 0 \rangle$ : Is the best known of an infinite tower of vacuum condensates, which characterize the QCD-vacuum itself, just as any other 'hadronic' state.

Recently this collection of correlators was substantially enlarged, namely by various non-local correlators. Correlators, which are non-local along the light cone coordinate

$$\langle P(p, s) | \bar{q}(-z^-, \mathbf{z}_\perp = \mathbf{0}) \gamma_\mu [-z, z] q(z, \mathbf{z}_\perp = \mathbf{0}) | P(p', s') \rangle \quad (2)$$

parametrize the Generalized Parton Distributions (GPDs), see [1] and references therein, which provide a comprehensive description of hadron structure, allowing to combine formerly unrelated information in a set of analytic functions, namely the GPDs. Finally correlators which are also non-local in the transverse direction

$$\langle P(p, s) | \bar{q}(-z^-, \mathbf{0}) \gamma_\mu [-z, \mathbf{0}; z, \mathbf{z}_\perp] q(z, \mathbf{z}_\perp) | P(p', s') \rangle \quad (3)$$

are intimately connected to various, surprisingly large spin-phenomena, as observed e.g. by the HERMES experiment, see [2]. (They actually challenge our current theoretical understanding of perturbative QCD.)

Obviously each of these (and many other) correlators would deserve a chapter on its own, but this would far exceed the scope of this small review.

To summarize: **The task is to calculate for each hadron the matrix elements of many different quark-gluon-operators.**

ii.) Obviously, this is an easy task to do, if one knows the exact many-particle hadron wave function. The latter is provided by lattice QCD, however, only in Euclidean space-time.

The basic idea is that by analytic continuation of the time-coordinate  $t \rightarrow -it_E$  the exponential weight in Eq.(1) becomes positive definite. (Note that  $\mathcal{L} \rightarrow -\mathcal{H}_E$  and thus  $iS \rightarrow -S_E$ .) If one then places some source, i.e. a combination of quarks and possibly gluons with the desired quantum numbers, on the lattice, Euclidean time evolution projects out the desired exact (in principle) hadron wave function. For the proton, one can choose, e.g., as source ( $C = i\gamma^2\gamma^4 = C^{-1}$  is the charge conjugation matrix):

$$\hat{B}_\alpha(t, \mathbf{p}) = \sum_{\mathbf{x}} e^{i\mathbf{p}\cdot\mathbf{x}} \epsilon_{ijk} \hat{u}_\alpha^i(x) \hat{u}_\beta^j(x) (C^{-1}\gamma_5)_{\beta\gamma} \hat{d}_\gamma^k(x) \quad (4)$$

and then gets

$$\begin{aligned} |B\rangle &\sim c_0|N\rangle + c_1|N'\rangle + c_2|N\pi\rangle + \dots \\ &\Rightarrow c_0 e^{-E_N t_E} |N\rangle + c_1 e^{-E_{N'} t_E} |N'\rangle + c_2 e^{-E_{N\pi} t_E} |N\pi\rangle + \dots \end{aligned} \quad (5)$$

For sufficiently large  $t_E$  this sum will obviously converge to the lowest energy state. Over the years rich experience was gained in the development of sources which maximize from the very beginning the overlap with a specific physical hadron state. For a (quenched) show-case example see Fig.1. (Note that to the right one sees the slope of the lowest nucleon resonance with negative parity.)

Once the propagation in imaginary time has projected the original source onto the physical wave function one can calculate physical correlators from

$$\frac{\tilde{\Gamma}_{\alpha\beta} \langle B_\beta(t, \mathbf{p}) \mathcal{O} \bar{B}_\alpha(0, \mathbf{p}) \rangle}{\Gamma_{\alpha\beta} \langle B_\beta(t, \mathbf{p}) \bar{B}_\alpha(0, \mathbf{p}) \rangle} \quad (6)$$

This procedure allows to calculate many of the quantities of interest, however, it is limited to those operators which contain only coordinate differences which are oriented either spatially or along the light cone direction in

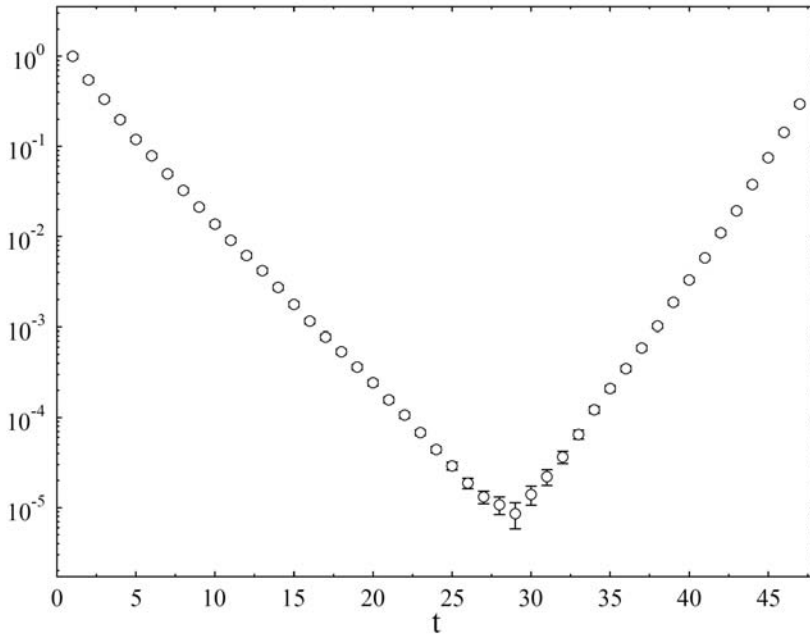


Figure 1: A show-case example for a clean exponential slope (nucleon, quenched Wilson fermions, QCDSF).

which the hadron is Lorentz-contracted (typically called  $z^-$ ). Otherwise the operator itself is affected by the analytic continuation to Euclidean times. Probably for many cases the resulting effects can be corrected for by making use of the analytic properties of the continuum expressions, but such efforts are, to the best of my knowledge, still in their infancy.

ii.) Linking lattice results and experiment is far more difficult than usually appreciated. It is only simple for very few cases, especially hadron masses, as these are direct experimental observables. However, reproducing known hadron spectra has only limited impact beyond fixing the quark masses. Basically it demonstrates that QCD is correct and that the technical aspects of lattice QCD are well understood, which nobody seriously doubts anyway. The real strength of lattice QCD is that it provides detailed direct information on the quark-gluon structure of hadrons. As the latter is not directly observable in experiment, it is crucial for the whole program of 'Hadron structure from lattice QCD' that one succeeds to link the correlators calculated on the lattice to experimental observables with help of perturbative QCD in the continuum. The latter has made tremendous progress in recent years.

Presently NLO calculations are the standard and NNLO calculations and beyond start to become common. Furthermore, resummation techniques have been developed which allow to improve very significantly the phenomenological agreement and to reduce the estimated systematic uncertainties. Unfortunately, this is not the place to give justice to these developments. Let me stress, however, one point which is specific to the lattice: lattice propagators differ from their continuum form. They contain periodic functions, as known from Brillouin zones from solid state lattices. Therefore, also the radiative corrections and thus the renormalization effects differ. The problem is aggravated by the fact that the discrete hypercubic symmetry group is much smaller than the continuous Lorentz group, such that on the lattice operators mix, further complicating the renormalization issues. Finally, lattice results correspond to all order calculations in perturbation theory and can, therefore, only be compared meaningfully to fixed order continuum results to the extent that the latter converge.

The bottom line of this section is that **the control of all theoretical uncertainties is today the main theme of modern hadron theory, both on and off the lattice.**

## 2 The choice of lattice actions

This question which discretization of Eq.(1), i.e. which lattice action is the best choice is often debated with close to religious fervor. As the computer resources absorbed by lattice-QCD add up world-wide to many millions of Euros per year, this is not just a question of academic interest, but a major issue for all universities and laboratories involved. In the following I will not argue for our position in this debate, but instead I will show examples from different groups without any assessment of the different actions used. I would like, however, to caution the reader that typically the unknown systematic uncertainties are largest for those choices for which the purely statistically uncertainties cited by the different groups are smallest. Otherwise the choice of the 'best' action would obviously not require any debate. One might, in fact, conclude from the fact that many highly experienced groups favor so many different choices, that presently no choice is clearly superior to any other, and that a mixture of strategies is in fact the wisest decision.

Some of the presently used fermion actions are:

**Chiral fermions:** Overlap fermions are the only realization with exact chiral symmetry presently used. For all other actions chiral symmetry is more or less heavily violated and only recovered in the limit of vanishing lattice constant  $a \rightarrow 0$ . Note that in practice the range of  $a$  reachable by numerical

simulations is very limited. Therefore, if the  $a$ -dependencies are not well described by simple linear fits, one faces a most severe problem.

**Approximately chiral fermions:** The best known example are domain wall fermions, which introduce a fifth space dimension. In the limit that the extension of this fifth lattice direction goes to infinity, chiral symmetry becomes exact. More severe approximations are involved in the construction of the 'Chirally Improved'- and 'Perfect Action' - fermions, which on the other hand are computationally substantially less expensive.

**Fermion actions with remnants of chiral symmetry:** Staggered fermions are certainly the most controversial choice. For them the continuum limit  $a \rightarrow 0$  and the chiral limit  $m_\pi \rightarrow 0$  do not commute, instead of the pion one gets 5 varieties of particles with different masses, quadratically divergent contributions to propagators (for finite  $a$ ), etc. Therefore, the validity of this approach depends crucially on the availability and control of the corresponding 'Staggered Chiral Perturbation Theory' which so far is only given for the meson, but not the baryon sector. On the other hand, however, staggered fermion simulations seem to provide the phenomenologically most impressive results.

Twisted-mass fermions have also pions of different masses, due to the addition of an additional isospin dependent term (vanishing in the continuum limit). This construction allows, however, to reach very small quark masses and the authors argue quite convincingly that the isospin violating effects are small in the baryon sector and anyway quite well under control.

**Fermion actions without chiral symmetry:** Some of the most used actions are variants of Wilson fermions, for which chiral symmetry is broken explicitly. They are in general very well understood and do not invoke any fundamental problems. There exist extremely efficient algorithms for Wilson and the results are in general phenomenologically satisfactory, with the exception of a few disturbing puzzles.

### 3 Some recent results

For hadron spectroscopy the quark masses are basically free parameters, which are determined by the optimal fit of the physical hadron masses. In view of the discussion above, quark masses in the continuum depend on the renormalization/factorization scheme and the chosen scale(s). By general convention one cites today typically the values in the  $\overline{MS}$ -scheme and at the scale  $\mu = 2$  GeV. Fig. 2 gives a recent compilation from [3] for the strange quark mass. Here  $N_f = 2$  and  $N_f = 2 + 1$  refers to the number of dynamical

quarks. For  $N_f = 2$  only up and down quark-antiquark fluctuations are taken into account, for  $N_f = 2 + 1$  also strange ones. Note that the results are generally smaller than the values used by many model-builders.

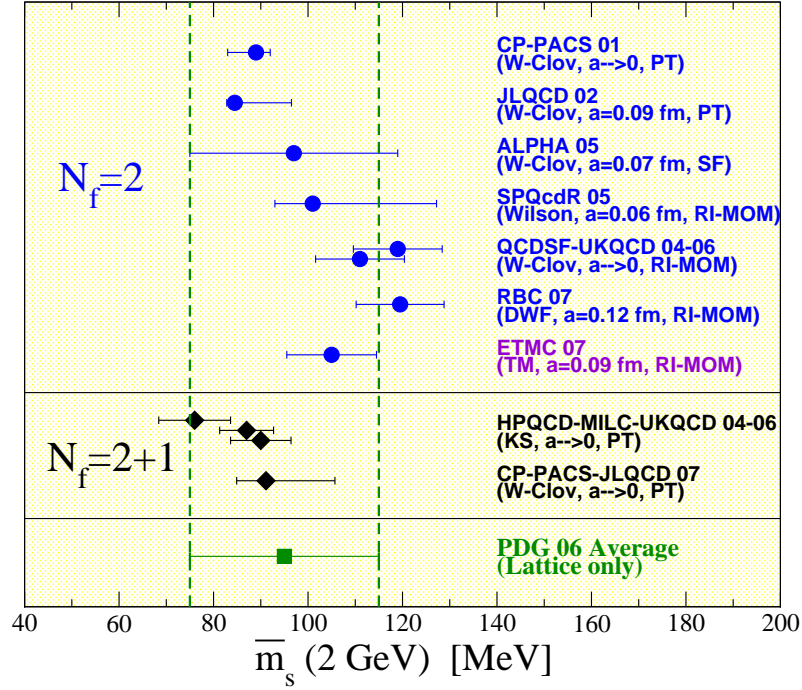


Figure 2: A recent compilation of lattice results for the strange quark mass.

Technically the next difficult observables are two-point functions, which provide coupling constants as well as moments of parton distribution amplitudes. The  $\rho$  coupling constants to the vector and tensor quark currents are defined e.g. by

$$\langle 0 | \bar{q}_2(0) \gamma^\mu q_1(0) | \rho(p; \lambda) \rangle = f_\rho m_\rho \varepsilon_\lambda^\mu \quad (7)$$

$$\langle 0 | \bar{q}_2(0) \sigma^{\mu\nu} q_1(0) | \rho(p; \lambda) \rangle = i f_\rho^T(\mu) (\varepsilon_\lambda^\mu p^\nu - \varepsilon_\lambda^\nu p^\mu), \quad (8)$$

Fig.3 shows recent result obtained by the UKQCD+RBC collaboration with domain wall fermions (hence the residual mass  $m_{res}$ , which is associated with the fifth dimension and has to be extrapolated to zero.)

The result is

$$\frac{f_\rho^T}{f_\rho} = 0.681(20) \quad (9)$$

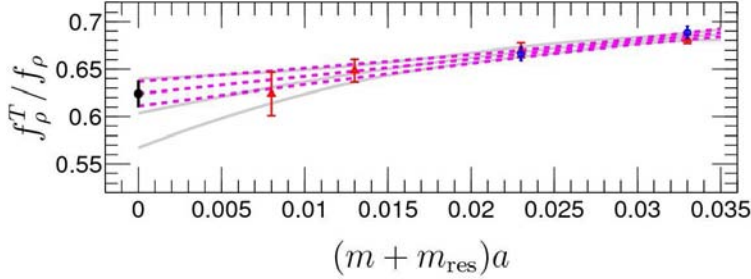


Figure 3: Chiral extrapolations for  $f_\rho^T/f_\rho$  for a UKQCD/RBC simulation with domain-wall fermions. The broken red lines represent a linear fit to the mass behavior and the solid grey lines a quadratic fit. Taken from [4]

which is somewhat smaller than earlier results from the BGR collaboration,  $0.742 \pm 0.014$ , which used quenched Chirally Improved fermions, see [5].

The calculation of many different decay constants for heavy quark systems is the main emphasis of the Fermilab/MILC collaboration, which uses staggered quarks. These results are important for the analysis of BABAR and BELLE results. Instead of discussing these in detail we show in Fig.4 another result of this collaboration, namely the  $D$  to  $K$  decay formfactor. Note that the lattice paper cited here actually antedated the experimental one, see [6].

Distribution amplitudes are the  $k_\perp$  integrals of the exact wave functions, e.g., for pseudoscalar hadrons one defines

$$\phi_\Pi(x, \mu^2) = Z_2(\mu^2) \int^{|k_\perp| < \mu} d^2 k_\perp \phi_{\Pi,BS}(x, k_\perp). \quad (10)$$

when  $\phi_{\Pi,BS}$  is the Bethe-Salpeter wave function of the pseudoscalar.  $\phi_\Pi(x, \mu^2)$  contains as valuable information as distribution functions, which are given by the  $k_\perp$  integrals of the squares of the wave functions. Phenomenologically, distribution amplitudes play a major role in the description of exclusive reactions. With the definitions

$$\begin{aligned} \langle 0 | \bar{q}(-z) \gamma_\mu \gamma_5 [-z, z] u(z) | \Pi^+(p) \rangle &= i f_\Pi p_\mu \int_{-1}^1 d\xi e^{-i\xi p \cdot z} \phi_\Pi(\xi, \mu^2) \\ \phi_\Pi(\xi, \mu^2) &= \frac{3}{4} (1 - \xi^2) \left( 1 + \sum_{n=1}^{\infty} a_n^\Pi(\mu^2) C_n^{3/2}(\xi) \right). \end{aligned} \quad (11)$$

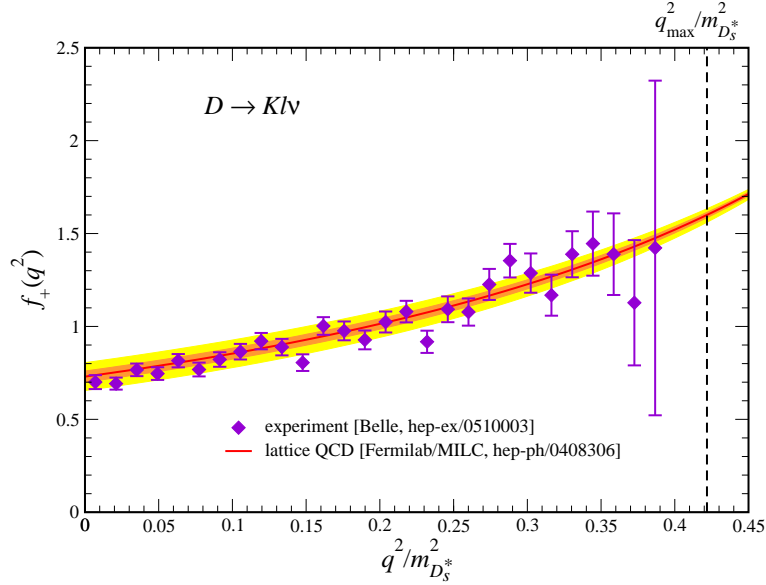


Figure 4: Form factor  $f_+(q^2)$  for  $D \rightarrow Kl\nu$  vs.  $q^2/m_{D_s^*}^2$  compared with Belle data.

the tasks reduces to the calculation of matrix elements of the operators

$$\mathcal{O}_{\{\mu_0 \dots \mu_n\}} = \bar{q} \gamma_{\{\mu_0} \gamma_5 \overleftrightarrow{D}_{\mu_1} \dots \overleftrightarrow{D}_{\mu_n\}} u \quad (12)$$

which give directly the  $\xi^n$ -moments of the distribution amplitude and thus allow to fix the expansion coefficients  $a_n^\Pi$ . Fig. 5 shows QCDSF results [7] for the pion, obtained with improved  $N_f = 2$  Wilson fermions.

The final result is  $[a_2^\pi(\mu^2 = 4 \text{ GeV}^2) = 0.201(114)]$  in rough agreement with the results from analyses of QCD sumrules, B-decays and transition formfactors, which give  $a_2^\pi(4 \text{ GeV}^2) = 0.17 \pm 0.15$

All of the examples given so far are only appetizers for the richness of present day lattice results. To finish this overview let us discuss one specific more complex example. Transverse asymmetries, observed in e.g. by HERMES [2], can be related by perturbative QCD to the so-called Boer-Mulders functions, which in turn are related to the spatial distribution of quarks in the transverse plane (perpendicular to its momentum direction), which in turn is parametrized by GPDs, moments of which can be calculated on the lattice. Some recent QCDSF results are shown in Fig.6. For details see [8,9]. These results were obtained with dynamical improved Wilson fermions.

Another example for the power of the GPD framework is given in Fig.7, where recent LHPC results for the spin and orbital angular momentum struc-

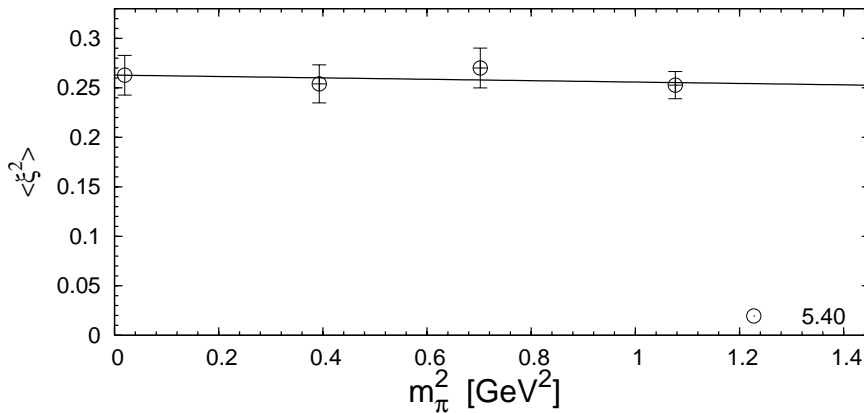


Figure 5: Chiral extrapolation of  $\langle \xi^2 \rangle_\pi$  for  $\beta = 5.40$  for  $\mathcal{O}_{412}^a$  in the  $\overline{\text{MS}}$  scheme at  $\mu^2 = 4 \text{ GeV}^2$

ture of the nucleon are shown. These results were obtained with a mixed action, combining a staggered fermion sea with domain wall valence quarks, see [10].

## 4 Conclusion

Lattice QCD, perturbative QCD, chiral perturbation theory (a topic which was barely addressed but is also of crucial importance) and experiment have reached in the last years such an accuracy that finally detailed questions regarding the quark gluon structure of hadrons can be precisely answered with controlled theoretical uncertainties. A few examples were given, to illustrate the wealth of information to be expected from lattice calculations in the near future. All of this promises to change the nature of hadron physics as QCD-motivated models will be more and more replaced by full-fledged QCD calculations.

## 5 Acknowledgements

This work was supported by BMBF, GSI and DFG.

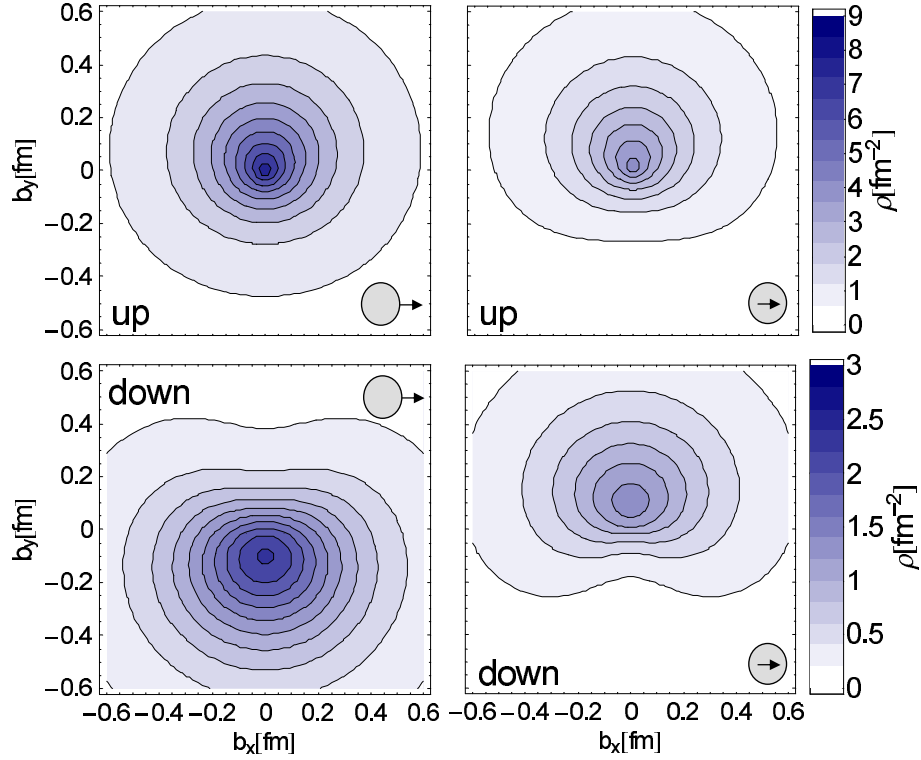


Figure 6: Transverse distribution of up and down quarks in a nucleon (integrated over the longitudinal momentum fraction  $x$ ) for different relative orientations of quark (inner arrow) and nucleon (outer arrow) spins. The nucleon is moving towards the observer

## References

- [1] M. Diehl, Phys. Rept. **388** (2003) 41 [arXiv:hep-ph/0307382].
- [2] A. Airapetian *et al.* [HERMES Collaboration], Phys. Rev. Lett. **94** (2005) 012002
- [3] B. Blossier *et al.*, [European Twisted Mass Collaboration] arXiv:0709.4574 [hep-lat].
- [4] bibitemAntonio:2007xr D. Antonio *et al.*, [UKQCD and Riken-Brookhave-Columbia collaboration arXiv:0710.0869 [hep-lat].
- [5] V. M. Braun *et al.*, [Bern-Graz-Regensburg collaboration] Phys. Rev. D **68** (2003) 054501 [arXiv:hep-lat/0306006].

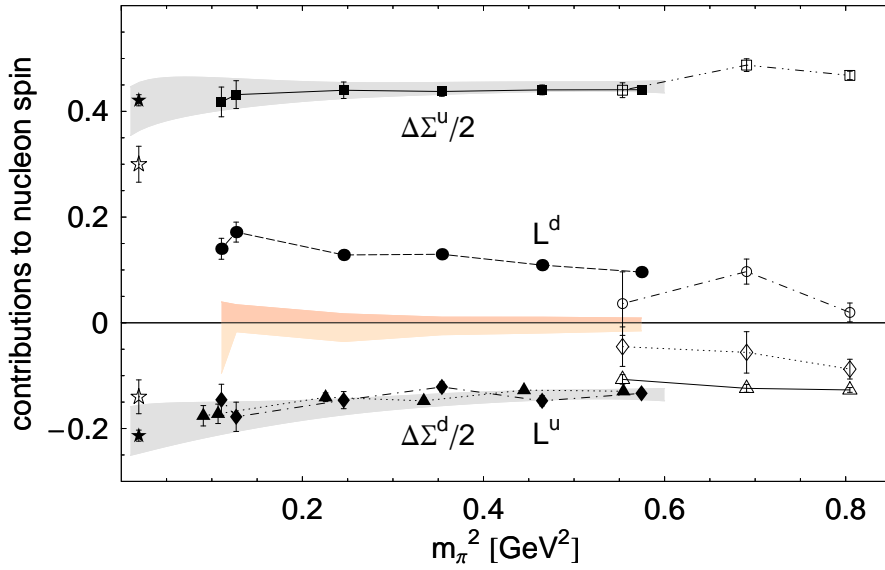


Figure 7: LHPC results for the nucleon spin structure. Filled stars: HERMES result

- [6] A. S. Kronfeld [Fermilab Lattice Collaboration], J. Phys. Conf. Ser. **46** (2006) 147 [arXiv:hep-lat/0607011].
- [7] V. M. Braun *et al.*, [QCDSF collaboration], Phys. Rev. D **74** (2006) 074501 [arXiv:hep-lat/0606012].
- [8] M. Göckeler *et al.* [QCDSF Collaboration], Phys. Rev. Lett. **98** (2007) 222001 [arXiv:hep-lat/0612032].
- [9] D. Brömmel *et al.* [QCDSF Collaboration], arXiv:0708.2249 [hep-lat].
- [10] Ph. Hägler *et al.* [LHPC Collaborations], arXiv:0705.4295 [hep-lat].

# Plenary Session III

**Session Chair:**

Hans Ströher

Structure of Baryons

*Mathias Lutz*

Physics Program at MAMI-C

*P. Achenbach*

Baryon Spectroscopy - Recent results from the Crystal

Barrel Experiment at ELSA

*Ulrike Thoma*

Baryon Resonances Observed at BES

*Bin-Song Zou*

**Session Chair:**

Jürg Gasser

Evidence for  $\Theta^+$  Photo-Production at LEPS

*T. Nakano*

Baryon Spectroscopy with Inelastic Channels:

Crystal Ball Experience

*A. Starostin*

Scaling in Charged Pion Photoproduction From Nucleon

*H. Gao*

## THE PHYSICS PROGRAM AT MAMI-C

*Patrick Achenbach*  
Institut für Kernphysik  
Johannes Gutenberg-Universität  
J.-J.-Becher-Weg 45  
D-55099 Mainz, Germany  
Email: patrick@kph.uni-mainz.de

### Abstract

In February 2007, the fourth stage of the Mainz Microtron, MAMI-C, started operations with a first experiment. The new Harmonic Double-Sided Microtron delivers an electron beam with energies up to 1.5 GeV while preserving the excellent beam quality of the previous stages. The experimental program at MAMI is focused on studies of the hadron structure in the domain of non-perturbative QCD. In this paper, a few prominent selections of the extensive physics program at MAMI-C will be presented.

## 1 The new 1.5 GeV Harmonic Double-Sided Microtron as the Fourth Stage of MAMI

The Mainz Microtron MAMI is a unique facility in Europe to study the hadron structure with the electromagnetic probe at small momentum transfers. MAMI comprises a cascade of three race-track microtrons (RTM), delivering since 1991 a high-quality 855 MeV, 100  $\mu$ A cw-electron beam, which was energy upgraded by a fourth stage, MAMI-C, in recent years. Realizing the fourth stage as another RTM was evidently impossible: the two 180°-bending magnets would have had a weight of approx.  $2 \times 2000$  tons for an end-point energy of 1.5 GeV. However, for the next higher polytron configuration, the Double-Sided Microtron (DSM), this weight is reduced by a factor of four. By operating at 4.90 GHz, the first harmonic of the fundamental 2.45 GHz radio-frequency (rf), the necessary coherent energy gain per turn for the two normal conducting linacs is reduced to get a moderate power consumption [1]. For achieving a simple transverse optics the strong vertical fringe field defocusing of the four 90°-bending magnets is compensated by a clam-shell field geometry. In this configuration uncritical longitudinal beam

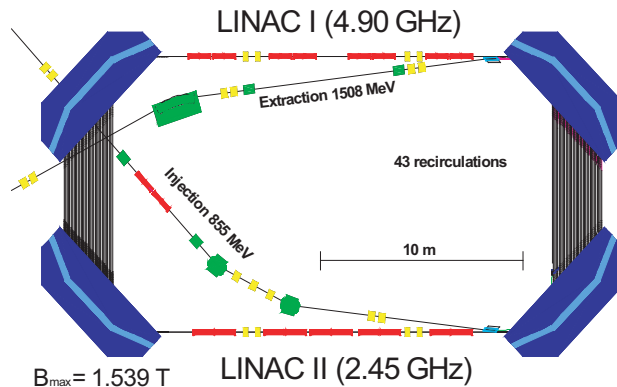


Figure 1: Scheme of the Harmonic Double-Sided Microtron for MAMI- C [2].

dynamics is achieved by operating one of the two linacs at the fundamental rf. The acceleration by two different rf in the Harmonic Double-Sided Microtron (HDSM) is possible because in one of its linacs only every second 4.90 GHz-bucket is occupied [2]. A scheme for the HDSM is given in Fig. 1.

The commissioning of the HDSM started in autumn 2006 with the first full turn through the HDSM. The acceleration along the full 43 recirculations was first operational at the end of 2006, and since February 2007 MAMI-C is delivering a 1.5 GeV high power beam of polarized electrons to the experimental areas.

## 2 Selection A: Polarized $\eta$ Electroproduction

The electromagnetic production of  $\eta$  mesons is a selective probe to study the resonance structure of the nucleon. The polarized target asymmetry was measured in Bonn at the PHOENICS experiment [3]. This measurement showed a surprising angular structure, which cannot be described by the existing phenomenological models. A detailed model-independent study [4] showed that one possibility to describe these data is to include a strong phase shift between  $s$ - and  $d$ -waves.

A measurement of two helicity-dependent polarizations and one helicity-independent polarization in  $\eta$  electroproduction on the proton was performed at the three spectrometer set-up of the A1 collaboration [5]. At  $Q^2 = 0.1 \text{ GeV}^2/c^2$  the kinematics of the experiment was chosen for an invariant mass  $W$  of the  $D_{13}(1520)$  resonance. Neglecting longitudinal multipoles and their interferences the helicity-independent polarizations are dominated by

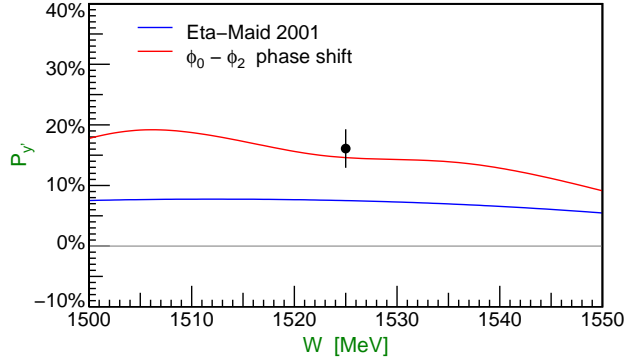


Figure 2: Recoil polarization observable  $P_{y'}$  as a function of the c.m. energy  $W$  at  $\theta = 120^\circ$ ,  $Q^2 = 0.1 \text{ GeV}^2/c^2$ , and  $\epsilon = 0.718$  from Ref. [5]. The solid line shows the prediction of Eta-MAID [6], the dashed line shows the same model prediction with the energy dependent phase shift of Ref. [4].

the structure functions  $R_T^{y'0} \approx \sin \theta \Im \{ E_{0+}^* (3 \cos \theta (E_{2-} - 3M_{2-}) - 2M_{1-}) \}$  and  ${}^c R_{TT}^{y'0} \approx 3 \sin \theta \cos \theta \Im \{ E_{0+}^* (E_{2-} + M_{2-}) \}$ . Thus, the interference with  $E_{0+}$  amplifies the sensitivity to the  $d$ -wave multipoles  $E_{2-}$  and  $M_{2-}$ . In particular,  ${}^c R_{TT}^{y'0}$  is proportional to the sine of the phase difference between  $E_{0+}$  and  $E_{2-} + M_{2-}$ .

The measured double polarization observables  $P_{x'}^h$  and  $P_{z'}^h$ , dominated by  $|E_{0+}|^2$ , are well described by the Eta-MAID model. The measured single polarization observable  $P_{y'}$  disagrees with the model, see Fig. 2 (solid line). However, if a strong phase change between  $E_{0+}$  and  $E_{2-} + M_{2-}$ , as discussed in Ref. [4], is applied, the data point is in good agreement with the model. Such a strong phase change is not easy to achieve if one assumes a standard Breit-Wigner behavior for the  $S_{11}(1535)$  resonance.

### 3 Selection B: Physics with the Photon Beam

In order to deal with the MAMI-C end-point energy increase, the photon tagging system has been extended and refurbished. The Crystal Ball detector, a photon spectrometer consisting of 672 NaI crystals, has been installed at the photon beam-line in recent years. It is now being used regularly with an inner detector for tracking and the forward photon spectrometer TAPS for a  $4\pi$  angular coverage, shown in Fig. 3. A new data acquisition system with high-rate performance is in operation and has successfully taken high statistics data [7]. Further, a new frozen spin target of liquid  ${}^1\text{H}$  and  ${}^2\text{H}$  is now

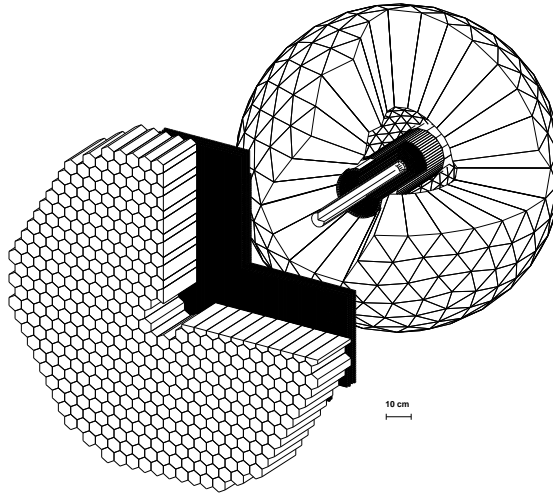


Figure 3: The Crystal Ball detector with the inner tracker and TAPS as forward wall [7].

being commissioned, with the cryostat temperature of 70 mK first reached in June 2007. This target, in particular, provides a unique opportunity to measure the partial contributions to the GDH sum rule on a neutron target. An incomplete list of several topics being addressed by this instrumentation is given here, details can be found in Ref. [1]:

Chiral perturbation theory has been successfully applied to pion photoproduction at threshold. Especially extensions to three flavors urgently require precision data for kaon production processes. Experiments will focus in particular on the following topics: tests of chiral perturbation theory with  $\gamma p \rightarrow \pi^0 p$  and  $\gamma n \rightarrow \pi^0 n$ ; photoinduced kaon production processes close to thresholds;  $\gamma p \rightarrow \eta' p$  at threshold; and low energy constants of baryon chiral perturbation theory with dispersion analysis of pion electroproduction.

A deeper understanding of the nature of resonances requires a reliable determination not only of the mass spectrum but also of coupling constants and decay vertexes. An essential prerequisite is the exploration of polarization degrees in photoinduced meson production: exploration of the Roper resonance  $P_{11}(1440)$  in  $\gamma \mathbf{p} \rightarrow \pi^0 p$ ;  $S_{11}(1535)$  and  $D_{13}(1520)$  in the target asymmetry for the  $\gamma p \rightarrow \eta p$  reaction; the role of the  $D_{15}(1675)$  and  $P_{11}(1710)$  in  $\eta$  photoproduction on the neutron; magnetic moment of the  $S_{11}(1535)$  in  $\gamma p \rightarrow \eta p \gamma'$ ;

and properties of the  $S_{11}(1535)$  and  $D_{33}(1700)$  resonances in the  $\gamma p \rightarrow \eta\pi^0 p$  reaction.

The dominant hadronic decay modes  $\eta, \eta' \rightarrow 3\pi$  only occur due to the isospin violating quark mass difference  $m_u - m_d$  or small electromagnetic effects. A systematic study of such decays offers an alternative way to study symmetries and symmetry breaking patterns in strong interactions. Experiments will concentrate on the main neutral decay channels of  $\eta$  and  $\eta'$  mesons:  $\pi\pi$  and  $\pi\eta$  interactions by a Dalitz plot analysis of the  $\eta \rightarrow 3\pi^0$ ,  $\eta' \rightarrow 3\pi^0$  and  $\eta' \rightarrow \eta\pi^0\pi^0$  decays; cusp at the opening of the  $\pi^0\pi^0 \rightarrow \pi^+\pi^-$  threshold in  $\eta' \rightarrow \eta\pi^0\pi^0$  and the  $\pi\pi$  scattering length; and anomalous  $\eta$  decays and corrections to the Wess-Zumino-Witten action at  $O(p^6)$ .

## 4 Selection C: Spectrometry of Kaons

The spectrometer facility in Mainz consists of three vertically deflecting magnetic spectrometers freely rotatable around a common pivot. However, the detection of kaons under small scattering angles is not possible with these spectrometers due to the short lifetime of the kaons ( $c\tau_K = 3.71$  m) and the long flight path (close to 10 m for spectrometer C), and their limited forward acceptance (5.6 msr and 28 msr). Therefore, reaction products with strangeness under forward scattering angles need to be analyzed with a short-orbit spectrometer.

KAOS is a very compact magnetic dipole spectrometer with a large acceptance in solid angle,  $\Omega \approx 50$  msr, and in momentum,  $p_{max}/p_{min} \approx 2$ , making it suitable especially for the detection of kaons. It was used (as KaoS) in heavy ion induced experiments at the SIS facility (GSI) in the 1990s [8]. For the use at the spectrometer facility in Mainz a new, flexible concept for a support structure was needed, based on a compact, mobile and adjustable platform on hydraulic positioning feet. The platform with the spectrometer is being moved from a installation position to a measurement position via a displacement system of hydraulic pressure cylinders on skid-tracks. A return to its parking position enables the complete coverage of the forward angle region through the vertical spectrometers. The mechanical parts for this complex installation were designed and constructed from 2003–6.

In November 2007 a first coincidence experiment was performed with KAOS as hadron arm and spectrometer B as electron arm. However, a series of measurements, among them the detection of hypernuclei at very forward angles, will be made possible only by the use of KAOS as a double spectrometer. Experiments will be performed close to production thresholds leaving very small center-of-mass energies to the reaction particles, so that those are

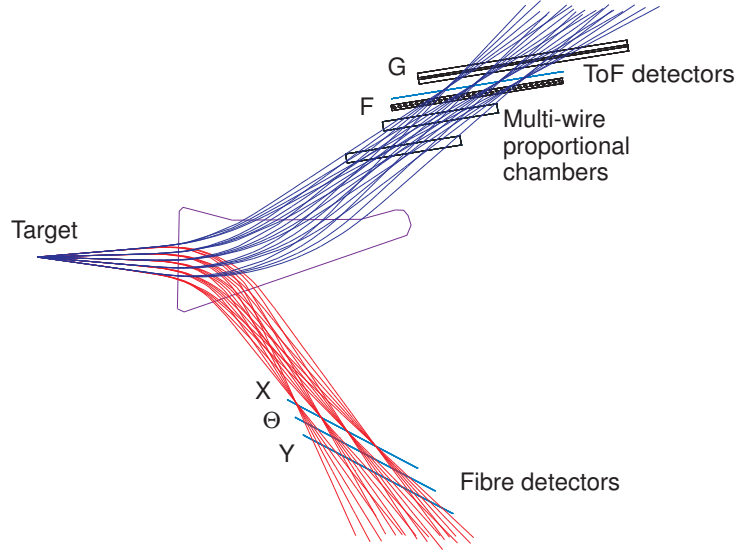


Figure 4: For the operation of KAOS as a double spectrometer trajectories of positively ( $p = 600, 675, 750, 825 \text{ MeV}/c$ ) and negatively charged ( $p = 280, 310, 340, 370 \text{ MeV}/c$ ) particles were simulated. The position of the focal planes with respect to the pole shoe contour is indicated.

moving with approximate center-of-mass velocity. The operation of KAOS as a double spectrometer benefits of the accessibility of both pole face edges. Simulated trajectories of positively and negatively charged particles of four different momenta are shown in Fig. 4. The developments for the instrumentation of the electron arm are well advanced [9].

## 5 Selection D: $\phi$ Meson Electroproduction

The question of how properties of hadrons change once they are embedded in nuclei is of fundamental interest. In particular the  $\phi$  meson provides an appealing probe for this field. Its properties in nuclei are intimately connected to the way kaons and anti-kaons are modified in a nuclear medium [11, 12] and may provide information on the in-medium strange-quark condensate  $\langle s\bar{s} \rangle$  [13].  $\phi$  mesons decaying within nuclei can be studied via the  $e^+e^-$  as well as the  $K^+K^-$  decay channels. Electrons practically do not interact with the nuclear medium while the kaons interact strongly with the nucleus themselves. Thus, studying  $\phi$  decays under well defined conditions may allow us to disentangle medium properties of the  $\phi$  meson on one hand and properties of kaons propagating within a nucleus on the other hand. Concerning the exper-

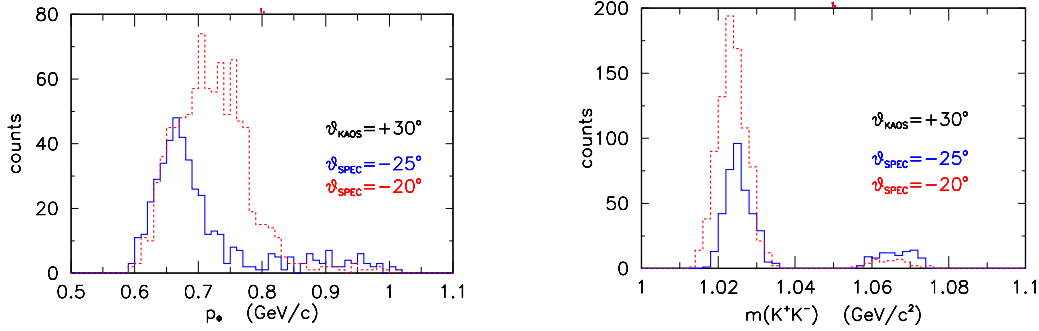


Figure 5: Left: momentum distribution of  $\phi$  mesons reconstructed via the  $K^+K^-$  decay channel. KAOS is positioned at an in-plane angle of  $\vartheta = 30^\circ$  and spectrometer C placed at  $-20^\circ$  (dashed histogram) or  $-25^\circ$  (solid histogram). Right: reconstructed  $K^+K^-$  invariant mass.

imental side, the natural width of the  $\phi$  is rather narrow ( $\Gamma = 4.26 \text{ MeV}/c^2$ ) and it is not masked by other neighboring resonances. Consequently, even the small medium modifications of typically few percent expected for the  $\phi$  mass at normal nuclear density [4, 12, 15] may be observable.

Although the maximum beam energy of MAMI-C does not allow the direct associated production of  $K^+K^-$  pairs on an individual nucleon at rest, the study of the coherent production of  $K^+K^-$  pairs with KAOS is possible. With the beam energy being so close to threshold, the production of  $K^+K^-$  pairs will be dominated by intermediate  $\phi$  meson production [16, 17]. Because of the small momentum of the  $\phi$  ( $\langle p \rangle \approx 800 \text{ MeV}/c$ ) and in view of the small transverse momentum transfer, the two kaons are kinematically constrained and the relative azimuth angle of the two kaons peaks at  $180^\circ$ . The experiment will take advantage of this strong azimuthal correlation and of the large solid angle of KAOS.

In order to explore the feasibility of a measurement of coherent  $\phi$  production at the multi-spectrometer facility of MAMI, a schematic Monte Carlo study assuming coherent production on a deuterium nucleus was performed. In the left panel of Fig. 5 the momentum distribution of the produced  $\phi$  mesons are presented which are detected within this set-up. As expected, the experimental conditions at MAMI-C allow the detection of  $\phi$  mesons with rather low average momentum of approximately  $0.75 \text{ GeV}/c$ . The right panel of Fig. 5 shows the reconstructed  $K^+K^-$  invariant mass. The two separated peaks correspond to  $\phi$  decays inside (right) and outside (left) of the nucleus. The shift of the left peaks with respect to the free  $\phi$  mass of  $1.019 \text{ GeV}/c^2$  reflects a bias caused by the finite momentum and angular acceptances for

the kaons. Comparing the dashed and solid histograms, one recognizes that by changing the positions of the two spectrometers the in-nucleus decays can be enhanced relative to decays outside of the nucleus.

## 6 Selection E: Two-Photon Exchange

Recently, the discussion about second-order processes in the electromagnetic interaction was nourished by the observation that the ratio of proton Sachs form factors,  $R^2 = (\mu_p G_E^p / G_M^p)^2$ , is different if measured by the method of Rosenbluth separation as compared to the extraction from the ratio of the transverse to longitudinal polarizations of the recoiling proton [18, 19]. A contribution from two-photon corrections was discussed as a possible explanation for this observation [20]. The two-photon contributions can be parameterized by the real part of the amplitudes  $\hat{G}_E$ ,  $\hat{G}_M$  and  $\hat{F}_3(s, Q^2)$ , where these amplitudes are modifications of the usual Born approximation electromagnetic form factors.

The beam normal spin asymmetry  $A_\perp$  is an asymmetry in the cross section for the elastic scattering of electrons with spin parallel ( $\sigma_\uparrow$ ) and spin anti-parallel ( $\sigma_\downarrow$ ) to the normal polarization vector. The evaluation of  $A_\perp$  yields a dependence on the imaginary part of  $\hat{F}_3(s, Q^2)$ . In contrast, the two-photon exchange contribution to the cross section is proportional to the real part of  $\hat{F}_3(s, Q^2)$ . A direct ab initio calculation of the real part of  $\hat{F}_3(s, Q^2)$  does not seem to be feasible. It would involve the knowledge of the off-shell form factors of the proton in the intermediate state and also of all contributing excitations and their off-shell transition form factors.

The A4 collaboration has contributed to the study of the imaginary part of the two-photon exchange amplitude by a measurement of the beam normal spin asymmetry,  $A_\perp$  [21]. The two lower panels of Fig. 6 show the results of measurements of  $A_\perp$  with the forward angle set-up ( $\theta_e \sim 30^\circ - 40^\circ$ ) for beam energies of 570 MeV and 854 MeV together with calculations by B. Pasquini. The upper panel contains new data at backward angles ( $\theta_e \sim 140^\circ - 150^\circ$ ) for a beam energy of 315 MeV [1]. While the discrepancy between measured and calculated values of  $A_\perp$  at forward angles could be explained by imperfect knowledge of higher mass intermediate states, the backward angle asymmetry should be dominated by the pure  $\Delta(1232)$  excitation only. The exploration of  $A_\perp$  by a series of measurements at different beam energies on proton and deuteron targets is foreseen at MAMI-C, and further studies of the induced recoil polarization,  $P_y$ , forbidden in one-photon exchange, are under consideration [1].

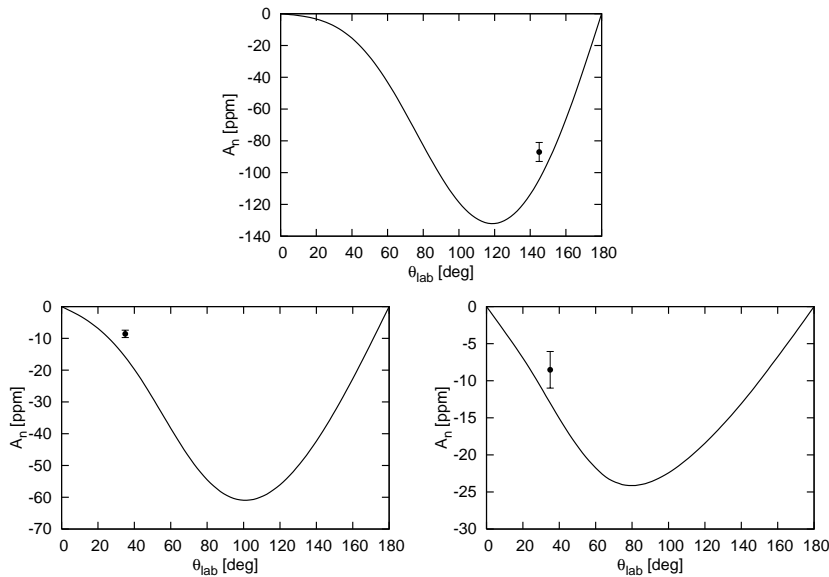


Figure 6: Results on  $A_{\perp}$  at backward angles for a beam energy of 315 MeV (upper panel) [1] and forward angles for 510 MeV and 855 MeV (lower panels) [21]. The full line is a calculation by B. Pasquini.

## 7 The Physics Potential of MAMI-C

The commissioning of the new 1.5 GeV Harmonic Double-Sided Microtron as the fourth stage of MAMI is a great success in accelerator research and technology. Only a few selections from the wide range of the physics potential at MAMI-C could be presented in this paper. Embedded in the MAMI-C research profile, there are further programs for testing effective field theories, *e.g.* the study of the polarizability of the nucleon and the pion, and of generalized polarizabilities of the proton, programs for testing models of the NN interaction, reaction mechanisms and for models of nuclei, *e.g.* the study of few-body systems, and last but not least programs for studying the electromagnetic and strange form factors of the nucleon.

## Acknowledgments

The physics program at MAMI is supported by the Deutsche Forschungsgemeinschaft (DFG) via the Sonderforschungsbereich SFB443 and the European Community Research Infrastructure Activity under the FP6 program HadronPhysics (RII3-CT-2004- 506078).

## References

- [1] *Funding proposal for Collaborative Research Centre 443: Many-body structure of strongly interacting systems*, Joh. Gutenberg-University (Mainz, 2007).
- [2] A. Jankowiak, *Eur. Phys. J.* **A28**, sup. 1, 149 (2006).
- [3] A. Bock *et al.*, *Phys. Rev. Lett.* **81**, 534 (1998).
- [4] L. Tiator *et al.*, *Phys. Rev.* **C60**, 035210 (1999).
- [5] H. Merkel *et al.*, *Phys. Rev. Lett.* **99**, 132301 (2007).
- [6] W.-T. Chiang *et al.*, *Nucl. Phys.* **A700**, 429 (2002).
- [7] H.-J. Arends, in *Proc. 9th Conf. on Intersections of Particle and Nuclear Physics*, *AIP Conf. Proc.* **870**, 481 (2006).
- [8] P. Senger *et al.*, *Nucl. Inst. Meth. in Phys. Res.* **A327**, 393 (1993).
- [9] P. Achenbach *et al.*, in *Proc. IX. Intern. Symp. on Detectors for Particle, Astroparticle and Synchrotron Radiation Experiments*, 144 (2006).
- [10] A. I. Titov, M. Fujiwara and T.S.H. Lee, *Phys. Rev.* **C66**, 02202 (2002).
- [11] H. W. Barz and M. Zétényi, *Phys. Rev.* **C69**, 024605 (2004).
- [12] P. Mühlich *et al.*, *Phys. Rev.* **C67**, 024605 (2003).
- [13] T. Hatsuda and S.H. Lee, *Phys. Rev.* **C46**, 34 (1992).
- [14] F. Klingl, T. Waas and W. Weise, *Phys. Lett.* **B431**, 254 (1998).
- [15] D. Cabrera and M.J. Vicente Vacas, *Phys. Rev.* **C69**, 065204 (2004).
- [16] J. Barth *et al.*, *Eur. Phys. J.* **A17**, 269 (2003).
- [17] A. Sibirtsev *et al.*, *Eur. Phys. J.* **A29**, 209 (2006).
- [18] M. K. Jones *et al.*, *Phys. Rev. Lett.* **84**, 1398 (2000).
- [19] O. Gayou *et al.*, *Phys. Rev. Lett.* **88**, 092301 (2002).
- [20] P. A. M. Guichon and M. Vanderhaeghen, arXiv:hep-ph/0306007.
- [21] F. Maas *et al.*, *Phys. Rev. Lett.* **94**, 152001 (2005).

# BARYON RESONANCES OBSERVED AT BES

*B. S. Zou*

Institute of High Energy Physics, Chinese Academy of Sciences,  
 P.O.Box 918(4), Beijing 100049, China

## Abstract

The  $\psi$  decays provide a novel way to explore baryon spectroscopy and baryon structure. The baryon resonances observed from  $\psi$  decays at BES are reviewed. The implications and prospects at upgraded BESIII/BEPCII are discussed.

## 1 Introduction

Although the quark model achieved significant successes in the interpretation of a lot of static properties of nucleons and the excited resonances, our present knowledge on baryon spectroscopy is still in its infancy [1]. Many fundamental issues in baryon spectroscopy are still not well understood [2].

On theoretical side, an unsolved fundamental problem is: what are proper effective degrees of freedom for describing the internal structure of baryons? Several pictures based on various effective degrees of freedom are shown in Fig.1.

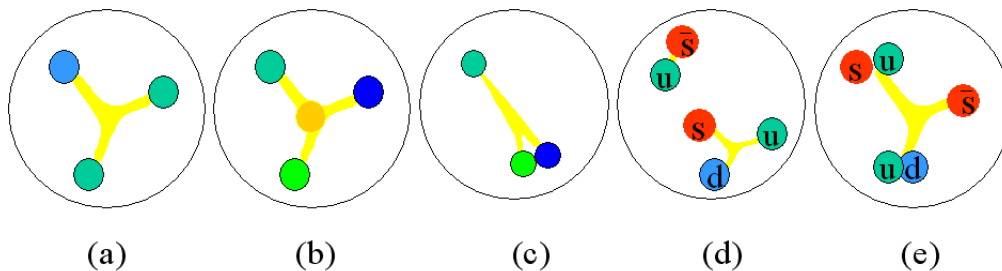


Figure 1: Various pictures for internal quark-gluon structure of baryons: (a)  $3q$ , (b)  $3qg$  hybrid, (c) diquark, (d) meson-baryon state, (e) pentaquark with diquark clusters.

The classical simple 3q constituent quark model as shown by Fig.1(a) has been very successful in explaining the static properties, such as mass and magnetic moment, of the spatial ground states of the flavor SU(3) octet and decuplet baryons. Its predicted  $\Omega$  baryon with mass around 1670 MeV was discovered by later experiments. However its predictions for the spatial excited baryons are not so successful. In the simple 3q constituent quark model, the lowest spatial excited baryon is expected to be a ( $uud$ )  $N^*$  state with one quark in orbital angular momentum  $L = 1$  state, and hence should have negative parity. Experimentally [1], the lowest negative parity  $N^*$  resonance is found to be  $N^*(1535)$ , which is heavier than two other spatial excited baryons :  $\Lambda^*(1405)$  and  $N^*(1440)$ . In the classical 3q constituent quark model, the  $\Lambda^*(1405)$  with spin-parity  $1/2^-$  is supposed to be a ( $uds$ ) baryon with one quark in orbital angular momentum  $L = 1$  state and about 130 MeV heavier than its  $N^*$  partner  $N^*(1535)$ ; the  $N^*(1440)$  with spin-parity  $1/2^+$  is supposed to be a ( $uud$ ) state with one quark in radial  $n = 1$  excited state and should be heavier than the  $L = 1$  excited ( $uud$ ) state  $N^*(1535)$ , noting the fact that for a simple harmonic oscillator potential the state energy is  $(2n + L + 3/2)\hbar\omega$ . So for these three lowest spatial excited baryons, the classical quark model picture is already failed.

The second outstanding problem in the classical 3q quark model is that in many of its forms it predicts a substantial number of ‘missing  $N^*$  states’ around 2 GeV/ $c^2$ , which have not so far been observed [2]. Since the more number of effective degrees of freedom the more predicted number of excited states, the ‘missing  $N^*$  states’ problem is argued in favor of the diquark picture as shown in Fig.1(c) which has less degree of freedom and predicts less  $N^*$  states [3]. For example, in diquark models, the two quarks forming the diquark are constrained to be in the relative S-wave, and hence cannot combine the third quark to form  $(20, 1_2^+)$ -multiplet baryons. Experimentally, not a single  $(20, 1_2^+)$ -multiplet baryon has been identified yet [1]. However, non-observation of these ‘missing  $N^*$  states’ does not necessarily mean that they do not exist. In the limit that the  $\gamma$  or  $\pi$  couples to one quark in the nucleon in the  $\gamma N$  or  $\pi N$  reactions, the  $(20, 1_2^+)$ -multiplet baryon cannot be produced [4]. Considering higher order effects, they may have weak coupling to  $\pi N$  and  $\gamma N$ , but maybe too weak to be produced by presently available  $\pi N$  and  $\gamma N$  experiments [2, 4]. Other production processes should be explored. Moreover the diquark models are only successful for very limited aspects.

The third outstanding problem for the classical 3q quark model is that from deep inelastic scattering and Drell-Yan experiments the number of  $\bar{d}$  is found to be more than the number of  $\bar{u}$  by 0.12 in the proton [5]. This is argued in favor of a mixture of the meson-baryon states as shown by Fig.1(d). With this picture, the excess of  $\bar{d}$  over  $\bar{u}$  in the proton is explained by a

mixture of  $n\pi^+$  with the  $\pi^+$  composed of  $u\bar{d}$  [6]; the  $N^*(1535)$  and  $\Lambda^*(1405)$  are ascribed as quasi-bound states of  $K\Sigma$  and  $\bar{K}N$ , respectively [7]. The extreme of this picture is that only the ground state baryon-octet  $1/2^+$  and baryon-decuplet  $3/2^+$  are dominated by  $qqq$  while all excited baryons are generated by meson-baryon coupled channel dynamics [8, 9]. However the mixture of the pentaquark components with diquark clusters as shown by Fig.1(e) can also explain these properties [10–13].

Another possible configuration for baryons is  $gqqq$  hybrid as shown by Fig.1(b) with various phenomenological models reviewed by Ref. [14].

In reality for a baryon state around 2 GeV, it could be a mixture of all five configurations shown in Fig.1.

On experimental side, our present knowledge of baryon spectroscopy came almost entirely from partial-wave analyses of  $\pi N$  total, elastic, and charge-exchange scattering data of more than twenty years ago [1]. Only recently, the new generation of experiments on  $N^*$  physics with electromagnetic probes at CEBAF at JLAB, ELSA at Bonn, GRAAL at Grenoble and SPRING8 at JASRI have been producing some nice results. However, a problem for these experiments is that above 1.8 GeV there are too many broad resonances with various possible quantum numbers overlapping with each other and it is rather difficult to disentangle them. Moreover resonances with weak couplings to  $\pi N$  and  $\gamma N$  will not show up in these experiments.

Joining the new effort on studying the excited nucleons,  $N^*$  baryons, BES started a baryon resonance program [15] at Beijing Electron-Positron Collider (BEPC). The  $J/\psi$  and  $\psi'$  experiments at BES provide an excellent place for studying excited nucleons and hyperons –  $N^*$ ,  $\Lambda^*$ ,  $\Sigma^*$  and  $\Xi^*$  resonances [16].

Comparing with other facilities, our baryon program has advantages in at least three obvious aspects:

(1) We have pure isospin  $1/2$   $\pi N$  and  $\pi\pi N$  systems from  $J/\psi \rightarrow \bar{N}N\pi$  and  $\bar{N}N\pi\pi$  processes due to isospin conservation, while  $\pi N$  and  $\pi\pi N$  systems from  $\pi N$  and  $\gamma N$  experiments are mixture of isospin  $1/2$  and  $3/2$ , and suffer difficulty on the isospin decomposition;

(2)  $\psi$  mesons decay to baryon-antibaryon pairs through three or more gluons. It is a favorable place for producing hybrid ( $qqqg$ ) baryons, and for looking for some “missing”  $N^*$  resonances, such as members of possible  $(20, 1_2^+)$ -multiplet baryons, which have weak coupling to both  $\pi N$  and  $\gamma N$ , but stronger coupling to  $g^3 N$ ;

(3) Not only  $N^*$ ,  $\Lambda^*$ ,  $\Sigma^*$  baryons, but also  $\Xi^*$  baryons with two strange quarks can be studied. Many QCD-inspired models [2] are expected to be more reliable for baryons with two strange quarks due to their heavier quark mass. More than thirty  $\Xi^*$  resonances are predicted where only two such states are well established by experiments. The theory is totally not chal-

lenged due to lack of data.

In this paper, we review baryon resonances observed by BES I and BES II, and discuss the prospects for baryon spectroscopy at BES III.

## 2 Baryon Spectroscopy at BES I and BES II

BES I started data-taking in 1989 and collected 7.8 million  $J/\psi$  events and 3.7 million  $\psi'$  events. BES II has collected 58 million  $J/\psi$  events and 14 million  $\psi'$  events since 1998.

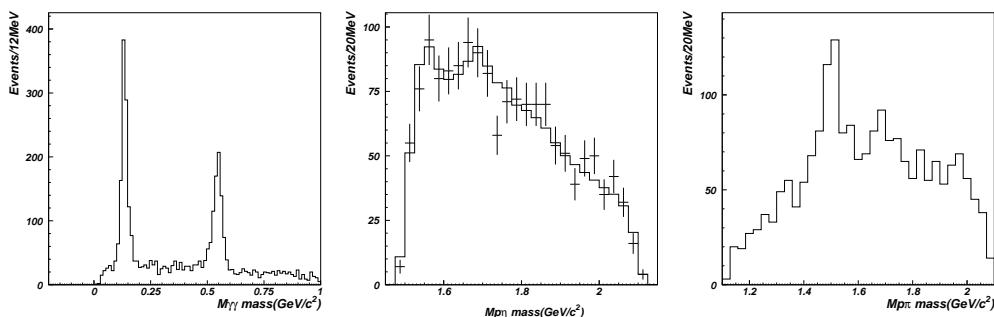


Figure 2: BES I data for  $\gamma\gamma$  invariant mass of  $J/\psi \rightarrow \bar{p}p\gamma\gamma$  (left);  $p\eta$  (middle) and  $p\pi$  (right) invariant mass spectra of  $J/\psi \rightarrow \bar{p}p\eta$  and  $\bar{p}p\pi^0$ .

Based on 7.8 million  $J/\psi$  events collected at BES I from 1990 to 1991, the events for  $J/\psi \rightarrow \bar{p}p\pi^0$  and  $\bar{p}p\eta$  have been selected and reconstructed with  $\pi^0$  and  $\eta$  detected in their  $\gamma\gamma$  decay mode [15]. The invariant mass of  $\gamma\gamma$  is shown in Fig. 2 (left) with two clear peaks corresponding to  $\pi^0$  and  $\eta$ . The  $p\eta$  invariant mass spectrum is shown in Fig. 2 (middle) with two peaks at 1540 and 1650 MeV. Partial wave analysis has been performed for the  $J/\psi \rightarrow \bar{p}p\eta$  channel [15] using the effective Lagrangian approach [17, 18] with Rarita-Schwinger formalism [19–22] and the extended automatic Feynman Diagram Calculation (FDC) package [23]. There is a definite requirement for a  $J^P = \frac{1}{2}^-$  component at  $M = 1530 \pm 10$  MeV with  $\Gamma = 95 \pm 25$  MeV near the  $\eta N$  threshold. In addition, there is an obvious resonance around 1650 MeV with  $J^P = \frac{1}{2}^-$  preferred,  $M = 1647 \pm 20$  MeV and  $\Gamma = 145^{+80}_{-45}$  MeV. These two  $N^*$  resonances are believed to be the two well established states,  $S_{11}(1535)$  and  $S_{11}(1650)$ , respectively. In the higher  $p\eta(\bar{p}\eta)$  mass region, there is an evidence for a structure around 1800 MeV; with BES I statistics one cannot determine its quantum numbers. The  $p\pi^0$  invariant

mass spectrum from  $J/\psi \rightarrow p\bar{p}\pi^0$  is shown in Fig. 2 (right) with two clear peaks around 1500 and 1670 MeV, and some weak structure around 2 GeV.

With 58 million new  $J/\psi$  events collected by BESII of improved detecting efficiency, one order of magnitude more reconstructed events can be obtained for each channel. Results for  $J/\psi$  to  $p\bar{n}\pi^- + c.c.$ ,  $pK^-\bar{\Lambda} + c.c.$  and  $\Lambda\bar{\Sigma}\pi + c.c.$  channels are shown in Figs.3,4,5, respectively. These are typical channels for studying  $N^*$ ,  $\Lambda^*$  and  $\Sigma^*$  resonances. For  $J/\psi \rightarrow p\bar{p}\pi^0$  channel, the  $N\pi$  invariant mass spectrum looks similar to the BESII data, but with much higher statistics.

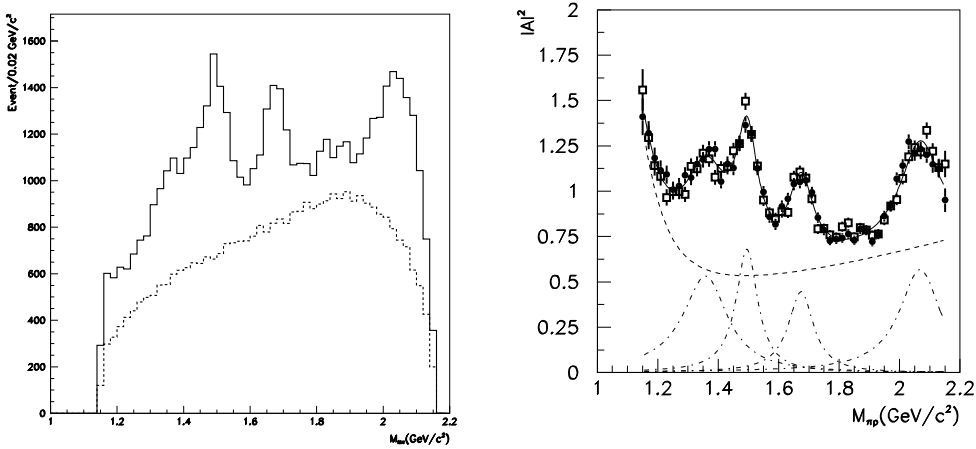


Figure 3:  $p\pi^-$  invariant mass spectrum for  $J/\psi \rightarrow p\pi^-\bar{n}$  compared with phase space distribution (left); And data divided by MC phase space vs  $p\pi^-$  invariant mass for  $J/\psi \rightarrow p\pi^-\bar{n}$  (solid circle) and  $p\pi^+n$  (open square).

For  $J/\psi \rightarrow p\bar{n}\pi^-$  channel, proton and  $\pi^-$  are detected [24]. With some cuts of backgrounds, the missing mass spectrum shows a very clean peak for the missing antineutron. In the  $p\pi^-$  invariant mass spectrum as shown in Fig.3 (left), besides two well known  $N^*$  peaks at 1500 and 1670 MeV, there are two new clear  $N^*$  peaks around 1360 and 2030 MeV. Its charge conjugate channel  $p\pi^+n$  gives very similar results.

To investigate the behavior of the amplitude squared as a function of invariant mass, one should remove the phase space factor and efficiency factor from the invariant mass distribution by dividing the data by Monte Carlo phase space times the detection efficiency. The results are shown in Fig. 3 (right). At low  $p\pi^-$  invariant mass, the tail from nucleon pole term, expected from theoretical considerations [25,26], is clearly seen. There are clearly four peaks around 1360 MeV, 1500 MeV, 1670 MeV and 2065 MeV. Note that the well known first resonance peak ( $\Delta(1232)$ ) in  $\pi N$  and  $\gamma N$  scattering data does not show up here due to the isospin filter effect of our  $J/\psi$  decay. While

the two peaks around 1500 MeV and 1670 MeV correspond to the well known second and third resonance peaks observed in  $\pi N$  and  $\gamma N$  scattering data, the two peaks around 1360 MeV and 2065 MeV have never been observed in  $\pi N$  invariant mass spectra before. The one around 1360 MeV should be from  $N^*(1440)$  MeV which has a pole around 1360 MeV [1,27,28] and which is usually buried by the strong  $\Delta$  peak in  $\pi N$  and  $\gamma N$  experiments; the other one around 2065 MeV may be due to the long sought “missing”  $N^*$  resonance(s). For the decay  $J/\psi \rightarrow \bar{N}N^*(2065)$ , the orbital angular momentum of  $L = 0$  is much preferred due to the suppression of the centrifugal barrier factor for  $L \geq 1$ . For  $L = 0$ , the spin-parity of  $N^*(2065)$  is limited to be  $1/2+$  and  $3/2+$ . This may be the reason that the  $N^*(2065)$  shows up as a peak in  $J/\psi$  decays while only much broader structures show up for  $\pi N$  invariant mass spectra above 2 GeV in  $\pi N$  and  $\gamma N$  production processes [29] which allow all  $1/2\pm$ ,  $3/2\pm$ ,  $5/2\pm$  and  $7/2\pm$   $N^*$  resonances around 2.05 GeV to overlap and interfere with each other there. A simple Breit-Wigner fit [24] gives the mass and width for the  $N^*(1440)$  peak as  $1358 \pm 6 \pm 16$  MeV and  $179 \pm 26 \pm 50$  MeV. Very recently, CELSIUS-WASA Collaboration [30] also observed the  $N^*(1440)$  peak in the  $n\pi^+$  invariant mass spectrum for their  $pp \rightarrow pn\pi^+$  reaction and obtained mass and width consistent with ours. For the new  $N^*$  peak above 2 GeV the fitted mass and width are  $2068 \pm 3_{-40}^{+15}$  MeV and  $165 \pm 14 \pm 40$  MeV, respectively. A partial wave analysis indicates that the  $N^*(2065)$  peak contains both spin-parity  $1/2+$  and  $3/2+$  components [24].

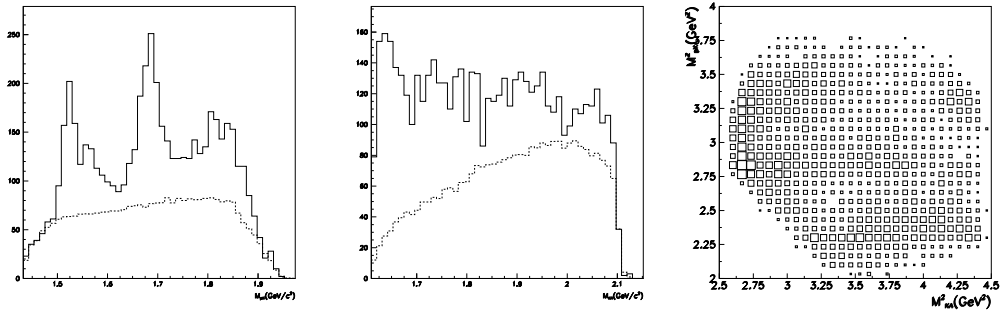


Figure 4:  $pK$  (left) and  $K\Lambda$  (middle) invariant mass spectra for  $J/\psi \rightarrow pK^-\bar{\Lambda}+c.c.$ , compared with phase space distribution; right: Dalitz plot for  $J/\psi \rightarrow pK^-\bar{\Lambda}+c.c.$

For  $J/\psi \rightarrow pK^-\bar{\Lambda}$  and  $\bar{p}K^+\Lambda$  channels [31], there are clear  $\Lambda^*$  peaks at 1.52 GeV, 1.69 GeV and 1.8 GeV in  $pK$  invariant mass spectrum, and  $N^*$  peaks near  $K\Lambda$  threshold, 1.9 GeV and 2.05 GeV for  $K\Lambda$  invariant mass spectrum. The  $N^*$  peak near  $K\Lambda$  threshold is most probably due to  $N^*(1535)$

which was found to have large coupling to  $K\Lambda$  [9, 12]. The SAPHIR experiment at ELSA [32] also observed a  $N^*$  peak around 1.9 GeV for  $K\Lambda$  invariant mass spectrum from photo-production, and the fit [33] to the data reveals large  $1/2^-$  near-threshold enhancement mainly due to the  $N^*(1535)$ . The  $N^*$  peak at 2.05 GeV is compatible with that observed in  $N\bar{N}\pi$  channels.

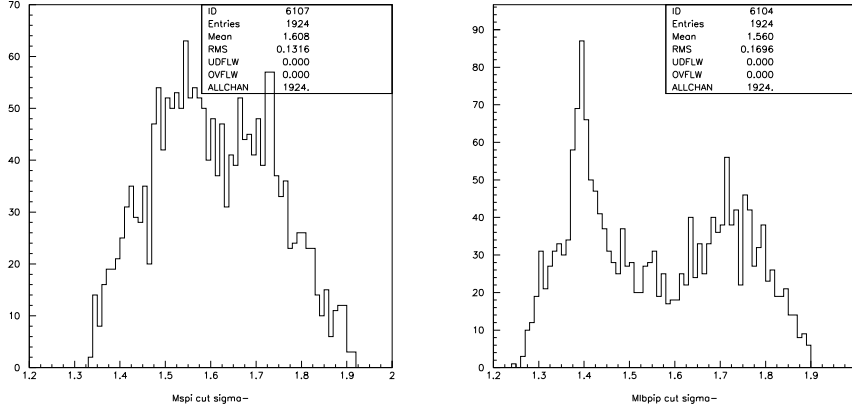


Figure 5:  $\bar{\Sigma}\pi$  (left) and  $\Lambda\pi$  (right) invariant mass spectrum for  $J/\psi \rightarrow \Lambda\bar{\Sigma}^+\pi^-$ . Preliminary BESII data [34]

For  $J/\psi \rightarrow \Lambda\Sigma\pi$  channels [34], it seems also  $\Lambda^*$  peaks at 1.52 GeV, 1.69 GeV and 1.8 GeV in  $\Sigma\pi$  invariant mass spectra, similar to those in the  $pK\Lambda$  channel, although less clear. In  $\Lambda\pi$  invariant mass spectra, there is a very clear peak around 1.385 GeV corresponding to the well-established  $\Sigma(1385)$  resonance and there is also another  $\Sigma^*$  peak around 1.72 GeV.

In order to get more useful information about properties of the baryon resonances involved, such as their  $J^{PC}$  quantum numbers, mass, width, production and decay rates, etc., partial wave analysis (PWA) is necessary. We use event-based standard maximum likelihood method with partial wave amplitudes constructed by the effective Lagrangian approach [17, 18] with Rarita-Schwinger formalism [19–22].

### 3 Baryon spectroscopy Prospects at BESIII

Recently, empirical indications for a positive strangeness magnetic moment and positive strangeness radius of the proton suggest that the 5-quark components in baryons may be largely in colored diquark cluster configurations rather than mainly in “meson cloud” configurations [10, 11]. The diquark

cluster picture also gives a natural explanation for the excess of  $\bar{d}$  over  $\bar{u}$  in the proton with a mixture of  $[ud][ud]\bar{d}$  component in the proton. More precise measurements and analyses of the strange form factors are needed to examine the relative importance of the meson-cloud components and  $q^2q^2\bar{q}$  components in the proton.

For excited baryons, the excitation energy for a spatial excitation could be larger than to drag out a  $q\bar{q}$  pair from gluon field with the  $q$  to form diquark cluster with a valence quark. Hence the 5-quark components could be dominant for some excited baryons.

The diquark cluster picture for the 5-quark components in baryons also gives a natural explanation for the longstanding mass-reverse problem of  $N^*(1535)$ ,  $N^*(1440)$  and  $\Lambda^*(1405)$  resonances as well as the unusual decay pattern of the  $N^*(1535)$  resonance with a large  $[[ud][us]\bar{s}] >$  component [10, 12].

The diquark cluster picture predicts the existence of the SU(3) partners of the  $N^*(1535)$  and  $\Lambda^*(1405)$ , *i.e.*, an additional  $\Lambda^* 1/2^-$  around 1570 MeV, a triplet  $\Sigma^* 1/2^-$  around 1360 MeV and a doublet  $\Xi^* 1/2^-$  around 1520 MeV [13]. There is indeed evidence for all of them in the data of  $J/\psi$  decays at BES. Fig. 4 (left) shows the  $pK$  invariant mass spectrum for  $J/\psi \rightarrow pK^-\bar{\Lambda}+c.c.$  and Fig. 5 (right)  $\Lambda\pi$  invariant mass spectrum for  $J/\psi \rightarrow \Lambda\bar{\Sigma}^+\pi^-$  from BES [34]. In the  $pK$  invariant mass spectrum, under the narrow  $\Lambda^*(1520) 3/2^-$  peak, there is a quite obvious broader peak around 1570 MeV. Preliminary partial wave analysis [35] gave its spin-parity as  $1/2^-$ . This  $\Lambda^*(1570) 1/2^-$  resonance fits in the new scheme for the  $1/2^-$  SU(3) baryon nonet very well. In the  $\Lambda\pi$  invariant mass spectrum, under the  $\Sigma^*(1385) 3/2^+$  peak, there is also a broader peak around 1360 MeV. No partial wave analysis has been performed for this channel yet. But there is a good reason to reckon that there may be  $1/2^-$  component underneath the  $\Sigma^*(1385) 3/2^+$  peak.

According to PDG [1], the branching ratios for  $J/\psi \rightarrow \bar{\Sigma}^-\Sigma^*(1385)^+$  and  $J/\psi \rightarrow \bar{\Xi}^+\Xi^*(1530)^-$  are  $(3.1 \pm 0.5) \times 10^{-4}$  and  $(5.9 \pm 1.5) \times 10^{-4}$ , respectively. These two processes are SU(3) breaking decays since  $\Sigma$  and  $\Xi$  belong to SU(3)  $1/2^+$  octet while  $\Sigma^*(1385)$  and  $\Xi^*(1530)$  belong to SU(3)  $3/2^+$  decuplet. Comparing with the similar SU(3) breaking decay  $J/\psi \rightarrow \bar{p}\Delta^+$  with branching ratio of less than  $1 \times 10^{-4}$  and the SU(3) conserved decay  $J/\psi \rightarrow \bar{p}N^*(1535)^+$  with branching ratio of  $(10 \pm 3) \times 10^{-4}$ , the branching ratios for  $J/\psi \rightarrow \bar{\Sigma}^-\Sigma^*(1385)^+$  and  $J/\psi \rightarrow \bar{\Xi}^+\Xi^*(1530)^-$  are puzzling too high. A possible explanation for this puzzling phenomena is that there were substantial components of  $1/2^-$  under the  $3/2^+$  peaks but the two branching ratios were obtained by assuming pure  $3/2^+$  contribution. This possibility

should be easily checked with the high statistics BESIII data in near future.

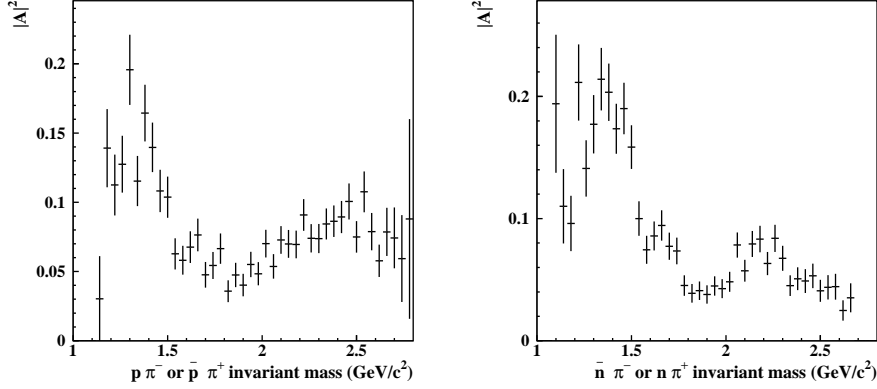


Figure 6: Data divided by efficiency and phase space vs  $p\pi^-$  (or  $\bar{p}\pi^+$ ) and  $\bar{n}\pi^-$  (or  $n\pi^+$ ) invariant mass for  $\psi' \rightarrow p\bar{n}\pi^- + c.c.$  candidate events [36].

With two order of magnitude more statistics at BESIII, plenty important channels for baryon spectroscopy can be studied from both  $J/\psi$  and  $\psi'$  decays. The  $\psi'$  data will significantly extend the mass range for the study of baryon spectroscopy. For example, for  $\psi' \rightarrow p\bar{n}\pi^- + c.c.$  events collected at BESII [36], there are obvious structures for  $M_{N\pi} > 2$  GeV in the  $N\pi$  invariant mass spectra as shown in Fig. 6. However due to low statistics at BESII, no conclusive information can be drawn for the  $N^*$  resonances with mass above 2 GeV from  $\psi'$  decays [36, 37]. With BESIII statistics, determination of properties for these high mass  $N^*$  resonances can be done. The BESIII  $\psi'$  data will enable us to complete the  $\Lambda^*$ ,  $\Sigma^*$  and  $\Xi^*$  spectrum and examine various pictures for their internal structures, such as simple 3q quark structure and more complicated structure with pentaquark components dominated.

Table 1: Measured  $J/\psi$  decay branching ratios ( $\text{BR} \times 10^3$ ) for channels involving baryon anti-baryon and meson(s) [1, 24]

$p\bar{n}\pi^-$	$p\bar{p}\pi^0$	$p\bar{p}\pi^+\pi^-$	$p\bar{p}\eta$	$p\bar{p}\eta'$	$p\bar{p}\omega$
$2.4 \pm 0.2$	$1.1 \pm 0.1$	$6.0 \pm 0.5$	$2.1 \pm 0.2$	$0.9 \pm 0.4$	$1.3 \pm 0.3$
$\Lambda\bar{\Sigma}^-\pi^+$	$pK^-\bar{\Lambda}$	$pK^-\bar{\Sigma}^0$	$\bar{p}p\phi$	$\Delta(1232)^{++}\bar{p}\pi^-$	$pK^-\bar{\Sigma}(1385)^0$
$1.1 \pm 0.1$	$0.9 \pm 0.2$	$0.3 \pm 0.1$	$0.045 \pm 0.015$	$1.6 \pm 0.5$	$0.51 \pm 0.32$

The measured  $J/\psi$  decay branching ratios for channels involving baryon anti-baryon plus meson(s) are listed in Table 1. With  $10^{10}$   $J/\psi$  events, all

these channels will get enough statistics for partial wave analysis. Among these channels, the  $\Sigma\bar{\Lambda}\pi + c.c.$  channels should have high priority for pinning down the lowest  $1/2^-$   $\Sigma^*$  and  $\Lambda^*$  as well as other higher excited  $\Sigma^*$  and  $\Lambda^*$  states. Another very important channel is  $K^-\Lambda\bar{\Xi}^+ + c.c.$  which is the best channel for finding the lowest  $1/2^-$   $\Xi^*$  resonance and many other “missing”  $\Xi^*$  states with  $\Xi^* \rightarrow K\Lambda$ . This channel should be rather easy to be reconstructed by BESIII. One can select events containing  $K^-$  and  $\Lambda$  with  $\Lambda \rightarrow p\pi^-$ , then from missing mass spectrum of  $K^-\Lambda$  one should easily identify the very narrow  $\bar{\Xi}^+$  peak.

For  $10^9$   $\psi'$  events, the  $K^-\Lambda\bar{\Xi}^+ + c.c.$  and  $p\bar{p}\phi$  channels should have high priority. These two channels are strongly limited by phase space in  $J/\psi$  decays. From  $\psi'$  decays, the phase space is much increased. The  $K^-\Lambda\bar{\Xi}^+ + c.c.$  channel should allow us to discover many “missing”  $\Xi^*$  resonances, while the  $p\bar{p}\phi$  channel should allow us to find those  $N^*$  resonances with large coupling to  $N\phi$  [39] and hence large 5-quark components.

After analyzing the easier 3-body final states, 4-body and 5-body channels should also be investigated. Among them,  $\Delta(1232)^{++}\bar{p}\pi^-$  in  $p\bar{p}\pi^+\pi^-$  and  $\Delta(1232)^{++}\bar{\Sigma}^-K^-$  in  $p\bar{\Sigma}^-\pi^+K^-$  are very good channels for finding “missing”  $\bar{\Delta}^{*-}$  decaying to  $\bar{p}\pi^-$  and  $\bar{\Sigma}^-K^-$ , respectively. The spectrum of isospin  $3/2$   $\Delta^{++*}$  resonances is of special interest since it is the most experimentally accessible system composed of 3 identical valence quarks. Recently, the lowest  $1/2^-$  baryon decuplet is proposed to contain large vector-meson-baryon molecular components [40]. In the new scheme, the  $\Xi^*(1950)$  is predicted to be  $1/2^-$  resonance with large coupling to  $\Lambda K^*$ . The  $\psi' \rightarrow \bar{\Xi}\Lambda K^*$  will provide a very good place to look for “missing”  $\Xi^*$  with large coupling to  $\Lambda K^*$ .

In summary, BESIII data can play a very important role in studying excited nucleons and hyperons, i.e.,  $N^*$ ,  $\Lambda^*$ ,  $\Sigma^*$ ,  $\Xi^*$  and  $\Delta^{*++}$  resonances.

## References

- [1] Particle Data Group, *Phys. Rev.* **D66**, 010001 (2002).
- [2] S.Capstick and W.Robert, *Prog. Part. Nucl. Phys.* **45**, S241 (2000), and references therein.
- [3] K.F.Liu and C.W.Wong, *Phys. Rev.* **D28** (1983) 170; M.Anselmino et al., *Rev. Mod. Phys.* **65**, 1199 (1993).
- [4] Q.Zhao and F.E.Close, *Phys. Rev.* **D74**, 094014 (2006).

- 
- [5] G.T.Garvey, J.C.Peng, *Prog. Part. Nucl. Phys.* **47** (2001) 203, and references therein.
- [6] J.P.Speth and A.W.Thomas, *Adv. Nucl. Phys.* **24** (1997) 93, and references therein.
- [7] N.Kaiser et al., *Phys. Lett.* **B362**, 23 (1995); *Nucl. Phys.* **A612**, 297 (1997).
- [8] M.F.M.Lutz and E.E.Kolomeitsev, *Nucl. Phys.* **A700**, 193 (2002); *ibid.* **A730**, 392 (2004).
- [9] E.Oset et al., *Int. J. Mod. Phys.* **A18**, 387 (2003); *Phys. Lett.* **B527**, 99 (2002); L. Roca et al., *Phys. Rev.* **C73**, 045 (2006).
- [10] B.S.Zou, *Nucl. Phys.* bf A790, 110c (2007) and reference therein.
- [11] B. S. Zou and D. O. Riska, *Phys. Rev. Lett.* **95** (1005) 072001; C. S. An, B. S. Zou and D. O. Riska, *Phys. Rev.* **C73** (2006) 035207.
- [12] B.C. Liu and B.S. Zou, *Phys. Rev. Lett.* **96**, 042002 (2006); *ibid.* **98**, 039102 (2007).
- [13] A.Zhang et al., *High Energy Phys. Nucl. Phys.* **29**, 250 (2005).
- [14] T.Barnes, in \*Juelich 2000, Baryon excitations\* 121-131, and reference therein; P.Page, *Int. J. Mod. Phys.* **A20**, 1791 (2005).
- [15] BES Collaboration, *Phys. Lett.* **B510**, 75 (2001); H.B.Li et al. (BES), *Nucl. Phys.* **A675**, 189c (2000); B.S.Zou et al. (BES), *Excited Nucleons and Hadronic Structure, Proc. of NSTAR2000 Conf. at JLab, Feb 2000*. Eds. V.Burkert et al., World Scientific (2001) p.155.
- [16] B.S.Zou, *Nucl. Phys.* **A684**, 330 (2001); *Nucl. Phys.* **A675**, 167 (2000).
- [17] M.Benmerrouche, N.C.Mukhopadhyay and J.F.Zhang, *Phys. Rev. Lett.* **77**, 4716 (1996); *Phys. Rev.* **D51**, 3237 (1995).
- [18] M.G.Olsson and E.T.Osypowski, *Nucl. Phys.* **B87**, 399 (1975); *Phys. Rev.* **D17**, 174 (1978); M.G.Olsson et al., *ibid.* **17**, 2938 (1978).
- [19] W.Rarita and J.Schwinger, *Phys. Rev.* **60**, 61 (1941).
- [20] C.Fronsdal, *Nuovo Cimento Suppl.* **9**, 416 (1958); R.E.Behrends and C.Fronsdal, *Phys. Rev.* **106**, 345 (1957).

- [21] S.U.Chung, *Spin Formalisms*, CERN Yellow Report 71-8 (1971); Phys. Rev. **D48**, 1225 (1993); J.J.Zhu and T.N.Ruan, *Communi. Theor. Phys.* **32**, 293, 435 (1999).
- [22] W.H.Liang, P.N.Shen, J.X.Wang and B.S.Zou, *J. Phys.* **G28** (2002) 333.
- [23] J.X.Wang, *Comput. Phys. Commun.* **77**, 263 (1993).
- [24] BES Collaboration, *Phys. Rev. Lett.* 97 (2006) 062001.
- [25] R. Sinha and S. Okubo, *Phys. Rev. D*30 (1984) 2333.
- [26] W.H.Liang, P.N.Shen, B.S.Zou and A.Faessler, *Euro. Phys. J. A*21 (2004) 487.
- [27] R.A. Arndt et al., *Phys.Rev.C*69, 035213 (2004); M.Manley, talk at NSTAR2004, Grenoble, March 2004.
- [28] T.P.Vrana, S.A.Dytman and T.S.H.Lee, *Phys. Rep.* 328 (2000) 181.
- [29] L.Y.Zhu et al., *Phys. Rev. Lett* 91 (2003) 022003.
- [30] H.Clement et al. (CELSIUS-WASA Collaboration), *nucl-ex/0612015*.
- [31] H.X.Yang et al., (BES Collaboration), *Int. J. Mod. Phys. A*20 (2005) 1985; BES Collaboration, *Phys. Rev. Lett.* 93 (2004) 112002.
- [32] K.H.Glander et al., *Euro. Phys. J.* **A19**, 251 (2004); R.Lawall et al., *Euro. Phys. J.* **A24**, 275 (2005).
- [33] G.Penner and U.Mosel, *Phys. Rev.* **C66**, 055211 (2002); *ibid.* **C66**, 055212 (2002); V.Shklyar, H.Lenske and U.Mosel, *Phys. Rev.* **C72**, 015210 (2005); B.Julia-Diaz et al., *Phys. Rev.* **C73**, 055204 (2006).
- [34] B.S.Zou (for BES), *Proc. of NSTAR2004, Grenoble, France*. Eds. J.P.Bocquet et al., World Scientific (2004) p.271.
- [35] H.X.Yang, IHEP Ph.D thesis (2001).
- [36] BES Collaboration, *Phys.Rev.* D74 (2006) 012004.
- [37] BES Collaboration, *Phys.Rev.* D71 (2005) 072006.
- [38] S. Capstick and N. Isgur, *Phys. Rev. D*34 (1986) 2809.
- [39] F.Huang, Z.Y.Zhang and Y.W.Yu, *Phys. Rev.* **C73**, 025207 (2006); J.J.Xie, B.S.Zou and H.C.Chiang, arXiv:0705.3950 [nucl-th].

- [40] J.J.Xie and B.S.Zou, Phys. Lett. **B649** (2007) 405.

# $K^+$ PHOTOPRODUCTION AND $\pi^0$ PHOTOPRODUCTION BY LINEARLY POLARIZED PHOTONS AT SPring-8/LEPS

M.Sumihama<sup>\*,1</sup>, J.K. Ahn<sup>%</sup>, H. Akimune<sup>#</sup>, Y. Asano<sup>⊥</sup>, W.C. Chang<sup>§</sup>,  
S. Daté<sup>⊥</sup>, H. Ejiri<sup>⊥</sup>, H. Fujimura<sup>&</sup>, M. Fujiwara<sup>\*</sup>, K. Hicks<sup>+</sup>, T. Hotta<sup>\*</sup>,  
K. Imai<sup>&</sup>, T. Ishikawa<sup>±</sup>, T. Iwata<sup>⊞</sup>, H. Kawai<sup>×</sup>, K. Kino<sup>\*</sup>, H. Kohri<sup>\*</sup>, N.  
Kumagai<sup>⊥</sup>, S. Makino<sup>⊗</sup>, T. Matsumura<sup>\*</sup>, N. Matsuoka<sup>\*</sup>, T. Mibe<sup>+</sup>,  
M. Miyabe<sup>&</sup>, M. Morita<sup>\*</sup>, N. Muramatsu<sup>\*</sup>, T. Nakano<sup>\*</sup>, M. Niiyama<sup>&</sup>,  
M. Nomachi<sup>°</sup>, Y. Ohashi<sup>⊥</sup>, H. Ohkuma<sup>⊥</sup>, T. Ooba<sup>×</sup>, D.S. Oshuev<sup>§</sup>,  
C. Rangacharyulu<sup>•</sup>, A. Sakaguchi<sup>°</sup>, T. Sato<sup>°</sup>, P.M. Shagin<sup>‡</sup>, Y. Shiino<sup>×</sup>,  
H. Shimizu<sup>±</sup>, Y. Sugaya<sup>°</sup>, H. Toyokawa<sup>⊥</sup>, C.W. Wang<sup>§</sup>, S.C. Wang<sup>§</sup>, K.  
Yonehara<sup>#</sup>, T. Yorita<sup>\*</sup>, M. Yosoi<sup>\*</sup>, R.G.T. Zegers<sup>⊥</sup>

\* Research Center for Nuclear Physics, Osaka University, Ibaraki, Japan

%Department of Physics, Pusan National University, Busan, Korea

#Department of Physics, Konan University, Kobe, Japan

⊥Japan Synchrotron Radiation Research Institute, Sayo, Hyogo, Japan

§Institute of Physics, Academia Sinica, Taipei, Taiwan

&Department of Physics, Kyoto University, Kyoto, Japan

+Department of Physics and Astronomy, Ohio University, Athens, Ohio, USA

±Laboratory of Nuclear Science, Tohoku University, Sendai, Japan

⊞Department of Physics, Yamagata University, Yamagata, Japan

×Graduate School of Science and Technology, Chiba University, Chiba, Japan

⊗Wakayama Medical College, Wakayama, Japan

°Department of Physics, Osaka University, Toyonaka, Japan

•Department of Physics and Engineering Physics, University of Saskatchewan,  
Saskatoon, Saskatchewan, Canada

‡School of Physics and Astronomy, University of Minnesota, Minneapolis,  
Minnesota

⊥National Superconducting Cyclotron Laboratory, Michigan State University,  
Michigan, USA

## Abstract

$K^+$  photoproduction and  $\pi^0$  photoproduction have been measured by linearly polarized photons from 1.5 GeV to 2.4 GeV at the SPring-8/LEPS facility. Differential cross sections and photon beam asymmetries for the  $\gamma p \rightarrow K^+\Lambda$ ,  $\gamma p \rightarrow K^+\Sigma^0$ , and  $\gamma p \rightarrow p\pi^0$  reactions have been obtained.

<sup>1</sup>E-mail address: sumihama@rcnp.osaka-u.ac.jp

## 1 Introduction

The spectroscopy of  $N^*$  and  $\Delta^*$  resonances has been studied both experimentally and theoretically. Many baryon resonances were found and their characteristics were determined at the total energy,  $W < 1.7$  GeV [1]. However many higher-mass resonances are still not well established, which are called “missing resonances” [1, 2]. A huge number of baryon resonances are predicted in the constituent quark models, but only a part of these expected resonances is experimentally observed [2]. Identification of the missing resonances is important to understand the quark-gluon structure of a nucleon.

Quark model studies suggest some of these missing resonances may couple to strange channels, such as  $K\Lambda$  and  $K\Sigma$  channels [2].  $\Lambda$  and  $\Sigma^0$  hyperons have the isospins of 0 and 1, respectively. Accordingly, intermediate states of  $K^+\Lambda$  have the isospin  $\frac{1}{2}$  whereas intermediate states of  $K^+\Sigma^0$  can have both the isospins of  $\frac{1}{2}$  and  $\frac{3}{2}$ . It is very interesting to study the  $\gamma p \rightarrow K^+\Lambda$  and  $\gamma p \rightarrow K^+\Sigma^0$  reactions to further our understanding of the role that nucleon resonances play in non-pionic reactions.

Valuable information on baryon resonances has been obtained primarily from the studies of pion channels. There still remains a possibility to obtain new information on baryon resonances in pion photoproduction by measuring polarization observables at high energies. Some weakly excited resonances are obscured due to other strong resonances which have large decay widths, making it difficult to demonstrate their existence only from the cross section data. Alternatively, polarization observables are useful to extract such hidden resonances [3].

At very forward (backward) angles, the production mechanism is expected to be dominated by  $t$ -channel ( $u$ -channel) contributions. In general, differential cross sections of meson photoproduction are well described using a simple equation of  $s^{2\alpha(t)-2}$  ( $s^{2\alpha(u)-2}$ ) on basis of the Regge theory at high energies  $E_\gamma > 3$  GeV [4, 5]. Unfortunately, the applicability of Regge theory is not well demonstrated at lower energies due to the lack of experimental data at backward angles. Such experimental data are obtained at the LEPS facility with photons at  $E_\gamma = 1.5 - 2.4$  GeV, and provide a good means to understand the reaction mechanism. We measured  $K^+$  photoproduction in  $t$ -channel kinematics, and  $\pi^0$  photoproduction in  $u$ -channel kinematics.

## 2 Experiment

The experiment was carried out at the Laser-Electron-Photon beam line of the Super Photon ring 8-GeV facility (SPring-8/LEPS) [6, 7]. A multi-

GeV photon beam was produced by backward-Compton scattering (BCS) between Ar-ion laser photons with a 351-nm wave length and the circulating 8-GeV electrons in the storage ring. The linearly polarized photon beam was obtained from the BCS process with linearly-polarized laser photons. The polarization of the photon beam was about 95% at the maximum energy, 2.4 GeV and about 55% at the lowest energy, 1.5 GeV. The photon beam energy was determined by measuring the recoil electron energy from Compton scattering with a tagging counter which consisted of 2 layers of a combination of a hodoscope and a silicon strip detector. The photon energy resolution was 15 MeV in root-mean-square (RMS). The photon intensity, integrated from 1.5 GeV to 2.4 GeV, was  $5 \times 10^5$ /s. Half of the data was taken with vertically polarized photons and the other half with horizontally polarized photons. A liquid hydrogen target with a thickness of 5.6 cm was used.

Charged hadrons were detected by the LEPS spectrometer covering forward angles. The spectrometer consisted of a plastic-scintillation start counter (SC), a silica-aerogel Čerenkov counter (AC), a silicon vertex detector, a dipole magnet, three multi-wire drift chambers, and a time-of-flight (TOF) wall. The field strength of the dipole magnet was 0.7 T at its center. The angular coverage of the spectrometer was about  $\pm 0.4$  rad and  $\pm 0.2$  rad in the horizontal and vertical directions, respectively. The SC determined the trigger timing for the data acquisition system. The AC with a refractive index of 1.03 was used to reject  $e^+e^-$  events at the trigger level.

Charged particles were momentum analyzed by using information from the silicon vertex detector and the three drift chambers. Tracks fitted within a 98% confidence level were accepted for further analysis. The TOF measurement was performed by using the RF signal from the 8-GeV electron storage ring as the start timing and signals of 40 plastic scintillators in the TOF wall as the stop timing. The particle mass was determined using the momentum, the path length and the time-of-flight.

After selecting  $K^+$  particles in the spectrometer, the missing mass of the  $\gamma p \rightarrow K^+ X$  reaction was calculated. The left plot in figure 1 shows the missing mass spectrum of  $K^+$  photoproduction. Peaks corresponding to  $\Lambda(1116)$ ,  $\Sigma^0(1193)$  and hyperon resonances are observed. In the analysis of  $\pi^0$  photoproduction, protons were selected and the missing mass of the  $\gamma p \rightarrow p X$  reaction was obtained to identify  $\pi^0$  particles. The missing mass spectrum for the  $\gamma p \rightarrow p X$  reaction is shown in the right plot of figure 1. Peaks due to  $\pi^0$ ,  $\eta$  and  $\omega/\rho^0$  photoproduction are observed.

The spectrometer acceptance, including the efficiency for detectors and track reconstruction, was obtained using a Monte Carlo simulation with the GEANT3 code. The systematic uncertainty of the target thickness, due to fluctuations of the temperature and pressure of the liquid hydrogen, was esti-

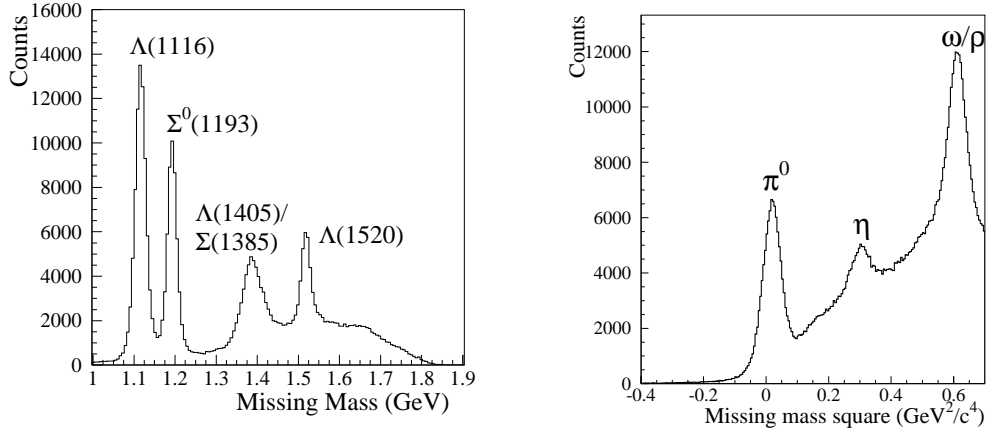


Figure 1: Left; Missing mass of the  $\gamma p \rightarrow K^+ X$  reaction. Right; Missing mass square of the  $\gamma p \rightarrow p X$  reaction.

mated to be 1.0%. The systematic error of the photon number normalization was 3.0%. The systematic uncertainty of the aerogel Čerenkov counter (AC) due to accidental vetoes and  $\delta$ -rays was measured to be lower than 1.6%.

## 3 Results

### 3.1 $K^+$ photoproduction

Figure 2 shows the experimental results of the differential cross sections and the photon beam asymmetries as a function of  $\cos\Theta_{c.m.}$  for the  $K^+\Lambda$  and  $K^+\Sigma^0$  reactions. The signs of the photon beam asymmetries for both reactions were found to be positive. The positive sign means that  $K^+$  particles are emitted preferentially in the orthogonal direction to the photon polarization. In both reactions the photon beam asymmetry increases with increasing photon energy and shows an angular distribution flat below  $W = 2.0$  GeV. Compared to the  $K^+\Lambda$  channel, the photon beam asymmetries for the  $K^+\Sigma^0$  channel exhibits a flatter dependence on angle.

The LEPS data of differential cross sections connect smoothly to the CLAS data. It is seen that the  $K^+\Lambda$  cross section increases at forward angles while the  $K^+\Sigma^0$  cross section decreases except for the low energy regions of  $W = 1.947$  and  $2.029$  GeV. The experimental data for the  $K^+\Lambda$  and  $K^+\Sigma^0$  reactions are compared with Mart and Bennhold's model calcu-

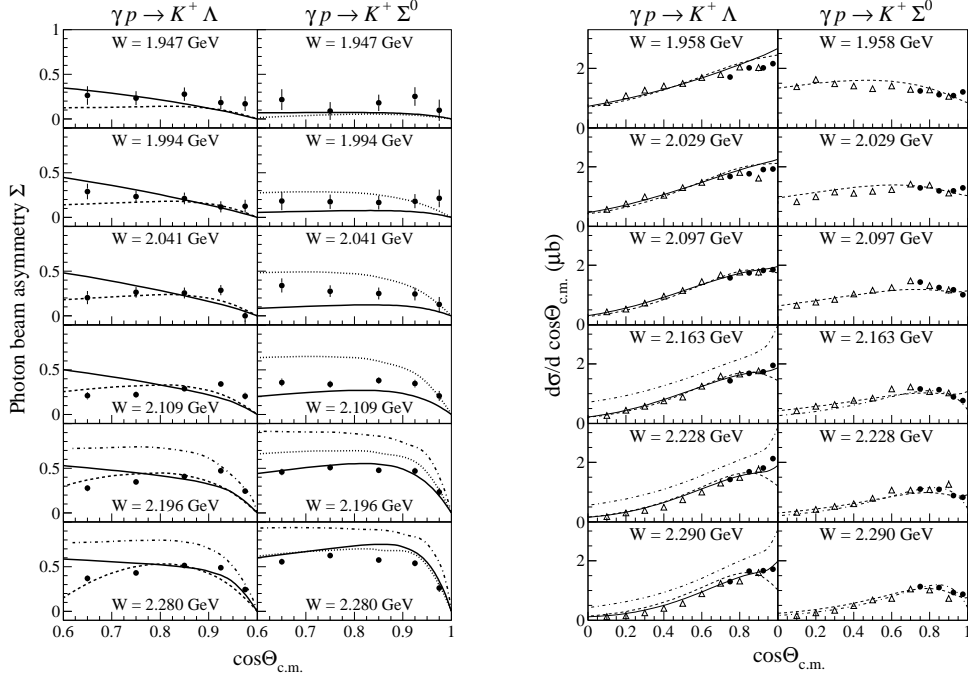


Figure 2: Angular dependence of photon beam asymmetries (left) and differential cross sections (right) for the  $\gamma p \rightarrow K^+ \Lambda$  and  $\gamma p \rightarrow K^+ \Sigma^0$  reactions. Closed circles are LEPS data and open triangles are CLAS data. Dot-dashed, dashed and solid curves are the theoretical calculations with the Regge model, the Feynman diagram and the mixing model of the Regge model and the Feynman diagram, respectively [8].

lation in figure 2. The mixing model calculation agrees with the data for the  $K^+ \Lambda$  reaction while the calculation of the Feynman diagram only agrees with the data for the  $K^+ \Sigma^0$  reaction. The calculations of the Feynman diagram increase as the scattering angle becomes smaller, then they drop at  $\cos\Theta_{c.m.} > 0.85$  for both reactions. The model calculation without inclusion of Regge amplitudes cannot explain the observed angular distributions for the  $K^+ \Lambda$  reaction. The Regge model calculation shows steep increase for the  $K^+ \Lambda$  while it drops for the  $K^+ \Sigma^0$  at  $\cos\Theta_{c.m.} > 0.9$ . In the Regge model, the  $K$  exchange contribution is large for the  $K^+ \Lambda$  but is small for the  $K^+ \Sigma^0$  at forward angles. In the high energy data measured at  $W > 3.2$  GeV at SLAC, the  $K^+ \Lambda$  shows a forward peak but the  $K^+ \Sigma^0$  does not [9]. This result was discussed in terms of the dominance of the  $K$  exchange for the  $K^+ \Lambda$  [5]. In our data the same feature is seen at  $W = 2.1$  to  $2.3$  GeV.

### 3.2 $\pi^0$ photoproduction

Figure 3 shows differential cross sections as a function of the  $\pi^0$  scattering angle. The cross sections measured in the present experiment agree mostly with previously published data [10–12]. The data show a backward peaking at  $\cos\Theta_{c.m.} < -0.85$  above 1.9 GeV while the data do not show the backward peaking below 1.9 GeV. The backward peaking suggests that the  $u$ -channel contribution is not negligibly small. The  $u$ -channel nucleon exchange process is expected to produce the backward peaking at high energies.

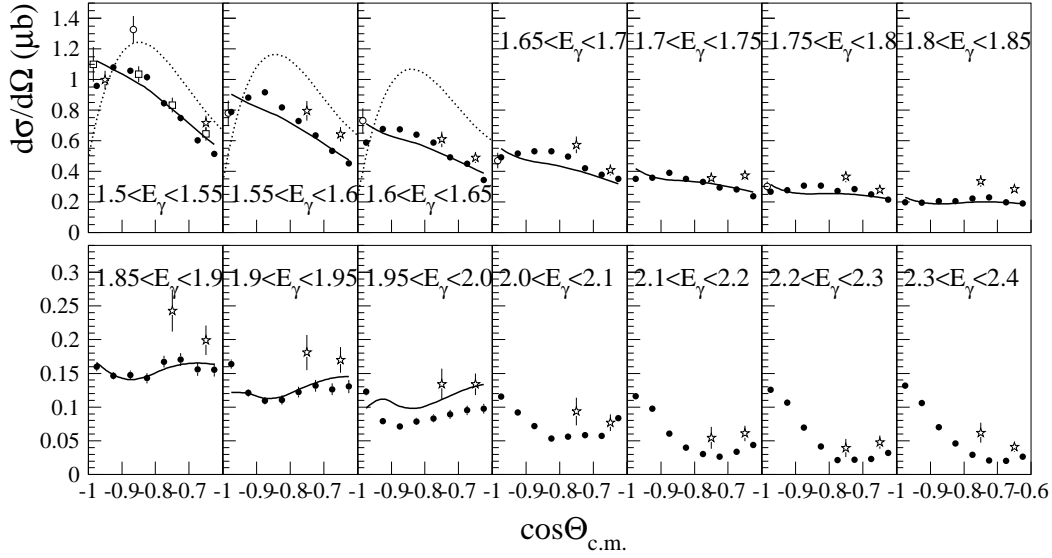


Figure 3: Differential cross sections as a function of the  $\pi^0$  scattering angle,  $\cos\Theta_{c.m.}$ . The closed circles are the results of the present analysis. Only statistical errors are plotted. Most of them are smaller than the size of symbols. The open squares, open stars and open circles are the GRAAL data [10], the ELSA data [11], and the Bonn data in 1979 [12], respectively. The solid and dotted curves are the results of the SAID [13] and the MAID2007 [14], respectively.

The LEPS data mostly agree with the SAID results. A small enhancement structure appears around  $\cos\Theta_{c.m.} = -0.7$  at  $E_\gamma = 1.85$ – $1.95$  GeV in the LEPS data which have not been clearly observed in the previous data due to the poor statistics. The enhancement is well reproduced by the SAID analysis. However, the SAID calculations do not reproduce the backward

peaking at  $E_\gamma = 1.9\text{--}2.0$  GeV. The MAID2007 results overestimate the data at  $\cos\Theta_{c.m.} > -0.9$  and underestimate the data at the most backward angles. The discrepancy becomes larger as the photon energy goes higher. Further improvement of the theoretical calculations will be expected at higher energies and backward angles by including the present data.

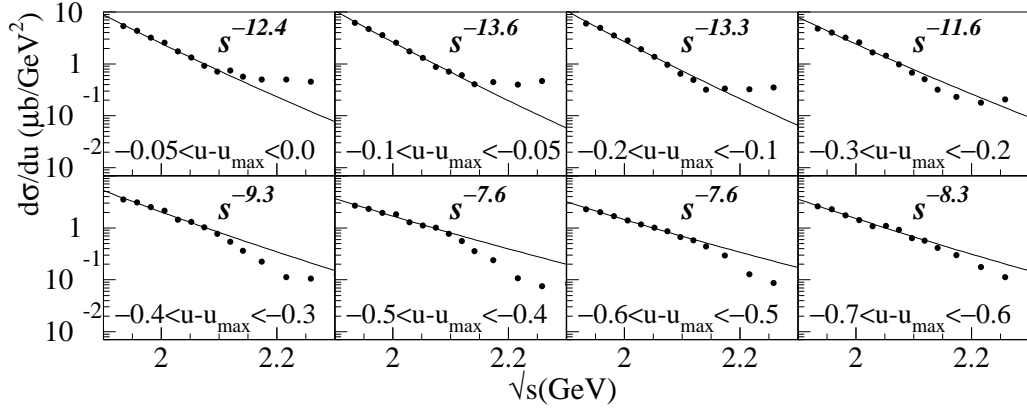


Figure 4: Differential cross sections as a function of the total energy,  $\sqrt{s}$ , for the  $\gamma p \rightarrow \pi^0 p$  reaction. The closed circles are the results of the present analysis. The curves are the fitting results of  $A s^{-x}$  for the data at  $\sqrt{s} < 2.1$  GeV, where  $A$  and  $x$  are fitting parameters [4].

Figure 4 shows differential cross sections as a function of the total energy,  $\sqrt{s}$  at eight bins of  $u - u_{\max}$  [GeV<sup>2</sup>]. The maximum value,  $u_{\max}$ , occurs when the proton goes forward at  $0^\circ$  from the photon beam direction. The energy-dependent slope of the cross sections for  $\pi^0$  production has been determined for the first time in this energy region. The curves are the results of fitting the data from  $\sqrt{s} = 1.93$  GeV (the lowest energy) to 2.1 GeV using a function of  $A s^{-x}$ . The slope parameter,  $x$ , obtained from the fitting is indicated in each plot.

The slope parameter,  $x$ , becomes smaller at larger  $|u - u_{\max}|$ . The LEPS photon energy sits in the transition region from nucleon-meson degrees of freedom to quark-gluon degrees of freedom. The cross sections are known to approximately follow the constituent counting rules above the resonance region and at large scattering angles [15]. If the scaling starts in this photon energy region, the data should follow the counting rule,  $s^{2-n}$ . The quantity  $n$  is the total number of interacting photon and quarks. The value  $n$  is 9 for

$\pi^0$  photoproduction. The data becomes closer to the scaling behavior,  $s^{-7}$ , at the larger  $|u - u_{\max}|$  where the momentum transfer is large. Although the LEPS photon energy is slightly lower than the onset of scaling, the LEPS data provide information on the early onset of scaling.

The differential cross sections sharply decrease for  $\sqrt{s}$  below 2.1 GeV. Above 2.1 GeV, the cross sections do not agree with the fitting curves determined by the data at lower  $\sqrt{s}$ . In order to explain the current data in the  $u$  channel kinematics, new mechanisms would be necessary.

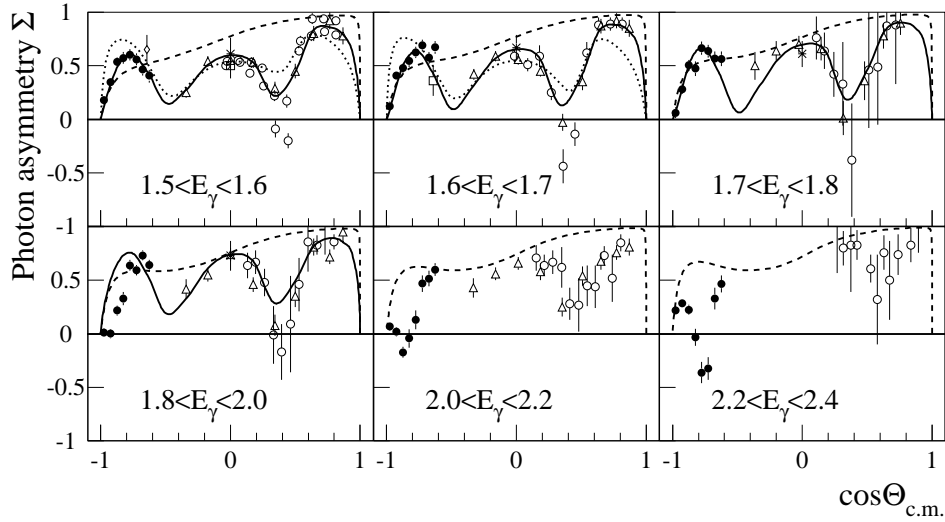


Figure 5: Photon beam asymmetries  $\Sigma$  as a function of the  $\pi^0$  scattering angle,  $\cos\Theta_{c.m.}$ . The closed circles are the results of the present analysis. The other plots are the data from other facilities,  $\square$  [16],  $\triangle$  [17],  $\circ$  [18],  $*$  [19]. The solid and dotted curves are the SAID results [13] and the MAID2007 results [14], respectively. The dashed curves are the calculations of the Born (non-resonant) term by the SL model [20].

The photon beam asymmetry is sensitive to the interference of different diagrams. Resonances can be studied from the photon beam asymmetry combined with cross section data. Figure 5 shows the photon beam asymmetries. The photon asymmetries indicate a bump structure around  $\cos\Theta_{c.m.} = -0.8$  at  $E_\gamma < 1.8$  GeV. Two bumps are observed around  $\cos\Theta_{c.m.} = 0$  and  $0.75$  in the data from other facilities. A similar angular distribution of the photon

asymmetries has been obtained at  $E_\gamma < 1.5$  GeV by the GRAAL collaboration [10]. The MAID2007 calculation including 13 resonances reproduces these bump structures. The SAID calculation agrees with the photon beam asymmetry data, and reproduces the bump structures up to  $E_\gamma = 1.8$  GeV, even though the LEPS data are not used for a fit in the analysis. Therefore, below 1.8 GeV, the LEPS data are explained by the well-known resonances.

The angular distribution changes above  $E_\gamma = 1.8$  GeV as well as the differential cross sections. A strong angular dependence appears at  $E_\gamma > 2.0$  GeV; The photon asymmetries show a dip structure around  $\cos\Theta_{c.m.} = -0.8$ , and the data drop to a negative sign, and then rise up to a positive sign. The discrepancy between the LEPS data and the SAID results becomes large at  $E_\gamma = 1.8$ – $2.0$  GeV. The SL model with the Born terms only shows a positive sign and does not reproduce the dip structure. To explain this strong angular dependence, new mechanism or new resonances are required. There are some candidates of resonances above 2.0 GeV.

## 4 Summary

$K^+$  photoproduction and  $\pi^0$  photoproduction have been studied by using linearly polarized photons at the SPring-8/LEPS facility with 1.5–2.4 GeV. Differential cross sections and photon beam asymmetries have been measured. The differential cross sections for the  $\gamma p \rightarrow K^+\Lambda$  reaction rise at forward angles while the cross sections for the  $\gamma p \rightarrow K^+\Sigma^0$  reaction drop. The exchanged meson in  $t$ -channel will be studied using the LEPS data at forward angles.

The differential cross sections for  $\pi^0$  photoproduction at  $E_\gamma > 1.9$  GeV show a backward peaking. It is suggested that the  $u$ -channel contribution is important. In addition, photon beam asymmetries have been obtained. Above 2.0 GeV, a strong angular distribution is found around  $\cos\Theta_{c.m.} = -0.8$ . In order to explain this structure, the presence of new high-mass resonances combined with the  $u$ -channel diagrams is required.

## 5 References

### References

- [1] Particle Data Group, <http://pdg.lbl.gov>.
- [2] S. Capstick and W. Roberts, *Phys. Rev.* **D49**, 4570 (1994);  
S. Capstick and W. Roberts, *Phys. Rev.* **D58**, 074011 (1998).

- [3] D. Dutta, H. Gao, T.-S. H. Lee, *Phys. Rev.* **C65**, 044619 (2002).
- [4] R.W. Clifft, *et al.*, *Phys. Lett.* **B72**, 144 (1977).
- [5] M. Guidal, M. Laget, M. Vanderhaeghen, *Nucl. Phys.* **A627**, 645 (1997).
- [6] T. Nakano, *Nucl. Phys.* **A721**, 112c (2003).
- [7] R.G.T. Zegers, M. Sumihama, *et al.*, *Phys. Rev. Lett.* **91**, 092001 (2003);  
M. Sumihama, *et al.*, *Phys. Rev.* **C73** 035214 (2006).
- [8] T. Mart and C. Bennhold, ‘Kaon photoproduction in the Feynman and Regge theories,’ arXiv:nucl-th/0412097.
- [9] A.M. Boyarski, F. Bulos, W. Busza, R. Diebold, S.D. Ecklund, G.E. Fischer, Y. Murata, J.R. Rees, B. Richter, and W.S. C. Williams, *Phys. Rev. Lett.* **22**, 1131 (1969).
- [10] O. Bartalini, *et al.*, *Eur. Phys. J.* **A26**, 399 (2005).
- [11] O. Bartholomy, *et al.*, *Phys. Rev. Lett.* **94**, 012503 (2005).
- [12] K.H. Althoff, *et al.*, *Z. Phys.* **C1**, 327 (1979).
- [13] R. Arndt, W. J. Briscoe, I. I. Strakovsky, R. L. Workman, *Phys. Rev.* **C66**, 055213 (2002);  
<http://gwdac.phys.gwu.edu/>.
- [14] L. Tiator, S. Kamalov, Proceedings of NSTAR2005, nucl-th/0603012;  
D. Drechsel, O. Hanstein, S.S. Kamalov, L. Tiator, *Nucl. Phys.* **A645** 145 (1999);  
<http://www.kph.uni-mainz.de/MAID/maid2007/>.
- [15] S.J. Brodsky, G.R. Farrar, *Phys. Rev. Lett.* **31**, 1153 (1973).
- [16] L.O. Abrahamian, *et al.*, *Phys. Lett.* **B48**, 463 (1974).
- [17] P.J. Bussey, *et al.*, *Nucl. Phys.* **B154**, 492 (1979).
- [18] P.J. Bussey, *et al.*, *Nucl. Phys.* **B104**, 253 (1976).
- [19] J. Alspector, *et al.*, *Phys. Rev. Lett.* **28**, 140. (1972)
- [20] T. Sato, T.-S. H. Lee, *Phys. Rev.* **C54**, 2660 (1996);  
T. Sato, T.-S. H. Lee, *Phys. Rev.* **C63**, 055201 (2001).

# BARYON SPECTROSCOPY WITH INELASTIC CHANNELS

*A. Starostin<sup>1</sup> and S. Prakhov*

Department of Physics and Astronomy  
University of California, Los Angeles  
Los Angeles, CA 90095-1547, USA

## Abstract

Many properties of QCD in the non-perturbative regime remain unknown. Baryon spectroscopy plays a vital role in understanding the confinement mechanism and origin of mass. Two series of successful experiments in the area of baryon spectroscopy have been conducted with the Crystal Ball detector with the pion and kaon beams of Brookhaven AGS. New high accuracy total and differential cross sections as well as hyperon polarizations are presented for the reactions  $K^-p \rightarrow \pi^0\Sigma$ ,  $K^-p \rightarrow \pi^0\Lambda$ , and  $K^-p \rightarrow \bar{K}^0n$ . The Crystal Ball program continues at the upgraded Mainz Microtron, which provides a high intensity beam of linearly and circularly polarized real photons up to the maximum energy of 1.5 GeV. Some preliminary MAMI-C results are shown.

## 1 Introduction

While QCD gives a good description of the strong interactions at short distances in the asymptotic region [1], processes in the non-perturbative regime cannot be analytically calculated due to the strong increase of the running coupling constant at large distances. For example, it is still insufficiently understood how the asymptotically observed hadrons, including their rich resonance spectrum, are created from QCD dynamics [2]. This is one of the reasons why one makes use of phenomenological, QCD-inspired, approaches to the description of hadron interaction at low and intermediate energies. The accurate experimental determination of the resonance parameters is a vital factor in our understanding of the nature of hadrons. Among the least studied is the hyperon sector [3]. Kaon beams are not readily available and there are experimental difficulties in detecting the complex decays of the  $\Lambda^*$

---

<sup>1</sup>E-mail:starost@ucla.edu

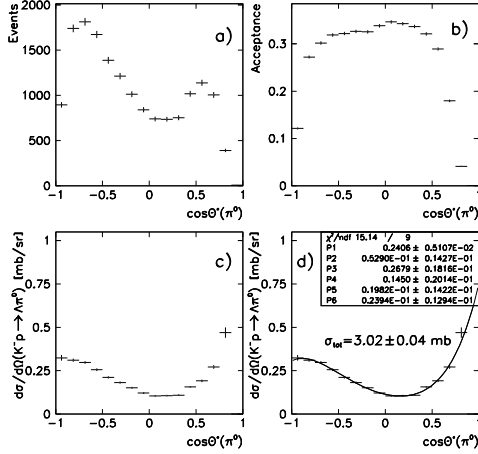


Figure 1: Angular distributions of the  $\Lambda$  in the center-of-mass for the reaction  $K^-p \rightarrow \pi^0\Lambda$  at a beam momentum of 714 MeV/c. (a) event distribution as measured, (b) acceptance, (c) differential cross section, (d) Legendre polynomial fit to our data and the resulting total cross section.

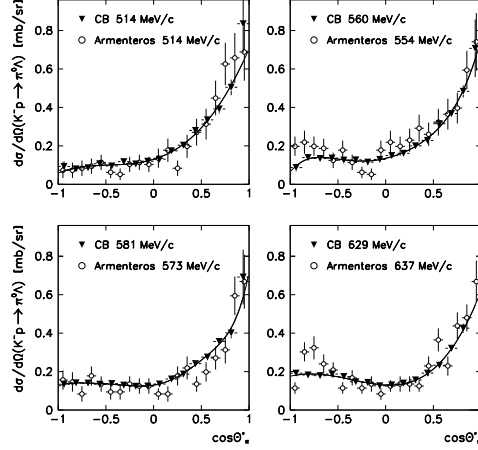


Figure 2: The CB differential cross sections for  $K^-p \rightarrow \pi^0\Lambda$  compared to the results by Armenteros [5].

and  $\Sigma^*$ . Most of the existing hyperon data come from old bubble chamber experiments (see Refs [4, 5], for example) and suffer from statistical limitations.

The last experiment studying excited  $\Lambda^*$  and  $\Sigma^*$  was conducted at Brookhaven National Laboratory (BNL). The experiment utilized the Crystal Ball multiphoton spectrometer installed at a secondary beam line of the Alternative Gradient Synchrotron (AGS). The details of the experimental setup as well as the analysis technique are described in Refs. [6–9]. Here we present new results on the total and the differential cross sections for  $K^-p \rightarrow \pi^0\Sigma$ ,  $K^-p \rightarrow \pi^0\Lambda$ , and  $K^-p \rightarrow \bar{K}^0 n$ . We have also measured the polarization of the hyperon in the reactions  $K^-p \rightarrow \pi^0\Sigma$ ,  $K^-p \rightarrow \pi^0\Lambda$ .

## 2 Kaon induced reactions

The candidates for reactions  $K^-p \rightarrow \pi^0\Lambda$  and  $K^-p \rightarrow \bar{K}^0n$  were selected from the four- and five-cluster events. For the four-cluster events it was assumed that all clusters originate from photons and the neutron is the missing particle. The five-cluster events were analyzed as if the neutron was detected in the Ball. The events were fitted to the hypotheses  $K^-p \rightarrow K_S^0 \rightarrow 2\pi^0n \rightarrow 4\gamma n$  and  $K^-p \rightarrow \pi^0\Lambda \rightarrow 2\pi^0n \rightarrow 4\gamma n$  for all possible permutations of four photons, or four photons and a neutron. The  $z$  coordinate of the interaction vertex and the decay length of the  $\Lambda$  and the  $K_S^0$  were the free parameters of the fit. The combination with the largest confidence level (CL) was used to reconstruct the kinematics of the reactions assuming that the CL is larger than 5%. In some cases an event satisfies both hypothesis. Such event was used only if the CL for one of the reaction exceeded the CL for the another reaction by a factor of two. This procedure allowed to decrease the background from misidentification to less than 4%, while retaining the optimum number of good event candidates. Figure 1 shows the intermediate steps and the final differential cross section for the  $K^-p \rightarrow \pi^0\Lambda$  at the kaon beam momenta of 714 MeV/c. For the cross section calculations we used the PDG branching ratio of  $BR(\Lambda \rightarrow \pi^0n) = 0.358 \pm 0.005$  and  $BR(K_S^0 \rightarrow \pi^0\pi^0) = 0.3139 \pm 0.0028$  [10]. The examples of the resulting differential cross sections for the reactions  $K^-p \rightarrow \pi^0\Lambda$  and  $K^-p \rightarrow \bar{K}^0n$  are shown in Figs. 2 and 3. The systematical uncertainty of about 7% comes from the uncertainty in the number of kaons in the beam and from the uncertainty in the fraction of good events lost due to pile-up in the CB. The systematical uncertainty is not shown on Figs 2, 3, and 5. The details of the data analysis are given in Ref. [11]. The polarization of the  $\Lambda$  was measured via its decay asymmetry as described in Ref. [5]. Examples of our results for the  $\Lambda$  polarization multiplied by the differential cross section of  $K^-p \rightarrow \pi^0\Lambda$  are shown in Fig. 4 in comparison with the results from Ref. [5].

The candidates for the reaction  $K^-p \rightarrow \pi^0\Sigma$  were selected from five-cluster (photons only) and six-cluster (photons and the neutron) events. All possible permutations were examined with the  $K^-p \rightarrow \pi^0\Sigma^0 \rightarrow \pi^0\gamma\Lambda \rightarrow 2\pi^0\gamma n \rightarrow 5\gamma n$  hypothesis. The events with at least one combination satisfying the hypothesis at 5% CL were accepted. Some examples of the  $K^-p \rightarrow \pi^0\Sigma$  differential cross sections and the  $\Sigma$  polarization are shown on Figs. 5 and 6.

While demonstrating superior quality the Crystal Ball data agrees with the existing data for the reactions  $K^-p \rightarrow \pi^0\Lambda$  and  $K^-p \rightarrow \bar{K}^0n$ . The discrepancy between the CB and the existing data for the differential cross

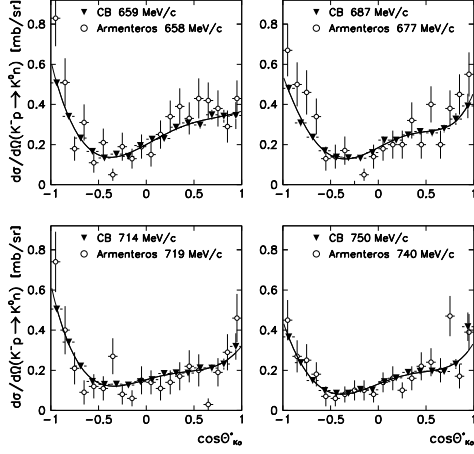


Figure 3: The CB differential cross sections for  $K^-p \rightarrow \bar{K}^0 n$  compared to the results by Armenteros [5].

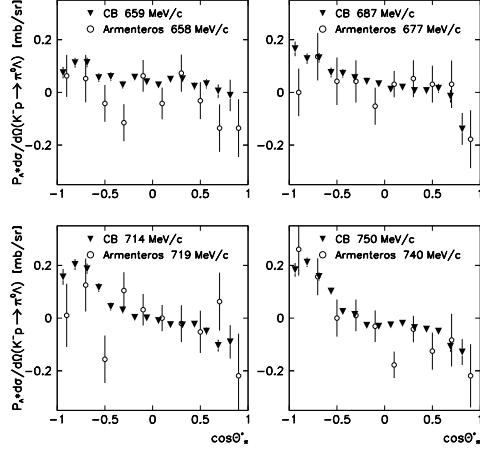


Figure 4: The product of the  $\Lambda$  polarization and the differential cross section for  $K^-p \rightarrow \pi^0 \Lambda$ . The CB results are compared to the ones from Ref. [5].

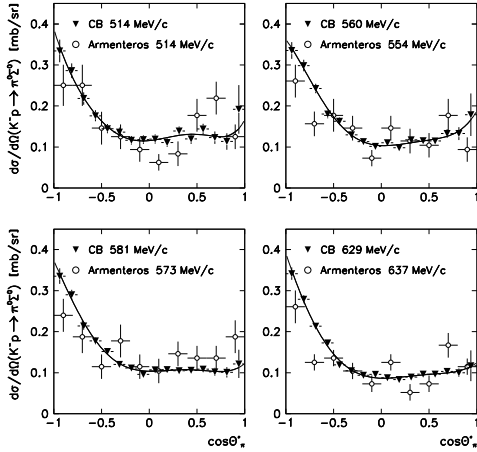


Figure 5: The CB differential cross sections for  $K^-p \rightarrow \pi^0 \Sigma^0$  compared to the results by Armenteros [5].

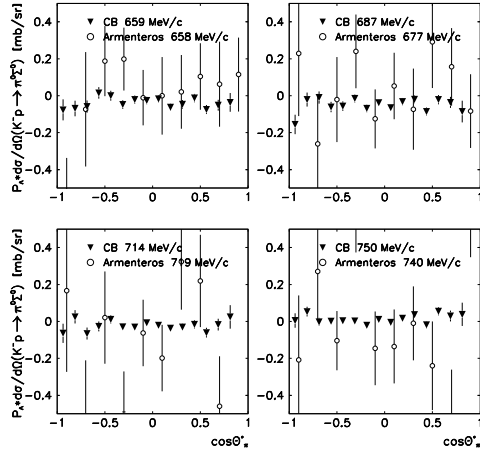


Figure 6: The product of the  $\Sigma^0$  polarization and the differential cross section for  $K^-p \rightarrow \pi^0 \Sigma^0$ . The CB results are compared to the ones from Ref. [5].

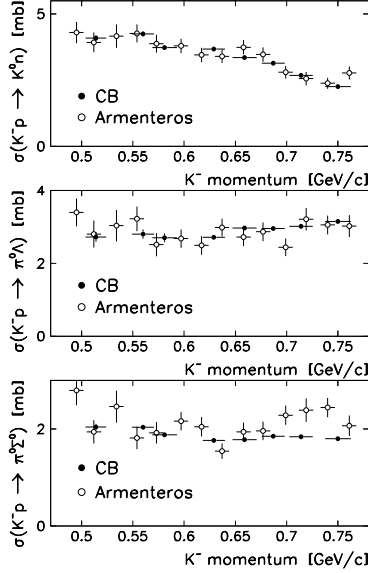


Figure 7: The CB results for the total cross section of reactions  $K^-p \rightarrow \bar{K}^0 n$ ,  $K^-p \rightarrow \pi^0 \Lambda$  and  $K^-p \rightarrow \pi^0 \Sigma^0$  at different beam momenta compared to Armenteros [5].

sections  $K^-p \rightarrow \pi^0 \Sigma^0$  can be due to the difficulties in detecting a  $\Sigma^0$  directly in a bubble chamber. It can lead to undersubtraction of the  $\pi^0 \Lambda$  and especially the  $\pi^0 \pi^0 \Lambda$  backgrounds. A similar discrepancy is observed in the total cross sections of the reaction  $K^-p \rightarrow \pi^0 \Sigma^0$  for the different beam momenta with the corresponding results by Armenteros [5]. This comparison is given in Fig. 7 for all three reactions. The agreement between the total cross sections of the CB and of Armenteros [5] for the two other reactions is good. The measured total cross section do not indicate any significant structures from particular resonances. The resonances in this energy region are  $\Lambda(1600)_{\frac{1}{2}}^+$ ,  $\Lambda(1670)_{\frac{1}{2}}^-$ ,  $\Lambda(1690)_{\frac{3}{2}}^-$ ,  $\Sigma(1580)_{\frac{3}{2}}^-$ ,  $\Sigma(1620)_{\frac{1}{2}}^-$ ,  $\Sigma(1660)_{\frac{1}{2}}^+$ , and  $\Sigma(1670)_{\frac{3}{2}}^-$ . A more sophisticated partial-wave analysis is needed in order to extract the resonance parameters from the data.

### 3 Photoproduction of light mesons

A new experimental program studying light-meson photoproduction is under way at the Mainz Microtron Facility. Recently the MAMI microtron was upgraded to 1.508 GeV giving access to  $\sqrt{s}$  up to 1.93 GeV. The scope of the physics topics is broad and includes: (i) measurement of the in-medium  $\omega$  mass; (ii) tests of Chiral Perturbation Theory and  $C$  and  $CP$  invariance in  $\eta$  decays; (iii) tests of Chiral Perturbation Theory and  $C$  invariance in  $\eta'$

decays; (iv) study of the reaction  $\gamma p \rightarrow \eta \gamma' p$  and the magnetic moment of the  $S_{11}^+(1535)$  resonance; (v) measurement of the polarization of the recoil nucleon in photoproduction; (vi) measurement of the photon asymmetry of the  $^{16}\text{O}(\gamma, pp)$  reaction for photons energies up to 400 MeV; (vii) determination of the helicity dependence of meson photoproduction off the proton; (viii) measurement of the  $G$  asymmetry in  $\gamma p \rightarrow p\pi^0$  and  $\gamma p \rightarrow n\pi^+$ ; (ix) determination of the helicity dependence of single and double pion photoproduction processes and the GDH integral on the neutron; (x) photoproduction of the  $\eta$ -meson on the neutron including the angular distributions and the double polarization observable  $E$ ; (xi) photoproduction of neutral pseudoscalar mesons on the neutron; (xii) measurement of the polarization observables in coherent  $\pi^0$  photoproduction off deuterium; (xiii)  $K^0\Sigma^+$  photoproduction.

The experimental setup includes the Crystal Ball detector with the TAPS spectrometer used as a forward wall. The central tracker located inside the Crystal Ball cavity consists of two layers of the cylindrical wire chamber surrounded by the particle identification detector (PID). The PID is a barrel made of 24 plastic strips. The beam photons are tagged in the upgraded Glasgow–Mainz tagger, which allows the determination of the beam photon energy with a typical accuracy of  $\pm 2$  MeV. A separate tagger ladder with fine segmentation called microscope can be used to improve the energy resolution to about  $\pm 0.5$  MeV.

The first MAMI-C run with real photons took place in March 2007. By October 2007 about 700 hours of data has been collected. One goal of the first months of running was to collect sufficient statistics for the experiments studying the decays of  $\eta$  and  $\eta'$ . Figure 8 shows the invariant mass of two photons in  $\gamma p \rightarrow \gamma\gamma p$  obtained with the MAMI-C photon beam. The two peaks correspond to the  $\pi^0 \rightarrow \gamma\gamma$  and  $\eta \rightarrow \gamma\gamma$  decays. The resolution for the  $\eta$  peak is about 5%. Figure 9 shows the invariant mass of  $\pi^0\gamma$ ; the peak is from  $\omega \rightarrow \pi^0\gamma$  and the background under the peak is from the  $\gamma p \rightarrow \pi^0\pi^0 p$  reaction.

One of the major goals of the first stage of the MAMI-C experiment is to collect the world largest samples of  $\eta$  and  $\eta'$ . The  $\eta$  sample will be used to calculate with high precision the slope parameter  $\alpha$  of the  $\eta \rightarrow 3\pi^0$  Dalitz plot [9] and the branching ratio and the matrix element of the  $\eta \rightarrow \pi^0\gamma\gamma$  decay [6]. Both measurements will be used to test the Chiral Perturbation Theory predictions. The sample of  $\eta'$  events will allow an investigation of the  $\eta' \rightarrow \eta\pi^0\pi^0$  and  $\eta' \rightarrow 3\pi^0$  Dalitz plots [12]. Those distributions carry information on the  $\pi\pi$  and  $\eta\pi$  interactions and potentially can be used to measure the  $\pi\pi$  scattering length [13].

The invariant mass of  $\pi^0\pi^0\pi^0$  is shown on Fig. 10. The resolution of the peak is about 5 MeV after the fit to the  $\gamma p \rightarrow 3\pi^0 p$  hypothesis. The

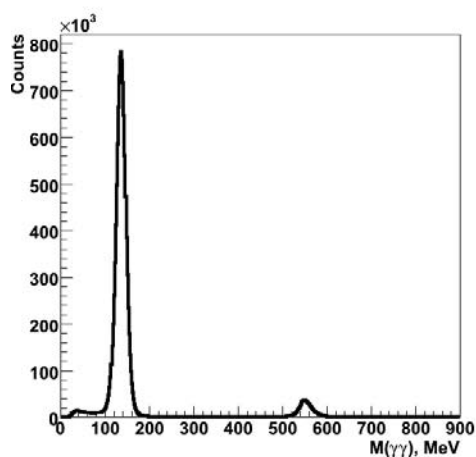


Figure 8: The invariant mass of two photons in  $\gamma p \rightarrow \gamma\gamma p$  obtained with the MAMI-C photon beam. The two peaks correspond to the  $\pi^0 \rightarrow \gamma\gamma$  and  $\eta \rightarrow \gamma\gamma$  decays. The resolution for the  $\eta$  peak is about 5%.

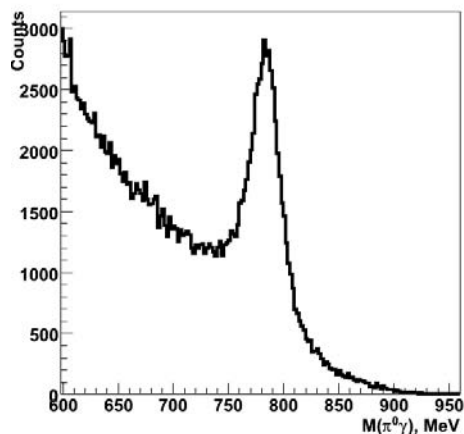


Figure 9: The invariant mass of  $\pi^0\gamma$ ; the peak is from the  $\omega \rightarrow \pi^0\gamma$  and the background under the peak is from  $\pi^0\pi^0$  production.

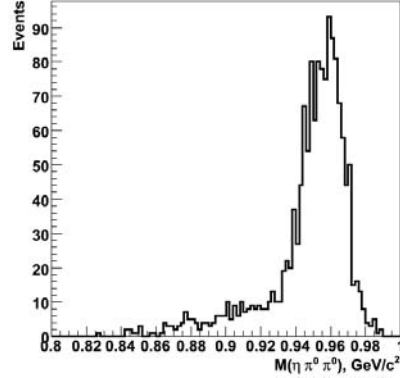
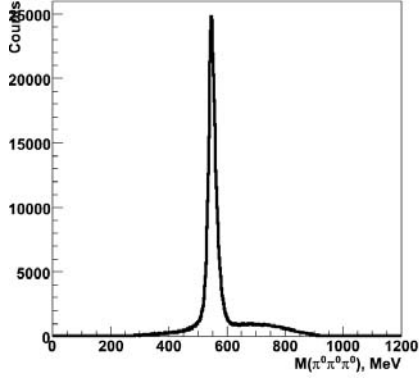


Figure 10: The invariant mass of  $3\pi^0$  in  $\gamma p \rightarrow 3\pi^0 p$  obtained at the MAMI-C. The peak is from the  $\eta \rightarrow 3\pi^0$  decay. The resolution for the  $\eta$  peak is about 5 MeV after the fit. The background under the peak is from the direct production of  $3\pi^0$ 's.

Figure 11: The invariant mass of  $\eta\pi^0\pi^0$ ; the peak is from the  $\eta' \rightarrow \eta\pi^0\pi^0$  decay.

background under the peak is from the direct production of the three  $\pi^0$ 's via the cascade decay of the resonances. The experimental acceptance for the reaction is about 40% detecting all six photons and the proton. The total number of about  $5 \times 10^6$  reconstructed  $\eta \rightarrow 3\pi^0$  events is already collected in the experiment. Currently this is a world largest sample of such events.

The invariant mass of  $\eta\pi^0\pi^0$  is shown on Fig. 11. The data shown here represent about 20% of the available statistics. The largest world sample of about 5000 events was collected by the GAMS2000 collaboration [12], therefore our sample is already comparable to the GAMS2000. The background under the peak comes from the direct production of  $3\pi^0$ . Figure 13 shows the Dalitz plot of the  $\eta' \rightarrow \eta\pi^0\pi^0$  decays. The Dalitz plot is uniform as expected.

Another important reaction to study is  $\gamma p \rightarrow \pi^0\pi^0 p$ . This process is one of the dominant ones in the MAMI-C energy range and carries valuable information about dynamics of  $\pi\pi$  and  $\pi N$  interaction. An example of the Dalitz plot for the reaction is shown on Fig.12. The structure of the Dalitz plot is significantly different from the similar distribution obtained in  $\pi^- p \rightarrow \pi^0\pi^0 n$  [7]. Finally Fig. 14 shows the first attempt to calculate the total cross section of the  $\gamma p \rightarrow \pi^0 p$  reaction for the photon beam energies from 600 MeV to 1500 MeV. The Crystal Ball results are compared to the data obtained

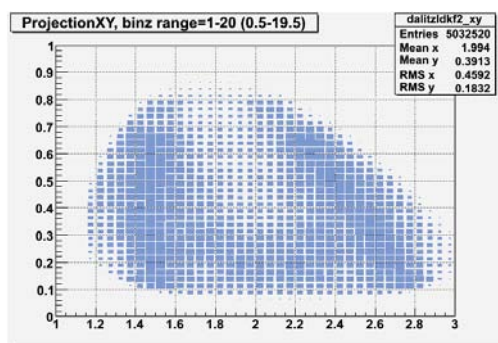


Figure 12: Dalitz plot distribution for the reaction  $\gamma p \rightarrow \pi^0 \pi^0 p$ . Each event has two entries. The structure of the Dalitz plot is significantly different from the similar distribution in  $\pi^- p \rightarrow \pi^0 \pi^0 n$  [7].

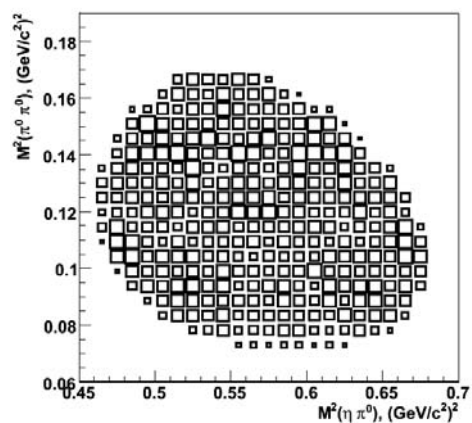


Figure 13: Dalitz plot distribution for the decay  $\eta' \rightarrow \eta \pi^0 \pi^0$ . The total number of events is about 1100. Each event has two entries because of the two identical  $\pi^0$ . The sample represent about 20% of the available statistics.

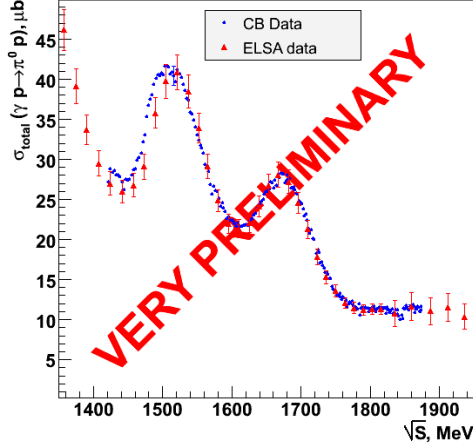


Figure 14: Preliminary results for the total cross section of  $\gamma p \rightarrow \pi^0 p$  in the MAMI-C beam energy range obtained during the first round of the experiment. The Crystal Ball cross sections is normalized to the ELSA data at  $\sqrt{s} = 1.5$  GeV.

with the Crystal Barrel/TAPS setup at ELSA. The Crystal Ball data are normalized to the ELSA results at  $\sqrt{s} = 1.5$  GeV. The Crystal Ball results show superior quality of the data in statistical accuracy and the beam energy resolution. The high beam intensity and good energy resolution of the tagger allows a detailed investigation of the total cross section with the energy step of about 4 MeV. The energy resolution could be further improved by using the tagger microscope.

## 4 Summary

In summary, the Crystal Ball detector is a universal instrument, which makes possible precise measurements of multi-photon neutral states. The detector was successfully used with pion and kaon beams and in this paper we present the new high statistics, low-systematics measurement of the three kaon induced reactions:  $K^- p \rightarrow \pi^0 \Sigma$ ,  $K^- p \rightarrow \pi^0 \Lambda$ , and  $K^- p \rightarrow \bar{K}^0 n$ . Besides the differential and total cross section we have measurement the polarization of the recoil hyperon for the reactions  $K^- p \rightarrow \pi^0 \Sigma$  and  $K^- p \rightarrow \pi^0 \Lambda$ . While of superior quality, the new data shows reasonable agreement with existing measurements. A complete partial-wave analysis is needed to extract the parameters of the  $\Lambda^*$  ( $\Lambda(1600)_{\frac{1}{2}}^+$ ,  $\Lambda(1670)_{\frac{1}{2}}^-$ ,  $\Lambda(1690)_{\frac{3}{2}}^-$ ) and  $\Sigma^*$  ( $\Sigma(1580)_{\frac{3}{2}}^-$ ,  $\Sigma(1620)_{\frac{1}{2}}^-$ ,  $\Sigma(1660)_{\frac{1}{2}}^+$ ,  $\Sigma(1670)_{\frac{3}{2}}^-$ ) from the data.

The experiments with the Crystal Ball are continued at Mainz Microtron. In early 2007 we have started the new series of measurements with the upgraded MAMI-C machine which provides the high intensity high resolution beam of real photons with the maximum energy up to 1.5 GeV. The prelim-

inary MAMI-C results indicate early success of the program.

## References

- [1] G. Altarelli, *Ann. Rev. Nucl. Part. Sci.* **39** (1989) 357.
- [2] D. J. Gross, *Nucl. Phys. Proc. Suppl.* **74** (1999) 426.
- [3] B. M. K. Nefkens, "Concluding Comments" talk in this proceeding.
- [4] T. Dombeck *et al.*, *Phys. Rev. D* **7** (1973) 1331.
- [5] R. Armenteros *et al.*, *Nucl. Phys.* **B21** (1970) 15.
- [6] S. Prakhov *et al.* *Phys. Rev. C* **72** (2005) 025201.
- [7] S. Prakhov *et al.* *Phys. Rev. C* **69** (2004) 045202.
- [8] A. Starostin *et al.* *Phys. Rev. C* **64** (2001) 55205.
- [9] W. B. Tippens *et al.* *Phys. Rev. Lett.* **87** (2001) 193001.
- [10] W-M Yoa *et al.*, *J. Phys. G* **33** (2006) 1.
- [11] S. Prakhov, Crystal Ball report CB-05-002 at <http://bmkn8.physics.ucla.edu/Crystalball/Docs/documentation.html>.
- [12] D. Alde *et al.*, *Phys. Lett. B* **177** (1986) 115; D. Alde *et al.*, *Z. Phys. C* **36** (1987) 603.
- [13] N. Cabibbo, *Phys. Rev. Lett.* **93** (2004) 121801.

# CHARGED PION PHOTOPRODUCTION AND SCALING

*H. Gao*<sup>1</sup>

Department of Physics and Triangle Universities Nuclear Laboratory  
Duke University  
Durham, NC 27516, U.S.A.

## Abstract

The  $\gamma n \rightarrow \pi^- p$  and  $\gamma p \rightarrow \pi^+ n$  reactions are essential probes of the transition from meson-nucleon degrees of freedom to quark-gluon degrees of freedom in exclusive processes. The cross sections of these processes are also advantageous, for the investigation of oscillatory behavior around the quark counting rule prediction, since they decrease relatively slower with energy compared with other photon-induced processes. In this talk, we discuss recent results on the  $\gamma p \rightarrow \pi^+ n$  and  $\gamma n \rightarrow \pi^- p$  processes from Jefferson Lab experiment E94-104. We also discuss the CLAS g10 analysis on the  $\gamma n \rightarrow \pi^- p$  process.

## 1 Introduction

The interplay between the nucleonic and partonic pictures of the strong interaction represents one of the major issues in contemporary nuclear physics. Although standard nuclear models are successful in describing the interactions between hadrons at large distances, and Quantum Chromodynamics (QCD) accounts well for the quark interactions at short distances, the physics connecting the two regimes remains unclear. In fact, the classical nucleonic description must break down once the probing distances become comparable to those separating the quarks. The challenge is to study this transition region by looking for the onset of some experimentally accessible phenomena naturally predicted by perturbative QCD (pQCD).

The simplest is the constituent counting rule (CCR) for high energy exclusive reactions [1] at fixed center-of-mass angles, in which  $d\sigma/dt \propto s^{-n+2}$ , with  $n$  the total number of point-like particles and gauge fields in the initial plus final states. Here  $s$  and  $t$  are the invariant Mandelstam variables for the total energy squared and the four-momentum transfer squared, respectively.

---

<sup>1</sup>Science Drive, Box 90308, Durham, NC 27516, U.S.A.

Many exclusive reactions [2] at high energy and large momentum transfer appear to obey the CCR and in recent years, a similar trend, i.e. global scaling behavior, has been observed in deuteron photo-disintegration experiments [3] - [6] at a surprisingly low transverse momentum value of  $\sim 1.1$  (GeV/c)<sup>2</sup>.

The same dimensional analysis which predicts the quark counting rule also predicts hadron helicity conservation for exclusive processes at high energy and large momentum transfers. However, polarization measurements on deuteron photo-disintegration [7], recently carried out in Hall A at Jefferson Lab (JLab), show disagreement with hadron helicity conservation in the same kinematic region where the quark counting behavior is apparently observed. These paradoxes make it essential to understand the exact mechanism governing the early onset of scaling behavior. Towards this goal, it is important to look closely at claims of agreement between the differential cross section data and the quark counting prediction. Historically, the elastic proton-proton ( $pp$ ) scattering at high energy and large momentum transfer has played a very important role. In fact, the re-scaled 90° center-of-mass  $pp$  elastic scattering data,  $s^{10} \frac{d\sigma}{dt}$  show substantial oscillations about the power law behavior. Oscillations are not restricted to the  $pp$  sector; they are also seen in  $\pi p$  fixed angle scattering [8].

Recently, a number of new developments have generated renewed interest in this topic. Zhao and Close [9] have argued that a breakdown in the locality of quark-hadron duality results in oscillations around the scaling curves predicted by the counting rule. They explain that the smooth behavior of the scaling laws arises due to destructive interference between various intermediate resonance states in exclusive processes at high energies. However, at lower energies this cancellation due to destructive interference breaks down locally and gives rise to oscillations about the smooth behavior. On the other hand, Ji *et al.* [10] have derived a generalized counting rule based on a pQCD inspired model, by systematically enumerating the Fock components of a hadronic light-cone wave function. Their generalized counting rule for hard exclusive processes include parton orbital angular momentum and hadron helicity flip, thus they provide the scaling behavior of the helicity flipping amplitudes. The interference between the different helicity flip and non-flip amplitudes offers a new mechanism to explain the oscillations in the scaled cross-sections. The counting rule for hard exclusive processes has also been shown to arise from the correspondence between the anti-de Sitter space and the conformal field theory [11], the so-called string/gauge duality. Brodsky *et al.* [12] have used this anti-de Sitter/Conformal Field Theory correspondence or string/gauge duality to compute the hadronic light front wave functions. This yields an equivalent generalized counting rule without

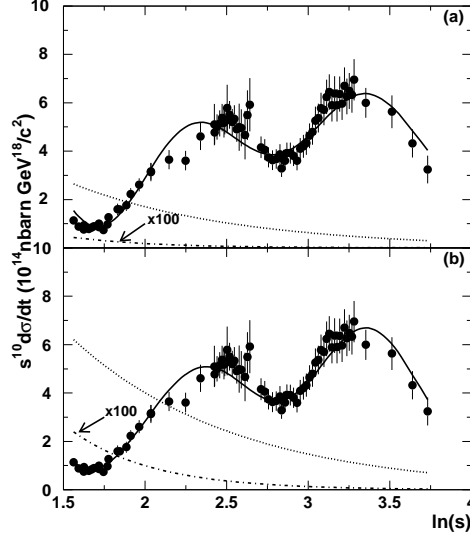


Figure 1: (a) The fit to  $pp$  scattering data at  $\theta_{cm} = 90^\circ$  when helicity flip amplitudes are included as described in [13]. The parameters for the energy dependent phase was kept same as the earlier fit of Ralston and Pire [14]. The solid line is the fit result, the dotted line is contribution from the helicity flip term  $\sim s^{-11}$ , the dot-dashed line is contribution from the helicity flip term  $\sim s^{-12}$ . The  $\sim s^{-12}$  contribution has been multiplied by 100 for display purposes. (b) The same data fitted to the form described in [13] but with the new more general parametrization of the Landshoff amplitude.

the use of a perturbative theory.

Recently, it has been shown [13] that the generalized counting rule of Ji *et al.* [10] along with the Landshoff terms and associated interferences does a better job of describing the oscillations about the quark counting rule, in the  $pp$  elastic scattering data at  $\theta_{cm} = 90^\circ$ . Fig 1 shows the results of such a fit and also shows the explicit contributions from the  $s^{-11}$  and  $s^{-12}$  terms due to the helicity-flipping amplitudes in this approach. The value of  $\Lambda_{QCD}$  was fixed at 100 MeV in the fit. This new fit is in much better agreement with the data. This is specially true in the low energy region ( $s < 10 \text{ GeV}^2$ ). The helicity flip amplitudes (mostly the term  $\sim s^{-4.5}$ ) are significant at low energies and seem to help in describing the data at low energies. The contributions from helicity flipping amplitudes which are related to quark orbital angular momentum, seem to play an important role at these low energies, which is reasonable given that the quark orbital

angular momentum is non-negligible compared to the momentum scale of the scattering process. It is interesting to note that among the helicity flip amplitudes the one with the lower angular momentum dominates. Similarly the spin-correlation  $A_{NN}$  [15] in polarized  $pp$  elastic scattering data can be better described [13] by including the helicity flipping amplitude along with the Landshoff amplitude and their interference.

Exclusive  $\gamma N \rightarrow \pi N$  processes are essential probes to study the transition from meson-nucleon degrees of freedom to quark-gluon degrees of freedom. The cross sections of these processes are also advantageous, for investigation of the possible oscillatory behavior around the quark counting prediction, since they decrease relatively slower with energy compared with other photon-induced processes. For the  $\gamma n \rightarrow \pi^- p$  process, no cross section data exist above a photon energy of 2.0 GeV prior to the recent Jefferson Lab experiment E94-104 [16].

## 2 Jefferson Lab Experiment E94-104

Experiment E94-104 was carried out in Hall A [17] at the Thomas Jefferson National Accelerator Facility (JLab). The continuous electron beam, at a current around 30  $\mu\text{A}$  and energies from 1.1 to 5.5 GeV, impinged on a 6% copper radiator and generated an untagged bremsstrahlung photon beam. The production data were taken with the 15 cm cryogenic liquid hydrogen (LH2) target for singles  $p(\gamma, \pi^+)n$  measurement, and with the liquid deuterium (LD2) target for coincidence  $d(\gamma, \pi^-p)p$  measurement. The two High Resolution Spectrometers (HRS) in Hall A were used to detect the outgoing pions and recoil protons. Two new aerogel Čerenkov detectors in the left spectrometer were constructed for this experiment to provide particle identification for positive particles, mainly pions and protons, since the time-of-flight technique fails at high momentum. Details of the Hall A spectrometers can be found [17].

Based on two-body kinematics, the incident photon energy was reconstructed from final states, i.e. the momentum and angle of the  $\pi^+$  in the singles measurement, momenta and angles of the  $\pi^-$  and  $p$  in the coincidence measurement. A 100 MeV bin with the center of the bin 75 MeV from the beam energy, was chosen for the data analysis, where the multi-pion contribution was negligible. The data after background subtraction, with cuts on trigger type, coincidence timing, PID (particle identification), acceptance and photon energy, were compared to a modified Monte Carlo simulation code for this experiment based on MCEEP [18] with the same cuts on acceptance and photon energy. The raw cross section was extracted by comparing

data and simulation. The distributions of acceptance, reconstructed momentum and photon energy were in good agreement with results obtained from simulations. Details on the simulation and the bremsstrahlung photon flux calculation can be found [19].

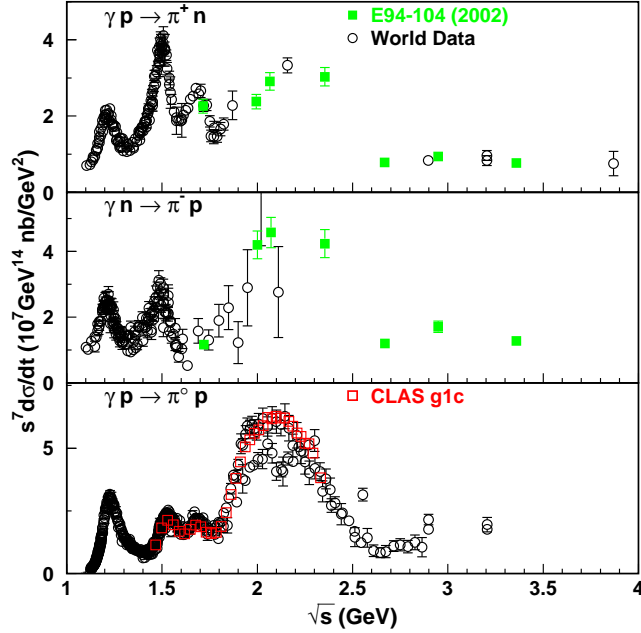


Figure 2: Scaled differential cross-section  $s^7 \frac{d\sigma}{dt}$  as a function of center-of-mass energy  $\sqrt{s}$  for a pion center-of-mass angles of  $90^\circ$ . The upper panel is for the  $\gamma p \rightarrow \pi^+ n$  process, the middle panel is for the  $\gamma n \rightarrow \pi^- p$  process, and the lower panel is for the  $\gamma p \rightarrow \pi^0 p$  process. The green solid squares are results from [16], and results from Dugger *et al.* [20] on the neutral pion production are shown as red open squares. All other world data [22] are shown as black open circles.

The new results from E94-104 on  $\gamma n \rightarrow \pi^- p$  greatly extend the existing measurements and exhibit, for the first time, a global scaling behavior at high energy for this reaction at  $90^\circ$ . The scaling behavior in  $\pi^-$  production is similar to that in  $\pi^+$  production. Results from experiment E94-104 also show dramatic change in the scaled differential cross-section from the  $\gamma n \rightarrow \pi^- p$  and  $\gamma p \rightarrow \pi^+ n$  processes in the center of mass energy between 1.8 GeV to about 2.4 GeV and a new resonance structure has been suggested by the data around 2.1 GeV at a pion center-of-mass angle of  $90^\circ$ . Fig. 2 shows the scaled differential cross-section  $s^7 \frac{d\sigma}{dt}$  as a function of center-of-mass energy  $\sqrt{s}$  for a pion center-of-mass angles of  $90^\circ$  for three different channels.

The upper panel is for the  $\gamma p \rightarrow \pi^+ n$  process, the middle panel is for the  $\gamma n \rightarrow \pi^- p$  process, and the lower panel is for the  $\gamma p \rightarrow \pi^0 p$  process. The green solid squares are results from [16], the red open squares are results from Dugger *et al.* [20] on neutral pion production. In both the  $\gamma p \rightarrow \pi^+ n$  and the  $\gamma p \rightarrow \pi^0 p$  channel, one sees clearly the  $\Delta$  resonance, the N(1500) and the N(1700) nucleon resonances. In the  $\gamma n \rightarrow \pi^- p$  channel, while one also sees the  $\Delta$  resonance and the N(1500) resonance, the existing data do not allow for a definitive statement about the N(1700) resonance in the scaled differential cross-section. There are two distinct features shown in the data for all three channels: broad resonance structure around a center-of-mass energy of 2.1 GeV, and a drastic fall-off of the differential cross-section in a narrow energy window of about 300 MeV. The second feature was first suggested by Jefferson Lab experiment E94-104 [16] (shown as green solid squares), and the  $\pi^- p$  total scattering cross section data [21]. This has now been established by preliminary results from g10 on the  $\gamma n \rightarrow \pi^- p$  which we will discuss next. The error bars for E94-104 include both statistical and systematic uncertainties, and neutral pion data [20] show only statistical uncertainties. All other world data are collected from Ref. [22] and are shown as black open circles.

The observed enhancement around 2.2 GeV might be related to some unknown baryon resonances. Several baryon resonances are predicted to be in this energy region by the constituent quark model [23], but have not been seen experimentally, i.e. the so called “missing resonances”. There has been some evidence for the N(2070)D<sub>15</sub> resonance both from the  $\pi^0$  [24] and  $\eta^0$  [25] photoproduction off the proton. Recently, a global analysis [26] of charged pion photoproduction based on Regge model has been carried out for photon energies between 3 to 8 GeV where nucleon resonance contributions are expected to be negligible. This allows for the extraction of the non-resonant background which can then be used to make prediction for photon energies below 3 GeV. The deviation between the data and the prediction can then be interpreted as possible signatures for excited baryon resonances, particularly in the case of polarization observables and differential cross-section in the case of  $\pi^-$  photoproduction from the neutron.

The observed enhancement might be associated with the strangeness production threshold [27,28]. They could also be related to the  $\phi$ -N bound state which has been predicted recently [29,30]. The sudden drop in the scaled differential cross-section may shed light on the transition between the aforementioned physical pictures. To test the onset of the scaling behavior in charged photopion production process, and to understand the enhancement and the dramatic drop aforementioned, it is important to investigate the detailed scaling behavior in a center-of-mass energy of 1.8 GeV to 2.5 GeV

in very fine photon energy bins. Recently, we have carried out a detailed study of the differential cross-section of the  $\gamma n \rightarrow \pi^- p$  process from a high statistics data sample obtained by the Jefferson Lab CLAS detector.

### 3 CLAS g10 analysis of the $\gamma n \rightarrow \pi^- p$ process

The experiment was carried out at the Thomas Jefferson National Accelerator Facility (Jefferson Lab) in Hall B with the CEBAF Large Acceptance Spectrometer (CLAS) [31]. The CLAS detector was designed to provide near  $4\pi$  coverage of charged particles. Details about the CLAS can be found in Ref. [31]. For the CLAS g10 experiment [32], a 24 cm long liquid deuterium target was employed with the target cell positioned 25 cm upstream from the CLAS nominal center. A tagged photon beam was used which was generated by an electron beam with an incident beam energy of 3.8 GeV, corresponding to a maximum  $\sqrt{s}$  of 2.8 GeV for the process of interest. The event trigger required at least two charged particles in different sectors. Two magnetic field settings were used during the experiment corresponding to a low-field setting (with torus current  $I=2250$  A) and a high field setting ( $I=3375$  A) which provided different angular coverage and momentum resolution. About 10 billion triggers were collected during the g10 running period of two months. The results from high field settings are consistent with those from the low field setting within systematic uncertainties.

The raw data collected from the experiment were first processed to calibrate and convert the information from the detector subsystem to physical variables such as energy, momentum, position and timing. This process generated about 40 Tera-bytes data. For the process of interest, the  $\gamma n \rightarrow \pi^- p$  quasifree process from the deuteron, only events with one proton and one  $\pi^-$  were selected. The vertex times of both proton and  $\pi^-$  were required to be within 1 ns of the photon vertex time. For this quasifree process detected, only the neutron inside the deuteron was coupled to the photon, and the spectator proton was left intact. The spectator proton is usually moving with a momentum below 200 MeV/c, and is usually not detected by the CLAS. To select this channel from other background channels, the 4-momentum of the spectator proton is reconstructed by energy-momentum conservation. Only events with missing mass around the proton mass were selected to make sure the missing particle was the spectator proton. Further, a missing momentum cut of below 200 MeV/c was used in the analysis to select the quasifree events of  $\gamma n \rightarrow \pi^- p$  from the deuterium target.

Monte Carlo simulations have been carried out to determine the acceptance and efficiency of the CLAS detector. Many practical factors, such as

the geometry and inefficiencies of the detectors, result in loss of events during the experiment. This has to be recovered by simulations in order to extract cross sections. A virtual CLAS detector (GSIM) was built based on GEANT, which simulates an ideal CLAS detector with all the subsystem working perfectly. Millions of events were generated and passed through the GSIM and then the simulated data were processed to incorporate the subsystem efficiencies and resolutions extracted from the experiment. All the simulated data were then processed by the same softwares used in the real data processing and analysis. The ratio between the events passed the simulation and the generated events is the product of the acceptance and the efficiency of the detector. Since deuteron is used as an effective neutron target in this experiment, the final state interaction (FSI) effects must be taken into account before one extracts cross sections. The FSI correction is estimated according to the Glauber formulation [33] which relates the nuclear transparency to the total cross section of final state particle with nucleons inside the nucleus.

Preliminary CLAS g10 results suggest the approach of the scaling region in the more backward angle kinematics:  $70^\circ$  to  $110^\circ$ . They also confirm the existence of a broad resonance structure around a center-of-mass energy of 2.2 GeV at a pion center-of-mass angle of  $90^\circ$ . The preliminary results also confirm the drastic drop in differential cross-section by a factor of 15 in an energy window of about 300 MeV from 2.2 GeV to 2.5 GeV at  $90^\circ$ . Further, preliminary g10 results show a very interesting angular dependent resonance structure, i.e. the center-of-mass energy location of this resonance structure depends on the pion center-of-mass angle. Detailed analysis of the angular distribution of the data as a function of the center-of-mass energy will be carried out in the near future to better understand the nature of the observed resonance structure.

## Acknowledgments

I thank Bill Briscoe, Wei Chen, Dipankar Dutta, Patrizia Rossi, A. Sibirtsev, Igor Strakovsky, Stepan Stepanyan, and Lingyan Zhu for helpful conversations. This work is supported in part by the U.S. Department of Energy under contract number DE-FG02-03ER41231.

## References

- [1] S.J. Brodsky and G.R. Farrar, Phys. Rev. Lett.**31**, 1153 (1973); Phys. Rev. D **11**, 1309 (1975); V. Matveev *et al.*, Nuovo Cimento Lett. **7**, 719

- (1973);
- [2] R. L. Anderson *et al.*, Phys. Rev. D **14**, 679 (1976); C. White *et al.*, Phys. Rev. D **49**, 58 (1994).
- [3] J. Napolitano *et al.*, Phys. Rev. Lett. **61**, 2530 (1988); S.J. Freedman *et al.*, Phys. Rev. C **48**, 1864 (1993); J.E. Belz *et al.*, Phys. Rev. Lett. **74**, 646 (1995).
- [4] C. Bochna *et al.*, Phys. Rev. Lett. **81**, 4576 (1998).
- [5] E.C. Schulte, *et al.*, Phys. Rev. Lett. **87**, 102302 (2001);
- [6] P. Rossi *et al.*, Phys. Rev. Letts. **94**, 012301 (2005); M. Mirazita *et al.*, Phys. Rev. C **70**, 014005 (2004).
- [7] K. Wijesooriya, *et al.*, Phys. Rev. Lett. **86**, 2975 (2001).
- [8] H. Genzel, P. Joos, and W. Pfeil, Photoproduction of Elementary Particles (Springer-Verlag, Berlin, 1973), Group I Volume 8 of Numerical Data and Functional Relationships in Science and Technology, edited by K.-H. Hellwege.
- [9] Q. Zhao and F. E. Close, Phys. Rev. Lett. **91**, 022004 (2003).
- [10] X. Ji, J.-P. Ma and F. Yuan, Phys. Rev. Lett. **90**, 241601 (2003).
- [11] J. Polchinski and M.J. Strassler, Phys. Rev. Lett. **88**, 031601 (2002); R.C. Brower and C.I. Tan, Nucl. Phys. B **662**, 393 (2003); O. Andreev, Phys. Rev. D **67**, 046001 (2003).
- [12] S. J. Brodsky and G. F. de Teramond, Phys. Lett. **B582**, 211 (2004); S. J. Brodsky, J. R. Hiller, D. S. Hwang and V. A. Karmanov, Phys. Rev. D **69**, 076001 (2004).
- [13] D. Dutta and H. Gao, Phys. Rev. C **71**, 032201(R) (2005).
- [14] J. P. Ralston and B. Pire, Phys Rev. Lett. **49**, 1605 (1982); B. Pire and J. P. Ralston, Phys. Lett. B **117**, 233 (1982).
- [15] G.R. Court *et al.*, Phys. Rev. Lett. **57**, 507 (1986); T.S. Bhatia *et al.*, Phys. Rev. Lett. **49**, 1135 (1982); E.A. Crosbie *et al.*, Phys. Rev. D **23**, 600 (1981).
- [16] L. Y. Zhu *et al.*, Phys. Rev. Lett. **91**, 022003 (2003); L. Y. Zhu *et al.*, Phys Rev. C, **71**, 044603 (2005).

- [17] J. Alcorn *et al.*, Nucl. Instrum. Methods A522, 294 (2004).
- [18] P. Ulmer *et al.*,  
<http://www.physics.odu.edu/~ulmer/mceep/mceep.html>.
- [19] L.Y. Zhu, Ph.D. thesis, February, 2004, Massachusetts Institute of Technology (unpublished).
- [20] M. Dugger *et al.*, Phys. Rev. C **76**, 025211 (2007).
- [21] [http://pdg.lbl.gov/2007/hadronic-xsections/hadronicrpp\\_page13.pdf](http://pdg.lbl.gov/2007/hadronic-xsections/hadronicrpp_page13.pdf).
- [22] The GWU CNS Database, [http://gwdac.phys.gwu.edu/analysis/pr\\_analysis.html](http://gwdac.phys.gwu.edu/analysis/pr_analysis.html)
- [23] S. Capstick, Phys. Rev. D **46**, 2864 (1992); S. Capstick and W. Roberts, Phys. Rev. D **49**, 4570 (1994).
- [24] O. Bartholomy *et al.*, Phys. Rev. Lett **94**, 012003 (2005).
- [25] V. Crede *et al.*, Phys. Rev. Lett **94**, 012004 (2005).
- [26] A. Sibirtsev, J. Haidenbauer, S. Krewald, T.-S.H. Lee, U.-G. Meissner, and A.G. Thomas, Nucl-th/07060183.
- [27] S. J. Brodsky, and G. F. de Teramond, Phys. Rev. Lett. **60**, 1924 (1988).
- [28] S.J. Brodsky, I.A. Schmidt, G.F. de Teramond, Phys. Rev. Lett. **64**, 1011 (1990).
- [29] H. Gao, T.S.-H. Lee, and V. Marinov, Phys. Rev. C **63**, 022201(R) (2001).
- [30] F. Huang, Z.Y. Zhang, and Y.W. Yu, Phys. Rev. C **73**, 025207 (2006).
- [31] B. Mecking and the CLAS Collaboration, The Cebaf Large Acceptance Spectrometer, *Nucl. Instr. & Meth.* **503/3** 513 (2003)
- [32] B. McKinnon, K. Hicks *et al.*, Phys. Rev. Lett. **96**, 212001 (2006); S. Nicolai, M. Mirazita, P. Rossi *et al.*, Phys. Rev. Lett. **97**, 032001 (2006).
- [33] H. Gao, R.J. Holt, and V.R. Pandharipande, Phys. Rev. C **54**,2779 (1996).

# Plenary Session IV

**Session Chair:**

Bing-Son Zou

Decay of Open Charm Hadrons

*M. B. Voloshin*

Charmed Hadrons from B-Decay

*R. Christov*

Hadronic B-Decays

*Walter Toki*

On the Brink of Major Discoveries in Weak Charm Decays

- a Bismarckian Chance to Make History

*Ikaros Bigi*

**Session Chair:**

T. Nakano

Three-Nucleon System Dynamics Studied via d-p Breakup

*St. Kistryn*

Three Nucleon Scattering Experiments from RIKEN

*Kimiko Sekiguchi*

Chiral Effective Theory Calculations of Electron and Photon

Scattering from Light Nuclei

*Daniel R. Phillips*

# HADRONIC B DECAYS INTO NEW CHARMONIUM LIKE STATES

Walter Toki<sup>1</sup>  
Dept. of Physics<sup>2</sup>  
Colorado State University  
Fort Collins, CO 80523  
USA

## Abstract

The new charmonium-like states,  $X(3872)$ ,  $Y(3940)$ , and  $Z^\pm(4430)$ , produced in B meson decays from the Belle and BaBar B-factories are reviewed. These mesons are observed in final states with the  $J/\psi$  or the  $\psi(2S)$ , and they do not fit into the conventional  $q\bar{q}$  meson or charmonium models. They are potential candidates of 4-quark, molecule, or hybrid  $gq\bar{q}$  models.

## 1 Introduction

The evidence for charmonium-like [1] states began with the Belle announcement in the 2003 Lepton and Photon Conference of the discovery [2] of the  $X(3872)$  in the decay  $X(3872) \rightarrow J/\psi\pi^+\pi^-$  in  $B \rightarrow X(3872)K$ . Following confirmations from the CDF, D0, and BaBar collaborations, there has been enormous interest in this state as a non- $q\bar{q}$  or exotic meson. Now more charmonium-like states from the Belle and BaBar B-factories have been discovered. All of these new charmonium-like states do not appear to fit into the conventional  $q\bar{q}$  meson spectroscopy of  $u, d, s, c$  quarks and they are possible candidates for exotic states such as molecules, 4-quark states, hybrids, etc. In this ten page experimental review we discuss the latest results on the new charmonium-like states, the  $X(3872)$ , the  $Y(3940)$  and the  $Z(4430)^\pm$  observed in B hadronic decays from the Belle and BaBar B-factories. We begin with a brief description of the simple quark model and the charmonium model and a summary of the different production mechanisms of charmonium states in the B-factories. Then we discuss in detail the recent evidence up to September 2007, for the new charmonium-like states, the  $X(3872)$ , the  $Y(3940)$  and the  $Z(4430)^\pm$ .

---

<sup>1</sup>Representing the BaBar Collaboration and email: Walter.Toki@ColoState.EDU.

<sup>2</sup>Work supported by the Dept. of Energy, contract, DE-FG03-93ER40788

## 2 $q\bar{q}$ meson model, charmonium model and Production

### 2.1 $q\bar{q}$ meson model

Essentially all of the experimentally observed mesons, with perhaps the exception of the light quark scalars mesons, have been fit into the simple  $q\bar{q}'$  model of meson. A meson is a bound state of the spin 1/2, quark  $q$  and anti-quark  $\bar{q}'$ , where  $q$  and  $\bar{q}'$  may be different flavors. The quark and anti-quark pair form states with total spin,  $S = 0$  or 1, orbital angular momentum of  $L = 0, 1, 2, \dots$ , and total angular momentum,  $J$ , where  $|L - S| < J < |L + S|$ . The parity of the state is  $P = (-1)^{L+1}$  and the charge conjugation for neutral  $q\bar{q}$  mesons is  $C = (-1)^{L+S}$ . With these simple rules, mesons are predicted using quark - antiquark combinations of  $\{u, d, s, c, b\} \times \{\bar{u}, \bar{d}, \bar{s}, \bar{c}, \bar{b}\}$ . Most of the predictions have been successfully observed with the correct masses, decay modes, and  $J^{PC}$ 's. A recent listing is given in the Quark Model review from the Particle Data Group [3].

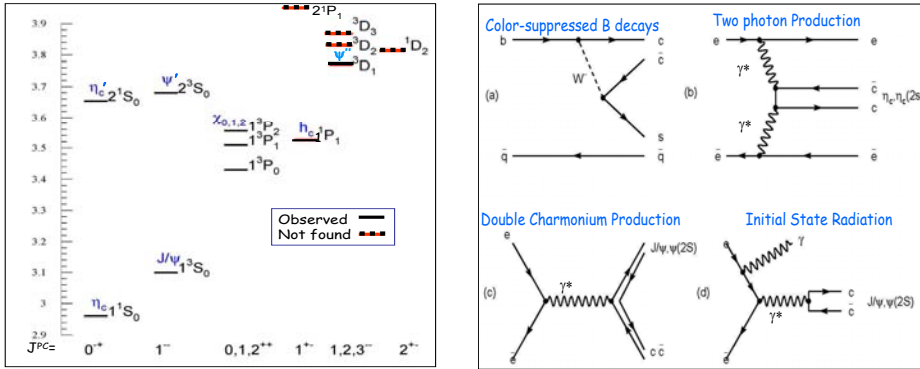


Figure 1: (Left) Charmonium Mass level diagram of observed (solid lines) and predicted states (dashed lines) and (Right) Feynman diagrams of charmonium production in B-factories.

The extensions of the  $q\bar{q}$  meson model relevant to the charmonium-like states include the four-quark, molecule, and hybrid models. Some of these models were used to explain the light quark scalars and the unusual states observed in radiative  $J/\psi$  decays and recently these models have been applied to the new charmonium-like states. In the four-quark model [4] the  $q\bar{q}q\bar{q}$  state forms  $SU(3)$  color singlets and the simplest configurations would have S-wave  $0^-$  and  $1^-$   $q\bar{q}$  pairs that would lead to predictions of  $J^P = 0^+, 1^+, 2^+$  four-

quark states. Recent variants of the four-quark or tetraquark model include di-quarks [5]. Given that the deuteron forms a molecule, the existence of mesons forming molecules [6] might be expected. Candidate meson molecules would likely have masses near the threshold of the two meson masses and its decays could violate isospin and G-parity. A recent molecule prediction [7] of the  $X(3872)$  is a  $D\bar{D}^*$  molecule that decays into  $J/\psi\pi^+\pi^-$  and  $J/\psi\omega$ . Another model was the hybrid model [8] which formed bound states of gluons and  $q\bar{q}$ . The hybrid models [9] have recently been applied to charmonium-like states and predict masses in the  $\sim 4.3$  GeV/ $c^2$  region.

## 2.2 Charmonium Model

The Charmonium model of  $c\bar{c}$  mesons is analogous to the positronium model of  $e^+e^-$  bound states. The charmonium potential models are non-relativistic, since the charm quarks have heavy masses, and models assume simple phenomenological potentials such the Cornell potential [10],  $V(r) = -\kappa/r + r/a^2$ , where  $\kappa = 0.61$ ,  $m_C = 1.84$  GeV/ $c^2$ , and  $a = 2.38$  GeV $^{-1}$ . These lead to fairly accurate predictions of masses, transition rates, and branching fractions. The mass predictions are drawn on the left in Fig.1 with  $N^{2S+1}L_J$  labels, where we use spectroscopic notation to represent N the principle quantum number, S the total spin, L the total orbital angular momentum, and J the total angular momentum. The solid lines are the observed masses and the dashed masses are predictions of charmonium states not yet observed. The most recent charmonium state discovery is the  $^1P_1$ , called the  $h_C$ , observed by the CLEO group [11].

## 2.3 Production of charmonium-like states in B-factories

The four different production diagrams for states with charmonium,  $c\bar{c}$ , are shown in the diagrams on the right side in Fig.1. The Fig.1(a) is the color-suppressed B meson decay where the  $b$  quark decays via  $b \rightarrow c\bar{c}s$ . The Fig.1(b) is the two photon production of the  $c\bar{c}$  states via the collision of two virtual photons. The Fig.1(c) is the production of a pair of  $c\bar{c}$  states via a virtual photon from the  $e^+e^-$  collision that decays into  $c\bar{c}$  quark pairs along with the creation of a  $c\bar{c}$  sea quarks. The Fig.1(d) is the production of  $c\bar{c}$  via initial state radiation (ISR) where either the electron or positron radiates a photon and creates a lower center of mass energy collision between the electron-positron pair that annihilates into a virtual photon that decays into a  $c\bar{c}$  state. In this paper we review the charmonium-like states created via color-suppressed B meson decays as shown in Fig.1(a).

### 3 $X(3872) \rightarrow J/\psi\pi^+\pi^-$

The  $X(3872)$  was the first charmonium-like state observed in color-suppressed  $B$  hadronic decays by Belle [2] in the decay,  $B \rightarrow X K, X \rightarrow J/\psi\pi^+\pi^-$ . It was subsequently confirmed in the same final state,  $X \rightarrow J/\psi\pi^+\pi^-$ , by the CDF, D0, and BaBar collaborations [12]. A recent remeasurement by Belle [13] of the  $X(3872)$  was performed with higher statistics and the resulting  $J/\psi\pi^+\pi^-$  invariant masses are shown in Figs.2(a) and (b), in the modes,  $B^\pm \rightarrow X K^\pm, X \rightarrow J/\psi\pi^+\pi^-$  and  $B^0 \rightarrow X K^0, X \rightarrow J/\psi\pi^+\pi^-$ , respectively. The two striking properties of the  $X(3872)$  were its mass, given in Table 1, which was observed right at  $D^{0*}\bar{D}^0$  mass threshold, and its narrow width. The sum [14] of the  $D^0$  and  $D^{*0}$  masses is  $3871.80 \pm 0.35 \text{ MeV}/c^2$

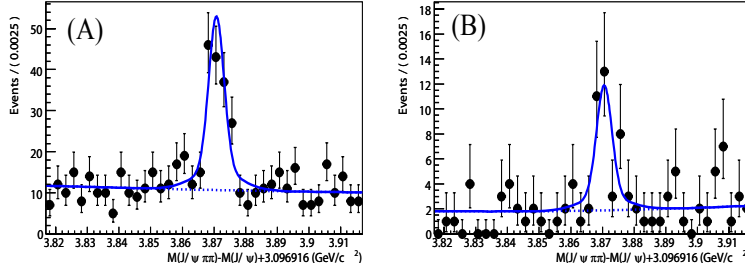


Figure 2: Recent Belle  $J/\psi\pi^+\pi^-$  mass plots of  $X$  produced from charged (a) and neutral (b)  $B$  decays in  $B \rightarrow XK$ .

Table 1: Measured  $X(3872)$  Masses ( $\text{MeV}/c^2$ )

Collaboration	$J/\psi\pi^+\pi^-$	$D\bar{D}^*$
Belle	$3872 \pm 0.6 \pm 0.5$	$3875.2 \pm 0.7^{+0.3}_{-1.6} \pm 0.8$
Babar	$3873.4 \pm 1.4$	$3875.1 \pm 1.1 \pm 0.5$
CDF	$3871.3 \pm 0.7 \pm 0.4$	
D0	$3871.8 \pm 3.1 \pm 3.0$	

and hence the observed  $X$  mass is  $\sim 1 \text{ MeV}/c^2$  above this mass threshold. The mass width was less than the detector resolution and an upper limit of the width,  $\Gamma(X) < 2.3 \text{ MeV}/c^2$ , was provided by Belle.

The search for other  $X$  charmonium decay modes led to evidence in the  $X \rightarrow \gamma J/\psi$  by Belle [15] and BaBar [16]. Since the  $X$  decays into  $\gamma J/\psi$  it

must have C-parity  $+$ , so the  $\pi^+\pi^-$  pair in the  $X \rightarrow J/\psi\pi^+\pi^-$  decay, must form a C-parity  $-$  state with  $L=\text{odd}$  orbital angular momentum. The  $\pi^+\pi^-$  mass has been observed by the Belle, CDF, and BaBar collaborations. The Belle [15] and CDF [17] groups find the  $\pi^+\pi^-$  mass distributions consistent with  $\rho^0$  mass shape where the  $J/\psi - \rho^0$  are in a relative S-wave. Further studies of the angular distributions indicate a preference for  $J^{PC} = 1^{++}$  or  $2^{-+}$  by CDF [17] and Belle [15] assuming only  $J = 0, 1, \text{ or } 2$  ruled out all assignments except  $J^{PC} = 1^{++}$  and  $2^{++}$ . Hence the combined evidence favors  $J^{PC} = 1^{++}$  for the  $X$ .

Other interesting possible  $X$  decay modes include final states such as,  $\omega J/\psi$ ,  $D^{*0}\bar{D}^0$ , and possibly charged partners. Belle [15] searched for  $X \rightarrow J/\psi 3\pi$  and observed evidence for an  $X$  signal when the  $3\pi$  mass is above  $750 \text{ MeV}/c^2$ . The rate relative to the  $J/\psi\pi^+\pi^-$  is observed to be comparable,  $B(X \rightarrow J/\psi 3\pi)/B(X \rightarrow J/\psi\pi^+\pi^-) = 1.0 \pm 0.4 \pm 0.3$ . Since the  $X$  is barely above the  $D^{*0}\bar{D}^0$  mass threshold, a search was performed for the direct decay,  $X \rightarrow D^{*0}\bar{D}^0$  and evidence [18] was found by Belle and BaBar. In Fig.3 (a) and (c) is evidence for these modes and in (b) is evidence for  $B \rightarrow \psi(3770)K$ ,  $\psi(3770) \rightarrow D\bar{D}$ . The mass and product branching fractions are given in Table 1. The masses in the  $D^{*0}\bar{D}^0$  final state appear to be about  $3 \text{ MeV}/c^2$  above of the nominal  $X$  mass that is observed in the  $J/\psi\pi^+\pi^-$  final state. This apparent mass shift could be explained [19] as a shift of the  $D^{*0}\bar{D}^0$  final state mass which is sensitive to its orbital angular momentum due to the closeness of the  $D^{*0}\bar{D}^0$  mass threshold.

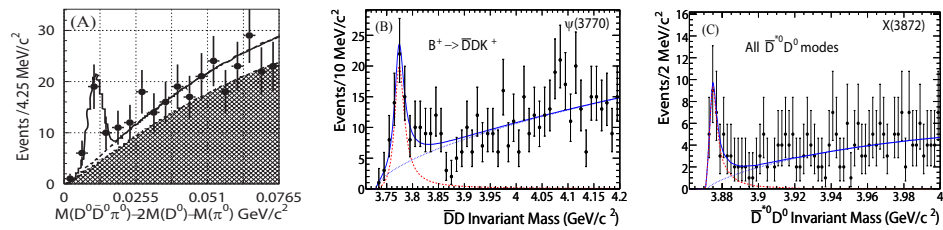


Figure 3: (a) The Belle  $M(D^0\bar{D}^0\pi^0) - M(D^0\bar{D}^0)$  mass difference in  $B \rightarrow D^0\bar{D}^0\pi^0 K$ . (b) The BaBar  $M(D^0\bar{D}^0)$  mass in  $B \rightarrow D^0\bar{D}^0 K$  and (c) the  $M(D^0\bar{D}^0\pi^0)$  mass in  $B \rightarrow D^0\bar{D}^0\pi^0 K$ .

## 4 $Y(3940) \rightarrow J/\psi\omega$

The  $Y(3940)$  was the second charmonium-like particle to be observed in  $B$  decays. This was first observed by the Belle collaboration [20], produced in  $B \rightarrow YK^+$  and  $YK_S$  with  $Y \rightarrow J/\psi\omega$ . This has been recently confirmed by the BaBar collaboration. The Belle analysis, using  $275 \times 10^6 B\bar{B}$  pairs, selected  $B \rightarrow J/\psi\pi^+\pi^-\pi^0K^+/K_S$  event candidates. Evidence for the three body final decay,  $B \rightarrow J/\psi\omega K^+/K_S$ , was apparent when signal peaks in the  $M_{BC}$ ,  $\Delta E$ , and  $3\pi$  mass distributions were observed. After restricting  $0.760 < M(3\pi) < 0.805$  GeV to select  $\omega$  candidates and requiring the event candidates to have the correct  $M_{BC}$  and  $\Delta E$  values, a Dalitz plot was created which is shown in Fig.4(a). The Dalitz plot has  $K\omega$  events  $M^2(K\omega) \sim 2$  (GeV/c<sup>2</sup>)<sup>2</sup> and Belle interprets this from strange mesons, such as the  $K_1(1270)$ ,  $K_1(1400)$ , or  $K_2^*(1430)$ , decaying into  $K\omega$ . To remove these possible backgrounds a  $M(K\omega) < 1.6$  GeV cut is applied as shown in Fig.4(a) by the vertical line. The event candidates are selected in twelve 40 MeV wide bins of  $M(J/\psi\omega)$  starting at 3.880 GeV and their  $M_{BC}$  mass distributions are fit with a gaussian signal function and an ARGUS background function. The number of signal events and its error for each  $M(J/\psi\omega)$  bin is plotted in Fig.4 (b). The binned  $M(J/\psi\omega)$  distributions represent pure signal events, when the  $\omega$  mass is restricted to  $0.760 < M(3\pi) < 0.805$  GeV. A large enhancement in the first three 40 MeV bins is visible at threshold. A pure phase space curve starting near zero at 3.880 MeV is drawn in Fig.4(B). The mass distribution is fit with a Breit-Wigner curve producing a signal yield of  $58 \pm 11$  events, a mass of  $M = 3942 \pm 11$  MeV, and a width of  $\Gamma = 87 \pm 22$  MeV. The resulting signal fit is shown in Fig.4 (c). The BaBar collabora-

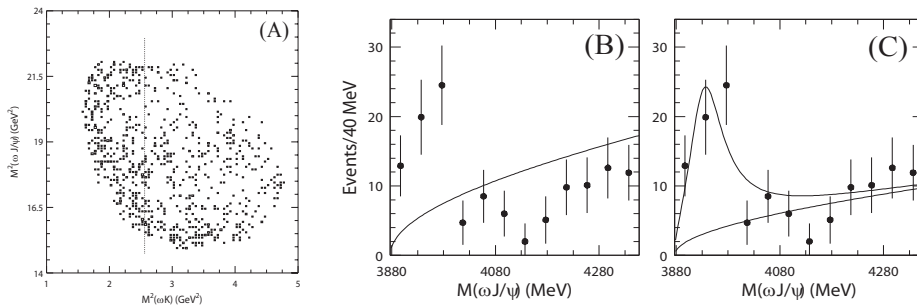


Figure 4: (a) Belle Dalitz plot of the three body decay  $B \rightarrow J/\psi\omega K$  with  $M^2(\omega J/\psi)$  versus  $M^2(K\omega)$ . (b) The mass plot  $M(J/\psi\omega)$  with a pure phase space curve and (c) a signal Breit-Wigner curve plus a pure phase space curve.

tion [21] has recently confirmed the evidence for the  $Y \rightarrow J/\psi\omega$  with higher statistics based on a  $350 \text{ fb}^{-1}$  data sample. The  $B \rightarrow J/\psi\pi^+\pi^-\pi^0K^+/K_S$  events are selected with  $0.7695/0.7605 < M(3\pi) < 0.7965/0.8055 \text{ GeV}$  for the  $B^+/B^0$  modes. The  $M_{ES}$  distributions contained in each  $M(J/\psi\omega)$  bin are fit to extract the number of  $B \rightarrow J/\psi\pi^+\pi^-\pi^0K^+/K_S$  signals. Since a narrow structure appears near threshold, the  $M(J/\psi\omega)$  bins are chosen to be ten narrow 10 MeV bins from 3882.5 to 3982.5 MeV and sixteen wider 50 MeV bins starting at 3982.5 MeV. Evidence for a signal near threshold appears in the charged and neutral  $B$  meson modes. The acceptance corrected plot for the charged and neutral  $B$  decay modes are shown in Fig.5. The

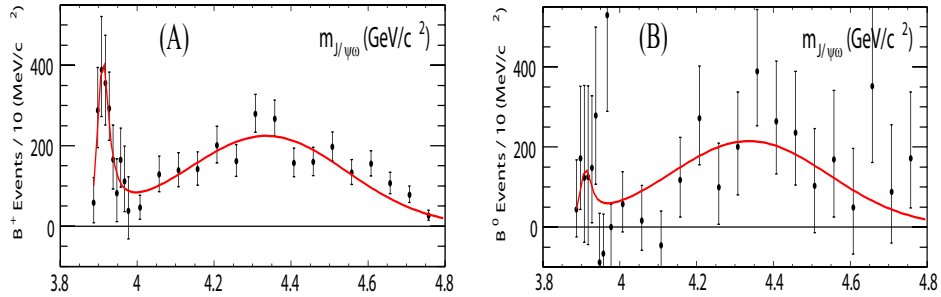


Figure 5: The BaBar  $M(J/\psi\omega)$  mass distributions from (a)  $B^+ \rightarrow J/\psi\omega K^+$  and (b)  $B^0 \rightarrow J/\psi\omega K_S$ .

two mass distributions are fit simultaneously with a Breit-Wigner curve producing a signal,  $Y \rightarrow J/\psi\omega$ , with a mass of  $M = 3914.6^{+3.8}_{-3.4}(\text{stat.})^{+1.9}_{-1.9}(\text{syst.}) \text{ MeV}/c^2$ , and a width of  $\Gamma = 33^{+12}_{-8}(\text{stat.})^{+5}_{-5}(\text{syst.}) \text{ MeV}/c^2$ . The higher statistics BaBar  $Y$  results compared with the Belle results, have narrower and lower mass values.

## 5 $Z^\pm(4430) \rightarrow \psi(2S)\pi^\pm$

The  $Z^\pm(4430)$  particle is the latest discovery announced by Belle [22] at the 2007 Lepton-Photon Conference. The remarkable aspect of this candidate state is a final state,  $\psi(2S)\pi^\pm$ , which is a charged charmonium-like state. The conventional quark model does not permit mesons to strongly decay into a charged state with hidden charm (or strangeness). Of course weak decays into final states such as  $D_S^+ \rightarrow \phi\pi^+$  or  $B^+ \rightarrow J/\psi K^+$  are predicted and observed, but no strong or  $OZI$ -allowed decays can create charged hidden charm and none until now have been observed. Hence this candidate is a *smoking gun* or irrefutable evidence for an exotic meson.

This particle is produced in color-suppressed  $B$  decays,  $B \rightarrow \psi(2S) \pi^\pm K^\mp/K_S$ . The events are based on an Belle integrated data sample of  $605 \text{ fb}^{-1}$ . The Dalitz plot of this three body decay is shown Fig.6(a). There is visual evidence for at least three quasi-twobody decays,  $B \rightarrow \psi(2S)K^*(890)$  with  $K^* \rightarrow K\pi$ ,  $B \rightarrow \psi(2S)K_2^*(1430)$  with  $K_2^* \rightarrow K\pi$ , and a new state,  $B \rightarrow Z^\pm(4430)K$  with  $Z^\pm \rightarrow \psi(2S)\pi^\pm$ . The obvious vertical bar at  $M(K\pi)^2 \approx 0.8 \text{ (GeV}/c^2)^2$  is the decay,  $K^*(890) \rightarrow K\pi$  and a weaker wide vertical line at  $M(K\pi)^2 \approx 2 \text{ (GeV}/c^2)^2$  may be the  $K_2^*(1430) \rightarrow K\pi$ . A horizontal line is evident near  $M(\psi(2S)\pi^\pm)^2 \approx 19.6 \text{ (GeV}/c^2)^2$  indicating a  $\psi(2S)\pi^\pm$  resonance with mass  $\sim 4.4 \text{ GeV}/c^2$ . The  $\psi(2S)\pi^\pm$  mass plot is shown in Fig.6(b) and a peak is evident at  $\sim 4.43 \text{ GeV}/c^2$  over a broad background which is presumably due to the  $B \rightarrow \psi(2S)K^*(890)$  signal. This  $4.43 \text{ GeV}/c^2$  state was named by Belle, the  $Z(4430)$ . In a related mode, BaBar has studied,  $B \rightarrow J/\psi K^*$ , and observed that the  $K^*$  resonances include the  $K^*(890)$ ,  $K_2^*(1430)$ , and a broad S-wave  $K\pi$  in the  $1.1\text{-}1.3 \text{ GeV}/c^2$  mass region. We would expect the similar  $K^*$  resonances produced in  $B \rightarrow \psi(2S)K^*$ . It is possible that in the Dalitz plot the  $Z^\pm$  interferes with the S-wave  $K\pi$  as the intensity of the events along  $19.6 \text{ (GeV}/c^2)^2$  horizontal line varies. Belle fit

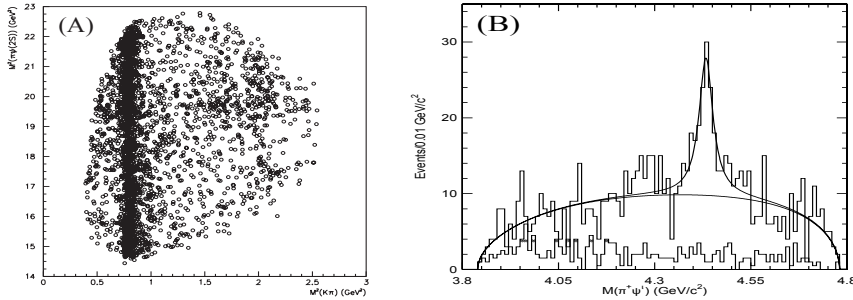


Figure 6: (a) The Belle Dalitz plot of  $M^2(\psi(2S)\pi^\pm)$  versus  $M^2(K\pi^\pm)$ . (b) The Belle  $M(\psi(2S)\pi^\pm)$  mass plot.

the  $M(\psi(2S)\pi^\pm)$  mass plot and obtained a mass of  $4433 \pm 4(\text{stat}) \pm 1(\text{syst}) \text{ GeV}/c^2$ , a width of  $44^{+17}_{-13}(\text{stat})^{+30}_{-11}(\text{syst}) \text{ GeV}/c^2$ , and a branching fraction of  $BF(B \rightarrow KZ^\pm, Z^\pm \rightarrow \psi(2S)\pi^\pm) = 4.1 \pm 1.0(\text{stat}) \pm 1.3(\text{syst}) \times 10^{-5}$ .

Since the evidence for the  $Z^\pm$  is very recent, we discuss some implications of this new candidate state. In the color-suppressed  $B$  decay into three bodies,  $\psi(2S)\pi^\pm K^\mp$ , we would expect and observe the conventional quasi-twobody decay to be the  $B \rightarrow \psi(2S)K^*$ ,  $K^* \rightarrow \pi^\pm K^\mp$  as shown in Fig.7 (a). The alternate combination in Fig.7 (b), would indicate the  $Z^\pm$  is formed with  $c\bar{c}u\bar{d}$  quarks or perhaps two mesons containing this combination of four

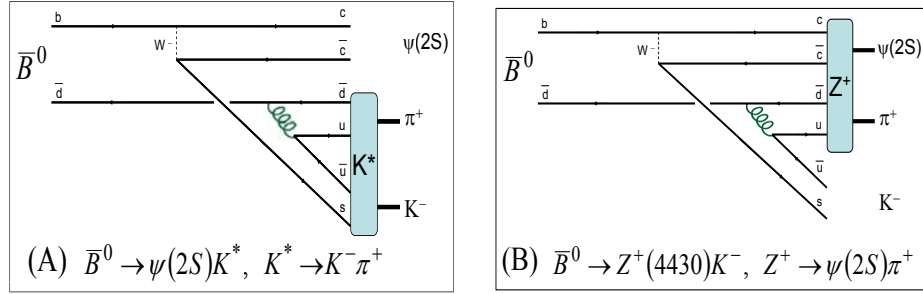


Figure 7: The Feynman diagram for color-suppressed  $B$  decay, (a)  $\bar{B}^0 \rightarrow \psi(2S)\bar{K}^{*0}, \bar{K}^{*0} \rightarrow K^-\pi^+$  and (b)  $\bar{B}^0 \rightarrow Z^+K^-, Z^+ \rightarrow \psi(2S)\pi^+$ .

quarks. The  $Z^\pm$  may be a bound state [23] of  $c\bar{c}u\bar{d}$  quarks. Since the mass of the  $Z^\pm$  is near the sum of the masses of the  $D^*(2010)$  and  $D_1(2420)$ , the  $Z^\pm$  may be a molecule [24] formed with these two mesons. If the  $\psi(2S)$  and  $\pi^\pm$  are in a relative  $L=0$  wave, then the  $Z^\pm$  has  $J^P = 1^+$ , and we might expect other  $Z^\pm$  decays to include  $\eta_C\rho$  and  $D\bar{D}^*$ . If the  $\psi(2S)$  and  $\pi^\pm$  are in a relative  $L=1$  wave, then the  $Z^\pm$  could be  $J^P = 0^-, 1^-,$  or  $2^-$ , and we might expect other  $Z^\pm$  decays to include  $J/\psi a_0(980), \eta_C b_1(1235), h_C\pi$ , and  $D\bar{D}_1(2420)$ . Assuming isospin is not severely violated we would expect to find the neutral decay,  $Z^0(4430) \rightarrow \psi(2S)\pi^0$ . A mysterious question is why the simpler and experimentally easier to detect decays such as  $Z^\pm \rightarrow J/\psi\pi^\pm$  or  $Z^\pm \rightarrow J/\psi\rho^\pm$  [25] have not been found. If it indeed turns out to be the case that  $Z^\pm \rightarrow J/\psi\pi^\pm$  is suppressed whereas  $Z^\pm \rightarrow \psi(2S)\pi^\pm$  is allowed, this perhaps may be related to the longstanding  $\rho\pi$  puzzle [26] in hadronic  $J/\psi$  and  $\psi(2S)$  decays where experimentally we observe  $J/\psi \rightarrow \rho\pi$ , but for unknown reasons  $\psi(2S) \rightarrow \rho\pi$  is highly suppressed.

## 6 Summary

In summary we discussed the new charmonium-like particles, the  $X(3872)$ , the  $Y(3940)$ , and the  $Z(4430)$ . These new discoveries observed in experiments at the B-factories and Tevatron collider, are candidates for non- $q\bar{q}$  or exotic mesons. The narrow  $X(3872)$  due to its mass proximity to  $D\bar{D}^*$  is likely to be a molecular meson. The  $Y(3940)$  may be a candidate for a hybrid charmonium. The  $Z(4430)$ , if confirmed, is perhaps the most compelling exotic meson found to date, being a state with charged hidden charm that must be a four-quark state or possibly a molecule. With more data expected, confirmations and new results are possible in the next two years.

## Acknowledgments

The BaBar collaboration acknowledges the extraordinary efforts of the PEP-II collider group for providing the excellent luminosity. The author would like to thank the MENU conference organizers for a fine meeting at the Forschungszentrum in Juelich. In preparation for the talk and this manuscript, the author had valuable communications with A. Gabareen-Mohktar, W. Dunwoodie, S. Olsen, and M. Voloshin. The conference talk by the author was supported by the Dept. of Energy contract DE-FG03-93ER40788.

## References

- [1] By charmonium-like, we mean a resonance whose a final state contains a charmonium,  $c\bar{c}$ , meson such as the  $J/\psi$ ,  $\psi(2S)$ ,  $\eta_C$ ,  $\chi_C$ , etc., but is not a predicted by the conventional charmonium model.
- [2] Belle Collaboration, S.K. Choi *et al.*, Phys. Rev. Lett. **91**, 262001 (2003).
- [3] See tables 14.2 and 14.3 in Quark Model review in the Particle Data tables in W.-M. Yao *et al.*, Journal of Physics **G33**, 1 (2006).
- [4] R.L. Jaffe, Phys. Rev. **D15**, 267 (1977).
- [5] L. Maiani, F. Piccinini, A.D. Polosa, and V. Riquer, Phys. Rev. **D71**, 014028(2005).
- [6] N. Tornqvist, Phys. Rev. Lett. **49**, 624 (1982); M.B. Voloshin and L.B. Okun, JETP Lett **23**, 333 (1976).
- [7] E.S. Swanson, Phys. Lett. **B588**, 189 (2004).
- [8] T. Barnes, F.E. Close, F. de Viron, J. Weyers, Nucl. Phys. **B224** 241 (1983); M. Chanowitz and S. Sharpe, Phys. Lett. **B132**, 413(1983).
- [9] F. E. Close and P. R. Page, Phys. Lett. **B628**, 215(2005).
- [10] For recent models see Eichten, Lane, Quigg, Phys. Rev. Lett., **89**, 162002 (2002) and Phys. Rev.**D69**, 094019 (2004).
- [11] CLEO collaboration, J. L. Rosner *et al.*, Phys. Rev. Lett. **95**, 102003 (2005).

- [12] CDF collaboration, D. Acosta *et al.*, Phys. Rev. Lett., **93**, 072001 (2004); D0 collaboration, V.M. Abazov *et al.*, Phys. Rev. Lett., **93**, 162002 (2004); BaBar collaboration, B. Aubert *et al.*, Phys. Rev. **D71**, 071103 (2004).
- [13] Belle collaboration, Belle-CONF-0711, August 2007.
- [14] The  $D\bar{D}^*$  mass sum is estimated using the recent Particle Data Group values of  $M(D^0) = 1864.84 \pm 0.17$  MeV/c<sup>2</sup> and  $M(D^*) - M(D^0) = 142.12 \pm 0.07$  MeV/c<sup>2</sup>. The error on the sum,  $2[M(D^0)] + [M(D^*) - M(D^0)]$ , assumes the errors are uncorrelated,
- [15] Belle collaboration, K. Abe *et al.*, hep-ex/0505037, May 2005.
- [16] BaBar collaboration, B. Aubert *et al.*, Phys. Rev. **D74**, 071101 (2006).
- [17] CDF collaboration, A. Abulencia *et al.*, Phys. Rev. Lett. **96**, 102002 (2006), and A. Abulencia *et al.*, Phys. Rev. Lett. **98**, 132002 (2007).
- [18] Belle collaboration, G. Gokhroo *et al.*, Phys. Rev. Lett. **97**, 162002 (2006); BaBar collaboration, B. Aubert *et al.*, submitted to Phys. Rev. **D**, Rapid Communications.
- [19] W. Dunwoodie and V. Zielger, SLAC-PUB-12934, arXiv:0710.5191v1, October 26, 2007.
- [20] Belle collaboration, S.K. Choi *et al.*, Phys. Rev. Lett., **94**, 182002 (2005).
- [21] BaBar collaboration, submitted to Phys. Rev. Lett.
- [22] Belle collaboration, K. Abe *et al.*, arXiv:0708.1790v1 [hep-ex], August 14, 2007; S.-K. Choi, S.L. Olsen *et al.*, arXiv:0708.1790v2 [hep-ex], October 23, 2007, submitted to Phys. Rev. Lett.
- [23] L. Maiani, A.D. Polosa, V. Riquer, arXiv:0708.3997v1 [hep-ph], August 29, 2007.
- [24] C. Meng and K. T. Chao, arXiv:0708.4222 [hep-ph], August 30, 2007; J. Rosner, arXiv:0708.3496v3 [hep-ph] August 31, 2007.
- [25] See Dalitz plot in figure 2, in BaBar Collaboration, B. Aubert *et al.*, Phys. Rev. **D71**, Rapid Communications, 031501 (2005).
- [26] W. Toki, SLAC-PUB-5093, Int. Symp. on Heavy Quark Physics, Ithaca, N.Y., Jun 13-17, 1989. Published in Cornell Heavy Quark 1989:317-324.

# ON THE BRINK OF MAJOR DISCOVERIES IN WEAK CHARM DECAYS – A BISMARCKIAN CHANCE TO MAKE HISTORY

*Ikaros Bigi*

Department of Physics, University of Notre Dame du Lac  
Notre Dame, IN 46556, USA  
Email: [ibigi@nd.edu](mailto:ibigi@nd.edu)

## Abstract

The recently obtained strong evidence for  $D^0 - \bar{D}^0$  oscillations from the  $B$  factories provides an important benchmark in our search for New Physics in charm transitions. While the theoretical verdict on the observed values of  $x_D$  and  $y_D$  is ambiguous – they could be fully generated by SM dynamics, yet could contain also a sizable contribution from New Physics – such oscillations provide a new stage for **CP** violation driven by New Physics. After emphasizing the unique role of charm among up-type quarks, I describe in some detail the **CP** phenomenology for charm decays.

## Prologue

While the sub-division of research in fundamental physics is the natural result of history, it makes eminent sense to consider periodically, whether its specific form is still optimal. This conference has assembled a majority of people from Middle Energy Physics with a sizable contingent from High Energy Physics. I have noticed during the talks that both communities share a dual goal in their research, namely to validate theoretical control over the Standard Model (SM) dynamics – most talks at this conference are devoted to this topic – and to search for New Physics. The latter is conducted at three frontiers: (i) The ‘High Energy Frontier’, which will be pushed into new territories with the operation of the LHC beginning next year; (ii) the ‘High Accuracy Frontier’, for which the analysis of the muon’s  $g - 2$  is the most impressive example, and (iii) the ‘High Sensitivity Frontier’ best illustrated by the probe of **CP** invariance in the decays of  $K$ ,  $B$  and  $D$  mesons. Items (ii) and (iii) represent indirect searches for New Physics. The greatly

enhanced experimental sensitivities for  $K$ ,  $B$  and  $D$  transitions and the typically moderate size contributions anticipated from New Physics mandate that the aspects of high accuracy and high sensitivity get combined in those studies, although not on the level of  $g-2$ . It is on this new combined frontier where in my view the Middle Energy and High Energy communities can and should form new alliances.

## 1 Introduction

While the study of strange dynamics was instrumental in the formation of the SM and that of charm transitions central for the SM being accepted, the analysis of  $B$  decays almost completed its validation through the establishment of CKM dynamics as the dominant source of the observed **CP** violation; ‘almost’, since the Higgs boson has not been observed yet. Now the race is on to see which of these areas together with top quark decays – will first reveal an incompleteness of the SM in flavour dynamics. If the evidence for  $D^0 - \bar{D}^0$  oscillations with  $x_D, y_D \sim 0.005 - 0.01$  listed below gets confirmed, then the detailed probe of **CP** symmetry in charm decays is a close second behind the race leader, namely the even more detailed study of  $B$  decays.

The signal for  $D^0 - \bar{D}^0$  oscillations is a *tactical* draw: while the observed values  $x_D$  and  $y_D$  might be generated by SM forces alone, they could contain large contributions from New Physics. Yet a *strategic* breakthrough is in sight: future probes of **CP** symmetry in  $D$  decays can decide, whether New Physics manifests itself in charm transitions. I would like to draw a historical analogy based on my personal experience. Sanda and myself had been talking about large **CP** asymmetries in certain  $B$  decays [1] without much resonance – till  $B_d - \bar{B}_d$  oscillations were found by the ARGUS collaboration in 1987 [2], i.e. twenty years ago. Since the oscillation parameter  $x_D$  is about two orders of magnitude smaller than  $x_B$ , **CP** asymmetries in  $D$  decays will be much smaller than what was found in  $B$  decays. However we should note that the ‘background’ from SM dynamics is even tinier – meaning the New Physics signal to ‘SM noise’ ratio might actually be considerably better than in  $B$  decays. I would also count on our experimentalists having become more experienced and thus being able to extract smaller signals.

## 2 New Physics Scenarios & the Uniqueness of Charm

New Physics in general induces flavour changing neutral currents (FCNC). It was actually one of the formative challenges for the SM to reproduce the observed great suppression of strangeness changing neutral currents. One should note that the couplings of FCNC could be substantially less suppressed for up-type than for down-type quarks. This actually happens in some models which ‘brush the dirt’ of FCNC in the down-type sector under the ‘rug’ of the up-type sector. *Among up-type quarks it is only charm that allows the full range of probes for FCNC and New Physics in general:* (i) Top quarks decay *before* they can hadronize [3]. Without top *hadrons*  $T^0 - \bar{T}^0$  oscillations cannot occur. This limits our options to search for **CP** asymmetries, since one cannot call on oscillations to provide the required second amplitude. (i) Hadrons built with  $u$  and  $\bar{u}$  quarks like  $\pi^0$  and  $\eta$  are their own antiparticle; thus there can be no  $\pi^0 - \pi^0$  etc. oscillations as a matter of principle. Furthermore they possess so few decay channels that **CPT** invariance basically rules out **CP** asymmetries in their decays.

I will show below that only very recently have experiments reached a range of sensitivity, where one can realistically expect **CP** violation to show up in charm transitions. My basic contention is as follows: *Charm transitions are a unique portal for obtaining novel access to flavour dynamics with the experimental situation being a priori favourable apart from the absence of Cabibbo suppression.*

## 3 On the Evidence for $D^0 - \bar{D}^0$ Oscillations

Oscillations are described by the normalized mass and width splittings:  $x_D \equiv \frac{\Delta M_D}{\Gamma_D}$ ,  $y_D \equiv \frac{\Delta \Gamma_D}{2\Gamma_D}$ . While the SM predicts similar numbers for  $x_D$  and  $y_D$  with the data showing the same trend, we should note that  $\Delta M_D$  and  $\Delta \Gamma_D$  reflect rather different dynamics:  $\Delta M_D$  is produced by *off-shell* transitions making it naturally sensitive to New Physics unlike  $\Delta \Gamma_D$ , which is generated by *on-shell* modes.

### 3.1 The Data

I will list here only those data that show an effect with the strongest significance.

- Finding different lifetimes in the decays of neutral  $D$  mesons constitutes

an unequivocal manifestation of  $D^0$  oscillations. BELLE obtains a 3.2  $\sigma$  signal for a difference in the effective lifetimes for  $D^0 \rightarrow K^+K^-$  and  $D^0 \rightarrow K^-\pi^+$  [4]:

$$y_{CP} = \frac{\tau(D^0 \rightarrow K^-\pi^+)}{\tau(D^0 \rightarrow K^+K^-)} - 1 = (1.31 \pm 0.32 \pm 0.25) \cdot 10^{-2} \quad (1)$$

In the limit of **CP** invariance (a good approximation for charm decays as explained later) the two mass eigenstates of the  $D^0 - \bar{D}^0$  complex are **CP** eigenstates as well.  $D^0 \rightarrow K^+K^-$  yields the width for the **CP** even state and  $D^0 \rightarrow K^-\pi^+$  the one averaged over the **CP** even and odd states and thus:  $y_{CP} = y_D = \frac{\Delta\Gamma_D}{2\Gamma_D}$ .

- The selection rule  $\Delta C = \Delta S$  is violated in the SM by doubly Cabibbo suppressed  $c \rightarrow d\bar{s}u$  transitions (DCSD). By analyzing the decay rate evolution as a function of (proper) time, one can disentangle the two sources for ‘wrong-sign’ kaons:

$$\frac{\text{rate}(D^0(t) \rightarrow K^+\pi^-)}{\text{rate}(D^0(t) \rightarrow K^-\pi^+)} = \frac{|T(D^0 \rightarrow K^+\pi^-)|^2}{|T(D^0 \rightarrow K^-\pi^+)|^2} \cdot [1 + Y_{K\pi}(t\Gamma_D) + Z_{K\pi}(t\Gamma_D)^2] \quad (2)$$

$$Y_{K\pi} \equiv \frac{y_D}{\text{tg}^2\theta_C} \text{Re} \left( \frac{q}{p} \hat{\rho}_{K\pi} \right) + \frac{x_D}{\text{tg}^2\theta_C} \text{Im} \left( \frac{q}{p} \hat{\rho}_{K\pi} \right), \quad Z_{K\pi} \equiv \frac{x_D^2 + y_D^2}{4\text{tg}^4\theta_C} |\hat{\rho}_{K\pi}|^2 \quad (3)$$

where we have used the notation

$$\frac{T(\bar{D}^0 \rightarrow K^+\pi^-)}{T(D^0 \rightarrow K^+\pi^-)} = \frac{1}{\text{tg}^2\theta_C} \hat{\rho}_{K\pi} \quad (4)$$

to emphasize that the *non*-oscillation amplitude is doubly Cabibbo suppressed. The first and third term in the square brackets represent the pure DCSD and oscillation terms, respectively, and the second one their interference. The latter receives a nonzero contribution from  $\text{Im} \left( \frac{p}{q} \frac{\hat{\rho}_{K\pi}}{|\hat{\rho}_{K\pi}|} \right)$ , if there is a *weak* phase, which leads to CP violation as discussed later, and/or if a *strong* phase is present due to different FSI in  $D^0 \rightarrow K^+\pi^-$  and  $\bar{D}^0 \rightarrow K^+\pi^-$ . One has to allow for such a difference since the latter is a pure  $\Delta I = 1$  transition, while the former is given by a combination of an enhanced  $\Delta I = 0$  and a suppressed  $\Delta I = 1$  amplitude. This strong phase  $\delta$  can be absorbed into modified expressions for  $x_D$  and  $y_D$ :

$$x'_D \equiv x_D \cos\delta + y_D \sin\delta, \quad y'_D \equiv -x_D \sin\delta + y_D \cos\delta \quad (5)$$

yielding  $(x'_D)^2 + (y'_D)^2 = x_D^2 + y_D^2$  to obtain

$$Y_{K\pi} = \frac{y'_D}{\text{tg}^2\theta_C} \left| \frac{q}{p} \hat{\rho}_{K\pi} \right| \quad (6)$$

Since a priori there is no reason why  $\delta$  should be particularly small, one better keeps the difference between  $(x_D, y_D)$  and  $(x'_D, y'_D)$  in mind. BABAR has found [5]

$$y'_D = (0.97 \pm 0.44 \pm 0.31) \cdot 10^{-2}, \quad (x'_D)^2 = (-2.2 \pm 3.0 \pm 2.1) \cdot 10^{-4} \quad (7)$$

representing a  $3.9 \sigma$  signal for  $[y'_D, (x'_D)^2] \neq [0, 0]$  due to the correlations between  $y'_D$  and  $(x'_D)^2$ . This reaction is a prime candidate for revealing **CP** violation due to new Physics, and we will discuss it in more detail later.

- Analyzing the time *dependent* Dalitz plot for  $D^0(t) \rightarrow K_S \pi^+ \pi^-$  BELLE finds [6]

$$x_D \equiv \frac{\Delta M_D}{\Gamma_D} = (0.80 \pm 0.29 \pm 0.17) \cdot 10^{-2}, \quad y_D = (0.33 \pm 0.24 \pm 0.15) \cdot 10^{-2}, \quad (8)$$

which amounts to a  $2.4 \sigma$  signal for  $x_D \neq 0$ .<sup>1</sup>

While all these findings are most intriguing, they do not (yet) establish the existence of  $D^0$  oscillations. A ‘preliminary’ average by the Heavy Flavour Averaging Group over all relevant data yields  $5 \sigma$  significance for  $[x_D, y_D] \neq [0, 0]$  with  $x_D$  and  $y_D$  in the range  $0.5 - 1\%$  – and the caveat that averaging over the existing data sets has to be taken with quite a grain of salt at present due to the complicated likelihood functions.

Establishing  $D^0 - \bar{D}^0$  oscillations would provide a novel insight into flavour dynamics. After having discovered oscillations in *all three* mesons built from *down*-type quarks –  $K^0$ ,  $B_d$  and  $B_s$  – it would be the first observation of oscillations with *up*-type quarks; it would also remain the only one (at least for three-family scenarios), as explained above.

---

<sup>1</sup>BELLE extracts from its analysis the ratio between doubly Cabibbo suppressed and favoured amplitudes for kaon resonances of increasing mass. The trend of strongly increasing ratios given in their analysis can, however, hardly be correct on theoretical grounds [7]. The values extracted for  $x_D$  and  $y_D$  are probably not very sensitive to this shortcoming in their Dalitz plot model.

### 3.2 The Inconclusive Theoretical Interpretation

The history of the predictions on  $D^0$  oscillations does not provide a tale of consistently sound judgment by theorists, when they predicted  $x_D \leq \text{few} \times 10^{-4}$ . Yet scientific progress is not made by majority vote, although that codifies it in the end. Within the SM two reasons combine to make  $x_D$  and  $y_D$  small in contrast to the situation for  $B^0 - \bar{B}^0$  and  $K^0 - \bar{K}^0$  oscillations: (i) The amplitude for  $D^0 \leftrightarrow \bar{D}^0$  transitions is twice Cabibbo suppressed and therefore  $x_D, y_D \propto \sin^2 \theta_C$ . The amplitudes for  $K^0 \leftrightarrow \bar{K}^0$  and  $B^0 \leftrightarrow \bar{B}^0$  are also twice Cabibbo and KM suppressed – yet so are their decay widths. (ii) Due to the GIM mechanism  $\Delta M = 0 = \Delta \Gamma$  in the limit of flavour symmetry. Yet  $K^0 \leftrightarrow \bar{K}^0$  is driven by  $SU(4)_{Fl}$  breaking characterised by  $m_c^2 \neq m_u^2$ , which represents no suppression on the usual hadronic scales. In contrast  $D^0 \leftrightarrow \bar{D}^0$  is controlled by  $SU(3)_{fl}$  breaking. Having two Cabibbo suppressed classes of decays one concludes for the overall oscillation strength:  $\frac{\Delta M_D}{\Gamma_D}$ ,  $\Delta \Gamma_D \sim SU(3)_{fl}$  breaking  $\times 2\sin^2 \theta_C < \text{few} \times 0.01$ . The proper description of  $SU(3)_{fl}$  breaking thus becomes the central issue. While  $x_D \lesssim y_D$  is a natural finding in the SM,  $x_D \ll y_D$  would not be although it cannot be ruled out. For if  $D^0 \rightarrow f \rightarrow \bar{D}^0$  can occur for an on-shell final state  $f$  thus contributing to  $\Delta \Gamma_D$ , then  $D^0 \rightarrow "f" \rightarrow \bar{D}^0$  is possible for "f" taken off-shell; i.e.,  $\Delta M_D$  and  $\Delta \Gamma_D$  are related by a dispersion relation.

One can invoke two complementary treatments to evaluate  $\Delta M_D$  and  $\Delta \Gamma_D$  in the SM. One approach [8] relies on an operator product expansion (OPE) in terms of quark and gluon operators including nonperturbative contributions, which yield contributions in powers of  $m_s/m_c$  and  $\mu_{\text{had}}/m_c$ , where  $m_s$  and  $m_c$  denote the mass of strange and charm quarks, respectively, and  $\mu_{\text{had}}$  hadronic condensates. Terms of order  $m_s^2 \mu_{\text{had}}^4 / m_c^6$  yield the largest contributions rather than the formally leading term  $m_s^4 / m_c^4$ , and one finds

$$x_D(SM)|_{OPE}, y_D(SM)|_{OPE} \sim \mathcal{O}(10^{-3}) \quad (9)$$

with a preference for  $|x_D(SM)|_{OPE} < y_D(SM)|_{OPE}$ . It is unlikely that this prediction can be sharpened numerically. It should also be noted that limitations to quark-hadron duality due to the proximity of hadronic thresholds could enhance in particular  $y_D$ .

The authors of Refs. [9] find similar numbers, albeit in a quite different approach: (i) They estimate the amount of  $SU(3)_{fl}$  breaking for  $\Delta \Gamma_D$  from phase space differences alone for two-, three- and four-body  $D$  modes and arrive at  $y_D(SM) \sim 0.01$ . The proximity of hadronic thresholds is reflected in this number; it thus attempts to incorporate limitations in quark-hadron duality in the language of the OPE treatment. (ii) They infer  $x_D$  from  $y_D$

via a dispersion relation arriving at  $0.001 \leq |x_D(SM)| \leq 0.01$  with  $x_D$  and  $y_D$  of opposite sign.

A priori it would have been conceivable to measure  $y_D \ll x_D \sim \text{few} \times 0.01$  thus establishing an indirect manifestation of New Physics. This has not happened: we are in a grey zone, where the observed strengths of both  $y_D$  and  $x_D$  might be produced by SM forces alone – or could contain significant contributions from New Physics. Even in the former case one should probe these oscillations as accurately as possible first establishing  $[x_D, y_D] \neq [0, 0]$  and then determining  $x_D$  vs.  $y_D$ .

A future theoretical breakthrough might allow us to predict  $\Delta M_D|_{SM}$  and  $\Delta\Gamma_D|_{SM}$  more accurately and thus resolve the ambiguity in our interpretation, but I would not count on it. Rather than wait for that to happen the community should become active in the catholic tradition of ‘active repentance’ and search for **CP** violation in  $D$  decays.

## 4 CP Violation – the Decisive Stage

Probing **CP** invariance for manifestations of New Physics is not a ‘wild goose chase’. For we know that CKM dynamics is completely irrelevant for baryogenesis; i.e., we need **CP** violating New Physics to understand the Universe’s observed baryon as a dynamically generated quantity rather than an arbitrary initial value. Charm decays offer several pragmatic advantages in such searches: (i) While we do not know how to reliably compute the strong phase shifts required for direct **CP** violation to emerge in partial widths, we can expect them to be in general large, since charm decays proceed in a resonance domain. (ii) The branching ratios into relevant modes are relatively large. (iii) **CP** asymmetries can be linear in New Physics amplitudes thus enhancing sensitivity to the latter. (iv) The ‘background’ from known physics is small: within the SM the effective weak phase is highly diluted, namely  $\sim \mathcal{O}(\lambda^4)$ . *Without* oscillations only direct **CP** violation can occur, and it can arise only in singly Cabibbo suppressed transitions, where one expects them to reach no better than the 0.1 % level; significantly larger values would signal New Physics. *Almost any* asymmetry in Cabibbo allowed or doubly suppressed channels requires the intervention of New Physics, since – in the absence of oscillations – there is only one weak amplitude. The exception are channels containing a  $K_S$  (or  $K_L$ ) in the final state like  $D \rightarrow K_S\pi$ . There are two sources for a **CP** asymmetry from known dynamics: (i) Two transition amplitudes are actually involved, namely a Cabibbo favoured and a doubly suppressed one,  $D \rightarrow \bar{K}^0\pi$  and  $D \rightarrow K^0\pi$ , respectively. Their relative weak CKM phase is given by  $\eta A^2\lambda^6 \sim \text{few} \cdot 10^{-5}$ , which seems to be well beyond observability.

(ii) While one has  $|T(D \rightarrow \bar{K}^0 \pi)| = |T(\bar{D} \rightarrow K^0 \pi)|$ , the well-known **CP** impurity  $|p_K| \neq |q_K|$  in the  $K_S$  wave function introduces a difference between  $D^{0,+} \rightarrow K_S \pi^{0,+}$  and  $\bar{D}^{0,-} \rightarrow \bar{K}_S \pi^{0,-}$  of  $\frac{|q_K|^2 - |p_K|^2}{|q_K|^2 + |p_K|^2} = (3.32 \pm 0.06) \cdot 10^{-3}$  [10].

With oscillations on an observable level – and it seems  $x_D, y_D \sim 0.005 - 0.01$  satisfy this requirement – the possibilities for **CP** asymmetries proliferate. Even if New Physics is not the main engine for  $\Delta M_D$ , it could well be the leading source of **CP** violation in  $\mathcal{L}(\Delta C = 2)$ . This would be analogous to the very topical case of  $B_s$  oscillations.  $\Delta M(B_s)$  has been observed to be consistent with the SM prediction within mainly theoretical uncertainties; yet since those are still sizable, we cannot rule out that New Physics impacts  $B_s - \bar{B}_s$  oscillations significantly. This issue, which is unlikely to be resolved theoretically, can be decided experimentally by searching for a time dependent **CP** violation in  $B_s(t) \rightarrow \psi\phi$ . For within the SM one predicts [1] a very small asymmetry not exceeding 4% in this transition since on the leading CKM level quarks of only the second and third family contribute. Yet in general one can expect New Physics contributions to  $B_s - \bar{B}_s$  oscillations to exhibit a weak phase that is not particularly suppressed. Even if New Physics affects  $\Delta M(B_s)$  only moderately, it could greatly enhance the time dependent **CP** asymmetry in  $B_s(t) \rightarrow \psi\phi$ . This analogy is of course qualitative rather than quantitative with  $D^0 - \bar{D}^0$  oscillations being (at best) quite slow.

#### 4.1 Oscillations – the New Portal to CP Violation

In the presence of  $D^0 - \bar{D}^0$  oscillations *time-dependent CP* asymmetries can arise in  $D^0$  decays on the Cabibbo allowed ( $D^0 \rightarrow K_S \phi, K_S \rho^0, K_S \pi^0$ ), once forbidden ( $D^0 \rightarrow K^+ K^-$ ) and doubly forbidden ( $D^0 \rightarrow K^+ \pi^-$ ) levels. Let me list just two prominent examples from the last two categories. Since  $y_D, x_D \ll 1$ , it suffices to give the decay rate evolution to first order in those quantities only (the general expressions can be found in Ref. [10]).

$$\Gamma(D^0(t) \rightarrow K^+ K^-) \propto e^{-\Gamma_1 t} |T(D^0 \rightarrow K^+ K^-)|^2 \times \left[ 1 + y_D \frac{t}{\tau_D} \left( 1 - \text{Re} \frac{q}{p} \bar{\rho}_{K^+ K^-} \right) - x_D \frac{t}{\tau_D} \text{Im} \frac{q}{p} \bar{\rho}_{K^+ K^-} \right]$$

$$\Gamma(\bar{D}^0(t) \rightarrow K^+ K^-) \propto e^{-\Gamma_1 t} |T(\bar{D}^0 \rightarrow K^+ K^-)|^2 \times \left[ 1 + y_D \frac{t}{\tau_D} \left( 1 - \text{Re} \frac{p}{q} \frac{1}{\rho_{K^+ K^-}} \right) - x_D \frac{t}{\tau_D} \text{Im} \frac{p}{q} \frac{1}{\rho_{K^+ K^-}} \right] \quad (10)$$

The usual three types of **CP** violation can arise, namely the direct and indirect types –  $|\bar{\rho}_{K^+K^-}| \neq 0$  and  $|q| \neq |p|$ , respectively – as well as the one involving the interference between the oscillation and direct decay amplitudes –  $\text{Im} \frac{q}{p} \bar{\rho}_{K^+K^-} \neq 0$  leading also to  $\text{Re} \frac{q}{p} \bar{\rho}_{K^+K^-} \neq 1$ . Assuming for simplicity  $|T(D^0 \rightarrow K^+K^-)| = |T(\bar{D}^0 \rightarrow K^+K^-)|^2$  and  $|q/p| = 1 - \epsilon_D$  one has  $(q/p)\bar{\rho}_{K^+K^-} = (1 - \epsilon_D)e^{i\phi_{K\bar{K}}}$  and thus

$$A_\Gamma = \frac{\Gamma(\bar{D}^0(t) \rightarrow K^+K^-) - \Gamma(D^0(t) \rightarrow K^+K^-)}{\Gamma(\bar{D}^0(t) \rightarrow K^+K^-) + \Gamma(D^0(t) \rightarrow K^+K^-)} \simeq x_D \frac{t}{\tau_D} \sin\phi_{K\bar{K}} - y_D \frac{t}{\tau_D} \epsilon_D \cos\phi_{K\bar{K}}. \quad (11)$$

where I have assumed  $|\epsilon_D| \ll 1$ . BELLE has found [4]

$$A_\Gamma = (0.01 \pm 0.30 \pm 0.15)\% \quad (12)$$

While there is no evidence for **CP** violation in the transition, one should also note that the asymmetry is bounded by  $x_D$ . For  $x_D, y_D \leq 0.01$ , as indicated by the data,  $A_\Gamma$  could hardly exceed the 1% range. I.e., there is no real bound on  $\phi_D$  or  $\epsilon_D$  yet. The good news is that if  $x_D$  and/or  $y_D$  indeed fall into the 0.5 - 1 % range, then any improvement in the experimental sensitivity for a **CP** asymmetry in  $D^0(t) \rightarrow K^+K^-$  constrains New Physics scenarios – or could reveal them [11].

Another promising channel for probing **CP** symmetry is  $D^0(t) \rightarrow K^+\pi^-$ : since it is doubly Cabibbo suppressed, it should a priori exhibit a higher sensitivity to a New Physics amplitude. Furthermore it cannot exhibit direct **CP** violation in the SM. With

$$\frac{q T(D^0 \rightarrow K^+\pi^-)}{p T(D^0 \rightarrow K^-\pi^+)} \left[ \frac{p T(\bar{D}^0 \rightarrow K^-\pi^+)}{q T(\bar{D}^0 \rightarrow K^+\pi^-)} \right] \equiv -\frac{1}{\text{tg}^2\theta_C} (1 - [+]\epsilon_D) |\hat{\rho}_{K\pi}| e^{-i(\delta - [+]\phi_{K\pi})} \quad (13)$$

one expresses an asymmetry as follows:

$$\frac{\Gamma(\bar{D}^0(t) \rightarrow K^-\pi^+) - \Gamma(D^0(t) \rightarrow K^+\pi^-)}{\Gamma(\bar{D}^0(t) \rightarrow K^-\pi^+) + \Gamma(D^0(t) \rightarrow K^+\pi^-)} \simeq \left( \frac{t}{\tau_D} \right) |\hat{\rho}_{K\pi}| \left( \frac{y'_D \cos\phi_{K\pi} \epsilon_D - x'_D \sin\phi_{K\pi}}{\text{tg}\theta_C^2} \right) + \left( \frac{t}{\tau_D} \right)^2 |\hat{\rho}_{K\pi}|^2 \frac{\epsilon_D (x_D^2 + y_D^2)}{2\text{tg}\theta_C^4} \quad (14)$$

---

<sup>2</sup>CKM dynamics is expected to induce an asymmetry not exceeding 0.1%.

where I have again assumed for simplicity  $|\epsilon_D| \ll 1$  and *no direct CP* violation.

BABAR has also searched for a time dependent **CP** asymmetry in  $D^0 \rightarrow K^+\pi^-$  vs.  $\overline{D}^0(t) \rightarrow K^-\pi^+$ , yet so far has not found any evidence for it [5]. Again, with  $x'_D$  and  $y'_D$  capped by about 1%, no nontrivial bound can be placed on the weak phase  $\phi_{K\pi}$ . On the other hand any further increase in experimental sensitivity could reveal a signal.

## 4.2 CP Asymmetries in Final State Distributions

Decays to final states of *more than* two pseudoscalar or one pseudoscalar and one vector meson contain more dynamical information than given by their widths; their distributions as described by Dalitz plots or **T-odd** moments can exhibit **CP** asymmetries that can be considerably larger than those for the width. All **CP** asymmetries observed so far in  $K_L$  and  $B_d$  decays except one concern partial widths, i.e.  $\Gamma(P \rightarrow f) \neq \Gamma(\overline{P} \rightarrow \overline{f})$ . The one notable exception can teach us important lessons for future searches both in charm and  $B$  decays, namely the **T** odd moment found in  $K_L \rightarrow \pi^+\pi^-e^+e^-$ . Denoting by  $\phi$  the angle between the  $\pi^+\pi^-$  and  $e^+e^-$  planes one has

$$\frac{d\Gamma}{d\phi}(K_L \rightarrow \pi^+\pi^-e^+e^-) = \Gamma_1 \cos^2\phi + \Gamma_2 \sin^2\phi + \Gamma_3 \cos\phi \sin\phi \quad (15)$$

Comparing the  $\phi$  distribution integrated over two quadrants one obtains a **T** odd moment:

$$\langle A \rangle = \frac{\int_0^{\pi/2} d\phi \frac{d\Gamma}{d\phi} - \int_{\pi/2}^{\pi} d\phi \frac{d\Gamma}{d\phi}}{\int_0^{\pi} d\phi \frac{d\Gamma}{d\phi}} = \frac{2\Gamma_3}{\pi(\Gamma_1 + \Gamma_2)} \quad (16)$$

$\langle A \rangle$  is measured to be  $0.137 \pm 0.015$  [12] in full agreement with the prediction of  $0.143 \pm 0.013$  [13]. Most remarkably this large asymmetry is generated by the tiny **CP** impurity parameter  $\eta_{+-} \simeq 0.0024$ ; i.e., the impact of the latter is magnified by a factor of almost a hundred – for the price of a tiny branching ratio of about  $3 \cdot 10^{-7}$ !

This trading of asymmetry against branching ratio can be attempted also in the so far unobserved rare charm mode  $D_L \rightarrow K^+K^-\mu^+\mu^-$ , where  $D_L$  denotes the **CP** odd longer lived mass eigenstate. The **CP** impurity parameter  $\epsilon_D$  that controls  $D_L \rightarrow K^+K^-$  can get enhanced by almost two orders of magnitude in the **T** odd moment defined analogous to  $\langle A \rangle$  in Eq.(16) [14]. The required  $D_L$  beam can be prepared through a EPR correlation [15] in  $e^+e^- \rightarrow \gamma^* \rightarrow D_S D_L$  near threshold, where the shorter lived  $D_S$  is tagged through  $D_S \rightarrow K^+K^-, \pi^+\pi^-$ .

The same effects can be probed also by comparing the  $\phi$  distributions in  $D^0 \rightarrow K^+K^-\mu^+\mu^-$  vs.  $\bar{D}^0 \rightarrow K^+K^-\mu^+\mu^-$  or in  $D^0 \rightarrow K^+K^-\pi^+\pi^-$  vs.  $\bar{D}^0 \rightarrow K^+K^-\pi^+\pi^-$  [16]. The aforementioned huge enhancement factor, however, does not arise then.

### 4.3 CP Violation in Semileptonic $D^0$ Decays

$|q/p| \neq 1$  unambiguously reflects **CP** violation in  $\Delta C = 2$  dynamics. It can be probed most directly in semileptonic  $D^0$  decays leading to ‘wrong sign’ leptons:

$$a_{SL}(D^0) \equiv \frac{\Gamma(D^0(t) \rightarrow l^- X) - \Gamma(\bar{D}^0 \rightarrow l^+ X)}{\Gamma(D^0(t) \rightarrow l^- X) + \Gamma(\bar{D}^0 \rightarrow l^+ X)} = \frac{|q|^4 - |p|^4}{|q|^4 + |p|^4} \quad (17)$$

The corresponding observable has been studied in semileptonic decays of neutral  $K$  and  $B$  mesons. With  $a_{SL}$  being controlled by  $(\Delta\Gamma/\Delta M)\sin\phi_{weak}$ , it is predicted to be small in both cases, albeit for different reasons: (i) While  $(\Delta\Gamma_K/\Delta M_K) \sim 1$  one has  $\sin\phi_{weak}^K \ll 1$  leading to  $a_{SL}^K = \delta_l \simeq (3.32 \pm 0.06) \cdot 10^{-3}$  as observed. (ii) For  $B^0$  on the other hand one has  $(\Delta\Gamma_B/\Delta M_B) \ll 1$  leading to  $a_{SL}^B < 10^{-3}$ .

For  $D^0$  both  $\Delta M_D$  and  $\Delta\Gamma_D$  are small, yet  $\Delta\Gamma_D/\Delta M_D$  is not: present data indicate it is about unity or even larger;  $a_{SL}$  is given by the smaller of  $\Delta\Gamma_D/\Delta M_D$  or its inverse multiplied by  $\sin\phi_{weak}^D$ , which might not be that small: i.e., while the rate for ‘wrong-sign’ leptons is small in semileptonic decays of neutral  $D$  mesons, their **CP** asymmetry might not be at all, if New Physics intervenes to generate  $\phi_{weak}^D$ .

## 5 Conclusions and Outlook

It is of great importance to firmly establish the existence of  $D^0 - \bar{D}^0$  oscillations and determine  $x_D$  vs.  $y_D$ . My main message is that we must go after **CP** violation in charm transitions in all of its possible manifestations, both time dependent and independent, in partial widths and final state distributions, and on all Cabibbo levels down to the  $10^{-3}$  or even smaller level. The present absence of any **CP** asymmetry is not telling. Comprehensive and detailed studies of charm decays provide a novel and possibly unique window onto flavour dynamics.

For that purpose we need the statistical muscle of LHCb. Charm studies constitute a worthy challenge to LHCb, for which  $D^0 \rightarrow K^+K^-$ ,  $\pi^+\pi^-$ ,  $K^+\pi^-$ ,  $K^+K^-\mu^+\mu^-$  represent good channels. Yet I feel we have to go after

even more statistics and more channels. This brings me to my second main message adapted from Cato the Elder:

”Ceterum censeo fabricam super saporis esse faciendam!”  
 ”Moreover I advise a super-flavour factory has to be built!”

Bismarck, who exhibited a flexibility concerning morality similar to Cato’s, once declared: ” ... it is the role of the statesman to grab the mantle of history when he feels it passing by.” Likewise it is the task of the physicist to make the greatest use of a special gift from Nature.  $D^0 - \bar{D}^0$  oscillations are such a gift; it is therefore our duty to make the most complete use of it – and there is fame within our grasp.

**Acknowledgments:** This work was supported by the NSF under the grant number PHY-0355098. I am grateful to Profs. Krewald and Machner for inviting me to this fine meeting and for making it possible that most participants could stay in the great city of Aachen.

## References

- [1] I.I. Bigi, A.I. Sanda, *Nucl.Phys.***B 193** (1981) 85.
- [2] ARGUS Collab., H. Albrecht *et al.*, *Phys.Lett.***B192** (1987) 245.
- [3] I.I. Bigi *et al.*, *Phys. Lett.* **B181** (1986) 157.
- [4] BELLE Collab., M. Staric *et al.*, *Phys.Rev.Lett.* **98** (2007) 211803.
- [5] BABAR Collab., B. Aubert *et al.*, hep-ex/0703020.
- [6] BELLE Collab., L.M. Zhang *et al.*, *Phys.Rev.Lett.* **99** (2007) 131803.
- [7] I.I. Bigi *et al.*, in preparation.
- [8] I.I. Bigi, N.G. Uraltsev, *Nucl.Phys.***B592** (2001) 92.
- [9] A. Falk *et al.*, *Phys.Rev.* **D65** (2002) 054034; *Phys.Rev.* **D69** (2004) 114021.
- [10] S. Bianco *et al.*, *La Rivista del Nuov. Cim.* **26**, # 7 - 8 (2003).
- [11] Y. Grossman, A. Kagan, Y. Nir, *Phys.Rev.* **D75** (2007) 036008.

- [12] PDG, *Review of Particle Physics, Journal of Physics G* **33** (2006) 1.
- [13] L.M. Sehgal, M. Wanninger, *Phys.Rev.* **D46** (1992) 1035; *ibid.* **D46** (1992) 5209 (E).
- [14] I.I. Bigi, A. Paul, in preparation.
- [15] A. Einstein, B. Podolsky, N. Rosen, *Phys.Rev.* **47** (1935) 777.
- [16] FOCUS Collab., J.M. Link *et al.*, *Phys.Lett.* **B622** (2005) 239.

# THREE NUCLEON SYSTEM DYNAMICS STUDIED VIA d-p BREAKUP

St. Kistryn<sup>\*,1</sup>, E. Stephan<sup>%</sup>, N. Kalantar-Nayestanaki<sup>#</sup>

<sup>\*</sup>Institute of Physics, Jagiellonian University, PL-30059 Kraków, Poland

<sup>%</sup>Institute of Physics, University of Silesia, PL-4007 Katowice, Poland

<sup>#</sup>Kernfysisch Versneller Instituut, NL-9747 Groningen, The Netherlands

## Abstract

Three-nucleon ( $3N$ ) system is the simplest non-trivial testing ground in which the quality of modern nucleon-nucleon ( $NN$ ) interaction models can be probed quantitatively by means of rigorous technique of solving the Faddeev equations. It has been found that a proper description of the experimental data cannot be achieved with the use of  $NN$  forces alone. This indicates a necessity of including additional dynamics: subtle effects of suppressed degrees of freedom, introduced by means of genuine three-nucleon forces.

A large set of high precision, exclusive cross-section and analyzing power data for the  $^1\text{H}(d,pp)n$  breakup reaction at 130 MeV deuteron energy, obtained in a dedicated experiment at KVI Groningen, contribute significantly to constrain the physical assumptions underlying the theoretical models. Comparison of nearly 1800 cross-section data points with the predictions using nuclear interactions generated in various ways (semi-phenomenological meson exchanges, coupled barion channels approach, chiral perturbation theory), allowed to establish for the first time a clear evidence of importance of the  $3N$  forces in the breakup process. Moreover, the results confirmed predictions of sizable influences of the Coulomb force in this reaction. Studies of the relativistic effects, another dynamical ingredient only recently introduced in the theoretical treatment of the breakup process, are under way.

## 1 Theoretical Foundations

Exploring the details of the nucleon-nucleon ( $NN$ ) interaction is one of the most intensive activities of nuclear physics. An exact knowledge of all features of the two nucleon ( $2N$ ) system dynamics would provide a natural basis

---

<sup>1</sup>E-mail address: stanislaw.kistryn@uj.edu.pl

for understanding of properties and interactions of nuclei. This optimistic presumption has to be verified by applying models of the  $NN$  interaction to describe properties of many-nucleon systems with increasing complexity. Obviously, the least complicated non-trivial environment is the one composed of three nucleons.

Dynamics of the three-nucleon ( $3N$ ) system can be comprehensively studied by means of the nucleon-deuteron ( $Nd$ ) breakup reaction. Its final state, constrained by only general conservation laws, provides a rich source of information to test the  $3N$  Hamiltonian details. It is of particular importance when components of the models which account for subtle effects, like three-nucleon force (3NF) contributions to the potential energy of the  $3N$  system, are under investigation. Nowadays precise predictions for observables in the  $3N$  system can be obtained via exact solutions of the  $3N$  Faddeev equations for any nucleon-nucleon interaction, even with the inclusion of a 3NF model [1, 2].

Models of  $NN$  forces describe the long range interaction part according to the meson-exchange picture (see Fig. 1), while the short range is based on phenomenology, adjusted by fitting a certain number of parameters to the  $NN$  scattering data. The most widely used in few-nucleon studies, so called realistic  $NN$  potentials are Argonne  $v_{18}$  (AV18), charge dependent (CD) Bonn, Nijmegen I and II (Nijm I, Nijm II). Their full equivalence with the phase shift analysis guarantees that all two-body aspects of the interaction are taken into account, what is reflected by the quality of the description which they provide for all  $pp$  and  $np$  observables below 350 MeV, expressed by a  $\chi^2$  per degree of freedom very close to 1.

In a more fundamental approach the strong forces between the nucleons should be considered as interactions between their constituent quarks and treated by quantum chromodynamics (QCD). However, the  $NN$  interaction at low energies is intrinsically non-perturbative, causing that a direct QCD approach is not practical. The link between QCD and the  $NN$  interaction phenomenology is provided by effective field theories. Chiral perturbation theory (ChPT), the expansion scheme for the nuclear systems, has been first outlined by Weinberg [3]. Its application to the two nucleon system opened the way to construct an effective  $NN$  potential consistent with the (broken) chiral symmetry of QCD. The nuclear potential is expressed by an expansion in terms of  $(Q/\Lambda_\chi)^\nu$ , with  $Q$  describing generic nucleon momentum,  $\Lambda_\chi$  representing the chiral symmetry breaking scale of about 1 GeV and  $\nu$  giving the expansion order. Within the ChPT framework a complete description of the  $NN$  and  $3N$  system has been established at the next-to-next-to-leading (NNLO) order [4–7]. Calculations for the  $NN$  system have been also performed at the next higher order, N<sup>3</sup>LO ( $\nu \leq 4$ ) [8, 9], what results in a

description of the  $NN$  data as perfect as the traditional, phenomenological models. Alas, at this order no  $3N$  contributions are included yet.

High quality models of the  $NN$  potentials, when applied to calculate observables in the  $3N$  system, revealed discrepancies between the pure pairwise dynamics and the experimental results. They have been observed in binding energies of the few-nucleon systems and, most abundantly, in various observables of the  $Nd$  elastic scattering (for a detailed list of references see e.g. Ref. [10]). The most promising and widely investigated explanation of those disagreements is the presence of a genuine three-nucleon interactions. The realistic potentials are therefore supplemented by 3NF models, usually refined versions of the Fujita-Miyazawa force, in which one of the nucleons is excited into an intermediate  $\Delta$  via a  $2\pi$ -exchange with both remaining nucleons. The most popular version of such an interaction is the Urbana IX force. The Tucson-Melbourne (TM) 3NF extends this picture by allowing for additional processes contributing to the rescattering of the exchanged mesons on the intermediate excited nucleon. Schematically the structures of the 3NF models are depicted in Fig. 1. An alternative mechanism of generating a 3NF is based on the so-called explicit  $\Delta$ -isobar excitation [11–13]. Calculations are performed in a coupled-channels approach in which the  $NN$  potential and effective 3NF is generated (together with other  $\Delta$ -isobar induced effects) due to the explicit treatment of the degrees of freedom of a single  $\Delta$ . Within the ChPT framework the 3NF appears naturally at NNLO and is handled on completely equal footing as graphs of the  $NN$  interaction. This leads to consistent  $NN$  and  $3N$  forces and also strongly constrains the

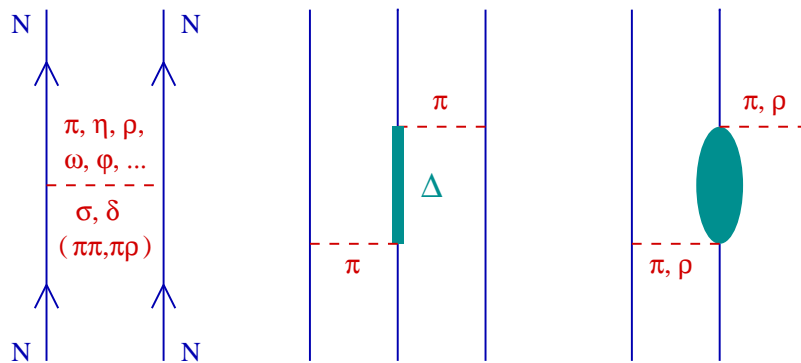


Figure 1: Schematic diagrams of the structure of the nucleon-nucleon interaction (left) and of the three-nucleon force (middle and right) in the meson exchange picture.

parameters of the 3NF.

Unfortunately, the comparisons of various elastic  $Nd$  scattering data with theoretical predictions lead to ambiguous conclusions. Sometimes inclusion of 3NF improves the agreement, but quite often (especially in the case of polarization observables) additional dynamics does not help, or even drives the predictions away from data. It is clear that the theoretical models need more constraints from the experimental data. It is therefore natural to extend the investigations of the  $3N$  system to the  $Nd$  breakup reaction. The continuum of the final states, which has to be simultaneously described in its full richness by the assumed dynamical models of  $NN$  and  $3N$  interactions, provides a lot of information to pin down the details of those theoretical models.

Additional difficulty in interpretation of the results are two features inherently present in the experimental data and until very recently missing in the theoretical formalisms. The first missing feature is the Coulomb interaction: the experiments are performed mainly for the deuteron-proton system while all calculations are strictly neglecting any long-range forces. Only in the last two years a significant step forward has been made in including the Coulomb force effects for the breakup reaction within the coupled-channels approach [14,15]. Contrary to the former expectations, the influence of the Coulomb force on the breakup observables can be quite significant. Similarly, until last year all the calculations for the breakup reaction have been performed using a nonrelativistic framework and nonrelativistic kinematics. Pioneering study on incorporating relativity in the calculation of the breakup reaction [16] showed that the effects can be sizable, again in contrast to a parallel drawn from the  $Nd$  elastic scattering case.

## 2 Experiment

Reliable breakup data sets, covering possibly large regions of the phase space, are urgently needed. Unfortunately, it still remains difficult to perform such measurements at the required level of precision. The experimental coverage is concentrated at lower energies, below 30 MeV nucleon energy – see Refs. [2,17] for references. In the recent years some revival of the activity can be noticed (see Ref. [10] for listing of papers), but again only few kinematical configurations are usually studied. Consequently, the conclusions of the studies are still rather unclear - the details of missing dynamics are waiting to be revealed.

The project dedicated towards improving the status of the breakup database has been undertaken by the Polish-Dutch collaboration. The worldwide first extensive set of the breakup cross-section data, spanned on a systematic

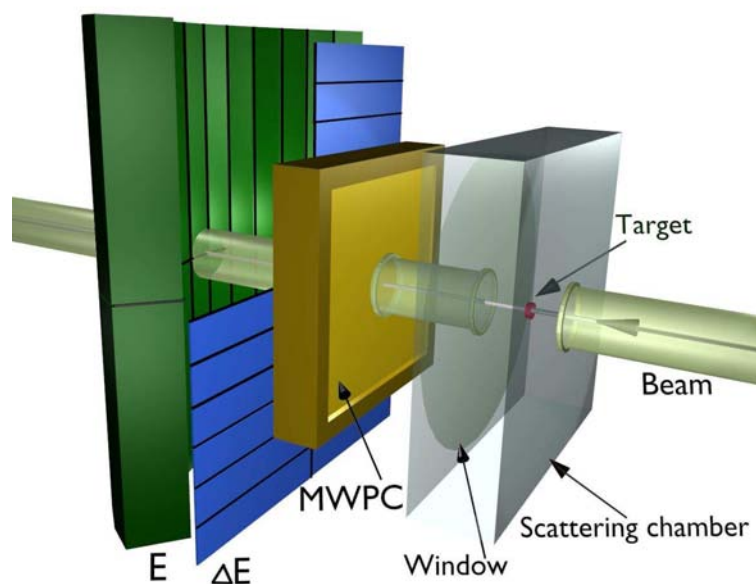


Figure 2: Schematic view of the detection system. Positions of the MWPC, the scintillation detectors and the scattering chamber with its exit window are shown and the central beam line is indicated. To allow some insight over the  $E$  detector wall 6  $\Delta E$  elements (one sector) are removed from the arrangement.

grid of kinematical variables, has been obtained in a dedicated measurement at 130 MeV of the deuteron beam. Along with the progress in a tedious data analysis the obtained results have been successively presented [18–20], amounting to a total of nearly 1800 cross-section data points. The analyzing power values are forthcoming, as well as the results for other energies [21–23].

The experimental data were acquired in measurements performed at the Kernfysisch Versneller Instituut (KVI), Groningen, The Netherlands. The deuteron beam with energy of 130 MeV was focused to a spot of approximately 2 mm diameter on a liquid hydrogen target of 4 mm thickness. The experimental setup consisted of a three-plane multi-wire proportional chamber (MWPC) and of two layers of a segmented scintillator hodoscope: horizontal transmission  $\Delta E$  and vertical stopping  $E$  detectors. Each layer consisted of 24 elements, as shown in Fig. 2.

Position information from the MWPC was used for precise reconstruction of the particle emission angles, while the hodoscope allowed to identify the charged reaction products (protons vs. deuterons) and to determine their energies. Segmentation of the detector allowed to suppress accidental coincidences and to define on-line trigger conditions with the help of special

programmable logic units.

The  $\Delta E$ -E wall covered a substantial fraction of the phase-space: from about  $10^\circ$  to  $35^\circ$  for the polar angles  $\theta$  and the full ( $2\pi$ ) range of the azimuthal angles  $\phi$ . Registered were coincidences of the charged reaction products: the two protons emitted from the breakup reaction or proton and deuteron from the elastic scattering. More details on the experimental setup and procedures, as well as on the data analysis are given in Refs. [18, 19].

### 3 Cross Section Results

The main purpose of the here discussed part of the project was a *systematic* study of the quality with which the breakup cross sections can be reproduced by theoretical predictions. The investigation spans a significant fraction of the breakup reaction phase space, with the attainable geometries defined by the experimental conditions. In the attempted systematic approach of scanning the phase space, the cross-section data are presented on a regular grid of polar and azimuthal angles with a constant step in the arclength variable  $S$ . Polar angles of the two protons  $\theta_1$  and  $\theta_2$  are changed between  $15^\circ$  and  $30^\circ$  with the step of  $5^\circ$  (with an additional set for  $\theta_1 = \theta_2 = 13^\circ$ ) and their relative azimuthal angle  $\phi_{12}$  is taken in the range from  $40^\circ$  to  $180^\circ$ , with the step of  $20^\circ$ . For each combination of the central values  $\theta_1$ ,  $\theta_2$  and  $\phi_{12}$  the experimental data were integrated within the limits of  $\pm 1^\circ$  for the polar angles and of  $\pm 5^\circ$  for the relative azimuthal angle. The bin size along the kinematic curve  $S$  was 4 MeV. Such limits allowed to reach sufficient statistical accuracy while keeping the angle and energy integration effects to a minimum, not affecting the comparison with the theoretical predictions.

The cross-section results for all 80 kinematical configurations of the  ${}^1\text{H}(d,pp)n$  breakup reaction were compared with three sets of theoretical predictions: the realistic potential approach without and with TM 3NF, the ChPT predictions and the calculations performed within the coupled-channels formalism. The detailed discussion concentrated on the influence of three-nucleon forces is given in Refs. [10, 18, 19]. A summary is shown in Fig. 3 in form of a global comparison, as the ratio of  $\chi_{2N}^2$  to  $\chi_{2N+3N}^2$  in order to magnify the influence of the 3NF effects. The  $\chi^2$  values are calculated for all data points with respect to various theoretical predictions, without and with inclusion of 3NF effects. One finds that the consistency between the predictions of the CD Bonn potential and the data is improved by adding the TM 3NF in configurations with relatively large  $\phi_{12}$  angles (ratio above 1). On the other hand, for  $\phi_{12} < 120^\circ$  including the 3NF into the calculations drives the results away from the data. This behavior is qualitatively confirmed

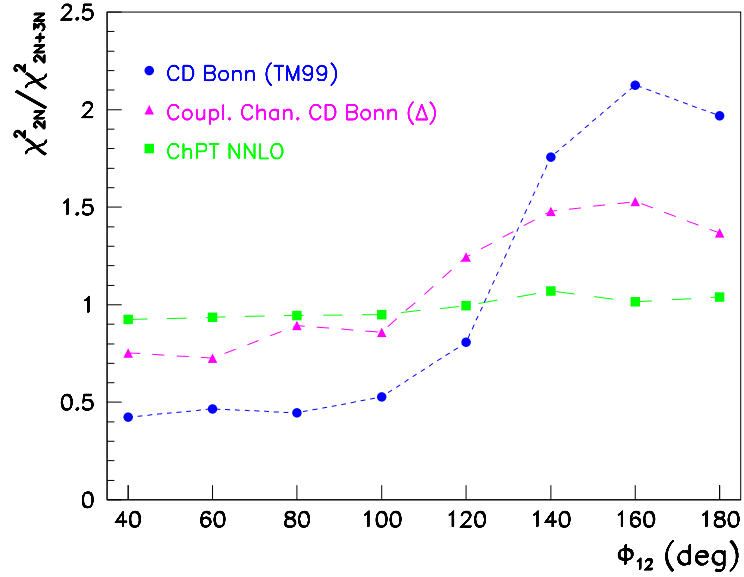


Figure 3: Ratios of  $\chi^2$  values for calculations without and with the 3NF contributions. The cross-section data with the experimental absolute normalization were used in computing the  $\chi^2_{2N}$  and  $\chi^2_{2N+3N}$  values for groups of kinematical configurations with the same  $\phi_{12}$  angle. The results of data comparison with the calculations with realistic potentials, within the coupled-channels and ChPT approaches are shown by dots, triangles and squares, respectively. Lines connecting the points are to guide the eye only.

by the coupled-channels calculations, however the amplitude of the changes induced by including the  $\Delta$ -isobar excitation contributions is smaller. For the ChPT calculations essentially no effect is present, the ratio stays close to 1 for all values of  $\phi_{12}$ , what is due to large theoretical uncertainties of the ChPT predictions at NNLO. We were able to conclude, that inclusion of 3NF (in the realistic potential approach) leads to a global better description of the data, quantified by a decrease of the  $\chi^2$  value by about 40%.

In comparisons of our results we were faced with quite substantial disagreements at low polar angles. Only with the inclusion of the Coulomb force into the calculations in the coupled-channels approach they were mostly explained and removed - see Fig. 4. Only with such a large set of the breakup data significance of the Coulomb effects could have been proved and their behavior traced over the phase space. More details on this topic are given in Refs. [10,20]. It has been also established that even after including Coulomb effects, there is still room for 3NF effects. Final conclusion, however, will be possible only when calculations treating simultaneously all the effects will

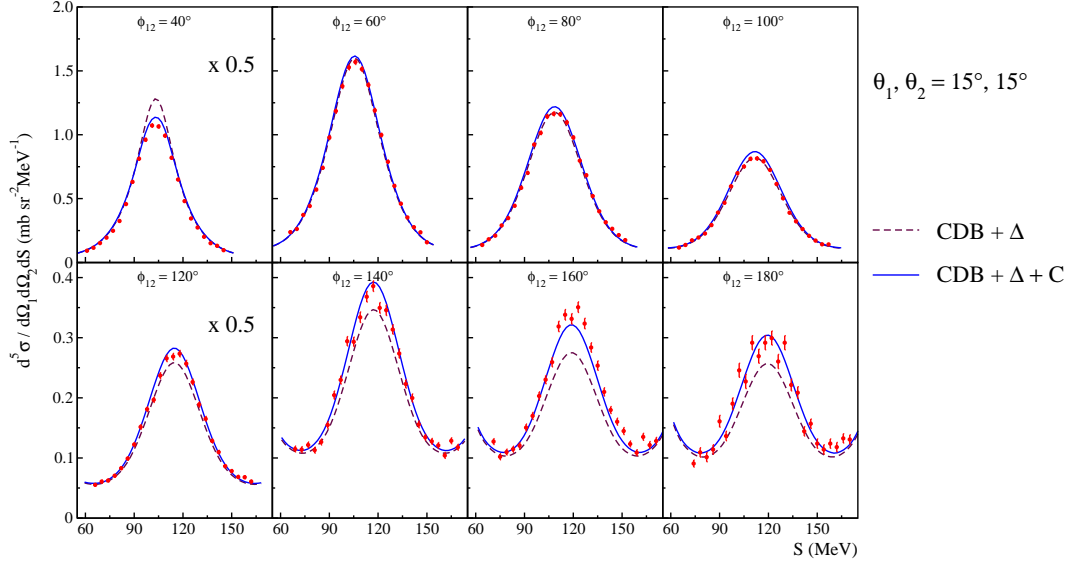


Figure 4: Differential cross sections of the deuteron-proton breakup at 130 MeV deuteron energy, plotted as a function of the arc length  $S$  along the kinematical curve. The data are shown for 8 kinematical configurations characterized by the proton polar angles  $\theta_1 = \theta_2 = 15^\circ$  and various relative azimuthal angles  $\phi_{12}$ , as indicated in the individual panels. Experimental data are compared to the results of calculations with the coupled-channels CD Bonn +  $\Delta$  potential, without (dashed lines) and with (solid lines) inclusion of the Coulomb interaction. The data and calculations in the leftmost panels are normalized to the common vertical axis by the indicated factor.

become available.

## 4 Conclusions

The described project is the first extensive and systematic study, covering a large fraction of the breakup phase space. Global comparisons of the whole cross section data set with various theoretical predictions show that the present day models of the  $3N$  system dynamics reproduce the majority of the data with satisfactory precision. In many cases in which the predicted effects due to genuine  $3NF$  are non-negligible, their inclusion tends to improve the agreement with the data. However, thanks to the applied experimental technique of covering a significant fraction of the breakup phase space with a highly symmetric detection system, it has been shown that there are also systematic regularities in discrepancies of the measured cross sections

and the predictions of all the theoretical approaches. These established disagreements are to a large extent explained by including Coulomb effects into the calculations. This is an important step towards a precise and complete description of the breakup observables, which should eventually include all aspects of the medium-energy reaction mechanism.

The theoretical predictions show that the effects of the Coulomb force, relativity and of the 3N interaction affect the breakup observables in different ways and with varying strength when inspecting the full reaction phase space. Such selectivity makes possible tracing the details of certain effects in regions where the others are proved to have relatively small influences. This is e.g. true for studies of the 3N forces - even if the Coulomb effects in the breakup cross sections are large, there are regions in which their influence is much smaller than the expected effects of the additional nuclear dynamics. With even larger experimental coverage of the breakup phase space with respect to several observables and for various beam energies, the eventually established pattern of discrepancies between the data and the calculations might help to improve the understanding of the full dynamics of the 3N system.

## Acknowledgments

This report is given on behalf of the whole Collaboration working on the described project. Indispensable contributions from all experimentalists and theoreticians are sincerely acknowledged, as well as the help of KVI technical staff. Financial support for the project has been provided in parts by several Polish, Dutch and European Institutions. The presenting author expresses thanks to the MENU 2007 Organizers for invitation and support.

## References

- [1] W. Glöckle, *The Quantum Mechanical Few-Body Problem*, (Springer-Verlag, Berlin Heidelberg, 1983, ISBN 3-540-12587-6).
- [2] W. Glöckle *et al.*, *Phys. Rep.* **274**, 107 (1996).
- [3] S. Weinberg, *Physica A* **96**, 327 (1979); *Phys. Lett.* **B295**, 114 (1992).
- [4] E. Epelbaum *et al.*, *Phys. Rev. C* **66**, 064001 (2002).
- [5] D. R. Entem and R. Machleidt, *Phys. Lett. B* **524**, 93 (2002).
- [6] E. Epelbaum, W. Glöckle, and U.-G. Meißner, *Eur. Phys. J. A* **19**, 125 (2004); *ibid.* **19**, 401 (2004).

- [7] E. Epelbaum, *Rep. Prog. Nucl. Phys.* **57**, 654 (2006).
- [8] D. R. Entem and R. Machleidt, *Phys. Rev. C* **66**, 014002 (2002); *ibid.* **68**, 041001(R) (2003).
- [9] E. Epelbaum, W. Glöckle, and U.-G. Meißner, *Nucl. Phys.* **A747**, 362 (2005).
- [10] St. Kistryn, *Three-Nucleon Force Effects in the Deuteron-Proton Breakup Reaction*, (habilitation thesis, DjaF Kraków 2005, ISBN 83-86774-42-8).
- [11] K. Chmielewski *et al.*, *Phys. Rev. C* **67**, 014002 (2003).
- [12] A. Deltuva, K. Chmielewski, and P. U. Sauer, *Phys. Rev. C* **67**, 034001 (2003).
- [13] A. Deltuva, R. Machleidt, and P. U. Sauer, *Phys. Rev. C* **68**, 024005 (2003).
- [14] A. Deltuva, A. C. Fonseca, and P. U. Sauer, *Phys. Rev. Lett.* **95**, 092301 (2005); *Phys. Rev. C* **72**, 054004 (2005).
- [15] A. Deltuva, A. C. Fonseca, and P. U. Sauer, *Phys. Rev. C* **73**, 057001 (2006).
- [16] H. Witała, J. Golak, and R. Skibiński, *Phys. Lett. B* **634** 374 (2006).
- [17] J. Kuroś-Żołnierczuk *et al.*, *Phys. Rev. C* **66**, 024004 (2002).
- [18] St. Kistryn *et al.*, *Phys. Rev. C* **68**, 054004 (2003).
- [19] St. Kistryn *et al.*, *Phys. Rev. C* **72**, 044006 (2005).
- [20] St. Kistryn *et al.*, *Phys. Lett. B* **641**, 23 (2006).
- [21] A. Biegun *et al.*, *Acta Phys. Pol. B* **37**, 213 (2006).
- [22] H. Mardanpour *et al.*, *Nucl. Phys.* **A790**, 426c (2007).
- [23] R. Sworst *et al.*, to appear in *Phys. Lett. B*.

# THREE NUCLEON SCATTERING EXPERIMENTS FROM RIKEN

*Kimiko Sekiguchi*

RIKEN Nishina Center, Saitama, 351-0198, Japan

## Abstract

Recent progress on three nucleon force study with three nucleon scattering at intermediate energies ( $E/A \approx 100$  MeV) are presented, especially focusing on the experimental work on deuteron-proton elastic scattering and breakup reactions at RIKEN. The first signature of three nucleon forces was identified in the cross section minimum for deuteron-proton elastic scattering by direct comparison between the precise data and state of the art Faddeev calculations based on the nucleon-nucleon forces plus the  $2\pi$ -exchange three nucleon forces. However the polarization observables are not always properly described by adding the three nucleon forces, indicating that components other than  $2\pi$ -exchange three nucleon forces are required to describe the data.

## 1 Introduction

A main interest of nuclear physics is to understand the forces acting between nuclear constituents. One recent topic of nuclear force study is to explore the properties of three nucleon forces (3NFs) that appear in the system more than two nucleons ( $A \geq 3$ ). The 3NFs arise naturally in the standard meson exchange picture, the main ingredient of which is considered to be  $2\pi$ -exchange with  $\Delta$ -isobar excitations [1], as well as in the more recent concept of chiral effective field theory. However the effects of the 3NFs are easily masked by those of nucleon-nucleon (NN) forces. Therefore it is hard to approach and find evidences for them experimentally.

The three nucleon (3N) scattering has been studied for a long time as one of the most promising tool to explore the properties of 3NFs since this system provides a rich set of energy dependent spin observables and differential cross sections. At lower energies ( $E/A \lesssim 20$  MeV), very high precision measurements were carried out in proton-deuteron ( $pd$ ) and neutron-deuteron ( $nd$ ) scattering, including elastic and breakup reactions. However theoretically predicted 3NF effects are rather small and a generally good description

of  $Nd$  elastic scattering data is obtained by exact solutions of 3N Faddeev equations employing NN forces only [2, 3]<sup>1</sup>. The situation of the 3NF study has changed since the end of 1990's. The following advances have made us possible to extract the 3NF effects in the 3N scattering.

(i) Establishments of the so-called modern NN forces, e.g. AV18 [4], CD-Bonn [5], Nijmegen I, II and 93 [6], which reproduce a rich set of experimental NN data up to a laboratory energy of 350 MeV with accuracy of  $\chi^2/\text{datum} \sim 1$ .

(ii) Achievements of rigorous numerical Faddeev calculations based on the modern NN potentials below the  $\pi$ -threshold energy (the incident nucleon energy  $E/A \leq 215$  MeV) [2].

(iii) Developments of experimental techniques to obtain precise data of 3N scattering at intermediate energies ( $E/A \approx 100$  MeV).

In 1998 indication of 3NF effects in the 3N scattering was first pointed out in the cross section minima for  $Nd$  elastic scattering at intermediate energies by the two theory groups [7, 8]. Since then experimental studies of the intermediate-energy  $pd$  and  $nd$  elastic scattering have been performed intensively by the several facilities, RIKEN, RCNP, KVI, IUCF and Uppsala, providing precise data of cross sections and a variety of spin observables [9–14]. The situation would be more interesting in complete  $dp$  breakup ( $d + p \rightarrow p + p + n$ ) reactions since they cover different kinematic conditions. By selecting one kinematic configuration, one hopes to enhance the effects which are sensitive to specific amplitudes of the 3NFs. Then the study of  $dp$  breakup reactions has followed as the second step of investigation of the 3NF dynamics.

The significance of 3NFs has also been pointed out in other nuclear environments than 3N scattering, e.g. descriptions of the binding of light mass nuclei and the empirical saturation point of the symmetric nuclear matter density. Microscopic calculations, such as the Green's function Monte Carlo [15, 16] and the *ab initio* no-core shell model [17] have been applied to light mass nuclei  $A \lesssim 12$  with realistic two- and three- nucleon forces, highlighting the necessity of including 3NFs to explain the binding energies of these nuclei. As for the density of the symmetric nuclear matter it has been reported that all NN potentials provide larger saturation points, and the 3NF is taken as one candidate to shift the theoretical results to the empirical point [18].

The current status is in the very beginning of the test ground of the 3NF model. In the following sections, the experimental challenges on  $dp$  scattering

---

<sup>1</sup>Exceptions are the vector analyzing powers  $A_y$  and  $iT_{11}$  and the deuteron breakup in the space star configuration.

at RIKEN [9] are presented.

## 2 Experiment

### 2.1 $dp$ Elastic Scattering

The experiments for  $dp$  elastic scattering have been performed at the RIKEN Accelerator Research Facility (RARF). The observables we have covered are cross sections and all deuteron analyzing powers ( $A_y^d$ ,  $A_{yy}$ ,  $A_{xx}$ ,  $A_{xz}$ ) in the angular range of  $\theta_{\text{c.m.}} = 10^\circ - 180^\circ$  at 70 – 135 MeV/A (deuteron energies of  $E_d = 140 - 270$  MeV). Later we have extended the measurement to the deuteron to proton polarization transfer coefficients ( $K_y^{y'}$ ,  $K_{xx}^{y'} - K_{yy}^{y'}$ , and  $K_{xz}^{y'}$ ) and the proton induced polarization  $P^{y'}$  at the angles  $\theta_{\text{c.m.}} = 90^\circ - 180^\circ$  at 135 MeV/A. Note, the  $P^{y'}$  is equivalent with the proton analyzing power  $A_y^p$  for the time-reversed reaction  ${}^2\text{H}(\mathbf{p}, p){}^2\text{H}$ .

The vector and tensor polarized deuteron beams [19] were accelerated by the AVF and Ring cyclotrons and they bombarded a liquid hydrogen or polyethylene ( $\text{CH}_2$ ) target. Either scattered deuteron or recoil proton was momentum analyzed by the magnetic spectrograph SMART (Swinger and Magnetic Analyzer with Rotator and Twister) [20] depending on the scattering angle and detected at the focal plane (see Fig. 1). For the polarization transfer measurement, the polarization of the elastically scattered protons from the hydrogen target was measured with the focal-plane polarimeter DPOL [21]. The beam polarizations were monitored with the beam line polarimeter by using the analyzing powers for  $dp$  elastic scattering. To obtain the absolute values of the deuteron beam polarizations, the analyzing powers for  $dp$  elastic scattering were calibrated by using the  ${}^{12}\text{C}(d, \alpha){}^{10}\text{B}^* [2^+]$  reaction, the  $A_{yy}(0^\circ)$  of which is exactly  $-1/2$  because of parity conservation [22]. In all the measurements the actual magnitudes of the polarizations were 60–80% of the theoretical maximum values.

### Determination of Absolute Values of Cross Section

It is essential to get precise absolute values of the cross section to compare with state of the art Faddeev calculations. However, it is usually difficult to know experimentally the systematic uncertainty. We performed the cross section measurements with the three different experimental setups and tried to estimate the systematic uncertainties. The procedure is in the following. First, we made a measurement at RIKEN with the proton beam at 135 MeV and a  $\text{CD}_2\text{-CH}_2$  sandwiched solid target at the angles where the  $pp$

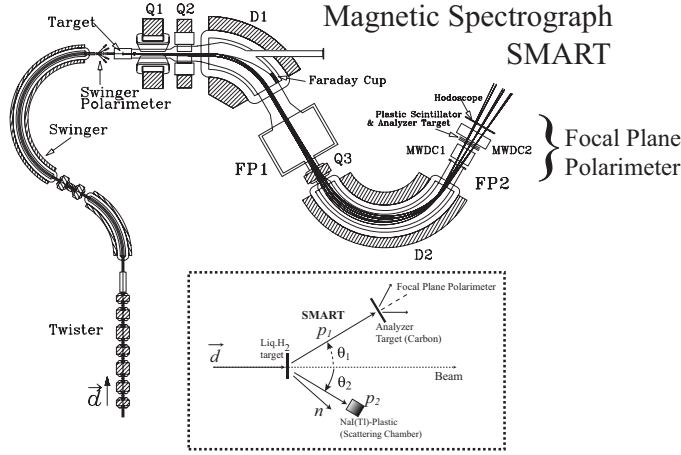


Figure 1: Schematic view of the experimental setup for the measurements on  $dp$  elastic and breakup processes at RIKEN.

and  $pd$  elastic scattering were simultaneously measured with the magnetic spectrograph SMART. Using the well-known elastic  $pp$  cross sections we can estimate the overall systematic uncertainty for the  $pd$  cross section. Secondly, to confirm the angular distribution we measured with 135 MeV/A deuterons, a  $\text{CH}_2$  solid target, and the SMART system. In the measurement we tried to check the fluctuations of the target thickness during the experiment by measuring the  $dp$  scattering at the fixed angle  $\theta_{\text{c.m.}} = 69.7^\circ$ , where the scattered deuterons and recoil protons were detected in coincidence in the scattering chamber. For the same purpose, the cross section at  $\theta_{\text{c.m.}} = 165.1^\circ$  was measured with the SMART system over several times during the experiment. Lastly, we performed a totally independent measurement at the Research Center for Nuclear Physics (RCNP) of Osaka University, using a 135 MeV proton beam and deuterated polyethylene target. The absolute normalization of the cross sections has been performed by taking data with a  $\text{D}_2$  gas target and the double slit system for which the RCNP group has already established the procedure to obtain the absolute  $pd$  cross section [10]. All the experimental results are shown in Fig. 2. The data taken at RCNP are shown with black solid diamonds. The open squares are the data measured with the proton beam at RIKEN and the open circles are the data with the deuteron beam at the same laboratory. Only statistical errors are presented. The very good agreement between the independent measurements allows us to conclude that the systematic uncertainty due to the detection setup is small [9].

## 2.2 $dp$ Breakup Reaction

The breakup experiment was also performed with the SMART spectrograph using polarized deuteron beams at 135 MeV/A. The measurement was focused on the deuteron to proton polarization transfer coefficient  $K_{yy}^{y'}$  and all deuteron analyzing powers for the specific coplanar configurations to study the model dependence of 3NFs. The angle sets of the two scattered protons ( $p_1, p_2$ ) were ( $\theta_1 = 27^\circ\text{--}33^\circ$ ,  $\theta_2 = 31^\circ$ ,  $\phi_1 - \phi_2 = 180^\circ$ ). The two emerging protons were detected in coincidence to identify the  $dp$  breakup events. The  $p_1$  was momentum analyzed by the magnetic spectrograph SMART and its polarizations were measured with the focal plane polarimeter. The  $p_2$  was detected by the  $E$ - $dE$  counters consisting of NaI(Tl) and plastic scintillators installed in a scattering chamber (see Fig. 1). The kinetic energies were covered from 164 MeV–180 MeV for the  $p_1$  and 30 MeV–75 MeV for the  $p_2$ , respectively.

## 3 Results and Discussion

### 3.1 Cross Section in elastic $dp$ scattering

In Fig. 2, the cross section data for elastic  $dp$  scattering at 135 MeV/A are compared with the Faddeev calculations by the Bochum-Cracow-KIT (BCK) group. The light (dark) shaded bands in the figure are the calculations with (w/o) Tuscon-Melbourne 99 (TM99) [23] based on the modern NN potentials, namely CDBonn, AV18, Nijmegen I, II. The solid lines are the calculation based on the AV18 potential plus the Urbana IX 3NF [24]. Note the main ingredients of these two 3NFs are  $2\pi$ -exchange with  $\Delta$ -isobar excitations. Based on the comparison between the data and the NN force predictions, the clear discrepancies are found in the angular range where the cross sections take minimum at the measured incident energies 70 and 135 MeV/A (the data at 70 MeV/A are not shown here). They become larger as an incident energy increases. The discrepancies are explained by taking into account the  $2\pi$  exchange type 3NF models (TM99, and Urbana IX). All  $2\pi$ -exchange 3NF potentials considered here provide 3NF effects for the cross section which are comparable in magnitude and sign.

Another alternative theoretical predictions have been reported by the Hannover-Lisbon group in which the  $\Delta$ -isobar excitations are explicitly included in the coupled-channel approach [25]. The contributions are based on all meson exchanges, i.e.  $\pi$ ,  $\rho$ ,  $\sigma$ , and  $\omega$  exchanges contained in the coupled-channel approach. Thus the  $\pi$ - $\pi$ ,  $\pi$ - $\rho$ ,  $\rho$ - $\rho$  with  $\Delta$ -isobar excitations as well as the Illinois type [16] many- $\pi$  rings are incorporated effectively. The CD-

Bonn potential was taken as the NN interaction. Recently this group has succeeded in incorporating the Coulomb forces via the screening and renormalization approach in the momentum-space framework [26]. The results are shown in Fig. 2. The dashed curves are the coupled-channel approach obtained with the  $\Delta$ -isobar excitations and the dotted curves are the predictions in which the Coulomb interactions are additionally included. The predictions with the NN forces only are not shown in the figures since they provide the similar results to those on the CDBonn potential by the BCK group. The  $\Delta$ -isobar effects improve the agreement in the angular range where the cross sections take minimum as is similar to the results by the BCK group. It should be noted that taking into account the Coulomb forces provides a good agreement at the very forward angles.

The theoretical approach to estimate the effects other than 3NFs is also in progress. The BCK group have recently reported the calculations with the Lorentz boosted NN potentials [27,28] to estimate the relativistic effects in 3N scattering. For the cross section in elastic  $Nd$  scattering their effects are restricted at the very backward angles, indicating that the 3NF is only a plausible mechanism to resolve the discrepancies between NN theory and the experimental data in the cross section minimum.

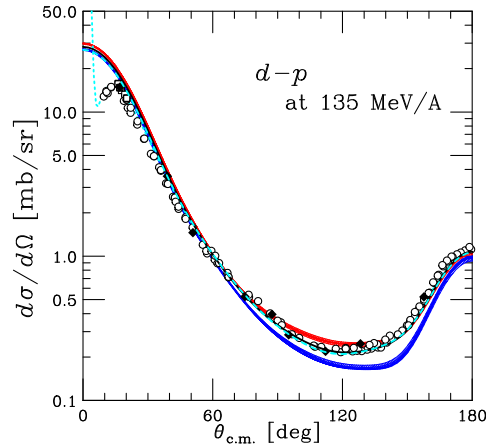


Figure 2: Cross section for  $dp$  elastic scattering at 135 MeV/A. For the descriptions of the theoretical predictions, see text.

### 3.2 Polarization Observables in Elastic $dp$ Scattering

Parts of the polarization observables in  $dp$  elastic scattering are shown with open circles in Fig. 3. The statistical errors are only shown in the figure

and their values are less than 0.03 for all the measured observables. Generally, the discrepancies between the data and the pure NN force predictions (dark shaded bands) are clearly seen at the angles where the cross sections take minimum. However the predictions based on NN + 3NF not always provide better descriptions of the data. The agreements are improved by incorporating the TM99 or Urbana IX 3NF for the proton analyzing power  $A_y^p$  and the polarization transfer coefficient  $K_{xx}^{y'} - K_{yy}^{y'}$ , while for the tensor analyzing powers  $A_{xx}$  and  $A_{yy}$ , differences between the data and the NN force predictions are not reproduced by adding the 3NFs. The  $\Delta$ -isobar effects (dotted curves) are similar to those of the TM99 and Urbana IX 3NFs for almost all observables except for the tensor analyzing power  $A_{xx}$  for which the prediction with the  $\Delta$ -isobar has a better agreement.

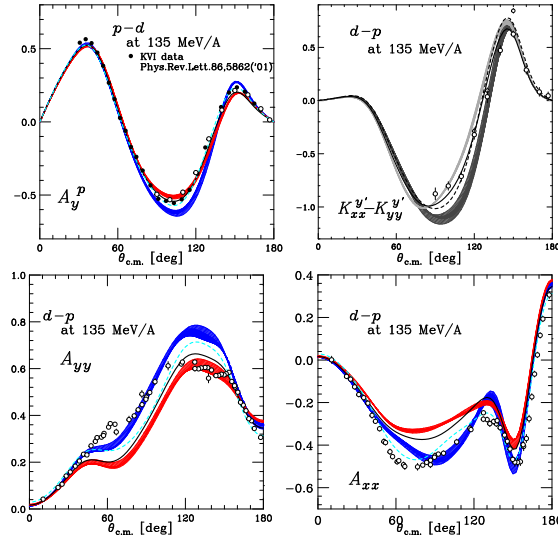


Figure 3: Proton and deuteron analyzing powers and polarization transfer coefficients for  $dp$  elastic scattering at 135 MeV/A. For the descriptions of the theoretical predictions, see text.

### 3.3 Polarization Observables in $dp$ Breakup Reactions

In Fig. 4 the experimental results are shown with open circles along with the kinematic curves of the emerging two protons (S-curve). The statistical errors are only shown and they are less than 0.03 for all the measured observables. The data were obtained with the S-curve energy bin of 8 MeV for the analyzing powers and 12 MeV for the polarization transfer coefficients. The predictions shown here are averaged over the S-curve energy bin of 8 and/or

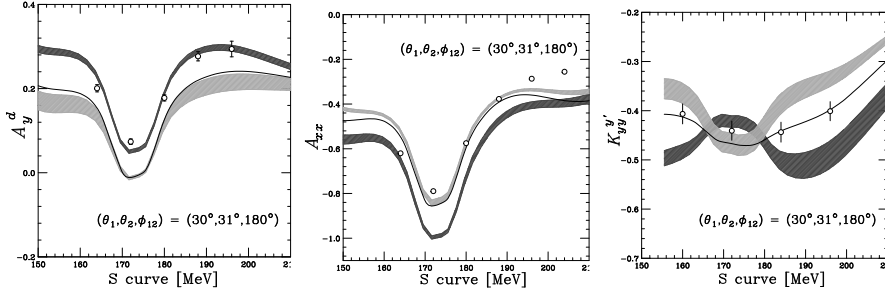


Figure 4: Analyzing powers ( $A_y^d$ ,  $A_{xx}$ ) and deuteron to proton polarization transfer coefficient  $K_{yy}^{y'}$  for the  $dp$  breakup reaction at 135 MeV/A. For the descriptions of the theoretical predictions, see text.

12 MeV for the direct comparison between the data and the calculations. For the polarization transfer  $K_{yy}^{y'}$ , the inclusions of the 3NFs change the shapes of the predictions from those on the pure NN forces (a dark shaded band) drastically. The different results are predicted between the TM99 3NF (a light shaded band) and the Urbana IX 3NF (a solid curve). The data rather support the predictions with the Urbana IX 3NF. For the tensor analyzing power  $A_{xx}$  the agreements are improved by adding the TM99 or Urbana IX 3NFs, however for the vector analyzing power  $A_y^d$  the agreement is deteriorated by taking into account the 3NFs. The data are well reproduced by the predictions with the NN forces only.

The cross section data for elastic  $dp$  scattering have opened up a new possibility to explore 3NFs via the 3N scattering at intermediate energies. The results of spin observables both for  $dp$  elastic and breakup reactions indicate insufficient understanding of spin dependent parts of 3NFs. It would be interesting to see how well the theoretical approaches, e.g. addition of 3NFs other than  $2\pi$  exchange types, relativistic treatment, and the potentials based on chiral effective field theory [29] describe these obtained data.

## 4 Summary

The 3NFs are now taken as key elements to understand various nuclear phenomena, such as the binding of light mass nuclei and the empirical saturation point of nuclear matter density. The  $Nd$  scattering provide rich sources to explore the properties of 3NF such as momentum and spin dependences. Since the end of 1990's extensive experimental challenges on proton–deuteron and neutron–deuteron elastic scattering at intermediate energies

( $E/A \approx 100$  MeV) have been performed at several facilities. Study of  $Nd$  breakup reactions has followed as the second step. In this talk, the experimental work on  $dp$  elastic scattering and  $dp$  breakup reactions at RIKEN was presented. Comparing the data with state of the art Faddeev calculations the cross section data for elastic  $dp$  scattering are explained by incorporating  $2\pi$ -exchange 3NFs, which is the first clear signature of 3NF effects in the three nucleon scattering. However polarization observables are not always properly described by adding the 3NFs, indicating that additional components are required to describe the data. To understand these spin observables, theoretical approaches incorporating 3NFs other than  $2\pi$  exchange types, relativistic treatment, incorporating of coulomb effects, and completely new approach based on chiral effective field theory are now in progress.

## Acknowledgments

This work has been performed in collaboration with RIKEN, the University of Tokyo, RCNP, Tokyo Institute of Technology, KVI, Kyushu University, Saitama University, Jagiellonian University, Ruhr-Universität Bochum, Kyushu Institute of Technology, Forschungszentrum of Jülich, Universität Hannover, and Universidade de Lisboa.

## References

- [1] J. Fujita, and H. Miyazawa, Prog. Theor. Phys. **17**, 360 (1957).
- [2] W. Glöckle, H. Witała, D. Hüber, H. Kamada and J. Golak, Phys. Rep. **274**, 107 (1996).
- [3] A. Kievsky, M. Viviani, and S. Rosati, Phys. Rev. C **64**, 024002 (2001).
- [4] R. B. Wiringa *et al.*, Phys. Rev. C **51**, 38 (1995).
- [5] R. Machleidt, Phys. Rev. C **63**, 024001 (2001).
- [6] V. G. J. Stoks *et al.*, Phys. Rev. C **49**, 2950 (1994).
- [7] H. Witała *et al.*, Phys. Rev. Lett. **81**, 1183 (1998).
- [8] S. Nemoto *et al.*, Phys. Rev. C **58**, 2599 (1998).
- [9] N. Sakamoto *et al.*, Phys. Lett. B **367**, 60 (1996); H. Sakai *et al.*, Phys. Rev. Lett. **84**, 5288 (2000); K. Sekiguchi *et al.*, Phys. Rev. C **65**, 034003

- (2002); K. Sekiguchi *et al.*, Phys. Rev. C **70**, 014001 (2004); K. Sekiguchi *et al.*, Phys. Rev. Lett **95**, 162301 (2005).
- [10] K. Hatanaka *et al.*, Phys. Rev. C **66**, 044002 (2002).
- [11] R. Bieber *et al.*, Phys. Rev. Lett. **84**, 606 (2000); K. Ermisch *et al.*, Phys. Rev. Lett. **86**, 5862 (2001); K. Ermisch *et al.*, Phys. Rev. C **68**, 051001 (2003); K. Ermisch *et al.*, Phys. Rev. C **71**, 064004 (2005); H. R. Amir-Ahmadi *et al.*, Phys. Rev. C **75**, 041001 (2007); H. Mardanpour *et al.*, Eur. Phys. J. A **31**, 383 (2007).
- [12] E. J. Stephenson *et al.*, Phys. Rev. C **60**, 061001 (1999); R. V. Cadman *et al.*, Phys. Rev. Lett. **86**, 967 (2001); B. v. Przewoski *et al.*, Phys. Rev. C **74**, 064003 (2006).
- [13] P. Mermod *et al.*, Phys. Rev. C **72**, 061002 (2005).
- [14] Y. Maeda *et al.*, Phys. Rev. C **76**, 014004 (2007).
- [15] R. B. Wiringa *et al.*, Phys. Rev. C **62**, 014001 (2000).
- [16] S. C. Pieper *et al.*, Phys. Rev. C. **64**, 014001 (2001).
- [17] P. Navrátil and W. E. Ormand, Phys. Rev. C **68**, 034305 (2003).
- [18] see for example, A. Akmal *et al.*, Phys. Rec. C **58**, 1804 (1998).
- [19] H. Okamura *et al.*, AIP Conf. Proc. **293**, 84 (1994).
- [20] T. Ichihara *et al.*, Nucl. Phys. **A569**, 287c (1994).
- [21] S. Ishida *et al.*, AIP Conf. Proc. **343**, 182 (1995).
- [22] K. Suda *et al.*, Nucl. Instrum. Methods Phys. Res. A **572**, 745 (2007).
- [23] S. A. Coon and H. K. Han, Few Body Syst., **30**, 131 (2001).
- [24] B. S. Pudliner *et al.*, Phys. Rev. C **56**, 1720 (1997).
- [25] A. Deltuva *et al.*, Phys. Rev. C **68**, 024005 (2003).
- [26] A. Deltuva *et al.*, Phys. Rev. C **71**, 054005 (2005).
- [27] H. Kamada *et al.*, Phys. Rev. C **66**, 044010 (2002).
- [28] H. Witała *et al.*, Phys. Rev. C **71**, 054001 (2005).
- [29] E. Epelbaum Prog. Part. Nucl. Phys. **57**, 654 (2006).

# ELECTROMAGNETIC REACTIONS ON LIGHT NUCLEI USING CHIRAL EFFECTIVE THEORY

*D. R. Phillips*

Department of Physics and Astronomy  
Ohio University  
Athens, OH 45701  
USA.

## Abstract

I describe the use of chiral effective theory ( $\chi$ ET) to compute electromagnetic reactions in two- and three-nucleon systems. I first explain how chiral perturbation theory can be extended to the few-nucleon sector. I then explain the predictions of the resulting  $\chi$ ET for electron-deuteron scattering, and how they will be tested by forthcoming data from BLAST. I conclude by displaying predictions for elastic Compton scattering from deuterium and Helium-3 nuclei. These computations, in concert with future data from MAX-Lab and HI $\gamma$ S, should give significant new information on neutron polarizabilities, and hence yield insight into the structure of the nucleon.

## 1 Introduction

Chiral perturbation theory ( $\chi$ PT) is the effective theory of the strong interaction at low energies. In  $\chi$ PT quantum-mechanical amplitudes for the interaction of pions and photons with each other and with nucleons are expanded in powers of the small parameter  $P$ , where  $P \equiv \frac{p, m_\pi}{\Lambda_{\chi SB}}$ . The scale  $\Lambda_{\chi SB} \sim m_\rho, 4\pi f_\pi$  in the meson sector, but is somewhat lower for reactions involving baryons unless additional degrees of freedom (in particular the Delta(1232)) are included explicitly in the theory.

The amplitudes we seek are computed using the technology of effective field theory (EFT), in which the field-theoretic Lagrangian is organized in an expansion in powers of  $P$  and loop calculations are then also organized via the same hierarchy. Computing the  $\chi$ PT result for a given process at a fixed order in  $P$  is simply a matter of writing down the Lagrangian up to that order and computing all the pertinent diagrams. An introduction to,

and explicit examples of, this strategy was given in Prof. Gasser’s talk at this meeting [1].

This approach has had much success in treating  $\pi\pi$  and  $\pi N$  interactions at energies below  $\Lambda_{\chi\text{SB}}$  (see Ref. [2] for a recent review). However, an obvious problem arises when we attempt to extend it to light nuclei: a perturbative expansion of amplitudes is not adequate to describe bound states. In 1990 Weinberg proposed that the fact that the nucleon mass,  $M \sim \Lambda_{\chi\text{SB}}$ , mandates resummation of diagrams with  $NN$  intermediate states, and so, when computing  $NN \rightarrow NN$ ,  $\chi$ PT should be applied not to the  $NN$  amplitude, but to the  $NN$  potential  $V$  [3]. In such an expansion the leading-order (LO)  $NN$  potential,  $V$ , is:

$$\langle \mathbf{p}' | V | \mathbf{p} \rangle = -\frac{g_A^2}{4f_\pi^2} \tau_1 \cdot \tau_2 \frac{\sigma_1 \cdot (\mathbf{p}' - \mathbf{p}) \sigma_2 \cdot (\mathbf{p}' - \mathbf{p})}{(\mathbf{p}' - \mathbf{p})^2 + m_\pi^2} + C, \quad (1)$$

where  $g_A$  and  $f_\pi$  are the nucleon’s axial charge and the pion-decay constant, and the constant(s)  $C$  (there is actually one for spin-singlet and one for spin-triplet  $NN$  states) is not determined by chiral symmetry and must be obtained from  $NN$  data.  $V$  is then inserted into the Schrödinger equation

$$\left( \frac{\hat{\mathbf{p}}^2}{M} + V \right) |\psi\rangle = E|\psi\rangle, \quad (2)$$

to generate bound and scattering states of two, or more, nucleons. This strategy, which has come to be known as “chiral effective theory” ( $\chi$ ET) produces a quantum-mechanical description of light nuclei, in which the potential  $V$  (and other operators too) have a systematic chiral expansion and a rigorous connection with the chiral symmetry of QCD and the pattern of its breaking.

Since the potential  $V$  is singular a cutoff,  $\Lambda$ , must be introduced. The constant  $C$  is then a function of  $\Lambda$ . The question arises as to whether this will be sufficient to renormalize the  $NN$  amplitude obtained by iterating  $V$ , i.e. whether there is significant residual  $\Lambda$ -dependence in  $NN$  observables after the value of  $C$  is adjusted to reproduce the very-low-energy  $NN$  data.

There has been much debate on this point over the past 10 years, but it has now been shown that a single constant  $C$  is sufficient to renormalize the  $NN$  problem in the  ${}^3\text{S}_1$ – ${}^3\text{D}_1$  channel at LO [4–6]. Moreover, these papers argue that it is necessary to solve the Schrödinger equation with the LO chiral potential precisely because that potential is not weak. In contrast to the  $A = 0$  and  $A = 1$  sectors a perturbative expansion for the  $NN$  interaction mediated by pions only converges for  $p \lesssim m_\pi$ : the one-pion exchange part of  $V$  is strongly attractive—singular even—in the  ${}^3\text{S}_1$ – ${}^3\text{D}_1$  channel.

More recently it has been pointed out that there are channels of higher angular momentum where the LO potential (1) is also singular and attractive,

but where the constant  $C$  is not operative [7]. Consequently it is impossible to generate  $\Lambda$ -independent predictions in those channels (e.g.  ${}^3P_0$ ) over a wide cutoff range. How wide a  $\Lambda$  range should be employed is still debated [8]. Ultimately renormalization-group techniques would seem the best way to determine what operators must be included to renormalize  $\chi$ ET to a given level of accuracy [6]. This is an ongoing discussion.

But its ultimate resolution should not have a significant impact on the results I present here, which are predominantly for deuterium, where this is a solved problem (at least at LO). In Sec. 2 I show results for deuteron electromagnetic form factors as a function of the cutoff  $\Lambda$  and demonstrate that cutoff artifacts indeed disappear as  $\Lambda \rightarrow \infty$ . I also describe how a chiral expansion for the deuteron charge operator generates precision predictions for the ratio  $G_C/G_Q$  that was recently measured at BLAST. In Sec. 3 I summarize  $\chi$ ET calculations of elastic photon scattering from deuterium and Helium-3 nuclei. And in Sec. 4 I provide a brief summary of other reactions involving light nuclei that have been successfully described in  $\chi$ ET.

## 2 Electron-deuteron scattering in $\chi$ ET

In Ref. [7] Eq. (2) was solved for the potential (1) in momentum space for  $\Lambda = 0.4\text{--}4$  GeV. In Ref. [5] the same problem was solved in co-ordinate space by converting  $C$  into a boundary condition on the wave function as  $r \rightarrow 0$  [5]. We now present results for deuteron electromagnetic form factors that show that the latter wave function can be regarded as the  $\Lambda \rightarrow \infty$  limit of the Fourier transform of the momentum-space wave functions [9].

The deuteron charge and quadrupole form factors  $G_C$  and  $G_Q$  involve matrix elements of the (Breit-frame) deuteron charge operator  $J_0$  between these wave functions (for formulae see, e.g. Refs. [10, 11]). Here we will compare  $\chi$ ET predictions for  $G_C$  with extractions from data for the deuteron structure function  $A$  and the tensor-polarization observable  $T_{20}$  [12]. For this purpose we use the deuteron current operator

$$\langle \mathbf{p}' | J_0(\mathbf{q}) | \mathbf{p} \rangle = |e| \delta^{(3)}(p' - p - q/2) G_E^{(s)}(Q^2), \quad (3)$$

with  $G_E^{(s)}$  the nucleon's isoscalar electric form factor. This is the result for  $J_0$  up to corrections suppressed by  $P^3$  (apart from some small effects that have coefficients  $\sim 1/M^2$ ). The strict LO  $\chi$ ET result for deuteron form factors is found by taking  $G_E^{(s)} = 1$ . However, here we wish to test  $\chi$ ET's predictions for deuteron structure, so we adopt ‘‘experimental’’ data for  $G_E^{(s)}$  (the parameterization of Belushkin *et al.* [13]) and compute  $G_C$ . Up to the order we work to this is equivalent to computing the ratio  $G_C/G_E^{(s)}$  in  $\chi$ ET.

The results are shown in the left panel of Fig. 1. Here the value of  $C$  is adjusted to ensure that the deuteron binding energy is reproduced, but the calculation contains no other free parameters. We observe that as  $\Lambda \rightarrow \infty$  the momentum-space wave functions produce a  $G_C$  that converges to a definite result (although asymptopia is not reached in  $G_C$  until  $\Lambda \approx 10 \text{ fm}^{-1}$ ). This result is consistent with that found using the co-ordinate space approach of Ref. [5]. The agreement with experimental data at low- $|\mathbf{q}|$  is quite good, but the LO wave functions predict a minimum in  $G_C$  at too large a  $Q^2$ . These trends are even more pronounced in  $G_Q$  (not shown), where we are within a few per cent of the asymptotic result at  $\Lambda = 4 \text{ fm}^{-1}$ , and the agreement with experimental data is excellent to a surprisingly large value of  $|\mathbf{q}|$ .

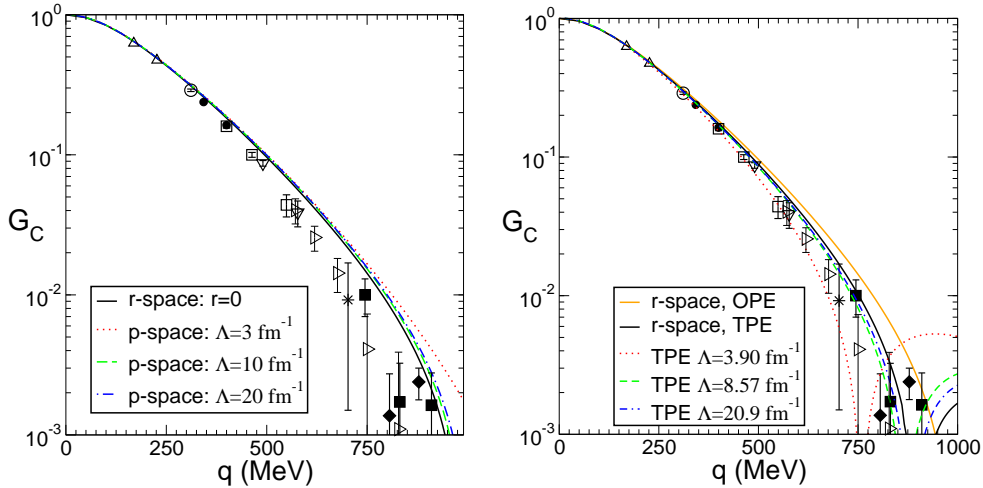


Figure 1: Predictions for  $G_C$  with LO wave functions (left panel) and wave functions including two-pion exchange (right panel). In each case results for four different regulators are shown. Data are taken from Ref. [12].

To go beyond LO we must consider corrections to the  $NN$  potential  $V$ , and to the charge operator  $J_0$ . When the two-pion-exchange mechanisms that define  $V$  up to  $\mathcal{O}(P^3)$  [14] are included the renormalization becomes a little more complicated since there are two undetermined parameters summarizing deuteron physics at scales  $> \Lambda_{\chi SB}$ . Here these constants are adjusted to reproduce the deuteron properties  $B = 2.22457 \text{ MeV}$ ,  $A_S = 0.885 \text{ fm}^{-1/2}$  and  $\eta = 0.0256$  [9]. Once again we see that convergence to the  $\Lambda \rightarrow \infty$  result is somewhat slow, but a smooth  $\Lambda \rightarrow \infty$  limit does exist. We also see that the two-pion-exchange corrections to  $V$  result in only a small shift in  $G_C$  in the range  $|\mathbf{q}| < 800 \text{ MeV}$ . This lends credence to the idea that these corrections could be treated in perturbation theory—at least in the  ${}^3S_1$ - ${}^3D_1$  channel. It is also significant that these corrections shift the  $G_C$  minimum to

the left as compared to the LO result, thereby improving the agreement with experiment. This suggests that electron-deuteron data provide evidence for the presence of two-pion-exchange pieces in the  $\chi$ ET potential  $V$ .

The existence of the minimum in  $G_C$  provides an opportunity to examine the impact on  $G_C$  of the meson-nucleon dynamics that enters the chiral  $NN$  potential. In particular, different choices of the  $\pi$ N LECs  $c_i$  that enter  $V$  produce minima in somewhat different locations [9]. However, it is difficult to draw any real conclusion as regards the preference of existing  $G_C$  data for a particular set of  $c_i$ 's, since the  $\mathcal{O}(P^3)$  corrections to  $J_0$  that were not included in Eq. (3) have an impact on the position of the minimum of  $G_C$  that is at least as large as the effect of choosing different sets of  $c_i$ 's.

We close this section by pointing out that this type of analysis, when carried out to higher orders in  $\chi$ ET, results in a precise prediction for the ratio of deuteron form factors  $G_C/G_Q$  in the kinematic range of forthcoming data from BLAST. In Ref. [11] all contributions to  $J_0$  (including two-body effects) up to order  $P^3$  relative to leading were computed. A variety of wave functions that included all the two-pion-exchange effects up to  $\mathcal{O}(P^3)$  were also employed. Significant sensitivity to short-distance  $NN$  physics was found in the resulting deuteron quadrupole moment  $Q_d$ : it varied by 2% when the cutoff in the  $NN$  system was changed by  $\sim 100\%$ . Intriguingly, this is roughly the magnitude of the discrepancy between the  $Q_d$  predicted at  $\mathcal{O}(eP^3)$  and the experimental value  $Q_d = 0.2859(3)$  fm<sup>2</sup>. This encouraged us to include in our analysis a short-distance operator that represents the contribution of modes above  $\Lambda_{\chi\text{SB}}$  to  $G_Q$ . This operator has much slower  $Q^2$ -dependence than the one-body mechanisms that give the LO contribution to  $G_Q$ , so we can constrain its impact by demanding that its coefficient is such that the experimental  $Q_d$  is reproduced. This vitiates our ability to predict  $G_Q$  at  $Q^2 = 0$ , but we can still predict the  $Q^2$ -dependence of  $G_Q$ . The prediction's remaining theoretical uncertainty—which comes from the  $Q^2$ -dependence of short-distance  $NN$  physics—is small, being only 3% at  $|\mathbf{q}| = 2$  fm<sup>-1</sup>. It is important to note that the  $\chi$ ET predictions for  $G_C/G_Q$  [11] have a rather different  $Q^2$ -dependence to those obtained in potential models (see, e. g., Fig. 11 of Ref. [10]), and so the BLAST data will provide a significant test of this approach to deuteron electromagnetic structure.

### 3 Compton scattering on $A = 2$ and 3 nuclei

Now we turn our attention to Compton scattering from the deuteron. The first calculation of this process in  $\chi$ ET computed the  $\gamma$ d amplitude

$$\mathcal{A} \equiv \langle \psi_d | \hat{\mathcal{O}} | \psi_d \rangle \quad (4)$$

by considering the operator  $\hat{O}$  up to  $\mathcal{O}(e^2P)$  [NLO] and using a variety of phenomenological deuteron wave functions [15]. At this order  $\chi$ ET makes a prediction for  $\mathcal{A}$ , and hence for the  $\gamma d$  differential cross section (dcs) [15], as well as single- and double-polarization observables [16].

For photon energies  $\omega$  such that  $\frac{m_\pi^2}{M} \ll \omega \sim m_\pi$ ,  $\hat{O}$  begins at  $\mathcal{O}(e^2)$  with the proton Thomson amplitude  $\sim \frac{-e^2}{M}$ . At  $\mathcal{O}(e^2P)$   $\hat{O}$  includes ‘‘pion-cloud’’ mechanisms that generate the leading contribution to the nucleon’s electric and magnetic polarizabilities,  $\alpha$  and  $\beta$ . It also includes analogous two-nucleon mechanisms where the incoming and outgoing photons couple to what can be thought of as the deuteron’s pion cloud, i.e. the exchanged pions that generate the LO  $\chi$ PT potential. These exchange currents are large, providing about 50% of the  $\gamma d$  dcs at  $\omega = 65$  MeV. At these energies the  $\chi$ ET prediction is in good agreement with data (see left panel of Fig. 2). However, the agreement with data at 95 MeV is not good (see right panel of Fig. 2). Later  $\chi$ ET calculations extended the calculation of  $\hat{O}$  to  $\mathcal{O}(e^2P^2)$  and used  $\chi$ ET wave functions [17]. However, this leads to very little improvement in the description of the 95 MeV data.

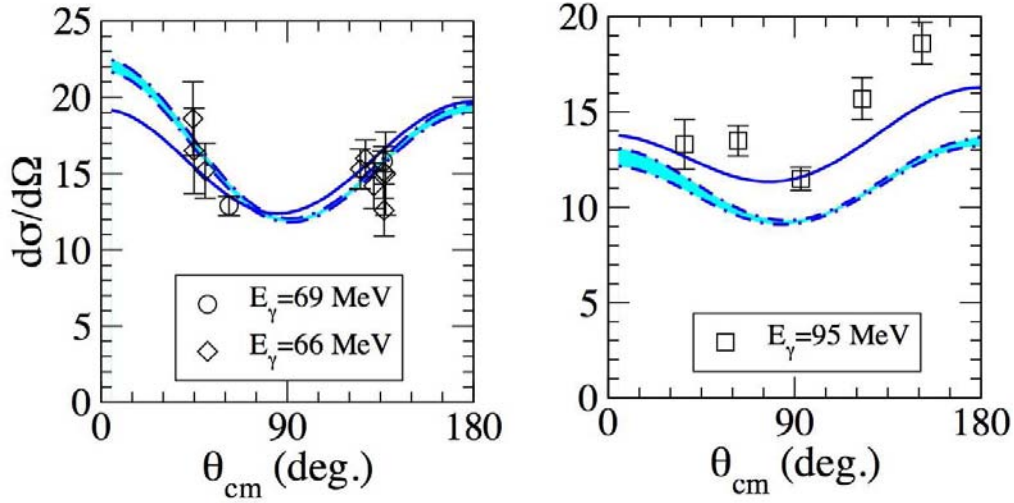


Figure 2: Centre-of-mass frame  $\gamma d$  dcs at  $\omega = 67$  and  $94.5$  MeV respectively. The dot-dashed line is the prediction at  $\mathcal{O}(e^2P)$ , with the band an estimate of the uncertainty due to short-distance  $NN$  physics. The solid line is a fit at  $\mathcal{O}(e^2P^2)$ . Adapted from Ref. [17], which includes references to data.

The rapid rise in the  $\gamma d$  dcs at backward angles is now understood to be due to M1 excitation of the Delta(1232) resonance [18]. Chiral EFTs that include this resonance as an explicit degree of freedom describe the backward-angle 95 MeV data well [19]. At the same time the power counting

in  $\chi$ ET for  $\omega \sim \frac{m_\pi^2}{M}$  has been worked out. In this domain additional diagrams that ensure that the low-energy theorem for  $\gamma d$  at  $\omega = 0$  is obeyed must be included, and these have now been computed [20]. But these diagrams are formally and numerically sub-leading for  $\omega \sim m_\pi$ . If they are included in the computation of  $\hat{O}$  for  $\omega \approx 90$  MeV the variation in the cross section due to short-distance physics in the  $NN$  system is reduced to 1–2% [19,20].

Therefore the elements needed for a  $\chi$ ET calculation of the  $\gamma d$  dcs in the range  $\omega = 50$ – $100$  MeV with an accuracy  $\sim 3\%$  are now understood. This ability of  $\chi$ ET to calculate the  $NN$  dynamics in such a controlled way motivates experimental efforts that aim to use new  $\gamma d$  data to extract the isoscalar combinations of nucleon electric and magnetic polarizabilities  $\alpha_N \equiv (\alpha_p + \alpha_n)/2$  and  $\beta_N \equiv (\beta_p + \beta_n)/2$  [19]. One such experiment is underway at the MAX-Lab facility at Lund, and will significantly increase the world data-base on the  $\gamma d$  reaction [21]. When this new data is used in concert with a new, precision  $\chi$ ET calculation of  $\gamma d$  it should yield an extraction of  $\alpha_N - \beta_N$  with an accuracy comparable to that with which  $\alpha_p - \beta_p$  is presently known. This will provide important constraints on the interplay between the pion-cloud mechanisms that generate the dominant piece of the nucleon's electric polarizability and other mechanisms that contribute to  $\alpha_N$  and  $\beta_N$ .

Recently it has been pointed out that elastic Compton scattering from the Helium-3 nucleus also provides access to information on neutron polarizabilities [22]. In this case the presence of two protons in the nucleus significantly enhances the Compton cross section. It also enhances (in absolute terms) the impact of  $\alpha_n$  and  $\beta_n$  on observables, because in coherent  $\gamma^3\text{He}$  scattering the polarizability effects in the single-nucleon Compton amplitude interfere with *two* proton Thomson terms.

We have performed  $\chi$ ET calculations of  $\gamma^3\text{He}$  scattering at  $\mathcal{O}(e^2P)$  [NLO] [22]. These calculations employ the same operator  $\hat{O}$  as was used for  $\gamma d$  scattering in Ref. [15], as well as a variety of  $\chi$ ET three-nucleon wave functions that are consistent with  $\hat{O}$  at this order in  $\chi$ ET. This is the first consistent  $\chi$ ET calculation of an electromagnetic reaction on the three-body system (but see also Ref. [23] for static electromagnetic properties of the trinucleons) and—so far as I am aware—the first calculation of  $\gamma^3\text{He}$  scattering. Once again,  $\chi$ ET makes a prediction for Compton observables at this order, with the impact of  $\alpha_n$  and  $\beta_n$  on the dcs shown in Fig. 3.

We can also predict the asymmetries that would be obtained were circularly polarized photons to scatter from Helium-3 nuclei polarized parallel ( $\Sigma_z$ ) or perpendicular ( $\Sigma_x$ ) to the incoming beam. In the Helium-3 nucleus, the two protons are predominantly in a  $^1S_0$  state, and so the double-polarization observables are dominated by the contribution from the neutron

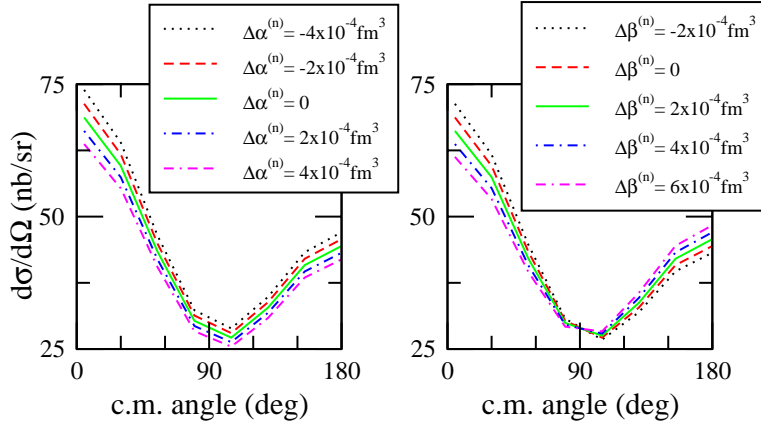


Figure 3: Centre-of-mass frame differential cross section for  $\gamma^3\text{He}$  scattering at 80 MeV as predicted at  $\mathcal{O}(e^2P)$ , with the addition of shifts in  $\alpha_n$  (left panel) and  $\beta_n$  (right panel). Taken from Ref. [22].

that is (mostly) carrying the spin of the polarized Helium-3. For photon energies above 100 MeV we find significant sensitivity in  $\Sigma_z$  and  $\Sigma_x$  to neutron spin polarizabilities [24]. Experiments that will measure these asymmetries are planned for the HI $\gamma$ S facility at the Triangle Universities Nuclear Laboratory [25], and will provide important new constraints on low-energy neutron spin structure.

## 4 Other reactions on light nuclei in $\chi$ ET: briefly

The dynamics of mesons and nucleons that is the focus of these meetings has significant consequences for nuclear physics. In particular, the  $\pi N$  interactions that are encoded in  $\chi$ PT are now being used as the basis for a quantitative understanding of few-nucleon systems. In this talk I have discussed only the portion of this understanding that pertains to electromagnetic reactions. But the  $\chi$ ET approach to nuclear dynamics has also had significant success in describing both elastic scattering and breakup reactions in neutron-deuteron and proton-deuteron experiments [26]. For comprehensive reviews of the application of  $\chi$ ET to few-nucleon systems see Refs. [27].

Meanwhile,  $\chi$ ET has also been used with significant success in understanding low-energy weak processes [28]. The fact that the chiral Lagrangian provides a connection between these reactions and pionic processes such as  $\pi^-d \rightarrow nn\gamma$  [29] is now being exploited to yield new, more precise calculations of the latter process [30]. Furthermore, several contributions to this conference described progress in pionic reactions on deuterium [31]. The re-

sulting calculations are evidence of the power of a description which allows us to trace the consequences of QCD's chiral symmetry and the pattern of its breaking through into predictions for experiments involving light nuclei.

## Acknowledgments

I thank the organizers of MENU2007 for a very stimulating and efficiently run meeting. I am also grateful for enjoyable and educative collaborations with those who worked with me on the research described here. Responsibility for any aberrant views and/or omissions in this paper is, however, entirely mine. This work was supported by DOE grant DE-FG02-93ER40756.

## References

- [1] J. Gasser, these proceedings.
- [2] V. Bernard and U.-G. Meißner, arXiv:hep-ph/0611231.
- [3] S. Weinberg, *Nucl. Phys.* **B363**, 3 (1991); *Phys. Lett.* **B251**, 288 (1990).
- [4] S. R. Beane, P. F. Bedaque, M. J. Savage, and U. van Kolck, *Nucl. Phys.* **A700**, 377 (2002).
- [5] M. P. Valderrama and E. R. Arriola, *Phys. Rev. C* **72**, 054002 (2005); *Phys. Rev. C* **74**, 054001 (2006).
- [6] M. C. Birse, *Phys. Rev. C* **74**, 014003 (2006).
- [7] A. Nogga, R.G.E. Timmermans and U. van Kolck, *Phys. Rev. C* **72**, 054006 (2005).
- [8] E. Epelbaum and U.-G. Meißner, arXiv:nucl-th/0609037.
- [9] M. P. Valderrama, A. Nogga, D. R. Phillips, and E. R. Arriola, in preparation.
- [10] M. Garcon and J. W. van Orden, *Adv. Nucl. Phys.* **26**, 293 (2001).
- [11] D. R. Phillips, *J. Phys. G* **34**, 365 (2007).
- [12] D. Abbott *et al.* [JLAB t20 Collaboration], *Eur. Phys. J.* **A7**, 421 (2000).
- [13] M. A. Belushkin, H.-W. Hammer and U.-G. Meißner, *Phys. Rev. C* **75**, 035202 (2007).

- [14] C. Ordonéz, L. Ray, and U. van Kolck, *Phys. Rev. C* **53**, 2086 (1996); N. Kaiser, R. Brockmann, and W. Weise, *Nucl. Phys.* **A625**, 758 (1997); E. Epelbaum, W. Glöckle, and U. Meißner, *Nucl. Phys.* **A671**, 295 (1999).
- [15] S. R. Beane, M. Malheiro, D. R. Phillips and U. van Kolck, *Nucl. Phys.* **A656**, 367 (1999).
- [16] D. Choudhury and D. R. Phillips, *Phys. Rev. C* **71**, 044002 (2005).
- [17] S. R. Beane, M. Malheiro, J. A. McGovern, D. R. Phillips and U. van Kolck, *Phys. Lett.* **B567**, 200 (2003); *Nucl. Phys.* **A747**, 311 (2005).
- [18] R. P. Hildebrandt, H. W. Griebhammer, T. R. Hemmert and D. R. Phillips, *Nucl. Phys.* **A748**, 573 (2005).
- [19] H. W. Griebhammer, these proceedings.
- [20] R. P. Hildebrandt, H. W. Griebhammer, and T. R. Hemmert, arXiv:nucl-th/0512063.
- [21] K. Fissum, in Proceedings of the 5th International Workshop on Chiral Dynamics, Theory and Experiment”, Durham, NC, 2006 (World Scientific, Singapore, to be published).
- [22] D. Choudhury *et al.*, *Phys. Rev. Lett.* **98**, 232303 (2007).
- [23] Y.-H. Song *et al.*, arXiv:0705.2657 [nucl-th].
- [24] S. Ragusa, *Phys. Rev. D* **47**, 3757 (1993).
- [25] H. Gao, in Proceedings of the 5th International Workshop on Chiral Dynamics, Theory and Experiment”, Durham, NC, 2006. (Ref. [21].)
- [26] St. Kistryn, these proceedings; K. Sekiguchi, these proceedings.
- [27] S. R. Beane *et al.*, arXiv:nucl-th/0008064; P. F. Bedaque and U. van Kolck, *Ann. Rev. Nucl. Part. Sci.* **52**, 339 (2002); E. Epelbaum, *Prog. Nucl. Part. Phys.* **57**, 654 (2006).
- [28] T.-S. Park *et al.*, *Phys. Rev. C* **67**, 055206 (2003), and references therein.
- [29] A. Gårdestig and D. R. Phillips, *Phys. Rev. Lett.* **96**, 232301 (2006).
- [30] A. Gårdestig and D. R. Phillips, these proceedings.
- [31] V. Lensky, these proceedings; V. Baru, these proceedings; S. Nakamura, these proceedings.

# Plenary Session V

**Session Chair:**

Anthony W. Thomas

The Japanese Proton Accelerator Facility  
Hadrons in Medium - Theory Meets Experiment  
Towards Polarized Antiprotons at FAIR

*N. Saito*  
*Ullrich Mosel*  
*Paolo Lenisa*

**Session Chair:**

Ullrich Mosel

Hadron Physics with Anti-Protons  
Overview of CLAS Physics  
Future Scientific Opportunities at Jefferson Lab

*Johan G. Messchendorp*  
*Günther Rosner*  
*Anthony W. Thomas*

**Session Chair:**

Rudolf Meier

Dynamics, Symmetries and Hadron Properties  
The Transverse Partonic Structure of the Proton  
Concluding Remarks

*Craig Roberts*  
*Mauro Anselmino*  
*Bernard M. K. Nefkens*

# HADRONS IN MEDIUM – THEORY MEETS EXPERIMENT

*U. Mosel*<sup>1</sup>

Institut für Theoretische Physik  
Universität Giessen  
Giessen, Germany, D-35392

## Abstract

In this talk I give a short review of theoretical results on the properties of hadrons in cold, equilibrium nuclear matter. I then discuss the observable consequences of any changes of these properties inside the medium in actual experiments. I demonstrate that any experimental verification of in-medium effects requires a state-of-the-art treatment of the reaction dynamics and, in particular, also the final state interactions.

## 1 Introduction

The interest in in-medium properties of hadrons has been growing over the last decade because of a possible connection with broken symmetries of QCD and their partial restoration inside nuclear matter. Already two decades ago Bernard and Meissner predicted on the basis of the NJL model that the scalar strength should drop considerably inside nuclei whereas the vector mesons were only little affected in that approach [1]. Somewhat later there were theoretical predictions that masses of vector mesons should generally decrease in medium as a function of density due to a partial restoration of chiral symmetry [2,3]. In addition, there existed well-worked out predictions that the scalar  $2\pi$  strength should decrease in medium and that the vector meson masses should drop [4,5]. All of these calculations were performed for idealized situations (infinite cold nuclear matter at rest) and little attention was paid to the actual observability of these predicted changes. At the same time experiments (CERES, TAPS) seemed to show the predicted behavior. The CERES results indicated a significant broadening of the  $\rho$  meson in medium [6], whereas the TAPS results on the  $2\pi$  strength exhibited the predicted lowering of the  $\sigma$  strength inside nuclei [7]. Most recently, the

---

<sup>1</sup>mosel@physik.uni-giessen.de

CBELSA/TAPS experiment has also obtained an indication for a lowering of the  $\omega$  meson mass in nuclei [8]. Other interesting data in this context have been obtained by groups at JLAB [9], KEK [10] and CERN [11].

Motivated by these developments we have concentrated our theoretical work on in-medium properties along two different lines. First, we have performed state-of-the-art calculations of vector meson spectral functions in cold nuclear matter. Second, we have followed closely the CBELSA/TAPS experiment and have performed various feasibility studies and analyses of this experiment searching for in-medium changes of the  $\omega$  meson in medium. In a third step we have also analyzed the lowering of scalar strength in nuclei observed by the TAPS experiment.

## 2 In-Medium Properties of Vector Mesons

On the first aspect we have initially finished a major calculation on the in-medium properties of the  $\pi$ ,  $\rho$  and  $\eta$  mesons [12]. In this work we have generated the in-medium selfenergies of these mesons by nucleon-hole and resonance-hole excitations which in turn are affected by the changed in-medium properties of the mesons. This self-consistency problem has been solved here for the first time. Special care was taken to respect the analyticity of the spectral functions and to take into account effects from short-range correlations both for positive and negative parity states.

Our model has been shown to produce sensible results for pion and  $\Delta$  dynamics in nuclear matter, as a test. For the  $\rho$  meson we find a strong interplay with the D13(1520), which moves spectral strength of the  $\rho$  spectrum to smaller invariant masses and simultaneously leads to a broadening of the baryon resonance. The strong interplay between the  $\rho$  meson and the D13(1520)-nucleon hole excitation leads to a dominant lower hump in the  $\rho$  spectral function also in this relativistic and selfconsistent calculation; it confirms our earlier result obtained in a more simplified approach. Whereas the longitudinal component of the  $\rho$  meson only broadens somewhat, the transverse component shows a major distortion which evolves as a function of the  $\rho$  momentum (see Fig. 1). At the same time, the D13(1520) resonance broadens considerably due to the opening of phase-space for  $\rho$ -decay. For the  $\eta$  meson the optical potential resulting from our model is rather attractive whereas the in-medium modifications of the S11(1535) are found to be quite small.

These studies also allow us to assess the validity range of the often used low-density approximation. We find that this depends very much on the special couplings involved and thus varies from meson to meson. Whereas

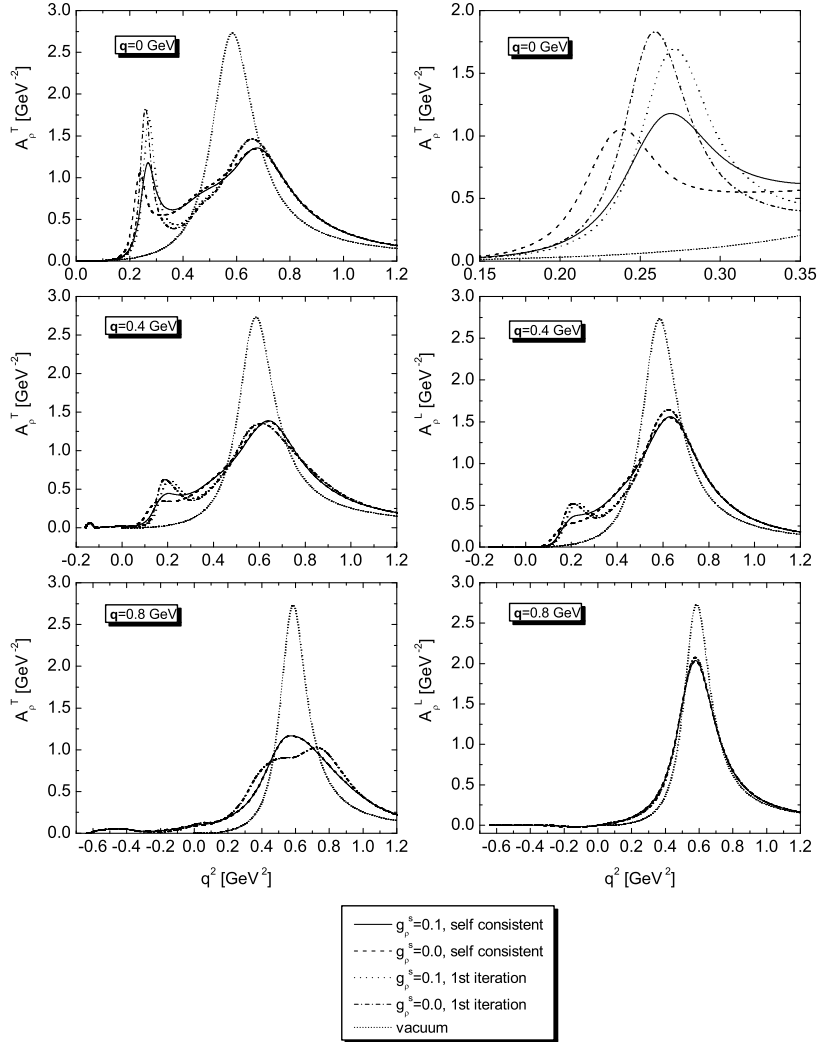


Figure 1: Spectral function of the  $\rho$  meson in nuclear matter at density  $\rho_0$  for various momenta indicated in the figure. The left column shows the transverse spectral function, the right column that of longitudinally polarized  $\rho$  mesons. The thin dotted line in each figure is the vacuum spectral function, the other curves give the effect of selfconsistency and short-range correlations (from [12]).

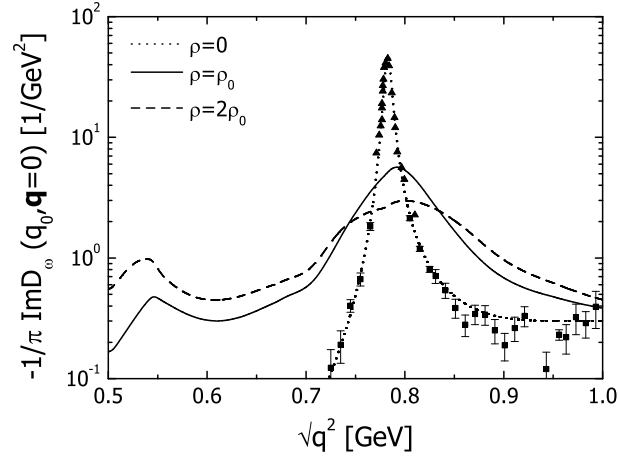


Figure 2: Spectral function of the  $\omega$  meson in nuclear matter at rest, at densities 0,  $\rho_0$  and  $2\rho_0$  (from [13]).

for the  $\eta$  meson the validity ranges up to a density of  $\rho_0$ , for the  $\rho$  meson it already breaks down at about  $0.3\rho_0$ . This may serve as a warning sign for many in-medium calculations that use the low-density approximation without any further proof of its reliability.

Bearing this in mind we have recently also performed a calculation of the selfenergy of the  $\omega$  meson in medium. This calculation is based on a unitary coupled channel analysis of all existing  $\pi N$  and  $\gamma N$  data up to an invariant mass of 2 GeV [13]. The coupled channel character of this calculation is of utmost importance here because it is the only way to include experimental constraints on the  $2\pi$  decay channel that was found to be dominant in [4]. This analysis and thus also the selfenergy of the  $\omega$  meson extracted from the  $\omega N$  scattering amplitude gives a broadening of about 60 MeV at  $\rho_0$  and a small upward shift of the peak mass. In addition, due to a nonzero coupling of the  $\omega$  to the S11(1535) resonance the  $\omega$  spectral function exhibits a small peak at a mass of around 550 MeV. This calculation gives, for the first time, the  $\omega$  selfenergy also for nonzero momenta (which corresponds to the experimental situation) and it takes the experimental constraints on the important  $2\pi$  channel into account because it is based on a unitary  $K$ -matrix analysis of 'real' data. The result of this calculation is shown in Fig. 2. For vanishing  $\omega$  momentum this result qualitatively agrees with that of [14] in that it yields a lower mass structure in the spectral function at an invariant mass of 500 - 600 MeV and only a very small shift of the main peak; the latter is in contrast to the results of [4] (for a recent discussion of the results obtained in [4] see [15]) and of [16]. The latter was based on a relativistic

mean-field model and does not contain any dispersive effects.

Our second line of approach to the problem of in-medium selfenergies has concentrated on an analysis of the recent CBELSA/TAPS data [8]. Since the experiment looks for the channel  $\gamma + A \rightarrow A^* + \omega \rightarrow A^* + \gamma + \pi^0$  it is mandatory to control the effects of final state interactions on the  $\pi^0$  in a quantitative way. The only method available for this is that of coupled channel semiclassical transport calculations which – as we had shown earlier in extensive work – can give a consistent description of many experimental phenomena, both in heavy-ion [18] as well as in nucleon-, pion- [19], photon- [20] and neutrino-induced reactions [21]. For any reaction on nuclei with hadrons in the final state a state-of-the-art transport calculation of the final state interactions is an indispensable part of the theory. We have, therefore, spent significant effort on developing a new code, dubbed 'GiBUU', for the transport calculations. This code is written in object-oriented FORTRAN 95/2003 and incorporates all the experience we have gained with earlier numerical implementations at Giessen over the last 20 years [17].

With this method we have first analysed both results on the experimental determination of the nuclear transparency ratio for  $\phi$  mesons [22], measured by a group at SPRING8. This transparency gives directly the imaginary part of the meson's selfenergy in medium; using a low-density approximation one can then extract the inelastic  $\omega N$  cross section. In this way an unexpectedly large inelastic cross section for  $\phi N$  interactions was extracted. We have found that indeed cross sections about a factor 3 larger than those theoretically expected are needed to explain the mentioned data, in line with a simple Glauber analysis by the SPRING8 group.

For  $\omega$  mesons the CBELSA/TAPS collaboration has measured the nuclear transparency [23]. We have shown that our calculations reproduce the measured attenuation quite well if – similar to the  $\phi N$  case – the inelastic cross section is increased by about a factor of 3 beyond earlier theoretical expectations. A fit to the data can actually also determine the momentum-dependence of this cross section [24].

A major effort has gone into an analysis of the  $\omega$  photo-production experiment at CBELSA/TAPS. Fig. 3 shows the result of such an analysis together with the data of the CBELSA/TAPS collaboration. Our simulations give a full event analysis and thus allow to calculate also background contributions on the same footing as the actual signal. They also allow insight into the effects of rescattering of the pions produced in the decay of the  $\omega$  meson and have suggested a method to suppress the rescattered pion background that has actually been adopted by the experimental group. The result of this analysis is that the data can be explained if a lowering of the  $\omega$  meson mass in medium by about 16 % is assumed together with the appropriate

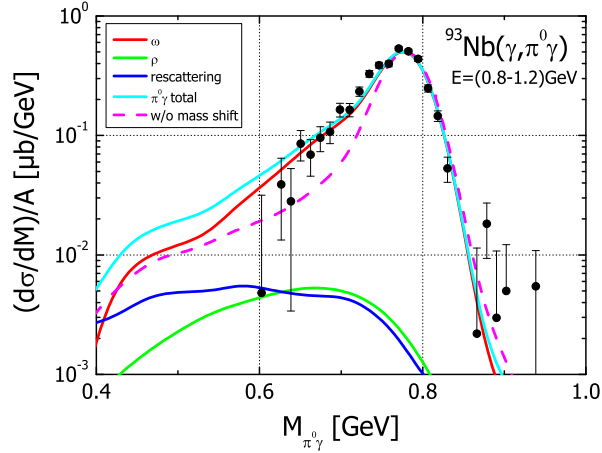


Figure 3: Comparison of CBELSA/TAPS data on  $\omega$  production on different targets in the energy range  $E_\gamma = 0.8 - 1.2$  GeV [8]. The dashed line shows a comparison of the GiBUU transport calculation with free  $\omega$  meson spectral functions (using the experimental mass resolution) and the solid line at the top gives the results of a calculation with mass-shift and collisional broadening. The solid line at the bottom gives the contribution of rescattered pions to the reconstructed spectral function and the grey line at the bottom gives the contribution of the decay channel  $\rho \rightarrow \pi^0\gamma$ . The top curve shows the sum of all contributions (from [24]).

collisional broadening.

A problem in this context is that the experiment does not determine the spectral function of the  $\omega$  meson itself. Instead, we have noted that the result of the experimental analysis is the product of the primary production cross section with the spectral function and the partial decay probability into the channel under study ( $\pi^0\gamma$  here). If the first and the latter depend strongly on the invariant mass itself, as it does for the CBELSA/TAPS experiment, then significant distortions of the spectral function may arise. This is a topic under intensive study by us presently [25]

### 3 In-Medium Properties of Scalar Mesons

Finally, we have analyzed the TAPS data on  $2\pi^0$  photoproduction on nuclei. The motivation for this experiment was a prediction that – due to chiral symmetry restoration in nuclei – the scalar strength of the  $\sigma$  meson should be lowered in nuclei [5]. The TAPS collaboration had indeed initially seen an effect as predicted in the  $2\pi^0$  data, whereas a comparison measurement in the

$\pi^0\pi^\pm$  channel did not seem to show such an effect [7]. Various explanations for these findings have been advanced by the Valencia group [26] and by a group in Lyon [27] in terms of chiral symmetry restoration or  $\pi - \pi$  correlations in nuclei, based on a chiral effective field theory model.

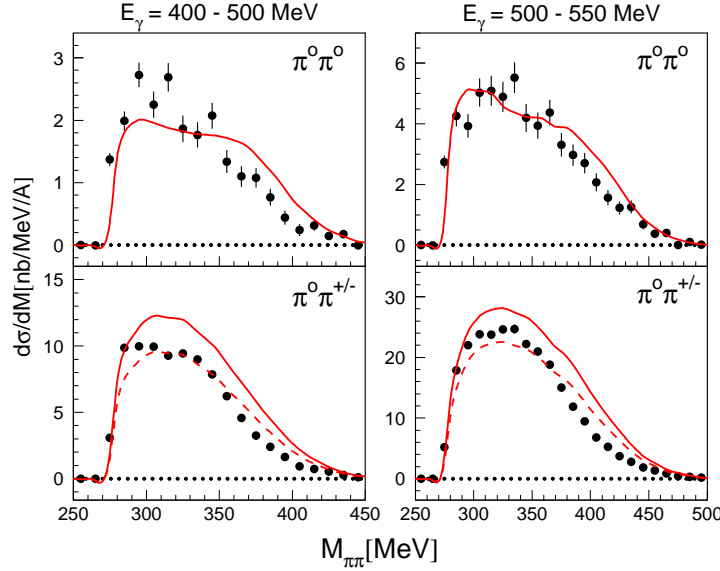


Figure 4: Data of the TAPS collaboration (Bloch et al.) for  $2\pi^0$  photoproduction on a  $^{40}\text{Ca}$  target for two different photon energies. The solid curve gives the result of a GiBUU calculation [28], the dashed curves in the semicharged  $2\pi$  channel are normalized to the data (see text). Data from [29].

None of these calculations, however, did look into the simplest possible explanation of the observed effects in terms of mundane pion rescattering. We have, therefore, performed such calculations [19] using the GiBUU method which is ideally suited for this task. These calculations, which did not contain any effects connected with  $\pi\pi$  correlations, could reproduce the observed effect for the  $\pi^0\pi^0$  channel, but they also predicted a similar effect in the semi-charged channel where it had not been seen experimentally. However, a more recent analysis with higher statistics by Bloch et al. [29] yielded a result for both charge channels that is in perfect agreement with our calculations (see Fig. 4; the dashed lines in this figure are normalized in height to the data, this normalization reflects uncertainties in the elementary cross sections). In particular the yield in the semi-charged channel is strongly influenced by a coupled-channel effect, the charge transfer in  $\pi N$  interactions; Glauber based absorption models miss this contribution. This illustrates that a very

sophisticated treatment of final state interactions is absolutely mandatory when looking for more 'exotic' effects in nuclei. We conclude that any analysis of the  $2\pi^0$  data with respect to a lowering of the scalar strength in nuclei has to take the pion rescattering effects into account. Present day's data are all consistent with simple rescattering.

## 4 Summary

The main message we have learned from the studies reported here is that it is important to calculate not only in-medium properties under idealized conditions (static, uniform matter in equilibrium), but to also explore the influence of these properties on actual observables. The spectral function itself, which contains the information on in-medium selfenergies, in particular in-medium masses and widths, is not directly observable. Instead, both the creation of the studied hadron as well as its decay influence the observables as much as the spectral function itself and thus have to be under good control. The same holds for the final state interactions on hadronic decay products. Here a state-of-the-art treatment of final state interactions is mandatory. There is now general agreement on the amount of collisional broadening of vector mesons in medium, but the verification of an actual mass-shift still requires more work, both theoretical and experimental.

## References

- [1] V. Bernard, U. G. Meissner and I. Zahed, Phys. Rev. Lett. **59** (1987) 966; V. Bernard and U. G. Meissner, Nucl. Phys. A **489** (1988) 647.
- [2] T. Hatsuda, S. H. Lee and H. Shiomi, Phys. Rev. C **52**, 3364 (1995) [arXiv:nucl-th/9505005].
- [3] G. E. Brown and M. Rho, Phys. Rev. Lett. **66** (1991) 2720.
- [4] F. Klingl and W. Weise, Nucl. Phys. A **606** (1996) 329; F. Klingl, N. Kaiser and W. Weise, Nucl. Phys. A **624** (1997) 527 [arXiv:hep-ph/9704398].
- [5] K. Yokokawa, T. Hatsuda, A. Hayashigaki and T. Kunihiro, Phys. Rev. C **66** (2002) 022201 [arXiv:hep-ph/0204163].
- [6] G. Agakishiev *et al.* [CERES Collaboration], Phys. Rev. Lett. **75** (1995) 1272.

- 
- [7] J. G. Messchendorp *et al.*, Phys. Rev. Lett. **89**, 222302 (2002) [arXiv:nucl-ex/0205009].
- [8] D. Trnka *et al.* [CBELSA/TAPS Collaboration], Phys. Rev. Lett. **94**, 192303 (2005) [arXiv:nucl-ex/0504010].
- [9] R. Nasseripour, M. H. Wood, C. Djalali, D. P. Weygand, C. Tur, U. Mosel, P. Muehlich, CLAS Collaboration, Phys. Rev. Lett. (2007) in press [arxiv.org/abs/0707.2324v3].
- [10] S. Yokkaichi *et al.* [KEK-PS325 Collaboration], Int. J. Mod. Phys. A **22**, 397 (2007).
- [11] S. Damjanovic *et al.* [NA60 Collaboration], Nucl. Phys. A **783** (2007) 327 [arXiv:nucl-ex/0701015].
- [12] M. Post, S. Leupold and U. Mosel, “Hadronic spectral functions in nuclear matter,” Nucl. Phys. A **741**, 81 (2004) [arXiv:nucl-th/0309085].
- [13] P. Muehlich, V. Shklyar, S. Leupold, U. Mosel and M. Post, “The spectral function of the omega meson in nuclear matter from a coupled-channel resonance model,” Nucl. Phys. A **780**, 187 (2006) [arXiv:nucl-th/0607061].
- [14] M. F. M. Lutz, G. Wolf and B. Friman, Nucl. Phys. A **706** (2002) 431 [Erratum-ibid. A **765** (2006) 431] [arXiv:nucl-th/0112052].
- [15] F. Eichstaedt, S. Leupold, U. Mosel and P. Muehlich, Prog. Theor. Phys. Suppl. **168**, 495 (2007) [arXiv:0704.0154 [nucl-th]].
- [16] K. Saito, K. Tsushima, D. H. Lu and A. W. Thomas, Phys. Rev. C **59**, 1203 (1999) [arXiv:nucl-th/9807028].
- [17] for details see: <http://gibuu.physik.uni-giessen.de/GiBUU/>
- [18] A. B. Larionov, O. Buss, K. Gallmeister and U. Mosel, Phys. Rev. C **76** (2007) 044909 [arXiv:0704.1785 [nucl-th]].
- [19] O. Buss, L. Alvarez-Ruso, A. B. Larionov and U. Mosel, Phys. Rev. C **74**, 044610 (2006) [arXiv:nucl-th/0607016].
- [20] O. Buss, T. Leitner, U. Mosel and L. Alvarez-Ruso, Phys. Rev. C **76**, 035502 (2007) [arXiv:0707.0232 [nucl-th]].

- 
- [21] T. Leitner, L. Alvarez-Ruso and U. Mosel, Phys. Rev. C **73**, 065502 (2006) [arXiv:nucl-th/0601103].  
T. Leitner, L. Alvarez-Ruso and U. Mosel, Phys. Rev. C **74**, 065502 (2006) [arXiv:nucl-th/0606058].
- [22] P. Muehlich and U. Mosel, “Attenuation of Phi mesons in gamma A reactions,” Nucl. Phys. A **765**, 188 (2006) [arXiv:nucl-th/0510078].
- [23] V. Metag, arXiv:0711.4709 [nucl-ex].
- [24] P. Muehlich, “Mesons in Nuclei and Nuclear Reactions”, PhD Dissertation, University of Giessen, 2007, <http://theorie.physik.uni-giessen.de/documents/dissertation/muehlich.pdf>
- [25] K. Gallmeister, M. Kaskulov and U. Mosel, arXiv:0712.2200 [nucl-th].
- [26] L. Roca, E. Oset and M. J. Vicente Vacas, Phys. Lett. B **541**, 77 (2002) [arXiv:nucl-th/0201054].
- [27] G. Chanfray, Z. Aouissat, P. Schuck and W. Noerenberg, Phys. Lett. B **256**, 325 (1991).
- [28] O. Buss, L. Alvarez-Ruso, P. Muehlich and U. Mosel, Eur. Phys. J. A **29** (2006) 189 [arXiv:nucl-th/0603003].
- [29] F. Bloch *et al.*, Eur. Phys. J. A **32** (2007) 219 [arXiv:nucl-ex/0703037].

# TOWARDS POLARIZED ANTIPROTONS AT FAIR

*P. Lenisa*

Dipartimento di Fisica  
Università di Ferrara  
44100 Ferrara, Italy

*F. Rathmann*

Institut für Kernphysik,  
Forschungszentrum Jülich  
52425 Jülich, Germany

## Abstract

In the framework of the FAIR project the PAX Collaboration has suggested new experiments using polarized protons and antiprotons. In order to provide polarized antiprotons, the polarization build-up by spin-dependent interaction (spin-filtering) must be studied. The goal of these investigations is to understand the physics of the spin-filtering process with stored protons at COSY, and shed light into the role of polarized electrons for the polarization buildup. Later on the dependence of the proton-antiproton interaction will be investigated at the Antiproton Decelerator ring (AD) at CERN.

## 1 Motivation

An entirely new chapter in the study of the spin structure of the proton might unfold with the advent of a polarized antiproton beam at the Facility for Antiproton and Ion Research (FAIR) at GSI, Darmstadt. A cornerstone of the hadronic physics program at FAIR is the collection, cooling, storing and acceleration of antiprotons in the 15 GeV High Energy Storage Ring (HESR). The PAX Collaboration [1] has suggested to convert HESR into an asymmetric polarized proton-polarized antiproton collider. The study of double polarized antiproton-proton Drell-Yan reactions will allow the first direct measurement of transversity. No other existing or future facility will be ever able to directly measure the transversity in a competitive way. The physics case for experiments with polarized antiprotons is outstanding and covers additional items like the measurement of the modules and absolute

phases of the electromagnetic form-factors in the time-like region; measurements of double-polarized proton-antiproton hard scattering. Also hadron spectroscopy studies will definitely benefit from polarization of beam and/or target particles, because the initial spin state of the system can be prepared at will.

## 2 Polarized Antiprotons

For more than two decades, physicists have tried to produce beams of polarized antiprotons, generally without success. Conventional methods like atomic beam sources (ABS), appropriate for the production of polarized protons and heavy ions cannot be applied, since antiprotons annihilate with matter. Polarized antiprotons have been produced from the decay in flight of hyperons at Fermilab. The intensities achieved with antiproton polarizations  $P > 0.35$  never exceeded  $1.5 \times 10^5 s^{-1}$ . Scattering of antiprotons off a liquid hydrogen target could yield polarizations of  $P \approx 0.2$ , with beam intensities of up to  $2 \times 10^3 s^{-1}$ . Unfortunately, both approaches do not allow efficient accumulation in a storage ring, which would greatly enhance the luminosity. Spin splitting using the Stern-Gerlach separation of the given magnetic sub-states in a stored antiproton beam was proposed in 1985, but it has never been experimentally demonstrated. Different methods to polarize antiprotons have been recently reviewed in a Workshop held at Daresbury (UK), August 29-31, 2007 [2].

There is only one viable method demonstrated so far that could yield a beam of polarized antiprotons: namely spin-filtering of a stored beam through repetitive interaction with a polarized internal target.

### 2.1 Spin filtering

Spin filtering is based on the effect of selective removal of (anti)protons of a stored beam by a polarized target. The total cross section consists of a transverse and a longitudinal part:

$$\sigma_{tot} = \sigma_0 + \sigma_{\perp} \mathbf{P} \cdot \mathbf{Q} + \sigma_{\parallel} (\mathbf{P} \cdot \mathbf{k})(\mathbf{Q} \cdot \mathbf{k}) \quad (1)$$

In equation 1  $\mathbf{P}$  and  $\mathbf{Q}$  represent the beam and target polarization respectively, while  $\mathbf{k}$  the beam momentum direction. For an initially equally populated  $\uparrow$  ( $m = +\frac{1}{2}$ ) and  $\downarrow$  ( $m = -\frac{1}{2}$ ) states in the beam, the cross sections for the transverse and longitudinal cases become:

$$\sigma_{tot\pm} = \sigma_0 \pm \sigma_{\perp} Q \quad \sigma_{tot\pm} \sigma_0 \pm (\sigma_{\perp} + \sigma_{\parallel}) Q \quad (2)$$

Experimental evidence for spin filtering has been given in 1992 in an experiment at the Test Storage Ring (TSR) at MPI Heidelberg where an initially unpolarized 23 MeV proton beam has been polarized by spin-dependent interaction with a polarized hydrogen gas target [3]. The measured polarization cross section was  $\sigma_{\perp} = 72.5 \pm 5.8$  mbarn.

In 1994 Horowitz and Meyer explained this result by three effects [4]: selective scattering of protons out of the acceptance of the storage ring; scattering of target protons into the acceptance of the storage ring and spin transfer from polarized target electrons. The theoretically calculated cross section by Meyer and Horowitz was  $\sigma_{\perp} = 65$  mbarn. On the other hand the 2005 scrutiny of the filtering process by Milstein and Strakhovenko [5] and Nikolaev and Pavlov [6] suggests a cancellation of the electron contribution to the polarization of the transmitted stored beam and beam particles elastically scattered off electrons. In this second scenario only the nuclear interaction would contribute to spin filtering. The estimated cross section is  $\sigma_{\perp} = 85.6$  mbarn, also in fair agreement with the measured one.

Understanding which of these scenario is really at work is crucial to progress towards the goal to eventually produce stored polarized antiproton beams.

## 3 Experiments at COSY

### 3.1 Polarization build-up experiments

The ideal solution to distinguish between the two scenarios would be the null experiment with two hyperfine states in the Polarized Internal Target (PIT) such that the net nuclear polarization of the target is zero, while the net electron polarization is large. This requires operating the PIT with longitudinal target polarization in a strong longitudinal guide field, where the stable beam spin direction must be aligned longitudinally at the target as well to preserve the longitudinal polarization of the stored protons.

Two possible null experiments can be performed. The first, by injecting two hyperfine states with identical electron and opposite nuclear polarization, will evidence the pure electron interaction, while the second, for the pure nuclear mechanism, can be performed by injecting two hyperfine states with identical proton polarizations and opposite electron polarizations. The situation is summarized in Table 1

In a single hyperfine state mode, one could rely upon the different energy dependencies of the electron and nuclear mechanisms. This point is made clear by the expected energy dependence of the effective polarization cross

Table 1: Polarization build-up experiments with one or two H hyperfine states injected. By injecting in the target cell two states in a strong field pure electron ( $P_e$ ) or nuclear polarization  $P_z$  can be obtained.

Injected states	$P_e$	$P_z$	Interaction	Holding field	
$ 1\rangle$	+1	+1	Elm.+had	transv. and long.	weak (20 G)
$ 1\rangle +  4\rangle$	0	+1	only had.	long.	strong (30 kG)
$ 1\rangle +  2\rangle$	+1	0	only elm.		

section, shown in the left plot of Fig. 1. In the right plot of Fig. 1, we show the predictions from the Budker-Jülich model for the energy dependence of the polarization of stored protons after filtering for 2 to 5 beam lifetimes both using the ANKE and new a PIT at TP1.

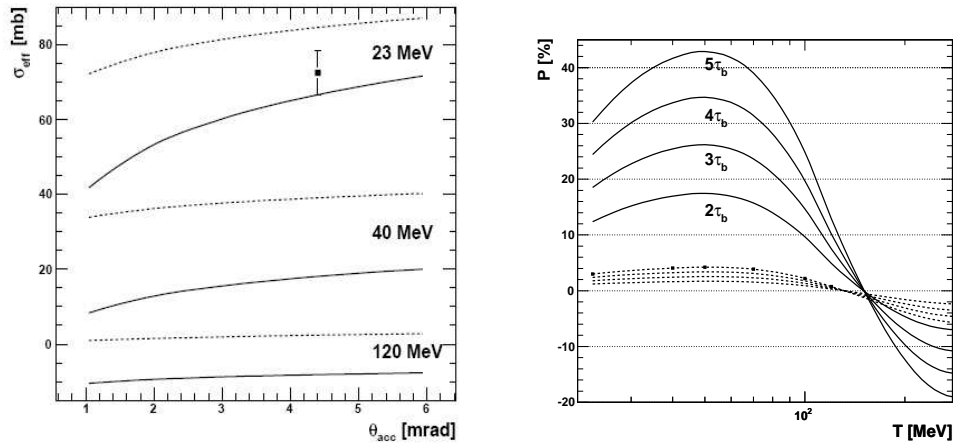


Figure 1: Polarization build-up studies with a single hyperfine state injected. Left plot: Calculated polarization cross section as a function of the ring acceptance for the Meyer-Horowitz (solid line) and Nikolaev and Pavlov (dots) models. Right plot: Comparison of the expected polarization buildup at the ANKE IP and in a new IP at TP1 of COSY for the Nikolaev and Pavlov model.

### 3.2 Depolarization experiments

A different approach to address the contribution of the polarized electrons consists in reversing the role of the beam and target polarizations: from the viewpoint of the kinetics of the spin-filtering, depolarization of polarized

stored protons in an unpolarized electron target is equivalent to the buildup of the polarization of the initially unpolarized beam proton by multiple passage through the polarized electron target.

### Gas target as unpolarized electron target

A possible way to provide an unpolarized electron target is to make use of a  $D_2$  cluster target. An advantage of this target is that at COSY injection energy (45 MeV) elastic polarized p-d scattering provides good counting rates and analyzing power and it can be used to measure the beam polarization.

The experimental task is to determine the polarization lifetime of COSY together with the depolarizing effect predicted by Meyer-Horowitz (MH) due to the unpolarized electrons in the  $D_2$  target. The total polarization lifetime ( $\tau_p^{total}$ ) can be written as:

$$\frac{1}{\tau_p^{total}} = \frac{1}{\tau_p^{COSY}} + \frac{1}{\tau_p^{MH}} \quad (3)$$

where  $\tau_p^{COSY}$  denotes the polarization lifetime of COSY alone, while  $\tau_p^{MH}$  is attributed to the depolarizing effect due to the target electrons.

To avoid possible systematic variations,  $\tau_p^{COSY}$  should be traced simultaneously with the measurements. Thus, a proper measuring cycle has to be introduced composed of three parts of duration  $T = T_1 + T_2 + T_3$ , during  $T_1$ , the  $D_2$  target is switched on, during  $T_2$ , the target is switched off, and during  $T_3$  the target is again switched on. From cycle to cycle the beam spin will be alternated from  $\uparrow$  to  $\downarrow$  to zero.

The p-d elastic scattering will be detected by two Silicon Tracking Telescopes (STT) left and right of the target area. The detectors are placed to cover the region, where the Factor of Merit (FOM) exhibits a maximum. The  $FOM = d\sigma/d\Omega(\theta_{cm}) \cdot A_y(\theta)^2$  has been evaluated on the basis of experimental data and for an energy of 45 MeV has been found to maximum near  $\theta_{lab}^{proton} = 80^\circ$ . The count rates have been determined on the basis of Monte Carlo simulations and show that a significance of 4-5  $\sigma$  in 4 weeks of data taking can be reached (Figure 2).

### Electron cooler beam as unpolarized electron target

A slightly different approach from the one reported in previous paragraph is the use of the electron cooler beam as unpolarized electron target with low relative energy with respect to the proton beam. This approach is motivated by a recent publication of Walcher et al. [7] describing a new QED calcula-

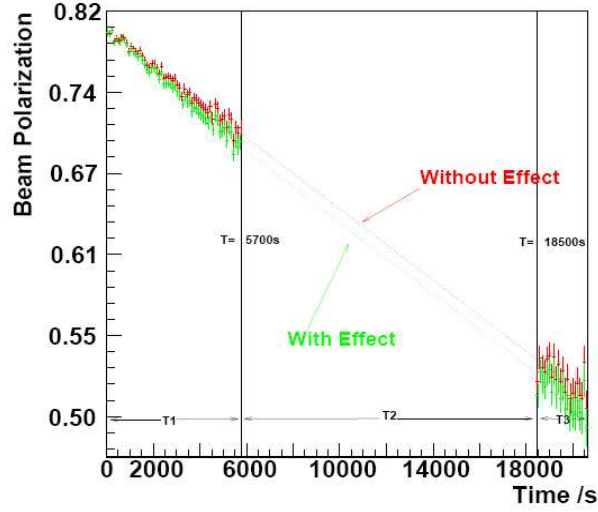


Figure 2: Depolarization study by using a  $D_2$  cluster target. Resulting accuracy of the time dependent beam polarization vs measuring time. The cycle is composed by three parts of duration  $T = T_1 + T_2 + T_3 = 20600$  s, target-off times are  $5700 \text{ s} < t < 18500 \text{ s}$ .

tion which extends the calculation of Meyer to very low relative velocities of protons and electrons.

A dedicated set of measurements is foreseen at COSY to directly determine the spin-exchange cross section by using a stored polarized proton beam and the unpolarized electron cooler beam. Although the electron cooler has a much smaller thickness compared to a gas target, the new calculation suggests a very large cross-section for the spin-exchange between protons and electrons. As an example for an electron energy of 1 keV in the rest frame of the proton, i.e. at a relative velocity  $v/c \approx 0.001$ , the predicted spin-exchange cross section amounts to  $\langle \sigma_{P_{zz}} \rangle \approx 2 \cdot 10^{13}$  barn.

By a measurement of the beam polarization lifetime as a function of the relative energy between proton and electron beams, we will be able to measure the spin-exchange cross section responsible for the beam depolarization. The variation of the relative energy of the two beams can be obtained by varying the acceleration potential of the electron cooler beam.

A possible complication arises from the fact that although the cooling force is small when the electron beam is detuned, the proton beam will nevertheless slowly change its momentum until again the velocities are matched. Therefore, one has to detune the cooler voltage for a short period of time and return to the nominal voltage to make sure that the proton beam remains

well-cooled. The measuring cycle will be realized by alternating the cooler voltage between *nominal* and *detuned*.

Figure 3 shows the reachable accuracy in the determination of the depolarization cross section as a function of the measured depolarization.

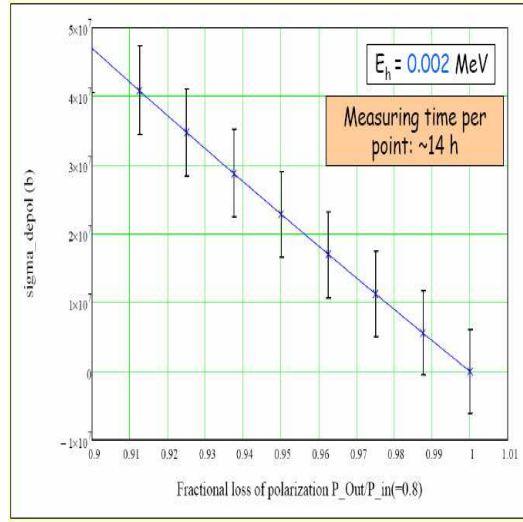


Figure 3: Depolarization study by using the electron cooler beam. Depolarizing cross section as a function of the measured fractional loss of polarization.

## 4 Experiments at AD

The experimental basis for predicting the polarization build-up in a stored antiproton beam is practically non-existent. The AD facility at CERN is a unique facility at which stored antiprotons in the appropriate energy range are available and whose characteristics meet the requirements for the first ever antiproton polarization build-up studies.

The two physics observables which can be measured by the spin-filtering technique, are the spin-dependent cross sections  $\sigma_{\perp}$  and  $\sigma_{\parallel}$  adopted in the parametrization of the hadronic cross section presented in equation 1. Such observables would improve substantially the modern phenomenology of the proton-antiproton interactions based on the experimental data gathered at LEAR.

## 5 Experimental setup for spin filtering

The commissioning of a spin filtering experiment in a storage ring requires the design, production and installation of three major components: a low-beta section, a polarized internal target making use of a storage cell and a detector system.

The design of the elements is taking into account their utilization both in the COSY ring environment for the experiments with protons and in the AD ring for the subsequent experiments with antiprotons.

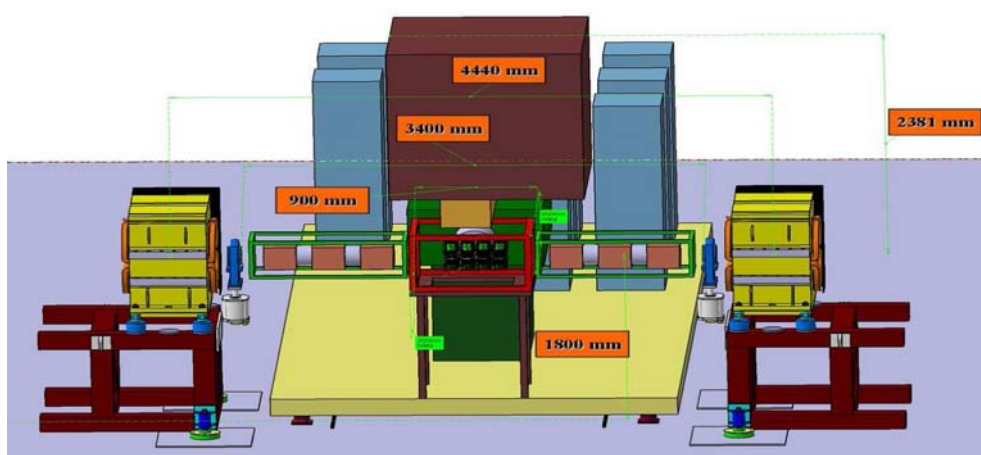


Figure 4: Layout of the interaction region for spin-filtering experiments. On top the Polarized Atomic Beam Source. Left and right to the scattering chamber, two sets of three quadrupoles are shown. Inside the scattering chamber, the silicon detectors are visible.

### 5.1 Low-beta section and polarized internal target

The insertion of a polarized target using a storage cell in the COSY and AD rings requires the redesign of the magnetic lattice of the ring. The solution which has been developed for the COSY (AD) ring foresees the substitution of one of the existing quadrupoles in a straight section of the ring with two sets of two (three) quadrupoles before and behind the target.

The polarized source used formerly at the HERMES experiment (DESY-Hamburg) has been transported to Jülich and its operation restored.

The operation of the AD ring requires injection of an uncooled antiproton beam at 3.5 GeV and subsequent cooling and deceleration to the experiment energies. Prior to the cooling process the beam occupies the whole acceptance

of the machine. Under these conditions, the size of the beam is so large that it requires the use of an openable cell that should not limit the machine acceptance at injection. In order to allow for the detection of low-energy recoil protons ( $T_{rec} < 8MeV$ ) the cell walls will be realized with a thin ( $5\mu m$ ) Teflon foil.

## 5.2 Detector

The detector for the spin-filtering experiments constitutes a multipurpose device which should work as beam polarimeter and recoil detector for the measurement of the spin-dependent cross-sections, cope with a broad range of beam energies (50-500 MeV), and fit into the lattices of the COSY and AD rings. The final configuration of the detector foresees the use of (at least) three series of four silicon telescopes in a diamond-shaped configuration, properly displaced along the storage cell (see Figure 5). Each telescope consists of two sensors.

The choice of the sensors has fallen on the TIGRE sensors from Micron-Semiconductors. These are,  $97 \times 97 mm^2$  double sided detectors, of  $300 \mu m$  thickness and a pitch of  $758 \mu m$ . The same sensors have been also used for the recoil detector of the HERMES experiment (DESY, Hamburg).

A complete simulation has been performed in order to evaluate the obtainable vertex resolution and the covered acceptance. A vertex resolution better than 2 mm has been obtained for all three vertex coordinates. This resolution allows the separation of the tracks coming from the gas target from the ones originating in the cells wall that constitute the background. The resolution is limited by the multiple scattering in the cell walls and in the sensors themselves. The right plot of Figure 5 shows the covered acceptance for elastic events in antiproton-proton scattering for a beam energy of 120 MeV. The detector acceptance is about 0.17. By using the obtainable luminosity in the AD ring, this translates 10 events/s.

## 6 Conclusions and timeline

Spin-filtering represents at the moment the only credible technique which might lead to the first beam of polarized antiprotons. To better understand its principles and define the basis for its practical exploitation, measurements with protons are foreseen at COSY in the next two years and at the AD ring starting in 2010.

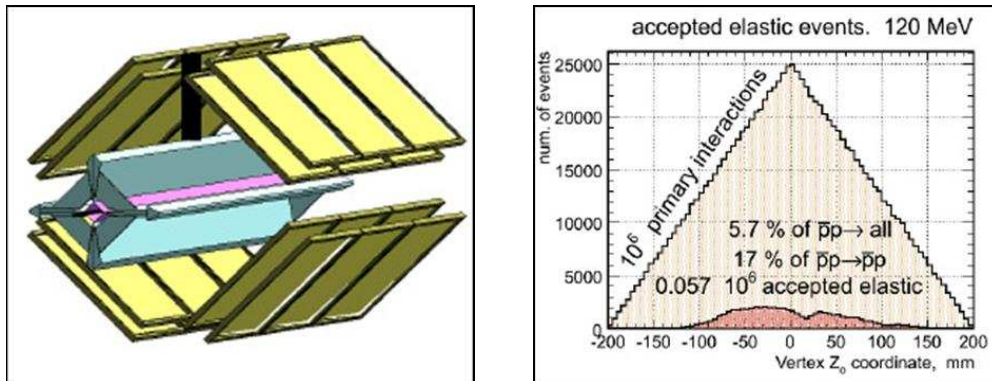


Figure 5: Left plot: layout of the detector for the spin-filtering experiments. The storage cell is shown in the center of the detector. Right plot: event distribution along the longitudinal  $z$  coordinate in the cell with the number of generated and accepted events in the detector.

## References

- [1] The proposals of the PAX Collaboration can be found at the PAX website at: <http://www.fz-juelich.de/ikp/pax>.
- [2] The presentation of the workshop can be downloaded from the site: <http://www.cockcroft.ac.uk/Polanti-p/Presentations>.
- [3] F. Rathmann et al., *Phys. Rev. Lett.* **71**, 1379 (1993).
- [4] C.J. Horowitz and H.O. Meyer *Phys. Rev. Lett.* **72**, 3981 (1994).
- [5] A.I. Milstein and V.M. Strakhovenko *Phys. Rev. E* **72**, 066503 (2005).
- [6] N.N. Nikolaev and F. Pavlov *Spin filtering of Stored (Anti)protons: from FILTEX to COSY to AD to FAIR*, e-Print Archive:hep-ph/0701175.
- [7] Th. Walcher et al., *A Surprising Mehtod for Polarizing Antiprotons*, arXiv:0706.3765.

# HADRON PHYSICS WITH ANTI-PROTONS: The $\bar{P}$ ANDA EXPERIMENT AT FAIR

*J.G. Messchendorp for the  $\bar{P}$ ANDA collaboration*  
Kernfysisch Versneller Instituut  
University of Groningen  
Groningen, NL-9747 AA  
The Netherlands  
mail: messchendorp@kvi.nl

## Abstract

The theory of Quantum Chromo Dynamics (QCD) reproduces the strong interaction at distances much shorter than the size of the nucleon. At larger distance scales, the generation of hadron masses and confinement cannot yet be derived from first principles on basis of QCD. The  $\bar{P}$ ANDA experiment at FAIR will address the origin of these phenomena in controlled environments. Beams of antiprotons together with a multi-purpose and compact detection system will provide unique tools to perform studies of the strong interaction. This will be achieved via precision spectroscopy of charmonium and open-charm states, an extensive search for exotic objects such as glueballs and hybrids, in-medium and hypernuclei spectroscopy, and more. An overview is given of the physics program of the  $\bar{P}$ ANDA collaboration.

## 1 Introduction

The fundamental building blocks of QCD are the quarks which interact with each other by exchanging gluons. QCD is well understood at short-distance scales, much shorter than the size of a nucleon ( $< 10^{-15}$  m). In this regime, the basic quark-gluon interaction is sufficiently weak. In fact, many processes at high energies can quantitatively be described by perturbative QCD. Perturbation theory fails when the distance among quarks becomes comparable to the size of the nucleon. Under these conditions, in the regime of non-perturbative strong QCD, the force among the quarks becomes so strong that they cannot be further separated. As a consequence of the strong coupling, we observe the relatively heavy mass of hadrons, such as protons and

neutrons, which is two orders of magnitude larger than the sum of the masses of the individual quarks. This quantitatively yet-unexplained behavior is related to the self-interaction of gluons leading to the formation of gluonic flux tubes connecting the quarks. As a consequence, quarks have never been observed as free particles and are confined within hadrons, i.e. the baryons containing three valence quarks or mesons containing a quark-antiquark pair.

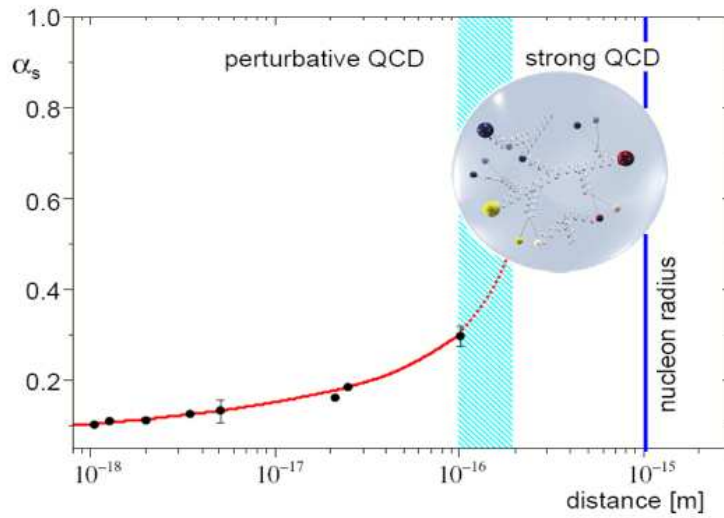


Figure 1: *The strong coupling constant,  $\alpha_s$ , as a function of the distance scale. Towards larger distances, QCD becomes non-perturbative, and gives rise to spectacular phenomena such as the generation of hadron masses.*

The physics program of the  $\bar{\text{P}}\text{ANDA}$  (anti-Proton ANnihilation at DArmstadt) collaboration [1] will address various questions related to the strong interactions by employing a multi-purpose detector system at the High Energy Storage Ring for anti-protons (HESR) of the upcoming Facility for Anti-proton and Ion Research (FAIR) [2]. The  $\bar{\text{P}}\text{ANDA}$  collaboration aims to connect the perturbative and the non-perturbative QCD regions, thereby providing insight in the mechanisms of mass generation and confinement. For this purpose, a large part of the program will be devoted to

- charmonium spectroscopy;
- gluonic excitations, e.g. hybrids and glueballs;
- open and hidden charm in nuclei.

In addition, various other physics topics will be studied with  $\bar{\text{P}}\text{ANDA}$  such as

- the hyperon-nucleon and hyperon-hyperon interactions via  $\gamma$ -ray spectroscopy of hypernuclei;
- CP violation studies exploiting rare decays in the D and/or  $\Lambda$  sectors;
- studies of the structure of the proton by measuring Generalized Parton Distributions (Drell-Yan and Virtual-Compton Scattering), "spin" structure functions using polarized anti-protons, and electro-magnetic form factors in the time-like region.

## 2 $\bar{P}$ ANDA physics topics

The key ingredient for the  $\bar{P}$ ANDA physics program is a high-intensity and a high-resolution beam of antiprotons in the momentum range of 1.5 to 15 GeV/c. Such a beam gives access to a center-of-mass energy range from 2.2 to 5.5 GeV/c<sup>2</sup> in  $\bar{p}p$  annihilations. In this range, a rich spectrum of hadrons with various quark configurations can be studied as is illustrated in Fig. 2. In particular, hadronic states which contain charmed quarks and gluon-rich matter become experimentally accessible.

### 2.1 Charmonium Spectroscopy

The level scheme of lower-lying bound  $\bar{c}c$  states, charmonium, is very similar to that of positronium. These charmonium states can be described fairly well in terms of heavy-quark potential models. Precision measurements of the mass and width of the charmonium spectrum give, therefore, access to the confinement potential in QCD. Extensive measurements of the masses and widths of the  $1^- \Psi$  states have been performed at  $e^+e^-$  machines where they can be formed directly via a virtual-photon exchange. Other states, which do not carry the same quantum number as the photon, cannot be populated directly, but only via indirect production mechanisms. This is in contrast to the  $\bar{p}p$  reaction, which can form directly excited charmonium states of all quantum numbers. As a result, the resolution in the mass and width of charmonium states is determined by the precision of the phase-space cooled beam momentum distribution and not by the (significantly poorer) detector resolution.

The combination of the much better mass resolution with the ability to detect hadronic final states which have up to two orders of magnitude higher branching fractions than - for instance - the  $\gamma\gamma$  decay channel will permit high-precision investigations of charmonium states. The need for such a tool becomes evident by reviewing the many open questions in the charmonium

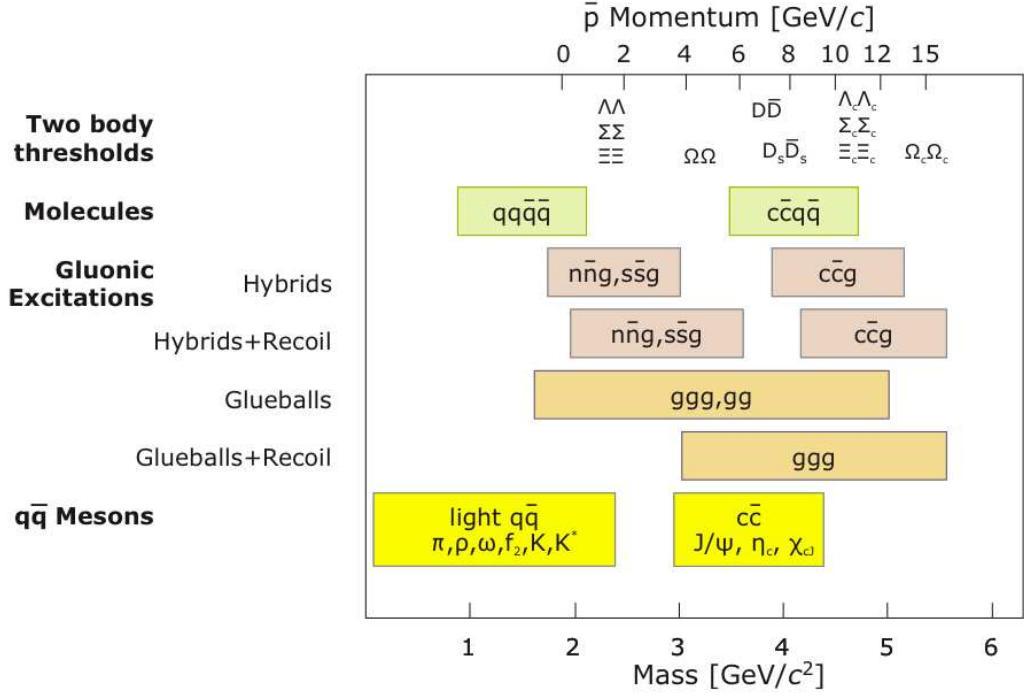


Figure 2: *An overview of the various quark and gluon configurations of hadrons and their corresponding mass range. The  $\bar{P}$ ANDA experiment will exploit masses up to  $5.5 \text{ GeV}/c^2$  in antiproton-proton collisions, thereby having access to glueballs, charmed hybrids, and charmed-rich four-quark states.*

sector. For instance, our knowledge of the ground state,  $\eta_c$ , is surprisingly poor. The existing data [3–7] do not present a consistent picture, and only a small fraction of the total decay width has been measured via specific decay channels. Furthermore, radial excitations, such as the  $\eta'_c$ , which was only recently discovered [8], are not simple recursions of the ground state, as was observed in the hadronic decays of the  $\Psi$  states. Another open question is the spin-dependence of the  $q\bar{q}$  potential. For this, a precise measurement of the mass and decay channels of the singlet-P resonance,  $h_c$ , is of extreme importance. The available data for the  $h_c$  are of poor precision [9, 10]. Due to the narrow width,  $\Gamma < 1 \text{ MeV}$ , of this state, only  $\bar{p}p$  formation experiments will be able to measure the width and perform systematic investigations of the decay modes. Finally, our understanding of the states above the  $D\bar{D}$  threshold is very poor and needs to be explored in more detail. Recent experimental evidences (see review [11]) hint at a whole series of surprisingly narrow states with masses and properties which, so-far, cannot be interpreted

consistently by theory.

Besides the spectroscopy of charmonium states,  $\bar{P}$ ANDA will also provide the capability to perform open-charm spectroscopy as the analog of the hydrogen atom in QED (heavy-light system). Striking discrepancies of recently discovered  $D_{sJ}$  states by BaBar [12] and CLEO [13] with model calculations have been observed. Precision measurements of the masses and widths of these states using antiprotons and by performing near-threshold scans are needed to shed light on these open problems.

## 2.2 Hybrids, glueballs, and other exotics

The self-coupling of gluons in strong QCD has an important consequence, namely that QCD predicts hadronic systems consisting of only gluons, glueballs, or bound systems of quark-antiquark pairs with a strong gluon component, hybrids. These systems cannot be categorized as "ordinary" hadrons containing valence  $q\bar{q}$  or  $qqq$ . The additional degrees of freedom carried by gluons allow glueballs and hybrids to have spin-exotic quantum numbers,  $J^{PC}$ , that are forbidden for normal mesons and other fermion-antifermion systems. States with exotic quantum numbers provide the best opportunity to distinguish between gluonic hadrons and  $q\bar{q}$  states. Exotic states with conventional quantum numbers can be identified by measuring an overpopulation of the meson spectrum and by comparing properties, like masses, quantum numbers, and decay channels, with - for instance - predictions from Lattice Quantum Chromodynamics (LQCD) calculations.

The first hints for gluonic hadrons came from antiproton annihilation experiments. Two particles, first seen in  $\pi N$  scattering with exotics  $J^{PC}=1^{-+}$  quantum numbers,  $\pi_1(1400)$  [14] and  $\pi_1(1600)$  [15] are clearly seen in  $\bar{p}p$  at rest and are considered as hybrid candidates. In the search for glueballs, a narrow state at  $1500 \text{ MeV}/c^2$ , discovered in antiproton annihilations by the Crystal Barrel collaboration [16–19] is considered the best candidate for the glueball ground state ( $J^{PC}=0^{++}$ ). However, the mixing with nearby conventional scalar  $q\bar{q}$  states makes a unique interpretation difficult.

The most promising energy range to discover unambiguously hybrid states and glueballs is in the region of  $3\text{-}5 \text{ GeV}/c^2$ , in which narrow states are expected to be superimposed on a structureless continuum. In this region, LQCD predicts an exotic  $1^{-+} \bar{c}c$ -hybrid state with a mass of  $4.2\text{-}4.5 \text{ GeV}/c^2$  and a glueball state around  $4.5 \text{ GeV}/c^2$  with an exotic quantum number of  $J^{PC}=0^{+-}$  [20, 21]. The  $\bar{p}p$  production cross section of these exotic states are similar to conventional states and in the order of  $100 \text{ pb}$ . All other states with ordinary quantum numbers are expected to have cross sections of about  $1 \mu\text{b}$ .

### 2.3 Hadrons in the nuclear medium

One of the challenges in nuclear physics is to study the properties of hadrons and the modification of these properties when the hadron is embedded in a nuclear many-body system. Only recently it became experimentally evident that the properties of mesons, such as masses of  $\pi$ ,  $K$ , and  $\omega$  mesons, change in a dense environment [22–25]. The  $\overline{\text{PANDA}}$  experiment provides a unique possibility to extend these studies towards the heavy-quark sector by exploiting the  $\overline{p}A$  reaction. For instance, an in-medium modification of the mass of the  $D$  meson would imply a modification of the energy threshold for the production of  $D$  mesons, compared to a free mass. In addition, a lowering of the  $D$ -meson mass could cause charmonium states which lie just below the  $D\overline{D}$  threshold for the  $\overline{p}p$  channel to reside above the threshold for the  $\overline{p}A$  reaction. In such a case, the width of the charmonium state will drastically increase, which can experimentally be verified. Although this is intuitively a simple picture, in practice the situation is more complicated since the mass of various charmonium states might also change inside the nuclear medium.

Besides the indirect in-medium studies as described above,  $\overline{\text{PANDA}}$  will be capable to directly measure the in-medium spectral shape of charmonium states. This can be achieved by measuring the invariant mass of the di-lepton decay products. For the  $\Psi(3770)$ , for instance, models predict mass shifts of the order of  $-100$  MeV [26], which are experimentally feasible to observe.

### 2.4 Hypernuclei

Nuclei in which one or more of the constituent nucleons are replaced by hyperons, hypernuclei, are promising laboratories to study the hyperon-nucleon and hyperon-hyperon interactions. Single and double  $\Lambda$ -hypernuclei were discovered 50 [27] and 40 [28] years ago, respectively, of which only 6 double  $\Lambda$ -hypernuclei are presently known. With a dedicated setup of  $\overline{\text{PANDA}}$  and its antiproton beam, a copious production of double  $\Lambda$ -hypernuclei is expected to be observed, providing a precision investigation of the  $\Lambda$ - $\Lambda$  interaction. For this purpose, antiprotons at a moderate momentum of 3 GeV/c will interact with a primary target to produce large numbers of  $\Xi\overline{\Xi}$  pairs. The  $\overline{\Xi}$  decay provides a unique signature for the production. The corresponding  $\Xi$  particle will be stopped and captured in a secondary target. In case the  $\Xi$  is absorbed inside the nucleus, it will yield a  $\Lambda$  pair with very small (relative) energy. A (double) hypernucleus can be formed whose decay is observed with spectroscopic precision using Germanium detectors.

## 2.5 Other Topics

So far, this paper has concentrated on only a few of the topics which will be addressed by the  $\overline{\text{P}}\text{ANDA}$  collaboration. There exists, however, a large variety of other physics topics which can ideally be studied with the  $\overline{\text{P}}\text{ANDA}$  setup at the antiproton facility at FAIR.

In one of these “side” activities, symmetry violation experiments are being proposed which will open a window onto physics beyond the Standard Model of particle physics. This includes experimental studies of lepton flavor number violation using rare decay of  $D$  mesons and, in addition, CP violation studies by asymmetry measurements of  $(D\overline{D})$  pairs near their production threshold in  $\overline{p}p \rightarrow \Psi(3770) \rightarrow D\overline{D}$  and  $\overline{p}p \rightarrow \Psi(4040) \rightarrow D\overline{D}$  reactions.

There is growing interest within the  $\overline{\text{P}}\text{ANDA}$  collaboration to make use of electro-magnetic probes, photons and leptons, in antiproton-proton annihilation. These probes will be used to study the structure of the proton by measuring Generalized Parton Distributions (GPDs), to determine quark distribution functions via Drell-Yan processes, and to obtain time-like electro-magnetic form factors by exploiting the  $\overline{p}p \rightarrow e^+e^-$  reaction with an intermediate massive virtual photon. For example, estimates [29] of the count rates predict a few thousand  $\gamma\gamma$  events per month for a luminosity of  $2 \cdot 10^{32} \text{ cm}^{-2}\text{s}^{-1}$  at an energy of  $\sqrt{s} = 3.2 \text{ GeV}/c^2$  for the crossed-channel Compton scattering process, which will be used to obtain GPDs. This indicates that such studies are feasible using beams of antiprotons together with a nearly- $4\pi$  electro-magnetic calorimeter, as foreseen with  $\overline{\text{P}}\text{ANDA}$ .

## 3 The experimental facility

The  $\overline{\text{P}}\text{ANDA}$  detector will be installed at the High Energy Storage Ring, HESR, at the future Facility for Antiproton and Ion Research, FAIR. FAIR provides a storage ring for beams of phase-space cooled antiprotons with unprecedented quality and intensity [30]. Antiprotons will be transferred to the HESR where internal-target experiments in the beam momentum range of  $1.5 - 15 \text{ GeV}/c$  can be performed. Electron and stochastic phase space cooling will be available to allow for experiments with either high momentum resolution of about  $\sim 10^{-5}$  at reduced luminosity or with high luminosity up to  $2 \times 10^{32} \text{ cm}^{-2}\text{s}^{-1}$  with an enlarged momentum spread of  $\sim 10^{-4}$ .

The  $\overline{\text{P}}\text{ANDA}$  detector is designed as a large acceptance multi-purpose setup. The experiment will use internal targets. It is conceived to use either pellets of frozen  $\text{H}_2$  or cluster jet targets for the  $\overline{p}p$  reactions, and wire targets for the  $\overline{p}A$  reactions.

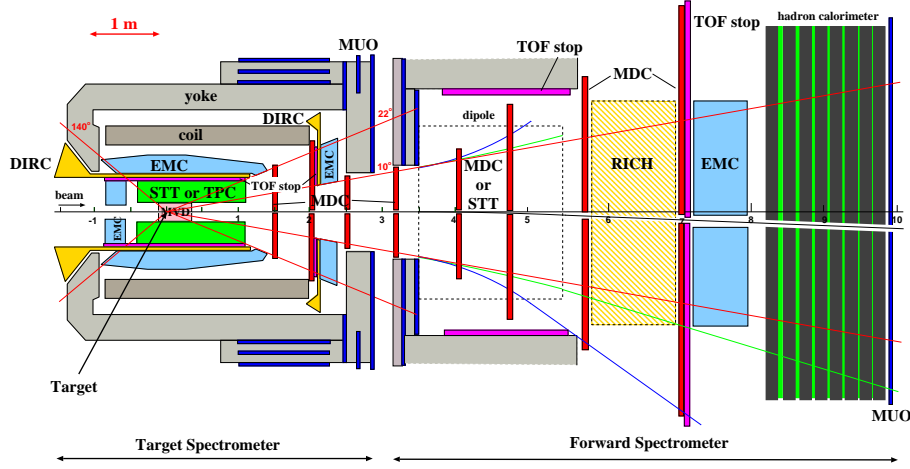


Figure 3: A schematic side view of the  $\bar{P}$ ANDA detector. The different components are abbreviated as DIRC (Detection of internally reflected Cherenkov photons), EMC (Electromagnetic calorimeter), STT (Straw-tube tracker), TPC (Time-projection chambers), MVD (Micro Vertex Detector), MDC (Mini drift chambers), MUO (Muon Detectors), RICH (Ring-imaging Cherenkov detectors), TOF (Time-of-flight detectors). Not shown are the recent plans to include Gas Electron Multipliers (GEMs).

In order to address the different physics topics, the detector needs to cope with a variety of final states and a large range of particle momenta and emission angles. At present, the detector is being designed to handle high rates of  $10^7$  annihilations/s, with good particle identification and momentum resolution for  $\gamma$ ,  $e$ ,  $\mu$ ,  $\pi$ ,  $K$ , and  $p$  with the ability to measure  $D$ ,  $K_S^0$ , and  $\Lambda$  which decay at displaced vertices. Furthermore, the detector will have an almost  $4\pi$  detection coverage both for charged particles and photons. This is an essential requirement for an unambiguous partial wave analysis [31] of resonance states. Various design studies are ongoing [32], partly making use of a dedicated computing framework for simulations and data analysis [33]. A schematic overview of the detector is given in Fig. 3.

## 4 Summary

The  $\bar{P}$ ANDA experiment at FAIR will address a wide range of topics in the field of QCD, of which only a small part could be presented in this paper. The physics program will be conducted by using beams of antiprotons together with a multi-purpose detection system, which enables experiments

with high luminosities and precision resolution. This combination provides unique possibilities to study hadron matter via precision spectroscopy of the charmonium system and the discovery of new hadronic matter, such as charmed hybrids or glueballs, as well as by measuring the properties of hadronic particles in dense environments. New insights in the structure of the proton will be obtained by exploiting electromagnetic probes. Furthermore, the next generation of hypernuclei spectroscopy will be conducted by the  $\bar{P}$ ANDA collaboration and at the J-PARC facility in Japan [34]. To summarize,  $\bar{P}$ ANDA has the ambition to provide valuable and new insights in the field of hadron physics which would bridge our present knowledge obtained in the field of perturbative QCD with that of non-perturbative QCD and nuclear structure.

## Acknowledgments

The author thanks N. Kalantar-Nayestanaki, H. Löhner, O. Scholten, and R.G.E. Timmermans for their comments and input to this paper. The  $\bar{P}$ ANDA collaboration acknowledges the support of the European Community under the FP6 Design Study program. The present work has been performed with financial support from the University of Groningen and the Gesellschaft für Schwerionenforschung mbH (GSI), Darmstadt.

## References

- [1] Technical Progress Report for  $\bar{P}$ ANDA,  
[http://www-panda.gsi.de/archive/public/panda\\_tpr.pdf](http://www-panda.gsi.de/archive/public/panda_tpr.pdf)
- [2] <http://www.gsi.de/fair/index.html>
- [3] P. Partridge *et al.*, *Phys. Rev. Lett.* **45**, 1150 (1980).
- [4] T. Himel *et al.*, *Phys. Rev. Lett.* **45**, 1146 (1980).
- [5] R.M. Baltrusaitis *et al.*, *Phys. Rev.* **D33**, 629 (1986)..
- [6] D. Bisello *et al.*, *Phys. Lett.* **B179**, 294 (1986).
- [7] J.Z. Bai *et al.*, *Phys. Rev.* **D62**, 072001 (2000).
- [8] S.-K. Choi *et al.*, *Phys. Rev. Lett.* **89**, 102001 (2002).
- [9] J.L. Rosner *et al.*, *Phys. Rev. Lett.* **95**, 102003 (2005).

- 
- [10] P. Rubin *et al.*, *Phys. Rev.* **D72**, 092005 (2005).
- [11] T. Barnes, *hep-ph/0608103*.
- [12] B. Aubert *et al.*, *Phys. Rev. Lett.* **90**, 242001 (2003).
- [13] D. Besson *et al.*, *Phys. Rev.* **D68**, 032002 (2003).
- [14] A. Abele *et al.*, *Phys. Lett.* **B423**, 175 (1998).
- [15] J. Reinnarth, *Nucl. Phys.* **A692**, 268c (2001).
- [16] C. Amsler *et al.*, *Phys. Lett.* **B342**, 433 (1995).
- [17] C. Amsler *et al.*, *Phys. Lett.* **B353**, 571 (1995).
- [18] A. Abele *et al.*, *Phys. Lett.* **B385**, 425 (1996).
- [19] A. Abele *et al.*, *Eur. Phys. J.* **C19**, 667 (2001).
- [20] C. Morningstar and M. Peardon, *Phys. Rev.* **D60**, 034509 (1999).
- [21] G.S. Bali, *Eur. Phys. J.* **A19**, 1 (2004).
- [22] K. Suzuki *et al.*, *Phys. Rev. Lett.* **92**, 072302 (2004).
- [23] R. Barth *et al.*, *Phys. Rev. Lett.* **78**, 4007 (1997).
- [24] F. Laue *et al.*, *Phys. Rev. Lett.* **82**, 1640 (1999).
- [25] D. Trnka *et al.*, *Phys. Rev. Lett.* **94**, 192303 (2005).
- [26] S.H. Lee, *nucl-th/0310080*.
- [27] M. Danysz and J. Pniewski, *Phil. Mag.* **44**, 348 (1953).
- [28] M. Danysz *et al.*, *Nucl. Phys.* **49**, 121 (1963).
- [29] A. Freund, A. Radyushkin, A. Schäfer, and C. Weiss, *Phys. Rev. Lett.* **90**, 092001 (2003).
- [30] The High Energy Storage Ring, <http://www.fz-juelich.de/ikp/hesr/>
- [31] R.G.E. Timmermans *et al.*, *Phys. Rev.* **C50**, 48 (1994).
- [32] K. Föhl, contribution to these proceedings.
- [33] A. Wronska, contribution to these proceedings.
- [34] N. Saito, contribution to these proceedings.

# FUTURE SCIENTIFIC OPPORTUNITIES AT JEFFERSON LAB

*A. W. Thomas*

Jefferson Lab, 12000 Jefferson Ave.,  
Newport News VA 23606 USA

## Abstract

Nuclear physics requires at least one major facility world-wide which is capable of fully exploiting the properties of the electro-weak force to investigate precisely the structure of strongly interacting systems. At its current maximum energy of 6 GeV Jefferson Lab has provided a wealth of important information on the structure of nucleons and nuclei. However, the plans to double the energy over the next seven years promise to open new frontiers in nuclear and particle physics. We briefly describe the plans for the 12 GeV Upgrade and the associated physics opportunities.

## 1 Introduction

The first 10 years of operation of the Continuous Electron Beam Accelerator Facility (CEBAF) at JLab have seen a number of important new results, which have advanced our knowledge of nucleon and nuclear structure as well as our understanding of non-perturbative QCD and the limits on possible physics beyond the Standard Model. The exploitation of parity violating electron scattering has given new meaning to the term precision electroweak measurements. In terms of that precision and its kinematic reach CEBAF is a truly world leading facility. However, the nuclear science community in the United States has realized that by doubling its energy at a relatively modest cost, one can open new frontiers of investigation, from the existence and properties of so-called exotic mesons to three-dimensional imaging of the nucleon to new searches for physics beyond the Standard Model which rival the precision achieved at LEP. Indeed, this 12 GeV Upgrade project has been recognized in the new Long Range Plan as the highest priority for nuclear science in the United States. In what follows we briefly outline what will be done as part of this project as well as the science which it is expected to enable.

## 2 The 12 GeV Upgrade at Jefferson Lab

CEBAF was designed to permit exploration of the detailed structure of nucleons and nuclei using continuous beams of 4 GeV electrons and nuclear physics research began there in 1995. The accelerator represents the world's first successful large-scale utilization of superconducting radio-frequency (SRF) accelerating structures. Advances in SRF technology have made it possible to increase the beam energy to 6 GeV without installing new equipment. Further developments have led to performance that will permit us to increase the energy to 12 GeV (double the present energy and triple the original) by installing a small number of new accelerating structures but without changing the basic configuration of the facility. Research at 12 GeV is to begin around 2014. We begin by describing the accelerator upgrade plans as well as the experimental equipment planned to exploit the new research opportunities.

### 2.1 Accelerator upgrade

A new 12 GeV beam to Hall D and beams of up to 11 GeV for Halls A, B, and C are needed for the desired research program. To provide them, the accelerator must be upgraded to 2.2 GeV/pass (1.1 GV/linac) and the beam transport system upgraded and expanded. The following summarizes the planned work:

- 1.1 GV/linac: Increase each linac's voltage by 0.5 GV by adding 5 new high-performance superconducting radio-frequency (SRF) accelerating systems and new RF system for each; the present 5kW@2K cryogenics plant will be roughly doubled to support the increased load;
- Add a tenth recirculation arc, thereby permitting a sixth pass of acceleration through the North Linac and direction of beam toward Hall D;
- Upgrade the capabilities of the present beam transport system to handle the increased beam energies; there will be extensive re-use of existing hardware;
- Add beam transport to Hall D.

### 2.2 Gluex Experiment in Hall D

Hall D will initially house the equipment for the GlueX experiment and will be situated at the northeast corner of the CEBAF accelerator. The

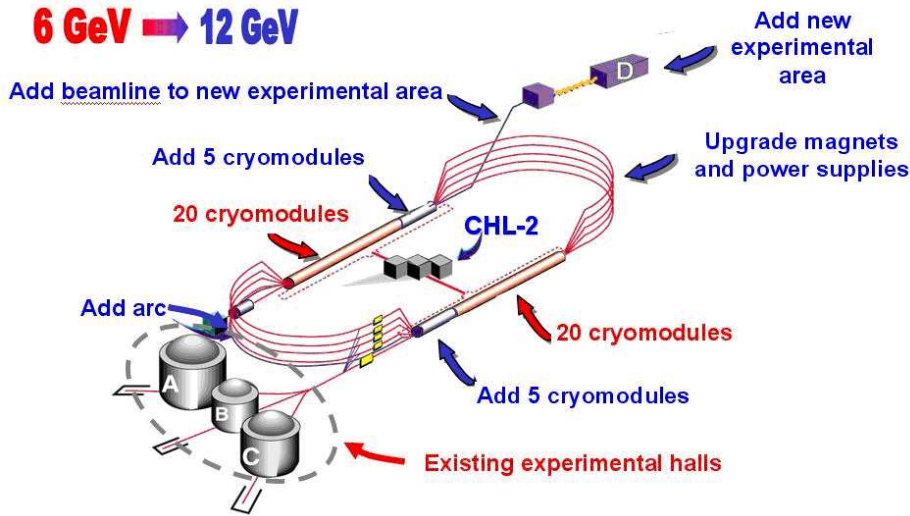


Figure 1: Illustration of the changes to the accelerator facility associated with the Upgrade of CEBAF from 6 to 12 GeV.

design, fabrication and installation of detector components will be performed. System integration and checkout will be performed, including interfacing of detector systems to trigger, data acquisition, slow controls, and monitoring systems. Features of this nearly-hermetic spectrometer include:

- A large solenoid magnet, which in concert with large-area drift chambers provides momentum and vertex measurements for multiple charged particles;
- Reconstruction capability for energy and direction of multiple photons using large-area calorimetry;
- Particle identification for charged particles via time-of-flight, electromagnetic shower calorimeters, Cerenkov detectors, and energy loss;
- A facility for producing a beam of polarized photons of known energies;
- A data acquisition system capable of handling data from a flux of  $10^7$  photons per second on a hydrogen target, with an architecture which is capable of being upgraded to ten times higher capacity.

### 2.3 Hall A, B and C Equipment

- In Hall A the beamline will be upgraded to achieve the capability of delivering the maximum energy 5-pass beam to the existing spectrom-

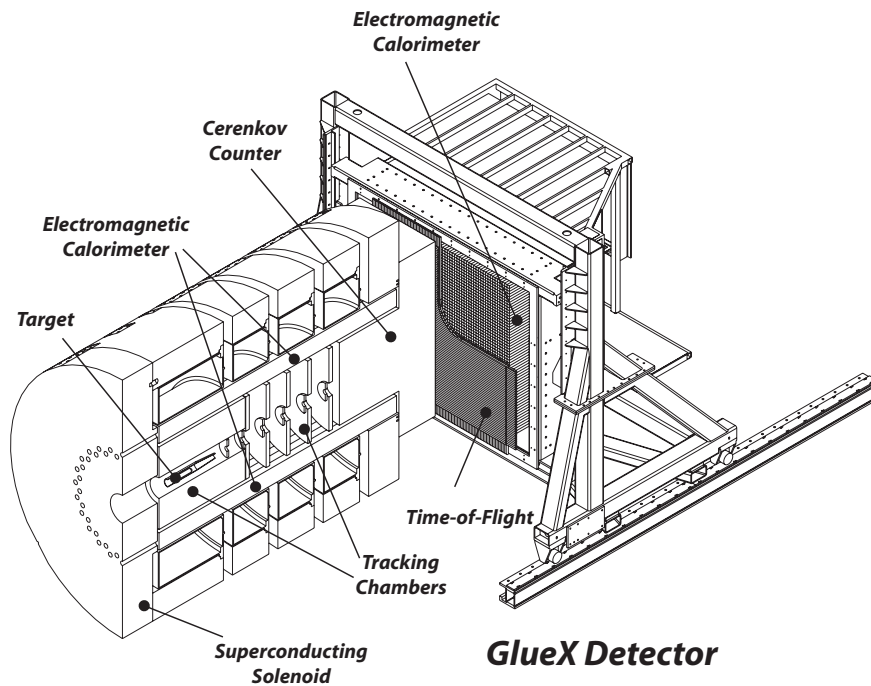


Figure 2: The GlueX detector, specifically optimized to permit reliable partial wave analysis for multi-meson final states, to be installed in Hall D.

eters. Some electronics will also be upgraded to improve data-taking at higher data acquisition rates.

- In Hall B CLAS, the existing large acceptance detector in Hall B will be extensively upgraded with new magnets and detectors to capture the more forward-focused reaction products at the increased luminosity. Features of this upgraded spectrometer include:
  - Toroidal magnetic field, which in concert with large-area drift chambers and silicon vertex detectors provides momentum and vertex measurements for multiple charged particles;
  - Reconstruction of energy and direction of multiple photons in the forward direction using large-area calorimetry;
  - Identification of charged particles via time-of-flight, electromagnetic shower calorimeters, and Cerenkov detectors;
  - Flexibility to accommodate a variety of target types; and
  - Magnetic shielding of Moller electrons adequate to permit measurements with a luminosity of  $10^{35} \text{ cm}^{-2}\text{s}^{-1}$ , and

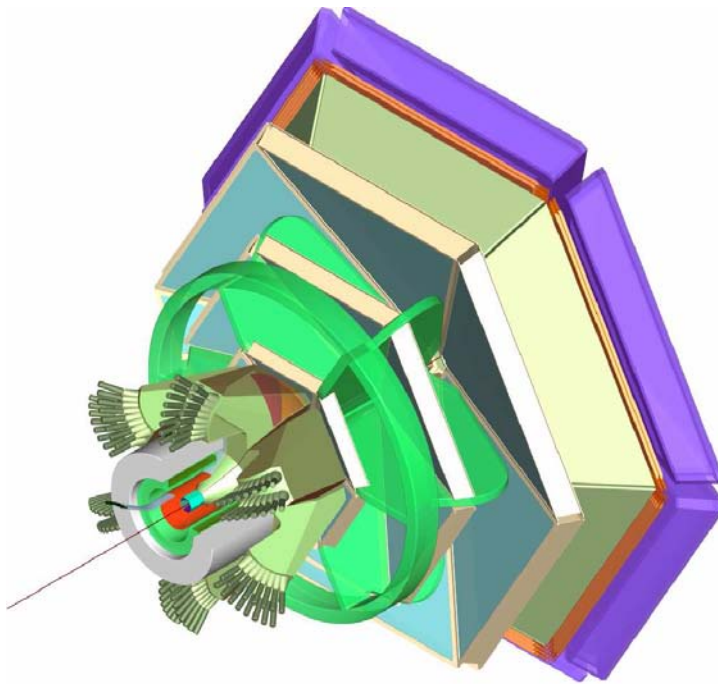


Figure 3: The new CLAS 12 detector to be installed in Hall B.

- A data acquisition system capable of absorbing the resulting data.
- In Hall C we will install a new focusing spectrometer system, called the Super High Momentum Spectrometer (SHMS) with central momentum up to 11 GeV/c will enable measurements of particles scattered at up to full beam momentum. It will be used together with the existing High Momentum Spectrometer (HMS). Features of the SHMS include:
  - High precision and reproducibility due to a rigid attachment to a central pivot and a robust support and transport structure;
  - Ability to analyze charged particles up to the full 5-pass beam energy;
  - Excellent momentum resolution for charged particles;
  - Particle identification for charged particles via time-of-flight, electromagnetic shower calorimeters, and Cerenkov detectors;
  - Flexibility to accommodate a variety of target types; and
  - Capability to use luminosities of  $10^{38} \text{ cm}^{-2}\text{s}^{-1}$ .

In addition there is, of course, a great deal of civil construction to house the new GlueX experiment.

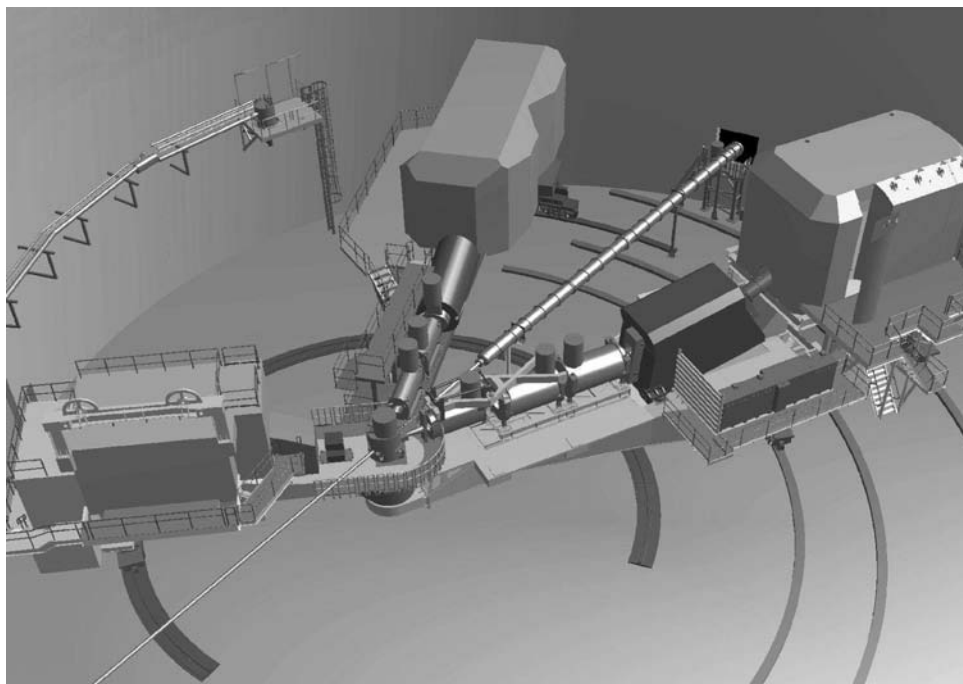


Figure 4: The Super High Momentum Spectrometer (SHMS) planned for Hall C is shown together with the two existing spectrometers. The capability of either using SHMS alone, or in combination with the HMS, presents an extremely versatile and powerful set of tools for investigating deep hadron structure.

### 3 Outline of the science to be explored at 12 GeV

In the process of reaching CD-1, we have defined a clear set of physics priorities for the first 5 years of operation after the completion of construction [1,2]. These priorities were judged to be outstanding, with significant discovery potential, by the independent DOE review [3] (in April 2005). This judgement was re-affirmed by the nuclear science community in the United States as part of the Long Range Planning exercise in early 2007. It will, of course, continue to be subject to peer review and re-evaluation. However, there is no known or planned facility which can address those scientific challenges and it is difficult to imagine their importance diminishing in the intervening period.

The major physics aims of the first 5 years of operation are:

- Revolutionize our knowledge of spin and flavor dependence of valence

## PDFs

- Revolutionize our knowledge of the distribution of charge and current within the nucleon
- Provide a totally new view of hadron (and nuclear) structure through the Generalized Parton Distributions (GPDs).
- Explore QCD in the nonperturbative regime. In particular, establish the existence and properties of exotic mesons and hence explore the mechanism of quark confinement.
- Establish a new paradigm for nuclear physics through the quest to understand nuclear structure in terms of QCD. In particular, the unique features of this new facility will enable us to explore the spin and flavor dependence of the famous EMC effect. We will also be able to study the propagation of quarks through nuclear matter.
- Make precision tests of the Standard Model.

We now briefly outline the main themes associated with each of these topics.

### 3.1 Exotic mesons and the origin of confinement

Unlike any area of physics hitherto explored, QCD has the property that the force carriers themselves, the gluons, can by themselves form new structures. In combination with quark-anti-quark pairs, gluons can also give rise to new particles whose quantum numbers cannot be made from a quark-anti-quark pair alone. The former are known as glueballs and the challenge to find them has been the lack of any distinct quantum numbers, at least in the low mass regime, and the fact that they almost certainly mix strongly with normal mesons. Exotic mesons, on the other hand, are expected to occur at low mass and, precisely because of the signature of their quantum numbers, be readily identifiable. Indeed, the best available theory suggests as many as three nonets of these “exotic mesons” in the mass range 1.5 to 2.5 GeV. The choice of 12 GeV was precisely in order to make this mass region accessible with a proton target. The GlueX detector was specifically designed to have extremely high efficiency for detecting the multi-meson final states resulting from the decay of these exotic mesons. Sophisticated techniques for making the partial wave analysis (PWA) needed to recognize an exotic meson signal have been underway at Indiana University for some years, with recent support at Jefferson Lab.

The physics interest in these states arises because the unique quantum numbers have their origin in excitations of the flux tube or string joining the quark-anti-quark pair. This flux tube is intimately connected with the nature of the QCD vacuum and the origin of confinement itself. Establishing the existence and properties of these exotics is a crucial step to understanding whether QCD really is the full theory of the strong interaction.

### 3.2 Spin and flavor dependence of PDFs

It is an astonishing fact that more than 30 years after the discovery of scaling we still do not know the distribution of the momentum of the proton on valence down quarks [4, 5]. For Bjorken  $x$  beyond 0.6, the uncertainty in  $d(x)$  rapidly grows to 100%. It is crucial to measure the large  $x$  behavior of  $d(x)$  in order to understand the relative importance of short and long distance di-quark correlations in the valence structure of the proton. It is at least equally important to understand how the spin of the proton is carried by its constituents [6]. With the 12 GeV Upgrade Jefferson Lab will be able to unambiguously map out the distribution of momentum and spin on the valence  $u$  and  $d$  quarks in the proton. It will also be possible to explore the sea down to Bjorken  $x$  of order 0.1.

### 3.3 Distribution of charge and current in the nucleon

Over the past 8 years, Jefferson Lab has mapped the electromagnetic form factors of the proton and neutron with great precision, out to a momentum transfer of order  $4 \text{ GeV}^2$  [6]. The 12 GeV Upgrade will permit the exploration to momentum transfers of order  $14 \text{ GeV}^2$ , an increase in spatial resolution by a factor of two.

### 3.4 Generalized parton distributions

The GPDs will yield unique, tomographic information on the three-dimensional structure of nucleons and nuclei [8,9] with particular sensitivity to the orbital angular momentum carried by specific quark flavors [10]. The latter feature is of particular importance in the light of advances made towards resolving the famous proton spin crisis over the past twenty years. We now know that the quarks carry roughly one third of the spin of the proton (rather than the value near zero originally suggested). In addition, it seems likely that the spin carried by polarized gluons in the proton is far too small to play a major role in resolving the discrepancy between modern data and theoretical expectations. Rather, important aspects of the non-perturbative structure

of the nucleon, such as the pion cloud and the one-gluon-exchange hyperfine interaction, are sufficient to resolve the remaining problem – see Ref. [11] for a summary. These new mechanisms imply that much of the spin of the proton is actually carried by quarks and anti-quarks in the proton as orbital angular momentum – most likely in the range of Bjorken- $x$  covered by the 12 GeV Upgrade. This clearly makes the GPD program even more relevant and important.

### 3.5 The QCD basis of nuclear structure

In more than 20 years since the discovery of the EMC effect (European Muon Collaboration) [12], which showed a dramatic change of the parton distribution functions of nuclei compared with free nucleons, no consensus has been reached as to the underlying physical origin of the effect [13]. It seems clear, however, that standard nuclear binding and kinematic corrections cannot explain the data and one is actually exploring the change in structure of the nucleon-like clusters when imbedded in the nuclear medium [14–16]. These are extremely important questions, going to the heart of how QCD itself yields nuclear matter [17, 18]. It is quite clear that precise data exploring the flavor and spin dependence of this effect [14, 15] will be crucial in choosing amongst the various theoretical models so far proposed to explain it.

There will also be a possibility to explore the interaction of fast quarks with nuclear matter, yielding new insights into the process of hadronization, the nature of confinement and the change of the structure of the QCD vacuum in-medium.

### 3.6 Beyond the Standard Model

The precise studies of parity violating electron scattering at JLab (as well as Mainz and Bates) have already led to a remarkable increase in the lower bound on the mass scale associated with possible new physics beyond the Standard Model – from roughly 0.4 to 0.9 TeV [19]. This success has also served to emphasize the discovery potential of the Qweak experiment, which will run just before the shutdown, to build the 12 GeV Upgrade [20]. This important experience at the high precision frontier means that the community is ideally placed to exploit the new possibilities opened by the Upgrade. For example, precise measurements of parity violation, in Moller scattering and in hadronic deep inelastic scattering have complementary sensitivities. One can in fact probe new physics, such as supersymmetry, additional gauge bosons and so on, at energy scales far beyond what can be explored directly at high energy facilities. A number of experiments are under consideration

and the choice will be made on the highest impact possible with the beam characteristics provided through the Upgrade.

## 4 Concluding Remarks

At present the project has undergone the reviews necessary to obtain CD-2 before the end of 2007 and we anticipate the award of CD-3, which signals the start of construction, late in 2008.

The science which has already been identified as part of the 12 GeV Upgrade represents a rich program of great breadth and importance for our field. Much of what has been outlined here will be achieved within the first 5 years of operation. We remain completely open to new ideas from anyone, with access to the facility determined by an independent Program Advisory Committee on the basis of scientific feasibility and impact. With an active and growing user base of more than 1,200 scientists we can be certain that many of the best ideas are yet to come!

## Acknowledgments

This work was supported by DOE contract DE-AC05-06OR23177, under which Jefferson Science Associates operates Jefferson Lab.

## References

- [1] [http://www.jlab.org/div\\_dept/physics\\_division/GeV/doe\\_review/](http://www.jlab.org/div_dept/physics_division/GeV/doe_review/)
- [2] [http://www.jlab.org/div\\_dept/physics\\_division/GeV/doe\\_review/CDR\\_for\\_Science\\_Review.pdf](http://www.jlab.org/div_dept/physics_division/GeV/doe_review/CDR_for_Science_Review.pdf)
- [3] [http://www.jlab.org/div\\_dept/physics\\_division/GeV/doe\\_review/science\\_review.pdf](http://www.jlab.org/div_dept/physics_division/GeV/doe_review/science_review.pdf)
- [4] W. Melnitchouk and A. W. Thomas, Phys. Lett. B **377**, 11 (1996) [arXiv:nucl-th/9602038].
- [5] M. Botje, Eur. Phys. J. **C14**, 285 (2000)
- [6] X. Zheng *et al.* [Jefferson Lab Hall A Collaboration], Phys. Rev. C **70**, 065207 (2004) [arXiv:nucl-ex/0405006].

- 
- [7] C. E. Hyde-Wright and K. de Jager, *Ann. Rev. Nucl. Part. Sci.* **54**, 217 (2004) [arXiv:nucl-ex/0507001].
- [8] X. Ji, *Ann. Rev. Nucl. Part. Sci.* **54**, 413 (2004).
- [9] A. V. Belitsky and A. V. Radyushkin, *Phys. Rept.* **418**, 1 (2005) [arXiv:hep-ph/0504030].
- [10] P. Hoodbhoy, X. D. Ji and W. Lu, *Phys. Rev. D* **59**, 014013 (1999) [arXiv:hep-ph/9804337].
- [11] F. Myhrer and A. W. Thomas, “Resolution of the Proton Spin Problem,” arXiv:0709.4067 [hep-ph].
- [12] J. J. Aubert *et al.* [European Muon Collaboration], *Phys. Lett. B* **123**, 275 (1983).
- [13] D. F. Geesaman, K. Saito and A. W. Thomas, *Ann. Rev. Nucl. Part. Sci.* **45**, 337 (1995).
- [14] I. C. Cloët, W. Bentz and A. W. Thomas, *Phys. Rev. Lett.* **95**, 052302 (2005) [arXiv:nucl-th/0504019].
- [15] I. C. Cloet, W. Bentz and A. W. Thomas, *Phys. Lett. B* **642**, 210 (2006) [arXiv:nucl-th/0605061].
- [16] J. R. Smith and G. A. Miller, *Phys. Rev. C* **72**, 022203 (2005) [arXiv:nucl-th/0505048].
- [17] W. Bentz and A. W. Thomas, *Nucl. Phys. A* **696**, 138 (2001) [arXiv:nucl-th/0105022].
- [18] P. A. M. Guichon and A. W. Thomas, *Phys. Rev. Lett.* **93**, 132502 (2004) [arXiv:nucl-th/0402064].
- [19] R. D. Young, R. D. Carlini, A. W. Thomas and J. Roche, *Phys. Rev. Lett.* **99**, 122003 (2007) [arXiv:0704.2618 [hep-ph]].
- [20] W. T. H. van Oers [Qweak Collaboration], “The Qweak Experiment – A search for new physics at the TeV Scale,” arXiv:0708.1972 [nucl-ex].

# DYNAMICS, SYMMETRIES AND HADRON PROPERTIES

*I.C. Cloët,\* A. Krassnigg† and C.D. Roberts\**

\* Physics Division, Argonne National Laboratory,  
Argonne, Illinois 60439, United States of America

† Institut für Physik, Karl-Franzens-Universität Graz,  
A-8010 Graz, Austria

## Abstract

We provide a snapshot of Dyson-Schwinger equation applications to the theory and phenomenology of hadrons. Exact results for pseudoscalar mesons are highlighted, with details relating to the  $U_A(1)$  problem. Calculated masses of the lightest  $J = 0, 1$  states are discussed. We recapitulate upon studies of nucleon properties and give a perspective on the contribution of quark orbital angular momentum to the spin of a nucleon at rest.

## 1 Introduction

Numerous salient features exhibited by the physics of mesons and nucleons arise nonperturbatively in QCD. Two phenomena strike one immediately: confinement and dynamical chiral symmetry breaking (DCSB). DCSB is the better understood of these emergent phenomena; e.g., it explains the origin of constituent-quark masses and underlies the success of chiral effective field theory. Confinement, on the other hand, remains only an empirical fact; viz., colored objects have not hitherto been observed in isolation. A fact too often ignored is that the potential between infinitely heavy quarks measured in numerical simulations of quenched lattice-QCD – the static potential – is not related in any known way to light-quark confinement.

## 2 DCSB

Understanding DCSB within QCD proceeds from the gap equation [1]; namely, the Dyson-Schwinger equation (DSE) for the dressed-quark propagator:

$$S(p)^{-1} = Z_2 (i\gamma \cdot p + m^{\text{bm}}) + Z_1 \int_q^\Lambda g^2 D_{\mu\nu}(p-q) \frac{\lambda^a}{2} \gamma_\mu S(q) \Gamma_\nu^a(q,p), \quad (1)$$

where  $\int_q^\Lambda$  represents a Poincaré invariant regularization of the integral, with  $\Lambda$  the regularization mass-scale,  $D_{\mu\nu}$  is the dressed-gluon propagator,  $\Gamma_\nu$  is the dressed-quark-gluon vertex, and  $m^{\text{bm}}$  is the quark's  $\Lambda$ -dependent bare current-mass. The vertex and quark wave-function renormalization constants,  $Z_{1,2}(\zeta^2, \Lambda^2)$ , depend on the gauge parameter.

The solution of Eq. (1) can be written:

$$S(p) = \frac{1}{i\gamma \cdot p A(p^2, \zeta^2) + B(p^2, \zeta^2)} = \frac{Z(p^2, \zeta^2)}{i\gamma \cdot p + M(p^2)}, \quad (2)$$

wherein  $Z(p^2; \zeta^2)$  is the wave-function renormalization and  $M(p^2)$  is the mass function. The latter is independent of the renormalization point,  $\zeta$ . The dressed propagator is obtained from Eq. (1) augmented by the renormalization condition  $S(p)^{-1}|_{p^2=\zeta^2} = i\gamma \cdot p + m(\zeta^2)$ , where  $m(\zeta^2)$  is the running mass:  $Z_2(\zeta^2, \Lambda^2) m^{\text{bm}}(\Lambda) = Z_4(\zeta^2, \Lambda^2) m(\zeta^2)$ , with  $Z_4$  the Lagrangian-mass renormalization constant. In QCD the chiral limit is strictly defined by [1]:  $Z_2(\zeta^2, \Lambda^2) m^{\text{bm}}(\Lambda) \equiv 0, \forall \Lambda^2 \gg \zeta^2$ , which states that the renormalization-point-invariant current-quark mass  $\hat{m} = 0$ .

Only in the chiral limit is it possible to unambiguously define the gauge invariant vacuum quark condensate in terms of  $S(p)$  [1–3]. This emphasizes that gauge covariant quantities contain gauge invariant information. The condensate is the order parameter most commonly cited in connection with DCSB. Nonetheless,  $M(p^2)$  is a more fundamental indicator: the condensate is only a small part of the information it contains.

In perturbation theory it is impossible in the chiral limit to obtain  $M(p^2) \neq 0$ : the generation of mass from *nothing* is an essentially nonperturbative phenomenon. On the other hand, it is a longstanding prediction of non-perturbative DSE studies that DCSB will occur so long as the integrated infrared strength possessed by the gap equation's kernel exceeds some critical value [4]. There are strong indications that this condition is satisfied in QCD [5, 6]. It follows that the quark-parton of QCD acquires a momentum-dependent mass function, which at infrared momenta is  $\sim 100$ -times larger than the current-quark mass. This effect owes primarily to a dense cloud of gluons that clothes a low-momentum quark [7].

A great deal has been learnt from the gap equation alone. To highlight only one recent example [3], realistic *Ansätze* for the the gap equation's kernel indicate that there is a critical current-quark mass,  $\hat{m}_{\text{cr}}$ , above which  $M(p^2)$  does not possess an expansion in  $\hat{m}$  around its chiral-limit value. For a pion-like meson constituted from a quark,  $f$ , with mass  $\hat{m}_{\text{cr}}$  and an equal-mass different-flavor antiquark,  $\bar{g}$ ,  $m_{\bar{g}f}^{0^-} = 0.45 \text{ GeV}$ . Since physical observables, such as the leptonic decay constant, are expressed in terms of  $M(p^2)$ , it

follows that a chiral expansion is meaningful only for  $(m_{gf}^{0-})^2 \lesssim 0.2 \text{ GeV}^2$ . This entails, e.g., that it is only valid to employ chiral perturbation theory to fit and extrapolate results from lattice-regularized QCD when the simulation parameters provide for  $m_\pi^2 \lesssim 0.2 \text{ GeV}^2$ . Lattice results at larger pion masses are not within the domain of convergence of chiral perturbation theory.

### 3 Mesons

For  $0^-$  mesons the axial-vector Ward-Takahashi identity is of fundamental importance, and recently its implications for neutral pseudoscalars and  $\eta$ - $\eta'$  mixing have been elucidated [8]. In the general case the identity is written

$$P_\mu \Gamma_{5\mu}^a(k; P) = \mathcal{S}^{-1}(k_+) i\gamma_5 \mathcal{F}^a + i\gamma_5 \mathcal{F}^a \mathcal{S}^{-1}(k_-) - 2i\mathcal{M}^{ab} \Gamma_5^b(k; P) - \mathcal{A}^a(k; P), \quad (3)$$

wherein:  $\{\mathcal{F}^a | a = 0, \dots, N_f^2 - 1\}$  are the generators of  $U(N_f)$ ; the dressed-quark propagator  $\mathcal{S} = \text{diag}[S_u, S_d, S_s, S_c, S_b, \dots]$ ;  $\mathcal{M}(\zeta)$  is the matrix of running current-quark masses and  $\mathcal{M}^{ab} = \text{tr}_F[\{\mathcal{F}^a, \mathcal{M}\}\mathcal{F}^b]$ , where the trace is over flavour indices. The inhomogeneous axial-vector vertex in Eq. (3),  $\Gamma_{5\mu}^a(k; P)$ , where  $P$  is the total momentum of the quark-antiquark pair and  $k$  the relative momentum, satisfies a Bethe-Salpeter equation (BSE), and likewise the pseudoscalar vertex,  $\Gamma_5^b(k; P)$ . The final term in Eq. (3) expresses the axial anomaly. It involves

$$\mathcal{A}_U(k; P) = \int d^4x d^4y e^{i(k_+ \cdot x - k_- \cdot y)} N_f \langle \mathcal{F}^0 q(x) \mathcal{Q}(0) \bar{q}(y) \rangle, \quad (4)$$

wherein the matrix element represents an operator expectation value in full QCD and  $\mathcal{Q}(x) = i\frac{\alpha_s}{8\pi} \epsilon_{\mu\nu\rho\sigma} F_{\mu\nu}^a F_{\rho\sigma}^a(x) = \partial_\mu K_\mu(x)$  is the topological charge density operator, where  $F_{\mu\nu}^a$  is the gluon field strength tensor.<sup>1</sup>

In considering the  $U_A(1)$ -problem one need only focus on the case  $\mathcal{A}^0 \neq 0$  because if that is false, then following Ref. [1] it is clear that the  $\eta'$  is certainly a Goldstone mode.  $\mathcal{A}^0$  is a pseudoscalar vertex and can therefore be expressed

$$\begin{aligned} \mathcal{A}^0(k; P) = & \mathcal{F}^0 \gamma_5 [i\mathcal{E}_A(k; P) + \gamma \cdot P \mathcal{F}_A(k; P) \\ & + \gamma \cdot k k \cdot P \mathcal{G}_A(k; P) + \sigma_{\mu\nu} k_\mu P_\nu \mathcal{H}_A(k; P)]. \end{aligned} \quad (5)$$

Equation (3) can now be used to derive a collection of chiral-limit, point-wise Goldberger-Treiman relations, important amongst which is the identity

<sup>1</sup>NB. While  $\mathcal{Q}(x)$  is gauge invariant, the associated Chern-Simons current,  $K_\mu$ , is not. Thus in QCD no physical state can couple to  $K_\mu$ . Hence, physical states cannot provide a resolution of the so-called  $U_A(1)$ -problem; namely, they cannot play any role in ensuring that the  $\eta'$  is not a Goldstone mode.

Table 1: Masses (GeV) of the lightest  $J = 0, 1$  states produced by the rainbow-ladder DSE truncation of Refs. [17, 18] with the parameter values:  $\omega = 0.4 \text{ GeV}$ ,  $\omega D = (0.72 \text{ GeV})^3$ ; and current-quark masses  $m_{u,d}(1 \text{ GeV}) = 5.45 \text{ MeV}$ ,  $m_s(1 \text{ GeV}) = 125 \text{ MeV}$ . The rainbow-ladder kernel gives ideal flavour mixing for all states. See the text for further discussion.

$J^{PC}$	$0^{-+}$	$1^{--}$	$0^{++}$	$1^{+-}$	$1^{++}$	$0^{--}$	$1^{-+}$	$0^{+-}$
$\bar{u}u$	139	740	670	830	900	860	1000	1040
$\bar{s}s$	695	1065	1080	1165	1240	1170	1310	1385

$2f_{\eta'} E_{\eta'}(k; 0) = 2B_0(k^2) - \mathcal{E}_{\mathcal{A}}(k; 0)$ , where  $B_0(k^2)$  is obtained in solving the chiral-limit gap equation. It is plain that if

$$\mathcal{E}_{\mathcal{A}}(k; 0) = 2B_0(k^2), \quad (6)$$

then  $f_{\eta'} E_{\eta'}(k; 0) \equiv 0$ . This being true, then the homogeneous Bethe-Salpeter equation for the  $\eta'$  does not possess a massless solution in the chiral limit. The converse is also true. Hence Eq. (6) is a necessary and sufficient condition for the absence of a massless  $\eta'$  bound-state. The chiral limit is being discussed, in which case  $B_0(k^2) \neq 0$  if, and only if, chiral symmetry is dynamically broken. Thus the absence of a massless  $\eta'$  bound-state is only assured through the existence of an intimate connection between DCSB and an expectation value of the topological charge density. A relationship between the mechanism underlying DCSB and the absence of a ninth Goldstone boson was also discussed in Ref. [9].

Reference [8] also derives corollaries, amongst which are mass formulae for neutral pseudoscalars, and presents an *Ansatz* for the Bethe-Salpeter kernel that enables their illustration. The model is elucidative and phenomenologically efficacious; e.g., it predicts  $\eta$ - $\eta'$  mixing angles of  $\sim -15^\circ$  and  $\pi^0$ - $\eta$  angles of  $\sim 1^\circ$ ; and suggests a strong neutron-proton mass difference of  $0.75(m_d - m_u)$ .

The use of DSEs to study meson phenomena is empowered by the existence of a systematic, nonperturbative and symmetry-preserving truncation scheme [10, 11]. It means that exact results, such as those indicated above, and others related to radial excitations and/or hybrids [12–14], and heavy-light [15] and heavy-heavy mesons [16], can be proved and illustrated.

In the latter connection, the renormalization-group-improved rainbow-ladder truncation of the gap and Bethe-Salpeter equations introduced in Refs. [17, 18] has been widely employed. To exemplify that, in Table 1 we

report calculated results for the masses of the lightest  $J = 0, 1$  states [19]. It is true in general that the truncation is accurate for the  $0^{-+}$  and  $1^{--}$  light-quark meson ground states. In these channels it can be seen algebraically that contributions beyond rainbow-ladder largely cancel between themselves owing to Eq. (3) [11, 20–22]. The remaining columns in the table deserve special attention because they show clearly the path toward improvement.

Terms beyond the rainbow-ladder truncation are known to add constructively in the  $0^{++}$  channel [23]. Hence the leading order truncation is *a priori* not expected to provide a good approximation. Further understanding is provided by an exploration of the contribution from two-pion intermediate states to the mass and width of this lowest-mass scalar. A rudimentary analysis shows that a realistic description is attainable therewith [25]; viz., it gives a pole position  $\sqrt{s_\sigma} = (0.578 - i0.311)$  GeV. This is not the end of the scalar story but it is a sensible path to follow, in particular because a QCD-level mechanism is precisely specified.<sup>2</sup>

Compared with experiment, the masses of the axial-vector mesons  $1^{+\pm}$  are poorly described by the rainbow-ladder truncation:  $\sim 400$  MeV of repulsion is missing from the kernel. A cruder model does better [26, 27]. The latter studies and a more recent analysis [28] indicate that at least part of the defect owes to the absence of spin-flip contributions at leading-order. Such contributions appear at all higher orders and are enhanced by the strongly dressed quark mass function. It is in this way that the meson spectrum can be used to probe the long-range part of the light-quark interaction and thereby to chart the nonperturbative behavior of QCD's  $\beta$ -function.

The last three columns describe systems with so-called exotic quantum numbers. Of course, these states are exotic only in the context of the naive constituent quark model. In QCD they correspond simply to interpolating fields with some gluon content and are easily accessible via the BSE [29]. Nonetheless, while the rainbow-ladder truncation binds in these channels, the shortcomings encountered in the  $1^+$  channels are also evident here, for much the same reasons. Reliable predictions for the masses of such states will only be obtained once improved kernels are developed. At the very least, one must have reliable predictions for axial-vector masses before drawing any conclusions about the so-called exotics.

One might pose the question of whether, in the context of bound-state studies in which model assumptions are made regarding the nature of the long-range interaction between light quarks, anything is gained by working solely with Schwinger functions. This means, in part, constraining oneself to

---

<sup>2</sup>In rainbow-ladder truncation, at least up to the c-quark mass, the ordering of meson masses is  $0^{-+}(1S) < 0^{++}(1S) < 0^{-+}(2S) < 0^{++}(2S)$  [24].

work only with information obtained from the DSEs at spacelike momenta.<sup>3</sup> According to a recent study [30] the answer is no. It analysed the capacity of Schwinger functions to yield information about bound states, and established that for the ground state in a given channel the mass and residue are accessible via rudimentary methods. However, simple methods cannot provide dependable information about more massive states in a given channel. Indeed, there is no easy way to extract such information. An approach based on a correlator matrix can be successful but only if the operators are carefully constructed so as to have large overlap with states of interest in a given channel and statistical errors can be made small; viz.,  $\sim 1\%$ . While it is possible in principle to satisfy these constraints, doing so is labor intensive and time consuming. That is only justified in the absence of model-dependence.

## 4 Nucleons

The discussion of DSEs at MENU04 did not describe the study of nucleons, stating only that it was feasible [31]. Material progress has been made in the interim. We now possess a level of expertise roughly equivalent to that we had with mesons approximately ten years ago; viz., phenomenology constrained by the significant body of knowledge we have gained in meson applications.

The nucleon appears as a pole in a six-point quark Green function. The pole's residue is proportional to the nucleon's Faddeev amplitude, which is obtained from a Poincaré covariant Faddeev equation that adds-up all possible quantum field theoretical exchanges and interactions that can take place between three dressed-quarks. Poincaré covariance is crucial because modern experimental facilities employ large momentum transfer reactions.

A tractable truncation of the Faddeev equation is based [32] on the observation that an interaction which describes mesons also generates colour- $\bar{3}$  diquark correlations [33]. For ground state octet and decuplet baryons the dominant correlations are  $0^+$  and  $1^+$  diquarks because, e.g.: the associated mass-scales are smaller than the baryons' masses [26,34,35], namely (in GeV)  $m_{[ud]_{0^+}} = 0.7 - 0.8$ ,  $m_{(uu)_{1^+}} = m_{(ud)_{1^+}} = m_{(dd)_{1^+}} = 0.9 - 1.0$ ; and the electromagnetic size of these correlations is less than that of the proton [36] –  $r_{[ud]_{0^+}} \approx 0.7$  fm, which implies  $r_{(ud)_{1^+}} \sim 0.8$  fm based on the  $\rho$ -meson/ $\pi$ -meson radius-ratio [37,38].

The Faddeev equation's kernel is completed by specifying that the quarks

---

<sup>3</sup>Lattice-regularized QCD provides a background to this question. That approach is grounded on the Euclidean space functional integral. Schwinger functions; i.e., propagators and vertices at spacelike momenta, are all that it can directly provide. It can only be useful if methods are found so that the question can be answered in the affirmative.

are dressed, with two of the three dressed-quarks correlated always as a colour- $\bar{3}$  diquark. Binding is then effected by the iterated exchange of roles between the bystander and diquark-participant quarks. A Ward-Takahashi-identity-preserving electromagnetic current for the baryon thus constituted is subsequently derived [39]. It depends on the electromagnetic properties of the axial-vector diquark correlation.

A study of the nucleon's mass and the effect on this of a pseudoscalar meson cloud are detailed in [40]. Lessons learnt were employed in a series of studies of nucleon properties, including form factors [41–44]. The calculated ratio  $\mu_p G_E^p(Q^2)/G_M^p(Q^2)$  passes through zero at  $Q^2 \approx 6.5 \text{ GeV}^2$  [42]. For the neutron, in the neighbourhood of  $Q^2 = 0$ ,  $\mu_n G_E^n(Q^2)/G_M^n(Q^2) = -\frac{r_n^2}{6} Q^2$ , where  $r_n$  is the neutron's electric radius [43]. The evolution of  $\mu_p G_E^p(Q^2)/G_M^p(Q^2)$  and  $\mu_n G_E^n(Q^2)/G_M^n(Q^2)$  on  $Q^2 \gtrsim 2 \text{ GeV}^2$  are both primarily determined by the quark-core of the nucleon. While the proton ratio decreases uniformly on this domain [41, 42], the neutron ratio increases steadily until  $Q^2 \simeq 8 \text{ GeV}^2$  [43]. A comparison of the Pauli/Dirac form factor ratios for the neutron and proton is presented in Ref. [7].

Of significant interest is the distribution of an hadron's *spin* over the quark constituents and their angular momentum. In a Poincaré covariant approach that can be calculated in any frame. The rest frame is physically most natural. The pion was considered in Ref. [16]. The answer is more complicated for the spin- $\frac{1}{2}$  nucleon. In the truncation just described a nucleon's Faddeev wave-function is expressed through eight scalar functions: no more are needed, no number fewer is complete. Two are associated with the  $0^+$  diquark correlation:  $\mathcal{S}_{1,2}$ , and six with the  $1^+$  correlation:  $\mathcal{A}_{1,\dots,6}$ . In the rest frame in this basis one can derive the following “good” angular momentum and spin assignments, which add vectorially to give a  $J = \frac{1}{2}$  nucleon:<sup>4</sup>

$$\begin{array}{c|c|c|c} L = 0, S = \frac{1}{2} & L = 1, S = \frac{1}{2} & L = 1, S = \frac{3}{2} & L = 2, S = \frac{3}{2} \\ \mathcal{S}_1, \mathcal{A}_2, \mathcal{B}_1 & \mathcal{S}_2, \mathcal{A}_1, \mathcal{B}_2, & \mathcal{C}_2 & \mathcal{C}_1 \end{array}, \quad (7)$$

$$\begin{aligned} B_1 &= \frac{1}{3}A_3 + \frac{2}{3}A_5, & B_2 &= \frac{1}{3}A_4 + \frac{2}{3}A_6, \\ C_1 &= A_3 - A_5, & C_2 &= A_4 - A_6. \end{aligned} \quad (8)$$

These assignments are straightforward to demonstrate and understand; e.g. in the rest frame of a relativistic constituent quark model the  $\mathcal{S}_{1,2}$  terms correspond, respectively, to the upper and lower components of the nucleon's spinor.

To exhibit the importance of the various  $L$ - $S$  correlations within the nucleon's Faddeev wave-function we report the breakdown of contributions to

<sup>4</sup>Equation (3.35) or Ref. [45] contradicts Fig. 6 of that reference. Equation (8) herein describes the correct assignments.

the nucleon's canonical normalization:<sup>5</sup>

	$\mathcal{S}_1$	$\mathcal{A}_2$	$\mathcal{B}_1$	$\mathcal{S}_2$	$\mathcal{A}_1$	$\mathcal{B}_2$	$\mathcal{C}_2$	$\mathcal{C}_1$
$\mathcal{S}_1$	0.62	-0.01	0.07	0.25				-0.02
$\mathcal{A}_2$	-0.01		-0.06		0.05	0.04	0.02	-0.16
$\mathcal{B}_1$	0.07	-0.06	-0.01		0.01	0.13	-0.01	
$\mathcal{S}_2$	0.25			0.06				
$\mathcal{A}_1$		0.05	0.01			-0.07	-0.07	0.02
$\mathcal{B}_2$		0.04	0.13		-0.07	-0.10	-0.02	0.13
$\mathcal{C}_2$		0.02	-0.01		-0.07	-0.02	-0.11	0.37
$\mathcal{C}_1$	-0.02	-0.16			0.02	0.13	0.37	-0.15

(9)

To illustrate how to read Eq. (9) we note that the largest single entry is associated with  $\mathcal{S}_1 \otimes \mathcal{S}_1$ , which represents the quark outside the scalar diquark correlation carrying all the nucleon's spin. That is the  $u$ -quark in the proton. However, it is noteworthy that a contribution of similar magnitude is associated with the axial-vector diquark correlations, expressing mixing between  $p$ - and  $d$ -waves; viz.,  $\mathcal{C}_1 \otimes \mathcal{C}_2 + \mathcal{C}_2 \otimes \mathcal{C}_1$ . With  $\mathcal{C}_2$  all quark spins are aligned with that of the nucleon and the unit of angular momentum is opposed, while with  $\mathcal{C}_1$  all quark spins are opposed and the two units of angular momentum are aligned. This contribution is more important than those associated with  $\mathcal{S}_2$ ; namely, scalar diquark terms with the bystander quark's spin antiparallel. Finally, for the present, in this context one single number is perhaps most telling: the contribution to the normalization from  $(L = 0) \otimes (L = 0)$  terms is only 37% of the total.

## 5 Coda

The DSEs provide a natural vehicle for the exploration of confinement and DCSB. DCSB is a remarkably effective mass generating mechanism. For light-quarks it is far more important than the Higgs mechanism. It is understood via QCD's gap equation, which delivers a quark mass function with a momentum-dependence that connects the perturbative domain with the non-perturbative, constituent-quark domain. The existence of a sensible truncation scheme enables the proof of exact results using the DSEs. The scheme is also tractable. Hence the results can be illustrated and predictions made for observables. The consequent opportunities for rapid feedback between

<sup>5</sup>The entry in location  $\mathcal{S}_1 \otimes \mathcal{S}_1$  indicates the integrated contribution associated with  $\mathcal{S}_1^2$ . The entries are reweighted such that the sum of the squares of the entries equals one. Positions without an entry are zero to two decimal places.

experiment and theory brings within reach an intuitive understanding of nonperturbative strong interaction phenomena.

It can be argued that confinement is expressed in the analyticity properties of dressed Schwinger functions [4]. To build understanding it is essential to work toward an accurate map of the confinement force between light-quarks. Among the rewards are a clear connection between confinement and DCSB, an accounting of the distribution of mass within hadrons, and a realistic picture of hybrids and exotics.

It is important to understand the relationship between parton properties on the light-front and the rest frame structure of hadrons. This is a challenge because, e.g., DCSB, a keystone of low-energy QCD, has not been realized in the light-front formulation. Parton distribution functions must be calculated in order to learn their content. Parametrization is insufficient. It would be very interesting to know how, if at all, the distribution functions of a Goldstone mode differ from those of other hadrons. Answers to these and kindred questions are being sought using the DSEs [46, 47].

## Acknowledgments

CDR is grateful to the organizers for their hospitality and support. This work was supported by the Department of Energy, Office of Nuclear Physics, contract no. DE-AC02-06CH11357; the Austrian Science Fund FWF under Schrödinger-Rückkehrstipendium Nr. R50-N08; and benefited from the facilities of the ANL Computing Resource Center.

## References

- [1] P. Maris, C. D. Roberts and P. C. Tandy, *Phys. Lett.* **B 420**, 267 (1998).
- [2] K. Langfeld, *et al.*, *Phys. Rev. C* **67**, 065206 (2003).
- [3] L. Chang, *et al.*, *Phys. Rev. C* **75**, 015201 (2007).
- [4] C. D. Roberts and A. G. Williams, *Prog. Part. Nucl. Phys.* **33**, 477 (1994).
- [5] P. O. Bowman, *et al.*, *Phys. Rev.* **D 71**, 054507 (2005).
- [6] M. S. Bhagwat and P. C. Tandy, *AIP Conf. Proc.* **842**, 225 (2006).
- [7] M. S. Bhagwat, I. C. Cloët and C. D. Roberts, “Covariance, Dynamics and Symmetries, and Hadron Form Factors,” arXiv:0710.2059 [nucl-th].

- 
- [8] M. S. Bhagwat, *et al.*, *Phys. Rev.* **C 76**, 045203 (2007).
- [9] A. E. Dorokhov and W. Broniowski, *Eur. Phys. J.* **C 32**, 79 (2003).
- [10] H. J. Munczek, *Phys. Rev.* **D 52**, 4736 (1995).
- [11] A. Bender, C. D. Roberts and L. Von Smekal, *Phys. Lett.* **B 380**, 7 (1996).
- [12] A. Höll, A. Krassnigg and C. D. Roberts, *Phys. Rev.* **C 70**, 042203(R) (2004).
- [13] A. Höll, *et al.*, *Phys. Rev.* **C 71**, 065204 (2005).
- [14] C. McNeile and C. Michael [UKQCD Collaboration], *Phys. Lett.* **B 642**, 244 (2006).
- [15] M. A. Ivanov, Yu. L. Kalinovsky and C. D. Roberts, *Phys. Rev.* **D 60**, 034018 (1999).
- [16] M. S. Bhagwat, *et al.*, *Eur. Phys. J.* **A 31**, 630 (2007).
- [17] P. Maris and C. D. Roberts, *Phys. Rev.* **C 56**, 3369 (1997).
- [18] P. Maris and P. C. Tandy, *Phys. Rev.* **C 60**, 055214 (1999).
- [19] In preparing this table, we benefited from discussions with P. Maris.
- [20] A. Bender, *et al.*, *Phys. Rev.* **C 65**, 065203 (2002).
- [21] M. S. Bhagwat, *et al.*, *Phys. Rev.* **C 70**, 035205 (2004).
- [22] H. H. Matevosyan, A. W. Thomas and P. C. Tandy, *Phys. Rev.* **C 75**, 045201 (2007).
- [23] C. D. Roberts, Confinement, diquarks and Goldstone's theorem, in *Proc. 2nd Int. Conf. on Quark Confinement and the Hadron Spectrum*, eds. N. Brambilla and G. M. Prosperi (World Scientific, Singapore, 1997) p. 224.
- [24] A. Krassnigg, C. D. Roberts and S. V. Wright, *Int. J. Mod. Phys.* **A 22**, 424 (2007).
- [25] A. Höll, *et al.*, *Nucl. Phys. Proc. Suppl.* **161**, 87 (2006).
- [26] C. J. Burden, *et al.*, *Phys. Rev.* **C 55**, 2649 (1997).

- [27] J. C. R. Bloch, *et al.*, *Phys. Rev.* **D 60**, 111502(R) (1999).
- [28] P. Watson, W. Cassing and P. C. Tandy, *Few Body Syst.* **35**, 129 (2004).
- [29] C. J. Burden and M. A. Pichowsky, *Few Body Syst.* **32**, 119 (2002).
- [30] M. S. Bhagwat, *et al.*, *Few Body Syst.* **40**, 209 (2007).
- [31] A. Höll, *et al.*, *Int. J. Mod. Phys.* **A 20**, 1778 (2005).
- [32] R. T. Cahill, C. D. Roberts and J. Praschifka, *Austral. J. Phys.* **42**, 129 (1989).
- [33] R. T. Cahill, C. D. Roberts and J. Praschifka, *Phys. Rev.* **D 36**, 2804 (1987).
- [34] C. Hanhart and S. Krewald, *Phys. Lett.* **B 344**, 55 (1995).
- [35] P. Maris, *Few Body Syst.* **32**, 41 (2002).
- [36] P. Maris, *Few Body Syst.* **35**, 117 (2004).
- [37] P. Maris and P. C. Tandy, *Phys. Rev.* **C 62**, 055204 (2000).
- [38] M. S. Bhagwat and P. Maris, “Vector meson form factors and their quark-mass dependence,” arXiv:nucl-th/0612069.
- [39] M. Oettel, M. Pichowsky and L. von Smekal, *Eur. Phys. J.* **A 8**, 251 (2000).
- [40] M. B. Hecht, *et al.*, *Phys. Rev.* **C 65**, 055204 (2002).
- [41] R. Alkofer, *et al.*, *Few Body Syst.* **37**, 1 (2005).
- [42] A. Höll, *et al.*, *Nucl. Phys.* **A 755**, 298 (2005).
- [43] M. S. Bhagwat, *et al.*, *Nucl. Phys.* **A 790**, 10 (2007).
- [44] A. Höll, C. D. Roberts and S. V. Wright, *AIP Conf. Proc.* **857**, 46 (2006).
- [45] M. Oettel, *et al.*, *Phys. Rev.* **C 58**, 2459 (1998).
- [46] M. B. Hecht, C. D. Roberts and S. M. Schmidt, *Phys. Rev.* **C 63**, 025213 (2001).
- [47] I. C. Cloët, W. Bentz and A. W. Thomas, “Transversity quark distributions in a covariant quark-diquark model,” arXiv:0708.3246 [hep-ph].

## CONCLUDING REMARKS

*Ben Nefkens<sup>1</sup> and Aleksandr Starostin*  
Department of Physics and Astronomy  
University of California, Los Angeles  
Los Angeles, CA 90095-1547, USA

### Abstract

Hadron Physics is undergoing a renaissance witnessed the extraordinarily large number of participants to this conference, MENU 2007. The physics thrust now is nonperturbative QCD, specifically tackling the problem of the occurrence of exotic hadronic matter and the existence, or not of the missing states, which are ordinary three-quark states predicted to exist by various quark models, but not observed experimentally. Conclusive searches are possible in the framework of the Flavor Symmetry of QCD.

A brief overview is given of new and upgraded accelerators. This is followed by a status report on the existence of various baryon and meson species; a comparison is made with the status at the time of the first MENU Conference in 1983.

Next we outline the Flavor Symmetry of QCD and its origin in the QCD Lagrangian. We illustrate its existence with different experimental tests. Encouraged by its success we use Flavor Symmetry for a successful comparison of charmed  $\Lambda_c$  hyperons with the ordinary, strange,  $\Lambda$  states. Finally we touch on the diverging modern views on the structure of the nucleon.

## 1 Introduction

The future of hadron physics looks bright seen in the light of new and upgraded facilities. IUPAP has just produced the much anticipated booklet on the properties of all accelerators in the world available for hadron physics. The major new workplace is going to be FAIR (Facility for Antiproton and Ion Research) at GSI in Darmstadt, Germany, featuring an intense 29 GeV proton beam. Especially attractive is the 15 GeV antiproton storage ring with a large  $4\pi$ -acceptance detector PANDA. It is particularly suited for investigating the light mesons and the lightest baryons: the old, the new, the

---

<sup>1</sup>E-mail: nefkens@physics.ucla.edu

exotic and the “missing” ones. Unfortunately, at present there are no plans for a secondary meson beam.

The JLab (Newport News, USA) 12 GeV upgrade has just passed some major approval hurdles. An important aim is to find exotic hadrons. They will be searched for with a new detector that has near  $4\pi$  acceptance and includes a magnetic field. There is plenty of room for baryon physics and other stuff.

Good progress is being made with the construction of J-PARC (Japan Proton Accelerator Research Complex) in Japan. This is a 50 GeV proton accelerator with a few modest, low energy, secondary beams of pions and kaons. It is geared toward hypernuclear physics such as searching for double  $\Lambda$  hypernuclei. BESII in Beijing is a  $e^+e^-$  collider in the  $J/\Psi$  region. It has just undergone an important upgrade in intensity. It produces a large number of charmed baryons and mesons. MAMI in Mainz Germany is an electron accelerator with a high resolution, high intensity photon tagger upgraded to 1.5 GeV. It has a large program for polarized beams and polarized targets. The KLOE group at DAFNE is making a case for a substantial intensity upgrade of the machine and a possible upgrade of the maximum c. m. energy to 2.5 GeV. There are  $e^-$  laser backscattering photon beam facilities, SPring-8 in Japan and MAX-Lab in Lund, they are successfully used for nuclear and particle physics experiments. We will miss GRAAL as well as the charming contributions of CESAR and the beautiful work in spectroscopy done at BaBar and Belle.

We like to give a special merit citation to WASA at COSY. It an outstanding example of an international collaboration at the forefront of technology. Especially interesting is the novel pellet target. Our compliments to all who have made its possible.

Key physics to be investigated with the new facilities is QCD in the non-perturbative region. We need to find an appropriate description of the complicated structure of the nucleon. Also important are the searches for exotica and missing states.

For decades the experimentalists have directed much effort toward establishing the extend of isospin symmetry. Now that interest has changed to measuring the magnitude of the breaking of isospin symmetry in different systems. It is a way to experimentally investigating the validity of QCD in the nonperturbative regime.

For many years the determination of the  $\pi N$ - resonance properties was dominated by three large  $\pi N$  partial wave analyses (PWA), those of Carnegie-Mellon-Lawrence-Berkeley, Karlsruhe-Helsinki and SAID (Blacksburg). These analyses are based mainly on  $\pi^\pm p$  elastic scattering and pion charge exchange. Promising new efforts on a modern analysis of new scattering data are under-

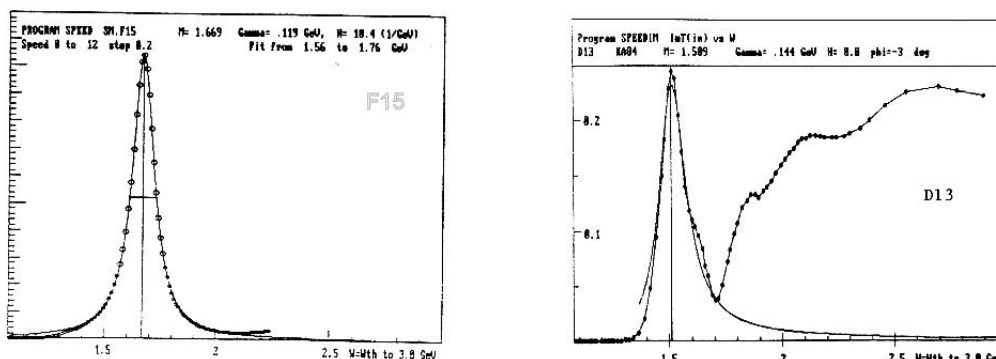


Figure 1: Examples of the speed plots for the  $F_{15}$  (left) and  $D_{13}$  (right) partial amplitudes from Ref. [2].

way at Mainz, JLab, and ANL. GWU is continuing with the SAID program. Restricted, but important results are coming from Giessen, Bonn–Gatchina and other places. Improvements include the inclusion of major inelastic channels and the use of coupled channel techniques. The latter are effectively promoted by the EBAC Group at JLab [1]. Unfortunately,  $\pi$  and  $K^-$  meson beams are no longer available in Europe and the U.S. Badly needed data on  $\pi N$  and  $KN$  interactions at intermediate energies are not in the cards in the near future. We are happy to note that extensive work in meson photoproduction is now being carried out at JLab, MAMI and ELSA. There are also important contributions from smaller facilities, which use back scattered laser photons. A complete photoproduction program should include linearly and circularly polarized photons as well as transversely and longitudinally polarized proton and deuteron targets.

## 2 The Status of Hadron Families

The energy dependence of the  $\pi N$  and  $KN$  partial wave amplitudes,  $A(W)$ , contains the full information on the dynamics of the light–quark resonances.  $W$  is the total energy in the c. m. frame. A useful quantity is the speed,  $SP$ , of the  $W$ –dependence of the scattering amplitudes:

$$SP(W) = |dA/dW| \quad (1)$$

as emphasized long ago by the pioneers of scattering theory [3]. A pronounced maximum in a speed plot corresponds to a maximum in the time

Table 1: Status of baryon spectroscopy. Comparison of the number of three- and four-star states available to the 1st and 11th MENU conferences.

state	number in 1983	number in 2007
$N^*$	18	14
$\Delta^*$	13	10
$\Lambda^*$	15	14
$\Sigma^*$	12	9
$\Xi^*$	4	4
$\Omega^-$	1	2
$B_c$	1	14
$B_b$	0	1
Dibaryon	3	0
Total	67	68

delay between the arrival and departure of the incident wave packet. It is a direct indication of the formation of an unstable particle in the intermediate state. It is a valuable alternative to the use of poles in the complex scattering plane. Since the speed plot is not well known to many we present two examples in Fig. 1. The speed plot of an elastic resonance has a smooth peak described by a Breit-Wigner. In most cases, but not always, the peak value agrees well with the pole position.

In the history of hadron physics there was a time around 1970 that it was generally assumed that the strong resonances were broad states like the  $\rho$ -meson or the  $\Delta$ -baryon. There was little incentive to search for the existence of narrow hadrons. That picture changed dramatically with the discovery of the  $J/\Psi$ -meson in 1974. It is not expected that history will repeat itself. There is at present no good theoretical reason for expecting the existence of small and narrow nucleon resonances which could lead to a small and narrow peak in a pseudo speed plot for the photoproduction of  $\pi^0$ ,  $\eta$ ,  $\eta'$ , *etc.* But a serious search for this has never been carried out. The necessary experimental tools – a high resolution tagged photon beam and a  $4\pi$  photon detector – are now available. Making such a search should now be considered.

MENU2007 is the eleventh conference in this series. It started out in 1983. It could be revealing to compare the resonance population then and now. For input we use the Review of Particle Properties then [5] and now [4]. We should limit the comparison to three- and four-star states as they are considered to be genuine states and not some statistical fluctuation. Listed in Table 1 are the number of the three- and four-star baryon family members then and now. The total number of genuine baryon resonances has barely

Table 2: Spectroscopy of mesonic states. Number of various mesons in 1983 and 2007 Review of Particle Properties. “Bullet” states only are shown.

Flavor	number in 1983	number in 2007
$s = c = b = 0$	24	44
$s = \pm 1; c = b = 0$	7	12
$b, s, c = \pm 1$	0	14
$c\bar{c}$	10	13
$b\bar{b}$	4	12
<i>Total</i>	46	95

changed, only 2%. But we have lost some three-star  $N^*$  and  $\Delta^*$  states. This loss is compensated by the discovery of 13 charmed baryons. These states are quite narrow and are therefore easy to find. However, the direct determination of spin and parity is very challenging and only done indirectly by flavor symmetry of QCD, see Sect. 3.

It should be pointed out that the spin and parity of all  $N^*$ ,  $\Delta^*$ ,  $\Lambda^*$  and  $\Sigma^*$  follow directly from the fabric of a PWA. For these states the number of stars reflects the quality of various data sets and the fits to the data. This approach does not work for the  $\Xi$  and  $\Omega$  states, which are otherwise readily discovered as a large, genuine peak in the appropriate missing mass or invariant mass distributions. The known  $\Xi$  resonances are quite narrow in contrast to the  $N^*$ ,  $\Delta^*$ ,  $\Lambda^*$  and  $\Sigma^*$  states, which tend to be broad. Spin and parity of new  $\Xi$  states can be investigated in a Byers–Fenster analysis, or from selected decays, such as the determination of the spin of the  $\Omega^-$  from the decay  $\Xi_c^0 \rightarrow \Omega^- K^+$  by Veronique Ziegler using BaBar data [6].

The star system was not made for cascade hyperons. We recommend to use four stars only if spin and parity have been measured directly, or reliably indirectly. Three stars should be awarded for a peak in excess of  $5\sigma$  and some kind of spin/parity assessment. Finding a five standard deviation peak only with no information on spin and parity gets only two stars. A  $4\sigma$  peak is rewarded with only one star.

Table 2 shows the comparison of the meson population in 1983 [5] and now [4]. A comprehensive evaluation of the quality of different meson states is not available. The only selection we can make is to limit the Table to mesons, which have been marked with a bullet in the Review of Particle Properties. The criteria for a bullet are not clear. The table caption in the Review of Particle Properties reads: “A bullet indicates particles that appear in the preceding Meson Summary Table. We do not regard the other entries as being established.” We count 95 accepted mesons in 2007 and half in 1983.

The increase is in all families.

One of the mysteries seen in all hadronic states is their relative simplicity: all baryon resonances can be satisfactorily described as three quark bound states. There is no indication that we need a gluon degree of freedom. All but a few mesons can be characterized as a quark–antiquark pair, again there is no requirement for gluons in meson spectroscopy. Neither is there at present evidence for color and/or flavor correlations. More spectroscopy data is needed to settle this.

### 3 The Flavor Symmetry of QCD

The interactions of quarks and gluons with one another are adequately described by the theory of Quantum Chromodynamics, QCD. Its Lagrangian,  $L_{\text{QCD}}$  has only two components, the chiral part,  $L_0$ , and the mass part,  $L_m$ . In other words,

$$L_{\text{QCD}} = L_0 + L_m \quad (2)$$

$L_0$  and  $L_m$  are very different.  $L_0$  has chiral symmetry and it depends primarily on the quark fields,  $\psi_q$ , and gluon fields  $A_\nu$ . There is only one coupling constant,  $g_s$ , for all interactions, this is the manifestation of the universality of the strong interactions. The detailed expressions for  $L_{\text{QCD}}$  are given in the Appendix.

The important property of  $L_0$ , aside from chiral symmetry, is that of Flavor Symmetry, FS. It means that  $L_0$  is the same for all six quark flavors,  $d$ ,  $u$ ,  $s$ ,  $c$ ,  $b$  and  $t$ .

The second component of  $L_{\text{QCD}}$  is the mass term  $L_m$ , it depends only on the quark fields and the quark masses,  $m_q$

$$L_m = - \sum_q \bar{\psi}_i m_q \psi_{qi}. \quad (3)$$

$L_m$  is responsible for Flavor Symmetry Breaking, FSB. Flavor Symmetry, which applies to all quarks, is the generalization of isospin symmetry, which concerns only up and down quarks. In the theoretical limit of massless quarks we have  $L_m = 0$  thus  $L_{\text{QCD}} = L_0$  and  $L_{\text{QCD}}$  will have FS.

Isospin symmetry leads to many relations of masses, cross sections, polarizations and decay branching ratios. Flavor symmetry features even more such relations. Examples will be discussed in the next section.

Exotica, such as hybrids, meson–baryon bound states, pentaquarks, glueballs and so forth are defined as resonances that do not obey flavor symmetry. Furthermore, they can be searched for by measuring various of flavor–symmetry relations.

## 4 Applications of Flavor Symmetry

The minimum content of any baryon is three quarks. FS implies that there are 27 different three-flavor combinations grouped in four  $SU(3)$  multiplets:

$$3 \otimes 3 \otimes 3 = 1_a + 8_m + 8_m + 10_s. \quad (4)$$

Every baryon belongs to a large family that consists of one singlet that is antisymmetric under flavor interchange, two octets with mixed symmetries and one fully symmetric decuplet.

FS implies that there must be a  $\Lambda^*$  octet state,  $\Lambda_8^*$ , with the same spin/parity for every  $N^*$  (since all  $N^*$  are octet members). The mass of the  $\Lambda_8^*$  is heavier than the  $J^P$ -corresponding  $N^*$  by the mass difference between the  $d$  and  $s$  constituent quarks. For every  $\Lambda_8^*$  there should be a singlet  $\Lambda_1^*$ . There is an important exception here: when the *color* part of the  $\Lambda$  statefunction is fully antisymmetric than Fermi statistics forbid the existence of a particle with an antisymmetric *flavor* statefunction. Thus FS predicts *absence* of a  $\Lambda_{\frac{1}{2}}^{1+}$  singlet, ground state particle.

For the  $d - s$  quark mass difference we will use the following

$$m(s) - m(d) = 1/3[m(\Omega) - m(\Delta)] = 147 \text{ MeV}. \quad (5)$$

Shown in Table 3 are the properties of 14 established  $N^*$  (three- and four-star) states. They have been arranged in order of increasing mass. The first column gives the name of each resonance as listed in RPP [4]. Followed are  $SU(3)$  classification and the experimentally determined  $J^P$ . In the right side part we have listed the  $\Lambda^*$  states (three- and four-star only) by name and the measured  $SU(3)$  classification and  $J^P$ . The next two columns show the prediction of the  $\Lambda^*$  mass as the sum of the mass of the matching  $N^*$  state and the quark mass correction,  $M_{predicted}(\Lambda^*) = M_{measured}(N^*) + 147 \text{ MeV}$ , followed by the measured  $\Lambda^*$  mass. The good agreement between all predictions based on FS and experiment is stunning.

There are four unseen  $\Lambda^*$  states they could be named the FS based “missing”  $\Lambda^*$  resonances. There are no unmatched  $\Lambda^*$ 's, so no unseen  $N^*$ 's. This does not mean that there could not be missing  $N^*$ 's at higher mass.

FS relates all  $SU(3)$  connected processes. For instance, FS predicts that at the appropriate beam momenta we must have

$$d\sigma(\pi^- p \rightarrow \eta n) = \Phi_1 d\sigma(K^- p \rightarrow \eta \Lambda), \quad (6)$$

where  $\Phi_1$  is a numerical factor that combines the Clebsch-Gordan factor and a correction factor for the different kinematics of the two processes. Relation 6 is very well fulfilled [7].

Table 3: Application of flavor symmetry to  $N^*$  and  $\Lambda^*$ 

$N^*$			$\Lambda^*$				
name	SU(3)	$J^P$	name	SU(3)	$J^P$	mass, (MeV/ $c^2$ )	
						predicted	measured
$n$	8	$\frac{1}{2}^+$	$\Lambda(1116)$	8	$\frac{1}{2}^+$	1086	$1115 \pm 1$
$N(1440)$	8	$\frac{1}{2}^+$	$\Lambda(1600)$	8	$\frac{1}{2}^+$	1587	$1600 \pm 40$
$N(1520)$	8	$\frac{3}{2}^-$	$\Lambda(1690)$	8	$\frac{3}{2}^-$	1667	$1690 \pm 10$
$N(1535)$	8	$\frac{1}{2}^-$	$\Lambda(1670)$	8	$\frac{1}{2}^-$	1682	$1670 \pm 10$
$N(1650)$	8	$\frac{1}{2}^-$	$\Lambda(1800)$	8	$\frac{1}{2}^-$	1797	$1800 \pm 50$
$N(1675)$	8	$\frac{5}{2}^-$	$\Lambda(1830)$	8	$\frac{5}{2}^-$	1822	$1830 \pm 10$
$N(1680)$	8	$\frac{5}{2}^+$	$\Lambda(1820)$	8	$\frac{5}{2}^+$	1817	$1820 \pm 5$
$N(1700)$	8	$\frac{3}{2}^-$	missing	8	$\frac{3}{2}^-$	1847	missing
$N(1710)$	8	$\frac{1}{2}^+$	$\Lambda(1810)$	8	$\frac{1}{2}^+$	1857	$1810 \pm 40$
$N(1720)$	8	$\frac{3}{2}^+$	$\Lambda(1890)$	8	$\frac{3}{2}^+$	1867	$1890 \pm 20$
$N(2190)$	8	$\frac{7}{2}^-$	missing	8	$\frac{7}{2}^-$	2337	missing
$N(2220)$	8	$\frac{9}{2}^+$	$\Lambda(2350)$	8	$\frac{9}{2}^+$	2367	$2350 \pm 15$
$N(2250)$	8	$\frac{9}{2}^-$	missing	8	$\frac{9}{2}^-$	2397	missing
$N(2600)$	8	$\frac{11}{2}^-$	missing	8	$\frac{11}{2}^-$	2747	missing
			$\Lambda(1405)$	1	$\frac{1}{2}^-$	no predic.	$1406 \pm 4$
			$\Lambda(1520)$	1	$\frac{3}{2}^-$	no predic.	$1519.5 \pm 1.0$
			$\Lambda(2100)$	1	$\frac{7}{2}^-$	no predic.	$2100 \pm 10$

Table 4: Application of flavor symmetry to  $\Lambda^*$  and  $\Lambda_c^*$ . Note that  $\Lambda_c(2765)^+$  can be in fact  $\Sigma_c(2765)$ ,  $\Lambda_c(2880)^+$  also can be a  $\Sigma_c^*$  state [4].

$\Lambda^*$			$\Lambda_c^*$				
name	SU(3)	$J^P$	name	SU(3)	$J^P$	mass, (MeV/ $c^2$ )	
						predicted	measured
$\Lambda(1116)$	8	$\frac{1}{2}^+$	$\Lambda_c^+$	?	$\frac{1}{2}^+$	input	$2284.46 \pm 0.14$
$\Lambda(1405)$	1	$\frac{1}{2}^-$	$\Lambda_c(2593)^+$	?	$\frac{1}{2}^-$	2575	$2595.4 \pm 0.6$
$\Lambda(1520)$	1	$\frac{3}{2}^-$	$\Lambda_c(2625)^+$	?	$\frac{3}{2}^-$	2690	$2628.1 \pm 0.6$
$\Lambda(1600)$	8	$\frac{1}{2}^+$	$\Lambda_c(2765)^+$	?	$\frac{1}{2}^+$	2770	$2766.6 \pm 2.4$
$\Lambda(1690)$	8	$\frac{3}{2}^-$	$\Lambda_c(2880)^+$	?	$\frac{3}{2}^-$	2840	$2882.5 \pm 2.2$
$\Lambda(1670)$	8	$\frac{1}{2}^-$	missing	?	$\frac{1}{2}^-$	2860	missing

One of the remarkable predictions of FS is the relation

$$d^5\sigma(\pi^-p \rightarrow \pi^0\pi^0n) = \Phi_2 d^5\sigma(K^-p \rightarrow \pi^0\pi^0\Lambda) \neq \Phi_3 d^5\sigma(K^-p \rightarrow \pi^0\pi^0\Sigma). \quad (7)$$

This has been verified as well [8–10].

Among the static relations following from FS are the Gell–Mann and Gell–Mann–Okuba mass relations.

## 5 Flavor Symmetry and the Spin/Parity of Charmed Baryons

Buoyed by the success of FS shown in Table 3 we like to make a straight forward application of FS to charmed baryons. FS implies that for every  $\Lambda$ -hyperon there should exist a charmed  $\Lambda$  called  $\Lambda_c^+$  with the same spin parity and  $SU(3)$  classification, but more massive due to the large charm–strange quark mass difference. Taking  $m_c - m_s$  to be the mass difference of the ground states,  $\Lambda_c(2285)^+ - \Lambda(1116)^0 = 1169$  MeV, the predicted masses of the known  $\Lambda_c^+$  states are listed in column seven of Table 4. The measured  $\Lambda_c^+$  masses are given in the last column of Table 4. Included are  $\Lambda_c(2266)^+$  and  $\Lambda_c(2882)^+$  whose isospin have not yet been determined. The agreement is excellent. Apparently, the huge mass correction resulting from the 1169 MeV mass difference of the  $c$  and  $s$  quarks has little effect on the dynamics, which is driven by the  $L_0$  component of  $L_{\text{QCD}}$ . Table 4 can be used to justify assigning the spin/parity of the  $\Lambda_c^*$  states to those of the corresponding  $\Lambda^*$  states. This practice is employed by the Review of Particle Properties [4]. Note in Table 4 that the  $\Lambda_c(2595)^+$  and  $\Lambda_c(2628)^+$  are  $SU(3)$  singlet states.

This is easier to verify than the spin/parity of the  $\Lambda_c^*$  states. That task still needs to be done by a direct spin/parity determination.

Applying a similar treatment to other charmed hyperons, the  $\Sigma_c^*$ ,  $\Xi_c^*$  and  $\Omega_c^*$ , has several pitfalls such as the fact that the  $\Xi$  and  $\Omega$  have more than one  $s$  quark, only one of which is changed to a  $c$  quark when making a  $\Xi_c$  or  $\Omega_c$ . Thus the  $\Xi_c$  and  $\Omega_c$  spectra do not have a one to one correspondence to those of the  $\Xi$  and  $\Omega$ .

## 6 The Structure of the Nucleon

When Otto Stern measured the magnetic dipole moment of the proton to be +2.79 Bohr magnetons back in 1932 it implied that the proton is not a point-like particle that obeys the Dirac equation as many famous theorists were hoping. Instead the proton is a particle that has a physical size and structure. After 75 years the structure is still not known and probing it is high on the priority list of nuclear physics. There are two points of view:

(a) The high energy perspective in which a proton consists of partons, which are a mixture of three colored “valence” quarks and many colored gluons, which can turn into a quark–antiquark pair. The probes are high energy polarized muons, electrons, neutrinos and polarized protons. The ease in which energy can turn into  $(q\bar{q})$ ’s has brought P.A.M. Dirac to question the meaning of an elementary particle in this case in the following quote: “The notion of an elementary particle has become more vague. One may at any time create a particle and an antiparticle, ..., and you can no longer say that they were present in the original matter. You can no longer describe in any simple way what are the ultimate constituents of matter” [11]. Note that lepton probes have no strong interactions, they are colorless. Lepton scattering is thus not sensitive to correlations of color.

(b) The spectroscopist’s view: all baryons consist of three valence quarks that have “absorbed” the gluon degrees of freedom. Mesons are simple quark–antiquark pairs of color–anticolor.

## 7 Epilogue

As evidenced by the record-breaking large number of registered participants (351) MENU 2007 has been a roaring success. The singularly large participation is an obvious testimony to the great interest of the physics community in non-perturbative QCD and in particular in baryon spectroscopy. But the main reason for the success lies in the effective and creative organization by

the Organizing Committee. It was expertly run under the guidance of the two co-chairmen Sigi Krewald and Hartmut Machner together with Conference Secretary Su Schadmand who dedicated great efforts to the well-being and happiness of all participants. Thanks on behalf of the participants for all the work of the entire Organizing Committee and the efforts of dedicated secretaries.

MENU 2007 will go in history and be remembered for its excellent physics, stimulating presentations, happy reunion with old friends and colleagues, in other words for being a very successful conference.

## 8 Appendix: Specifics of the QCD Lagrangian

$$L_{QCD} = L_0 + L_m \quad (8)$$

$$L_0 = -\frac{1}{4}F_{\mu\nu}^{(a)} \cdot F^{(a)\mu\nu} + i \sum_q \bar{\psi}_q^i \gamma^\mu (D_\mu)_{ij} \psi_q^j \quad (9)$$

$$L_m = - \sum_q \bar{\psi}_i m_q \psi_{qi} \quad (10)$$

$$F_{\mu\nu}^{(a)} = \partial_\mu A_\nu^a - \partial_\nu A_\mu^a - g_s f_{abc} A_\mu^b A_\nu^c \quad (11)$$

$$(D_\mu)_{ij} = \delta_{ij} \partial_\mu + i g_s \sum_a \frac{\lambda_{i,j}^a}{2} A_\mu^a \quad (12)$$

$f_{abc}$  are the SU(3) structure constants.

$A_\nu$  = gluon field

$\psi$  = quark field

$g_s$  = strong coupling constant

Note that  $L_0$  depends only on the quark and gluon fields. It is the same for all massless quarks. This is the famous flavor symmetry of QCD. This symmetry is broken by  $L_m$  which depends only on the quark field and the quark mass.

## References

- [1] A. Matsuyama, T. Sato and T.-S.H. Lee, Phys. Rept. 439 (2007) 193.

- [2] G. Höhler and A. Schulte,  $\pi N$  Newsletter Rept. No. 7 (1992) 94.
- [3] E.P. Wigner, Phys. Rev. **98** (1955) 145.
- [4] W-M Yoa *et al.*, J. Phys. G **33** (2006) 1.
- [5] M. Roos. *et al.*, Phys. Lett. 111B (1982) 1.
- [6] V. Ziegler, presentation at this conference.
- [7] A. Starostin *et al.* Phys. Rev. C **64** (2001) 55205.
- [8] S. Prakhov *et al.* Phys. Rev. C **69** (2004) 045202.
- [9] S. Prakhov *et al.* Phys. Rev. C **69** (2004) 042202.
- [10] S. Prakhov *et al.* Phys. Rev. C **70** (2004) 034605.
- [11] P.A.M. Dirac, Crane Lecture, University of Michigan, April 1978.

# Invited Talks

MENU 2007  
11th International Conference  
on Meson-Nucleon Physics and  
the Structure of the Nucleon  
September 10-14, 2007  
IKP, Forschungszentrum Jülich, Germany

# PION–DEUTERON SCATTERING LENGTH IN CHIRAL PERTURBATION THEORY UP TO ORDER $\chi^{3/2}$

V. Baru<sup>\*,1</sup>, J. Haidenbauer<sup>%</sup>, C. Hanhart<sup>%</sup>, A. Kudryavtsev<sup>\*</sup>, V. Lensky<sup>\*,%</sup>  
and U.-G. Meißner<sup>%,#</sup>

<sup>\*</sup>Institute of Theoretical and Experimental Physics, 117259,  
B.Cheremushkinskaya 25, Moscow, Russia

<sup>%</sup>Institut für Kernphysik, Forschungszentrum Jülich GmbH, D–52425  
Jülich, Germany

<sup>#</sup>Helmholtz-Institut für Strahlen- und Kernphysik (Theorie), Universität  
Bonn, Nußallee 14-16, D–53115 Bonn, Germany

## Abstract

A complete calculation of the corrections to pion-deuteron scattering length up to order  $\chi^{3/2}$  with  $\chi = m_\pi/M_N$ , is performed. The calculation includes the dispersive contributions and corrections due to the explicit treatment of the  $\Delta$  resonance. s-wave pion-nucleon scattering parameters are extracted from a combined analysis of modern experimental data.

## 1 Introduction

The pion-nucleon ( $\pi N$ ) scattering lengths are fundamental quantities of low-energy hadron physics since they test the QCD symmetries and the pattern of chiral symmetry breaking. As stressed by Weinberg long time ago, chiral symmetry suppresses the isoscalar  $\pi N$  scattering length  $a^+$  substantially compared to its isovector counterpart  $a^-$ . Thus, a precise determination of  $a^+$  demands in general high accuracy experiments.

Here pion-deuteron ( $\pi d$ ) scattering near threshold plays an exceptional role for  $\text{Re}(a_{\pi d}) = 2a^+ + (\text{few-body corrections})$ . The first term  $\sim a^+$  is simply generated from the impulse approximation (scattering off the proton and off the neutron) and is independent of the deuteron structure. Thus, if one is able to calculate the few-body corrections in a controlled way,  $\pi d$

---

<sup>1</sup>E-mail address: baru@itep.ru

scattering is a prime reaction to extract  $a^+$  (most effectively in combination with pionic hydrogen measurements).

A method how to calculate processes on few nucleon systems with external probes was proposed by Weinberg in one of his classical papers [1]. As a first step the perturbative transition operators need to be calculated using the rules of ChPT. Then those transition operators must be convoluted with the appropriate  $NN$  wave functions. This scheme was already applied to a large number of reactions like  $\pi d \rightarrow \pi d$  [2],  $\gamma d \rightarrow \pi^0 d$  [3, 4],  $\pi^3\text{He} \rightarrow \pi^3\text{He}$  [5],  $\pi^- d \rightarrow \gamma nn$  [6], and  $\gamma d \rightarrow \pi^+ nn$  [7], where only the most recent references are given. The standard expansion parameter  $\chi = m_\pi/M_N$ , where  $m_\pi$  ( $M_N$ ) is the pion (nucleon) mass, was used in most of these references.

It was also Weinberg who calculated the leading order few body corrections to the  $\pi d$  system, the most important of which – the diagram when pion rescatters on two nucleons with the Weinberg-Tomozawa (WT) vertices – is almost as large as the experimental value for the  $\pi d$  scattering length. The diagrams at leading order were calculated in the fixed center kinematics, i.e. with static nucleons. An accounting for the nucleon recoils leads to potentially sizable corrections of order of  $\chi^{1/2}$  in the standard Weinberg counting. The non-analyticity of this correction is related to the few-body singularities that are employed in some pion-few-nucleon diagrams as demonstrated in Refs. [7, 8]. It was the main result of Ref. [8] that the importance of the resulting effect of all recoil terms is directly connected to the Pauli principle for the nucleons in the intermediate state. In particular, if the s-wave NN-state is not allowed by quantum numbers, which is fulfilled in the  $\pi d$  process, the net effect of the recoil correction is to be small due to a cancellation of individually large terms. At next-to-leading (NLO) order there are basically the same diagrams as at LO but with subleading vertices. The calculation performed in Ref. [2] showed that the sum of diagrams contributing at NLO vanishes. Furthermore, the solution for  $\{a^+, a^-\}$  was found in Ref. [2] from a common intersection of three bands corresponding to the shift and width of pionic hydrogen atom [9] and to the shift of pionic deuterium [10]. Due to a cancellation of terms at orders  $\chi^{1/2}$  and  $\chi$  the results for  $\{a^+, a^-\}$  extracted in ChPT [2] turned out to be quite similar to the phenomenological calculations [11, 12]. However, the recent measurement of the width of  $\pi^- p$  atom with much better accuracy [13] seriously changes the picture. The problem is that an intersection region of the three bands and thus a unique solution for  $\{a^+, a^-\}$  does not exist anymore. This finding means that something important is missing in our understanding of the  $\pi d$  system. This could be isospin symmetry breaking (ISB) effects that were recently found in Ref. [14] to give a huge effect to the  $\pi d$  scattering although with large uncertainty. Another possibility is that higher order effects to the transition operators

could be important. In this presentation we discuss both possibilities. The influence of ISB effects on the extraction of the s-wave  $\pi N$  scattering lengths is considered in sec. 2. In sec. 3 and 4 we discuss corrections to the  $\pi d$  scattering length emerging at order  $N^{3/2}\text{LO}$  ( $\chi^{3/2}$ ). At this order two new classes of diagrams start to contribute. One of them, the so-called dispersive correction due to the process  $\pi d \rightarrow NN \rightarrow \pi d$  is the subject of sec. 3. In sec. 4 we discuss the effect of the  $\Delta$  isobar as explicit degree of freedom. The main results are summarized in sec. 5.

## 2 ISB effects and s-wave $\pi N$ scattering lengths

Since the leading one-body contribution ( $\sim a^+$ ) to the  $\pi d$  scattering length is chirally suppressed the role of ISB effects in this process becomes significant. For the  $\pi^- d$  system so far only leading ISB corrections were evaluated [14]. They were found to give a very large effect of order of 40% to the  $\pi^- d$  scattering length. In this section we would like to investigate the influence of this correction on the combined analysis of experimental data and thus on the s-wave  $\pi N$  scattering lengths. To account for the ISB correction at leading order we should replace  $2a^+$  by  $a_{\pi^- p} + a_{\pi^- n}$  in the expression for  $a_{\pi d}$ , which agrees to the former only, if isospin were an exact symmetry. The expressions for the  $\pi N$  amplitudes with inclusion of ISB effects were derived in Ref. [14]:

$$\begin{aligned} a_{\pi^- p} &= a^+ + a^- + \frac{1}{4\pi(1+\chi)} \left( \frac{4(m_\pi^2 - m_{\pi^0}^2)}{F_\pi^2} c_1 - \frac{e^2}{2} (4f_1 + f_2) \right), \\ a_{\pi^- n} &= a^+ - a^- + \frac{1}{4\pi(1+\chi)} \left( \frac{4(m_\pi^2 - m_{\pi^0}^2)}{F_\pi^2} c_1 - \frac{e^2}{2} (4f_1 - f_2) \right). \end{aligned} \quad (1)$$

Here  $m_\pi(m_{\pi^0})$  is the charged (neutral) pion mass,  $F_\pi = 92.4$  MeV and  $c_1$  and  $f_1, f_2$  correspond to the strong and electromagnetic LECs. Whereas  $f_2$  and  $c_1$  are known more or less well ( $f_2 = -(0.97 \pm 0.38)$  GeV $^{-1}$  [15] and  $c_1 = -0.9_{-0.5}^{+0.2}$  GeV $^{-1}$  [16]) the value for  $f_1$  ( $|f_1| \leq 1.4$  GeV $^{-1}$ ) is very uncertain – a naive dimensional analysis was used in Ref. [14] to fix the latter. At the same time it is  $f_1$  and  $c_1$  that give the largest contribution to the ISB correction for  $\pi d$  scattering thus introducing a large uncertainty in the extraction of  $\{a^+, a^-\}$  from the data. At this stage we would like to note that the parameters  $a^+, c_1$  and  $f_1$  enter the expressions for  $a_{\pi^- p}$  and  $a_{\pi^- n}$  in the same linear combination (see Eq. (1)). Note that the expression for the charge exchange amplitude  $\pi^- p \rightarrow \pi^0 n$  does not depend on the LECs  $c_1$  and

$f_1$  at all. Therefore let us introduce the quantity  $\tilde{a}^+$  which is defined as

$$\tilde{a}^+ = a^+ + \frac{1}{4\pi(1+\chi)} \left( \frac{4(m_\pi^2 - m_{\pi^0}^2)}{F_\pi^2} c_1 - 2e^2 f_1 \right). \quad (2)$$

The leading isospin breaking terms that are also the main source of the uncertainty<sup>2</sup> are contained now in  $\tilde{a}^+$ . Using this the expressions for  $a_{\pi^-p}$ ,  $a_{\pi^-n}$  and  $\text{Re } a_{\pi d}$  take the form

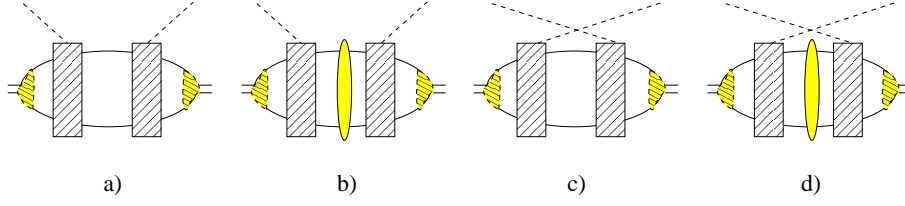
$$\begin{aligned} a_{\pi^-p} &= \tilde{a}^+ + a^- - \frac{1}{4\pi(1+\chi)} \frac{e^2}{2} f_2, \\ a_{\pi^-n} &= \tilde{a}^+ - a^- + \frac{1}{4\pi(1+\chi)} \frac{e^2}{2} f_2, \\ \text{Re } a_{\pi d} &= 2\tilde{a}^+ + \langle \text{few-body corrections } (a^-) \rangle, \end{aligned} \quad (3)$$

Thus, we get a system of three equations for  $a_{\pi^-p}$ ,  $\text{Re } a_{\pi d}$  and  $a_{\pi^-p \rightarrow \pi^0 n}$  (the explicit expression for the latter is given in Ref. [14]) to determine  $\tilde{a}^+$  and  $a^-$ . Once this determination is performed and provided that new and less uncertain information about the LECs  $c_1$  and  $f_1$  is available from elsewhere, one will be able to extract  $a^+$  directly without doing the analysis of pionic data once again. Let us discuss Eq. (3) in more detail. Note that the equations for the hydrogen and deuterium shifts ( $a_{\pi^-p}$  and  $\text{Re } a_{\pi d}$  respectively) written in terms of  $\tilde{a}^+$  and  $a^-$  and including ISB effects at leading order are very close to those obtained in the isospin symmetric case in Ref. [2] in terms of  $a^+$  and  $a^-$ . The difference basically consists in the term proportional to  $f_2$  for the pionic hydrogen shift that gives a relatively small effect. Thus the main modification due to the inclusion of ISB effects at leading order consists in the replacement of  $a^+$  by  $\tilde{a}^+$ . At the same time we know that for the isospin symmetric case there is no unique solution for  $\{a^+, a^-\}$  if the new data for the hydrogen width are utilized. Thus we conclude that the system of equations for  $\{\tilde{a}^+, a^-\}$  does not have a unique solution either at least as long as the few body corrections of Ref. [2] are used. In the following sections we present the recent progress in this sector.

### 3 Dispersive corrections

Experimental measurement of the  $\pi d$  scattering length shows that its imaginary part is relatively large, about 1/4 of its real part [10]. The imaginary

<sup>2</sup>The idea of using some linear combinations of observables to reduce the uncertainty was suggested in Refs [14, 17]. In particular the combination  $2a_{\pi^-p} - a_{\pi^-d}$  that depends solely on  $a^-$  was considered in Ref. [17].

Figure 1: Dispersive corrections to the  $\pi d$  scattering length.

part can be expressed in terms of the  $\pi d$  total cross section through the optical theorem. One gets

$$4\pi\text{Im}(a_{\pi d}) = \lim_{q \rightarrow 0} q \{ \sigma(\pi d \rightarrow NN) + \sigma(\pi d \rightarrow \gamma NN) \} , \quad (4)$$

where  $q$  denotes the relative momentum of the initial  $\pi d$  pair. The ratio  $R = \lim_{q \rightarrow 0} (\sigma(\pi d \rightarrow NN)/\sigma(\pi d \rightarrow \gamma NN))$  was measured to be  $2.83 \pm 0.04$  [18]. At low energies diagrams that lead to a sizable imaginary part of some amplitude are expected to contribute also significantly to its real part. Those contributions are called dispersive corrections. As a first estimate Brückner speculated that the real and imaginary part of these contributions should be of the same order of magnitude [19]. This expectation was confirmed within Faddeev calculations in Refs. [20]. Here we present the first consistent ChPT calculation of the dispersive corrections that emerge from the hadronic  $\pi d \rightarrow NN \rightarrow \pi d$  and photonic  $\pi d \rightarrow \gamma NN \rightarrow \pi d$  processes [21]. We define dispersive corrections as contributions from diagrams with an intermediate state that contains only nucleons, photons and at most real pions. Therefore, all the diagrams shown in Fig. 1 are included in our work. All these diagrams contribute at order  $\chi^{3/2}$  as compared to the leading double scattering diagram (see Ref. [21] for details). The hatched blocks in the diagrams of Fig. 1 refer to the relevant transition operators for the reaction  $NN \rightarrow NN\pi$  that consist of the direct and rescattering mechanisms. Note that the latter is to be calculated with the on-shell  $\pi N \rightarrow \pi N$  vertices ( $2m_\pi$ ) as was derived in Ref. [22]. Using the CCF potential [23] for the  $NN$  distortions we found for the dispersive correction from the purely hadronic transition

$$\delta a_{\pi d}^{disp} = (-6.5 + 1.3 + 2.4 - 0.2) \times 10^{-3} m_\pi^{-1} = -3.0 \times 10^{-3} m_\pi^{-1} , \quad (5)$$

where the numbers in the first bracket are the individual results for the diagrams shown in Fig. 1, in order. Note that the diagrams with intermediate  $NN$  interactions and the crossed ones (diagram (c) and (d)), neither of them were included in most of the previous calculations, give significant

contributions. When repeating the calculation with the four different phenomenological  $NN$  potentials CD Bonn [24], Paris [25], AV18 [26] we find

$$\delta a_{\pi d}^{\text{disp}} = (-2.9 \pm 1.4) \times 10^{-3} m_{\pi}^{-1}, \quad (6)$$

where the first number is the mean value for the various potentials and the second number reflects the theoretical uncertainty of this calculation estimated conservatively — see Ref. [21] for details. Note that the same calculation gave very nice agreement for the corresponding imaginary part [21].

In Ref. [21] also the electromagnetic contribution to the dispersive correction was calculated. It turned out that the contribution to the real part was tiny —  $-0.1 \times 10^{-3} m_{\pi}^{-1}$  — while the sizable experimental value for the imaginary part was described well.

## 4 Role of the Delta resonance

From phenomenological studies it is well known that the delta isobar  $\Delta(1232)$  plays a very special role in low energy nuclear dynamics [27] as a consequence of the relatively large  $\pi N \Delta$  coupling and the quite small delta–nucleon mass difference  $\Delta = M_{\Delta} - M_N \simeq 2m_{\pi}$ , where  $M_{\Delta}$  denotes the mass of the delta. In the present section we investigate the role of the  $\Delta$  isobar in the reaction  $\pi d \rightarrow \pi d$  at threshold in EFT. In the delta-less theory the effect of the  $\Delta$  resonance is hidden in the LEC  $c_2$  which is the leading term in the so-called boost correction to the  $\pi d$  scattering length [2]. This correction is known to be quite sizable ( $\sim 10\text{-}20\%$  of  $a_{\pi d}$ ) although very model dependent. The pertinent one–body operator scales with the square of the nucleon momentum and therefore the corresponding expectation value is proportional to the nucleon kinetic energy inside the deuteron — this quantity is strongly model-dependent [28]. However, the value of  $c_2$  is reduced by a large factor once the delta contribution is taken out [29, 30] so that the residual boost correction becomes negligible [31].

The reason why the explicit inclusion of the delta in pionic reactions on the two–nucleon system is beneficial is that the dynamical treatment of the  $\Delta$  allows to improve the convergence of the transition operators. Let us, for example, focus on the one–body terms with the delta (see, e.g., second diagram in Fig. 2). Then the corresponding  $\pi N \rightarrow \pi N$  transition potential is proportional to  $p^2/(m_{\pi} - \Delta - \mathbf{p}^2/M_N)$ . For static deltas, the nucleon–delta propagator reduces to  $1/(m_{\pi} - \Delta)$ . Thus, in the latter case the transition operator behaves like  $\mathbf{p}^2$ , whereas in the former it approaches a constant for momenta larger than  $|\mathbf{p}_{\Delta}| \sim \sqrt{(\Delta - m_{\pi})M_N} \sim 2.7m_{\pi}$  with the effect that the static amplitude is much more sensitive to the short range part of the

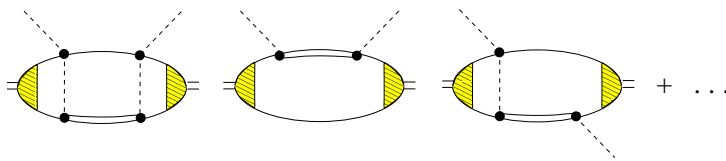


Figure 2: Diagrams with the  $\Delta$  resonance at order  $\chi^{3/2}$ . Crossed terms are not shown explicitly but included in the calculation (see Ref. [31]).

deuteron wave function and must be balanced by appropriate counter terms. The value of  $p_\Delta$  is numerically very close to  $p_{\text{thr}} = \sqrt{M_N m_\pi} \sim 2.6 m_\pi$  — the minimum initial momentum for the reaction  $NN \rightarrow NN\pi$  (for a recent review of this class of reactions see Ref. [32]). This automatically puts the delta contributions in the same order as the dispersive corrections [31]. In Fig. 2 we show diagrams with the  $\Delta$  isobar that contribute at order  $\chi^{3/2}$ . Diagrams with crossed external pions are not shown explicitly but are taken into account in the calculation. The resulting correction is [31]

$$\delta a_{\pi d}^\Delta = (2.38 \pm 0.40) \times 10^{-3} m_\pi^{-1}, \quad (7)$$

where the central value is the arithmetic average of the results for the seven different potentials and the uncertainty reflects the variations in the results. Note that we used phenomenological  $NN$  models without [24–26] and with [23] explicit delta degree of freedom, as well as three variants of  $NN$  wave functions derived within EFT [33]. These numbers were obtained with the  $\pi N\Delta$  coupling constant  $h_A = 2.77$ . In contrast to earlier treatments of the boost correction, the results we found with the explicit treatment of the  $\Delta$  depend only very weakly on the  $NN$  model used. In Ref. [31] also a detailed comparison to previous phenomenological works is given.

## 5 Results and Conclusions

We performed a complete calculation of the isospin-conserving corrections to the pion-deuteron scattering length up to order  $\chi^{3/2}$ . The calculation includes the dispersive contributions and corrections due to the dynamical treatment of the  $\Delta$  resonance. Although these corrections are quite significant individually the net effect of the diagrams that contribute at order  $\chi^{3/2}$  is very small:

$$\delta a_{\pi d}^\Delta + \delta a_{\pi d}^{\text{disp}} = (-0.6 \pm 1.5) \times 10^{-3} m_\pi^{-1}. \quad (8)$$

However, an important consequence of our investigations is that once the  $\Delta$  is treated dynamically, as it is done here, the so-called boost corrections contribute insignificantly to the  $\pi d$  scattering length.

Also we analyzed the role of ISB effects at leading order in the combined analysis of pionic data. It was observed that the LEC  $f_1$ , that is known very poorly, appears in the expressions for  $a_{\pi^-p}$  and  $a_{\pi^-n}$  in the same linear combination with  $a^+$  and the LEC  $c_1$ . We called it  $\tilde{a}^+$ . Thus, the inclusion of ISB effects at leading order consists basically in the replacement of  $a^+$  by  $\tilde{a}^+$  in the combined analysis of pionic data. This drastically reduces the uncertainty of the analysis that originates mainly from our ignorance regarding  $f_1$ . The solution for the s-wave  $\pi N$  parameters  $\{\tilde{a}^+, a^-\}$  is shown in Fig. 3. The black band stems from the analysis of the pionic hydrogen shift [13]. The blue vertical band corresponds to the new preliminary data for the pionic hydrogen width [34]. The red solid and dashed bands correspond to the pion deuteron scattering length calculated with and without corrections at order  $\chi^{3/2}$ . Also the boost correction was not included in the full calculation corresponding to the solid red band as a consequence of the explicit treatment of the  $\Delta$  resonance. It is basically the latter effect that improves the situation resulting in some intersection region for all three bands. However, it still remains to be seen if the corrections at NLO of the isospin violation do not distort this picture. Corrections at this order for the  $\pi^-p$  system were evaluated in Refs. [15,35] and turned out to be quite sizable, especially those that come from the pion mass difference. In order to push also the calculation for the  $\pi d$  system to a similar level of accuracy in isospin violation, the  $\pi^-n$  scattering amplitude as well as some virtual photon exchanges in the  $\pi^-d$  system are still to be calculated.

## Acknowledgments

This research is part of the EU Integrated Infrastructure Initiative Hadron Physics Project under contract number RII3-CT-2004-506078, and was supported also by the DFG-RFBR grant no. 05-02-04012 (436 RUS 113/820/0-1(R)) and the DFG SFB/TR 16 "Subnuclear Structure of Matter". V. B and A. K. acknowledge the support of the Federal Agency of Atomic Research of the Russian Federation.

## References

- [1] S. Weinberg, Phys. Lett. B **295**, 114 (1992).
- [2] S. R. Beane, V. Bernard, E. Epelbaum, U.-G. Meißner and D. R. Phillips, Nucl. Phys. A **720**, 399 (2003) [arXiv:hep-ph/0206219].

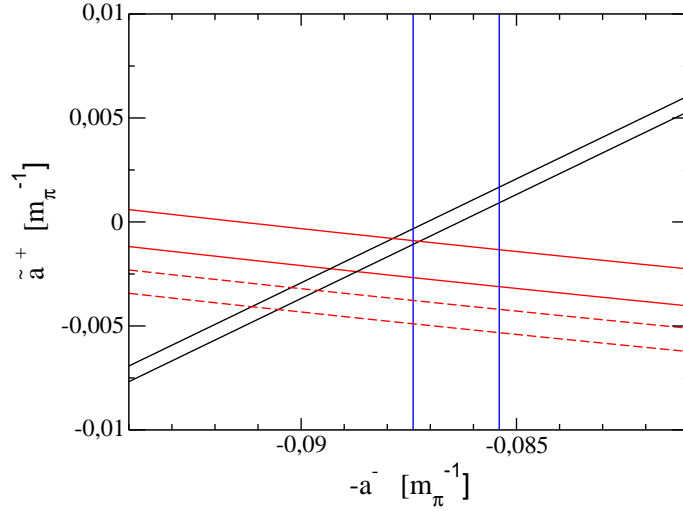


Figure 3: The solution for  $\{\tilde{a}^+, a^-\}$  from the combined analysis of experimental data. See text for details.

- [3] S. R. Beane, V. Bernard, T. S. H. Lee, U.-G. Meißner and U. van Kolck, Nucl. Phys. A **618**, 381 (1997) [arXiv:hep-ph/9702226].
- [4] H. Krebs, V. Bernard and U.-G. Meißner, Eur. Phys. J. A **22**, 503 (2004) [arXiv:nucl-th/0405006].
- [5] V. Baru, J. Haidenbauer, C. Hanhart and J. A. Niskanen, Eur. Phys. J. A **16**, 437 (2003) [arXiv:nucl-th/0207040].
- [6] A. Gårdestig and D. R. Phillips, Phys. Rev. C **73** 014002 (2006); Phys. Rev. Lett. **96**, 232301 (2006), [arXiv:nucl-th/0603045].
- [7] V. Lensky, V. Baru, J. Haidenbauer, C. Hanhart, A. E. Kudryavtsev and U.-G. Meißner, Eur. Phys. J. A **26**, 107 (2005) [arXiv:nucl-th/0505039].
- [8] V. Baru, C. Hanhart, A. E. Kudryavtsev and U.-G. Meißner, Phys. Lett. B **589**, 118 (2004) [arXiv:nucl-th/0402027].
- [9] H. C. Schröder *et al.*, Eur. Phys. J. C **21**, 473 (2001).
- [10] P. Hauser *et al.*, Phys. Rev. C **58**, 1869 (1998).
- [11] V. Baru, A. Kudryavtsev, Phys. Atom. Nucl., **60**, 1476 (1997).
- [12] T. E. O. Ericson, B. Loiseau, A. W. Thomas, Phys. Rev. C **66**, 014005 (2002) [arXiv:hep-ph/0009312].

- [13] D. Gotta, *Int. J. Mod. Phys. A* **20**, 349 (2005).
- [14] U.-G. Meißner, U. Raha and A. Rusetsky, *Phys. Lett. B* **639**, 478 (2006) [arXiv:nucl-th/0512035].
- [15] J. Gasser, M. A. Ivanov, E. Lipartia, M. Mojzis and A. Rusetsky, *Eur. Phys. J. C* **26**, 13 (2002) [arXiv:hep-ph/0206068].
- [16] U.-G. Meißner, *PoS LAT2005*, 009 (2006) [arXiv:hep-lat/0509029].
- [17] A. Rusetsky, Talk given at the International Workshop on Exotic Hadronic Atoms, Deeply Bound Kaonic Nuclear States and Antihydrogen, Trento, Italy, 19-24 Jun 2006; [arXiv: hep-ph/0610201]
- [18] V. C. Highland et al., *Nucl. Phys. A* **365**, 333 (1981).
- [19] K. Brückner, *Phys. Rev.* **98**, 769 (1955).
- [20] I.R. Afnan and A.W. Thomas, *Phys. Rev. C* **10**, 109 (1974); D.S. Koltun and T. Mizutani, *Ann. Phys. (N.Y.)* **109**, 1 (1978).
- [21] V. Lensky, V. Baru, J. Haidenbauer, C. Hanhart, A. E. Kudryavtsev and U.-G. Meißner, *Phys. Lett. B* **648**, 46 (2007) [arXiv:nucl-th/0608042].
- [22] V. Lensky, V. Baru, J. Haidenbauer, C. Hanhart, A. E. Kudryavtsev and U.-G. Meißner, *Eur. Phys. J. A* **27**, 37 (2006) [arXiv:nucl-th/0511054].
- [23] J. Haidenbauer, K. Holinde, M.B.Johnson, *Phys. Rev. C* **48**, 2190 (1993).
- [24] R. Machleidt, *Phys. Rev. C* **63**, 024001 (2001) [arXiv:nucl-th/0006014].
- [25] M. Lacombe et al., *Phys. Rev. C* **21**, 861 (1980).
- [26] R. B. Wiringa, V. G. J. Stoks and R. Schiavilla, *Phys. Rev. C* **51**, 38 (1995) [arXiv:nucl-th/9408016].
- [27] T. Ericson und W. Weise, *Pions and Nuclei* (Clarendon Press, Oxford, 1988).
- [28] A. Nogga and C. Hanhart, *Phys. Lett. B* **634**, 210 (2006) [arXiv:nucl-th/0511011].
- [29] V. Bernard, N. Kaiser and U.-G. Meißner, *Nucl. Phys. A* **615**, 483 (1997) [arXiv:hep-ph/9611253].

- [30] H. Krebs, E. Epelbaum and U.-G. Meißner, *Eur. Phys. J. A* **32**, 127 (2007) [arXiv:nucl-th/0703087].
- [31] V. Baru, J. Haidenbauer, C. Hanhart, A. Kudryavtsev, V. Lensky and U.-G. Meißner, arXiv:0706.4023 [nucl-th], *Phys. Lett. B*, in print.
- [32] C. Hanhart, *Phys. Rep.* **397**, 155 (2004) [arXiv:hep-ph/0311341].
- [33] E. Epelbaum, W. Glöckle and U.-G. Meißner, *Nucl. Phys. A* **747**, 362 (2005) [arXiv:nucl-th/0405048].
- [34] T. Strauch, Talk given at MENU 2007, Jülich, Germany, 10-14 Sep 2007.
- [35] N. Fettes and U.-G. Meißner, *Nucl. Phys. A* **693**, 693 (2001) [arXiv:hep-ph/0101030].

## PROGRESS IN $NN \rightarrow NN\pi$

V. Baru<sup>\*,1</sup>, J. Haidenbauer<sup>%</sup>, C. Hanhart<sup>%</sup>, A. Kudryavtsev<sup>\*</sup>, V. Lensky<sup>\*,%</sup>  
and U.-G. Meißner<sup>%,#</sup>

<sup>\*</sup>Institute of Theoretical and Experimental Physics, 117259,  
B. Chermushkinskaya 25, Moscow, Russia

<sup>%</sup>Institut für Kernphysik, Forschungszentrum Jülich GmbH, D-52425  
Jülich, Germany

<sup>#</sup>Helmholtz-Institut für Strahlen- und Kernphysik (Theorie), Universität  
Bonn, Nußallee 14-16, D-53115 Bonn, Germany

### Abstract

We survey the recent developments in the reaction  $NN \rightarrow NN\pi$  in effective field theory. We show that the proper construction of the production operator needs a careful separation of irreducible pieces from reducible ones. The result of this consideration is a complete cancellation of all loops in the production operator at NLO. Moreover, we show that this procedure brings the leading Weinberg-Tomozawa vertex on-shell, thus enhancing the corresponding contribution to the transition amplitude by a factor of 4/3 as compared to the commonly used value. We also discuss the role of the  $\Delta(1232)$  for the  $s$ -wave pion production. Being relatively sizable individually the direct and rescattering mechanisms of the  $\Delta$  excitation at NLO cancel each other to a large extent. Thus, we conclude that the net effect of the  $\Delta$  at NLO is very small.

## 1 Introduction

Understanding the dynamics of pion production in nucleon-nucleon collisions near threshold is a challenge for theoreticians. Knowledge of the pion production mechanism in the isospin symmetric case is an important step to the study of isospin violation in few-nucleon processes [1,2], which provides a test for chiral perturbation theory (ChPT). Furthermore, success in the description of the charged pion production reactions is a necessary condition for a calculation of the dispersive correction to  $\pi d$  scattering [3], which is one of the most uncertain and at the same time important corrections to this

---

<sup>1</sup>E-mail address: baru@itep.ru

process. When accurate data for the total cross-section close to threshold appeared in 1990 [4], existing models [?, 6] failed to describe the data by a factor of five to ten for the channel  $pp \rightarrow pp\pi^0$  and a factor of two for the channels  $pp \rightarrow pn\pi^+$  and  $pp \rightarrow d\pi^+$ . To cure this discrepancy, many phenomenological mechanisms were proposed — for a recent review see Ref. [7]. Also various groups started to investigate  $NN \rightarrow NN\pi$  using ChPT. As a big surprise, however, it turned out that using the original power counting proposed by Weinberg [8] leads to even larger discrepancy between data and theory at next-to-leading order (NLO) for  $pp \rightarrow pp\pi^0$  [9] as well as for  $pp \rightarrow d\pi^+$  [10]. Even worse, the corrections at one-loop order (next-to-next-to-leading order (N<sup>2</sup>LO) in the standard counting) turned out to be even larger than the tree level NLO corrections, putting into question the convergence of the chiral expansion [11, 12].

At the same time it was already realized that a modified power counting is necessary to properly take care of the large momentum transfer characteristic for pion production in  $NN$  collisions [13–16]. The expansion parameter in this case is

$$\chi = \frac{|\mathbf{p}_{\text{thr}}|}{M_N} = \sqrt{\frac{m_\pi}{M_N}} \quad (1)$$

where  $m_\pi$  ( $M_N$ ) is the pion (nucleon) mass and  $|\mathbf{p}_{\text{thr}}|$  is the initial nucleon momentum at threshold. As a consequence the hierarchy of diagrams changes and some one-loop diagrams start to contribute already at NLO. In this presentation we discuss the charged pion production where the produced pion is in an s-wave relative to the final NN pair up to NLO in ChPT. In sec. 2 we discuss the pion production operators involving only pionic and nucleonic degrees of freedom. We start from the concept of reducibility that is necessary to distinguish between the production operator, which should consist of all irreducible pieces, and the NN wave functions. The proper treatment of this concept allows to avoid double counting in the calculation and thus is extremely important. We discuss in detail the special case of diagrams with the energy dependent vertices originating from, e.g., the Weinberg-Tomozawa (WT) term. In this case some diagrams that seem to be purely reducible from the general rules acquire an important irreducible contribution. In sec. 3 we discuss the role of the Delta resonance for the s-wave pion production near threshold. The corresponding diagrams start to contribute at NLO and thus are relevant for the present study. The main results are summarized in sec. 4.

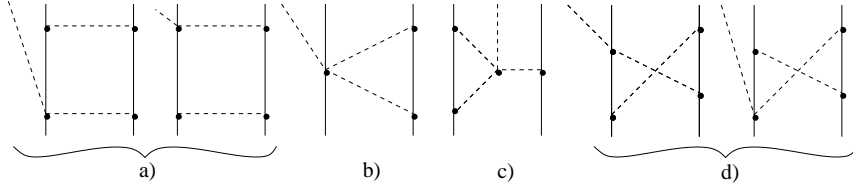


Figure 1: Leading loop diagrams for  $NN \rightarrow NN\pi$ . Here dashed lines denote pions and solid lines denote nucleons.

## 2 Nucleonic amplitudes up to NLO

A method how to calculate processes on few nucleon systems with external probes was proposed by Weinberg [8]: here the transition (production) operators are to be calculated using ChPT. Then those transition operators must be convoluted with the appropriate  $NN$  wave functions — in full analogy to the so-called distorted wave Born approximation traditionally used in phenomenological calculations [5].

Therefore it is necessary to disentangle those diagrams that are part of the wave function from those that are part of the transition operator. In complete analogy to  $NN$  scattering, the former are called reducible and the latter irreducible. The distinction stems from whether or not the diagram shows a two-nucleon cut. Thus, in accordance to this rule, the one-loop diagrams shown in Fig. 1(b)–(d) are irreducible, whereas diagrams (a) seem to be reducible. This logic was used in the paper by Hanhart and Kaiser [16] to single out the irreducible loops contributing at NLO. The findings of Ref. [16] were:

- For the channel  $pp \rightarrow pp\pi^0$  the sum of diagrams (b)–(d) of Fig. 1 vanished due to a cancellation between individual diagrams
- For the channel  $pp \rightarrow d\pi^+$  the same sum gave a finite answer<sup>2</sup>:

$$A_{pp \rightarrow d\pi^+}^{b+c+d} = \frac{g_A^3}{256 f_\pi^5} (-2 + 3 + 0) |\mathbf{q}| = \frac{g_A^3 |\mathbf{q}|}{256 f_\pi^5}. \quad (2)$$

The latter amplitude grows linearly with increasing final  $NN$ -relative momentum  $|\mathbf{q}|$ , which leads to a large sensitivity to the final  $NN$  wave function, once the convolution of those with the transition operators is evaluated. However, the problem is that such a sensitivity is not allowed in a consistent field

<sup>2</sup>The connection of the amplitude  $A$  to the observables is given, e.g., in Ref [17]

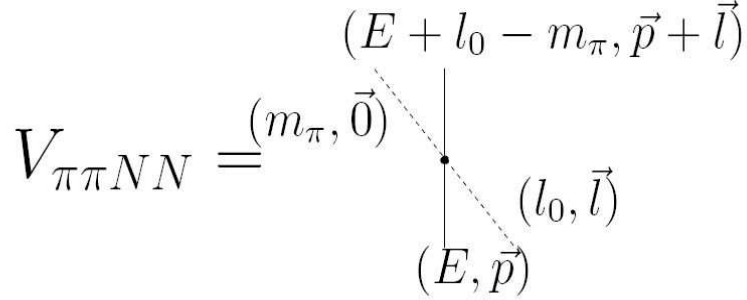


Figure 2: The  $\pi N \rightarrow \pi N$  transition vertex: definition of kinematic variables as used in the text.

theory as was stated in Ref. [18]. The solution of this problem was presented in Ref. [17] and will be discussed in this presentation.

It is the main point of this section that diagrams (a) contain a genuine irreducible piece due to the energy dependence of the leading  $\pi N \rightarrow \pi N$  vertex. Specifically, the energy dependent part of the WT vertex cancels one of the intermediate nucleon propagators, resulting in the additional irreducible contribution at NLO from diagrams (a). This additional contribution compensates the linear growth of diagrams (b)–(d) thus solving the problem. To demonstrate this, we write the expression for the  $\pi N \rightarrow \pi N$  vertex in the notation of Fig. 2 as

$$\begin{aligned}
 V_{\pi\pi NN} &= l_0 + m_\pi - \frac{\mathbf{l} \cdot (2\mathbf{p} + \mathbf{l})}{2M_N} \\
 &= \underbrace{2m_\pi}_{\text{on-shell}} + \underbrace{\left( l_0 - m_\pi + E - \frac{(\mathbf{l} + \mathbf{p})^2}{2M_N} \right)}_{(E' - H_0) = (S')^{-1}} - \underbrace{\left( E - \frac{\mathbf{p}^2}{2M_N} \right)}_{(E - H_0) = S^{-1}}. \quad (3)
 \end{aligned}$$

For simplicity we skipped the isospin part of the amplitude. The first term in the last line denotes the transition in on-shell kinematics, the second the inverse of the outgoing nucleon propagator and the third the inverse of the incoming nucleon propagator. Note that for on-shell incoming and outgoing nucleons, the  $\pi N \rightarrow \pi N$  transition vertex takes its on-shell value  $2m_\pi$  — even if the incoming pion is off-shell. This is in contrast to standard phenomenological treatments [5], where  $l_0$  is identified with  $m_\pi/2$  — the energy transfer in on-shell kinematics — and the recoil terms are not considered. Note, since  $p_{thr}^2/M_N = m_\pi$  the recoil terms are to be kept. A second consequence of Eq. (3) is even more interesting: when the rescattering diagram with the  $\pi N \rightarrow \pi N$  vertex gets convoluted with  $NN$  wave functions, only

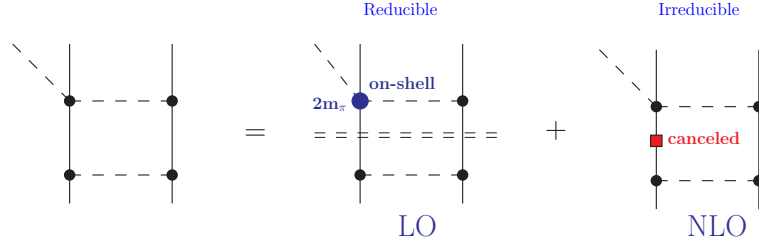


Figure 3: Reducible and irreducible parts of the box diagram. The square indicates that the corresponding nucleon propagator is cancelled. The double dashed line shows the two-nucleon cut.

the first term leads to a reducible diagram. The second and third terms, however, lead to irreducible contributions, since one of the nucleon propagators gets cancelled. This is illustrated in Fig. 3 on the example of the second diagram of Fig. 1a. It was shown explicitly in Ref. [17] that those induced irreducible contributions cancel the finite remainder of the NLO loops ((b)-(d)) in the  $pp \rightarrow d\pi^+$  channel. Thus, up to NLO only the diagrams

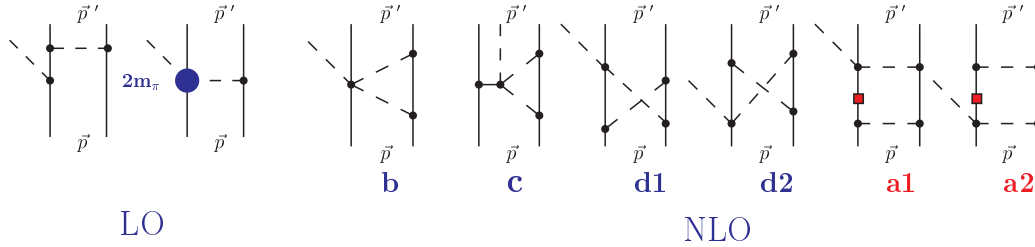


Figure 4: Complete set of nucleonic diagrams up to NLO. Note that sum of all loops at NLO vanishes.

appearing at LO, as shown in Fig. 4, contribute to  $pp \rightarrow d\pi^+$ , with the rule that the  $\pi N \rightarrow \pi N$  vertex is put on-shell. This enhances the dominating isovector  $\pi N$ -rescattering amplitude by a factor of  $4/3$  as compared to the traditionally used value, which leads to a good description of the experimental data for  $pp \rightarrow d\pi^+$ . The result found in Ref. [17] is shown in Fig. 5 as the solid line whereas the dashed line is the result of the model by Koltun and Reitan [5] that basically corresponds to our LO calculation with  $3/2m_\pi$  for the  $\pi N \rightarrow \pi N$  vertex. The data sets are from TRIUMF [19], IUCF [20], COSY [21] and PSI [22].

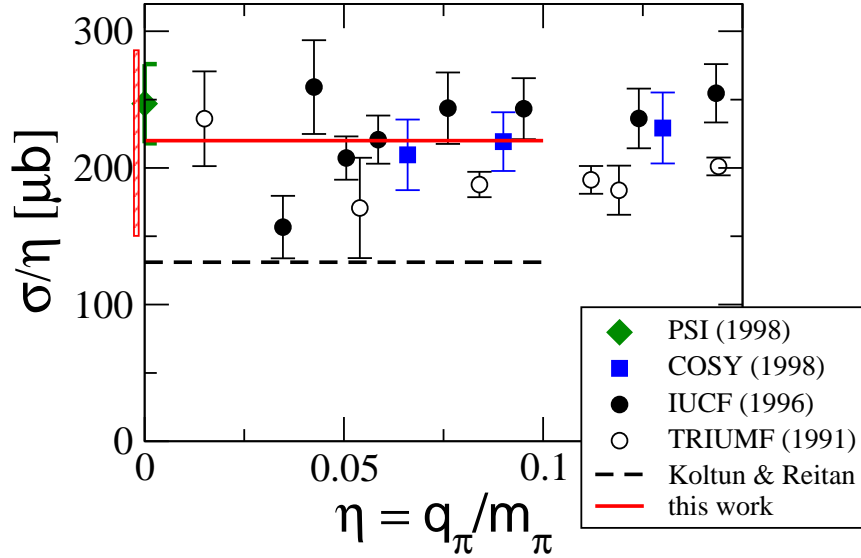


Figure 5: Comparison of our results to experimental data for  $NN \rightarrow d\pi$  (see text for the details).

### 3 Role of the Delta resonance

In this section we would like to discuss the influence of the  $\Delta$  resonance on the s-wave pion production cross section. The effect of the Delta has been extensively studied in the literature both in the phenomenological framework and using EFT. However, the current situation in the literature is quite contradictory. In particular, in phenomenological study by Niskanen [23] it was shown that the inclusion of the  $\Delta$  isobar leads to an enhancement of the total cross section in  $pp \rightarrow d\pi^+$  by almost a factor of 3. This enhancement is governed by the process where  $\Delta$  in the intermediate state emits a p-wave pion which is then rescattered on the nucleon in an s-wave, i.e. the diagrams analogous to the box diagrams of Fig.1 a) but with the  $\Delta$  instead of the nucleon in the intermediate state. However, the finding of Ref. [23] was not confirmed in the model calculation by Hanhart et al. [24]. The authors of this work have found that the direct pion emission from the  $\Delta$  increases the cross section by about 30% whereas the rescattering process is negligible. The Jülich meson-nucleon model [25] was applied in Ref. [24] to generate the off-shell  $\pi N \rightarrow \pi N$  transition T-matrix and the coupled channel CCF model [26] was employed to take into account the  $N\Delta$  and  $NN$  distortions in the initial and final states. In contrary to these results the direct pion production from the  $\Delta$  was shown to be negligible in the EFT calculation

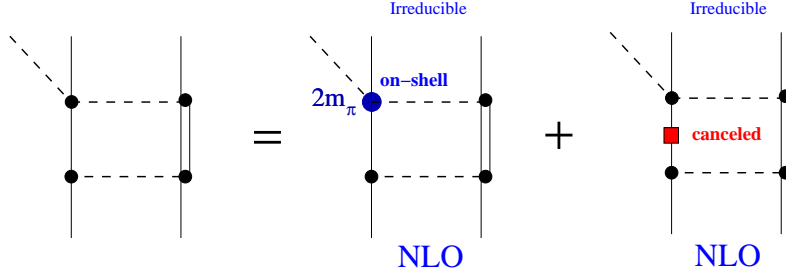


Figure 6: Rescattering diagram with the  $\Delta$  isobar. Pattern of separation on two parts due to the energy dependent WT vertex.

by da Rocha *et al.* [27]. However, the  $NN \rightarrow N\Delta$  transition in Ref [27] was approximated by one-pion exchange only, and the  $NN \rightarrow N\Delta$  contact interaction that contributes at the same order was not taken into account. At the same time it is known from phenomenology that heavy  $\rho$  meson exchange which plays the role of this contact term in phenomenological calculations is significant [26]. In addition the static  $\Delta$  propagator is used in Ref. [27] which leads to the large model dependence of the results. The similar problem with the use of the static  $\Delta$  propagator for the  $\pi d$  scattering was investigated in Ref. [28]. Let us now discuss in more detail the  $\pi N$  rescattering diagrams with the  $\Delta$ . First of all, due to the small mass difference between the nucleon and  $\Delta$ ,  $\Delta M = M_\Delta - M_N \simeq 2m_\pi$ , the  $N\Delta$  propagator behaves as

$$\frac{1}{m_\pi - \Delta M - p^2/2M_{N\Delta}} \sim \frac{1}{m_\pi}, \quad (4)$$

where  $M_{N\Delta}$  is the reduced mass of the  $N\Delta$  system, i.e. in full analogy with the counting rules for the NN propagator. Secondly, these rescattering diagrams contain the energy dependent WT vertex, and thus the method developed in the previous section for the diagrams with nucleons can be applied here as well. In particular, these diagrams can be also divided into two parts, as demonstrated in Fig. 6: the first one goes with the on shell  $\pi N$  vertex and in the second one the nucleon propagator cancels the corresponding piece in the vertex. In contradistinction from the diagrams of Fig. 3 both these parts contribute at NLO and both are irreducible. Furthermore, in the recent paper by Hanhart and Kaiser [16] the full set of one-loop diagrams with the  $\Delta$  contributing at NLO was studied in EFT. In particular, it was shown that those parts of the rescattering diagrams, in which the nucleon propagator is canceled, take part in a cancellation with other loop diagrams (see Fig. 4 in Ref. [16]). Thus, the only remainders contributing at NLO are the direct pion production and the rescattering process with the on shell  $\pi N$

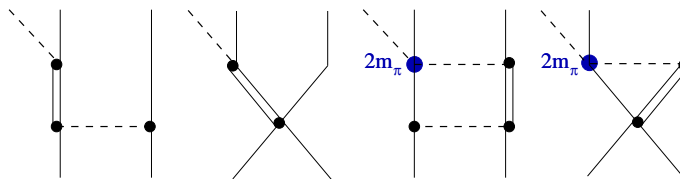


Figure 7: Non vanishing diagrams with the  $\Delta$  isobar contributing at NLO.

vertex as shown in Fig. 7. We evaluated these diagrams in a manner similar to our recent study of the role of the  $\Delta$  in pion-deuteron scattering [28]. The calculation revealed that each of these diagrams gives about a 10-15% correction to the transition amplitude but they enter with opposite signs – the direct contribution increases the cross section in line with the finding of Ref. [24] whereas the rescattering piece leads to a reduction by almost the same amount. Thus, there is a significant cancellation between different mechanisms involving the  $\Delta$  excitation and the resulting contribution of the  $\Delta$  resonance at NLO is very small. The calculation was done with the CCF [26] and the Hannover [29] coupled-channel NN models, and the pattern of cancellation was the same for both models although the individual contributions were slightly different.

## 4 Summary

We reported about recent developments in the reaction  $NN \rightarrow NN\pi$  in the effective field theory. Within the counting scheme that acknowledges the large momentum transfer between the initial and the final nucleons we have calculated the transition operator for this reaction up to NLO. We discussed how to implement properly the reducibility concept for the pion production process. In particular it was shown how to identify the irreducible contribution of the formally reducible loop diagrams with the energy dependent vertices. As a result we obtained that the irreducible loops at NLO cancel altogether, and the leading order  $\pi N$ -rescattering amplitude is enhanced by a factor of  $4/3$  as compared to the commonly used value. This enhancement leads to a good description of the experimental data for  $pp \rightarrow d\pi^+$ . We also investigated the effect of the  $\Delta$  isobar on the s-wave pion production. Being relatively sizable individually the direct and rescattering mechanisms of the  $\Delta$  excitation at NLO cancel each other to a large extent. Thus, we conclude that the net effect of the  $\Delta$  at NLO is very small.

The theoretical uncertainty of our NLO calculation was estimated con-

servatively using the dimensional arguments. The large uncertainty of about  $2m_\pi/M_N \approx 30\%$  for the cross section is a consequence of the rather large expansion parameter. Thus, a computation at NNLO is necessary for drawing more solid conclusions on the pion production mechanism, especially if one wants to learn more about the charge-symmetry breaking effects.

## Acknowledgments

This research is part of the EU Integrated Infrastructure Initiative Hadron Physics Project under contract number RII3-CT-2004-506078, and was supported also by the DFG-RFBR grant no. 05-02-04012 (436 RUS 113/820/0-1(R)) and the DFG SFB/TR 16 "Subnuclear Structure of Matter". V. B and A. K. acknowledge the support of the Federal Agency of Atomic Research of the Russian Federation.

## References

- [1] U. van Kolck, J. A. Niskanen, and G. A. Miller, Phys. Lett. **B 493**, 65 (2000).
- [2] A. Gårdestig *et al.*, Phys. Rev. **C 69**, 044606 (2004).
- [3] V. Lensky, V. Baru, J. Haidenbauer, C. Hanhart, A. E. Kudryavtsev and U. G. Meißner, Phys. Lett. **B 648**, 46 (2007) [arXiv:nucl-th/0608042].
- [4] H. O. Meyer *et al.*, Phys. Rev. Lett. **65**, 2846 (1990).
- [5] D. Koltun and A. Reitan, Phys. Rev. **141**, 1413 (1966).
- [6] G. A. Miller and P. Sauer, Phys. Rev. **C 44**, 1725 (1991).
- [7] C. Hanhart, Phys. Rep. **397**, 155 (2004) [arXiv:hep-ph/0311341].
- [8] S. Weinberg, Phys. Lett. **B 295**, 114 (1992).
- [9] B.Y. Park *et al.*, Phys. Rev. **C 53**, 1519 (1996) [arXiv:nucl-th/9512023].
- [10] C. Hanhart, J. Haidenbauer, M. Hoffmann, U.-G. Meißner and J. Spet Phys. Lett. **B 424**, 8 (1998) [arXiv:nucl-th/9707029].
- [11] V. Dmitrašinović, K. Kubodera, F. Myhrer and T. Sato, Phys. Lett. **B 465**, 43 (1999) [arXiv:nucl-th/9902048].
- [12] S. I. Ando, T. S. Park and D. P. Min, Phys. Lett. **B 509**, 253 (2001) [arXiv:nucl-th/0003004].

- 
- [13] T. D. Cohen, J. L. Friar, G. A. Miller and U. van Kolck, Phys. Rev. **C 53**, 2661 (1996) [arXiv:nucl-th/9512036].
- [14] C. da Rocha, G. Miller and U. van Kolck, Phys. Rev. **C 61**, 034613 (2000) [arXiv:nucl-th/9904031].
- [15] C. Hanhart, U. van Kolck, and G. Miller, Phys. Rev. Lett. **85**, 2905 (2000) [arXiv:nucl-th/0004033].
- [16] C. Hanhart and N. Kaiser, Phys. Rev. **C 66**, 054005 (2002) [arXiv:nucl-th/0208050].
- [17] V. Lensky, V. Baru, J. Haidenbauer, C. Hanhart, A. E. Kudryavtsev and U. G. Meißner, Eur. Phys. J. **A 27**, 37 (2006) [arXiv:nucl-th/0511054].
- [18] A. Gårdestig, talk presented at ECT\* workshop *Charge Symmetry Breaking and Other Isospin Violations*, Trento, June 2005; A. Gårdestig, D. R. Phillips and C. Elster, Phys. Rev. **C 73**, 024002 (2006) [arXiv:nucl-th/0511042].
- [19] D. A. Hutcheon *et al.*, Nucl. Phys. **A 535**, 618 (1991).
- [20] P. Heimberg *et al.*, Phys. Rev. Lett. **77**, 1012 (1996).
- [21] M. Drochner *et al.*, Nucl. Phys. **A 643**, 55 (1998).
- [22] P. Hauser *et al.*, Phys. Rev. **C 58**, 1869 (1998).
- [23] J. A. Niskanen, Phys. Rev. **C 53**, 526 (1996). [arXiv:nucl-th/9502015].
- [24] C. Hanhart, J. Haidenbauer, O. Krehl and J. Speth, Phys. Lett. **B 444**, 25 (1998). [arXiv:nucl-th/9808020].
- [25] C. Schutz, J. W. Durso, K. Holinde and J. Speth, Phys. Rev. **C 49**, 2671 (1994).
- [26] J. Haidenbauer, K. Holinde, and M.B. Johnson, Phys. Rev. **C 48**, 2190 (1993).
- [27] C. da Rocha, G. Miller and U. van Kolck, Phys. Rev. **C 61**, 034613 (2000) [arXiv:nucl-th/9904031].
- [28] V. Baru, J. Haidenbauer, C. Hanhart, A. Kudryavtsev, V. Lensky and U. G. Meißner, arXiv:0706.4023 [nucl-th], Phys. Lett. B, in print.
- [29] C. Hajduk, P. U. Sauer and W. Struve, Nucl. Phys. **A 405**, 581 (1983).

MENU 2007  
11th International Conference  
on Meson-Nucleon Physics and  
the Structure of the Nucleon  
September 10-14, 2007  
IKP, Forschungszentrum Jülich, Germany

## $\sigma$ CHANNEL LOW-MASS ENHANCEMENT IN DOUBLE-PIONIC FUSION – IS A DIBARYON RESONANCE THE REASON FOR THE ABC EFFECT?

M. Bashkanov<sup>\*1</sup>, C. Bargholtz<sup>%</sup>, D. Bogoslawsky<sup>#</sup>, H. Calen<sup>⊥</sup>, F. Cappellaro<sup>§</sup>, H. Clement<sup>\*</sup>, L. Demiroers<sup>+</sup>, E. Doroshkevich<sup>\*</sup>, D. Duniec<sup>§</sup>, C. Ekström<sup>⊥</sup>, K. Franssen<sup>⊥</sup>, L. Geren<sup>%</sup>, L. Gustafsson<sup>§</sup>, B. Höistad<sup>§</sup>, G. Ivanov<sup>#</sup>, M. Jacewicz<sup>§</sup>, E. Jiganov<sup>#</sup>, T. Johansson<sup>§</sup>, M. Kaskulov<sup>\*</sup>, O. Khakimova<sup>\*</sup>, S. Keleta<sup>§</sup>, I. Koch<sup>§</sup>, F. Kren<sup>\*</sup>, S. Kullander<sup>§</sup>, A. Kupść<sup>⊥</sup>, A. Kuznetsov<sup>#</sup>, K. Lindberg<sup>%</sup>, P. Marciniewski<sup>⊥</sup>, R. Meier<sup>\*</sup>, B. Morosov<sup>#</sup>, C. Pauly<sup>‡</sup>, H. Petterson<sup>§</sup>, Y. Petukhov<sup>#</sup>, A. Povtorejko<sup>#</sup>, A. Pricking<sup>\*</sup>, K. Schönning<sup>§</sup>, W. Scobel<sup>+</sup>, B. Schwartz<sup>±</sup>, T. Skorodko<sup>\*</sup>, V. Sopov<sup>‡</sup>, J. Stepeniak<sup>¶</sup>, P.-E. Tegner<sup>%</sup>, P. Thörngren-Engblom<sup>§</sup>, V. Tikhomirov<sup>#</sup>, G. J. Wagner<sup>\*</sup>, M. Wolke<sup>‡</sup>, A. Yamamoto<sup>□</sup>, J. Zabierowski<sup>▷</sup>, I. Zartova<sup>%</sup>, J. Złomanczuk<sup>§</sup>

<sup>\*</sup>Physikalisches Institut der Universität Tübingen, D-72076 Tübingen, Germany

<sup>%</sup>Department of Physics, Stockholm University, Stockholm, Sweden

<sup>#</sup>Joint Institute for Nuclear Research, Dubna, Russia

<sup>⊥</sup>The Svedberg Laboratory, Uppsala, Sweden

<sup>§</sup>Uppsala University, Uppsala, Sweden

<sup>+</sup>Hamburg University, Hamburg, Germany

<sup>±</sup>Budker Institute of Nuclear Physics, Novosibirsk, Russia

<sup>‡</sup>Institute of Theoretical and Experimental Physics, Moscow, Russia

<sup>‡</sup>Forschungszentrum Jülich, Germany

<sup>□</sup>High Energy Accelerator Research Organization, Tsukuba, Japan

<sup>¶</sup>Soltan Institute of Nuclear Studies, Warsaw, Poland

<sup>▷</sup>Soltan Institute of Nuclear Studies, Lodz, Poland

---

<sup>1</sup>E-mail address: bashkano@pit.physik.uni-tuebingen.de

### Abstract

The ABC effect - a puzzling low-mass enhancement in the  $\pi\pi$  invariant mass spectrum - is known from inclusive measurements of two-pion production in nuclear fusion reactions. First exclusive measurements carried out at CELSIUS-WASA for the fusion reactions to d and  ${}^3\text{He}$  in the final state reveal this effect to be a  $\sigma$  channel phenomenon associated with the formation of a  $\Delta\Delta$  system in the intermediate state. The total cross sections obtained for the  $pn \rightarrow d\pi^0\pi^0$  reaction exhibit a resonance-like behavior. Both this intriguing energy dependence and the differential distributions for the  $\pi^0\pi^0$  channels can be well described, if a quasibound state in the  $\Delta\Delta$  system leading to a resonance in the  $pn$  and  $d\pi^0\pi^0$  systems is assumed.

## 1 Introduction

The ABC effect - first observed by Abashian, Booth and Crowe [1] - in the double pionic fusion of deuterons and protons to  ${}^3\text{He}$ , stands for an unexpected enhancement at low masses in the  $M_{\pi\pi}$  spectrum. Follow-up experiments [2–11] revealed this effect to be of isoscalar nature and to show up in cases, when the two-pion production process leads to a bound nuclear system. With the exception of low-statistics bubble-chamber measurements [4, 8] all experiments conducted on this issue have been inclusive measurements carried out preferentially with single-arm magnetic spectrographs for the detection of the fused nuclei.

Initially the low-mass enhancement had been interpreted as an unusually large  $\pi\pi$  scattering length and evidence for the  $\sigma$  meson, respectively [1]. Since the effect showed up particularly clearly at beam energies corresponding to the excitation of two  $\Delta$ s in the nuclear system, the ABC effect was interpreted later on by a  $\Delta\Delta$  excitation in the course of the reaction process leading to both a low-mass and a high-mass enhancement in isoscalar  $M_{\pi\pi}$  spectra [12–16]. In fact, the missing momentum spectra from inclusive measurements have been in support of such predictions. It has been shown [17] that these structures can be enhanced considerably in theoretical calculations by including  $\rho$  exchange and short-range correlations.

## 2 Experiment

In order to shed more light on this issue, exclusive measurements of the reactions  $pd \rightarrow pd\pi^0\pi^0$  ( $T_p = 1.03$  and  $1.35$  GeV) and  $pd \rightarrow {}^3\text{He}\pi\pi$  ( $T_p = 0.893$  GeV) have been carried out in the energy region of the ABC effect

at CELSIUS using the  $4\pi$  WASA detector setup including the pellet target system [18]. The selected energies are close to the maximum of the ABC effect observed in the respective inclusive measurements. The  $pd \rightarrow pd\pi^0\pi^0$  reaction proceeds as quasifree  $pn \rightarrow d\pi^0\pi^0$  reaction with a spectator proton of very small four-momentum. Since all ejectiles except of the spectator have been measured, the spectator momentum has been reconstructed by kinematical fits with three overconstraints. The experimental results on the  $pd \rightarrow {}^3\text{He}\pi^0\pi^0$  and  $pd \rightarrow {}^3\text{He}\pi^+\pi^-$  reactions have been published already elsewhere [20, 21].

### 3 Experimental results

Results of our measurements are shown in Figs. 1 - 4. Fig.1 shows the Dalitz plot of the squares of invariant masses  $M_{d\pi^0}$  versus  $M_{\pi^0\pi^0}$  for the quasifree reaction process  $pn \rightarrow d\pi^0\pi^0$  at a nominal beam energy of  $T_p = 1.03$  GeV. Note that due to Fermi motion of the nucleons in the target deuteron the quasifree reaction process proceeds via a continuum of effective collision energies in the range 0.94 - 1.18 GeV with according kinematical smearing in the differential distributions. This smearing may be reduced strongly by dividing the data into narrow bins of effective collision energy at the cost of statistics. In Fig.1 the Dalitz plot for the quasifree  $pn \rightarrow d\pi^0\pi^0$  reaction is shown both for data and Monte Carlo (MC) simulation of a model description discussed in the next section. Note that the measurements cover practically the full phase space.

The  $\pi^0\pi^0$  channel, which is free of any isospin  $I=1$  contributions, exhibits a pronounced low-mass enhancement (ABC effect) in the  $M_{\pi^0\pi^0}$  spectrum both in the fusion process to the deuteron and in the one leading to  ${}^3\text{He}$  [20, 21]. Fig. 2 depicts the spectra of the invariant masses  $M_{\pi^0\pi^0}$  and  $M_{d\pi^0}$  for the quasifree  $pn \rightarrow d\pi^0\pi^0$  reaction at the beam energy  $T_p = 1.03$  GeV. We note in passing that in the  ${}^3\text{He}\pi^+\pi^-$  channel the threshold enhancement is observed [20] too, however, somewhat less pronounced. The reason for this is that this channel contains also isovector contributions - as may be seen [22] by the small shifts between the  $\Delta$  peaks in the  $M_{3\text{He}\pi^+}$  and  $M_{3\text{He}\pi^-}$  spectra [20, 21]. However, the main point is that in these spectra we see that indeed two  $\Delta$ s are excited simultaneously in this reaction, which supports the hypothesis of the excitation of a  $\Delta\Delta$  system in the course of the double pionic fusion process. .

Angular distributions are shown in Fig. 3 for the quasifree  $pn \rightarrow d\pi^0\pi^0$  reaction. For the  ${}^3\text{He}$  cases they are given in Refs. [20, 21]. The distribution of the opening angle  $\delta_{\pi^0\pi^0}$  between the two pions in the overall center-of-mass

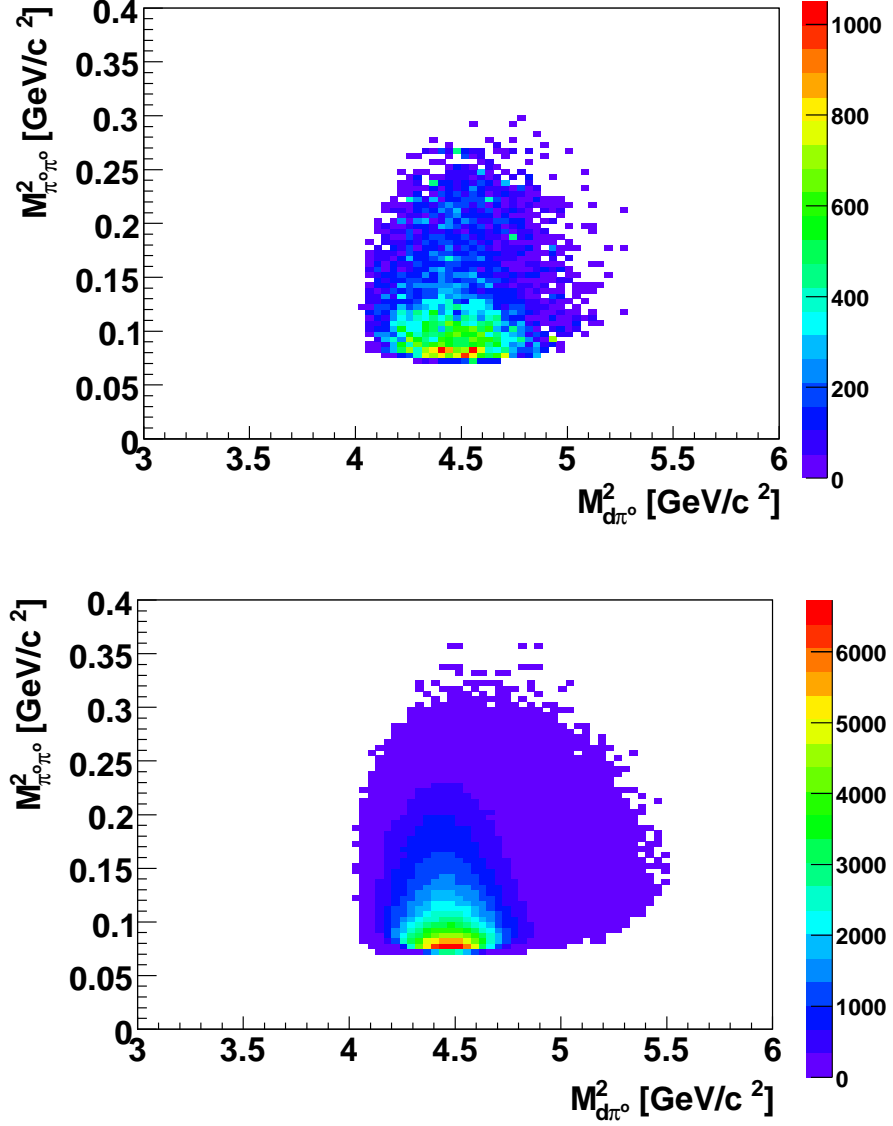


Figure 1: Dalitz plot of the invariant mass distributions for  $M_{d\pi^0}$  versus  $M_{\pi^0\pi^0}$  for the quasi free reaction process  $pn \rightarrow d\pi^0\pi^0$  in the range 0.94 - 1.18 GeV of effective collision energies. Top: data, bottom: MC simulation of a quasi bound state in the  $\Delta\Delta$  system leading to a resonance in the  $pn$  and  $d\pi^0\pi^0$  systems.

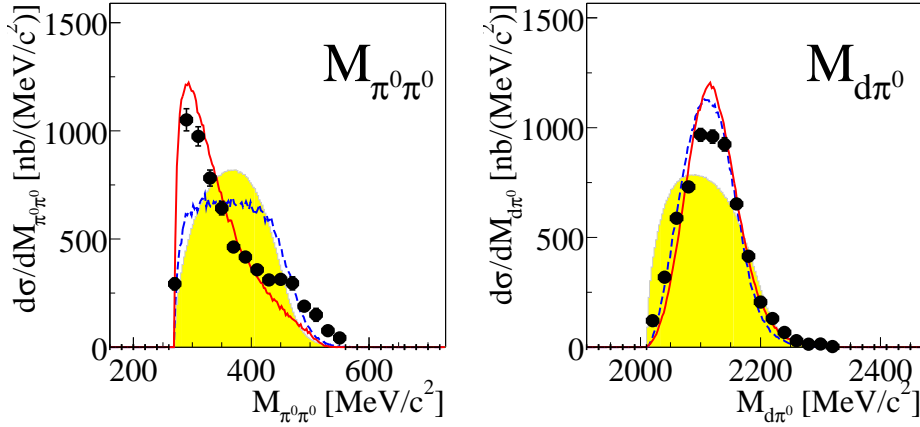


Figure 2: Distributions of the invariant masses  $M_{\pi^0\pi^0}$  and  $M_{d\pi^0}$  from the exclusive measurement of the quasifree  $pn \rightarrow d\pi^0\pi^0$  reaction at a beam energy  $T_p = 1.03$  GeV. The shaded areas show the pure phase space distributions. Solid and dashed curves give  $\Delta\Delta$  calculations with and without the assumption of a quasibound state in the  $\Delta\Delta$  system leading to a resonance in the  $pn$  and  $d\pi^0\pi^0$  systems.

system (cms) peaks at small angles, in particular if we select events with  $M_{\pi^0\pi^0} \leq 0.34$  GeV/c<sup>2</sup>. This means that the low-mass enhancement is associated with pions leaving the interaction vertex in parallel. The distributions of the deuteron polar angles  $\Theta_d^{d\pi^0\pi^0}$  in the overall cms (i.e. the full  $d\pi^0\pi^0$  system) and of the pion polar angles  $\Theta_{\pi^0}^{\pi^0\pi^0}$  and  $\Theta_{\pi^0}^{d\pi^0}$  in  $d\pi^0$  and  $\pi^0\pi^0$  subsystems, respectively, are symmetric about 90° and anisotropic. The anisotropy observed for the latter (not shown in Fig. 2) corresponds just to the one expected from  $\Delta$  decay. The anisotropy in the  $\pi^0$  angular distribution in the  $\pi\pi$  subsystem signals some admixture from higher partial waves. It gets strongly reduced, if we consider only data with  $M_{\pi^0\pi^0} \leq 0.34$  GeV/c<sup>2</sup>, i.e. in the region of the low-mass enhancement. From this we deduce that the threshold enhancement (ABC-effect) is of scalar nature.

Finally we show in Fig. 4 the energy dependence of the total cross section of the double-pionic fusion to Deuterium. Depicted are the results for the  $pn \rightarrow d\pi^+\pi^-$  reaction from bubble chamber measurements at DESY [4] and JINR [8] together with our preliminary results from measuring the quasifree  $pn \rightarrow d\pi^0\pi^0$  reaction at two incident energies, which have been binned into narrow ranges of effective collision energies providing thus four entries at lower energies and two entries at higher energies. Since  $\pi^+\pi^-$  and  $\pi^0\pi^0$  channels are related by an isospin factor of two, we have plotted our results in Fig.4

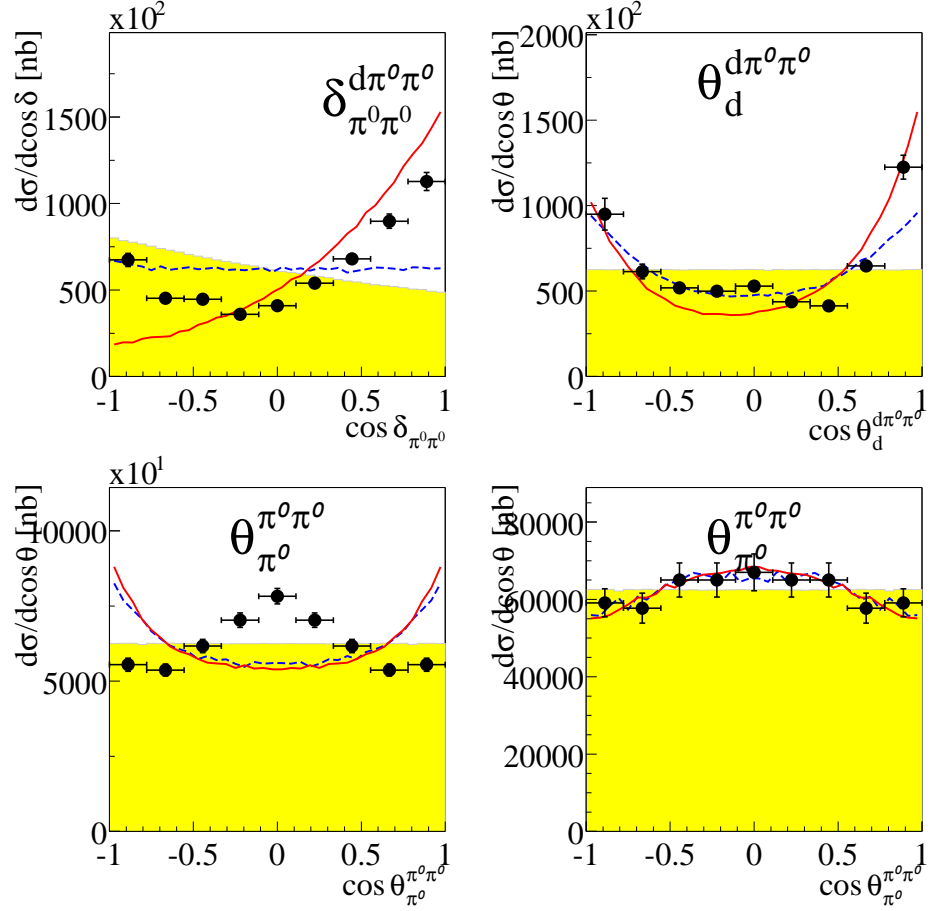


Figure 3: Angular distributions in the quasifree reaction  $pn \rightarrow d\pi^0\pi^0$  at the nominal beam energy of  $T_p = 1.03$  GeV for the opening angle  $\delta_{\pi^0\pi^0}^{d\pi^0\pi^0}$  between the two pions, the angle of the deuteron  $\Theta_d^{d\pi^0\pi^0}$  - all in the overall cms of the  $d\pi^0\pi^0$  system - as well as the pion angle  $\Theta_{\pi^0}^{\pi^0\pi^0}$  in the  $\pi^0\pi^0$  subsystem (Jackson frame), respectively. This angular distribution is plotted also with the constraint  $M_{\pi^0\pi^0} < 0.34$  GeV/ $c^2$  (bottom, right). The shaded areas show the pure phase space distributions. Solid and dashed curves give  $\Delta\Delta$  calculations with and without the assumption of a quasibound state in the  $\Delta\Delta$  system leading to a resonance in the  $pn$  and  $d\pi^0\pi^0$  systems.

by multiplying them by this isospin factor, in order to make them directly comparable to the  $\pi^+\pi^-$  results.

## 4 Discussion and Interpretation of Experimental Results

The  $\pi\pi$  low-mass enhancements observed in the exclusive data for the  $\pi^0\pi^0$  channels turn out to be much larger than predicted in previous  $\Delta\Delta$  calculations [12, 14, 16]. As an example we show by the dashed lines in Figs. 2 and 3 and by dotted lines in Fig. 4 calculations in the model ansatz of Ref. [12], where we additionally included the pion angular distribution in  $\Delta$  decay and the Fermi smearing of the nucleons bound in the final nucleus. Contrary to these predictions the data also do not exhibit any high-mass enhancement that had been supported by the inclusive measurements, too. As suspected already in Ref. [9] the high-mass bump observed in inclusive spectra rather turns out to be associated with  $\pi\pi\pi$  production and  $I=1$  contributions.

Since on the one hand the available  $\Delta\Delta$  calculations obviously fail, but on the other hand the data clearly show the  $\Delta\Delta$  excitation in their  $M_{N\pi}$  spectra, a profound physics piece appears to be missing. Such a missing piece may be provided by a strong  $\Delta\Delta$  attraction or even a boundstate condition, as we demonstrated in Refs. [20, 21, 23, 24]. With these assumptions we are able to describe the exclusively measured data for d and  $^3\text{He}$  fusion as well as the inclusive spectra for double-pionic fusion to  $^4\text{He}$  amazingly well without modification of the  $\Delta\Delta$  interaction parameters. For the boundstate case we request the distribution of the relative momentum of the two  $\Delta$ s to follow that of a Hulthen type distribution. For the scattering case we take the Migdal-Watson [25, 26] ansatz for final state interactions with the  $\Delta\Delta$  scattering length as a parameter, which is adjusted for an optimal description of the data. Using an effective range of 2 fm, i.e. in the region of corresponding NN values, we find two equivalent solutions for the  $\Delta\Delta$  scattering length of -16 fm and +10 fm, respectively. The first value means that the interaction is strongly attractive and close to the one for isovector NN scattering, the second solution means that there is even a bound  $\Delta\Delta$  state. All these cases provide very similar descriptions of the observables and hence can not be discriminated by the present data base. However, these calculations still predict an energy dependence of the total cross section, which is only slightly steeper than that of  $\Delta\Delta$  calculations without mutual interaction, i.e., inconsistent with the total cross section data in Fig. 4.

In fact, the clue to the true nature of the ABC effect may be provided by

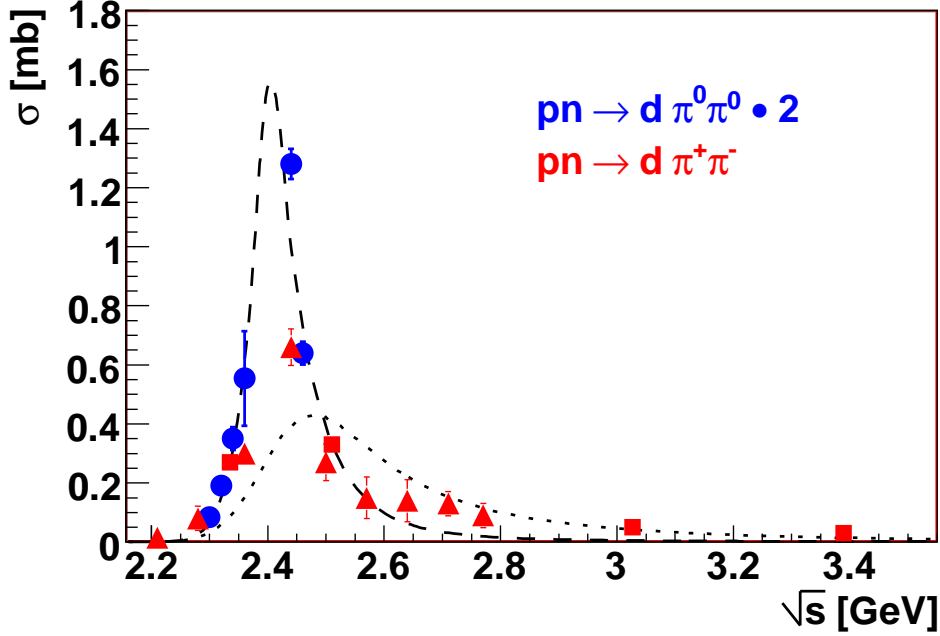


Figure 4: Energy dependence of the  $pn \rightarrow d\pi\pi$  reaction with preliminary results of this work for the  $\pi^0\pi^0$  channel (quasi-free measurements at two incident energies) and results for the  $\pi^+\pi^-$  channel from Ref. [8] (squares) and Fig. 2c of Ref. [4] (triangles). Dashed and dotted lines represent calculations with and without the assumption of a quasibound state in the  $\Delta\Delta$  system leading to a resonance in the  $pn$  and  $d\pi^0\pi^0$  systems.

the intriguing energy dependence of the double-pionic fusion in the isoscalar channel. On the one hand the isovector fusion channel  $pp \rightarrow d\pi^+\pi^0$ , which shows **no** ABC effect [27] despite a clear  $\Delta\Delta$  excitation signal in its differential spectra, exhibits an energy dependence [28] in its total cross section close to the dotted curve in Fig. 4. On the other hand the isoscalar fusion channel exhibits a much steeper energy-dependence resembling that of a pronounced resonance excitation with a width of roughly 100 MeV or even below, i.e. much smaller than twice the  $\Delta$  width expected from usual  $\Delta\Delta$  calculations. As is also borne out by the data in Fig. 4 the cross section maximum at  $\sqrt{s} \approx 2.41$  GeV means that the resonance mass is below twice the  $\Delta$  mass pointing to a quasibound state in the isoscalar  $\Delta\Delta$  system, which not only can decay into the  $pn$  system, but also into the isoscalar  $d\pi\pi$  system, because the  $\Delta$  decay width is larger than the binding of this state.

In fact, the Migdal-Watson ansatz with its dependence on the relative momentum  $q_{\Delta\Delta}$  between the two  $\Delta$ s can be easily upgraded to a Breit-Wigner term with a  $q_{\Delta\Delta}$  dependent width. Adjusting the width parameters to a correct reproduction of the  $M_{\pi^0\pi^0}$  differential distribution leads not only to a quantitative description of all differential data (solid curves in Figs. 2 and 3 as well as Dalitz plot in Fig.1) but also to a quantitative description of the energy dependence of the total cross section (dashed curve in Fig. 4) by providing automatically the correct width needed for the description of the total cross section data.

Since the model calculations for a quasibound state in the  $\Delta\Delta$  system, which assume the decay into this system to proceed via relative s-waves between the two  $\Delta$ s, describe the measured angular distributions very well, the spin-parity assignment to this isoscalar intermediate state has to be either  $J^P = 1^+$  or  $3^+$  taking into account that the two-fermion system has to be in an antisymmetric state.

## Acknowledgments

We acknowledge valuable discussions with E. Oset, C. Wilkin, Ch. Hanhart, A. Sibirtsev, L. Alvarez-Ruso, A. Kaidalov, L. Dakhno and V. Anisovitch on this issue. This work has been supported by BMBF (06TU201, 06TU261), COSY-FFE, DFG (Europ. Graduiertenkolleg 683), Landesforschungsschwerpunkt Baden-Württemberg and the Swedish Research Council. We also acknowledge the support from the European Community-Research Infrastructure Activity under FP6 "Structuring the European Research Area" programme (Hadron Physics, contract number RII3-CT-2004-506078).

## References

- [1] N. E. Booth, A. Abashian, K. M. Crowe, Phys. Rev. Lett. **7**, 35 (1961) ; **6** (1960) 258; Phys. Rev. **C132**, 2296ff (1963)
- [2] R. J. Homer *et al.*, Phys. Rev. Lett. **9**, 72 (1964)
- [3] J. H. Hall *et al.*, Nucl. Phys. **B12**, 573 (1969)
- [4] I. Bar-Nir *et al.*, Nucl. Phys. **B54**, 17 (1973)
- [5] J. Banaigs *et al.*, Nucl. Phys. **B67**, 1 (1973)
- [6] J. Banaigs *et al.*, Nucl. Phys. **B105**, 52 (1976)

- [7] F. Plouin *et al.*, Nucl. Phys. **A302**, 413 (1978)
- [8] A. Abdivaliev *et al.*, Sov. J. Nucl. Phys. **29**, 796 (1979)
- [9] F. Plouin, P. Fleury, C. Wilkin, Phys. Rev. Lett. **65**, 690 (1990)
- [10] R. Wurzinger *et al.*, Phys. Lett. **B445**, 423 (1999)
- [11] for a review see A. Codino and F. Plouin, LNS/Ph/94-06
- [12] T. Risser and M. D. Shuster, *Phys. Lett.* **43B**, 68 (1973)
- [13] I. Bar-Nir, T. Risser, M. D. Shuster, Nucl. Phys. **B87**, 109 (1975)
- [14] J. C. Anjos, D. Levy, A. Santoro, Nucl. Phys. **B67**, 37 (1973)
- [15] see, e.g., A. Gardestig, G. Fäldt, C. Wilkin, Phys. Rev. **C59**, 2608 (1999) and Phys. Lett. **B421**, 41 (1998)
- [16] C. A. Mosbacher, F. Osterfeld, nucl-th/990364
- [17] L. Alvarez-Ruso, *Phys. Lett.* **B452**, 207(1999); PhD thesis, Univ. Valencia 1999
- [18] J. Zabierowski *et al.*, Phys. Scripta **T99**, 159 (2002)
- [19] M. Bashkanov *et al.*, *Act. Phys. Slov.* **56**, 285 (2006)
- [20] M. Bashkanov *et al.*, Phys. Lett. **B637** 223 (2006)
- [21] M. Bashkanov, PhD thesis, Univ. Tübingen 2006, <http://tobias-lib.ub.uni-tuebingen.de/volltexte/2006/2636/>, urn:nbn:de:bsz:21-opus-26366
- [22] C. Wilkin, private communication 2007
- [23] M. Bashkanov *et al.*, Int. J. Mod. Phys. **A22**, 625 (2007)
- [24] O. Khakimova *et al.*, Int. J. Mod. Phys. **A22**, 617 (2007)
- [25] A. B. Migdal, JETP **28**, 1 (1955)
- [26] K. J. Watson, Phys. Rev. **88**, 1163 (1952)
- [27] F. Kren, PhD thesis Tübingen, in preparation
- [28] J. Bystricky *et al.*, J. Physique **48**, 1901 (1987)

# HOW WE DISCOVERED THE NONET OF LIGHT SCALAR MESONS

*Eef van Beveren*

Centro de Física Teórica, Departamento de Física, Universidade de Coimbra, P-3004-516 Coimbra, Portugal

*George Rupp*

Centro de Física das Interações Fundamentais, Instituto Superior Técnico, Universidade Técnica de Lisboa, Edifício Ciência, P-1049-001 Lisboa, Portugal.

## Abstract

As has been confirmed meanwhile by lattice-QCD calculations (see e.g. Ref. [1]), the confinement spectrum of non-exotic quark-antiquark systems has its ground state for scalar mesons well above 1 GeV in the Resonance Spectrum Expansion (RSE)<sup>1</sup>. For instance, in the  $S$ -wave  $K\pi$  RSE amplitude, a broad resonance was predicted slightly above 1.4 GeV [2], which is confirmed by experiment as the  $K_0^*(1430)$ . However, a complete nonet of light scalar mesons was predicted [3] as well, when a model strongly related to the RSE and initially developed to describe the  $c\bar{c}$  and  $b\bar{b}$  resonance spectra [4] was applied in the light-quark sector. Thus, it was found that the light scalar-meson nonet constitutes part of the ordinary meson spectrum, albeit represented by “*extraordinary*” [5] poles [2]. Similar resonances and bound states appear in the charmed sector [6], and are predicted in the  $B$ -meson spectrum [7, 8].

A recent work [9] confirmed the presence of light scalar-meson poles in the RSE amplitude for  $S$ -wave and  $P$ -wave  $\pi\pi$  and  $K\pi$  contributions to three-body decay processes measured by the BES, E791 and FOCUS collaborations.

## 1 Scattering poles

It is generally accepted that resonances in scattering are represented by poles in the “second” Riemann sheet of the complex energy plane [10]. Let us assume here that in a process of elastic and non-exotic meson-meson scattering

---

<sup>1</sup>The RSE was designed for the description of the complete resonance structure in meson-meson scattering, for both the heavy- and light-quark sectors.

one obtains scattering poles at

$$E = P_0, P_1, P_2, \dots \quad (1)$$

Simple poles in  $S$  may be considered simple zeros in its denominator. Hence, assuming a polynomial expansion, we may [11,12] represent the denominator  $D$  of  $S$  by

$$D(E) \propto (E - P_0)(E - P_1)(E - P_2)\dots \quad (2)$$

Unitarity then requires that the  $S$ -matrix be given by<sup>2</sup>

$$S(E) = \frac{(E - P_0^*)(E - P_1^*)(E - P_2^*)\dots}{(E - P_0)(E - P_1)(E - P_2)\dots} \quad (3)$$

If we assume that the resonances (1) stem from an underlying confinement spectrum, given by the real quantities

$$E = E_0, E_1, E_2, \dots \quad (4)$$

then we may represent the differences  $(P_n - E_n)$ , for  $n = 0, 1, 2, \dots$ , by  $\Delta E_n$ . Thus, we obtain for the unitary  $S$ -matrix the expression

$$S(E) = \frac{(E - E_0 - \Delta E_0^*)(E - E_1 - \Delta E_1^*)(E - E_2 - \Delta E_2^*)\dots}{(E - E_0 - \Delta E_0)(E - E_1 - \Delta E_1)(E - E_2 - \Delta E_2)\dots} \quad (5)$$

So we assume here that resonances occur in scattering because the two-meson system couples to confined states, usually of the  $q\bar{q}$  type, viz. in non-exotic meson-meson scattering. Let the strength of the coupling be given by  $\lambda$ . For vanishing  $\lambda$ , we presume that the widths and real shifts of the resonances also vanish. Consequently, the scattering poles end up at the positions of the confinement spectrum (4), and so

$$\Delta E_n \xrightarrow{\lambda \downarrow 0} 0 \quad \text{for } n = 0, 1, 2, \dots \quad (6)$$

As a result, the scattering matrix tends to unity, as expected in case there is no interaction.

---

<sup>2</sup>Note that we do not consider here a possible overall phase factor representing a background and stemming from the proportionality constant in formula (2).

An obvious candidate for an expression of the form (5) looks like

$$S(E) = \frac{1 + \lambda^2 \left\{ \sum_n \frac{G(E)^*}{E - E_n} \right\}}{1 + \lambda^2 \left\{ \sum_n \frac{G(E)}{E - E_n} \right\}}, \quad (7)$$

where  $G$  is a smooth complex function of energy  $E$ , and where, at least for small values of the coupling constant  $\lambda$ , one has

$$\Delta E_i \approx -\lambda^2 G(E_i) \quad \text{for } i = 0, 1, 2, \dots \quad (8)$$

Relation (8) can be easily understood, if we assume that for small  $\lambda$  poles show up in the vicinity of the energy values (4) of the confinement spectrum. As a consequence, at the zero  $P_i$  of the denominator, near the  $i$ -th recurrence of the confinement spectrum  $E_i$ , the term  $n = i$  dominates the summations in formula (7), i.e.,

$$0 = 1 + \lambda^2 \left\{ \sum_n \frac{G(P_i)}{P_i - E_n} \right\} \approx 1 + \lambda^2 \frac{G(E_i)}{\Delta E_i} \quad (9)$$

For larger values of  $\lambda$ , one cannot perform the approximation  $P_i \approx E_i$  in Eq. (9). In such cases, the left-hand part of Eq. (9) must be solved by other methods, usually numerically. However, since it is reasonable to assume that poles move smoothly in the lower half of the complex energy plane as  $\lambda$  varies, we may suppose that the left-hand part of Eq. (9) has solutions which, when the value of  $\lambda^2$  is continuously decreased, each correspond to one of the values out of the confinement spectrum (4).

When all scattering poles in expression (5) are known, one can — with unlimited accuracy — determine the function  $G$  in formula (7). Once  $G$  is known, one can search for poles by solving the left-hand part of Eq. (9). However, further restrictions can be imposed upon expression (7). For a two-meson system, there may exist bound states below the meson-meson scattering threshold. Such states are represented by poles in the analytic continuation of expression (7) to below threshold, on the real axis in the complex energy plane. Consequently, in the case that a confinement state, say  $E_0$ , comes out below threshold, its corresponding pole is, at least for small coupling, expected to be found on the real axis in the complex energy plane. Using formula (8), we obtain

$$G(E_0) \text{ real for } E_0 < \text{threshold.} \quad (10)$$

Moreover, in order to ensure that scattering poles come out in the lower-half of the complex energy plane, also using formula (8), we find that above threshold  $G$  must be complex, with a positive imaginary part.

## 2 Partial waves

In different partial waves, resonances come out at different masses. At threshold, where the total invariant mass of the two-meson system equals the sum of the two meson masses, one has additional conditions. For  $S$  waves, since cross sections are finite, we must demand that  $G$  do not vanish at threshold, whereas, for  $P$  and higher waves, as cross sections do vanish,  $G$  should vanish as well.

A possible expression that satisfies all imposed conditions reads

$$i pa j_\ell(pa) h_\ell^{(1)}(pa) \quad \text{for } \ell = 0, 1, 2, \dots, \quad (11)$$

where  $p$  represents the linear momentum in the two-meson system and  $a$  a scale parameter with the dimensions of a distance. The well-known scattering solutions  $j_\ell$  and  $h_\ell^{(1)}$  stand for the spherical Bessel function and the Hankel function of the first kind, respectively.

Thus, we arrive at a good candidate for a scattering amplitude of resonant scattering off a confinement spectrum, reading

$$T_\ell(E) = \frac{1}{2i} (S_\ell(E) - 1) = \frac{-2\lambda^2 \left\{ \sum_n \frac{g_{n\ell}^2}{E - E_n} \right\} \mu pa j_\ell^2(pa)}{1 + 2i\lambda^2 \left\{ \sum_n \frac{g_{n\ell}^2}{E - E_n} \right\} \mu pa j_\ell(pa) h_\ell^{(1)}(pa)}, \quad (12)$$

where we have introduced the two-meson reduced mass  $\mu$  and, moreover, relative couplings  $g_{n\ell}$ , which may be different for different recurrences of the confinement spectrum.

As it is written, formula (12) seems to allow a lot of freedom, through adjustments of the  $g_{n\ell}$  to experiment. In principle, it might even be useful to carry out such data fitting, so as to gain more insight into the details of the coupling between a two-meson system and a confined  $q\bar{q}$  state. However, experimental results are so far much too incomplete to make a detailed comparison to our expression possible.

The spin structure of quarks, besides being important for the spectrum of a  $q\bar{q}$  system, is also crucial for the short-distance dynamics, hence for the

properties of the coupling between  $q\bar{q}$  and meson-meson states. In the  ${}^3P_0$  model [13,14], it is assumed that a two-meson system couples to a  $q\bar{q}$  state via the creation or annihilation of a new  $q\bar{q}$  pair, with vacuum quantum numbers  $J^{PC} = 0^{++}$ . Under this assumption, all relative couplings can be determined from convolution integrals of the wave functions. In Refs. [15,16], such integrals have been calculated for general quantum numbers, including flavour. The latter results leave no freedom for the coupling constants in formula (12), except for an overall strength  $\lambda$ , which parametrises the probability of  $q\bar{q}$  creation/annihilation.

This way, the full spin structure of the two-meson system is entirely contained in the relative coupling constants  $g_{n\ell}$ . Yet, direct comparison of the results given in Refs. [15,16] to experiment would still be of great interest.

The relevant  $q\bar{q} \leftrightarrow MM$  coupling-constant book-keeping has been developed in Refs. [15,16]. The latter scheme not only eliminates any freedom, but also — by construction — restricts the number of possible  $MM$  channels that couple to a given  $q\bar{q}$  system. Nonetheless, the number of involved channels rapidly grows for higher radial and angular excitations of the  $q\bar{q}$  system.

### 3 Observables

The scattering matrix is not directly observable, but only through quantities like cross sections and production rates. It is straightforward to determine cross sections [17] and, after some algebra, production rates [18] from expression (12). However, a complete modelling of strong interactions is more complex. For example, a  $c\bar{c}$  vector state couples, via OZI-allowed decay, to  $D\bar{D}$ , but also to  $DD^*$ ,  $D^*D^*$ ,  $D_s\bar{D}_s$ , ... [4]. Consequently, the involved two-meson channels couple to one another as well. So the first extension necessary for a more proper description of strong interactions is the formulation of a multichannel equivalent of expression (12). This issue has been dealt with in Ref. [19]. It involves coupling constants similar to the ones discussed above, but now for each two-meson channel.

A meson-meson channel is characterised by quantum numbers, including flavour and isospin, and the meson masses. However, many of the needed masses are unknown yet, while most mesons only exist as resonances.

In experiment, one can concentrate on one specific channel. On the other hand, in a meaningful analysis all channels that couple must be taken into account. For example, one may argue that for the description of  $\pi\pi$  scattering below the  $KK$  threshold the channels  $KK$ ,  $\eta\eta$ , ... can be neglected. But then one ignores virtual two-meson channels, which may have a noticeable

influence below the  $KK$  threshold.

Furthermore,  $q\bar{q}$  states may couple to one another via meson loops. Typical examples are:  $c\bar{c}$  vector states, which become mixtures of  ${}^3S_1$  and  ${}^3D_1$  via loops of charmed mesons, and isoscalar  $q\bar{q}$  states, where kaon loops mix the  $u\bar{u} + d\bar{d}$  and  $s\bar{s}$  components. One then obtains different interplaying confinement spectra, which may become visible in production rates. The extension of expression (7) to more than one  $q\bar{q}$  channel has been considered in Refs. [3, 20], for the description of the  $\sigma$  and  $f_0(980)$  resonances.

## 4 The parameters

Besides the parameters  $\lambda$  and  $a$ , formula (12) contains an infinite number of parameters  $E_{nl}$ . These represent the unknown and even hypothetical spectra of confined  $q\bar{q}$  systems. From experiment, we only have data at our disposal for resonances in meson-meson scattering or production. Formulae like expression (12) are intended to interpolate between the observed resonances and the underlying — largely unknown — confinement spectrum.

In Fig. 2 of Ref. [21], we showed, for  $S$ -wave isodoublet  $K\pi$  scattering, how cross sections determined by the use of formula (12) vary with increasing values of the coupling  $\lambda$ . For small  $\lambda$ , the nonstrange-strange ( $n\bar{s}$ ) confinement spectrum is well visible in the latter figure, whereas for the model value of the  $q\bar{q} \leftrightarrow$  meson-meson coupling experiment is reproduced.

Furthermore, in Fig. 3 of Ref. [22] we showed a similar behavior as a function of  $\lambda$  for  $J^{PC} = 1^{--}$   $c\bar{c}$  states. For  $\lambda = 0$ , we find the theoretical ground state at 3.46 GeV, whereas for  $\lambda = 1$  it coincides with the experimentally observed  $J/\psi$  mass. The model employed to determine the results of this figure was a multichannel extension of formula (12), taking moreover into account the degeneracy of certain confined  $q\bar{q}$  states.

From these results we may conclude that, although there is some connection between the confinement spectrum ( $\lambda = 0$ ) and the resonances and bound states of two-meson systems ( $\lambda = 1$ ), it is not a simple one-to-one relation. Moreover, the level splittings of the confinement spectrum appear distorted in experiment. In particular, the experimental ground states show up much below the ground states of the hypothetical confinement spectrum.

Over the past decades, many models have been developed for the description of meson spectra. Only very few of those models are based on expressions for two-meson scattering or production. Here, it is stressed that no data for the spectra of confined  $q\bar{q}$  systems exist. We only dispose of data for resonances in meson-meson scattering or production [3, 4, 17]. Neverthe-

less, in order to unravel the characteristics of the  $q\bar{q}$  confinement spectrum, we must rely on results from experiment, even though the available data [23] are manifestly insufficient as hard evidence.

We observe from data that the average level splitting in  $c\bar{c}$  and  $b\bar{b}$  systems equals 350–400 MeV, when the ground states,  $J/\psi$ ,  $\eta_c$ ,  $\Upsilon(1S)$  and  $\eta_b$  are not taken into account [4]. Furthermore, mass differences in the positive-parity  $f_2$  meson spectrum, which are shown in Table 3 of Ref. [24], hint at level splittings of a similar size in the light  $q\bar{q}$  spectrum. In Ref. [24], possible internal flavor and orbital quantum numbers for  $f_2$  states were discussed.

Moreover, the few available mass differences for higher recurrences indicate that level splittings might turn out to be almost constant for states higher up in the  $q\bar{q}$  spectra as well [23,25], a property shared by the spectrum of a simple non-relativistic harmonic oscillator. Over the past thirty years, we have systematically discussed an ansatz for harmonic-oscillator confinement. A formalism which naturally leads to a harmonic-oscillator-like  $q\bar{q}$  confinement spectrum starting from QCD, by exploiting the latter theory's Weyl-conformal symmetry, can be found in Refs. [26,27].

Guided by the — not overwhelmingly compelling — empirical evidence that level splittings may be constant and independent of flavor, and given the obvious need to further reduce the parameter freedom in expression (12) for the two-meson elastic  $T$ -matrix, we simply choose here the  $q\bar{q}$  level splittings  $E_{(n+1)\ell} - E_{n\ell}$  to be constant and equal to 380 MeV, for all possible  $q\bar{q}$  flavor combinations. The remaining set of parameters  $E_{00}$ , different for each possible  $q\bar{q}$  flavor combination, can be further reduced [17], via the choice of effective valence flavor masses and a universal frequency  $\omega$ . In the future, when more data become available on the spectra of  $q\bar{q}$  systems, higher-order corrections to the harmonic-oscillator spectrum may be inferred. At present, this does not seem to be feasible.

## **$S$ -wave scattering for $I = 1/2$**

In Fig. 2 of Ref. [21], we compared the result of formula (12) to the data of Refs. [28,29]. We observed a fair agreement for total invariant masses up to 1.6 GeV. However, one should bear in mind that the LASS data must have larger error bars for energies above 1.5 GeV than suggested in Ref. [29], since most data points fall well outside the Argand circle. Hence, for higher energies, the model should better not follow the data too precisely.

Now, in order to have some idea about the performance of formula (12) for  $I = 1/2$   $S$ -wave  $\pi K$  scattering, we argue that, since in our model there is only one non-trivial eigenphase shift for the coupled  $\pi K + \eta K + \eta' K$  system, we may compare the phase shifts of our model for  $\eta K$  and  $\eta' K$  to the ex-

perimental phase shifts for  $K\pi$ . We did this comparison in Figs. 6 and 7 of Ref. [21], where, instead of the phase shifts, we plotted the cross sections, assuming no inelasticity in either case. The latter assumption is, of course, a long shot. Nevertheless, we observe an extremely good agreement.

Apparently, we may conclude that the phase motion in the coupled  $\pi K$ ,  $\eta K$  and  $\eta' K$  system is well reproduced by the model. In particular, one could have anticipated that  $\pi K$  and  $\eta K$  have very similar phase motions, because  $\eta K$  has been observed to almost decouple from  $\pi K$ . This implies that the corresponding  $T$ -matrix for a coupled  $\pi K + \eta K$  system is practically diagonal. Knowing, moreover, that this system has only one non-trivial eigenphase, we should then also find almost the same phase motion for  $\pi K$  and  $\eta K$ .

### The $I = 1/2$ $S$ -wave poles

Since the model reproduces fairly well the data for the  $I = 1/2$   $S$ -wave, it is justified to study its poles. In Table 1 we collect the five lowest zeros of formula (9). Only three of the five corresponding poles are anticipated from

Pole Position (GeV)	Origin
$0.77 - 0.28i$	continuum
$1.52 - 0.10i$	confinement
$1.79 - 0.05i$	confinement
$2.04 - 0.15i$	continuum
$2.14 - 0.07i$	confinement

Table 1: The five lowest zeros of formula (9).

the  $J^P = 0^+ n\bar{s}$  confinement spectrum, coming out at 1.39 GeV, 1.77 GeV, 2.15 GeV, ... . So we expected only three, but find five poles in the invariant-mass region below 2.2 GeV. This shows that the transition from formula (5) to formula (12), is not completely trivial. *A fortiori*, expression (9) even has more zeros than expression (2). It is amusing that Nature seems to agree with the form of the scattering matrix in formula (12). As a matter of fact, the latter expression can be obtained by a model for confinement [4, 30], whereas formula (5) only expresses one of the many possible ways to obtain poles in the scattering matrix at the positions (1).

The extra poles (*continuum* poles), which disappear towards negative imaginary infinity when the overall coupling  $\lambda$  is switched off, can be observed

in the experimental signal by noticing the shoulders at about 1.4 GeV in  $\pi K$  scattering (see Fig. 2 of Ref. [21]), and at about 1.9 GeV in  $\eta' K$  (see Figs. 6 and 7 of Ref. [21]). The shoulder in  $\pi K$  corresponds to the confinement state at 1.39 GeV, on top of the larger and broader bump of the continuum pole at  $(0.77 - 0.28i)$  GeV, while the shoulder in  $\eta' K$  corresponds to the continuum pole at  $(2.04 - 0.15i)$  GeV, on top of the larger and broader bump of the confinement state at 1.77 GeV. Such subtleties in the data may have been overlooked in the corresponding Breit-Wigner analyzes.

There is one more observation to be made at this stage. The central resonance peak of the lower enhancement in  $S$ -wave  $\pi K$  scattering (see Fig. 2 of Ref. [21]) is at about 830 MeV, whereas the real part of the associated pole is at 772 MeV. Hence, identifying the real part of the pole position with the central peak of a resonance may be quite inaccurate.

With respect to the positions of the poles given in Table 1, it must be stressed again that these are model dependent. So the model (12) only indicates the existence of such poles in the respective regions of total invariant mass. A more sophisticated model, which fits the data even better, will find the poles at somewhat different positions.

## Acknowledgements

This work was partly supported by the *Fundação para a Ciência e a Tecnologia* of the *Ministério da Ciência, Tecnologia e Ensino Superior* of Portugal, under contract no. PDCT/FP/63907/2005.

## References

- [1] H. Wada, T. Kunihiro, S. Muroya, A. Nakamura, C. Nonaka and M. Sekiguchi [SCALAR Collaboration], arXiv:hep-lat/0702023.
- [2] E. van Beveren and G. Rupp, Eur. Phys. J. **C 22**, 493 (2001) [arXiv:hep-ex/0106077].
- [3] E. van Beveren, T. A. Rijken, K. Metzger, C. Dullemond, G. Rupp and J. E. Ribeiro, Z. Phys. C **30**, 615 (1986).
- [4] E. van Beveren, C. Dullemond and G. Rupp, Phys. Rev. D **21**, 772 (1980) [Erratum-ibid. D **22**, 787 (1980)].
- [5] R. L. Jaffe, arXiv:hep-ph/0701038.
- [6] E. van Beveren and G. Rupp, Phys. Rev. Lett. **91**, 012003 (2003) [arXiv:hep-ph/0305035].

- 
- [7] E. van Beveren and G. Rupp, arXiv:hep-ph/0312078.
- [8] E. van Beveren and G. Rupp, Mod. Phys. Lett. **A 19**, 1949 (2004) [arXiv:hep-ph/0406242].
- [9] E. van Beveren and G. Rupp, J. Phys. **G 34**, 1789 (2007) [arXiv:hep-ph/0703286].
- [10] R. E. Peierls, in Proceedings of the Glasgow conference on Nuclear and Meson physics (Pergamon Press, New York, 1954), p. 296.
- [11] H. Q. Zheng, Z. Y. Zhou, G. Y. Qin and Z. Xiao, AIP Conf. Proc. **717**, 322 (2004) [arXiv:hep-ph/0309242].
- [12] F. Kleefeld, PoS **HEP2005**, 108 (2006) [arXiv:hep-ph/0511096].
- [13] A. Le Yaouanc, L. Oliver, O. Pène and J. C. Raynal, Phys. Rev. D **8**, 2223 (1973).
- [14] M. Chaichian and R. Kögerler, Annals Phys. **124**, 61 (1980).
- [15] E. van Beveren, Z. Phys. C **21**, 291 (1984) [arXiv:hep-ph/0602247].
- [16] E. van Beveren and G. Rupp, Phys. Lett. B **454**, 165 (1999) [arXiv:hep-ph/9902301].
- [17] E. van Beveren, G. Rupp, T. A. Rijken and C. Dullemond, Phys. Rev. D **27**, 1527 (1983).
- [18] E. van Beveren and G. Rupp, arXiv:0706.4119 [hep-ph].
- [19] E. van Beveren and G. Rupp, AIP Conf. Proc. **687**, 86 (2003) [arXiv:hep-ph/0306155].
- [20] E. van Beveren, D. V. Bugg, F. Kleefeld and G. Rupp, Phys. Lett. B **641**, 265 (2006) [arXiv:hep-ph/0606022].
- [21] E. van Beveren, F. Kleefeld and G. Rupp, AIP Conf. Proc. **814**, 143 (2006) [arXiv:hep-ph/0510120].
- [22] E. van Beveren, Nucl. Phys. Proc. Suppl. **21**, 43 (1991).
- [23] W.-M. Yao *et al.* [Particle Data Group Collaboration], J. Phys. **G 33**, 1 (2006).
- [24] E. van Beveren and G. Rupp, Eur. Phys. J. **A 31**, 468 (2007) [arXiv:hep-ph/0610199].

- [25] X. L. Wang, et al, [Belle Collaboration], arXiv:0707.3699 [hep-ex].
- [26] C. Dullemond, T. A. Rijken and E. van Beveren, Nuovo Cimento **80**, 401 (1984).
- [27] E. van Beveren, C. Dullemond and T. A. Rijken, Phys. Rev. D **30**, 1103 (1984).
- [28] P. Estabrooks, R. K. Carnegie, A. D. Martin, W. M. Dunwoodie, T. A. Lasinski and D. W. Leith, Nucl. Phys. B **133**, 490 (1978).
- [29] D. Aston *et al.* [LASS Collaboration], Nucl. Phys. B **296**, 493 (1988).
- [30] E. van Beveren and G. Rupp, Int. J. Theor. Phys. Group Theor. Nonlin. Opt. **11**, 179 (2006) [arXiv:hep-ph/0304105].

# THE HEXAQUARK-FLAVOURED ANTI-K-N-N STATE COMPUTED MICROSCOPICALLY WITH A CLUSTERIZED OCTOQUARK

*P. Bicudo*<sup>1</sup>

CFTP and Departamento de Física  
Instituto Superior Técnico  
1049-001 Lisboa  
Portugal

## Abstract

The possible production processes of the anti-K-NN are explored. We derive microscopically, with the RGM, the microscopic derivation of the K-N and anti-K-N interactions. We discuss the binding or not binding of the different anti-K-N and anti-K-NN systems. When binding occurs, the respective decay widths are also discussed.

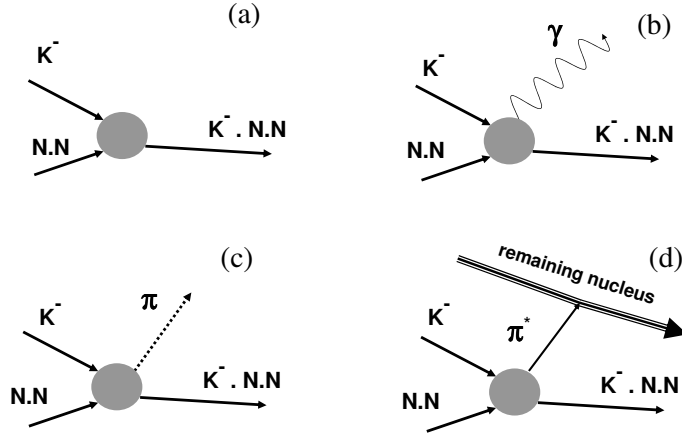
## 1 production processes

A possible molecular antikaon, nucleon and nucleon three-body system would be very interesting, both from the exotic hadronic physics perspective and from the few-body nuclear physics perspective.

Notice that the  $K^- \bullet N \bullet N$  can be produced with antikaon ( $K^-$ ) deuteron ( $p \bullet n$ ) scattering. Other exotic tetraquarks, pentaquarks or hexaquarks are also very plausible, but they are all harder to produce experimentally because they would need at least strangeness and charm. The several experiments dedicated to pentaquark searches (where not only the Kaon, but also the antikaon may interact with nuclei), or to antikaon-nuclear binding at RCNP, JLab, KEK, DAFNE and at many other laboratories, are already able to search for the proposed  $K^- \bullet N \bullet N$ . In particular evidence for  $K^- \bullet N \bullet N$  has already been found by the FINUDA collaboration at DAFNE [1]. In Fig. 1 different possible production mechanisms are depicted. They are similar

---

<sup>1</sup>bicudo@ist.utl.pt

Figure 1: Different  $K^- \bullet N \bullet N$  production mechanisms .

to the  $\Lambda(1405)$  production mechanisms, except that the  $K^-$  scatters on a deuterium nucleus, not on a hydrogen nucleus. The process in Fig. 1 (a) is only possible if the width of the  $K^- \bullet N \bullet N$  is of the order of its binding energy. The process in Fig. 1 (b) is always possible, but is suppressed by the electromagnetic coupling. Processes in Fig. 1 (c) , (d) are dominant.

## 2 From quarks to the $K \bullet N$

For the  $N \bullet N$  interaction we use the precise Nijmegen potentials [2].

We compute the  $K^- \bullet N$  interaction microscopically at the quark level. Here we assume a standard Quark Model (QM) Hamiltonian,

$$H = \sum_i T_i + \sum_{i < j, \bar{i} < \bar{j}} V_{ij} + \sum_{i, \bar{j}} A_{i\bar{j}} , \quad (1)$$

where each quark or antiquark has a kinetic energy  $T_i$  with a constituent quark mass, and the colour dependent two-body interaction  $V_{ij}$  includes the standard QM confining term and a hyperfine term,

$$V_{ij} = \frac{-3}{16} \lambda_i \cdot \lambda_j [V_{conf}(r) + V_{hyp}(r) \mathbf{S}_i \cdot \mathbf{S}_j] . \quad (2)$$

For the purpose of this paper the details of potential (2) are unimportant, we only need to estimate its matrix elements. The hadron spectrum is compatible with,

$$\langle V_{hyp} \rangle \simeq \frac{4}{3} (M_\Delta - M_N) \quad (3)$$

Moreover we include in the Hamiltonian (1) a quark-antiquark annihilation potential  $A_{i\bar{j}}$ . Notice that the quark-antiquark annihilation is constrained when the quark model produces spontaneous chiral symmetry breaking. In the  $\pi$  Salpeter equation, the annihilation potential  $A$  cancels most of the kinetic energy and confining potential  $2T + V$ ,

$$\langle A \rangle_{S=0} \simeq \langle 2T + V \rangle_{S=0} \simeq \langle V_{hyp} \rangle, \quad (4)$$

leading to a massless pion in the chiral limit. We stress that the QM of eq. (1) not only reproduces the meson and baryon spectra as quark and antiquark bound-states, but it also complies with the PCAC theorems.

We summarize [3–7] the effective potentials computed for the relevant channels,

$$\begin{aligned} V_{K \bullet N} &= c_K^2 \langle V_{hyp} \rangle \frac{23}{32} \left( 1 + \frac{20}{23} \tau_K \cdot \tau_N \right) |\phi_{000}^\alpha \rangle \langle \phi_{000}^\alpha|, \\ V_{\bar{K} \bullet N}(\mathbf{r}) &= -c_K^2 \langle V_{hyp} \rangle 2\sqrt{2} \left( 1 - \frac{4}{3} \tau_K \cdot \tau_N \right) e^{-r^2/\alpha^2}, \\ V_{\bar{K} \bullet N \leftrightarrow \pi \bullet \Lambda} &= c_\pi c_K \langle V_{hyp} \rangle \frac{9}{32} \left( 1 + \frac{4}{3} \tau_K \cdot \tau_N \right) |\phi_{000}^\alpha \rangle \langle \phi_{000}^\alpha|, \\ V_{\bar{K} \bullet N \leftrightarrow \pi \bullet \Sigma} &= c_\pi c_K \langle V_{hyp} \rangle \frac{-5}{8} \left( \frac{1+\sqrt{6}}{4} + \frac{-3+\sqrt{6}}{3} \tau_K \cdot \tau_N \right) \\ &\quad |\phi_{000}^\alpha \rangle \langle \phi_{000}^\alpha|, \end{aligned} \quad (5)$$

where  $\tau$  are  $1/2$  of the Pauli isospin matrices for the  $I = 0$  and  $I = 1$  cases, and  $c_\pi = \sqrt{E_\pi} f_\pi (\sqrt{2\pi\alpha})^{3/2} / \sqrt{3}$  is a PCAC factor, and  $\mathbf{r}$  is the relative coordinate. We calibrate our parameters in the two-body  $K \bullet N$  channels, where the diagonalization of the finite difference hamiltonian is straightforward.

### 3 Results and conclusion

It turns out that in the  $K^- \bullet N \bullet N$ ,  $I = 1/2$ ,  $S = 1$  channel there is no binding [8]. The groundstate has binding in the  $r_{12}$  coordinate, but no binding in the  $r_{123}$  coordinate. In particular, the  $r_{12}$  part of the wavefunction is localized and reproduces the deuteron wavefunction, while the  $r_{123}$  part is extended over the whole size of the large box where we quantize the wavefunction. In the limit where the size of the box is infinite, we get a bound deuteron  $p \bullet n$  and a free  $K^-$ .

In the  $S = 0$ ,  $K^- \bullet N \bullet N$  three-body system, we have binding because the attraction in the  $K^- \bullet N$  sub-systems is increased by a factor of  $5/3$  when compared with the  $S = 1$ ,  $K^- \bullet N \bullet N$  three-body system. In particular we find a binding energy  $M - m_K - 2m_N \in [-53.0, -14.2]$  MeV, and a decay width  $\Gamma \in [13.6, 28.3]$  MeV to the  $\pi \bullet \Sigma \bullet N$  and  $\pi \bullet \Lambda \bullet N$  channels [8]. The complex pole of this resonance is comparable to the one we get for the  $\Lambda(1405)$ .

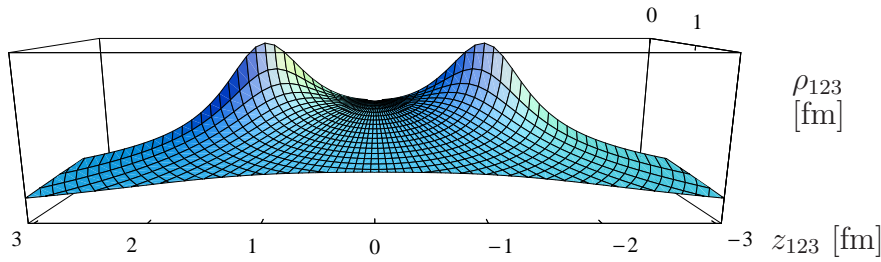


Figure 2: 3D perspective (color online) of the antikaon wavefunction, assuming two adiabatically frozen nucleons at the distance of  $r_{12} = 2.5$  fm.

## Acknowledgments

PB thanks Avraham Gal, Eulogio Oset, Paola Gianotti, Marco Cardoso and George Rupp for suggestions and discussions.

## 4 References

### References

- [1] M. Agnello *et al.* [FINUDA Collaboration], Phys. Rev. Lett. **94** (2005) 212303.
- [2] V. G. J. Stoks, R. A. M. Klomp, C. P. F. Terheggen and J. J. de Swart, Phys. Rev. C **49**, 2950 (1994) [arXiv:nucl-th/9406039]; *online codes at* <http://nn-online.org>.
- [3] P. Bicudo and J. E. Ribeiro, Z. Phys. C **38**, 453 (1988).
- [4] P. Bicudo, J. E. Ribeiro and J. Rodrigues, Phys. Rev. C **52**, 2144 (1995).
- [5] P. Bicudo, Nucl. Phys. A **748**, 537 (2005) [arXiv:hep-ph/0401106].
- [6] P. Bicudo, Phys. Rev. D **70**, 111504(R) (2004) [arXiv:hep-ph/0403146].
- [7] P. Bicudo, Phys. Rev. D **74**, 036008 (2006) [arXiv:hep-ph/0512041].
- [8] P. Bicudo, Phys. Rev. D **76**, 031502 (2007) [arXiv:hep-ph/0701008].

MENU 2007  
11th International Conference  
on Meson-Nucleon Physics and  
the Structure of the Nucleon  
September 10-14, 2007  
IKP, Forschungszentrum Jülich, Germany

## THREE-BODY FORCE EFFECTS IN NEUTRON-DEUTERON SCATTERING AT 95 MeV

*J. Blomgren, P. Mermod, C. Johansson, J. Klug, L. Nilsson, N. Olsson<sup>1</sup>,  
S. Pomp, U. Tippawan<sup>2</sup>, A. Öhrn, M. Österlund*  
Department of Neutron Research  
Uppsala University  
Uppsala, Sweden

*B. Bergenwall, P. Nadel-Turonski<sup>3</sup>*  
Department of Radiation Sciences  
Uppsala University  
Uppsala, Sweden

*O. Jonsson, A. Prokofiev, P.-U. Renberg*  
The Svedberg Laboratory  
Uppsala University  
Uppsala, Sweden

*Y. Maeda, H. Sakai, A. Tamii*  
Department of Physics  
Tokyo University  
Tokyo, Japan

### Abstract

Three-body force effects have been studied in neutron-deuteron scattering at 95 MeV. Three different experiments, performed with different experimental setups, have been used to provide data covering the full angular distribution with unprecedented precision in the region of the cross section minimum, where three-nucleon forces are expected to be significant. The use of different

---

<sup>1</sup>Also at Swedish Defence Research Agency, Stockholm, Sweden

<sup>2</sup>Also at Fast Neutron Research Facility, Chiang Mai University, Chiang Mai, Thailand

<sup>3</sup>Presently at George Washington University, Washington, D.C., USA

setups allow detailed studies of systematic effects in the experimental data. Measurements of the ratio between neutron-proton and neutron-deuteron scattering have been performed to provide data free from systematic uncertainties related to cross-section normalization. The data display significant deviations from predictions based on two-nucleon interactions only, while they are perfectly described by theories including three-nucleon forces.

## 1 Introduction

The nucleon-nucleon ( $NN$ ) interaction can be used as a basic tool to describe the properties and interactions of nuclei. For this purpose,  $NN$  potentials, which are based on meson-exchange theories, have been developed: the most widely used ones are the Paris potential [1], the Argonne AV18 potential [2], the CD-Bonn potential [3,4] and the Nijmegen potentials [5]. After proper adjustment of the free parameters, these models are able to describe very well a restricted  $pp$  and  $np$  data base below 350 MeV [6].

The next step to demonstrate the success of this approach is to test the  $NN$  potentials in three-nucleon ( $3N$ ) systems. Quantitative descriptions of  $3N$  systems can be provided rigorously by using  $NN$  potentials in the Faddeev equations [7]. However, theoretical considerations indicate that the description of systems made of more than two nucleons is not complete if three-body forces are not taken into account (and, in principle, also four-body forces, five-body forces, etc.). Formally,  $3N$  forces can be represented by introducing a  $3N$  potential in the Faddeev equations. The most widely used  $3N$  potentials are the Tucson-Melbourne [8,9] and Urbana [10,11] forces. As a first experimental evidence, the  ${}^3\text{H}$  and  ${}^3\text{He}$  binding energies can be reproduced model-independently taking  $3N$  forces into account [12], while calculations using only  $NN$  interactions underestimate them by typically half an MeV [3]. Interestingly, the  ${}^4\text{He}$  binding energy can also be described correctly with combined  $NN$  and  $3N$  forces [13], indicating that the role of four-nucleon forces is not significant.

The ultimate goal of nuclear physics would be to have a single consistent theory that could describe both nucleon and nuclear properties and dynamics. As pointed out in, e.g., Refs. [6] and [14], an appropriately tailored effective field theory, rooted in the symmetries of QCD, might be a tool powerful enough to succeed in such an ambitious program, at least for few-nucleon systems. In particular, chiral symmetry breaking can be analyzed in terms of an effective field theory, called chiral perturbation theory (CHPT). This model can be applied to describe consistently the interaction between pions and nucleons, as well as the pion-pion interaction. Calculations made within

the CHPT framework at next-to-next-to-leading order implicitly include  $3N$  forces [15, 16]. Calculations at the next higher order were made recently [17, 18], allowing for instance an excellent description of  $NN$  phase shifts.

Experimental investigations of three-nucleon systems are essential for determining the properties of  $3N$  forces. Besides the  ${}^3\text{H}$  and  ${}^3\text{He}$  binding energies, a number of observables that may reveal the effects of  $3N$  forces have been identified. We will concentrate our discussion to nucleon-deuteron scattering in the energy range 65–250 MeV. At these energies, significant  $3N$ -force contributions can potentially be seen in the elastic scattering angular distribution [19, 20] as well as for various spin-transfer observables in elastic scattering [7]. In addition, observables in the break-up process in various kinematical configurations are also expected to provide signatures of  $3N$  forces [21, 22]. Existing proton-deuteron elastic scattering data between 65 and 250 MeV can be found in Refs. [23–35], and proton-deuteron break-up data in Refs. [36–40]. Except for Refs. [23, 26], these data were obtained with polarized beams, and polarization observables could be extracted. Comparison of experimental analysing powers with theoretical predictions show a puzzling picture where data and predictions agree only partially with each other. Many of these results call for a better understanding of the spin structure of the three-nucleon forces: possible solutions could be a refinement of the  $3N$  force terms in CHPT [15] or the introduction of new types of diagrams in the  $3N$  potentials [41]. While polarization observables are extremely valuable especially for studying the details of the  $3N$  interactions, in order to validate the whole approach of introducing  $3N$  forces at all, an observable that would give a clear and unambiguous signal is desirable. As pointed out in, e.g., Ref. [19], the differential cross section of nucleon-deuteron elastic scattering is expected to reveal substantial effects of  $3N$  forces in the minimum region of the angular distribution. This can be understood in the following way: the contributions from  $NN$  interactions are strongly forward and backward peaked, while the contributions from  $3N$  interactions should be roughly isotropic. Thus, the  $3N$ -force contribution to the cross section would be particularly significant relative to  $NN$  interactions in the angular range of the cross-section minimum. Around 100 MeV, the effect of  $3N$  forces is expected to increase the cross section by about 30% in the minimum, as predicted [19] by Faddeev calculations including the Tucson-Melbourne  $3N$  force [8] with parameters adjusted to the triton binding energy.

Thus, both neutron-deuteron ( $nd$ ) and proton-deuteron ( $pd$ ) elastic scattering differential cross sections should provide robust investigations of  $3N$  forces. The existing  $pd$  elastic scattering data [23–29, 32–34] tend to show the expected effects in the cross-section minimum: the descriptions are generally improved when taking  $3N$  forces into account. The contribution from the

Coulomb interaction in  $pd$  scattering is not known with certainty to be negligible in the minimum region, thus complicating the interpretation of these results. Recent calculations suggest that Coulomb interactions should not result in significant effects in the minimum of the  $pd$  elastic scattering angular distribution above 65 MeV [42,43]. The question of Coulomb effects—and thus also the question of  $3N$  force effects—can be definitively settled by  $nd$  scattering experiments. There are  $nd$  data at 67 MeV [44] consisting essentially of an analyzing power measurement. Three  $nd$  experiments at 95 MeV, previously reported in Refs. [45–47], agree well with the predictions including  $3N$  forces. Existing data at 152 MeV [48] give the same picture. Recent data at 250 MeV [49], together with  $pd$  data at the same energy [33], reveal an effect in the cross-section minimum which is too large to be accounted for by any theory. At such large energies, part of the explanation for this failure could be the lack of a full relativistic treatment in the calculations. Pioneering studies [50,51] show that relativistic effects are expected to increase the cross section in the region of backward angles at large energies. At 95 MeV, the energy of the present work, such effects are not expected to contribute significantly.

In the present work, data from three  $nd$  scattering experiments are presented. By detecting either the scattered neutron or the recoil deuteron, we were able to cover the angular range from 15 to 160 degrees in the c.m. system. By using two different detector setups in various configurations, we could keep the systematic uncertainties under control. Additionally, by measuring the neutron-proton ( $np$ ) scattering differential cross section and, in the case where scattered neutrons were detected, also elastic scattering in carbon (i.e., the  $^{12}\text{C}(n,n)$  reaction), the systematic error due to uncertainties in the normalization factors was minimized.

The present  $np$  data give supplementary information about the  $np$  angular distribution at 95 MeV (for previous data, see, e.g., Refs. [52,53]). In many experiments, neutron cross sections are measured relative to the  $np$  cross section [53], i.e., it is used as a cross-section standard. Neutron-proton scattering plays an important role in nuclear physics, since it can be used to validate  $NN$  potentials and to derive a value of the absolute strength of the strong interaction. The extensive database of  $np$  differential cross sections is not always consistent and, not unrelated, there are still problems with the determination of a precise value of the  $\pi NN$  coupling constant [6,54,55].

In the  $nd$  experiment where the scattered neutrons were detected, we could also obtain elastic scattering angular distributions for carbon and oxygen at 95 MeV, which are not discussed further here. Besides their interest in fundamental nuclear theory, these data are relevant for medical treatment of tumors with fast neutrons as well as in dosimetry, since the human body

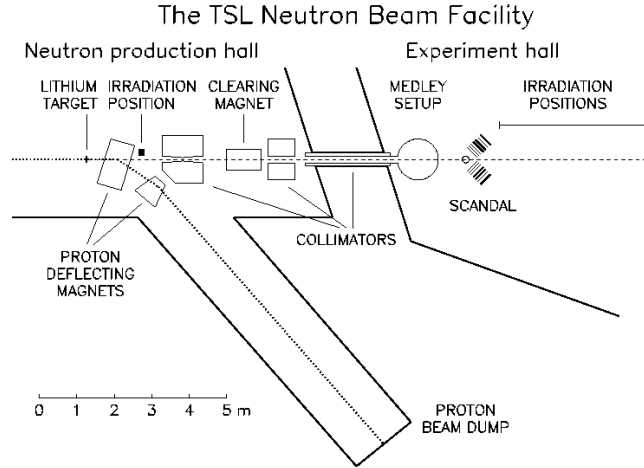


Figure 1: Schematic view of the Uppsala neutron beam facility before its upgrade in 2004.

contains significant amounts of carbon and oxygen. Recoil nuclei from elastic and inelastic scattering are expected to account for more than 10% of the cell damage, the rest being mainly due to  $np$  scattering and neutron-induced emission of light ions [57, 58]. The oxygen data may also be relevant for future incineration of nuclear waste in subcritical reactors fed by a proton accelerator, where the nuclear fuel might be in oxide form. These data were obtained as by-products of the target handling, e.g., due to the use of heavy water as deuterium target.

## 2 Experimental procedure

### 2.1 Neutron beam and detector setups

A full account of the experimental details and analysis procedures have been published in Ref. [47], and only an introduction is presented here. The present experiments were performed with the two experimental setups MEDLEY [59] and SCANDAL [60] at the neutron beam facility (before upgrade, see Fig. 1) at The Svedberg Laboratory in Uppsala, Sweden. This facility has been described in detail in Ref. [60], and therefore only a brief outline will be given here. The neutrons were produced with the  ${}^7\text{Li}(p,n){}^7\text{Be}$  reaction, using a 98

MeV proton beam of about  $5 \mu\text{A}$  hitting an 8 mm thick neutron production target consisting of lithium enriched to 99.98% in  ${}^7\text{Li}$ . The resulting neutron spectrum consisted of a high-energy peak at  $94.8 \pm 0.5$  MeV with an energy spread of 2.7 MeV (FWHM) and a low-energy tail which was suppressed by time-of-flight techniques. After the production target, the proton beam was bent into a well-shielded beam dump where the beam current was integrated in a Faraday cup for relative beam monitoring consistency checks. At the MEDLEY target position 9.15 m after the neutron production target, the neutron beam was about 8 cm in diameter and had an intensity of about  $5 \times 10^4 \text{ s}^{-1} \text{ cm}^{-2}$ . At the SCANDAL target position 10.70 m after the lithium target, the beam was about 9 cm in diameter and had an intensity of about  $4 \times 10^4 \text{ s}^{-1} \text{ cm}^{-2}$ . The neutron beam was transported in a vacuum system which was terminated with a 0.1 mm thick stainless steel foil at the exit of the MEDLEY chamber. Immediately after the foil, two fission detectors were mounted for relative monitoring of the neutron fluence: one monitor was based on thin-film breakdown counters (TFBC) [61] and the other one, which was more stable and had much better statistics, on an ionization chamber (ICM). The MEDLEY target, the vacuum chamber exit foil, and the neutron monitors were thin enough to consider the neutron beam as negligibly affected.

The MEDLEY vacuum chamber is a cylinder of 80 cm inner diameter. Targets were mounted onto frames attached to the center of the ceiling, with a remote control allowing to switch between up to three different frames without opening the vacuum chamber. Eight telescopes were placed on rails emerging radially at  $20^\circ$  separation from each other on a rotatable table. Two silicon detectors and one CsI detector could be mounted inside each telescope. Thin (50 or 60  $\mu\text{m}$  thickness) and thick (400 or 500  $\mu\text{m}$  thickness) silicon detectors were available. The CsI crystals were thick enough to detect protons with energies up to 110 MeV. This combination of silicon detectors and CsI crystals allowed light ion detection, identification and energy measurement in the energy range 3–110 MeV. In order to define precisely the active detection area (and solid angle), either active plastic scintillators or passive aluminum rings were used as collimators. A full description of the MEDLEY setup is given in Ref. [59].

The SCANDAL (SCattered Nucleon Detection AssembLy) setup, previously described in Ref. [60], consists of two identical arms that can be positioned on either side of the beam and rotated around the target position. Each SCANDAL arm was equipped with a 2 mm thick veto scintillator for charged-particle rejection, two converter scintillators of 20 mm and 10 mm thickness for neutron-proton conversion, a 2 mm thick  $\Delta E$  plastic scintillator for triggering, two drift chambers (DCH) giving two horizontal and

two vertical coordinates for proton tracking, another 2 mm thick  $\Delta E$  plastic scintillator for triggering, and an array of twelve CsI detectors that defined twelve angular bins. The CsI detectors as well as the plastic scintillators were read out by photomultiplier (PM) tubes. The CsIs had one PM tube each, and the scintillators two each, mounted adjacent to each other on one of the longer, horizontal sides. The proton energy resolution was on average 3.7 MeV (FWHM) [60], varying between the individual CsI crystals due to internal properties of the detectors. The setup could be used for direct detection of protons or deuterons coming from the target by simply removing the veto and converter scintillators. This option allowed to measure  $np$  and  $nd$  elastic scattering at backward angles. In proton/deuteron detection mode, a multitarget (MTGT) box permitted to use up to seven targets at the same time, sandwiched between multiwire proportional counters (MWPCs). In this way it was possible to determine in which target the reaction took place and to veto charged particles in the beam.

### 3 Results and discussion

The final results for  $np$  and  $nd$  scattering, recently reported in Refs. [45–47], are shown in Fig. 2. The  $nd$  differential cross section is shown in the middle panel. For the data in proton/deuteron detection mode, the ratio of  $nd$  to  $np$ —a quantity which is independent of the absolute normalization—is plotted in the bottom panel as a function of the proton/deuteron angle in the laboratory.

The  $np$  data are valuable in the sense that they increase the database in the intermediate energy region, where the systematic uncertainties are not always under satisfying control. Many applications involve measurements relative to the  $np$  cross section, and new data are therefore most welcome. The  $np$  data from the three present experiments are in good overall agreement with each other and with predictions based on modern  $NN$  interactions. This allows us to validate the quality of the  $nd$  data since the  $np$  and  $nd$  differential cross sections were measured under essentially the same conditions.

The  $nd$  data agree well with each other in the regions where they overlap. We can compare them with Faddeev calculations using various  $NN$  potentials, and see if the description is improved when including  $3N$  potentials. The curves obtained with the CD-Bonn  $NN$  potential [4] including (dashed line) and not including (solid line) the Tucson-Melbourne  $3N$  potential TM99 [9] are shown in Fig. 2. Predictions obtained with the Argonne AV18  $NN$  potential [2] and the Nijmegen potentials Nijm1 and Nijm2 [5], which can also be combined with the TM99  $3N$  potential, are not shown in

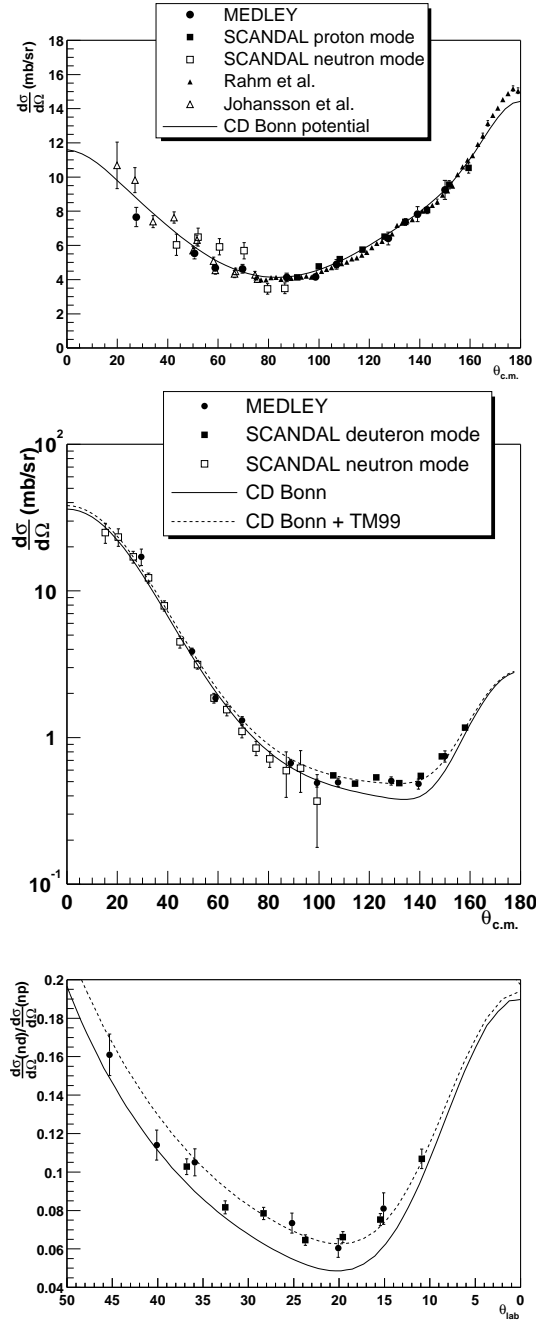


Figure 2: Combined data of the three present experiments, for the *np* (top panel), *nd* (middle panel) and the ratio between *nd* and *np* (bottom panel) elastic scattering differential cross sections at 95 MeV. The theoretical curves for *nd* scattering were obtained with Faddeev calculations [19] with the CD-Bonn (2001) potential [4] without 3*N* forces (solid line) and with the TM99 3*N* potential [9] (dashed line).

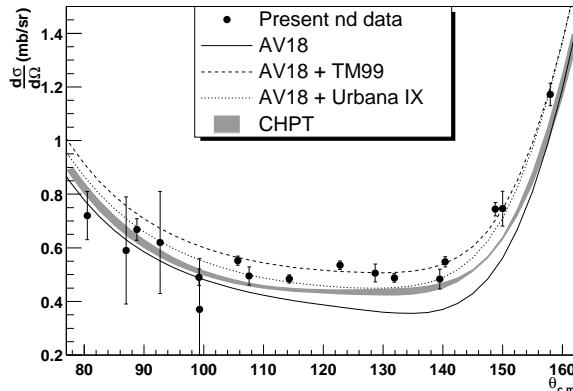


Figure 3: The present *nd* data (filled dots) in the angular range  $80^\circ < \theta_{c.m.} < 160^\circ$ . The solid, dashed, and dotted curves were obtained from Faddeev calculations with the Argonne AV18 potential [2] without  $3N$  forces, with the Tucson-Melbourne (TM99)  $3N$  potential [9], and with the Urbana IX  $3N$  potential [11], respectively. The gray band was obtained from chiral perturbation theory at next-to-next-to-leading order [15].

this figure since they give very similar predictions. In the minimum region, our data are well described by the Faddeev calculations including the TM99  $3N$  potential, while they are incompatible with the same calculations without  $3N$  forces. This behavior is also observed when considering the ratio of the *nd* to the *np* cross sections (bottom panel of Fig. 2), which is free from normalization uncertainties. The AV18 potential can also be combined with the Urbana IX  $3N$  potential [11]. The curve obtained with this choice for the  $3N$  force (shown as a dotted line in Fig. 3) gives a different description than the curve obtained with the TM99  $3N$  potential (dashed line). The theoretical prediction obtained from CHPT at next-to-next-to-leading order [15] is shown as a gray band in Fig. 3.

It is quantitatively illustrative to compute the reduced  $\chi^2$  between our data and the calculations for the *nd* differential cross section in the minimum, i.e., in the angular range  $80^\circ < \theta_{c.m.} < 160^\circ$  (the 17 data points shown in Fig. 3). The reduced  $\chi^2$  for different choices of the potentials used in the Faddeev calculations are listed in Table 1. When no  $3N$  forces are included, the  $\chi^2$  are unreasonably large, in minimum 18. The best description is given by the CD-Bonn potential (version 1996) with the TM99  $3N$  force, with a  $\chi^2$  of 2.1. With the AV18 potential, the *nd* differential cross section is slightly better described with the TM99  $3N$  potential ( $\chi^2 = 2.3$ ) than with

Table 1: Reduced  $\chi^2$  between the present measured  $nd$  differential cross section in the minimum ( $80^\circ < \theta_{c.m.} < 160^\circ$ , or all points shown in Fig. 3) and the Faddeev calculations with different models for the potentials, either without  $3N$  forces or combined with a  $3N$  potential.

$NN$ potential	Without $3N$	TM99 [9]	Urbana IX [11]
AV18 [2]	25	2.3	3.5
CD Bonn (1996) [3]	21	2.1	—
CD Bonn (2001) [4]	18	2.2	—
Nijm1 [5]	21	3.2	—
Nijm2 [5]	25	2.4	—

Table 2: Reduced  $\chi^2$  for the ratio of the  $nd$  to the  $np$  differential cross sections in the minimum ( $10^\circ < \theta_{lab} < 46^\circ$ , or all points shown in the bottom panel of Fig. 2). The present data are compared with calculations with different models for the potentials (for  $nd$  scattering, either without  $3N$  forces or combined with a  $3N$  potential).

$NN$ potential	Without $3N$	TM99 [9]	Urbana IX [11]
AV18 [2]	17	2.7	1.2
CD Bonn (1996) [3]	13	0.6	—
CD Bonn (2001) [4]	12	1.7	—
Nijm1 [5]	15	3.8	—
Nijm2 [5]	18	2.8	—

the Urbana IX potential ( $\chi^2 = 3.5$ ). The CHPT prediction at next-to-next-to-leading order gives a  $\chi^2$  of 6.5 (not given in the table). Note that the deviations from unity may be partly due to the normalization uncertainties in the data [46]. For this reason, the ratio of the  $nd$  differential cross section to the  $np$  differential cross section—in this ratio, many sources of uncertainties (including the uncertainty in the absolute normalization) are cancelled out—is a more practical observable for testing the models. The reduced  $\chi^2$  between our data (for the 13 data points shown in the bottom panel of Fig. 2) and calculations using different  $NN$  and  $3N$  potentials for  $nd$  scattering are listed in Table 2. When the ratio is considered, the AV18 potential combined with Urbana IX gives a near-perfect description ( $\chi^2 = 1.2$ ), and the best description is still given by CD-Bonn (1996) + TM99 ( $\chi^2 = 0.6$ ).

The present  $nd$  data can be compared with  $pd$  data at the same energy to examine the effects of the Coulomb force in  $pd$  scattering (see Fig. 4).

At 250 MeV, precise  $nd$  and  $pd$  data have been published, allowing a detailed analysis of Coulomb effects [62]. The data deviate significantly from

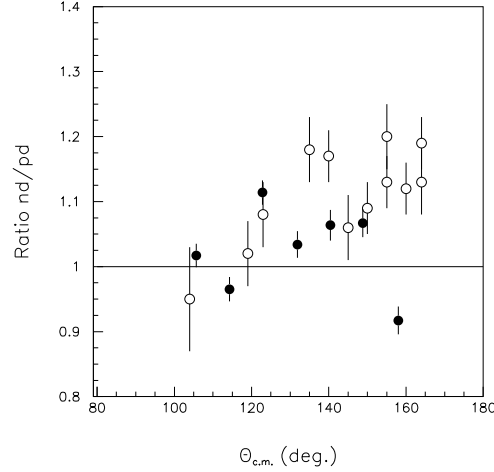


Figure 4: The ratio of *nd* and *pd* scattering cross sections at 95 MeV (filled symbols). The error bars display the full uncertainty, statistical and systematic, with respect to the *nd* data. An additional 5 % uncertainty should be attributed to the *pd* data. The *pd* data have been measured at 90 MeV, and have been scaled down by 8 % to take the energy dependence of the *pd* cross section into account. The unfilled symbols show the same ratio at 250 MeV [62].

the theory predictions. Overall, the ratio is close to unity, but there is an oscillatory behaviour, with *nd* cross sections about 20 % lower than *pd* around 90 degrees, and 20 % higher than *pd* around 120–160 degrees. If this is not due to experimental artifacts, one possible explanation could be isospin dependence in the  $2N$  or  $3N$  models, or both.

In Fig. 4, the ratio *nd/pd* data at 95 MeV is displayed. There is no high-quality *pd* experiment at 95 MeV, but recently data at 90 MeV have been published [63], and an experiment at 100 MeV is under analysis [64]. In the figure, the 90 MeV data have been used, scaled to 95 MeV (8 % reduction in cross section, derived from the energy dependence of predictions based on the AV18  $2N$  force [2] in combination with the U-IX  $3N$  force [11]). No theory prediction of the Coulomb correction is presently available at this energy.

It can be noted that like at 250 MeV, the *nd* data are above the *pd* data

at 95 MeV in the 100-160 degree range, although slightly less so. It should be noted, however, that, if the  $pd$  data are renormalized further down by 5 %, which is their reported systematic uncertainty, the effect is compatible with the situation at 250 MeV.

## 4 Conclusions

We have measured the full  $nd$  angular distribution at 95 MeV in three independent experiments, using the MEDLEY setup and the SCANDAL setup either in deuteron or neutron detection mode. The absolute normalization was obtained relative to either the  $np$  cross section or the total  $^{12}\text{C}(n,n)$  elastic scattering cross section, with an accuracy of  $\pm 4\%$ . We obtained excellent precision in the angular range of the  $nd$  cross-section minimum. The data are in good agreement with Faddeev calculations using modern  $NN$  potentials and including  $3N$  forces from a  $2\pi$ -exchange model, while the calculations without  $3N$  forces fail to describe the data. CHPT calculations at next-to-next-to-leading order represent an improvement compared to calculations with  $NN$  forces only, but still underestimate the data in the minimum region.

The present experimental work provides valuable pieces of information with the purpose of being able to describe nuclear interaction from the basic interactions between nucleons. The  $np$  and  $nd$  data help to refine the  $NN$  and  $3N$  potentials as well as effective field theories, which can be applied in systems of more than three nucleons. Thanks to the ongoing advances in computational resources, microscopic calculations directly producing nuclear shell structure from two- and three-nucleon potentials have become feasible and have been attempted for nuclear masses up to  $A=13$  [11, 65]. The inclusion of a  $3N$  potential in these calculations has generally a positive effect on the nuclear binding energy and on the level ordering and level spacing of the low-lying excitation spectra. The success of this method depends on the quality of the  $3N$  potentials, which can be effectively tested versus experimental data in three-nucleon systems.

## Acknowledgments

We wish to thank the technical staff of the The Svedberg Laboratory for enthusiastic and skillful assistance. We are very grateful to E. Epelbaum, W. Glöckle, H. Kamada and H. Witała for contributions concerning the theoretical part. We have appreciated the precious collaboration of K. Hatanaka and N. Kalantar-Nayestanaki. This work was supported by the Swedish Nuclear

Fuel and Waste Management Company, the Swedish Nuclear Power Inspectorate, Ringhals AB, the Swedish Defence Research Agency and the Swedish Research Council.

## 5 References

### References

- [1] M. Lacombe, B. Loiseau, J.M. Richard, R. Vinh Mau, J. Côté, P. Pirès, and R. de Tournel, *Phys. Rev. C* **21**, 861 (1980).
- [2] R.B. Wiringa, V.G.J. Stoks, and R. Schiavilla, *Phys. Rev. C* **51**, 38 (1995).
- [3] R. Machleidt, F. Sammarruca, and Y. Song, *Phys. Rev. C* **53**, R1483 (1996).
- [4] R. Machleidt, *Phys. Rev. C* **63**, 024001 (2001).
- [5] V.G.J. Stoks, R.A.M. Klomp, C.P.F. Terheggen, and J.J. de Swart, *Phys. Rev. C* **49**, 2950 (1994).
- [6] R. Machleidt and I. Slaus, *J. Phys. G* **27**, R69 (2001).
- [7] W. Glöckle, H. Witała, D. Hüber, H. Kamada, and J. Golak, *Phys. Rep.* **274**, 107 (1996).
- [8] S.A. Coon, M.D. Scadron, P.C. McNamee, B.R. Barrett, D.W.E. Blatt, and B.H.J. McKellar, *Nucl. Phys.* **A317**, 242 (1979); S.A. Coon and W. Glöckle, *Phys. Rev. C* **23**, 1790 (1981).
- [9] J.L. Friar, D. Hüber and U. van Kolck, *Phys. Rev. C* **59**, 53 (1999); S.A. Coon and H.K. Han, *Few-Body Syst.* **30**, 131 (2001).
- [10] J. Carlson, V.R. Pandharipande, and R.B. Wiringa, *Nucl. Phys.* **A401**, 59 (1983).
- [11] B.S. Pudliner, V.R. Pandharipande, J. Carlson, Steven C. Pieper, and R.B. Wiringa, *Phys. Rev. C* **56**, 1720 (1997).
- [12] A. Nogga, A. Kievsky, H. Kamada, W. Glöckle, L.E. Marcucci, S. Rosati, and M. Viviani, *Phys. Rev. C* **67**, 034004 (2003).

- 
- [13] A. Nogga, H. Kamada, W. Glöckle, and B.R. Barrett, Phys. Rev. C **65**, 054003 (2002).
- [14] Ulf-G. Meissner, Nucl. Phys. **A737**, 110 (2004).
- [15] E. Epelbaum, A. Nogga, W. Glöckle, H. Kamada, Ulf-G. Meissner, and H. Witała, Phys. Rev. C **66**, 064001 (2002).
- [16] P.F. Bedaque and U. van Kolck, Annu. Rev. of Nucl. Part. Sci. **52**, 339 (2002).
- [17] D.R. Entem and R. Machleidt, Phys. Rev. C **68**, 041001(R) (2003).
- [18] E. Epelbaum, W. Glöckle, and Ulf-G. Meissner, Nucl Phys. **A747**, 362 (2005).
- [19] H. Witała, W. Glöckle, D. Hüber, J. Golak, and H. Kamada, Phys. Rev. Lett. **81**, 1183 (1998).
- [20] S. Nemoto, K. Chmielewski, S. Oryu, and P.U. Sauer, Phys. Rev. C **58**, 2599 (1998).
- [21] L.D. Knutson, Phys. Rev. Lett. **73**, 3062 (1994).
- [22] J. Kuroś-Żołnierczuk, H. Witała, J. Golak, H. Kamada, A. Nogga, R. Skibiński, and W. Glöckle, Phys. Rev. C **66**, 024003 (2002).
- [23] O. Chamberlain and M.O. Stern, Phys. Rev. **94**, 666 (1954).
- [24] H. Postma and R. Wilson, Phys. Rev. **121**, 1229 (1961).
- [25] K. Kuroda, A. Michalowicz, and M. Poulet, Nucl. Phys. **88**, 33 (1966).
- [26] G. Igo, J.C. Fong, S.L. Verbeck, M. Goitein, D.L. Hendrie, J.C. Carroll, B. McDonald, A. Stetz, and M.C. Makino, Nucl. Phys. **A195**, 33 (1972).
- [27] R.E. Adelberger and C.N. Brown, Phys. Rev. D **5**, 2139 (1972).
- [28] H. Shimizu, K. Imai, N. Tamura, K. Nisimura, K. Hatanaka, T. Saito, Y. Koike and Y. Taniguchi, Nucl. Phys. **A382**, 242 (1982).
- [29] H. Sakai *et al.*, Phys. Rev. Lett. **84**, 5288 (2000).
- [30] R.V. Cadman *et al.*, Phys. Rev. Lett. **86**, 967 (2001).
- [31] K. Ermisch *et al.*, Phys. Rev. Lett. **86**, 5862 (2001).

- 
- [32] K. Sekiguchi *et al.*, Phys. Rev. C **65**, 034003 (2002).
- [33] K. Hatanaka *et al.*, Phys. Rev. C **66**, 044002 (2002).
- [34] K. Ermisch *et al.*, Phys. Rev. C **68**, 051001(R) (2003).
- [35] K. Sekiguchi *et al.*, Phys. Rev. C **70**, 014001 (2004).
- [36] M. Allet *et al.*, Phys. Rev. C **50**, 602 (1994).
- [37] M. Allet *et al.*, Phys. Lett. B **376**, 255 (1996).
- [38] J. Zejma *et al.*, Phys. Rev. C **55**, 42 (1997).
- [39] K. Bodek *et al.*, Few Body Syst. **30**, 65 (2001).
- [40] St. Kistryn *et al.*, Phys. Rev. C **68**, 054004 (2003);  
St. Kistryn *et al.*, Phys. Rev. C **72**, 044006 (2005).
- [41] L. Canton and W. Schadow, Phys. Rev. C **62**, 044005 (2000); L. Canton  
and W. Schadow, Phys. Rev. C **64**, 031001(R) (2001).
- [42] A. Kievsky, M. Viviani, and L.E. Marcucci, Phys. Rev. C **69**, 014002  
(2004).
- [43] A. Deltuva, A.C. Fonseca, and P.U. Sauer, Phys. Rev. C **71**, 054005  
(2005).
- [44] H. Rühl *et al.*, Nucl. Phys. **A524**, 377 (1991).
- [45] P. Mermod *et al.*, Phys. Lett. B **597**, 243 (2004).
- [46] P. Mermod *et al.*, Phys. Rev. C **72**, 061002(R) (2005).
- [47] P. Mermod *et al.*, Phys. Rev. C **74**, 054002 (2006).
- [48] J.N. Palmieri, Nucl. Phys. **A188**, 72 (1972).
- [49] Y. Maeda, Ph.D. thesis, University of Tokyo (2004), unpublished.
- [50] H. Witała, J. Golak, W. Glöckle, and H. Kamada, Phys. Rev. C **71**,  
054001 (2005).
- [51] K. Sekiguchi *et al.*, Phys. Rev. Lett. **95**, 162301 (2005).
- [52] J. Rahm *et al.*, Phys. Rev. C **63**, 044001 (2001).
- [53] C. Johansson *et al.*, Phys. Rev. C **71**, 024002 (2005).

- [54] J. Blomgren, N. Olsson, and J. Rahm, Phys. Scr. **T87**, 33 (2000).
- [55] M. Sarsour *et al.*, Phys. Rev. Lett. **94**, 082303 (2005).
- [56] J. Klug *et al.*, Phys. Rev. C **68**, 064605 (2003).
- [57] M.B. Chadwick, P.M. DeLuca Jr., and R.C. Haight, Radiat. Prot. Dosim. **70**, 1 (1997).
- [58] J. Blomgren and N. Olsson, Radiat. Prot. Dosim. **103**, 293 (2003).
- [59] S. Dangtip *et al.*, Nucl. Instr. Meth. **A 452**, 484 (2000).
- [60] J. Klug *et al.*, Nucl. Instr. Meth. **A 489**, 282 (2002).
- [61] A.N. Smirnov, V.P. Eismont, and A.V. Prokofiev, Rad. Meas. **25**, 151 (1995).
- [62] Y. Maeda, *et al.*, Phys. Rev. C **76**, 014004 (2007).
- [63] H.R. Amir-Ahmadi *et al.*, Phys. Rev. C **75**, 041001(R) (2007).
- [64] K. Hatanaka, private communication.
- [65] P. Navrátil and W.E. Ormand, Phys. Rev. C **68**, 034305 (2003).

## DECAYS OF $\eta$ AND $\eta'$

*B. Borasoy*

Helmholtz-Institut für Strahlen- und Kernphysik (Theorie),  
Universität Bonn Nußallee 14-16, D-53115 Bonn, Germany

### Abstract

Decays of the  $\eta$  and  $\eta'$  are suited to study symmetries and symmetry violations in QCD, e.g., the chiral anomalies and the axial U(1) anomaly in strong interactions, as well as isospin breaking due to the quark mass difference  $m_u - m_d$ . We present a theoretical framework which is suited to describe  $\eta, \eta'$  decays in a consistent and uniform manner. It is based on the combination of the chiral effective Lagrangian with a coupled-channels Bethe-Salpeter equation which satisfies unitarity constraints. Very good agreement with experimental data is achieved.

## 1 Introduction

Quantum chromodynamics (QCD) is the field theory of strong interactions. In low-energy hadron physics, however, it cannot be directly applied by means of a perturbative series in the strong coupling  $\alpha_s$  which is large in this case [1]. In the non-perturbative regime of QCD one must thus resort to alternative model-independent approaches.

A promising approach is provided by lattice simulations which are a numerical solution to QCD, see e.g. [2]. But due to limited computing resources lattice QCD simulations must be performed at finite lattice spacings and volumes and at unphysically large pion masses. The various extrapolations to the physical world remain a challenging task and imply systematic uncertainties.

Chiral perturbation theory (ChPT), the effective field theory of QCD at low energies, constitutes an alternative model-independent framework [3–5]. ChPT is based on the observation that at low energies the relevant, effective degrees of freedom of the strong interactions are hadrons composed of confined quarks and gluons. The QCD Lagrangian is replaced by an effective Lagrangian which is formulated in terms of the effective degrees of freedom. At sufficiently low energies these are the pions, kaons and the eta.

The effective Lagrangian incorporates all relevant symmetries and symmetry-breaking patterns of QCD, in particular, the (approximate)  $SU(3)_L \times SU(3)_R$  chiral symmetry which is broken down spontaneously to  $SU(3)_V$ .

The conventional  $SU(3)$  chiral effective Lagrangian is a function of the octet of Goldstone boson fields ( $\pi, K, \eta$ ). Making use of the hypothesis of the partially conserved axial vector current (PCAC) and Goldstone boson pole dominance one concludes that the interaction between the Goldstone bosons vanishes at zero momentum. A low-energy expansion can be formulated wherein the Green's functions are expanded in powers of Goldstone boson masses and small momenta: a *chiral counting scheme* is established.

Although the classical QCD Lagrangian is invariant under the extended group  $SU(3)_L \times SU(3)_R \times U(1)_A \times U(1)_V$  quantum effects destroy the  $U(1)_A$  symmetry of the classical Lagrangian: a so-called *anomaly* occurs.<sup>1</sup> Under axial  $U(1)$  transformations the path integral picks up an additional contribution from the fermion determinant such that the full quantum theory does not exhibit the classical axial  $U(1)$  symmetry [6]. The axial  $U(1)$  anomaly in QCD prevents the  $\eta'$  from being a Goldstone boson which is phenomenologically manifested in its relatively large mass of 958 MeV—much larger than the masses of the Goldstone boson octet. Hence, the  $\eta'$  is not included explicitly in conventional  $SU(3)$  ChPT, albeit its effects are hidden in coupling constants [5, 7]. Nonetheless, ChPT can be extended to include the  $\eta'$  as a dynamical degree of freedom [8]. In addition to the chiral expansion one can impose an expansion in  $1/N_c$ —where  $N_c$  is the number of colors—which allows for a rigorous counting scheme also in the presence of the  $\eta'$  and a perturbative loopwise expansion can be carried out [9].

However, large unitarity corrections due to final-state interactions, which are already substantial in  $\eta \rightarrow 3\pi$ , must be accounted for in a non-perturbative fashion [10, 11]. Final state interactions are expected to be even more important in  $\eta'$  decays due to larger phase space and the presence of nearby resonances. This cannot be accomplished within ChPT wherein unitarity is restored only perturbatively in the chiral expansion, but one must rather resort to non-perturbative methods. To this aim, the combination of the chiral effective Lagrangian with a coupled-channels Bethe-Salpeter equation (BSE) has proven useful. In this approach, unitarity corrections are taken into account by deriving the interaction kernel for meson-meson scattering from the effective Lagrangian and iterating it to infinite order by means of the BSE. Such chiral unitary approaches have been applied quite successfully in many investigations, see e.g. [12].

---

<sup>1</sup>The  $U(1)_V$  symmetry corresponds with baryon number conservation and is usually not presented explicitly.

We have applied this framework to various decays of  $\eta$  and  $\eta'$  [13–18]. For example, to the isospin violating decays  $\eta, \eta' \rightarrow 3\pi$  which can only occur due to an isospin breaking quark mass difference  $m_u - m_d$  or electromagnetic effects [13, 16, 17]. While for most processes isospin violation of the strong interactions is masked by electromagnetic effects, these corrections are expected to be small for the three pion decays of  $\eta$  and  $\eta'$  (Sutherland's theorem) [19]. Neglecting electromagnetic corrections the decay amplitude is directly proportional to  $m_u - m_d$ .

The chiral unitary method has also been applied to the dominant decay mode of the  $\eta'$ ,  $\eta' \rightarrow \eta\pi\pi$ , where the contributions from the resonances  $a_0(980)$ ,  $f_0(980)$  and the so-called  $\sigma$  can be studied [13, 16, 17].

Moreover, the decays  $\eta, \eta' \rightarrow \gamma\gamma$  and  $\eta, \eta' \rightarrow \pi^+\pi^-\gamma$  are phenomenological manifestations of the chiral anomaly of QCD and can provide important information on the violation of chiral symmetry in strong interactions [14, 15]. These investigations have recently been extended to the decays  $\eta, \eta' \rightarrow \pi^+\pi^-l^+l^-$  ( $l = e, \mu$ ) [18].

On the experimental side, there is renewed interest in  $\eta, \eta'$  decays which are investigated at WASA-at-COSY [20], MAMI [21], KLOE [22], CLEO at CESR [23] and by the VES collaboration [24, 25]. There is thus the necessity to provide a consistent and uniform theoretical description for these decays. We present here a framework which satisfies important theoretical requirements, while at the same time being in very good agreement with experimental data.

## 2 Outline of the approach

We start with the illustration of the hadronic decays  $\eta, \eta' \rightarrow 3\pi$  and  $\eta' \rightarrow \eta\pi\pi$  [13, 16]. The underlying idea of the approach is that the initial particle, i.e. the  $\eta$  or  $\eta'$ , decays into three mesons and that two out of these rescatter (elastically or inelastically) an arbitrary number of times, see Fig. 1 for illustration. All occurring vertices are derived from the effective Lagrangian and are thus constrained by chiral symmetry. Interactions of the third meson with the pair of rescattering mesons are neglected which turns out to be a good approximation, particularly for the decays  $\eta \rightarrow 3\pi$  and  $\eta' \rightarrow \eta\pi\pi$  [16].

Such an infinite meson-meson rescattering process can be generated by application of the Bethe-Salpeter equation. To this aim, the partial wave interaction kernels for meson meson scattering,  $A_l$ , are derived from the chiral effective Lagrangian and iterated in a Bethe-Salpeter equation which generates the propagator for two interacting particles in a covariant fashion. For each partial wave  $l$  the matrix-valued solution  $T_l$  of the BSE with coupled

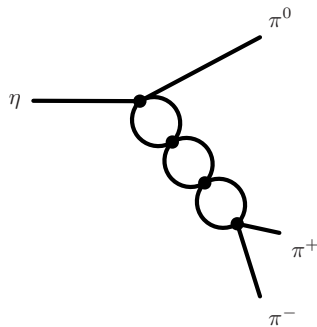


Figure 1: Shown is a possible contribution to final state interactions in the decay  $\eta \rightarrow \pi^+\pi^-\pi^0$ .

channels and on-shell interaction kernels is given by

$$T_l^{-1} = A_l^{-1} + G, \quad (1)$$

where the diagonal matrix  $G$  collects the scalar loop integrals of the different two-meson channels. The solution of the BSE satisfies exact unitarity for two-particle scattering and generates resonances dynamically by an infinite string of meson-meson rescattering processes, see also [12]. In the investigations discussed here we have restricted ourselves to  $s$ - and  $p$ -wave interaction kernels.

This approach can be extended to the anomalous decays  $\eta, \eta' \rightarrow \gamma^{(*)}\gamma^{(*)}$  [14] and  $\eta, \eta' \rightarrow \pi^+\pi^-\gamma$  [15] in a straightforward manner. In  $\eta, \eta' \rightarrow \gamma^{(*)}\gamma^{(*)}$ , e.g., the incoming pseudoscalar meson  $P$  can directly decay via a vertex of either the Wess-Zumino-Witten Lagrangian, which describes the chiral anomaly, or the unnatural-parity Lagrangian into one of the following three channels: two photons, a photon and two pseudoscalar mesons, or four pseudoscalar mesons. Pairs of mesons can then rescatter an arbitrary number of times before they eventually couple to a photon, see Fig. 2 for illustration. In order to implement the non-perturbative summation of loop graphs covered by the BSE in the decay processes under consideration, we treat the BSE  $T$ -matrix as an effective vertex for meson-meson scattering. The anomalous decays into  $\pi^+\pi^-\gamma$  are treated in the same way [15]. Most recently, the decays  $\eta, \eta' \rightarrow \pi^+\pi^-l^+l^-$  ( $l = e, \mu$ ) have been investigated in this approach, where the virtual photon couples to a lepton pair [18]. The results of [18] will soon be tested at KLOE at DAΦNE and WASA-at-COSY.

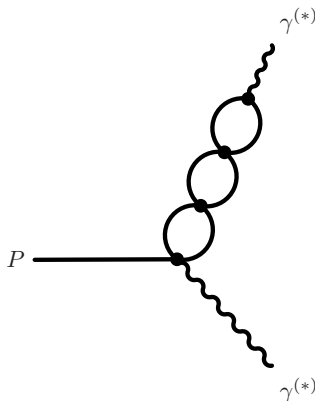


Figure 2: Sample rescattering process in the decay  $P \rightarrow \gamma^{(*)}\gamma^{(*)}$ .

### 3 Results

We now turn to the discussion of the numerical results, where for brevity we restrict ourselves to the hadronic decays [16], while the anomalous decays are discussed in [14,15]. The results of our calculation for the hadronic decays are obtained from a combined analysis of the decay widths, branching ratios, and slope parameters of the considered decays as well as phase shifts in meson-meson scattering. The widths of  $\eta \rightarrow 3\pi$  and  $\eta' \rightarrow \eta\pi\pi$  have been measured roughly at the 10% precision level, while for  $\eta' \rightarrow 3\pi^0$  the experimental uncertainty is considerably larger and only an upper limit exists for  $\Gamma(\eta' \rightarrow \pi^+\pi^-\pi^0)$  [26]. Moreover, some of these decay widths are constrained by the well-measured branching ratios

$$r_1 = \frac{\Gamma(\eta \rightarrow 3\pi^0)}{\Gamma(\eta \rightarrow \pi^+\pi^-\pi^0)}, \quad r_2 = \frac{\Gamma(\eta' \rightarrow 3\pi^0)}{\Gamma(\eta' \rightarrow \eta\pi^0\pi^0)}. \quad (2)$$

The squared absolute values of the decay amplitudes for  $\eta' \rightarrow \eta\pi\pi$  and the charged decay modes of  $\eta, \eta' \rightarrow 3\pi$ ,  $|A(x, y)|^2$ , are expanded in terms of the usual Dalitz variables  $x, y$ , as (see e.g. [16] for definitions of  $x$  and  $y$ )

$$|A(x, y)|^2 = |N|^2 [1 + ay + by^2 + cx^2 + dy^3 + \dots], \quad (3)$$

while for the decays into three identical particles Bose symmetry dictates the form

$$|A(x, y)|^2 = |N'|^2 [1 + g(y^2 + x^2) + \dots]. \quad (4)$$

For the Dalitz plot parameters  $a, b, c$  of  $\eta \rightarrow \pi^+\pi^-\pi^0$  the experimental situation is not without controversy. We employ the numbers of [27], since it is the most recent published measurement and the results appear to be

consistent with the bulk of the other experiments listed by the Particle Data Group [26]. They differ somewhat from the new preliminary results of the KLOE Collaboration [28] that has found a non-zero value for the third order parameter  $d$  which was not included in previous experimental parametrizations. Very recently the Dalitz plot parameters of  $\eta' \rightarrow \eta\pi^+\pi^-$  have been determined with high statistics by the VES experiment [25]. Note that the slope parameters of  $\eta' \rightarrow 3\pi$  have not yet been determined experimentally, but such a measurement is intended at WASA-at-COSY [20, 29].

From the unitarized partial-wave  $T$ -matrix one may also derive the phase shifts in meson-meson scattering. Hence, our approach is further constrained by the experimental phase shifts for  $\pi\pi \rightarrow \pi\pi, K\bar{K}$  scattering.

An intriguing feature of the fits is that they accommodate the large negative slope parameter  $g$  of the decay  $\eta \rightarrow 3\pi^0$  measured by the Crystal Ball Collaboration [30] which could not be met by previous theoretical investigations, see e.g. [31]. In particular, it is in sharp disagreement with the most recent two-loop calculation in conventional chiral perturbation theory [32] which provides a positive slope parameter. The experimental value of [30] has now been confirmed by the more recent but yet preliminary  $g$  value of the KLOE Collaboration [33].

It is of interest, in this respect, to mention that the revised  $g$  parameter of the KLOE collaboration [33] replaces a smaller  $|g|$  value of a previous analysis [22] which was in disagreement with Crystal Ball [30]. As a matter of fact, our approach is not able to accommodate the previous  $g$  value together with the KLOE slope parameters for the charged decay  $\eta \rightarrow \pi^0\pi^+\pi^-$  [22]. In this context, we have illustrated that utilizing the  $\Delta I = 1$  selection rule which relates both  $\eta \rightarrow 3\pi$  decays and taking the KLOE parametrization of the charged decay as input leads in a model-independent way to a  $g$  value not consistent with the previous KLOE  $g$  result [16]. This inconsistency appears to be settled now.

Let us turn our attention to the isospin-breaking quark mass difference  $m_d - m_u$ . An accurate way of extracting  $m_d - m_u$  is, in principle, given by the isospin-violating decays  $\eta, \eta' \rightarrow \pi^0\pi^+\pi^-$  and  $\eta, \eta' \rightarrow 3\pi^0$ . For this reason, it has been claimed in [34] that the branching ratio  $r = \Gamma(\eta' \rightarrow \pi^0\pi^+\pi^-)/\Gamma(\eta' \rightarrow \eta\pi^+\pi^-)$  can be utilized in a very simple manner to extract the light quark mass difference  $m_d - m_u$ . To this aim, it is assumed that

- a) the amplitude  $A(\eta' \rightarrow \pi^0\pi^+\pi^-)$  is determined by the corresponding amplitude  $A(\eta' \rightarrow \eta\pi^+\pi^-)$  via

$$A(\eta' \rightarrow \pi^0\pi^+\pi^-) = \epsilon A(\eta' \rightarrow \eta\pi^+\pi^-) \quad (5)$$

with  $\epsilon = (\sqrt{3}/4)(m_d - m_u)/(m_s - \hat{m})$  the  $\pi^0$ - $\eta$  mixing angle and  $\hat{m} = (m_d + m_u)/2$ . (Note that in [34] the difference  $m_s - \hat{m}$  has been

approximated by  $m_s$  in the denominator of  $\epsilon$ .) Eq. (5) implies that the decay  $\eta' \rightarrow \pi^0 \pi^+ \pi^-$  proceeds entirely via  $\eta' \rightarrow \eta \pi^+ \pi^-$  followed by  $\pi^0$ - $\eta$  mixing.

- b) both amplitudes are “*essentially constant*” over phase space (see the remark in front of Eq. (19) of Ref. [34]).

Based on these two assumptions one arrives at the relation

$$r = \frac{\Gamma(\eta' \rightarrow \pi^0 \pi^+ \pi^-)}{\Gamma(\eta' \rightarrow \eta \pi^+ \pi^-)} \simeq (16.8) \frac{3}{16} \left( \frac{m_d - m_u}{m_s} \right)^2, \quad (6)$$

where the factor 16.8 represents the phase space ratio. Comparison with experimental data—for which, so far, only an upper limit exists—would then lead to a prediction for the quark mass ratio  $(m_d - m_u)/(m_s - \hat{m}) \simeq (m_d - m_u)/m_s$ .

Utilizing the developed chiral unitary approach, we are in a position to critically examine these two assumptions which lead to the simple relation in Eq. (6). Our results clearly indicate that the two underlying assumptions *a*) and *b*) of [34] in order to arrive at a relation between  $r$  and  $(m_d - m_u)/(m_s - \hat{m})$  are not justified at all [17]. The results from the full chiral unitary approach are in plain disagreement with these two assumptions. This shows that sophisticated theoretical approaches, which take into account final-state interactions appropriately, are in general required to extract this quark mass ratio from  $\eta'$  decays.

From these discussions it becomes evident that in general more precise experimental data on  $\eta$  and  $\eta'$  decays are needed. An improvement of the experimental situation is foreseen in the near future due to the upcoming data from WASA-at-COSY [20], MAMI-C [21] and KLOE at DAΦNE [22].

## 4 Conclusions

To summarize, we have explained why  $\eta$  and  $\eta'$  decays provide a perfect opportunity to study symmetries and symmetry-breaking patterns of QCD. These are in more detail, isospin breaking due to different light quark masses  $m_u \neq m_d$ , explicit chiral symmetry breaking due to finite quark masses, the chiral anomalies as well as the axial U(1) anomaly which is closely related to the  $\eta'$ .

The simultaneous treatment of different  $\eta$  and  $\eta'$  decays poses tighter constraints on theoretical approaches. The recent VES data on the decay  $\eta' \rightarrow \eta \pi^+ \pi^-$ , e.g., implies important consequences on the decay  $\eta' \rightarrow \pi^0 \pi^+ \pi^-$

within our approach. In general, the importance of resonances in these decays can be studied unambiguously as they are generated dynamically via the Bethe-Salpeter equation and are not inserted by hand.

Moreover, the study of the  $\eta$ - $\eta'$  system may shed some light into the gluonic degrees of freedom in low-energy hadronic physics due to the close link to the axial U(1) anomaly. Finally, very rare  $\eta$  and  $\eta'$  decays can provide a window to physics beyond the Standard Model. The search for unexpectedly large branching ratios into those channels which cannot be explained within the Standard Model is another main goal of experimental efforts at the various facilities.

## Acknowledgments

The author wishes to thank the organizers for the pleasant conference. This research is part of the EU Integrated Infrastructure Initiative Hadron Physics Project under contract number RII3-CT-2004-506078. Work supported in part by DFG (SFB/TR 16, “Subnuclear Structure of Matter”, and BO 1481/6-1).

## References

- [1] D. J. Gross and F. Wilczek: Phys. Rev. Lett. **30**, 1343 (1973);  
H. D. Politzer: Phys. Rev. Lett. **30**, 1346 (1973).
- [2] I. Montvay and G. Münster, “Quantum fields on a lattice,” Cambridge University Press, Cambridge (1994);  
R. Gupta: [arXiv:hep-lat/9807028].
- [3] S. Weinberg: Physica **96** A, 327 (1979).
- [4] J. Gasser and H. Leutwyler: Ann. Phys. **158**, 142 (1984).
- [5] J. Gasser and H. Leutwyler: Nucl. Phys. B **250**, 465 (1985).
- [6] S. L. Adler, Phys. Rev. **177** (1969) 2426;  
J. S. Bell and R. Jackiw, Nuovo Cim. A **60** (1969) 47;  
W. A. Bardeen: Phys. Rev. **184**, 1848 (1969);  
K. Fujikawa: Phys. Rev. Lett. **42**, 1195 (1979).
- [7] G. Ecker, J. Gasser, A. Pich and E. de Rafael: Nucl. Phys. B **321**, 311 (1989).

- [8] E. Witten: *Ann. Phys. (N.Y.)* **128**, 363 (1980);  
P. di Vecchia and G. Veneziano: *Nucl. Phys. B* **171**, 253 (1980).
- [9] R. Kaiser and H. Leutwyler: *Eur. Phys. J. C* **17**, 623 (2000).
- [10] C. Roiesnel and T. N. Truong, *Nucl. Phys. B* **187** (1981) 293.
- [11] J. Gasser and H. Leutwyler, *Nucl. Phys. B* **250** (1985) 539.
- [12] J. A. Oller, E. Oset and A. Ramos, *Prog. Part. Nucl. Phys.* **45** (2000) 157.
- [13] N. Beisert and B. Borasoy, *Nucl. Phys. A* **716** (2003) 186.
- [14] B. Borasoy and R. Nißler, *Eur. Phys. J. A* **19** (2004) 367.
- [15] B. Borasoy and R. Nißler, *Nucl. Phys. A* **740** (2004) 362.
- [16] B. Borasoy and R. Nißler, *Eur. Phys. J. A* **26** (2005) 383.
- [17] B. Borasoy, U.-G. Meißner and R. Nißler, *Phys. Lett. B* **643** (2006) 41.
- [18] B. Borasoy and R. Nißler, *Eur. Phys. J. A* **33** (2007) 95.
- [19] D. G. Sutherland, *Phys. Lett.* **23** (1966) 384.
- [20] H. H. Adam *et al.* [WASA-at-COSY Collaboration], arXiv:nucl-ex/0411038.
- [21] H. J. Arends [A2 Collaboration], *AIP Conf. Proc.* **870** (2006) 481.
- [22] T. Capussela [KLOE Collaboration], *Acta Phys. Slov.* **56** (2005) 341.
- [23] A. Lopez *et al.* [CLEO Collaboration], arXiv:0707.1601 [hep-ex].
- [24] V. Nikolaenko *et al.* [VES Collaboration], *AIP Conf. Proc.* **796** (2005) 154.
- [25] V. Dorofeev *et al.* [VES Collaboration], [arXiv:hep-ph/0607044].
- [26] W.-M. Yao *et al.* [Particle Data Group Collaboration], *J. Phys. G* **33** (2006) 1.
- [27] A. Abele *et al.* [Crystal Barrel Collaboration], *Phys. Lett. B* **417** (1998) 197.
- [28] F. Ambrosino *et al.* [KLOE Collaboration], arXiv:0707.2355 [hep-ex].

- [29] B. R. Jany, arXiv:0709.2834 [nucl-ex]..
- [30] W. B. Tippens *et al.* [Crystal Ball Collaboration], Phys. Rev. Lett. **87** (2001) 192001.
- [31] J. Kambor, C. Wiesendanger and D. Wyler, Nucl. Phys. B **465** (1996) 215.
- [32] J. Bijnens and K. Ghorbani, arXiv:0709.0230 [hep-ph];  
J. Bijnens, these proceedings.
- [33] F. Ambrosino *et al.* [KLOE collaboration], arXiv:0707.4137 [hep-ex].
- [34] D. J. Gross, S. B. Treiman, and F. Wilczek, Phys. Rev. D **19** (1979) 2188.

# GENERALIZED PARTON DISTRIBUTIONS AND DEEPLY VIRTUAL COMPTON SCATTERING AT CLAS

*R. De Masi*<sup>1</sup> for the CLAS Collaboration

Institut de Physique Nucléaire

15, Rue G. Clemenceau

F-91406 Orsay, France

## Abstract

The deeply virtual Compton scattering is the simplest process to access the generalized parton distributions of the nucleon. A dedicated large statistics experiment for the measurement of deeply virtual Compton scattering with a 6 GeV polarized electron beam on a proton target has been performed at the Hall-B of Jefferson Laboratory with the CLAS spectrometer. The experiment covered a wide kinematic range, allowing the study of the beam spin asymmetry as function of the Bjorken variable  $x_B$ , the Mandelstam variable  $t$ , the virtual photon four-momentum squared  $Q^2$  and the angle  $\phi$  between leptonic and hadronic planes. The preliminary results are in agreement with previous measurements and with the predicted twist-2 dominance.

## 1 Physics Motivation

The **Generalized Parton Distributions** (GPDs) [1, 2] parametrize the structure of hadrons. They include form factors and parton distributions as special limit, and contain in addition information on the transverse momentum distribution of partons and the correlation between quarks.

The GPDs can be accessed in hard exclusive leptonproduction of photons ( **D**eeply **V**irtual **C**ompton **S**cattering - DVCS) and mesons ( $\pi$ ,  $\rho$ ,  $\omega$ ,  $\phi$ , etc.).

In the Bjorken limit, the scattering can be assumed to happen at the quark level, as depicted in the so called “handbag” diagram in Fig. 1.

In the reaction  $ep \rightarrow ep\gamma$  the DVCS interferes with the Bethe-Heitler process, where the real photon in the final state is radiated from the incoming

---

<sup>1</sup>presently at Institut Pluridisciplinaires Hubert Curien 23 Rue de Loess F-67037, Strasbourg, France.

or scattered electron. By using a longitudinally polarized electron beam, this interference has been studied via the beam spin asymmetry  $A = \frac{d\sigma^\uparrow - d\sigma^\downarrow}{d\sigma^\uparrow + d\sigma^\downarrow}$  where  $\uparrow$  ( $\downarrow$ ) indicates a positive (negative) beam helicity. The asymmetry shows an azimuthal dependence  $A = \frac{\alpha \sin\phi}{1 + \beta \cos\phi}$  where  $\phi$  is the angle between the leptonic and hadronic planes.

A first dedicated experiment [3] has shown the validity of the handbag description already at values of  $Q^2 \approx 1 \text{ GeV}^2$ .

## 2 The Experimental Set-up

For this experiment, the longitudinally polarized electron beam from CEBAF accelerator was used. 5.77 GeV electrons with 80% average polarization impinged on a 2.5 cm liquid hydrogen target. In order to detect all the particles in the final state the CLAS spectrometer [4] was used. CLAS is a large acceptance magnetic spectrometer, divided in six sectors. Each sector is equipped with drift chambers for momentum measurement and Cherenkov detector, calorimeter, time-of-flight detectors for particle identification. An additional lead-tungstate calorimeter (**I**nners **C**alorimeter - IC) was especially realized for this experiment and placed in the near forward region to increase the acceptance of photons emitted at small angles ( $4^\circ - 15^\circ$ ).

## 3 Analysis and Results

One electron, one proton and at least one photon are required. In addition the following cuts are applied to ensure the exclusivity of the event:

- missing transverse momentum ( $P_T^X < 90(150) \text{ MeV}/c$ );

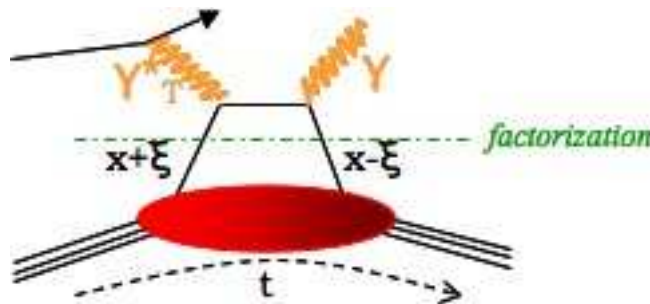


Figure 1: The handbag diagram for deeply virtual Compton scattering.

- angle between the predicted and measured photon direction  $< 1.2(2.7)^\circ$ ;
- coplanarity angle between  $\gamma p$  and  $\gamma^* p < \pm 1.5(3)^\circ$ ;
- missing energy  $E^X < 300(150)$  MeV;

Due to the different energy resolution between the IC and the standard CLAS calorimeter (EC), the cuts have been optimized depending on which calorimeter has measured the photon energy.

A further selection required  $Q^2 > 1$  GeV<sup>2</sup> and the  $\gamma^* p$  invariant mass  $W > 2$  GeV.

The events from  $\pi^0$  decay with one photon not reconstructed, were subtracted in each  $x_B - Q^2 - t - \phi$  bin and in each helicity state with a Monte Carlo based method.

The kinematic range in  $x_B - Q^2$  has been divided in 13 bins as shown in Figure 2 and each bin has further been binned in  $t$ . The variation of the coefficient  $\alpha$  in the decomposition of the beam spin asymmetry has been studied and it is shown in Figure 3.

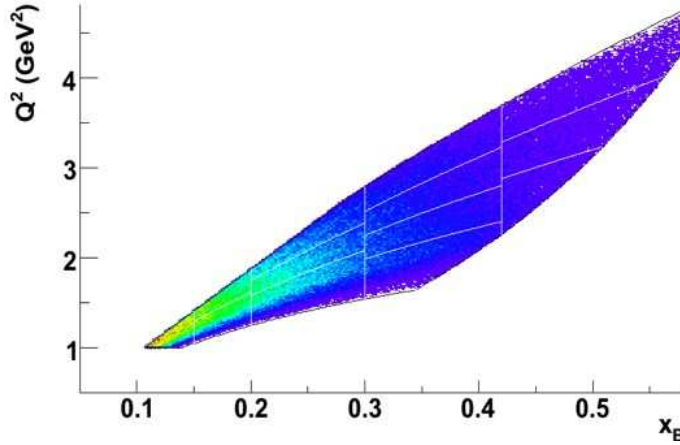


Figure 2: The kinematic region in  $x_B - Q^2$  covered by the experiment. The white lines define the bins studied in this analysis.

The data are in agreement with previous measurements from CLAS [5] and the JLAB Hall-A [3].

For a detailed description of this analysis see [6–8].

## References

- [1] X. Ji, *Phys. Rev. Lett.* **78**, 610 (1997); *Phys. Rev.* **D55**, 7114 (1997).
- [2] A. V. Radyuskin, *Phys. Lett.* **B380**, 417 (1996). *Phys. Rev.* **D56**, 5524 (1997).
- [3] C. Munoz Camacho *et al.*[Jefferson Lab Hall-A Collab.], *Phys. Rev. Lett.* **97**, 262002 (2006).
- [4] B. A. Mecking *et al.*[CLAS Collab.], *Nucl. Instr. Meth.* **503**, 513 (2003).
- [5] S. Stepanyan *et al.*[CLAS Collab.], *Phys. Rev. Lett.* **87**, 182002 (2001).
- [6] F.-X. Girod, *Thèse de Doctorat*, Université de Strasbourg (Dec. 20, 2006); <http://www.jlab.org/Hall-B/secure/e1-dvcs/fxgirod/These.pdf>;
- [7] F.-X. Girod *et al.*[CLAS Collab.], arXiv:0711.0755.
- [8] F.-X. Girod *et al.*[CLAS Collab.], in preparation.

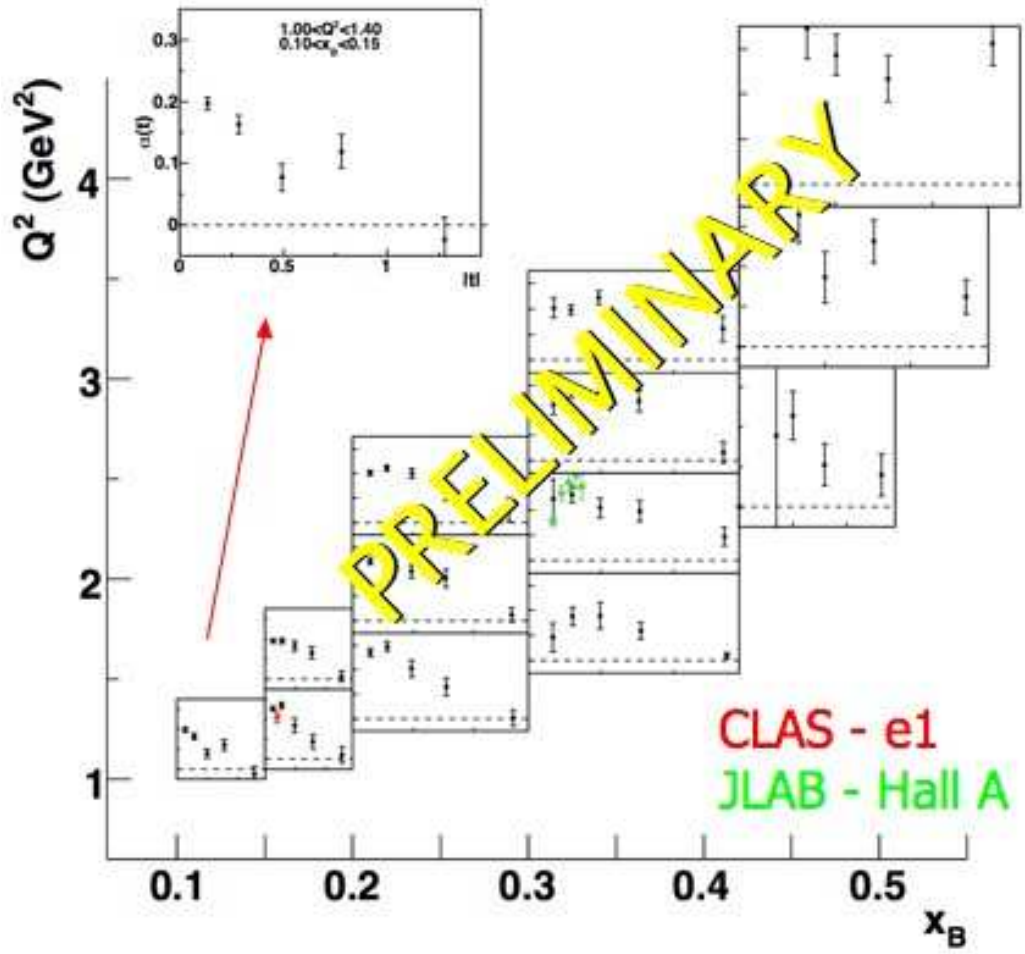


Figure 3:  $\alpha$  vs.  $t$  in .

# THE NATURE OF THE $N^*(1535)$

M. Döring<sup>\*</sup>, D. Jido<sup>%1</sup>, E. Oset<sup>#</sup>

<sup>\*</sup>Institut für Kernphysik, FZ-Jülich, D-52425 Jülich, Germany

<sup>%</sup>Yukawa Institute for Theoretical Physics, Kyoto University, Kyoto,  
606-8502, Japan

<sup>#</sup>Departamento de Física Teórica and IFIC, Universidad de Valencia-CSIC,  
Aptdo. 22085, 46071 Valencia, Spain

## Abstract

Electromagnetic properties provide independent tests of models of strongly interacting systems. In the unitary chiral approach, the  $N^*(1535)$  appears dynamically generated from the interaction of mesons and baryons. We evaluate the  $A_{1/2}$  and  $S_{1/2}$  helicity amplitudes as a function of the photon virtuality for the  $N^*(1535) \rightarrow \gamma^* N$  transition. Within the same formalism we evaluate the cross section for the reactions  $\gamma N \rightarrow \eta N$  and several ratios of observables. The global results provide a strong support to the idea of this resonance being dynamically generated, hence, largely built up from meson baryon components.

## 1 Introduction

The traditional picture of baryons as being made from three constituent quarks [1] is giving room in some cases to more complicated structures. One of the ideas which has caught strength in recent times is that low lying resonances of  $J^P = 1/2^-, 3/2^-$  seem to be well represented in terms of ordinary resonances generated by the meson baryon interaction in  $L = 0$ ; in the  $1/2^-$  case from the interaction of the octet of mesons of the  $\pi$  with the octet of baryons of the  $p$  [2–9] and in the  $3/2^-$  from the interaction of the same mesons with the decuplet of baryons of the  $\Delta(1232)$  [10, 11]. The  $\Lambda(1405)$ , which actually comes as two poles in chiral theories [6], with this two pole structure supported by experiment [12], has been for long thought of as a kind of meson baryon molecule of the  $\bar{K}N$  and  $\pi\Sigma$  states [13, 14], a structure similar to that provided by the chiral approaches mentioned above. The

---

<sup>1</sup>E-mail address: jido@yukawa.kyoto-u.ac.jp

$N^*(1535)$  is one more resonance that appears in the two octets and one singlet of dynamically generated resonances coming from the interaction of the octet of mesons of the  $\pi$  with the octet of baryons of the  $p$  [6]. In fact, it was early noted in [15], before the systematics of [6] was established, that the interaction provided by chiral Lagrangians put as kernel of the Lippmann Schwinger equation generated this resonance, which also appears in other works [16, 17] done along similar lines.

The  $N^*(1535)$  plays an important role in all processes of  $\eta$  production since it couples very strongly to  $\eta N$ . This feature is actually provided automatically by the chiral theories, one of the points of support for the nature of this resonance as dynamically generated. A recent study of the model dependence of the properties of this resonance is seen in [18].

From the point of view of a dynamically generated resonance the  $N^*(1535)$  leads to fair descriptions of the  $\pi N \rightarrow \eta N$  and  $\gamma N \rightarrow \eta N$  reactions [15, 17, 19] and produces reasonable numbers for the  $\eta N$  scattering lengths [2, 17]. Yet, it has been argued that one of the important tests of the nature of a resonance is its electromagnetic form factors. Indeed, a meson baryon resonance should get the  $Q^2$  dependence basically from the meson cloud. If this is a pion, this light particle has a fairly large extend in the wave function, as a consequence of which, the form factor of the resonance should fall relatively fast compared to ordinary quark models which confine the quarks at smaller distances. This is also the case for the proton at small  $Q^2$ , due to its meson cloud, which stabilizes later on at larger values of  $Q^2$  where the quark components take over, as shown in chiral quark models [20–22]. We shall see that something special happens for the  $N^*(1535)$ , but in any case this is a very stringent test, since the chiral theory provides the normalization and the  $Q^2$  dependence for the different transition form factors without any free parameter, once the parameters used in  $\pi N$  scattering with its coupled channels are fixed to scattering data.

Radiative decays of resonances from the point of view of their dynamically generated nature have been addressed in [23] for the  $\Lambda(1520)$ , in [24] for the  $\Delta(1700)$  and in [26] for the two  $\Lambda(1405)$  states. It concerns the decay of the resonances into a baryon and a real photon. Some work with virtual photons from this point of view is done in [2] for the electroproduction of  $\eta$  in the vicinity of the  $N^*(1535)$  resonance. Meanwhile experimental analyzes have succeeded in extracting the helicity transition form factors  $A_{1/2}$  and  $S_{1/2}$  for  $N^*(1535) \rightarrow N\gamma$ , for both  $N = p, n$ , in a relatively wide range of  $Q^2$  values [27].

We undertake the task [25] of evaluating these form factors from the point of view of the  $N^*(1535)$  as a dynamically generated resonance. For that purpose we shall extend the formalism of [24, 26] to virtual photons.

From the quark model point of view there is also much work done on these helicity form factors [28–32]. A comparison of their prediction with experiment plus a compilation of results from different experiments can be seen in [27]. There are appreciable differences from one quark model to another and relativistic effects seem to be important, particularly in the  $S_{1/2}$  helicity transition form factor.

In our approach the quarks enter through the meson and baryon components of the resonance and the  $Q^2$  dependence is tied to the meson and baryon form factors, which we take from experiment, plus the particular  $Q^2$  dependence of the loop functions from the meson baryon coupled channels that build up the resonance. Thus, the final  $Q^2$  dependence is a nontrivial consequence of chiral dynamics, which provides the coupling of the resonance to open and closed channels, the  $Q^2$  dependence of the different loops and the form factors of the mesons and baryons, particularly the mesons, as we shall see.

## 2 Formalism

In our approach, the  $N^*(1535)$  resonance is dynamically generated in the  $s$ -wave scattering of the coupled channels  $\pi N$ ,  $\eta N$ ,  $K\Lambda$ , and  $K\Sigma$ , for total charges of  $Q = 0$  and  $Q = 1$ . The scattering amplitudes for the  $N^*(1535)$  resonance are described in Ref. [17] by means of the Bethe-Salpeter equation for meson baryon scattering given formally by

$$T = V + VGT . \quad (1)$$

Based on the  $N/D$  method and the dispersion relation [5], this integral scattering equation can be reduced to a simple algebraic equation

$$T = \frac{1}{1 - VG}V \quad (2)$$

where the matrix  $V$  is the  $s$ -wave meson-baryon interaction provided by the lowest order of chiral perturbation theory, given by the Weinberg-Tomozawa interaction. The diagonal matrix  $G$  is the meson baryon loop function evaluated in dimensional regularization. It provides the right-hand cut of the scattering amplitude and ensures exact unitarity through its imaginary part. Furthermore, and this distinguishes the formalism from  $K$ -matrix approaches, it is analytic and thus has a real part. Provided attraction in a given channel, this leads to the formation of poles in the complex plane of the scattering energy  $s^{1/2}$ . The pole is identified with resonances and its residues provide the couplings  $g_i$  of the resonance to the channels that are included: in the

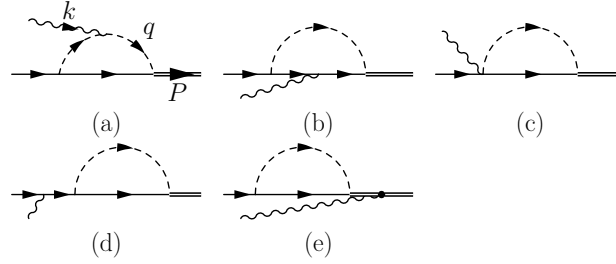


Figure 1: Feynman diagrams for the transition form factor of  $N(1535)$  at one loop level. The solid, dashed, wavy and double lines denote octet baryons, mesons, photon, and  $N^*(1535)$ , respectively.

transition from channel  $i \rightarrow j$ , the amplitude can be expanded around the pole as

$$T_{N^*}^{ij}(\sqrt{s}) = \frac{g_i g_j}{\sqrt{s} - M_R + i\Gamma_R/2} + T_{\text{BG}}. \quad (3)$$

The empirical evidence of larger coupling of  $N(1535)$  to  $\eta N$  than that to  $\pi N$  is reproduced in this model. In addition, the couplings to  $\Sigma K$  and  $\Lambda K$  are also large. This implies that the  $N(1535)$  has large components of strangeness. The basic model has been refined in Ref. [17] by including the  $\pi\pi N$  channel and form factors at higher energies. We leave these additional ingredients out, as they play a minor role in the  $S_{11}$  channel and their inclusion in the coupling to the photon is beyond the scope of this study.

## 2.1 Phototransition

In the meson-baryon picture of the  $N(1535)$  resonance, the photoproduction of the resonance from the nucleon is formulated through the well-known photon couplings to the mesons and baryons that constitute the resonance. Photon couplings and gauge invariance in the case of chiral unitary amplitudes are discussed in Ref. [33]. Here we follow a similar approach as developed in Refs. [23, 24, 26] for real photons, extending it to virtual ones. Feynman diagrams for the transition form factors at the one-loop level are shown in Fig.1. In the loops, all possible octet mesons and baryons contribute. In the diagrams (a) and (b), the photon attaches to the meson and baryon in the loop, respectively. The diagram (c) has the Kroll-Ruderman coupling which is the contact interaction of the photon, meson and baryon. The diagrams (d) and (e) have to be taken into account to keep gauge invariance.

We calculate the transition amplitudes both in non-relativistic and relativistic formulations. The momenta of the baryons are small enough to

describe the transition amplitudes in the non-relativistic formulation. In addition, as can be seen in Ref. [17], in the construction of the  $N^*(1535)$  in meson-baryon scattering, we have used the non-relativistic formulation in the elementary vertex and the baryon propagators. Therefore, to keep consistency of the calculation of the photon couplings with the construction of the  $N^*$  resonance, the non-relativistic calculation is preferable. Nevertheless, it is somewhat complicated to prove gauge invariance in the calculation of the amplitude, since one needs to take into account all the possible diagrams including negative energy contributions, which are referred to as Z-diagrams. To avoid this complication, we will perform the calculation of the amplitudes also in relativistic formulation, in which the negative energy contributions are automatically counted without introducing Z-diagrams, and we have shown that the relativistic calculation is exactly gauge invariant. This guarantees that each term in the  $1/M$  expansion is gauge invariant. Exploiting this fact, in the non-relativistic framework, we calculate diagrams for leading amplitudes relying upon gauge invariance and show that the next-to-leading terms are relatively small.

Lorentz invariance and momentum conservation require the transition current  $J^\mu$  to be written, in general, by the following three Lorentz scalar amplitudes:

$$J^\mu = (\mathcal{M}_1 \gamma^\mu + \mathcal{M}_2 P^\mu + \mathcal{M}_3 k^\mu) \gamma_5. \quad (4)$$

The gauge invariance  $k \cdot J = 0$ , tells us that there are only two independent amplitudes among these three amplitudes,  $\mathcal{M}_i$ , giving the following relation:

$$(M_{N^*} + M_N) \mathcal{M}_1 + k \cdot P \mathcal{M}_2 + k^2 \mathcal{M}_3 = 0. \quad (5)$$

Using the transition current (4), we evaluate the helicity amplitudes,  $A_{1/2}$  and  $S_{1/2}$ , in the rest frame of the  $N(1535)$  resonance. After some algebra, the helicity amplitudes are written in terms of the amplitude  $\mathcal{M}_2$  and  $\mathcal{M}_3$  by

$$A_{1/2} = \sqrt{\frac{2\pi\alpha}{q_R}} \sqrt{\frac{E_i + M_N}{2M_N}} \frac{1}{e} \frac{\sqrt{2}}{M_{N^*} + M_N} (k \cdot P \mathcal{M}_2 + k^2 \mathcal{M}_3) \quad (6)$$

$$S_{1/2} = \sqrt{\frac{2\pi\alpha}{q_R}} \sqrt{\frac{E_i + M_N}{2M_N}} \frac{1}{e} \frac{-|\mathbf{k}|}{M_{N^*} + M_N} (M_{N^*} \mathcal{M}_2 + (M_{N^*} - M_N) \mathcal{M}_3); \quad (7)$$

the result for the non-relativistic amplitudes is similar.

In the non-relativistic formulation, the leading terms of the  $1/M$  expansions are the diagrams (a) and (c) in Fig.1. The diagram (b) is found to be the next leading order due to the  $1/M$  factor in the  $\gamma BB$  coupling. In the

CM frame of the  $N^*$ , which we take for the non-relativistic calculation, the diagram (d) vanishes, since there is a direct transition of  $1/2^+$  to  $1/2^-$ . The diagram (e) has some contribution in this frame, but it is also found to be the next leading order, since the contribution to the diagram (e) is confirmed to vanish in the large  $M$  limit. One of the advantage that Eq. (5) provides is the fact that only the terms proportional to the external momenta  $k \cdot P$ ,  $k^2$  have to be considered. For the non-relativistic calculation this means that the loop integrals are finite for these terms. In Ref. [24] it has been shown that the consideration of these finite terms is equivalent to a calculation of all divergent loop diagrams for which the infinities cancel in the sum. In the present case, this is again the case for the charge  $Q = 0$  sector; for  $Q = 1$  one needs, however, higher order terms to cancel the infinities, as they are automatically provided in a fully relativistic calculation.

As mentioned above, the non-relativistic framework for the photon loops ensures consistence with the hadronic part of the model. The purpose of a relativistic calculation of these loops is to confirm gauge invariance of our formulation. Without the  $1/M$  expansion, which has been performed in the non-relativistic calculation, all the diagrams shown in Fig.1 have been calculated to make the amplitudes gauge-invariant at the one loop level. Each diagram has a divergence from the loop integral. It has been found that the divergence appears only in the  $\mathcal{M}_1$  term.

We have also included standard form factors for the virtual photon in the calculation, as well as a non-relativistic treatment of the anomalous magnetic momenta which introduce a small correction.

### 3 Results

In order to compare our results to the experimentally extracted helicity amplitude, there is an important caveat: The hadronic width of the resonance, as well as the branching ratio, enter the normalization of the experimentally extracted amplitudes [34–36]. It is, thus, the  $Q^2$ -dependence of the form factor rather than absolute numbers which should be considered, taking into account the large experimental uncertainties of the width of the  $N^*(1535)$ . In Fig. 2, the results for  $A_{1/2}$  and  $S_{1/2}$  are plotted. For  $A_{1/2}$ , the slope coincides well whereas the strength is underestimated, most probably due to the mentioned ambiguities in the experimental extraction of this quantity. A rescaling shows good agreement with data. Furthermore, the relativistic corrections are rather small in this case (dashed vs. unrescaled solid line). Note that in the most recent MAID analysis [41] a value of  $A_{1/2}(Q^2 = 0) = 66 \cdot 10^{-3} \text{ GeV}^{-1/2}$  is given, quite in agreement with the

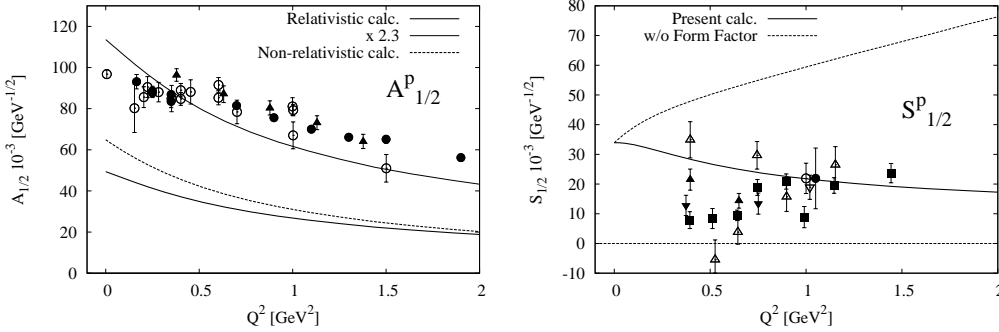


Figure 2: Modulus of  $A_{1/2}$  and  $S_{1/2}$ . The data are from Refs. [36–40]. See text for an explanation of the curves. The sign of  $S_{1/2}$  relative to  $A_{1/2}^p$  is negative, both in experiment and theory.

present findings. For  $S_{1/2}$ , we also observe good agreement. For comparison, the quantity  $S_{1/2}$  without form factors for the pions and kaons is also plotted (dashed line). The observed rise with  $Q^2$ , also present for  $A_{1/2}$  (not shown), comes from the momentum dependence of the photon loops from Fig. 1. The loops are responsible for the relatively slow fall-off of  $A_{1/2}$  with rising  $Q^2$ .

For a real photon at  $Q^2 = 0$  we obtain the ratio  $A_{1/2}^n/A_{1/2}^p = -0.79 + 0.11i$ , which is almost a real value, and its modulus 0.80. A multipole analysis [42] using the inclusive experimental data of Ref. [34] gives the negative sign value  $-0.84 \pm 0.15$  for  $A_{1/2}^n/A_{1/2}^p$ . Values of  $|A_{1/2}^n|/|A_{1/2}^p|$  which are extracted from the ratio of the eta photoproduction cross sections,  $\sigma_n/\sigma_p$ , are reported as  $0.82 \pm 0.04$  in Ref. [43] and  $0.819 \pm 0.018$  in Ref. [44]. The result obtained in our approach agrees with the experimental data in both sign and magnitude. This comparison is free from the normalization uncertainty.

As a boundary condition, we have also checked that our model reproduces  $\eta$  photoproduction data in the reaction  $\gamma p \rightarrow \eta p$ , although the resonance turns out relatively narrow. Furthermore, we could reasonably well reproduce the available data on the ratio of  $\eta$  photoproduction on the neutron over that on the proton,  $\sigma_n/\sigma_p$ .

## 4 Conclusions

In this work we have addressed the evaluation of the electromagnetic helicity form factors for the electroproduction of the  $N^*(1535)$  resonance considered as a dynamically generated resonance. The agreement with the  $A_{1/2}^p$  am-

plitude of the proton  $N^*(1535)$  resonance is good up to the normalization problem that we discussed. The slow fall-off of the slope is a consequence of the structure of the photon loops that provide the phototransition in the picture of dynamical generation.

The results obtained for the  $S_{1/2}$  amplitude are also in fair agreement with experiment, both in size and the relative sign to the  $A_{1/2}$  amplitude. As well, sign and size of  $A_{1/2}^n/A_{1/2}^p$  are in good agreement with data. We have also ensured that  $\eta$  photoproduction data and the associated ratio  $\sigma_n/\sigma_p$  are reasonably well reproduced.

Altogether, the information extracted in this study [25] provides support for the idea of the  $N^*(1535)$  resonance as being dynamically generated from the interaction of mesons and baryons, the dynamics of which seems to be well accounted for by chiral Lagrangians together with a proper coupled channels unitary treatment of the interaction, as provided by the chiral unitary approach.

## References

- [1] N. Isgur and G. Karl, Phys. Rev. D **18**, 4187 (1978); S. Capstick and N. Isgur, *ibid.* **34**, 2809 (1986); L. Y. Glozman and D. O. Riska, Phys. Rep. **268**, 263 (1996); L. Y. Glozman, Z. Papp, and W. Plessas, Phys. Lett. B **381**, 311 (1996); see also the review by S. Capstick and W. Roberts, Prog. Part. Nucl. Phys. **45**, S241 (2000), and references therein.
- [2] N. Kaiser, T. Waas and W. Weise, Nucl. Phys. A **612**, 297 (1997).
- [3] E. Oset and A. Ramos, Nucl. Phys. A **635**, 99 (1998).
- [4] E. Oset, A. Ramos and C. Bennhold, Phys. Lett. B **527**, 99 (2002) [Erratum-*ibid.* B **530**, 260 (2002)].
- [5] J. A. Oller and U. G. Meissner, Phys. Lett. B **500**, 263 (2001).
- [6] D. Jido, J. A. Oller, E. Oset, A. Ramos and U. G. Meissner, Nucl. Phys. A **725**, 181 (2003).
- [7] C. Garcia-Recio, J. Nieves, E. Ruiz Arriola and M. J. Vicente Vacas, Phys. Rev. D **67**, 076009 (2003).
- [8] C. Garcia-Recio, M. F. M. Lutz and J. Nieves, Phys. Lett. B **582**, 49 (2004).

- [9] T. Hyodo, S. I. Nam, D. Jido and A. Hosaka, *Phys. Rev. C* **68**, 018201 (2003).
- [10] E. E. Kolomeitsev and M. F. M. Lutz, *Phys. Lett. B* **585** (2004) 243 [arXiv:nucl-th/0305101].
- [11] S. Sarkar, E. Oset and M. J. Vicente Vacas, *Nucl. Phys. A* **750** (2005) 294 [Erratum-ibid. A **780** (2006) 78]
- [12] V. K. Magas, E. Oset and A. Ramos, *Phys. Rev. Lett.* **95** (2005) 052301
- [13] R. H. Dalitz and S. F. Tuan, *Phys. Rev. Lett.* **2**, 425 (1959).
- [14] R. H. Dalitz and S. F. Tuan, *Annals Phys.* **10**, 307 (1960).
- [15] N. Kaiser, P. B. Siegel and W. Weise, *Phys. Lett. B* **362** (1995) 23
- [16] J. Nieves and E. Ruiz Arriola, *Phys. Rev. D* **64** (2001) 116008
- [17] T. Inoue, E. Oset and M. J. Vicente Vacas, *Phys. Rev. C* **65** (2002) 035204
- [18] A. Kiswandhi, S. Capstick and S. Dytman, *Phys. Rev. C* **69** (2004) 025205
- [19] M. Döring, E. Oset and D. Strottman, *Phys. Rev. C* **73** (2006) 045209
- [20] A. W. Thomas, S. Theberge and G. A. Miller, *Phys. Rev. D* **24** (1981) 216.
- [21] E. Oset, R. Tegen and W. Weise, *Nucl. Phys. A* **426** (1984) 456 [Erratum-ibid. A **453** (1986) 751].
- [22] V. E. Lyubovitskij, T. Gutsche and A. Faessler, *Phys. Rev. C* **64** (2001) 065203
- [23] M. Döring, E. Oset and S. Sarkar, *Phys. Rev. C* **74** (2006) 065204
- [24] M. Döring, *Nucl. Phys. A* **786**, 164 (2007)
- [25] D. Jido, M. Döring, and E. Oset, to appear soon
- [26] L. S. Geng, E. Oset and M. Döring, *Eur. Phys. J. A* **32**, 201 (2007)
- [27] V. D. Burkert and T. S. H. Lee, *Int. J. Mod. Phys. E* **13** (2004) 1035
- [28] F. E. Close and Z. P. Li, *Phys. Rev. D* **42** (1990) 2194.

- [29] M. M. Giannini, E. Santopinto and A. Vassallo, *Prog. Part. Nucl. Phys.* **50** (2003) 263
- [30] D. Merten, U. Loring, K. Kretzschmar, B. Metsch and H. R. Petry, *Eur. Phys. J. A* **14** (2002) 477
- [31] S. Capstick and B. D. Keister, *Phys. Rev. D* **51** (1995) 3598
- [32] B.D. Keister, S. Capstick, *N\* Physics*, edited by T.-S. H. Lee, W. Roberts (World Scientific, Singapore, 1997) p. 58.
- [33] B. Borasoy, P. C. Bruns, U. G. Meissner and R. Nissler, *Phys. Rev. C* **72**, 065201 (2005) [arXiv:hep-ph/0508307].
- [34] B. Krusche *et al.*, *Phys. Rev. Lett.* **74** (1995) 3736.
- [35] C. S. Armstrong *et al.* [Jefferson Lab E94014 Collaboration], *Phys. Rev. D* **60**, 052004 (1999) [arXiv:nucl-ex/9811001].
- [36] H. Denizli *et al.* [CLAS Collaboration], *Phys. Rev. C* **76**, 015204 (2007) [arXiv:0704.2546 [nucl-ex]].
- [37] R. Thompson *et al.* [CLAS Collaboration], *Phys. Rev. Lett.* **86**, 1702 (2001) [arXiv:hep-ex/0011029].
- [38] F. W. Brasse *et al.*, *Nucl. Phys. B* **139**, 37 (1978); F. W. Brasse *et al.*, *Z. Phys. C* **22**, 33 (1984).
- [39] U. Beck *et al.*, *Phys. Lett. B* **51**, 103 (1974).
- [40] H. Breuker *et al.*, *Phys. Lett. B* **74**, 409 (1978).
- [41] S. Kamalov, talk at the NSTAR2007 Workshop, September 2007, Bonn.
- [42] N. C. Mukhopadhyay, J. F. Zhang and M. Benmerrouche, *Phys. Lett. B* **364**, 1 (1995) [arXiv:hep-ph/9510307].
- [43] P. Hoffmann-Rothe *et al.*, *Phys. Rev. Lett.* **78**, 4697 (1997).
- [44] J. Weiss *et al.*, *Eur. Phys. J. A* **16**, 275 (2003) [arXiv:nucl-ex/0210003].

# PHOTOPRODUCTION OF $\eta$ AND $\eta'$ MESONS FROM THE PROTON

*M. Dugger*  
(for the CLAS Collaboration)  
Department of Physics  
Arizona State University  
Tempe, AZ. USA 85287-1504

## Abstract

The excitation spectrum of the proton is comprised of many broad overlapping resonances, making investigations of these resonances very challenging. Two excellent tools in helping deconvolve the spectrum are  $\eta$  and  $\eta'$  meson photoproduction from the proton.

Since the beginning of this new millennium, much progress has been made in measuring  $\eta$  and  $\eta'$  meson photoproduction from the proton. These new measurements are largely in the form of differential cross sections that now cover the first and second resonance regions. In addition to differential cross section data, there have been a comparatively smaller number of beam asymmetry measurements for  $\eta$  photoproduction. However, these beam asymmetries cover the energy range up to only about  $E_\gamma = 1.5$  GeV. In this talk, I will present preliminary Jefferson Lab CLAS data on beam asymmetry for both the  $\eta$  and  $\eta'$ . I will also discuss how the new measurements will be useful in understanding the structure and excited states of the proton.

## 1 Motivation

Understanding the structure of the proton is challenging due to the great complexity of this strongly interacting multi-quark system [1]. Of particular utility in investigating nucleon structure are those production mechanisms and observables that help isolate individual excited states of the nucleon and determine the importance of specific contributions. Since the electromagnetic interaction is well understood, photoproduction offers one of the more powerful methods for studying the nucleon. Because the  $\eta$  and  $\eta'$  mesons have isospin 0,  $\eta N$  and  $\eta' N$  final states can only originate (in one-step processes) from isospin  $I = 1/2$  intermediate states. Therefore, the reactions

$\gamma p \rightarrow \eta p$  and  $\gamma p \rightarrow \eta' p$  isolate  $I = 1/2$  resonances, providing an “isospin filter” for the spectrum of broad, overlapping nucleon resonances, a useful simplification for theoretical efforts. Moreover, since the  $\eta'$  meson is the only flavor singlet of the fundamental pseudoscalar meson nonet, studies of the reaction can also help yield information on the role of glue states in nucleon excitations.

## 2 Recent results

Six experimental facilities have been or are providing new data on meson photoproduction from the proton: GRAAL [2], SAPHIR [3], CB-ELSA [4], CLAS [5], LNS [6], and MAMI [7]. Their contributions to  $\eta$  and  $\eta'$  photoproduction from the proton will be summarized here.

### 2.1 The reaction $\gamma p \rightarrow p\eta$

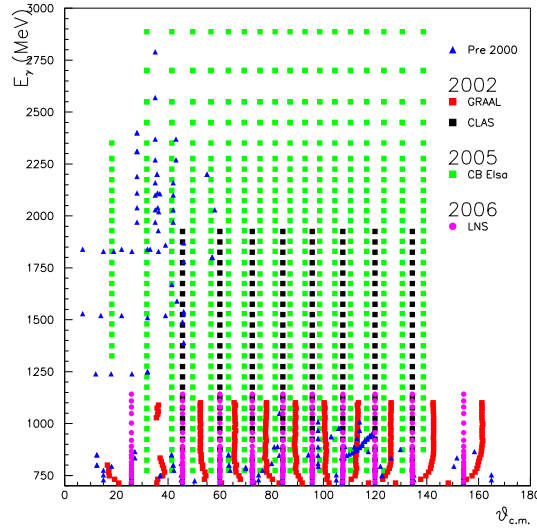


Figure 1: Coverage of differential cross section measurements for  $\gamma p \rightarrow p\eta$  in terms of incident photon energy and center of mass angle. Shown are measurements before 2000 (blue triangles), GRAAL [8] (red squares), CLAS [9] (black squares), CB-ELSA [10] (green squares), and LNS [11] (pink circles).

Before 2002 the world database for  $\gamma p \rightarrow p\eta$  differential cross sections was only well covered for  $E_\gamma$  from threshold (0.707 GeV) up to 0.8 GeV. More recently, the following groups have produced data

- In 2002, GRAAL published results on  $d\sigma/d\Omega$  for  $E_\gamma$  up to 1.1 GeV [8], and CLAS published  $d\sigma/d\Omega$  for  $E_\gamma$  up to 1.95 GeV [9].
- In 2005, CB-ELSA published  $d\sigma/d\Omega$  results for  $E_\gamma$  up to 3 GeV [10].
- In 2006, LNS published  $d\sigma/d\Omega$  results for  $E_\gamma$  up to 1.15 GeV [11].

Fig.1 shows the coverage of differential cross sections in terms of incident photon and center of mass angle. In addition to these published results, there are ongoing analyses for  $\eta$  differential cross sections from groups at MAMI and CLAS.

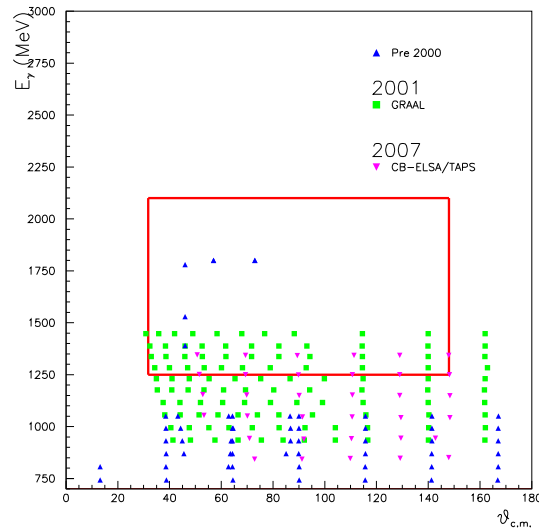


Figure 2: Coverage of beam asymmetry  $\Sigma$  measurements for  $\gamma p \rightarrow \eta p$  in terms of incident photon energy and center of mass angle. Shown are measurements before 2000 (blue triangles), GRAAL [13] (green squares), and CB-ELSA/TAPS [14] (pink triangles). The red box represents the region that CLAS is expected to cover.

Recent beam asymmetry  $\Sigma$  results for  $\gamma p \rightarrow p\eta$  include:

- In 1998, GRAAL published results for  $E_\gamma$  up to 1.050 GeV [12].
- In 2002, GRAAL published results that extended the energy range to 1.447 GeV [13].
- In 2007, CB-ELSA/TAPS produced results for energies up to 1.350 GeV [14].

During the summer of 2005, data were taken at CLAS for  $\Sigma$  that should allow extraction of that observable for  $\eta$  photoproduction from the proton for  $E_\gamma$  up to 2.1 GeV. Fig. 2 shows the coverage of beam asymmetry measurements in terms of incident photon energy and center of mass angle, including a rectangular box showing the region where the new CLAS measurements will provide coverage. A preview of some very preliminary CLAS results is shown in Fig. 3.

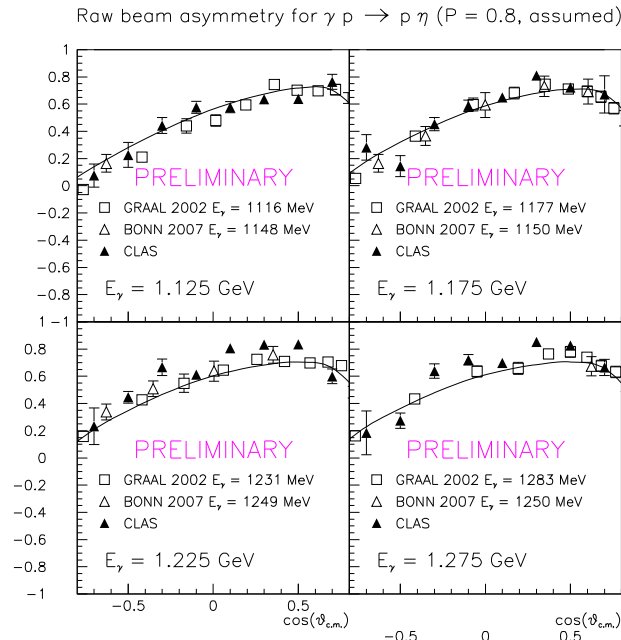


Figure 3: Beam asymmetries for  $\gamma p \rightarrow p \eta$ . The data points are from a preliminary CLAS analysis (filled triangles), Bonn CB-ELSA/TAPS [14] (open triangles), and GRAAL [13] (open squares). The curves are from SAID [15].

All other polarization observables are very sparsely covered in energy and angle. Future experiments are expected to enhance our knowledge of the polarization observables. In particular, an approved experiment at Jefferson Lab [16] will begin taking data later this Fall (2007) for double polarization observables (beam and target).

## 2.2 The reaction $\gamma p \rightarrow p\eta'$

Prior to 1998, only 18  $\eta'$  photoproduction events had been measured (11 events from the ABBHHM bubble chamber experiment [17], and 7 events from the AHHM streamer chamber experiment [18]). In 1998, the SAPHIR collaboration published results [19] extracted from an additional 250  $\eta'$  exclusive events. By contrast, the 2006 CLAS results [20] includes over  $2 \times 10^5$   $\eta'$  photoproduction events used to extract the differential cross sections shown in Fig. 4. Also shown in Fig. 4 are the results of theoretical fits to the data from K. Nakayama and H. Haberzettl (NH model [21], described in the next section) using five different sets of included resonances (see Table 1). The CLAS results span  $E_\gamma$  from 1.527 to 2.227 GeV.

No polarization observables have been published for this reaction. Therefore, the differential cross sections provide the only reported experimental data for the reaction  $\gamma p \rightarrow p\eta'$ . However, while there are currently no released data for  $\gamma p \rightarrow p\eta'$  beam asymmetries, Fig. 5 shows a sample of preliminary CLAS results, along with the predictions from the NH model for each of the five resonance sets given in Table 1. It is important to note that the NH model results shown in Figs. 4 and 5 were determined by fitting only to the differential cross section data.

## 3 Theoretical results

As noted above, there are many new differential cross section data for the reactions discussed here. However, these alone are not sufficient to constrain theoretical models such that contributing resonances can be uniquely determined. More data on the polarization observables are desperately needed, and a coupled channel approach is required, in order to determine conclusively the contributions of various resonances.

One step in this direction comes from a model [10, 22, 23] developed by A. V. Anisovich, E. Klempt, A. Sarantsev, and U. Thoma (Bonn-Gatchina model) that couples the reactions  $\gamma p \rightarrow p\pi^0$ ,  $n\pi^+$ , and  $p\eta$ . Bonn-Gatchina included published differential cross sections, as well as the recent GRAAL beam polarization observables. The model uses a  $K$  matrix approach for the  $S_{11}(1535)$  and the  $S_{11}(1650)$  resonances. The remaining resonances are described by Breit-Wigner amplitudes. The model also includes Reggeized  $u$ - and  $t$ -channel contributions. Results from their analysis [22] find evidence for a previously unseen  $D_{15}(2070)$  resonance, and indications for a new  $P_{13}(2200)$  resonance.

One model that considers the  $\eta'$  exclusively is the NH model mentioned

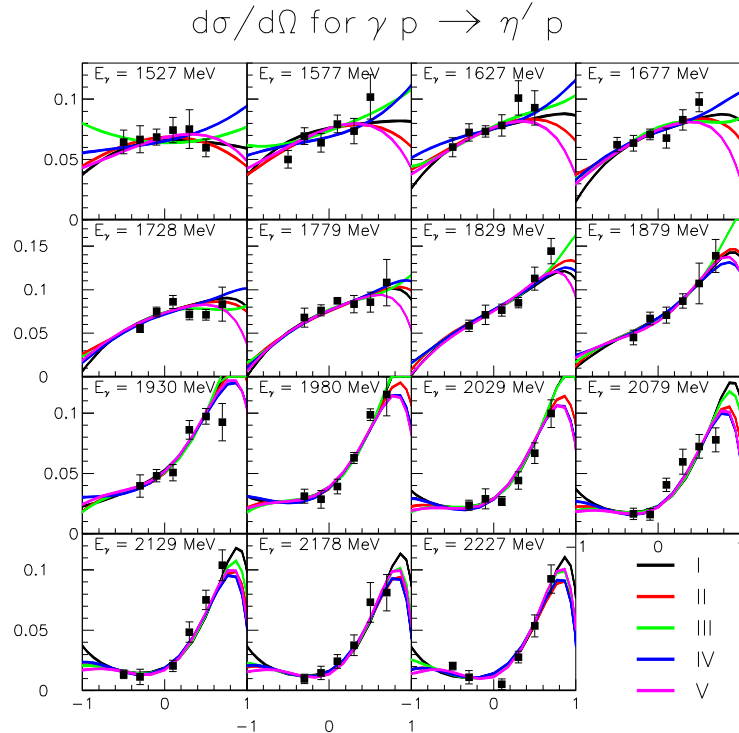


Figure 4: Differential cross sections for  $\gamma p \rightarrow p\eta'$ . The data points are from CLAS [20] and the curves are based on five different sets of resonances (see Table 1) using the NH model [21] described in the text.

above [21]. This model is based upon a relativistic meson-exchange model of hadronic interactions. Allowed processes include  $s$ -,  $t$ -, and  $u$ -channel contributions. The intermediate mesons for the  $t$ -channel exchange are the  $\omega$  and  $\rho^0$ . NH tried five different sets of resonances in their fits; the masses and widths of the included resonances were allowed to vary, except for those in set V which were set to PDG values. The observed  $u$ -channel contribution allows the  $g_{\eta'NN}$  coupling to be extracted (albeit in a model-dependent way). The five sets of included resonances, along with the  $g_{\eta'NN}$  fit parameter, are summarized in Table 1.

Since the  $\eta'$  meson is the only flavor singlet of the fundamental pseudoscalar meson nonet, studies of the reaction can also help yield information on the role of glue states in excitations of the nucleon. The flavor-singlet axial charge of the nucleon ( $G_A(0)$ ) is related to the  $\eta'$ -nucleon-nucleon and gluon-nucleon-nucleon coupling constants ( $g_{\eta'NN}$  and  $g_{GNN}(0)$ , respectively)

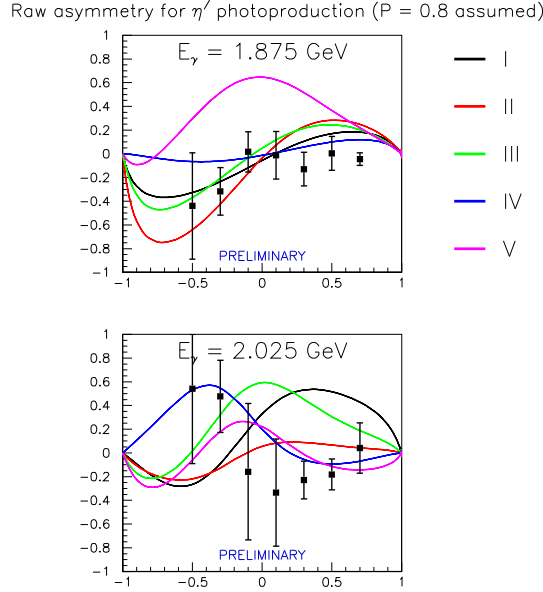


Figure 5: Beam asymmetries for  $\gamma p \rightarrow p\eta'$ . The data points are from a preliminary CLAS analysis, and the curves are based on five different sets of resonances (see Table 1) using the NH model [21].

through the flavor-singlet Goldberger-Treiman relation [24]:

$$2m_N G_A(0) = F g_{\eta' NN} - \frac{F^2 m_{\eta'}^2}{N_F} g_{GNN}(0), \quad (1)$$

where  $m_N$  is the mass of the nucleon,  $m_{\eta'}$  is the  $\eta'$  mass,  $F$  is an invariant decay constant that reduces to  $F_\pi$  (pion decay constant) if the  $U(1)_A$  anomaly is turned off [25], and  $N_F$  equals the number of flavors. When first measured [26], the singlet axial charge was found to have a value of  $G_A(0) = 0.20 \pm 0.35$ . (A more recent calculation [27] gives  $G_A(0) = 0.213 \pm 0.138$ .) At that time, the importance of the second term in Eq. 1 was unappreciated, and this low value of  $G_A(0)$  was surprising: Since  $g_{\eta' NN}$  is considered to be correlated with the fraction of the nucleon spin carried by its constituent quarks [28], that fraction would then be consistent with zero. Thus, neglecting the gluonic portion of Eq. 1 was one of the causes of the so-called “spin crisis.” However, when the gluonic degrees of freedom are included in Eq. 1, the value of  $g_{\eta' NN}$  can be large, provided that it is nearly canceled by  $g_{GNN}(0)$ . This equation then can be used to indirectly determine a value for  $g_{\eta' NN}$ .

By looking only at the differential cross sections, no particular set of resonances (from the five sets studied) appears to do much better in fitting the

Table 1: The five sets of resonances used in the NH model [21].

Set I	Set II	Set III	Set IV	Set V
$S_{11}(2090)$	$S_{11}(2090)$	$S_{11}(1535)$	$S_{11}(1535)$	$S_{11}(1535)$
		$S_{11}(1650)$		$S_{11}(1650)$
		$S_{11}(2090)$	$S_{11}(2090)$	$S_{11}(2090)$
$P_{11}(2100)$	$P_{11}(2100)$	$P_{11}(1710)$	$P_{11}(1710)$	$P_{11}(1710)$
		$P_{11}(2100)$	$P_{11}(2100)$	$P_{11}(2100)$
		$P_{11}(2400)$		
$P_{13}(1900)$ $D_{13}(1700)$	$P_{13}(1900)$ $D_{13}(1700)$ $D_{13}(2080)$	$P_{13}(1900)$		$P_{13}(1720)$
		$D_{13}(1700)$	$D_{13}(1700)$	$P_{13}(1900)$
		$D_{13}(2080)$	$D_{13}(2080)$	$D_{13}(1700)$ $D_{13}(2080)$
$g_{\eta'NN} = 0.43$	$g_{\eta'NN} = 0.25$	$g_{\eta'NN} = 1.33$	$g_{\eta'NN} = 0.002$	$g_{\eta'NN} = 1.91$

data than the others. The CLAS report on the differential cross sections [20] concentrated on resonance set III because the value of  $g_{\eta'NN}$  found from that particular NH fit was 1.33. As stated in that paper

Since differential cross sections alone do not provide sufficient constraints to this model, the  $g_{\eta'NN}$  values should be taken with caution. Nonetheless, this value is consistent with the analysis of T. Feldmann [25] which gives  $g_{\eta'NN} = 1.4 \pm 1.1$ .

Now, with the benefit of the preliminary beam asymmetry measurements shown in Fig. 5, it would appear that resonance set IV is much more consistent with the data. Resonance set IV, however, would yield a value of  $g_{\eta'NN} = 0.002$ , which is much smaller than would be expected. Since the NH fit needs to be redone to include the new beam asymmetry measurements, no definitive statements regarding the  $g_{\eta'NN}$  coupling constant can be made at this time. However, it is readily apparent that beam asymmetry measurements will be vital in determining which resonances significantly contribute to the process and in delimiting the value of  $g_{\eta'NN}$ .

## 4 Summary

While there has been much progress in obtaining differential cross section data for  $\eta$  and  $\eta'$  photoproduction from the proton, and some new beam

polarization ( $\Sigma$ ) measurements have become available, more polarization observables are needed in order to provide constraints for theoretical models. Such experiments are planned for the near future. A comprehensive program for single, double and even triple polarization measurements in photoproduction is in preparation at Jefferson Lab. From the data already taken, there appears to be evidence for a new  $D_{15}$  resonance at 2.09 GeV and indications of a new  $P_{13}$  at 2.20 GeV. In the future, when the  $g_{\eta'NN}$  coupling constant can be determined with a high degree of confidence, it can be used to indirectly determine the gluonic coupling to the proton through the flavor-singlet Goldberger-Treiman relation.

## Acknowledgments

The authors gratefully acknowledge the Jefferson Lab Accelerator Division staff. We thank H. Habertzettl and K. Nakayama for useful discussions and assistance. This work was supported by the National Science Foundation, the Department of Energy (DOE), the Deutsche Forschungsgemeinschaft (through an Emmy Noether grant to U.T.), the French Centre National de la Recherche Scientifique and Commissariat à l'Énergie Atomique, the Italian Istituto Nazionale di Fisica Nucleare, and the Korean Science and Engineering Foundation. Jefferson Science Associates (JSA) operates the Thomas Jefferson National Accelerator Facility for the United States Department of Energy under Contract No. DE-AC05-06OR23177.

## References

- [1] See, e.g., S. Capstick and W. Roberts, *Prog. in Part. and Nucl. Phys* **45**, S241 (2000).
- [2] F. Ghio, *et al.*, *Nucl. Instrum. Meth. A* **404**, 71 (1998).
- [3] W. J. Schwille, *et al.*, *Nucl. Instrum. Meth. A* **344**, 470 (1994).
- [4] E. Aker, *et al.*, *Nucl. Instrum. Meth. A* **321**, 69 (1992).
- [5] B. Mecking, *et al.*, *Nucl. Instrum. Meth. A* **503/3**, 513 (2003).
- [6] H. Okuno, *et al.*, *Nucl. Instrum. Meth. A* **365**, 352 (1995).
- [7] S. Hall, *et al.*, *Nucl. Instrum. Meth. A* **368**, 698 (1996).
- [8] F. Renard, *et al.*, *Phys. Lett. B* **528**, 215 (2002).

- 
- [9] M. Dugger, *et al.*, Phys. Rev. Lett. **89**, 222002 (2002).
- [10] V. Crede, *et al.*, Phys. Rev. Lett. **94**, 012004 (2005).
- [11] T. Nakabayashi, *et al.*, Phys. Rev. C **74**, 035202 (2006).
- [12] J. Ajaka, *et al.*, Phys. Rev. Lett. **81**, 1797 (1998).
- [13] A. Kuznetsov, *et al.*, pi N Newsletter **16**, 160 (2002).
- [14] D. Elsner, *et al.*, nucl-ex/0702032.
- [15] R. A. Arndt, W. J. Briscoe, I. I. Strakovsky, and R. L. Workman, Phys. Rev. C **66**, 055213 (2002).
- [16] Jefferson Lab Proposal E05-012, “Measurement of Polarization Observables in  $\eta$ -photoproduction with CLAS,” Spokespersons: E. Pasyuk (contact), M. Dugger (2005).
- [17] ABBHHM Collaboration, Phys. Rev. **175**, 1669 (1968).
- [18] AHHM Collaboration, Nucl. Phys. B **108**, 45 (1976).
- [19] R. Plötzke *et al.*, Phys. Lett. B **444**, 55 (1998).
- [20] M. Dugger, *et al.*, Phys. Rev. Lett. **96**, 062001 (2006).
- [21] K. Nakayama, and H. Haberzettl, Phys. Rev. C **73**, 045211 (2006).
- [22] O. Bartholomy *et al.*, Phys. Rev. Lett. **94**, 012003 (2005).
- [23] A.V.Anisovich, E.Klempt, A.Sarantsev, U.Thoma, hep-ph/0407211.
- [24] G.M. Shore, G. Veneziano, Nucl. Phys. **B381**, 23 (1992)
- [25] T. Feldmann, Int. J. Mod. Phys. A **15** 159 (2000); also available as hep-ph/9907491.
- [26] J. Ashman *et al.*, Nucl. Phys. B **328**, 1 (1989).
- [27] M. Hirai, S. Kumano, N. Saito, Phys. Rev. D **69** 054021 (2004); also available as hep-ph/0312112.
- [28] A. Sibirtsev, Ch. Elster, S. Krewald, and J. Speth, AIP Conf. Proc. **717**, 837 (2004); A. Sibirtsev, Ch. Elster, S. Krewald, and J. Speth, nucl-th/0303044.

# DELTA-RESONANCE CONTRIBUTIONS TO THE NUCLEAR FORCE

E. Epelbaum<sup>\*,†,1</sup>

<sup>\*</sup>IKP, Forschungszentrum Jülich, D-52425 Jülich, Germany

<sup>†</sup>HISKP, Universität Bonn, D-53115 Bonn, Germany

## Abstract

The  $\Delta$ -isobar is well known to play an important role in nuclear physics due to its low excitation energy,  $\Delta \equiv m_\Delta - m_N \simeq 293$  MeV, and the strong coupling to the  $\pi N$  system. I discuss the implications of treating the  $\Delta$  as a dynamical degree of freedom for two- and three-nucleon forces.

## 1 Introduction

Nuclear forces and few-nucleon dynamics based on chiral effective field theory (EFT) have been studied in great detail over the last decade, see [1, 2] for recent review articles. Most of the calculations in the few-nucleon sector carried out in this framework are based on the effective Lagrangian for pions and nucleons chirally coupled to external sources. The two-nucleon force (2NF) has been worked out up to next-to-next-to-next-to-leading order ( $N^3$ LO) in the chiral expansion and demonstrated to provide an accurate description of the low-energy two-nucleon observables [3, 4]. On the other hand, the chiral expansion for the 2NF is known to exhibit a somewhat unnatural convergence pattern. In particular, by far the most important two-pion exchange (TPE) contribution arises at next-to-next-to-leading order ( $N^2$ LO) [5]. The corresponding attractive central potential turns out to be one order of magnitude stronger than the (formally) dominant TPE contributions at at next-to-leading order (NLO).

The origin of the unnaturally strong subleading TPE potential can be traced back to the large values of the dimension-two low-energy constants (LECs)  $c_{3,4}$  which are also responsible for the numerical dominance of the subleading three-pion exchange [6] and charge-symmetry breaking TPE 2NF [7] over the corresponding leading contributions. The large values of the LECs  $c_i$  are well understood in terms of resonance saturation [8]. In particular, the

---

<sup>1</sup>E-mail address: e.epelbaum@fz-juelich.de

$\Delta$ -isobar provides the dominant (significant) contribution to  $c_3$  ( $c_4$ ). Given its low excitation energy,  $\Delta \equiv m_\Delta - m_N = 293$  MeV, and strong coupling to the  $\pi N$  system, the  $\Delta$ -isobar is known to play an important role in nuclear physics. One can, therefore, expect that the explicit inclusion of  $\Delta$  in EFT will allow to resum a certain class of important contributions and improve the convergence as compared to the delta-less theory, provided a proper power counting scheme such as the small scale expansion (SSE) [9] is employed. The SSE is a phenomenological extension of chiral perturbation theory in which the delta-nucleon mass splitting is counted as an additional small parameter. This improved convergence has been explicitly demonstrated for pion-nucleon scattering where the description of the phase shifts at third order in the SSE comes out superior (inferior) to the third (fourth) order chiral expansion in the delta-less theory [10].

In this talk I describe the structure of the nuclear force in EFT with explicit delta degrees of freedom and compare it with the one resulting in the delta-less theory. The manuscript is organized as follows. In section 2, I discuss the power counting and the effective Lagrangian. The determination of the relevant LECs is described in section 3. The contributions to the 2NF and three-nucleon force (3NF) up to N<sup>2</sup>LO are considered in sections 4 and 5, respectively. I end with a summary and outlook.

## 2 Power counting and the effective Lagrangian

Here and in what follows, I use Weinberg's power counting [11] utilizing the SSE. The low-momentum scale  $Q$  is set by external three-momenta of the nucleons, pion masses and the nucleon-delta mass splitting,  $Q \in \{p, M_\pi, \Delta\}$ . The irreducible<sup>2</sup> contributions to the scattering amplitude give rise to the nuclear force and can be obtained using the variety of schemes, see e.g. [5, 5, 11]. They are ordered according to the power  $\nu$  of the expansion parameter  $Q/\Lambda$  with  $\Lambda$  being the pertinent hard scale. For an irreducible  $N$ -nucleon diagram, the power  $\nu$  is given by [11]:

$$\nu = -2 + 2N + 2(L - C) + \sum_i V_i \Delta_i, \quad \Delta_i = d_i + \frac{1}{2}b_i - 2. \quad (1)$$

Here,  $L$ ,  $C$  and  $V_i$  refer to the number of loops, separately connected pieces and vertices of type  $i$ , respectively. Further,  $b_i$  is the number of baryon field operators and  $d_i$  is the number of derivative and/or insertions of  $M_\pi$ . The

<sup>2</sup>These are the contributions which are not generated through iteration of the dynamical equation.

nucleon mass  $m_N$  is counted in a special way via  $Q/m_N \sim Q^2/\Lambda^2$  which implies that  $m_N \gg \Lambda$  [5, 11]. Notice further that according to the above counting rules, the momentum scales associated with the real pion and delta production are treated as the hard scale,  $\sqrt{m_N M_\pi} \sim \sqrt{m_N \Delta} \sim \Lambda$ , and thus do not need to be explicitly kept track of. Clearly, such a framework is only applicable at energies well below the pion production threshold.

The effective Lagrangian needed to derive the 2NF up to N<sup>2</sup>LO ( $\nu = 3$ ) has the following form in the heavy-baryon formulation:

$$\begin{aligned} \mathcal{L}^{(0)} &= \frac{F_\pi^2}{4} \langle u_\mu u^\mu + \chi_+ \rangle + \bar{N} [i v \cdot D + g_A u \cdot S] N - \frac{1}{2} C_S (\bar{N} N) (\bar{N} N) \\ &\quad + 2 C_T (\bar{N} S_\mu N) (\bar{N} S^\mu N) - \bar{T}_\mu^i [i v \cdot D^{ij} - \Delta \delta^{ij} + \dots] g^{\mu\nu} T_\nu^j, \\ \mathcal{L}^{(1)} &= \bar{N} [c_1 \langle \chi_+ \rangle + c_2 (v \cdot u)^2 + c_3 u \cdot u + c_4 [S^\mu, S^\nu] u_\mu u_\nu] N \\ &\quad + \left( (b_3 + b_8) \bar{T}_\mu^i i P^{\mu\nu} \omega_{\nu\rho}^i v^\rho N + \text{h.c.} \right), \end{aligned} \quad (2)$$

where the superscripts of  $\mathcal{L}$  refer to the dimension  $\Delta_i$  defined in Eq. (1),  $N$  denotes the large component of the nucleon field and  $T_\mu^i$  with  $\mu$  ( $i$ ) being the Lorentz (isospin) index is the large component of the delta field. Further,  $U(x) = u^2(x)$  collects the pion fields,  $u_\mu = i(u^\dagger \partial_\mu u - u \partial_\mu u^\dagger)$ ,  $\chi_+ = u^\dagger \chi u^\dagger + u \chi^\dagger u$  includes the explicit chiral symmetry breaking,  $\langle \dots \rangle$  denotes a trace in flavor space and  $D_\mu (D_\mu^{ij})$  is the chiral covariant derivative for the nucleon (delta) fields. Furthermore,  $P_{\mu\nu}$  is the standard projector on the 3/2-components,  $P_{\mu\nu} = g_{\mu\nu} - v_\mu v_\nu - 4 S_\mu S_\nu / (1 - d)$ , with  $v_\mu$  the four-velocity,  $S_\mu$  the covariant spin vector and  $d$  the number of space-time dimensions. We also have  $w_\alpha^i = \langle \tau^i u_\alpha \rangle / 2$  and  $w_{\alpha\beta}^i = \langle \tau^i [\partial_\alpha, u_\beta] \rangle / 2$ . The LECs in the lowest-order Lagrangian involve the pion decay constant  $F_\pi = 92.4$  MeV, the nucleon axial-vector coupling  $g_A = 1.27$  and the  $\pi N \Delta$  axial coupling  $h_A$  and the constants  $C_{S,T}$  accompanying nucleon-nucleon contact interactions. At subleading order, five further LEC contribute, namely the subleading  $\pi N$  LECs  $c_i$  ( $i = 1, 2, 3, 4$ ) and the combination of  $\pi N \Delta$  LECs  $b_3 + b_8$ . Notice further that the 2NF at N<sup>2</sup>LO also involves subleading nucleon-nucleon contact interactions from  $\mathcal{L}^{(2)}$  which are not shown explicitly. It should also be emphasized that the derivative-less  $NNN\Delta$  contact interaction in  $\mathcal{L}^{(0)}$  vanishes due to the Pauli principle [12]. For more details on the notation, the reader is referred to [9, 10], see also [13] for a recent review article.

### 3 Determination of the LECs

The values of the LECs  $c_i$  are different in the delta-less and delta-full theories and can be naturally extracted from  $\pi N$  scattering. At subleading order,

which is sufficient for our purpose, the determination of  $c_i$  from the  $\pi N$  S- and P-wave threshold coefficients yields in the delta-less theory [14]

$$c_1 = -0.57, \quad c_2 = 2.84, \quad c_3 = -3.87, \quad c_4 = 2.89, \quad (3)$$

where only central values are given and the units are  $\text{GeV}^{-1}$ . The above values are somewhat smaller in magnitude than the ones obtained at higher orders, see e.g. [15]. Including the contributions from the  $\Delta$ , one finds

$$c_1 = -0.57, \quad c_2 = -0.25, \quad c_3 = -0.79, \quad c_4 = 1.33, \quad b_3 + b_8 = 1.40. \quad (4)$$

Notice that the LECs  $c_{2,3,4}$  are strongly reduced in magnitude when the  $\Delta$ -isobar is included. It should also be emphasized that the values of these LECs depend sensitively on  $h_A$ , which in the above case was set to  $h_A = 3g_A/(2\sqrt{2})$  from SU(4) (or large  $N_c$ ). The results for the threshold coefficients and the TPE potential are, however, rather stable [14]. Notice further that the description of the P-wave threshold parameters improves significantly upon inclusion of the delta-isobar.

## 4 Two-nucleon force

The structure of the 2NF in the delta-full and delta-less theories up to N<sup>2</sup>LO is depicted in Fig. 1. I will first briefly overview the various contributions in EFT without explicit  $\Delta$ .

- The lowest-order 2NF is due to the OPE potential and the leading contact interactions<sup>3</sup>:

$$V_{2N}^{(0)} = -\frac{g_A^2}{(2F_\pi)^2} \boldsymbol{\tau}_1 \cdot \boldsymbol{\tau}_2 \frac{\boldsymbol{\sigma}_1 \cdot \mathbf{q} \boldsymbol{\sigma}_2 \cdot \mathbf{q}}{q^2 + M_\pi^2} + C_S + C_T \boldsymbol{\sigma}_1 \cdot \boldsymbol{\sigma}_2, \quad (5)$$

where  $\mathbf{q} \equiv \mathbf{p}' - \mathbf{p}$  is the nucleon momentum transfer with  $\mathbf{p}$  ( $\mathbf{p}'$ ) being the initial (final) nucleon momenta in the center-of-mass system and  $\sigma_i$  ( $\boldsymbol{\tau}_i$ ) denote the Pauli spin (isospin) matrices of the nucleon ( $i$ ). Here and in what follows, the expressions for the potential are to be understood as operators in spin and isospin spaces and matrix elements with respect to momenta.

- The first corrections arise at order  $\nu = 2$  from TPE and subleading

---

<sup>3</sup>Alternative counting schemes for contact interactions are currently being explored.

	<i>Two-nucleon force</i>		<i>Three-nucleon force</i>	
	<i>Δ-less EFT</i>	<i>Δ-contributions</i>	<i>Δ-less EFT</i>	<i>Δ-contributions</i>
<b>LO</b>		—	—	—
<b>NLO</b>			—	
<b>NNLO</b>				—

Figure 1: Two- and three-nucleon forces in the delta-less and delta-full EFT. Dashed, solid and double-solid lines represent pions, nucleons and delta isobars, respectively. Solid dots, filled circles and squares denote vertices with  $\Delta_i = 0, 1$  and  $2$ . Only one representative topology is depicted in each case.

contact terms

$$\begin{aligned}
V_{2N}^{(2)} = & -\frac{\boldsymbol{\tau}_1 \cdot \boldsymbol{\tau}_2}{384\pi^2 F_\pi^4} L^\Lambda(q) \left[ 4M_\pi^2(5g_A^4 - 4g_A^2 - 1) + q^2(23g_A^4 - 10g_A^2 - 1) \right. \\
& \left. + \frac{48g_A^4 M_\pi^4}{4M_\pi^2 + q^2} \right] - \frac{3g_A^4}{64\pi^2 F_\pi^4} L^\Lambda(q) \left[ \sigma_1 \cdot \mathbf{q} \sigma_2 \cdot \mathbf{q} - \sigma_1 \cdot \sigma_2 q^2 \right] \\
& + C_1 (\mathbf{p} - \mathbf{p}')^2 + \frac{C_2}{4} (\mathbf{p} + \mathbf{p}')^2 + \dots
\end{aligned} \tag{6}$$

Here, the ellipses refer to further contact terms,  $C_i$  denote the LECs and the loop function  $L^\Lambda(q)$  has the form

$$L^{\tilde{\Lambda}}(q) = \frac{\omega}{2q} \ln \frac{\tilde{\Lambda}^2 \omega^2 + q^2 s^2 + 2\tilde{\Lambda} q \omega s}{4M_\pi^2 (\tilde{\Lambda}^2 + q^2)}, \quad \omega^2 = q^2 + 4M_\pi^2, \quad s^2 = \tilde{\Lambda}^2 - 4M_\pi^2,$$

where  $\tilde{\Lambda}$  is the cutoff in the spectral-function representation. Further contributions at this order resulting from renormalization of the OPE potential and the leading contact interactions only lead to shifts in the corresponding LECs.

- At N<sup>2</sup>LO, one has to take into account the subleading TPE potential

$$V_{2N}^{(3)} = -\frac{3g_A^2}{16\pi F_\pi^4}(2M_\pi^2(2c_1 - c_3) - c_3q^2)(2M_\pi^2 + q^2)A^{\tilde{\Lambda}}(q) \quad (7)$$

$$- \frac{g_A^2 c_4}{32\pi F_\pi^4} \boldsymbol{\tau}_1 \cdot \boldsymbol{\tau}_2 \left[ \sigma_1 \cdot \mathbf{q} \sigma_2 \cdot \mathbf{q} - q^2 \sigma_1 \cdot \sigma_2 \right] (4M_\pi^2 + q^2)A^{\tilde{\Lambda}}(q),$$

with the loop function  $A^{\tilde{\Lambda}}(q)$  given by

$$A^{\tilde{\Lambda}}(q) = \frac{1}{2q} \arctan \frac{q(\tilde{\Lambda} - 2M_\pi)}{q^2 + 2\tilde{\Lambda}M_\pi}.$$

Similarly to the previously considered case, OPE diagrams at this order only generate shifts in the corresponding LECs.

The inclusion of the  $\Delta$ -isobar as an explicit degree of freedom in the SSE leads to additional contributions to the TPE potential which are listed in Fig. 1. The leading TPE diagrams were first discussed by Ordóñez et al. [16] using old-fashioned time-ordered perturbation theory. These contributions were then calculated by Kaiser et al. [17] using the Feynman graph technique. The corrections at N<sup>2</sup>LO have also been worked out recently [14]. I do not list here all expressions for the  $\Delta$ -contributions but show the results for the isovector tensor TPE potential  $W_T$ , defined according to  $V_{2N} = \boldsymbol{\tau}_1 \cdot \boldsymbol{\tau}_2 \sigma_1 \cdot \mathbf{q} \sigma_2 \cdot \mathbf{q} W_T$ , which may be regarded as a representative example:

$$W_T^{(2)} = -\frac{h_A^2}{1296\pi^2 F_\pi^4 \Delta} \left[ 9\pi g_A^2 \omega^2 A^{\tilde{\Lambda}}(q) + h_A^2 (2L^{\tilde{\Lambda}}(q) + (4\Delta^2 + \omega^2)D^{\tilde{\Lambda}}(q)) \right],$$

$$W_T^{(3)} = -\frac{h_A^2 \Delta}{648\pi^2 F_\pi^4} \left[ (2(b_3 + b_8)g_A(\omega^2 - 12\Delta^2) - 9c_4(\omega^2 - 4\Delta^2))D^{\tilde{\Lambda}}(q) \right. \\ \left. + 6(3c_4 - 2(b_3 + b_8)h_A)L^{\tilde{\Lambda}}(q) \right]. \quad (8)$$

Here, the new loop function  $D^{\tilde{\Lambda}}(q)$  is defined via

$$D^{\tilde{\Lambda}}(q) = \frac{1}{\Delta} \int_{2M_\pi}^{\tilde{\Lambda}} \frac{d\mu}{\mu^2 + q^2} \arctan \frac{\sqrt{\mu^2 - 4M_\pi^2}}{2\Delta}. \quad (9)$$

The complete results for the  $\Delta$ -contributions can be found in Refs. [14, 17]. It is instructive to verify the consistency between the delta-full and delta-less theories which requires the contributions due to intermediate  $\Delta$ -excitations, expanded in powers of  $1/\Delta$ , to be absorbable into a redefinition of the LECs in the delta-less theory. This implies e.g. that the nonpolynomial (in momenta)

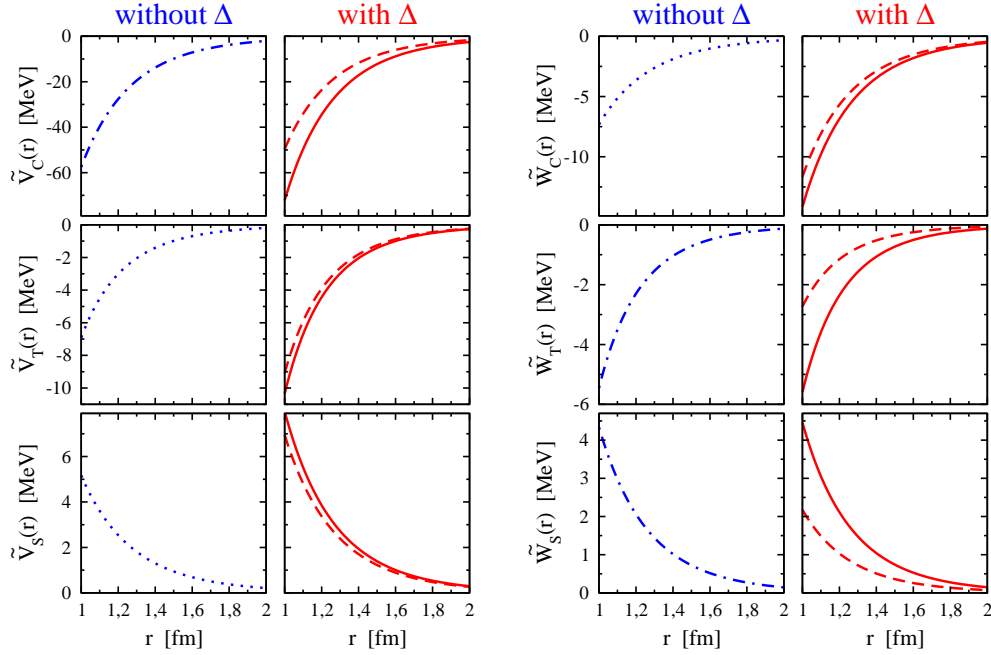


Figure 2: TPE potential in coordinate space for  $\tilde{\Lambda} = 700$  MeV. Dashed and solid (dotted and dashed-dotted) lines refer to the NLO and N<sup>2</sup>LO results in the delta-full (delta-less) theory, respectively. There are no contributions to  $\tilde{V}_C$  and  $\tilde{W}_{T,S}$  ( $\tilde{V}_{T,S}$  and  $\tilde{W}_C$ ) at NLO (N<sup>2</sup>LO) in the delta-less theory.

contributions up to N<sup>2</sup>LO resulting from such an expansion must have the same form as expressions in Eqs. (6, 7). This indeed turns out to be the case: all expanded nonpolynomial terms up to N<sup>2</sup>LO are exactly reproduced by the shift in the LECs  $c_{3,4}$ ,  $c_3 = -2c_4 = -4h_A^2/(9\Delta)$  in Eqs. (6, 7).

To get more insight into the strength of various contributions, it is useful to switch to coordinate space. The TPE potential can then be written as

$$\tilde{V}(r) = \tilde{V}_C + \boldsymbol{\tau}_1 \cdot \boldsymbol{\tau}_2 \tilde{W}_C + [\tilde{V}_S + \boldsymbol{\tau}_1 \cdot \boldsymbol{\tau}_2 \tilde{W}_S] \boldsymbol{\sigma}_1 \cdot \boldsymbol{\sigma}_2 + [\tilde{V}_T + \boldsymbol{\tau}_1 \cdot \boldsymbol{\tau}_2 \tilde{W}_T] S_{12}, \quad (10)$$

where  $S_{12} = 3\boldsymbol{\sigma}_1 \cdot \hat{r} \boldsymbol{\sigma}_2 \cdot \hat{r} - \boldsymbol{\sigma}_1 \cdot \boldsymbol{\sigma}_2$  is the tensor operator. The scalar functions  $\tilde{V}_i(r)$  and  $\tilde{W}_i(r)$  are plotted in Fig. 2 using the values for the LECs specified in section 3. As expected, one observes a much more natural convergence pattern in the theory with explicit delta with the N<sup>2</sup>LO contributions yielding typically only modest corrections to the NLO result. This is, clearly, not the case in the delta-less theory where the entire contributions to  $\tilde{V}_C$  and  $\tilde{W}_{T,S}$  are generated at N<sup>2</sup>LO. On the other hand, the N<sup>2</sup>LO TPE potential in the delta-less theory provides a surprisingly good approximation to the

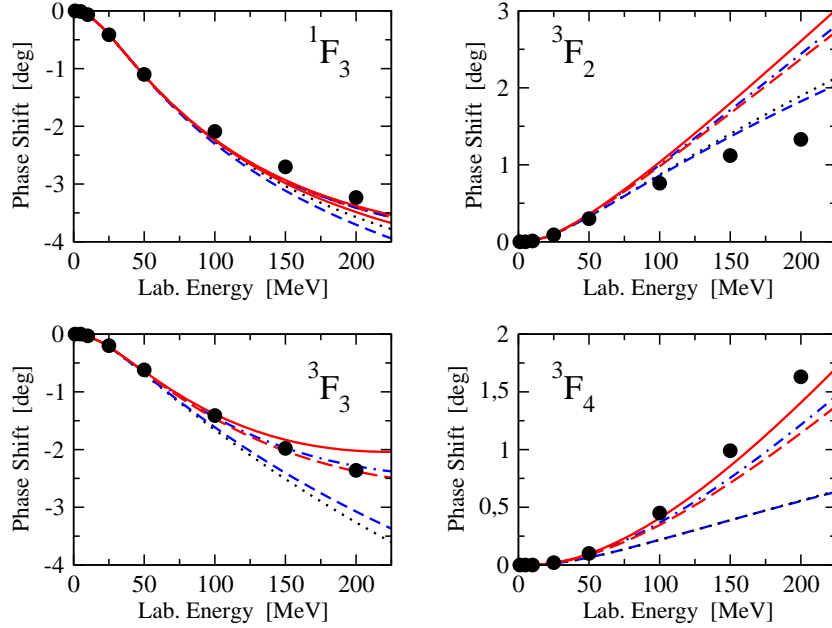


Figure 3: F-wave NN phase shifts for  $\tilde{\Lambda} = 700$  MeV. The dotted curve is the LO prediction, long-dashed (short-dashed) and solid (dashed-dotted) lines show the NLO and N<sup>2</sup>LO results with (without) the explicit  $\Delta$ -contributions. The filled circles depict the results from the Nijmegen PWA [18].

potential resulting at the same order in the delta-full theory. This indicates that the saturation of the LECs  $c_{3,4}$  is the most important effect of the  $\Delta$ -isobar at the considered order. The results for NN F- and other peripheral waves calculated using the Born approximation also clearly demonstrate the improved convergence in the theory with explicit  $\Delta$ , see Fig. 3.

## 5 Three-nucleon force

Chiral power counting in Eq. (1) implies that the 3NF first appears at NLO,  $\nu = 2$ . It is, however, well known that the corresponding terms in the delta-less theory vanish [1, 2], so that the 3NF only starts to contribute at N<sup>2</sup>LO, see Fig. 1. The situation is different in the delta-full theory where the leading contribution of the TPE type shows up already at NLO giving rise to the so-called Fujita-Miyazawa 3NF [19]. Notice that the expression for the  $\Delta$ -contribution to the TPE 3NF is exactly reproduced at N<sup>2</sup>LO in the delta-less theory via resonance saturation of the LECs  $c_{3,4}$ . There are no short-range 3NFs with intermediate  $\Delta$ -excitation since the corresponding

$NNN\Delta$  interaction is Pauli forbidden, see section 2. Interestingly, there are also no  $\Delta$ -contributions at  $N^2\text{LO}$ . The TPE diagrams with one insertion of the subleading  $\pi N\Delta$  vertex  $\propto b_3 + b_8$  lead to  $1/m_N$ -suppressed contributions due to the time derivative which enters this vertex. Despite the fact that both delta-full and delta-less theories produce the same expressions for the TPE 3NF at  $N^2\text{LO}$ , one should keep in mind that their strength might be different<sup>4</sup>. We found, however, that this difference is rather small ( $\sim 7\%$ ) [12].

## 6 Summary and outlook

In this talk, I discussed the structure of the nuclear force in EFT with and without delta degrees of freedom. Explicit expressions for two- and three-nucleon forces in the delta-full theory are currently available at the  $N^2\text{LO}$  in the SSE. As expected, EFT with explicit delta shows a more natural convergence pattern for the long-range nuclear forces, which is clearly visible in peripheral NN phase shifts. On the other hand, the obtained results demonstrate that the contributions of the  $\Delta$ -isobar to the 2NF and 3NF at  $N^2\text{LO}$  are well approximated by the shifts of the LECs  $c_{3,4}$  in the delta-less theory. In the future, these studies should be extended to low NN partial waves and few-nucleon observables. In addition, it would be very interesting to go to  $N^3\text{LO}$ . Based on the available results for the three-pion exchange 2NF [6], one would expect significant  $\Delta$ -contributions to the corresponding three- and four nucleon forces at this order.

## Acknowledgments

I am grateful to my collaborators on this subject, Hermann Krebs and Ulf-G. Meißner, and thank the organizers for the enjoyable conference.

## References

- [1] P. F. Bedaque and U. van Kolck, *Ann. Rev. Nucl. Part. Sci.* **52**, 339 (2002), nucl-th/0203055.
- [2] E. Epelbaum, *Prog. Part. Nucl. Phys.* **57**, 654 (2006), nucl-th/0509032.
- [3] D. R. Entem and R. Machleidt, *Phys. Rev.* **C68**, 041001 (2003), nucl-th/0304018.

---

<sup>4</sup>The extrapolation of the  $\pi N$  amplitude from threshold where the LECs are determined to the kinematical region relevant for the 3NF differs in both theories, see e.g. [20].

- [4] E. Epelbaum, W. Glöckle, and U.-G. Meißner, Nucl. Phys. **A747**, 362 (2005), nucl-th/0405048.
- [5] N. Kaiser, R. Brockmann, and W. Weise, Nucl. Phys. **A625**, 758 (1997), nucl-th/9706045.
- [6] N. Kaiser, Phys. Rev. **C63**, 044010 (2001), nucl-th/0101052.
- [7] E. Epelbaum and U.-G. Meißner, Phys. Rev. **C72**, 044001 (2005), nucl-th/0502052.
- [8] V. Bernard, N. Kaiser, and U.-G. Meißner, Nucl. Phys. **A615**, 483 (1997), hep-ph/9611253.
- [9] T. R. Hemmert, B. R. Holstein, and J. Kambor, J. Phys. **G24**, 1831 (1998), hep-ph/9712496.
- [10] N. Fettes and U.-G. Meißner, Nucl. Phys. **A679**, 629 (2001), hep-ph/0006299.
- [11] S. Weinberg, Nucl. Phys. **B363**, 3 (1991).
- [12] E. Epelbaum, H. Krebs, and U.-G. Meißner, in preparation .
- [13] V. Bernard, Prog. Part. Nucl. Phys. **60**, 82 (2008), arXiv:0706.0312 [hep-ph].
- [14] H. Krebs, E. Epelbaum, and U.-G. Meißner, Eur. Phys. J. **A32**, 127 (2007), nucl-th/0703087.
- [15] N. Fettes, U.-G. Meißner, and S. Steininger, Nucl. Phys. **A640**, 199 (1998), hep-ph/9803266.
- [16] C. Ordóñez, L. Ray, and U. van Kolck, Phys. Rev. **C53**, 2086 (1996), hep-ph/9511380.
- [17] N. Kaiser, S. Gerstendörfer, and W. Weise, Nucl. Phys. **A637**, 395 (1998), nucl-th/9802071.
- [18] V. G. J. Stoks, R. A. M. Klomp, M. C. M. Rentmeester, and J. J. de Swart, Phys. Rev. **C48**, 792 (1993).
- [19] F. Fujita and H. Miyazawa, Prog. Thepr. Phys. **17**, 360 (1957).
- [20] V. R. Pandharipande, D. R. Phillips, and U. van Kolck, Phys. Rev. **C71**, 064002 (2005), nucl-th/0501061.

# COULOMB EFFECTS IN FEW-NUCLEON SYSTEMS

*A. C. Fonseca*

Centro de Física Nuclear da Universidade de Lisboa  
Av. Prof. Gama Pinto 2, P-1649-003 Lisboa, Portugal

## Abstract

Recent progress on the solution of *ab initio* three- and four-nucleon scattering equations in momentum space that include the correct treatment of the Coulomb interaction is reviewed; results for specific observables in reactions initiated by  $p + d$ ,  $p + {}^3\text{He}$  and  $n + {}^3\text{He}$  are shown.

## 1 Introduction

In recent years considerable progress has been achieved in the study of nuclei up to  $A \leq 12$  through *ab initio* structure calculations based on the underlying concept that nucleons interact through pairwise forces fitted to nucleon-nucleon ( $NN$ ) scattering up to the pion production threshold plus a three-nucleon force [1, 2] when necessary. The same concept applies to *ab initio* scattering calculations but here restricted to three- [3, 4] or four-nucleon [5–7] reactions given the greater difficulty involved in the solution of many-body scattering equations, particularly in the presence of the repulsive Coulomb force between charged protons.

In the present review we account for the changes that have taken place since 2005, leading to fully converged *ab initio* calculations of  $p + d$  elastic scattering and breakup at energies up to the pion production threshold and all possible four-nucleon reactions initiated by  $n + {}^3\text{He}$ ,  $p + {}^3\text{H}$ ,  $d + d$ ,  $n + {}^3\text{H}$  and  $p + {}^3\text{He}$  below three-body breakup threshold.

## 2 Three-Nucleon Scattering with Two Protons

The treatment of the Coulomb interaction is based on the ideas proposed in Ref. [8] for the scattering of two charged particles and extended in Ref. [9]

for three-particle scattering. The Coulomb potential is screened, standard scattering theory for short-range potentials is used and the obtained results are corrected for the unscreened limit through the renormalization method proposed in Refs. [8,9]. Although the theory was well established, no reliable calculations existed due to the shortcomings of the practical implementation. In Refs. [10,11] we have demonstrated how one obtains fully converged calculations for  $p+d$  elastic scattering and breakup,  $p+d$  capture into  ${}^3\text{He}+\gamma$ , and two- and three-body photo and electro disintegration using realistic nucleon-nucleon interactions plus the Coulomb potential between protons.

One major difference relative to previous work is that we use a Coulomb potential  $w_R$ , screened around the separation  $r = R$  between two charged baryons which, in configuration space, reads

$$w_R(r) = w(r) e^{-(r/R)^n}, \quad (1)$$

with the true Coulomb potential  $w(r) = \alpha_e/r$ , where  $\alpha_e \approx 1/137$  is the fine structure constant and  $n$  controls the smoothness of the screening. We prefer to work with a sharper screening than the Yukawa screening ( $n = 1$ ) of Ref. [9]. We want to ensure that the screened Coulomb potential  $w_R$  approximates well the true Coulomb one  $w$  for distances  $r < R$  and simultaneously vanishes rapidly for  $r > R$ , providing a comparatively fast convergence of the partial-wave expansion. In contrast, the sharp cutoff ( $n \rightarrow \infty$ ) yields an unpleasant oscillatory behavior in the momentum-space representation, leading to convergence problems. We find that values  $3 \leq n \leq 6$  provide a sufficiently smooth, but at the same time a sufficiently rapid screening around  $r = R$ .

In addition to a different choice of screening function, our calculations are based on the definition of a “two-potential formula” where one separates the long range Coulomb amplitude between the proton and the center of mass (c.m.) of the deuteron from the remainder that constitutes the Coulomb modified short range contribution to the full scattering amplitude.

The starting point in our approach is the full three-body Alt, Grassberger and Sandhas (AGS) equation [12] for the transition operator  $U_{\beta\alpha}^{(R)}(Z)$  that depends parametrically on the screening radius  $R$

$$U_{\beta\alpha}^{(R)}(Z) = \bar{\delta}_{\beta\alpha} G_0^{-1}(Z) + \sum_{\sigma} \bar{\delta}_{\beta\sigma} T_{\sigma}^{(R)}(Z) G_0(Z) U_{\sigma\alpha}^{(R)}(Z), \quad (2a)$$

where the two-particle transition matrix  $T_{\sigma}^{(R)}$  is derived from the full channel interaction  $v_{\alpha} + w_{\alpha R}$

$$T_{\alpha}^{(R)}(Z) = (v_{\alpha} + w_{\alpha R}) + (v_{\alpha} + w_{\alpha R}) G_0(Z) T_{\alpha}^{(R)}(Z), \quad (2b)$$

$G_0(Z) = (Z - H_0)^{-1}$  is the free resolvent and  $\bar{\delta}_{\beta\alpha} = 1 - \delta_{\beta\alpha}$ . Of course, the full multichannel transition matrix  $U_{\beta\alpha}^{(R)}(Z)$  must contain the pure Coulomb transition matrix  $T_{\alpha R}^{\text{c.m.}}(Z)$  derived from the screened Coulomb potential  $W_{\alpha R}^{\text{c.m.}}$  between the spectator proton and the center of mass (c.m.) of the remaining neutron-proton pair in channel  $\alpha$ , that is,

$$T_{\alpha R}^{\text{c.m.}}(Z) = W_{\alpha R}^{\text{c.m.}} + W_{\alpha R}^{\text{c.m.}} G_{\alpha}^{(R)}(Z) T_{\alpha R}^{\text{c.m.}}(Z), \quad (3a)$$

$$G_{\alpha}^{(R)}(Z) = (Z - H_0 - v_{\alpha} - w_{\alpha R})^{-1}, \quad (3b)$$

with the  $pd$  channel being one of those channels  $\alpha$ . The same screening function is used for both Coulomb potentials  $w_{\alpha R}$  and  $W_{\alpha R}^{\text{c.m.}}$ . As shown in [10]  $[U_{\beta\alpha}^{(R)}(Z) - \delta_{\beta\alpha} T_{\alpha R}^{\text{c.m.}}(Z)]$  is a short range operator which after renormalization [9] has a well defined  $R \rightarrow \infty$  limit. Therefore, in the  $R \rightarrow \infty$  limit

$$\begin{aligned} \langle \mathbf{q}_{\beta} | U_{\beta\alpha} | \mathbf{q}_{\alpha} \rangle &= \delta_{\beta\alpha} \langle \mathbf{q}_{\beta} | T_{\alpha C}^{\text{c.m.}} | \mathbf{q}_{\alpha} \rangle \\ &+ \lim_{R \rightarrow \infty} (\mathcal{Z}_{\beta R}^{-\frac{1}{2}}(q_{\beta}) \langle \mathbf{q}_{\beta} | [U_{\beta\alpha}^{(R)}(Z) - \delta_{\beta\alpha} T_{\alpha R}^{\text{c.m.}}(Z)] | \mathbf{q}_{\alpha} \rangle \mathcal{Z}_{\alpha R}^{-\frac{1}{2}}(q_{\alpha})), \end{aligned} \quad (4)$$

where

$$\mathcal{Z}_{\alpha R}(q) = e^{-2i(\sigma_l^{\alpha}(q) - \eta_{lR}^{\alpha}(q))}, \quad (5)$$

with the diverging screened Coulomb  $pd$  phase shift  $\eta_{lR}^{\alpha}(q)$  corresponding to standard boundary conditions and the proper Coulomb one  $\sigma_l^{\alpha}(q)$  referring to the logarithmically distorted proper Coulomb boundary conditions;  $l$  is the  $pd$  relative orbital angular momentum. Likewise for breakup we show [10] that

$$\langle \mathbf{p}_f \mathbf{q}_f | U_{0\alpha} | \mathbf{q}_{\alpha} \rangle = \lim_{R \rightarrow \infty} \{ z_R^{-\frac{1}{2}}(p_f) \langle \mathbf{p}_f \mathbf{q}_f | U_{0\alpha}^{(R)}(Z) | \mathbf{q}_{\alpha} \rangle \mathcal{Z}_{\alpha R}^{-\frac{1}{2}}(q_{\alpha}) \}, \quad (6)$$

$$U_{0\alpha}^{(R)}(Z) = G_0^{-1}(Z) + \sum_{\sigma} T_{\sigma}^{(R)}(Z) G_0(Z) U_{\sigma\alpha}^{(R)}(Z), \quad (7)$$

where  $\mathcal{Z}_{\alpha R}(q_{\alpha})$  and  $z_R(p_f)$  are the corresponding  $pd$  and  $pp$  renormalizations factors. Equations (2a), (3a) and (7) are solved independently for each  $R$  and the corresponding on-shell amplitudes for nuclear plus Coulomb calculated in the  $R \rightarrow \infty$  limit through (4) and (6). In effect the convergence with  $R$  is obtained at small finite  $R$  as demonstrated in Ref. [10,11] for elastic scattering and breakup. All configurations converge at  $R = 20$  fm except the  $pp$ -FSI configuration where a  $pp$ -FSI peak in the absence of Coulomb, becomes a  $pp$ -FSI depression with zero cross section at  $E_{pp} = 0$  MeV when Coulomb is added. Although further details may be found in Refs. [10,11] we show in Figs. 1-3 three examples on how Coulomb effects in  $pd$  breakup and

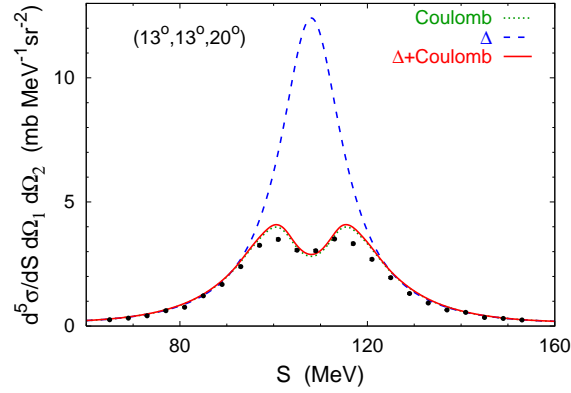


Figure 1: Fivefold differential cross section for  $dp$  breakup at  $E_d = 130$  MeV close to  $pp$ -FSI. The solid line corresponds to calculations with CD Bonn +  $\Delta$  + Coulomb, the dotted line to CD Bonn + Coulomb and the dashed line to CD Bonn +  $\Delta$ . The dots are data from Ref. [15].

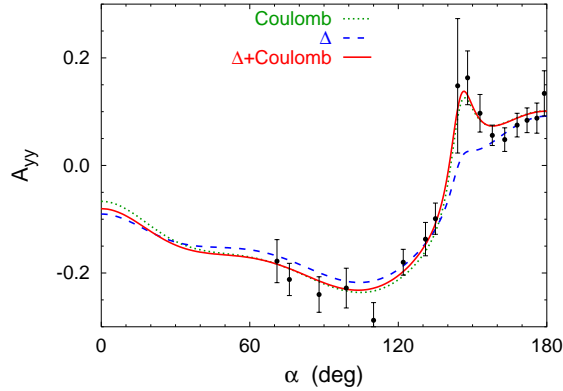


Figure 2: Same as in Fig. 1 for deuteron analyzing power  $A_{yy}$  resulting from  $dp$  breakup at  $E_d = 94.5$  MeV in SCRE geometry. The dots are data from Ref. [16].

three-body photo disintegration of  $^3\text{He}$  are paramount to describe the data. The calculations are based on the purely nucleonic charge-dependent CD-Bonn potential [13] and its coupled-channel extension, CD-Bonn +  $\Delta$  [14], allowing for a single virtual  $\Delta$  - isobar excitation and fitted to the experimental data with the same degree of accuracy as the CD-Bonn itself. In the three-nucleon system the  $\Delta$  isobar mediates an effective three-nucleon force and effective two- and three-nucleon currents, both consistent with the

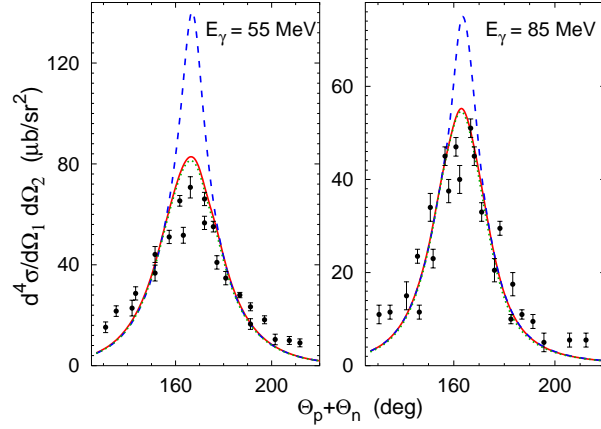


Figure 3: The semi-inclusive fourfold differential cross section for  ${}^3\text{He}(\gamma, pn)p$  reaction at 55- and 85-MeV photon lab energy as a function of the  $np$  opening angle  $\theta_p + \theta_n$  with  $\theta_p = 81^\circ$ . Curves as in Fig. 1. The experimental data are from Ref. [17].

underlying two-nucleon force.

### 3 Four-Nucleon Scattering

The four-nucleon ( $4N$ ) scattering problem gives rise to the simplest set of nuclear reactions that shows the complexity of heavier systems. The neutron- ${}^3\text{H}$  ( $n$ - ${}^3\text{H}$ ) and proton- ${}^3\text{He}$  ( $p$ - ${}^3\text{He}$ ) scattering is dominated by the total isospin  $\mathcal{T} = 1$  states while elastic deuteron-deuteron ( $d$ - $d$ ) scattering by the  $\mathcal{T} = 0$  states; the reactions  $n$ - ${}^3\text{He}$  and  $p$ - ${}^3\text{H}$  involve both  $\mathcal{T} = 0$  and  $\mathcal{T} = 1$  and are coupled to  $d$ - $d$  in  $\mathcal{T} = 0$ . Due to the charge dependence of the hadronic and electromagnetic interaction a small admixture of  $\mathcal{T} = 2$  states is also present. In  $4N$  scattering the Coulomb interaction is paramount not only to treat  $p$ - ${}^3\text{He}$  but also to separate the  $n$ - ${}^3\text{He}$  threshold from  $p$ - ${}^3\text{H}$  and at the same time avoid a second excited state of the  $\alpha$  particle a few keV below the lowest scattering threshold. All these complex features make the  $4N$  scattering problem a natural theoretical laboratory to test different force models of the nuclear interaction, after the  $3N$  system [3, 10].

The equations we solve are the four-body AGS equations of Ref. [18] which were used in Ref. [19] to study  $n$ - ${}^3\text{H}$  elastic scattering and in Ref. [20] to calculate  $p$ - ${}^3\text{He}$  with the Coulomb force included between all three-protons. As in (2a) the four-body AGS transition operators in the presence of screened Coulomb become  $R$  dependent. The transition operators  $\mathcal{U}_{(R)}^{\alpha\beta}$  where  $\alpha(\beta) = 1$

and 2 corresponds to initial/final 1 + 3 and 2 + 2 two-cluster states, respectively, satisfy the symmetrized AGS equations

$$\mathcal{U}_{(R)}^{11} = - (G_0 T^{(R)} G_0)^{-1} P_{34} - P_{34} U_{(R)}^1 G_0 T^{(R)} G_0 \mathcal{U}_{(R)}^{11} + U_{(R)}^2 G_0 T^{(R)} G_0 \mathcal{U}_{(R)}^{21}, \quad (8a)$$

$$\mathcal{U}_{(R)}^{21} = (G_0 T^{(R)} G_0)^{-1} (1 - P_{34}) + (1 - P_{34}) U_{(R)}^1 G_0 T^{(R)} G_0 \mathcal{U}_{(R)}^{11}. \quad (8b)$$

Here  $G_0$  is the four free particle Green's function and  $T^{(R)}$  the two-nucleon t-matrix derived from nuclear potential plus screened Coulomb between  $pp$  pairs. The operators  $U_{(R)}^\alpha$  obtained from

$$U_{(R)}^\alpha = P_\alpha G_0^{-1} + P_\alpha T^{(R)} G_0 U_{(R)}^\alpha, \quad (9a)$$

$$P_1 = P_{12} P_{23} + P_{13} P_{23}, \quad (9b)$$

$$P_2 = P_{13} P_{24}, \quad (9c)$$

are the symmetrized AGS operators for the 1 + (3) and (2) + (2) subsystems and  $P_{ij}$  is the permutation operator of particles  $i$  and  $j$ . Defining the initial/final 1 + (3) and (2) + (2) states with relative two-body momentum  $\mathbf{p}$

$$|\phi_\alpha^{(R)}(\mathbf{p})\rangle = G_0 T^{(R)} P_\alpha |\phi_\alpha^{(R)}(\mathbf{p})\rangle, \quad (10)$$

the amplitudes for 1 + 3  $\rightarrow$  1 + 3 and 1 + 3  $\rightarrow$  2 + 2 are obtained as  $\langle \mathbf{p}_f | T_{(R)}^{\alpha\beta} | \mathbf{p}_i \rangle = S_{\alpha\beta} \langle \phi_\alpha^{(R)}(\mathbf{p}_f) | \mathcal{U}_{(R)}^{\alpha\beta} | \phi_\beta^{(R)}(\mathbf{p}_i) \rangle$  with  $S_{11} = 3$  and  $S_{21} = \sqrt{3}$ .

In close analogy with  $pd$  elastic scattering, the full scattering amplitude, when calculated between initial and final  $p$ - $^3\text{He}$  states, may be decomposed as follows

$$T_{(R)}^{11} = T_R^{\text{c.m.}} + [T_{(R)}^{11} - T_R^{\text{c.m.}}], \quad (11)$$

with the long-range part  $T_R^{\text{c.m.}}$  being the two-body t-matrix derived from the screened Coulomb potential of the form (1) between the proton and the c.m. of  $^3\text{He}$ , and the remaining Coulomb distorted short-range part  $[T_{(R)}^{11} - T_R^{\text{c.m.}}]$  as demonstrated before for  $pd$ . Applying the renormalization procedure, i.e., multiplying both sides of Eq. (11) by the renormalization factor  $Z_R^{-1}$ , in the  $R \rightarrow \infty$  limit, yields the full 1 + 3  $\rightarrow$  1 + 3 transition amplitude in the presence of Coulomb

$$\langle \mathbf{p}_f | T^{11} | \mathbf{p}_i \rangle = \langle \mathbf{p}_f | T_C^{\text{c.m.}} | \mathbf{p}_i \rangle + \lim_{R \rightarrow \infty} \{ \langle \mathbf{p}_f | [T_{(R)}^{11} - T_R^{\text{c.m.}}] | \mathbf{p}_i \rangle Z_R^{-1} \}. \quad (12)$$

Although the limit in the second term of Eq. (12) is carried out numerically, it is reached for finite  $R$  as shown in Fig. 4, where one sees that Coulomb effects are large.

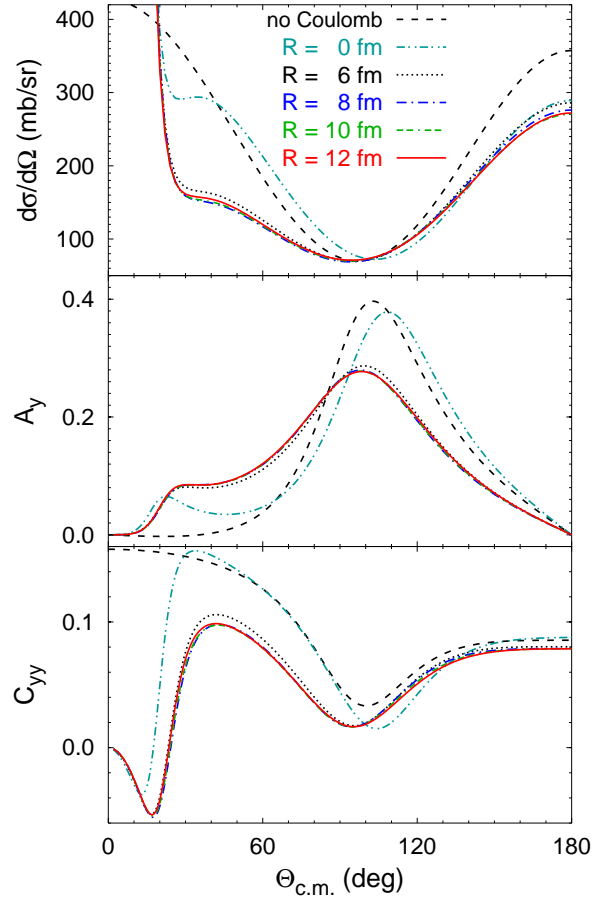


Figure 4: (Color online) Convergence of the  $p$ - ${}^3\text{He}$  scattering observables with screening radius  $R$ . Results for the differential cross section, proton analyzing power  $A_y$ , and  $p$ - ${}^3\text{He}$  spin correlation coefficient  $C_{yy}$  at 4 MeV proton lab energy obtained with screening radius  $R = 0$  fm (dashed-double-dotted curves), 6 fm (dotted curves), 8 fm (dashed-dotted curves), 10 fm (double-dashed-dotted curves), and 12 fm (solid curves) are compared. Results without Coulomb (dashed curves) are given as reference for the size of the Coulomb effect.

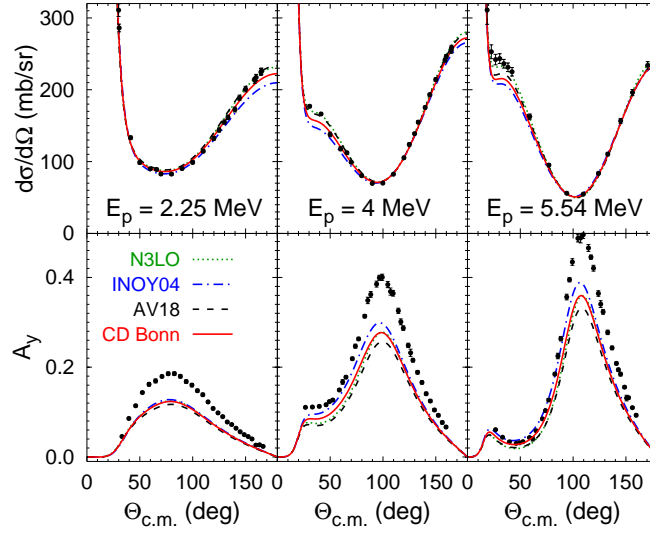


Figure 5: The differential cross section and proton analyzing power  $A_y$  of elastic  $p$ - ${}^3\text{He}$  scattering at 2.25, 4.0, and 5.54 MeV proton lab energy. Results including the Coulomb interaction obtained with potentials CD Bonn (solid curves), AV18 (dashed curves), INOY04 (dashed-dotted curves), and N3LO (dotted curves) are compared. The data are from Refs. [25–27].

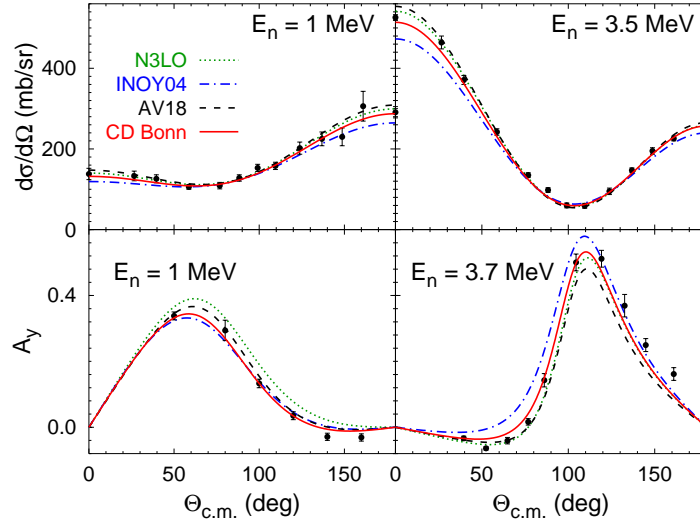


Figure 6: Differential cross section and neutron analyzing power of elastic  $n$ - ${}^3\text{He}$  scattering at 1, 3.5, and 3.7 MeV neutron lab energy. The curves as in Fig. 5. The cross section data are from Ref. [28],  $A_y$  data are from Ref. [29] at 1 MeV and from Ref. [30] at 3.7 MeV.

In Fig. 5-6 we show results for  $p$ - $^3\text{He}$  and  $n$ - $^3\text{He}$  elastic scattering respectively using AV18 [21], CD-Bonn [13], N3LO [22] and INOY04 [23] potentials between  $NN$  pairs plus Coulomb. No  $3N$  force is included at this time. Results indicate that in  $p$ - $^3\text{He}$  there is a stronger  $A_y$  deficiency than in  $n$ - $^3\text{He}$ . This finding may reveal the need for stronger isospin dependent forces but further studies are needed such as including a  $3N$  force. Other considerations and examples may be found in Refs. [20] and [24].

## 4 Conclusions

We have reviewed the most recent work on *ab initio* scattering calculations for three- and four-nucleon reactions using realistic pairwise interactions and the Coulomb force between protons. The calculations with the inclusion of the Coulomb potential are now as accurate as those without, and provide an opportunity for a comprehensive test of hadronic interactions by comparing theory with experimental results obtained with charge particle reactions where data is abundant and error bars smaller.

## References

- [1] S.C. Pieper, V.R. Pandharipande, R.B. Wiringa and J. Carlson, *Phys. Rev.* **C64**, 014001 (2001).
- [2] K. Varga, S.C. Pieper, Y. Suzuki and R.B. Wiringa, *Phys. Rev.* **C66**, 044310 (2002).
- [3] W. Glöckle *et al.*, *Phys. Rep.* **274**, 107 (1996).
- [4] A. Kievsky, M. Viviani and S. Rosati, *Phys. Rev.* **C64**, 024002 (2001); M. Viviani *et al.*, *Phys. Rev.* **C61**, 064001 (2000).
- [5] R. Lazauskas and J. Carbonell, *Phys. Rev.* **C70**, 044002 (2004).
- [6] R. Lazauskas *et al.*, *Phys. Rev.* **C71**, 034004 (2005).
- [7] M. Viviani *et al.*, *Phys. Rev. Lett.* **86**, 3739 (2001).
- [8] J.R. Taylor, *Nuovo Cimento* **B23**, 313 (1974); M.D. Semon and J.R. Taylor, *ibid.* **A26**, 48 (1975).
- [9] E.O. Alt, W. Sandhas and H. Ziegelmann, *Phys. Rev.* **C17**, 1981 (1978).

- [10] A. Deltuva, A.C. Fonseca and P. U. Sauer, *Phys. Rev.* **C71**, 054005 (2005); **C72**, 054004 (2005); **C73**, 057001 (2006).
- [11] A. Deltuva, A.C. Fonseca and P.U. Sauer, *Phys. Rev. Lett.* **95**, 092301 (2005).
- [12] E.O. Alt, P. Grassberger and W. Sandhas, *Nucl. Phys.* **B2**, 167 (1967).
- [13] R. Machleidt, *Phys. Rev.* **C63**, 024001 (2001).
- [14] A. Deltuva, R. Machleidt and P.U. Sauer, *Phys. Rev.* **C68**, 024005 (2003).
- [15] St. Kistryn *et al.*, *Phys. Lett.* **B641**, 23 (2006).
- [16] D.A. Low *et al.*, *Phys. Rev.* **C44**, 2276 (1991).
- [17] N. R. Kolb, P. N. Dezendorf, M. K. Brussel, B. B. Ritchie, and J. H. Smith, *Phys. Rev.* **C44**, 37 (1991).
- [18] P. Grassberger and W. Sandhas, *Nucl. Phys.* **B2**, 181 (1967); E. O. Alt, P. Grassberger, and W. Sandhas, JINR report No. E4-6688 (1972).
- [19] A. Deltuva and A.C. Fonseca, *Phys. Rev.* **C75**, 014005 (2007).
- [20] A. Deltuva and A.C. Fonseca, *Phys. Rev. Lett.* **98**, 162502 (2007).
- [21] R. B. Wiringa *et al.*, *Phys. Rev.* **C51**, 38 (1995).
- [22] D. R. Entem and R. Machleidt, *Phys. Rev.* **C68**, 041001 (2003).
- [23] P. Doleschall, *Phys. Rev.* **C69**, 054001 (2004).
- [24] A. Deltuva and A.C. Fonseca, *Phys. Rev.* **C76**, 021001(R) (2007).
- [25] B. M. Fisher *et al.*, *Phys. Rev.* **C74**, 034001 (2006).
- [26] D. G. McDonald, W. Haeberli, and L. W. Morrow, *Phys. Rev.* **133**, B1178 (1964).
- [27] M. T. Alley and L. D. Knutson, *Phys. Rev.* **C48**, 1890 (1993).
- [28] J. D. Seagrave, L. Cranberg, and J. E. Simmons, *Phys. Rev.* **119**, 1981 (1960).
- [29] P. Jany *et al.*, *Nucl. Phys.* **A483**, 269 (1988).
- [30] H. O. Klages *et al.*, *Nucl. Phys.* **A443**, 237 (1985).

# PRECISION EXTRACTION OF $a_{nn}$ FROM $\pi^- d \rightarrow nn\gamma$ USING CHIRAL PERTURBATION THEORY

*A. Gårdestig*

Department of Physics and Astronomy  
University of South Carolina  
Columbia, SC 29208  
U. S. A.

*D. R. Phillips*

Department of Physics and Astronomy  
Ohio University  
Athens, OH 45701  
U. S. A.

## Abstract

The neutron-neutron scattering length  $a_{nn}$  provides a sensitive probe of charge-symmetry breaking in the strong interaction. Here we summarize our recent efforts to use chiral perturbation theory in order to systematically relate  $a_{nn}$  to the shape of the neutron spectrum in the reaction  $\pi^- d \rightarrow nn\gamma$ . In particular we show how the chiral symmetry of QCD relates this process to low-energy electroweak reactions such as  $pp \rightarrow de^+\nu_e$ . This allows us to reduce the uncertainty in the extracted  $a_{nn}$  (mainly due to short-distance physics in the two-nucleon system) by a factor of more than three, to  $< 0.05$  fm. We also report first results on the impact that two-nucleon mechanisms of chiral order  $P^4$  have on the  $\pi^- d \rightarrow nn\gamma$  neutron spectrum.

## 1 Introduction

Quantum chromodynamics (QCD) is almost symmetric under the interchange of the up and down quarks. This is called charge symmetry, and is due to the fact that the mass difference  $m_d - m_u$  is much smaller than the QCD mass scale  $\Lambda \sim 1$  GeV. This symmetry, which is a subgroup of isospin symmetry  $SU(2)_V$ , is well-respected in strong interactions at low energies, but is

softly broken by quark-mass differences, and also by electromagnetic effects. The relevant dimensionless parameters governing charge-symmetry breaking are therefore  $(m_d - m_u)/\Lambda$  and  $\alpha_{em}/\pi$ , both of which are less than 1%. Although it is indeed generally of this small magnitude, charge-symmetry breaking (CSB) has many experimentally verifiable effects in hadronic and nuclear physics, such as the neutron-proton mass difference, rho-omega mixing, the binding-energy difference of mirror nuclei (e.g.,  ${}^3\text{He}$  and  ${}^3\text{H}$ ), the recently measured forward-backward symmetry for  $np \rightarrow d\pi^0$  [1], and the  $dd \rightarrow \alpha\pi^0$  reaction [2]. For comprehensive reviews of charge symmetry and its breaking see Ref. [3].

The difference between the strong-interaction parts of the  $nn$  and  $pp$  scattering lengths ( $a_{pp}^{\text{str}} - a_{nn}^{\text{str}}$ ) is particularly sensitive to CSB. The scattering length parameterizes the zero-energy  $NN$  scattering phase shift,  $\delta(p)$ , via:

$$a \equiv -\lim_{p \rightarrow 0} \frac{\delta(p)}{p}, \quad (1)$$

where  $p$  is the  $NN$  relative momentum. Hence the (strong)  $nn$  and  $pp$  scattering lengths would be equal in the limit of exact charge symmetry. Their difference is an important quantity for two, somewhat related reasons. Firstly, the nucleon-nucleon scattering lengths are unnaturally large compared to the pion Compton wavelength. This is indicative of fine tuning in the  $NN$  potential and in consequence the CSB piece of the  $NN$  potential has an impact on the scattering lengths that is greatly enhanced [3]:

$$\frac{a_{pp}^{\text{str}} - a_{nn}^{\text{str}}}{a} = (10 - 15) \frac{\Delta V_{\text{CSB}}}{V_{NN}}. \quad (2)$$

Measurements of  $a_{pp} - a_{nn}$  therefore provide significant constraints on CSB terms in modern phenomenological  $NN$  potentials, e.g., AV18 [4]. Secondly, when potentials fit to the currently accepted values  $a_{nn} = -18.59 \pm 0.4$  fm and  $a_{pp} = -17.3 \pm 0.4$  fm [5] are used to make predictions for binding energies of mirror nuclei, they very accurately reproduce the experimental binding-energy difference of, e.g., the aforementioned  ${}^3\text{H}$  and  ${}^3\text{He}$  [6].

Both  $a_{nn}$  and  $a_{pp}$  must have electromagnetic corrections applied to them in order to extract the strong-interaction part. This correction is huge for the  $pp$  case, but is under good theoretical control. In the  $nn$  case the electromagnetic correction is due to a magnetic-moment interaction and is  $\approx -0.3$  fm.

But on the  $nn$  side there is an experimental difficulty in obtaining dense enough free nucleon targets. There have been some attempts at doing direct  $nn$  measurements, the most recent one being pursued at the pulsed reactor YAGUAR [7]. However, the more promising approaches so far have been

based on indirect measurements, where final-state neutrons are detected in regions of phase space where they have low relative energy and hence observables are sensitive to the  $nn$  scattering length.

Unfortunately, the two most recent measurements employing the  $nd \rightarrow nnp$  reaction for this purpose extract very different  $a_{nn}$  values. Thus, a Bonn group reported  $a_{nn} = -16.1 \pm 0.4$  fm [8], while a group based at TUNL claimed  $a_{nn} = -18.7 \pm 0.7$  fm [9], a  $4\sigma$  disagreement.

However, experiments at different facilities based on the alternative process  $\pi^-d \rightarrow nn\gamma$  [10,11], have yielded consistent values for many years. Thus these results dominate the “accepted” value of  $a_{nn}$  quoted above. The scattering length is extracted by fitting the shape of the spectrum of neutrons emitted from the decay of the pionic deuterium atom. The theoretical uncertainty in the  $a_{nn}$  extracted using extant calculations [12,13] is  $\approx \pm 0.3$  fm, dominated by the uncertainties in the  $nn$  wave function at short distances.

In the present work we revisit these calculations for radiative pion capture on deuterium and take advantage of the modern development of effective field theory (EFT), in particular chiral perturbation theory ( $\chi$ PT). By using an EFT we have consistency between the wave functions and production/capture amplitudes, a recipe to estimate the theoretical error, and we can make systematic improvements when necessary. Also, in the case of  $\chi$ PT, we gain a close connection to the underlying theory QCD through QCD’s chiral symmetry. In the next section we describe the key elements of our  $\chi$ PT calculation of  $\pi^-d \rightarrow nn\gamma$ , and in Section 3 we present the results already obtained in recent publications [14–16], and also provide a first report on substantial improvements of these calculations.

## 2 Anatomy of the Calculation

EFTs circumvent the problem of the large QCD coupling constant at low energies. Instead one expands amplitudes in the ratio  $P/\Lambda$ , where  $P \sim m_\pi$  is a small energy/momentum of the problem and  $\Lambda \sim 1$  GeV is the scale of chiral-symmetry breaking. This power counting provides a hierarchy of quantum-mechanical amplitudes which allows for an systematic organization of the calculation. (We count the electron charge  $e$  as one power of  $P/\Lambda$ .)

In the application of chiral perturbation theory to nuclear processes, classes of graphs must be resummed in order to generate the nuclear bound states observed in nature. The original proposal for such resummation is due to Weinberg [17]. Applying it to the case at hand we see that the amplitude for  $\pi^-d \rightarrow nn\gamma$  should be calculated as:

$$\mathcal{A} = \langle \mathbf{p} | \hat{O} | \psi_d \rangle + \langle \mathbf{p} | T_{nn} G_0 \hat{O} | \psi_d \rangle, \quad (3)$$

where  $|\psi_d\rangle$  is the deuteron wave function (which is dominated by modes with momenta where  $\chi$ PT is applicable),  $|\mathbf{p}\rangle$  is a plane wave with the observed relative momentum of the two final-state neutrons,  $\mathbf{p}$ ,  $T_{nn}$  is the  $nn$  rescattering amplitude, and  $G_0$  the free  $nn$  Green function.

Meanwhile  $\hat{O}$  is the operator (technically the two-particle irreducible kernel) governing the transition  $\pi^-np \rightarrow nn\gamma$ . Weinberg proposed that  $\hat{O}$  has a well-behaved chiral expansion and so can be calculated in  $\chi$ PT. (For a summary of the successful application of this idea to electromagnetic processes see Ref. [18].)  $\hat{O}$  has one- and two-body pieces, with the one-body part in this case beginning at  $\mathcal{O}(P)$  with the Kroll-Ruderman term for  $\pi^-p \rightarrow n\gamma$ . Two-body pieces enter at  $\mathcal{O}(P^3)$ . In this work we report on calculations obtained from a partial  $\mathcal{O}(P^4)$  (next-to-next-to-next-leading order = N3LO) calculation of  $\hat{O}$ . Our calculation includes all mechanisms at  $\mathcal{O}(P^3)$  (N2LO), but only the dominant  $\mathcal{O}(P^4)$  two-body pieces of  $\hat{O}$ .

## 2.1 Chirally inspired wave functions

In order to reach the desired accuracy in the calculation of  $\mathcal{A}$ , the  $NN$  wave functions have to be calculated to an order that is consistent with that to which  $\hat{O}$  is obtained. Here this means that they must be computed up to  $\mathcal{O}(P^3)$  and thus include the leading- and sub-leading two-pion-exchange corrections to the chiral  $NN$  potential [19]. The necessary deuteron and  $nn$  scattering wave functions are derived starting from the asymptotic states, given by the asymptotic normalization  $A_S$  and  $D/S$  ratio for the deuteron and the effective-range expansion for  $nn$  scattering. These are integrated in from  $r = \infty$  using the Schrödinger equation with the chiral one- and two-pion exchange potentials. Eventually, we reach a region, at  $r = 1$ – $2$  fm, where the chiral expansion for the  $NN$  potential breaks down. We take the simple approach of introducing a cutoff  $R$  in this range and assume that the potential for  $r < R$  is given by a square well whose depth we adjust to enforce continuity of the wave function at  $r = R$ . This parameterizes and regularizes our ignorance of the short-distance  $NN$  physics. It is then important to ensure that the result is independent of the cutoff  $R$  to the order we are working, i.e., that the renormalization-group criteria are fulfilled.

## 2.2 One-body amplitudes to NNLO

The chiral one-body amplitudes have been calculated by Fearing *et al.* [20] up to  $\mathcal{O}(P^3)$ , fitting the available  $\gamma p \rightarrow \pi^+n$  and  $\pi^-p \rightarrow \gamma n$  data via the adjustment of  $\chi$ PT low-energy constants (LECs). A preliminary estimate

of the size of the N3LO one-body amplitude indicates that it has negligible influence on  $\pi^- d \rightarrow nn\gamma$  and hence we do not discuss it further here [21].

### 2.3 Two-body amplitudes to N3LO

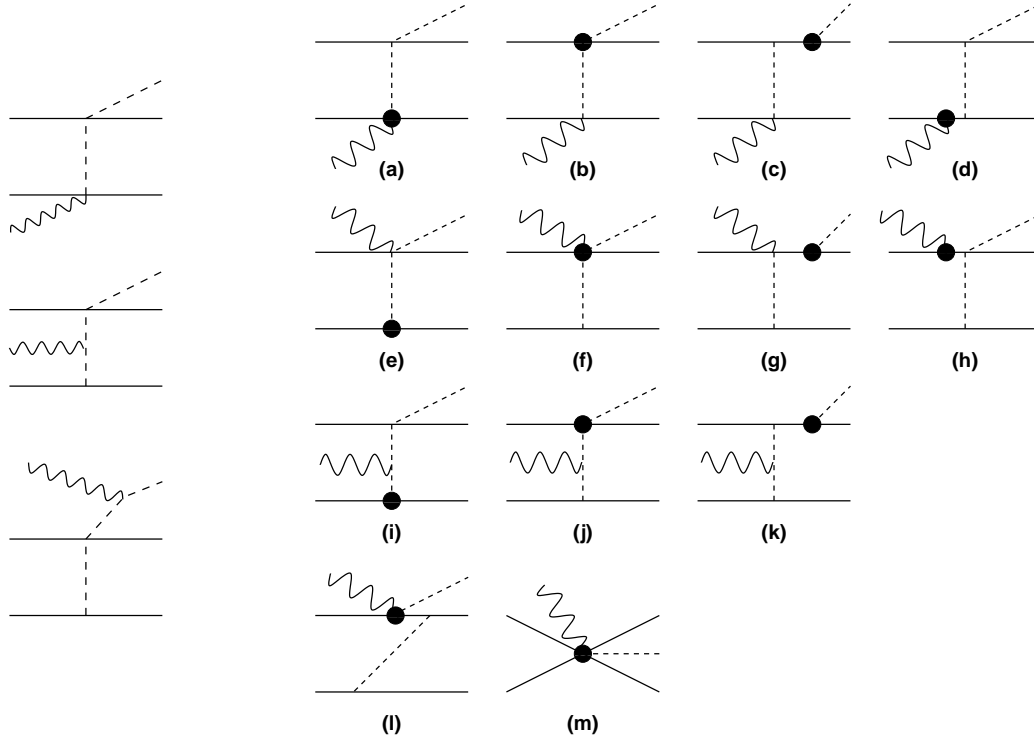


Figure 1: The two-body diagrams relevant for  $\pi^- d \rightarrow nn\gamma$ . Left:  $\mathcal{O}(P^3)$ . Right:  $\mathcal{O}(P^4)$ . Only one representative vertex ordering is given for each type of diagram. The black discs indicates insertions from  $\mathcal{L}_{\pi NN}^{(2)}$ .

At  $\mathcal{O}(P^3)$  (N2LO), there are the three diagrams given to the left in Fig. 1. The first is believed to be larger than the second since the pion mass disappears from its single propagator and the pion can go on-shell, while the second has, in addition, also one off-shell propagator. The third diagram vanishes in Coulomb gauge. At N3LO [ $\mathcal{O}(P^4)$ ], a slew of diagrams appear, given to the right in Fig. 1 and discussed in detail in [16]. The overall result for the neutron time-of-flight spectrum when all these graphs except for (l) are included is depicted in Fig. 3. Diagram (l) is related to the orthonormalization of the wave functions. Since this is suppressed by  $1/M$ , we expect that effects due to  $c_2$ - $c_4$ , which appear in the two-body currents computed in

Ref. [16] that are included in our calculation, will be substantially larger. A complete calculation of the  $\mathcal{O}(P^4)$  correction, including orthonormalization, is under way [21].

## 2.4 Constraining unknown short-distance physics

Fig. 3 shows that the neutron spectrum calculated at  $\mathcal{O}(P^4)$  with different values of the regulator radius  $R$  and a fixed value of the short-distance coefficient in diagram (m) is significantly different in the final-state-interaction (FSI) region. Since  $a_{nn}$  is extracted by fitting the shape of the spectrum in the FSI region [11] this sensitivity to unconstrained physics of the  $NN$  system seems to limit the accuracy with which  $a_{nn}$  can be obtained from  $\pi^-d \rightarrow nn\gamma$ . We now show how to remedy this problem.

The LO contribution to the matrix element in this region is given by

$$\mathcal{M}_{FSI} \equiv C \int_0^\infty dr u_{nn}(r; p) j_0\left(\frac{kr}{2}\right) u_d(r), \quad (4)$$

where  $k$  is the momentum of the outgoing photon,  $C$  is a constant that is fixed by  $e$ ,  $g_A$ ,  $f_\pi$ , etc.,  $j_0$  is the spherical Bessel function of zeroth order, and  $u_d$  [ $u_{nn}(r; p)$ ] is the radial S-wave wave function of the deuteron ( $^1S_0$ ) state. But the short-distance part of this matrix element is the same as that of the  $pp$  fusion matrix element

$$\mathcal{M}_{GT} \equiv \int_0^\infty dr u_{pp}(r) u_d(r). \quad (5)$$

This connection is shown empirically in Fig. 2, revealing a linear relationship between the Gamow-Teller matrix element  $\mathcal{M}_{GT}$ , and the FSI peak height in  $\pi^-d \rightarrow nn\gamma$ ,  $\Gamma_{FSI} \sim |\mathcal{M}_{FSI}|^2$ .

This can be understood from the structure of the chiral Lagrangian. It contains both one-nucleon and two-nucleon terms linear in the axial field  $u_\mu$ :

$$\begin{aligned} \mathcal{L} = & N^\dagger (i v \cdot D + g_A S \cdot u) N \\ & - 2d_1 N^\dagger S \cdot u N N^\dagger N + 2d_2 \epsilon^{abc} \epsilon_{\kappa\lambda\mu\nu} v^\kappa u^{\lambda,a} N^\dagger S^\mu \tau^b N N^\dagger S^\nu \tau^c N \dots, \end{aligned} \quad (6)$$

where

$$f_\pi u_\mu = -\tau^a \partial_\mu \pi^a - \epsilon^{3ba} V_\mu \pi^b \tau^a + f_\pi A_\mu + \mathcal{O}(\pi^3), \quad (7)$$

$V_\mu$  ( $A_\mu$ ) is an external vector (axial) field, and the  $d_i = \mathcal{O}(\frac{1}{Mf_\pi^2})$  are (a priori unknown) LECs. Since  $u_\mu$  contains the pion pseudovector coupling, as well as a pion-photon coupling and the axial field  $A_\mu$ , this is the chiral explanation behind the well-known Goldberger-Treiman (GT) relation and

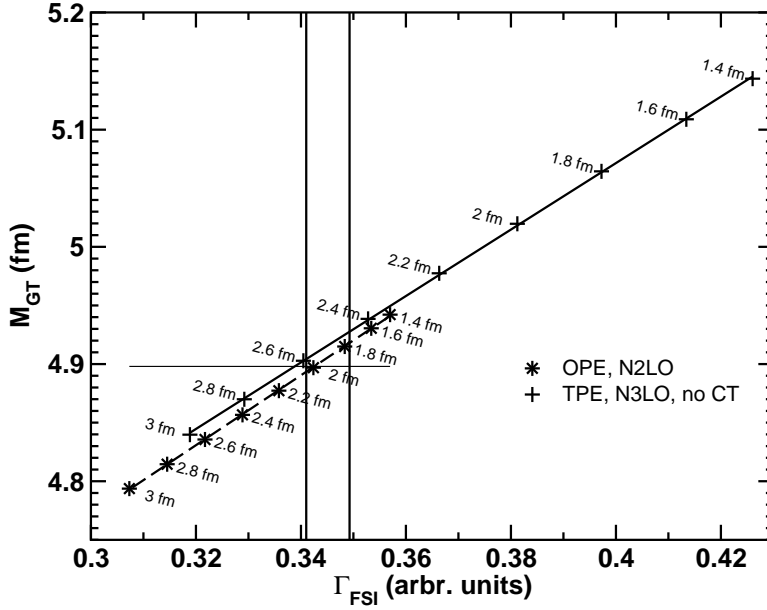


Figure 2: Gamow-Teller matrix element plotted against  $\pi^-d \rightarrow nn\gamma$  FSI peak height for various values of  $R$  and at different orders and wave functions. The points correspond to the values of  $R$  (in fm) indicated. The straight lines are linear fits to the points. The vertical lines show the range in  $\Gamma_{\text{FSI}}$  after renormalization, given the  $M_{\text{GT}}$  value indicated by the horizontal line.

Kroll-Ruderman (KR) terms. In the two-nucleon sector, the same features of  $u_\mu$  imply a connection between pion  $p$ -wave production, pion photoproduction on the  $NN$  system, and axial currents—two-body analogs of the GT and KR. The connection between pion production and electroweak processes is currently being investigated by Nakamura [22].

For Gamow-Teller ( $^1S_0 \leftrightarrow ^3S_1$ ) transitions, the LECs only appear in the combination

$$\hat{d} \equiv \hat{d}_1 + 2\hat{d}_2 + \frac{\hat{c}_3}{3} + \frac{2\hat{c}_4}{3} + \frac{1}{6}, \quad (8)$$

where  $g_A \hat{d}_i \equiv M f_\pi^2 d_i$  and  $\hat{c}_i \equiv M c_i$  [23]. This LEC also appears in  $p$ -wave pion production in  $NN$  collisions, tritium  $\beta$  decay,  $pp$  fusion,  $\nu d$  scattering,  $\mu^-d \rightarrow nn\nu_\mu$ , and the hep reaction. In addition, if the emitted pion couples to a third nucleon, this same operator and coefficient enters the leading chiral three-nucleon force. These and other implications are discussed further in Refs. [15, 16]. The key point in the context of this work is that chiral symmetry and gauge invariance together explain the linear correlation between  $pp$  fusion and the FSI peak height that is evident in Fig. 2.

Now, the solar  $pp$  fusion process has recently been calculated very accurately by constraining its unknown short-distance physics from precise calculations of tritium beta decay [23]. If we adjust the LEC that appears in diagram ( $m$ ) to reproduce this rate for  $pp \rightarrow de^+\nu_e$  we obtain a very precise prediction for the FSI peak height in  $\pi^-d \rightarrow nn\gamma$ , as shown in Fig. 2.

### 3 Results

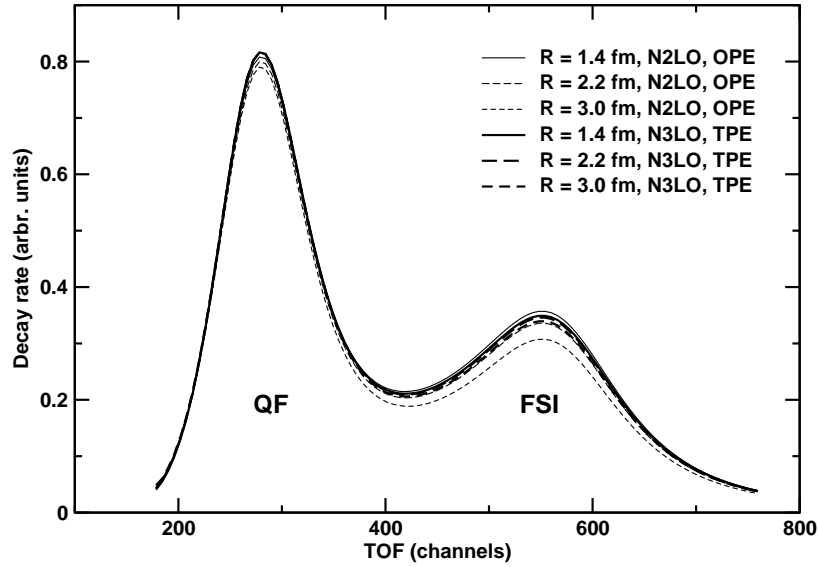


Figure 3: The neutron time-of-flight spectrum for  $\pi^-d \rightarrow nn\gamma$  at different cutoffs  $R$  and orders as indicated. The thin lines are for the N3LO calculation with wave functions calculated with the chiral one-pion exchange potential, while the thick lines include N3LO two-body currents and the chiral two-pion exchange potential as well. The latter coincide at the quasi-free (QF) peak and show a much reduced spread in the FSI peak.

The result of this renormalization can be seen in Fig. 3. Clearly the N3LO contribution reduces the cutoff dependence considerably compared to N2LO. The theoretical uncertainty due to unknown short-distance physics in the  $NN$  system is now negligible in the FSI region. A detailed analysis of the other theoretical uncertainties (see Ref. [14]) reveals that the total theoretical error in the extracted  $a_{nn}$  at N3LO is  $\pm 0.3$  fm when the entire spectrum is fitted and  $\pm 0.05$  fm if only the FSI peak is fitted.

## 4 Conclusions

Chiral perturbation theory relates the unknown short-distance physics of various electroweak two-body observables to pion  $p$ -wave production and pion photoproduction on two nucleons. (We can also constrain a piece of the chiral three-nucleon force from electroweak two-body observables.) This connection makes it possible to calculate  $\pi^- d \rightarrow nn\gamma$  to high precision, leading to a small theoretical error for the extraction of  $a_{nn}$ :  $\Delta a_{nn}^{\text{theory}} = \pm 0.05$  fm. This reduces that error by at least a factor of three compared to previous calculations.

A future publication [21] will contain a full description of the amplitudes and wave functions employed in our N3LO calculation. In that work we will also investigate the influence of higher-order electromagnetic corrections in the  $pp$  wave functions used for  $pp \rightarrow de^+\nu_e$  and whether we are justified in neglecting the N3LO one-body contribution. We also provide a full accounting of the  $1/M$  corrections to the two-body operators that are mandated by the unitary transformations used to obtain a Hermitian  $NN$  potential  $V$ .

In addition we are investigating the possibility to constrain  $\hat{d}$  directly from a two-body observable by calculating the  $\mu^- d \rightarrow nn\nu_\mu$  capture rate in the same framework [24]. This reaction is soon to be measured at the Paul Scherrer Institute to 1% precision [25]. It would also be interesting to revisit the neutrino-deuteron breakup reactions that are important for the SNO detector. Another possible direction would be to complete the circle by calculating tritium beta decay using chiral three-nucleon wave functions with the  $r$ -space regularization we have used in the  $NN$  sector.

## Acknowledgments

This work was supported by the Institute for Nuclear and Particle Physics at Ohio University, by DOE grant DE-FG02-93ER40756, and by NSF grant PHY-0457014.

## References

- [1] A. K. Opper *et al.*, *Phys. Rev. Lett.* **91**, 212302 (2003).
- [2] E. J. Stephenson *et al.*, *Phys. Rev. Lett.* **91**, 142302 (2003).
- [3] G. A. Miller, B. M. K. Nefkens, and I. Šlaus, *Phys. Rep.* **194**, 1 (1990); G. A. Miller and W. van Oers, arXiv:nucl-th/9409013; G. A. Miller, A. Opper, and E. J. Stephenson, *Ann. Rev. Nucl. Part. Sci.* **56**, 293 (2006).

- 
- [4] R. B. Wiringa, V. G. J. Stoks, and R. Schiavilla, *Phys. Rev. C* **51**, 38 (1995).
- [5] R. Machleidt and I. Slaus, *J. Phys. G* **27**, R69 (2001).
- [6] S. C. Pieper and R. B. Wiringa, *Annu. Rev. Nucl. Part. Sci.* **51**, 53 (2001).
- [7] W. I. Furman *et al.*, *J. Phys. G: Nucl. Part. Phys.* **28**, 2627 (2002).
- [8] V. Huhn *et al.*, *Phys. Rev. Lett.* **85**, 1190 (2000).
- [9] D. E. González Trotter *et al.*, *Phys. Rev. Lett.* **83**, 3788 (1999). *Phys. Rev. C* **73**, 034001 (2006).
- [10] B. Gabioud *et al.*, *Phys. Rev. Lett.* **42**, 1508 (1979); *Phys. Lett.* **103B**, 9 (1981); *Nucl. Phys.* **A420**, 496 (1984); O. Schori *et al.*, *Phys. Rev. C* **35**, 2252 (1987).
- [11] C. R. Howell *et al.*, *Phys. Lett. B* **444**, 252 (1998).
- [12] W. R. Gibbs, B. F. Gibson, and G. J. Stephenson, Jr., *Phys. Rev. C* **11**, 90 (1975); **16**, 322 (1977); **16**, 327 (1977).
- [13] G. F. de Téramond, *Phys. Rev. C* **16**, 1976 (1977); G. F. de Téramond, J. Páez, and C. W. Soto Vargas, *ibid.* **21**, 2542 (1980); G. F. de Téramond and B. Gabioud, *ibid.* **36**, 691 (1987).
- [14] A. Gårdestig and D. R. Phillips, *Phys. Rev. C* **73**, 014002 (2006).
- [15] A. Gårdestig and D. R. Phillips, *Phys. Rev. Lett.* **96**, 232301 (2006).
- [16] A. Gårdestig, *Phys. Rev. C* **74**, 017001 (2006).
- [17] S. Weinberg, *Nucl. Phys. B* **363**, 3 (1991); *Phys. Lett. B* **251**, 288 (1990).
- [18] D. R. Phillips, these proceedings.
- [19] C. Ordonéz, L. Ray, and U. van Kolck, *Phys. Rev. C* **53**, 2086 (1996); N. Kaiser, R. Brockmann, and W. Weise, *Nucl. Phys.* **A625**, 758 (1997); E. Epelbaum, W. Glöckle, and U.-G. Meißner, *Nucl. Phys.* **A671**, 295 (1999); M. C. M. Rentmeester, *et al.*, *Phys. Rev. Lett.* **82**, 4992 (1999).
- [20] H. W. Fearing *et al.*, *Phys. Rev. C* **62**, 054006 (2000).
- [21] A. Gårdestig and D. R. Phillips, (in preparation).

- [22] S. X. Nakamura, arXiv:0709.1239 [nucl-th] and these proceedings.
- [23] T.-S. Park *et al.*, *Phys. Rev. C* **67**, 055206 (2003).
- [24] A. Gårdestig, T.-S. Park, K. Kubodera, and F. Myhrer, (in preparation).
- [25] P. Kammel, talk at *International Conference on Muon Catalyzed Fusion and Related Topics*, Dubna, Russia (2007).

# QCD SYMMETRIES IN EXCITED HADRONS

*L. Ya. Glozman*

Institute for Physics, Theoretical Physics Branch

University of Graz

Universitätsplatz 5, A-8010 Graz, Austria

## Abstract

Recent developments for chiral and  $U(1)_A$  restorations in excited hadrons are reviewed. We emphasize predictions of the chiral symmetry restoration scenario for axial charges and couplings to Goldstone bosons. Using very general chiral symmetry arguments it is shown that strict chiral restoration in a given excited nucleon forbids its decay into the  $N\pi$  channel. We confront this prediction with the  $N^*N\pi$  coupling constants extracted from the decay widths and observe a 100 % correlation of these data with the spectroscopic parity doublet patterns. These results suggest that the lowest approximate chiral parity doublet is the  $N(1440) - N(1535)$  pair. In the meson sector we discuss predictions of the chiral symmetry restoration for still missing states and a signature of the higher symmetry observed in new  $\bar{p}p$  data. We conclude with the exactly solvable chirally symmetric and confining model that can be considered as a generalization of the 1+1 dimensional 't Hooft model to 4 dimensions. Complete spectra of  $\bar{q}q$  mesons demonstrate a fast chiral restoration with increasing  $J$  and a slow one with increasing  $n$ .

## 1 Introduction

In hadrons consisting of  $u$  and  $d$  quarks there are two crucially important properties of QCD - chiral symmetry and confinement. Their interrelations and mechanisms are not yet understood. What we do know theoretically is that at zero temperature and density in the confining phase chiral symmetry must be necessarily spontaneously broken in the vacuum [1]. Another conceptual and closely related issue is the generation of hadron mass in the light quark sector. It was considered almost self-evident that such a mass generation proceeds via the chiral symmetry breaking in the vacuum and the most important characteristics that determines the hadron mass is the quark

condensate of the vacuum. Indeed, it is firmly established both phenomenologically and on the lattice that to leading order the pion mass squared is proportional to the bare quark mass and the quark condensate [2]. In the baryon sector the very absence of the chiral partner to the nucleon implies that its mass is at least mostly related to the spontaneous breaking of chiral symmetry in the vacuum. This fact is supported by the Ioffe formula [3] that connects, though not rigorously, the nucleon mass with the quark condensate. Another obvious sign of the strong dynamical chiral symmetry breaking effects in the nucleon is the large pion-nucleon coupling constant. Indeed, it is well understood that the coupling of the Goldstone bosons to the nucleon is a direct consequence of the spontaneous chiral symmetry breaking and is a basis for nucleon chiral perturbation theory [4]. One more strong evidence for the chiral symmetry breaking in the nucleon is its large axial charge,  $g_A = 1.26$ .

A main message of this talk is that the mass generation mechanism in excited hadrons is essentially different - the quark condensate of the vacuum becomes less and less important with the excitation and the chiral as well as the  $U(1)_A$  symmetries get eventually approximately restored in the given hadron, even though they are strongly broken in the vacuum. This is referred to as effective restoration of chiral symmetry, for a review see ref. [10].

It is important to precisely characterize what is implied under effective restoration of chiral and  $U(1)_A$  symmetry in excited hadrons. A mode of symmetry is defined only by the properties of the vacuum. If a symmetry is spontaneously broken in the vacuum, then it is the Nambu-Goldstone mode and the whole spectrum of excitations on the top of the vacuum is in the Nambu-Goldstone mode. However, it may happen that the role of the chiral symmetry breaking condensates becomes progressively less important higher in the spectrum, because the valence quarks decouple from the quark condensates. This means that the chiral symmetry breaking effects become less and less important in the highly excited states and asymptotically the states approach the regime where their properties are determined by the underlying unbroken chiral symmetry (i.e. by the symmetry in the Wigner-Weyl mode). This effective restoration in excited hadrons should not be confused with the chiral symmetry restoration in the vacuum at high temperature/density. In the latter case the quark vacuum becomes trivial and the system is in the Wigner-Weyl mode. In the former case the symmetry is always broken in the vacuum, however this symmetry breaking in the vacuum gets irrelevant in the highly excited states.

## 2 Empirical evidence for chiral restoration in excited nucleons

The nucleon excitation spectrum is shown in Fig. 1. Only well-established states (i.e. without stars in boxes) should be seriously considered. It is well seen that there is no chiral partner to the nucleon. This necessarily implies that chiral symmetry is strongly broken in the nucleon and consequently is realized nonlinearly [5]. Obvious approximate parity doublets are observed in the region 1.7 GeV and higher. An absence of parity doublets for the lowest-lying states and their apparent appearance for (highly) excited states was taken in refs. [6–9] as evidence for chiral restoration in excited baryons, for a review see ref. [10]. The parity doublets in the 1.7 GeV region have been assigned to the  $(0, 1/2) + (1/2, 0)$  representation of the parity-chiral group because there are no approximately degenerate doublets in the same mass region in the spectrum of the delta-resonance [8, 10]. A clear testable prediction of the chiral symmetry restoration scenario is an existence of chiral partners of the well established high-lying resonances  $N(2190)$  and  $N(2600)$ . A dedicated experimental search of these missing states can be undertaken [11]. Similar situation takes place in the Delta-spectrum.

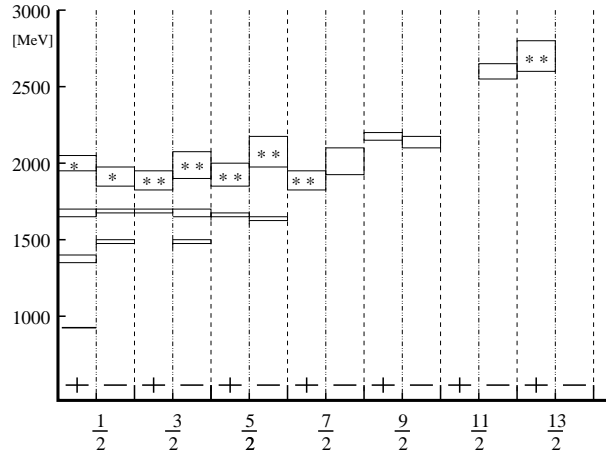


Figure 1: Low- and high-lying nucleons. Those states which are not yet established are marked by \*\* or \* according to the PDG classification.

While these parity doubling patterns are impressive, they are still only suggestive, because so far no other complementary experimental data would independently tell us that these parity doublets are due to effective chiral symmetry restoration. Strict chiral restoration in a given baryon would imply that its diagonal axial charge is zero and hence the diagonal coupling

constant to the pion must vanish [10, 12–15]. This is one of the most important implications of the chiral symmetry restoration and is reviewed below.

Assume that we have a free  $I = 1/2$  chiral doublet  $B$  in the  $(0, 1/2) + (1/2, 0)$  representation and there are no chiral symmetry breaking terms. This doublet is a column [16]

$$B = \begin{pmatrix} B_+ \\ B_- \end{pmatrix}, \quad (1)$$

where the bispinors  $B_+$  and  $B_-$  have positive and negative parity, respectively. The chiral transformation law under the  $(0, 1/2) \oplus (1/2, 0)$  representation provides a mixing of two fields  $B_+$  and  $B_-$ <sup>1</sup>

$$B \rightarrow \exp\left(i\frac{\theta_V^a \tau^a}{2}\right) B; \quad B \rightarrow \exp\left(i\frac{\theta_A^a \tau^a}{2} \sigma_1\right) B. \quad (2)$$

Here  $\sigma_i$  is a Pauli matrix that acts in the  $2 \times 2$  space of the parity doublet. Then the chiral-invariant Lagrangian of the free parity doublet is given as

$$\mathcal{L}_0 = i\bar{B}\gamma^\mu\partial_\mu B - m_0\bar{B}B = i\bar{B}_+\gamma^\mu\partial_\mu B_+ + i\bar{B}_-\gamma^\mu\partial_\mu B_- - m_0\bar{B}_+B_+ - m_0\bar{B}_-B_-.$$

Alternative forms for this Lagrangian can be found in refs. [17, 18].

A crucial property of this Lagrangian is that the fermions  $B_+$  and  $B_-$  are exactly degenerate and have a nonzero chiral-invariant mass  $m_0$ . In contrast, for usual (Dirac) fermions chiral symmetry in the Wigner-Weyl mode restricts particles to be massless, hence they acquire their mass only in the Nambu-Goldstone mode of chiral symmetry due to chiral symmetry breaking in the vacuum (i.e. via the coupling with the quark condensate of the vacuum). The chiral parity doublets have their chiral-invariant mass term already in the Wigner-Weyl mode and this mass term has no relation with the quark condensate.

From the axial transformation law (2) one can read off the axial charge matrix, which is  $\gamma_5\sigma_1$ . Hence the diagonal axial charges of the opposite parity baryons are exactly 0,  $g_+^A = g_-^A = 0$ , while the off-diagonal axial charge is 1,  $|g_{+-}^A| = |g_{-+}^A| = 1$ . This is another crucial property that distinguishes the parity doublets from the Dirac fermions where  $g^A = 1$ . The axial vector current conservation,  $q^\mu\langle B_\pm|A_\mu|B_\pm\rangle = 0$ , translates this axial charge matrix via the Goldberger-Treiman relation into the  $\pi B_\pm B_\pm$  coupling constants which are zero. Hence a small (vanishing) value of the pion-baryon coupling constant taken together with the large baryon mass would tell us that the

<sup>1</sup>Note that the axial transformation given in [16] is incorrect as it breaks chiral symmetry of the kinetic term. The correct axial transformation is given in ref. [10].

origin of this mass is not due to chiral symmetry breaking in the vacuum. An experimental verification of the smallness of the diagonal axial charges or smallness of the pion-baryon coupling constants would be a direct verification of the chiral symmetry restoration scenario in excited nucleons. It is unclear, however, how to measure experimentally these quantities.

There is rich experimental data on strong decays of excited hadrons. It turns out that the chiral restoration implies a very strong selection rule [19]. Namely, it predicts that if chiral symmetry is completely restored in a given excited nucleon ( $B$ ), then it cannot decay into the  $\pi N$  channel, i.e. the coupling constant  $f_{BN\pi}$  must vanish. This selection rule is based exclusively on general properties of chiral symmetry and hence is model-independent.

Let us prove this selection rule. Assume that a  $\pi N$  decay of an exact chiral doublet is possible. Then there must be a self-energy contribution  $B_{\pm} \rightarrow \pi N \rightarrow B_{\pm}$  into its mass. Then the axial rotation (2) would require that the S-wave  $\pi N$  state transforms into the P-wave  $\pi N$  state. However, in the Nambu-Goldstone mode the axial rotations of the pion and nucleon states are fixed - these are the nonlinear axial transformations [14,15]. Given these well known axial transformation properties of the Goldstone boson and nucleon [5] it is not possible to rotate the S-wave  $\pi N$  state into the P-wave  $\pi N$  state. Therefore, there cannot be any  $\pi N$  self-energy component in  $B_{\pm}$ . Hence a decay  $B_{\pm} \rightarrow \pi N$  is forbidden. However, a decay of the exact chiral doublet into e.g.  $N\rho$  or  $N\pi\pi$  is not forbidden. Hence, if a state is a member of an approximate chiral multiplet, then its decay into  $N\pi$  must be strongly suppressed,  $(f_{BN\pi}/f_{NN\pi})^2 \ll 1$ .

If, in contrast, the excited baryon has no chiral partner, then its mass, like in the nucleon case is exclusively due to chiral symmetry breaking in the vacuum. Its axial charge should be comparable with the nucleon axial charge. Then nothing forbids its strong decay into  $N\pi$ . One then expects that the decay coupling constant should be of the same order as the pion-nucleon coupling constant. These two extreme cases suggest that a magnitude of the  $BN\pi$  decay constant can be used as an indicator of the mass origin.

The decay constants  $f_{BN\pi}$  can be extracted from the  $B \rightarrow N + \pi$  decay widths, see e.g. [20,21]. The pion-nucleon coupling constant is well-known,  $f_{NN\pi} = 1.0$ . In Table 1 we show ratios  $(f_{BN\pi}/f_{NN\pi})^2$  for all well-established states. It is well seen that this ratio is  $\sim 0.1$  or smaller for approximate  $J = 1/2, 3/2, 5/2$  parity doublets. For the high-spin states this ratio is practically vanishing. This is consistent with the recent demonstration of the large J-rate of chiral restoration within the only known exactly solvable confining and chirally-symmetric model [22].

From Fig. 1 one can see that the only well established excited state which has no obvious chiral partner is  $3/2^-$ ,  $N(1520)$ . It decays very strongly into

Table 1: Chiral multiplets of excited nucleons. Comment: There are two possibilities to assign the chiral representation:  $(1/2, 0) \oplus (0, 1/2)$  or  $(1/2, 1) \oplus (1, 1/2)$  because there is a possible chiral pair in the  $\Delta$  spectrum with the same spin with similar mass.

Spin	Chiral multiplet	Representation	$(f_{B_+N\pi}/f_{NN\pi})^2 - (f_{B_-N\pi}/f_{NN\pi})^2$
1/2	$N_+(1440) - N_-(1535)$	$(1/2, 0) \oplus (0, 1/2)$	0.15 - 0.026
1/2	$N_+(1710) - N_-(1650)$	$(1/2, 0) \oplus (0, 1/2)$	0.0030 - 0.026
3/2	$N_+(1720) - N_-(1700)$	$(1/2, 0) \oplus (0, 1/2)$	0.023 - 0.13
5/2	$N_+(1680) - N_-(1675)$	$(1/2, 0) \oplus (0, 1/2)$	0.18 - 0.012
7/2	$N_+(?) - N_-(2190)$	see comment	? - 0.00053
9/2	$N_+(2220) - N_-(2250)$	see comment	0.000022 - 0.0000020
11/2	$N_+(?) - N_-(2600)$	see comment	? - 0.000000064
3/2	$N_-(1520)$	no chiral partner	2.5

$N\pi$ , indeed. This implies that a nature of mass of this state is rather different compared to approximate parity doublets. One observes a 100% correlation of the spectroscopic patterns with the  $N\pi$  decays, as predicted by the chiral symmetry restoration.

The Fig. 1 and the Table 1 suggest that the lowest approximate chiral doublet is  $N(1440) - N(1535)$ . If correct, the diagonal axial charges of these states must be small. While it is impossible to measure these charges experimentally, this can be done on the lattice. The axial charge of  $N(1535)$  has just been measured by Takahashi and Kunihiro and they report it to be surprisingly small, smaller than 0.2 [23]. Certainly lattice studies of other states are welcome.

### 3 Symmetries in excited mesons

Fig. 2 shows the spectra of the well established mesons from the PDG and new, not yet confirmed  $\bar{n}n$  states from the partial wave analysis [24, 25] of  $\bar{p}p$  annihilation at LEAR (CERN). Obvious high symmetry of the high-lying  $\bar{n}n$  states is seen. These data have been analysed in ref. [26] and it turned out that the high-lying  $\bar{n}n$  mesons perfectly fit all possible linear chiral multiplets of both  $SU(2)_L \times SU(2)_R$  and  $U(1)_A$  groups with a few still missing states. In particular, the chiral symmetry predicts a duplication of some of the  $J > 0$  states with the given quantum numbers, which is indeed observed in data. If the chiral symmetry is indeed responsible for positive-negative

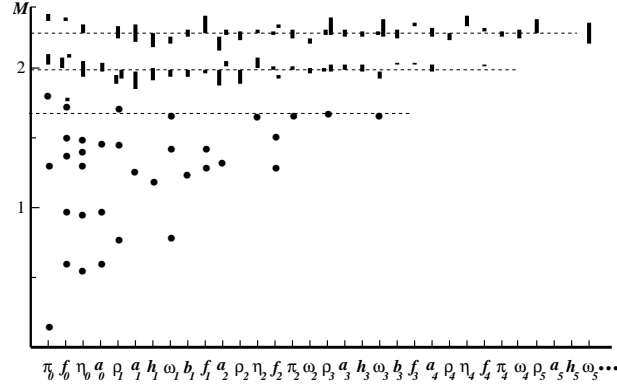


Figure 2: Masses (in GeV) of the well established states from PDG (circles) and new  $\bar{n}n$  states from the proton-antiproton annihilation (strips). Note that the well-established states include  $f_0(1500)$ ,  $f_0(1710)$ , which are the glueball and  $\bar{s}s$  states with some mixing and hence are irrelevant from the chiral symmetry point of view. Similar, the  $f_0(980)$ ,  $a_0(980)$  mesons most probably are not  $\bar{n}n$  states and also should be excluded from the consideration. The same is true for  $\eta(1475)$ , which is the  $\bar{s}s$  state and  $\eta(1405)$  with the unknown nature.

parity degeneracy of the states, then there should be chiral multiplets for the high-spin states at the levels  $M \sim 2$  GeV,  $M \sim 2.3$  GeV and, possibly, at  $M \sim 1.7$  GeV. These states are presently missing in refs. [24,25] and it would be extraordinary important to find them or to reliably exclude them. Note that such high-spin parity doublets are well seen in the nucleon spectrum - see Fig. 1.

The chiral and  $U(1)_A$  symmetries can connect only states with the same spin. Certainly we observe larger degeneracy, the states with different spins are also degenerate. The large degeneracy might be understood if, on top of chiral and  $U(1)_A$  restorations, a principal quantum number  $N = n + J$  existed.

There are suggestions in the literature to explain this large degeneracy without resorting to chiral symmetry, assuming the  $\mathbf{J} = \mathbf{L} + \mathbf{S}$  coupling scheme and that there is a principal quantum number  $N = n + L$ , where  $L$  is the *conserved* orbital angular momentum in the quark-antiquark system [27–29]. This suggestion is hard to reconcile with the Lorentz and chiral symmetries, however [30].

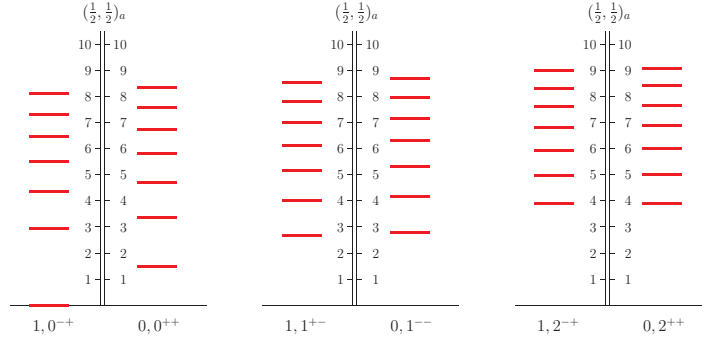


Figure 3: Spectra of the  $\bar{q}q$  mesons in the  $(1/2, 1/2)_a$  representations.

## 4 Chirally symmetric and confining solvable model

There exists only one known manifestly chirally-symmetric and confining model in four dimensions that is solvable [31], sometimes called Generalized Nambu and Jona-Lasinio model (GNJL). This model can be considered as a generalization of the 1+1 dimensional 't Hooft model, that is QCD in the large  $N_c$  limit [32]. It is postulated within the GNJL model that there exists a linear confining potential of the Coulomb type in four dimensions. The chiral symmetry breaking and the properties of the Goldstone bosons have been obtained from the solution of the Schwinger-Dyson and Bethe-Salpeter equations [33–38]. The complete spectrum of  $\bar{q}q$  mesons has been calculated only recently, in ref. [22], which exhibits restoration of the chiral symmetry.

Part of the spectra is shown in Fig. 3 and a fast chiral restoration with increasing of  $J$  is observed, while a slow rate is seen with respect to the radial quantum number  $n$ . It is possible to see directly a mechanism of the chiral restoration. The chiral symmetry breaking Lorentz-scalar dynamical mass of quarks  $M(q)$  arises via selfinteraction loops and vanishes fast at large momenta. When one increases the spin of the hadron  $J$ , or its radial quantum number  $n$ , one also increases the typical momentum of valence quarks. Consequently, the chiral symmetry violating dynamical mass of quarks becomes small and chiral symmetry gets approximately restored. This mechanism of chiral restoration is in accord with a general semiclassical analysis [9, 10, 39].

A higher degeneracy is recovered for  $J \rightarrow \infty$ . In this limit all states with the same  $J$  and  $n$  fall into reducible representation  $[(0, 1/2) \oplus (1/2, 0)] \times [(0, 1/2) \oplus (1/2, 0)]$ , hence the quantum loop effects become irrelevant and all

possible states with different quark chiralities become equivalent.

Support of the Austrian Science Fund through grant P19168-N16 is acknowledged.

## References

- [1] G. 't Hooft, in: Recent developments in Gauge Theories, Eds. G. 't Hooft et al, Plenum, New York, 1980; S. Coleman, E. Witten, Phys. Rev. Lett. **45**, 100 (1980).
- [2] M. Gell-Mann, R. J. Oakes, B. Renner, Phys. Rev. **175**, 2195 (1968).
- [3] B. L. Ioffe, Nucl. Phys. **B 188**, 317 (1981); E: **B 191**, 591 (1981).
- [4] U-G. Meissner, Chiral QCD: Baryon Dynamics, in: At the frontiers of Particle Physics. Handbook of QCD., edited by M. Shifman, v. 1, p. 417, World Sc. 2001.
- [5] S. Weinberg, Phys. Rev. **166**, 1568 (1968).
- [6] L. Ya. Glozman, Phys. Lett. B **475**, 329 (2000).
- [7] T. D. Cohen and L. Ya. Glozman, Phys. Rev. D **65**, 016006 (2002).
- [8] T. D. Cohen and L. Ya. Glozman, Int. J. Mod. Phys. A **17**, 1327 (2002).
- [9] L. Ya. Glozman, Int. J. Mod. Phys. A **21**, 475 (2006).
- [10] L. Ya. Glozman, Phys. Rep. **444**, 1 (2007).
- [11] A. Sibirtsev et al, arXiv: 0706.0183 [nucl-th].
- [12] T. D. Cohen and L. Ya. Glozman, Mod. Phys. Lett. **A 21**, 1939 (2006).
- [13] L. Ya. Glozman, A. V. Nefediev, Phys. Rev. **D 73**, 074018 (2006).
- [14] R. L. Jaffe, D. Pirjol, A. Scardicchio, Phys. Rev. **D 74**, 057901 (2006); Phys. Rev. Lett. **96**, 121601 (2006).
- [15] R. L. Jaffe, D. Pirjol, A. Scardicchio, Phys. Rep. **435**, 157 (2006).
- [16] B. W. Lee, Chiral Dynamics, Gordon and Breach, New York, 1972
- [17] C. DeTar, T. Kunihiro, Phys. Rev. **D 39**, 2805 (1989).

- [18] D. Jido, M. Oka, A. Hosaka, *Progr. Theor. Phys.* **106**, 873 (2001).
- [19] L. Ya. Glozman, arXiv:0706.3288 [hep-ph], *Phys. Rev. Lett.*, in print.
- [20] W. K. Cheng, C. W. Kim, *Phys. Rev.* **154**, 1525 (1967).
- [21] D. O. Riska and G. E. Brown, *Nucl. Phys. A* **679**, 577 (2001).
- [22] R. F. Wagenbrunn, L. Ya. Glozman, *Phys. Lett. B* **643**, 98 (2006); *Phys. Rev. D* **75**, 036007 (2007).
- [23] T. Takahashi and T. Kunihiro, talk at MENU2007.
- [24] A. V. Anisovich et al, *Phys. Lett. B* **491**, 47 (2000); *ibid.* **B 517**, 261 (2001); *ibid.* **B 542**, 8 (2002); *ibid.* **B 542**, 19 (2002); *ibid.* **B 513**, 281 (2001).
- [25] D. V. Bugg, *Phys. Rep.* **397**, 257 (2004).
- [26] L. Ya. Glozman, *Phys. Lett. B* **539**, 257 (2002); *ibid* **587**, 69 (2004).
- [27] S. S. Afonin, *Phys. Rev. C* **76**, 015202 (2007).
- [28] E. Klempt and A. Zaitsev, arXiv:0708.4016 [hep-ph].
- [29] M. Shifman and A. Vainshtein, arXiv:0710.0863 [hep-ph].
- [30] L. Ya. Glozman and A. V. Nefediev, arXiv:0704.2673 [hep-ph], to appear in *Phys. Rev. D*.
- [31] A. Le Yaouanc et al, *Phys. Rev. D* **29** (1984) 1233; **31** (1985) 137.
- [32] G. 't Hooft, *Nucl. Phys. B* **75** (1974) 461; I. Bars, M. B. Green, *Phys. Rev. D* **17** (1978) 537.
- [33] S. L. Adler and A. C. Davis, *Nucl. Phys. B* **244** (1984) 469.
- [34] R. Alkofer and P. A. Amundsen, *Nucl. Phys. B* **306** (1988) 305.
- [35] P. Bicudo and J. E. Ribeiro, *Phys. Rev. D* **42** (1990) 1611; 1625.
- [36] P. J. A. Bicudo and A. V. Nefediev, *Phys. Rev. D* **68** (2003) 065021.
- [37] F. J. Llanes-Estrada and S. R. Cotanch, *Phys. Rev. Lett.*, **84** (2000) 1102.
- [38] R. Alkofer et al, *Phys. Rev. Lett.*, **96**, 022001 (2006).
- [39] L. Ya. Glozman, A. V. Nefediev, J. Ribeiro, *Phys. Rev. D* **72** (2005) 094002.

# NEUTRON POLARIZABILITIES FROM DEUTERON COMPTON SCATTERING IN $\chi$ EFT

*Harald W. Griesshammer*

Center for Nuclear Studies, Department of Physics,  
The George Washington University, Washington DC 20052, USA

## Abstract

Chiral Effective Field Theory is for photon energies up to 200 MeV the tool to accurately determine the polarisabilities of the neutron from deuteron Compton scattering. A multipole analysis reveals that dispersive effects from an explicit  $\Delta(1232)$  prove in particular indispensable to understand the data at 95 MeV measured at SAL. Simple power-counting arguments derived from nuclear phenomenology lead to the correct Thomson limit and gauge invariance. At next-to-leading order, the static scalar dipole polarisabilities are extracted as identical for proton and neutron within the error-bar of available data:  $\bar{\alpha}^n = 11.6 \pm 1.5_{\text{stat}} \pm 0.6_{\text{Baldin}}$ ,  $\bar{\beta}^n = 3.6 \mp 1.5_{\text{stat}} \pm 0.6_{\text{Baldin}}$  for the neutron, in units of  $10^{-4} \text{ fm}^3$ , compared to  $\bar{\alpha}^p = 11.0 \pm 1.4_{\text{stat}} \pm 0.4_{\text{Baldin}}$ ,  $\bar{\beta}^p = 2.8 \mp 1.4_{\text{stat}} \pm 0.4_{\text{Baldin}}$  for the proton in the same framework. New experiments e.g. at MAXlab (Lund) will improve the statistical error-bar.

## 1 The Problem with Neutron Polarisabilities

As the nucleon is not a point-like spin- $\frac{1}{2}$  target with an anomalous magnetic moment, the photon field displaces in low-energy Compton scattering  $\gamma N \rightarrow \gamma N$  its charged constituents, inducing a non-vanishing multipole moment. These long-known nucleon-structure effects are for static external fields parameterised by the electric polarisability  $\bar{\alpha}$  and its magnetic counterpart  $\bar{\beta}$ . For the proton, the generally accepted static values are  $\bar{\alpha}^p \approx 12 \times 10^{-4} \text{ fm}^3$ ,  $\bar{\beta}^p \approx 2 \times 10^{-4} \text{ fm}^3$ , with error-bars of about  $1\% \times 10^{-4} \text{ fm}^3$ .<sup>1</sup>

Does the neutron react similarly under deformations,  $\bar{\alpha}^p \approx \bar{\alpha}^n$ ,  $\bar{\beta}^p \approx \bar{\beta}^n$ ? Different types of experiments report a range of values  $\bar{\alpha}^n \in [-4; 19]$ :

---

<sup>1</sup>It is customary to measure the scalar dipole-polarisabilities in  $10^{-4} \text{ fm}^3$ , so that the units are dropped in the following. Notice that the nucleon is quite stiff.

Coulomb scattering of neutrons off lead, and deuteron Compton-scattering  $\gamma d \rightarrow \gamma d$  with and without breakup, see e.g. [1] for a list. The latter should be a clean way to extract the iso-scalar polarisabilities  $\bar{\alpha}^s := \frac{1}{2}(\bar{\alpha}^p + \bar{\alpha}^n)$  and  $\bar{\beta}^s$  in analogy to determinations of the proton polarisabilities. Experiments were performed in Urbana at  $\omega = 49$  and  $69$  MeV, in Saskatoon (SAL) at  $94$  MeV, and in Lund (MAXlab) at  $55$  and  $66$  MeV. While all low-energy extractions are consistent with small iso-vectorial polarisabilities, the SAL data lead to conflicting analyses: The original publication [2] gave  $\bar{\alpha}^s = 8.8 \pm 1.0$ , using the Baldin sum-rule for the static nucleon polarisabilities. Without it, Levchuk and L'vov obtained  $\bar{\alpha}^s = 11 \pm 2$ ,  $\bar{\beta}^s = 7 \pm 2$  [3]; and Beane et al. found recently from all data  $\bar{\alpha}^s = 13 \pm 4$ ,  $\bar{\beta}^s = -2 \pm 3$  [4]. The extraction being very sensitive to the polarisabilities, this seems discouraging news.

These notes outline the resolution of the puzzle and report on a new high-accuracy determination of the nucleon polarisabilities from all Compton scattering data. There are two main ingredients: a better understanding of dispersive effects in the polarisabilities themselves as discussed in Sect. 2; and a model-independent determination of meson-exchange current effects with an error-estimate, Sect. 3. As customary in proceedings, I apologise for my biased view and refer to [1] at least for a better list of references.

## 2 Dynamical Polarisabilities

The nucleon-structure effects encoded by the polarisabilities are conveniently parameterised starting from the most general interaction between a nucleon  $N$  with spin  $\sigma/2$  and an electro-magnetic field of fixed, non-zero energy  $\omega$ :

$$\begin{aligned} \mathcal{L}_{\text{pol}} = & 2\pi N^\dagger \left[ \alpha_{E1}(\omega) \mathbf{E}^2 + \beta_{M1}(\omega) \mathbf{B}^2 + \gamma_{E1E1}(\omega) \sigma \cdot (\mathbf{E} \times \dot{\mathbf{E}}) \right. \\ & \left. + \gamma_{M1M1}(\omega) \sigma \cdot (\mathbf{B} \times \dot{\mathbf{B}}) - 2\gamma_{M1E2}(\omega) \sigma_i B_j E_{ij} + 2\gamma_{E1M2}(\omega) \sigma_i E_j B_{ij} + \dots \right] N \end{aligned} \quad (1)$$

Here, the electric or magnetic ( $X, Y = E, M$ ) photon undergoes a transition  $Xl \rightarrow Yl'$  of definite multipolarity  $l, l' = l \pm \{0, 1\}$ ;  $T_{ij} := \frac{1}{2}(\partial_i T_j + \partial_j T_i)$ . Its coefficients are the *energy-dependent* or *dynamical polarisabilities* of the nucleon [5]. Most prominently, there are six dipole-polarisabilities. The two spin-independent ones parameterise electric and magnetic dipole-transitions,  $\alpha_{E1}(\omega)$  and  $\beta_{M1}(\omega)$ . Particularly interesting are the four spin-polarisabilities  $\gamma_{E1E1}(\omega)$ ,  $\gamma_{M1M1}(\omega)$ ,  $\gamma_{E1M2}(\omega)$ ,  $\gamma_{M1E2}(\omega)$  as they parameterise the response of the nucleon-*spin* to the photon field. Contributions from higher ones like quadrupole polarisabilities are negligible in today's experiments.

Polarisabilities measure the global stiffness of the nucleon's internal degrees of freedom against displacement in an electric or magnetic field of def-

inite multipolarity and non-vanishing frequency  $\omega$  and are identified *at fixed energy* only by their different angular dependence. Nucleon Compton scattering provides thus a wealth of information about the internal structure of the nucleon. In contradistinction to most other electro-magnetic processes, the nucleon-structure effects in Compton scattering were however previously not analysed in terms of a multipole-expansion at fixed energies. Instead, one focused on the static electric and magnetic polarisabilities  $\bar{\alpha} := \alpha_{E1}(\omega = 0)$  and  $\bar{\beta} := \beta_{M1}(\omega = 0)$ , which are often called “the polarisabilities”. While quite different frameworks could provide a consistent picture for them, the underlying mechanisms are only properly revealed by the energy-dependence.

Clearly, the complete set of dynamical polarisabilities does – like in all multipole-decompositions – not contain more or less information about the temporal response of the nucleonic degrees of freedom than the Compton amplitudes. But the information is better accessible and easier to interpret, as each mechanism leaves a characteristic signature in a particular channel.

To investigate them in a model-independent framework, we employ the unique low-energy theory of QCD, namely Chiral Effective Field Theory  $\chi$ EFT. It contains only those low-energy degrees of freedom which are observed at the typical energy of the process, interacting in all ways allowed by the underlying symmetries of QCD. A momentum expansion of all forces allows for model-independent results of finite, systematically improvable accuracy and thus for an estimate of the theoretical uncertainties encountered by neglecting higher-order contributions. The resulting contributions at leading order (LO) are listed in Fig. 1 and easily motivated [5]:

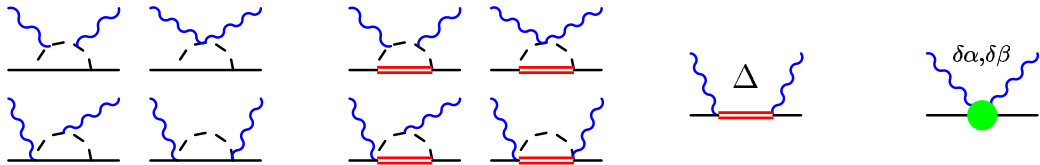


Figure 1: The LO contributions to the nucleon polarisabilities. Left to right: pion cloud around the nucleon and  $\Delta$ ;  $\Delta$  excitations; short-distance effects. Permutations and crossed diagrams not shown. From Ref. [5].

(1) Photons couple to the pions around the nucleon and around the  $\Delta$ , signalled by a characteristic cusp at the one-pion production threshold.

(2) It is well-known that the  $\Delta(1232)$  as the lowest nuclear resonance leads by the strong  $\gamma N \Delta$   $M1$ -transition to a para-magnetic contribution to the static magnetic dipole-polarisability  $\bar{\beta}_\Delta = +[7 \dots 13]$  and a characteristic resonance-shape, cf. the Lorentz-Drude model of classical electrodynamics.

**(3)** As the observed static value  $\bar{\beta}^p \approx 2$  is smaller by a factor of 5 than the  $\Delta$  contribution, a strong dia-magnetic component must exist. The resultant fine-tuning at zero photon-energy is unlikely to hold once the evolution with the photon energy is considered: If dia- and para-magnetism are of different origin, they involve different scales and hence different energy-dependences. We sub-sume this short-distance Physics which is at this order not generated by the pion or  $\Delta$  into two *energy-independent* low-energy coefficients  $\delta\alpha$ ,  $\delta\beta$ .

The cornucopia of Compton data on the proton below 200 MeV determines these to be indeed anomalously large,  $\delta\alpha = -5.9 \pm 1.4$ ,  $\delta\beta = -10.7 \pm 1.2$ , justifying their inclusion at leading order. As expected,  $\delta\beta$  is dia-magnetic. The resulting static proton polarisabilities

$$\bar{\alpha}^p = 11.0 \pm 1.4_{\text{stat}} \pm 0.4_{\text{Baldin}} \quad , \quad \bar{\beta}^p = 2.8 \mp 1.4_{\text{stat}} \pm 0.4_{\text{Baldin}} \quad (2)$$

compare both in magnitude and uncertainty favourably with other state-of-the-art results [5]. Higher-order corrections contribute an error of about  $\pm 1$  not displayed here as the statistics dominates the total error.

With the parameters now fixed, the energy-dependence of all polarisabilities is fixed.  $\chi\text{EFT}$  predicts them at LO to be identical for the proton and neutron. We will confirm this in Sect. 3. The dipole-polarisabilities show the expected behaviour. No low-energy degrees of freedom inside the nucleon are missing. Dispersion is large for  $\omega \in [80; 200]$  MeV where most experiments to determine polarisabilities are performed. Most notably even well below the pion-production threshold is the strong energy-dependence induced into  $\beta_{M1}(\omega)$  and all polarisabilities containing an  $M1$  photon by the unique signature of the  $\Delta$ -resonance: Truncating the Taylor-expansion at order  $\omega^2$  under-estimates  $\beta_{M1}(\omega = 95 \text{ MeV}) - \bar{\beta} \approx 1.7$  [3], while the multipole-analysis gives  $\approx 4$  (Fig. 2). The traditional approximation of  $\beta_{M1}(\omega)$  as “static-plus-small-slope”,  $\bar{\beta} + \omega^2\bar{\beta}_\nu$ , is inadequate. Not surprisingly, this contribution is most pronounced at large momentum-transfers, i.e. backward angles, and thus is the major source of confusion in deuteron Compton scattering, as Fig. 5 will show. Figure 2 reveals the good agreement between the measured value of  $\bar{\beta}^p$  and the prediction in  $\chi\text{EFT}$  without explicit  $\Delta$  as accidental: The pion is not dispersive enough to explain the energy-dependence of  $\beta_{M1}$ .

That the two short-distance parameters  $\delta\alpha$ ,  $\delta\beta$  suffice to describe the data up to  $\omega \approx 200$  MeV [5] leads to three constraints on their explanation:

- (1) Like  $\delta\alpha$ ,  $\delta\beta$ , the effect must be  $\omega$ -independent over a wide range.
- (2) Albeit it must lead to the values for  $\delta\alpha$ ,  $\delta\beta$  predicted in  $\chi\text{EFT}$ , it must be absent at least in the pure spin-polarisabilities  $\gamma_{E1E1}$ ,  $\gamma_{M1M1}$ .

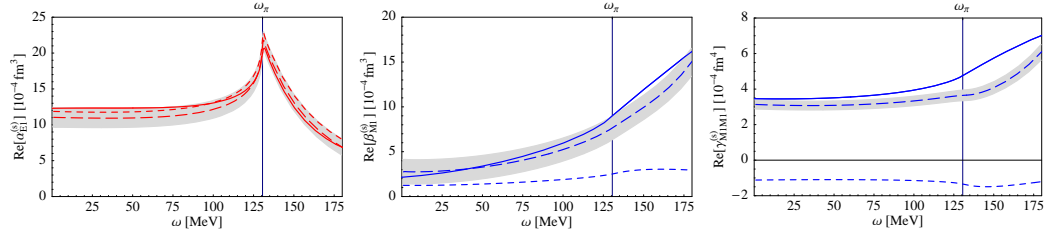


Figure 2: Spin-independent (left, right) and example of spin-dependent (right) dipole-polarisabilities, predicted by Dispersion Theory (solid) and  $\chi$ EFT with (dashed; band: fit-errors) and without (dotted) explicit  $\Delta$ .  $\omega_\pi$ : one-pion production threshold. From Ref. [5].

(3) Its prediction for the proton and neutron must be similar because iso-vectorial effects are small and energy-independent [5, 6].

### 3 Embedding the Nucleon in the Deuteron

Since free neutrons can often not be used in experiments, their properties are usually extracted from data taken on few-nucleon systems by dis-entangling nuclear-binding effects.  $\chi$ EFT allows to subtract two-body contributions from meson-exchange currents and wave-function dependence from data with minimal theoretical prejudice and an estimate of the theoretical uncertainties.

A consistent description must also give the correct Thomson limit, i.e. the exact low-energy theorem which is a consequence of gauge invariance [7, 8]. Its verification is straight-forward in the 1-nucleon sector, where the ampli-

$$\begin{array}{c}
 \begin{array}{c} \text{---} k \text{---} \\ \text{---} -k \text{---} \end{array} \begin{array}{c} \text{---} p \text{---} \\ \text{---} -p \text{---} \end{array} \\
 \text{---} \text{---} \\
 Q^m
 \end{array}
 =
 \begin{array}{c} \text{---} \text{---} \\ \text{---} \text{---} \\ Q^m \end{array}
 V_{NN}
 +
 \begin{array}{c} \text{---} \text{---} \\ \text{---} \text{---} \\ Q^{2m+3-2} \end{array}
 \begin{array}{c} \text{---} q \text{---} \\ \text{---} \text{---} \end{array}
 V_{NN}
 \end{array}
 \stackrel{!}{=}
 Q^m
 \implies m = -1$$

Figure 3: On the consistency of  $NN$  power-counting in  $\chi$ EFT. From Ref. [9].

tude is perturbative. In contradistinction, the two-nucleon amplitude must be non-perturbative to accommodate the shallow bound-state: All terms in the LO Lippmann-Schwinger equation of  $NN$ -scattering, Fig. 3, including the potential, must be of the same order when all nucleons are close to their non-relativistic mass-shell. Otherwise, one of them could be treated

as perturbation of the others and a low-lying bound-state would be absent. Picking the nucleon-pole in the energy-integration  $E \sim \frac{\mathbf{k}^2}{2M}$  leads therefore to the consistency condition that the  $NN$ -scattering amplitude  $T_{NN}$  must be of order  $Q^{-1}$ , irrespective of the potential used.  $Q$  is a typical low-momentum scale of the process under consideration, e.g. the inverse S-wave scattering length. It does therefore not suffice to determine the relative strength of forces and potentials in  $\chi$ EFT just by counting the number of momenta. This has long been recognised in “pion-less” EFT, but is only an emerging communal wisdom in the chiral version [9–11].

In deuteron Compton scattering, this mandates inclusion of  $T_{NN}$  for all graphs in which both nucleons propagate close to their mass-shell between photon absorption and emission, i.e. in which the photon energy  $\omega \lesssim 50$  MeV does not suffice to knock a nucleon far off its mass-shell [1, 9]. Figure 4 lists the contributions to Compton scattering off the deuteron to next-to-leading order NLO in  $\chi$ EFT. At higher photon energies  $\omega \gtrsim 60$  MeV, one can show that the nucleon is kicked far off its mass-shell,  $E \sim |\mathbf{k}|$ , and the amplitude becomes perturbative. This is intuitively clear, as the nucleon has only a very short time ( $\sim 1/\omega$ ) to scatter with its partner before the second photon has to be radiated to restore the coherent final state. The diagrams which contain  $T_{NN}$  in Fig. 4 are therefore less important for larger  $\omega$ , together with some of the other diagrams. Indeed, the nucleon propagator scales then as  $1/Q \sim 1/\omega$  and thus becomes static, with each re-scattering process in  $T_{NN}$  suppressed by an additional power of  $Q$ .

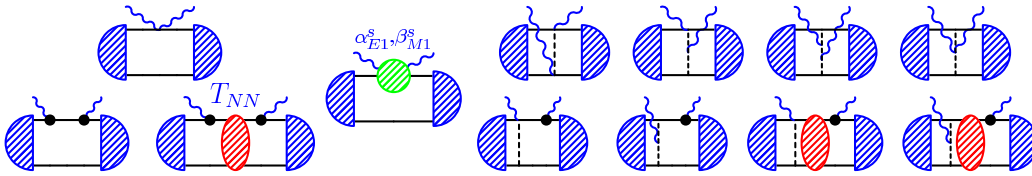


Figure 4: Deuteron Compton scattering in  $\chi$ EFT to NLO. Left: one-body part (dot: electric/magnetic coupling; blob: nucleon polarisabilities of Fig. 1). Right: two-body part (pion-exchange currents). Permutations and crossed graphs not shown. From Ref. [1].

We implemented rescattering by the Green’s function method described in [1, 3, 12]. The calculation is parameter-free when the short-distance coefficients  $\delta\alpha$ ,  $\delta\beta$  are taken over from the proton – as justified by the  $\chi$ EFT prediction that iso-vectorial contributions are suppressed by one order. The nucleon- and nuclear-structure contributions separate at this (and the next) order.

While the two-nucleon piece does not contain the  $\Delta(1232)$ -resonance in the intermediate state at this order as the deuteron is an iso-scalar target, this does not hold for the polarisabilities, as seen in Sect 2. Figure 5 also shows that the strong energy-dependence from the  $\Delta$  is indeed pivotal to reproduce both shape and normalisation of the 94 MeV data in particular at back-angles without significantly changing the static polarisabilities, but is negligible at lower energies. Thus, we argue that the discrepancy between the SAL data and experiments at lower energies is resolved [1, 6].

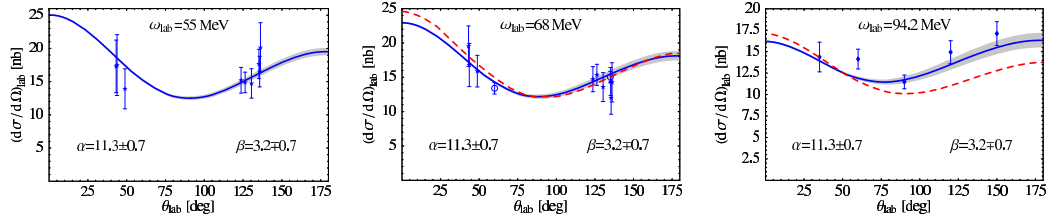


Figure 5: Examples for the 1-parameter fit result using the Baldin sum rule (solid, with stat. uncertainty), compared to  $\chi$ EFT without explicit  $\Delta(1232)$  ( $\mathcal{O}(p^3)$ , dashed). From Ref. [1].

The power-counting at the heart of  $\chi$ EFT implies several cross-checks: First, it must automatically reproduce the Thomson limit as an exact LO result, with all corrections cancelling order by order as  $\omega \rightarrow 0$  [7]. Fortunately, Arenhövel showed long before  $\chi$ EFT was formulated that it is indeed exactly recovered from the diagrams which  $\chi$ EFT classifies as LO at low energies, and that all diagrams which couple photons to meson-exchange currents sum up to zero at zero energy [8]. The numerical calculation confirms this [1].

Secondly,  $\chi$ EFT demotes at higher photon energies all graphs with  $T_{NN}$  in the intermediate state to higher orders. The difference to the previous  $\chi$ EFT calculations [4, 6] which were tailored to high photon energies should therefore decrease with increasing  $\omega$ . This is indeed found, see Fig. 6.

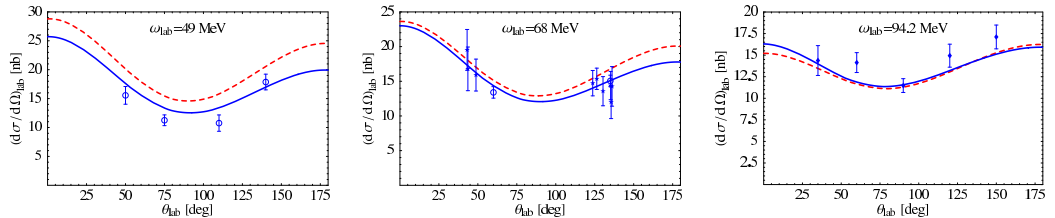


Figure 6: Examples of prediction using proton polarisabilities with (solid) and without (dashed)  $NN$ -rescattering in intermediate states. From Ref. [1].

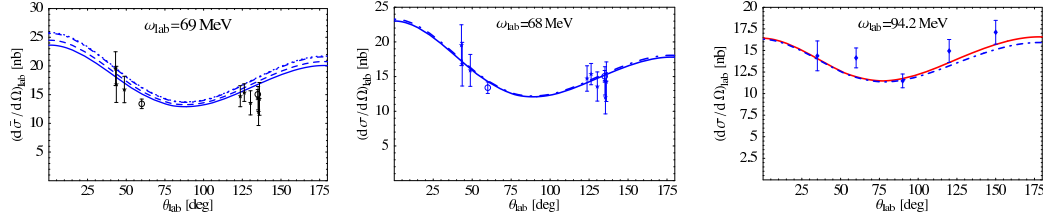


Figure 7: Examples of dependence on higher-order effects, with iso-scalar polarisabilities at proton values. Left (without  $T_{NN}$ ) and centre (with  $T_{NN}$ ): different deuteron wave-functions (solid: NNLO  $\chi$ EFT; dot-dashed: AV18; dashed: CD-Bonn; dotted: Nijmegen 93). Right: Dependence on the  $NN$ -potential for  $T_{NN}$  (solid: LO  $\chi$ EFT; dot-dashed: AV18). From Ref. [1].

Another consequence is a substantially reduced dependence on the deuteron wave-function, see Fig. 7. With the long-range part fixed by the deuteron binding energy and one-pion exchange, different wave-functions and potentials correspond to different assumptions about the short-distance dynamics of  $NN$ -scattering. Different answers would hence indict model-dependence, i.e. sensitivity to details of Physics at scales where a description in terms of the low-energy degrees of freedom breaks down. In the model-*independent* approach of  $\chi$ EFT, answers from different potentials and wave-functions agree within the theoretical accuracy, i.e. serve to estimate higher-order contributions. While the Thomson limit is universal for  $\omega \rightarrow 0$  [7, 8], the dependence on the deuteron wave-function used is now also at higher energies virtually eliminated compared to previous approaches [4, 6].

Figure 7 shows that the result is also quite insensitive to the potential from which  $T_{NN}$  is found. The maximal difference is smaller than 3% between constructing it from AV18 and a one-pion exchange with a crude parameterisation of short-distance effects as two point-like, momentum-independent contact operators. In  $\chi$ EFT, these differences come from  $NN$  interactions which are suppressed by  $Q^2 \approx (1/7)^2$ , in line with the spread found.

Finally, we test whether the neutron and proton polarisabilities are indeed similar by fitting the two short-distance parameters  $\delta\alpha$ ,  $\delta\beta$  to all deuteron Compton scattering data below 100 MeV [1]. The iso-scalar Baldin sum rule  $\bar{\alpha}^s + \bar{\beta}^s = 14.5 \pm 0.6$  is in excellent agreement with our 2-parameter fit, serving in the next step as input to model-independently determine the iso-scalar, spin-independent dipole polarisabilities of the nucleon at zero energy:

$$\bar{\alpha}^s = 11.3 \pm 0.7_{\text{stat}} \pm 0.6_{\text{Baldin}} \pm 1_{\text{th}}, \quad \bar{\beta}^s = 3.2 \mp 0.7_{\text{stat}} \pm 0.6_{\text{Baldin}} \pm 1_{\text{th}} \quad (3)$$

We estimate the theoretical error to be  $\pm 1$  from typical higher-order contri-

butions in the one- and two-nucleon sector. Comparing this with our analysis (2) of all proton Compton data below 170 MeV by the same method, we conclude that the proton and neutron polarisabilities are to this leading order identical within (predominantly statistical) errors and confirm the  $\chi$ EFT prediction. In particular, the proton and neutron show only a small but very similar deformation when put between the poles of a magnet:  $\bar{\beta}^p \approx \bar{\beta}^n \approx 3$ .

## 4 Concluding Questions

Dynamical polarisabilities test the global response of the nucleon to the electric and magnetic fields of a real photon with non-zero energy and definite multipolarity. They answer the question which internal degrees of freedom govern the structure of the nucleon at low energies and are defined by a multipole-expansion of the Compton amplitudes. While they do not contain more or less information than the corresponding Compton scattering amplitudes, the facts are more readily accessible and easier to interpret. Dispersive effects in particular from the  $\Delta(1232)$  are necessary to accurately extract the static polarisabilities of the nucleon from all data. Future work includes:

(i) The non-zero width of the  $\Delta$  and higher-order effects from the pion-cloud become crucial in the resonance region.

(ii) A multipole-analysis of Compton scattering at fixed energies from doubly-polarised, high-accuracy experiments provides a new avenue to extract the energy-dependence of the six dipole-polarisabilities per nucleon, both spin-independent and spin-dependent [5]. This will in particular further our knowledge on the spin-polarisabilities which characterise the spin-structure of the nucleon. A concerted effort of planned and approved experiments at  $\omega \lesssim 300$  MeV is under way: polarised photons on polarised protons, deuterons and  ${}^3\text{He}$  at TUNL/HI $\gamma$ S; tagged protons at S-DALINAC; polarised photons on polarised protons at MAMI. An unpolarised, running experiment on the deuteron at MAXlab covers a wide range of energies and angles. With at present only 29 (un-polarised) points for the deuteron in a small energy range of  $\omega \in [49;94]$  MeV and error-bars on the order of 15%, these high-quality data will provide better information on the neutron polarisabilities and allow one to zoom in on the proton-neutron differences.

(iii) Choudhury et al. found that Compton scattering on  ${}^3\text{He}$  also shows high sensitivity to the neutron polarisabilities [13]. In a coordinated effort, we now investigate which observables in proton, deuteron and  ${}^3\text{He}$  Compton scattering are most sensitive to combinations of polarisabilities in  $\chi$ EFT. Of particular interest are polarisation asymmetries because of their sensitivity to the experimentally practically undetermined dipole spin-polarisabilities.

Enlightening insight into the electro-magnetic structure of the nucleon has already been gained from combining Compton scattering off nucleons and few-nucleon systems with  $\chi$ EFT and the (energy-dependent) dynamical polarisabilities; and a host of activities should add to it in the coming years.

## Acknowledgements

I am grateful for financial support by the National Science Foundation (CAREER grant PHY-0645498), US Department of Energy (DE-FG02-95ER-40907) and Deutsche Forschungsgemeinschaft (GR1887/3-1). Foremost, I thank my collaborators – R.P. Hildebrandt, T.R. Hemmert, B. Pasquini and D.R. Phillips – for a lot of fun!

## References

- [1] R.P. Hildebrandt et al., [nucl-th/0512063], submitted to Phys. Rev. C; R.P. Hildebrandt, PhD thesis TU München Dec. 2005 [nucl-th/0512064].
- [2] D.L. Hornidge et al., Phys. Rev. Lett. **84**, 2334 (2000).
- [3] M.I. Levchuk and A.I. L’vov, Nucl. Phys. **A674**, 449 (2000).
- [4] S.R. Beane, et al., Nucl. Phys. **A656**, 367 (1999); S.R. Beane et al., Phys. Lett. **B567**, 200 (2003); erratum ibid. **B607**, 320 (2005); Nucl. Phys. **A747**, 311 (2005).
- [5] H. W. Griesshammer and T. R. Hemmert, Phys. Rev. **C65**, 045207 (2004); R. P. Hildebrandt et al., Eur. Phys. J. **A20**, 293 (2004); H. W. Griesshammer, Prog. Part. Nucl. Phys. **55**, 215 (2005).
- [6] R.P. Hildebrandt et al., Nucl. Phys. **A748**, 573 (2005).
- [7] J.L. Friar, Ann. of Phys. **95**, 170 (1975).
- [8] H. Arenhövel, Z. Phys. **A297**, 129 (1980); M. Weyrauch and H. Arenhövel, Nucl. Phys. **A408**, 425 (1983).
- [9] H.W. Griesshammer, forthcoming.
- [10] A. Nogga et al., Phys. Rev. **C72**, 054006 (2005); M.C. Birse, Phys. Rev. **C74**, 014003 (2006) and **76**, 034002 (2007).
- [11] H. W. Griesshammer, Nucl. Phys. **A760** 110 (2007).

- [12] J.J. Karakowski and G.A. Miller, Phys. Rev. **C60**, 014001 (1999);  
J.J. Karakowski, Ph.D. thesis U. of Washington 1999 [nucl-th/9901011].
- [13] D. Choudhury et al., Phys. Rev. Lett. **98**, 232303 (2007).

# RECENT BES RESULTS AND THE BESIII UPGRADE

*F. A. Harris*  
*for the BES Collaboration*  
Department of Physics and Astronomy  
University of Hawaii  
Honolulu, HI 96822  
USA

## Abstract

Using 58 million  $J/\psi$  and 14 million  $\psi(2S)$  events collected by the BESII detector at the BEPC, branching fractions or upper limits for the decays  $J/\psi$  and  $\psi(2S) \rightarrow \Lambda\bar{\Lambda}\pi^0$  and  $\Lambda\bar{\Lambda}\eta$  are measured, and the decays of  $J/\psi$  and  $\psi(2S)$  to  $nK_S^0\bar{\Lambda} + c.c.$  are observed and measured for the first time. Finally,  $R$  measurement data taken with the BESII detector at center-of-mass energies between 3.7 and 5.0 GeV are fitted to determine resonance parameters of the high mass charmonium states,  $\psi(3770)$ ,  $\psi(4040)$ ,  $\psi(4160)$ , and  $\psi(4415)$ .

The Beijing Electron Collider is being upgraded to a two-ring collider (BEPCII) with a design luminosity of  $1 \times 10^{33} \text{cm}^{-2} \text{s}^{-1}$  at 3.89 GeV and will operate between 2 and 4.2 GeV in the center of mass. With this luminosity, the new BESIII detector will be able to collect, for example, 10 billion  $J/\psi$  events in one year of running. BEPCII and BESIII are currently nearing completion, and commissioning of both is expected to begin in mid-2008.

## 1 Introduction

In this paper, some recent BESII results are reported based on 58 million  $J/\psi$  and 14 million  $\psi(2S)$  events collected by the BESII detector at the BEPC, and the status of BESIII/BEPCII is summarized. For much more detail, see the references.

## 2 Recent Results

### 2.1 $J/\psi$ and $\psi(2S)$ decays into $\Lambda\bar{\Lambda}\pi^0$ and $\Lambda\bar{\Lambda}\eta$

The isospin violating decay  $J/\psi \rightarrow \Lambda\bar{\Lambda}\pi^0$  was studied by DM2 [1] and BESII [2], and its average branching fraction is  $\mathcal{B}(J/\psi \rightarrow \Lambda\bar{\Lambda}\pi^0) = (2.2 \pm$

Table 1: Measured branching fractions or upper limits at the 90% confidence level (C.L.).

Channels	Number of events	MC efficiency (%)	Branching fraction ( $\times 10^{-4}$ )
$J/\psi \rightarrow \Lambda \bar{\Lambda} \pi^0$	$< 10$	0.75	$< 0.64$
$J/\psi \rightarrow \Lambda \bar{\Lambda} \eta$	$44 \pm 10$	1.8	$2.62 \pm 0.60 \pm 0.44$
$\psi(2S) \rightarrow \Lambda \bar{\Lambda} \pi^0$	$< 7.0$	2.5	$< 0.49$
$\psi(2S) \rightarrow \Lambda \bar{\Lambda} \eta$	$< 7.6$	2.9	$< 1.2$
$J/\psi \rightarrow \Sigma^+ \pi^- \Lambda$	$335 \pm 22$	2.3	$7.70 \pm 0.51 \pm 0.83$
$J/\psi \rightarrow \bar{\Sigma}^- \pi^+ \Lambda$	$254 \pm 19$	1.8	$7.47 \pm 0.56 \pm 0.76$

$0.6) \times 10^{-4}$  [3]. However, the isospin conserving process  $J/\psi \rightarrow \Lambda \bar{\Lambda} \eta$  has not been reported, and there are no measurements for  $\Lambda \bar{\Lambda} \pi^0$  and  $\Lambda \bar{\Lambda} \eta$  decays of  $\psi(2S)$ .

Here  $J/\psi \rightarrow \Lambda \bar{\Lambda} \pi^0$ ,  $J/\psi \rightarrow \Lambda \bar{\Lambda} \eta$ ,  $\psi(2S) \rightarrow \Lambda \bar{\Lambda} \pi^0$ , and  $\psi(2S) \rightarrow \Lambda \bar{\Lambda} \eta$ , where  $\Lambda$  decays to  $\pi^- p$  and  $\pi^0$  and  $\eta$  to  $\gamma\gamma$ , are studied. Candidate events must have four good charged tracks and at least two photons, two protons identified using particle identification, a satisfactory four constraint kinematic fit, and a  $\pi p$  mass consistent with the  $\Lambda$  mass. For  $J/\psi \rightarrow \Lambda \bar{\Lambda} \pi^0$ , the decay lengths of  $\Lambda$  and  $\bar{\Lambda}$  in the  $x - y$  plane must be larger than 0.05 m.

Possible backgrounds are studied using MC simulation. The most serious one is from  $J/\psi \rightarrow \Sigma^0 \pi^0 \bar{\Lambda} + c.c.$ , which contains  $\Lambda \bar{\Lambda} \pi^0$  with an additional photon in the final state. The branching fraction for this decay has not been previously measured. Since direct measurement of  $J/\psi \rightarrow \Sigma^0 \pi^0 \bar{\Lambda} + c.c.$  is difficult, we measure the branching fractions of its isospin partner and estimate the branching fraction assuming isospin symmetry.

The histogram in Fig. 1 shows normalized backgrounds from all background channels, and the dashed line in the figure shows the  $\pi^0$  signal from MC simulated  $J/\psi \rightarrow \Lambda \bar{\Lambda} \pi^0$ . The data in Fig. 1 are consistent with background, and the upper limit on the number of  $\pi^0$  events from  $J/\psi \rightarrow \Lambda \bar{\Lambda} \pi^0$  is determined. Figure 2 shows the  $\gamma\gamma$  invariant mass distribution for  $J/\psi \rightarrow \Lambda \bar{\Lambda} \eta$  candidates, where a clear  $\eta$  signal is observed. Figure 3 shows the  $\gamma\gamma$  invariant mass distribution for  $\psi(2S) \rightarrow \Lambda \bar{\Lambda} \pi^0$  and  $\Lambda \bar{\Lambda} \eta$  using similar selection criteria, and no significant  $\pi^0$  or  $\eta$  signals are seen.

Table 1 lists the results for  $J/\psi$  and  $\psi(2S)$  decay into  $\Lambda \bar{\Lambda} \pi^0$  and  $\Lambda \bar{\Lambda} \eta$ , as well as  $J/\psi \rightarrow \Sigma^+ \pi^- \bar{\Lambda} + c.c.$ . Except for  $J/\psi \rightarrow \Lambda \bar{\Lambda} \pi^0$  and  $J/\psi \rightarrow \Sigma^+ \pi^- \bar{\Lambda} + c.c.$ , the results are first measurements. Interestingly, the result of  $J/\psi \rightarrow \Lambda \bar{\Lambda} \pi^0$  presented here is much smaller than those of DM2 and BES1 [1,2]. Previously, the large contaminations from  $J/\psi \rightarrow \Sigma^0 \pi^0 \bar{\Lambda} + c.c.$

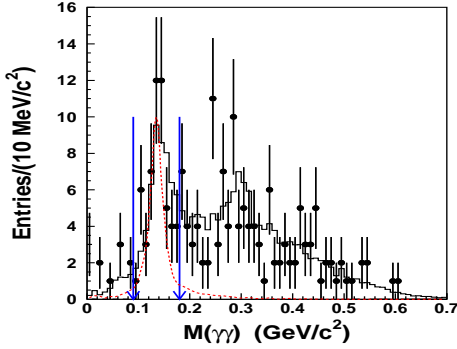


Figure 1: Invariant mass distribution of  $M(\gamma\gamma)$  for  $J/\psi \rightarrow \Lambda\bar{\Lambda}\pi^0 \rightarrow \Lambda\bar{\Lambda}\gamma\gamma$  candidates (dots with error bars) and normalized backgrounds (solid histogram). The dashed curves shows the  $\pi^0$  signal from MC simulated  $J/\psi \rightarrow \Lambda\bar{\Lambda}\pi^0$ .

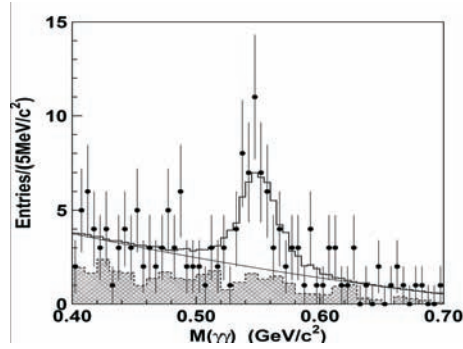


Figure 2: Fit to the  $\gamma\gamma$  invariant mass distribution of  $J/\psi \rightarrow \Lambda\bar{\Lambda}\eta \rightarrow \Lambda\bar{\Lambda}\gamma\gamma$  candidate events. Dots with error bars are data, the hatched histogram is the normalized background, and the solid histogram is the fit to data using a histogram of the signal shape from MC simulation plus a second order polynomial for background.

and  $J/\psi \rightarrow \Sigma^+\pi^-\bar{\Lambda} + c.c.$  were not considered, resulting in a large  $J/\psi \rightarrow \Lambda\bar{\Lambda}\pi^0$  branching fraction. The small branching fraction of  $J/\psi \rightarrow \Lambda\bar{\Lambda}\pi^0$  and relatively large branching fraction of  $J/\psi \rightarrow \Lambda\bar{\Lambda}\eta$  measured here indicate that the isospin violating decay in  $J/\psi$  decays is suppressed while the isospin conserving decays is favored, which is consistent with expectation. For more detail, see Ref. [4].

## 2.2 $J/\psi$ and $\psi(2S)$ decaying to $nK_S^0\bar{\Lambda} + c.c.$

In 2004, BESII reported the observation of an enhancement  $X(2075)$  near the threshold of the invariant mass spectrum of  $p\bar{\Lambda}$  in  $J/\psi \rightarrow pK^-\bar{\Lambda}$  decays. The mass, width, and product branching fraction of this enhancement are  $M = 2075 \pm 12$  (stat.)  $\pm 5$  (syst.) MeV/ $c^2$ ,  $\Gamma = 90 \pm 35$  (stat.)  $\pm 9$  (syst.) MeV/ $c^2$ , and  $B(J/\psi \rightarrow K^-X)B(X \rightarrow p\bar{\Lambda} + c.c.) = (5.9 \pm 1.4 \pm 2.0) \times 10^{-5}$  [5], respectively. The study of the isospin conjugate channel  $J/\psi \rightarrow nK_S^0\bar{\Lambda}$  is therefore important not only in exploring new decay modes of  $J/\psi$  but also in understanding the  $X(2075)$ .

$J/\psi$  and  $\psi(2S) \rightarrow nK_S^0\bar{\Lambda}$  with  $K_S^0 \rightarrow \pi^+\pi^-$  and  $\bar{\Lambda} \rightarrow \bar{p}\pi^+$  (and  $c.c.$ ) final states contain four charged tracks and an undetected neutron or anti-neutron.

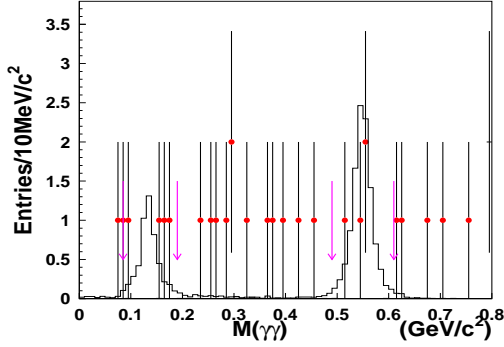


Figure 3: The  $\gamma\gamma$  invariant mass distribution for candidate  $\psi(2S) \rightarrow \gamma\gamma\Lambda\bar{\Lambda}$  events. Dots with error bars are data, and the histograms are MC simulated signal events. The arrows indicate the  $\pi^0$  and  $\eta$  signal regions.

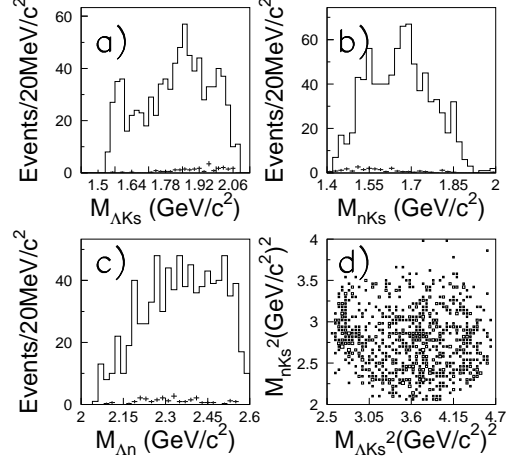


Figure 4: The invariant mass spectra of (a)  $\Lambda K_S^0$ , (b)  $nK_S^0$ , and (c)  $\bar{\Lambda}n(\Lambda\bar{n})$ , as well as (d) the Dalitz plot for candidate  $J/\psi \rightarrow nK_S^0\Lambda + c.c.$  events after all selection criteria. The crosses show the sideband backgrounds.

We require the candidate events to have four charged tracks with total charge zero. Secondary vertex fitting is used to identify the  $\pi^+\pi^-$  from the  $K_S^0$  and the  $p\pi$  from the  $\Lambda$ , and their masses are required to be consistent with those of the parent particles. To reject backgrounds from channels without a  $K_S^0$  or  $\Lambda$ , we require  $L_{xy}(\Lambda)$ , the distance from the reconstructed  $\Lambda$  vertex to the event origin, to be larger than 5 mm and  $L_{xy}(K_S^0) > 5$  mm. To suppress background and improve the resolution, a one constraint (1C) kinematic fit with a missing neutron is applied under the  $J/\psi \rightarrow \bar{p}n\pi^+\pi^-\pi^+$  hypothesis, and  $\chi_{1C}^2 < 5$  is required.

The invariant mass spectra of  $\Lambda K_S^0$ ,  $nK_S^0$ , and  $\bar{\Lambda}n(\Lambda\bar{n})$ , as well as the Dalitz plot for all selection requirements are shown in Fig. 4. In the  $\Lambda K_S^0$  invariant mass spectrum, an enhancement near  $\Lambda K_S^0$  threshold is evident, as is found in the  $\Lambda K$  mass spectrum in  $J/\psi \rightarrow pK^-\bar{\Lambda}$  [6]. The  $X(2075)$  signal which was seen in the  $p\bar{\Lambda}$  invariant mass spectrum in  $J/\psi \rightarrow pK^-\bar{\Lambda}$  is not significant here. Taking into account the systematic error, the upper limit of the near-threshold enhancement  $X(2075)$  in the  $n\bar{\Lambda}$  threshold is  $B(J/\psi \rightarrow K_S^0 X(2075)) \cdot B(X(2075) \rightarrow n\bar{\Lambda}) < 4.75 \times 10^{-5}$  (90% C.L.). Considering

the isospin factor, the branching fraction upper limit for  $B(J/\psi \rightarrow K_S^0 X) \cdot B(X \rightarrow n\bar{\Lambda} + c.c.)$  is not inconsistent with that for  $B(J/\psi \rightarrow KX) \cdot B(X \rightarrow p\bar{\Lambda} + c.c.)$  [5].

An  $N^*$  state at around 1.9 GeV/c<sup>2</sup> in the  $\Lambda K_S^0$  invariant mass spectrum and  $\Lambda^*$  states at around 1.5 and 1.7 GeV/c<sup>2</sup> in the  $nK_S^0$  invariant mass spectrum are present. A larger data sample and a partial wave analysis are needed to analyze these states.

We use the same criteria to select  $\psi(2S) \rightarrow nK_S^0\bar{\Lambda} + c.c.$  events from the BESII sample of 14M  $\psi(2S)$  events. The branching ratios obtained are:

$$\begin{aligned} Br(J/\psi \rightarrow nK_S^0\bar{\Lambda} + c.c.) &= (6.42 \pm 0.20 \pm 0.99) \times 10^{-4} \\ Br(J/\psi \rightarrow nK_S^0\bar{\Lambda}) &= (3.09 \pm 0.14 \pm 0.56) \times 10^{-4} \\ Br(J/\psi \rightarrow \bar{n}K_S^0\Lambda) &= (3.37 \pm 0.14 \pm 0.45) \times 10^{-4} \\ Br(\psi(2S) \rightarrow nK_S^0\bar{\Lambda} + c.c.) &= (0.77 \pm 0.11 \pm 0.13) \times 10^{-4}. \end{aligned}$$

The ratio of the branching ratios of  $\psi(2S)$  and  $J/\psi$  decaying to  $nK_S^0\bar{\Lambda} + c.c.$ ,  $Q_h = (12.0 \pm 3.2)\%$ , obeys the "12%" rule [7]. These results are preliminary; for more detail, see Ref. [8].

### 2.3 $\psi(3770)$ , $\psi(4040)$ , $\psi(4160)$ and $\psi(4415)$ resonance parameters

The total cross section for hadron production in  $e^+e^-$  annihilation is usually parameterized in terms of the ratio  $R$ , which is defined as  $R = \sigma(e^+e^- \rightarrow \text{hadrons})/\sigma(e^+e^- \rightarrow \mu^+\mu^-)$ , where the denominator is the lowest-order QED cross section,  $\sigma(e^+e^- \rightarrow \mu^+\mu^-) = \sigma_{\mu\mu}^0 = 4\pi\alpha^2/3s$ . At the open flavor thresholds where resonance structures show up,  $R$  measurements are used to determine resonance parameters. For the high mass charmonium resonances, the  $\psi(3770)$  was measured by MARK-I [9], DELCO [10], MARK-II [11] and BES [12] [13]; the  $\psi(4040)$  and  $\psi(4160)$  were measured by DASP [14]; and the  $\psi(4415)$  was measured by DASP [14] and MARK-I [15].

The most recent and precise  $R$  measurements between 2-5 GeV were made by BESII [16]. Experimentally,  $R$  for both the continuum and the wide resonance region is given by

$$R_{exp} = \frac{N_{had}^{obs} - N_{bg}}{\sigma_{\mu\mu}^0 L \epsilon_{trg} \epsilon_{had} (1 + \delta_{obs})}, \quad (1)$$

where  $N_{had}^{obs}$  is the number of observed hadronic events,  $N_{bg}$  is the number of the residual background events,  $L$  is the integrated luminosity,  $(1 + \delta_{obs})$  is the effective correction factor of the initial state radiation (ISR) [17,18],  $\epsilon_{had}$  is the detection efficiency for hadronic events determined by Monte Carlo

simulation without bremsstrahlung being simulated, and  $\epsilon_{trg}$  is the trigger efficiency.

Table 2: The resonance parameters of the high mass charmonia in this work together with the values in PDG2004 [19], PDG2006 [3] and K. Seth's evaluations [20] based on Crystal Ball and BES data.

		$\psi(3770)$	$\psi(4040)$	$\psi(4160)$	$\psi(4415)$
$M$ (MeV/ $c^2$ )	PDG2004	3769.9±2.5	4040±10	4159±20	4415±6
	PDG2006	3771.1±2.4	4039±1.0	4153±3	4421±4
	CB (Seth)	-	4037±2	4151±4	4425±6
	BES (Seth)	-	4040±1	4155±5	4455±6
	BES (this work)	3771.4±1.8	4038.5±4.6	4191.6±6.0	4415.2±7.5
$\Gamma_{tot}$ (MeV)	PDG2004	23.6±2.7	52±10	78±20	43±15
	PDG2006	23.0±2.7	80±10	103±8	62±20
	CB (Seth)	-	85±10	107±10	119±16
	BES (Seth)	-	89±6	107±16	118±35
	BES (this work)	25.4±6.5	81.2±14.4	72.7±15.1	73.3±21.2
$\Gamma_{ee}$ (keV)	PDG2004	0.26±0.04	0.75±0.15	0.77±0.23	0.47±0.10
	PDG2006	0.24±0.03	0.86±0.08	0.83±0.07	0.58±0.07
	CB (Seth)	-	0.88±0.11	0.83±0.08	0.72±0.11
	BES (Seth)	-	0.91±0.13	0.84±0.13	0.64±0.23
	BES (this work)	0.18±0.04	0.81±0.20	0.50±0.27	0.37±0.14
$\delta$ (degree)	BES (this work)	0	133±68	301±61	246±86

In the previous analysis [16], the determination of  $R$  values was done using PDG04 [19] resonance parameters for the high mass resonances. Here, the analysis uses the data to determine the resonance parameters. The determination of  $R$  values and resonance parameters are intertwined; the factor  $(1 + \delta_{obs})$  in Eq. (1) contains contributions from the resonances and depends on the resonance parameters. Therefore, the procedure to calculate  $(1 + \delta_{obs})$  requires a number of iterations before stable results can be obtained. We perform a global fit over the entire center-of-mass energy region from 3.7 to 5.0 GeV covering the four resonances,  $\psi(3770)$ ,  $\psi(4040)$ ,  $\psi(4160)$  and  $\psi(4415)$ , and include interference effects among the resonances. We also adopt energy-dependent full widths, and introduce relative phases between the resonances.

The resonant parameters of the high mass charmonia determined in this work, together with those in PDG2004, PDG2006 and the results given in Ref. [20] are listed in Table 2. The updated  $R$  values between 3.7 and 5.0 GeV and the fit curves are illustrated in Fig. 5.

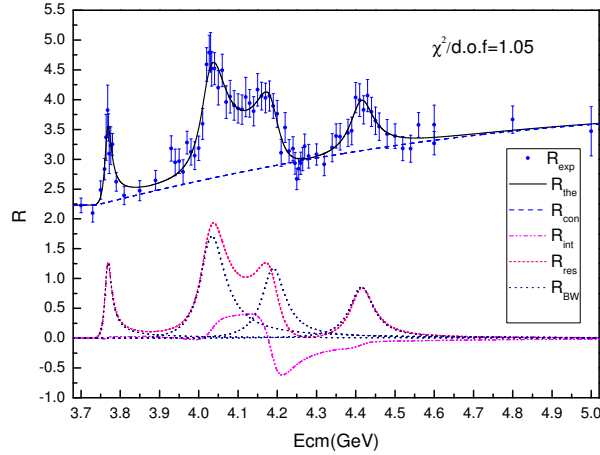


Figure 5: The fit to the  $R$  values in the high mass charmonium region. The dots with error bars are the updated  $R$  values. The solid curve shows the best fit, and the other curves show the contributions from each resonance  $R_{BW}$ , the interference  $R_{int}$ , the summation of the four resonances  $R_{res} = R_{BW} + R_{int}$ , and the continuum background  $R_{con}$  respectively.

It is worth noting that the change of the resonance parameters affects the effective initial state radiative correction factors, and thus affects the  $R$  values. In general the relative difference is within 3%, and for a few energy points the maximum difference is about 6%. Our resonance parameter results are in agreement with the previous experiments in most cases, but large differences are observed in some of the parameters, such as the mass of the  $\psi(4160)$ . This is mainly due to the reconsideration of the radiative correction factors, and the inclusion of interferences between the resonances. This work is preliminary; for more detail, see Ref. [21].

### 3 BEPCII and BESIII

In 2003, the Chinese Government approved the upgrade of the BEPC to a two-ring collider (BEPCII) with a design luminosity approximately 100 times higher than that of the BEPC. This will allow unprecedented physics opportunities in this energy region and contribute to precision flavor physics.

#### 3.1 BEPCII

BEPCII is a two-ring  $e^+e^-$  collider that will run in the tau-charm energy region ( $E_{cm} = 2.0 - 4.2$  GeV) with a design luminosity of  $1 \times 10^{33}$   $\text{cm}^{-2}\text{s}^{-1}$  at

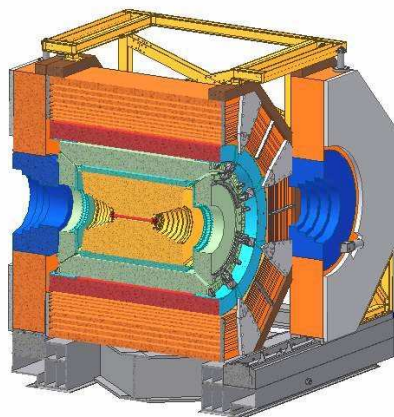


Figure 6: Schematic view of the BESIII detector.

a beam energy of 1.89 GeV, an improvement of a factor of 100 with respect to the BEPC. This is accomplished by using multi-bunches and micro-beta. The upgrade uses the existing tunnel.

The 2024 meter long linac has been upgraded with new klystrons, a new electron gun, and a new positron source to increase its energy and beam current; it can accelerate electrons and positrons up to 1.89 GeV with an positron injection rate of 50 mA/min. Its installation was completed in the summer of 2005.

There are two storage rings with lengths of 237.5 meters. The collider has new super-conducting RF cavities, power supplies, and control; super-conducting quadrupole magnets; beam pipes; magnets and power supplies; kickers; beam instrumentation; vacuum systems; and control. The old dipoles are modified and used in the outer ring. Electrons and positrons will collide at the interaction point with a horizontal crossing angle of 11 mrad and bunch spacing of 8 ns. Each ring has 93 bunches with a beam current of 9170 mA. The machine is already providing a high flux of synchrotron radiation at a beam energy of 2.5 GeV.

### 3.2 BESIII

The BESIII detector consists of a beryllium beam pipe, a helium-based small-celled drift chamber, Time-Of-Flight counters for particle identification, a CsI(Tl) crystal calorimeter, a super-conducting solenoidal magnet with a field of 1 Tesla, and a muon identifier using the magnet yoke interleaved with Resistive Plate Counters (RPC). Fig. 6 shows the schematic view of the BESIII detector, including both the barrel and endcap portions.

### 3.3 Physics in the tau-charm energy region

The tau-charm energy region makes available a wide variety of interesting physics. Data can be taken at the  $J/\psi$ ,  $\psi(2S)$ , and  $\psi(3770)$ , at  $\tau$  threshold, and at an energy to allow production of  $D_s$  pairs, as well as for an R-scan.

Table 3: Number of events expected for one year of running.

Physics channel	Center-of-mass Energy (GeV)	Peak Luminosity ( $10^{33} \text{ cm}^{-2} \text{ s}^{-1}$ )	Physics cross section (nb)	Number of Events per year
$J/\psi$	3.097	0.6	$\sim 3400$	$10 \times 10^9$
$\tau$	3.67	1.0	$\sim 2.4$	$12 \times 10^6$
$\psi(2S)$	3.686	1.0	$\sim 640$	$3.0 \times 10^9$
$D$	3.770	1.0	$\sim 5$	$25 \times 10^6$
$D_s$	4.030	0.6	$\sim 0.32$	$1.0 \times 10^6$
$D_s$	4.140	0.6	$\sim 0.67$	$2.0 \times 10^6$

BEPCII and BESIII are in the final stage of assembly, and commissioning will begin in summer 2008. The design luminosity of BESIII is  $1 \times 10^{33} \text{ cm}^{-2}$ . Clearly BESIII with higher luminosity will contribute greatly to precision flavor physics:  $V_{cd}$  and  $V_{cs}$  will be measured with a statistical accuracy of 1.6%.  $D^0 D^0$  mixing will be studied and CP violation will be searched for. Table 3 gives the numbers of events expected during one year of running at various energies. Huge  $J/\psi$  and  $\psi(2S)$  samples will be obtained. The  $\eta_C$ ,  $\chi_{CJ}$ , and  $h_C$  can be studied with high statistics, and the  $\rho\pi$  puzzle will be studied with better accuracy. For more detail, see Refs [22, 23].

## 4 References

### References

- [1] P. Henrard *et al.* [DM2 Collab.], *Nucl. Phys.B* **292**, 670 (1987).
- [2] J. Z. Bai *et al.* [BES Collab.], *Phys. Lett. B* **424**, 213 (1998).
- [3] W. M. Yao *et al.* [Particle Physics Group], *J. Phys. G* **33**, 1 (2006).
- [4] M. Ablikim *et al.* [BES Collab.], to appear in *Phys. Rev. D*, arXiv:0707.1127 [hep-ex].

- 
- [5] M. Ablikim *et al.* [BES Collab.], *Phys. Rev. Lett.* **93**, 112002 (2004).
- [6] Shan JIN for the BES Collab., *Int. J. Mod. Phys. A* **21**, 613 (2006).
- [7] T. Appelquist and H. D. Politzer, *Phys. Rev. Lett.* **34**, 43 (1975); A. De Rujula and S. L. Glashow, *ibid*, page 46.
- [8] M. Ablikim *et al.* [BES Collab.], submitted to *Phys. Lett. B*, arXiv:0710.3091 [hep-ex].
- [9] P. A. Rapidis *et al.* [MARK-I Collab.], *Phys. Rev. Lett.* **39**, 526 (1977).
- [10] W. Bacino *et al.* [DELCO Collab.], *Phys. Rev. Lett.* **40**, 671 (1978).
- [11] R. H. Schindler *et al.* [MARK-II Collab.], *Phys. Rev. D* **21**, 2716 (1980).
- [12] M. Ablikim *et al.* [BES Collab.], *Phys. Lett. B* **652**, 238 (2007).
- [13] M. Ablikim *et al.* [BES Collab.], *Phys. Rev. Lett.* **97**, 121801 (2006).
- [14] R. Brandelik *et al.* [DASP Collab.], *Phys. Lett. B* **76**, 361 (1978).
- [15] J. Siegrist *et al.* [MarkI Collab.], *Phys. Rev. Lett.* **36**, 700, (1976).
- [16] J. Z. Bai *et al.* [BES Collab.], *Phys. Rev. Lett.* **88**, 101802 (2002).
- [17] A. Osterfeld *et al.* [Crystal Ball Collab.], Report No. SLAC-PUB-4160 (1986) (unpublished).
- [18] H. M. Hu *et al.*, *High Energy Physics and Nuclear Physics* **25**, 701 (2001) (in Chinese).
- [19] S. Eidelman *et al.* [Particle Data Group], *Phys. Lett. B* **592**, 310 (2004).
- [20] K. K. Seth, *Phys. Rev. D* **72**, 017501 (2005).
- [21] M. Ablikim *et al.* [BES Collab.], submitted to *Phys. Lett. B*, arXiv:0705.4500 [hep-ex].
- [22] F. A. Harris, *Nucl. Phys. Proc. Suppl.* **162**, 345 (2006).
- [23] Weiguo Li, to be published in the Proceedings of 4th Flavor Physics and CP Violation Conference, hep-physics/0605158.

# KAON-NUCLEON AND ANTI-KAON-NUCLEON INTERACTIONS IN A CONSTITUENT QUARK MODEL

F. Huang <sup>\*, $\circ$ ,1</sup>, W.L. Wang  <sup>$\S$ , $\triangleright$</sup> , Z.Y. Zhang  <sup>$\triangleright$</sup>

<sup>\*</sup>Institut für Kernphysik (Theorie), Forschungszentrum Jülich, D-52428  
Jülich, Germany

<sup>$\circ$</sup> China Center of Advanced Science and Technology (CCAST, World Lab.),  
Beijing 100080, China

<sup>$\S$</sup> Institute of Particle Physics, Huazhong Normal University, Wuhan 430079,  
China

<sup>$\triangleright$</sup> Institute of High Energy Physics, Chinese Academy of Sciences, Beijing  
100049, China

## Abstract

A combined study of the  $KN$  and  $\bar{K}N$  interactions is performed within a chiral constituent quark model with the parameters fitted by the masses of the octet and decuplet baryon ground states. The  $S$ ,  $P$ ,  $D$ ,  $F$  wave  $KN$  phase shifts and the cross sections for  $K^-p$  scattering into  $K^-p$ ,  $K^0n$ ,  $\pi^+\Sigma^-$ ,  $\pi^-\Sigma^+$ ,  $\pi^0\Sigma^0$  and  $\pi^0\Lambda$  channels are dynamically calculated by solving a resonating group method (RGM) equation. A satisfactory agreement with the experimental data is obtained, and at the same time, the results show that both one-gluon exchange (OGE) and vector meson exchange are necessary to be included in the quark-quark interacting potentials if one tries to simultaneously describe the  $KN$  phase shifts and  $\bar{K}N$  cross sections in a constituent quark model.

## 1 Introduction

In the past few years, the chiral SU(3) quark model and the extended chiral SU(3) quark model have been quite successful in reproducing the energies of the octet and decuplet baryon ground states, the binding energy of

---

<sup>1</sup>E-mail address: f.huang@fz-juelich.de

the deuteron, the nucleon-nucleon ( $NN$ ) and kaon-nucleon ( $KN$ ) scattering phase shifts, and the hyperon-nucleon ( $YN$ ) cross sections [1–5]. In the original chiral SU(3) quark model, the short range quark-quark interaction is dominantly provided by one-gluon exchange (OGE) and quark exchange effects. In the extended chiral SU(3) quark model, the vector meson exchanges are included and consequently the OGE is largely reduced, thus the short range quark-quark interaction is dominantly provided by vector-meson exchange and quark exchange effects. In other words, the short range quark-quark interaction mechanisms in these two models are quite different. Using these two models, we have dynamically studied [1–9] the  $NN$  and  $KN$  scattering phase shifts and the  $\Omega\Omega$ ,  $N\bar{\Omega}$ ,  $\Delta K$ ,  $\Lambda K$  and  $\Sigma K$  interactions in the framework of the resonating group method (RGM). It was found that though the mechanisms of the short range quark-quark interaction are quite different, these two models give quite similar results for all those hadron-hadron systems. To get more definite information about the short range quark-quark interaction mechanisms, it seems interesting and necessary to investigate some special systems where the chiral SU(3) quark model and the extended chiral SU(3) quark model give quite different results.

One notices that the  $KN$  and  $\bar{K}N$  cases are of special interest, since OGE exists in  $KN$  system while vanishes in  $\bar{K}N$  system (which is because the OGE between two hadrons is always accompanied by simultaneous quark exchange between these two clusters due to the color of the gluon, but the quark content of  $\bar{K}N$  prevents such a quark exchange diagram), and on the hadron level the vector-meson exchanges in  $KN$  and  $\bar{K}N$  are related by a  $G$ -parity transition. Specially, the  $\omega$  exchange is repulsive for  $KN$  while attractive for  $\bar{K}N$ , because of the negative  $G$  parity of the  $\omega$  meson (on hadron level). Thus if OGE and vector meson exchange give similar contributions in  $KN$ , they must give quite different contributions in  $\bar{K}N$ , or vice versa.

In Refs. [3–5], we have dynamically studied the  $KN$  scattering in the chiral SU(3) quark model and the extended chiral SU(3) quark model, and got a satisfactory description of the  $S$ ,  $P$ ,  $D$ ,  $F$  wave  $KN$  phase shifts. Further in Ref. [10], a preliminary study of the  $\bar{K}N$  bound state problem is performed by use of the same models and parameters as in Refs. [3–5], and it is found that in the extended chiral SU(3) quark model the attractive  $\bar{K}N$  interaction can make for a bound state which appears as a  $\pi\Sigma$  resonance in the coupled-channel calculation, while the chiral SU(3) quark model cannot accommodate the existence of a  $\bar{K}N$  bound state.

In this work [11], we use three different constituent quark models to perform a combined study of the  $S$ ,  $P$ ,  $D$ ,  $F$  wave  $KN$  elastic scattering phase shifts and the cross sections for  $K^-p$  scattering into  $K^-p$ ,  $K^0n$ ,  $\pi^+\Sigma^-$ ,  $\pi^-\Sigma^+$ ,

$\pi^0\Sigma^0$  and  $\pi^0\Lambda$  channels by solving the RGM equation. These three different models are briefly introduced in the next section. The results of  $KN$  phase shifts and  $K^-p$  cross sections are shown in Sec. III, where some discussion is presented as well. Finally, the summary is given in Sec. IV.

## 2 Theoretical Frame

The three different constituent quark models are well described in Ref. [11], and we refer the reader to this work for details. Here we just give the salient features of those models.

In those three models, the total Hamiltonian is written as

$$H = \sum_i T_i - T_G + \sum_{i<j} V_{ij}. \quad (1)$$

Here  $T_G$  is the kinetic energy operator for the center-of-mass motion, and  $V_{ij}$  is the effective quark-quark interaction,

$$V_{ij} = V_{ij}^{\text{conf}} + V_{ij}^{\text{S}} + V_{ij}^{\text{PS}} + V_{ij}^{\text{SR}}, \quad (2)$$

where  $V_{ij}^{\text{conf}}$  is the confinement potential,  $V_{ij}^{\text{S}}$  and  $V_{ij}^{\text{PS}}$  represent the effective quark-quark potentials stemming from scalar and pseudo-scalar meson exchanges, respectively, and  $V_{ij}^{\text{SR}}$  denotes the short-range quark-quark interaction. In model I, i.e. the chiral SU(3) quark model,  $V_{ij}^{\text{SR}}$  is represented by OGE,

$$V_{ij}^{\text{SR}} = V_{ij}^{\text{OGE}}, \quad (3)$$

and in model II, i.e. the extended chiral SU(3) quark model,  $V_{ij}^{\text{SR}}$  is represented by vector meson exchange,

$$V_{ij}^{\text{SR}} = V_{ij}^{\text{V}}, \quad (4)$$

and in model III, both OGE and vector meson exchange are included,

$$V_{ij}^{\text{SR}} = V_{ij}^{\text{OGE}} + V_{ij}^{\text{V}}. \quad (5)$$

The expressions of these potentials can be found in the literature [3–5, 10, 11].

All the model parameters are fitted with the same method as in our previous work [1–9], and here we briefly give the procedure for the parameter determination. The three initial input parameters, i.e. the harmonic-oscillator width parameter  $b_u$ , the up (down) quark mass  $m_{u(d)}$  and the strange quark mass  $m_s$ , are taken to be the usual values:  $b_u = 0.5$  fm for model I and 0.45

Table 1: Model parameters. The meson masses and the cutoff masses:  $m_{\sigma'} = 980$  MeV,  $m_{\kappa} = 1430$  MeV,  $m_{\epsilon} = 980$  MeV,  $m_{\pi} = 138$  MeV,  $m_K = 495$  MeV,  $m_{\eta} = 549$  MeV,  $m_{\eta'} = 957$  MeV,  $m_{\rho} = 770$  MeV,  $m_{K^*} = 892$  MeV,  $m_{\omega} = 782$  MeV,  $m_{\phi} = 1020$  MeV,  $\Lambda = 1500$  MeV for  $\kappa$  and 1100 MeV for other mesons.

	Model I Without VME	Model II Without OGE	Model III With OGE and VME
$b_u$ (fm)	0.5	0.45	0.45
$m_u$ (MeV)	313	313	313
$m_s$ (MeV)	470	470	470
$g_u^2$	0.77	0	0.37
$g_s^2$	0.55	0	0.47
$g_{\text{ch}}$	2.62	2.62	2.62
$g_{\text{chv}}$	0	2.35	0.83
$f_{\text{chv}}$	0	0	3.33
$m_{\sigma}$ (MeV)	675	675	675
$a_{uu}^c$ (MeV/fm <sup>2</sup> )	52.9	56.4	60.2
$a_{us}^c$ (MeV/fm <sup>2</sup> )	76.0	104.1	95.1
$a_{uu}^{c0}$ (MeV)	-51.7	-86.4	-72.2
$a_{us}^{c0}$ (MeV)	-68.5	-72.2	-86.9

fm for models II and III,  $m_{u(d)} = 313$  MeV, and  $m_s = 470$  MeV. The coupling constant for scalar and pseudoscalar chiral field coupling,  $g_{\text{ch}}$ , is fixed by the relation

$$\frac{g_{\text{ch}}^2}{4\pi} = \left(\frac{3}{5}\right)^2 \frac{g_{NN\pi}^2}{4\pi} \frac{m_u^2}{M_N^2}, \quad (6)$$

with the empirical value  $g_{NN\pi}^2/4\pi = 13.67$ . The masses of the mesons are taken to be the experimental values, except for the  $\sigma$  meson. The  $m_{\sigma}$  is treated as a parameter, and we adjust it to fit the  $S$ -wave  $KN$  phase shifts. The OGE coupling constants and the strengths of the confinement potential are fitted by baryon masses and their stability conditions. All the parameters are tabulated in Table I, where the first, second and third sets are for models I, II and III, respectively. All these three sets of parameters can give good descriptions of the masses of octet and decuplet baryon ground states [11].

### 3 Results and Discussion

From Table I one sees that in model I, i.e. the original chiral SU(3) quark model, the vector meson exchange is not included and thus the short-range

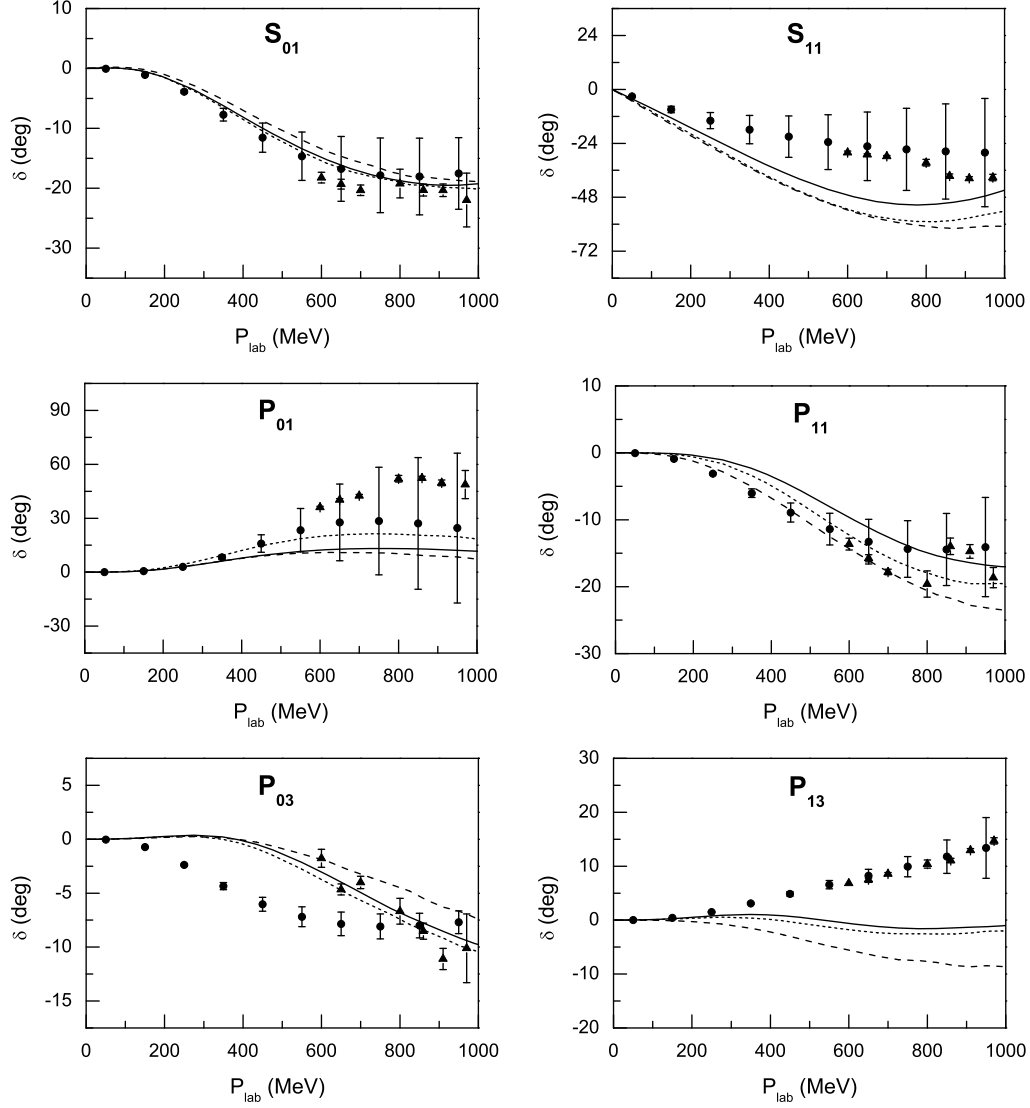
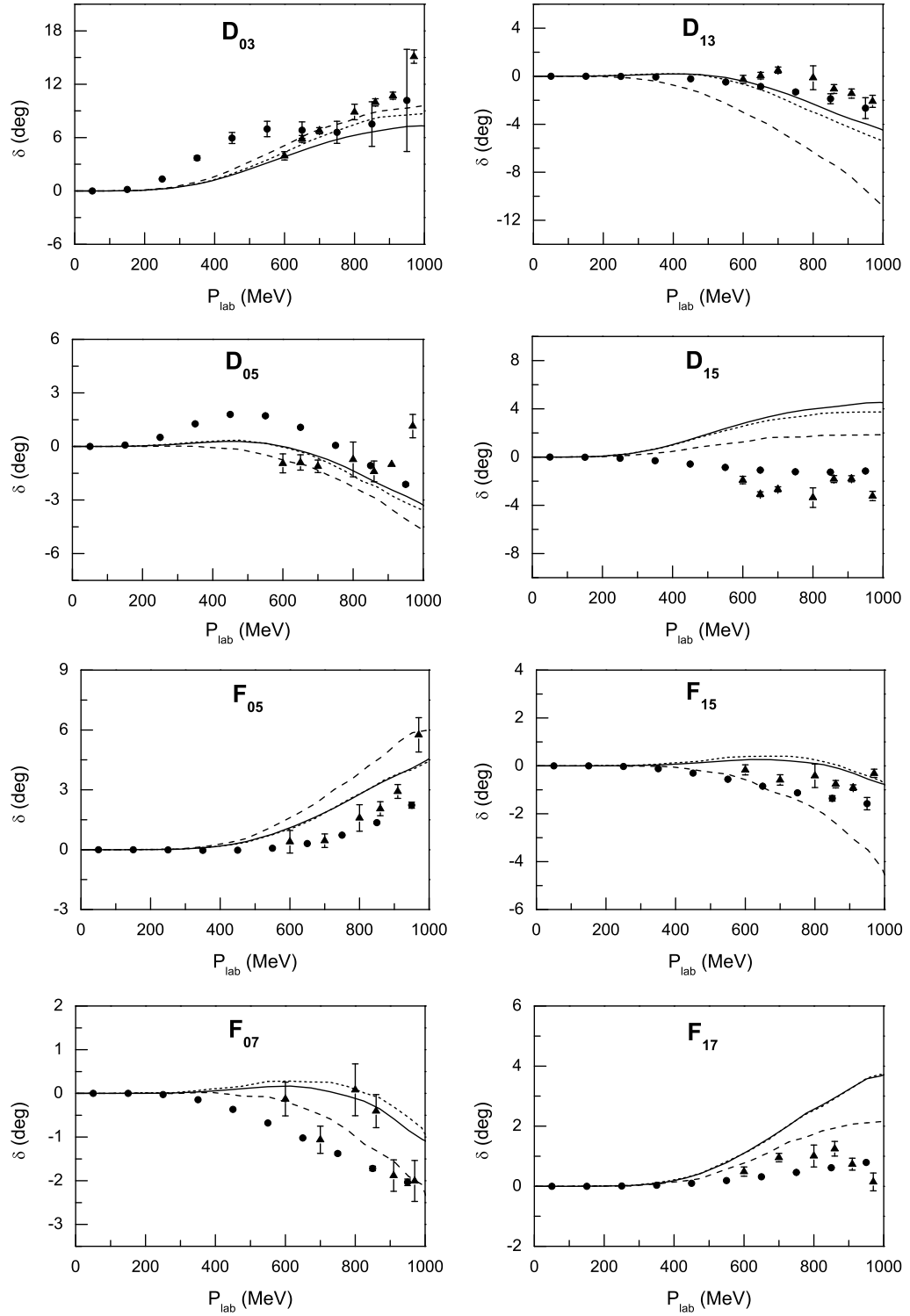


Figure 1:  $KN$   $S$ - and  $P$ -wave phase shifts as a function of the laboratory momentum of kaon meson. The short-dashed and dashed lines represent the results obtained in the chiral  $SU(3)$  quark model and the extended chiral  $SU(3)$  quark model, respectively. The solid curves show the phase shifts from the model including both OGE and vector meson exchange. The experimental data are taken from Refs. [12] (circles) and [13] (triangles).

Figure 2:  $KN$   $D$ - and  $F$ -wave phase shifts. Same notation as in Fig. 1.

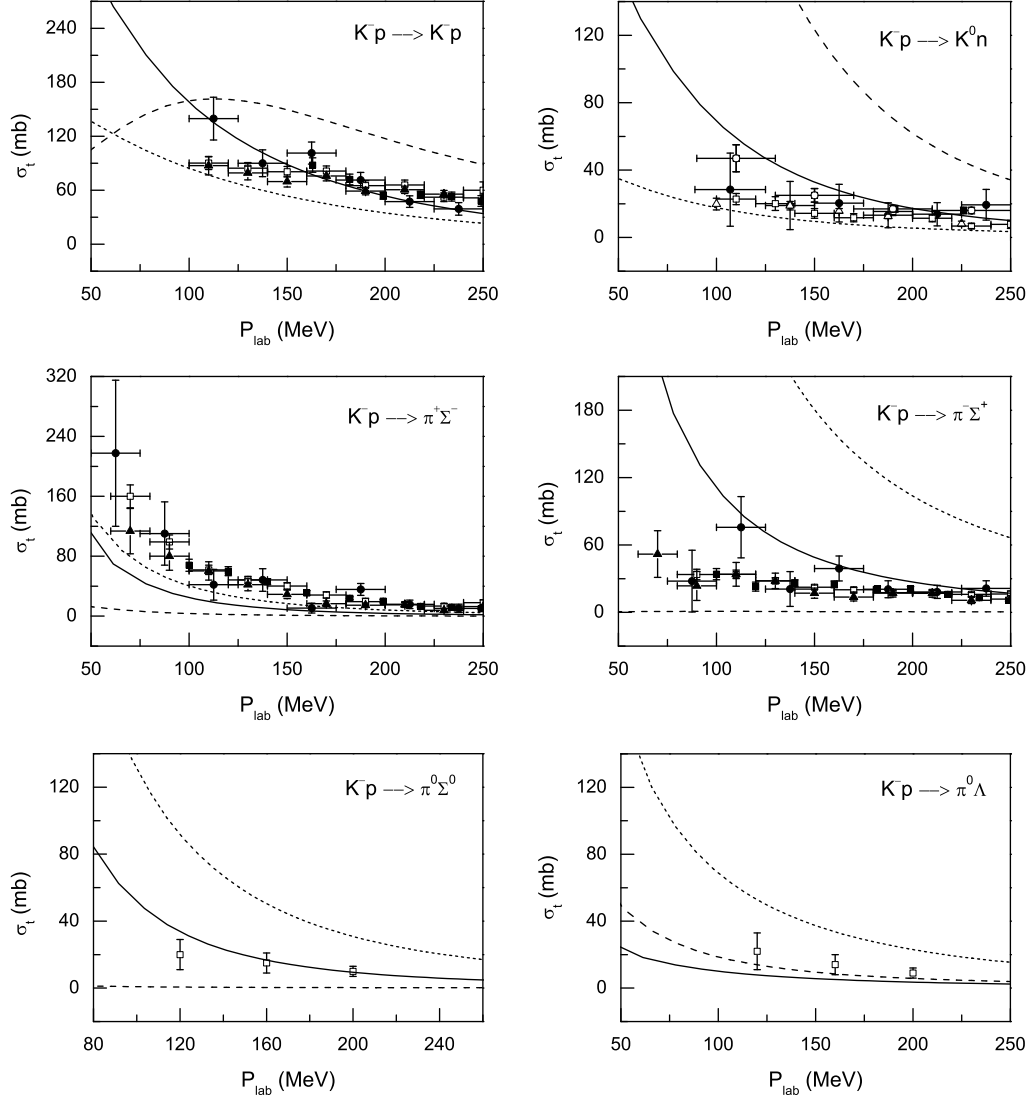


Figure 3: Total cross sections for  $K^-p$  scattering into various channels as a function of the laboratory momentum of  $K^-$  meson. The short-dashed and dashed lines correspond to the results from the chiral SU(3) quark model and the extended chiral SU(3) quark model, respectively. The solid curves represent the results from the model including both OGE and vector meson exchange. The experimental data are taken from Refs. [14] (empty circles), [15] (empty squares), [16] (empty triangles), [17] (filled circles), [18] (filled squares), and [19] (filled triangles).

quark-quark interaction is dominantly described by OGE; in model II, i.e. the extended chiral SU(3) quark model, the OGE is not included and thus the short-range quark-quark interaction is dominantly described by vector meson exchange; and in model III, both OGE and vector meson exchange are included. In other words, the short-range quark-quark interaction mechanisms are quite different in those three different models. We use those three models to perform a combined study of  $KN$  and  $\bar{K}N$  scattering processes in the framework of resonating group method (RGM). The results are shown in Figs. 1-3.

Figures 1 and 2 show the  $S$ -,  $P$ -,  $D$ -, and  $F$ -wave  $KN$  phase shifts calculated in our models. The short-dashed, dashed and solid lines represent the results from models I, II, and III, respectively. One notices that except for the  $P_{13}$  and  $D_{15}$  channels, our theoretical phase shifts for all partial waves are in good agreement with the experiment. One also sees that the phase shifts from those three different models are quite similar, even the short-range quark-quark interaction mechanisms are quite different in those three models. This means that for the  $KN$  system, the short range interaction can be identified as either OGE or vector meson exchange or both of them.

Figure 3 shows the cross sections for  $K^-p$  scattering into  $K^-p$ ,  $K^0n$ ,  $\pi^+\Sigma^-$ ,  $\pi^-\Sigma^+$ ,  $\pi^0\Sigma^0$  and  $\pi^0\Lambda$  channels. The solid lines show the results from model III. The short dashed and dashed lines represent the results from models I and II, respectively. One sees neither model I nor model II can give a satisfactory description of the  $K^-p$  cross sections. While in model III, the theoretical results are in qualitatively agreement with the experiment. This means that although for the  $KN$  system, all these three models can give satisfactory description of the data, for the  $\bar{K}N$  system, only the model with both OGE and vector meson exchange can describe the data. In other words, in order to give a unitary description of the  $KN$  phase shifts and  $\bar{K}N$  cross sections by use of one set of parameters, both OGE and vector meson exchanges are necessarily to be included in the quark-quark interactions.

## 4 Summary

We have performed a combined study of  $S$ -,  $P$ -,  $D$ -,  $F$ -wave  $KN$  phase shifts and the cross sections for  $K^-p$  scattering into  $K^-p$ ,  $K^0n$ ,  $\pi^+\Sigma^-$ ,  $\pi^-\Sigma^+$ ,  $\pi^0\Sigma^0$  and  $\pi^0\Lambda$  channels by use of three different constituent quark models and the resonating group method [11]. Some interesting results are obtained:

- we get a satisfactory description of the  $KN$  phase shifts for all partial waves except  $P_{13}$  and  $D_{15}$ ,

- the OGE and vector meson exchange give similar contributions to  $KN$  system, which is similar to the cases of  $NN$ ,  $\Omega\Omega$ ,  $N\bar{\Omega}$ ,  $\Delta K$ ,  $\Lambda K$  and  $\Sigma K$  systems,
- for the  $\bar{K}N$  system, the OGE and vector meson exchange give quite different contributions,
- both OGE and vector meson exchange are necessary to be included in the quark-quark potentials if one tries to simultaneously describe the  $KN$  phase shifts and  $\bar{K}N$  cross sections in a constituent quark model.

In the next step work, the effects of  $s$ -channel quark-anti-quark annihilation interaction and the coupling to a three-quark component will be investigated.

## Acknowledgments

This work was supported in part by the National Natural Science Foundation of China (Nos. 10475087 & 10775146) and China Postdoctoral Science Foundation (No. 20060400093). The author F. Huang is grateful to the support from Alexander von Humboldt Foundation.

## References

- [1] Z.Y. Zhang, Y.W. Yu, P.N. Shen, L.R. Dai, A. Faessler and U. Straub, *Nucl. Phys.* **A625**, 59 (1997).
- [2] L.R. Dai, Z.Y. Zhang, Y.W. Yu and P. Wang, *Nucl. Phys.* **A727**, 321 (2003).
- [3] F. Huang, Z.Y. Zhang, and Y.W. Yu, *Phys. Rev.* **C70**, 044004 (2004).
- [4] F. Huang and Z.Y. Zhang, *Phys. Rev.* **C70**, 064004 (2004).
- [5] F. Huang and Z.Y. Zhang, *Phys. Rev.* **C72**, 024003 (2005).
- [6] L.R. Dai, Z.Y. Zhang and Y.W. Yu, *Chin. Phys. Lett.* **23**, 3215 (2006).
- [7] D. Zhang, F. Huang, L.R. Dai, Y.W. Yu and Z.Y. Zhang, *Phys. Rev.* **C75**, 024001 (2007).
- [8] F. Huang, D. Zhang, Z.Y. Zhang and Y.W. Yu, *Phys. Rev.* **C71**, 064001 (2005).

- [9] F. Huang and Z.Y. Zhang, *Phys. Rev.* **C72**, 068201 (2006).
- [10] F. Huang, W.L. Wang, Z.Y. Zhang and Y.W. Yu, *Phys. Rev.* **C76**, 018201 (2007).
- [11] F. Huang, W.L. Wang and Z.Y. Zhang, A combined study of  $KN$  and  $\bar{K}N$  interactions in a constituent quark model, in preparation.
- [12] J.S. Hyslop, R.A. Arndt, L.D. Roper and R.L. Workman, *Phys. Rev.* **D46**, 961 (1992).
- [13] K. Hashimoto, *Phys. Rev.* **C29**, 1377 (1984).
- [14] D. Evans, J.V. Major, E. Rondio, J.A. Zakrzewski, J.E. Conboy, D.J. Miller and T. Tymieniecka, *J. Phys.* **G9**, 885 (1983).
- [15] J.K. Kim, *Phys. Rev. Lett.* **14**, 29 (1965).
- [16] W. Kittel, G. Otter and I. Wacek, *Phys. Lett.* **21**, 349 (1966).
- [17] W.E. Humphrey and R.R. Ross, *Phys. Rev.* **127**, 1305 (1962).
- [18] J. Ciborowski *et al.*, *J. Phys.* **G8**, 13 (1982).
- [19] M. Sakitt, T.B. Day, R.G. Glasser, N. Seeman, J. Friedman, W.E. Humphrey and R.R. Ross, *Phys. Rev.* **139**, B719 (1965).

MENU 2007  
11th International Conference  
on Meson-Nucleon Physics and  
the Structure of the Nucleon  
September 10-14, 2007  
IKP, Forschungszentrum Jülich, Germany

# DYNAMICAL COUPLED-CHANNEL MODEL ANALYSIS OF $\pi$ -N SCATTERING AND ELECTROMAGNETIC PION PRODUCTION REACTIONS

*B. Juliá-Díaz*

Departament de Estructura i Constituents de la Matèria,  
University of Barcelona,  
Spain, 08028

## Abstract

The ability of the coupled channel model (MSL) developed in recently in Ref. [1] to account simultaneously for the  $\pi N$  scattering data and the  $\pi$  photoproduction reactions on the nucleon is presented. An accurate description of  $\pi N$  scattering has been obtained. A preliminary description of  $\pi$  photoproduction is also discussed.

## 1 Introduction

Understanding the intricate dynamics leading to baryon resonance production and subsequent decay is essential to deepen our understanding on the confinement mechanisms of QCD. It is now well recognized that a coupled-channel approach is needed to extract the nucleon resonance ( $N^*$ ) parameters from the data of  $\pi N$  and electromagnetic meson production reactions. With the recent experimental developments [2,3], such a theoretical effort is needed to analyze the very extensive data from Jefferson Laboratory (JLab), Mainz, Bonn, GRAAL, and Spring-8. To cope with this challenge, a dynamical coupled-channel model (MSL) for meson-baryon reactions in the nucleon resonance region has been developed recently [1].

The details of the MSL model are given in Ref. [1] and will not be discussed here. Similar to the earlier works using meson-exchange models of pion-nucleon scattering, see Ref. [2] for a review, the starting point of the MSL model is a set of Lagrangians describing the interactions between mesons (including the photon) ( $M = \gamma, \pi, \eta, \rho, \omega, \sigma, \dots$ ) and baryons ( $B = N, \Delta, N^*, \dots$ ). By applying a unitary transformation method [4,5], an

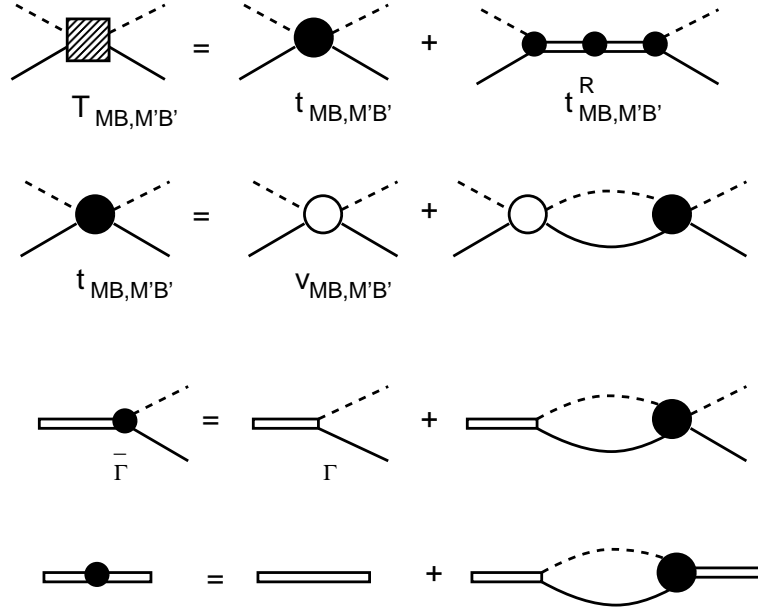


Figure 1: Graphical representation of Eqs.(1)-(8).

effective Hamiltonian is then derived from the considered Lagrangian. All of these interactions are *energy independent*, an important feature of the MSL formulation.

Once the Hamiltonian has been obtained, the coupled-channel equations for  $\pi N$  and  $\gamma N$  reactions are derived by using the standard projection operator technique [6], as given explicitly in Ref. [1]. The obtained scattering equations satisfy the two-body ( $\pi N, \eta N, \gamma N$ ) and three-body ( $\pi\pi N$ ) unitarity conditions. The  $\pi\Delta$ ,  $\rho N$  and  $\sigma N$  resonant components of the  $\pi\pi N$  continuum are generated dynamically.

The constructed model can describe up to now very well almost all of the empirical  $\pi N$  amplitudes in  $S, P, D$ , and  $F$  partial waves of SAID [7]. We will also show that the predicted differential cross sections and target polarization asymmetry are in good agreement with the original data of elastic  $\pi^\pm p \rightarrow \pi^\pm p$  and charge-exchange  $\pi^- p \rightarrow \pi^0 n$  processes.

## 2 Dynamical coupled-channel equations

The meson-baryon ( $MB$ ) scattering equations derived in Ref. [1] are illustrated in Fig. 1. Explicitly, they are defined by the following equations

$$T_{\alpha,\beta}(E) = t_{\alpha,\beta}(E) + t_{\alpha,\beta}^R(E), \quad (1)$$

where  $\alpha, \beta = \gamma N, \pi N, \eta N, \pi\pi N$ . The full amplitudes, e.g.  $T_{\pi N, \pi N}(E)$ ,  $T_{\eta N, \pi N}(E)$ ,  $T_{\pi N, \gamma N}(E)$  can be directly used to calculate  $\pi N$ ,  $\pi N \rightarrow \eta N$  and  $\gamma N \rightarrow \pi N$  scattering observables. The non-resonant amplitude  $t_{\alpha,\beta}(E)$  in Eq. (1) is defined by the coupled-channel equations,

$$t_{\alpha,\beta}(E) = V_{\alpha,\beta}(E) + \sum_{\delta} V_{\alpha,\delta}(E) G_{\delta}(E) t_{\delta,\beta}(E) \quad (2)$$

with

$$V_{\alpha,\beta}(E) = v_{\alpha,\beta} + Z_{\alpha,\beta}^{(E)}(E). \quad (3)$$

The second term in the right-hand-side of Eq. (1) is the resonant term defined by

$$t_{\alpha,\beta}^R(E) = \sum_{N_i^*, N_j^*} \bar{\Gamma}_{\alpha \rightarrow N_i^*}(E) [D(E)]_{i,j} \bar{\Gamma}_{N_j^* \rightarrow \beta}(E), \quad (4)$$

with

$$[D^{-1}(E)]_{i,j} = (E - M_{N_i^*}^0) \delta_{i,j} - \bar{\Sigma}_{i,j}(E), \quad (5)$$

where  $M_{N^*}^0$  is the bare mass of the resonant state  $N^*$ , and the self-energies are

$$\bar{\Sigma}_{i,j}(E) = \sum_{\delta} \Gamma_{N_i^* \rightarrow \delta} G_{\delta}(E) \bar{\Gamma}_{\delta \rightarrow N_j^*}(E). \quad (6)$$

The dressed vertex interactions in Eq. (4) and Eq. (6) are (defining  $\Gamma_{\alpha \rightarrow N^*} = \Gamma_{N^* \rightarrow \alpha}^\dagger$ )

$$\bar{\Gamma}_{\alpha \rightarrow N^*}(E) = \Gamma_{\alpha \rightarrow N^*} + \sum_{\delta} t_{\alpha,\delta}(E) G_{\delta}(E) \Gamma_{\delta \rightarrow N^*}, \quad (7)$$

$$\bar{\Gamma}_{N^* \rightarrow \alpha}(E) = \Gamma_{N^* \rightarrow \alpha} + \sum_{\delta} \Gamma_{N^* \rightarrow \delta} G_{\delta}(E) t_{\delta,\alpha}(E). \quad (8)$$

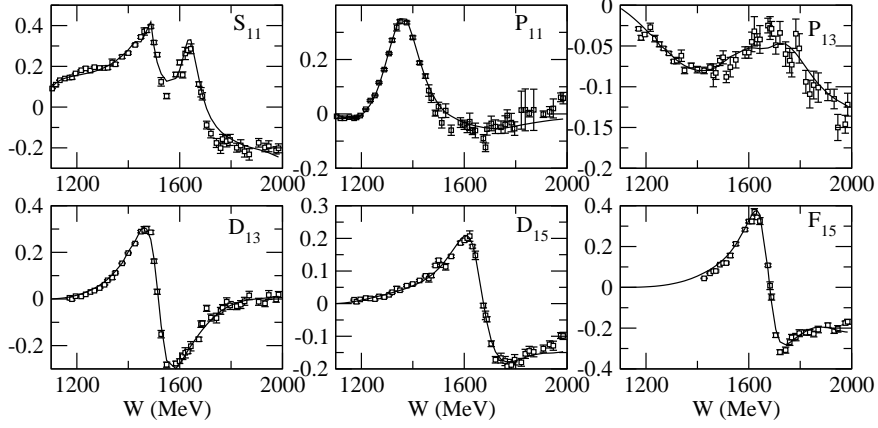


Figure 2: Real part of  $T_{\pi N, \pi N}$  for some isospin 1/2 partial waves compared to the SAID energy independent extraction.

### 3 Meson-baryon interaction

We proceed in the following way. First we consider the meson-baryon interactions involving  $\pi N, \eta N, (\pi\Delta, \sigma N, \rho N)$  and use the extensive database for  $\pi N \rightarrow \pi N$  (and also the  $\pi N \rightarrow \eta N$ ) to fix the non-resonant parameters entering in the phenomenological lagrangians. Once the meson-baryon is fixed we will, in a first stage, leave it unchanged and produce a first description of the single meson photoproduction data. In the next step a combined analysis will need to be performed.

To solve the coupled-channel integral equations, Eq. (2), without introducing any further simplification we need to regularize the matrix elements of  $v_{MB, M'B'}$ . We include at each meson-baryon-baryon vertex a form factor of the following form

$$F(\mathbf{k}, \Lambda) = \left[ \frac{|\mathbf{k}|^2}{|\mathbf{k}|^2 + \Lambda^2} \right]^2 \quad (9)$$

with  $\mathbf{k}$  being the meson momentum. For the meson-meson-meson the same form is used with  $\mathbf{k}$  being the momentum of the exchanged meson.

With the non-resonant amplitudes generated from solving Eq. (2), the resonant amplitude  $t_{MB, M'B'}^R$  Eq. (4) then depends on the bare mass  $M_{N^*}^0$  and the bare  $N^* \rightarrow MB$  vertex functions. It is worth recalling that the resonance amplitude will necessarily contain information about the non-resonant piece, as is apparent from Eq. (4). As discussed in Ref. [1], these bare  $N^*$  parameters

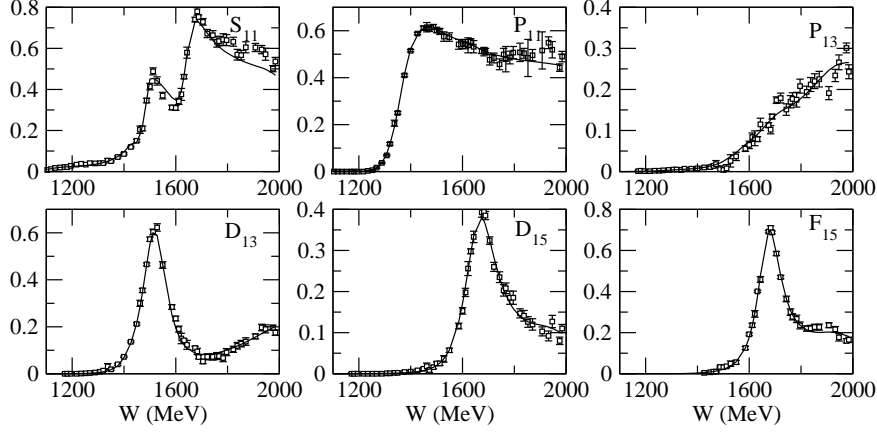


Figure 3: Imaginary part of  $T_{\pi N, \pi N}$  for some isospin 1/2 partial waves compared to the SAID energy independent extraction.

can perhaps be taken from a hadron structure calculation which *does not* include coupling with meson-baryon continuum states or meson-exchange quark interactions. Unfortunately, such information is not available to us. We thus use a parameterization given explicitly in Ref. [8].

In figures 2 and 3 we depict the real and imaginary part of  $T_{\pi N, \pi N}$  matrix compared to the energy independent extraction of the GWU group [7]. A comparison with experimental data for differential cross section and target polarization asymmetry is given in figures 4 and 5.

Our model is further checked by examining our predictions of the total cross sections  $\sigma^{tot}$  which can be calculated from the forward elastic scattering amplitudes by using the optical theorem.

The predicted  $\sigma^{tot}$  (solid curves) along with the resulting total elastic scattering cross sections  $\sigma^{el}$  compared with the data of  $\pi^-p$  reaction are shown in Fig. 6. Clearly, the model can account for the data very well within the experimental errors. Equally good agreement with the data for  $\pi^+p$  reaction is achieved. In the right side of Fig. 6, we show how the contributions from each channel add up to get the total cross sections.

The contributions from  $\pi\Delta$ ,  $\rho N$  and  $\sigma N$  intermediate states to the  $\pi^-p \rightarrow \pi\pi N$  total cross sections calculated from our model can be seen in the right side of Fig. 6. These predictions remain to be verified by the future experiments. The existing  $\pi N \rightarrow \pi\pi N$  data are not sufficient for extracting *model independently* the contributions from each unstable channel.

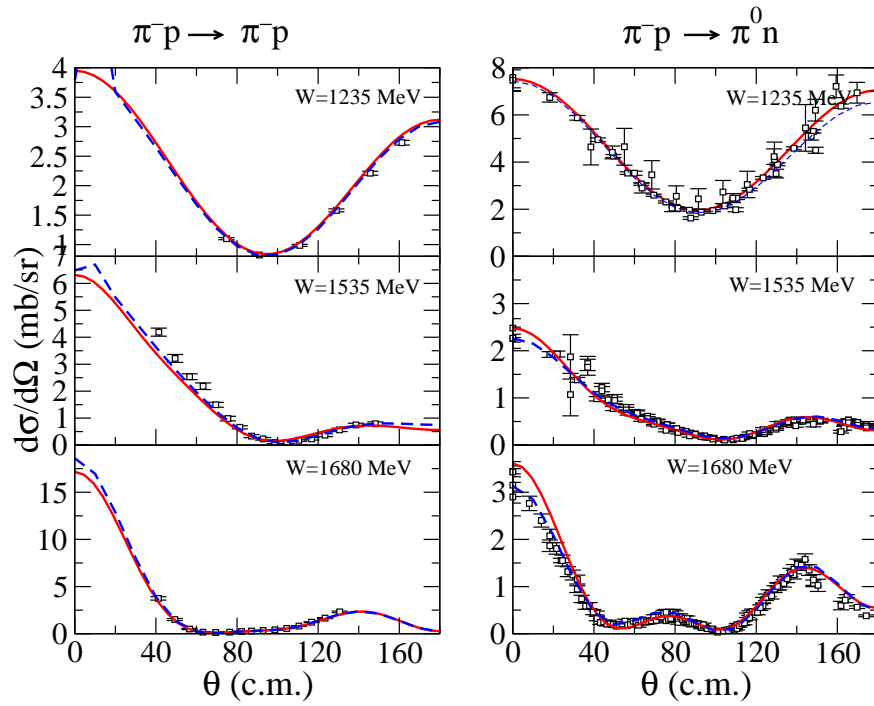


Figure 4: Differential cross section for several different center of mass energies. Solid red curve corresponds to our model while blue dashed lines correspond to the SP06 solution of SAID [7]. All data have been obtained through the SAID online applications. Ref. [11].

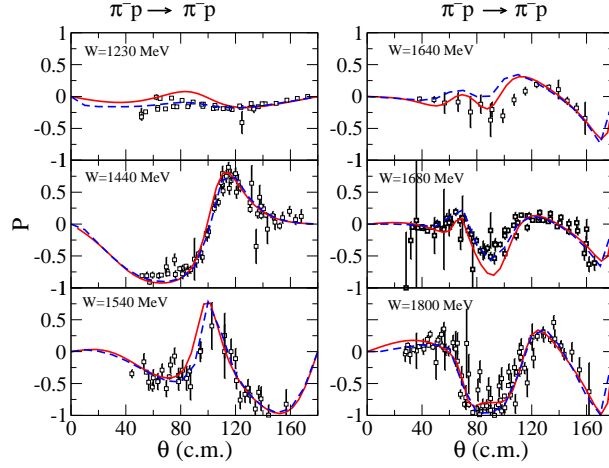


Figure 5: Target polarization asymmetry,  $P$ , for several different center of mass energies. Solid red curve corresponds to our model while blue dashed lines correspond to the SP06 solution of SAID [7]. All data have been obtained through the SAID online applications. Ref. [11].

As mentioned above, the fit to  $\pi N$  elastic scattering can not determine well the bare  $N^* \rightarrow \pi\Delta, \rho N, \sigma N$  parameters. Thus the results for these unstable particle channels must be refined by fitting the  $\pi N \rightarrow \pi\pi N$  data, this is currently being pursued [9].

## 4 Photoproduction reactions

With the hadronic parameters determined in the previous fit to meson-baryon experimental data we proceed to analyze the extensive data base of  $\pi$  photoproduction. Here the only parameters that need to be determined are the bare  $\gamma N \rightarrow N^*$  vertex interactions.

The strategy is to start with the bare helicity amplitudes of resonances at the values given by the PDG [10]. Then, we allow small variations with respect to those values and also in a preliminary step small variations of a selected set of non-resonant parameters. At the present stage we can only present preliminary results which are at the present time being further improved and will be reported elsewhere.

In figure 7 we present a comparison of the current model and the experimental differential cross section data for the reaction  $\gamma p \rightarrow \pi^+ n$  at a fixed

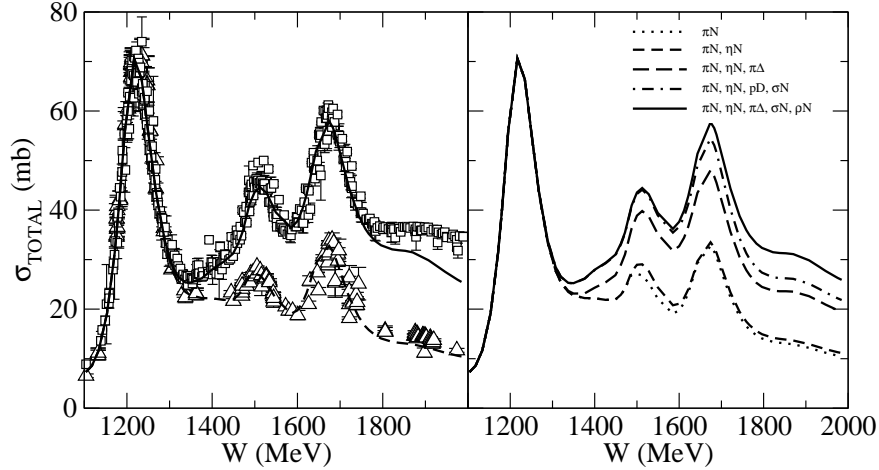


Figure 6: Left: The predicted total cross sections of the  $\pi^- p \rightarrow X$  (solid curve) and  $\pi^- p \rightarrow \pi^- p + \pi^0 n$  (dashed curve) reactions are compared with the data. Open squares are the data on  $\pi^- p \rightarrow X$  from Ref. [10], open triangles are obtained by adding the  $\pi^- p \rightarrow \pi^- p$  and  $\pi^- p \rightarrow \pi^0 n$  data obtained from Ref. [10] and SAID database [11] respectively. Right: Show how the predicted contributions from each channel are added up to the predicted total cross sections of the  $\pi^- p \rightarrow X$ .

angle,  $\theta = 90$  (deg). First, our main emphasis is put on understanding the region up to 1.6 GeV extending in that way previous works where only the  $\Delta(1232)$  region was studied [4, 12, 13]. In figure 8 we depict angular distributions for both  $\pi^+ n$  and  $\pi^0 p$  photoproduction in the  $\Delta(1232)$  region. The effect of intermediate meson-baryon states different from  $\pi N$  is also depicted. The importance of multi-step processes is clear and confirms previous studies done in similar frameworks.

## 5 Future Developments

The model described in detail in Refs. [1, 8] has already been used to study  $\pi N$  scattering and  $\pi$  photoproduction reactions as presented in this contribution. Being the main and most important interest of these studies the extraction and interpretation of baryon resonances by analyzing the extant photo and electro production experimental data we are now beginning to perform simultaneous studies of meson-baryon, single meson electro (photo)production [14]

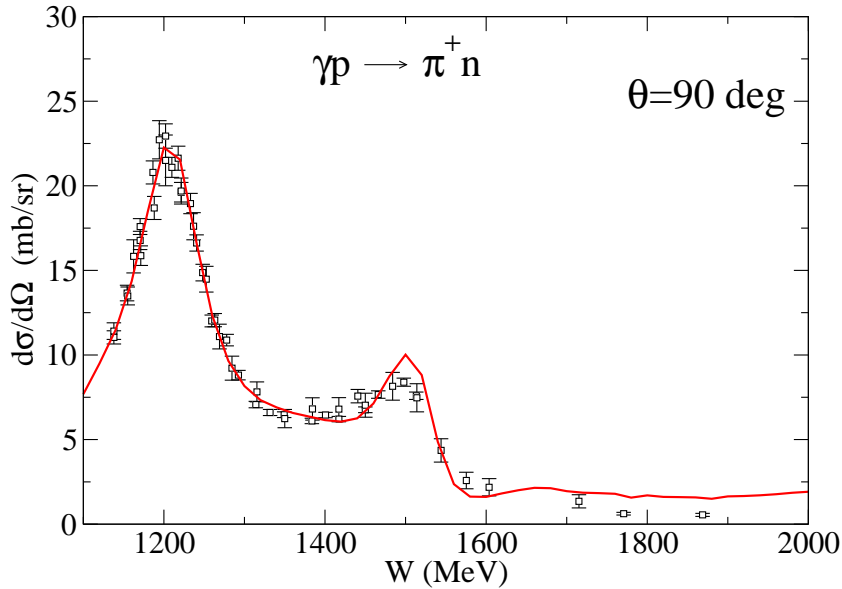


Figure 7: Differential cross section for the reaction  $\gamma p \rightarrow \pi^+ n$  at  $\theta = 90^\circ$  as function of the center of mass energy,  $W$ .

and two-meson photoproduction.

At the same time an important effort is being pursued to reliably extract meaningful resonance parameters from the coupled channel formalism [15].

The simultaneous consideration of other meson-baryon channels, such as  $\omega N$  [16] or kaon-hyperon channels is being pursued within the same framework.

## Acknowledgments

It is a pleasure to thank T.-S. H. Lee, A. Matsuyama and T. Sato who collaborated in everything presented here. I want to thank also the hospitality of the theory group at JLAB where part of this work was done. This work is partially supported by Grant No. FIS2005-03142 from MEC (Spain) and FEDER and European Hadron Physics Project RII3-CT-2004-506078. The computations were performed at NERSC (LBNL) and Barcelona Supercomputing Center (BSC/CNS) (Spain).

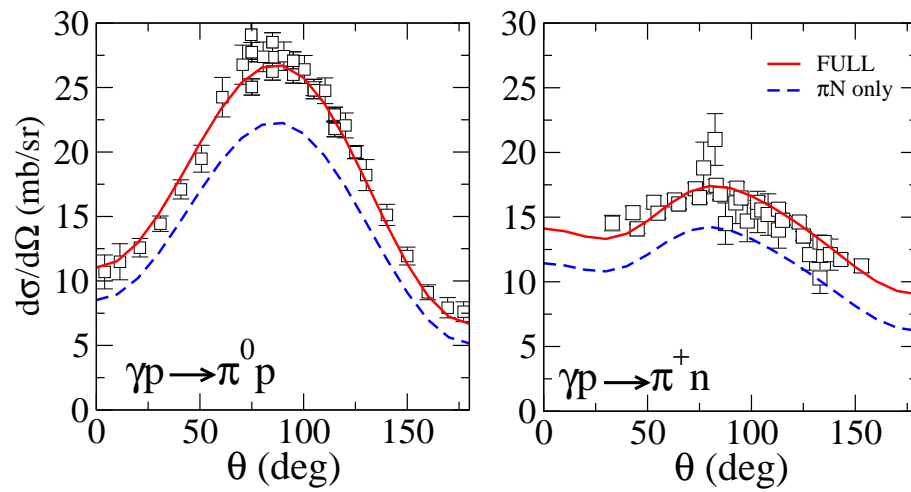


Figure 8: Differential cross section in the  $\Delta$  region. The full line corresponds to the current full model, the dashed line only considers intermediate  $\pi N$  intermediate states in the photoproduction process.

## References

- [1] A. Matsuyama, T. Sato, T.-S. H. Lee, *Phys. Rept.* **439**, 193 (2007).
- [2] V. Burkert and T.-S. H. Lee, *Int. J. of Mod. Phys.* **E13**, 1035 (2004).
- [3] T.-S. H. Lee and L.C. Smith, *J. Phys. G* **34**, 1 (2007).
- [4] T. Sato and T.-S. H. Lee, *Phys. Rev. C* **54**, 2660 (1996).
- [5] M. Kobayashi, T. Sato, and H. Ohtsubo, *Prog. Theor. Phys.* **98**, 927 (1997).
- [6] Herman Feshbach, *Theoretical Nuclear Physics, Nuclear Reactions* (Wiley, New York, 1992)
- [7] R.A. Arndt, I.I. Strakovsky, R.L. Workman, *Phys. Rev. C* **53**, 430 (1996); *Int. J. Mod. Phys.* **A18**, 449 (2003).
- [8] B. Julia-Diaz, T.-S. H. Lee, A. Matsuyama, and T. Sato, *arXiv:0704.1615*. To appear in *Phys. Rev. C*.
- [9] B. Julia-Diaz, H. Kamano, T.-S. H. Lee, A. Matsuyama, and T. Sato, in preparation.
- [10] W. M. Yao *et al.* [Particle Data Group], *J. Phys. G* **33**, 1 (2006).
- [11] CNS Data Analysis Center, GWU, <http://gwdac.phys.gwu.edu>.
- [12] T. Sato and T.-S. H. Lee, *Phys. Rev. C* **63**, 055201 (2001).
- [13] B. Julia-Diaz, T.-S. H. Lee, T. Sato and L. C. Smith, *Phys. Rev. C* **75**, 015205 (2007).
- [14] B. Julia-Diaz, T.-S. H. Lee, A. Matsuyama, T. Sato, L.C. Smith in preparation.
- [15] N. Suzuki, T. Sato and T.-S.H. Lee, in preparation.
- [16] M.W. Paris, T. Sato and T.-S.H. Lee, in preparation.

# VECTOR AND TENSOR ANALYZING POWERS OF THE ${}^1\text{H}(d,\gamma{}^3\text{He})$ CAPTURE REACTION

D. Kiselev<sup>\*,1</sup>, T. Klechneva<sup>\*</sup>, C. Carasco<sup>\*</sup>, I. Goussev<sup>#</sup>, M. Hauger<sup>\*</sup>, J. Jourdan<sup>\*</sup>, B. Krusche<sup>\*</sup>, H. Mühry<sup>\*</sup>, Ch. Normand<sup>\*</sup>, D. Seliverstov<sup>#</sup>, I. Sick<sup>\*</sup>, G. Warren<sup>\*</sup>, H. Wöhrle<sup>\*</sup>, M. Zeier<sup>\*</sup>

<sup>\*</sup>Institut für Physik, Universität Basel, 4056 Basel, Switzerland  
<sup>#</sup>PNPI, Gatchina, Russia

## Abstract

Precise measurements of the deuteron vector analyzing power  $A_y^d$  and the tensor analyzing power  $A_{yy}$  of the  ${}^1\text{H}(d,\gamma{}^3\text{He})$ -capture reaction have been performed at deuteron energies of 29 MeV and 45 MeV. The data have been compared to theoretical state-of-the-art calculations of the Bochum-Krakow, Hannover-Lisbon and the Pisa group. Due to the large sensitivity of polarization observables and the precision of the data small effects in the dynamics become visible.

## 1 Introduction

The three-body system is particularly interesting because its wave function can be exactly calculated in a non-relativistic framework. Ground and continuum states are treated on the same footing and realistic nucleon-nucleon potentials like CD Bonn or Argonne V18 are used. Even though the basic principles are the same for the three-body theoretical groups [1–6] the technique used to solve the Schrödinger equation are quite different. Therefore it is satisfying to see that their results on the one-body current level agree well to each other. Beyond the one-body current different descriptions of Meson Exchange Currents (MEC's) and three-body forces and different treatments of explicit inclusion of Coulomb interaction and relativistic corrections makes a comparison of the results from the Bochum-Krakow, Hannover-Lisbon and

---

<sup>1</sup>E-mail address: Daniela.Kiselev@psi.ch  
present address: Paul Scherrer Institut, 5232 Villigen, Switzerland  
former name: D. Rohe

Pisa group interesting. However, comparison to experimental data is mandatory. These data should be preferably sensitive to small effects in the dynamics and the error bars should be smaller than these effects.

The data taken by the Basel-PNPI collaboration at the Philips injector cyclotron at the Paul Scherrer Institut (PSI) which will be described in the following, fulfill these requirements. In polarization observables like the vector and tensor analyzing powers,  $A_y^d$  and  $A_{yy}$ , the dominant S-S transition in the radiative capture reaction  ${}^1\text{H}(\text{d},\gamma){}^3\text{He}$  is suppressed compared to the S-D amplitude. The latter is closely related to MEC's as it was shown in the measurement of e.g. the elastic form factors in the  $A=3$  system [8]. Therefore one can expect that measurements of polarization observables in capture reactions provide insight into the different roles played by nucleonic and mesonic degrees of freedom.

The deuteron analyzing powers  $A_y^d$  and  $A_{yy}$  are measured using a vector and tensor polarized deuteron beam with its spin perpendicular to the scattering plane. Then the cross section can be written as

$$\frac{d\sigma(\theta)}{d\Omega} = \frac{d\sigma_o(\theta)}{d\Omega} \left( 1 + \frac{3}{2}p_z A_y^d + \frac{1}{2}p_{zz} A_{yy} \right). \quad (1)$$

Here  $\sigma_o$  is the unpolarized cross section and  $\theta$  the center-of-mass (c.m.) angle of the deuteron-photon system. The vector and tensor polarizations of the beam,  $p_z$  and  $p_{zz}$ , have to be measured absolutely before the analyzing powers can be extracted.

The deuteron beam energy was chosen as 29 MeV and 45 MeV. At around 30 MeV the beam energy dependence of  $A_{yy}(\theta = 90^\circ)$  shows a maximum whereas at 50 MeV a zero crossing occurs as shown by both experimental data [9–15] and theory [2, 16]. The minimum of  $A_{yy}(\theta = 90^\circ)$  is expected to be particularly sensitive to interference effects. As it will become clear when comparing the data to the theoretical results the tensor analyzing powers at these two energies show rather different sensitivities to the underlying physics.

The full angular dependence of the analyzing powers up to the extreme angles were measured which is important because of the different sensitivity to MEC's. In the energy range of 10-50 MeV the  ${}^1\text{H}(\text{d},\gamma){}^3\text{He}$ -capture process is dominated by the electric dipole transition (E1). Although MEC's can give large contributions to the E1-transition, they can be taken into account implicitly when performing calculations with operators derived using the Siegert's theorem [17]. The Siegert theorem treats the two-body currents in (part of) the electric transitions only and disregards them in the magnetic transitions completely. Therefore at medium angles where the E1-E1 transition dominates ( $\propto \sin^2(\theta)$ ) it is expected that the Siegert theorem will

provide a good description of the data. At the extreme angles in forward and backward direction the small M1 amplitude is enhanced by the E1 amplitude in the M1-E1 interference term. In the M1 transition MEC's can contribute up to 50 % [13].

## 2 Experimental details

The experiment was performed at the Philips injector cyclotron (maximum proton energy 72 MeV) of the Paul Scherrer Institute (PSI) in Villigen (Switzerland) where a polarized deuteron beam prepared in the PSI atomic beam ion source [18] was available. With the two strong and one weak field radio frequency (RF) -transition units the nuclear polarization was induced. Depending on the combination of active RF-units 4 polarization states with  $p_z = \pm 1/3$  and  $p_{zz} = \pm 1$  could be obtained in addition to the unpolarized beam (= 5 modes). To minimize systematic errors the modes were cycled through with a repetition rate of 0.3 Hz.

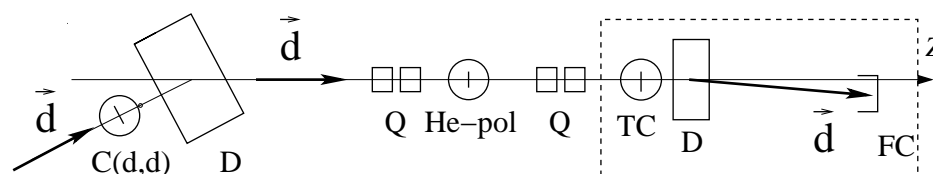


Figure 1: Schematic overview of the beam line in the experimental hall NE-C. Here C(d,d) - carbon scattering chamber, Q - quadrupole doublet, He-pol -  $^4\text{He}$ -polarimeter, TC - target chamber, D - dipole magnet to separate  $^3\text{He}$  and unscattered deuterons, FC - Faraday cup.

In fig. 1 a sketch of the experimental setup is shown. In a first a scattering chamber deuterons scatter elastically on a thin carbon foil and are detected using a fast scintillator. The signal relative to RF of the cyclotron gives online-information about the actual bunch structure of the beam. It was required to be less than 1.5 ns FWHM. After a dipole the deuterons passes a second scattering chamber which houses a polarimeter to measure the tensor and vector polarization of the beam. It consists of a  $^4\text{He}$  cell of 0.5 bar and two passivated implanted planar silicon (PIPS) detectors which detect the recoil  $^4\text{He}$  at  $\theta_{cm} = 150^\circ$  left and right from the beam line. The PIPS detectors allow to discriminate between  $\alpha$  particles and deuterons. At this angle the vector and tensor analyzing powers for elastic d- $\alpha$  scattering are high and precisely known [19]. Then the beam polarizations can be extracted

in a similar to eq. 1. In average the polarizations were  $p_z = 0.25$  and  $p_{zz} = 0.65$ , determined with accuracies of 2 -3%.

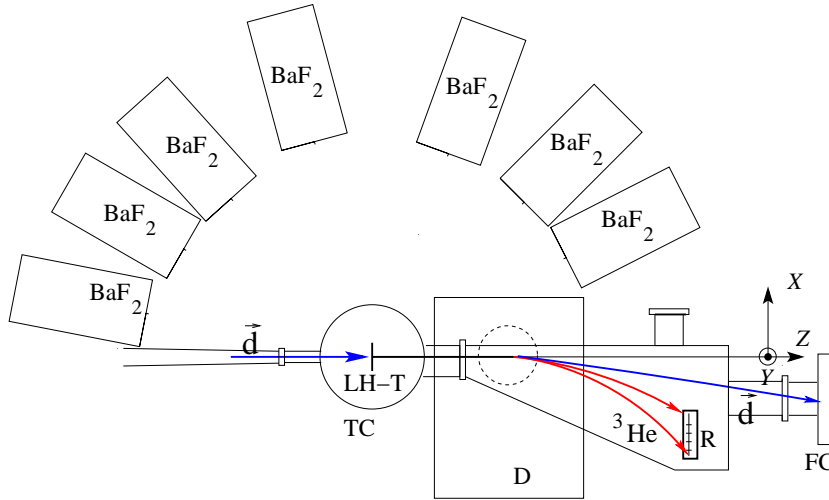


Figure 2: Schematic overview of the setup: LH-T - liquid hydrogen target, D - dipole magnet to separate  ${}^3\text{He}$  and unscattered deuterons, R - recoil-detectors, FC - Faraday cup.

Behind the beam polarimeter the setup for the capture experiment is located. It is shown in more detail in fig. 2. The deuteron beam hits first the liquid hydrogen target (16 K at 0.25 bar) with a thickness of  $14 \text{ mg/cm}^2$ . The conical beam entrance tube allows also for measurements at extreme backward angles. The capture photons are detected in four  $\text{BaF}_2$  crystals of dimension  $8\text{cm} \times 8\text{cm} \times 25\text{cm}$ . This crystal was chosen for its excellent timing characteristic and the high density ( $4.89 \text{ g/cm}^3$ ) which leads to a good efficiency for photons and an acceptable energy resolution of about 16%. Further the short component allows to discriminate between photons and neutrons generated by background reactions. Both performances are crucial considering the high background rate from hadronic reactions (in particular neutrons from the break-up reaction). In addition the crystals were shielded against background with 5 cm Pb on top, bottom and side as well as 5 cm Bor-plastic in the front.

The recoil  ${}^3\text{He}$  particles are detected in a segmented plastic scintillator of 1.2 mm thickness. The thickness is chosen such that  ${}^3\text{He}$  is stopped but protons and deuterons pass through. This helps distinguishing these particle types. The  ${}^3\text{He}$  recoil in a cone between  $0.4^\circ$  and  $2.6^\circ$  degrees. Without the C-shaped dipole it would be not possible to separate them from the deuteron beam downstream. The strength of the magnetic field was chosen such that

the  $^3\text{He}$  were separated from the deuteron beam by  $10^\circ$ . Simulations were performed to determine the path of the particles.

Finally a Faraday cup (FC) stopped the beam and measured the current for each polarization state.

### 3 Analysis and Results

The main challenge of the data analysis is to single out the few capture events from a huge background due to hadronic reactions. The signal to noise ratio (S/N) could be increased to one by a hardware coincidence (time window 25 ns) between the detected photon, the recoiling  $^3\text{He}$  and the RF of the cyclotron. After applying several 2-dimensional software cuts S/N was larger than 25. For a more detailed description of the software cuts see refs. [20, 21]. After applying all possible cuts the  $\gamma$  energy spectrum of the

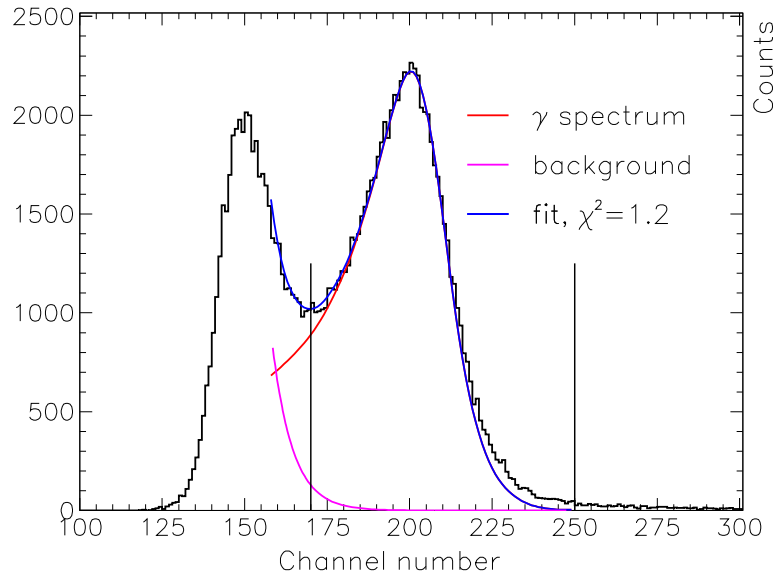


Figure 3: Final  $\gamma$  energy spectrum of the short component in  $\text{BaF}_2$ . Indicated are the integration limits set for the signal. Further the fit of the response function to the data is shown as well as the decomposition into background (magenta) and signal (red).

short component of  $\text{BaF}_2$  obtained is shown in fig. 3. Also indicated are

the integration limits from which the final asymmetries are derived. The asymmetries are diluted by the remaining background from the low energy photons leaking into the region of the integration limits. The final result has to be corrected for and therefore the background has to be determined. For this a fit function for the region between the integration limits is needed, i.e. a response function of  $\text{BaF}_2$  for photons of about 20 MeV must be known.

For this determination an additional experiment with monoenergetic  $\gamma$ -rays was performed at the Physics Institute of the University of Basel. Monoenergetic 20 MeV  $\gamma$ -rays were produced in a  ${}^3\text{H}(\text{p},\gamma){}^4\text{He}$  reaction with a 1 MeV proton beam provided by a Cockcroft-Walton accelerator. The detector was placed at 110 deg close to the maximum of the angular distribution of the photons in a similar geometry as in the  $\mathbf{d}-p$ -capture experiment. The measured short component of the  $\text{BaF}_2$  response function plus an exponential function representing the background were folded with a Gaussian and fitted with the peak position, the amplitude, the width of the Gaussian and the exponent of the exponential function as free parameters. The result of such a fit is shown in fig. 3. The background determined in this way contributes at maximum 4.6%. In addition it was verified that the background is unpolarized. Further various systematic checks were done to determine the systematic error. The resulting total systematic errors vary between 0.00044 and 0.00113 as compared to the statistical errors of 0.00187 to 0.00470.

## 4 Comparison to theory

The present data together with previous data taken at the same deuteron energies are compared to calculations from the Bochum-Krakow group [22], the Pisa group [23] and the Hannover-Lisbon group [24]. The calculations are all exact in the sense that they provide a full solution of the Schrödinger equation for a realistic nucleon-nucleon interaction for both the ground- and continuum states. The techniques applied in the calculations by the three groups are quite different. The Hannover-Lisbon group solves the Alt-Grassberger-Sandhas equation in momentum space via a Chebychev expansion of the two-baryon transition matrix. As N-N potential the CD-Bonn potential is used which is extended to include the excitation to a (static)  $\Delta$ . The latter produces an effective three-body force. The CD-Bonn +  $\Delta$  extension is as exact as CD-Bonn as it is also fitted to the experimental two-nucleon data up to 350 MeV [25]. The Pisa group solves the three-body Schrödinger equation in coordinate space by variational methods. The wave function is expanded by pair-correlated hyperspherical harmonics. The Bochum-Krakow group solves the Faddeev equation in momentum space. The Pisa and the

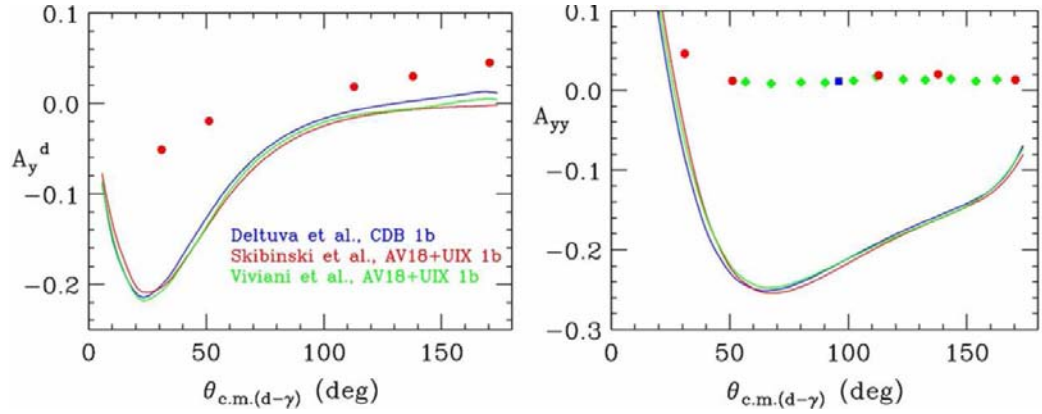


Figure 4:  $A_y^d$  (left) and  $A_{yy}$  (right) for 45 MeV incident deuteron energy as a function of the center-of-mass angle between deuteron and outgoing  $\gamma$ . Data of the present experiment ( $\bullet$ ) together with the data by Anklin *et al.* [14] ( $\circ$ ) and Jourdan *et al.* [13] ( $\square$ ) are compared to the one-body-calculations by Deltuva *et al.* (blue), Skibinski *et al.* (red) and Viviani *et al.* (green). The last two calculations also include the three-body force.

Bochum-Krakov group are using the Argonne V18 potential combined with the Urbana IX three-body force.

The data shown in the following are from the present experiment and from Anklin *et al.* [14] ( $\circ$ ) and Jourdan *et al.* [13] at incident deuteron energies of 29 and 45 MeV. The data themselves have non-visible error bars and are therefore also able to distinguish tiny effects. All three data sets are in

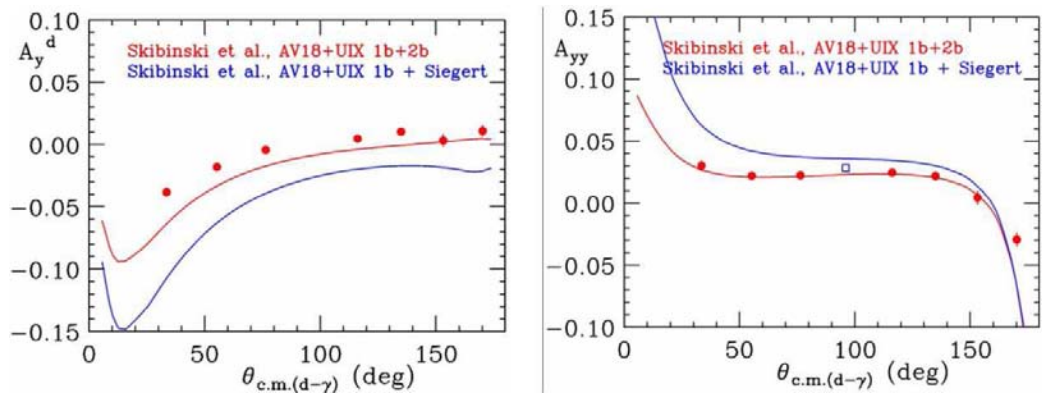


Figure 5: Similar to figure 4 but for 29 MeV. Here the data are compared to the calculations by Skibinski *et al.* with an explicit treatment of the exchange currents (red) and within the Siegert approach (blue).

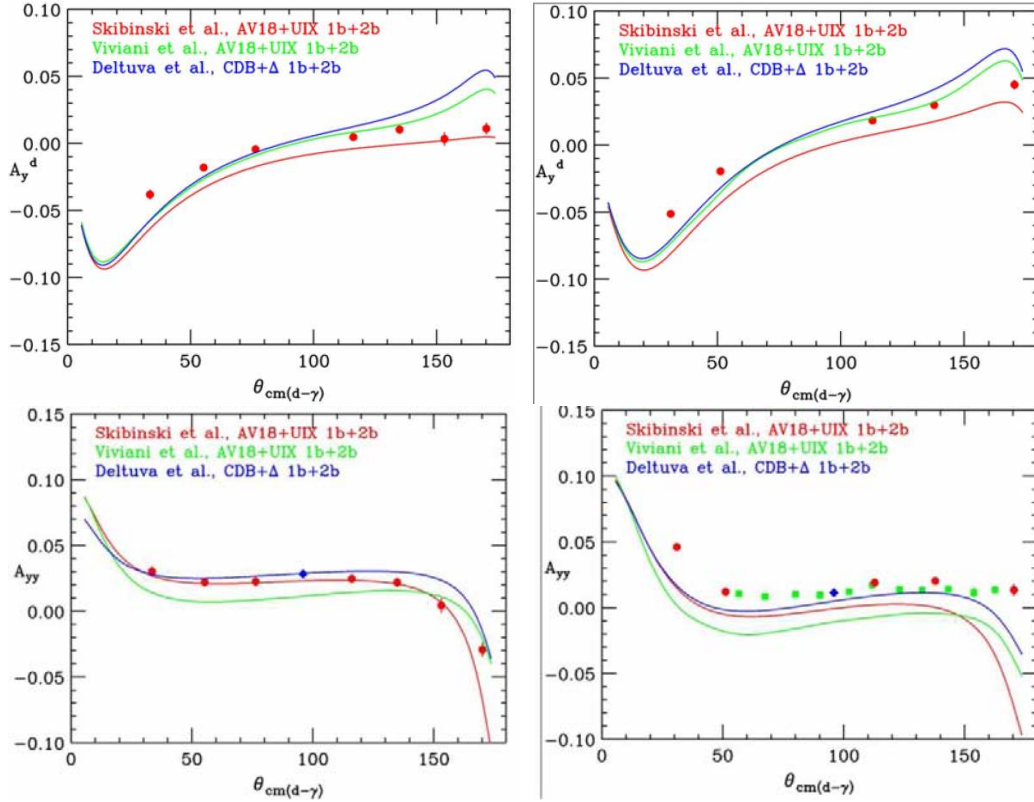


Figure 6:  $A_y^d$  (top) and  $A_{yy}$  (bottom) for 29 MeV (left) and 45 MeV (right). Data are the same as in fig. 4. They are compared to the calculations with the explicit treatment of the exchange currents and two- and three-body currents: Marcucci/Viviani *et al.* (green), Skibinski *et al.* (red) and Deltuva *et al.* (blue).

good agreement with each other. In fig. 4 the results for 45 MeV from the three theoretical groups are shown for the case of neglecting the two-body currents. The large deviation from the data demonstrates the importance of two-body currents. In contrast they contribute only 15% in the unpolarized cross section. Even though the calculations use different potentials, the CD-Bonn and the Argonne V18, the difference between the results are small. The calculations of the Bochum-Krakow and the Pisa group contain in addition the Urbana IX as three-body force. It seems already here that the effect of the three-body force is small. For an explicit comparison see below. The results at 29 MeV show the same features as at 45 MeV and therefore they are not shown here (s. ref. [20] for a more detailed comparison).

In sec. 1 the application of the Siegert theorem to the case of the cap-

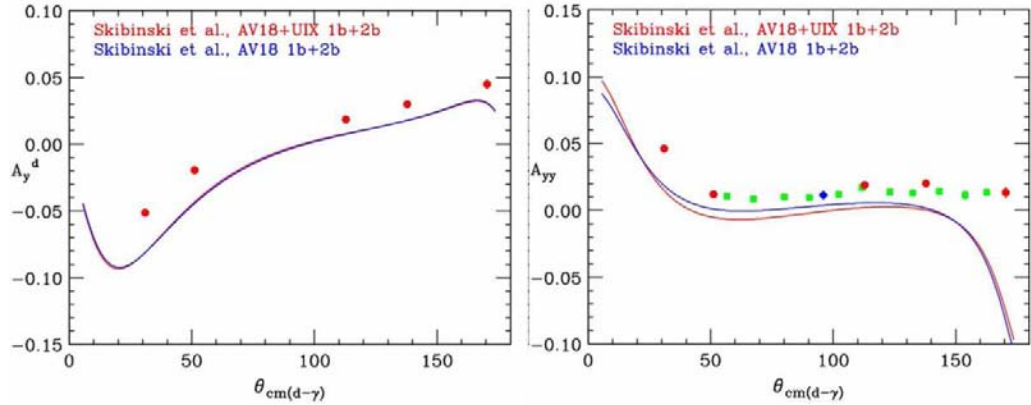


Figure 7: The data (s. fig. 4) for  $E = 45$  MeV are compared to the calculations by Skibinski *et al.* with one- and two-body currents only (blue) and with the Urbana IX as three-body force in addition (red).

ture reaction was discussed. The Bochum-Krakow group provided calculations where the two-body currents are approximated by the Siegert theorem (modified version in momentum space s. [2]), i.e. MEC's are neglected in the magnetic currents, and with an explicit treatment of MEC's using the Riska prescription [26]. While it was previously thought that the Siegert theorem would describe the data correctly at medium angles where the E1 transition is dominant, this is not the case as shown in fig. 5. On the other hand explicitly taking into account  $\pi$  and  $\rho$  currents via the Riska description improves the theoretical description of the data a lot.

In fig. 6 the calculations of the three groups including two- and three-body currents are shown. Whereas the Hannover-Lisbon and Bochum-Krakow group take the Riska prescription for the  $\pi$  and  $\rho$  exchange currents the Pisa group uses exchange currents for the  $\pi$ ,  $\rho$ ,  $\omega$  and  $\sigma$  currents consistent with the Argonne V18 potential [23]. In this case current conservation is preserved. Further the excitation to a  $\Delta$  as well as point Coulomb interaction are taken into account. For the tensor analyzing power at 29 MeV satisfactory agreement with the data is achieved. However, particularly at 45 MeV a deviation from the data at small and large angles is apparent.

The effect of the three-body force was studied by Skibinsky *et al.* for 45 MeV beam energy. As shown in fig. 7 its effect is small and the large discrepancy to the data at backward angles for  $A_{yy}$  remains unchanged.

A similar discrepancy presented a long standing puzzle in the 0 deg cross section of the *two-body* photodisintegration. Cambi, Mosconi, and Ricci [7] solved this puzzle demonstrating the importance of the relativistic spin-orbit contribution.

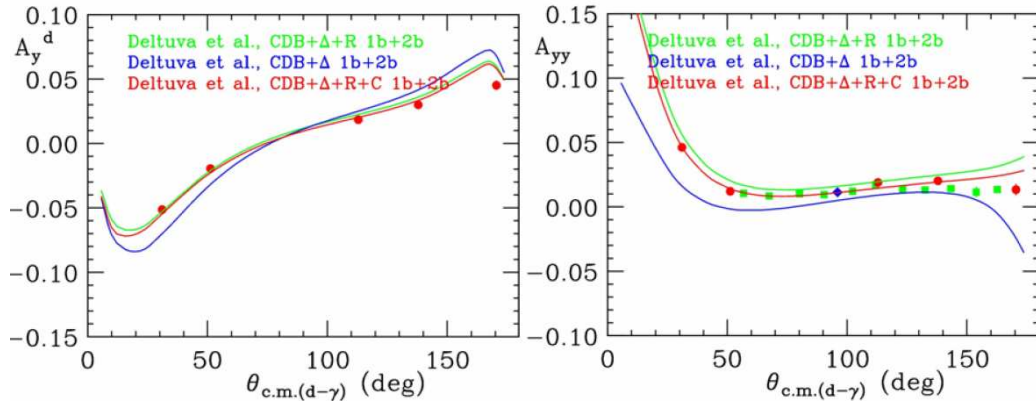


Figure 8: Comparison to the calculations by Deltuva *et al.* with two- and three-body currents (blue), plus relativistic corrections (green), and plus added Coulomb corrections (red).

Deltuva *et al.* included a relativistic correction of the order  $(k/m_N)^2$  in the current operator [24]. Here  $k$  is the nucleon momentum and  $m_N$  the nucleon mass. This calculation, shown in fig. 8, is in very good agreement with the data and also describes  $A_{yy}$  at backward angles for the first time. In addition the effect of the Coulomb interaction was studied. Inclusion of the Coulomb interaction into a calculation in momentum space is not straightforward as in configuration space. This problem was solved by using a screened Coulomb potential [16]. A benchmark calculation between the Pisa and Hannover-Lisbon group was performed for verification of the procedure [27]. The effect of the Coulomb interaction at 45 MeV is small (s. fig. 8).

## 5 Summary

Precise data for the vector and tensor analyzing powers,  $A_y^d$  and  $A_{yy}$ , have been measured at a deuteron beam energy of 29 and 45 MeV in a wide angular range for the capture reaction  ${}^1\text{H}(\text{d},\gamma){}^3\text{He}$ . These energies were chosen because at 29 MeV  $A_{yy}$  has a maximum whereas at 45 MeV it is close to the zero crossing.

The data were compared to exact calculations of three groups, the Hannover-Lisbon, the Bochum-Krakow and the Pisa group [22–24] which use different approaches and potentials. The calculations are in general in good agreement with each other, in particular when only one-body currents are included. Calculations disregarding the two-body currents are in large disagreement with the data demonstrating the sensitivity of the data to MEC. Further-

more the treatment of the MEC's using the Siegert theorem, i.e. by neglecting the MEC's in the magnetic part completely, is not sufficient to describe the data. While the sensitivity to the three-body force and the Coulomb interaction is small, relativistic corrections have to be included to get a satisfying agreement for  $A_{yy}$  at 45 MeV and backward angles.

## 6 Acknowledgements

We would like to thank A. Deltuva, P. Sauer, W. Glöckle, J. Golak, R. Skibinski, H. Witala, A. Kievsky, L.E. Marcucci, and M. Vivani, for providing us with the various calculations and A.C. Fonseca for valuable discussions during the conference. This work was supported by the Schweizerische Nationalfonds.

## References

- [1] W. Glöckle, H. Witala, D. Hüber, H. Kamada, and J. Golak. *Phys. Rep.* **274**, 107 (1996).
- [2] J. Golak *et al.*, *Phys. Rev. C* **62**, 054005 (2000).
- [3] A. Kievsky, M. Viviani, and S. Rosati, *Nucl. Phys.* **A577**, 51 (1994).
- [4] A. Kievsky, M. Viviani, and S. Rosati., *Phys. Rev. C* **64**, 024002 (2001).
- [5] A. Deltuva, K. Chmielewski, and P.U. Sauer, *Phys. Rev. C* **67**, 034001 (2003).
- [6] L.P. Yuan, K. Chmielewski, M. Oelsner, P.U. Sauer, A.C. Fonseca, and J. Adam Jr, *Few-Body Systems* **32**, 83 (2002).
- [7] A. Cambi, B. Mosconi, and P. Ricci *Phys. Rev. Lett.* **48**, 462 (1982).
- [8] A. Amroun *et al.*, *Nucl. Phys.* **A579**, 596 (1994).
- [9] A.A. Mehmandoost-Khajeh-Dad *et al.*, *Phys. Lett.* **B617**, 18 (2005).
- [10] G.J. Schmid, R.M. Chasteler, H.R. Weller, D.R. Tilley, A.C. Fonseca, and D.R. Lehman, *Phys. Rev. C* **53**, 35 (1996).
- [11] K. Sagara *et al.*, in Few Body Problems in Physics, *AIP Conf. Proc.* **334**, 467 (1995).

- [12] M.C. Vetterli, J.A. Kuehner, A.J. Trudel, C.L. Woods, R. Dymarz, A.A. Pilt, and H.R. Weller, *Phys. Rev. Lett.* **54**, 1129 (1985).
- [13] J. Jourdan *et al.*, *Nucl. Phys* **A453**, 220 (1986).
- [14] H. Anklin *et al.*, *Nucl. Phys* **A636**, 189 (1998).
- [15] W.K. Pitts *et al.*, *Phys. Rev. C* **37**, 1 (1988).
- [16] A. Deltuva, A.C. Fonseca, and P.U. Sauer, *Phys. Rev. C* **71**, 054005 (2005).
- [17] A.J.F. Siegert, *Phys. Rev.* **52**, 787 (1937).
- [18] D. Singy *et al.*, *Nucl. Instrum. Methods* **B47**, 167 (1990).
- [19] H. Anklin *et al.*, *Nucl. Instrum Methods* **A404**, 394 (1998).
- [20] T. Klechneva *et al.*, *Phys. Rev. C* **73**, 034005 (2006).
- [21] T. Klechneva, Phd thesis at the University of Basel, 2004, available on [http://pages.unibas.ch/diss/2004/DissB\\_6770.htm](http://pages.unibas.ch/diss/2004/DissB_6770.htm).
- [22] R. Skibinski, J. Golak, H. Kamada, H. Witala, W. Glockle, and A. Nogga, *Phys. Rev. C* **67**, 054001 (2003).
- [23] L.E. Marcucci, M. Viviani, R. Schiavilla, A. Kievsky, and S. Rosati, *Phys.Rev. C* **72**, 014001 (2005).
- [24] A. Deltuva, L.P. Yuan, J. Adam, A.C. Fonseca and P.U. Sauer, *Phys. Rev. C* **69**, 34004 (2004).
- [25] A. Deltuva, R. Machleidt, and P.U. Sauer, *Phys. Rev. C* **68**, 024005 (2003).
- [26] D.O. Riska, *Phys. Rep.* **181**, 207 (1989).
- [27] A. Deltuva, A.C. Fonseca, A. Kievsky, S. Rosati, P.U. Sauer, and M. Viviani, *Phys. Rev. C* **71**, 064003 (2005).

# ISOSPIN VIOLATING NUCLEON FORM FACTORS

Bastian Kubis  
 Helmholtz-Institut für Strahlen- und Kernphysik (Theorie)  
 Universität Bonn  
 D-53115 Bonn, Germany

## Abstract

A quantitative understanding of isospin violation is an increasingly important ingredient for the extraction of the nucleon's strange vector form factors. We present a theoretical analysis of the isospin violating form factors, both for single nucleons and for  $^4\text{He}$ .

## 1 Isospin Violation and Nucleon Strangeness

The investigation of strangeness contributions to static properties of the nucleon is particularly interesting as it gives unambiguous access to low-energy manifestations of virtual or sea quark effects. Different strangeness currents of the form  $\bar{s}\Gamma s$  test the strangeness component of different nucleon observables, such as mass ( $\Gamma = 1$ ), spin ( $\Gamma = \gamma_\mu \gamma_5$ ), or magnetic moment ( $\Gamma = \gamma_\mu$ ). Here we are concerned with the magnetic moment only, or, more generally, with the nucleon form factors of the vector current.

The standard model provides two different flavor combinations of the three light quark contributions to the electric ( $G_E$ ) and magnetic ( $G_M$ ) form factors due to the electromagnetic and the weak vector currents,

$$G_{E/M}^{\gamma,p} = \frac{2}{3}G_{E/M}^u - \frac{1}{3}(G_{E/M}^d + G_{E/M}^s), \quad (1)$$

$$G_{E/M}^{Z,p} = \left(1 - \frac{8}{3}\sin^2\theta_W\right)G_{E/M}^u - \left(1 - \frac{4}{3}\sin^2\theta_W\right)(G_{E/M}^d + G_{E/M}^s), \quad (2)$$

so in order to obtain a full flavor decomposition of the vector current, one has to invoke isospin (or charge) symmetry in the form

$$G_{E/M}^{u,n} = G_{E/M}^{d,p}, \quad G_{E/M}^{d,n} = G_{E/M}^{u,p}, \quad (3)$$

and use the neutron electromagnetic form factors as the third input. If one relaxes this assumption and allows for isospin violation, however, the relation

between weak vector form factors, electromagnetic form factors of proton and neutron, and strangeness is complicated by an additional term,

$$G_{E/M}^{Z,p} = (1 - 4 \sin^2 \theta_W) G_{E/M}^{\gamma,p} - G_{E/M}^{\gamma,n} - G_{E/M}^s - G_{E/M}^{u,d}, \quad (4)$$

where  $G_{E/M}^{u,d} = 2/3(G_{E/M}^{d,p} - G_{E/M}^{u,n}) - 1/3(G_{E/M}^{u,p} - G_{E/M}^{d,n})$ . In other words, the isospin violating form factors  $G_{E/M}^{u,d}$  generate “pseudo-strangeness”, and in order to reliably extract strangeness effects, the former have to be calculated from theory.

## 2 Theory of Isospin Violating Form Factors

Chiral perturbation theory (ChPT) is ideally suited for an analysis of isospin violation. It is tailor-made to analyze the dependence of low-energy observables on quark masses, in particular on the light quark mass difference  $m_u - m_d$ , and the consistent inclusion of electromagnetic effects is also well-understood. As the isospin violating form factors can be calculated in SU(2) ChPT, they are not affected by convergence problems to the extent the strangeness form factors are (see Ref. [1] for a brief review on the latter).

Particular emphasis will be put on the analysis of the leading moments of the isospin violating form factors, magnetic moment as well as electric and magnetic radius terms,

$$G_E^{u,d}(t) = \rho_E^{u,d} t + \mathcal{O}(t^2), \quad G_M^{u,d}(t) = \kappa^{u,d} + \rho_M^{u,d} t + \mathcal{O}(t^2). \quad (5)$$

The two radius terms are unaffected by low-energy constants up to leading ( $\rho_E^{u,d}$ ) and next-to-leading ( $\rho_M^{u,d}$ ) order and can be expressed entirely in terms of the neutron-to-proton mass difference  $\Delta m = m_n - m_p$  [2], with the result [3]

$$\rho_E^{u,d} = \frac{5\pi C}{6M_\pi m_N}, \quad \rho_M^{u,d} = \frac{2C}{3M_\pi^2} \left\{ 1 - \frac{7\pi}{4} \frac{M_\pi}{m_N} \right\}, \quad C = \frac{g_A^2 m_N \Delta m}{16\pi^2 F_\pi^2}. \quad (6)$$

It is remarkable that up to  $\mathcal{O}(p^4)$  for  $G_E^{u,d}$  and  $\mathcal{O}(p^5)$  for  $G_M^{u,d}$ , no photon loops contribute, nor are there two-loop effects, nor does the pion mass difference  $M_{\pi^+}^2 - M_{\pi^0}^2$  play a role.

In order to complete the chiral representation, we have to estimate the combination of low-energy constants entering  $\kappa^{u,d}$ . This is done by invoking resonance saturation: low-energy constants incorporate the effects of heavier states not included in the theory as explicit degrees of freedom. In our case, the relevant contributions are provided by vector mesons including  $\rho - \omega$  mixing:

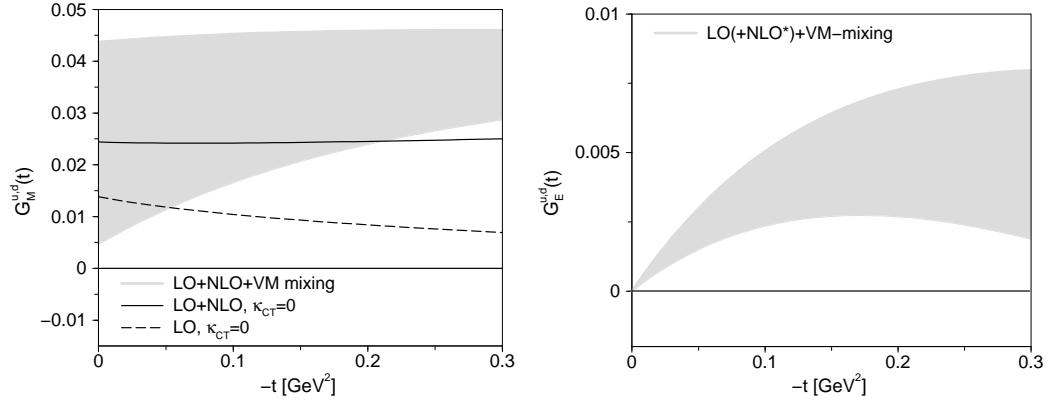


Figure 1: Isospin violating form factors. Figures taken from Ref. [3].

$$\begin{aligned}
 G_E^{u,d}(t) \Big|_{\text{mix}} &= \frac{\Theta_{\rho\omega} t}{M_V(M_V^2 - t)^2} \left[ \left(1 + \frac{\kappa_\omega M_V^2}{4m_N^2}\right) g_\omega F_\rho - \left(1 + \frac{\kappa_\rho M_V^2}{4m_N^2}\right) g_\rho F_\omega \right], \\
 G_M^{u,d}(t) \Big|_{\text{mix}} &= \frac{\Theta_{\rho\omega}}{M_V(M_V^2 - t)^2} \left[ (t + \kappa_\omega M_V^2) g_\omega F_\rho - (t + \kappa_\rho M_V^2) g_\rho F_\omega \right], \quad (7)
 \end{aligned}$$

where the necessary couplings can be extracted from experiment within certain errors; see Ref. [3] for details.

The total results for the isospin violating form factors are shown in Fig. 1. Isospin breaking remains at the percent level, the  $t$ -dependence of the form factors is rather moderate. We note that the symmetries of QCD do *not* dictate  $\kappa^{u,d}$  to vanish, indeed we find  $G_M^{u,d}(0) \neq 0$ . Table 1 compares the specific linear combinations of  $G_E^{u,d}$  and  $G_M^{u,d}$  at  $t \approx -0.1 \text{ GeV}^2$  with the experimentally extracted values for strangeness form factors.

Table 1: Comparison of selected experimental measurements of strange form factors from SAMPLE [4], A4 [5], and HAPPEX [6] to the results of Ref. [3] for the isospin violating form factors.

experiment	electric/magnetic	$G^s$	$G^{u,d}$
SAMPLE	$G_M$	$0.37 \pm 0.20 \pm 0.26 \pm 0.07$	$0.02 \dots 0.05$
A4	$G_E + 0.106 G_M$	$0.071 \pm 0.036$	$0.004 \dots 0.010$
HAPPEX	$G_E + 0.080 G_M$	$0.030 \pm 0.025 \pm 0.006 \pm 0.012$	$0.004 \dots 0.009$

### 3 Isospin Mixing in Helium-4

Parity-violating electron scattering on  ${}^4\text{He}$  gives clean access to the strange *electric* form factor  $G_E^s$ , as the  $J^\pi = 0^+$  target does not allow for magnetic or axial vector transitions. However, in addition to effects of the isospin violating electric form factor, an  $I = 1$  admixture in the  ${}^4\text{He}$  wave function yields a contribution to the measured asymmetry  $A_{PV}$  [7],

$$A_{PV} = -\frac{G_\mu t}{4\pi\alpha\sqrt{2}} \left\{ 4\sin^2\theta_W + \Gamma \right\}, \quad \Gamma = -2\frac{F^{(1)}}{F^{(0)}} - \frac{2G_E^I - G_E^s}{(G_E^p + G_E^n)/2}, \quad (8)$$

where  $F^{(0/1)}$  are the nuclear form factors corresponding to isoscalar/isovector charge operators, and  $G_E^I = (G_E^{u,p} - G_E^{d,n} - G_E^{d,p} + G_E^{u,n})/4$  is a different isospin breaking linear combination of single-nucleon form factors. The measured asymmetry  $A_{PV} = [+6.40 \pm 0.23_{\text{stat}} \pm 0.12_{\text{syst}}] \times 10^{-6}$  at  $t = -0.077 \text{ GeV}^2$  [8] leads to  $\Gamma = 0.010 \pm 0.038$ . Single-nucleon isospin violation contributes  $0.008 \pm 0.003$  to  $\Gamma$ , while isospin mixing in the  ${}^4\text{He}$  wave function amounts to  $\approx 0.003$ , leaving a mere strangeness contribution of  $G_E^s = -0.001 \pm 0.016$ .

### 4 Conclusions

The contributions of isospin violation are as yet smaller than some of the experimental uncertainties in extracting strange form factors, see Table 1, but in the case of the  ${}^4\text{He}$  experiment, they are sufficient to explain the central value of the measured asymmetry (again within larger error bounds). Clearly, isospin breaking effects will become an essential ingredient for future precision extractions of strangeness matrix elements.

### Acknowledgments

I would like to thank my coworkers Randy Lewis, Michele Viviani, and Rocco Schiavilla for the fruitful collaboration that led to the results presented here. This work is supported in part by the EU I3HP Project (RII3-CT-2004-506078), by the EU Contract No. MRTN-CT-2006-035482 (“FLAVIANet”), and by the DFG (SFB/TR 16).

### References

- [1] B. Kubis, *Eur. Phys. J.* **A24S2**, 97 (2005).
- [2] R. Lewis and N. Mobed, *Phys. Rev.* **D59**, 073002 (1999).

- [3] B. Kubis and R. Lewis, *Phys. Rev.* **C74**, 015204 (2006).
- [4] D. T. Spayde *et al.* [SAMPLE Collab.], *Phys. Lett.* **B583**, 79 (2004).
- [5] F. E. Maas *et al.* [A4 Collab.], *Phys. Rev. Lett.* **94**, 152001 (2005).
- [6] K. A. Aniol *et al.* [HAPPEX Collab.], *Phys. Lett.* **B635**, 275 (2006).
- [7] M. Viviani *et al.*, *Phys. Rev. Lett.* **99**, 112002 (2007).
- [8] A. Acha *et al.* [HAPPEX Collab.], *Phys. Rev. Lett.* **98**, 032301 (2007).

# PION SCALAR FORM FACTORS FROM $J/\psi$ DECAYS

*Timo A. Lähde*

Department of Physics, University of Washington,  
Seattle, WA 98195-1560, USA

## Abstract

The description of the decays  $J/\psi \rightarrow \phi\pi^+\pi^-$ ,  $J/\psi \rightarrow \omega\pi^+\pi^-$ ,  $J/\psi \rightarrow \phi K^+K^-$  and  $J/\psi \rightarrow \omega K^+K^-$  in terms of the scalar form factors of the light pseudoscalar mesons is reviewed. Key features in these decays include the  $S$ -wave resonances  $\sigma$  and  $f_0(980)$ , which appear prominently in the new data from the BES collaboration. These resonances are dynamically generated by resummation of the  $s$ -channel unitarity loops, after which the formalism is matched to the NLO expressions for the scalar form factors in Chiral Perturbation Theory (ChPT). This allows for an estimation of several low-energy constants (LECs) of ChPT, in particular the OZI-suppressed  $L_4^r$  and  $L_6^r$ .

## 1 Introduction

The decays of the  $J/\psi$  into a vector meson, such as  $\phi$  or  $\omega$ , via emission of a pair of light pseudoscalar mesons may yield insight into the dynamics of the pseudo-Goldstone bosons of QCD [1–3], and in particular into the final state interaction (FSI) between  $\pi\pi$  and  $K\bar{K}$  pairs, which is an essential component in a realistic description of the scalar form factors (FFs) of pions and kaons. Recently, the BES collaboration has published data with high statistics on  $J/\psi \rightarrow \phi\pi^+\pi^-$  and  $J/\psi \rightarrow \phi K^+K^-$ , as well as for  $J/\psi \rightarrow \omega\pi^+\pi^-$  and  $J/\psi \rightarrow \omega K^+K^-$  [4]. Additionally, a comprehensive partial-wave analysis (PWA) has been performed, which is particularly useful since a determination of the  $S$ -wave components of the  $\pi\pi$  and  $K\bar{K}$  invariant mass distributions is thus available.

A much more precise analysis in the spirit of Ref. [5] is thus possible, the key ingredient being a realistic treatment of the final state interaction (FSI) in the emitted pseudoscalar meson pair. It has been demonstrated in Ref. [6] that the FSI in the  $\pi\pi - K\bar{K}$  system can be well described by a coupled-channel Bethe-Salpeter approach using the lowest order ChPT amplitudes for

meson-meson scattering [7, 8]. In such an approach, the lightest resonances in the  $0^{++}$  sector are of dynamical origin, i.e. they arise due to the strong rescattering effects in the  $\pi\pi$  or  $K\bar{K}$  system. Such dynamically generated states include the  $\sigma$  and  $f_0(980)$  mesons, which are prominent in the BES data on the  $J/\psi$  decays in question [4].

The analysis of Ref. [9] uses the formalism introduced in Refs. [5, 6], which allows for a description of the scalar FFs which takes into account the final-state interaction (FSI) between pions and kaons up to  $\sqrt{s} \sim 1.2$  GeV. At higher energies, a number of pre-existing scalar resonances such as the  $f_0(1500)$  have to be accounted for, as well as the effects of multi-particle intermediate states, most importantly the  $4\pi$  state. The scalar FFs may then be constrained by matching to the next-to-leading-order (NLO) chiral expressions. This allows for a fit of the large  $N_c$  suppressed Low-Energy Constants (LECs)  $L_4^r$  and  $L_6^r$  of ChPT to the dimeson spectra of the  $J/\psi \rightarrow \phi\pi\pi$  and  $J/\psi \rightarrow \phi K\bar{K}$  decays, using the Lagrangian model of Ref. [5].

## 2 Description of $J/\psi \rightarrow VPP$ decays

From the considerations of Ref. [5], the matrix elements for  $\phi\pi^+\pi^-$  and  $\phi K^+K^-$  decay of the  $J/\psi$  are given, in terms of the strange and non-strange scalar operators  $\bar{s}s$  and  $\bar{n}n = (\bar{u}u + \bar{d}d)/\sqrt{2}$ , by

$$\mathcal{M}_\phi^{\pi\pi} = \sqrt{\frac{2}{3}} C_\phi \langle 0 | (\bar{s}s + \lambda_\phi \bar{n}n) | \pi\pi \rangle_{I=0}^* \quad (1)$$

$$\mathcal{M}_\phi^{KK} = \sqrt{\frac{1}{2}} C_\phi \langle 0 | (\bar{s}s + \lambda_\phi \bar{n}n) | K\bar{K} \rangle_{I=0}^* \quad (2)$$

in terms of the  $\pi\pi$  and  $K\bar{K}$  states with  $I = 0$ , which are related to the physical  $\pi^+\pi^-$  and  $K^+K^-$  states by the Clebsch-Gordan (CG) coefficients of the above expressions. In addition, the full transition amplitudes also contain the polarization vectors of the  $J/\psi$  and  $\phi$  mesons. The matrix elements for  $\omega\pi^+\pi^-$  and  $\omega K^+K^-$  may be obtained by replacement of the labels in Eqs. (1) and (2) according to  $\phi \rightarrow \omega$ . The matrix elements of the scalar operators are referred to as the strange and non-strange  $I = 0$  scalar FFs. The parameter  $\lambda_\phi$  measures the relative strengths of the singly ( $\bar{s}s$ ) and doubly ( $\bar{n}n$ ) OZI-violating contributions to the  $\phi\pi^+\pi^-$  decay.

In Ref. [5], ideal mixing in the  $\phi - \omega$  system was used to relate the parameters for  $\omega$  emission to those of the  $\phi$ , which enables a simultaneous description of the  $\phi\pi^+\pi^-$  and  $\omega\pi^+\pi^-$  final states. The explicit relations are

given by

$$C_\omega = \lambda_\phi C_\phi, \quad \lambda_\omega = \frac{\lambda_\phi + \sqrt{2}}{\sqrt{2}\lambda_\phi}, \quad (3)$$

such that the quantities to be determined from fits to the experimental spectra of Refs. [4] are  $C_\phi$  and  $\lambda_\phi$ . It is worth noting that in the limit  $\lambda_\phi = 0$ , the dimeson spectra for  $\phi$  and  $\omega$  emission are driven entirely by the strange scalar source  $\bar{s}s$  and the non-strange scalar source  $\bar{n}n$ , respectively.

### 3 Matching of FSI to NLO ChPT

The constraints imposed by unitarity on the pion and kaon scalar FFs, the inclusion of the FSI via resummation in terms of the Bethe-Salpeter (BS) equation, the channel coupling between the  $\pi\pi$  and  $K\bar{K}$  systems, and the matching of the scalar FFs to the NLO ChPT expressions have all been elaborated in great detail in Refs. [5, 6]. Within that framework, the scalar FFs are obtained from the algebraic coupled-channel equation

$$\begin{aligned} \Gamma(s) &= [I + K(s)g(s)]^{-1}R(s) \\ &= [I - K(s)g(s)]R(s) + \mathcal{O}(p^6), \end{aligned} \quad (4)$$

where the expansion in the second line can be used for matching the FSI to the NLO ChPT expressions for the scalar form factors. In Eq. (4), the loop function  $g(s)$  is divergent and requires a cut-off  $q_{\max} \sim 1$  GeV, which can be fixed using the mass of the  $f_0(980)$  resonance. The matching to ChPT implies that  $R(s)$  is given by the NLO chiral expression for the scalar form factor with the unitarity loop contributions removed. Finally  $K(s)$  denotes the (on-shell) LO chiral amplitude for  $\pi\pi$  and  $K\bar{K}$  scattering,

$$K_{11} = \frac{2s - m_\pi^2}{2f^2}, \quad K_{12} = K_{21} = \frac{\sqrt{3}s}{4f^2}, \quad K_{22} = \frac{3s}{4f^2}, \quad (5)$$

where the constant  $f$  is taken to equal the physical pion decay constant  $f_\pi$ , with the convention  $f_\pi = 0.0924$  GeV. Consideration of Eq. (4) yields the defining relations for  $R_i^n(s)$

$$\Gamma_i^n(s) = R_i^n(s) - \sum_{j=1}^2 K_{ij}(s)g_j(s)R_j^n(s) + \mathcal{O}(p^6), \quad (6)$$

with  $i = \pi, K$ , illustrated in Fig. 3, such that only contributions up to  $\mathcal{O}(p^4)$  are retained in the product  $KgR$ . The analogous expressions for the vectors  $R_i^s(s)$  associated with the strange scalar FFs  $\Gamma_i^s(s)$  can be obtained from the above relations by the substitutions  $\Gamma_i^n \rightarrow \Gamma_i^s$  and  $R_i^n \rightarrow R_i^s$ .

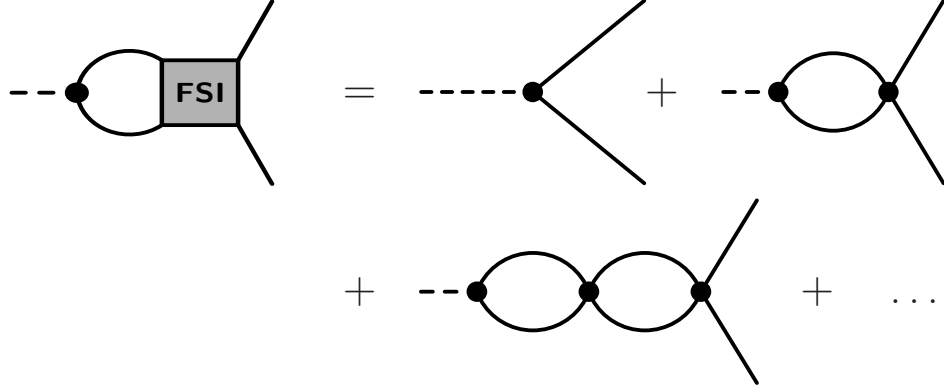


Figure 1: Resummation of unitarity loops in the  $s$ -channel for the pion and kaon scalar form factors. The leading term is given by the NLO ChPT expressions for  $\Gamma_i^n$  and  $\Gamma_i^s$ .

## 4 Fit Results

The results obtained in Ref. [5] involve a fit of the model parameters  $C_\phi$  and  $\lambda_\phi$  as well as the LECs  $L_4^r$ ,  $L_5^r$ ,  $L_6^r$  and  $L_8^r$  to the BES data on  $J/\psi$  decays to  $\phi\pi^+\pi^-$ ,  $\phi K^+K^-$  and  $\omega\pi^+\pi^-$ . The main results are shown in Fig. 2, and the resulting pion scalar FFs are given in Fig. 3. The optimal value of  $\lambda_\phi$ , which measures the OZI violation in the  $J/\psi \rightarrow \phi\pi^+\pi^-$  decay, is  $\lambda_\phi = 0.13 \pm 0.02$ , which indicates a significant contribution to  $\phi\pi^+\pi^-$  from the non-strange scalar FF, and a contribution to  $\omega\pi^+\pi^-$  from the strange one. In particular, a realistic description of the  $\omega\pi^+\pi^-$  spectrum close to the  $K\bar{K}$  threshold requires an interplay between the non-strange and strange scalar FFs.

### 4.1 Determination of $L_4^r$ and $L_6^r$

One of the main objectives of Refs. [5, 9] is the determination of the LECs  $L_4^r$  and  $L_6^r$  of ChPT. As discussed in Refs. [8, 10], where a set of standard estimates for the LECs of ChPT are given,  $L_4^r$  and  $L_6^r$  are expected, in terms of large  $N_c$  arguments, to vanish at some unknown scale in the resonance region of QCD, conventionally taken to be  $m_\rho$  or  $m_\eta$ . The values obtained from ‘‘Fit I’’ are  $(0.84 \pm 0.06) \times 10^{-3}$  for  $L_4^r$  and  $(0.03 \pm 0.16) \times 10^{-3}$  for  $L_6^r$ . These should be compared with the NNLO ChPT analyses of Refs. [11–13], where the  $L_i^r$  were extracted by fits to the available experimental data on  $K_{l4}$  decays. In that study, constraints on  $L_4^r$  and  $L_6^r$  were derived by requiring a

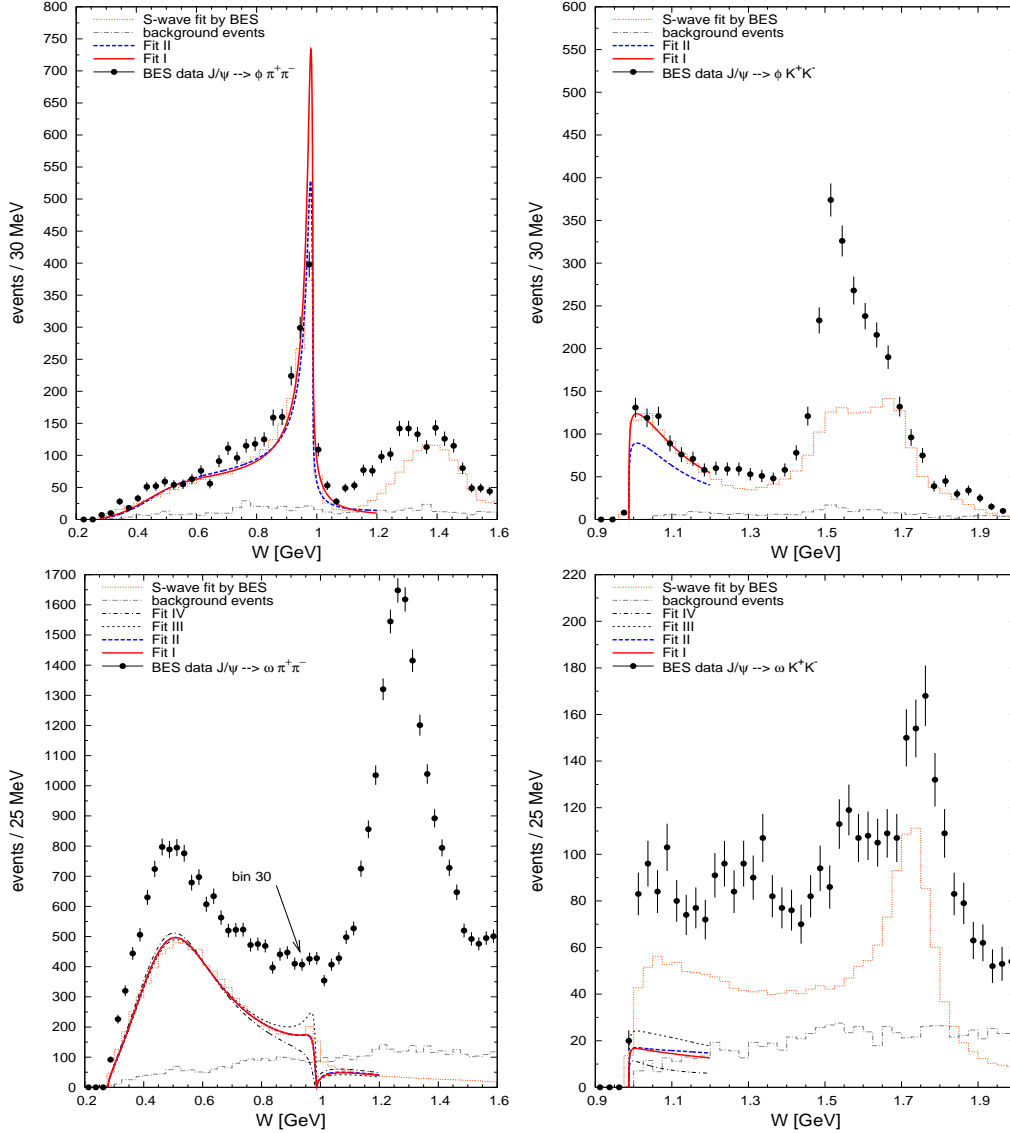


Figure 2: Fit results from Ref. [9] and BES data [4] for  $J/\psi \rightarrow \phi \pi^+ \pi^-$ ,  $J/\psi \rightarrow \phi K^+ K^-$  and  $J/\psi \rightarrow \omega \pi^+ \pi^-$ . The case of  $J/\psi \rightarrow \omega K^+ K^-$  is left as a prediction. The direct  $S$ -wave contribution from the BES PWA and the estimated background are denoted by the dashed and dotted histograms, respectively. Note in particular the strong  $\sigma$  contribution and the conspicuous lack of  $f_0(980)$  in  $\omega \pi^+ \pi^-$ . The main result is given by the solid curves labeled “Fit I”, the remaining fits II-IV are explained in Ref. [9].

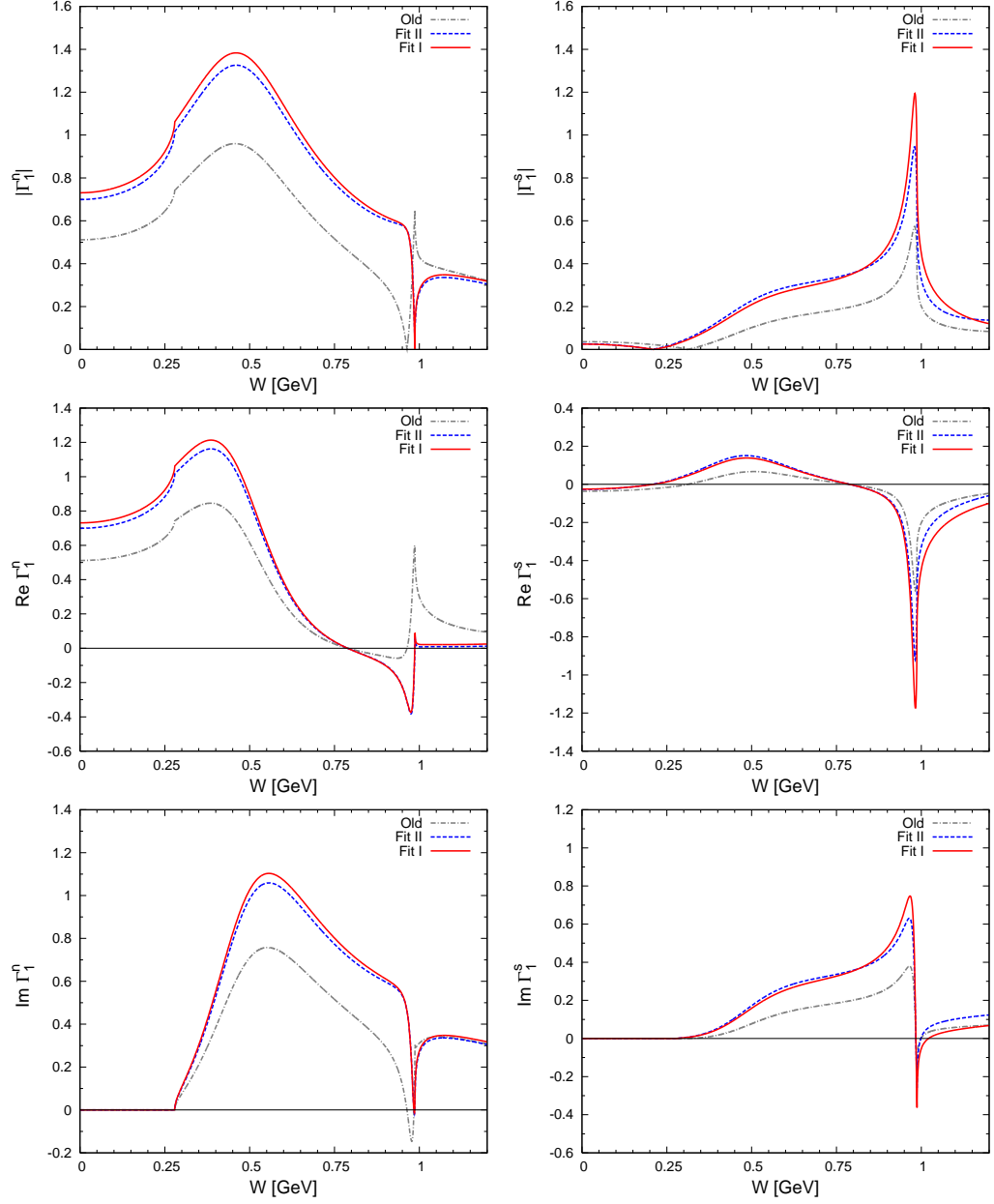


Figure 3: The non-strange and strange scalar FFs  $\Gamma_1^n$  and  $\Gamma_1^s$  of the pion. Moduli, real and imaginary parts are shown for the analysis of Ref. [9]. It should be emphasized that the FSI is identical for both FFs. The curves labeled “Old” show, for comparison, the scalar FFs obtained by Ref. [5]. The corresponding kaon FFs  $\Gamma_2^n$  and  $\Gamma_2^s$  can be found in Ref. [9].

properly convergent behavior of the chiral expansion up to NNLO for several quantities, such as the pseudoscalar meson masses and decay constants.

It was found that such a constraint can only be satisfied, within a NNLO ChPT analysis, in a rather small region centered around  $L_4^r = 0.2 \times 10^{-3}$  and  $L_6^r = 0.5 \times 10^{-3}$ . Also of interest in this context is the analysis based on QCD sum rules in Ref. [14], where  $L_6^r$  was constrained to be positive and in the region  $0.2 \times 10^{-3} \leq L_6^r \leq 0.6 \times 10^{-3}$ . Also, a significantly positive value of  $L_4^r = 0.4 \times 10^{-3}$  was obtained in Ref. [14], although with unknown error. Some updated results for the  $L_i^r$  are given in Ref. [15], and a recent analysis of  $\pi\pi$  and  $\pi K$  scattering is presented in Ref. [16], where the preferred values of  $L_4^r$  and  $L_6^r$  were found to be compatible with zero.

Further recent determinations of the  $L_i^r$  include the analyzes of Refs. [17, 18] and [19] in terms of the Inverse Amplitude Method (IAM) of Ref. [20]. In Ref. [19], a simultaneous fit to the  $\pi\pi$  and  $K\bar{K}$  partial wave amplitudes for  $I = 0, 1, 2$  was performed using the complete NLO ChPT amplitudes, which yielded a value of  $L_4^r$  equal to  $(0.2 \pm 0.1) \times 10^{-3}$ . The analysis of Ref. [18] considered all two-meson scattering amplitudes including the  $\eta\eta$  channel within the chiral IAM framework, which enabled the simultaneous extraction of the LECs  $L_1^r$  through  $L_8^r$ , the reported values of  $L_4^r$  and  $L_6^r$  being  $(-0.36 \pm 0.17) \times 10^{-3}$  and  $(0.07 \pm 0.08) \times 10^{-3}$ , respectively.

Finally, Lattice QCD also offers the possibility of studying the LECs of ChPT via Partially Quenched (PQ) Lattice QCD and PQChPT. For a theoretical background, see Refs. [21–24], and some recent Lattice QCD results for the  $L_i^r$  can be found in Refs. [25–27].

## 4.2 Results for $L_5^r$ and $L_8^r$

The values of  $L_5^r$  and  $L_8^r$  are much less controversial, as most studies are in reasonable agreement concerning their numerical values. In the previous work of Ref. [5] their values were kept fixed and were taken to coincide with those determined by the  $K_{l4}$  analysis of Ref. [13]. These values were quoted as  $L_5^r = (0.65 \pm 0.12) \times 10^{-3}$  and  $L_8^r = (0.48 \pm 0.18) \times 10^{-3}$ , respectively. However, it turned out in Ref. [9] to be advantageous to let these parameters adjust themselves to their optimal values. The values so obtained are  $L_5^r = (0.45 \pm 0.09) \times 10^{-3}$  and  $L_8^r = (0.33 \pm 0.17) \times 10^{-3}$ . Although they come out slightly smaller than the values of Ref. [13], it is encouraging to note that an optimal fit to data does not require extreme values of  $L_5^r$  and  $L_8^r$ .

The more recent fit in Ref. [15] has reported an updated set of LECs which compare slightly more unfavorably with the present values, namely  $L_5^r = (0.91 \pm 0.15) \times 10^{-3}$  and  $L_8^r = (0.62 \pm 0.20) \times 10^{-3}$ . However, it should be kept in mind that Ref. [15] was not able to determine  $L_4^r$  and  $L_6^r$  at the

same time. Moreover, the values for  $L_5^r$  and  $L_8^r$  obtained in Refs. [13, 15] are in much better agreement with the present results, than the NLO standard values  $L_5^r = (1.4 \pm 0.5) \times 10^{-3}$  and  $L_8^r = (0.9 \pm 0.3) \times 10^{-3}$  given in Ref. [10].

## 5 Conclusions

A good description of the  $\sigma$  and  $f_0(980)$  resonances in the  $J/\psi$  decays studied by BES was achieved in terms of the scalar form factors of the light pseudoscalar mesons. The results are consistent with significant OZI-violation in the scalar sector of QCD, with a clear signal for a  $\sigma$  contribution to the  $\phi\pi^+\pi^-$  final state, and hints at a possibly large value of the OZI-suppressed LEC  $L_4^r$  of ChPT. Further studies using the IAM method may yield improved insight into the latter issue.

## Acknowledgments

This research was supported by the U.S. Department of Energy under grant DE-FG-02-97ER41014, and is part of the EU Integrated Infrastructure Initiative Hadron Physics Project under contract number RII3 - CT - 2004 - 506078 and DFG (SBF/TR 16, ‘‘Subnuclear Structure of Matter’’). TL is grateful to Ulf-G. Meißner for a fruitful collaboration, and to B. Kubis and J.R. Peláez for stimulating discussions, and acknowledges a travel stipend from the Mikael Björnberg memorial foundation.

## References

- [1] K. L. Au, D. Morgan and M. R. Pennington, Phys. Rev. D **35**, 1633 (1987); D. Morgan and M. R. Pennington, Phys. Rev. D **48**, 1185 (1993); Phys. Rev. D **48**, 5422 (1993).
- [2] J. D. Weinstein and N. Isgur, Phys. Rev. Lett. **48**, 659 (1982); Phys. Rev. D **27**, 588 (1983); Phys. Rev. D **41**, 2236 (1990).
- [3] G. Janssen, B. C. Pearce, K. Holinde and J. Speth, Phys. Rev. D **52**, 2690 (1995) [arXiv:nucl-th/9411021].
- [4] M. Ablikim *et al.* [BES Collaboration], Phys. Lett. B **607**, 243 (2005) [arXiv:hep-ex/0411001]; Phys. Lett. B **598**, 149 (2004) [arXiv:hep-ex/0406038]; Phys. Lett. B **603**, 138 (2004) [arXiv:hep-ex/0409007].

- 
- [5] Ulf-G. Meißner and J. A. Oller, Nucl. Phys. A **679**, 671 (2001) [arXiv:hep-ph/0005253].
- [6] J. A. Oller and E. Oset, Nucl. Phys. A **620**, 438 (1997) [Erratum-ibid. A **652**, 407 (1999)] [arXiv:hep-ph/9702314].
- [7] S. Weinberg, Physica (Amsterdam) A **96**, 327 (1979).
- [8] J. Gasser and H. Leutwyler, Annals Phys. **158**, 142 (1984); Nucl. Phys. B **250**, 465 (1985); Nucl. Phys. B **250**, 517 (1985); Nucl. Phys. B **250**, 539 (1985).
- [9] T.A. Lähde and Ulf-G. Meißner, Phys. Rev. D **74**, 034021 (2006) [arXiv:hep-ph/0606133].
- [10] J. Bijnens, G. Ecker and J. Gasser, in: *The Second DAΦNE Physics Handbook*, edited by L. Maiani, G. Pancheri and N. Paver (INFN-LNF publications, Frascati (Italy), 1995), Vol. 1, pp. 125-144 [arXiv:hep-ph/9411232].
- [11] J. Bijnens, G. Colangelo and P. Talavera, JHEP **9805**, 014 (1998) [arXiv:hep-ph/9805389].
- [12] J. Bijnens and P. Dhonte, JHEP **0310**, 061 (2003) [arXiv:hep-ph/0307044].
- [13] G. Amorós, J. Bijnens and P. Talavera, Nucl. Phys. B **585**, 293 (2000) [Erratum-ibid. B **598**, 665 (2001)] [arXiv:hep-ph/0003258]; Phys. Lett. B **480**, 71 (2000) [arXiv:hep-ph/9912398].
- [14] B. Moussallam, Eur. Phys. J. C **14**, 111 (2000) [arXiv:hep-ph/9909292]; JHEP **0008**, 005 (2000) [arXiv:hep-ph/0005245].
- [15] G. Amorós, J. Bijnens and P. Talavera, Nucl. Phys. B **602**, 87 (2001) [arXiv:hep-ph/0101127].
- [16] J. Bijnens, P. Dhonte and P. Talavera, JHEP **0405**, 036 (2004) [arXiv:hep-ph/0404150]; JHEP **0401**, 050 (2004) [arXiv:hep-ph/0401039].
- [17] J. A. Oller, E. Oset and J. R. Peláez, Phys. Rev. D **59**, 074001 (1999) [Erratum-ibid. D **60**, 099906 (1999)] [arXiv:hep-ph/9804209].
- [18] A. Gómez Nicola and J. R. Peláez, Phys. Rev. D **65**, 054009 (2002) [arXiv:hep-ph/0109056].

- [19] F. Guerrero and J. A. Oller, Nucl. Phys. B **537**, 459 (1999) [Erratum-  
ibid. B **602**, 641 (2001)] [arXiv:hep-ph/9805334].
- [20] T. N. Truong, Phys. Rev. Lett. **61**, 2526 (1988); Phys. Rev. Lett. **67**,  
2260 (1991); A. Dobado, M. J. Herrero and T. N. Truong, Phys. Lett. B  
**235**, 134 (1990); J. A. Oller, E. Oset and J. R. Peláez, Phys. Rev. Lett.  
**80**, 3452 (1998) [arXiv:hep-ph/9803242].
- [21] A. Morel, J. Phys. (France) **48**, 1111 (1987);  
C. W. Bernard and M. F. L. Golterman, Phys. Rev. D **46**, 853 (1992)  
[arXiv:hep-lat/9204007]; S. R. Sharpe, Phys. Rev. D **46**, 3146 (1992)  
[arXiv:hep-lat/9205020].
- [22] C. W. Bernard and M. F. L. Golterman, Phys. Rev. D **49**, 486 (1994)  
[arXiv:hep-lat/9306005]; S. R. Sharpe and N. Shores, Phys. Rev. D **62**,  
094503 (2000) [arXiv:hep-lat/0006017]; Phys. Rev. D **64**, 114510 (2001)  
[arXiv:hep-lat/0108003].
- [23] J. Bijnens, N. Danielsson and T. A. Lähde, Phys. Rev. D **70**,  
111503 (2004) [arXiv:hep-lat/0406017]; Phys. Rev. D **73**, 074509 (2006)  
[arXiv:hep-lat/0602003].
- [24] S. Dürr, Eur. Phys. J. C **29**, 383 (2003) [arXiv:hep-lat/0208051];  
D. R. Nelson, G. T. Fleming and G. W. Kilcup, Phys. Rev. Lett. **90**,  
021601 (2003) [arXiv:hep-lat/0112029].
- [25] J. Heitger, R. Sommer and H. Wittig [ALPHA Collaboration], Nucl.  
Phys. B **588**, 377 (2000) [arXiv:hep-lat/0006026].
- [26] F. Farchioni, I. Montvay and E. Scholz [qq+q Collaboration], Eur. Phys.  
J. C **37**, 197 (2004) [arXiv:hep-lat/0403014].
- [27] C. Aubin *et al.* [MILC Collaboration], Phys. Rev. D **70**, 114501 (2004)  
[arXiv:hep-lat/0407028].

MENU 2007  
11th International Conference  
on Meson-Nucleon Physics and  
the Structure of the Nucleon  
September 10-14, 2007  
IKP, Forschungszentrum Jülich, Germany

# HERMES RESULTS ON HARD-EXCLUSIVE PROCESSES AND PROSPECTS USING THE NEW RECOIL DETECTOR

*Inti Lehmann, for the HERMES Collaboration*  
Department of Physics & Astronomy  
University of Glasgow  
Glasgow, G12 8QQ  
Scotland, UK

## Abstract

Hard exclusive processes provide access to the still unknown Generalized Parton Distributions (GPDs) which extend our description of the nucleon structure beyond the description by standard parton distributions. The HERMES experiment at DESY Hamburg studies hard exclusive processes using polarized electron or positron beams from HERA and an internal gas target.

Latest results are presented on Deeply Virtual Compton Scattering (DVCS) based on data taken with polarized hydrogen and deuterium targets, analyzing events in the forward magnetic spectrometer. In particular the asymmetry measured on a transversely polarized proton target is sensitive to the GPD  $E$ ; and it becomes possible to constrain the angular momentum fraction carried by  $u$  and  $d$  quarks.

Measuring the recoiling proton in addition to the forward scattered particles in those reactions reduces background and systematic uncertainties to a large extent. The newly built Recoil Detector was designed for this purpose. It was installed and commissioned at the beginning of 2006. First detector performance plots and an outlook of the physics topics addressed are given.

## 1 Physics Case

It has been known for decades that the nucleon can be described in all its quantum numbers by a combination of three quarks. However, it was then found that, in contrast to the naïve picture, the fraction of the spin  $1/2$  of the proton carried by the quarks is far below one. This caused considerable

excitement when first observed. By now this fraction is well established to be about  $1/3$  [1]. The remainder must be somehow shared between a contribution from the orbital angular momentum of the quarks and the total angular momentum of the gluons.

The structure of the nucleon as a system of quarks and gluons is traditionally described in terms of form factors and Parton Distribution Functions (PDFs). Elastic form factors describe the distribution of partons in impact parameter space while the PDFs describe their longitudinal momentum fraction. The theoretical framework of Generalized Parton Distributions (GPDs) [2–5] extends this to a more complete description of the nucleon. There are four main chirality conserving quark GPDs:  $H_q(x, \xi, t)$ ,  $E_q(x, \xi, t)$ ,  $\tilde{H}_q(x, \xi, t)$ ,  $\tilde{E}_q(x, \xi, t)$ , where  $x, \xi$ , and  $t$  are the momentum fraction carried by the struck parton, the skewness, and the Mandelstam variable  $t$ , i.e. the squared momentum transfer to the target proton, respectively (refer to Fig. 1). In fact, the PDFs  $q$  and  $\Delta q$  are kinematic limits as  $t \rightarrow 0$  of the GPDs  $H$  and  $\tilde{H}$  respectively. Elastic form factors of the nucleon can be obtained by calculating the first  $x$  moments of the four main GPDs.

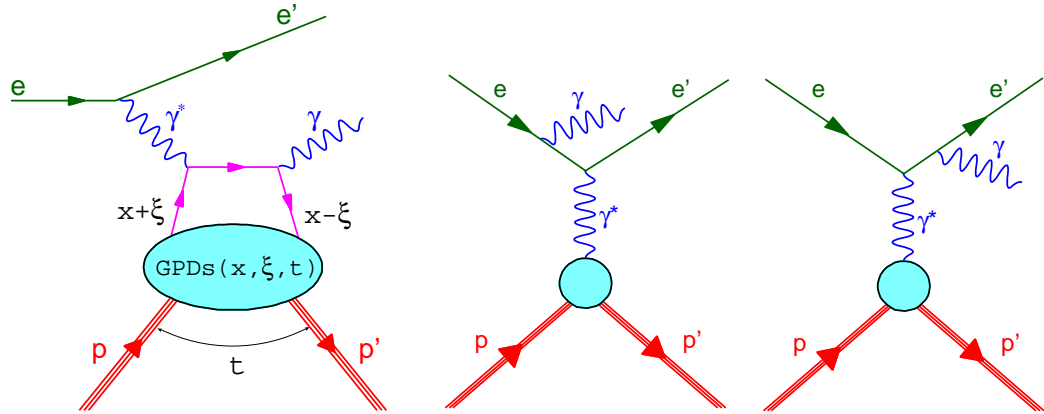


Figure 1: Left: Deeply Virtual Compton Scattering (DVCS). The incoming lepton emits a virtual photon, which scatters off a parton with momentum fraction  $x + \xi$ . This parton emits a real photon and returns to the nucleon with momentum fraction  $x - \xi$ . The momentum transfer between the initial and final nucleon state is  $\sqrt{t}$ . Right: the Bethe Heitler process (BH) is the dominant and indistinguishable experimental background which is, however, exactly calculable.

It has been noted that the total angular momentum of the quarks with flavor  $q$  is related to the GPDs  $H_q$  and  $E_q$  in the limit as  $t \rightarrow 0$  (known as

the Ji Sum Rule [4]):

$$J_q = \lim_{t \rightarrow 0} \frac{1}{2} \int_{-1}^{+1} x dx [H_q(x, \xi, t) + E_q(x, \xi, t)]. \quad (1)$$

Hence measurements constraining these GPDs provide access to the angular momentum of the quarks.

Generalized Parton Distributions can be studied measuring Deeply Virtual Compton Scattering processes. DVCS processes involve a ‘hard part’ which can be described perturbatively and a ‘soft part’ which is described by GPDs. The hard part describes the scattering of the virtual photon off a parton with subsequent emission a hard real photon. In the soft part, GPDs describe the correlation between kinematic variables of the parton before interacting with the virtual photon and after emission of the real photon. (See Fig. 1.) This description is valid in the kinematical domain of large momentum transfer by the virtual photon  $Q^2$  and small  $t$ .

The Bethe-Heitler (BH) process, i.e. the initial or final state radiation of a hard photon, leads to the same final state and cannot be distinguished by measurement at all. The total cross section measured experimentally is then given by

$$d\sigma(eN \rightarrow eN\gamma) \propto |T_{\text{DVCS}}|^2 + |T_{\text{BH}}|^2 + \underbrace{T_{\text{DVCS}} T_{\text{BH}}^* + T_{\text{DVCS}}^* T_{\text{BH}}}_{\text{InterferenceTerm}}. \quad (2)$$

Although the BH amplitude  $T_{\text{BH}}$  is the dominant contribution in the kinematic conditions of the measurements, it is precisely calculable from measured elastic form factors of the nucleon. Thus one can extract the DVCS amplitude  $T_{\text{DVCS}}$  from a measurement of cross sections using the Interference Term of Eq. 2.

Experimentally these amplitudes can be accessed through the measurement of asymmetries. The four most important ones are: the Beam Spin Asymmetry (BSA)

$$A_{LU} = \frac{d\sigma(e^{\rightarrow}, \phi) - d\sigma(e^{\leftarrow}, \phi)}{d\sigma(e^{\rightarrow}, \phi) + d\sigma(e^{\leftarrow}, \phi)} \propto \text{Im } m(\mathcal{H}) \sin(\phi), \quad (3)$$

the Beam Charge Asymmetry (BCA):

$$A_C = \frac{d\sigma(e^+, \phi) - d\sigma(e^-, \phi)}{d\sigma(e^+, \phi) + d\sigma(e^-, \phi)} \propto \Re e(\mathcal{H}) \cos(\phi), \quad (4)$$

the Longitudinal Target Spin Asymmetry:

$$A_{UL} = \frac{d\sigma(p^{\rightarrow}, \phi) - d\sigma(p^{\leftarrow}, \phi)}{d\sigma(p^{\rightarrow}, \phi) + d\sigma(p^{\leftarrow}, \phi)} \propto \text{Im } m(\tilde{\mathcal{H}}) \sin(\phi), \quad (5)$$

and the Transverse Target Spin Asymmetry:

$$\begin{aligned}
A_{UT} &= \frac{d\sigma(p^\uparrow, \phi) - d\sigma(p^\downarrow, \phi)}{d\sigma(p^\uparrow, \phi) + d\sigma(p^\downarrow, \phi)} \propto \\
&\quad \text{Im } m(F_2\mathcal{H} - F_1\mathcal{E}) \sin(\phi - \phi_S) \cos(\phi) \\
&\quad + \text{Im } m(F_2\tilde{\mathcal{H}} - F_1\xi\tilde{\mathcal{E}}) \cos(\phi - \phi_S) \sin(\phi),
\end{aligned} \tag{6}$$

where the arrows denote the polarisation of the beam electron  $e^-$  (positron  $e^+$ ) or target proton  $p$ . These asymmetries are to leading order proportional to the real and imaginary parts of the Compton Form Factors (CFFs)  $\mathcal{H}$ ,  $\tilde{\mathcal{H}}$ ,  $\mathcal{E}$ ,  $\tilde{\mathcal{E}}$ , and trigonometric functions of the angle  $\phi$  between the lepton plane and the plane which is spanned by the virtual and real photons.  $F_1$  and  $F_2$  are the Dirac and Pauli Form Factors respectively. The Transverse Target Spin Asymmetry also depends on another azimuthal angle  $\phi_S$  which relates the target spin vector to the lepton plane. At leading order in  $\alpha_S$  the real and imaginary parts of the CFFs directly relate to the GPDs at  $x = \pm\xi$  through:

$$\begin{aligned}
\text{Im } m\mathcal{F}(\xi, t) &= \pi \sum_q e_q^2 [F_q(\xi, \xi, t) \mp F_q(-\xi, \xi, t)] \quad \text{and} \\
\Re e\mathcal{F}(\xi, t) &= - \sum_q e_q^2 \left[ P \int_{-1}^{+1} dx F_q(\xi, \xi, t) \left( \frac{1}{x - \xi} \mp \frac{1}{x + \xi} \right) \right],
\end{aligned} \tag{7}$$

where the  $\mathcal{F}(\xi, t)$  correspond to the CCFs  $\mathcal{H}, \mathcal{E}$  and  $\tilde{\mathcal{H}}, \tilde{\mathcal{E}}$  for  $(-)$  and  $(+)$  respectively [6]. Similarly,  $F_q(x, \xi, t)$  are substitutes for the GPDs  $H_q(x, \xi, t)$ ,  $E_q(x, \xi, t)$ ,  $\tilde{H}_q(x, \xi, t)$ , and  $\tilde{E}_q(x, \xi, t)$ .  $P$  denotes Cauchy's principal value.

## 2 Results from HERMES

The HERMES experiment at DESY Hamburg [7] has been investigating the quark and gluon structure of the nucleon using electrons or positrons with 27.6 GeV energy from HERA scattered off protons or heavier nuclei. HERMES is an experiment consisting of a forward magnetic spectrometer and a storage cell target using gases ranging from Hydrogen to Krypton. Hydrogen and Deuterium targets can be polarised transversely or longitudinally.

The selection of the DVCS/BH process at HERMES requires events with exactly one photon and one charged track, identified as the scattered lepton, with  $Q^2 > 1 \text{ GeV}^2$ . In the dataset where the recoiling proton has not been detected (before 2006), exclusive events are identified by requiring the missing mass  $M_X$  of the reaction  $ep \rightarrow e\gamma X$  to correspond to the proton mass. Due

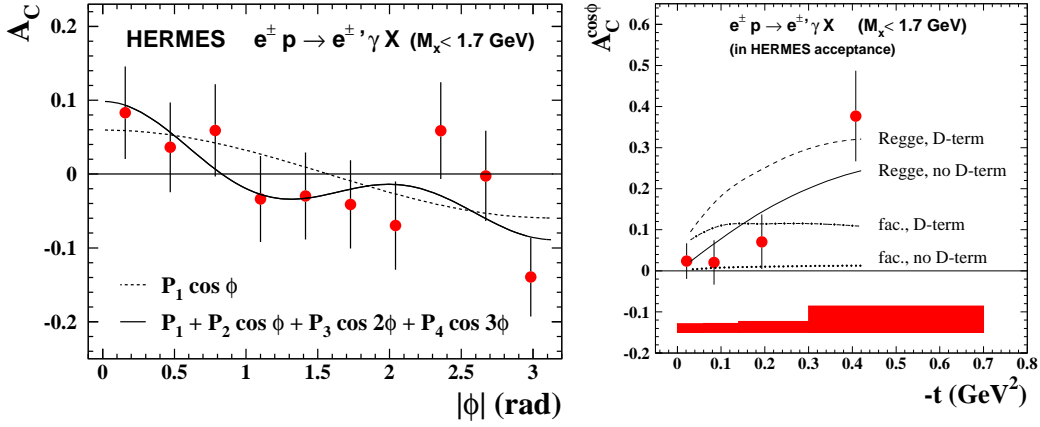


Figure 2: Left: Beam Charge Asymmetry  $A_C$  as a function of the azimuthal angle  $\phi$  before background correction. The dashed curve shows the angular dependence extracted from the 4 parameter fit (solid line). Right: obtained  $\cos \phi$  amplitude as a function of  $-t$ . These data restrict GPD models [10] shown as curves. Please refer to text and Ref. [11] for details.

to the finite energy resolution, the exclusive sample is selected in the region  $-1.5 < M_X < 1.7$  GeV, based on signal-to-background studies using Monte Carlo simulations.

HERMES and CLAS were the first experiments to measure the Beam-Spin Asymmetry  $A_{LU}$  in hard exclusive reactions [8, 9]. The Beam-Charge Asymmetry  $A_C$  has been measured on a proton target for the first time. The data disfavour a certain GPD model with the non-factorised  $t$  dependence (Regge) and including the D-term [10]. For details please refer to Fig. 2 and Ref. [11]. In Fig. 2 and the top panel of Fig. 3 the error bars and bands at the bottom of the panels represent the statistical and systematic uncertainties, respectively.

The Transverse Target Spin Asymmetry  $A_{UT}$  is the only asymmetry on a proton target where the contribution of the GPD  $E$  is not suppressed, i.e. the  $\mathcal{H}$  term in Eq. 6 is smaller than the  $\mathcal{E}$  term. The latter term is sensitive to the angular momentum of the quarks while the former is not [12]. The measured amplitude  $A_{UT}^{\sin(\phi-\phi_S) \cos(\phi)}$  can be compared with a GPD model [13] varying the angular contribution of  $u$  and  $d$  quarks separately. An example of the variation of the  $u$  quark contribution is shown in the top panel of Fig. 3. In the bottom panel the resulting contour plot for an one-sigma band obtained from the data is shown. For further information please refer to Refs. [12, 14].

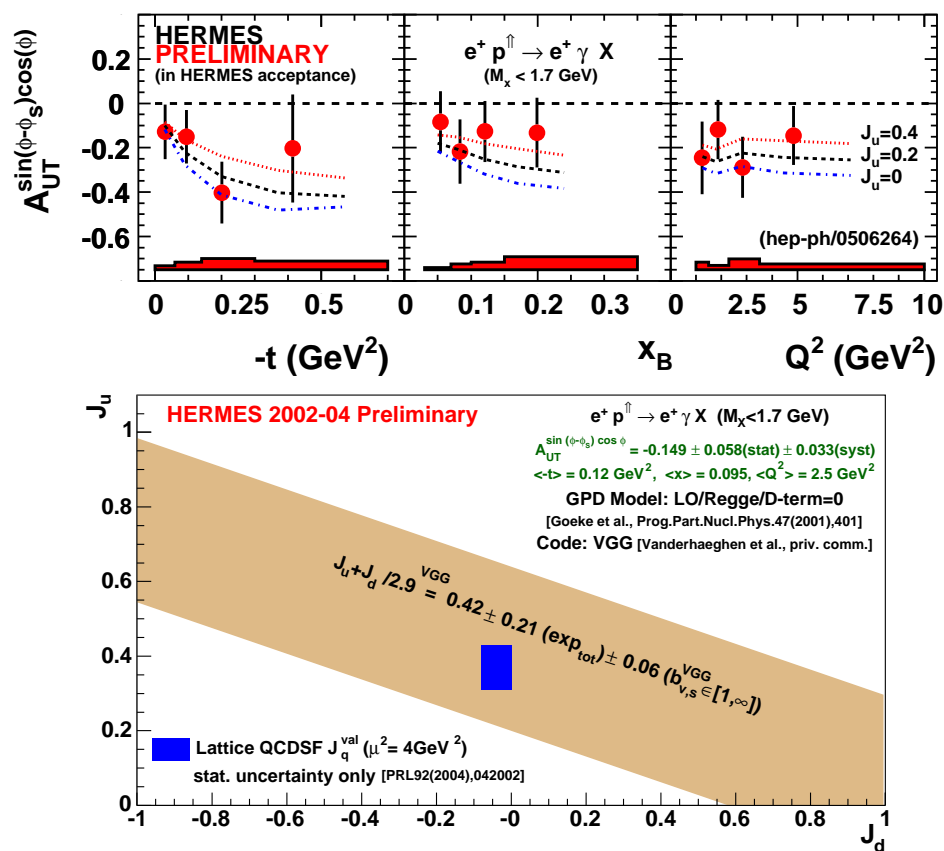


Figure 3: Top: the  $A_{UT}^{\sin(\phi - \phi_S) \cos \phi}$  moment as a function of  $-t$ ,  $x_B$  or  $Q^2$  compared to predictions based on the VGG model. Bottom: model dependent constraint on  $J_u$  and  $J_d$  obtained from a fit of this amplitude to a GPD model [13]. Please refer to Refs. [12, 14] for details.

New lattice gauge theory results [15] are consistent with these experimental findings within one sigma. Measurements from JLab Hall A on the neutron provide complementary results [16].

### 3 Recoil Detector at HERMES

In January 2006 the HERMES spectrometer was extended by the installation of the Recoil Detector [17], a new magnetic spectrometer surrounding the target. It consists of three detector systems:

- two layers of Silicon Strip Detectors inside the vacuum of HERA,
- two barrels of Scintillating Fibre Trackers,
- a Photon Detector of stacked lead and scintillator layers.

These are mounted inside a superconducting solenoid surrounding a storage cell target with unpolarised gases.

The main purpose of this apparatus is the measurement of the previously undetected recoiling proton from the DVCS process. The Recoil Detector is expected to reduce the background from associated BH/DVCS (intermediate  $\Delta$ -production) and from semi-inclusive processes from 17% to 1%. The  $t$  resolution at small  $t$  is improved and high luminosities are achieved as unpolarised targets are used.

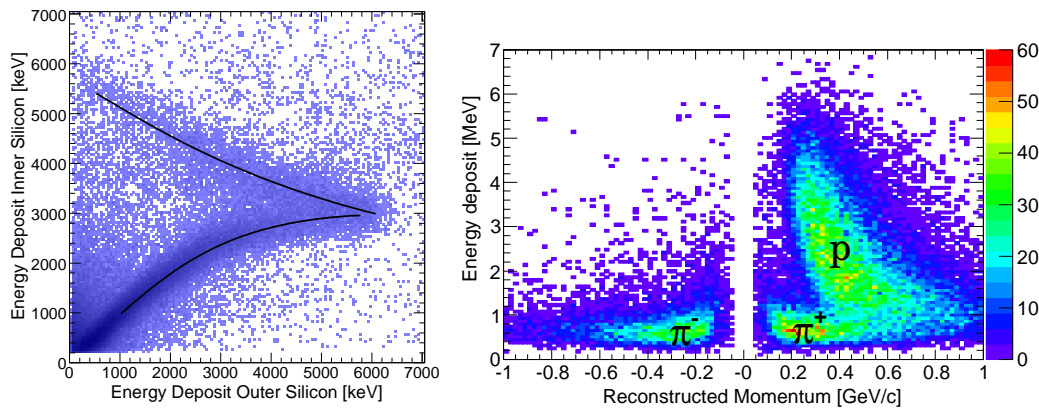


Figure 4: Left: experimental data of the energy deposited in the first and second layers of the Silicon Strip Detector. Clearly visible is the band from protons in the detectors. Also shown is the parametrisation of the expected energy deposit from Monte-Carlo studies (solid curves). Right: experimental data of energy deposited in the Scintillating Fibre Tracker versus reconstructed momentum by the curvature in the magnetic field.

The detector has been successfully commissioned in spring 2006. Data with electron and positron beams were collected, the latter data sample being

significantly larger. After first calibrations and with a preliminary momentum reconstruction in place already clean signals from protons and pions can be observed. In the left panel of Fig. 4 the band from experimental data is in good agreement with the expected energy deposit for protons obtained from Monte-Carlo studies (solid curves). From plotting the average energy losses versus the momentum reconstructed in the magnetic field of the solenoid, clear bands are observed (see right panel in Fig. 4). Thus we can clearly identify protons and pions of positive and negative charge. Currently, fine calibrations, Monte-Carlo studies and first analysis steps are being carried out.

## 4 Summary and Outlook

Within the framework of Generalized Parton Distributions, the measurement of hard exclusive reactions has the potential to provide access to the distributions of momentum and angular momentum of partons in the nucleon, in particular on how the spin is shared between the quarks and gluons.

The HERMES experiment has made a crucial contribution to this field already, of which only a small fraction can be presented here. Much data are still to be analysed. A large sample of data was taken in 2006 and 2007 with the new Recoil Detector, providing an almost background free exclusive data sample on Deeply Virtual Compton Scattering with improved  $t$ -resolution at small  $t$ . In particular, the large data set will allow the Beam Spin Asymmetry to be determined more precisely. Many physics results from the HERMES collaboration can be expected to emerge in the coming years.

## References

- [1] A. Airapetian *et al.* [HERMES Collaboration], Phys. Rev. D **75** (2007) 012007 [Erratum-ibid. D **76** (2007) 039901].
- [2] D. Mueller *et al.*, Fortsch. Phys. **42** (1994) 101.
- [3] A. V. Radyushkin, Phys. Rev. D **56** (1997) 5524.
- [4] X. D. Ji, Phys. Rev. Lett. **78** (1997) 610;
- [5] M. Diehl *et al.*, Eur. Phys. J. C **39** (2005) 1.
- [6] W. D. Nowak, Conf. Proc. St. Andrews, Scotland, Sep. 2004, [arXiv:hep-ex/0503010].

- [7] K. Ackerstaff *et al.* [HERMES Collaboration], Nucl. Instrum. Meth. A **417** (1998) 230; and  
K. Rith, Prog. Part. Nucl. Phys. **49** (2002) 245.
- [8] A. Airapetian *et al.* [HERMES Collaboration], Phys. Rev. Lett. **87** (2001) 182001.
- [9] S. Stepanyan *et al.* [CLAS Collaboration], Phys. Rev. Lett. **87** (2001) 182002.
- [10] M. Vanderhaeghen, P. A. M. Guichon and M. Guidal, Phys. Rev. D **60** (1999) 094017.
- [11] A. Airapetian *et al.* [HERMES Collaboration], Phys. Rev. D **75** (2007) 011103.
- [12] F. Ellinghaus, W. D. Nowak, A. V. Vinnikov and Z. Ye, Eur. Phys. J. C **46**, 729 (2006).
- [13] K. Goeke, M. V. Polyakov and M. Vanderhaeghen, Prog. Part. Nucl. Phys. **47** (2001) 401.
- [14] Z. Ye [HERMES Collaboration], PoS **HEP2005** (2006) 120 [arXiv:hep-ex/0512010]; arXiv:hep-ex/0606061.
- [15] Ph. Hagler *et al.* [LHPC Collaborations], arXiv:0705.4295 [hep-lat].
- [16] M. Mazouz *et al.* [Jefferson Lab Hall A Collaboration], arXiv:0709.0450 [nucl-ex].
- [17] [HERMES Collaboration], Technical Design Report, HERMES Internal Note 02-003 (2002); and  
B. Seitz [HERMES Collaboration], Nucl. Instr. Meth. A **535**, 538 (2004).

# ILLUMINATING THE $1/x$ MOMENT OF PARTON DISTRIBUTION FUNCTIONS

Stanley J. Brodsky <sup>\*</sup>, Felipe J. Llanes-Estrada<sup>%</sup> and Adam P. Szczepaniak<sup>#</sup>

<sup>\*</sup> Theory Group, Stanford Linear Accelerator Center, 2575 Sand Hill Road,  
94025 Menlo Park, California, USA. [sjbth@slac.stanford.edu](mailto:sjbth@slac.stanford.edu)

<sup>%</sup> Depto. Física Teórica I, Fac. Cc. Físicas, Universidad Complutense de  
Madrid, 28040 Madrid, Spain. <sup>1</sup>. [fllanes@fis.ucm.es](mailto:fllanes@fis.ucm.es)

<sup>#</sup> Nuclear Theory Center, Indiana University, 2401 Milo Sampson Lane,  
Bloomington, IN 47408 Indiana, USA. [aszczepa@indiana.edu](mailto:aszczepa@indiana.edu)

## Abstract

The Weisberger relation, an exact statement of the parton model, elegantly relates a high-energy physics observable, the  $1/x$  moment of parton distribution functions, to a nonperturbative low-energy observable: the dependence of the nucleon mass on the value of the quark mass or its corresponding quark condensate. We show that contemporary fits to nucleon structure functions fail to determine this  $1/x$  moment; however, deeply virtual Compton scattering can be described in terms of a novel  $F_{1/x}(t)$  form factor which illuminates this physics. An analysis of exclusive photon-induced processes in terms of the parton-nucleon scattering amplitude with Regge behavior reveals a failure of the high  $Q^2$  factorization of exclusive processes at low  $t$  in terms of the Generalized Parton-Distribution Functions which has been widely believed to hold in the past. We emphasize the need for more data for the DVCS process at large  $t$  in future or upgraded facilities.

## 1 The Weisberger relation

The importance of the  $1/x$  moment of parton distribution functions (pdf's) was stressed in a 1972 paper by W. Weisberger [1]. There he derived a relation between the  $1/x$  moment and the derivative of the squared proton mass with

---

<sup>1</sup>Talk and poster presented at MeNu07, part of a work in preparation.

respect to the squared parton mass defined at the same renormalization scale  $\mu$ . In modern notation and normalization [2], Weisberger's result reads

$$\frac{\delta M_N^2}{\delta m_i^2(\mu)} = \int_0^1 \frac{dx}{x} (f_i(x)_\mu + \bar{f}_i(x)_\mu) . \quad (1)$$

Here  $f_i$  is the  $i$ th-quark distribution function, and since CPT invariance implies that the mass of quark and antiquark are equal and must be varied together, we have also included the antiquark pdf  $\bar{f}$ .

With the advent of QCD and the Hellmann-Feynman theorem, one can see that Weisberger's result holds simply by noting that in light front quantization the Hamiltonian contains a kinetic energy term

$$M_{\text{kin}}^2 = \sum_i \frac{k_\perp^2 + m_i^2}{x_i} . \quad (2)$$

where  $x = k^+/P^+ = (k^0 + k^z)/(P^0 + P^z)$  is the light-front momentum fraction. After regularization and renormalization [3], a  $c_8$  mass counterterm appears, but no mass dependence in any of the other counterterms, so that the formal manipulation of the Hellmann-Feynman theorem remains valid in the regulated Hamiltonian.

Upon taking the expectation value  $\langle \delta M^2 / \delta m_i^2 \rangle_\psi$ , the trivial integration over the  $k_\perp$  transverse variables leads to the  $\int f/x$  result. Thus the Weisberger relation Eq. 1 relates the variation of the proton mass to the quark mass terms which appear specifically in the LF kinetic energy. (The Weisberger relation is an exact statement of the parton model, but in full QCD there could be an additional term due to an implicit mass dependence of the fields, which is under investigation).

In chiral perturbation theory the quark mass dependence of the nucleon mass is parameterized in terms of a contact term with an unknown constant  $c_1$  [4]

$$M_N(m_q) = M_N(0) - 4c_1 m_\pi^2 - \frac{3g_A^2 m_\pi^3}{32\pi f_\pi^2} + O(m_\pi^4) . \quad (3)$$

The constant counterterm  $4c_1 m_\pi^2$  is related to the  $\sigma$  term of the nucleon, the expectation value of a scalar current. The accurate determination of the  $1/x$  moment of pdf's, including its scale dependence, would thus allow a determination of the  $\sigma$  term independently of chiral perturbation theory, or alternatively, provide a constraint between high and low-energy physics which tests the way mass terms enter the QCD Hamiltonian. One can also combine independent evaluations of the  $\sigma = \hat{m} \partial m_N / \partial \hat{m}$  term and the  $1/x$

moment to provide an evaluation of the quark mass via (for isospin averaged light quarks)

$$\hat{m}^2 = \frac{M_N \sigma}{\langle 1/x \rangle} . \quad (4)$$

The spontaneous chiral symmetry breaking pattern of QCD also allows us to write down a new sum rule for the pion distribution function by combining the Weisberger relation with the Gell-Mann-Oakes-Renner relation, which links the quark mass to the quark condensate in the chiral limit:

$$\int_0^1 \frac{dx}{x} f_u^\pi(x) = \frac{\langle \bar{\Psi}\Psi \rangle_{m=0}^2}{m_\pi^2 f_\pi^4} . \quad (5)$$

The left and right-hand sides vary with the scale in the same way (since  $m\langle\bar{\psi}\psi\rangle$  is renormalization-group invariant). This result is independent of the light-front formalism since  $\delta M_N^2/\delta m_q^2$  can be studied in any framework. The light-front formalism, however, provides the tools needed to demonstrate the relation. This new sum rule can be of use to constrain models of the pion as well as Deep Inelastic Scattering data.

## 2 Regularization of the Weisberger relation

The parton distribution functions measured in deep inelastic lepton scattering are observed to diverge at small  $x_{bj}$  due to the Regge behavior of the forward virtual Compton amplitude and simple analytic arguments. In fact, modern fits to deep inelastic scattering data at small  $Q^2$  routinely employ a parameterization of pdf's which is a simple variation of the Kuti-Weisskopf model [5], namely

$$x f_i(x) = A_i x^{\eta_i} (1-x)^{\lambda_i} (1 + \gamma_i \sqrt{x} + \epsilon_i x) \quad (6)$$

where all parameters are left free for the fit. The phenomenology of deep inelastic scattering generally requires  $\eta$  to be smaller than 1 for several pdf's. In fact, for the valence flavors,  $\eta_i = 1 - \alpha(0)$ , a typical Regge intercept  $\alpha(0) = 1/2$  makes the integral in eq. 1 to be manifestly divergent. This is the case for the GRV98 pdf set [6] which has exponents  $-0.85$  and  $-0.52$  for the light sea and valence pdf's respectively. Notice that the  $\sqrt{x}$  in eq. 6 gives rise to subleading Regge power laws. For the MRST98 [2] pdf sets, an also widely used alternative, the power-law exponents have higher variation around classical Regge theory and the  $u$  proton's valence component has a somewhat high intercept  $\alpha_u(0) \in (0.53, 0.59)$ , the  $d$  valence component being definitely at odds with other phenomenology with  $\alpha_d(0) \simeq 0.73$  as large as

the sea component. The subleading Regge behavior is also given by the  $\sqrt{x}$  factor in eq. 6, and having an intercept larger than zero, it also causes a divergence. In both GRV98, MRST98 sets the gluon pdf behaves as a valence-like parton with a very small intercept at this low scale, indication of the gluon degrees of freedom being truncated at low energy [7].

The Weisberger relation is thus formally divergent and needs to be properly regulated. This can be done either by analytical continuation from large  $t$  where the amplitudes are convergent [8] or by studying the spectral representation of the parton-nucleon scattering amplitude which underlie the parton-distribution functions. Both topics will be discussed briefly below, but meanwhile let us give the correctly regulated relation as found by Brodsky, Close, and Gunion(BCG) [9],

$$\begin{aligned} \frac{\delta M_N^2}{\delta m_i^2} &= \int_0^1 \frac{dx}{x} \left( f_i - f_i^{\text{Regge}} + \bar{f}_i - \bar{f}_i^{\text{Regge}} \right) (x) - \sum_{\alpha} \frac{\gamma_{\alpha}}{\alpha(0)} - \sum_{\bar{\alpha}} \frac{\bar{\gamma}_{\bar{\alpha}}}{\bar{\alpha}(0)} \quad (7) \\ f_i^{\text{Regge}}(x) &= \sum_{\alpha} \gamma_{\alpha} x^{-\alpha(0)} \quad \alpha(0) > 0 \\ \bar{f}_i^{\text{Regge}}(x) &= \sum_{\bar{\alpha}} \bar{\gamma}_{\bar{\alpha}} x^{-\bar{\alpha}(0)} \quad \bar{\alpha}(0) > 0 . \end{aligned}$$

Notice that the particular form of this subtraction entails that there can be no Regge pole with exactly  $\alpha = 0$  in the input fit (this is set by the BCG choice of the subtraction point in the parton-nucleon scattering matrix formalism). As a consequence we cannot currently examine the pion sum rule with standard pion distribution functions [10] since  $\alpha = 0$  constant terms do appear in those parametrizations. It may be possible to develop an equivalent formula with a different subtraction point to avoid this inconvenience.

The result of computing the properly regularized  $1/x$  moment from Eq. 7 for a few standard pdf sets is given in table 1. As can be seen, there is considerable spread in the results, and much room for improvement in the determination of the moments.

### 3 The $1/x$ Form Factor of the Nucleon

An important empirical way to access the  $1/x$  moment of parton distribution functions is by utilizing the forward limit of the generalized parton distribution (GPD) functions measured in deeply virtual Compton scattering (DVCS); specifically,

$$H(x, \zeta = 0, t = 0) = f(x) \quad (8)$$

Table 1: Weisberger integral  $\int_0^1 dx \frac{f(x)}{x}$  for MRST98 [2] and GRV parton distribution functions. Following BCG, we have analytically continued in  $t$  as in eq. (7) by adding and subtracting the divergent Regge terms. The sets are taken at low-energy input scales  $1\text{GeV}^2$  (MRST) and  $0.26(0.4)\text{GeV}^2$  for the LO(NLO) GRV set. The latter has no strange sea component at this low scale.

quark flavor	MRST	MRST	MRST	LO	NLO
	Low gluon	Central gluon	Upper gluon	GRV	GRV
$u$	34	8.6	12	133	26
$\bar{u}$	-1.3	-5.2	-7.1	62	5.8
$\frac{\delta M_N^2}{\delta m_u^2}$	33	3.4	4.9	195	32
$d$	0.98	-0.4	0.33	-20	-5.7
$\bar{d}$	-0.46	-0.75	-1.8	-62	-17
$\frac{\delta M_N^2}{\delta m_d^2}$	0.52	-1.1	-1.5	-82	-22
$s$	-0.43	-1.5	-2.2	0	0
$\frac{\delta M_N^2}{\delta m_s^2}$	-0.86	-3.0	-4.4	0	0
$g$	$\simeq 600$	$\simeq 400$	$\simeq 2900$	10	12

so that the  $F_{1/x}(t)$  form factor defined by

$$F_{1/x}(t) = \sum e_q^2 \int_0^1 dx \frac{H(x, 0, t)}{x} \quad (9)$$

should take in the  $t \rightarrow 0$  limit a value given by a sum of the  $1/x$  moments for various flavors. Unfortunately this equation is known to be rigorously valid for sizeable  $t$  only. In that case, the  $F_{1/x}(t)$  form factor is accessible via DVCS; the required DVCS amplitude in the GPD-collinear factorization formalism is given by

$$\mathcal{M}^{++}(s, t, Q^2) = \frac{-e_q^2 \sqrt{1-\zeta}}{2} \frac{1-\zeta/2}{1-\zeta/2} \int_{\zeta-1}^1 dx \left[ \frac{1}{x-i\epsilon} + \frac{1}{x-\zeta+i\epsilon} \right] H(x, \zeta, t) . \quad (10)$$

(Here we have ignored the contribution of the  $E(x, \zeta, t)$  GPD, and work in the asymmetric frame).

The experimental determination of the  $F_{1/x}(t)$  form factor would in principle allow an analytic continuation in  $t$  to  $t = 0$ , thus providing  $1/x$  moment. However, as noted in the next section, it is not trivial to carry out such an extrapolation through the low  $t$  region due to Regge divergences.

A prediction for the  $1/x$  form factor of the nucleon has been given for a

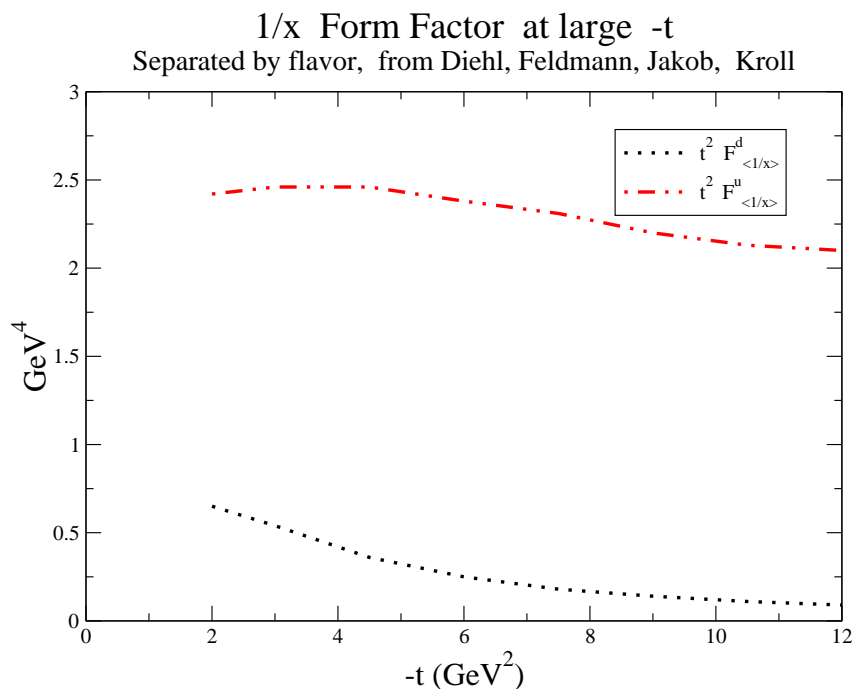


Figure 1: An evaluation of the  $1/x$  form factor of the proton assuming the Gaussian light-front constituent quark model utilizing flavor-separated form factors obtained from a set of GPD's fit to a number of conventional Dirac and Pauli form factors. Data from [11] is given only at large  $-t$  by direct calculation.

particular model, the Gaussian light-front constituent quark model; this is illustrated in figure 1.

## 4 Loss of collinear factorization in deeply virtual Compton scattering

It has been recently shown [12, 13] that the DVCS amplitudes can be most efficiently described in terms of  $t$ -channel Regge exchanges. The analysis proceeds along the lines of ref. [9] by employing a representation of the leading twist amplitude as an integral over the underlying parton-nucleon scattering amplitude [14]. The DVCS amplitude can then be written in terms of a

subtracted spectral representation

$$A^\pm = \sum_n c_n (2\pi)^4 \int dm^2 \left[ \frac{\rho_n}{s_{pp} - m^2 + i\epsilon} - \frac{\rho_R^n}{-m^2 + i\epsilon} \pm (s_{pp} \rightarrow u_{pp}) \right] f(k^2, k'^2) \quad (11)$$

The convergence needed for the handbag diagram is provided by the regularization procedure  $I_n = (m^2)^n \frac{d^n}{(dm^2)^n}$ ,  $n > 1$  and the functional form of  $f$ . The Regge behavior follows from the form  $\rho^R \propto (m^2)^{\alpha(t)}$  (under the assumption that the quark-nucleon matrix element has standard hadronic physics properties [14]).

At large  $t$ , one can eschew Regge behavior and think of such representation as a dispersive integral over diquark exchanges of varying mass. The form of the resulting nucleon GPDs (see figure 2) are similar to those found in ref. [15] and ref. [16] for the GPD of the pion.

However, if one now proceeds to study the low- $t$  region, one finds Regge poles at the break-points of the GPD, for example, approaching  $x = \zeta$  from higher values of  $x$  one finds

$$H(x \rightarrow \zeta^+, \zeta, t \simeq 0) \rightarrow \left[ \pi^2 m_q^2 I_{n-1} \beta \int_0^\infty \frac{d\phi \phi^\alpha}{(\phi^2 + m_q^2)^2} \right] \left[ \frac{(1-\zeta)^\alpha}{1+\alpha} (x-\zeta)^{-\alpha} - \frac{\zeta^{-\alpha}}{1+\alpha} \right] \quad (12)$$

where the function on the left bracket will be discussed in detail in our upcoming publication. The function on the right however shows clearly the Regge pole  $(x-\zeta)^{-\alpha}$ . As a result, whereas the DVCS amplitude correctly exhibits Regge scaling in  $s$ , its  $Q^2$  dependence does not track with the same power; the amplitude at nonzero- $t$  thus cannot scale with Bjorken  $\zeta$  alone. Such Regge contributions were not contemplated in the original proof of the collinear factorization theorem [18] and thus apparently make it fail. Current models, such as the one presented in in figure 2, which have soft behavior at the break-points also must be improved.

## 5 The $J = 0$ fixed-pole in Compton Scattering.

In Regge theory, hadron scattering amplitudes scale as  $s^\alpha(t)$ , where the exponent of the Regge pole evolves with  $t$ . A fixed pole at  $J = \alpha = 0$  corresponds to a constant real amplitude. Such behavior was proposed [19] and found [8] in Compton scattering in the late sixties. In their analysis Damashek and Gilman [8] used the forward dispersion relation for the Compton amplitude and measurements of total photoabsorption cross section  $\sigma(\gamma p \rightarrow X)$  to show

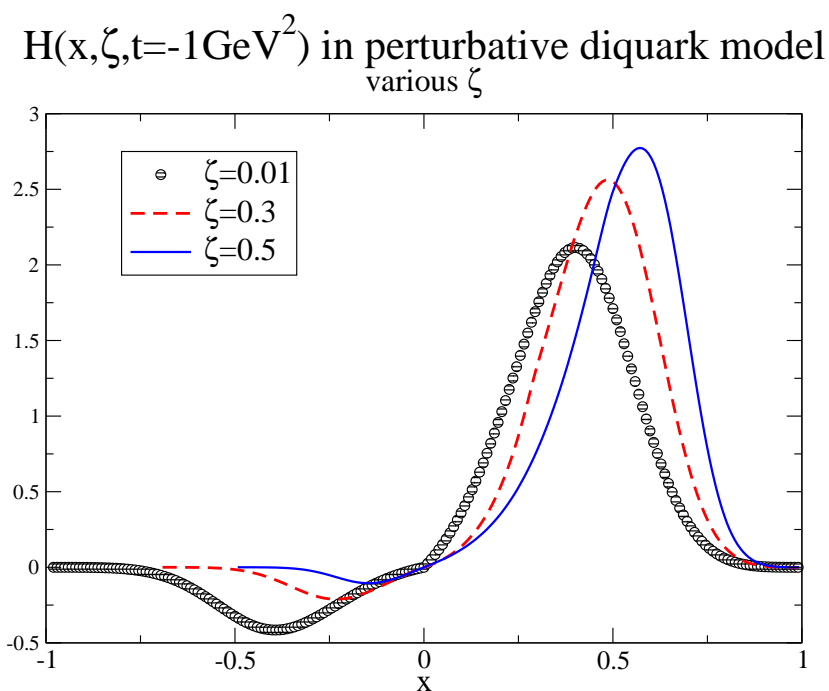


Figure 2: The GPD  $H(x, \zeta, t)$  at fixed  $-t = 1\text{GeV}^2$  in a perturbative quark-diquark model [17] with masses  $400\text{ MeV}$  and  $800\text{ MeV}$  for the quark and diquark, a vertex coupling  $g = 25$  and both  $u$  and  $s$  channel exchanges (the latter, covering the antiquark region  $x < 0$ , have been suppressed by an ad-hoc 0.2 factor since this is a valence-like model)

that the forward Compton scattering on the proton has a  $J = 0$  contribution. A formal proof that the Compton amplitude must present fixed pole behavior was given in ref. [20]. Physically it arises from the local four-point seagull interaction in scalar QCD or from the instantaneous fermion exchange interaction in the light-front QCD Hamiltonian [21, 22]. The  $J = 0$  contribution to the DVCS amplitude is thus independent of  $s$  for any photon virtuality and any momentum transfer  $t$ .

In general, the contribution to Compton scattering (real or virtual) which is directly sensitive to the  $1/x$  moment can be identified with the “handbag” diagram in QCD where the incoming and outgoing photons interact on the same valence quark line. Note that in the case of fixed  $\theta_{CM}$  angle Compton scattering, where  $t, u$ , and  $s$  are all large, the outgoing photon can be equally well emitted by another valence quark (see figure 3). Therefore, Compton

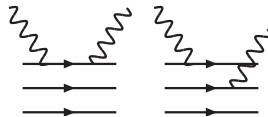


Figure 3: In the handbag mechanism the left diagram dominates the cross-section over all others such as, say, the right one. This is testable through the ratio of the Compton scattering cross sections of the neutron over the proton.

scattering at fixed angle does not isolate the handbag diagram. The optimum experimental approach is thus to work in the Regge regime for DVCS. As shown in ref. [9], the  $J = 0$  fixed pole has  $t$  dependence given precisely by the  $1/x$  form factor.

Thus, a good experimental strategy to extract the  $J = 0$   $F_{1/x}(t)$  form factor is to fix  $t$  and let  $s$  increase until only the constant fixed-pole amplitude remains. Since the contribution to the DVCS amplitude is real, it can be extracted from interference with the Bethe-Heitler amplitude [21]. In addition, if one wants to interpret this form factor in terms of a moment of GPD's, one needs to demand  $Q^2 \gg -t$ . An upgraded Jefferson Laboratory with a 12 GeV beam should be able to reach perhaps  $s \simeq 40 \text{ GeV}^2$ ,  $Q^2 \simeq 6 \text{ GeV}^2$ ,  $t \simeq -3 \text{ GeV}^2$  and thus should be able to report a first measurement in a regime where the virtual Compton amplitude should become  $Q^2$  and  $s$  independent. The extracted  $t$  dependence would provide the first

measurement of the  $F_{1/x}(t)$  nucleon form factor. It is also possible that current measurements by the Hall A collaboration at JLab [23] of  $R_V(t)$  in real Compton scattering also yield the same physics, but there is no kinematic limit where one can perform the needed checks. The kinematically stringent Regge limit of DVCS at sizeable  $t$  provides further motivation for a future electron-proton collider.

## Acknowledgments

We are indebted to many colleagues for valuable discussions, among them Tim Londergan. Work supported by grants FPA 2004-02602, 2005-02327, PR27/05-13955-BSCH (Spain), DOE contracts DE-FG0287ER40365 DE-AC02-76SF00515, and NSF under grant PHY-0555232 (USA).

## References

- [1] W. I. Weisberger, Phys. Rev. D **5**, 2600 (1972).
- [2] A. D. Martin, R. G. Roberts, W. J. Stirling and R. S. Thorne, Eur. Phys. J. C **4**, 463 (1998) [arXiv:hep-ph/9803445].
- [3] S. A. Paston, V. A. Franke and E. V. Prokhvatilov, Theor. Math. Phys. **120**, 1164 (1999) [Teor. Mat. Fiz. **120**, 417 (1999)] [arXiv:hep-th/0002062].
- [4] B. Kubis, arXiv:hep-ph/0703274. B. Borasoy and U. G. Meissner, Annals Phys. **254**, 192 (1997) [arXiv:hep-ph/9607432].
- [5] J. Kuti and V. F. Weisskopf, Phys. Rev. D **4**, 3418 (1971).
- [6] M. Gluck, E. Reya and A. Vogt, Eur. Phys. J. C **5**, 461 (1998) [arXiv:hep-ph/9806404].
- [7] R. Alkofer, P. Bicudo, S. R. Cotanch, C. S. Fischer and F. J. Llanes-Estrada, arXiv:nucl-th/0601032.
- [8] M. Damashek and F. J. Gilman, Phys. Rev. D **1**, 1319 (1970).
- [9] S. J. Brodsky, F. E. Close and J. F. Gunion, Phys. Rev. D **8**, 3678 (1973).
- [10] P. J. Sutton, A. D. Martin, R. G. Roberts and W. J. Stirling, Phys. Rev. D **45**, 2349 (1992).

- [11] M. Diehl, T. Feldmann, R. Jakob and P. Kroll, Eur. Phys. J. C **39**, 1 (2005) [arXiv:hep-ph/0408173].
- [12] A. P. Szczepaniak and J. T. Londergan, Phys. Lett. B **643**, 17 (2006) [arXiv:hep-ph/0604266].
- [13] A. P. Szczepaniak, J. T. Londergan and F. J. Llanes-Estrada, arXiv:0707.1239 [hep-ph].
- [14] P. V. Landshoff, J. C. Polkinghorne and R. D. Short, Nucl. Phys. B **28**, 225 (1971).
- [15] B. C. Tiburzi and G. A. Miller, Phys. Rev. D **67** 113004, (2003).
- [16] C.-R. Ji, Y. Mischenko and A. Radyushkin, Phys. Rev. D **73** 114013 (2006).
- [17] S. J. Brodsky and F. J. Llanes-Estrada, Eur. Phys. J. C **46**, 751 (2006) [arXiv:hep-ph/0512247].
- [18] J. C. Collins and A. Freund, Phys. Rev. D **59**, 074009 (1999) [arXiv:hep-ph/9801262].
- [19] M. J. Creutz, S. D. Drell and E. A. Paschos, Phys. Rev. **178**, 2300 (1969).
- [20] A. Zee, Phys. Rev. D **5**, 2829 (1972) [Erratum-ibid. D **6**, 938 (1972)].
- [21] S. J. Brodsky, F. E. Close and J. F. Gunion, Phys. Rev. D **5**, 1384 (1972).
- [22] S. J. Brodsky, H. C. Pauli and S. S. Pinsky, Phys. Rept. **301**, 299 (1998) [arXiv:hep-ph/9705477].
- [23] A. Danagoulian *et al.* [Hall A Collaboration], Phys. Rev. Lett. **98**, 152001 (2007) [arXiv:nucl-ex/0701068].

# STUDIES OF CHARGE SYMMETRY BREAKING REACTIONS AT COSY

*A. Magiera*  
Institute of Physics  
Jagiellonian University  
Reymonta 4, 30-059 Cracow, Poland

## Abstract

Investigations of the charge symmetry breaking become the most important topic for WASA detector at COSY. The planned studies concentrate on charge symmetry forbidden reaction  $d + d \rightarrow \alpha + \pi^0$  and decays of  $\eta'$  meson. The experimental results will be compared with Chiral Perturbation Theory ( $\chi$ PT) predictions, providing information on up and down quarks mass difference. For  $d + d \rightarrow \alpha + \pi^0$  reaction various mechanisms within  $\chi$ PT were considered and it was found that the leading process is suppressed due to the selection rules. It is shown that another (not yet investigated) charge symmetry forbidden reaction,  $d + d \rightarrow d + d + \pi^0$ , may deliver new information on such leading process. In this case the use of tensor polarized deuteron beam will be especially important, allowing extraction of contributing amplitudes. The physical issues of charge symmetry breaking in  $\mathbf{d} + d \rightarrow d + p + n$  reaction, which may be measured simultaneously, are presented. Feasibility to perform measurements of these reactions with WASA at COSY is discussed.

## 1 Introduction

The observed experimentally similarities in proton and neutron masses and interactions led Heisenberg to introduce isospin, which allows treating both these particles as two states of the nucleon. This concept gave way to a more general proposition on isospin and charge symmetry, described as the invariance of the hadron system under rotations in the isospin space. After discovery of various hadrons this idea was followed by introducing the SU3 symmetry, allowing to group them into multiplets. A direct consequence of this observation was the concept of quarks - elementary particles building all hadrons.

Since the masses and interactions of different hadrons belonging to the same SU3 multiplet are not the same, the charge and isospin symmetries

are not exact. Therefore, until discovery of quarks, these symmetries were considered as accidental. Presently the appearance of these symmetries may be explained by the up and down quark mass difference and by their different electromagnetic interaction. Therefore, the observation of isospin or/and charge symmetry violation for hadrons opens a unique window to study the quark mass term of the QCD.

Despite that the isospin and charge symmetries are approximate, they were widely applied in various nuclear and particle physics investigations. Consequently, the searches for charge symmetry breaking (CSB) and isospin symmetry breaking (ISB) were performed very intensively (see ref. [1] for a review). However, it was not possible to relate the observed CSB and ISB to the elemental level of the QCD. Recently CSB was discovered by observation of the charge symmetry forbidden reaction  $d + d \rightarrow \alpha + \pi^0$  [2] and of forward-backward asymmetry in the  $p + n \rightarrow d + \pi^0$  reaction [3]. This triggered intensive theoretical calculations in the frame of Chiral Perturbation Theory (ChPT) [4–6]. Significant progress has been obtained in the theoretical analysis (see [7] for a review), however, still more experimental data are necessary.

## 2 Existing data and its implications

Major effect of ISB have the origin in the static symmetry breaking due to hadron mass differences. In the case of pions the origin of the mass difference is predominantly due to electromagnetic quark interaction. In order to have access to the dynamical symmetry breaking it is more favorable to study effect of CSB, where the pion mass difference does not contribute. However, the observation of CSB is difficult since these effects are very small. Therefore the best choice for studying the CSB are processes forbidden by charge symmetry invariance. This is the case for  $d + d \rightarrow \alpha + \pi^0$  reaction, recently observed at the beam energies close to the kinematical threshold [2]. The total cross section values measured for two beam energies ( $\sigma = 12.7 \pm 2.2$  pb at  $T_d = 228.5$  MeV and  $15.1 \pm 3.1$  pb at 231.8 MeV) are in agreement with the  $S$ -wave production. The difficulties in observation of CSB in allowed reactions is demonstrated in studies of the forward-backward asymmetry in the  $p + n \rightarrow d + \pi^0$  reaction [3]. The final result  $A_{fb} = [17.2 \pm 8(stat) \pm 5.5(sys)] \cdot 10^{-4}$  due to large uncertainties is a less convincing demonstration of CSB effects. Both recent experiments on CSB are under analysis using the ChPT [7]. A theory collaboration group, aiming at calculating the CSB effects in  $\pi^0$  production reactions, has been formed [8] and the work on the theoretical frontier is in progress.

In the case of CSB in the  $p + n \rightarrow d + \pi^0$  reaction the calculations within meson exchange coupled channel model [9] showed that the CSB effects are induced by  $\pi^0 - \eta$  mixing. However, this results in negative  $A_{fb}$  value in disagreement with the experimental observation. The calculations performed using ChPT [4] lead to positive values of forward-backward asymmetry, as observed experimentally. In this case the CSB is driven by charge symmetry violation in  $\pi^0$ -nucleon interaction. The predicted effect is much larger than observed experimentally. Therefore further theoretical analysis is required and more precise data on CSB in this reaction are necessary.

The first calculations using ChPT were performed for the  $d + d \rightarrow \alpha + \pi^0$  reaction [5]. It was found that at the leading order (LO) only charge symmetry violation in pion rescattering contributes. There is no NLO order contribution and some NNLO contributions were identified. Calculations of the cross section were performed using plane wave approximation in the entrance channel and simplified  $\alpha$  particle wave function. It was found that the contribution from the LO term becomes negligibly small due to spin-isospin selection rules and the symmetry of  $\alpha$  wave function. The NNLO terms result in the cross section by a factor of two larger than the experimentally observed. It necessitates, however, in surprisingly large value of the graph used to estimate the influence of the short range physics. Without this graph the cross section will be reduced to a value by one order of magnitude smaller than the experimental one. More reliable calculations were performed using realistic four body wave functions in the entrance and exit channels [6]. It was confirmed that the LO contribution is negligible and that at NNLO the first non vanishing contribution gives the cross section of the same order of magnitude as the observed experimentally. At NNLO new terms with unknown strength contribute to  $s$ -wave pion production in the  $d + d \rightarrow \alpha + \pi^0$  reaction. In order to fix the strength of the isospin violating  $\pi NN$  constant a new measurement for  $p$ -wave production is planned at COSY [10]. A dramatic influence of the initial state interaction was identified. Therefore new experimental constraints for deuteron-deuteron interaction becomes of great importance. This will be delivered by new measurements performed at COSY for charge symmetry conserving reactions  $d + d \rightarrow {}^3A + N + \pi$  at threshold [11] and substantially above the threshold [10].

Advanced analysis of CSB effect using ChPT will profit also from data for other CSB reactions that may be studied at COSY. These other possible measurements comprise investigations of charge symmetry forbidden reaction  $d + d \rightarrow d + d + \pi^0$  and polarization observables in deuteron break-up  $d + d \rightarrow d + p + n$ . The  $d + d \rightarrow d + d + \pi^0$  reaction was never observed and it may deliver direct information on the LO term not accessible in the  $d + d \rightarrow \alpha + \pi^0$  reaction. The use of polarized deuteron beam will enable to

evaluate the contributions from various transition amplitudes directly from the experimental data, without any theoretical assumptions. Comparison of the polarization observables for the  $d - p$  and  $d - n$  coincidences as well as data on  $p - n$  coincidences in deuteron break-up may deliver information on CSB in the entrance channel. This may be crucial in understanding of the CSB effect in pion production reactions.

### 3 Partial wave expansion

The use of polarization observables allows to measure directly the transition amplitudes for the  $d + d \rightarrow \alpha + \pi^0$  and  $d + d \rightarrow d + d + \pi^0$  reactions. This unique feature is due to the identical bosons in the entrance channel and the spin zero particles in the exit channel.

The identical bosons in the entrance channel require that their wave function has to be symmetric. The entrance channel spin  $s_i$  (parity  $\pi_s$ ) and angular momentum  $l_i$  (parity  $\pi_l$ ) couple to total angular momentum  $J$  (parity  $\pi$ ). For particles with spin-parity  $1^+$  only certain combinations  $(s_i^\pi, l_i^{\pi_l}) \rightarrow J^\pi$  are allowed:  $(0^+, 0^+) \rightarrow 0^+$ ,  $(0^+, 2^+) \rightarrow 2^+$ ,  $(1^+, 1^-) \rightarrow 0^- - 2^-$ ,  $(2^+, 0^+) \rightarrow 2^+$ ,  $(2^+, 2^+) \rightarrow 0^+ - 4^+$ .

Conservation of total angular momentum  $J$  and parity leads to a limited number of partial wave amplitudes allowed for the given angular momentum  $l_f$  and the total spin  $s_f$  in the exit channel. For the  $d + d \rightarrow \alpha + \pi^0$  reaction the exit channel spin is  $s_f = 0^-$  and the only allowed amplitudes are: for  $s$ -wave -  $a_{11000}$  and for  $p$ -wave -  $a_{22110}$  (subscripts denote values  $l_i, s_i, J, l_f$  and  $s_f$ ). In the case of the  $d + d \rightarrow d + d + \pi^0$  reaction one has to take into account the identity of the two deuterons in the exit channel. Then, considering only  $s$ -wave in the exit channel, the total spin is limited to  $s_f = 0$  and  $s_f = 2$ . Therefore for this reaction in  $s$ -wave there are three transition amplitudes:  $b_{11000}$ ,  $b_{11202}$  and  $b_{31202}$ .

The unpolarized cross section  $d\sigma_0$  and the analyzing powers  $T_{11}$ ,  $T_{20}$  and  $T_{22}$  may be written in terms of derived allowed transition amplitudes (the common factor is  $4\pi(2s_a + 1)(2s_b + 1)$ , where  $s_a = 1$  and  $s_b = 1$  are spins of particles in the entrance channel). For the  $d + d \rightarrow \alpha + \pi^0$  reaction in  $s$  and  $p$  waves one obtains the expressions:

$$\begin{aligned}
36\pi\sigma_0 &= \frac{1}{3} a_{11000}^2 + \frac{9}{10} a_{22110}^2 \sin^2 \theta \\
36\pi\sigma_0 iT_{11} &= \frac{3}{2\sqrt{10}} \text{Im} (a_{11000} a_{22110}^*) \sin \theta \\
36\pi\sigma_0 T_{20} &= \frac{1}{3\sqrt{2}} a_{11000}^2 - \frac{9}{20\sqrt{2}} a_{22110}^2 \sin^2 \theta \\
36\pi\sigma_0 T_{22} &= \frac{9\sqrt{3}}{40} a_{22110}^2 \sin^2 \theta
\end{aligned} \tag{1}$$

By measuring angular distributions of unpolarized cross section  $\sigma_0$  and analyzing powers  $T_{11}$ ,  $T_{20}$  and  $T_{22}$  it is possible to unambiguously determine two complex amplitudes. Since amplitude  $a_{11000}$  is strongly suppressed at LO, the observables  $\sigma_0$ ,  $T_{20}$  and  $T_{22}$  may be dominated by  $p$ -wave amplitude  $a_{22110}$ . However, the measurement of interference term in  $T_{11}$  should deliver information on the  $a_{11000}$  amplitude.

For the  $d + d \rightarrow d + d + \pi^0$  reaction in just  $s$  wave the cross section and analyzing powers are:

$$\begin{aligned}
36\pi\sigma_0 &= \frac{1}{3} b_{11000}^2 + \frac{5}{3} b_{11202}^2 + \frac{5}{7} b_{31202}^2 - \frac{2\sqrt{2}}{3} \Re (b_{11000} b_{11202}^*) + \\
&\quad + \frac{2}{\sqrt{7}} \Re (b_{11000} b_{31202}^*) \\
36\pi\sigma_0 T_{20} &= \frac{1}{3\sqrt{2}} b_{11000}^2 + \frac{1}{6\sqrt{2}} b_{11202}^2 + \frac{2}{7\sqrt{2}} b_{31202}^2 - \frac{2}{3} \Re (b_{11000} b_{11202}^*) + \\
&\quad + \frac{\sqrt{2}}{7} \Re (b_{11000} b_{31202}^*) - \frac{3}{\sqrt{7}} \Re (b_{11202} b_{31202}^*)
\end{aligned} \tag{2}$$

The amplitude  $b_{11000}$  is strongly suppressed at LO (similarly as  $a_{11000}$  due to the same spin structure). Therefore the measurement of the unpolarized cross section and analyzing power  $T_{20}$  for the  $d + d \rightarrow d + d + \pi^0$  reaction will deliver information on the LO allowed amplitudes  $b_{11202}$  and  $b_{31202}$ .

## 4 Break-up reaction $d + d \rightarrow d + p + n$

The break-up reaction  $d + d \rightarrow d + p + n$  conserves charge symmetry since it cannot be distinguished from the process with all protons exchanged to neutrons and vice versa. Studies of this reaction offer many advantages over other processes in which CSB may be investigated [13]. One of the important topics is systematic investigation of the CSB induced by the Coulomb effects. Therefore a deconvolution of these effects from CSB induced by strong interaction might be possible. This will be of great importance for the analysis of CSB in the  $d + d \rightarrow \alpha + \pi^0$  and  $d + d \rightarrow d + d + \pi^0$  reactions. Using simplified

model it was shown [14] that the entrance channel Coulomb interaction in the  $d + d \rightarrow \alpha + \pi^0$  reaction may lead to CSB comparable in magnitude to the contributions from other effects.

Up to now the charge symmetry breaking in this reaction was studied only at very low energy [13]. The measurement for beam energy of 12 MeV was performed for very limited range of angular configurations of the coinciding particles (only in the region close to quasi-free scattering). With quite low statistic it was not possible to derive final conclusion on observation of CSB effects.

If charge symmetry holds, all observables should demonstrate proper symmetries under exchange of all protons to neutrons and vice versa. However, a precise comparison of the cross sections is not possible, since they are affected by efficiency of the detection system, introducing large systematic uncertainty. Therefore the best observables to search CSB are analyzing powers. They are measured always relatively, therefore most of the systematic uncertainties cancel and high precision data may be obtained. If charge symmetry holds, all analyzing powers  $T_{ij}$  for  $d - p$  and  $d - n$  coincidences should be equal along the kinematical curve (described by the arc length  $S$ ) for given polar and azimuthal angles  $\theta_d$  for deuterons and  $\theta_p, \phi_p$  and  $\theta_n, \phi_n$  for protons and neutrons:

$$T_{ij}(\theta_d, \theta_p = \theta, \phi_p = \phi, S) = T_{ij}(\theta_d, \theta_n = \theta, \phi_n = \phi, S). \quad (3)$$

In the case of  $p - n$  coincidences the tensor analyzing powers should be symmetric while the vector analyzing power should be antisymmetric about the point where proton and neutron energies  $E_p$  and  $E_n$  are equal:

$$\begin{aligned} T_{ij}(\theta_p = \theta, \theta_n = -\theta, E_p = E_1, E_n = E_2) = \\ = (-1)^i T_{ij}(\theta_p = \theta, \theta_n = -\theta, E_p = E_2, E_n = E_1). \end{aligned} \quad (4)$$

## 5 Measurements with WASA at COSY

### 5.1 $d + d \rightarrow \alpha + \pi^0$ reaction

A possibility to perform measurements of the  $d + d \rightarrow \alpha + \pi^0$  reaction at WASA at COSY was studied very intensively [15]. The WASA detection system allows to measure both outgoing particles, registering  $\alpha$  particles and two  $\gamma$  quants from  $\pi^0$  decay. This kinematically over-constrained measurement put strong requirements for the analysis of the reaction of interest. However, due to the small cross section of few picobarn for the goal reaction,

the background conditions are of great importance. The major background problem arises from particle misidentification for  $\alpha$  from the investigated reaction and  ${}^3\text{He}$  produced with a large cross section in the  $d+d \rightarrow {}^3\text{He}+n+\pi^0$  reaction. It was shown [15] that this background may be efficiently reduced by applying all possible cuts and using kinematical constraints. This leads to the background contribution of only 3% in the observables identifying the  $d+d \rightarrow \alpha + \pi^0$  reaction.

## 5.2 $d + d \rightarrow d + d + \pi^0$ reaction

Similar studies were performed for the  $d+d \rightarrow d+d+\pi^0$  reaction. In this case the reaction will be identified by detecting two deuterons and two  $\gamma$  quanta from  $\pi^0$  decay. Also in this case the major background originates from the particles misidentification between deuterons and protons or tritons produced in the charge symmetry allowed  $d+d \rightarrow t+p+\pi^0$ ,  $d+d \rightarrow d+p+n+\pi^0$  and  $d+d \rightarrow p+p+n+n+\pi^0$  reactions. Since the measurement of the  $d+d \rightarrow d+d+\pi^0$  reaction is planned close to the threshold, a careful choice of the incident deuteron momentum may substantially reduce this background. The threshold beam momentum for the reaction of interest is 1.052 GeV/c and for the background reactions are: 1.035 GeV/c for the  $d+d \rightarrow t+p+\pi^0$ , 1.061 GeV/c for the  $d+d \rightarrow d+p+n+\pi^0$  and 1.071 GeV/c for the  $d+d \rightarrow p+p+n+n+\pi^0$  reactions. Therefore for the beam momentum of 1.061 GeV/c the only allowed background reaction is  $d+d \rightarrow t+p+\pi^0$ . At this beam momentum the available energy for the investigated reaction is  $Q=2.2$  MeV, while for the background reaction  $Q=6.2$  MeV. Then the expected ratio of the cross sections is  $\sigma(tp\pi^0)/\sigma(dd\pi^0) = 10^5$ . The background may be produced only when both deuterons are misidentified, one with triton and second with proton. This requirement leads to background reduction by a factor of  $10^4$ . Further reduction is obtained by proper cuts on the energy of the detected particles. It is shown in Fig. 1 that the  $d+d \rightarrow d+d+\pi^0$  reaction may be clearly distinguished from background by accepting deuterons with the energies within the interval where particles from the background reaction are not allowed. Such requirement eliminates the background completely and limits the acceptance for the investigated reaction only to about 50%.

## 5.3 $d + d \rightarrow d + p + n$ reaction

This reaction will be measured by detecting deuteron and proton in coincidence. Comparison of the analyzing powers for  $d-p$  and  $d-n$  coincidences will be performed for many angular configurations. Also tests of the symmetry of the tensor analyzing powers and antisymmetry of the vector analyzing

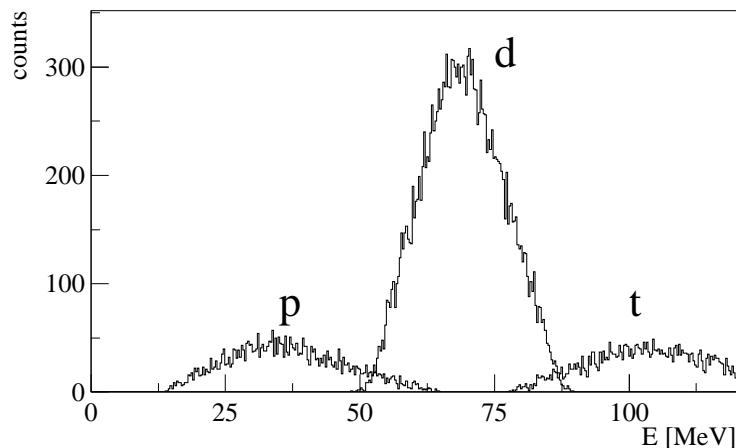


Figure 1: Energy of deuterons from the  $d + d \rightarrow d + d + \pi^0$  reaction and energies of tritons and protons from the  $d + d \rightarrow t + p + \pi^0$  background reaction. Cuts on particle identification and kinematical constraints were applied.

power will be performed for  $p - n$  coincidences. The energy and angles of the not detected neutron for  $d - n$  and  $p - n$  coincidences will be deduced from the registered proton and deuteron, respectively. The limited angular acceptance and threshold for deuteron and proton detection lead to an inhomogeneous acceptance. However, as seen in Fig. 2, almost the whole allowed region on the Dalitz plot is covered. Therefore the investigation of CSB in the whole kinematical region by comparison of  $d - p$  and  $d - n$  coincidences as well as for  $p - n$  coincidences is possible.

The features of the WASA at COSY offer very good conditions for CSB studies in deuteron break-up on deuteron target. The measurement may be performed simultaneously for all possible kinematical configurations. The CSB effect will be traced by comparison of the analyzing powers for various coincidences. The measurement will be relative, therefore knowledge of the beam intensity and polarization is not required and all systematic uncertainties cancel. Cross section for the break-up reaction is of the order of a millibarn, therefore large statistic may be reached. At beam energies close to the pion production threshold this break-up reaction is the only dominant process, therefore there will be virtually no background. Considering all these arguments implies that high precision may be reached, allowing to study CSB with exceptional precision.

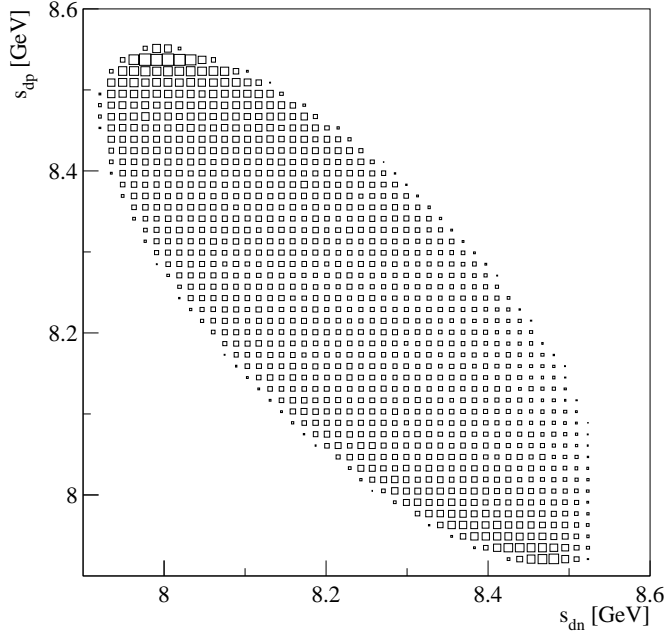


Figure 2: Dalitz plot for  $s_{dp}$  versus  $s_{dn}$  for the  $d + d \rightarrow d + p + n$  reaction. All cuts on angular acceptance and detection threshold were applied.

## 6 Summary

The experiments searching for charge symmetry breaking with WASA at COSY are discussed. The existing data on CSB and the theoretical analysis performed up to now show that new data on charge symmetry allowed reactions and on CSB reactions for the  $d + d$  system at higher beam momenta than available are badly needed. This defines the experimental strategy for CSB searches at COSY. The data for the charge symmetry allowed  $d + d \rightarrow {}^3A + N + \pi$  reaction, measured close to threshold, will be soon analyzed. The new measurement of this reactions, substantially above threshold, will be performed. In the next step, the charge symmetry forbidden reactions  $d + d \rightarrow \alpha + \pi^0$  and  $d + d \rightarrow d + d + \pi^0$  will be investigated. The vector and tensor polarized beam will be used, what enables a model independent extraction of the partial wave amplitudes for these reactions. Simultaneously, the analyzing powers for the break-up  $d + d \rightarrow d + p + n$  reaction in the whole kinematical region will be measured. It is demonstrated that WASA at COSY is an unique detection system that may deliver high quality data for all these reactions. By completing this investigation program, an extensive set of experimental data for reactions initiated from the  $d + d$  entrance chan-

nel will be provided. These data, together with a proper analysis within the chiral perturbation theory, will enable to understand the charge symmetry breaking effects on the quark level.

## References

- [1] G.A. Miller, B.M.K. Nefkens, I. Slaus, Phys. Rep. 194, 1 (1990).
- [2] E.J. Stephenson *et al.*, Phys. Rev. Lett. 91, 142302 (2003).
- [3] A.K. Opper *et al.*, Phys. Rev. Lett. 91, 212302 (2003).
- [4] U. van Kolck, J.A. Niskanen, G.A. Miller, Phys. Lett. B493, 65 (2000).
- [5] A. Gårdestig *et al.*, Phys. Rev. C 69, 044606 (2004).
- [6] A. Nogga *et al.*, Phys. Lett. B 639, 465 (2006).
- [7] G.A. Miller, A.K. Opper, E.J. Stephenson, Ann. Rev. Nucl. Part. Sci. 56, 253 (2006).
- [8] [www.physics.arizona.edu/~vankolck/coolerCSBtheory.html](http://www.physics.arizona.edu/~vankolck/coolerCSBtheory.html).
- [9] J.A. Niskanen, Few-body Systems 26, 241 (1999).
- [10] V. Hejny, A. Magiera, COSY Proposal 173.
- [11] V. Hejny, A. Magiera, COSY Proposal 139.
- [12] H.H. Adam *et al.* [WASA-at-COSY Collaboration], arXiv:nucl-ex/0411038.
- [13] C.R. Howell *et al.*, Phys. Rev. C48, 2855 (1993).
- [14] T.A. Lähde, G.A. Miller, Phys. Rev. C75, 055204 (2007).
- [15] P. Podkopał, AIP Conf. Proc. 950, 261 (2007).

# LATTICE APPROACH TO LIGHT SCALARS

*Craig McNeile*<sup>1</sup>

Department of Physics and Astronomy  
The Kelvin Building  
University of Glasgow  
Glasgow G12 8QQ  
U.K.

## Abstract

I report on lattice QCD calculations that study the properties of the  $a_0$  and  $f_0$  mesons.

## 1 Introduction

I review the recent lattice results for the light  $J^{PC} = 0^{++}$  scalar mesons. The interpretation of many  $0^{++}$  mesons in terms of quark and glue degrees of freedom is still not clear [1,2]. The  $0^{++}$  mesons potentially contain glueball, tetraquark, meson molecule or even quark-antiquark degrees of freedom. I have recently written a review [3] of light meson spectroscopy from lattice QCD, that contains more detail on many of the topics covered here.

### 1.1 Background to lattice QCD

The physical picture behind lattice QCD calculations is that an interpolating operator creates a hadron in the QCD vacuum and after a specific time interval the hadron is destroyed. The choice of interpolating operator is particularly important for hadrons where it is not clear how the hadron is built out of quarks and gluons.

For example, to create a light flavour singlet  $0^{++}$  hadron, possible interpolating operators are

$$O_1 = \bar{q}q \tag{1}$$

$$O_2 = \bar{q}\gamma_5 q \bar{q}\gamma_5 q \tag{2}$$

$$O_3 = U_{plaq} \tag{3}$$

---

<sup>1</sup>Current address.

Group	$n_f$	$m_{K_0}$ GeV
Prelovsek et al. [11]	2	$1.6 \pm 0.2$
McNeile and Michael [12]	2	1.1 – 1.2
Mathur et al. [13]	0	$1.41 \pm 0.12$
SCALAR [10]	0	$\sim 1.7$

Table 1: Lightest strange-light  $0^+$  meson from lattice QCD.

where  $U_{plaq}$  is a spatial plaquette of gauge fields with  $0^{++}$  symmetry, and  $q$  is a light quark operator.

The majority of recent lattice QCD calculations include the dynamics of sea quarks and have pion masses as low as 300 MeV [3]. The results I will present for scalar mesons largely use the last generation of lattice QCD calculations that are quenched or dynamical QCD calculations with pion masses above 500 MeV [4, 5].

There are a number of reasons that lattice calculations of the light scalar mesons are challenging. The lattice QCD correlators for scalar mesons are more noisy than for  $\rho$  and  $\pi$  mesons. The light scalar mesons decay via S-wave decays, and current lattice QCD calculations are in the quark mass regime where some decay channels to two mesons are open.

Eventually, the issue of dealing with resonances in lattice QCD will be dealt with by Lüscher's formalism [6] that produces scattering phase shifts. This year Lüscher's technique for resonances was applied to the  $\rho$  meson for the first time, by the CP-PACS collaboration [7].

## 1.2 The flavour non-singlet $0^{++}$ and $0^+$ mesons.

Although I am going to loop through the lattice results for the lightest  $0^{++}$  and  $0^+$  mesons, it is important to classify the states into SU3 multiplets or some other classification based on tetraquarks for example.

In the PDG the lightest strange-light  $0^+$  meson is the  $K_0(1430)$  [1]. There have also been claims that experimental data is consistent with  $0^+$   $I = 1/2$  meson called the  $\kappa$  with a mass of 660 MeV [9]. The existence of the  $\kappa$  is controversial, see [1, 2, 10] for a discussion.

In table 1 I collect results for the mass of the lightest  $0^+$   $\bar{s}q$  meson from lattice QCD calculations. The lattice results in table 1 are consistent with experimental mass of the  $K_0^*(1430)$ , but mostly miss the controversial  $\kappa$  particle. All the lattice calculations used  $\bar{s}q$  interpolating operators, so may have missed the  $\kappa$  state, if it is mostly a tetraquark state, with no overlap with  $\bar{s}q$  interpolating operators.

Experimentally the lightest  $I = 1$   $0^{++}$  mesons are the  $a_0(980)$  and the

Group	$n_f$	$m_{a_0}$ GeV
Bardeen et al. [14]	0	1.34(9)
Burch et al. [15]	0	$\sim 1.45$
Hart et al. [16]	2P	1.0(2)
Prelovsek et al. [11]	2	1.58(34)
Prelovsek et al. [11]	2P	1.51(19)
Mathur et al. [13]	0	1.42(13)

Table 2: A collection of results from lattice QCD for the mass of the lightest non-singlet  $0^{++}$  meson. The P stands for a partially quenched analysis.

$a_0(1450)$  [1]. There have been speculations that the  $a_0(980)$  meson is a molecule or tetraquark state [1, 2], so it is interesting to see whether lattice QCD calculations with  $\bar{q}q$  interpolating operators couple to the  $a_0(980)$  meson. In quenched QCD there is a ghost contribution [14], due to the  $\eta\pi$  contribution, to the scalar correlator that needs to be subtracted off the lattice data. I collect together some recent results for the mass of the light  $0^{++}$  meson from lattice QCD in table 2. I only include quenched data where the  $\eta\pi$  contribution has been corrected for [14].

McNeile and Michael [12], in an unquenched lattice QCD calculation focused on the mass difference (in the hope that systematics cancel), between the  $1^{+-}$  and the  $0^{++}$  mesons. The lattice calculation used gauge configurations from UKQCD [4] and CP-PACS [5]. The mass of the light  $1^{+-}$  state was always higher than the  $0^{++}$  meson. The final result was  $m_{b_1} - m_{a_0} = 221(40)$  MeV, compared to the experimental result of 245 MeV. Lang et al. recently reported masses for the lightest flavour non-singlet  $0^{++}$  consistent with the mass of the  $a_0(980)$  meson, from an unquenched lattice QCD calculation using chirally improved fermions [17].

The previous lattice QCD calculations, discussed in this section, were in a regime where the quark masses were large enough that the decay  $a_0 \rightarrow \eta\pi$  was forbidden. Now I discuss the new lattice QCD calculations where the decay  $a_0 \rightarrow \eta\pi$  is energetically allowed.

The MILC collaboration [18] originally claimed that they had evidence for  $a_0$  decay to  $\pi\eta$  from their calculations with improved staggered fermions. Other decays are discussed in [19]. Later work by the MILC [19] and UKQCD [20] collaborations showed that the lightest state in the flavour non-singlet  $0^{++}$  channel was actually below the  $\pi\eta$  threshold, with improved staggered fermions. This was puzzling, because experimentally the  $a_0 \rightarrow \pi\pi$  decay is forbidden by G parity.

In [21], Prelovsek explained the behaviour of the flavour non-singlet  $0^{++}$  correlator with improved staggered fermions using staggered chiral pertur-

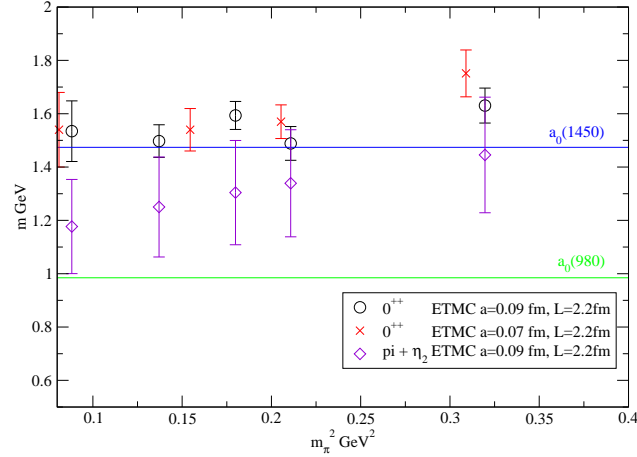


Figure 1: Mass of lightest state in  $0^{++}$  channel with  $\pi\eta_2$  decay threshold.

bation theory. Bernard, DeTar, Fu, and Prelovsek [22] extended the original analysis by Prelovsek, and also applied it to the flavour singlet  $f_0$  meson. A larger study, with more sea quark masses, is required to say something specific about the mass of the lightest  $a_0$  meson.

The ETM collaboration have preliminary results for the mass of the light  $0^{++}$  meson from a  $n_f=2$  unquenched lattice QCD calculation with twisted mass fermions [23–25]. In figure 1 I plot the mass of the light  $0^{++}$  meson and the  $\pi + \eta_2$  decay threshold as a function of the square of the pion mass. The mass of the  $\eta_2$  was computed by Michael and Urbach [24]. Figure 1 shows some evidence for the mass of the  $0^{++}$  tracking the  $\pi + \eta_2$  threshold, or at least for it being an open decay channel. The mass of  $0^{++}$  state is relatively independent of mass and consistent with the mass of  $a_0(1450)$  meson. As noted by Mathur et al. [13], the mass independence of  $0^{++}$  is consistent with closeness of the experimental masses of the  $a_0(1450)$  and  $K_0(1430)$ , if they are both part of the same  $SU3$  octet.

Although the preliminary results from the ETM collaboration are inconsistent with the results by Michael and McNeile [12], some caution is required. We are only just starting to deal with mesons with open decay channels in unquenched lattice QCD calculations. There is a of order 250 MeV difference between the mass of the lightest flavour singlet pseudoscalar meson in lattice QCD calculations with  $n_f = 2$  and  $n_f = 2 + 1$  sea quark flavours [3] and this will be important for the decay thresholds.

There are other quantities, other than masses, that can help determine the quark and glue content of scalar mesons. For example, Narison [26]

proposed to use the leptonic decay constant of the non-singlet  $0^{++}$  mesons to determine the structure of the  $a_0$  meson. The  $f_{a_0}$  decay constant of the light flavour non-singlet  $0^{++}$  meson has been computed using unquenched lattice QCD [12].

$$\langle 0 | \bar{q}q | a_0 \rangle = M_{a_0} f_{a_0} \quad (4)$$

See [12, 27, 28] for a further discussion of this decay constant and the connection with the electroweak current.

A molecule of two mesons should have a very small "wave-function" at the origin, hence  $f_{a_0}$  should be small. The definition of  $f_{a_0}$  is similar to that of the pion decay constant. Hence we mean "small" relative to 130 MeV. The other measured decay constants of pseudoscalar mesons are within a factor of 2.5 to the pion decay constant [1]. The only exception is the decay constant of the  $\pi(1300)$  that is suppressed [29, 30]. A large value for decay constant  $f_{a_0}$  does not rule out a  $\bar{q}q\bar{q}q$  multi-quark meson.

Using gauge configurations from UKQCD and CP-PACS, McNeile and Michael computed  $f_{a_0} \sim 480$  MeV. Sum rule and model estimates find  $f_{a_0}$  in the range 290 to 440 MeV [26, 28, 31, 32]. The  $f_{a_0}$  decay constant depends on the scale and this should be specified for a more detailed comparison.

Computing the decay width of a hadron is also very a valuable way of identifying a state on the lattice. In [12], it was reported that the experimental hadron coupling for the decays  $a_0(980) \rightarrow K\bar{K}$  and  $a_0(1450) \rightarrow K\bar{K}$  were 0.9 and 0.5 respectively. A lattice calculation [12] found that the lightest hadron in the  $0^{++}$  correlator had a coupling to  $K\bar{K}$  of  $\approx 1$ , thus providing additional evidence that the lightest state was the  $a_0(980)$ .

Pennington [33] has recently extracted the two photon decay width of the  $\sigma$  from experiment to be  $\Gamma(\sigma \rightarrow \gamma\gamma) \sim 4$  keV. Pennington notes that value of  $\Gamma(\sigma \rightarrow \gamma\gamma)$  can depend quite sensitively on the quark content of the  $\sigma$  [33]. Recently a formalism to compute two photon widths on the lattice has been developed [34]. Dudek and Edwards have computed  $\Gamma(\chi_0 \rightarrow \gamma\gamma) = 2.4 \pm 1.0$  keV, from a quenched QCD calculation [34]. It would be interesting to do a similar calculation for light scalar mesons.

### 1.3 Flavour singlet $0^{++}$ mesons

The spectrum of the light flavor singlet  $0^{++}$  mesons is where the  $0^{++}$  glueball is thought to be hiding out. The lightest flavor singlet  $0^{++}$  mesons listed in the PDG [1] are:  $f_0(600)$ ,  $f_0(980)$ ,  $f_0(1370)$ ,  $f_0(1500)$ , and  $f_0(1710)$ . There are claims that the  $f_0(980)$  is a molecule or tetraquark [1], so it may not couple to  $\bar{q}q$  interpolating operators.

Morningstar and Peardon [35] obtained  $M_{0^{++}} = 1730(50)(80)$  MeV for

the mass of the lightest  $0^{++}$  glueball from quenched QCD. Chen et al. [36] recently found  $M_{0^{++}} = 1710(50)(80)$  MeV. The quark model predicts that there should only be two  $0^{++}$  mesons between 1300 and 1800 MeV, so if the mixing between the glueball and  $\bar{q}q$  operators is weak, then the  $0^{++}$  glueball is hidden inside the  $f_0(1370)$ ,  $f_0(1500)$  and  $f_0(1710)$  mesons.

Weingarten and Lee [37] used quenched lattice QCD to estimate the mixing matrix between the glue and  $\bar{q}q$  states. Weingarten and Lee [37] predicted that the  $f_0(1710)$  meson was 74(10)%  $0^{++}$  glueball, and hence the mixing between the  $0^{++}$  glueball and  $\bar{q}q$  states was weak.

There are claims [38] that continuum phenomenology is more consistent with a sizable contributions from the  $0^{++}$  glueball to the  $f_0(600)$  and  $f_0(980)$  mesons.

The SESAM collaboration studied the glueball spectrum on unquenched lattices [39]. McNeile and Michael studied the light  $0^{++}$  spectrum with unquenched QCD [40] at a coarse lattice spacing and found the mass of the lightest flavour singlet  $0^{++}$  meson was very light. Using  $0^{++}$  glueball operators, Hart and Teper [41] found that

$$M_{0^{++}UNquenched} = 0.85(3)M_{0^{++}Quenched} \quad (5)$$

at a fixed lattice spacing of 0.1 fm. The UKQCD collaboration [20] separately studied  $0^{++}$  glueball and  $0^{++}$   $\bar{q}q$  operators on improved staggered gauge configurations, however higher statistics and an analysis similar to the one by Bernard et al. is required [22].

Unfortunately, the existing unquenched lattice QCD calculations of the flavour singlet  $0^{++}$  mesons don't have the range of lattice spacings where a continuum extrapolation can be attempted. In quenched QCD it was found that the lattice spacing dependence of the mass of the  $0^{++}$  glueball was strong. The use of a Symanzik improved gauge action by Chen et al. [36] and, Morningstar and Peardon [35], produced a slightly smaller slope with lattice spacing of the scalar  $0^{++}$  glueball mass, than for calculations that used the Wilson plaquette action. This is relevant to unquenched calculations, because any suppression of the mass of the flavour singlet  $0^{++}$  mass may be due to lattice spacing effects.

The SCALAR collaboration [42], used unquenched lattice QCD, with Wilson fermions and the Wilson gauge action, to study the  $0^{++}$  mesons. At a single lattice spacing a  $\sim 0.2$  fm, with  $\bar{q}q$  interpolating operators only, they obtain  $m_{\bar{q}q} \sim m_\rho$ . The lattice spacing dependence of this result needs to be quantified.

In unquenched QCD, both glue and  $\bar{q}q$  states will couple to singlet  $0^{++}$  mesons, so it is better to do a variational fit with both types of operators

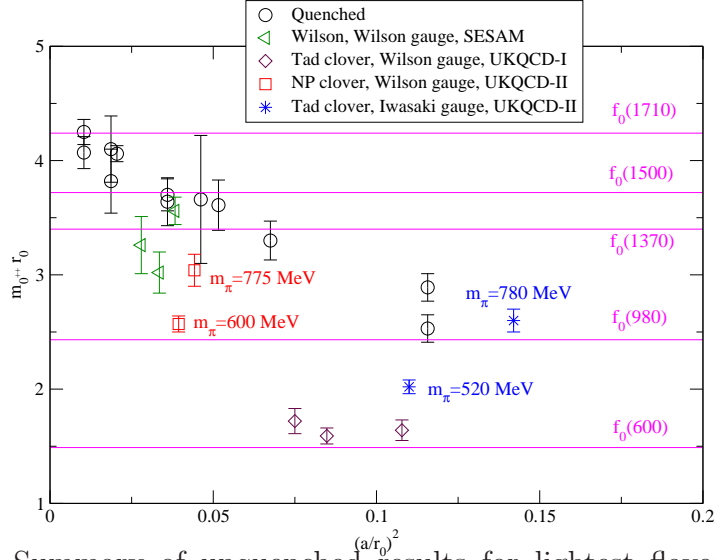


Figure 2: Summary of unquenched  $(a/r_0)^2$  results for lightest flavor singlet  $0^{++}$  mesons from [43]. The unquenched results are from SESAM [39], UKQCD-I [40], and UKQCD-II [43].

as basis interpolating operators. The variational technique analysis of the singlet  $0^{++}$  mesons was done by Hart et al. [43]. A combined fit to  $0^{++}$  glue and  $\bar{q}q$  interpolating operators with two types of spatial smearing sources was done. The calculation used the non-perturbative improved clover action at a single lattice spacing [4]. Configurations from CP-PACS [5] with the Iwasaki gauge action and tadpole improved clover action were also used in the analysis, because this calculation should be less affected by lattice artifacts. A summary plot of the results, in units of  $r_0$  ( $1/r_0 \sim 400$  MeV) is in figure 2 (updated from [43]). The data with the bursts and squares (with the pion masses written near them) in figure 2 shows an additional reduction of the mass of the  $0^{++}$  state over the pure glueball operators, as used by Hart and Teper [41].

Mathur et al. [13] recently claimed to get a result for the mass of the  $f_0(600)$  ( $\sigma$ ) from quenched lattice QCD with pion masses as low as 180 MeV. Using the interpolating operator  $\bar{\psi}\gamma_5\psi\bar{\psi}\gamma_5\psi$  they obtain  $m_{f_0(600)} \sim 550$  MeV. The key part of this work is a three state fit ( $\pi(p=0)\pi(p=0)$ ,  $f_0(600)$ ,  $\pi(p=\frac{2\pi}{L})\pi(p=\frac{-2\pi}{L})$ ) using the Bayes adaptive curve fitting algorithm [44]. They studied the finite volume effects to distinguish the signal for the resonance from the  $\pi\pi$  scattering states [45]. Mathur et al.'s [45] calculation is discussed in slightly more detail in [3]. The effect of sea quarks on this calculation needs to be quantified.

There has also been a recent quenched QCD study [46] of light  $0^{++}$  states with  $qq\bar{q}\bar{q}$  interpolating operators that did not see resonant states in the quark mass regime they explored.

In [43] an attempt was made to compute the decay width for  $f_0$  decay to two pions. Unfortunately much higher statistics will be required to obtain an accurate value for that width.

## 2 Conclusions

There is still no consensus as to whether  $\bar{q}q$  operators in lattice QCD calculations are coupling to the  $a_0(980)$  meson. To clear up the many questions about the spectrum of the  $0^{++}$  scalar mesons, unquenched lattice QCD calculations with tetraquark interpolating operators are required. There is “some” evidence that the flavour singlet  $0^{++}$  interpolating operators, in unquenched lattice QCD calculations, are coupling to states around or below 1 GeV [43]. Although a continuum extrapolation is required for definite results. Recent lattice QCD calculations that include the dynamics of the sea quarks are working with light enough quarks that the two meson decays of some scalar mesons are allowed [3, 24, 25].

## Acknowledgments

I thank Chris Michael for reading the paper. I thank the ETM collaboration for allowing me to use preliminary results for the  $a_0$  masses.

## References

- [1] K.F. Liu, (2007), arXiv:0706.1262 [hep-ph],
- [2] M.R. Pennington, Int. J. Mod. Phys. A21 (2006) 747, hep-ph/0509265,
- [3] C. McNeile, (2007), arXiv:0710.0985 [hep-lat],
- [4] UKQCD, C.R. Allton et al., Phys. Rev. D65 (2002) 054502, hep-lat/0107021,
- [5] CP-PACS, A. Ali Khan et al., Phys. Rev. D65 (2002) 054505, hep-lat/0105015,
- [6] M. Luscher, Nucl. Phys. B364 (1991) 237,

- [7] CP-PACS, S. Aoki et al., (2007), arXiv:0708.3705 [hep-lat],
- [8] Particle Data Group, W.M. Yao et al., J. Phys. G33 (2006) 1,
- [9] S. Descotes-Genon and B. Moussallam, Eur. Phys. J. C48 (2006) 553, hep-ph/0607133,
- [10] H. Wada et al., (2007), hep-lat/0702023,
- [11] S. Prelovsek et al., Phys. Rev. D70 (2004) 094503, hep-lat/0407037,
- [12] UKQCD, C. McNeile and C. Michael, Phys. Rev. D74 (2006) 014508, hep-lat/0604009,
- [13] N. Mathur et al., (2006), hep-ph/0607110,
- [14] W.A. Bardeen et al., Phys. Rev. D65 (2002) 014509, hep-lat/0106008,
- [15] T. Burch et al., Phys. Rev. D73 (2006) 094505, hep-lat/0601026,
- [16] UKQCD, A. Hart, C. McNeile and C. Michael, Nucl. Phys. Proc. Suppl. 119 (2003) 266, hep-lat/0209063,
- [17] R. Frigori et al., (2007), arXiv:0709.4582 [hep-lat],
- [18] C.W. Bernard et al., Phys. Rev. D64 (2001) 054506, hep-lat/0104002,
- [19] C. Aubin et al., Phys. Rev. D70 (2004) 094505, hep-lat/0402030,
- [20] E.B. Gregory et al., PoS LAT2005 (2006) 027, hep-lat/0510066,
- [21] S. Prelovsek, Phys. Rev. D73 (2006) 014506, hep-lat/0510080,
- [22] C. Bernard et al., (2007), arXiv:0707.2402 [hep-lat],
- [23] ETM, P. Boucaud et al., Phys. Lett. B650 (2007) 304, hep-lat/0701012,
- [24] ETM, .C. Michael and C. Urbach, (2007), arXiv:0709.4564 [hep-lat],
- [25] C. Urbach, (2007), arXiv:0710.1517 [hep-lat],
- [26] S. Narison, Phys. Rev. D73 (2006) 114024, hep-ph/0512256,
- [27] M. Diehl and G. Hiller, JHEP 06 (2001) 067, hep-ph/0105194,
- [28] H.Y. Cheng, C.K. Chua and K.C. Yang, Phys. Rev. D73 (2006) 014017, hep-ph/0508104,

- 
- [29] A. Holl, A. Krassnigg and C.D. Roberts, Phys. Rev. C70 (2004) 042203, nucl-th/0406030,
- [30] UKQCD, C. McNeile and C. Michael, Phys. Lett. B642 (2006) 244, hep-lat/0607032,
- [31] K. Maltman, Phys. Lett. B462 (1999) 14, hep-ph/9906267,
- [32] C.M. Shakin and H. Wang, Phys. Rev. D63 (2001) 074017,
- [33] M.R. Pennington, Mod. Phys. Lett. A22 (2007) 1439, arXiv:0705.3314 [hep-ph],
- [34] J.J. Dudek and R.G. Edwards, Phys. Rev. Lett. 97 (2006) 172001, hep-ph/0607140,
- [35] C.J. Morningstar and M.J. Peardon, Phys. Rev. D60 (1999) 034509, hep-lat/9901004,
- [36] Y. Chen et al., Phys. Rev. D73 (2006) 014516, hep-lat/0510074,
- [37] W.J. Lee and D. Weingarten, Phys. Rev. D61 (2000) 014015, hep-lat/9910008,
- [38] G. Mennessier et al., (2007), arXiv:0707.4511 [hep-ph],
- [39] TXL, G.S. Bali et al., Phys. Rev. D62 (2000) 054503, hep-lat/0003012,
- [40] UKQCD, C. McNeile and C. Michael, Phys. Rev. D63 (2001) 114503, hep-lat/0010019,
- [41] UKQCD, A. Hart and M. Teper, Phys. Rev. D65 (2002) 034502, hep-lat/0108022,
- [42] SCALAR, T. Kunihiro et al., Phys. Rev. D70 (2004) 034504, hep-ph/0310312,
- [43] UKQCD, A. Hart et al., Phys. Rev. D74 (2006) 114504, hep-lat/0608026,
- [44] Y. Chen et al., (2004), hep-lat/0405001,
- [45] N. Mathur et al., Phys. Rev. D70 (2004) 074508, hep-ph/0406196,
- [46] H. Suganuma et al., (2007), arXiv:0707.3309 [hep-lat],

# LOCAL QUARK-HADRON DUALITY IN ELECTRON SCATTERING

*W. Melnitchouk*  
Jefferson Lab  
Newport News, VA 23606  
USA

## Abstract

We present some recent developments in the study of quark-hadron duality in structure functions in the resonance region. To understand the workings of local duality we introduce the concept of truncated moments, which are used to describe the  $Q^2$  dependence of specific resonance regions within a QCD framework.

## 1 Introduction

Deep inelastic lepton-nucleon scattering is one of the most effective tools to study the quark and gluon substructure of the nucleon. Since the early days of QCD, deep inelastic scattering data have been successfully analyzed within the framework of the operator product expansion (OPE). At large photon virtuality  $Q^2$  and energy transfer  $\nu$ , the structure functions can be interpreted in terms of universal parton (quark and gluon) distribution functions.

Much of the initial focus was on reaching higher  $Q^2$  and exploring the small- $x$  region, where  $x = Q^2/2M\nu$  is the Bjorken scaling variable and  $M$  is the nucleon mass. However, recently attention has turned towards understanding the onset of scaling behavior in structure functions, and the dynamics of the transition from the region dominated by nucleon resonances at low hadron final state masses  $W$ . This has been motivated in part by the observation of the intriguing phenomenon of *Bloom-Gilman duality*, in which structure functions measured in the resonance region are found on average to be approximately equivalent to the scaling function which describes the high-energy data [1,2]. The equality between the resonance region (characterized by hadronic bound states) and the deep inelastic continuum (characterized by scattering from free quarks) is also referred to as *quark-hadron duality*.

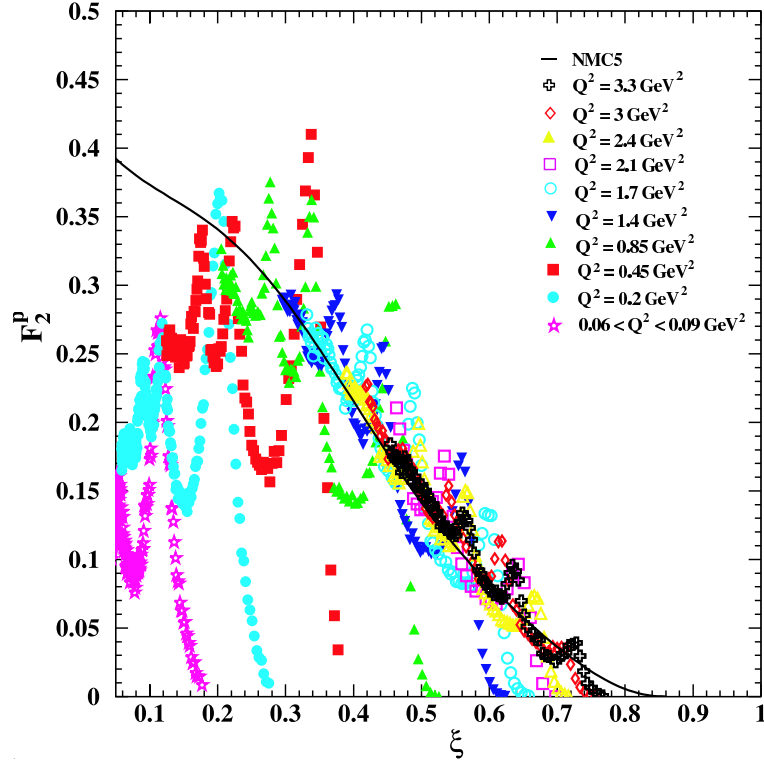


Figure 1: Proton  $F_2^p$  structure function data from Jefferson Lab and SLAC in the resonance region in the range  $0.06 < Q^2 < 3.30 \text{ GeV}^2$ , as a function of the Nachtmann scaling variable  $\xi$  [2]. The solid curve is a fit to deep inelastic data at the same  $\xi$  but higher ( $W^2, Q^2$ ), shown here at  $Q^2 = 5 \text{ GeV}^2$ .

First observed by Bloom and Gilman in the late 1960s [1], the duality between resonance and scaling functions has been spectacularly confirmed by recent high-precision data from Jefferson Lab on unpolarized and polarized structure functions. These have enabled the global and local aspects of Bloom-Gilman duality to be quantified, including its flavor, spin and nuclear medium dependence (see Ref. [3] for a review). Data on the proton  $F_2^p$  structure functions are illustrated in Fig. 1 in the resonance region for various  $Q^2$  values as a function of the Nachtmann scaling variable  $\xi = 2x/(1 + \sqrt{1 + 4M^2x^2/Q^2})$  [4]. The data strongly suggest that duality works remarkably well for each of the prominent, low-lying resonances to rather low values of  $Q^2$  ( $\sim 1 \text{ GeV}^2$ ).

The appearance of *global* duality in structure functions (*i.e.*, the weak  $Q^2$  dependence of moments at low  $Q^2$ ) implies strong cancellations between nucleon resonances, resulting in the dominance of the leading twist contribution

to the moments. Within the OPE the existence of duality is understood in terms of the suppression of higher twist ( $\propto 1/Q^{2n}$  with  $n \geq 1$ ) contributions to moments of structure functions [5, 6]. However, while the OPE can be used to describe the global aspects of duality in terms of moments, the similarity of the resonance and scaling functions in individual resonance regions, over restricted regions of  $x$  (or  $W$ ) — termed *local* duality — is difficult to understand from QCD.

To see how such cancellations may take place, simple models have been considered recently [7–9], in which the resonance transitions can be evaluated exactly and the degree to which duality holds quantified. Although this can yield clues as to how local duality can arise in nature, the connection with QCD is still not very clear. In this talk, we describe a new approach to local Bloom-Gilman duality, in terms of *truncated* moments of structure functions, which allow one to follow the  $Q^2$  evolution of specific resonances, or resonance regions, explicitly [10, 12–17]. With the evolution equations obtained from perturbative QCD, the analysis in terms of truncated moments offers the first direct connection between local duality and QCD.

## 2 Duality and the OPE

Before the advent of QCD, quark-hadron duality in structure functions was interpreted in the context of finite-energy sum rules, in analogy with the  $s$ - and  $t$ -channel duality observed in hadron-hadron scattering. In QCD, this duality is understood in the language of the operator product expansion, in which moments of structure functions are organized in powers of  $1/Q^2$ . For the  $F_2$  structure function, for example, one has for the  $n$ -th moment:

$$M_2^{(n)}(Q^2) = \int_0^1 dx x^{n-2} F_2(x, Q^2) \quad (1)$$

$$= \sum_{\tau=2}^{\infty} \frac{A_{\tau}^{(n)}(\alpha_s(Q^2))}{Q^{\tau-2}}, \quad (2)$$

where  $A_{\tau}^{(n)}$  are the matrix elements of operators with twist  $\leq \tau$  (where twist is defined as the mass dimension minus the spin,  $n$ , of the operator).

The leading term in Eq. (2) is associated with free quark scattering, and is responsible for the scaling of structure functions, while the  $1/Q^{\tau-2}$  terms involve nonperturbative, long-distance interactions between quarks and gluons. The weak  $Q^2$  dependence of the low moments of the structure function is then interpreted as indicating that the non-leading,  $1/Q^2$ -suppressed, interaction terms do not play a major role even at low  $Q^2$ .

An important consequence of duality is that the strict distinction between the resonance and deep inelastic regions becomes entirely artificial. To illustrate this, consider that at  $Q^2 = 1 \text{ GeV}^2$  around 2/3 of the total cross section comes from the resonance region,  $W < 2 \text{ GeV}$  [6]. However, the resonances and the deep inelastic continuum conspire to produce only about a 10% higher-twist correction to the lowest moment of the scaling  $F_2$  structure function at the same  $Q^2$ . Even though each resonance is built up from a multitude of twists, when combined the resonances interfere in such a way that they resemble the leading-twist component [8].

This by itself is quite a remarkable observation. But how can it be made useful in practice? If the degree to which duality holds, or the extent to which duality is violated, is understood, then the resonance data, when properly averaged, can be used to extract information on the leading-twist (scaling) parts of structure functions. Furthermore, if the inclusive–exclusive connection via local duality is taken seriously, one can relate structure functions measured in the resonance region to electromagnetic transition form factors [1, 11].

### 3 Truncated Moments

While “global duality” — the duality for structure function moments — can be analyzed in terms of the OPE, a simple interpretation of “local duality” — the  $x$  dependence of the functions themselves, or for integrals over restricted regions of  $x$  — is elusive. Attempts have been made to understand the emergence of a scaling function from resonances within QCD-inspired models of the nucleon, which have shed some light on the possible dynamics behind the emergence of local duality [7–9].

Recently it was found that local quark-hadron duality can be studied within a perturbative QCD context in terms of *truncated* moments of structure functions, which are integrals of structure functions over restricted intervals of  $x$  (or  $W$ ) [10, 12–17]. For the  $F_2$  structure function, the  $n$ -th truncated moment for the interval  $x_{\min} \leq x \leq x_{\max}$  is defined as:

$$\mathcal{M}^{(n)}(x_{\min}, x_{\max}, Q^2) = \int_{x_{\min}}^{x_{\max}} dx x^{n-2} F_2(x, Q^2) . \quad (3)$$

In the limit  $x_{\min} \rightarrow 0$  and  $x_{\max} \rightarrow 1$ , one recovers the usual (full) moment of Eq. (1),  $\mathcal{M}^{(n)}(0, 1, Q^2) \rightarrow M_2^{(n)}(Q^2)$ .

The remarkable feature of the truncated moments is that they obey  $Q^2$  evolution equations which are similar to the DGLAP evolution equations for parton distribution functions. In particular, the evolution equation for the

$n$ -th truncated moment can be written as [10, 15]:

$$\frac{d\mathcal{M}_n(x_{\min}, x_{\max}, Q^2)}{dt} = \frac{\alpha_s(Q^2)}{2\pi} (P'_n \otimes \mathcal{M}_n)(x_{\min}, x_{\max}, Q^2), \quad (4)$$

where  $\otimes$  denotes convolution, and  $P'_n$  is defined in terms of the QCD splitting function  $P$  as:

$$P'_n(z, \alpha_s(Q^2)) = z^n P(z, \alpha_s(Q^2)). \quad (5)$$

The truncated moments therefore satisfy DGLAP-like evolution with a modified splitting function  $P \rightarrow P'_n$ .

The truncated moments can be used to determine the extent to which nucleon structure function data in specific regions in  $x$  (or  $W$ ) are dominated by leading twists [10]. This is done by constructing empirical truncated moments and evolving then to a different  $Q^2$  using the evolution equations in Eq. (4). Deviations of the evolved moments from the experimental data at the new  $Q^2$  then reveal any higher twist contributions in the original data.

Psaker *et al.* [10] have analyzed recent data on the proton  $F_2$  structure function from Jefferson Lab, from which moments were constructed at a range of  $Q^2$  values, from  $Q^2 \sim 1 \text{ GeV}^2$  up to  $9 \text{ GeV}^2$ . The data at low  $Q^2$  contain significant contributions arising from kinematical effects associated with finite values of  $Q^2/\nu^2 = 4M^2x^2/Q^2$ . These so-called “target mass corrections” are formally related to twist-two operators, and hence contain no additional information on nonperturbative multi-parton correlations. In the literature there are well known approaches for how to remove the target mass effects, and here this is done by applying the standard TMC prescription from Ref. [18] (see also Ref. [19] for a recent review).

To determine the extent to which the  $F_2$  data at low  $Q^2$  are dominated by leading twist, one assumes that the data at the highest  $Q^2$  value available, namely  $Q^2 = 9 \text{ GeV}^2$ , contain only twist-2 contributions. After evolving down to  $Q^2 = 1 \text{ GeV}^2$  and applying the target mass corrections, the truncated moments are compared with the actual data at  $1 \text{ GeV}^2$ . Preliminary results indicate the presence of higher twists in the data at  $Q^2 = 1 \text{ GeV}^2$ . To quantify the higher twist content of the truncated moments in various resonance regions, several intervals in  $W$  are considered:  $W_{\text{th}}^2 \leq W^2 \leq 1.9 \text{ GeV}^2$ , corresponding to the  $\Delta(1232)$  (or first) resonance region (where  $W_{\text{th}} = M + m_\pi$  is the inelastic threshold);  $1.9 \leq W^2 \leq 2.5 \text{ GeV}^2$  for the  $S_{11}(1535)$  (or second) resonance region; and  $2.5 \leq W^2 \leq 3.1 \text{ GeV}^2$  for the  $F_{15}(1680)$  (or third) resonance region.

The results for the  $n = 2$  moment generally indicate deviations from leading twist behavior at the level of  $\lesssim 20\%$  for all  $Q^2 \geq 0.75 \text{ GeV}^2$ , with

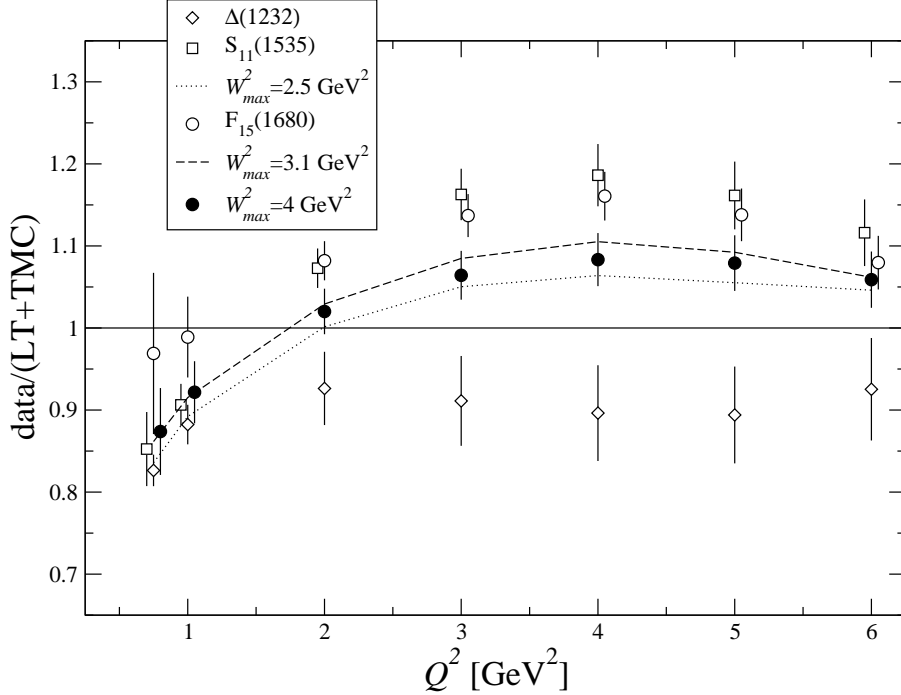


Figure 2:  $Q^2$  dependence of the ratio of truncated moments  $\mathcal{M}_2$  calculated from the data and from leading twist evolution from  $Q^2 = 9 \text{ GeV}^2$  (including target mass corrections), for various intervals in  $W$ . (Some of the points are offset slightly for clarity.) From Psaker *et al.* [10].

significant  $Q^2$  dependence for  $Q^2 \lesssim 3 \text{ GeV}^2$ , decreasing at larger  $Q^2$ . In the  $\Delta$  region (diamonds), the higher twist contributions are approximately  $-10\%$  of the total. For the  $S_{11}$  region (squares), on the other hand, the higher twists constitute  $\lesssim +15\%$  of the total moment (except at  $Q^2 \leq 1 \text{ GeV}^2$ , where the higher twists change sign). Combined, the higher twist contribution from first two resonance regions (dotted curve) is  $\approx 5\%$  at  $Q^2 = 4 \text{ GeV}^2$ . The higher twist content of the  $F_{15}$  region (open circles) appears to be similar to the  $S_{11}$  within errors, and the first three resonance regions combined (dashed curve) contribute  $\lesssim 10\%$  for  $Q^2 > 1 \text{ GeV}^2$ . Integrating up to  $W_{\text{max}}^2 = 4 \text{ GeV}^2$ , the data on the  $n = 2$  truncated moment are found to be leading twist dominated at the level of  $90 - 95\%$  for  $Q^2 > 1 \text{ GeV}^2$ .

The overall magnitude of the higher twists for the higher moments is

qualitatively similar to the  $n = 2$  moments, however, the  $Q^2$  values at which they start decreasing in importance are larger. At low  $Q^2$  values the higher twist contributions are also relatively larger for higher moments: at  $Q^2 = 1 \text{ GeV}^2$ , for example, the magnitude of the higher twist component of the  $W^2 < 4 \text{ GeV}^2$  region increases from  $\sim 15\%$  for the  $n = 2$  moment, to  $\sim 25\%$  for  $n = 4$ , and  $> 40\%$  for  $n = 6$ . This behavior can be understood from the relatively greater role played by the nucleon resonances and the large- $x$  region, which is emphasized more by the higher moments.

The relatively small size of the higher twists at scales  $\sim 1 \text{ GeV}^2$  is consistent with the qualitative observations made in earlier data analyses about the approximate validity of Bloom-Gilman duality [2]. The truncated moment analysis is able to for the first time quantify the degree to which this duality holds as a function of  $Q^2$ . The fact that duality works better (*i.e.* higher twists are smaller) when more resonances are included has also been borne out in quark model studies [7–9] (see also Ref. [3] and references therein).

## 4 Conclusion

Structure functions at low  $Q^2$  provide fertile ground for studying the transition from perturbative to nonperturbative QCD dynamics. The dramatic empirical confirmation of Bloom-Gilman duality in inclusive electron–nucleon scattering has stimulated considerable interest in understanding the dynamical origins of duality and of low  $Q^2$  physics in general.

We have outlined here how the operator product expansion can be used to understand the qualitative features of global duality in terms of moments of structure functions. The phenomenon of quark-hadron duality appears to go further beyond this, however, and a non-trivial connection is found to exist between resonance and scaling functions for individual resonance regions. Understanding the emergence of this *local* duality from first principles is considerably more challenging, and to date the only attempts to do so have been within QCD-inspired models of the nucleon — which at best can only serve to give us clues as to the underlying dynamics.

In this talk we have described a new approach to local duality in terms of *truncated* moments of structure functions. The crucial feature of these moments is that they obey  $Q^2$  evolution equations similar to the DGLAP equations obeyed by parton distribution functions. The same techniques for evolving the parton distributions can therefore be used for the truncated moments.

We find that at a scale of  $Q^2 = 1 \text{ GeV}^2$  the  $\Delta$  resonance region contains about  $-10\%$  higher twist contributions to the total  $n = 2$  moment. The

higher twists in the first and second resonance regions are positive, each contributing  $\lesssim +15\%$  higher twist to the moment. Combined, the entire nucleon resonance region up to  $W_{\max}^2 = 4 \text{ GeV}^2$  contains about 5 – 10% higher twist for  $Q^2 > 1 \text{ GeV}^2$ . Similar behavior is found also for the  $n = 4$  and  $n = 6$  truncated moment ratios, where the relatively greater role played by the resonances due to the large- $x$  enhancement means larger higher twists at the same  $Q^2$ .

These results represent the first quantitative determination of higher twists in individual resonance regions within a QCD framework. This work thus opens the way to further study of local duality in other structure functions, such as the longitudinal structure function  $F_L$  or spin-dependent structure functions.

## Acknowledgments

I thank Ales Psaker, Thia Keppel and Eric Christy for their collaboration on the truncated moment analysis present here. This work is supported by the U.S. DOE Contract No. DE-AC05-06OR23177, under which Jefferson Science Associates, LLC operates the Thomas Jefferson National Accelerator Facility.

## References

- [1] E. D. Bloom and F. J. Gilman, *Phys. Rev. Lett.* **25**, 1140 (1970).
- [2] I. Niculescu *et al.*, *Phys. Rev. Lett.* **85**, 1182, 1186 (2000).
- [3] W. Melnitchouk, R. Ent and C. Keppel, *Phys. Rept.* **406**, 127 (2005).
- [4] O. Nachtmann, *Nucl. Phys.* **B 63**, 237 (1973).
- [5] A. De Rujula, H. Georgi and H. D. Politzer, *Phys. Rev.* **D 15**, 2495 (1977).
- [6] X. D. Ji and P. Unrau, *Phys. Rev.* **D 52**, 72 (1995).
- [7] F. E. Close and N. Isgur, *Phys. Lett.* **B 509**, 81 (2001).
- [8] N. Isgur, S. Jeschonnek, W. Melnitchouk and J. W. Van Orden, *Phys. Rev.* **D 64**, 054005 (2001).
- [9] F. E. Close and W. Melnitchouk, *Phys. Rev.* **C 68**, 035210 (2003).

- [10] A. Psaker, W. Melnitchouk, M. E. Christy and C. E. Keppel, in preparation.
- [11] W. Melnitchouk, *Phys. Rev. Lett.* **86**, 35 (2001).
- [12] S. Forte and L. Magnea, *Phys. Lett.* **B 448**, 295 (1999).
- [13] S. Forte, L. Magnea, A. Piccione and G. Ridolfi, *Nucl. Phys.* **B 594**, 46 (2001).
- [14] A. Piccione, *Phys. Lett.* **B 518**, 207 (2001).
- [15] D. Kotlorz and A. Kotlorz, *Acta Phys. Polon.* **B 36**, 3023 (2005).
- [16] D. Kotlorz and A. Kotlorz, *Eur. Phys. J.* **C 48**, 457 (2006).
- [17] D. Kotlorz and A. Kotlorz, *Phys. Lett.* **B 644**, 284 (2007).
- [18] H. Georgi and H. D. Politzer, *Phys. Rev.* **D 14**, 1829 (1976).
- [19] I. Schienbein *et al.*, arXiv:0709.1775 [hep-ph], to appear in *J. Phys. G*.

## TWO-PION-EXCHANGE EFFECTS IN $pp \rightarrow pp\pi^0$ REACTION

*F. Myhrer*

Dept. of Physics and Astronomy  
University of South Carolina  
Columbia, SC 29208, USA

### Abstract

We study the  $pp \rightarrow pp\pi^0$  reaction near threshold based on heavy-baryon chiral perturbation theory. We show that the two-pion-exchange diagrams give much larger contribution than the one-pion-exchange diagram which is of lower chiral order in Weinberg's counting scheme. We also discuss the relation of our results to the momentum counting scheme.

The near-threshold  $pp \rightarrow pp\pi^0$  reaction has been attracting much theoretical attention, ever since experimental data of extremely high quality became available [1]. The heavy-baryon chiral perturbation theory (HB $\chi$ PT) offers a possible systematic approach to the investigation of this reaction. A motivation of this study may be stated in reference to the generic  $NN \rightarrow NN\pi$  processes near threshold. Although HB $\chi$ PT presupposes the small size of its expansion parameter  $Q/\Lambda_\chi$ , the pion-production reactions involve somewhat large energy- and three-momentum transfers even at threshold ( $\mathbf{p}^2 \sim m_\pi m_N$ ). Therefore, the application of HB $\chi$ PT to the  $NN \rightarrow NN\pi$  reactions may involve some delicate aspects, but this also means that these processes may serve as a good test case for probing the limit of applicability of HB $\chi$ PT. Apart from this general issue, a specific aspect of the  $pp \rightarrow pp\pi^0$  reaction makes its study particularly interesting. For most isospin channels, the  $NN \rightarrow NN\pi$  amplitude near threshold is dominated by the pion rescattering diagram where the  $\pi N$  scattering vertex is given by the Weinberg-Tomozawa term, which represents the lowest order contribution. However, a quantitatively reliable description of the  $NN \rightarrow NN\pi$  reactions obviously requires detailed examinations of the corrections to this dominant amplitude. Meanwhile, since the Weinberg-Tomozawa vertex does not contribute to the pion-nucleon rescattering diagram for  $pp \rightarrow pp\pi^0$ , this reaction is particularly sensitive to higher order contributions and hence its study is expected to

provide valuable information to guide us in formulating a quantitative description of all the  $NN \rightarrow NN\pi$  reactions.

At threshold the strong (and Coulomb)  $pp$  initial and final state interactions have to be considered in these reactions. In our DWBA evaluation the nuclear transition operators are derived using HB $\chi$ PT, whereas the initial and final state nuclear wave functions are calculated in the standard nuclear physics approach (SNPA). A serious problem encountered in performing such a *hybrid*  $\chi$ PT (for short called EFT\* below) calculation of pion production is that the calculation involves uncomfortably high momentum components which are present in the nuclear wave functions. The occurrence of these high-momentum components goes against the tenet of  $\chi$ PT, which presupposes the existence of a momentum cutoff scale,  $\Lambda_\chi \simeq 1$  GeV/c. The high momenta arise from two sources. The first source is the large momentum components contained in the distorted initial and final wave functions generated by a so-called high-precision phenomenological NN-potential,  $V_{NN}$ ; see e.g. Ref. [2](b). The second source of the high momentum behavior originates from higher powers of momentum terms which appear in the transition amplitudes generated by higher  $\chi$ PT diagrams [3,4]. Below we will focus our discussion on these transition amplitudes.

In order to eliminate from the  $NN$  wave functions the high-momentum components that lie above the original cutoff scale of  $\chi$ PT, a suitably parameterized cutoff factor is introduced (we make certain the observables are independent of this cut-off). This is admittedly an operational remedy, the foundation of which needs to be examined from a formal point of view. It is also informative and of practical value to examine the use of the “low-momentum regime NN potential”,  $V_{low-k}$  [5–7].  $V_{low-k}$  is derived from  $V_{NN}$  by integrating out the high-momentum components contained in  $V_{NN}$ . Since  $V_{low-k}$  by construction is free from high-momentum components, its use in an EFT\* calculations for pion production should alleviate the “high momentum problem” that plagued the past DWBA calculations. From a purist’s point of view this may not be a totally satisfactory approach but we believe that this “pragmatic” method still has its merits. We remark that, as is well known,  $V_{low-k}$ s generated from any realistic phenomenological potential lead to practically equivalent half-off-shell NN K-matrices and hence the same NN wave function.

We derived the TPE transition amplitude operators [3] using Weinberg’s chiral counting scheme with expansion parameter  $\epsilon \simeq m_\pi/m_N \simeq 0.15$ . We isolated the high-momentum components of these amplitudes using an asymptotic expansion, see Refs. [8,9]. Hanhart and Kaiser [4] used the

momentum counting scheme (MCS) [10, 11] to evaluate TPE diagrams for the reaction  $NN \rightarrow NN\pi$ . The MCS has the expansion parameter  $\tilde{\epsilon} \simeq (m_\pi/m_N)^{1/2} \simeq 0.39$ . Unlike Weinberg’s chiral counting a subtlety in MCS is that loop diagrams of a given order  $\nu$  in  $\tilde{\epsilon}$  not only contains a contribution of order  $\nu$  (the “leading” part) but, in principle, can also involve contributions of higher order in  $\tilde{\epsilon}$  (“sub-leading” parts). Hanhart and Kaiser evaluated the “leading” part of the lowest MCS-order TPE diagrams and showed that the “leading” parts of the two-pion exchange diagrams, when summed up, cancel among themselves, see also Ref. [12]. We [14] identified the “leading” part of our TPE operators [3] and confirmed this cancellation [8, 9]. As will be discussed below, we have found however that the remainder, or the “sub-leading” parts, of the TPE amplitudes can be at least as large as the one-pion rescattering amplitude [8, 9]. We consider it important to re-examine the behavior of MCSOs “sub-leading” parts of these TPE diagrams in order to see whether they can still be as large as indicated by the phenomenological SNPA success of the Lee-Riska heavy-meson exchange mechanism. In a forthcoming publication [13] we will also consider other chiral correction amplitudes including the contributions from counter-terms needed to regulate the UV behavior of the TPE loop diagrams.

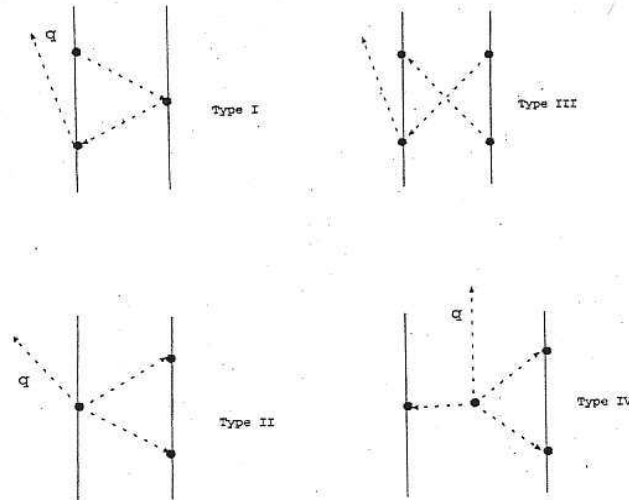


Figure 1: The two-pion-exchange loop-diagrams discussed in the text.

The one-pion loop  $pp \rightarrow pp\pi^0$  transition operators were evaluated analytically by Ref. [3] using HB $\chi$ PT. When these operators are sandwiched with phenomenological determined distorted initial and final  $NN$  wave functions,

we find that the momentum integrals convergence very slowly [8, 14]. This slow convergence can easily be understood when we adopt the threshold fixed kinematics approximation (*FKA*) to evaluate the amplitudes. We impose the *FKA* on the analytic expressions for the transition operators of the different TPE diagrams are given in Ref. [3] and make an asymptotic expansion in the two-nucleon momentum transfer  $\mathbf{k}$ , i.e.  $|\mathbf{k}| = |\mathbf{p} - \mathbf{p}'| \rightarrow \infty$ . The transition operator matrix  $T$  of the TPE diagrams is of the form

$$T = \left( \frac{g_A}{f_\pi} \right) (\boldsymbol{\Sigma} \cdot \mathbf{k}) t(p, p', x) \quad (1)$$

where  $x = \hat{p} \cdot \hat{p}'$ . The generic *asymptotic* behavior for  $t(p, p', x)$  is [14]:

$$t(p, p', x) \stackrel{k \rightarrow \infty}{\sim} t_1 (g_A / (8f_\pi^2))^2 |\mathbf{k}| + t_2 \ln[\Lambda^2 / |\mathbf{k}|^2] + t_3 + \delta t(p, p', x), \quad (2)$$

where  $t_3$  is asymptotically  $k$ -independent, and  $\delta t(p, p', x)$  is  $\mathcal{O}(k^{-1})$ . For each of Types I  $\sim$  IV, analytic expressions for  $t_i$ 's ( $i = 1, 2, 3$ ) can be extracted [14] from the amplitudes  $T$  given in Ref. [3]. The first term with  $t_1$  in eq.(2) is the ‘‘leading’’ term in MCS discussed by HK [4], whereas the remaining terms, which we refer to as the ‘‘sub-leading’’ terms, were not considered by HK.

Table 1: For the four types of TPE diagrams,  $K = \text{I, II, III and IV}$ , the second row gives the value of  $t_1$  defined in eq.(2), and the third row gives the ratio  $R_K = T_K / T_{Resc}$ , where  $T_K$  is the plane-wave matrix element of  $T$  in eq.(1) for Type  $K$ , and  $T_{Resc}$  is the lowest chiral order one-pion-exchange rescattering (Resc) amplitude. The last row gives  $R_K^* = T_K^* / T_{Resc}$ , where  $T_K^*$  is the plane-wave matrix element of  $T$  in eq.(1) with the  $t_1$  term in eq.(2) subtracted.

Type of diagrams : $K =$	I	II	III	IV	Sum
$(t_1)_K \propto$	0	-1	-1/2	3/2	0
$R_K$	-0.70	-6.54	-6.60	9.19	-4.65
$R_K^*$	-0.70	-0.82	-3.73	0.60	-4.65

In Table 1, the second row shows that the ‘‘leading’’ parts in the MCS  $\propto t_1$  of the TPE diagrams I  $\sim$  IV sum to zero. This confirms the finding of Hanhart and Kaiser [4]. In the third row marked  $R_K$ , and using *FKA*, we give the values of the ratio of the transition amplitude in Ref. [3] to the rescattering amplitude in the plane wave approximation for the four TPE amplitudes. We note that the sum of the TPE amplitudes are non-zero. The magnitude of the sum reflects the size of the ‘‘sub-leading’’ parts of the TPE amplitudes. In the fourth row we have removed the ‘‘leading’’ term,  $t_1$  from  $t(p, p', x)$  in Eq.(1) and then evaluated the similar ratio  $R_K^*$ . We observe that

the sum of the four modified TPE amplitudes (II, III and IV) is larger than the rescattering amplitude [8]. This can also be inferred from the  $R_K$  row of the table where the ratios of the amplitudes II:III:IV are about -2:-2:3, whereas the ratios of the corresponding amplitudes  $\tilde{O}$  “leading” terms are -2:-1:3. However, the evaluations of the different diagrams appear to confirm that the magnitudes of the different diagrams follow the momentum counting rule as indicated in Table 11 of Ref. [15].

Next we investigate the behavior of the TPE diagrams as we go beyond the plane-wave approximation by using distorted waves (DW) for the initial- and final-state NN wave functions. For formal consistency we should use the NN potential recently derived from HB $\chi$ PT [16,17], but as discussed earlier we adopt here EFT\*. As argued earlier, in order to stay close to the spirit of HB $\chi$ PT, we introduce a Gaussian momentum regulator,  $\exp(-p^2/\Lambda_G^2)$ , in the initial and final distorted wave integrals, suppressing thereby the high momentum components of the phenomenological NN potentials, e.g. the Bonn [18] or Nijmegen potential [19]. We require that  $\Lambda_G$  be larger than the characteristic momentum scale of the  $NN \rightarrow NN\pi$  reactions,  $|\mathbf{p}| \sim \sqrt{m_\pi m_N} \simeq 360$  MeV/c, but it should not exceed the chiral scale  $\Lambda_\chi \sim 1$  GeV/c. Part of the work to implement the idea of utilizing a low-momentum regime NN potential has been published [20] where use was made of  $V_{low-k}$ . One issue regarding the use of Stony Brook’s  $V_{low-k}$  in the present context is that it is derived with a rather low value of the cutoff parameter,  $p_{max} = 2$  fm $^{-1}$ , which is very close to the threshold momentum for the  $NN \rightarrow NN\pi$  reactions. We therefore have extended the  $V_{low-k}$  potential to cases where the momentum cut-off  $p_{max}$  is allowed to be larger than the original Stony Brook value up to 5 fm $^{-1}$  (this value corresponds to the chiral scale,  $\Lambda_\chi \simeq 1$  GeV/c $^2$ ). This extended  $V_{low-k}$  has been used in our recent study of the two-pion-exchange (TPE) amplitudes for the  $pp \rightarrow pp\pi^0$  reaction [9].

To evaluate the  $pp \rightarrow pp\pi^0$  reaction at threshold using HB $\chi$ PT, the impulse approximation (I.A.) and the one-pion-exchange (Resc) diagrams are the lowest order amplitudes (diagrams) according to Weinberg counting. However, the typical momentum for this reaction at threshold is  $p \sim \sqrt{m_\pi m_N}$ , which implies that for this reaction we have to take Weinberg chiral counting with a grain of salt. It was shown early on that in HB $\chi$ PT the I.A. and Resc amplitudes interfere destructively resulting in a very small cross sections [2,10]. We therefore expect sizeable contributions to this reaction from the TPE diagrams. In Table 2 we show examples, taken from Ref. [9], of DWBA evaluations for a typical energy  $T_{lab} = 281$  MeV. Since the  $t_1$  terms add to zero and to improve the numerical convergence, we drop the  $t_1$  terms in our calculations as was done in the fourth row of Table 1.

Thus, in Eq.(1), we use  $t^*(p, p', x)$  instead of  $t(p, p', x)$ , where  $t^*(p, p', x)$  is obtained from  $t(p, p', x)$  by suppressing the  $t_1$  term in Eq.(2). The partial-wave projected form of  $t^*(p, p', x)$  in a DWBA calculation is written as:

$$J = - \left( \frac{m_N m_\pi}{8\pi} \right) \int_0^\infty p^2 dp \int_{-1}^1 p'^2 dp' \int_{-1}^1 dx \psi_{1S_0}(p') t^*(p, p', x) (p - p'x) \psi_{3P_0}(p) \quad (3)$$

In Table 2 we show the values of the  $J$  amplitudes for each TPE diagram.

Table 2: The values of  $J$ , Eq.(3), corresponding to the TPE diagrams of Types I  $\sim$  IV, evaluated in a DWBA calculation for  $T_{lab} = 281$  MeV. The column labeled ‘‘Sum’’ gives the combined contributions of Types I  $\sim$  IV, and the last column gives the value of  $J$  for  $1\pi$ -Resc. For the Nijm93 potential case, the results for three different choices of  $\Lambda_G$  (in MeV/c) are shown. For the case with  $V_{low-k}$ , CD-4 (CD-5) represents  $V_{low-k}$  generated from the CD-Bonn potential with a momentum cut-off  $\Lambda_{low-k} = 4 \text{ fm}^{-1}$  ( $5 \text{ fm}^{-1}$ ). The last row gives the results obtained in plane-wave approximation.

	I	II	III	IV	Sum	$1\pi$ -Resc
$V_{\text{Nijm}} : \Lambda_G = 600$	-0.12	-0.12	-0.57	0.07	-0.74	0.20
$V_{\text{Nijm}} : \Lambda_G = 700$	-0.12	-0.11	-0.57	0.06	-0.74	0.21
$V_{\text{Nijm}} : \Lambda_G = 800$	-0.12	-0.11	-0.55	0.04	-0.74	0.22
$V_{low-k} \text{ (CD-4)}$	-0.12	-0.09	-0.46	0.03	-0.65	0.23
$V_{low-k} \text{ (CD-5)}$	-0.09	-0.06	-0.30	-0.01	-0.46	0.22
Plane-waves	-0.06	-0.07	-0.30	0.05	-0.37	0.080

Table 2 shows that the DW amplitudes from the TPE diagrams are only roughly of the order of the one-pion rescattering amplitude tabulated in the last column. Evidently, when we compare to the plane wave amplitudes, the DWBA treatment does affect the relative magnitudes of the various diagrams differently. In the last row we show the plane wave amplitudes and we note that the ‘‘sub-leading’’ part of diagram III is a factor three or more larger than the other amplitudes. The MCS indicates that the ‘‘sub-leading’’ parts of the TPE amplitudes should be of the same order as the one-pion rescattering amplitude. Furthermore, the expansion parameter in MCS,  $\tilde{\epsilon} \simeq 0.4$ , ideally speaking should be the ratio of the amplitudes from the different orders in the MCS. When comparing the results in Table 1 and Table 2, we find that the ‘‘leading’’ part of diagrams II and IV are almost an order of magnitude larger than their ‘‘sub-leading’’ parts. Clearly, as seen in Table 2, we find, as expected in the MCS, that the amplitudes from the ‘‘sub-leading’’ parts of diagrams II, IV and from the one-pion rescattering diagram are about the

same magnitude. However, diagram III (the “cross-box” diagram) appears not follow the expected MCS behavior. The plane wave amplitude for the “sub-leading” part of diagram III is less than 50% than the “leading” part of diagram III. Moreover, the amplitude of the “sub-leading” part of diagram III is more than a factor  $\tilde{\epsilon}^{-1}$  larger than what is expected in the MCS. One explanation could be that we evaluate diagram III using HB $\chi$ PT’s heavy nucleon propagators and not the nucleon propagator which is advocated for the MCS [15]. This issue will be resolved in the near future. A final note, the lowest- and next-chiral-order (diagram VII in Ref. [3]) one-pion-exchange diagrams were found to be same order of magnitude as expected in MCS.

We have demonstrated [9] that, as expected, the two-pion-exchange loop diagrams give very large contributions to the  $pp \rightarrow pp\pi^0$  reaction at threshold, and that these diagrams will give important contributions to other  $NN \rightarrow NN\pi$  reaction channels.

## Acknowledgments

This research has been done in a close collaboration with Drs. Y. Kim, K. Kubodera and T. Sato. This work is supported in part by the National Science Foundation, Grant No. PHY-0457014.

## References

- [1] H. O. Meyer *et al.*, Phys. Rev. Lett. **65**, 2846 (1990).
- [2] B.-Y. Park, F. Myhrer, J.R. Morones, T. Meissner and K. Kubodera, Phys. Rev. C, **53**, 1519 (1996); T. Sato, T.-S.H. Lee, F. Myhrer and K. Kubodera, Phys. Rev. C, **56**, 1246 (1997).
- [3] V. Dmitrašinović K. Kubodera, F. Myhrer and T. Sato, Phys. Lett. **B 465**, 43 (1999).
- [4] C. Hanhart and N. Kaiser, Phys. Rev. C, **66**, 054005 (2002); [nucl-th/0208050].
- [5] E. Epelbaum, W. Glöckle and U.-G. Meissner, Phys. Lett. B, **439**, 1 (1998); E. Epelbaum, W. Glöckle, A. Krüger and U.-G. Meissner, Nucl. Phys. A, **645**, 413 (1999).
- [6] M.C. Birse, J.A. McGovern and K.G. Richardson, Phys. Lett. B, **464**, 413 (1999); T. Barford and M.C. Birse, AIP Conf. Proc. **603**, 229 (2001)

- [7] S. Bogner, T.T.S. Kuo and L. Coraggio, Nucl.Phys. A, **684**, 432c (2001); S.K. Bogner *et al.*, Phys. Lett. B, **576**, 265 (2003) [nucl-th/0108041]; S. Bogner *et al.* Phys. Rept. **386**, 1 (2003); J.D. Holt *et al.*, Nuc. Phys. A, **733**, 153 (2004).
- [8] F. Myhrer, “Large two-pion-exchange contributions to the  $pp \rightarrow pp\pi^0$  reaction”, *to appear in* Proc. Intern. Workshop *Chiral Dynamics 2006*, Eds. M.W. Ahmed *et al.*, World Scientific) [nucl-th/0611051].
- [9] Y. Kim, T. Sato, F. Myhrer and K. Kubodera, Phys. Lett. B, to appear; arXiv:0704.1342 [nucl-th] (2007).
- [10] T.D. Cohen, J.L. Friar, G.A. Miller and U. van Kolck, Phys. Rev. C, **53**, 2662 (1996).
- [11] C. Hanhart, G.A. Miller and U. van Kolck, Phys. Rev. Lett. **85**, 2905 (2000).
- [12] V. Lensky, J. Haidenbauer, C. Hanhart, V. Baru, A. Kudryavtsev and U.-G. Meissner, Eur. Phys. J. **A27**, 37 (2006) [nucl-th/0511054]; V. Lensky *et al.*, [nucl-th/0609007]
- [13] Y. Kim, T. Sato, F. Myhrer and K. Kubodera, “Two-pion-exchange and the  $pp \rightarrow pp\pi^0$  cross section”, manuscript in preparation.
- [14] T. Sato and F. Myhrer, private communication (1999).
- [15] C. Hanhart, Phys. Rep. **397**, 155 (2004)
- [16] P.F. Bedaque and U. van Kolck, Ann. Rev. Nucl. Part. Sci. **52**, 339 (2002), and references therein.
- [17] E. Epelbaum, Prog. Part. Nucl. Phys. **57**, 654 (2006), and references therein.
- [18] R. Machleidt, K. Holinde and C. Elster, Phys. Rep. **149**, 1 (1987); R. Machleidt, Phys. Rev. C, **63**, 024001 (2001).
- [19] V.G.J. Stoks, R.A.M. Klomp, C.P.F. Terheggen and J.J. de Swart, Phys. Rev. C, **21**, 861 (1980); Phys. Rev. C, **49**, 2950 (1994).
- [20] Y Kim, I. Danchev, K. Kubodera, F. Myhrer and T. Sato, Phys. Rev. C, **73**, 025202 (2006).

MENU 2007  
11th International Conference  
on Meson-Nucleon Physics and  
the Structure of the Nucleon  
September 10-14, 2007  
IKP, Forschungszentrum Jülich, Germany

# MESON PRODUCTION IN NN COLLISIONS

K. Nakayama<sup>a,b,1</sup>, Yongseok Oh<sup>a,2</sup>, H. Haberzettl<sup>c</sup>

<sup>a</sup>Department of Physics and Astronomy, University of Georgia, Athens, GA 30602, USA

<sup>b</sup>Institut für Kernphysik, Forschungszentrum Jülich, 52425 Jülich, Germany

<sup>c</sup>Center for Nuclear Studies, Department of Physics, George Washington University, Washington DC 20052, USA

## Abstract

Meson production in  $NN$  collisions is discussed in conjunction with more basic two-body reactions. In particular, the production of  $\eta$  mesons in both the photo- and hadro-induced reactions are investigated in a combined analysis in order to learn about the relevant production mechanisms for this meson. We consider the nucleonic, mesonic and nucleon resonance currents constructed within an effective Lagrangian approach.

## 1 Introduction

The primary motivation for studying the production of mesons off nucleons and nuclei is to investigate the structure and properties of the nucleon resonances and, in the case of heavier meson productions, to learn about hadron dynamics at short range. In particular, we still know relatively little about the production mechanism of heavier mesons. Apart from pion production, the majority of theoretical investigations of meson production processes are performed within phenomenological meson-exchange approaches. Such approaches force us to correlate as many independent processes as possible within a single model, if one is to extract meaningful physics information. Here, we concentrate on our investigation of  $\eta$  meson production in both the photo- and hadro-induced reactions. More specifically, we perform a

---

<sup>1</sup>E-mail address: nakayama@uga.edu

<sup>2</sup>Current address: Cyclotron Institute and Department of Physics, Texas A&M University, College Station, TX 77843.

combined analysis of the

$$\begin{aligned}
 \gamma + N &\rightarrow N + \eta, \\
 \pi + N &\rightarrow N + \eta, \\
 N + N &\rightarrow N + N + \eta
 \end{aligned}
 \tag{1}$$

reactions. The photoproduction reaction is calculated by considering the  $s$ -,  $u$ - and  $t$ -channel Feynman diagrams plus the generalized contact terms [1] which ensure the gauge invariance of the total amplitude, in addition to accounting for the final state interaction (FSI) effects [2]. The  $\pi + N \rightarrow N + \eta$  reaction is calculated in the tree-level approximation including the  $s$ -,  $u$ -, and  $t$ -channels. To the extent that this reaction is dominated by the excitation of the  $S_{11}(1535)$  resonance at least for energies close to threshold, this should be a reasonable approximation if one confine oneself to energies not too far from threshold. For higher energies, effects of the  $\pi\pi N$  channel becomes important [3]. The  $N + N \rightarrow N + N + \eta$  process is calculated in the DWBA approximation, where both the  $NN$  FSI and the initial state interaction (ISI) are taken into account [4]. The  $NN$  FSI is known to be responsible for the dominant energy dependence observed in the total cross section apart from that due to the phase space. As for the basic meson production amplitude, our model includes the nucleonic, mesonic and nucleon resonance currents which are derived from relevant effective Lagrangians [1, 4]. The free parameters of our model — the resonance parameters, the  $NN\eta$  coupling constant, and the cutoff parameter at the photon vertex in the  $t$ -channel meson exchange currents — are fixed such as to reproduce the available data in a global fitting procedure of the three reaction processes listed in (1).

## 2 Results

In this section we discuss the results of our model calculation according to the procedure outlined above. The calculation is basically the same to that reported in [1] for  $\eta'$ , except that here we consider the production of  $\eta$  and that there is an additional reaction channel,  $\pi N \rightarrow N\eta$ .

### 2.1 $\gamma p \rightarrow p\eta$

For photoproduction of  $\eta$  off nucleons the amount of available data is considerable, in particular, for proton target. We have available not only the total and differential cross sections over a wide range of energy starting from

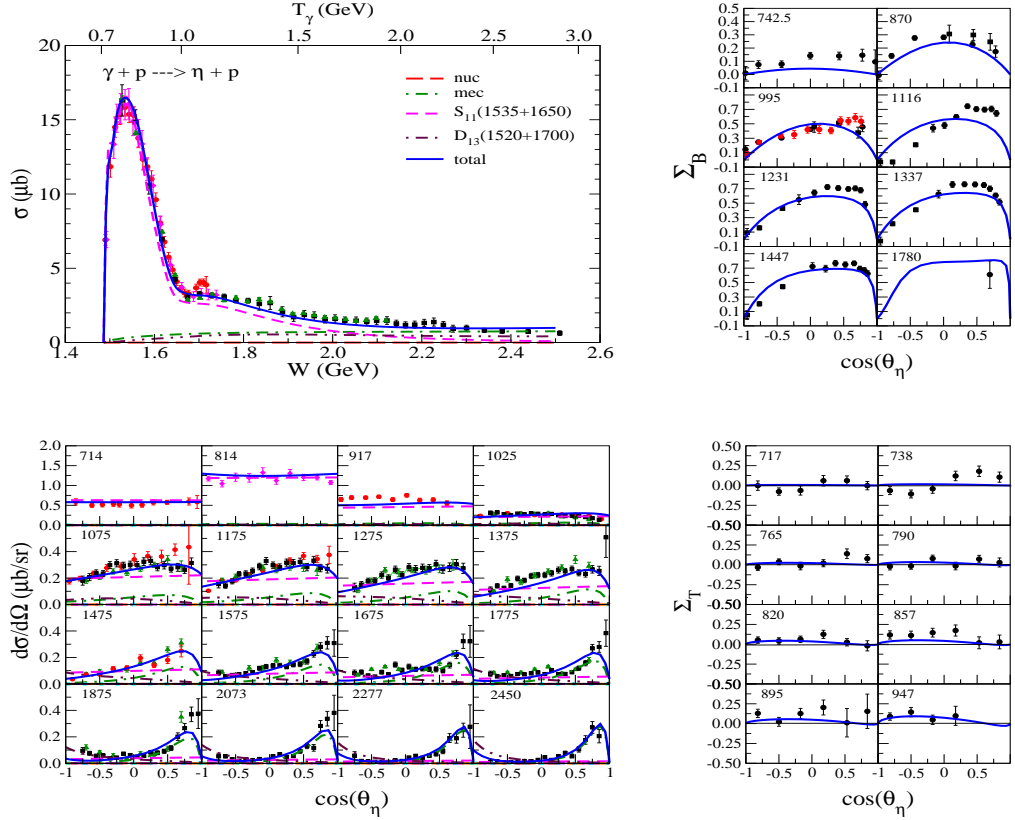


Figure 1: Results for  $\gamma p \rightarrow \eta p$ . Upper left panel: total cross section as a function of the total energy  $W$  of the system. Lower left panel:  $\eta$  angular distribution in the center-of-mass frame. Upper right panel: beam asymmetry,  $\Sigma_B$ . Lower right panel: target asymmetry,  $\Sigma_T$ . The data are from [6].

threshold, but also the beam and target asymmetries. The recent data on neutron target from GRAAL [5] have attracted much interest in this reaction in connection with the possibility of the existence of a narrow (exotic) baryon resonance with mass near 1.68 GeV. Here, we restrict our discussion to the  $\gamma p \rightarrow p\eta$  reaction. The results are shown in Fig. 1. As far as the resonance currents are concerned, we follow the strategy adopted in [1] to include the resonances one by one until a reasonable fit is achieved. We found that a reasonable fit quality of  $\chi^2/N \approx 3.7$  is achieved by considering the  $S_{11}(1535)$ ,  $S_{11}(1650)$ ,  $D_{13}(1520)$ , and  $D_{13}(1700)$  resonances if only the photoproduction reaction is considered. In a global fit with all the three reaction processes (1) considered, we have  $\chi^2/N \approx 5.7$ . For the photoproduction process, the inclusion of more resonances did not change the fit quality in any major way.

In particular, we found that no higher spin resonances ( $D_{15}$  and  $F_{15}$ ) were necessary to reproduce the existing data, including the beam asymmetry. However, we were unable to reproduce the measured target asymmetry. This requires a further detailed study. The spin-3/2 resonances are important in reproducing the measured angular distributions in the range of  $T_\gamma = 1.07\text{--}1.6$  GeV and the beam asymmetry. We emphasize that the resonance parameter values in our model are highly correlated with each other and that the existing data are insufficient to establish a unique set of these parameters. The relatively small cross sections measured at higher energies and backward angles constrain the nucleonic current contribution to be very small, so that the  $NN\eta$  coupling constant is compatible with zero.

## 2.2 $\pi^- p \rightarrow n\eta$

As displayed in the upper left panel of Fig. 2, the total cross section for  $\pi^- p \rightarrow n\eta$  is nicely reproduced up to  $W \approx 1.6$  GeV, where it is dominated by the  $S_{11}$  resonances, especially, the  $S_{11}(1535)$ . We underpredict the measured total cross section at higher energies due to the absence of the  $\pi\pi N$  contribution via the coupled channel [3] in our model. The corresponding differential cross section results are shown in the upper right panel of Fig. 2. We note that the model doesn't quite reproduce the structure exhibited by the data at higher energies. The  $P_{13}(1720)$  resonance is important in reproducing this structure as illustrated in the lower right panel in Fig. 2.

## 2.3 $NN \rightarrow NN\eta$

The results for  $NN \rightarrow NN\eta$  are shown in Fig. 3. This process is particularly relevant in connection with the role of the  $\eta N$  FSI. Most of the existing calculations take into account the effects of the  $NN$  FSI in one way or another which is well known to influence the energy dependence of the cross section near threshold. Calculations which include the  $\eta N$  FSI to lowest order reproduce the bulk of the energy dependence exhibited by the data. However, they fail to reproduce the  $pp$  invariant mass distribution measured by the COSY-TOF [9] and COSY-11 collaborations [10]. In Ref. [11], it has been emphasized the importance of the three-body nature of the final state in the  $S$ -wave in order to account for the observed  $pp$  invariant mass distribution. Other authors have suggested an extra energy dependence in the basic production amplitude [12] to reproduce the existing data. Yet another possibility has been offered which is based on a higher partial wave ( $P$ -wave) contribution [13]. We observe that all what is required to reproduce the measured  $pp$  invariant mass distribution is an extra  $p'^2$  dependence, where

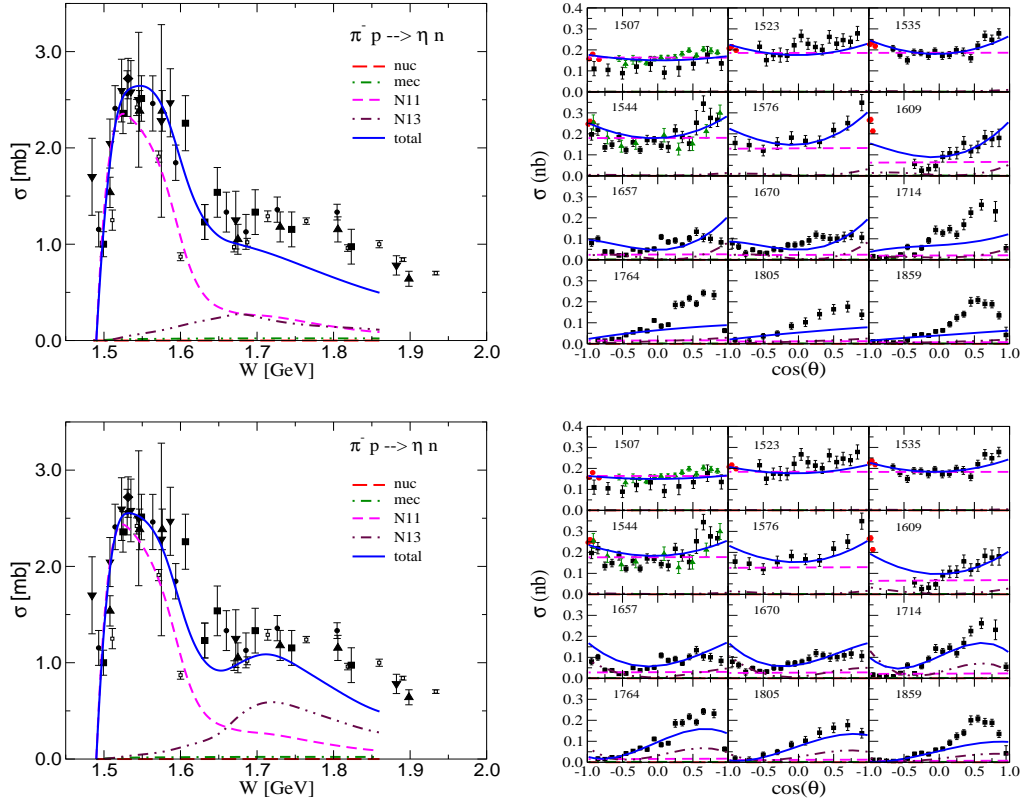


Figure 2: Results for  $\pi^- p \rightarrow \eta n$ . Upper left panel: total cross section as a function of the total energy of the system  $W$ . Upper right panel:  $\eta$  angular distribution in the center-of-mass frame. Here,  $N11$  stands for  $S_{11}(1535) + S_{11}(1650)$  contribution and  $N13 = D_{13}(1520) + D_{13}(1700)$  contribution. Lower panels: same as the upper panels except for the inclusion of the additional  $P_{13}(1720)$  resonance, i.e.,  $N13 = D_{13}(1520) + D_{13}(1700) + P_{13}(1720)$ . The data are from [7]

$p'$  denotes the relative momentum of the final  $pp$  subsystem. Obviously, this can be achieved either by an  $S$ -wave or by a  $P$ -wave contribution. Note that the  $NN$   $P$ -wave ( ${}^3P_0$ ) can also yield a flat proton angular distribution as observed in the corresponding data. In any case, as pointed out in Ref. [13], the measurement of the spin correlation functions should help settle the question of the  $S$ - versus  $P$ -wave contributions in a model-independent way.

Although the model calculation of [13], based on a stronger  $P$ -wave contribution, reproduces nicely the shape of the measured  $pp$  invariant mass distributions, it underpredicts the total cross section data near threshold

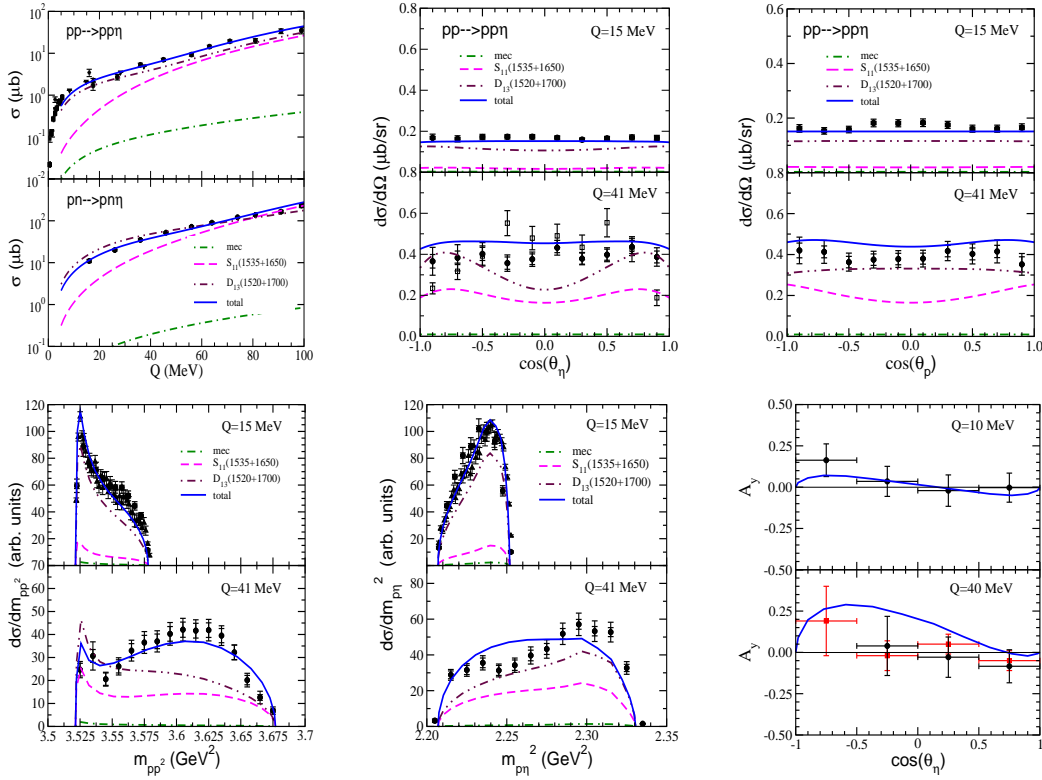


Figure 3: Results for  $NN \rightarrow \eta NN$ . Upper left panel: total cross section as a functions of the excess energy  $Q$  in  $pp$  and  $pn$  collisions. Upper middle panel:  $\eta$  angular distribution in the overall center-of-mass frame. Upper right panel: final proton angular distribution. Lower left panel:  $pp$  invariant mass distribution. Lower middle panel:  $pn$  invariant mass distribution. Lower right panel: Analyzing power. The data are from [8–10].

( $Q < 30\text{MeV}$ ). Here we show the new results, based on a combined analysis of the  $\gamma p \rightarrow p\eta$ ,  $\pi^- p \rightarrow n\eta$  and  $NN \rightarrow NN\eta$  reactions, which reproduce the currently existing data on  $NN \rightarrow NN\eta$ . The major difference from the previous calculation [13] is a much stronger spin-3/2 resonance contribution. In contrast to the  $S_{11}$  resonances, the  $D_{13}$  contributions follow more closely the empirically observed energy dependence of the total cross section. It should be emphasized, however, that whether or not the dominance of the  $D_{13}$  resonances discussed above is indeed the case still remains to be seen. The reason for this is that, in the present calculation, the coupling constants at the  $D_{13}Nv$  vertices ( $v = \rho, \omega$ ) have been fitted to reproduce the  $NN\eta$  data. Therefore, the consistency of these coupling constants with

other independent reaction processes involving the  $D_{13}Nv$  vertices needs to be checked. For this purpose, processes such as  $NN \rightarrow NNv$  and  $\gamma N \rightarrow Nv$  are of particular interest.

In Ref. [13], where the dominant  $\eta$  production mechanism is the excitation of the  $S_{11}(1535)$  resonance via the pion-exchange, the analyzing power,  $A_y$ , exhibits a zero around  $\cos(\theta_\eta) = 0$ . In the present calculation, where the dominant production mechanism is the  $D_{13}$  resonance excitation, the zero of  $A_y$  is shifted toward forward angles. Unfortunately, the data are not accurate enough to disentangle these two mechanisms. More accurate data can, therefore, impose more stringent constraints so as to help distinguish the two results.

### 3 Summary

The progress in the study of meson production processes in  $NN$  collisions, both experimentally and theoretically, has reached such a level that it allows us to address certain concrete physics issues, especially, when they are investigated in conjunction with other independent reactions. This has been illustrated here for the specific case of  $\eta$  production where some information on the nucleon resonances may be extracted. In particular, the consideration of meson production processes in  $NN$  collisions in conjunction with more basic photo- and (two-body) hadro-induced reactions aiming at a resonance parameters extraction, should help impose more stringent constraints on these extracted parameters. This is especially relevant given the fact that the existing data on meson production (other than pion) in two-body hadronic reactions are rather scarce and of relatively low accuracy. Currently, no facilities are available to improve/extend the corresponding database. On the other hand, the available data on meson production in  $NN$  collisions are much more accurate and this database can be and is being expanded especially at the COSY facility.

### Acknowledgments

This work is partly supported by the FFE grant no.41445282.

### References

- [1] K. Nakayama and H. Haberzettl, Phys. Rev. **C 69**, 065212 (2004); *ibid.* **C73**, 045211 (2006).

- 
- [2] H. Haberzettl, K. Nakayama, and S. Krewald, Phys. Rev. **C74**, 045202 (2006).
- [3] A. Gasparyan, Ch. Hanhart, J. Haidenbauer, and J. Speth, Phys. Rev. **C74**, 045202 (2006).
- [4] K. Nakayama, J. Speth, and T.-S. H. Lee, Phys. Rev. **C65**, 045210 (2002).
- [5] V. Kuznetsov *et al.*, Phys. Lett. **B647**, 23 (2007).
- [6] M. Dugger *et al.*, Phys. Rev. Lett. **89**, 222002 (2002); V. Crede *et al.*, Phys. Rev. Lett. **94**, 012004 (2005); T. Nakabayashi *et al.*, Phys. Rev. **C74**, 035202 (2006); F. M. Renard *et al.*, Phys. Lett. **B528**, 215 (2002); J. Ajaka, Phys. Rev. Lett. **81**, 1797 (1998); V. Kouznetsov *et al.*,  $\pi N$  NewsLetter **16**, 160 (2002); A. Bock *et al.*, Phys. Rev. Lett. **81**, 534 (1998).
- [7] R. M. Brown *et al.*, Nucl. Phys. **B153**, 89 (1979); F. Bulos *et al.*, Phys. Rev. Lett. **13**, 486 (1964); F. Bulos *et al.*, Phys. Rev. **187**, 1827 (1969); W. Deinet *et al.*, Nucl. Phys. **B11**, 495 (1969); J. Feltesse *et al.*, Nucl. Phys. **B93**, 242 (1975); B. W. Richards *et al.*, Phys. Rev. **D 1**, 10 (1970); T. Morrison, Ph.D. thesis, The George Washington University, (1999); N. C. Debenham *et al.*, Phys. Rev. **D 12**, 2545 (1975).
- [8] E. Chiavassa *et al.*, Phys. Lett. **B322**, 270 (1994); H. Calén *et al.*, Phys. Rev. Lett. **79**, 2642 (1997); F. Hibou *et al.*, Phys. Lett. **B438**, 41 (1998); J. Smyrski *et al.*, Phys. Lett. **B474**, 180 (2000); B. Tatischeff *et al.*, Phys. Rev. **C62**, 054001 (2000); H. Calén *et al.*, Phys. Rev. **C58**, 2667 (1998); H. Calén *et al.*, Phys. Lett. **B458**, 190 (1999); H. Calén *et al.*, Phys. Lett. **B366**, 39 (1996); H. Calén *et al.*, Phys. Rev. Lett. **80**, 2069 (1998); P. Winter *et al.*, Phys. Lett. **B544** 251 (2002); Erratum-*ibid.* **B553**, 339 (2003). P. Moskal *et al.*, Phys. Lett. **B482**, 356 (2000). R. Czyzykiewicz *et al.*, Phys. Rev. Lett. **98**, 122003 (2007).
- [9] M. Abdel-Bary *et al.*, Eur. Phys. J. **A 16**, 127 (2003).
- [10] P. Moskal *et al.*, Phys. Rev. **C69**, 025203 (2004).
- [11] A. Fix and H. Arenhövel, Phys. Rev. **C69**, 014001 (2004).
- [12] A. Deloff, Phys. Rev. **C69**, 035206 (2004).
- [13] K. Nakayama, J. Haidenbauer, C. Hanhart, and J. Speth, Phys. Rev. **C68**, 045201 (2003).

# THE NATURE OF THE LIGHT SCALAR MESONS FROM THEIR RADIATIVE DECAYS

*A. V. Nefediev*

Institute of Theoretical and Experimental Physics, Moscow, Russia<sup>1</sup>

## Abstract

The nature of the light scalar mesons is one of the most intriguing open challenges in hadronic spectroscopy. It is argued that radiative decays involving these scalars can serve as an important decisive tool in establishing their nature. In particular, special emphasis is made on the radiative decays of the scalars themselves (in addition to the radiative decays of the  $\phi$ -meson with the scalars appearing in the final state), including their two-photon decays. All the above mentioned processes are considered in detail in the (point-like) kaon molecule model of the scalars and explicit predictions for the decay widths are made. In addition, finite-range corrections to the point-like results are investigated, with a special attention paid to gauge invariance of the decay amplitude. Finally, the conclusion is made that experimental data on the radiative decays with the light scalar mesons involved strongly support the molecule assignment for the latter.

## 1 Introduction

Understanding the properties of light scalar mesons is one of the most challenging problems of the hadrons spectroscopy. In particular, investigations of the nature of the  $a_0(980)$  and  $f_0(980)$  mesons attract considerable theoretical and experimental efforts. This interest should not come as a surprise since the given states reside at the very kaon–antikaon threshold and thus the admixture of the kaon molecular component in the wave function is expected to be large. Indeed, experimental data [1–3] unambiguously show a prominent  $K\bar{K}$  contribution. Other assignments for these mesons are also suggested and studied in the literature, such as the genuine  $q\bar{q}$  assignment [4],

---

<sup>1</sup>Institute of Theoretical and Experimental Physics, 117218, B.Chermushkinskaya 25, Moscow, Russia.

or the compact four–quark assignment [5, 6]. Many experimental tests have been suggested so far in order to distinguish between these assignments and thus to disclose the nature of the scalars  $a_0/f_0(980)$ . For example, the importance of measurements of the radiative decays of the  $\phi(1020)$  to scalar mesons was argued in [7]. In the meantime, another class of radiative decays — the radiative decays of the scalars themselves — can be studied as well and provide new important data. As compared to the radiative decays  $\phi \rightarrow \gamma S$  ( $S = a_0/f_0$ ), the decays  $S \rightarrow \gamma V$  ( $V = \rho, \omega, \gamma$ ) possess a number of advantages, such as a considerable phasespace in the final state and a possibility to probe the nonstrange component of the scalars w.f. These radiative decays can serve therefore as a complementary source of information and to deliver decisive information on the structure of these long–debated objects [8].

Both types of radiative decays can be described with the single vertex function  $VS\gamma$ . Gauge invariance imposes quite restrictive constraints on the structure of the transition matrix element:  $iW^{\mu\nu} = M(m_V^2, m_S^2)[P_V^\mu P_\gamma^\nu - g^{\mu\nu}(P_V P_\gamma)]$ , where  $P_V$  and  $P_\gamma$  are the vector and the photon four-momenta.

## 2 Evaluation of the decay widths in various assignments for the scalars

In the quark–antiquark assignment, the  $a_0/f_0(980)$  mesons are treated as the genuine quark–antiquark  $^3P_0$  states. Their radiative decays can be studied in the framework of nonrelativistic quark models [9, 10] yielding the width of 125 keV, for the decays  $a_0 \rightarrow \gamma\omega$  and  $f_0 \rightarrow \gamma\rho$ , 14 keV, for the decays  $a_0 \rightarrow \gamma\rho$  and  $f_0 \rightarrow \gamma\omega$ , and 4.5 keV, for the decays  $a_0/f_0 \rightarrow \gamma\gamma$ . The radiative decays widths of the genuine quark–antiquark mesons  $f_1(1285)$  ( $\Gamma(f_1(1285)) \rightarrow \gamma\rho) = 1320 \pm 312\text{keV}$ ) and  $f_2(1270)$  ( $\Gamma(f_2(1270) \rightarrow \gamma\gamma) = 2.61 \pm 0.30\text{ keV}$ ) were used here in order to fix the radial w.f. matrix element [8].

In the molecule assignment for the scalars, the radiative decays proceed via a kaon loop, and the scales involved into the problem possess the hierarchy  $\varepsilon \ll m \lesssim \beta$ , where  $\beta$  is the intrinsic scale of the binding force,  $m$  is the kaon mass, and  $\varepsilon = 2m - m_S$  is the binding energy. It was argued in [11] that, for the realistic values of the parameters ( $\beta \approx m_\rho \approx 800\text{ MeV}$ ,  $m = 495\text{ MeV}$ , and  $\varepsilon = 10\text{ MeV}$ ), this hierarchy can be achieved starting from the point-like limit of  $\beta \rightarrow \infty$  and taking into account finite-range corrections in the inverse power of  $\beta$ . The point-like  $SK\bar{K}$  coupling constant,  $g_S^2/(4\pi) = 32m\sqrt{m\varepsilon} \approx 1.12\text{ GeV}^2$  was obtained in [12]. The two remaining couplings can be obtained from the  $\rho\pi\pi$  constant ( $g_V = g_\rho = g_\omega = \frac{1}{2}g_{\rho\pi\pi} \approx 2.13$ ) and from the total width of the  $\phi$  ( $g_\phi^2/(4\pi) \approx 1.77$ ). Then the point-like

Table 1: The widths (in keV) of the radiative decays involving scalars;  $\theta$  is the (small)  $\phi - \omega$  mixing angle.

	Quark–antiquark	Molecule	Data (PDG)
$\phi \rightarrow \gamma a_0$	$0.37 \sin^2 \theta$	0.6	$0.32 \pm 0.02$
$\phi \rightarrow \gamma f_0(\bar{n}n)/f_0(\bar{s}s)$	$0.04 \sin^2 \theta/0.18$	0.6	$0.47 \pm 0.03$
$a_0 \rightarrow \gamma\gamma$	$2 \div 5$	0.22	$0.30 \pm 0.10$
$f_0 \rightarrow \gamma\gamma$	$2 \div 5$	0.22	$0.29^{+0.07}_{-0.09}$
$a_0\gamma\omega/\rho$	125/14	3.4	pending
$f_0(\bar{n}n)\gamma\rho/\omega$	125/14	3.4	
$f_0(\bar{s}s)\gamma\rho/\omega$	$0/31 \sin^2 \theta$	3.4	

predictions for the widths are  $\Gamma(\phi \rightarrow \gamma S) = 0.6$  keV,  $\Gamma(S \rightarrow \gamma V) = 3.4$  keV, and  $\Gamma(S \rightarrow \gamma\gamma) = 0.22$  keV. It can be demonstrated explicitly that no large corrections to these results, of order  $\mathcal{O}(m^2/\beta^2)$ , appear [11–13]. Thus one concludes that inclusion of the finite–range corrections does not change these prediction appreciably, giving only moderate (of order  $10 \div 20\%$  in the amplitude) corrections, provided they are included in a self-consistent and gauge-invariant way [11–13].

### 3 Conclusions

In Table 1 we give the widths for the radiative decays involving scalars. Comparing the predictions made in the quark–antiquark and molecule assignment with the experimental data we conclude that the molecule picture is strongly supported by the data (Belle reports the new result  $\Gamma(f_0 \rightarrow \gamma\gamma) = 0.205^{+95+0.147}_{-0.83-0.117}$  keV [14] which is in even better agreement with the molecule prediction). An important property revealed by the radiative decays of the scalars is that the theoretical predictions for these decays differ drastically depending on the assignment made for the nature of the scalars. This makes such radiative decays an important tool in establishing the structure of the  $a_0/f_0(980)$  mesons. We conclude that experimental data on the radiative decays  $a_0/f_0 \rightarrow \gamma\rho/\omega$  are strongly needed, as an important, and possibly decisive, source of information about the scalar mesons.

## Acknowledgments

This work was supported by the Federal Agency for Atomic Energy of Russian Federation and by grants NSh-843.2006.2, DFG-436 RUS 113/820/0-1(R), RFFI-05-02-04012-NNIOa, and PTDC/FIS/70843/2006-Fisica.

## References

- [1] M. N. Achasov *et al.*, *Phys. Lett.* **B440**, 442 (1998); M. N. Achasov *et al.*, *Phys. Lett.* **B485**, 349 (2000).
- [2] R. R. Akhmetshin *et al.* [CMD-2 Collab.], *Phys. Lett.* **B462**, 380 (1999).
- [3] A. Aloisio *et al.* [KLOE Collab.], *Phys. Lett.* **B536**, 209 (2002); A. Aloisio *et al.*, *Phys. Lett.* **B537**, 21 (2002).
- [4] S. Godfrey and N. Isgur, *Phys. Rev.* **D32**, 189 (1985); M. Kroll, R. Ricken, D. Merten, B. Metsch, and H. Petry, *Eur. Phys. J.* **A9**, 73 (2000); A. M. Badalyan and B. L. G. Bakker, *Phys. Rev.* **D66**, 034025 (2002); A.M. Badalian, *Phys. Atom. Nucl.* **66**, 1342 (2003).
- [5] R. L. Jaffe, *Phys. Rev.* **D15**, 267, 281 (1977).
- [6] N. N. Achasov, S. A. Devyanin, and G. N. Shestakov, *Phys. Lett.* **B96**, 168 (1980); D. Black, A. H. Fariborz, F. Sannino, and J. Schechter, *Phys. Rev.* **D59**, 074026 (1999); M. Alford and R. L. Jaffe, *Nucl. Phys.* **B578**, 367 (2000); L. Maiani, F. Piccinini, A. D. Polosa, and V. Riquer, *Phys. Rev. Lett.* **93**, 212002 (2004).
- [7] N. N. Achasov and V. N. Ivanchenko, *Nucl. Phys.* **B315**, 465 (1989).
- [8] J. Haidenbauer, C. Hanhart, Yu. S. Kalashnikova, A. E. Kudryavtsev, and A. V. Nefediev, *Phys. Rev.* **C73**, 045203 (2006).
- [9] W. Kwong and J. L. Rosner, *Phys. Rev.* **D38**, 279 (1988).
- [10] R. Barbieri, R. Gatto, and R. Kogerler, *Phys. Lett.* **B60**, 183 (1976).
- [11] C. Hanhart, Yu. S. Kalashnikova, A. E. Kudryavtsev, and A. V. Nefediev, *Phys. Rev.* **D75**, 074015 (2007).
- [12] J. Haidenbauer, C. Hanhart, Yu. S. Kalashnikova, A. E. Kudryavtsev, and A. V. Nefediev, *Eur. Phys. J.* **A24**, 437 (2005).

[13] V.E. Markushin, *Eur. Phys. J.* **A8**, 389 (2000).

[14] T. Mori *et. al* [Belle Collab.], *Phys. Rev.* **D75**, 051101 (2007).

MENU 2007  
11th International Conference  
on Meson-Nucleon Physics and  
the Structure of the Nucleon  
September 10-14, 2007  
IKP, Forschungszentrum Jülich, Germany

# SCALAR RADIUS OF THE PION AND TWO PHOTONS INTO TWO PIONS. STRONG S-WAVE FINAL STATE INTERACTIONS

*J. A. Oller, L. Roca*  
Departamento de Física  
Universidad de Murcia  
Spain, E-30071

*C. Schat*  
Departamento de Física, FCEyN,  
Universidad de Buenos Aires  
Ciudad Universitaria, Pab.1,  
(1428) Buenos Aires, Argentina.

## Abstract

The quadratic pion scalar radius,  $\lambda r^2 \rightarrow_s^\pi$ , plays an important role for present precise determinations of  $\pi\pi$  scattering. The solution of the Muskhelishvili-Omnès equations for the non-strange null isospin ( $I$ ) pion scalar form factor determines that  $\lambda r^2 \rightarrow_s^\pi = 0.61 \pm 0.04 \text{ fm}^2$ . However, by using an Omnès representation of this form factor, Ynduráin recently obtains  $\lambda r^2 \rightarrow_s^\pi = 0.75 \pm 0.07 \text{ fm}^2$ . A large discrepancy between both values, given the precision, then results. We show that Ynduráin's method is indeed compatible with the determinations from the Muskhelishvili-Omnès equations once a zero in the scalar form factor for some S-wave  $I = 0$   $T$ -matrices is considered. Once this is accounted for, the resulting value is  $\lambda r^2 \rightarrow_s^\pi = 0.63 \pm 0.05 \text{ fm}^2$ .

On the other hand, we perform a theoretical study of the reaction  $\gamma\gamma \rightarrow \pi^0\pi^0$  based on dispersion relations. The large source of uncertainty for  $\sqrt{s} \gtrsim 0.5 \text{ GeV}$ , due to variations in the phase used in the Omnès function above the  $K\bar{K}$  threshold, is removed by taking one more subtraction in the dispersion relation. This allows us to make sharper predictions for the cross section so that one could use this reaction to distinguish between different low energy  $\pi\pi$  parameterizations, once independent experiments are available. We also study the role played by the  $\sigma$  or  $f_0(600)$  meson in this reaction and determine its width to two photons.

## 1 Introduction

Here we summarize the two papers [1, 2] that mainly handle with the strong influence of the  $I = 0$  S-wave meson-meson final state interactions. We concentrate here on the non-strange  $I = 0$  scalar form factor of the pion [1] and  $\gamma\gamma \rightarrow \pi^0\pi^0$  [2]. Both processes can be formulated in a way that has in common the same basic function in order to take care of the strong final state interactions in the  $I = 0$  S-wave. This function has been recently the origin of large uncertainties in its implementation in the literature, both for the scalar form factor of the pion [3–5] and for  $\gamma\gamma \rightarrow \pi^0\pi^0$  [6].

The scalar form factor of the pion,  $\Gamma_\pi(t)$ , corresponds to the matrix element

$$\Gamma_\pi(t) = \int d^4x e^{-i(q'-q)x} \lambda\pi(q') | (m_u \bar{u}(x)u(x) + m_d \bar{d}(x)d(x)) | \pi(q) \rightarrow , \quad t = (q'-q)^2 . \quad (1)$$

Performing a Taylor expansion around  $t = 0$ ,

$$\Gamma_\pi(t) = \Gamma_\pi(0) \left\{ 1 + \frac{1}{6} t \lambda r^2 \rightarrow_s^\pi + \mathcal{O}(t^2) \right\} , \quad (2)$$

where  $\lambda r^2 \rightarrow_s^\pi$  is the quadratic scalar radius of the pion. The quantity  $\lambda r^2 \rightarrow_s^\pi$  contributes around 10% to the values of the S-wave  $\pi\pi$  scattering lengths  $a_0^0 = 0.220 \pm 0.005 M_\pi^{-1}$  and  $a_0^2 = -0.0444 \pm 0.0010 M_\pi^{-1}$ , as determined in Ref. [7] by solving the Roy equations with constraints from two loop Chiral Perturbation Theory (CHPT). If one takes into account that one has a precision of 2.2% in the scattering lengths, a 10% of contribution from  $\lambda r^2 \rightarrow_s^\pi$  is a large one. Related to that,  $\lambda r^2 \rightarrow_s^\pi$  is also important in  $SU(2) \times SU(2)$  CHPT since it gives the low energy constant  $\bar{\ell}_4$  that controls the departure of  $F_\pi$  from its value in the chiral limit [8, 9] at next-to-leading order.

Based on one loop  $\chi PT$ , Gasser and Leutwyler [8] obtained  $\lambda r^2 \rightarrow_s^\pi = 0.55 \pm 0.15 \text{ fm}^2$ . This calculation was improved later on by the same authors together with Donoghue [10], who solved the corresponding Muskhelishvili-Omnès equations with the coupled channels of  $\pi\pi$  and  $K\bar{K}$ . The update of this calculation, performed in Ref. [7], gives  $\lambda r^2 \rightarrow_s^\pi = 0.61 \pm 0.04 \text{ fm}^2$ . Mousallam [11] employs the same approach and obtains values in agreement with the previous result. One should notice that solutions of the Muskhelishvili-Omnès equations for the scalar form factor rely on non-measured  $T$ -matrix elements or on assumptions about which are the channels that matter. Other independent approaches are then most welcome. In this respect we quote the works [12–14], and Ynduráin's ones [3–5]. These latter works have challenged the previous value for  $\lambda r^2 \rightarrow_s^\pi$ , shifting it to the larger  $\lambda r^2 \rightarrow_s^\pi =$

$0.75 \pm 0.07 \text{ fm}^2$ . If this is translated to the scattering lengths above, employing an equation of Ref. [7], it implies a shift of  $+0.006 M_\pi^{-1}$  for  $a_0^0$  and  $-0.001 M_\pi^{-1}$  in  $a_0^2$ . Thus, one is referring to a shift of slightly more than one sigma. Refs. [3,4] emphasize that one should have a precise knowledge of the  $I = 0$  S-wave phase shifts,  $\delta_0(s)$ , for  $s \geq 4M_K^2 \text{ GeV}^2$ ,  $M_K$  is the kaon mass, to disentangle which of the values, either that of Ref. [7] or [3], is the right one. However, this point is based on an unstable behaviour of the solution of Ref. [3] with respect to the value of  $\delta_0(4M_K^2)$ . Once this instability is cured, as shown below, the resulting  $\lambda r^2 \rightarrow_s^\pi$  only depends weakly on  $\delta_0(s)$ ,  $s \geq 4M_K^2$ , and is compatible with the value of Ref. [7].

Regarding the reaction  $\gamma\gamma \rightarrow \pi^0\pi^0$  one has to emphasize that due to the absence of the Born term (as the  $\pi^0$  is neutral), this reaction is specially sensitive to final state interactions. For energies below 0.6 GeV or so, only the S-waves matter, which have  $I = 0$  or 2. It is in this point where both the study of this reaction and the scalar form factor match. Recently, Ref. [6] updated the dispersive approach of Ref. [15] to calculate  $\sigma(\gamma\gamma \rightarrow \pi^0\pi^0)$ . Here one finds a large uncertainty in the results for  $\sqrt{s} \geq 0.5 \text{ GeV}$  that at around 0.6 GeV is already almost 200%. Again, this is due to the lack of a precise knowledge of the phase of the  $\gamma\gamma \rightarrow \pi\pi$   $I = 0$  S-wave amplitude above  $4m_K^2$ .

We showed in Refs. [1,2] that one can improve largely this situation by employing an appropriate Omnès function in the  $I = 0$  S-wave. The key point is that this function should be continuous under changes in the phase functions used above 1 GeV, a point overlooked in the previous studies.

## 2 The scalar form factor

Ref. [3] makes use of an Omnès representation for the pion scalar form factor,

$$\Gamma_\pi(t) = P(t) \exp \left[ \frac{t}{\pi} \int_{4M_\pi^2}^{\infty} ds' \frac{\phi_0(s')}{s'(s' - t - i\epsilon)} \right]. \quad (3)$$

Here,  $P(t)$  is a polynomial in  $t$  normalized such that  $P(0) = \Gamma_\pi(0)$  and whose zeroes are those of  $\Gamma_\pi(t)$ . On the other hand,  $\phi_0(t)$  is the continuous phase of  $\Gamma_\pi(t)/P(t)$ . Then Refs. [3,4] make use of asymptotic QCD which predicts that the scalar form factors should go as  $-1/t$  times a positive smooth factor for  $t \rightarrow +\infty$ , so that the phase of the form factor should tend to  $+\pi$  in the same limit. At this point, Refs. [3,4] make an assumption that is not always necessarily fulfilled. Namely, to identify  $\phi_0(t)$  with the phase of  $\Gamma_\pi(t)$ , that we denote in the following as  $\rho(t)$ . If this identification is done, as in Refs. [3,4], it follows that  $P(t)$  must be a constant,  $\Gamma_\pi(0)$ , because the behaviour for

$t \rightarrow +\infty$  that follows from Eq. (3) is

$$\Gamma_\pi(t) \rightarrow (-1)^{-\phi(\infty)/\pi} t^n t^{-\phi(\infty)/\pi} \Gamma_\pi(0) , \quad (4)$$

with  $n$  the degree of  $P(t)$ . As QCD implies in this assumption that  $\phi(\infty)/\pi = 1$ , then  $n = 0$  and hence  $P(t) = \Gamma_\pi(0)$ , just a constant. One must be aware that in Eq. (3)  $\phi_0(t)$  is the phase of  $\Gamma_\pi(t)/P(t)$ . Notice that the phase of  $\Gamma_\pi(t)$  is not continuous when crossing a zero located at  $t_1 \in \mathbb{R}$ , as there is a flip in the sign when passing through. However, the phase of  $\Gamma_\pi(t)/P(t)$  is continuous, since the zero is removed. This is the phase one should use in the Omnès representation, Eq. (3), because it results from a dispersion relation of  $\log \Gamma_\pi(t)/P(t)$ , and then  $\phi(t)$  must be continuous (but not necessarily  $\rho(t)$ ).

As stated, Ref. [3] took

$$\Gamma_\pi(t) = \Gamma_\pi(0) \exp \left[ \frac{t}{\pi} \int_{4M_\pi^2}^{\infty} ds' \frac{\rho(s')}{s'(s' - t - i\epsilon)} \right] . \quad (5)$$

So that the scalar form factor is given by,

$$\lambda r^2 \xrightarrow{s} \pi = \frac{6}{\pi} \int_{4M_\pi^2}^{+\infty} \frac{\rho(s)}{s^2} ds . \quad (6)$$

The phase  $\rho(s)$  is fixed in Refs. [3,4] by invoking Watson's final state theorem. For  $s < s_K$ ,  $s_K = 4M_K^2$ , it implies that  $\rho(s) = \delta_0(s)$ , where neglecting inelasticity due to multipion states, an experimental fact. For  $1.42 > \sqrt{s} \gtrsim 1.1$  GeV, Ref. [3] stressed the interesting fact that experimentally the inelasticity turns out to be small and hence Watson's final state theorem can be applied approximately again. In the narrow region between  $2M_K$  and 1.1 GeV inelasticity cannot be neglected but Ref. [3] argues that, as it is so narrow, its contribution to Eq. (6) is small anyhow and, furthermore, that the elasticity parameter  $\eta$  is not so small, so that one could still apply Watson's final state theorem with corrections. Thus, for  $s_K < s < 2 \text{ GeV}^2$ , Ref. [3] identifies again  $\rho(s) \simeq \delta_0(s)$ . Finally, for  $s > s_0 = 2 \text{ GeV}^2$  Ref. [3] takes a linear extrapolation from  $\delta_0(s_0)$  to  $\pi$ . One should here criticize that it is still a long way to run from values of  $\delta_0(s_0) \lesssim 2\pi$  up to  $\pi$  at  $s \rightarrow +\infty$ . With all these ingredients, and some error estimates, the value  $\lambda r^2 \xrightarrow{s} \pi = 0.75 \pm 0.07 \text{ fm}^2$  results [3,4].

As discussed above in the lines of Ref. [1], the steps performed in Ref. [3] are not always compatible. In Ref. [1] we took as granted the assumption that Watson's final state theorem can be approximately applied for  $1.5 \text{ GeV} > \sqrt{s} > 2M_K$ . Our assumption is in agreement with any explicit calculation of the pion non-strange  $I = 0$  scalar form factor [7,10,11,13] and it is the proper

generalized version of the assumption of Refs. [3,4] of identifying  $\rho(s) \simeq \delta_0(s)$ . Now, Watson's final state theorem implies that  $\phi(s) = \varphi(s)$  (modulo  $\pi$ ), with  $\varphi(s)$  the phase of the  $I = 0$  S-wave  $\pi\pi$  amplitude,  $t_{\pi\pi} = (\eta e^{2i\delta_0} - 1)/2i$ . It occurs, as stressed in Refs. [4, 16], that  $\varphi(s)$  can be either  $\sim \delta_0(s)$  or  $\sim \delta_0(s) - \pi$  depending on whether  $\delta_0(s_K) > \pi$  or  $< \pi$ , respectively, for  $s_K < s < 2 \text{ GeV}^2$ . The latter case corresponds to the calculation in Ref. [7], while the former is the preferred one in Ref. [4] and arguments are put forward for this preference in this reference.

Let us evolve continuously from one situation ( $\delta_0(s_K) < \pi$ ) to the other ( $\delta_0(s_K) > \pi$ ). In the first case  $\varphi(s)$  has an abrupt drop for  $s > s_K$  simply because then  $\eta < 1$  and while the real part of  $t_{\pi\pi}$  rapidly changes sign, its imaginary part is positive ( $> 0$ ). The rapid movement in the real part is due to the swift one in  $\delta_0(s)$  in the  $K\bar{K}$  threshold due to the  $f_0(980)$  resonance. As a result for  $s \lesssim s_K$ ,  $\varphi(s) = \delta_0(s) \simeq \pi$  and for  $s \gtrsim s_K$  then  $\varphi(s) < \pi/2$ . This rapid movement gives rise to a rapid drop in the Omnès function, Eq. (5), so that the modulus of the form factor has a deep minimum around  $s_K$ . Here, one is using Watson's final state theorem with  $\phi_0(s) = \varphi(s)$  and the form factor of Ref. [10] is reproduced. Notice as well that in this case the function  $\phi(s)$  approaches  $\pi$  from below for asymptotic  $s$  and then  $P(t) = \Gamma_0(0)$  in Eq. (3). Now, we consider the limit  $\delta_0(s) \rightarrow \pi^-$  for  $s \rightarrow s_K^-$ . The superscript  $- (+)$  indicates that the limit is approached from below(above). In the limit, the change in sign in the real part of  $t_{\pi\pi}$  occurs precisely at  $s_K$ , so that for  $s = s_K^-$ ,  $\varphi(s) = \pi$  and for  $s = s_K^+$  then  $\varphi(s) < \pi/2$  (indeed it can be shown from unitarity that must be 0). As a result one has a drop by  $-\pi$  in  $\varphi(s)$  which gives rise to a zero in the Omnès representation of the scalar form factor. Thus, the deep has evolved to a zero when  $\delta_0(s_K) \rightarrow \pi^-$ . Because of this zero the proper Omnès representation now involves a  $P(t) = \Gamma_\pi(0)(1 - t/s_K)$  and  $\phi(s)$  is no longer  $\varphi(s)$  but  $\simeq \varphi(s) + \pi \simeq \delta_0(s)$  for  $2.25 \text{ GeV}^2 > s > s_K$ . This follows simply because  $\phi(s)$  is continuous. Thus, we go into a new realm where  $\phi(s) \simeq \delta_0(s)$  and the degree of  $P(t)$  is 1, so that  $\Gamma_\pi(t)$  has a zero at the point  $s_1$  where  $\delta_0(s_1) = \pi$  and  $s_1 < s_K$ . Note that only at  $s_1$  the imaginary part of  $\Gamma_\pi(t)$  is zero and this fixes the position of the zero [1]. We should emphasize here that if one uses Eq. (5) with  $\phi(s) \simeq \delta_0(s)$ , as in Refs. [3, 4], then in the limit  $\delta_0(s) \rightarrow \pi^+$  for  $s \rightarrow s_K^+$  the Omnès representation would give rise to  $|\Gamma_\pi(s_K)| = \infty$ , while in the previously discussed limit of  $\delta_0(s) \rightarrow \pi^-$  for  $s \rightarrow s_K^-$  one has  $|\Gamma_\pi(s_K)| = 0$ . This discontinuity was corrected in Ref. [1] and it is the benchmark for a jump by one unit in the degree of  $P(t)$ , a discrete function, in Eq. (3).

Hence for  $\delta_0(s_K) \geq \pi$  one has to use

$$\Gamma_\pi(t) = \Gamma_\pi(0) \left( 1 - \frac{t}{s_K} \right) \exp \left[ \frac{t}{\pi} \int_{4M_\pi^2}^{\infty} ds' \frac{\phi(s')}{s'(s' - t - i\epsilon)} \right], \quad (7)$$

with  $\phi(s) \simeq \delta_0(s)$  for  $s < 2.25 \text{ GeV}^2$ . The uncertainties in this approximation for  $s > s_K$  are discussed in Ref. [1] and included in the final error in  $\lambda r^2 \rightarrow_s^\pi$ . The estimation is based in diagonalizing the  $I = 0$  S-wave S-matrix for  $s < 2.25 \text{ GeV}^2$ , so that two elastic channels can be singled out [4]. We also remark that now  $\phi(s)$  for  $\delta_0(s_K) \geq \pi$  must tend to  $2\pi$  asymptotically so as to match with the asymptotic behaviour of  $\Gamma_\pi(t)$  as  $-1/t$ . In this way we have now a very soft matching with asymptotic QCD since for  $s$  around  $2.25 \text{ GeV}^2$ ,  $\delta_0(s) \simeq 2\pi$ . This was not the case in Ref. [3,4]. Notice that from our work it follows that the precise knowledge of the asymptotic behaviour of the phase of the form factor is not relevant as  $\phi(s)$  can tend either to  $2\pi$  ( $\delta_0(s_K) > \pi$ ) or to  $\pi$  ( $\delta_0(s_K) < \pi$ ), and the results are very similar.

Our final value is

$$\lambda r^2 \rightarrow_s^\pi = 0.63 \pm 0.05 \text{ fm}^2. \quad (8)$$

The error takes into account different  $\pi\pi$   $I = 0$  S-wave parameterizations, namely those of Refs. [7] and [17], the error in the application of Watson's final state theorem above 1 GeV and up to 1.5 GeV, and the uncertainties in  $\phi(s)$  given by asymptotic QCD for  $s > 2.25 \text{ GeV}^2$ . This value is compatible with that of Ref. [7],  $\lambda r^2 \rightarrow_s^\pi = 0.61 \pm 0.04 \text{ fm}^2$ , and also with  $\lambda r^2 \rightarrow_s^\pi = 0.64 \pm 0.06 \text{ fm}^2$  of Ref. [13] calculated from Unitary CHPT.

### 3 The $\gamma\gamma \rightarrow \pi^0\pi^0$ reaction

In this section we briefly review Ref. [2]. This reference extended the approach of Refs. [6, 15] so as to be less sensitive to the phase of the  $I = 0$  S-wave  $\gamma\gamma \rightarrow \pi\pi$  amplitude above  $s_K$ . For this phase one has a similar situation to that of the scalar form factor of the pion, it can be either  $\sim \delta_0(s)$  or  $\sim \delta_0(s) - \pi$  for  $1 \lesssim s \lesssim 2.25 \text{ GeV}^2$  [2,6]. In the approach of Ref. [6] this originates an uncertainty that raises dramatically with energy above 0.5 GeV, such for  $\sqrt{s} \simeq 0.6 \text{ GeV}$  it is already 200%.

Let us denote by  $F_I(s)$  the S-wave  $I = 0$   $\gamma\gamma \rightarrow \pi\pi$  amplitude. The approach of Ref. [6, 15] is based on isolating the left hand cut contribution of  $F_I$  which is denoted by  $L_I$ . These authors also employ the Omnès function

$$\Omega_I(s) = \exp \left[ \frac{s}{\pi} \int_{4M_\pi^2}^{+\infty} ds' \frac{\phi_I(s')}{s'(s' - s)} \right], \quad (9)$$

where  $\phi_I(s')$  is the phase of  $F_I(s)$ . For  $I = 2$  by the application of Watson's final state theorem one has that  $\phi_2(s) = \delta_2(s)$ . For  $I = 0$  and  $s < s_K$ ,  $\phi_0(s) = \delta_0(s)$ . In the interval  $1.5 > \sqrt{s} > 1.1$  GeV,  $\phi_0 = \delta_0$  (modulo  $\pi$ ) because inelasticity is small again, as already remarked. Similarly as in the scalar form factor one can have because of the onset of inelasticity above  $2M_K$  and up to 1.1 GeV, that  $\phi_0$  is given either by  $\sim \delta_0$  or  $\sim \delta_0 - \pi$ .

Ref. [6] then performed a twice subtracted dispersion relation of the function  $(F_I(s) - L_I(s))/\Omega_I(s)$ . An important point to realize is that the previous function has no left hand cut and that  $F_I/\Omega_I$  has no right hand cut. Making use of the Low's theorem, which implies that  $L_I(s)$  is given by the Born term  $B_I(s)$  for  $s \rightarrow 0$ , one is only left with two subtraction constants to be fixed. One of these constants can be fixed by requiring that the  $\gamma\gamma \rightarrow \pi^0\pi^0$  S-wave amplitude,  $F_N(s)$ , has an Adler zero around  $M_\pi^2$ . The other one was fixed in Ref. [6] by requiring that the  $\gamma\gamma \rightarrow \pi^+\pi^-$  S-wave amplitude,  $F_C(s)$ , tends to the Born term  $B_C(s)$  for  $s \rightarrow 0$  up to  $\mathcal{O}(s^2)$ . One has to say that Ref. [6] did not include axial vector exchanges which indeed give rise to a term that vanishes for  $s \rightarrow 0$  only linearly in  $s$ . This gives rise to a difference in the cross section of around a 30% at  $\sqrt{s} \simeq 0.5$  GeV.

In order to better handle the ambiguities in  $\phi_0(s)$  above 1 GeV, Ref. [2] only uses  $\Omega_0(s)$  of Eq. (9)<sup>1</sup> for  $\phi_0(s) \sim \delta_0(s) - \pi$  for  $s > 1$  GeV<sup>2</sup>. For the case  $\phi_0(s) \sim \delta_0(s)$  above 1 GeV Ref. [2] employs

$$\tilde{\Omega}_0(s) = \left(1 - \frac{s}{s_1}\right) \exp \left[ \frac{s}{\pi} \int_{4M_\pi^2}^{+\infty} ds' \frac{\phi_I(s')}{s'(s' - s)} \right], \quad (10)$$

and then a twice dispersion relation of  $(F_0 - L_0)/\tilde{\Omega}_0$  is performed. It is important to realize, as stressed in Ref. [2], that because of the first order polynomial in front of the exponential in Eq. (10), one indeed has a *three* times subtracted dispersion relation for  $(F_0 - L_0)/\Omega_0$ . Recall that the latter is the original function used in Refs. [6, 15].

Because of this extra subtraction one can reduce dramatically the sensitivity to the  $\phi_0(s)$  above 1 GeV. The conditions used to fix the at most three subtraction constants that appear in our scheme are: i)  $F_N(s) \rightarrow 0$  for  $s \rightarrow 0$  with the slope fixed by one loop CHPT [18] (with an uncertainty of around 15%), ii)  $F_C(s) \rightarrow B_C(s) + \mathcal{O}(s)$  with the rest fixed by one loop CHPT (with the same 15% of estimated uncertainty). The third condition is an upper bound to the value of the resulting cross section in the  $f_0(980)$  region so that it is smaller than 200 nb. Notice that its experimental value is smaller than 40 nb and, hence, we take here a very conservative uncertainty.

<sup>1</sup>We already know about the lack of continuity of  $\Omega_0(s)$  when  $\delta_\pi(s_K)$  crosses  $\pi$  when taking  $\phi_0(s)$  given by  $\varphi(s)$  as in the case of the scalar form factor.

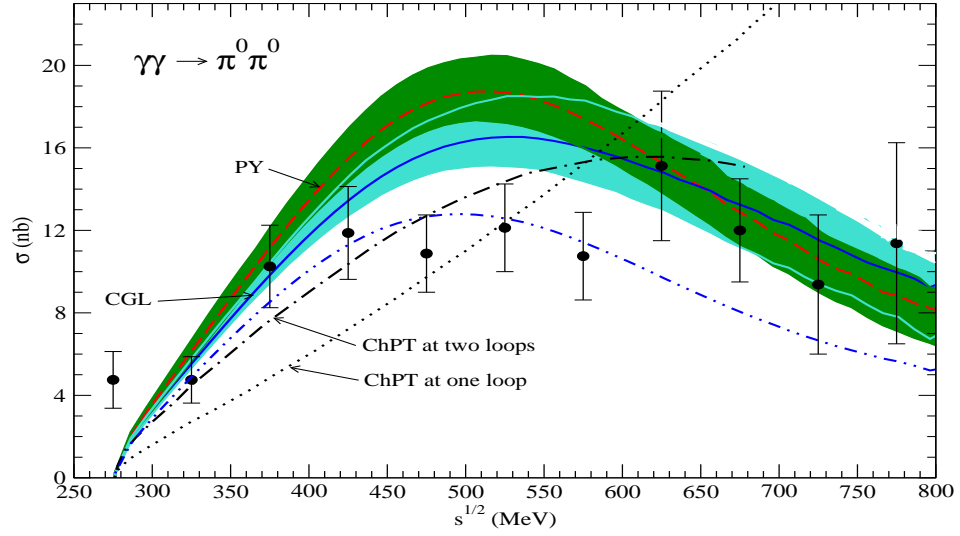


Figure 1: Final results for the  $\gamma\gamma \rightarrow \pi^0\pi^0$  cross section. Experimental data are from the Crystal Ball Coll. [19], scaled by  $1/0.8$ , as  $|\cos\theta| < 0.8$  is measured and S-wave dominates. The lighter band corresponds to Ref. [7] while the darker one to Ref. [17]. The dot-dot-dashed line results after removing the axial vector exchange contributions, as in Ref. [6] with  $\phi_0(s) \sim \delta_0(s) - \pi$  for  $s > 1 \text{ GeV}^2$ . The band along each line represents the theoretical uncertainty. The dotted line is the one loop  $\chi$ Pt result [18] and the dot-dashed one the two loop calculation [20].

We show in Fig. 1 our results together with the experimental points from Ref. [19]. The darker band corresponds to employ Ref. [17] for  $\delta_0(s)$  below  $1 \text{ GeV}$  and the lighter one to use Ref. [7]. One sees that now with more precise data one should be able to distinguish between different low energy  $\delta_0(s)$  parameterizations as the theoretical uncertainty is much reduced. The widths of the bands correspond to the uncertainties related to the  $\delta_0(s)$  and  $\delta_2(s)$  parameterizations used, those in fixing the three subtraction constants and in employing Watson's final state theorem for  $s > 1 \text{ GeV}^2$ , and it also includes the uncertainty in the asymptotic  $\phi_I(s)$  employed. In the figure we also show with the dotted line the one loop CHPT result [18] and with the dash-dotted line the two loop one [20]. There is a clear improvement when going from one to two loops in CHPT, though to have a perfect agreement with our results some higher order corrections are still needed. Finally, the dash-double-dotted line corresponds to the result of Ref. [6] with  $\phi_0(s) \sim \delta_0(s) - \pi$  for  $s > 1 \text{ GeV}^2$ . Let us recall that Ref. [6] does not include axial vector exchanges. Were they included, the results of this reference would fall inside the bands shown by our results.

By analytical continuation on the complex plane one can determine the coupling of the  $\sigma$  to  $\gamma\gamma$ ,  $g_{\sigma\gamma\gamma}$ , and calculate the width to  $\gamma\gamma$  of this resonance [2]. We then obtain for the ratio of couplings  $\left|\frac{g_{\sigma\gamma\gamma}}{g_{\sigma\pi\pi}}\right| = (2.1 \pm 0.2) \times 10^{-3}$ , with  $g_{\sigma\pi\pi}$  the  $\sigma$  coupling to two pions. The result of [6] corresponds to this ratio being 20% bigger at  $(2.53 \pm 0.09) \times 10^{-3}$ . Half of this difference is due to the omission of the exchanges of axial vector resonances in [6], and the other half comes from improvements delivered by our extra subtraction and our slightly different inputs. As a result, using the same value for  $|g_{\sigma\pi\pi}|$  as in [6], our resulting value for  $\Gamma(\sigma \rightarrow \gamma\gamma)$  would be around a 40% smaller than that in [6]. Taking into account different choices of  $|g_{\sigma\pi\pi}|$  we end with  $\Gamma(\sigma \rightarrow \gamma\gamma)$  in the interval 1.8 – 3 KeV.

## 4 Conclusions

We have shown that both Ynduráin's method [3] and the solution of the Muskhelishvili-Omnés equations [7, 10] provide compatible results for the quadratic scalar radius of the pion. The origin of the discrepancy between Refs. [3] and [7] was due to overlooking a zero in the scalar form factor in the former reference. We finally obtain [1]  $\lambda r^2 \rightarrow_s^\pi = 0.63 \pm 0.05 \text{ fm}^2$  and  $\bar{\ell}_4 = 4.5 \pm 0.3$ . These numbers are in good agreement with  $\lambda r^2 \rightarrow_s^\pi = 0.61 \pm 0.04 \text{ fm}^2$  and  $\bar{\ell}_4 = 4.4 \pm 0.2$  of Ref. [7].

We have also studied the  $\gamma\gamma \rightarrow \pi^0\pi^0$  reaction for energies  $\sqrt{s} \lesssim 0.7 \text{ GeV}$ , where S-waves dominate. We have extended the original approach of Ref. [6, 15] by performing a three times subtracted dispersion relation [2], instead of the twice subtracted originally employed. The sensitivity of the results with respect to the phase of the  $I = 0$   $\gamma\gamma \rightarrow \pi\pi$  S-wave above  $4M_K^2$  is then largely reduced. A key point is to properly handle the contribution of the  $f_0(980)$  resonance, at least at the level of the order of magnitude. Importantly, one can then use this reaction to distinguish between different low energy  $\pi\pi$  parameterizations once new data on  $\sigma(\gamma\gamma \rightarrow \pi^0\pi^0)$  are available. The  $\Gamma(\sigma \rightarrow \gamma\gamma)$  width is estimated in the range 1.8 – 3 KeV [2].

## Acknowledgments

This work has been supported in part by the MEC (Spain) and FEDER (EC) Grants FPA2004-03470 and Fis2006-03438, the Fundación Séneca (Murcia) grant Ref. 02975/PI/05, the European Commission (EC) RTN Network EURIDICE Contract No. HPRN-CT2002-00311 and the HadronPhysics I3 Project (EC) Contract No RII3-CT-2004-506078.

## References

- [1] J. A. Oller and L. Roca, *Phys. Lett.* **B651**, 139 (2007).
- [2] J. A. Oller, L. Roca and C. Schat, *arXiv:0708.1659 [hep-ph]*. To appear in *Phys. Lett.* **B**.
- [3] F. J. Ynduráin, *Phys. Lett.* **B578**, 99 (2004); (E)-*ibid* **B586**, 439 (2004).
- [4] F. J. Ynduráin, *Phys. Lett.* **B612**, 245 (2005).
- [5] F. J. Ynduráin, *arXiv:hep-ph/0510317*.
- [6] M. R. Pennington, *Phys. Rev. Lett.* **97**, 011601 (2006).
- [7] G. Colangelo, J. Gasser and H. Leutwyler, *Nucl. Phys.* **B603**, 125 (2001).
- [8] J. Gasser and H. Leutwyler, *Phys. Lett.* **B125**, 325 (1983).
- [9] G. Colangelo and S. Dür, *Eur. Phys. J.* **C33**, 543 (2004).
- [10] J. F. Donoghue, J. Gasser and H. Leutwyler, *Nucl. Phys.* **B343**, 341 (1990).
- [11] B. Moussallam, *Eur. Phys. J.* **C14**, 111 (2000).
- [12] J. Gasser and U.-G. Meißner, *Nucl. Phys.* **B357**, 90 (1991).
- [13] U. G. Meißner and J. A. Oller, *Nucl. Phys.* **A679**, 671 (2001).
- [14] J. Bijnens, G. Colangelo and P. Talavera, *JHEP* **9805**, 014 (1998).
- [15] D. Morgan and M. R. Pennington, *Phys. Lett.* **B272**, 134 (1991); *Z. Phys.* **C37**, 431 (1988) [Erratum-*ibid.* **C 39**, 590 (1988)].
- [16] B. Ananthanarayan, I. Caprini, G. Colangelo, J. Gasser and H. Leutwyler, *Phys. Lett.* **B602**, 218 (2004).
- [17] J. R. Peláez and F. J. Ynduráin, *Phys. Rev.* **D68**, 074005 (2003); *ibid* **D71**, 074016 (2005).
- [18] J. Bijnens and F. Cornet, *Nucl. Phys.* **B296**, 557 (1988). J. F. Donoghue, B. R. Holstein and Y. C. Lin, *Phys. Rev.* **D37**, 2423 (1988).
- [19] H. Marsiske *et al.* [Crystal Ball Collab.], *Phys. Rev.* **D41**, 3324 (1990).
- [20] S. Bellucci, J. Gasser and M. E. Sainio, *Nucl. Phys.* **B423**, 80 (1994); J. Gasser, M. A. Ivanov and M. E. Sainio, *Nucl. Phys.* **B728**, 31 (2005).

# PHOTOPRODUCTION OF $\omega$ AND $\omega$ IN THE NUCLEAR MEDIUM

E. Oset<sup>a</sup>, M. Kaskulov<sup>b</sup>, H. Nagahiro<sup>c</sup>, E. Hernandez<sup>d</sup> and S. Hirenzaki<sup>e</sup> <sup>1</sup>

<sup>a</sup>Dpto. Fisica Teorica and IFIC<sup>2</sup>

<sup>b</sup> Institut für Physik, Giessen, Germany

<sup>c</sup> Research Center for Nuclear Physics, Osaka University, Ibaraki, Osaka

<sup>d</sup> Facultad de Ciencias, Universidad de Salamanca, Salamanca, Spain

<sup>e</sup> Department of Physics, Nara Women's University, Nara 630-8506 Japan

## Abstract

We reanalyze data from ELSA on  $\omega$  production in nuclei, from where claims of a large shift of the mass were made earlier, which are tied to a certain election of the background in nuclei, very different in shape to the one on the proton. The reanalysis shows that the data demand a very large width of the  $\omega$  in the medium, with no need for a shift of the mass, for which the experiment is quite insensitive. We study possible  $\omega$  bound states in the nucleus and find that, even assuming a small width, they could not be observed with the present ELSA resolution. Finally we show that, due to the interplay of background and  $\omega$  signal, a two bump structure appears with the ELSA set up for the  $(\gamma, p)$  reaction that should not be misidentified with a signal of a possible  $\omega$  bound state in the nucleus.

## 1 Introduction

The interaction of vector mesons with nuclei has captured for long the attention of the hadron community. Along these lines, an approach has been followed by the CBELSA/ TAPS collaboration by looking at the  $\gamma\pi^0$  coming from the  $\omega$  decay, where a recent work [1] claims evidence for a decrease of the  $\omega$  mass in the medium of the order of 100 MeV from the study of the modification of the mass spectra in  $\omega$  photoproduction. Here we present the reanalysis of the data of [1] done in [2], where one concludes that the distribution is compatible with an enlarged  $\omega$  width of about 90 MeV at

---

<sup>1</sup>IFIC, Universidad de Valencia, Spain.

<sup>2</sup>IFIC, Institutos de Investigacion, Universidad de Valencia, apdo 22085, 46071 Valencia, Spain.

nuclear matter density and no shift in the mass and at the same time we show the insensitivity of the results to a mass shift. We also show results for the  $(\gamma, p)$  reaction searching for possible  $\omega$  bound states in the nucleus concluding that even in the case of a sufficiently attractive potential and small width no peaks can be seen with the present experimental resolution of about  $50\text{MeV}$  at ELSA. We also discuss the origin of a two peak structure of the  $(\gamma, p)$  cross section which should not be misidentified with evidence for an  $\omega$  bound state in the nucleus.

## 2 Preliminaries

We consider the photonuclear reaction  $A(\gamma, \omega \rightarrow \pi^0\gamma)X$  in two steps - production of the  $\omega$ -mesons and propagation of the final states. In the laboratory, where the nucleus with the mass number  $A$  is at rest, the nuclear total cross section of the inclusive reaction  $A(\gamma, \omega)X$ , including the effects of Fermi motion and Pauli blocking, plus effects of final state interaction of the particles produced, can be calculated as shown in [2].

The  $\omega$ -mesons are produced according to their spectral function  $S_\omega$  at a local density  $\rho(r)$

$$S_\omega(m_\omega, \tilde{m}_\omega, \rho) = -\frac{1}{\pi} \frac{\text{Im}\Pi_\omega(\rho)}{\left(\tilde{m}_\omega^2 - m_\omega^2 - \text{Re}\Pi_\omega(\rho)\right)^2 + \left(\text{Im}\Pi_\omega(\rho)\right)^2}, \quad (1)$$

where  $\Pi_\omega$  is the in-medium selfenergy of the  $\omega$ . The width of the  $\omega$  in the nuclear medium is related to the selfenergy by  $\Gamma_\omega(\rho, \tilde{m}_\omega) = -\text{Im}\Pi_\omega(\rho, \tilde{m}_\omega)/E_\omega$ . It includes the free width  $\Gamma_{free} = 8.49$  MeV and an in-medium part  $\Gamma_{coll}(\rho)$  which accounts for the collisional broadening of the  $\omega$  due to the quasielastic and absorption channels. In Eq. (1)  $\text{Re}\Pi_\omega = 2E_\omega \text{Re}V_{opt}(\rho)$ , where  $V_{opt}(\rho)$  is the  $\omega$  nucleus optical potential accounts for a possible shift of the  $\omega$  mass in the medium and we shall make some considerations about it latter on.

We also consider the situation when the energy of the incident photon beam is not fixed but constrained in some energy interval  $E_\gamma^{\min} < E_\gamma < E_\gamma^{\max}$ , and also take into account the photon flux produced at the ELSA facility.

## 3 The Monte Carlo simulation procedure

The computer MC simulation proceeds in close analogy to the actual experiment. At first, the multiple integral involved in the evaluation of the cross

section is carried out using the MC integration method. This procedure provides a random point  $\mathbf{r}$  inside the nucleus where the photon collides with the nucleon, also randomly generated from the Fermi sea with  $|\mathbf{p}_N| \leq k_F(\mathbf{r})$ . For the sample event in the MC integral the mass  $\tilde{m}_\omega$  of the  $\omega$  respects the spectral function  $S_\omega$  at local density  $\rho(r)$ , see Eq. (1). Inside the nucleus the  $\omega$ -mesons moving with the three momentum  $\mathbf{p}_\omega^{lab}$  necessarily interact with the nucleons in their way out of the nucleus. In the MC simulation the  $\omega$ -mesons are allowed to propagate a distance  $\delta\mathbf{L} = \frac{\mathbf{p}_\omega^{lab}}{|\mathbf{p}_\omega^{lab}|} \delta L$  and at each step,  $\delta L \simeq 0.1$  fm, the reaction probabilities for different channels like the decay of the  $\omega$  into  $\pi^0\gamma$  and  $\pi\pi\pi$  final states, quasielastic scattering and in-medium absorption are properly calculated. Details of the simulation can be seen in [2].

We use the following parameterization for the width,  $\Gamma_{abs} = \Gamma_0 \frac{\rho(r)}{\rho_0}$ , where  $\rho_0 = 0.16$  fm $^{-3}$  is the normal nuclear matter density.

The propagation of pions in nuclei is done using a MonteCarlo simulation procedure. In their way out of the nucleus pions can experience the quasielastic scattering or can be absorbed. The intrinsic probabilities for these reactions as a function of the nuclear matter density are calculated using the phenomenological model of Refs [3], which also includes higher order quasielastic cuts and the two-body and three-body absorption mechanisms. Details for the present case are described in [2].

## 4 In-medium $\omega$ -meson width and nuclear transparency

In this section we discuss an extraction of the in-medium inelastic width of the  $\omega$  in the photonuclear experiments. As a measure for the  $\omega$ -meson width in nuclei we employ the so-called nuclear transparency ratio

$$\tilde{T}_A = \frac{\sigma_{\gamma A \rightarrow \omega X}}{A \sigma_{\gamma N \rightarrow \omega X}} \quad (2)$$

i.e. the ratio of the nuclear  $\omega$ -photoproduction cross section divided by  $A$  times the same quantity on a free nucleon.  $\tilde{T}_A$  describes the loss of flux of  $\omega$ -mesons in the nuclei and is related to the absorptive part of the  $\omega$ -nucleus optical potential and thus to the  $\omega$  width in the nuclear medium.

We have done the MC calculations for the sample nuclear targets:  ${}^{12}_6\text{C}$ ,  ${}^{16}_8\text{O}$ ,  ${}^{24}_{12}\text{Mg}$ ,  ${}^{27}_{13}\text{Al}$ ,  ${}^{28}_{14}\text{Si}$ ,  ${}^{31}_{15}\text{P}$ ,  ${}^{32}_{16}\text{S}$ ,  ${}^{40}_{20}\text{Ca}$ ,  ${}^{56}_{26}\text{Fe}$ ,  ${}^{64}_{29}\text{Cu}$ ,  ${}^{89}_{39}\text{Y}$ ,  ${}^{110}_{48}\text{Cd}$ ,  ${}^{152}_{62}\text{Sm}$ ,  ${}^{208}_{82}\text{Pb}$ ,  ${}^{238}_{92}\text{U}$ . In the following we evaluate the ratio between the nuclear cross sections in heavy nuclei and a light one, for instance  ${}^{12}\text{C}$ , since in this way, many other nuclear effects not related to the absorption of the  $\omega$  cancel in the ratio,  $T_A$ .

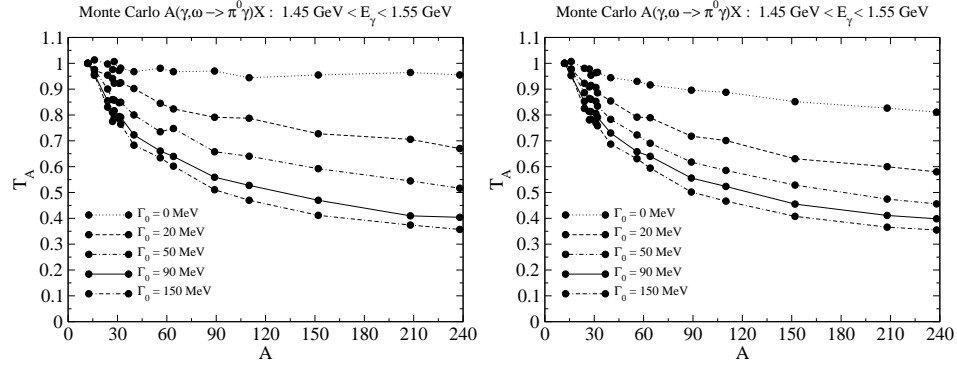


Figure 1: The result of the Monte Carlo method for the  $A$ -dependence of the nuclear transparency ratio  $T_A$  without (left panel) and with (right panel) FSI of outgoing pions. A lower cut  $T_\pi > 150$  MeV on the kinetic energy of the outgoing pions has been used to suppress the contribution of the distorted events due to FSI. The incident photon beam was constrained in the range  $1.45 \text{ GeV} < E_\gamma < 1.55 \text{ GeV}$ . The carbon  $^{12}\text{C}$  was used as the reference target in the ratio of the nuclear cross sections. With  $\Gamma_{abs} = \Gamma_0 \frac{\rho(r)}{\rho_0}$ , where  $\rho_0$  is the normal nuclear matter density, the dotted, dashed, dash-dotted, solid and dash-dash-dotted curves correspond to  $\Gamma_0 = 0 \text{ MeV}$ ,  $\Gamma_0 = 20 \text{ MeV}$ ,  $\Gamma_0 = 50 \text{ MeV}$ ,  $\Gamma_0 = 90 \text{ MeV}$  and  $\Gamma_0 = 150 \text{ MeV}$ , respectively.

The results of the MC calculation for the  $A$ -dependence of the nuclear transparency ratio  $T_A$  are presented in Fig. 1. The incident photon beam was constrained in the range  $1.45 \text{ GeV} < E_\gamma < 1.55 \text{ GeV}$  - a region which is considered in the analysis of the CBELSA/TAPS experiment [4, 5]. In Fig. 1 (left panel) we show the results for the transparency ratio when the collisional broadening and FSI of the  $\omega$  are taken into account but without FSI of the pions from  $\omega \rightarrow \pi^0\gamma$  decays inside the nucleus. The right panel corresponds to considering in addition the FSI of the pions.

By using these results and taking into account the preliminary results of CBELSA/TAPS experiment [5] we get an estimate for the  $\omega$  width  $\Gamma_{abs} \simeq 90 \times \frac{\rho(r)}{\rho_0} \text{ MeV}$ . This estimate must be understood as an average over the  $\omega$  three momentum.

## 5 In-medium $\omega$ -meson mass and CBELSA/TAPS experiment

The first thing one should note is that the  $\omega$  line shape reconstructed from  $\pi^0\gamma$  events strongly depends on the background shape subtracted from the bare  $\pi^0\gamma$  signal. In Ref. [1] the shape of the background was chosen such that

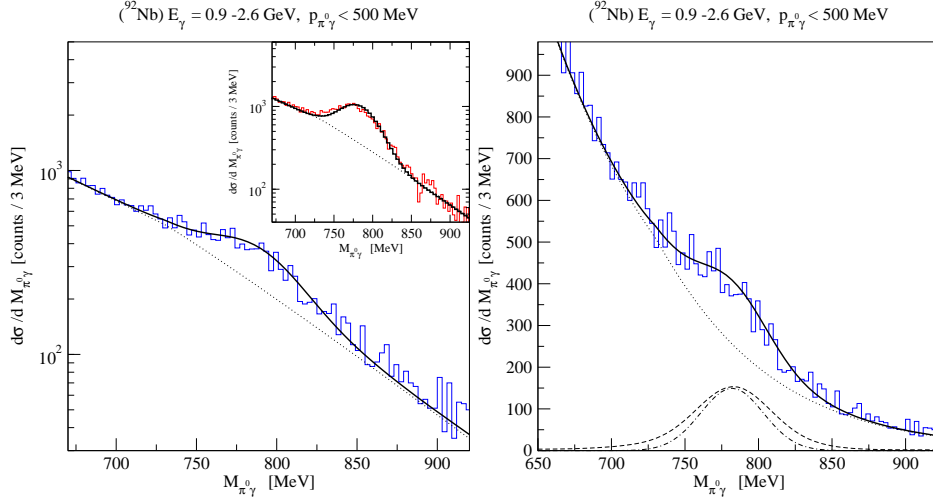


Figure 2: Left panel: Invariant mass spectra reconstructed from the  $\pi^0\gamma$  events in the  $(\gamma, \pi^0\gamma)$  reaction from Nb target (solid curve). The experimental data are from Ref. [1]. The incident photon beam has been constrained in the range  $0.9 \text{ GeV} < E_{\gamma}^{in} < 2.6 \text{ GeV}$ . Dotted curve is an uncorrelated  $\pi^0\gamma$  background (see the text). Right panel: Same but in linear scale. The dashed and dash-dash-dotted curves correspond to the  $\omega \rightarrow \pi^0\gamma$  events with and without the kinematic cut  $|\mathbf{p}_{\pi^0\gamma}| < 500 \text{ MeV}$ , respectively. The normalization without cut is arbitrary. The solid line corresponds to the sum of the background and the dashed line. Inset (left panel): The  $\pi^0\gamma$  invariant mass spectra in the elementary  $p(\gamma, \pi^0\gamma)p$  reaction. Same background line shape (dotted curve) as for the Nb target has been used. The solid line is the sum of the background and  $\omega \rightarrow \pi^0\gamma$  events.

it accounted for all the experimental strength at large invariant masses. This choice was done both for the elementary  $\gamma p \rightarrow \pi^0\gamma p$  reaction as well as for nuclei. As we shall show, this choice of background in nuclei implies a change of the shape from the elementary reaction to that in the nucleus for which no justification was given. We shall also show that when the same shape for the background as for the elementary reaction is chosen, the experiment in nuclei shows strength at invariant masses higher than  $m_{\omega}$  where the choice of [1] necessarily produced no strength. We will also see that the experimental data can be naturally interpreted in terms of the large in-medium  $\omega$  width discussed above without the need to invoke a shift in the  $\omega$  mass in the medium.

In Fig. 2 we show the experimental data (solid histogram) for the  $\pi^0\gamma$  invariant mass spectra in the reaction  $(\gamma, \pi^0\gamma)$  [1] from  $^{92}_{41}\text{Nb}$  target. The inset (left panel) corresponds to the  $\pi^0\gamma$  spectra from the hydrogen target. In our MC calculations the incident photon beam has been constrained in the range  $0.9 \text{ GeV} < E_{\gamma}^{in} < 2.6 \text{ GeV}$ . The higher momentum cut  $|\mathbf{p}_{\pi^0\gamma}| =$

$|\mathbf{p}_{\pi^0} + \mathbf{p}_\gamma| < 500$  MeV on a three momentum of the  $\pi^0\gamma$  pair was imposed as in the actual experiment. First, we use the hydrogen target, see inset in Fig. 2 (left panel), to fix the contribution of the uncorrelated  $\pi^0\gamma$  background (dotted curve) which together with the  $\pi^0\gamma$  signal from  $\omega \rightarrow \pi^0\gamma$  decay, folded with the Gaussian experimental resolution of 55 MeV as in Ref. [1], gives a fair reproduction of the experimental spectra. Then we assume the same shape of the  $\pi^0\gamma$  background in the photonuclear reaction. The weak effect of the FSI of the pions found in the calculation, with the cuts imposed in the experiment, strongly supports this assumption.

In the following we use the  $\omega$  inelastic width of  $\Gamma_0 = 90$  MeV at  $\rho_0$ . The exclusive  $\omega \rightarrow \pi^0\gamma$  MC spectra is shown by the dashed curve (right panel). The solid curve is the reconstructed  $\pi^0\gamma$  signal after applying the cut on  $\pi^0\gamma$  momenta and adding the background fixed when using the hydrogen target (dotted curve). Note that the shape of the exclusive  $\pi^0\gamma$  signal without applying a cut on  $\pi^0\gamma$  momenta (dash-dotted curve) is dominated by the experimental resolution and no broadening of the  $\omega$  is observed. This is in agreement with data of Ref. [1]. But applying the cut one increases the fraction of in-medium decays coming from the interior of the nucleus where the spectral function is rather broad and as a result the broadening of the  $\pi^0\gamma$  signal with respect to the signal (without cut) can be well seen. The resulting MC spectra (solid curve) shows the accumulation of the  $\pi^0\gamma$  events from the left and right sides of the mass spectra, and it is consistent both with our choice of the uncorrelated  $\pi^0\gamma$  background and experimental data.

We have also done the exercise of seeing the sensitivity of the results to changes in the mass. As shown in [2], a band corresponding to having the  $\omega$  mass in between  $m_\omega \pm 40\rho/\rho_0$  MeV is far narrower than the statistical fluctuations. In other words, this experiment is too insensitive to changes in the mass to be used for a precise determination of the shift of the  $\omega$ -mass in the nuclear medium. We should also note that the peak position barely moves since it is dominated by the decay of the  $\omega$  outside the nucleus.

## 6 Production of bound $\omega$ states in the $(\gamma, p)$ reaction

Here we evaluate the formation rate of  $\omega$  bound states in the nucleus by means of the  $(\gamma, p)$  reaction. We use the Green function method [6] to calculate the cross sections for  $\omega$ -mesic states formation as described in Refs. [7] in detail. The theoretical model used here is exactly same as that used in these references.

The  $\omega$ -nucleus optical potential is written here as  $V(r) = (V_0 + iW_0)\frac{\rho(r)}{\rho_0}$ , where  $\rho(r)$  is the nuclear experimental density for which we take the two parameter Fermi distribution. We consider three cases of the potential strength as:  $(V_0, W_0) = -(0, 50)$ ,  $-(100, 50)MeV$  and  $-(156, 29)MeV$ . The last of the potentials is obtained by the linear density approximation with the scattering length  $a = 1.6 + 0.3i$  fm [8]. This potential is strongly attractive with weak absorption and hence should be the ideal case for the formation of  $\omega$  mesic nuclei. No  $\omega$  bound states are expected for the first potential which has only an absorptive part. The second potential has a strong attraction with the large absorptive part as indicated in Ref. [4]. For the first two potentials we find no visible peaks in the spectrum since the width is so large. For the third potential we observe peaks but they are washed out when folded with the experimental resolution of about  $50MeV$  of ELSA.

## 7 Monte Carlo simulation of the reaction of the $(\gamma, p)$ reaction

We next apply the MonteCarlo simulation explained above to describe the  $(\gamma, p)$  reaction studied at ELSA. Because our MC calculations represent complete event simulations it is possible to take into account the actual experimental acceptance of ELSA [4] (see details in [9]).

We start our MC analysis with the cross section of the elementary reaction  $\gamma p \rightarrow \omega p \rightarrow \pi^0 \gamma p$ . With this we determine the cross section for  $\omega$  formation and follow the fate of the protons at the same time.

There are also sources of background like from  $\gamma p \rightarrow \pi^0 \pi^0 p$ , or  $\gamma p \rightarrow \pi^0 \eta p$ , where one of the two photons from the decay of the  $\pi^0$  or the  $\eta$  is not measured. We show in Fig. 3 the cross section  $d\sigma/dE_{\pi^0\gamma}$  coming from the  $\gamma p \rightarrow \pi^0 \pi^0 p$  reaction followed by the decay  $\pi^0 \rightarrow \gamma\gamma$  of either of the  $\pi^0$  (left panel) and from the  $\gamma p \rightarrow \pi^0 \eta p$  reaction followed by the decay  $\eta \rightarrow \gamma\gamma$  (right panel). As one can see, the contribution from the  $\pi^0 \pi^0$  photoproduction to the background is the dominant one among the two. The important thing, thus, is that these two sources of background, with the cuts imposed, produce a background peaked at -100 MeV. For the exclusive  $\pi^0 \gamma$  events coming from  $\gamma p \rightarrow \omega p \rightarrow \pi^0 \gamma p$  an experimental resolution of 50 MeV was imposed, see Ref. [1]. We obtain a factor of two bigger strength at the  $\omega$  peak than at the peak from the  $\gamma p \rightarrow \pi^0 \pi^0 p$  background. Experimentally, this seems to be also the case from the preliminary data of CBELSA/TAPS,

In the following we assume that the inclusive  $\pi^0 \gamma$  background scales with respect to the target nucleus mass number  $A$  like  $\sigma_A \simeq A \sigma_{elem}$ . But this

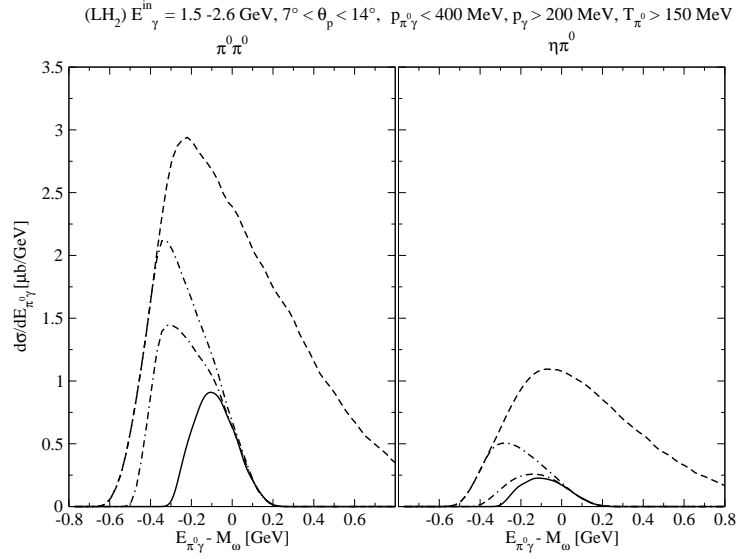


Figure 3: The differential cross section  $d\sigma/dE_{\pi^0\gamma}$  of the reactions  $\gamma p \rightarrow \pi^0\pi^0 p$  (left panel) and  $\gamma p \rightarrow \pi^0\eta p$  (right panel) followed by the decay  $\pi^0(\eta) \rightarrow \gamma\gamma$  as a function of the  $E_{\pi^0\gamma} - m_\omega$  where  $E_{\pi^0\gamma} = E_{\pi^0} + E_\gamma$ . The following cuts were imposed:  $E_\gamma^{in} = 1.5 \div 2.6$  GeV and  $7^\circ < \theta_p < 14^\circ$  (dashed curves);  $E_\gamma^{in} = 1.5 \div 2.6$  GeV,  $7^\circ < \theta_p < 14^\circ$  and  $|\mathbf{p}_{\pi^0} + \mathbf{p}_\gamma| < 400$  MeV (dash-dotted curves); plus the cut  $T_{\pi^0} > 150$  MeV (dash-dash-dotted curves) and plus the cut  $|\mathbf{p}_\gamma| > 200$  MeV (solid curves).

is not the case for the exclusive  $\pi^0\gamma$  events coming from the decay of the  $\omega \rightarrow \pi^0\gamma$ , since the rather strong absorption of the  $\omega$  inside the nucleus changes the scaling relation and  $\sigma_A(\omega \rightarrow \pi^0\gamma) \simeq A^\alpha \sigma_{elem}(\omega \rightarrow \pi^0\gamma)$ , where the attenuation parameter  $\alpha < 1$ .

In Fig. 4 we show the result of the MC simulation for the  $E_{\pi^0\gamma} - m_\omega$  spectra reconstructed from the  $\pi^0$  and  $\gamma$  events. The calculations are performed for the sample nuclear targets  $^{12}\text{C}$ ,  $^{40}\text{Ca}$ ,  $^{92}\text{Nb}$  and  $^{208}\text{Pb}$ . The kinematic and acceptance cuts discussed before have been already imposed. The MC distributions are normalized to the nuclear mass number  $A$ . The solid curves correspond to the sum of the inclusive  $\pi^0\gamma$  background (dash-dotted curve), and the exclusive  $\pi^0\gamma$  events coming from the direct decay of the  $\omega \rightarrow \pi^0\gamma$ . The contributions of the exclusive  $\omega \rightarrow \pi^0\gamma$  events are shown by the dashed curves. We note a very strong attenuation of the  $\omega \rightarrow \pi^0\gamma$  signal with respect to the background contribution with increasing nuclear mass number  $A$ . This is primary due to the stronger absorption of the  $\omega$ -mesons with increasing nuclear matter density. The former exercise indicates that given the

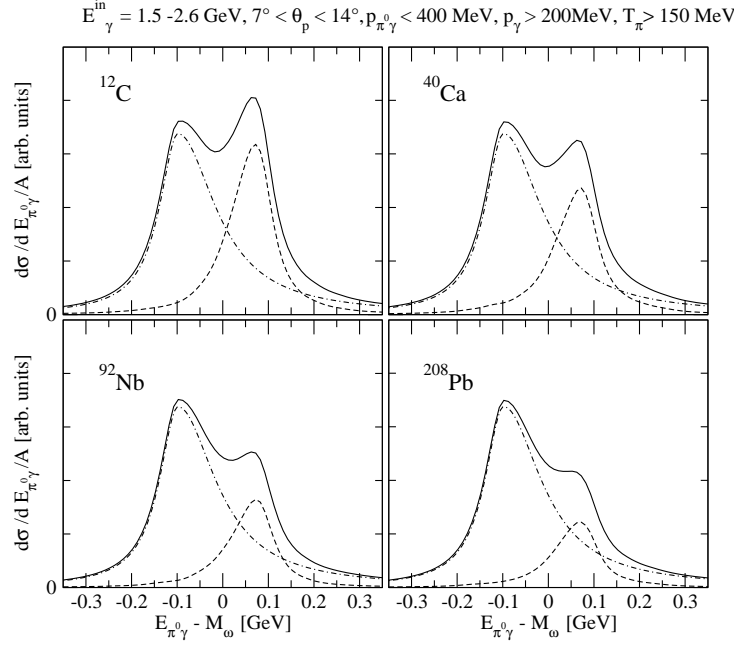


Figure 4: The differential cross section  $d\sigma/dE_{\pi^0\gamma}$  of the reaction  $A(\gamma, \pi^0\gamma)X$  as a function of  $E_{\pi^0\gamma} - m_\omega$  from  $^{12}\text{C}$ ,  $^{40}\text{Ca}$ ,  $^{92}\text{Nb}$  and  $^{208}\text{Pb}$  nuclear targets. The reconstructed exclusive events from the  $\omega \rightarrow \pi^0\gamma$  decay are shown by the dashed curves. The  $\pi^0\gamma$  background is shown by the dash-dotted curves. The sum of the two contributions is given by the solid curves. The following cuts were imposed:  $E_\gamma^{\text{in}} = 1.5 \div 2.6 \text{ GeV}$ ,  $7^\circ < \theta_p < 14^\circ$ ,  $|\mathbf{p}_{\pi^0} + \mathbf{p}_\gamma| < 400 \text{ MeV}$ ,  $|\mathbf{p}_\gamma| > 200 \text{ MeV}$  and  $T_\pi > 150 \text{ MeV}$ . The exclusive  $\omega \rightarrow \pi^0\gamma$  signal has been folded with the 50 MeV experimental resolution. All spectra are normalized to the corresponding nuclear mass numbers  $A$ .

particular combination of  $\pi^0\gamma$  from an uncorrelated background and from  $\omega$  decay, and the different behaviour of these two sources in the  $\pi^0\gamma$  production in nuclei, a double hump structure is unavoidable in nuclei with this set up, and one should avoid any temptation to associate the lower energy peak to a possible bound state in the nucleus.

## 8 Conclusions

The studies done in [2] and [9] show that: 1) The ELSA results on inclusive  $\omega$  production in nuclei can be interpreted in terms of a large  $\omega$  width in the medium without the need of a mass shift. 2) The results are very insensitive to a mass shift in matter. 3) With the large medium  $\omega$  width

derived from the ELSA data no visible peaks for  $\omega$  bound states are seen, even with hypothetical large  $\omega$  binding. 4) Even in the hypothetical case of small widths, the possible  $\omega$  bound states would not be resolved with the present ELSA resolution. 5) When looking at the  $(\gamma, p)$  reaction with the present ELSA experimental set up, a double hump structure appears in the calculation from the interplay of the  $\omega$  signal and the background. The peak at lower energies is related to the background, with the cuts imposed, and should not be misidentified with a possible  $\omega$  bound state in the nucleus.

## Acknowledgments

This work is partly supported by DGICYT contract number BFM2003-00856, the Generalitat Valenciana, the projects FPA2004-05616 (DGICYT) and SA016A07 (Junta de Castilla y Leon). This research is part of the EU Integrated Infrastructure Initiative Hadron Physics Project under contract number RII3-CT-2004-506078.

## 9 References

### References

- [1] D. Trnka *et al.* [CBELSA/TAPS Collaboration], Phys. Rev. Lett. **94** (2005) 192303
- [2] M. Kaskulov, E. Hernandez and E. Oset, Eur. Phys. J. A **31** (2007) 245
- [3] L. L. Salcedo, E. Oset, M. J. Vicente-Vacas and C. Garcia-Recio, Nucl. Phys. A **484** (1988) 557.
- [4] D. Trnka, PhD Thesis, University of Giessen, 2006.
- [5] M. Kotulla, [arXiv:nucl-ex/0609012].
- [6] O. Morimatsu, K. Yazaki, Nucl. Phys. A **435** (1985) 727;
- [7] D. Jido, H. Nagahiro, S. Hirenzaki, Phys. Rev. C **66** (2002) 045202;
- [8] F. Klingl, T. Waas and W. Weise, Nucl. Phys. A **650** (1999) 299
- [9] M. Kaskulov, H. Nagahiro, S. Hirenzaki and E. Oset, Phys. Rev. C **75** (2007) 064616

# SCALAR MESONS FROM UNITARIZED CHIRAL PERTURBATION THEORY: $N_c$ AND QUARK MASS DEPENDENCES

*José R. Peláez and G. Ríos*  
*Departamento de Física Teórica II. Facultad de CC. Físicas.*  
*Universidad Complutense*  
*28040 Madrid, SPAIN*

## Abstract

We review recent studies of light scalar meson properties by means of unitarization techniques, obtained from dispersion theory, and applied to the Chiral Perturbation Theory expansion. In particular, light scalars do not follow the  $N_c$  dependence of  $\bar{q}q$  states although a subdominant  $\bar{q}q$  component may be observed to arise for the  $f_0(600)$  around 1 GeV, where another  $\bar{q}q$  multiplet is believed to exist. Finally, we present our preliminary results on the quark mass dependence of the  $f_0(600)$  and  $\rho(770)$  resonances.

## 1 Introduction

Light hadron spectroscopy lies outside the applicability range of QCD perturbative calculations. Still, in this low energy region one can use Chiral Perturbation Theory (ChPT) [1] to obtain a model independent description of the dynamics of pions, kaons and etas. These particles are the Goldstone Bosons (GB) associated to the QCD spontaneous breaking of Chiral Symmetry and ChPT is built as a low energy expansion that contains those fields in the terms of a Lagrangian that respect all QCD symmetries, including its symmetry breaking pattern. The small quark masses of the three lightest flavors can be treated systematically within the perturbative chiral expansion and thus ChPT becomes a series in momenta and meson masses, generically  $O(p^2/\Lambda^2)$ . At lowest order there are no free parameters apart from masses and  $f_\pi$ , the pion decay constant, that sets the scale  $\Lambda \equiv 4\pi f_\pi$ . The chiral expansion can be renormalized order by order by absorbing the loop divergences in higher order counterterms, known as low energy constants (LEC), whose values depend on the specific QCD dynamics. That is, other theories

with spontaneous chiral symmetry breaking at the same scale will have the same leading order, but will differ in the values of the LEC.

The renormalized LEC have to be determined from experiment, since they cannot be calculated from perturbative QCD. However, thanks to the fact that ChPT has the same symmetries than QCD and that it should couple to different kind of currents in the same way, it is still possible to determine *in a model independent way* how the constants that appear in ChPT, and therefore the observables, depend on some QCD parameters. This is indeed the case of the leading dependence on the number of colors  $N_c$  and of the dependence on the quark masses.

## 2 Unitarization and dispersion theory

The unitarity of the  $S$  matrix implies that, for physical values of  $s$ , partial waves  $t^{IJ}$  of definite isospin  $I$  and angular momenta  $J$  for *elastic* meson-meson scattering should satisfy

$$\text{Im } t^{IJ} = \sigma |t^{IJ}|^2 \Rightarrow \text{Im } \frac{1}{t^{IJ}} = -\sigma \quad (1)$$

where  $\sigma = 2p/\sqrt{s}$ , and  $p$  is the CM momenta of the two mesons. Note that unitarity implies that  $|t^{IJ}| \leq 1/\sigma$ , and a strong interaction is characterized precisely by the saturation of this unitarity bound.

However, partial waves are obtained within ChPT as a low energy expansion  $t \simeq t_2 + t_4 + t_6 + \dots$ , (To simplify the notation, from now on we will drop the  $IJ$  indices.) where  $t_{2k} \equiv O(p/(4\pi f_\pi))^{2k}$ , and thus they cannot satisfy unitarity exactly, but just perturbatively, i.e:

$$\text{Im } t_2 = 0, \quad \text{Im } t_4 = \sigma t_2^2, \quad \text{etc...} \quad (2)$$

Unitarization methods extend the ChPT series to high energies by using the fact, remarked in eq.(1), that *the imaginary part of the inverse amplitude is known exactly*. Hence, we can approximate the real part of  $\text{Re } t^{-1} \simeq t_2^{-2}(t_2 + \text{Re } t_4 + \dots)$  with ChPT, and find that

$$t \simeq = \frac{1}{\text{Re } t^{-1} - i\sigma} = \frac{t_2}{1 - t_4/t_2} \quad (3)$$

This is known as the one-channel Inverse Amplitude Method [2, 3]. A usual complaint is that the ChPT series is only valid at low energies, and there is no reason to use it beyond that regime.

However, not only the complete  $t$ , but also the *inverse amplitude*  $1/t$  and the ChPT series to next to leading order (NLO) and beyond, have an

analytic structure with a “physical cut” extending from threshold to  $\infty$  and a “left cut” from  $-\infty$  up to the highest value of  $s$  allowed in the crossed channel ( $s = 0$  if the two mesons are identical). It is then possible to write the following dispersion relation [3] for  $t_4$

$$t_4 = b_0 + b_1 s + b_2 s^2 + \frac{s^3}{\pi} \int_{s_{th}}^{\infty} \frac{\text{Im } t_4(s') ds'}{s'^3 (s' - s - i\epsilon)} + LC(t_4). \quad (4)$$

where “LC” stands for a similar integral over the left cut and we have three subtractions to ensure convergence. A similar dispersion relation can be written for the function  $G \equiv t_2^2/t$ , by simply replacing  $t_4$  by  $G$  and changing the name of the subtraction constants. Since  $t_2$  is real, these two functions have opposite imaginary parts on the physical cut so that their contributions from the “physical cut” integral are *exactly* opposite. Their subtraction constants correspond to the value of these functions at  $s = 0$  where it is perfectly justified to use the ChPT expansion. And finally, their contributions from the left cut are also opposite from each other, but this time only up to the NNLO ChPT terms. This guarantees a good description of the integrand only at low energies, but that is precisely the region that has been weighted by the three subtractions.

Therefore, note that the IAM is actually exact on the physical region and only uses the ChPT approximations for the subtraction constants at  $s = 0$ , where the use of ChPT is totally justified, and for the left cut, where the use of ChPT might not be justified at large  $|s'|$ , but the influence of this region is dumped by the subtractions. The use of the IAM is even more justified if used sufficiently far from this left cut, since this has an additional  $(s - s')$  suppression. In summary, there are no model dependencies in the approach, but just approximations to a given order in ChPT, and indeed the IAM can be derived not only at NLO but also at NNLO.

Remarkably, the simple formula of the IAM, eq.(3), is able to describe the  $\pi\pi$  and  $\pi K$  scattering data not only at low energies, where it reproduces the ChPT series, but also in the resonance region. This is done with values of the ChPT parameters that are compatible with the values obtained within standard ChPT.

In addition, the IAM generates the poles [3,4] associated to the resonances in the second Riemann sheet. This is of relevance since, in particular, the scalar resonances are the subject of intense debate that has been lasting for several decades, and as we have seen, the IAM is able to generate their poles from first principles like unitarity, analyticity and the QCD chiral symmetry breaking, without introducing these resonances by hand. Thus, we can study, without any a priori assumption, the nature of these states as follows from first principles and QCD.

### 3 $N_c$ behavior

The QCD  $1/N_c$  expansion [5] allows for a clear identification of a  $\bar{q}q$  resonance, since it becomes a bound state, whose width follows an  $O(1/N_c)$  behavior, whereas its mass should behave as  $O(1)$ . For our purposes, the relevant observation is that the leading  $1/N_c$  behavior of the ChPT constants is known in a model independent way. Thus, in order to know the leading  $N_c$  behavior of the resonances generated with the IAM, we just have to change the ChPT parameters according to their established  $N_c$  scaling properties. For instance, the pion decay constant scales as  $O(\sqrt{N_c})$ , and we thus substitute  $f_\pi$  by  $f_\pi\sqrt{N_c}/3$ . Similar replacements, but according to their respective  $N_c$  scaling, have to be done with all ChPT parameters.

This procedure [4, 6] was first applied to the coupled channel IAM [4, 7] using the one loop SU(3) ChPT amplitudes, that also include kaons and etas, and the result was that the light vector resonances  $\rho(770)$  and  $K^*(982)$  followed remarkably well the expected behavior of  $\bar{q}q$  states. In contrast, the members of the light scalar nonet, namely, the sigma or  $f_0(600)$ , the kappa or  $K_0(800)$ , as well as the  $f_0(980)$  and  $a_0(980)$  resonances, all showed a behavior at odds with that of  $\bar{q}q$  states (Only the  $a_0(980)$  could display a  $\bar{q}q$  behavior in a limited corner of parameter space). It follows that *the dominant component of light scalar mesons does not have a  $\bar{q}q$  nature*.

Very recently [8] we have extended the analysis to two loops in SU(2) ChPT, using the IAM one-channel formalism just described above to NNLO. In addition, we have developed a quantitative measure of how close a resonance is to a  $\bar{q}q$  behavior: Taking into account subleading orders, to consider a resonance a  $\bar{q}q$  state, it is enough that

$$M_{N_c}^{\bar{q}q} = \widetilde{M} \left( 1 + \frac{\epsilon_M}{N_c} \right), \quad \Gamma_{N_c}^{\bar{q}q} = \frac{\widetilde{\Gamma}}{N_c} \left( 1 + \frac{\epsilon_\Gamma}{N_c} \right), \quad (5)$$

where  $\widetilde{M}$  and  $\widetilde{\Gamma}$  are unknown but  $N_c$  independent and the subleading terms have been gathered in  $\epsilon_M, \epsilon_\Gamma \simeq 1$ , since we expect *generically* 30% uncertainties at  $N_c = 3$ . Thus, for a  $\bar{q}q$  state, the *expected*  $M_{N_c}$  and  $\Gamma_{N_c}$  can be obtained from those at  $N_c - 1$  generated by the IAM, as follows

$$M_{N_c}^{\bar{q}q} \simeq M_{N_c-1} \left[ 1 + \epsilon_M \left( \frac{1}{N_c} - \frac{1}{N_c-1} \right) \right] \equiv M_{N_c-1} + \Delta M_{N_c}^{\bar{q}q}, \quad (6)$$

$$\Gamma_{N_c}^{\bar{q}q} \simeq \frac{\Gamma_{N_c-1}(N_c-1)}{N_c} \left[ 1 + \epsilon_\Gamma \left( \frac{1}{N_c} - \frac{1}{N_c-1} \right) \right] \equiv \frac{\Gamma_{N_c-1}(N_c-1)}{N_c} + \Delta \Gamma_{N_c}^{\bar{q}q}.$$

Note the  $\bar{q}q$  index for quantities obtained *assuming* a  $\bar{q}q$  behavior. The reason to write the  $N_c$  values from those at  $N_c - 1$  is to be able to calculate from

what  $N_c$  a resonance starts behaving as a  $\bar{q}q$ , which is of interest to search for subdominant  $\bar{q}q$  components. Thus, we can define an *averaged*  $\bar{\chi}_{\bar{q}q}^2$  to check how close a resonance is to a  $\bar{q}q$  behavior, as follows:

$$\bar{\chi}_{\bar{q}q}^2 = \frac{1}{2n} \sum_{N_c=4}^n \left[ \left( \frac{M_{N_c}^{\bar{q}q} - M_{N_c}}{\Delta M_{N_c}^{\bar{q}q}} \right)^2 + \left( \frac{\Gamma_{N_c}^{\bar{q}q} - \Gamma_{N_c}}{\Delta \Gamma_{N_c}^{\bar{q}q}} \right)^2 \right] \quad (7)$$

When this quantity is smaller than one, it indicates a  $\bar{q}q$  behavior, whereas a larger value indicates that it does not behave predominantly as such. Note also that imposing the minimization of the  $\bar{\chi}^2$  in eq.(7) we could try to force a given  $\bar{q}q$  behavior for a given resonance when fitting data.

When evaluating eq.(7) above, one has to be careful not to consider too large  $N_c$  values. The reason is that, after all, we are interested in the physical state at  $N_c = 3$  and, most likely, states are a mixture of different components with different  $N_c$  behavior. By allowing for too large values of  $N_c$  we could be altering too radically the nature of the state, and, since  $\bar{q}q$  states are expected to survive in the large  $N_c$  limit, whereas other kind of states, like tetraquarks, glueballs, etc... do not, even insignificant admixtures of  $\bar{q}q$  at  $N_c = 3$  could become dominant for sufficiently large  $N_c$ . Thus, the most relevant information will come from  $N_c$  not too far from  $N_c = 3$  and we consider  $N_c$  values smaller than one order of magnitude its physical value of 3, let us say  $N_c < 20$ .

In this respect, J.A. Oller raised an interesting concern at the end of my talk in this conference, about the absence of  $\eta'(980)$  in our calculations. Certainly, the  $\eta'$  mass is due to the  $U_A(1)$  anomaly, and decreases like  $1/\sqrt{N_c}$ . If we were to consider very large  $N_c$ , this particle should be definitely included in our calculations, because it would become the most relevant degree of freedom of QCD at very large  $N_c$ . However, if we limit ourselves to, say  $N_c = 20$ , its mass would be  $950 \text{ MeV} \times \sqrt{3/20} \simeq 370 \text{ MeV}$ , so, it is still much heavier than the pions that can still be considered as the only low energy degrees of freedom of the theory (Furthermore, its contribution would be similar to that of kaon loops, although there are both neutral and charged kaon loops, whereas we only have one  $\eta'$ ). This is an additional reason why it would be just wrong to consider too large values of  $N_c$  to draw conclusions about the nature of the sigma.

Therefore, with the measure in eq.(7) and  $n = 20$ , we are able to quantify the deviation of the  $f_0(600)$  from the  $\bar{q}q$  behavior: at NLO, even in the most favorable case when we try to impose that it behaves as a  $\bar{q}q$ , the data fit yields a  $\bar{\chi}_{\bar{q}q}^2 = 125$  for the  $f_0(600)$ .

When using the NNLO (two loop ChPT calculation), we have many more ChPT parameters, which are not well known, and give a great deal of free-

dom. For the NNLO low energy constants (LECS) we thus use standard estimates [9] with a 100% uncertainty. Still, there are large correlations and some very weak dependences on some of these parameters that can be driven far from their standard values for negligible improvements in the  $\chi^2$  of the data fit. For that reason we stabilize the values of the LECS, imposing also the minimization of a  $\chi_{LECS}^2$  together with that of the data. Also, using eq.(7), we impose the  $\rho(770)$ , which is a well established  $\bar{q}q$  state, to behave as such. Thus, at two loops, we find that the  $f_0(600)$  comes out with  $\bar{\chi}_{\bar{q}q}^2 = 4$  in the most favorable case when we try to impose it to behave as a  $\bar{q}q$ . Even relaxing the  $\rho$   $\bar{q}q$  behavior, we still get  $\bar{\chi}_{\bar{q}q}^2 = 3.5$  for the  $f_0(600)$ . In conclusion, *the two loop IAM confirms once again that the  $f_0(600)$  does not behave predominantly as a  $\bar{q}q$  state*, whereas that behavior is nicely followed by the  $\rho$ , whose  $\bar{\chi}_{\bar{q}q}^2 < 0.35$  at NLO and  $\bar{\chi}_{\bar{q}q}^2 = 0.93$  at NNLO.

We show in Fig.1 the NNLO behavior of the  $\rho$  and  $f_0(600)$  mass and width. In the top figure, we show the  $N_c = 3$  behavior of the  $\rho$ . The full dots represent the values, for different  $N_c$ , of its "pole mass",  $M$ , whereas the empty dots represent its "pole width",  $\Gamma$ , both normalized to their physical values at  $N_c = 3$ . It can be clearly seen that, already for very low  $N_c$ ,  $M/M_3$  starts behaving as  $O(1)$  and  $\Gamma/\Gamma_3$  as  $O(1/N_c)$ , as expected for a  $\bar{q}q$  state. As commented above, the behavior shown in this plot yields  $\bar{\chi}_{\bar{q}q}^2 = 0.93$  for the  $\rho$ . In contrast, in the bottom figure, and with the same conventions, we show the  $N_c$  behavior of the  $\sigma$  or  $f_0(600)$ . This time we are also imposing in the fit minimization that it should behave as a  $\bar{q}q$  state. Obviously it does not, at least until  $N_c \simeq 8$ , and its  $\bar{\chi}_{\bar{q}q}^2 = 4$ . Despite the  $\sigma$  is still not behaving predominantly as a  $\bar{q}q$  state, the price due to trying to impose such behavior is that the fit suffers a clear deterioration, since the data now has a  $\chi^2/dof = 1.5$  (compared to 1.1 before) and the  $\rho$  now has  $\bar{\chi}_{\bar{q}q}^2 = 1.3$ , thus with a much worse  $\bar{q}q$  behavior.

Remarkably, it is also clear that the  $\sigma$  or  $f_0(600)$  follows a  $\bar{q}q$  behavior for  $N_c > 8$  or 10. This suggests the existence of a *subdominant*  $\bar{q}q$  behavior in the  $\sigma$  or  $f_0(600)$  that originates at a mass around twice that of the sigma  $\simeq 1\text{GeV}$ , where a  $\bar{q}q$  nonet is usually located.

## 4 Quark mass dependence

We now present our very preliminary work [10] on the quark mass dependence of the mass and widths of the  $\sigma$  and  $\rho$  mesons, which could be of interest to compare with lattice studies, where the small physical masses of light quarks are hard to implement.

With the IAM we can also study the quark mass dependence of the light

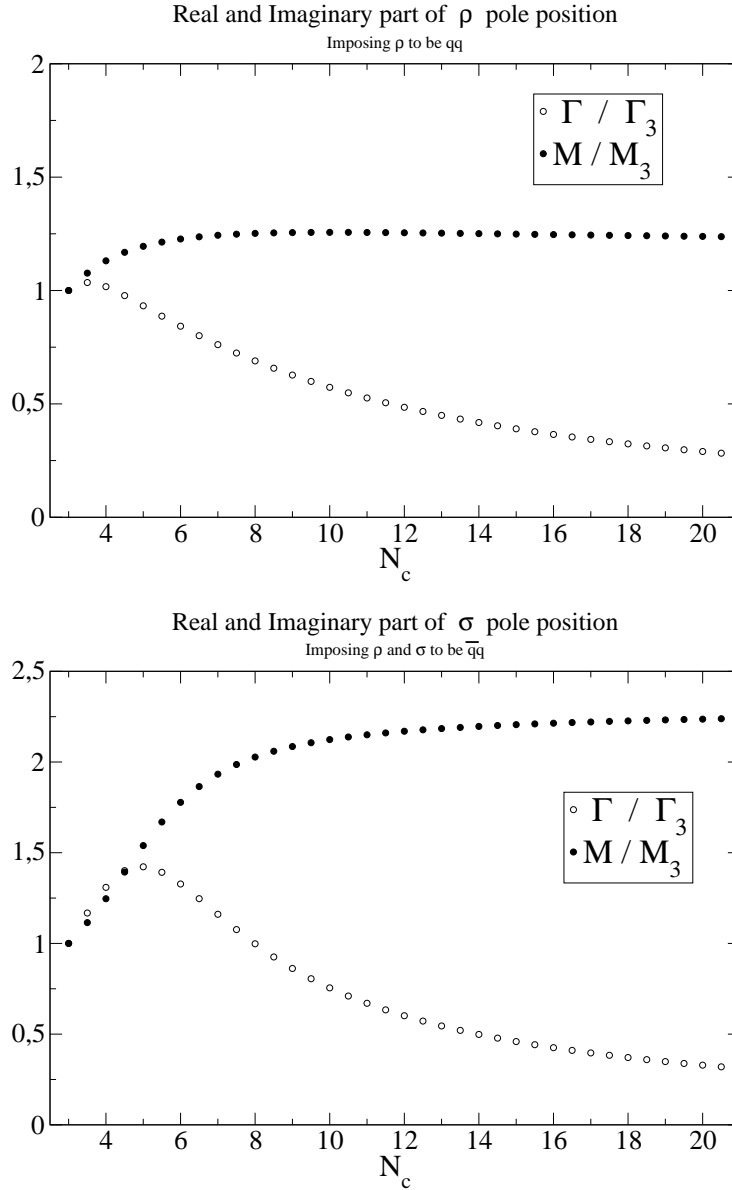


Figure 1: Mass and width dependence on  $N_c$  for the  $\rho$  (Top) and  $\sigma$  (Bottom) resonances. We have normalized all  $M$  and  $\Gamma$  to their respective physical values at  $N_c = 3$ . Note that, already for  $N_c$  close to 3, the  $\rho$  mass and width follow nicely the respective  $O(1)$  and  $O(1/N_c)$  behavior expected for a  $\bar{q}q$  state. In contrast, the  $\sigma$  does not behave predominantly as such, but only develops, above  $N_c = 8$  or 10, a *subdominant*  $\bar{q}q$  behavior with a mass  $\simeq 1$  GeV.

resonances by changing the meson masses in the amplitudes, which is equivalent to change quark masses, since, to leading order  $M_\pi^2 \sim m_q + \dots$ . We have done this in  $SU(2)$  Unitarized ChPT at NLO. In  $\pi\pi$  scattering at NLO there appear four LECs  $l_1, \dots, l_4$ . Phase shifts are almost insensitive to  $l_3^r$  and  $l_4^r$ , for which we take the values in [1]:  $l_3^r = 0.8 \pm 3.8$ ,  $l_4^r = 6.2 \pm 5.7$ , evaluated at a renormalization scale of  $\mu = 770$  MeV. In contrast, we make a data fit for  $l_1^r$  and  $l_2^r$ , finding  $l_1^r = -3.7 \pm 0.2$ ,  $l_2^r = 5.0 \pm 0.4$ , in fairly good agreement with standard values. Finally, when changing pion masses we have to take into account that amplitudes are customarily written [1] in terms of the  $\mu$  independent LECs  $\bar{l}$  [1] and the physical pion decay constant  $f_\pi = f_0 \left(1 + \frac{M_\pi^2}{16\pi^2 f_0^2} \bar{l}_4 + \dots\right)$  that depend explicitly on the pion mass.

We have taken two criteria to set the applicability limit of our method, that is, the maximum value of the pion mass we can use. First, we do not want to spoil the chiral expansion, and second, we do not want the two-pion threshold to reach the  $K\bar{K}$  threshold. Taking into account that  $SU(3)$  ChPT works well with a kaon mass of  $\sim 495$  MeV, and that, according to NLO ChPT, if we set  $M_\pi \simeq 500$  MeV the kaon mass becomes  $\sim 600$  MeV, this means that for 500 MeV pions,  $\pi\pi$  scattering is still elastic for about 200 MeV above threshold. Hence the above criteria impose an applicability bound of  $M_\pi \simeq 500$  MeV. To go beyond that we would need a coupled channel  $SU(3)$  formalism.

We show in Fig.2 how the  $\rho$  and  $f_0(600)$  poles in the second Riemann sheet move as  $M_\pi$  changes. Both the  $\rho$  and  $\sigma$  mass increase with the pion mass, but that of the  $\sigma$  grows faster. In addition, both widths decrease, partly due to phase space reduction (the two-pion threshold grows faster than both resonance masses). When the two-pion threshold reaches the  $\sigma$  mass, its pole remains for a short while on the second sheet with a non-zero width but quickly reaches the real axis where it meets its conjugate partner from the upper plane and splits again into two poles corresponding to virtual bound states located on the real axis below threshold. As the pion mass keeps increasing, one of those "virtual state" poles moves toward threshold and jumps into the first sheet, whereas the other one remains in the second sheet. Although, of course, this happens for very large  $M_\pi$  masses, such an analytic structure, with two very asymmetric poles in different sheets of an angular momentum zero partial wave, may be a signal of molecular structure, as discussed by M. Pennington in this conference.

Finally, as the pion mass increases, the  $\rho$  pole moves toward the real axis and just when threshold reaches its mass it jumps into the real axis on the first sheet, thus becoming a traditional bound state, while its conjugate partner remains on the second sheet practically at the very same position as

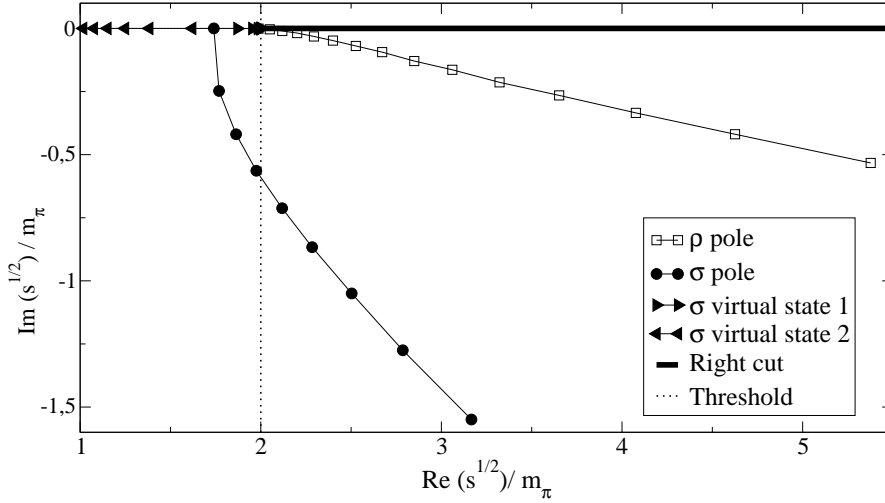


Figure 2:  $\rho$  and  $\sigma$  complex plane pole movement with increasing pion mass. To ease the comparison of the pole position relative to the two-pion threshold we normalize by the pion mass that is changing. Note how the sigma pole moves toward the real axis below threshold where it splits in two virtual states, whereas the  $\rho$  pole just moves toward threshold.

the one in the first.

A publication with further details is in preparation [10] including results of the  $f_0(600)$  and  $\rho(770)$  mass and width evolution with the pion mass as well as a comparison with other works and lattice results. Estimates of uncertainties and possibly an extension to the SU(3) coupled channel case are presently in progress.

## Acknowledgments

J.R. Peláez thanks the MENU07 organizers for their kind invitation and the great scientific organization. We also thank J.A. Oller and C. Hanhart for useful discussions and comments.

Research partially funded by Spanish CICYT contracts FPA2005-02327, BFM2003-00856 as well as Banco Santander/Complutense contract PR27/05-13955-BSCH, and part of the EU integrated infrastructure initiative HADRON-PHYSICS PROJECT, under contract RII3-CT-2004-506078.

## References

- [1] S. Weinberg, *Physica* **A96** (1979) 327. J. Gasser and H. Leutwyler, *Annals Phys.* **158** (1984) 142; *Nucl. Phys. B* **250** (1985) 465.
- [2] T. N. Truong, *Phys. Rev. Lett.* **61** (1988) 2526. *Phys. Rev. Lett.* **67**, (1991) 2260; A. Dobado, M.J.Herrero and T.N. Truong, *Phys. Lett.* **B235** (1990) 134.
- [3] A. Dobado and J. R. Pelaez, *Phys. Rev. D* **47** (1993) 4883. *Phys. Rev. D* **56** (1997) 3057.
- [4] J. R. Pelaez, *Mod. Phys. Lett. A* **19**, 2879 (2004)
- [5] G. 't Hooft, *Nucl. Phys. B* **72** (1974) 461. E. Witten, *Annals Phys.* **128** (1980) 363.
- [6] J. R. Pelaez, *Phys. Rev. Lett.* **92**, 102001 (2004)
- [7] F. Guerrero and J. A. Oller, *Nucl. Phys. B* **537** (1999) 459 [Erratum-ibid. *B* **602** (2001) 641]. A. Gómez Nicola and J. R. Peláez, *Phys. Rev. D* **65** (2002) 054009 and *AIP Conf. Proc.* **660** (2003) 102 [hep-ph/0301049].
- [8] J. R. Pelaez and G. Rios, *Phys. Rev. Lett.* **97**, 242002 (2006)
- [9] J. Bijnens *et al.*, *Nucl. Phys. B* **508**, 263 (1997)
- [10] C. Hanhart, J.R. Peláez and G. Ríos, *in preparation*.

# RECENT RESULTS FROM THE COMPASS EXPERIMENT AT CERN

*S. Platchkov*<sup>1</sup>  
DAPNIA/SPhN  
F-91191, Gif-sur-Yvette  
France

## Abstract

Recent data from the COMPASS experiment at CERN, including inclusive and semi-inclusive double-spin asymmetries are presented. The gluon and the valence quarks spin distributions are determined from the data.

## 1 Introduction

Understanding the nucleon spin structure is one of the main objectives of the COMPASS experiment [1] at CERN. In the years 2002-2006, COMPASS collected a large amount of data on inclusive, semi-inclusive, and transverse spin asymmetries. In this talk two of our new results are presented: the shape of the gluon spin distribution, as inferred from a Next-to-Leading order QCD fit to the inclusive asymmetries, and the valence quarks spin distribution, as determined from the semi-inclusive data.

## 2 The polarized gluon distribution

Deep-inelastic scattering cross section asymmetries were measured [2] for values of the Bjorken variable  $x$  ranging from 0.004 to 0.7 and for four-momenta  $Q^2$  between 1 and 100  $(GeV/c)^2$ . The deuteron spin structure function  $g_1^d(x)$  is determined from the experimental asymmetries, by taking into account the beam and the target polarizations, the target dilution factor, the ratio of the longitudinal to transverse cross sections and the  $F_2(x)$  unpolarized structure function. The data are in good agreement with previous results on  $g_1^d(x)$  from SMC [3]. The statistical accuracy is significantly improved, particularly in the lowest  $x$  region, where  $g_1^d(x)$  is found to be compatible with zero.

---

<sup>1</sup>On behalf of the COMPASS collaboration.

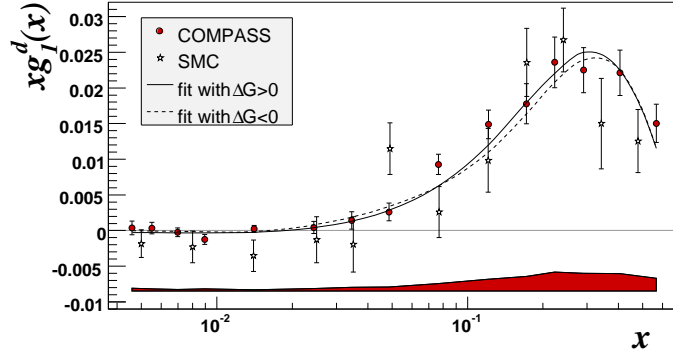


Figure 1: The deuteron  $g_1^d$  structure function, as measured by COMPASS and by SMC [3]. The solid and the dashed curves are the QCD fits to the data for the solution with  $\Delta G > 0$  and  $\Delta G < 0$  respectively.

A Next-to-Leading Order QCD fit of the world proton, deuteron and  $^3\text{He}$  data available (see Ref. [2] and references therein) was carried out, based on two different approaches: in the  $(x, Q^2)$  space and in the space of moments. Both approaches use the QCD evolution equations, in which the  $Q^2$  dependence of the nucleon polarized structure function is described in terms of singlet  $\Delta\Sigma(x)$ , non-singlet  $\Delta q_3(x)$  and  $\Delta q_8(x)$ , and gluon  $\Delta G(x)$  distributions. The fits are performed in the  $\overline{MS}$  renormalization and factorization scheme at the reference  $Q_0^2$  value of 3  $(\text{GeV}/c)^2$ . In total, 230 data points were used, out of which 43 are from COMPASS.

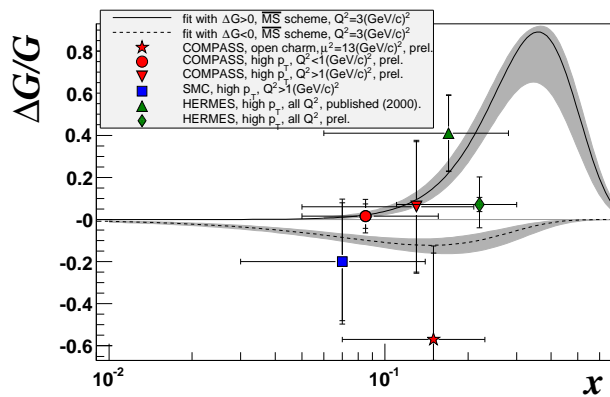


Figure 2: QCD fit results for the gluon distribution, together with the available  $\Delta G/G$  measurements from COMPASS, SMC, and HERMES [5].

Each of the two analyses of  $g_1^d(x)$  provide us with two different solutions, one with  $\Delta G < 0$  and the other with  $\Delta G > 0$ . The two solutions (Fig. 1) yield comparable  $\Delta\Sigma(x)$ ,  $\Delta q_3(x)$ , and  $\Delta q_8(x)$  distributions with nearly identical  $\chi^2$  probabilities. In spite of the sign difference, the two fits to  $g_1^d(x)$  are hardly distinguishable all over the measured range in  $x$ . They start to differ only for the very low values of  $x$  and have different behavior when  $x$  tends to zero.

The first moments  $\eta_G$  for each of the two gluon distributions are small for both solutions and nearly equal in absolute values, i.e.  $|\eta_G| \approx 0.2 - 0.3$ . The available measurements [5] of  $\Delta G/G$ , all obtained via the Photon-Gluon Fusion (PGF) process, are compared to the fits results in Fig. 2. Within the present statistical errors, the PGF measurements are compatible with either of the two solutions.

From the difference between  $\Delta\Sigma(x)$  and  $\Delta q_8(x)$  we also determine the strange quark distribution. It is negative, peaks at high  $x$ , and contributes to the nucleon spin for  $\Delta s + \Delta\bar{s} = -0.10 \pm 0.01(stat.) \pm 0.01(evol.)$ .

### 3 Polarized valence quark distribution

Additional insight into the nucleon spin structure is obtained through the correlation between the flavor of the struck quark, and the outgoing hadron detected in coincidence with the scattered lepton. In the period 2002-2004, COMPASS has measured [6] semi-inclusive asymmetries for both positive and negative hadrons. The asymmetries are in good agreement with previous data from SMC [3] and HERMES [4] experiments, and show improved statistics, particularly in the region of low  $x$  ( $x < 0.04$ ).

From the positive and negative hadron spin asymmetries we define the difference asymmetry. At leading order the difference asymmetry is not sensitive to the fragmentation functions, which cancel out in the cross-section ratio. Since for a deuteron target both pion and kaon difference asymmetries are related to the valence quark polarization  $\Delta u_v + \Delta d_v$ , no particle identification is required.

The valence quark spin distribution is determined from the difference asymmetries by using the unpolarized valence distribution from Ref. [7] and correcting for the deuteron D-state. The results are shown in Fig. 3. For values of  $x > 0.3$  inclusive data points are also displayed. Since in this region the contribution of the unpolarized sea quarks becomes negligible, all the polarization is due to the valence quarks. The inclusive results agree with the semi-inclusive data, and have better statistical errors.

The first moment of the valence quark spin distribution has the value

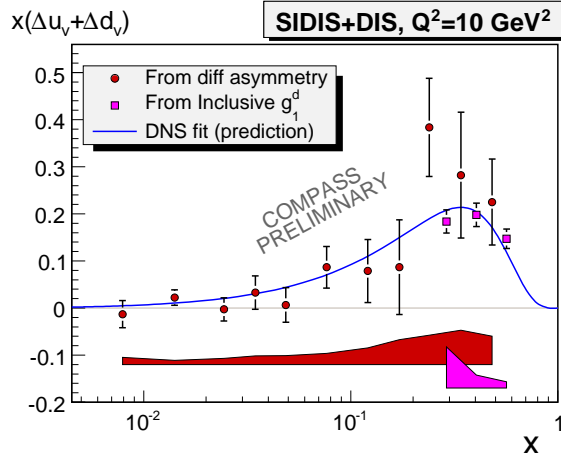


Figure 3: Valence quark spin distribution, evolved to  $Q^2 = 10 \text{ (GeV/c)}^2$ . The square points at  $x > 0.3$  are obtained from the inclusive measurements on  $g_1^d$ . The line is a fit result prediction from Ref. [8].

$0.41 \pm 0.07(\text{stat.}) \pm 0.05(\text{syst.})$ . The contribution of the unmeasured regions to this value was found to be negligible. Combining the valence quarks first moment with the first moment of  $g_1(x)$ , for which both valence and sea quarks contribute, we derive the light quark polarized sea contribution. The result  $(0.0 \pm 0.04(\text{stat.}) \pm 0.03(\text{syst.}))$  indicates that if  $\Delta\bar{u}(x)$  and  $\Delta\bar{d}(x)$  are different from zero, they should have an opposite sign. The polarized sea should be then flavor asymmetric:  $\Delta\bar{u}(x) = -\Delta\bar{d}(x)$ , at the two  $\sigma$  level.

## References

- [1] P. Abbon, *et al.*[COMPASS Collab.], Nucl. Instrum. Methods **A577**, 455 (2007).
- [2] V. Alexakhin, *et al.*[COMPASS Collab.], *Phys. Lett.* **B647**, 330 (2007).
- [3] B. Adeva, *et al.*[SMC Collab.], *Phys. Lett.* **B420**, 180 (1998).
- [4] A. Airapetian, *et al.*[HERMES Collab.], *Phys. Rev.* **D71**, 012003 (2005).
- [5] R. Kuhn, talk at this conference and references therein.
- [6] M. Alekseev, *et al.*[COMPASS Collab.], CERN-PH-EP/2007-024.
- [7] A. Martin, W. Stirling and R. Thorne, *Phys. Rev.* **B636**, 259 (2006).

- [8] D. de Florian, G. Navarro, R. Sassot, *Phys. Rev. D* **71** 094018 (2005).

## NEW RESULTS ON THE RARE DECAY

$$\eta \rightarrow \pi^0 \gamma \gamma$$

*S. Prakhov (for the Crystal Ball Collaboration at AGS and the Crystal Ball Collaboration at MAMI)*<sup>1</sup>

Department of Physics and Astronomy  
University of California, Los Angeles  
BOX 951547, Los Angeles, California 90095-1547, USA

### Abstract

New results on the rare, doubly-radiative decay  $\eta \rightarrow \pi^0 \gamma \gamma$  have been obtained from a reanalysis of the Crystal Ball experiment performed at the AGS and the first analysis of a recent Crystal Ball experiment at MAMI-B. The analyses have yielded the first results on the dependence of the decay width on the two-photon invariant mass squared,  $d\Gamma(\eta \rightarrow \pi^0 \gamma \gamma)/dm^2(\gamma \gamma)$ . The new values for the full decay width are:  $\Gamma(\eta \rightarrow \pi^0 \gamma \gamma) = 0.285 \pm 0.031_{\text{stat}} \pm 0.049_{\text{syst}}$  eV for the AGS reanalysis, and  $\Gamma(\eta \rightarrow \pi^0 \gamma \gamma) = 0.290 \pm 0.059_{\text{stat}} \pm 0.022_{\text{syst}}$  eV for the MAMI experiment. The results of the AGS and MAMI measurements are in good agreement with each other, and they are close to the calculations of Chiral Perturbation Theory assuming vector-meson dominance.

## 1 Introduction

The rare, doubly-radiative decay

$$\eta \rightarrow \pi^0 \gamma \gamma \tag{1}$$

is attracting much attention as there are large uncertainties in its experimental measurements and in calculations that are based on Chiral Perturbation Theory ( $\chi$ PTh).

The experimental challenges in measuring  $\eta \rightarrow \pi^0 \gamma \gamma$  are formidable because of the smallness of doubly-radiative processes, which is typically of order  $\alpha^2 = 1/137^2$ . Major backgrounds, which can mimic  $\eta \rightarrow \pi^0 \gamma \gamma$  events, come from  $\eta \rightarrow 3\pi^0$  decays with overlapping photon showers and  $\eta \rightarrow \gamma \gamma$  decays with split-off showers. Since  $BR(\eta \rightarrow 3\pi^0) = 0.325$  and

---

<sup>1</sup>E-mail: prakhov@bmnk8.physics.ucla.edu

$BR(\eta \rightarrow \gamma\gamma) = 0.394$ , the background from these  $\eta$  decay modes is very significant. Another large background, which also needs to be suppressed, comes from  $\pi^0\pi^0$  production.

The uncertainties in  $\chi$ PTh calculations of the  $\eta \rightarrow \pi^0\gamma\gamma$  decay amplitude are related to the fact that the leading  $\mathcal{O}(\mathbf{p}^2)$  term and the  $\mathcal{O}(\mathbf{p}^4)$  tree contribution are absent because neither  $\pi^0$  nor  $\eta$  can emit a photon. Very small contributions come from the  $\mathcal{O}(\mathbf{p}^4)$  pion and kaon loops as they are greatly suppressed by G-parity invariance and the large mass of kaons, respectively. The main contribution to the  $\eta \rightarrow \pi^0\gamma\gamma$  decay amplitude comes from the  $\mathcal{O}(\mathbf{p}^6)$  counterterms that are needed in  $\chi$ PTh to cancel various divergences. However, the coefficients of these counterterms are not determined by  $\chi$ PTh itself and depend on the model used for the calculations. Since any  $\chi$ PTh calculation yields the decay amplitude and width, a reliable experimental measurement of the  $\eta \rightarrow \pi^0\gamma\gamma$  branching ratio and Dalitz plot is important for testing  $\chi$ PTh calculations and the determination of the coefficients for the  $\mathcal{O}(\mathbf{p}^6)$  counterterms.

Early attempts to measure and calculate the  $\eta \rightarrow \pi^0\gamma\gamma$  decay have been reviewed in Ref. [1]. An experimental break-through was achieved in 1981 with the GAMS experiment [2,3], which used a wall of 1400 Cerenkov counters that provided good energy and spatial resolution for high-energy photons.  $6 \times 10^5$   $\eta$  mesons were produced in reaction  $\pi^- p \rightarrow \eta n$ , improving the statistics compared to previous experiments by two orders of magnitude. A narrow peak of 40 events in the  $\pi^0\gamma\gamma$  invariant-mass spectrum located at the mass value of the  $\eta$  meson was interpreted as the  $\eta \rightarrow \pi^0\gamma\gamma$  signal. Much attention was paid to suppressing the  $\eta \rightarrow 3\pi^0$  background. For two decades, the GAMS result,  $\Gamma(\eta \rightarrow \pi^0\gamma\gamma) = 0.84 \pm 0.17$  eV [3], was the favored experimental value for this decay width. It brought much interest to theoretical calculations that were trying to reproduce the surprisingly large  $\eta \rightarrow \pi^0\gamma\gamma$  decay width. According to [4–7], the  $\chi$ PTh calculations, which were based on vector-meson dominance (VMD) with additional contributions like scalar, tensor,  $C$ -odd axial-vector resonances and other smaller ones, give about half of the GAMS value. Only the calculations using quark-box diagrams [8,9] got close to the experimental value for  $\Gamma(\eta \rightarrow \pi^0\gamma\gamma)$ .

After 2001 the experimental situation for measuring the  $\eta \rightarrow \pi^0\gamma\gamma$  decay changed greatly. New experiments reported decay-width values which were two to three times smaller than the GAMS result and were in better agreement with  $\chi$ PTh calculations. The Crystal Ball (CB) collaboration at the AGS conducted an experiment devoted to investigations of rare  $\eta$ -meson decays with a total of  $2.8 \times 10^7$   $\eta$  mesons produced in reaction  $\pi^- p \rightarrow \eta n$  near threshold [10–12], which ended up with  $\Gamma(\eta \rightarrow \pi^0\gamma\gamma) = 0.45 \pm 0.12$  eV. An independent analysis [13] of the same CB data yielded the relative branching

ratio  $B_1 = (8.3 \pm 2.8_{\text{stat}} \pm 1.4_{\text{syst}}) \times 10^{-4}$  with respect to  $BR(\eta \rightarrow 3\pi^0)$ , this implies  $\Gamma(\eta \rightarrow \pi^0\gamma\gamma) = 0.35 \pm 0.13$  eV. Meanwhile, the SND collaboration at VEPP-2M reported  $\Gamma(\eta \rightarrow \pi^0\gamma\gamma) = 0.27_{-0.25}^{+0.49}$  eV [1]. However, their signal was just  $7.0_{-6.5}^{+12.9}$  events. Most recent  $\chi$ PTh calculations of  $\Gamma(\eta \rightarrow \pi^0\gamma\gamma)$ , which revised earlier ones, resulted in  $0.47 \pm 0.10$  eV [14] and  $0.45\text{--}0.53$  eV [15], showing good agreement with the new experimental values.

Surprisingly low, in comparison with all earlier measurements and  $\chi$ PTh calculations, is the recent result of the KLOE collaboration [16],  $\Gamma(\eta \rightarrow \pi^0\gamma\gamma) = 0.108 \pm 0.035_{\text{stat}} \pm 0.029_{\text{syst}}$  eV, which is based on a signal of  $68 \pm 23$  events. Hypothetically, such a small decay width could be the result of destructive interference between the vector-meson and other meson contributions. To check this experimentally, one should also measure the  $\eta \rightarrow \pi^0\gamma\gamma$  Dalitz plot, the density of which reflects the decay amplitude. Instead of a Dalitz plot,  $\chi$ PTh calculations usually depict the  $d\Gamma(\eta \rightarrow \pi^0\gamma\gamma)$  dependence on the invariant mass (or the invariant mass squared) of the two photons from the  $\eta \rightarrow \pi^0\gamma\gamma$  decay. In Fig. 1, we illustrate the predictions for both the  $m(\gamma\gamma)$  and  $m^2(\gamma\gamma)$  spectra, which are obtained from the decay amplitudes described in detail in Refs. [5, 8]. The prediction based only on the vector-

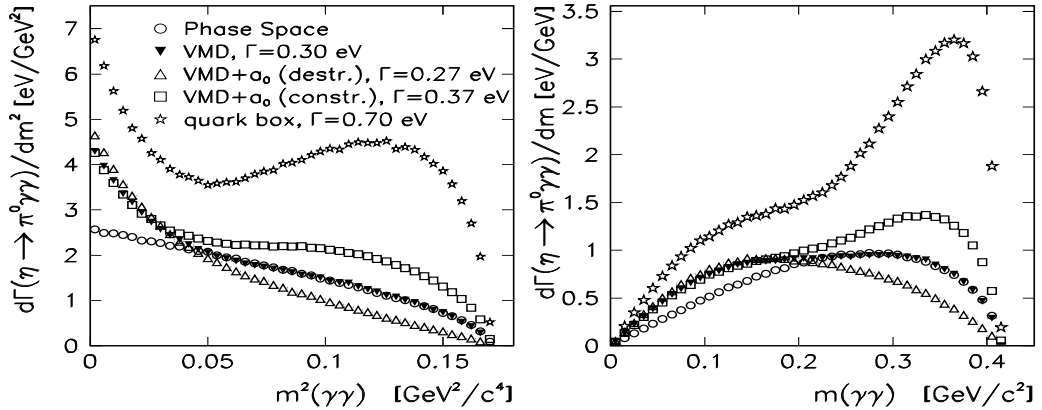


Figure 1: Comparison of different  $\chi$ PTh calculations of Refs. [5, 8] for the dependence of the  $\eta \rightarrow \pi^0\gamma\gamma$  decay width on  $m^2(\gamma\gamma)$  (left) and on  $m(\gamma\gamma)$  (right).

meson contribution gives the basic decay width and two-photon invariant-mass spectrum, which is close to phase space when  $m^2(\gamma\gamma) > 0.05$   $\text{GeV}^2/c^4$ . Note that the “pure” VMD prediction for  $d\Gamma(\eta \rightarrow \pi^0\gamma\gamma)/dm(\gamma\gamma)$  is very similar for most of the existing calculations [4–7, 14]. Adding other contributions to the vector-meson part, for example  $a_0$ -meson exchange, changes the decay width and the invariant-mass spectrum depending on the sign of the

interference term. As shown in Fig. 1, there is a typical correlation between the change of the decay width and the change in the two-photon invariant-mass spectrum. Evidently, increasing the total decay width occurs mostly due to the rise in the  $d\Gamma(\eta \rightarrow \pi^0\gamma\gamma)$  spectrum at high  $m(\gamma\gamma)$  masses.

In light of the above, an experimental measurement of the  $d\Gamma(\eta \rightarrow \pi^0\gamma\gamma)/dm(\gamma\gamma)$  distribution is needed as it provides a unique test of  $\chi$ PTh calculations and the information necessary for the determining the coefficients of the  $\mathcal{O}(p^6)$  counterterms.

In this conference proceeding, we present the first results for the  $d\Gamma(\eta \rightarrow \pi^0\gamma\gamma)/dm^2(\gamma\gamma)$  distribution and a new value for the  $\eta \rightarrow \pi^0\gamma\gamma$  branching ratio.

## 2 Experimental arrangements

The experiments at the AGS (in 1998) and at MAMI (in 2004) were performed with the Crystal Ball multiphoton spectrometer which consists of 672 optically isolated NaI(Tl) crystals that are arranged in two hemispheres covering 93% of  $4\pi$  steradians. Details about the CB detector at the AGS and the analyses of its data can be found in Refs. [17–19]. Details of measuring  $\eta \rightarrow \pi^0\gamma\gamma$  at the AGS are given in Ref. [12]. The reanalysis of these data mostly revised the fitting procedure of the experimental distributions that allowed obtaining the  $d\Gamma(\eta \rightarrow \pi^0\gamma\gamma)/dm^2(\gamma\gamma)$  distribution and an improved value for  $BR(\eta \rightarrow \pi^0\gamma\gamma)$ .

The AGS experiment used a momentum-analyzed beam of negative pions incident on a 10-cm-long liquid hydrogen (LH<sub>2</sub>) target located in the center of the CB. The mean value of the incident momentum spectrum at the center of the LH<sub>2</sub> target was 716 MeV/ $c$  (that is just above the  $\pi^-p \rightarrow \eta n$  threshold), the momentum spread was  $\sim 12$  MeV/ $c$ , and the momentum resolution of an individual beam particle was  $\sim 0.6\%$ . The number of  $\pi^-p \rightarrow \eta n$  events produced in our experiment was determined using the  $\eta \rightarrow \gamma\gamma$  decay mode and equals  $(27.64 \pm 0.19) \times 10^6$ . The quality of the data analysis and Monte Carlo (MC) simulation is illustrated in Ref. [12].

In our analysis of the AGS data, we searched for the process  $\pi^-p \rightarrow \eta n \rightarrow \pi^0\gamma\gamma n \rightarrow 4\gamma n$  in four-cluster events, assuming that all clusters in the CB were produced by the electromagnetic showers of the final-state photons. The neutron was analyzed as being the missing particle. Since the  $\pi^-p \rightarrow \eta n$  reaction was measured near the production threshold where the majority of the final-state neutrons left through the downstream tunnel of the CB, the fraction of the  $\eta$  events with the neutron detected in the CB comprised only 5%.

The experiment at MAMI was conducted with the beam of Bremsstrahlung photons from MAMI-B (multistage electron accelerator with maximum energy of  $\sim 883$  MeV) that were incident on a 5-cm-long  $\text{LH}_2$  target located in the center of the CB. To cover the exit beam tunnel of the CB, the TAPS photon detector [20] was installed 1.75 m downstream of the CB center. In this experiment, TAPS consisted of 510 individual  $\text{BaF}_2$  detectors that are hexagonally shaped with an inner diameter of 6 cm and a length of 25 cm (corresponding to 12 radiation lengths). The typical energy resolution for electromagnetic showers in TAPS is  $\Delta E/E = 0.018 + 0.008/(E[\text{GeV}])^{0.5}$ . Due to the long distance between the CB and TAPS, the resolution of TAPS in the polar angle  $\theta$  was better than  $1^\circ$ . The resolution in azimuthal angle  $\phi$  is better than  $1/R$  radian, where  $R$  is the distance in [cm] from the TAPS center to the point on the TAPS surface corresponding to the  $\theta$  angle. The incident photons were tagged with the Bremsstrahlung recoil electrons detected by the Tagger spectrometer. The Tagger consisted of a momentum-dispersed magnet [21] focusing the electrons on the focal plane detector of 353 half-overlapping plastic scintillators [22]. The energy resolution of the tagged photon beam, which is defined by the overlap region of two scintillation counters, is about 1 MeV. The maximum energy for tagging the beam photon with the Tagger was 820 MeV.

In the analysis of the MAMI data, we searched for the process  $\gamma p \rightarrow \eta p \rightarrow \pi^0\gamma\gamma p \rightarrow 4\gamma p$  in events with five clusters detected in the CB and TAPS in coincidence with the prompt signal from the Tagger. The detection of the recoil proton was required to improve the experimental resolution and the signal-to-background ratio compared to the AGS-data analysis. The number of the  $\eta \rightarrow \gamma\gamma$  decays observed was based on  $\sim 10^7$   $\gamma p \rightarrow \eta p$  events produced in the experiment. More details on the experimental set-up and data analysis can be found in Ref. [23].

### 3 Selection of the $\eta \rightarrow \pi^0\gamma\gamma$ candidates

The search for a signal from the  $\eta \rightarrow \pi^0\gamma\gamma$  decays is similar for the AGS and MAMI data. The signal should be seen as a peak in the invariant-mass spectrum of the  $\pi^0\gamma\gamma$  final state at the position corresponding to the  $\eta$ -meson mass value. This means that one has to search for process  $\pi^-p \rightarrow \pi^0\gamma\gamma n \rightarrow 4\gamma n$  in the AGS data and process  $\gamma p \rightarrow \pi^0\gamma\gamma p \rightarrow 4\gamma p$  in the MAMI data. Since the major contribution to the four-photon final states comes from direct  $\pi^0\pi^0$  production, this reaction must be suppressed in our analysis. The kinematic-fitting technique was used for testing hypotheses on the necessary processes and selecting event candidates based on the fit

confidence level (CL). The  $\pi^0\pi^0$  background was suppressed by discarding all events that satisfied the  $\pi^0\pi^0$  hypothesis with probability greater than 0.001%. Further suppression of the background processes can be done by requiring a cut on the confidence level of the  $\pi^0\gamma\gamma$  hypothesis itself. Our typical cut on this was at the 10% CL (i.e., with a probability greater than 10%). Besides the “smooth” background from the  $\pi^0\pi^0$  production in the  $m(\pi^0\gamma\gamma)$  spectrum, there are contributions from other neutral  $\eta$  decays that can mimic the  $\eta \rightarrow \pi^0\gamma\gamma$  signal. The  $\eta \rightarrow 3\pi^0$  decay produces four clusters because of overlapping photon showers and the  $\eta \rightarrow \gamma\gamma$  decay does the same because of split-off showers. The kinematic-fit cuts on CL are not enough for sufficient suppression of these background contributions. As illustrated in Ref. [12], further suppression of the  $\eta \rightarrow \gamma\gamma$  and  $\pi^0\pi^0$  background contributions can be reached by applying a cut on  $m(\pi^0\gamma)$  with respect to  $m(\pi^0\gamma\gamma)$ . The overlapping clusters can be partially separated from the normal single-photon ones by testing their radius as a function of the cluster energy. The

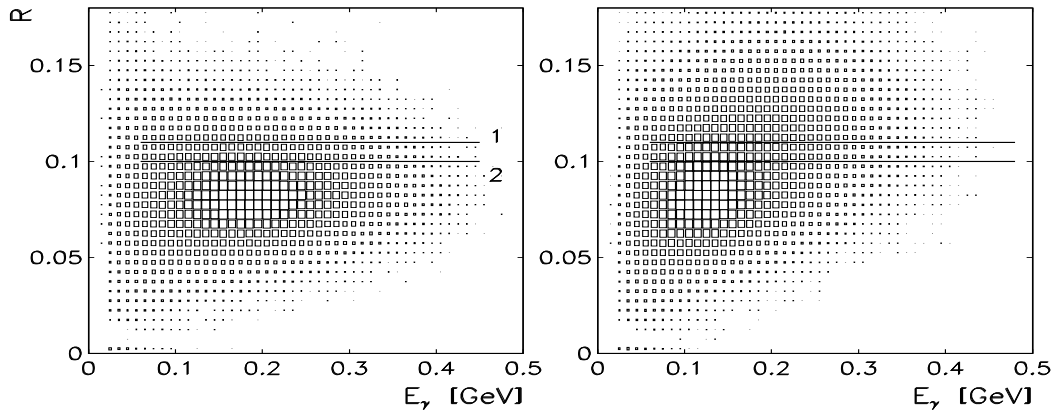


Figure 2: Two-dimensional distributions of the effective cluster radius  $R$  versus the cluster energy of the photons for events selected as  $\pi^-p \rightarrow \pi^0\gamma\gamma n$  candidates: (left) MC simulation for  $\pi^-p \rightarrow \eta n \rightarrow \pi^0\gamma\gamma n$ , (right) MC for  $\pi^-p \rightarrow \eta n \rightarrow 3\pi^0 n$ . The lines in the distributions show the cuts on  $R$ . The cuts require discarding all events for which a cluster energy is greater than 0.06 GeV and  $R$  is above the line. Cut #2 is tighter than #1.

so-called effective radius  $R$  of a cluster containing  $k$  crystals with energy  $E_i$  deposited in crystal  $i$  is defined as  $R = \sqrt{\sum_i^k E_i \cdot (\Delta r_i)^2 / \sum_i^k E_i}$ , where  $\Delta r_i$  is the opening angle (in radians) between the cluster direction and the crystal axis. As seen in Fig. 2, the cluster radii for the  $\eta \rightarrow 3\pi^0$  background events are systematically larger compared to the ones for  $\eta \rightarrow \pi^0\gamma\gamma$  events.

Since the length of the LH<sub>2</sub> targets was not insignificant, we could improve the angular resolution using the  $z$  coordinate of the event vertex as a free parameter in the kinematic fit. For background reactions, the resulting  $z$ -coordinate distribution does not correspond to the real vertex distribution. Thus applying a cut on the  $z$  coordinate, which was obtained from the kinematic-fit output, allowed further improvement of the signal-to-background ratio.

The typical acceptance for  $\eta \rightarrow \gamma\gamma$  events after applying our standard selection criteria was about 15% for the AGS-data analysis and 8% for MAMI-B. A lower acceptance for MAMI-B is due to the requirement that the recoil proton must be detected. Note also that the detection efficiency for the recoil protons is smaller than for the photons, as low energy protons do stop in the material located between the target and the crystals.

## 4 Determination of $d\Gamma(\eta \rightarrow \pi^0\gamma\gamma)/dm^2(\gamma\gamma)$

To determine the  $d\Gamma(\eta \rightarrow \pi^0\gamma\gamma)/dm^2(\gamma\gamma)$  spectrum, we divided our experimental and MC-simulated data in seven subsamples depending on the  $m^2(\gamma\gamma)$  value, which was obtained as a result of testing the  $\pi^0\gamma\gamma$  hypothesis. Then, from the experimental spectra of  $m(\pi^0\gamma\gamma)$ , we subtracted the background spectra from the MC simulation of the  $\eta \rightarrow 3\pi^0$  and  $\eta \rightarrow \gamma\gamma$  events. The fraction of these remaining backgrounds, which depends on the selection cuts used, was determined from the ratio of the number of these  $\eta$  decays observed in the experiment itself to the number of events generated for these decays in our MC simulation. The resulting  $m(\pi^0\gamma\gamma)$  spectra were fitted to a smooth polynomial function for the remaining background plus a Gaussian for the expected signal. The initial parameters for the polynomial function were determined from the fit of the MC simulation for the  $\pi^0\pi^0$  background; the mean value and sigma for the Gaussian were fixed according to the fit of the MC simulation for the  $\eta \rightarrow \pi^0\gamma\gamma$  events. Examples of the fits of some  $m^2(\gamma\gamma)$  ranges are illustrated in Fig. 3 for both the AGS and MAMI-B data. Note that the MAMI-B spectra have smaller statistics but better signal-to-background ratios.

The results on the  $\eta \rightarrow \pi^0\gamma\gamma$  decay width as a function of  $m^2(\gamma\gamma)$  are shown in Fig. 4 for both the AGS and MAMI-B data. The analysis was repeated several times using different criteria for event selection. In order to illustrate the variation of results in each  $m^2(\gamma\gamma)$  interval, they are all plotted in the same Figure. The acceptance in each  $m^2(\gamma\gamma)$  interval was determined using the phase-space simulation of the  $\eta \rightarrow \pi^0\gamma\gamma$  decay. The decay-width calculation was based on the experimental ratio of the  $\eta \rightarrow \pi^0\gamma\gamma$

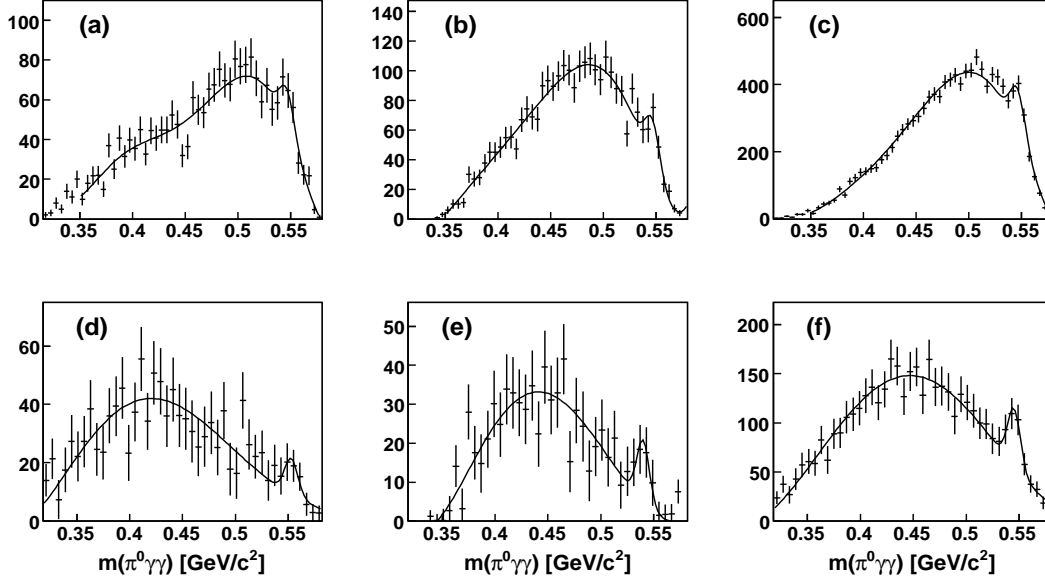


Figure 3: Fit of the  $m(\pi^0 \gamma \gamma)$  spectra for the AGS (top) and MAMI-B (bottom): (a,d)  $0.027 < m^2(\gamma \gamma) < 0.04 \text{ GeV}^2/c^4$ ; (b,e)  $0.04 < m^2(\gamma \gamma) < 0.06 \text{ GeV}^2/c^4$ ; (c,f) full  $m^2(\gamma \gamma)$ .

and  $\eta \rightarrow 3\pi^0$  events measured, and using the branching ratio for  $\eta \rightarrow 3\pi^0$  and the full width  $\Gamma(\eta \rightarrow \text{all}) = 1.29 \pm 0.07 \text{ keV}$  from the latest edition of the Review of Particle Physics [24]. In Fig. 4, we also depict the VMD prediction for the  $d\Gamma(\eta \rightarrow \pi^0 \gamma \gamma)/dm^2(\gamma \gamma)$  distribution based on the calculations of Ref. [5]. This VMD prediction matches our results better if we normalize it to  $\Gamma(\eta \rightarrow \pi^0 \gamma \gamma) = 0.33 \text{ eV}$  for the AGS results and to  $0.37 \text{ eV}$  for MAMI-B. Our results are in reasonable agreement with  $\chi$ PTh predictions based on the vector-meson contribution only. However, we do not pretend that other contributions are absent. So, to enable one to fit our results to other models, we calculated the average of the results for  $d\Gamma(\eta \rightarrow \pi^0 \gamma \gamma)/dm^2(\gamma \gamma)$  in each  $m^2(\gamma \gamma)$  interval and listed them in Table 1. Note that the  $m^2(\gamma \gamma)$  range between  $0.011$  and  $0.027 \text{ GeV}^2/c^4$  is absent because of zero acceptance after the suppression of the  $\pi^0 \pi^0$  background. Since the measurements with different selection criteria are correlated, the uncertainties of the values were calculated by adding in quadrature the average of the individual errors in each  $m^2(\gamma \gamma)$  interval and the r.m.s. of the results themselves. Note that the AGS results for the  $d\Gamma(\eta \rightarrow \pi^0 \gamma \gamma)/dm^2(\gamma \gamma)$  distribution are in agreement within the error bars with the MAMI-B results. More precise measurements of this distribution require significantly higher experimental statistics, which is expected from the CB experiments at MAMI-C. On the other hand, as seen

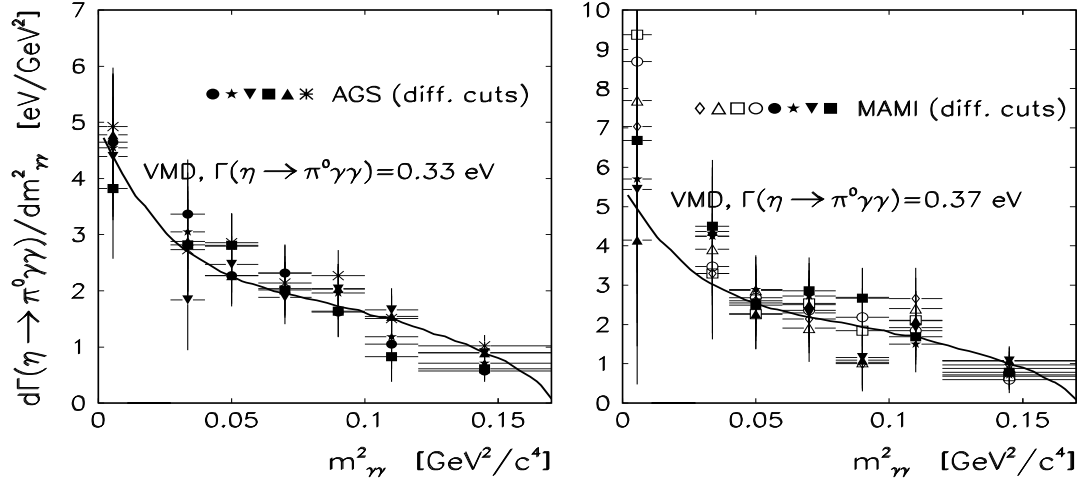


Figure 4: The  $d\Gamma(\eta \rightarrow \pi^0\gamma\gamma)/dm^2(\gamma\gamma)$  results obtained for different selection criteria of the AGS (left) and MAMI-B (right) data. The VMD prediction (solid line) is calculated according to Ref. [5] and normalized to  $\Gamma(\eta \rightarrow \pi^0\gamma\gamma) = 0.33$  eV for the AGS results and to 0.37 eV for MAMI-B.

Table 1: The  $d\Gamma(\eta \rightarrow \pi^0\gamma\gamma)/dm^2(\gamma\gamma)$  results (in units [eV/GeV<sup>2</sup>]) for seven intervals of  $m^2(\gamma\gamma)$  calculated from the average of the measurements shown in Figs. 4.

$m^2(\gamma\gamma)$ [GeV <sup>2</sup> /c <sup>4</sup> ]	0.—0.011	0.027—0.04	0.04—0.06	0.06—0.08
$d\Gamma/dm^2(\gamma\gamma)$ (AGS)	$4.5 \pm 1.2$	$2.8 \pm 1.1$	$2.58 \pm 0.59$	$2.12 \pm 0.51$
$d\Gamma/dm^2(\gamma\gamma)$ (MAMI)	$6.8 \pm 4.0$	$3.9 \pm 1.6$	$2.58 \pm 0.90$	$2.41 \pm 0.90$
$m^2(\gamma\gamma)$ [GeV <sup>2</sup> /c <sup>4</sup> ]	0.08—0.1	0.1—0.12	0.12—0.17	
$d\Gamma/dm^2(\gamma\gamma)$ (AGS)	$1.93 \pm 0.51$	$1.30 \pm 0.52$	$0.78 \pm 0.25$	
$d\Gamma/dm^2(\gamma\gamma)$ (MAMI)	$1.71 \pm 1.00$	$2.03 \pm 0.83$	$0.85 \pm 0.39$	

from the fits of our samples to the full  $m^2(\gamma\gamma)$  range (shown in Figs. 3(c,f)), the present statistics are high enough for the determination of the full decay width for  $\eta \rightarrow \pi^0\gamma\gamma$ . Based on our  $d\Gamma(\eta \rightarrow \pi^0\gamma\gamma)/dm^2(\gamma\gamma)$  results, we simulated the  $\eta \rightarrow \pi^0\gamma\gamma$  decay according to the VMD amplitude of Ref. [5], and used this Monte Carlo simulation for the determination of our overall acceptance. The average of our results from the fits to our  $m(\pi^0\gamma\gamma)$  spectra, which were obtained for different selection criteria, yielded for the AGS and MAMI-B analyses

$$BR_{\text{AGS}}(\eta \rightarrow \pi^0\gamma\gamma) = (2.21 \pm 0.24_{\text{stat}} \pm 0.38_{\text{syst}}) \times 10^{-4} = (2.21 \pm 0.45_{\text{tot}}) \times 10^{-4},$$

$$BR_{\text{MAMI-B}}(\eta \rightarrow \pi^0\gamma\gamma) = (2.25 \pm 0.46_{\text{stat}} \pm 0.17_{\text{syst}}) \times 10^{-4} = (2.25 \pm 0.49_{\text{tot}}) \times 10^{-4}.$$

By the “statistical” uncertainty, we mean the average uncertainty based on the fit errors; the systematic uncertainty comes from the r.m.s. of all results obtained for different selection criteria. The corresponding values for the decay width are

$$\begin{aligned}\Gamma_{\text{AGS}}(\eta \rightarrow \pi^0\gamma\gamma) &= 0.285 \pm 0.031_{\text{stat}} \pm 0.049_{\text{syst}} = 0.285 \pm 0.058_{\text{tot}} \text{ eV}, \\ \Gamma_{\text{MAMI-B}}(\eta \rightarrow \pi^0\gamma\gamma) &= 0.290 \pm 0.059_{\text{stat}} \pm 0.022_{\text{syst}} = 0.290 \pm 0.063_{\text{tot}} \text{ eV}.\end{aligned}$$

Our new AGS value for the  $\eta \rightarrow \pi^0\gamma\gamma$  decay width is somewhat smaller than  $\Gamma(\eta \rightarrow \pi^0\gamma\gamma) = 0.45 \pm 0.12 \text{ eV}$  reported earlier by us in Ref. [12], but both values overlap within the error bars. For the most part, we explain this difference by the uncertainty in the definition of the  $\pi^0\pi^0$  background shape under the  $\eta \rightarrow \pi^0\gamma\gamma$  signal. From the comparison of the previous AGS data analysis with the present one, we have found that a small discrepancy in the shape between the real  $\pi^0\pi^0$  background and the MC-simulated one resulted in some gain of the weight factor for the  $\eta \rightarrow \pi^0\gamma\gamma$  signal spectrum in our binned maximum-likelihood fits. In the new fitting procedure, we fixed only the  $\eta \rightarrow \pi^0\gamma\gamma$  peak parameters, taking them according to the MC simulation, while the parameters for the  $\pi^0\pi^0$  background were free, but initialized from a fit of the  $\pi^0\pi^0$  MC simulation. Our new AGS result for  $\Gamma(\eta \rightarrow \pi^0\gamma\gamma)$  supersedes the results reported earlier in Refs. [10–12].

## 5 Summary and conclusions

New results on the rare, doubly-radiative decay  $\eta \rightarrow \pi^0\gamma\gamma$  have been obtained from a reanalysis of the Crystal Ball experiment performed at the AGS and the first analysis of a new Crystal Ball experiment at MAMI-B. The analyses have yielded the first results on the dependence of the decay width on the two-photon invariant mass squared,  $d\Gamma(\eta \rightarrow \pi^0\gamma\gamma)/dm^2(\gamma\gamma)$ , and new values for the  $\eta \rightarrow \pi^0\gamma\gamma$  branching ratio. The results of the AGS and MAMI measurements are in good agreement with each other, and they are close to the calculations of Chiral Perturbation Theory assuming vector-meson dominance.

All our results that are presented in this conference contribution are close to final, but should still be classified as preliminary.

## References

- [1] M. M. Achasov *et al.* [SND Collab.], *Nucl. Phys.* **B600**, 3 (2001).

- [2] F. Binon *et al.* [GAMS Collab.], *Yad. Fiz.* **33**, 1534 (1982) also *Lett. Nuovo Cim.* **A71**, 497 (1982).
- [3] D. Alde *et al.* [GAMS Collab.], *Z. Phys.* **C25**, 225 (1984).
- [4] Ll. Ametller, J. Bijnens, A. Bramon and F. Cornet, *Phys. Lett.* **B276**, 185 (1992).
- [5] J.N. Ng and D.J. Peters, *Phys. Rev.* **D46**, 5034 (1992).
- [6] P. Ko, *Phys. Rev.* **D47**, 3933 (1993).
- [7] M. Jetter, *Nucl. Phys.* **B459**, 283 (1996).
- [8] J.N. Ng and D.J. Peters, *Phys. Rev.* **D47**, 4939 (1993).
- [9] Y. Nemoto, M. Oka, and M. Takizawa, *Phys. Rev.* **D54**, 6777 (1996).
- [10] S. Prakhov [for Crystal Ball Collab.], *Phys. of Atom. Nucl.* **65**, 2238 (2002).
- [11] B.M.K. Nefkens and J.W. Price, “Eta Physics Handbook” *Physica Scripta* **T99**, 114 (2002).
- [12] S. Prakhov *et al.* [Crystal Ball Collab.] *Phys. Rev.* **C72**, 025201 (2005).
- [13] N. Knecht *et al.*, *Phys. Lett.* **B589**, 14 (2004).
- [14] E. Oset, J.R. Pelaez, and L. Roca, *Phys. Rev.* **D67**, 073013 (2003).
- [15] A.E. Radzhabov and M.K. Volkov, *Phys. Rev.* **D74**, 113001 (2006).
- [16] B.Di Micco *et al.* [KLOE Collab.], *Acta Phys. Slov.* **56**, 403 (2006).
- [17] W. B. Tippens *et al.* [Crystal Ball Collab.] *Phys. Rev. Lett.* **87**, 192001 (2001).
- [18] S. Prakhov *et al.* [Crystal Ball Collab.] *Phys. Rev.* **C69**, 045202 (2004).
- [19] M.E. Sadler *et al.* [Crystal Ball Collab.] *Phys. Rev.* **C69**, 055206 (2004).
- [20] R. Novotny, *IEEE Trans. Nucl. Sci.* **38**, 379 (1991).
- [21] I. Anthony *et al.*, *NIM* **A301**, 230 (1991).
- [22] S.J. Hall *et al.*, *NIM* **A368**, 698 (1996).
- [23] J.W. Brudvik, *Ph.D. Thesis*, University of California Los Angeles(2007).
- [24] A. B. Balantekin *et al.* [Particle Data Group], *J. Phys. G: Nucl. Part. Phys.* **33**, 1 (2006).

# SPIN PHYSICS WITH CLAS AT JEFFERSON LABORATORY

*Y. Prok*<sup>1</sup> for the CLAS Collaboration  
Laboratory for Nuclear Science  
77 Massachusetts Avenue, Bldg. 26-505  
Massachusetts Institute of Technology  
Cambridge, MA 02139, USA

## Abstract

Inelastic scattering using polarized nucleon targets and polarized charged lepton beams allows the extraction of spin structure functions that provide information about the spin structure of the nucleon. A program designed to study such processes at low and intermediate  $Q^2$  for the proton and deuteron has been pursued by the CLAS Collaboration at Jefferson Lab since 1998.

The data with high statistical precision and extensive kinematic coverage allows us to better constrain the polarized parton distributions and to accurately determine various moments of  $g_1$  as a function of  $Q^2$ . The latest results are presented, illustrating our contribution to the world data, with comparisons of the data with NLO global fits, phenomenological models, chiral perturbation theory, the GDH and Bjorken sum rules, and tests of global duality.

## 1 Spin Structure Functions

For several decades spin structure functions have been measured using polarized nucleon targets and polarized lepton beams. In particular, the photon-nucleon asymmetry  $A_1^p(x, Q^2)$ , the structure function  $g_1^p(x, Q^2)$  and its first moment  $\Gamma_1(Q^2)$  have been investigated. The photon-nucleon asymmetry  $A_1^p(x, Q^2)$  reflects the valence spin structure of the proton. In lowest order

---

<sup>1</sup>present address: Department of Physics, Computer Science, and Engineering  
Christopher Newport University  
Gosnold Hall, 1 University Place  
Newport News, VA 23606, USA

in the quark parton model,  $A_1^p$  is given by the ratio of the spin-dependent to spin-independent quark distribution functions [1]:

$$A_1 = \frac{\sum_i e_i^2 [q_i^\uparrow - q_i^\downarrow]}{\sum_i e_i^2 [q_i^\uparrow + q_i^\downarrow]}. \quad (1)$$

Assuming that the nucleon obeys SU(6) symmetry at large  $x$  generates the prediction that  $A_1^p = 5/9$ . The symmetry is strongly broken, which is particularly evident at large  $x$ . Several non-perturbative mechanisms have been used to account for this observation by explicitly breaking SU(6) at the quark level, which results in different weighting of components of the wavefunction, and consequently different  $x$  dependencies for the spin and flavor distributions. Mapping  $A_1^p$  as a function of  $x$  can help differentiate between the various models.

The spin structure function  $g_1$  is important in understanding the quark and gluon spin components of the nucleon spin, and their relative contributions in different kinematic regions. At high  $Q^2$ ,  $g_1$  provides information on how the nucleon spin is composed of the spin of its constituent quarks and gluons. At low  $Q^2$ , hadronic degrees of freedom become more important and dominate the measurements. Besides its  $Q^2$ -dependence,  $g_1$  depends also on the fraction of momentum,  $x$  carried by the struck parton. The DGLAP equations [2] predict that  $g_1^p$  increases logarithmically with  $Q^2$  at low  $x$ , and decreases with  $Q^2$  at high  $x$ .

There is particular interest in the first moment of  $g_1$ ,  $\Gamma_1(Q^2) = \int_0^{1-} g_1(x, Q^2) dx$ , which is constrained at low  $Q^2$  by the Gerasimov-Drell-Hearn sum rule [3] and at high  $Q^2$  by the Bjorken sum rule [4] and previous deep inelastic scattering (DIS) experiments. In our definition the upper limit of the integral does not include the elastic peak. Ji and Osborne [5] have shown that the GDH sum rule can be generalized to all  $Q^2$  via

$$S_1(\nu = 0, Q^2) = \frac{8}{Q^2} [\Gamma_1(Q^2) + \Gamma_1^{el}(Q^2)], \quad (2)$$

where  $S_1(\nu, Q^2)$  is the spin-dependent virtual photon Compton amplitude.  $S_1$  can be calculated in Chiral Perturbation Theory ( $\chi$ PT) at low  $Q^2$  and with perturbative QCD (pQCD) at high  $Q^2$ . Therefore,  $\Gamma_1$  represents a calculable observable that spans the entire energy range from hadronic to partonic descriptions of the nucleon.

Another topic of interest is the phenomenon of quark-hadron duality, an observation that the hadronic and partonic degrees of freedom can sometimes both be successfully used to describe the structure of hadrons. This phenomena was discovered experimentally by Bloom and Gilman [6], who

observed that the spin averaged structure function  $F_2(\nu, Q^2)$  measured in the resonance region was on average equivalent to the 'scaling' deep inelastic one, if averaged over the variable  $w' = (2M\nu + M^2)/Q^2$ . This phenomenon has recently been studied with high precision in the unpolarized  $F_2^p$  structure function [7]. Quark-hadron duality has not been extensively tested in the case of the polarized structure functions.

## 2 Measurements and Data Analysis

$g_1$  was extracted from measurements of the double spin asymmetry  $A_{\parallel}$  in inclusive  $ep$  scattering:

$$g_1 = \frac{F_1}{1 + \gamma^2} [A_{\parallel}/D + (\gamma - \eta)A_2], \quad (3)$$

where  $F_1$  is the unpolarized structure function,  $A_2$  is the virtual photon asymmetry, and  $\gamma$ ,  $D$  and  $\eta$  are kinematic factors.  $F_1$  and  $A_2$  are calculated using a parametrization of the world data, and  $A_{\parallel}$  is measured. The spin asymmetry for  $ep$  scattering is given by:

$$A_{\parallel} = \frac{N_- - N_+}{N_- + N_+} \frac{C_N}{f P_b P_t f_{RC}} + A_{RC}, \quad (4)$$

where  $N_-(N_+)$  is the number of scattered electrons normalized to the incident charge with negative (positive) beam helicity,  $f$  is the dilution factor needed to correct for the electrons scattering off the unpolarized background,  $f_{RC}$  and  $A_{RC}$  correct for radiative effects, and  $C_N$  is the correction factor associated with polarized  $^{15}\text{N}$  nuclei in the target.  $A_{\parallel}$  was measured by scattering polarized electrons off polarized nucleons using a cryogenic solid polarized target and CLAS in Hall B. The raw asymmetries were corrected for the beam charge asymmetry, the dilution factor and radiative effects. Since the elastic peak is within the acceptance range, the product of beam and target polarization was determined from the known  $ep$  elastic asymmetry.

The longitudinally polarized electrons were produced by a strained  $GaAs$  electron source with a typical beam polarization of  $\sim 70\%$ . Two solid polarized targets were used:  $^{15}\text{ND}_3$  for polarized deuterons and  $^{15}\text{NH}_3$  for polarized protons. The targets were polarized using the method of Dynamic Nuclear Polarization, with the typical polarization of 70-90% for protons, and 10-35% for deuterons. Besides the polarized targets, three unpolarized targets ( $^{12}\text{C}$ ,  $^{15}\text{N}$ , liquid  $^4\text{He}$ ) were used for background measurements. The scattered electrons were identified using the CLAS package [8], consisting

of drift chambers, Cherenkov detector, time-of-flight counters and electromagnetic calorimeters. Data were taken with beam energies of 1.6, 2.4, 4.2 and 5.7 GeV, covering a kinematic range of  $0.05 < Q^2 < 4.5 \text{ GeV}^2$  and  $0.8 < W < 3.0 \text{ GeV}$ . The data include multi-particle final states, making it possible to investigate exclusive and semi-inclusive pion production, deeply virtual Compton scattering and other exclusive channels.

### 3 Results

#### 3.1 Large $x$ behavior of $A_1(x, Q^2)$

The photon-nucleon asymmetry  $A_1^d$  is shown in Figure 1. Along with the recent CLAS data, the plot shows results from previous experiments, and predictions from several models. The models [9] include the suppression

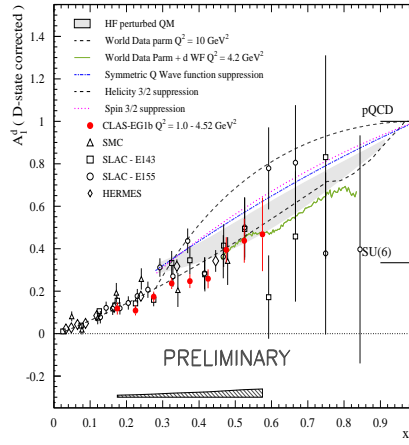


Figure 1: Asymmetry  $A_1^d$  plotted vs  $x$  could differentiate between the different models of valence spin structure of the nucleons.

of transitions to states in the lowest even and odd parity multiplets with combined quark spin  $S = \frac{3}{2}$ , the suppression of transitions to states with helicity  $h = \frac{3}{2}$ , and the suppression of transitions to the states which couple only through symmetric components of the spin-flavor wavefunction. Also shown is the prediction of the hyperfine-perturbed quark model, which involves spin-spin interaction between quarks, mediated by one gluon or pion exchange [10]. Our data show a preference for the pQCD limit as  $x \rightarrow 1$ , and are also consistent with the hyperfine-perturbed quark model.

### 3.2 Moments of $g_1(x, Q^2)$

The first moments of  $g_1^p$  and  $g_1^d$  are shown in Figure 2. The parametrization of world data is used to include the unmeasured contribution to the integral down to  $x = 0.001$ . Only the  $Q^2$  bins in which the measured part constitutes at least 50% of the total integral are included. For the proton, the parametrization at high  $x$  ( $1.09 < W < 1.14$  (1.15) GeV) is used for the low (high) energy data). For the deuteron, the integration is carried out up to the nucleon pion production threshold at high  $x$ , excluding the quasi-elastic and electro-disintegration contributions. The integral is observed to turn over at low  $Q^2$ , consistent with the slope predicted by the GDH sum rule. In general the data are well described by the phenomenological models of Burkert and Ioffe [14] and Soffer and Teryaev [15].

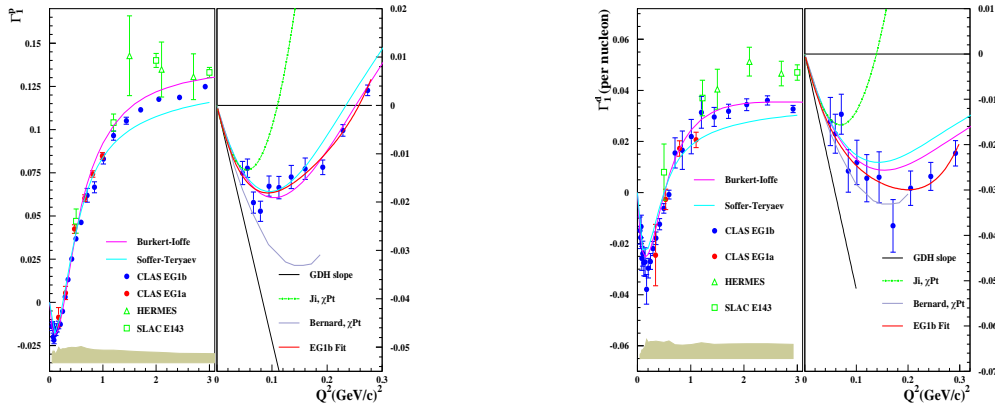


Figure 2: Left:  $\Gamma_1^p$  as a function of  $Q^2$ . Right:  $\Gamma_1^d$  as a function of  $Q^2$ . The EG1a [11], SLAC [12] and Hermes data [13] are shown for comparison. The filled circles represent the present data, including an extrapolation over the unmeasured part of the  $x$  spectrum using a model of world data.

The low  $Q^2$   $\Gamma_1$  data are shown in more detail in the right-hand panels of Figs. 2. It is possible to make a quantitative comparison between our results for  $\Gamma_1^p$  and  $\Gamma_1^d$  at low  $Q^2$  and the next-to-leading order  $\chi$ PT calculation by Ji, Kao and Osborne [16], who find  $\Gamma_1^p(Q^2) = -\frac{\kappa_p^2}{8M^2}Q^2 + 3.89Q^4 + \dots$  and  $\Gamma_1^n(Q^2) = -\frac{\kappa_n^2}{8M^2}Q^2 + 3.15Q^4 + \dots$ . Treating the deuteron as the incoherent sum of a proton and a neutron and correcting for the D-state,

$$\Gamma_1^d(Q^2) = \frac{1}{2}(1 - 1.5\omega_D) \{ \Gamma_1^p(Q^2) + \Gamma_1^n(Q^2) \}, \quad (5)$$

one finds that  $\Gamma_1^d(Q^2) = -0.451Q^2 + 3.26Q^4$ . The low  $Q^2$  results for  $\Gamma_1^p$  and  $\Gamma_1^d$  have been fit to a function of the form  $aQ^2 + bQ^4 + cQ^6 + dQ^8$  where  $a$  is fixed at  $-0.455$  (proton) and  $-0.451$  (deuteron) by the GDH sum rule. For the proton,  $b = 3.81 \pm 0.31$  (stat)  $+0.44 - 0.57$  (syst) is extracted and for the deuteron,  $b = 2.91 \pm 0.52$  (stat)  $\pm 0.69$  (syst) was obtained, both consistent with the  $Q^4$  term predicted by Ji *et al.*

Our fit is shown in the right-hand panel of plots in Figs. 2 along with Ji's prediction. We find that the  $Q^6$  term becomes important even below  $Q^2 = 0.1$  GeV<sup>2</sup> and that this term needs to be included in the  $\chi$ PT calculations in order to extend the range of their validity beyond roughly  $Q^2 = 0.06$  GeV<sup>2</sup>.

### 3.3 Test of global duality

The data for both the proton and the deuteron were used to examine quark-hadron duality in  $g_1$ .

The test is performed by averaging both data and DIS models for  $g_1$  over a  $Q^2$ -dependent interval corresponding to the resonance region, and comparing the two. The averages were determined as

$$\langle g_1(Q^2) \rangle = \frac{\int_{x_l}^{x_h} g_1(x, Q^2) dx}{x_h - x_l}, \quad (6)$$

where  $x_l$  and  $x_h$  correspond respectively to the maximum and minimum values of  $W$  in the considered interval, at a given value of  $Q^2$  (using the definition  $x^{-1} = 1 + (W^2 - M^2)/Q^2$ ). The  $x$ -averaged values of  $g_1$  for the entire resonance region (scaled by  $Q^2$ ) are plotted as a function of  $Q^2$  in Figure 3 for both targets. Hatched bands represent the range of the averages calculated with the next-to-leading order twist-2 PDF predictions [17], [18]. Each version of the pQCD calculation has been corrected for the target mass effects [19], taking into account the fact that the measurements were taken at a low  $Q^2$ . The data for both targets exhibit a power-law-type deviation from the scaling curves at low  $Q^2$ , but show good agreement above  $Q^2=1.7$  GeV<sup>2</sup>/c<sup>2</sup> within the systematic errors of the data and models. The onset of duality in this happens at a slightly higher value than it does in the case of spin-averaged structure function [7]. An effect of adding the elastic contribution to the numerator was also tested, with the elastic contribution evaluated from the elastic form factors [20]. Inclusion of elastic contribution extends the region of agreement to a lower  $Q^2 = \text{GeV}^2/c^2$ . The results are similar in case of  $g_1^p$  and  $g_1^d$ , indicating no large effects from different isospin projections [21].

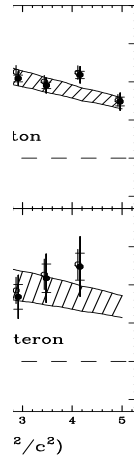


Figure 3: The  $Q^2$ -dependence of  $Q^2 g_1(x, Q^2)$  averaged over a region in  $x$  corresponding to  $1.08 < W < 2$  GeV (solid circles) for a) proton; b) deuteron. the open circles represent our data after adding the contribution from  $ep$  elastic ( $ed$  quasi-elastic) scattering at  $x = 1$  for the proton (deuteron).

## Acknowledgments

This research is supported by the US Department of Energy under grant DE-FG02-96ER40960.

## References

- [1] P. Renton, *Electroweak Interactions*, (Cambridge University Press, 1990).
- [2] G. Altarelli and G. Parisi, *Nucl. Phys.* **B126**, 298 (1977).
- [3] S. Drell and A. Hearn, *Phys. Rev. Lett.* **16**, 908 (1966); S. Gerasimov, *Yad. Fiz.* **2**, 598 (1965).
- [4] J. D. Bjorken *et al.* *Phys. Rev.* **148**, 1467 (1966)
- [5] X. Ji and J. Osborne *J. Phys. G: Nucl. Part. Phys.* **27**, 127 (2001)
- [6] E. Bloom and F. Gilman, *Phys. Rev. D* **4**, 2901 (1971).
- [7] I. Niculescu *Phys. Rev. Lett* **85**, 1182 (2000)
- [8] B. A. Mecking *et al.*, *Nucl. Instr. Meth* **503/3**, 513 (2003).

- [9] F.E.Close and W. Melnitchouk *Phys. Rev. C* **68**, 035210 (2003).
- [10] N. Isgur *Phys. Rev. D* **59**, 034013 (1999).
- [11] R. Fatemi *et al.*, *Phys. Rev. Lett* **91**, 222002 (2003)
- [12] K. Abe *et al.*, *Phys. Rev. Lett* **78**, 815 (1997)
- [13] M. Amarian *et al.*, *Phys. Rev. Lett* **93**, 152301 (2004)
- [14] V. D. Burkert and B. L. Ioffe, *Phys. Lett B* **296**, 223 (1992)
- [15] J. Soffer and O. V. Teryaev *Phys. Lett B* **545**, 323 (2002)
- [16] X. Ji *et al.*, *Phys. Lett. B* **472**, 1 (2000)
- [17] M. Gluck, E. Reya, M. Stratmann and W. Vogelsang *Phys. Rev. D* **63**, 014505 (2001).
- [18] M. Hirai *et al.*, *Phys. Rev. D* **69**, 054021 (2004).
- [19] J. Blumlein and A. Tkabladze, *Nucl. Phys. B* **553**, 427 (1999).
- [20] P. Bosted, *Phys. Rev. C* **51**, 409 (1995).
- [21] P. Bosted *et al.* *Phys. Rev. C* **75**, 035203 (2007).

# RENORMALIZING THE SCHRÖDINGER EQUATION FOR NN SCATTERING

*E. Ruiz Arriola, A. Calle Cordón, M. Pavón Valderrama*<sup>1</sup>

Departamento de Física Atómica, Molecular y Nuclear  
Universidad de Granada  
E-18071 Granada, Spain.

## Abstract

The renormalization of the Schrödinger equation with regular One Boson Exchange and singular chiral potentials including One and Two-Pion exchanges is analyzed within the context of NN scattering.

## 1 Introduction

One traditional view of NN force has been through One Boson Exchange (OBE) Models [1, 2]. Recent developments have shown how chiral symmetry may provide NN forces of practical interest in nuclear physics [?, 4, 5]. Remarkably, chiral expansions, based on assuming a large scale suppression on the parameters  $4\pi f_\pi \sim M_N \sim 1\text{GeV}$  necessarily involve singular potentials at short distances, i.e.  $r^2|V(r)| \rightarrow \infty$  for  $r \rightarrow 0$ . If we take the limit  $r \ll 1/m_\pi$  (or equivalently large momenta) pion mass effects are irrelevant and hence at some fixed order of the expansion one has

$$V(r) \sim \frac{M_N}{(4\pi f_\pi)^{2n} M_N^m} \frac{1}{r^{2n+m}} \quad (1)$$

(the only exception is the singlet channel-OPE case which behaves as  $\sim m_\pi^2/f_\pi^2 r$ , see below). The dimensional argument is reproduced by loop calculations in the so called Weinberg dimensional power counting [6, 7]. Thus, much of our understanding on the physics deduced from chiral potentials might be related to a proper interpretation of these highly singular potentials. Renormalization is the most natural tool provided 1) we expect the potential is realistic at long distances and 2) we want short distance details not to be essential in the description. This is precisely the situation we

---

<sup>1</sup>Institut für Kernphysik, Forschungszentrum Jülich, 52425 Jülich, Germany

face most often in nuclear physics. Knowledge on the attractive or repulsive character of the singularity turns out to be crucial to successfully achieve this program and ultimately depends on the particular scheme or power counting used to compute the potential. We illustrate our points for the simpler OBE potential in the  $^1S_0$  channel and then review some results for chiral OPE and TPE potentials for all partial waves and the deuteron bound state.

## 2 Renormalization of OBE potentials

The singularity of chiral potentials raises suspicions and, quite often, much confusion. However, if properly interpreted and handled they do not differ much from the standard well-behaved regular potentials one usually encounters in nuclear physics. Actually, we digress here that renormalization may provide useful insights even if the potential is not singular at the origin ( $r^2V(r) \rightarrow 0$ !). For definiteness, let us analyze as an illustrative example the phenomenologically successful  $^1S_0$  OBE potential [1, 2] (we take  $m_\rho = m_\omega$ )

$$V(r) = -\frac{g_{\pi NN}^2 m_\pi^2}{16\pi M_N^2} \frac{e^{-m_\pi r}}{r} - \frac{g_{\sigma NN}^2}{4\pi} \frac{e^{-m_\sigma r}}{r} + \frac{g_{\omega NN}^2}{4\pi} \frac{e^{-m_\omega r}}{r} + \dots \quad (2)$$

where for simplicity we neglect nucleon mass effects and a tiny  $\eta$  contribution. We take  $m_\pi = 138\text{MeV}$ ,  $M_N = 939\text{MeV}$ ,  $m_\omega = 783\text{MeV}$  and  $g_{\pi NN} = 13.1$  which seem firmly established. Actually, Eq. (2) looks like a long distance expansion of the potential. NN scattering in the elastic region below pion production threshold involves CM momenta  $p < p_{\text{max}} = 400\text{MeV}$ . Given the fact that  $1/m_\omega = 0.25\text{fm} \ll 1/p_{\text{max}} = 0.5\text{fm}$  we expect heavier mesons to be irrelevant, and  $\omega$  itself to be marginally important. In the traditional approach, however, this is not so [1, 2]. Actually, the problem is essentially handled by solving the Schrödinger equation (S-wave)

$$-u_p''(r) + MV(r)u_p(r) = p^2 u_p(r) \quad (3)$$

with the *regular* solution at the origin,  $u_p(0) = 0$ . This boundary condition implicitly assumes taking also the potential all the way down to the origin. The asymptotic condition for  $r \gg 1/m_\pi$  is taken to be

$$u_p(r) \rightarrow \frac{\sin(pr + \delta_0(p))}{\sin \delta_0(p)} \quad (4)$$

where  $\delta_0(p)$  is the phase-shift. For the potential in Eq. (2) the phase shift is an analytic function of  $p$  with the closest branch cut located at  $p = \pm im_\pi/2$ ,

so that one can undertake an effective range expansion,

$$p \cot \delta_0(p) = -\frac{1}{\alpha_0} + \frac{1}{2}r_0p^2 + v_2p^4 + \dots \quad (5)$$

within a radius of convergence  $|p| \leq m_\pi/2$ . A similar expansion for the wave function  $u_p(r) = u_0(r) + p^2u_2(r) \dots$  means solving the set of equations

$$-u_0''(r) + MV(r)u_0(r) = 0, \quad (6)$$

$$u_0(r) \rightarrow 1 - r/\alpha_0,$$

$$-u_2''(r) + U(r)u_2(r) = u_0(r), \quad (7)$$

$$u_2(r) \rightarrow (r^3 - 3\alpha_0r^2 + 3\alpha_0r_0r) / (6\alpha_0),$$

where, again, the *regular* solutions,  $u_0(0) = u_2(0) = 0$  are taken. With this normalization the effective range  $r_0$  is computed from the standard formula

$$r_0 = 2 \int_0^\infty dr [(1 - r/\alpha_0)^2 - u_0(r)^2]. \quad (8)$$

In the usual approach [1,2] *everything* is obtained from the potential assumed to be valid for  $0 \leq r < \infty$ . In practice, strong form factors are included mimicking the finite nucleon size and reducing the short distance repulsion of the potential, but the regular boundary condition is always kept.<sup>2</sup> As it is well known the  $^1S_0$  scattering length is unnaturally large  $\alpha_0 = -23.74(2)\text{fm}$ , while  $r_0 = 2.77(4)\text{fm}$ . Let us assume we have fitted the potential, Eq. (2), to reproduce  $\alpha_0$ . Under these circumstances a tiny change in the potential  $V \rightarrow V + \Delta V$  has a dramatic effect on  $\alpha_0$ , since one obtains

$$\Delta\alpha_0 = \alpha_0^2 M_N \int_0^\infty \Delta V(r) u_0(r)^2 dr. \quad (9)$$

As a result, potential parameters must be fine tuned. In particular, the resulting  $\omega$ -repulsive contribution is well determined with an unnaturally large coupling,  $g_{\omega NN} \sim 16$ . [1,2]. In our case, with no form factors nor relativistic corrections, a fit to Ref. [8] yields  $g_{\omega NN} = 12.876(2)$ ,  $g_{\sigma NN} = 12.965(2)$  and  $m_\sigma = 554.0(4)\text{MeV}$  with  $\chi^2/\text{DOF} = 0.26$ . Note the small uncertainties, as expected from our discussion and Eq. (9). As mentioned above  $1/m_\omega = 0.25\text{fm} \ll 1/p_{\text{max}} = 0.5\text{fm}$  so  $\omega$  should not be crucial at least for CM momenta  $p \ll p_{\text{max}}$ . Thus, despite the undeniable success in fitting the data this sensitivity to short distances looks counterintuitive.

<sup>2</sup>Calculations solving the equivalent Lippmann-Schwinger equation in momentum space for regular potentials correspond always to choose the regular solution for the Schrödinger equation in coordinate space.

The renormalization viewpoint *refuses* to access physically the very short distance region, but encodes it through low energy parameters described by the effective range expansion, Eq. (5), as renormalization conditions (RC's). In the case of only one RC where  $\alpha_0$  is fixed one proceeds as follows [9, 10]:

- For a given  $\alpha_0$  integrate in the zero energy wave function  $u_0(r)$ , Eq. (6), down to the cut-off radius  $r_c$ . This is the RC.
- Implement self-adjointness through the boundary condition

$$u'_p(r_c)u_0(r_c) - u'_0(r_c)u_p(r_c) = 0, \quad (10)$$

- Integrate out the finite energy wave function  $u_p(r)$ , from Eq. (3) and determine the phase shift  $\delta_0(p)$  from Eq.(4).
- Remove the cut-off  $r_c \rightarrow 0$  to strive for model independence.

This allows to compute  $\delta_0$  (and hence  $r_0, v_2$ ) from  $V(r)$  and  $\alpha_0$  as *independent* information. Note that this is equivalent to consider, in addition to the regular solution, the *irregular* one <sup>3</sup>. A beautiful result is the universal low energy theorem which highlights this de-correlation between the potential and the scattering length [10]

$$r_0 = 2 \int_0^\infty dr(1 - u_{0,0}^2) - \frac{4}{\alpha_0} \int_0^\infty dr(r - u_{0,0}u_{0,1}) + \frac{2}{\alpha_0^2} \int_0^\infty dr(r^2 - u_{0,1}^2), \quad (11)$$

based on the superposition principle of boundary conditions, i.e. writing  $u_0(r) = u_{0,0}(r) - u_{0,1}(r)/\alpha_0$  with  $u_{0,n}(r) \rightarrow r^n$  and using Eq.(8). A fit of the potential (2) with  $g_{\omega NN} = 0$  to the effective range yields (Fig. 1) a strong correlation between  $m_\sigma$  and  $g_{\sigma NN}$ . Over-imposing this correlation to  $r_0 = 2.670(4)\text{fm}$ , a fit to Ref. [8] yields  $m_\sigma = 493(12)\text{MeV}$ ,  $g_{\sigma NN} = 8.8(2)$ ,  $g_{\omega NN} = 0(5)$  with  $\chi^2/\text{DOF} = 0.24$  (Fig. 1). Note the larger uncertainties, although correlations allow  $g_{\omega NN} \sim 9$  and  $m_\sigma \sim 520\text{MeV}$  within  $\Delta\chi^2 = 1$ . Contrary to common wisdom, but according to our naive expectations, no strong short range repulsion is essential. The moral is that building  $\alpha_0$  *from* the potential is equivalent to absolute knowledge at short distances and in the  $^1S_0$  channel a strong fine tuning is at work. Of course, a more systematic analysis should be pursued in all partial waves and relativistic corrections might be included as well, but this example illustrates our point that the renormalization viewpoint may tell us to what extent short distance physics may be less well determined than the traditional approach assumes. This opens up a new perspective to the phenomenology of OBE potentials in cases where the strong  $\omega$ -repulsion has proven to be crucial at low energies [12].

<sup>3</sup>In momentum space this can be shown to be equivalent to introduce one counterterm in the cut-off Lippmann-Schwinger equation, see Ref. [11] for a detailed discussion.

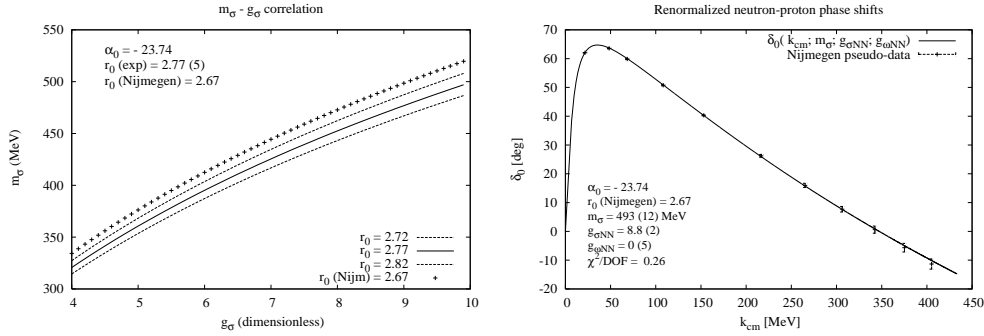


Figure 1: Results in the  $^1S_0$  channel for the renormalized OBE potential. Left: Effective range correlation between  $g_{\sigma NN}$  and  $m_\sigma$  for  $g_{\omega NN} = 0$ . Right: Renormalized phase shift (in degrees) as a function of the CM momentum (in MeV) in the OBE ( $\pi + \sigma + \omega$ ) model. The data are an average of [8].

### 3 Renormalization of chiral potentials

The generalization of the above method to the singular chiral potentials [6, 7] has been implemented in [10] with promising results for One- and Two Pion Exchange (OPE and TPE). We illustrate again the case of pn scattering in the  $^1S_0$ -channel. For the simplest situation with one RC, corresponding to fix the scattering length as an independent parameter, the method outlined above may be directly applied to singular potentials *provided* they are attractive, i.e.  $V(r) \rightarrow -C_n/r^n$  with  $n \geq 2$ <sup>4</sup>. The result for zero energy wave functions as well as the effective range can be seen at Fig. 2. NNLO corresponds to the TPE potential of Ref. [6]. As we see the Nijmegen result  $r_0 = 2.67$ fm is *almost* saturated by the TPE potential yielding  $r_0 = 2.87$ fm already at  $r_c \sim 0.5$ fm. Calculations with TPE to N3LO with one RC show convergence but no improvement [11] without or with  $\Delta$  explicit degrees of freedom. Thus, some physics is missing, perhaps  $3\pi$  effects. If, in addition to  $\alpha_0$ , we want to fix  $r_0 = 2.67$ fm [8] as a RC we must solve Eqs. (6) and (7). The matching condition at the boundary  $r = r_c$  becomes energy dependent [13]

$$\frac{u'_p(r_c)}{u_p(r_c)} = \frac{u'_0(r_c) + p^2 u'_2(r_c) + \dots}{u_0(r_c) + p^2 u_2(r_c) + \dots}. \quad (12)$$

The generalization to arbitrary order is straightforward. For  $N$  RC's we have  $u_p(r) = \sum_{n=0}^N p^{2n} u_{2n}(r)$  and using the natural extension of the matching relation in Eq. (12) as well as the superposition principle of boundary conditions

<sup>4</sup>If the potential was singular and repulsive one cannot fix any low energy parameters; doing so yields non-converging phase shifts.

one can show the following formula

$$p \cot \delta_0(p) = \frac{\sum_{n=0}^N a_n \mathcal{A}_n(p, r_c)}{\sum_{n=0}^N a_n \mathcal{B}_n(p, r_c)}, \quad (13)$$

where the coefficients  $a_n$  can be related to the effective range parameters  $a_0 = 1$ ,  $a_1 = -1/\alpha_0$ ,  $a_2 = r_0$ ,  $a_3 = v_2$  etc. and  $\mathcal{A}_n(p, r_c)$  and  $\mathcal{B}_n(p, r_c)$  are functions which are finite in the limit  $r_c \rightarrow 0$  and depend *solely* on the potential. In Eq. (13) the dependence on the low energy parameters used as input is displayed explicitly and can be completely separated from the long range potential [13]. The coupled channel case can be analyzed in terms of eigenpotentials although the result is cumbersome. In Fig. 3 we show the phase shift for the  $^1S_0$  channel when the potential is considered at LO, NLO and NNLO and either one RC (fixing  $\alpha_0$ ) or two RC's (fixing  $\alpha_0$  and  $r_0$ ) are considered. LO+1C, NLO+2C and NNLO+2C fix the same number of RC's as LO, NLO and NNLO of the Weinberg counting respectively. As we see, our NNLO+2C does not improve over NLO+2C.

It is worth mentioning that the innocent-looking energy dependent matching condition, Eq. (12), is quite unique since this is the only representation guaranteeing finiteness of results for singular potentials [13]. Polynomial expansions in  $p^2$  such as suggested e.g. in Ref. [7] do not work for  $r_c \rightarrow 0$ . A virtue of the coordinate over momentum space is that these results can be deduced analytically. For instance, the equivalent representation of Eq.(13) in momentum space may likely exist, but is so far unknown. Actually, the usual polynomial representation of short distance interactions in momentum space  $V_S(k', k) = C_0 + C_2(k^2 + k'^2) + \dots$  of standard NLO and NNLO Weinberg counting is renormalizable only when  $C_2 \rightarrow 0$  for  $\Lambda \rightarrow \infty$  [11].

## 4 Renormalization of the Deuteron

In the  $^3S_1 - ^3D_1$  channel, the relative proton-neutron state for negative energy is described by the coupled equations

$$\begin{pmatrix} -\frac{d^2}{dr^2} + M_N V_s(r) & M_N V_{sd}(r) \\ M_N V_{sd}(r) & -\frac{d^2}{dr^2} + \frac{6}{r^2} + M_N V_d(r) \end{pmatrix} \begin{pmatrix} u \\ w \end{pmatrix} = -\gamma^2 \begin{pmatrix} u \\ w \end{pmatrix}. \quad (14)$$

Here  $\gamma = \sqrt{M_M B}$ , with  $B = 2.24\text{MeV}$  is the deuteron binding energy and  $u(r)$  and  $w(r)$  are S- and D-wave reduced wave functions respectively. At long distances they satisfy,

$$\begin{pmatrix} u \\ w \end{pmatrix} \rightarrow A_S e^{-\gamma r} \begin{pmatrix} 1 \\ \eta \left[ 1 + \frac{3}{\gamma r} + \frac{3}{(\gamma r)^2} \right] \end{pmatrix}. \quad (15)$$

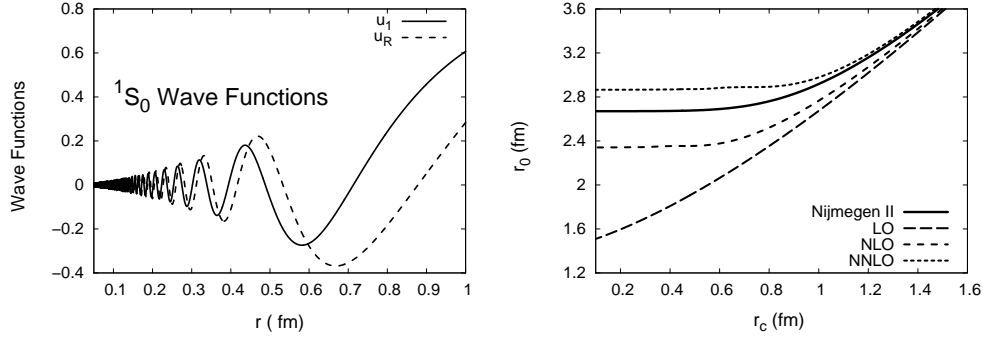


Figure 2: (Left panel) Zero-energy,  $^1S_0$  linearly independent wave functions at NNLO;  $u_1 \rightarrow 1$  and  $u_r \rightarrow r$  for  $r \rightarrow \infty$ . (Right Panel) Effective range  $r_0$  as a function to the cut-off for the same channel and different orders; using  $r_0(r_c) = 2 \left( \int_0^\infty (1 - r/\alpha_0)^2 dr - \int_{r_c}^\infty u_0^2 dr \right)$ , with  $\alpha_0 = -23.74\text{fm}$  [8].

where  $\eta$  is the asymptotic D/S ratio parameter and  $A_S$  is the asymptotic normalization factor, which is such that the deuteron wave functions are normalized to unity. The OPE  $^3S_1 - ^3D_1$  potential is given by  $M_N V_s = U_C$ ,  $M_N V_{sd} = 2\sqrt{2}U_T$ ,  $M_N V_d = U_C - 2U_T$  where for  $r \geq r_c > 0$  we have

$$U_C = -\frac{m_\pi^2 M_N g_A^2}{16\pi f_\pi^2} \frac{e^{-m_\pi r}}{r}, \quad U_T = U_C \left( 1 + \frac{3}{m_\pi r} + \frac{3}{(m_\pi r)^2} \right). \quad (16)$$

The tensor force generates a  $1/r^3$  singularity at the origin in coupled channel space. This behavior of the potential is strong enough to overcome the centrifugal barrier at short distances, thus modifying the usual threshold behavior of the wave functions. The interesting aspect of this potential is that after diagonalization it has one positive (repulsive) and one (negative) attractive eigenvalue. The proper normalization of the wave functions in the limit  $r_c \rightarrow 0$  implies that one can only fix one free parameter, e.g. the deuteron binding energy [10]. Other properties may be predicted, for instance one gets  $\eta_{\text{OPE}} = 0.0263$  (exp. 0.0256(4)). The TPE chiral potentials of Ref. [6] have also been renormalized [10], yielding a rather satisfactory picture of the deuteron. The results described here have been reproduced in momentum space [14]. The required cut-off in momentum space is larger than a naive estimate  $r_c \sim 1/\Lambda$  because the regularization influences both the counterterms as well as the potential. Deuteron form factors, probing some off-shellness of the potential, have been computed describing surprisingly well the data up to momenta  $q \sim 800\text{MeV}$  when LO currents are considered <sup>5</sup>.

<sup>5</sup>See talk of D. R. Phillips in this conference

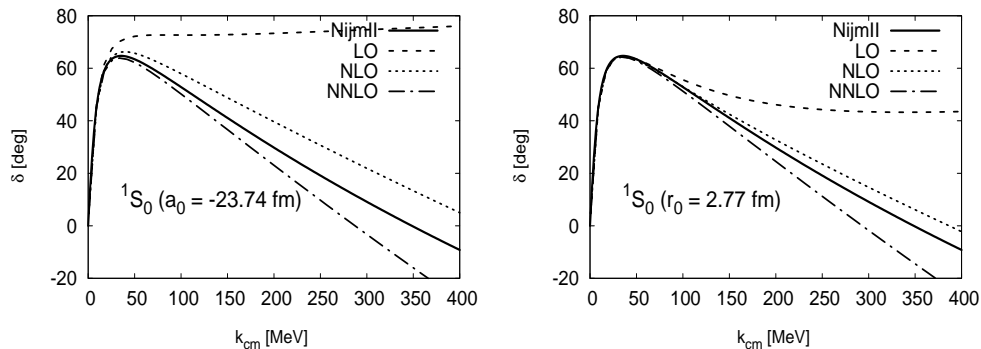


Figure 3: Renormalized  $^1S_0$  phase shifts (in degrees) for chiral LO, NLO and NNLO potentials fixing  $\alpha_0 = -23.74\text{fm}$  (Left panel) or  $\alpha_0 = -23.74\text{fm}$  and  $r_0 = 2.77\text{fm}$  (Right panel) as input parameters. The data are from [8].

## 5 Power counting and renormalization

The question on how a sensible hierarchy for NN interactions should be organized remains so far open, because it is not obvious if one should renormalize or not and how [10, 15–17]. However, for a given long distance potential, we know *whether* and, in positive case, *how* this can be made compatible with the desired short distance insensitivity [10]. Not all chiral interactions fit into this scheme, and thus it is sometimes preferred to keep finite cut-offs despite results being often strongly dependent on the choice at scales  $r_c \sim 0.5 - 1\text{fm}$  similar to the ones we want to probe in NN scattering [10, 15]. Renormalizability of chiral potentials developing a singularity such as Eq. (1) requires that one must choose the regular solution in which case the wave function behaves as  $u_p(r) \sim (r4\pi f_\pi)^{\frac{2n+m}{4}}$  and thus increasing insensitivity is guaranteed as the power of the singularity increases. Converging renormalized TPE calculations show insensitivity for reasonable scales of  $r_c \sim 0.5\text{fm}$  [10].

The Weinberg counting based in a heavy baryon approach at LO [5] for  $^1S_0$  and  $^3S_1 - ^3D_1$  states turns out to be renormalizable. There is at present no necessity argument why this ought to be so, for the simple reason that power counting does not anticipate the sign of the interaction at short distances. When one goes to NLO the short distance  $1/r^5$  singular repulsive character of the potential makes the deuteron unbound [10]. Finally, NNLO potentials diverge as  $-1/r^6$  and are, again, compatible with Weinberg counting in the deuteron [10]. More failures have been reported in Refs. [11, 15]. Relativistic potentials subjected to different power counting have been renormalized in Ref. [18] yielding much less counterterms due to their different short distance

$1/r^7$  singularities and slightly better overall description, although the  $^1S_0$  phase is not improved as compared to the heavy baryon formulation. These complications in the more fundamental chiral potentials contrast with the simplicity of the  $\sigma + \pi$  OBE renormalized results (see Figs. 1 and 3).

In the present state of affairs a clue might come from a remarkable analogy between the NN interaction in the chiral quark model and the Van der Waals molecular interactions in the Born-Oppenheimer approximation [10]. For non-relativistic constituent quarks the direct NN interaction is provided by the convoluted OPE quark-quark potential. Second order perturbation theory in OPE among quarks generates TPE between nucleons yielding

$$V_{NN} = \langle NN | V_{\text{OPE}} | NN \rangle + \sum_{HH' \neq NN} \frac{|\langle NN | V_{\text{OPE}} | HH' \rangle|^2}{E_{NN} - E_{HH'}} + \dots \quad (17)$$

When  $HH' = N\Delta$  and  $HH' = \Delta\Delta$  this resembles Ref. [19] which for  $2\text{fm} < r < 3\text{fm}$  behaves as  $\sigma$  exchange with  $m_\sigma = 550\text{MeV}$  and  $g_{\sigma NN} = 9.4$ . Moreover, the second order perturbative character suggests that the potential becomes singular  $\sim 1/r^6$  and attractive, necessarily being renormalizable with an arbitrary number of counterterms through energy dependent boundary conditions [13]. Clearly, the renormalization of such a scheme where the  $N\Delta$  splitting is treated as a small scale deserves further investigation [20].

## 6 Conclusion

Renormalization is the mathematical implementation of the appealing physical requirement of short distance insensitivity and hence a convenient tool to search for model independent results. In a non-perturbative setup such as the NN problem, renormalization imposes rather tight constraints on the interplay between the unknown short distance physics and the perturbatively computable long distance interactions. This viewpoint provides useful insights and it is within such a framework that we envisage a systematic and model independent description of the NN force based on chiral interactions.

## Acknowledgments

We thank R. Higa, D. Entem, R. Machleidt, A. Nogga and D. R. Phillips for collaboration and the Spanish DGI and FEDER funds grant no. FIS2005-00810, Junta de Andalucía grants no.FQM225-05, EU Integrated Infrastructure Initiative Hadron Physics Project grant no. RII3-CT-2004-506078, DFG (SFB/TR 16) and Helmholtz Association grant no. VH-NG-222 for support.

## References

- [1] R. Machleidt, K. Holinde and C. Elster, Phys. Rept. **149**, 1 (1987).
- [2] R. Machleidt, Phys. Rev. C **63** (2001) 024001
- [3] P. F. Bedaque, U. van Kolck, Ann. Rev. Nucl. Part. Sci. **52**, 339 (2002)
- [4] R. Machleidt and D. R. Entem, J. Phys. G **31** (2005) S1235
- [5] E. Epelbaum, Prog. Part. Nucl. Phys. **57**, 654 (2006)
- [6] N. Kaiser, R. Brockmann and W. Weise, Nucl. Phys. A **625**, 758 (1997)
- [7] M. C. M. Rentmeester, R. G. E. Timmermans, J. L. Friar and J. J. de Swart, Phys. Rev. Lett. **82** (1999) 4992 [arXiv:nucl-th/9901054].
- [8] V. G. J. Stoks, R. A. M. Klomp, C. P. F. Terheggen and J. J. de Swart, Phys. Rev. C **49** (1994) 2950. (<http://nn-online.org>).
- [9] M. Pavon Valderrama and E. Ruiz Arriola, Phys. Lett. B **580** (2004) 149; Phys. Rev. C **70** (2004) 044006
- [10] M. Pavon Valderrama and E. Ruiz Arriola, Phys. Rev. C **72**, 054002 (2005), C **74**, 054001 (2006) C **74**, 064004 (2006) [Erratum-ibid. C **75**, 059905 (2007)]
- [11] D. R. Entem, E. Ruiz Arriola, M. Pavon Valderrama and R. Machleidt, arXiv:0709.2770 [nucl-th].
- [12] A. Calle Cordón and E. Ruiz Arriola (in preparation).
- [13] M. Pavon Valderrama and E. Ruiz Arriola, arXiv:0705.2952 [nucl-th].
- [14] M. Pavon Valderrama, A. Nogga, E. Ruiz Arriola and D. R. Phillips (in preparation).
- [15] A. Nogga, R. G. E. Timmermans and U. van Kolck, Phys. Rev. C **72** (2005) 054006 [arXiv:nucl-th/0506005].
- [16] E. Epelbaum and U. G. Meissner, arXiv:nucl-th/0609037.
- [17] M. C. Birse, Phys. Rev. C **74** (2006) 014003 [arXiv:nucl-th/0507077].
- [18] R. Higa, M. Pavon Valderrama and E. Ruiz Arriola, arXiv:0705.4565
- [19] N. Kaiser, S. Gerstendorfer, W. Weise, Nucl. Phys. A **637** (1998) 395
- [20] M. Pavon Valderrama and E. Ruiz Arriola (in preparation).

# EFFECTIVE FIELD THEORY FRAMEWORK FOR $\bar{K}d$ SCATTERING

*B. Borasoy, U.-G. Meißner, R. Nißler, A. Rusetsky*

Helmoltz-Institut für Strahlen- und Kernphysik,

Universität Bonn,

Nußallee 14-16, 53115 Bonn, Germany

*U. Raha*

Department of Physics and Astronomy,

University of Basel

Klingelbergstrasse 82, CH-4056 Basel, Switzerland

## Abstract

An effective field theory framework is proposed to study  $\bar{K}d$  scattering at threshold. At lowest order, the approach reproduces the well-known result obtained by the re-summation of the multiple-scattering series in the static limit. It has been demonstrated that the approach enables one to systematically evaluate corrections to the lowest-order result.

The SIDDHARTA experiment at LNF-INFN [1] is aimed at a high-precision measurement of the energy shift and the decay width of the ground-state of the kaonic hydrogen at a few percent accuracy in 2008. Moreover, the collaboration plans the first ever measurement of the ground state energy shift and width of the kaonic deuterium. Together, these two independent measurements in principle suffice to determine the values of two complex  $\bar{K}N$  scattering lengths  $a_0$  and  $a_1$  in the isospin symmetry limit. In order to extract these from the experimental data, however, one needs in addition the theory that links the observables of the hadronic atoms to  $a_0$  and  $a_1$  in a model-independent manner and to the accuracy that matches the experimental precision.

The main stumbling point that should be addressed in the theory, is the relation of  $a_0$  and  $a_1$  to the  $\bar{K}d$  scattering length  $A_{\bar{K}d}$ , which is directly extracted from the experimental data on kaonic deuterium. For a long time, the only framework to study this problem was provided by the potential scattering model, which enables one to calculate  $A_{\bar{K}d}$  through solving Faddeev

equations with input “realistic”  $\overline{K}N$  and  $NN$  potentials. Explicit hyperonic channels ( $Y = \Lambda, \Sigma$ ) are shown to contribute only up to a few percent in Faddeev calculations of  $A_{\overline{K}d}$  and can therefore be safely neglected [2]. Moreover, assuming the nucleons to be static, it is possible to give an explicit expression of  $A_{\overline{K}d}$  through  $a_0$  and  $a_1$  in a form of the re-summed multiple-scattering series [3]. In most cases, these series reproduce the result of the full Faddeev calculation with a reasonable accuracy (see, e.g. [4]).

The above approach, however, suffers from obvious deficiencies:

- It is very difficult to control the systematic error, arising from the model-dependent input and the approximations done.
- The Faddeev equations relate  $A_{\overline{K}d}$  to  $a_0$  and  $a_1$  only indirectly. The result of numerical calculations can not be straightforwardly used for the extraction of  $a_0$  and  $a_1$  from the data.

In recent years, investigations of the problem within the framework of effective field theories have started to appear [5]. At lowest order (static nucleons, no derivative couplings) the approach readily reproduces the re-summed multiple scattering series of the potential model. One may expect that the lowest order is already reasonably accurate for the description of  $A_{\overline{K}d}$  and perturbation theory must be applicable beyond the leading order. This conjecture, however, still has to be confirmed by actual calculations.

Below we give a schematic description of the proposed framework. In this framework,  $\overline{K}$  and nucleons are described by a non-relativistic effective Lagrangian. Particle creation/annihilation is forbidden, as well as explicit coupling to the hyperonic channels. Both these effects are implicitly contained in the couplings of the effective Lagrangian.

Further, the  $\overline{K}N$  interaction, as well as the three-body force in the  $\overline{K}NN$  system is described by local Lagrangians containing any number of space derivatives acting on the fields (the terms with higher derivatives are suppressed by inverse powers of a heavy scale). Dimensional regularization is used to tame the ultraviolet divergences arising in the calculation of the Feynman diagrams. The couplings in the  $\overline{K}N$  sector are related to the effective range parameters of  $\overline{K}N$  scattering – the scattering lengths  $a_I$ , the effective ranges  $r_I$ , etc – through the matching procedure (here,  $I = 0, 1$ ). For this reason, the perturbative expansion in the non-relativistic effective theory coincides with the multiple-scattering expansion.

Finally, the  $NN$  interaction is described by a non-local energy-independent potential, calculated in chiral effective theories (see, e.g. [6]). Within the present framework, the explicit form of the potential is assumed to be given.

The following conclusions can be drawn:

1. As already pointed out, assuming static nucleons and retaining only leading-order (non-derivative)  $\overline{K}N$  vertices, one reproduces the re-summed multiple scattering series of the potential model. In addition, in the field-theoretical approach the physical meaning of the re-summation becomes crystal clear. Namely, it can be shown that the difference between the re-summed and conventional multiple scattering series has the same form as the terms emerging from the 3-body Lagrangian and can therefore be removed by renormalization of the 3-body couplings. In other words, the re-summation of the multiple scattering series can only be justified in the presence of the 3-body force.
2. The 3-body force is the main source of the systematic uncertainty in the present approach. One may estimate the imaginary part of the 3-body contribution from experimental data on the two-nucleon absorption of  $K^-$  on the deuteron. Owing to the fact that the total two-nucleon absorption rate is equal to  $1.22 \pm 0.09\%$  [7], one may expect that the systematic uncertainty due to the three-body force in  $A_{\overline{K}d}$  should not exceed a few percent.
3. Despite the large isospin-breaking in the  $\overline{K}N$  amplitudes, the net isospin-breaking effect in  $A_{\overline{K}d}$  is small (the same result has been obtained in Ref. [3] within the potential approach). The reason for this can be immediately seen from the explicit expression of  $A_{\overline{K}d}$ . Although the individual  $\overline{K}N$  amplitudes in this expression possess the unitary cusp that leads to the large isospin-breaking effect, the final expression has no cusp.
4. Going beyond the leading-order approximation, the derivative couplings in the  $\overline{K}N$  sector can be considered (finite-range corrections). Due to the presence of the sub-threshold  $\Lambda(1405)$  one could *a priori* expect rapid variations of the  $\overline{K}N$  amplitudes in the vicinity of threshold, resulting in an enhancement of the effective range term. Our calculations, however, show that this is not the case. The net effect amounts up to a few percent.
5. The most interesting (and difficult) application of the present framework are calculations beyond the static limit, together with the non-perturbative re-summation of the multiple scattering series. We construct the perturbation theory in the parameter  $\xi = M_K/m_N$ . The

expansion of a particular matrix element proceeds in powers of  $\xi^{1/2}$  and can be performed by applying the threshold expansion technique [8] to the Feynman integral, which defines this matrix element. The cancellation of the retardation corrections, which have been widely discussed in the literature (see, e.g. [9]), in the new language is equivalent to the cancellation of the leading contributions in  $\xi$  and can be studied by using the powerful technique of Ref. [8].

Why does the static approximation in the Faddeev approach work so well, even if  $\xi \simeq 0.5$  in real world? We plan to address this question in our subsequent investigations.

## Acknowledgments

The authors would like to thank E. Epelbaum, E. Oset and C. Wilkin for the interesting discussions. Partial financial support from the EU Integrated Infrastructure Initiative Hadron Physics Project (contract number RII3-CT-2004-506078), DFG (SFB/TR 16, “Subnuclear Structure of Matter”) and the EU Contract No. MRTN-CT-2006-035482 “FLAVIANet” is acknowledged.

## References

- [1] C. Curceanu *et al.*, *Eur. Phys. J.* **A31**, 537 (2007).
- [2] L.H. Schick and B.F. Gibson, *Z. Phys.* **A288**, 307 (1978); G. Toker, A. Gal and J.M. Eisenberg, *Nucl. Phys.* **A362**, 405 (1981).
- [3] R. Chand and R.H. Dalitz, *Ann. Phys.* **20**, 1 (1962).
- [4] A. Gal, *Int. J. Mod. Phys.* **A22**, 226 (2007).
- [5] S.S. Kamalov, E. Oset and A. Ramos, *Nucl. Phys.* **A690**, 494 (2001); U.-G. Meißner, U. Raha and A. Rusetsky, *Eur. Phys. J.* **C47**, 473 (2006).
- [6] E. Epelbaum, *Prog. Part. Nucl. Phys.* **57**, 654 (2006).
- [7] V.R. Veirs and R.A. Burnstein, *Phys. Rev.* **D1**, 1883(1970).
- [8] M. Beneke and V.A. Smirnov, *Nucl. Phys.* **B522**, 321 (1998) [arXiv:hep-ph/9711391].
- [9] G. Fäldt, *Phys. Scripta* **16**, 81 (1977); V. Baru, C. Hanhart, A. E. Kudryavtsev and U. G. Meißner, *Phys. Lett.* **B589**, 118 (2004).

# TETRAQUARK SPECTROSCOPY

*E. Santopinto*

Department of Physics  
INFN and University of Genova  
via Dodecaneso 33, Genova, Italy 16146

*G. Galatà*

Department of Physics  
University of Genova  
via Dodecaneso 33, Genova, Italy 16146

## Abstract

A complete classification of tetraquark states in terms of the spin-flavor, color and spatial degrees of freedom was constructed. The permutational symmetry properties of both the spin-flavor and orbital parts of the quark-quark and antiquark-antiquark subsystems are discussed. This complete classification is general and model-independent, and is useful both for model-builders and experimentalists. The total wave functions are also explicitly constructed in the hypothesis of ideal mixing; this basis for tetraquark states will enable the eigenvalue problem to be solved for a definite dynamical model. This is also valid for diquark-antidiquark models, for which the basis is a subset of the one we have constructed. An evaluation of the tetraquark spectrum is obtained from the Iachello mass formula for normal mesons, here generalized to tetraquark systems. This mass formula is a generalization of the Gell-Mann Okubo mass formula, whose coefficients have been upgraded by means of the latest PDG data. The ground state tetraquark nonet was identified with  $f_0(600)$ ,  $\kappa(800)$ ,  $f_0(980)$ ,  $a_0(980)$ . The mass splittings predicted by this mass formula are compared to the KLOE, Fermilab E791 and BES experimental data. The diquark-antidiquark limit was also studied.

## 1 Introduction

Light meson spectroscopy, in particular the nature of the scalar nonet, is still an open problem. Recently the KLOE, E791 and BES collaborations have provided evidence of the low mass resonances  $f_0(600)$  [1] [2] [3] and  $\kappa(800)$

[2] [3]. The quark-antiquark assignment to P-waves [4] has never worked for the lowest lying scalar mesons,  $f_0(980)$ ,  $a_0(980)$ ,  $\kappa(800)$  and  $f_0(600)$  [5]. Maiani *et al.* in Ref. [6] have suggested that these mesons could be described as a tetraquark nonet, in particular as a diquark-antidiquark system. In the traditional quark-antiquark scheme, the  $f_0(980)$  is made up of non-strange quarks [4] and so it is difficult to explain both its higher mass respect to the other components of the nonet and its decay properties (see Refs. [5] [6]). Already in the seventies Jaffe [5] suggested the tetraquark structure of the scalar nonet and proposed a four quark bag model. Other identifications, in particular as quasimolecular states in Ref. [7] and as dynamically generated resonances in Ref. [8], have been proposed (for a complete review see Refs. [9–11] and references therein).

We present here a complete classification scheme of the two quark-two antiquark states in terms of  $SU(6)_{sf}$  from Ref. [12], as well as an evaluation of the tetraquark spectrum for the lowest scalar meson nonet, obtained from a generalization, to the tetraquark case, of the Iachello mass formula for normal mesons published in Ref. [13].

Since the classification of the states is general, it is valid whichever dynamical model for tetraquarks is chosen. As an application, in section 4 we develop a simple diquark-antidiquark model with no spatial excitations inside diquarks. In this case the states are a subset of the general case.

## 2 The classification of tetraquark states

In the construction of the classification scheme we shall make use of symmetry principles without, for the moment, introducing any explicit dynamical model. We are constrained by two conditions: the tetraquark wave functions should be a colour singlet, as all physical states, and the tetraquarks states must be antisymmetric for the exchange of the two quarks and the two antiquarks.

First we begin with the internal (color, flavor and spin) degrees of freedom. The allowed  $SU(3)_f$  representations for the  $qq\bar{q}\bar{q}$  system are obtained by means of the product  $[3] \otimes [3] \otimes [\bar{3}] \otimes [\bar{3}] = [1] \oplus [8] \oplus [1] \oplus [8] \oplus [27] \oplus [8] \oplus [8] \oplus [10] \oplus [\bar{10}]$ . The allowed isospin values are  $I = 0, \frac{1}{2}, 1, \frac{3}{2}, 2$ , while the hypercharge values are  $Y = 0, \pm 1, \pm 2$ . The values  $I = \frac{3}{2}, 2$  and  $Y = \pm 2$  are exotic, which means that they are forbidden for the  $q\bar{q}$  mesons. The allowed  $SU(2)_s$  representations are obtained by means of the product  $[2] \otimes [2] \otimes [2] \otimes [2] = [1] \oplus [3] \oplus [1] \oplus [3] \oplus [3] \oplus [5]$ . The tetraquarks can have an exotic spin  $S = 2$ , value forbidden for normal  $q\bar{q}$  mesons. The  $SU(6)_{sf}$ -spin-flavour classification is obtained by  $[6] \otimes [6] \otimes [\bar{6}] \otimes [\bar{6}] = [1] \oplus [35] \oplus [405] \oplus [1] \oplus [35] \oplus [189] \oplus [35] \oplus$

$[280] \oplus [35] \oplus [\overline{280}]$ . In Appendices A and B of Ref. [12] all the flavor and spin states in the  $qq\bar{q}\bar{q}$  configuration are explicitly written in terms of the single quark and antiquark states. The flavor states are also written in the ideal mixing hypotheses, i.e. as a superposition of the SU(3)-symmetrical states in such a way to have defined strange quark and antiquark numbers. The ideal mixing is essentially a consequence of the OZI rule and, while it has not been proved yet, it is used by all the authors working on  $q\bar{q}$  mesons and tetraquarks.

We can now describe the spatial degrees of freedom. The tetraquark is a system made up of four objects. Thus, we have to define three relative coordinates that we choose as in Ref. [14]: a relative coordinate between the two quarks, another between the two antiquarks and the third relative coordinate between the centers of mass of the two  $q$  and the two  $\bar{q}$ . We associate to each coordinate an orbital angular momentum,  $L_{13}$ ,  $L_{24}$  and  $L_{12-34}$  respectively. We obtain the total angular momentum  $J$  by combining the four different spins and the three orbital angular momenta. The parity for a tetraquark system is the product of the intrinsic parities of the quarks (+) and the antiquarks (-) times the factors coming from the spherical harmonics [14]. The result is  $P = P_q P_q P_{\bar{q}} P_{\bar{q}} (-1)^{L_{13}} (-1)^{L_{24}} (-1)^{L_{12-34}} = (-1)^{L_{13}+L_{24}+L_{12-34}}$ . Using these coordinates, the charge conjugation eigenvalues can be calculated by following the same steps as in the  $q\bar{q}$  case, considering a tetraquark as a  $Q\bar{Q}$  meson, where  $Q$  represents the couple of quarks and  $\bar{Q}$  the couple of antiquarks, with total “spin”  $S$  and relative angular momentum  $L_{12-34}$ . Only the states for which  $Q$  and  $\bar{Q}$  have opposite charges are  $C$  eigenvectors, with eigenvalues [14]  $C = (-1)^{L_{12-34}+S}$ . A discussion of G parity and its eigenvalues can be found in Ref. [12]. Tetraquark mesons do not have forbidden  $J^{PC}$  combinations. Because of the Pauli principle, the tetraquark states must be antisymmetric for the exchange of the two quarks and the two antiquarks and it is, thus, necessary to study the permutational symmetry (i.e. the irreducible representations of the group  $S_2$ ) of the color, flavor, spin and spatial parts of the wave functions of each subsystem. Moreover we have another constraint: only the singlet colour states are physical states. We have seen that there are two colour singlets allowed to the tetraquarks. It is better to write them by underlining their permutational  $S_2$  symmetry, antisymmetric (A) or symmetric (S):  $(qq)$  in  $[\underline{3}]_C (A)$  and  $(\bar{q}\bar{q})$  in  $[3]_C (A)$ , or  $(qq)$  in  $[6]_C (S)$  and  $(\bar{q}\bar{q})$  in  $[\underline{6}]_C (S)$ . Then we have to study the permutational symmetry of the spatial part of the two quarks (two antiquarks) states and the permutational symmetry of the SU(6)<sub>sf</sub> representations for a couple of quarks (antiquarks). The spatial, flavor, color and spin parts with given permutational symmetry ( $S_2$ ) must then be combined together to obtain completely antisymmetric states under the exchange of the two quarks and

the two antiquarks. The resulting states are listed in Table III of Ref. [12]. In Table V, VI, VII and VIII of Ref. [12] we write the possible flavor, spin and  $J^{PC}$  values for different orbital angular momenta.

### 3 The tetraquark spectrum

In Ref. [13] Iachello, Mukhopadhyay and Zhang developed a mass formula for  $q\bar{q}$  mesons,

$$M^2 = (N_n M_n + N_s M_s)^2 + a\nu + bL + cS + dJ + e M_{ijj'j'}^{\prime 2} + f M_{ijj'j'}^{\prime\prime 2}, \quad (1)$$

where  $N_n$  is the non-strange quark and antiquark number,  $M_n \equiv M_u = M_d$  is the non-strange constituent quark mass,  $N_s$  is the strange quark and antiquark number,  $M_s$  is the strange constituent quark mass,  $\nu$  is the vibrational quantum number,  $L$ ,  $S$  and  $J$  are the total orbital angular momentum, the total spin and the total angular momentum respectively,  $M_{ijj'j'}^{\prime 2}$  and  $M_{ijj'j'}^{\prime\prime 2}$  are two phenomenological terms which act only on the lowest pseudoscalar mesons. The first acts only on the octet and encodes the unusually low masses of the eight Goldstone bosons, while the second acts on the  $\eta$  and  $\eta'$  mesons and encodes the non-negligible  $q\bar{q}$  annihilation effects that arise when the lowest mesons are flavour diagonal. The flavor states are considered in the ideal mixing hypothesis, with the exception of the lowest pseudoscalar nonet whose mixing angle can be found in Ref. [13]. During the many years that have passed from the publication in 1991 of Iachello's article the values of the mesons masses reported by the PDG are changed in a considerable way. Thus, we have decided to update the fit of the Iachello model using the latest values reported by the PDG [11] for the light  $q\bar{q}$  mesons. The resulting parameters are reported in Ref. [12]. The Iachello mass formula

Table 1: The candidate tetraquark nonet. Experimental data and quantum numbers

Meson	$I^G(J^{PC})$	$N_s$	Mass (GeV)	Source
$a_0(980)$	$1^-(0^{++})$	2	$0.9847 \pm 0.0012$	PDG [11]
$f_0(980)$	$0^+(0^{++})$	2	$0.980 \pm 0.010$	PDG [11]
$f_0(600)$	$0^+(0^{++})$	0	$0.478 \pm 0.024$	KLOE [1]
$k(800)$	$\frac{1}{2}(0^+)$	1	$0.797 \pm 0.019$	E791 [15]

was developed for  $q\bar{q}$  mesons. In order to describe uncorrelated tetraquark systems by means of an algebraic model one should use a new spectrum generating algebra for the spatial part, i.e.  $U(10)$  since we have nine spatial

degrees of freedom. We have not addressed this difficult problem yet, but we chose to write the internal degrees of freedom part of the mass formula in the same way as it was done for the  $q\bar{q}$  mesons. The splitting inside a given flavor multiplet, to which is also associated a given spin, can be described by the part of the mass formula that depends on the numbers of strange and non-strange quarks and antiquarks. Thus we can use, with the only purpose of determining the mass splitting of the candidate tetraquark nonet, see Ref. [12],

$$M^2 = \text{const} + (N_n M_n + N_s M_s)^2, \quad (2)$$

where *const* is a constant that includes all the spatial and spin dependence of the mass formula, and  $M_n$  and  $M_s$  are the masses of the constituent quarks as obtained from the previously discussed upgrade of the parameters of the Iachello mass formula. We set the energy scale, i. e. we determine the constant *const*, by applying Eq.(2) to the best-known candidate tetraquark,  $a_0(980)$ , see Ref. [12]. Thus, the masses of the other mesons belonging to the same tetraquark nonet, predicted with our simple formula, are  $M(\kappa(800)) = 0.726 \text{ GeV}$ ,  $M(f_0(600)) = 0.354 \text{ GeV}$  and  $M(f_0(980)) = 0.984 \text{ GeV}$ . These values do not seem in very good agreement with the experimental values, even if, before reaching any conclusion, new experiments, especially on the poorly known  $\kappa(800)$  and  $f_0(600)$ , are mandatory.

## 4 Diquark-antidiquark model

We think of the constituent diquark<sup>1</sup> as two correlated constituent quarks with no internal spatial excitations, or at least we hypothesize that their internal spatial excitations will be higher in energy than the scale of masses of the resonances we will consider. The tetraquark mesons are described in this model as composed of a constituent diquark,  $(qq)$ , and a constituent antidiquark,  $(\bar{q}\bar{q})$ . The diquark  $SU(3)_c$  color representations are  $[\bar{3}]_c$  and  $[6]_c$ , while the antidiquark ones are  $[3]_c$  and  $[\bar{6}]_c$ , using the standard convention of denoting color and flavor by the dimensions of their representation. As the tetraquark must be a color singlet, the possible diquark-antidiquark color combinations are

$$\text{diquark in } [\bar{3}]_c, \text{ antidiquark in } [3]_c \quad (3a)$$

$$\text{diquark in } [6]_c, \text{ antidiquark in } [\bar{6}]_c \quad (3b)$$

Diquarks (and antidiquarks) are made up of two identical fermions and so they have to satisfy the Pauli principle. Since we consider diquarks with

<sup>1</sup>For a discussion about the existence or not of the diquark degree of freedom and its importance in our model, please see Ref. [12] and references therein.

no internal spatial excitations, their color-spin-flavor wave functions must be antisymmetric. This limits the possible representations to being only

$$\text{color in } \overline{[3]} \text{ (AS), spin-flavor in } [21]_{sf} \text{ (S)} \quad (4a)$$

$$\text{color in } [6] \text{ (S), spin-flavor in } [15]_{sf} \text{ (AS)} \quad (4b)$$

The decomposition of these  $SU_{sf}(6)$  representations in terms of  $SU(3)_f \otimes SU(2)_s$  is (in the notation [flavor repr., spin])

$$[21]_{sf} = \overline{[3]}, 0 \oplus [6], 1 \quad (5a)$$

$$[15]_{sf} = \overline{[3]}, 1 \oplus [6], 0 \quad (5b)$$

Using the notation [flavor repr., color repr., spin], the diquark states corresponding to color  $\overline{[3]}_c$  and  $[6]_c$  respectively, are

$$|[\overline{3}]_f, [\overline{3}]_c, 0\rangle, |[6]_f, [\overline{3}]_c, 1\rangle \quad (6)$$

$$|[\overline{3}]_f, [6]_c, 1\rangle, |[6]_f, [6]_c, 0\rangle \quad (7)$$

The antidiquark states are the conjugate of the above states.

Following Refs. [16, 17] or Ref. [18], we expect that color-sextet diquarks will be higher in energy than color-triplet diquarks or even that they will not be bound at all. Thus, we will consider only diquarks and antidiquarks in  $\overline{[3]}_c$  and  $[3]_c$  color representations.

The tetraquark color-spin flavor states, obtained combining the allowed diquark and antidiquark states, are reported in Table XI of Ref. [12]. Since diquarks are considered with no internal spatial excitations, the tetraquark states in this model are a subset of the tetraquark states previously derived. In particular they corresponds to the subset with  $L_{13} = L_{24} = 0$ , and color  $\overline{[3]}_c \otimes [3]_c$ . The relative orbital angular momentum between the diquark and the antidiquark is denoted by  $L_{12-34}$ ;  $S_{dq}$  and  $S_{d\bar{q}}$  are respectively the spin of the diquark and the spin of the antidiquark, and  $S_{tot}$  is the total spin;  $J$  is the total angular momentum.

Table XII of Ref. [12] shows the corresponding flavor tetraquark states for each diquark and antidiquark content in the ideal mixing hypothesis.

We have also determined the  $J^{PC}$  quantum numbers of the tetraquarks in the diquark-antidiquark limit. We start from the possible quantum numbers classified for the uncorrelated tetraquark states and then apply the restrictions for the diquark-antidiquark limit,  $L_{13} = L_{24} = 0$  and color  $\overline{[3]}_c \otimes [3]_c$ . Thus, the parity of a tetraquark in the diquark-antidiquark limit is  $P = (-1)^{L_{12-34}}$ , while the charge conjugation (obviously only for its eigenstates) is  $C = (-1)^{L_{12-34} + S_{tot}}$ . In Ref. [12] is also discussed the  $G$  parity in the diquark-antidiquark limit.

The possible  $J^{PC}$  combinations and diquark content of diquark-antidiquark systems with  $L_{12-34} = 0$ ,  $L_{12-34} = 1$  and  $L_{12-34} = 2$  are reported in Ref. [12], in Tables XIII, XIV and XV respectively.

#### 4.1 The tetraquark nonet spectrum in the diquark-antidiquark model.

In the diquark-antidiquark limit we can use  $U(4) \otimes SU(3)_f \otimes SU(2)_s \otimes SU(3)_c$  as spectrum generating algebra, by analogy with what was done by Iachello *et al.* in Ref. [13, 19] for the normal mesons. The analogy between the tetraquark in the diquark-antidiquark limit and the  $q\bar{q}$  mesons is even more evident if we consider that in a string model, as we can see in Refs. [20, 21] the slopes of the Regge trajectories depend only on the color representation of the constituent particles. Thus the slope of the trajectories of tetraquarks made up of a diquark in  $[\bar{3}]_c$  and an antidiquark in  $[3]_c$  is the same as the slope of the trajectories of  $q\bar{q}$  mesons.

Following all these considerations, it is evident that for the tetraquark in the diquark-antidiquark model we can use the same mass formula developed for the normal mesons, with the only difference that we have to replace the masses of the quark and the antiquark with those of the diquark and the antidiquark:

$$M^2 = (M_{qq} + M_{\bar{q}\bar{q}})^2 + a \cdot n + b \cdot L_{12-34} + c \cdot S_{tot} + d \cdot J, \quad (8)$$

where  $M_{qq}$  and  $M_{\bar{q}\bar{q}}$  are the diquark and antidiquark masses,  $n$  is a vibrational quantum number,  $L_{12-34}$  the relative orbital angular momentum,  $S_{tot}$  the total spin and  $J$  the total angular momentum.

The diquark masses are unknown parameters and are determined by fitting the mass formula Eq.(8) with the mass values of the tetraquark candidate nonet<sup>2</sup>  $a_0(980)$ ,  $f_0(980)$ ,  $f_0(600)$  and  $\kappa(800)$ . We consider the candidate tetraquark nonet as the fundamental tetraquark multiplet and so it contains the lighter diquarks, i.e. scalar diquarks.

The masses of the scalar diquarks resulting from the fit are:

$$M_{[n,n]} = 0.275 \text{ GeV}, \quad M_{[n,s]} = 0.492 \text{ GeV} \quad (9)$$

From the fit we obtain also the following masses of the candidate tetraquark

---

<sup>2</sup>This nonet has quantum numbers  $n = L_{12-34} = S_{tot} = J = 0$ , so we do not need to know the parameters  $a$ ,  $b$ ,  $c$  and  $d$ .

Table 2: Quantum numbers of the candidate tetraquark nonet.  $\kappa(800)$  corresponds to  $[n, n][\bar{n}, \bar{s}]$  and also to its conjugate.

Meson	Mass (GeV)	Diquark content	$I^G(J^{PC})$	Source
$a_0(980)$	$0.9847 \pm 0.0012$	$[n, s][\bar{n}, \bar{s}]$	$1^-(0^{++})$	PDG [11]
$f_0(980)$	$0.980 \pm 0.010$	$[n, s][\bar{n}, \bar{s}]$	$0^+(0^{++})$	PDG [11]
$f_0(600)$	$0.478 \pm 0.024$	$[n, n][\bar{n}, \bar{n}]$	$0^+(0^{++})$	KLOE [1]
$\kappa(800)$	$0.797 \pm 0.019$	$[n, n][\bar{n}, \bar{s}]$	$\frac{1}{2}(0^+)$	E791 [15]

nonet:

$$M_{a_0(980)} = M_{f_0(980)} = 0.984 \text{ GeV} \quad (10a)$$

$$M_{f_0(600)} = 0.550 \text{ GeV} \quad (10b)$$

$$M_{\kappa(800)} = 0.767 \text{ GeV}. \quad (10c)$$

These masses are much closer to the experimental values reported in Table

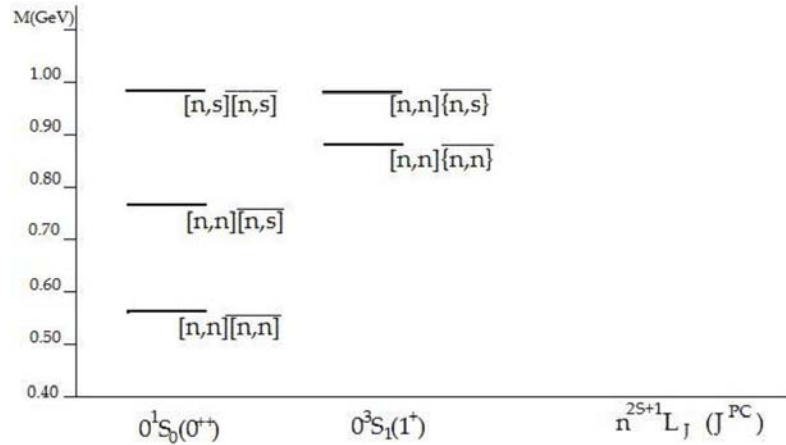


Figure 1: Lowest part (below 1 GeV) of the tetraquark spectrum in the diquark-antidiquark model.

2 than the masses obtained in the uncorrelated tetraquark model of Section 3. However we again underline that, before reaching any conclusion, new experiments are necessary also to be sure of the existence of all the states of the scalar nonet. If the existence of only some states of the nonet will be confirmed a different kind of clusterization will emerge, and we have still not studied this limit in the algebraic framework. Moreover, we have still not

studied the decays of these states and the study of their decay properties can give a better insight into their nature.

The mass formula Eq. 8 can be used to predict all the spectrum of the tetraquarks in the diquark-antidiquark model. In Fig. 1 we include as a preview of this work (still in progress) the lowest (below 1 GeV) part of this spectrum.

## References

- [1] A. Aloisio *et al.*, *Phys. Lett.* **B537**, 21 (2002).
- [2] E. M. Aitala *et al.*, *Phys. Rev. Lett.* **86**, 770 (2001).
- [3] M. Ablikim *et al.* (2005), hep-ex/0506055.
- [4] N. A. Tornqvist, *Z. Phys.* **C68**, 647 (1995).
- [5] R. L. Jaffe, *Phys. Rev.* **D15**, p. 267 (1977).
- [6] L. Maiani, F. Piccinini, A. D. Polosa and V. Riquer, *Phys. Rev. Lett.* **93**, p. 212002 (2004).
- [7] J. D. Weinstein and N. Isgur, *Phys. Rev. Lett.* **48**, p. 659 (1982).
- [8] J. A. Oller and E. Oset, *Nucl. Phys.* **A620**, p. 438 (1997).
- [9] C. Amsler and N. A. Tornqvist, *Phys. Rept.* **389**, 61 (2004).
- [10] F. E. Close and N. A. Tornqvist, *J. Phys.* **G28**, R249 (2002).
- [11] S. Eidelman *et al.* [Particle Data Group collaboration], *Phys. Lett.* **B592**, p. 1 (2004).
- [12] E. Santopinto and G. Galatà, *Phys. Rev.* **C75**, 045206 (2007).
- [13] F. Iachello, N. C. Mukhopadhyay and L. Zhang, *Phys. Lett.* **B256**, 295 (1991).
- [14] F. J. Llanes-Estrada, *ECONF* **c0309101**, p. FRWP011 (2003).
- [15] E. M. Aitala *et al.*, *Phys. Rev. Lett.* **89**, p. 121801 (2002).
- [16] R. L. Jaffe, *Phys. Rept.* **409**, p. 1 (2005).
- [17] R. L. Jaffe (1999), hep-ph/0001123.

- [18] D. B. Lichtenberg, R. Roncaglia and E. Predazzi (1996), hep-ph/9611428.
- [19] F. Iachello, N. C. Mukhopadhyay and L. Zhang, *Phys. Rev.* **D44**, 898 (1991).
- [20] K. Johnson and C. B. Thorn, *Phys. Rev.* **D13**, 1934 (1976).
- [21] G. 't Hooft, *Nucl. Phys.* **B75**, 461 (1974).

MENU 2007  
11th International Conference  
on Meson-Nucleon Physics and  
the Structure of the Nucleon  
September 10-14, 2007  
IKP, Forschungszentrum Jülich, Germany

# POSITIVE AND NEGATIVE PARITY CHARMED MESONS IN HEAVY HADRON CHIRAL PERTURBATION THEORY

R.P. Springer\*,<sup>1</sup>

\*Duke University, Durham, NC, USA

## Abstract

Using heavy hadron chiral perturbation theory (HH $\chi$ PT), we present (to order  $Q^3$ ) the masses, strong decays, and electromagnetic decays of the lowest lying even and odd parity charmed mesons. Here,  $Q \sim \Lambda_{QCD}/m_c, m_\pi/\Lambda_\chi$ . We find: the unusually low masses of the positive parity charmed strange states are consistent with reasonably sized HH $\chi$ PT parameters; the parity-doubling model parameters are RG stable in HH $\chi$ PT; and the positive parity charmed strange states are unlikely to be “molecular” bound states of lower mass mesons. We present some typical fit parameters.

## 1 Introduction

The relevant portion of the charmed meson spectrum is shown in Fig. 1 [1]. The important points to notice from this figure are: (a) the positive parity (0,1) pair have the same ( $\sim 140$  MeV) hyperfine splitting as the negative parity (0,1) pair. This is not required by QCD. It could be an accident, or it could be evidence in favor of the so-called parity doubling model [2]. (b) The positive parity charmed-strange states exist at unexpectedly low energies. Related to this may be (c) the unusually small ( $\sim 10$  MeV) SU(3) breaking, when it is expected to be  $\sim 100$  MeV (as it is elsewhere in this spectrum), and the narrowness of the even parity charmed-strange states. Were the  $D_{s0}(D'_{s1})$  heavy enough to decay to a  $D(D^*)$  and a kaon, they would be as broad as their non-strange partners. Instead, they decay through an isospin violating channel.

---

<sup>1</sup>E-mail address: rps@phy.duke.edu; on leave at University of Maryland, College Park, MD, USA

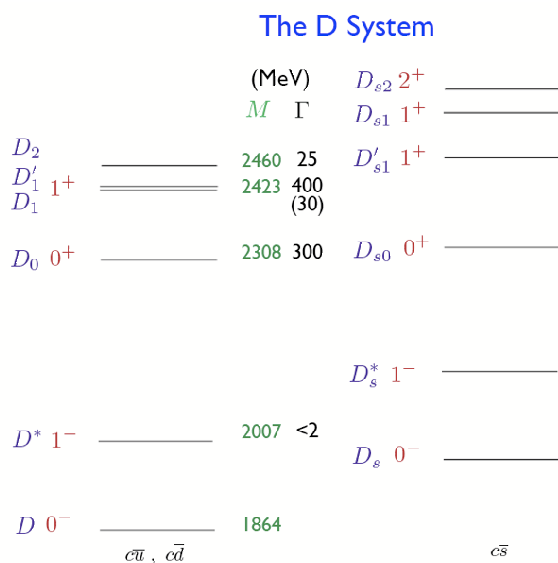


Figure 1: The lowest masses in the charmed meson spectrum [1]

## 2 Heavy Hadron Chiral Perturbation Theory for the $(0^-, 1^-)$ and $(0^+, 1^+)$ charmed mesons

We wish to determine whether these unexpected characteristics of the charmed mesons are consistent with Heavy Hadron Chiral Perturbation Theory (HH $\chi$ PT) [3]. HH $\chi$ PT incorporates two limits of QCD where there exist enhanced symmetries. If we live in a world that is perturbatively close to these limits, then operators in the HH $\chi$ PT Lagrangian can be categorized by how large we expect them to be in this perturbative expansion. In the limit that the up, down, and strange quark masses are taken to zero, QCD exhibits a chiral symmetry. The octet of pions, kaons, and eta are taken to be the pseudo-Goldstone bosons of this spontaneously broken symmetry. Explicit breaking is included as an expansion in  $m_\pi/\Lambda_\chi$ , where  $\Lambda_\chi \sim 1$  GeV is the chiral symmetry breaking scale. In the limit that the charm (and bottom) quark masses are taken to infinity, QCD exhibits a heavy quark spin-flavor symmetry. Corrections to this appear as an expansion in  $1/m_Q$ , where  $m_Q$  is the charm or bottom quark mass. So long as momentum transfers in the problem are “small” compared to  $\Lambda_\chi$  and  $m_Q$ , the theory should be predictive.

Heavy quark spin-flavor symmetry is made manifest by redefining the heavy quark field to make it explicitly velocity-dependent. The effect is to remove the portion of the heavy quark’s momentum that is not relevant to

the process being considered. After that redefinition, derivatives of the heavy quark fields will yield only the off-shell momentum small compared to  $m_Q$  and not include  $m_Q v$  factors that would spoil the perturbative expansion [3]:

$$\mathcal{L}_{QCD}^{heavy} = \bar{Q}(i\not{D} - m_Q)Q \rightarrow \bar{h}_v^{(Q)} i v \cdot D h_v^{(Q)} , \quad (1)$$

where  $Q = e^{-im_Q v \cdot x} (h_v^{(Q)} + \xi_v^{(Q)})$  and  $\xi_v^{(Q)}$  is the ‘‘small’’ component of the heavy quark spinor when  $p_Q^\mu = m_Q v^\mu + k^\mu$ .

Invoking this symmetry in the hadron language, the heavy meson multiplets are contained in [3, 4]:

$$H_a = \frac{1 + \not{v}}{2} [P_a^{*\mu} \gamma_\mu - P_a \gamma_5] , \quad (2)$$

$$S_a = \frac{1 + \not{v}}{2} [P_a^{*\mu} \gamma_\mu \gamma_5 - \mathcal{P}_a] , \quad (3)$$

where  $P_a \sim (D^{0,+}, D_s)$  and  $P_a^{*\mu} \sim (D^{*(0,+)}, D_s^*)$  contain the odd parity multiplet ( $a$  is the flavor label of the light quark) and  $\mathcal{P}_a \sim (D_0^{(0,+)}, D_{s0})$  and  $P_a^{*\mu} \sim (D_1^{(0,+)}, D_{s1}')$  contain the even parity multiplet.

The leading order kinetic and strong interaction terms are contained in [5]

$$\begin{aligned} \mathcal{L}_{axial} = & -\text{Tr}[\bar{H}_a (i v \cdot D_{ab} - \delta_H) H_b] + \text{Tr}[\bar{S}_a (i v \cdot D_{ab} - \delta_S) S_b] \\ & + g \text{Tr}[\bar{H}_a H_b \not{A}_{ba} \gamma_5] + g' \text{Tr}[\bar{S}_a S_b \not{A}_{ba} \gamma_5] \\ & + h (\text{Tr}[\bar{H}_a S_b \not{A}_{ba} \gamma_5] + h.c.) \end{aligned} \quad (4)$$

where the pion, kaon, and  $\eta$  fields are in the 3x3 matrix  $M$ ,  $\xi = e^{iM/f}$ ,  $D^\mu = \partial^\mu + V^\mu$ ,  $V^\mu = \frac{1}{2}(\xi \partial^\mu \xi^\dagger + \xi^\dagger \partial^\mu \xi)$ , and  $A^\mu = \frac{i}{2}(\xi \partial^\mu \xi^\dagger - \xi^\dagger \partial^\mu \xi)$ . This portion of the Lagrange density contains a number of unknown parameters. Were we able to solve QCD we could match it to this effective Lagrange density and predict the parameters. Instead, we must rely on either lattice determinations or experimental measurements. The parameters are:  $g$ , the coupling between odd-parity heavy mesons and light mesons;  $g'$ , the coupling between even-parity heavy mesons and light mesons;  $h$ , the coupling between an odd-parity meson, an even-parity meson, and light mesons; and  $\delta_S - \delta_H$ , the shift between the center of mass of the even-parity and odd-parity heavy mesons.

The mass terms appear in [6, 7]

$$\begin{aligned}
\mathcal{L}_v^{\text{mass}} = & -\frac{\Delta_H}{8} \text{Tr}[\bar{H}_a \sigma^{\mu\nu} H_a \sigma_{\mu\nu}] + \frac{\Delta_S}{8} \text{Tr}[\bar{S}_a \sigma^{\mu\nu} S_a \sigma_{\mu\nu}] \\
& + a_H \text{Tr}[\bar{H}_a H_b] m_{ba}^\xi - a_S \text{Tr}[\bar{S}_a S_b] m_{ba}^\xi \\
& + \sigma_H \text{Tr}[\bar{H}_a H_a] m_{bb}^\xi - \sigma_S \text{Tr}[\bar{S}_a S_a] m_{bb}^\xi \\
& - \frac{\Delta_H^{(a)}}{8} \text{Tr}[\bar{H}_a \sigma^{\mu\nu} H_b \sigma_{\mu\nu}] m_{ba}^\xi + \frac{\Delta_S^{(a)}}{8} \text{Tr}[\bar{S}_a \sigma^{\mu\nu} S_b \sigma_{\mu\nu}] m_{ba}^\xi \\
& - \frac{\Delta_H^{(\sigma)}}{8} \text{Tr}[\bar{H}_a \sigma^{\mu\nu} H_a \sigma_{\mu\nu}] m_{bb}^\xi + \frac{\Delta_S^{(\sigma)}}{8} \text{Tr}[\bar{S}_a \sigma^{\mu\nu} S_a \sigma_{\mu\nu}] m_{bb}^\xi, \quad (5)
\end{aligned}$$

where  $m_{ba}^\xi = \frac{1}{2}(\xi m_q \xi + \xi^\dagger m_q \xi^\dagger)_{ba}$ , and  $m_q = \text{diag}(m_u, m_d, m_s)$ . The unknown parameters here are  $\Delta_H$  and  $\Delta_S$ , giving hyperfine splitting;  $a_H$  and  $a_S$ ,  $\mathcal{O}(m_q)$  corrections but spin-symmetry preserving; and  $\Delta_H^{(a)}$ ,  $\Delta_S^{(a)}$ ,  $\Delta_H^{(\sigma)}$ , and  $\Delta_S^{(\sigma)}$ ,  $\mathcal{O}(m_q)$  and spin-symmetry violating.

Leading order electromagnetic decays are dictated by [8–10]

$$\begin{aligned}
\mathcal{L} = & \frac{e\beta}{4} \text{Tr}[\bar{H}_a H_b \sigma^{\mu\nu}] F_{\mu\nu} Q_{ba}^\xi + \frac{e\tilde{\beta}}{4} \text{Tr}[\bar{H}_a S_b \sigma^{\mu\nu}] F_{\mu\nu} Q_{ba}^\xi \\
& + \frac{e\beta_s}{4} \text{Tr}[\bar{S}_a S_b \sigma^{\mu\nu}] F_{\mu\nu} Q_{ba}^\xi \quad (6)
\end{aligned}$$

where  $Q_{ba}^\xi = \frac{1}{2}(\xi Q \xi^\dagger + \xi^\dagger Q \xi)_{ba}$  and  $Q = \text{diag}(2/3, -1/3, -1/3)$ .

### 3 Masses and the Parity Doubling Model

If isospin symmetry is imposed, there are eight independent masses among the even and odd parity multiplets. The non-strange even parity masses have large errors associated with them, and these are the unusually low masses that might challenge HH $\chi$ PT. At leading order, there are eight parameters and these may be fit to the eight masses. At order  $Q^3$ ,  $g$ ,  $h$ , and  $g'$  also enter. Those expressions are given in Ref. [7].

What can HH $\chi$ PT say about the viability of the parity doubling model to explain the near equality of the hyperfine splittings within the even and odd parity multiplets? A one-loop renormalization analysis yields the following equations [7]:

$$\begin{aligned}
\mu^2 \frac{d}{d\mu^2} (\Delta_S - \Delta_H) = & \frac{4}{9\pi^2 f^2} (g'^2 \Delta_S^3 - g^2 \Delta_H^3) \\
& + \frac{2h^2}{3\pi f^2} (\Delta_S - \Delta_H) * \mathcal{F}[\delta_S - \delta_H, \Delta_S - \Delta_H] \quad (7)
\end{aligned}$$

$$\begin{aligned}\mu \frac{d}{d\mu}(g + g') &= -\frac{9}{4\pi^2 f^2}(\delta_H - \delta_S)(g + g') \\ \mu \frac{d}{d\mu}(g - g') &= -\frac{7}{4\pi^2 f^2}(\delta_H - \delta_S)(g - g')\end{aligned}\quad (8)$$

$$(m_{S_3^*} - m_{S_3}) - (m_{H_3^*} - m_{H_3}) = \frac{g'^2}{f^2}(\dots) - \frac{g^2}{f^2}(\dots) \quad , \quad (9)$$

where  $\mathcal{F}$  is a (known) function of  $(\delta_S - \delta_H)$  and  $(\Delta_S - \Delta_H)$  and the  $(\dots)$  in the last equation indicate identical (at this order) expressions. The significance of the above equations is that if at any point in the RG evolution  $|g| = |g'|$  and  $\Delta_H = \Delta_S$ , they remain so; and the mass splitting between  $S_3^*$  and  $S_3$  remains the same as the splitting between  $H_3^*$  and  $H_3$ . This means that, from the point of view of HH $\chi$ PT, the parity doubling model is stable to one loop.

## 4 Electromagnetic and Strong Decays

Present values for electromagnetic decays from the even-parity to odd-parity states are [11]:

$$\begin{aligned}\frac{D_{s0}(2317) \rightarrow D_s^* \gamma}{D_{s0}(2317) \rightarrow D_s \pi^0} &< 0.059 \\ \frac{D'_{s1}(2460) \rightarrow D_s^* \gamma}{D'_{s1}(2460) \rightarrow D_s^* \pi^0} &< 0.16 \\ \frac{D'_{s1}(2460) \rightarrow D_s \gamma}{D'_{s1}(2460) \rightarrow D_s^* \pi^0} &= 0.27 \text{ to } 0.55\end{aligned}\quad (10)$$

With this information, along with data on strong and electromagnetic decays within the odd-parity multiplet and a limit on electromagnetic decay within the even-parity multiplet, we have fit to HH $\chi$ PT parameters to order  $Q^3$ . There are still not enough experiments to constrain these parameters. So all we can say at this point is that the data is consistent with an HH $\chi$ PT description of the physics. This is important because if the power counting in HH $\chi$ PT is correct, we expect its predictions to agree with those of QCD. An example of a parameter fit yielding electromagnetic decays at the limit of their experimental values (when only limits are available) is [10]:

$$\begin{aligned}g \sim 0.5, \quad g' \sim 0.5, \quad h \sim -0.96, \quad \frac{h'}{m_c} \sim -0.29, \quad g' \sim -0.64, \\ \beta \sim 1.5 \text{ GeV}^{-1}, \quad \beta_s \sim -6 \text{ GeV}^{-1}, \quad \tilde{\beta} \sim 0.004 \text{ GeV}^{-1}, \quad \tilde{\beta}' \sim 0.001, \end{aligned}\quad (11)$$

where  $h'$  contributes to the isospin violating decay from  $D_{s0}(D'_{s1})$  to  $D_s(D_s^*)$ ,  $\tilde{\beta}$  and  $\tilde{\beta}'$  come with higher order electromagnetic operators, and those parameters whose values do not significantly affect the result are not shown.

## 5 Testing the Molecular Hypothesis

One hypothesis for why the  $D_{s0}$  and  $D'_{s1}$  are found at masses just below threshold to decay to  $DK$  and  $D^*K$ , respectively, is that they are in fact bound states of these mesons. Mehen and I investigated this possibility by calculating what the electromagnetic decay ratios would be if the  $D^{(*)}$  and  $K$  were bound nonrelativistically. We did not solve for this bound state, but took the wavefunction components as unknowns. Keeping the expansion to leading order in the three momentum of the constituents leaves only the wavefunction at the origin, which cancels in the ratio of electromagnetic to strong decays. Even if the errors in the estimate are near 40%, it would be hard to reproduce the experimental measurements/limits with this molecular model. In particular, the dependence of the cross section on the photon energy is  $E_\gamma^3$  in the  $HH\chi$ PT treatment but only  $E_\gamma$  in the molecular interpretation. Clearly the data favor a strong scaling with  $E_\gamma$ . There are those who disagree with this conclusion [12] so it will be useful to investigate further.

## 6 The B meson spectrum

One way to increase the amount of experimental information available to fit unknown parameters is to utilize the flavor part of the spin-flavor symmetry of  $HH\chi$ PT. Further decay information on the  $b$  analogues of the even-parity and odd-parity  $c$  mesons is expected. In the meantime we have the following mass information [1]:

$$m_{H_1}^{(b)} = 5279 \text{ MeV} \quad m_{H_1^*}^{(b)} = 5325 \text{ MeV} \quad (12)$$

$$m_{H_3}^{(b)} = 5366 \text{ MeV} \quad m_{H_3^*}^{(b)} = 5412 \text{ MeV} \quad (13)$$

From HQET operators we know that [13]:

$$\begin{aligned} \bar{m}_S^{(b)} - \bar{m}_H^{(b)} &= \bar{m}_S^{(c)} - \bar{m}_H^{(c)} + \mathcal{O}(1/m_Q) \\ \frac{m_{H^*}^{(b)} - m_H^{(b)}}{m_{H^*}^{(c)} - m_H^{(c)}} &= \frac{m_{S^*}^{(b)} - m_S^{(b)}}{m_{S^*}^{(c)} - m_S^{(c)}} = \frac{m_c}{m_b} + \mathcal{O}\left(\frac{1}{m_Q}\right), \end{aligned} \quad (14)$$

where  $\bar{m}_{H,S}^{(Q)} = (3m_{H^*,S^*}^{(Q)} + m_{H,S}^{(Q)})/4$  from which we expect, with errors at the  $\pm 30$  MeV level:  $m_{S_1}^{(b)} = 5709$  MeV,  $m_{S_1^*}^{(b)} = 5746$  MeV,  $m_{S_3}^{(b)} = 5716$  MeV,

and  $m_{S_3}^{(b)} = 5763$  MeV. Not unexpectedly, this exercise predicts that the even-parity strange-beauty mesons will lie low in mass like their charmed partners. D0 has seen evidence of an excited  $B_1$  mass near 5724 MeV [14].

## 7 Conclusion

To summarize, we conclude that HH $\chi$ PT predictions to  $\mathcal{O}(Q^3)$  for strong and electromagnetic decays are consistent with the available data, but we need more data to further constrain the unknown parameters. We find the molecular interpretation of the  $D_{s0}$  and  $D'_{s1}$  to be disfavored given the available electromagnetic decay data. A one loop renormalization group analysis indicates that the parity doubling model is stable. We make predictions for the spectrum of excited  $B$  mesons. We look forward to future experimental measurements on both the  $c$  and  $b$  excited meson systems.

## 8 Index

## Acknowledgments

This work was supported by DOE grant DE-FG02-05ER41368. RPS thanks the hospitality of Bonn University and the University of Maryland, where some of this work was prepared.

## References

- [1] W. M. Yao *et al.* [Particle Data Group], *J. Phys. G* **33**, 1 (2006), and pdgLive.
- [2] For a recent review of the history and concept, see, e.g., S. S. Afonin, arXiv:0704.1639 [hep-ph].
- [3] M. B. Wise, *Phys. Rev. D* **45**, 2188 (1992);  
G. Burdman and J. F. Donoghue, *Phys. Lett. B* **280**, 287 (1992);  
T. M. Yan, H. Y. Cheng, C. Y. Cheung, G. L. Lin, Y. C. Lin and H. L. Yu, *Phys. Rev. D* **46**, 1148 (1992) [Erratum-ibid. D **55**, 5851 (1997)].
- [4] A. F. Falk, *Nucl. Phys. B* **378**, 79 (1992).

- 
- [5] A. F. Falk and M. E. Luke, *Phys. Lett. B* **292**, 119 (1992).
- [6] E. Jenkins, *Nucl. Phys. B* **412**, 181 (1994).
- [7] T. Mehen and R. P. Springer, *Phys. Rev. D* **72**, 034006 (2005) [arXiv:hep-ph/0503134].
- [8] I. W. Stewart, *Nucl. Phys. B* **529**, 62 (1998) [arXiv:hep-ph/9803227].
- [9] T. Mehen and R. P. Springer, *Phys. Rev. D* **70**, 074014 (2004) [arXiv:hep-ph/0407181].
- [10] T.B. Bunton and R. P. Springer, in preparation.
- [11] D. Besson *et al.* [CLEO Collaboration], *Phys. Rev. D* **68**, 032002 (2003).  
P. Krokovny *et al.* [Belle Collaboration], *Phys. Rev. Lett.* **91**, 262002 (2003).  
K. Abe *et al.*, [Belle Collaboration] *Phys. Rev. Lett.* **92**, 012002 (2004).
- [12] E. van Beveren and G. Rupp, *Phys. Rev. Lett.* **91**, 012003 (2003) [arXiv:hep-ph/0305035];  
E. E. Kolomeitsev and M. F. M. Lutz, *Phys. Lett. B* **582**, 39 (2004) [arXiv:hep-ph/0307133];  
J. Hofmann and M. F. M. Lutz, *Nucl. Phys. A* **733**, 142 (2004) [arXiv:hep-ph/0308263];  
M. F. M. Lutz and M. Soyeur, arXiv:0710.1545 [hep-ph];  
A. Faessler, T. Gutsche, V. E. Lyubovitskij and Y. L. Ma, *Phys. Rev. D* **76**, 014005 (2007) [arXiv:0705.0254 [hep-ph]].  
C. Hanhart, private communication.
- [13] A. V. Manohar and M. B. Wise, *Cambridge Monogr. Part. Phys. Nucl. Phys. Cosmol.* **10**, 1 (2000).
- [14] D0 Collab., *Study of excited B-mesons*, D0-note 4517 (<http://www-d0.fnal.gov>).

# QUARK MODEL: RECENT ISSUES

*Fl. Stancu*

Institute of Physics, B.5  
University of Liège  
Sart Tilman, B-4000 Liège 1  
Belgium

## Abstract

In the first part I briefly survey recent issues in constituent quark models raised by the observation of unusual hadronic states. In particular I discuss the role of higher Fock components in the wave function of baryons and the possible interpretation of open charm and of new charmonium-type resonances as tetraquarks. In the second part I show support for the quark model dynamics obtained in a model independent way from the  $1/N_c$  expansion approach of QCD which proved to be successful in describing baryon properties.

## 1 Introduction

The organizers asked me to talk about recent issues in the quark model (QM). This is a vast subject and I had to make a selective choice. My talk contains two distinctive parts. The first is devoted to specific issues in the QM related to the recent observation (since 2003) of unusual hadronic states. In this context I present a few aspects of the QM developments in the light of the newly found resonances. The second part is devoted to a comparison between QM results and the  $1/N_c$  expansion approach of QCD, both being successful in baryon spectroscopy, the latter being closer to QCD and model independent.

## 2 The QM and the newly found resonances

Here I refer to constituent quark (or potential) models. The basic assumptions are that the Hamiltonian consists of a kinetic (non-relativistic or relativistic) part, a confinement part and a hyperfine interaction of a one-gluon

exchange (OGE) type, a Goldstone boson exchange (GBE) type or resulting from an instanton induced interaction (III), or a mixture of them.

The quark models are generally successful in reproducing baryon spectra. Relativistic effects turn out to be specially important in describing electromagnetic or axial form factors of light baryons. The strong decays of baryons remain problematic in all potential models. The decay widths are generally underestimated in OGE or GBE models [1] as well as in III models [2]. These are results based on the description of the baryons as a system of three valence quarks. Till recently most of mesons were well described as  $q\bar{q}$  systems.

The discovery of new exotic resonances starting from 2003 brought new aspects into the standard treatment of hadrons. These are: 1) higher Fock components in the wave function of some baryons 2) additional spin-orbit term in mesons with non-identical quark masses or the interpretation of some of them as tetraquarks, for example.

## 2.1 Higher Fock components in baryon states

The debate on the existence of pentaquarks lead to the study of the role of five quark components ( $q^4\bar{q}$ ) in the wave function of the nucleon whenever there is a problem in the description of a baryon as a  $q^3$  system. For example, the implication of such components has been analyzed in connection with experiments on parity violation in electron-proton scattering which suggest that the strangeness magnetic moment  $\mu_s$  of the proton is positive. So far calculations gave either positive or negative values. A positive value was obtained [3] by including in the wave function a positive parity component  $uuds\bar{s}$  with one quark in the  $uuds$  subsystem excited to the  $p$ -shell. The most favorable configuration is  $[31]_O[22]_F[22]_S$ , the same as for positive parity pentaquarks [4] with a flavor-spin dependent GBE interaction.

Also, it is known that the QM, irrespective of the hyperfine interaction included in the Hamiltonian model, cannot explain the low mass of the  $\Lambda(1405)$  resonance. Recently dynamical calculations based on the  $q^4\bar{q}$  configurations have been performed [5]. These studies require an embedded  $q^3$  pole in the continuum and a coupling between  $q^3$  and  $q^4\bar{q}$  configurations which remains an open problem.

Finally, there is the suggestion that a  $uuds\bar{s}$  component in the wave function of the  $N^*(1535)$  resonance could lead to a larger coupling to  $N\eta$  and  $N\eta'$  channels [6], in agreement to experiment.

## 2.2 Tetraquarks

Since 2003 an important number of exotic meson-like resonances have been discovered. These are open charm resonances:  $D_s(2317)$ ,  $D_s(2460)$ ,  $D_s(2690)$ ,  $D_s(2860)$  and charmonium type (hidden charm) resonances:  $X(3872)$ ,  $X(3940)$ ,  $Y(3940)$ ,  $Z(3930)$ ,  $Y(4260)$ ,  $Z^\pm(4433)$ .

While for open charm resonances a canonical interpretation as  $c\bar{s}$  systems is still possible [7,8] through the addition of a spin-orbit term which vanishes for equal quark and antiquark masses, in the case of hidden charm resonances one has to assume more complicated structures as: tetraquarks  $(c\bar{c})(q\bar{q})$ ,  $D\bar{D}^*$  molecules, hybrids, glueballs, etc. (for a review see for example Refs. [9,10]). The tetraquark interpretation of  $X(3872)$  is quite attractive [11–13]. The quark model [13] gives twice more states than the diquark model [11]. However much work is still needed in the framework of QM or other approaches in order to understand the exotic hidden charm resonances.

## 3 Compatibility of the quark model and the $1/N_c$ expansion approach

The QM still remains the basic tool in hadron spectroscopy. In addition, it has played an important role in the evolution of ideas towards QCD. However there is no known way to derive the QM from QCD. Each constituent quark model is based on a given Hamiltonian which contains a number of dynamical assumptions. The results are obviously model dependent. Therefore it is very important to establish a connection between QM results and another approach, also successful in baryon spectroscopy, but model independent and much more closely related to QCD. This is the  $1/N_c$  expansion method described below.

### 3.1 The $1/N_c$ expansion method

In 1974 't Hooft [14] extended QCD from  $SU(3)$  to  $SU(N_c)$ , where  $N_c$  is an arbitrary number of colors and suggested a perturbative expansion in the parameter  $1/N_c$ , applicable to all QCD regimes. Witten applied the approach to baryons [15] and derived power counting rules which lead to a powerful  $1/N_c$  expansion method to study static properties of baryons, as for example, masses, magnetic moments, axial currents, etc. The method is systematic and predictive. It is based on the discovery that, in the limit  $N_c \rightarrow \infty$ , QCD possesses an exact contracted  $SU(2N_f)$  symmetry [16,17] where  $N_f$  is the

number of flavors. This symmetry is only approximate for finite  $N_c$  so that corrections have to be added in powers of  $1/N_c$ .

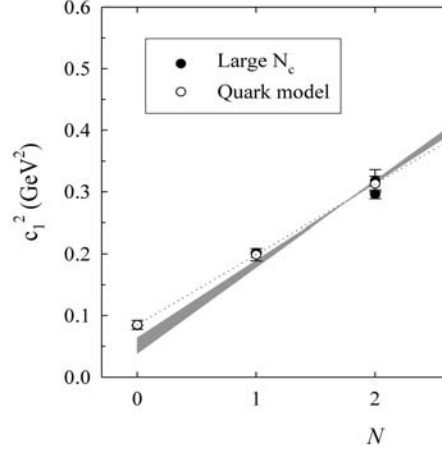


Figure 1:  $c_1^2$  from the  $1/N_c$  expansion mass formula, Eq. (1), and the QM result, Eq. (8). (for details on the large  $N_c$  points see Ref. [23]).

In the  $1/N_c$  expansion approach the mass operator has the general form

$$M = \sum_i c_i O_i + \sum_i d_i B_i, \quad (1)$$

where each sum extends over a finite number of terms. The operators  $O_i$  are invariants under SU(6) transformations and the operators  $B_i$  explicitly break SU(3)-flavor symmetry. The coefficients  $c_i$  and  $d_i$  encode the quark dynamics and are fitted to the experimental data. In the case of nonstrange baryons, only the operators  $O_i$  contribute while  $B_i$  are defined such as their expectation values are zero. The building blocks of  $O_i$  and  $B_i$  are the SU(6) generators:  $S_i$  ( $i = 1, 2, 3$ ) acting on spin and forming an su(2) subalgebra,  $T^a$  ( $a = 1, \dots, 8$ ) acting on flavor and forming an su(3) subalgebra, and  $G^{ia}$  acting both on spin and flavor subspaces. For orbitally excited states, also the components  $\ell_i$  of the angular momentum, as generators of SO(3), and the tensor operator  $\ell^{ij}$  are necessary to build  $O_i$  and  $B_i$ . Examples of  $O_i$  and  $B_i$  can be found in Refs. [18–21]. Each operator  $O_i$  or  $B_i$  carries an explicit factor of  $1/N_c^{n-1}$  resulting from the power counting rules [15], where  $n - 1$  represents the minimum of gluon exchanges to generate the operator. In the matrix elements there are also compensating factors of  $N_c$  when one sums coherently over  $N_c$  quark lines. In practice it is customary to drop higher order corrections of order  $1/N_c^2$ .

The discussion below concerns the coefficients  $c_1$ ,  $c_2$  and  $c_4$  in Eq. (1) related to the following operators

$$O_1 = N_c, \quad O_2 = \ell_i S_i, \quad O_4 = \frac{1}{N_c} S_i S_i. \quad (2)$$

These are the spin-isospin independent, the spin-orbit and the spin-spin operators respectively. The analysis is straightforward for resonances described by symmetric states [56,  $\ell$ ]. For mixed symmetric states [70,  $\ell$ ] the procedure is more complicated due to the separation of the system into a symmetric core and an excited quark. In principle one can use a simpler approach in order to avoid such separation [22].

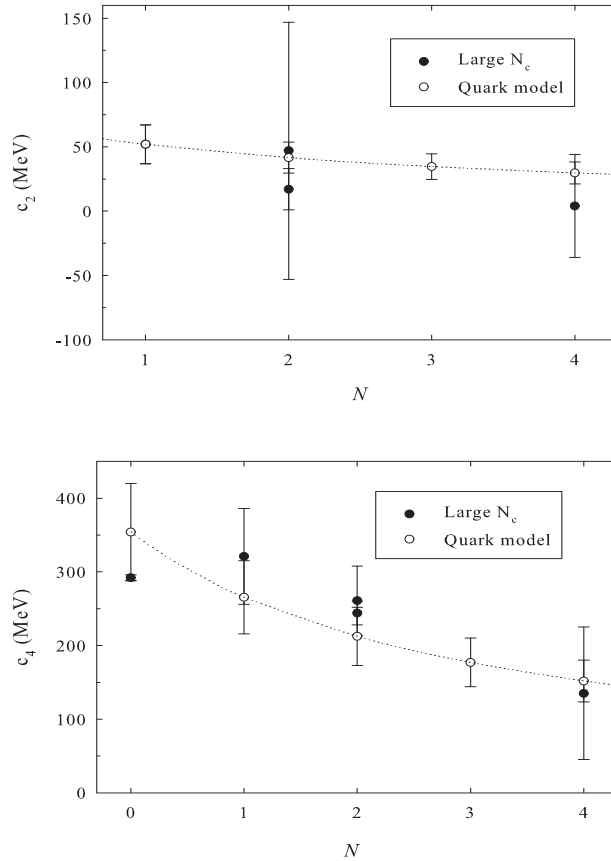


Figure 2: The coefficients  $c_2$  and  $c_4$  in the large  $N_c$  and QM approaches (for details see Ref. [23]). The dotted line passes through QM results.

For strange baryons one has to include both  $O_i$  and  $B_i$  operators in Eq.

(1). The contribution to each strange quark to the mass, denoted by  $\Delta M_s$ , is given by

$$n_s \Delta M_s = \sum_i d_i B_i \quad (3)$$

where  $n_s$  is the number of strange quarks in a baryon.

### 3.2 The quark model

We follow the approach of Ref. [23] and start from the spinless Salpeter Hamiltonian

$$H = \sum_{i=1}^3 \sqrt{p_i^2 + m_i^2} + V_Y; \quad V_Y = a \sum_{i=1}^3 |\mathbf{x}_i - \mathbf{x}_T| \quad (4)$$

where  $m_i$  is the current mass,  $a$  the string tension and  $\mathbf{x}_T$  the Toricelli point. Our purpose is to obtain an approximate analytical form of the eigenvalues of the Hamiltonian (4). To a good approximation for the Y-junction [24] one can replace  $H$  by

$$H_0 = \sum_{i=1}^3 \sqrt{p_i^2 + m_i^2} + \frac{a}{2} \left[ \sum_{i=1}^3 |\mathbf{x}_i - \mathbf{R}| + \frac{1}{2} \sum_{i<j}^3 |\mathbf{x}_i - \mathbf{x}_j| \right] \quad (5)$$

where  $\mathbf{R}$  is the position of the center of mass. The next step is to use the auxiliary field formalism [25] which allows to replace a semirelativistic by a nonrelativistic kinetic energy and a linear by a quadratic confinement. The eigenvalue problem becomes exactly solvable. By minimizing with respect to the auxiliary fields one obtains a good approximation to the exact mass. This is [26]

$$M_0 = 6\mu_0. \quad (6)$$

where

$$\mu_0 = \left[ \frac{a}{3} Q(N+3) \right]^{1/2}, \quad Q = 1/2 + \sqrt{3}/4. \quad (7)$$

Here  $N = 2n + \ell$ , as in a harmonic oscillator potential, and represents the band number used in phenomenology. Adding perturbatively Coulomb-type and self-energy corrections to the squared mass of Eq. (6) one obtains

$$M_0^2 = 2\pi\sigma(N+3) - \frac{4}{\sqrt{3}}\pi\sigma\alpha_s - \frac{12}{(2+\sqrt{3})}f\sigma. \quad (8)$$

provided one makes the scaling  $12aQ = 2\pi\sigma$  where  $\sigma$  is the standard strength tension,  $\alpha_s$  is the strong coupling constant and  $f$  a parameter varying between 3 and 4.

In the auxiliary field formalism, one expects that  $c_2 \propto \mu_0^{-2}$  and  $c_4 \propto \mu_0^{-2}$ . Thus, using Eq. (7), one obtains

$$c_2 = \frac{c_2^0}{N+3}, \quad c_4 = \frac{c_4^0}{N+3}. \quad (9)$$

where the coefficients  $c_2^0$  and  $c_4^0$  have to be fitted.

As a matter of fact, the proof that the band number  $N$  can be considered a good quantum number for baryons including both strange and nonstrange quarks is more involved (for details see Ref. [27]).

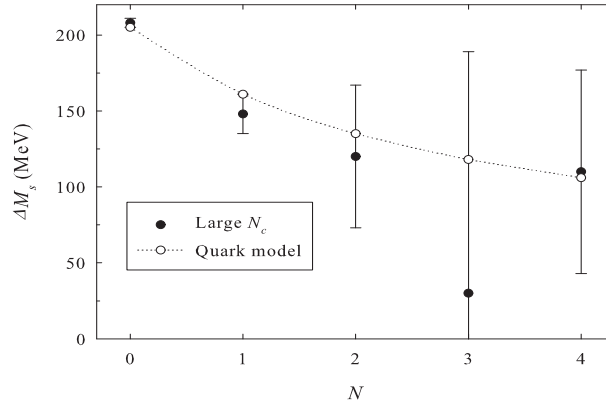


Figure 3:  $\Delta M_s$  from the  $1/N_c$  expansion mass formula, Eq. (1) and the QM mass result (for details see Ref. [27]).

### 3.3 Comparison of the two approaches

In the real world we have  $N_c = 3$ . Thus we have to compare the coefficient  $c_1^2$  of Eq. (1) with  $M_0^2/9$  where  $M_0^2$  comes from Eq. (8). This comparison is made in Fig. 1 for the bands  $N = 0, 1, 2, 3, 4$  studied within the  $1/N_c$  approach. From the best fit one has  $\sigma = 0.163 \pm 0.004 \text{ GeV}^2$ ,  $\alpha_s = 0.4$ , and  $f = 3.5$ , as very standard values. One can see a remarkable agreement between the two approaches. In both cases the points follow the same straight line (Regge trajectory). If the value of  $\sigma$  is chosen in the common phenomenological interval  $\sigma = 0.17$  (0.20)  $\text{GeV}^2$  one obtains the shaded area.

For the upper part of Fig. 2 we chose  $c_2^0 = 208 \pm 60 \text{ MeV}$  so that the large  $N_c$  point at  $N = 1$ , for which the uncertainty is minimal, is exactly reproduced. This coefficient is related to the contribution of the spin-orbit

operator  $O_2$  which turns out to be very small in both approaches. For the lower part of Fig. 2 a good fit to all points gave  $c_4^0 = 1062 \pm 198$  MeV. Note that  $c_4^0 \gg c_2^0$  which indicates that the spin-spin contribution dominates over the spin-orbit term. This justifies the quark model assumption that the spin-spin is the dominant contribution to the hyperfine interaction. Details of this comparison can be found in Ref. [23].

The comparison between the QM and large  $N_c$  results for  $\Delta M_s$  is shown in Fig. 3. The point at  $N = 2$  is from Ref. [27]. The points corresponding to  $N = 0, 1$  and 3 are taken from Ref. [28]. Except for  $N = 3$ , the central values of  $\Delta M_s$  in the large  $N_c$  approach are close to the quark model results. The QM results show a smooth behavior. This suggests that the  $N = 3$  point in the  $1/N_c$  expansion must be re-analyzed. The accuracy of the  $1/N_c$  expansion results depends on the quality and quantity of experimental data on strange baryons, which is very scarce for various reasons [29]. More data are highly desired.

## 4 Conclusions

The key tool in the comparison of QM and large  $N_c$  approaches is the band number  $N$  which turns out to be a good and relevant quantum number in the classification of baryons. It leads to Regge trajectories where  $M^2 \propto N$ . The basic conclusion is that the large  $N_c$  approach supports the quark model assumptions as the relativistic kinetic energy, Y-junction confinement, dominant spin-spin interaction, vanishing spin-orbit contribution, etc. At the same time, the QM can give some physical insight into the coefficients  $c_i$  and  $d_i$  which encode the QCD dynamics. Similar studies are needed for heavy baryons.

## Acknowledgments

I am grateful to C. Semay, F. Buisseret and N. Matagne for an enjoyable collaboration and to the MENU07 Conference organizers for their invitation.

## References

- [1] B. Sengl, T. Melde and W. Plessas, *Phys. Rev.* **D76** 054008 (2007).
- [2] B. Metsch, these proceedings.
- [3] B. S. Zou and D. O. Riska, *Phys. Rev. Lett.* **95**, 072001 (2005).

- 
- [4] Fl. Stancu, *Phys. Rev.* **D58** 111501 (1998).
- [5] S. Takeuchi and K. Shimizu, *Phys. Rev.* **C76**, 035204 (2007) and these proceedings.
- [6] B. S. Zou, these proceedings.
- [7] R. Cahn and J. D. Jackson, *Phys. Rev.* **D68**, 037502 (2003).
- [8] F. E. Close, C. E. Thomas, O. Lakhina, E. S. Swanson, *Phys. Lett.* **B647**, 159 (2007); O. Lakhina, E. S. Swanson, *Phys. Lett.* **B650**, 159 (2007).
- [9] J. L. Rosner, *J. Phys.* **G34**, S127 (2007).
- [10] E. Swanson, *Phys. Rept.* **429**, 243 (2006).
- [11] L. Maiani, F. Piccini, A. D. Polosa and V. Riquer, *Phys. Rev.* **D71**, 014028 (2005).
- [12] H. Hogaasen, J. -M. Richard and P. Sorba, *Phys. Rev.* **D73**, 05403 (2006).
- [13] Fl. Stancu, On the existence of heavy tetraquarks, in *Proc. 11th International Conference on Nuclear Reaction Mechanisms*, ed. E. Gadioli, (Università degli Studi di Milano, Ricerca Scientifica ed Educazione Permanente, Supplemento no. 126, 2006, p. 319, hep-ph/0607077.
- [14] G. 't Hooft, *Nucl. Phys.* **B72**, 461 (1974).
- [15] E. Witten, *Nucl. Phys.* **B160**, 57 (1979).
- [16] J. L. Gervais and B. Sakita, *Phys. Rev. Lett.* **52**, 87 (1984); *Phys. Rev.* **D30**, 1795 (1984).
- [17] R. Dashen and A. V. Manohar, *Phys. Lett.* **B315**, 425 (1993); **B315**, 438 (1993) .
- [18] J. L. Goity, C. Schat and N. N. Scoccola, *Phys. Rev.* **D66**, 114014 (2002).
- [19] N. Matagne and Fl. Stancu, *Phys. Rev.* **D71**, 014010 (2005).
- [20] N. Matagne and Fl. Stancu, *Phys. Lett.* **B631**, 7 (2005).
- [21] N. Matagne and Fl. Stancu, *Phys. Rev.* **D74**, 034014 (2006).
- [22] N. Matagne and Fl. Stancu, hep-ph/0610099.

- [23] C. Semay, F. Buisseret, N. Matagne, Fl. Stancu, *Phys. Rev.* **D75**, 096001 (2007).
- [24] B. Silvestre-Brac, C. Semay, I. M. Narodetskii, and A. I. Veselov, *Eur. Phys. J.* **C32**, 385 (2004).
- [25] Yu. A. Simonov, *Phys. Lett.* **B226**, 151 (1988); **B228**, 413 (1989).
- [26] F. Buisseret and C. Semay, *Phys. Rev.* **D73**, 114011 (2006).
- [27] C. Semay, F. Buisseret, Fl. Stancu, hep-ph/0708.3291.
- [28] J. L. Goity and N. Matagne, *Phys. Lett.* **B** in press, hep-ph/0705.3055.
- [29] W. M. Yao et al. (PDG), *J. Phys.* **G33**, 1 (2006).

# PARTIAL-WAVE ANALYSIS AND SPECTROSCOPY: FROM $\pi$ -N SCATTERING TO PION-ELECTROPRODUCTION

R. Arndt, W. Briscoe, I. Strakovsky<sup>1</sup>, R. Workman

Center for Nuclear Studies, Department of Physics, The George  
Washington University, Washington, D.C. 20052, U.S.A.

## Abstract

We have analyzed data from  $\pi$ N elastic scattering along with single pion photo- and electroproduction. The main focus is the study of low-lying resonances. Here we concentrate on some difficulties associated with resonance identification, in particular the Roper and higher  $P_{11}$  states.

## 1 Introduction

Many of our fits to scattering data have been motivated by ongoing studies of the  $N^*$  properties [1]. Most of these require, as input, amplitudes extracted from elastic  $\pi$ N scattering data [2, 3]. Our pion photoproduction multipoles are determined using a K-matrix formalism, based upon  $\pi$ N partial-wave amplitudes [4, 5]. Further, the electroproduction analysis is anchored to our  $Q^2 = 0$  photoproduction results, with additional factors intended to account for the  $Q^2$  variation [6].

One of the most convincing ways to study the spectroscopy of non-strange baryons is through  $\pi$ N partial-wave analysis (PWA). The main sources of the Review of Particle Physics (RPP)  $N^*$  Listings [1] are the PWA of the KH, CMB, and GW/VPI groups. The analysis of  $\pi$ N scattering data is still crucial in this respect.

In  $\pi$ N PWA, we found resonances through a search for poles in the complex energy plane. These were not put in by hand, contrary to the Breit-Wigner (BW) parameterization. We have also given the results of a BW parameterization, mapping  $\chi^2[W_R, \Gamma]$  while searching all other partial-wave parameters. Some subjectivity is involved, such as: (i) energy binning, (ii)

---

<sup>1</sup>E-mail address:igor@gwu.edu

the strength of constraints, and (iii) the choice of partial waves to be searched. We should stress that the standard PWA reveals resonances with widths of order 100 MeV, but not too wide ( $\Gamma > 500$  MeV) or possessing too small a branching ratio ( $\text{BR} < 4\%$ ), tending (by construction) to miss narrow resonances with  $\Gamma < 30$  MeV. The partial waves of solution KA84 [7] and the single-energy solutions (SES) associated with our SP06 results agree reasonably well over the full range of SP06 (Figs. 4–7 from [2]). However, this does not lead to agreement on the resonance content. For instance, our study [2] does not support several  $N^*$  and  $\Delta^*$  reported by PDG [1]. It is important here to remember that during last 20 years,  $\pi N$  database has increased by a factor of 3–4.

## 2 $P_{11}$ Puzzle

These states have been controversial for many years. The prominent  $N(1440)P_{11}$  resonance is clearly evident in both KH and GW/VPI analyzes (Figs. 4–7 from [2]), but occurs very near the  $\pi\Delta$ ,  $\eta N$ , and  $\rho N$  thresholds (Fig. 8 from [3]), making a BW fit questionable. The  $N(1440)$  is the single resonance which manifests itself through two poles on different Riemann sheets (with respect to the  $\pi\Delta$ -cut). Due to the nearby  $\pi\Delta$  threshold, both  $P_{11}$  poles are not far from physical region. There is a shift between pole positions at two sheets, due to a non-zero jump at the  $\pi\Delta$ -cut. Our conclusion is that a simple BW parametrization cannot account for such complicated structure.

There is recent evidence for a direct measurement of the  $N(1440)$  (at BES in  $e^+e^- \rightarrow J/\psi \rightarrow p\pi^-\bar{n} + n\pi^+\bar{p}$  [8], at SATURNE II in  $\alpha p \rightarrow \alpha'X$  [9], at Uppsala in  $pp \rightarrow np\pi^+$  [10], and at JLab in  $ep \rightarrow e'X$  [11]). They found peaks different from the BW interpretation of  $\pi N$  elastic scattering. This could indicate that a difference is due to the complex structure described above.

Indeed, the  $P_{11}$  partial wave wraps around the center of the Argand diagram (Fig. 1). As a result, small changes in the amplitude can produce large changes in the phase, though these changes have little influence on the fit to data. For the  $\pi N$  elastic scattering, we conclude that there is no sensitivity to resonance in  $P_{11}$  above 1500 MeV except possible states with small  $\Gamma_{el}$  [12].

In fitting the electroproduction database, we extrapolate from the relatively well determined  $Q^2 = 0$  point. The photoproduction multipoles can be parametrized using a form containing the Born terms and phenomenological pieces maintaining the correct threshold behavior and Watson's theorem below the two-pion production threshold. The  $\pi N$  T-matrix connects each

multipole to structure found in the elastic scattering analysis.

The difference between MAID and GW/VPI amplitudes tends to be small but resonance content may be essentially different (Figs. 13 and 14 from [5]).

Ongoing fits incorporate all available electroproduction data, with modifications to our fitting procedure implemented as necessary. Useful comparisons will require those involved in this effort to make available all amplitudes obtained in any new determination of  $R_{EM}$  and  $R_{SM}$ . A major database problem is that most data are from unpolarized measurements. There are no  $\pi^0 n$  data and very few  $\pi^- p$  data (no polarized measurements). This does not allow a determination of the neutron couplings.

## Acknowledgments

This work was supported in part by the U. S. Department of Energy Grant DE-FG02-99ER41110 and by funding from Jefferson Laboratory.

## References

- [1] W.-M. Yao *et al.* [Review of Particle Physics], *J. Phys.* **G33**, 1 (2006).
- [2] R. A. Arndt *et al.*, *Phys. Rev.* **C74**, 045205 (2006).
- [3] R. A. Arndt *et al.*, *Phys. Rev.* **C69**, 035213 (2004).
- [4] R. A. Arndt *et al.*, *Phys. Rev.* **C66**, 055213 (2002).
- [5] M. Dugger *et al.* [CLAS Collab.], *Phys. Rev.* **C76**, 025211 (2007).
- [6] R. A. Arndt *et al.*, in *Proc. Workshop on Shape of Hadrons, Athens, Greece, 2006*, eds. C. N. Papanicolas and A. M. Bernstein, *AIP Conf. Proc.* **904**, 269 (2007).
- [7] R. Koch, *Z. Phys.* **C29**, 597 (1985); G. Höhler, *Pion-Nucleon Scattering*, Landoldt-Börnstein Vol. **I/9b2**, ed. H. Schopper (Springer-Verlag, 1983).
- [8] M. Ablikim *et al.* [BES Collab.], *Phys. Phys. Lett.* **97**, 062001 (2006).
- [9] H. P. Morsch and P. Zupranski, *Phys. Rev.* **C61**, 024002 (2006).
- [10] H. Clement *et al.*, nucl-ex/0612015.
- [11] F. R. Wesselmann *et al.*, *Phys. Phys. Lett.* **98**, 132003 (2007).
- [12] R.A. Arndt *et al.*, *Phys. Rev.* **C69**, 035208 (2004).

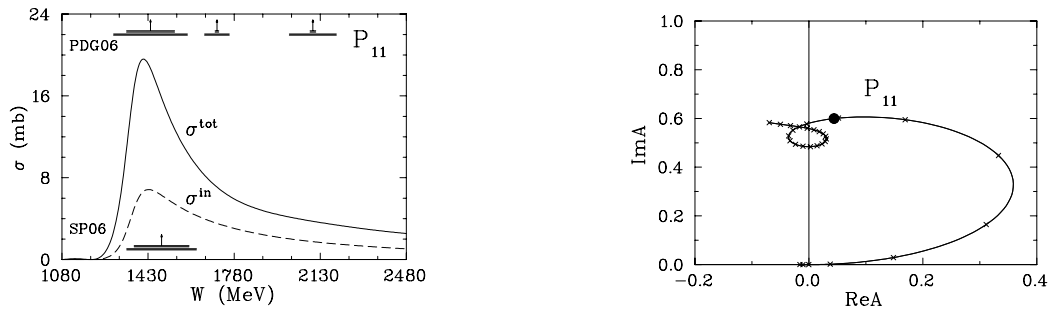


Figure 1: Left panel:  $P_{11}$  contribution to total cross sections. Vertical arrows indicate resonance  $W_R$  values and horizontal bars show full  $\Gamma$  and partial  $\Gamma_{\pi N}$  widths. The lower BW resonance symbols are associated with the SP06 values; upper symbols give PDG values. Right panel: Argand plot for partial-wave amplitude from threshold (1080 MeV) to  $\bar{W} = 2.5$  GeV. Crosses indicate 50 MeV steps in  $W$ . Solid circle corresponds to BW  $W_R$ .

## ON AMBIGUITIES AND UNCERTAINTIES IN PWA

*A. Švarc*<sup>1</sup>, *S. Ceci*, *B. Zauner*  
Rudjer Bošković Institute, Zagreb, Croatia

Establishing a well defined point of comparison between experimental results and theoretical predictions has for decades been one of the main issues in hadron spectroscopy, and the present status is still not satisfactory. Experiments, via partial wave (PWA) and amplitude analysis (AA), can give reliable information on scattering matrix singularities, while quark model calculations usually give information on resonant states spectrum in the first order impulse approximation (bare/quenched mass spectrum). And these two quantities are by no means the same. Up to now, in the absence of a better recipe, these quantities have usually been directly compared, but the awareness has ripened that the clear distinction between the two has to be made. One either has to dress quark-model resonant states spectrum and compare the outcome to the experimental scattering matrix poles, or to try to take into account all self-energy contributions which are implicitly included in the measured scattering matrix pole parameters, make a model independent undressing procedure and compare the outcome to the impulse approximation quark-model calculations. The first option seems to be feasible but complicated [1], but the latter one seems to be impossible [2] due to very general field-theory considerations [3, 4].

Hence, it seems fairly reasonable to focus our interest onto investigating detailed features of scattering matrix singularities.

The general structure of all coupled-channel models is identical: the same type of Dyson-Schwinger integral equation is always solved, but the channel-resonance vertex interaction is treated differently - the approach varies from phenomenological to microscopic [5]. Consequently, all coupled-channel models contain two types of scattering matrix singularities: full and bare. While the full scattering matrix singularities are unanimously identified with "measurable" scattering matrix poles, the interpretation of bare poles, related to the vertex interaction, have not yet been reached. Desirous ones attempt to relate them to quark-model resonant states: in [6-8] the possibility has been opened that  $\gamma N \rightarrow \Delta$  helicity amplitudes and transition form factors of constituent quark models should be compared to the bare coupled-channel functions, in [9] a simple well defined model is devised for understanding

---

<sup>1</sup>E-mail address: svarc@irb.hr

Roper and  $\Delta$  resonances in terms of Cloudy Bag Model form factors [10], and in [11, 12] this idea is used for understanding charmed/strange resonant states in meson-meson scattering sector. Second, more cautious ones give them certain measure of physical importance, but strongly refrain from giving them such a tempting physical meaning. The main reason for such a disagreement lies in believing that the poles of the interaction potential do arise only from the assumed model, and as such do not reveal much dynamics of the interaction [2, 13].

Here we discuss various modes how to numerically quantify both types of scattering matrix singularities, bare and dressed ones. First we focus onto dressed scattering matrix singularities.

## Dressed scattering matrix singularities

Dressed scattering matrix poles are nowadays quantified in two dominant ways: either as Breit-Wigner parameters, i.e. parameters of a Breit-Wigner function which is used to locally represent the experimentally obtainable T-matrix, or as scattering matrix poles (either T or K). In spite of the fact that it is since Hoehler's analysis [14] quite commonly accepted that Breit-Wigner parameters are necessarily model dependent quantities, they are still widely used to quantify the scattering matrix poles. Only recently the scattering matrix poles are being shown in addition [15].

The possibility to define model independent "Breit-Wigner like" parameters by parameterizing K-matrix poles with a Breit-Wigner function has been discussed by our group [16], but in this contribution we focus the presentation on extracting the dressed scattering matrix poles as complex numbers in the complex energy plane, quantities which are to be extracted by knowing only real and imaginary part of the scattering matrix on the real energy axes. We analyze the reliability of the speed-plot technique in particular.

As a self-consistency test to extracting the scattering matrix pole positions using the inherent multi-channel analytic continuation methods [17], we have applied the standard speed plot technique (single-channel) to the amplitudes which describe various different-channel reactions. Surprisingly, we obtained the values which differed from those obtained when using the original method. In addition, the obtained parameters were not identical for different channel processes. This anomalous behavior challenged common sense and the conclusion was drawn that either our partial-wave analysis or the applied pole extraction methods were incorrect. The single-channel extraction methods were carefully examined, and those methods were determined to be at fault. This effort resulted in a new model-independent

Table 1: The  $N^*$  resonance pole parameters obtained by the analytic continuation method and speed plot in various channels. The  $N(????)$  stands for resonances unnamed in the RPP.

$N^*$	$L_{2I2J}$	Continuation method		SPEED PLOT METHOD					
		Re $\mu$ (MeV)	-2 Im $\mu$ (MeV)	$\pi N$ ELASTIC		$\eta N \rightarrow \eta N$		$\pi N \rightarrow \eta N$	
				Re $\mu$ (MeV)	-2 Im $\mu$ (MeV)	Re $\mu$ (MeV)	-2 Im $\mu$ (MeV)	Re $\mu$ (MeV)	-2 Im $\mu$ (MeV)
$N(1535)$	$S_{11}$	1517	190	1506	83	1531	388	-	-
$N(1650)$	$S_{11}$	1642	203	1657	183	1601	208	1632	179
$N(2090)$	$S_{11}$	1785	420	1764	133	-	-	1917	423
$N(1440)$	$P_{11}$	1359	162	1355	154	st <sup>2</sup>	st <sup>a</sup>	st <sup>a</sup>	st <sup>a</sup>
$N(1710)$	$P_{11}$	1728	138	1722	121	1733	154	1679	151
$N(????)$	$P_{11}$	1708	174	-	-	-	-	-	-
$N(2100)$	$P_{11}$	2113	345	2131	394	2122	357	2116	360
$N(1720)$	$P_{13}$	1686	235	1706	219	1617	289	1641	252
$N(1520)$	$D_{13}$	1505	123	1505	129	1527	129	-	-
$N(1700)$	$D_{13}$	1805	130	1953	290	1809	129	-	-
$N(2080)$	$D_{13}$	1942	476	1960	270	-	-	-	-
$N(1675)$	$D_{15}$	1657	134	1657	136	1651	149	1620	108
$N(2200)$	$D_{15}$	2133	439	2134	375	2141	422	2130	401

extraction method free from this anomaly.

Using the speed plot technique we have extracted the pole parameters from the coupled-channel amplitudes of ref. [17] for  $\pi N \rightarrow \pi N$ ,  $\eta N \rightarrow \eta N$  and  $\pi N \rightarrow \eta N$  processes. We summarized the results in Table 1, and compared them to the pole parameters of analytic continuation method. To our surprise, in some partial waves the obtained pole positions turned out to be different for each process, and shifted with respect to analytic continuation method by a few tens of MeV. And that is in obvious contradiction with the input, because the pole positions in ref. [17] are manifestly identical for all T-matrix matrix elements by the very construction. Therefore, something was wrong.

In order to understand, explain and remedy this, we devise a new single-channel method: the T-matrix regularization procedure, the method in which the speed-plot technique is nothing but the first order approximation.

We start with a very general set of assumptions.

Let there be an analytic function  $T(z)$  of complex variable  $z$  which has a first-order pole at some complex point  $\mu$ . The function  $T(z)$  can be any of

the T-matrix matrix elements, and variable  $z$  can be either Mandelstam  $s$  or center-of-mass energy  $\sqrt{s}$ . In order to achieve a full correspondence with the speed plot technique, from now on we are going to use the latter choice. Since all physical processes occur for real energy values, we are allowed to directly determine only  $T(x)$  for  $x$  being a real number. To be able to successfully continue  $T(x)$  into complex energy plane (to search for its poles), we should regularize this function (i.e. remove the pole). In that case, any simple expansion of the regularized function would converge in the proximity of the removed pole.

The T-matrix matrix amplitudes are parameterized as:

$$T(z) = \underbrace{\frac{r}{\mu - z}}_{\text{resonant part}} + \underbrace{\left(T(z) - \frac{r}{\mu - z}\right)}_{\text{smooth background}}, \quad (1)$$

where  $\mu$  and  $r$  are pole position and pole residue, and the variable  $z$  stands for center-of-mass energy ( $\sqrt{s}$ ).

The function  $T(z)$  with a simple pole at  $\mu$ , is regularized by multiplying it with a simple zero at  $\mu$ :

$$f(z) = (\mu - z)T(z). \quad (2)$$

From this definition and Eq. (1), it is evident that the value of  $f(\mu)$  is equal to the residue  $r$  of  $T(z)$  at point  $\mu$ . As we have the access to the function values on real axis only, the Taylor expansion of  $f$  is done over some real  $x$  to give the value (residue) in the pole  $\mu$  (where background is highly suppressed)

$$f(\mu) = \sum_{n=0}^N \frac{f^{(n)}(x)}{n!} (\mu - x)^n + R_N(x, \mu). \quad (3)$$

The expansion is explicitly written to the order  $N$ , and the remainder is designated by  $R_N(x, \mu)$ . Using the mathematical induction one can show that the  $n$ th derivative of  $f(x)$ , given by Eq. (2), is given as:

$$f^{(n)}(x) = (\mu - x)T^{(n)}(x) - nT^{(n-1)}(x). \quad (4)$$

Insertion of this derivative into Taylor expansion conveniently cancels all consecutive terms in the sum, except the last one

$$f(\mu) = \frac{T^{(N)}(x)}{N!} (\mu - x)^{N+1} + R_N(x, \mu), \quad (5)$$

where  $T^{(N)}(x)$  is the  $N$ th energy derivative of T-matrix element. To simplify the notation, the pole can be written as a general complex number  $\mu = a + ib$ .

Table 2: The comparison of  $N^*$  resonance pole parameters obtained by the analytic continuation method, and the Regularization method for  $\pi N$ ,  $\eta N \rightarrow \eta N$  and  $\pi N \rightarrow \eta N$  processes. Numbers in subscript are the expansion order required to obtain convergent result.

N*	$L_{2I2J}$	Analytic Contin.		Regularization Method					
		Re $\mu$ (MeV)	-2 Im $\mu$ (MeV)	$\pi N \rightarrow \pi N$		$\pi N \rightarrow \eta N$		$\eta N \rightarrow \eta N$	
				Re $\mu$ (MeV)	-2 Im $\mu$ (MeV)	Re $\mu$ (MeV)	-2 Im $\mu$ (MeV)	Re $\mu$ (MeV)	-2 Im $\mu$ (MeV)
N(1535)	S <sub>11</sub>	1517	190	1522 <sub>(7)</sub>	146 <sub>(7)</sub>	-	-	-	-
N(1650)	S <sub>11</sub>	1517	203	1647 <sub>(7)</sub>	203 <sub>(7)</sub>	1645 <sub>(10)</sub>	211 <sub>(10)</sub>	-	-
N(2090)	S <sub>11</sub>	1785	420	-	-	-	-	-	-
N(1440)	P <sub>11</sub>	1359	162	1354 <sub>(8)</sub>	162 <sub>(8)</sub>	st <sup>3</sup>	st <sup>a</sup>	st <sup>a</sup>	st <sup>a</sup>
N(1710)	P <sub>11</sub>	1728	138	1729 <sub>(8)</sub>	150 <sub>(8)</sub>	1733 <sub>(5)</sub>	133 <sub>(5)</sub>	1728 <sub>(7)</sub>	142 <sub>(7)</sub>
N(????)	P <sub>11</sub>	1708	174	-	-	-	-	-	-
N(2100)	P <sub>11</sub>	2113	345	2120 <sub>(6)</sub>	347 <sub>(6)</sub>	2120 <sub>(6)</sub>	347 <sub>(6)</sub>	2120 <sub>(6)</sub>	347 <sub>(6)</sub>
N(1720)	P <sub>13</sub>	1686	235	1691 <sub>(5)</sub>	235 <sub>(5)</sub>	1691 <sub>(5)</sub>	234 <sub>(5)</sub>	1691 <sub>(5)</sub>	235 <sub>(5)</sub>
N(1520)	D <sub>13</sub>	1505	123	1506 <sub>(4)</sub>	124 <sub>(4)</sub>	-	-	-	-
N(1700)	D <sub>13</sub>	1805	130	1806 <sub>(5)</sub>	132 <sub>(5)</sub>	1806 <sub>(4)</sub>	130 <sub>(4)</sub>	-	-
N(2080)	D <sub>13</sub>	1942	476	-	-	-	-	-	-
N(1675)	D <sub>15</sub>	1657	134	1658 <sub>(5)</sub>	138 <sub>(5)</sub>	1657 <sub>(3)</sub>	137 <sub>(3)</sub>	1658 <sub>(5)</sub>	138 <sub>(5)</sub>
N(2200)	D <sub>15</sub>	2133	439	2145 <sub>(6)</sub>	439 <sub>(6)</sub>	2144 <sub>(4)</sub>	435 <sub>(4)</sub>	2144 <sub>(6)</sub>	438 <sub>(6)</sub>

Once the Taylor series converges the remainder  $R_N(x, \mu)$  can be disregarded, and the absolute value of both sides of Eq. (5) is given as:

$$|f(\mu)| = \frac{|T^{(N)}(x)|}{N!} |a + ib - x|^{(N+1)}. \quad (6)$$

To keep the form as simple as possible, Eq. (6) is raised to the power of  $2/(N+1)$ . After simple rearrangement of terms, in which we have collected the information on the T-matrix values on the right hand side, and the information on the pole position and residuum on the left hand side, the elemental second-order polynomial emerges:

$$\frac{(a-x)^2 + b^2}{\sqrt[N+1]{|f(\mu)|^2}} = \sqrt[N+1]{\frac{(N!)^2}{|T^{(N)}(x)|^2}}, \quad (7)$$

This is the equation which enables us to directly extract the pole position ( $a = \text{Re } \mu$ ,  $b = \text{Im } \mu$ ) and the absolute value of the function residue  $|f(\mu)|$

from the T-matrix values at the real axes, namely from the quantities directly attainable from the energy-dependent partial wave analysis and evaluated at factual energy points  $x$ .

What we actually do is the following: we first find the  $N$ -th derivative of the T-matrix, and then we calculate the right-hand side of Eq. (7). Observe that the *exact* knowledge of the right-hand side of Eq. (7) *in only three points* uniquely determines the pole parameters. The problem is that we can never know the right-hand side of Eq. (7) exactly. Therefore, we have two options: either i) to take various three-point sets, evaluate the right-hand side of Eq. (7), solve the equation for pole parameters, and make a statistical analysis of obtained results; or ii) to fit the right-hand side of Eq. (7) with the three parameter parabolic function. We have chosen the latter option, and the obtained fitting parameters are our final result.

The pole parameters attained in this way, with the subscript  $N$  denoting the number of required Taylor series terms, are for all three calculated processes given in Table 2. Discrepancies are eliminated.

Observe:

The standard speed plot method turns out to be the “regularization” method in the first order approximation! (To get the speed plot, one should reduce the expansion given by Eq. (3) to  $N = 1$  term.) The developed regularization method represents an improvement of contemporary single-channel pole extraction methods. We demonstrate that it successfully finds resonance pole parameters from a T-matrix in a model-independent way, i.e. without having to assume a specific T-matrix functional form.

## Bare scattering matrix singularities

Coupled-channel T-matrix formalisms (CC\_T) [17, 19, 20] by construction distinguish between scattering-matrix poles and bare Green function (bare propagator) poles. The bare Green function poles, which are the subset of CC\_T model fit parameters, can not be detected experimentally. To become observable they have to interact. Through the formalism described by resolvent Dyson-Schwinger equation the self-energy term is generated; the self-energy term shifts the initial real-value bare propagator poles into the complex energy plane; and eventually the measurable complex scattering-matrix poles are generated as dressed Green function poles.

Following the ideas formulated in a dynamical coupled-channel model of refs. [6, 21], but baring in mind controversies raised in ref. [2], we propose that in any CMB type model one should as well try to identify the position of a bare Green function pole with the mass of a quark-model resonant state (QMRS), and to correlate the imaginary part of the scattering-matrix pole

(SMP), which is created when the interaction effects shift QMRS into the complex energy plane, with its decay width.

Such an identification simultaneously solves two problems: establishes a missing link between QMRS and SMP offering a better control over the missing-resonance problem, and at the same time creates a mechanism how to distinguish between genuine scattering-matrix resonant states (SMRS) being states which are produced by a nearby bare propagator pole, and dynamically generated ones which are only an interference effect of distant ones. By accepting this assumptions, we are able to: a) identify which QMRS are needed to explain a chosen collection of experimental data; b) determine a nature of a given SMRS (genuine or dynamic).

Even before showing the results, we want to warn the reader that the simplicity of the model, i.e. the fact that we are effectively using only three out of at least seven accessible and contributing channels, will produce only qualitative results. Complexity of the coupled-channel model (simultaneous mixing of all channels) requires considerable number of parameters, and we expect that the absence of constraining data in more than two channels will necessarily produce instabilities in obtained fitting solutions.

The first four partial waves in  $I=1/2$  channel ( $S_{11}$ ,  $P_{11}$ ,  $P_{13}$  and  $D_{13}$ ) were analyzed. We use a model with three channels: two physical two-body channels  $\pi N$  and  $\eta N$ , while the third, effective channel represents all remaining two- and three-body processes in a form of a two-body process.

For the  $\pi N$  elastic partial waves we used the VPI/GWU single-energy solutions [22, 23].

For the  $\pi N \rightarrow \eta N$  partial-wave data we used the coupled-channel amplitudes from Batinić *et al.* [17], but instead of using smooth theoretical curves, we constructed the data points by normally distributing the model input (see ref. [16]).

Fitting strategy was taken over from ref. [16].

The obtained curves correctly reproduce all input partial wave data for  $\pi N$  elastic and  $\pi N \rightarrow \eta N$  process, but are because of lack of space given elsewhere [24].

In Fig. 1 we show two groups of results: scattering matrix poles for two lowest negative and two lowest positive parity partial waves.

First group of results, the two lowest negative parity partial waves  $S_{11}$  and  $D_{13}$ , pretty well confirm our assumption. All three bare propagator poles for both partial waves can be naturally identified with lowest QMRS of refs. [25]. We do see some discrepancies in mass position, but each required bare propagator pole does qualitatively correspond to a particular QMRS, and all lowest QMRS have found their bare propagator counter partners.

The obtained CC-T scattering-matrix pole positions correspond reason-

ably well to the experimental values reported in ref. [15]. The only disagreement, the unexpected position of the third SMP of the  $S_{11}$  partial wave (too far in the complex energy plane), is again a consequence of the fit-results instability, and is expected to disappear with including more channels. All three experimentally detected SMPs for the  $D_{13}$  partial wave are reproduced, but the lowest two are somewhat shifted in mass.

We also symbolically visualize the influence of the interaction upon bare propagator poles, and their “journey” from the initial QMRS to the final SMP positions. In the world without interaction mixing matrices  $\gamma$  vanish, we have no “dressing”, and bare propagator and scattering-matrix poles are identical. In the real world, in the world with interaction, the  $\gamma$  matrices are non-vanishing, and are obtained by fitting the partial wave data. Arrows represent the way how bare propagator poles travel from the world without interaction ( $\gamma=0$ ) to the real world scattering-matrix singularities ( $\gamma \neq 0$ ).

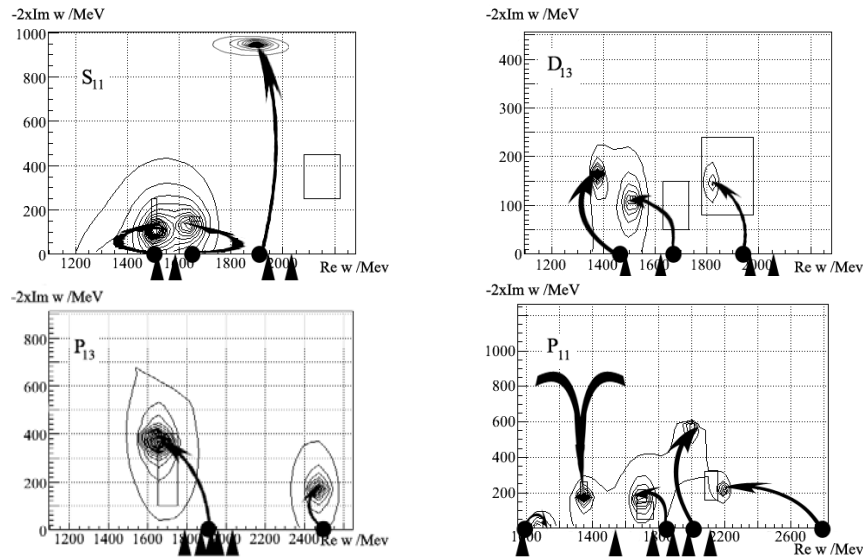


Figure 1: Scattering-matrix singularities and bare propagator pole positions. Full dots denote bare propagator pole positions, triangle arrows denote the few lowest quark-model resonant state masses of refs. [25].

Next group of results, the two lowest positive parity partial waves  $P_{13}$  and  $P_{11}$ , is still consistent with the hypothesis of the article, but some problems appear. Only one out of five QMRS of ref. [25] for the  $P_{13}$  partial wave is identified with the bare propagator pole, while other states remain yet to be identified. The second required bare propagator pole should either be identified with one of the higher lying QMRS, or will be shifted downwards

when results of the fit stabilize.

The notoriously problematic  $P_{11}$  partial wave, however, remains a troublemaker as in majority of theoretical considerations. First, we needed four bare propagator poles in order to achieve acceptable fit to the input data. Having in mind that we should identify bare propagator poles with *all* quark-model states (resonant *and* bound), we have fixed the value of the first bare propagator pole to the mass of the sub-threshold nucleon pole, and left the remaining three poles unconstrained.

Problems start with the identification of QMRS with bare propagator pole position. In ref. [16] we have demonstrated that the presence of inelastic channels directly produces the  $N(1710)$   $P_{11}$  SMP, and in Fig. 1 we show that it is generated by dressing the 1.854 GeV bare propagator pole. This pole can be directly associated with one of the quark-model states of ref. [25], either 1.770 or 1.880. The nucleon state is producing an insignificant, sub threshold and experimentally inaccessible pole at 1.1 GeV; remaining two poles at 2.018 and 2.759 produce SMP of 2.2 GeV which can be identified with poorly determined  $N(2100)$   $P_{11}$ , and an experimentally not yet established state at 2 GeV.

However, our model with constraining data in only two channels shows two very interesting features for  $P_{11}$  partial wave: *i) no bare propagator pole which would correspond to the 1.540 quark-model state is needed; ii) one of experimentally confirmed SMPs, namely the  $N(1440)$   $P_{11}$  state - Roper resonance, is not produced by any nearby bare propagator pole as it was the case for all other scattering-matrix poles; it is generated differently.*

The CMB model in conjunction with our interpretation of physical meaning of bare propagator poles offers us a natural way to characterize the nature of scattering-matrix resonant state. We propose a criteria: the *genuine* SMRS is a state which is produced by a nearby bare propagator pole; the *dynamic* SMRS is a state which is created out of distant bare propagator poles through the interaction mechanism itself.

According to this definition, we have no need for such an entity as the “Roper quark-model resonant state”, in our model Roper resonance is a dynamic resonant state.

## References

- [1] S. Capstick, Unquenching the Quark Model, presentation given on BRAG 2007, September 4, 2007, University of Bonn, Germany, <http://www.kph.uni-mainz.de/MAID/BRAG2007/contributions/>.
- [2] C. Hanhart, What we can learn from spectroscopy and what not, presen-

- tation given on BRAG 2007, September 4, 2007, University of Bonn, Germany, <http://www.kph.uni-mainz.de/MAID/BRAG2007/contributions/>.
- [3] H. W. Fearing and S. Scherer, *Phys. Rev. C* **62**, 034003 (2000).
- [4] M. Gell-Mann and M. L. Goldberger, *Phys. Rev.* **96**, 1433 (1954); R. Haag, *Phys. Rev.* **112**, 669 (1958); J. S. R. Chisholm, *Nucl. Phys.* **26**, 469 (1961); S. Kamefuchi, L. O'Raiheartaigh, and A. Salam, *Nucl. Phys.* **28**, 529 (1961); S. Coleman, J. Wess, and B. Zumino, *Phys. Rev.* **177**, 2239 (1969); B. K. Jennings, *Phys. Lett.* **196**, 307 (1987).
- [5] T.-S. H. Lee, Proceedings of the Workshop on the Physics of Excited Nucleons (NSTAR 2005), Tallahassee, Florida, 10-15 Oct 2005, World Scientific 2006, Pg. 1 - 16.
- [6] T. Sato and T. -S. H. Lee, *Phys. Rev. C* **54**, 2660 (1996).
- [7] T. Sato and T.-S. H. Lee, *Phys. Rev. C*, **63**, 055201 (2001).
- [8] L. Tiator, D. Drechsel, S. Kamalov, M.M. Giannini, E. Santopinto, A. Vassallo, *Eur.Phys.J.* **A19** (2004) 55-60.
- [9] I.R. Afnan, *Acta Physica Polonica* **8**, 2397 (1998).
- [10] A.W. Thomas, *Adv. Nucl. Phys.* **13**, 1 (1984).
- [11] Dae Sung Hwang and Do-Won Kim, *Phys. Lett. B* **601**, 137 (2004).
- [12] Yu. S. Kalashnikova, *Phys. Rev. D* **72**, 034010 (2005).
- [13] P.J. Fink, Jr., G. H. R. H. Landau and J.W. Schnick, *Phys. Rev. C* **41** (1990) 2720.
- [14] G. Höhler,  *$\pi N$  Newslett.* **10**, 320 (1997); **14**, 168 (1998), and references therein.
- [15] W.-M. Yao *et al.* (*Particle data Group*), *J. Phys.G: Nucl. Part. Phys.* **33**, 1 (2006).
- [16] S. Ceci, A. Švarc and B. Zauner, Multichannel Anomaly of the Resonance Pole Parameters Resolved, *arXiv:hep-ph/0609236*.
- [17] M. Batinić, *et al.*, *Phys. Rev. C* **51**, 2310 (1995); M. Batinić, *et al.*, *Physica Scripta* **58**, 15, (1998).
- [18] G. Höhler,  *$\pi N$  Newslett.* **9**, 1 (1993).
- [19] R.E. Cutkosky, C.P. Forsyth, R.E. Hendrick and R.L. Kelly, *Phys. Rev. D* **20**, 2839 (1979).
- [20] T.P. Vrana, S.A. Dytman and T.S.-H. Lee, *Phys. Rep.* **328**, 181 (2000).
- [21] A. Matsuyama, T. Sato and T. -S. H. Lee, *Physics Report* **493**, 193 (2007).
- [22] [http://gwdac.phys.gwu.edu/analysis/pin\\_analysis.html](http://gwdac.phys.gwu.edu/analysis/pin_analysis.html).
- [23] R. A. Arndt, W.J. Briscoe, I.I. Strakovsky, R.L. Workman, and M.M. Pavan, *Phys. Rev. C* **69**, 035213 (2004).
- [24] S. Ceci, A. Švarc and B. Zauner, Phys. *lanl.arXiv.org preprint arXiv:hep-ph/0701224*.
- [25] Capstick and W. Roberts, *Prog. Part. Nucl. Phys.* **45**, S241-S331 (2000), and references therein.

# NUCLEON AND PION-NUCLEON FORM FACTORS FROM LATTICE QCD

*A. Tsapalis*

Institute of Accelerating Systems and Applications, University of Athens  
Athens, Greece

## Abstract

The isovector Nucleon electromagnetic form factors  $G_E(q^2)$  and  $G_M(q^2)$  are evaluated in Lattice QCD using Wilson fermions. A lattice of spatial extent 3 fm is used in the quenched theory allowing the extraction of the form factors for momentum transfer squared between 0.1 and 2 GeV<sup>2</sup> for lowest pion mass of about 400 MeV. The calculation is also performed using two degenerate dynamical flavors of Wilson quarks for pion masses comparable to those in the quenched theory allowing a direct comparison. An effective chiral theory is used for the extrapolation of the magnetic moment and isovector radii at the physical limit.

In addition, we present recent results from the calculation of the momentum dependence of the axial form factors  $G_A(q^2)$  and  $G_p(q^2)$  along with the calculation of the  $G_{\pi NN}$  form factor on the same set of lattices. This enables us to test the Goldberger-Treiman relation and compare to the experimental value of the pion-nucleon strong coupling constant  $g_{\pi NN}$ .

## 1 Introduction

Form factors maintain a central role in the study of hadron structure. They yield information on the size, magnetization and charge distribution in hadrons. They are functions of the Lorentz invariant momentum transfer squared probing the interaction of a hadron with a current. The electromagnetic structure of the nucleon is probed by the coupling of a photon with a quark, a process parameterized by the electric,  $G_E$ , and the magnetic,  $G_M$  form factor. A photon exchanging momentum  $\mathbf{q}$  probes a length scale of roughly  $1/|\mathbf{q}|$  and therefore a range of momentum transfers is required in order to map the full spatial distribution. The traditional picture of the nucleon electric and magnetic form factors having similar  $q^2$  dependence based on data using Rosenbluth separation has been revised recently by precise

polarization measurements [1], which indicate an approximately linear  $q^2$  dependence of the ratio of  $G_E(q^2)/G_M(q^2)$ .

Lattice QCD enables a non-perturbative study of these fundamental quantities using directly the fundamental theory of strong interactions. State-of-the-art lattice calculations can reach pion masses as low as 350 MeV where chiral effective theories begin to be applicable. Having reliable predictions from chiral theories on the dependence of physical quantities on the pion mass [2, 3] provides the bridge connecting lattice results to experiment.

The exchange of a W or Z boson probes different dynamics inside the nucleon. Two additional form factors enter, namely the axial-vector  $G_A(q^2)$  and the induced pseudoscalar  $G_p(q^2)$ . Chiral symmetry breaking and the associated partial conservation of the axial current (PCAC) constrains the behavior of these form factors. Pion pole dominance is directly reflected in the  $q^2$ -dependence of  $G_p$  while both form factors are related to the pseudoscalar nucleon form factor,  $G_{\pi NN}(q^2)$ , defined through the pion-nucleon vertex. Quasi-elastic neutrino scattering [4] and pion electroproduction experiments [5, 6] are consistent with a dipole  $q^2$ -dependence for  $G_A$  up to 1 GeV<sup>2</sup>.  $G_p$  is less well known, with muon capture experiments [7] being the main source of measurements of  $G_p(-0.88m_\mu^2)$  and pion electroproduction probing the  $q^2$  dependence. At small  $q^2$  [6] the data are well represented with a dipole *Ansatz*. In this work we present the calculation of the isovector nucleon electromagnetic form factors [8] in quenched QCD and using two degenerate flavors of dynamical Wilson fermions. Optimal techniques are employed allowing the evaluation on a large range of momenta with reduced statistical error. In addition we evaluate the axial-vector form factors and the  $\pi - N$  pseudoscalar form factor [9] for a range of momenta transfers up to 2 GeV<sup>2</sup>, which allows us to examine the validity of pion dominance and the associated Goldberger-Treiman (GT) relation. Recent studies of these quantities in Lattice QCD with dynamical quarks using different discretizations [10, 11] yield comparable results to ours. Consistency among the different approaches is indicative that lattice artifacts are under control.

It is worth mentioning that additional information on the nucleon structure is contained in the transition form factors of the nucleon to the  $\Delta(1232)$  resonance. Recent precise pion electroproduction experiments and theoretical calculations in lattice QCD including three dynamical flavors [12] have established the existence of quadrupole strength in the electromagnetic transition, connected to a deformation in the nucleon and/or Delta wavefunctions. Calculations of the axial-vector [13] and pseudoscalar  $N - \Delta$  transition form factors [9] have addressed pion pole dominance in the  $N - \Delta$  system and the validity of the associated non-diagonal GT relation.

## 2 Nucleon matrix elements and form factors

### 2.1 Electromagnetic form factors

The nucleon electromagnetic matrix element for real or virtual photons is parameterized in terms of the Dirac,  $F_1$ , and Pauli,  $F_2$ , form factors,

$$\langle N(p', s') | j_\mu | N(p, s) \rangle = i \bar{u}(p', s') \left[ \gamma_\mu F_1(q^2) + \frac{i \sigma_{\mu\nu} q^\nu}{2M_N} F_2(q^2) \right] u(p, s) \quad (1)$$

where  $p(s)$  and  $p'(s')$  denote initial and final nucleon momentum (spin) and  $M_N$  is the nucleon mass. The form factors depend only on the momentum transfer squared,  $q^2 = (p'_\mu - p_\mu)(p'^\mu - p^\mu)$ . The value of the Dirac form factor at the real photon point,  $F_1(0)$ , is equal to the charge of the proton (neutron) while the Pauli form factor value at the origin,  $F_2(0)$ , measures the anomalous magnetic moment. They are connected to the electric,  $G_E$ , and magnetic,  $G_M$ , Sachs form factors by the relations

$$\begin{aligned} G_E(q^2) &= F_1(q^2) + \frac{q^2}{(2M_N)^2} F_2(q^2) \\ G_M(q^2) &= F_1(q^2) + F_2(q^2) \end{aligned} \quad (2)$$

where  $G_M(0)$  measures the nucleon magnetic moment,  $\mu_p = 2.79$  for the proton and  $\mu_n = -1.91$  for the neutron.

The isoscalar contribution of the electromagnetic current requires the calculation of disconnected loop diagrams. Such diagrams require the evaluation of the quark propagator from *all-to-all* lattice space-time points, a notoriously difficult task given current resources. As done in all current lattice computations on form factors we neglect disconnected contributions. Therefore we can only calculate directly the isovector transition matrix element. In the isospin limit the following equality holds

$$\langle p | (\frac{2}{3} \bar{u} \gamma^\mu u - \frac{1}{3} \bar{d} \gamma^\mu d) | p \rangle - \langle n | (\frac{2}{3} \bar{u} \gamma^\mu u - \frac{1}{3} \bar{d} \gamma^\mu d) | n \rangle = \langle p | (\bar{u} \gamma^\mu u - \bar{d} \gamma^\mu d) | p \rangle. \quad (3)$$

Calculation of the isovector matrix element therefore provides the *isovector* nucleon form factors which measure the difference of the respective proton and neutron form factors

$$\begin{aligned} G_E(q^2) &= G_E^p(q^2) - G_E^n(q^2), \\ G_M(q^2) &= G_M^p(q^2) - G_M^n(q^2). \end{aligned} \quad (4)$$

## 2.2 Axial-vector and pseudoscalar form factors

The axial vector and pseudoscalar density are defined by

$$A_\mu^a(x) = \bar{\psi}(x)\gamma_\mu\gamma_5\frac{\tau^a}{2}\psi(x) \quad , \quad P^a(x) = \bar{\psi}(x)\gamma_5\frac{\tau^a}{2}\psi(x) \quad (5)$$

where  $\tau^a$  are the three Pauli-matrices acting in flavor space and  $\psi$  is the isospin doublet of u- and d- quarks. The matrix element of the axial vector current between nucleon states can be written in the form

$$\langle N(p', s') | A_\mu^3 | N(p, s) \rangle = i \bar{u}(p', s') \left[ \gamma_\mu\gamma_5 G_A(q^2) + \frac{q_\mu}{2M_N}\gamma_5 G_p(q^2) \right] \frac{\tau^3}{2} u(p, s) \quad (6)$$

where  $G_A$  is the axial vector form factor and  $G_p$  the induced pseudoscalar form factor.

The value  $G_A(0)$  defines the axial vector charge of the nucleon, obtained through nucleon  $\beta$ -decay measurements,  $g_A = G_A(0) = 1.2695(29)$ .

Spontaneous breaking of chiral symmetry leads to the relation  $\partial^\mu A_\mu^a = f_\pi m_\pi^2 \pi^a$  between the pion field and the axial vector current. In QCD the corresponding relation is known as the Ward-Takahashi identity  $\partial^\mu A_\mu^a = 2m_q P^a$  where  $m_q$  is the averaged light flavor doublet quark mass. The pion field is therefore proportional to the pseudoscalar density,  $\pi^a = 2m_q P^a / f_\pi m_\pi^2$ .

Taking the nucleon matrix element of the pseudoscalar current defines the pseudoscalar (or pion - nucleon) form factor  $G_{\pi NN}(q^2)$

$$2m_q \langle N(p', s') | P^3 | N(p, s) \rangle = \frac{f_\pi m_\pi^2 G_{\pi NN}(q^2)}{m_\pi^2 - q^2} \bar{u}(p', s') i\gamma_5 \frac{\tau^3}{2} u(p, s). \quad (7)$$

The value  $G_{\pi NN}(0)$  defines the low energy pion nucleon strong coupling constant,  $g_{\pi NN} = G_{\pi NN}(0) = 13.2(1)$  measured from low energy pion - nucleon scattering. PCAC relates the nucleon axial form factors to  $G_{\pi NN}$ : taking the divergence of Eq. (6) leads to

$$G_A(q^2) + \frac{q^2}{4M_N^2} G_p(q^2) = \frac{1}{2M_N} \frac{2G_{\pi NN}(q^2) f_\pi m_\pi^2}{m_\pi^2 - q^2} . \quad (8)$$

The pion pole appearing in the right hand side of Eq. 8 implies a similar pole in  $G_p$ :

$$\frac{1}{2M_N} G_p(q^2) \sim \frac{2G_{\pi NN}(q^2) f_\pi}{m_\pi^2 - q^2} . \quad (9)$$

Substituting the expression for  $G_p$  in Eq. (8) leads to the Goldberger-Treiman relation

$$G_{\pi NN}(q^2) f_\pi = M_N G_A(q^2) . \quad (10)$$

Eq. (10) is satisfied for  $q^2 = 0$  at the 2% level, as  $g_{\pi NN} f_\pi = M_N g_A$ .

### 3 Lattice techniques

The evaluation of the matrix elements in Eqs. (1), (6) and (7) is performed using standard techniques in Lattice QCD. Three point functions of the nucleon interpolating operators interacting with the fermionic bilinear are calculated using the *sequential inversion through the sink* technique. With this technique, the nucleon source and sink operators are fixed at well separated Euclidean time slices and bilinear operator insertions of arbitrary momentum can be calculated at all intermediate Euclidean time slices. We stress the importance of exploiting particular linear combinations of the source and sink fields which maximize the number of allowed lattice momenta insertions and therefore determine the form factors at maximal accuracy in a rotationally symmetric fashion [8,9]. Appropriate ratios of three point functions and nucleon two point functions are constructed, which in the limit of large Euclidean time separation between the current and the nucleon sources converge to the desired matrix element. Smearred quark fields and gauge links are utilized in order to enhance the overlap of the interpolating field to the nucleon state and minimize the contamination from excited states.

### 4 Results

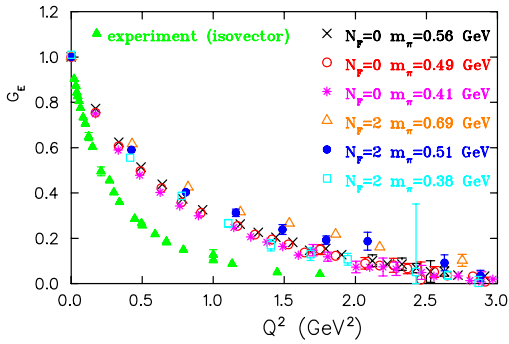


Figure 1:  $G_E$  as a function of  $Q^2$ . Filled triangles show extracted experimental results for the isovector electric form factor

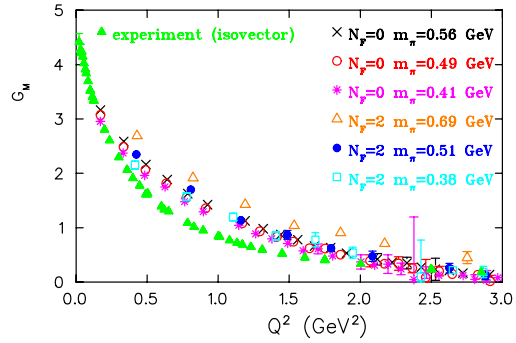


Figure 2: The isovector magnetic form factor,  $G_M$ , as a function of  $Q^2$ . The notation is the same as in Fig. 1.

An ensemble of 200 quenched ( $N_F = 0$ ) configurations on a lattice of size  $32^3 \times 64$  is utilized at three Wilson quark mass parameters corresponding to pion masses of 0.56, 0.49 and 0.41 GeV respectively. The spatial extent of 3.2 fm is large enough to ensure that finite volume effects are small. The lattice spacing obtained using the nucleon mass at the physical limit is  $a = 0.09$  fm.

In addition, the study is performed on  $(1.9 \text{ fm})^3$  ensembles which include a dynamical doublet of light (u,d) Wilson quarks [14, 15] and corresponding pion masses of 0.69, 0.51 and 0.38 GeV.

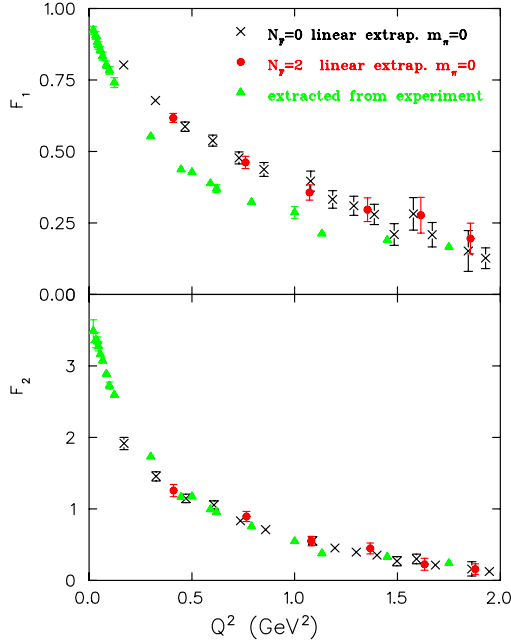


Figure 3:  $F_1$  (upper) and  $F_2$  (lower) as a function of  $Q^2$  at the chiral limit. Results extracted from experiment are shown by the filled triangles.

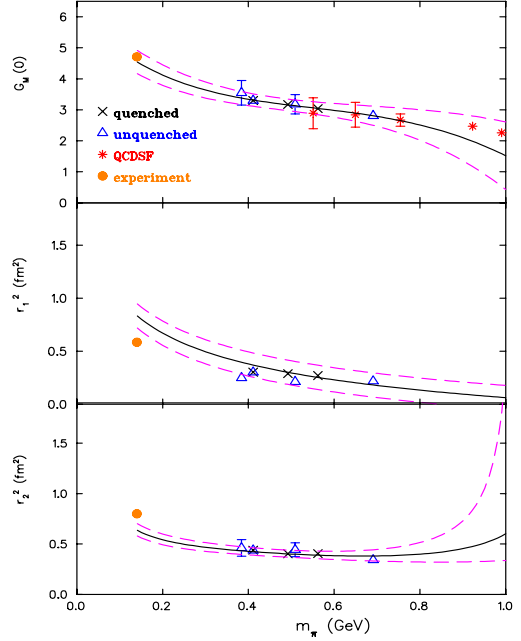


Figure 4: Chiral extrapolation of  $G_M(0)$  and the rms radii  $r_1$  and  $r_2$ . The dashed lines show the maximal error band using the errors on the fitted parameters.

In order to compare the calculated isovector form factors to experiment, we deduce the isovector part of the form factors from the available experimental data via Eqs. (4).  $G_E^p$  is well described by the dipole *Ansatz*,  $G_d(Q^2) = 1/(1 + Q^2/0.71)^2$  while for the neutron the Galster parametrization is assumed

$$G_E^n(Q^2) = \frac{-\mu_n \tau}{1 + 5.6\tau} G_d(Q^2), \quad (11)$$

where  $Q^2 = -q^2 > 0$ ,  $\tau = Q^2/4M_N^2$  and  $\mu_n = -1.91$ . Both  $G_M^p$  and  $G_M^n$  are interpolated to the same  $q^2$  value using  $G_d$ . In Figures 1, 2 we show the isovector form factors for all the lattices compared to the extracted experimental isovector data. The Lattice data show a weak quark mass dependence for both  $G_E$  and  $G_M$  while unquenching effects are small.  $G_E$  shows a larger deviation to experiment than  $G_M$ . For the pion masses considered here the decreasing tendency as  $m_\pi$  becomes smaller is well described by a linear dependence in  $m_\pi^2$ . Using a linear extrapolation scheme the form factors  $F_1$  and

$F_2$  are obtained at the chiral limit and shown in Fig. 3.  $F_2$  is in agreement with experiment while  $F_1$  clearly remains above.

Assuming a dipole Ansatz for  $G_E$  and  $G_M$  we can extrapolate to zero  $q^2$ , to extract the magnetic moment  $\mu = G_M(0)$ . The isovector Dirac and Pauli rms radii are related to the dipole masses  $M_i$  via

$$\langle r_i^2 \rangle = -\frac{6}{F_i(Q^2)} \frac{dF_i(Q^2)}{dQ^2} \Big|_{Q^2=0} = \frac{12}{M_i^2}, \quad i = 1, 2 \quad (12)$$

The dependence of  $\mu$ ,  $\langle r_1^2 \rangle$  and  $\langle r_2^2 \rangle$  on the pion mass has been studied within a chiral effective theory including the  $\Delta$  resonance in [2]. Varying consistently the parameters in the expressions we obtain the results shown in Fig. 4. Quenched and dynamical data for  $\mu$  are well described by the effective theory and extrapolate nonlinearly to the physical value. The Dirac radii on the other hand miss the physical value as expected from the fact that  $F_1$  is decreasing slower than experiment in the low  $Q^2$  regime.

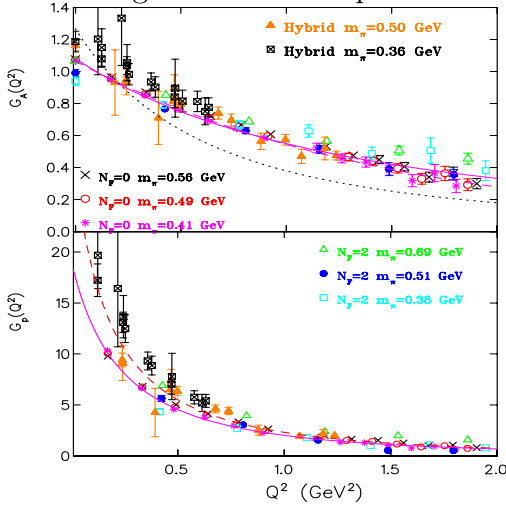


Figure 5:  $G_A(Q^2)$  (upper) and  $G_p(Q^2)$  (lower) for the Wilson lattices. Hybrid results are taken from Hägler *et al.* [11].

Our results for the nucleon axial form factors  $G_A$  and  $G_p$  are shown in Fig. 5. Results using MILC configurations and domain wall fermions [11] at similar pion masses are included. The dotted line in the upper plot is a fit to the experimental results taking a dipole Ansatz  $G_A(q^2) = g_A / \left(1 - \frac{q^2}{M_A^2}\right)^2$ , with an axial mass,  $M_A = 1.026 \pm 0.0021$  GeV. The lattice results fall off slower than experiment and although described well by dipole fits, the fitted dipole masses are considerably larger than experiment. The hybrid data deviate from the Wilson data at low  $Q^2$  and approach the expected  $g_A$  value at

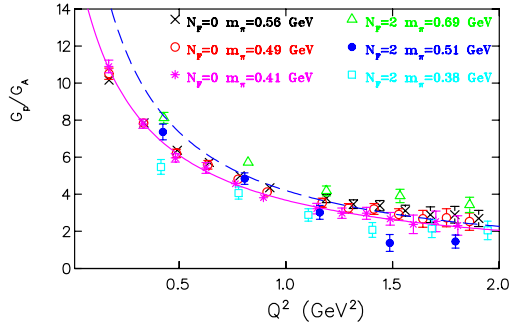


Figure 6:  $G_p(Q^2)/G_A(Q^2)$  for the Wilson lattices. Pion pole dominance prediction for the 0.41 GeV pion quenched data is shown by the dashed line. The solid line is the fit to monopole form with fitted pion pole mass.

the origin.  $G_p$  data are presented in the lower plot where a similar deviation between full and quenched results at low  $q^2$  is seen. If pion pole dominance holds, the ratio  $G_p(Q^2)/G_A(Q^2)$  is completely fixed from Eqs. (9), (10):

$$\frac{G_p(Q^2)}{G_A(Q^2)} = \frac{4M_N^2}{m_\pi^2 + Q^2}. \quad (13)$$

In Fig. 6 we show the ratio  $G_p/G_A$  together with the prediction using pion pole dominance as given in Eq. 13 for the smallest pion mass in the quenched theory (dashed line). As can be seen the lattice data show weaker  $q^2$  dependence. Allowing the pion mass in the monopole form to vary in the fit achieves a good description of the data as shown with the solid line.

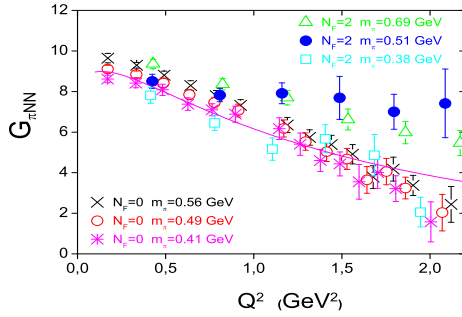


Figure 7:  $G_{\pi NN}(Q^2)$  form factor for the Wilson theory quarks. The solid line is the fit of the 0.41 GeV pion data to Eq. (14).

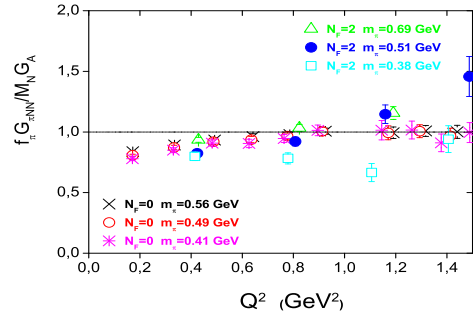


Figure 8:  $f_\pi G_{\pi NN}/M_N G_A$  as a function of  $Q^2$ . If the GT relation holds exactly this ratio should be unity (solid line).

The pseudoscalar form factor  $G_{\pi NN}(Q^2)$  is extracted from Eq. (7). The quark mass  $m_q$  and pion decay constant  $f_\pi$  which enter Eq. (7) are calculated from appropriate two point functions [9] of the axial and pseudoscalar current through the Ward-Takahashi identity  $\partial^\mu A_\mu^a = 2m_q P^a$  and  $\langle 0|A_\mu^a(0)|\pi^b(p)\rangle = if_\pi p_\mu \delta^{ab}$  respectively. In Fig. (7)  $G_{\pi NN}(Q^2)$  is shown for all the Wilson quark lattices. These results are described well by a fit function

$$G_{\pi NN}(Q^2) = K_N \frac{Q^2/m_\pi^2 + 1}{(Q^2/m_A^2 + 1)^2(Q^2/m^2 + 1)} \quad (14)$$

where  $m_A$  is the mass in the dipole *Ansatz* of  $G_A$ ,  $m$  is the mass in the monopole fit of  $G_p/G_A$  and  $K_N$  an overall fit constant. The fit of the  $m_\pi = 0.41$  GeV quenched data is shown by the solid line in Fig. (7) and the extrapolated value at  $Q^2 = 0$  underestimates the experimental value. The fact that at low  $Q^2$  the observed behavior is different than the one expected is

reflected in the plot of the  $f_\pi G_{\pi NN}(Q^2)/M_N G_A(Q^2)$  ratio (Fig. 8) which is expected to be unity if the GT relation is valid. It is indeed observed that in the quenched theory this ratio is less than one for small  $Q^2$  but becomes one for  $Q^2 \gtrsim 0.5 \text{ GeV}^2$ . The dynamical Wilson theory shows an approximately similar behavior for the two heaviest pion masses. If on the other hand the validity of the GT relation  $f_\pi G_{\pi NN} = M_N G_A$  is assumed at low  $Q^2$ , the lightest pion data in the quenched theory extrapolate to  $g_{\pi NN} = 11.8 \pm 0.3$ , closer to the experimentally extracted 13.2(1) value.

## 5 Conclusions

Rapid progress in Lattice QCD has recently allowed calculations of nucleon structure in the pion mass regime where chiral effective theory is applicable allowing reliable extrapolations to the chiral limit. We have calculated the isovector electromagnetic, axial and pseudoscalar form factors of the nucleon with optimal techniques in a wide range of momenta transfers and pion masses down to 380 MeV in the Wilson theory. Assuming that finite spacing effects are under control, the linear extrapolation of  $F_1$  and  $F_2$  to the chiral limit shows small unquenching effects and results to higher values for  $F_1$  compared to experiment. The magnetic moment data extrapolate to the physical value via the one loop chiral effective theory prediction. The isovector radii are underestimated as  $F_1$  and  $F_2$  increase slower than experiment at low  $Q^2$ , a result of truncated pion cloud effects at the heavy quark mass lattice simulations. The importance of chiral symmetry breaking and the associated pion pole dominance in the axial vector transition is also studied. It is observed that  $G_p/G_A$  is described by a monopole form with a pole mass heavier than the corresponding pion mass.  $G_A$  is well described by a dipole *Ansatz*, in agreement to experiment, *albeit* requiring dipole masses  $\gtrsim 1.5 \text{ GeV}$  as compared to  $m_A \sim 1.1 \text{ GeV}$  observed in experiment. Large unquenching effects are observed for both  $G_A$  and  $G_p$  when we compare to the 350 MeV pion mass hybrid lattices [11] confirming expectations for the importance of pion cloud effects at low  $Q^2$ . The pseudoscalar form factor  $G_{\pi NN}$  also increases less rapidly than the expected from the Goldberger-Treiman relation dipole form at low  $Q^2$ . This results to an underestimation of the strong coupling constant  $g_{\pi NN}$  as compared to experiment. We plan to further investigate the behavior of this quantity using different lattice discretization schemes for fermions in order to check lattice cut off effects while approaching lighter pion masses.

## Acknowledgments

I am indebted to C. Alexandrou, G. Koutsou, Th. Leontiou and J. W. Negele for the very enjoyable and fruitful collaboration on the topics covered in this talk. The authors of [14,15] are acknowledged for providing the unquenched configurations used in this work. I acknowledge support by the University of Cyprus and the program "Pythagoras" of the Greek Ministry of Education. Computer resources were provided by NERSC under contract No. DE-AC03-76SF00098.

## References

- [1] M. Jones, *et al.*, *Phys. Rev. Lett.* **84**, 1398 (2000); O. Gayou, *et al.*, *Phys. Rev.* **C64**, 038202 (2001); O. Gayou *et al.*, *Phys. Rev. Lett.* **88**, 092301 (2002).
- [2] M. Gockeler *et al.*, [QCDSF Collab.] *Phys. Rev.* **D71**, 034508 (2005).
- [3] T. R. Hemmert and W. Weise, *Eur. Phys. J.* **A15**, 487 (2002).
- [4] A. L. Ahrens *et al.*, *Phys. Lett.* **B202**, 284 (1988).
- [5] V. Bernard, N. Kaiser and U.-G. Meissner, *Phys. Rev. Lett.* **69**, 1877 (1992).
- [6] S. Choi *et al.*, *Phys. Rev. Lett.* **71**, 3927 (1993).
- [7] T. Goringe and H. W. Fearing, *Rev. Mod. Phys.* **76**, 31 (2004).
- [8] C. Alexandrou, G. Koutsou, J. W. Negele and A. Tsapalis, *Phys. Rev.* **D74** 034508 (2006); C. Alexandrou, hep-lat/0608025.
- [9] C. Alexandrou *et al.*, *Phys. Rev.* **D76** 094511 (2007) ; C. Alexandrou *et al.*, *PoS(LATTICE2007) 162*, 2007.
- [10] M. Gockeler *et al.*, [UKQCDSF Collab.] *PoS(LATTICE2007) 161*, 2007.
- [11] Ph. Hägler *et al.*, arXiv:0705.4295 ; D. Richards, arXiv: 0711.2048.
- [12] C. Alexandrou *et al.*, *Phys. Rev. Lett.* **94**, 021601 (2005) ; C. Alexandrou *et al.*, *Phys. Rev.* **D69**, 114506 (2004) ; C. Alexandrou *et al.*, arXiv: 0710.4621 (2007).
- [13] C. Alexandrou, Th. Leontiou, J. W. Negele and A. Tsapalis, *Phys. Rev. Lett.* **98**, 052003 (2006) ; C. Alexandrou, arXiv:0710.1202 (2007); C. Alexandrou *et al.*, *PoS(LAT2006) 115*, 2006.
- [14] B. Orth, Th. Lippert and K. Schilling [T $\chi$ L Collaboration], *Phys. Rev.* **D72**, 014503 (2005); Th. Lippert *et al.*, *Nucl. Phys. Proc. Suppl.***60A**, 311 (1998).
- [15] C.Urbach *et al.*, *Comput. Phys. Commun.* **174**, 87(2006).

# Participants

Patrick Achenbach	Johannes Gutenberg-Universität Mainz
Sergey Afonin	St. Petersburg State University
Miguel Albaladejo	Universidad de Murcia
Hamoud Alharbi	National Center for Mathematics and Physics at KACST
Mauro Anselmino	University and INFN, Torino
David Armstrong	College of William and Mary
Shahin Atashbar Tehrani	Persian Gulf University
Urnaa Badarch	University Giessen
Gunnar Bali	Universität Regensburg
Fouad Ballout	FZ Jülich
Luca Barion	FZ Jülich
Sergey Barsov	FZ Jülich
Vadim Baru	Institute for Theoretical and Experimental Physics, Moscow, Russia
Mikhail Bashkanov	Univ. Tübingen
Gerhard Baur	FZ Jülich
Silas Beane	University of New Hampshire
Ulf Bechstedt	FZ Jülich
Matthias Behler	Mainz University
Falco Beijer	Pfeiffer Vacuum GmbH
Himani Bhatt	Indian Institute of Technology, Bombay
Pedro Bicudo	IST, Lisboa
Ikaros Bigi	University of Notre Dame
Roelof Bijker	Instituto de Ciencias Nucleares
Johan Bijmens	Lund University, Lund, Sweden
Cesare Bini	Sapienza Università' di Roma and INFN Roma
Michael Birse	University of Manchester
Andrea Bizzeti	Università' di Modena e Reggio Emilia and INFN Sezione di Firenze
Jan Blomgren	Uppsala University, Dept of Neutron Research
Harald Bongen	FZ Jülich
Norbert Bongers	FZ Jülich
Bugra Borasoy	Bonn University
Ekaterina Borodina	FZ Jülich
Robert Bradford	University of Rochester
Ronald Brings	FZ Jülich
Kai Brinkmann	IKTP, TU Dresden
William Briscoe	The George Washington University
Markus Büscher	FZ Jülich
Maxim Bychkov	University of Virginia
Hans Calen	Uppsala University
Kavita Chandwani	Indian Institute of Technology Bombay
Wen-Chen Chang	Institute of Physics, Academia Sinica, Taiwan

David Chiladze	FZ Jülich
Rsulan Chistov	ITEP Moscow
Ales Cieply	Institute of Nuclear Physics, Rez near Pragü, Czechia
Heinz Clement	Univ. Tübingen
Tom Cohen	University of Maryland
Marialaura Colantoni	Universita' del Piemonte Orientale e INFN-Torino
Catalina Curceanu	Laboratori Nazionali di Frascati dell'INFN
Rafal Czyzykiewicz	Jagellonian University, Cracow and FZ Jülich
Rita De Masi	Institut de Physique Nucleaire Orsay
Jean-Pierre Didelez	Institut de Physique Nucleaire Orsay
Jürgen Dietrich	FZ Jülich
Michael Doering	University of Valencia
Heinz Dohmen	Oerlikon Leybold Vacuum GmbH
Frank Dohrmann	FZ Dresden-Rossendorf
Alessandro Drago	University of Ferrara
Michael Dugger	Arizona State University
Alexey Dzyuba	FZ Jülich
Bruno El-Bennich	LPNHE Univ. Pierre et Marie Curie, Paris
Sergey Eliseev	Laboratory of Theoretical Physics, R, Dubna
Ralf Engels	FZ Jülich
Evgeny Epelbaum	FZ Jülich and Bonn University
Franz-Josef Etzkorn	FZ Jülich
Riccardo Fabbri	DESY-ZEUTHEN
Amir Fariborz	SUNY Institute of Technology
Pavel Fedorets	ITEP Moscow
Olaf Felden	FZ Jülich
Robert Fersch	College of William and Mary
Detlef Filges	FZ Jülich
Christian Fischer	Institut für Kernphysik, TU Darmstadt
Klaus Foehl	University of Edinburgh
Antonio Fonseca	Centro Fisica Nuclear da Universidade Lisboa
Aida Galoyan	LPP JINR, Dubna
Gurjav Ganbold	JINR, Dubna and Institute of Physics and Technology, Ulaanbaatar
Haiyan Gao	Duke University and TUNL
Anders Gardestig	University of South Carolina
Archil Garishvili	FZ Jülich
Jürg Gasser	Univ. Bern
Werner Gast	FZ Jülich
Daniel Gazda	Institute of Nuclear Physics, Rez near Prague
Ralf Gebel	FZ Jülich
Albrecht Gillitzer	FZ Jülich
Derek Glazier	University of Edinburgh
Leonid Glozman	University of Graz

Alexander Glushkov	Odessa University
Frank Goldenbaum	FZ Jülich
Detlev Gotta	FZ Jülich
Harald Griebhammer	George Washington University
Kirill Grigoriev	FZ Jülich
Vera Grishina	FZ Jülich
Frank Grümmer	FZ Jülich
Peter Gründschloss	Calplus GmbH
Dieter Grzonka	FZ Jülich
Ali Murat Guler	Middle East Technical University
Helmut Haberzettl	George Washington University
Dietrich Habs	LMU Garching
Johann Haidenbauer	FZ Jülich
Rene Halver	FZ Jülich
Guido Hamacher	Pfeiffer Vacuum GmbH
Hans-Werner Hammer	Bonn University
Christoph Hanhart	FZ Jülich
Fred Harris	University Hawaii
Michael Hartmann	FZ Jülich
Hassan Hassanabadi	Shahrood University of Technology
Martin Hausner	FZ Jülich
Jun He	CEA-Saclay
Volker Hejny	FZ Jülich
Thomas Hemmert	Physik Dep. T39, TU München
Kurt Henn	FZ Jülich
Frank Hinterberger	Bonn University
Aye Thandar Htay	FZ Jülich
Jie Hu	Duke University
Fei Huang	China Center of Advanced Science and Technology
Fabian Hüggling	FZ Jülich
Tetsuo Hyodo	Yukawa Institute for Theoretical Physics, Kyoto
Yoichi Ikeda	Department of Physics, Osaka University
Takashi Inoue	Dept. Phys. Sophia University, Tokyo
Tomoichi Ishiwatari	Stefan Meyer Institut für subatomare Physik, Wien
Sergiy Ivashyn	National Science Center, Kharkov
Herbert Jäger	FZ Jülich
Marco Jagodzinska	FZ Jülich
Brajesh K. Jain	Mumbai University
Harald Janssen	Calplus GmbH
Michal Janusz	FZ Jülich and Jagiellonian University, Krakow
Benedykt R. Jany	FZ Jülich and Nuclear Physics Department, Jagiellonian University, Krakow
Vishwajeet Jha	Nuclear Physics Division, BARC, Mumbai
Bruno Julia-Diaz	University of Barcelona

Stefan Jurk	iseg Spezialelektronik GmbH
Andro Kacharava	Erlangen University
Mardy Karnadi	FZ Jülich
Irakli Keshelashvili	FZ Jülich
Olena Khakimova	Univ. Tübingen
Dimitry Khaneft	FZ Jülich
Olga Khetselius	Nucl.Spectr.Lab., Odessa University
Alfons Khoukaz	IKP, Universität Münster
Anatoly Khrykin	JINR, Dubna
Kurt Kilian	FZ Jülich
Daniil Kirillov	FZ Jülich
Matthias Kirsch	Struck Innovative Systeme GmbH
Daniela Kiselev	Paul Scherrer Institut
Stanislaw Kistryn	Jagiellonian University, Krakow
Pawel Klaja	FZ Jülich
Vera Kleber	Bonn University
Eberhard Klempt	Bonn University
Rüdiger Koch	FZ Jülich
Stefan Kölling	FZ Jülich
Evgeni Kolomeitsev	GSI Darmstadt
Polina Kravchenko	PNPI, S.Petersburg
Gastao Krein	Instituto de Fisica Teorica
Siegfried Krewald	FZ Jülich
Bernd Krusche	Basel University
Bastian Kubis	HISKP (Theorie), Bonn University
Eberhard Kuhlmann	Institut für Kern- und Teilchenphysik, TU Dresden
Roland Kuhn	Technische Universität München, Physik Department
Pawel Kulesa	FZ Jülich and Institute of Nuclear Physics Cracow
Viacheslav Kulikov	ITEP, Moscow
Andrzej Kupsc	Department of Nuclear And Particle Physics, Uppsala University
Alexander Kvinikhidze	Razmadze Mathematical Institute, Tbilisi
Valentyn Kyryanchuk	FZ Jülich
Timo Lahde	Department of Physics, University of Washington, Seattle, WA
Jens Soeren Lange	Universität Giessen
Inti Lehmann	University of Glasgow
Andreas Lehrach	FZ Jülich
Paolo Lenisa	Universita' di Ferrara and INFN - Ferrara
Horst Lenske	U. Giessen
Vadim Lensky	FZ Jülich
Vladimir Leontyev	FZ Jülich
Felipe Llanes Estrada	Depto. Fisica Teorica I, Universidad Complutense Madrid
Markus Lochno	Tektronix GmbH
Bernd Lorentz	FZ Jülich

Alfredo Luccio	Brookhaven National Laboratory
Matthias F.M. Lutz	GSI Darmstadt
Valery Lyubovitskij	Institute of Theoretical Physics, University of Tübingen
Nikolay Lyutorovich	St. Petersburg State University
Frank Maas	CNRS/IN2P3/Institut de Physique Nucleaire Orsay
Alexander Machavariani	JINR Dubna and HEPI Tbilisi
Hartmut Machner	FZ Jülich
Andrzej Magiera	Institute of Physics, Jagiellonian University
Rudolf Maier	FZ Jülich
Alberto Martinez Torres	IFIC-Universidad de Valencia
Sergio Mauro	WIENER, Plein & Baus GmbH
Judith McGovern	University of Manchester
Bryan McKinnon	University of Glasgow
Craig McNeile	University of Glasgow
Ulf-G. Meißner	FZ Jülich and Bonn University
Wally Melnitchouk	Jefferson Lab
Marius Mertens	FZ Jülich
Johan Messchendorp	KVI/RuG, Groningen
Pekko Metsae	University of Helsinki
Bernard Metsch	Bonn University
Malte Mielke	IKP, Universität Münster
Maxim Mikirtychyants	Petersburg Nuclear Physics Institute and FZ Jülich
David Minossi	FZ Jülich
Hans-Peter Morsch	Soltan Institute for Nuclear Studies, Warsaw
Ulrich Mosel	University of Giessen
Pawel Moskal	Jagellonian University and FZ Jülich
Fred Myhrer	University of South Carolina
Satoshi Nakamura	TRIUMF
Takashi Nakano	RCNP, Osaka University
Kanzo Nakayama	University of Georgia
Mariana Novoa	University of Giessen
Alexey Nefediev	ITEP Moscow
Ben Nefkens	University California Los Angeles
Mikhail Nekipelov	FZ Jülich
Dominik Nickel	Technische Universität Darmstadt
Nikolai Nikolaev	L.D.Landau Institute for Theoretical Physics and FZ Jülich
Victor Nikonov	HISKP Bonn, PNPI Gatchina
Mikheil Niroadze	High Energy Physics Institute of Tbilisi State University
Tetsuo Nishikawa	Tokyo Institute of Technology
Jouni Niskanen	University of Helsinki
Andreas Nogga	FZ Jülich
Walter Oelert	FZ Jülich
Dieter Oellers	FZ Jülich

Henner Ohm	FZ Jülich
Hiroaki Ohnishi	RIKEN
Vitaly Okorokov	MEPhI - Moscow Engineering Physics Institute
Jose A. Oller	Universidad de Murcia
Eulogio Oset	University of Valencia
Simone Pacetti	LNF-INFN Frascati and CSR Enrico Fermi, Roma
Michael Papenbrock	IKP, Universität Münster
Mark W. Paris	EBAC @ Jefferson Lab
Vladimir Pascalutsa	ECT* Trento
Christian Pauly	FZ Jülich
Fedor Pavlov	FZ Jülich
Jose R. Pelaez	University Complutense de Madrid
Mario Pelliccioni	Universita' degli Studi di Torino, INFN
Michael Pennington	IPPP, Durham University
Henrik Pettersson	IKP, Uppsala University
Daniel Phillips	Ohio University
Jerzy Pietraszko	GSI Darmstadt
Stephane Platchkov	CEA Saclay
Henk Polinder	FZ Jülich
Maxim Polyakov	Ruhr-University Bochum
Sergey Prakhov	University California Los Angeles
Dieter Prasuhn	FZ Jülich
Elisabetta Prencipe	University of Ferrara and INFN
Annette Pricking	Univ. Tübingen
Joanna Przerwa	FZ Jülich
Piotr Raczka	University of Warsaw
Ali A. Rajabi	Shahrood University of Technology
Frank Rathmann	FZ Jülich
Christoph Redmer	FZ Jülich
David Richards	Jefferson Laboratory
James Ritman	FZ Jülich
Craig Roberts	Argonne National Laboratory
Eduard Roderburg	FZ Jülich
David Rodriguez Entem	University of Salamanca and IUFFyM
Günther Rosner	University of Glasgow
Anatoli Rouba	Research Institute for Nuclear Problems, Minsk
Ankhi Roy	IIT Bombay
Enriqü Ruiz Arriola	Universidad de Granada
Akaki Rusetsky	HISKP, Bonn University
Michael Sadler	Abilene Christian University
Mikko Sainio	Helsinki Institute of Physics
Naohito Saito	KEK
Elena Santopinto	INFN

Andrei Sarantsev	Bonn University
Pavel Saviankou	FZ Jülich
Susan Schadmand	FZ Jülich
Andreas Schäfer	University of Regensburg
Wo. Schäfer	FZ Jülich
D. Schoenfelder	FZ Jülich
Joseph Schechter	Physics Department, Syracuse University
Ralf Schleichert	FZ Jülich
Herbert Schneider	FZ Jülich
Karin Schoenning	Uppsala University
Wolfgang Schroeder	FZ Jülich and Erlangen University
Otto Schult	FZ Jülich
Martin Schulte-Wissermann	TU Dresden
Thomas Sefzick	FZ Jülich
Kimiko Sekiguchi	RIKEN
Marc Sellschopp	Pfeiffer Vacuum GmbH
Kirill Semenov-Tian-Shansky	Ruhr Universität Bochum and St. Petersburg State University
Valeriy Serdyuk	FZ Jülich
Hellmut Seyfarth	FZ Jülich
Neha Shah	Indian Institute of Technology Bombay
Kiyotaka Shimizu	Department of Physics, Sophia University
Vitaly Shklyar	Inst. für Theor. Physik I, Universität Giessen
Mohammad R. S. K. Sofla	Shahrood University of Technology
Alexander Sibirtsev	HISKP, Universität Bonn
Regina Siudak	Institute of Nuclear Physics, Cracow,
Tatiana Skorodko	Uni. Tübingen
Tytus Smolinski	FZ Jülich and Jagiellonian University, Cracow
Andrey Sokolov	FZ Jülich
Josef Speth	FZ Jülich
Dirk Spoelgen	FZ Jülich
Roxanne Springer	Duke University
Jugoslav Stahov	University of Tuzla
Florica Stancu	University of Liege
Aleksandr Starostin	University of California Los Angeles
Rolf Stassen	FZ Jülich
Hans-Joachim Stein	FZ Jülich
Joanna Stepaniak	Institute for Nuclear Studies, Warsaw
Günter Sterzenbach	FZ Jülich
Hans Stockhorst	FZ Jülich
Tobias Stockmanns	FZ Jülich
Igor Strakovsky	The George Washington University
Thomas Strauch	FZ Jülich
Hans Stroehrer	FZ Jülich

Viktorin Sumachev	Petersburg Nuclear Physics Institute
Mizuki Sumihama	Osaka University RCNP
Yury Surovtsev	Bogoliubov Laboratory of Theoretical Physics, JINR, Dubna
Nobuhiko Suzuki	Department of Physics, Osaka University
Takatoshi Suzuki	RIKEN
Alfred Svarc	Rudjer Boskovic Institute
Antoni Szczurek	Institute of Physics and University of Rzeszow
Berhan Taddesse	Jacobs University Bremen
Fatemeh Taghavi Shahri	IUST
Toru Takahashi	Yukawa Institute for Theoretical Physics, Kyoto University
Sachiko Takeuchi	Japan College of Social Work
Makoto Takizawa	Showa Pharmaceutical University
Setsuo Tamenaga	RCNP, Osaka University
Ulrike Thoma	Bonn University
Anthony Thomas	Jefferson Lab
Raimund Tölle	FZ Jülich
Walter Toki	Colorado State University
Tamer Tolba	FZ Jülich
Laura Tolos	FIAS. University of Frankfurt
Sergey Trusov	FZ Jülich
Antonios Tsapalis	University of Athens
Kay Ulbrich	Bonn University
Wolfgang Ullrich	TU Dresden
Maurizio Ungaro	Jefferson Lab
Yury Valdau	FZ Jülich
Eef van Beveren	Coimbra University
Brandon Van der Ventel	Stellenbosch University
David van Niekerk	Stellenbosch University
Willem van Oers	University of Manitoba, Winnipeg
Galina Vankova-Kirilova	Sofia University
Tsvetanova Raghava Varma	Indian Institute of Technology Bombay
Peter Vlasov	FZ Jülich
Mikhail Voloshin	FTPI, University of Minnesota
Michael von Düring	CAEN GmbH
Fan Wang	Nanjing University
Rainer Wanke	Mainz University
Wojciech Węglorz	FZ Jülich
Christian Weidemann	FZ Jülich
Herbert Weigel	Fachbereich Physik, Siegen University
Dominic Welsch	FZ Jülich
Eberhard Widmann	Stefan Meyer Institute for Subatomic Physics, Vienna
Uwe-Jens Wiese	Institute for Theoretical Physics, Bern University
Alexander Winnemöller	IKP, Universität Münster

Peter Wintz	FZ Jülich
Andreas Wirzba	FZ Jülich
Magnus Wolke	FZ Jülich
Aleksandra Wronska	Jagiellonian University, Cracow
Xiaohua Yuan	FZ Jülich
Leonid Yurev	FZ Jülich
Zhongdong Zhang	FZ Jülich
Qiang Zhao	IHEP Beijing
Veronique Ziegler	SLAC
Bing-song Zou	IHEP Beijing
Pawel Zupranski	The Andrzej Soltan Institute for Nuclear Studies
Izabella Zychor	IPJ Swierk



# Program

<b>Registration</b>		
<i>Plenary Session Monday, Sep. 10, 2007 9:00 - 12:30</i>		
<i>chair: S. Krewald</i>		
Welcome ( <i>H. Machner</i> )		
Welcome to the Research Center ( <i>U. Samm</i> )		
W. van Oers	Department of Physics and Astronomy University of Manitoba	Opening Remarks (IUPAP)
J. Gasser	Univ. Bern, Switzerland	Chiral Effective Field Theory
C. Curceanu	Laboratori Nazionali di Frascati dell'INFN	Kaonic Atoms Experimental Studies at DAPHNE
<i>chair: J. Ritman</i>		
R. Wanke	Mainz University	Wigner-Cusp in Kaon Decays and Determination of $\pi\pi$ Scattering Lengths
J. Bijnens	Lund University, Lund, Sweden	Eta and Eta' Physics
M. Wolke	FZ Juelich	Eta Meson Decays with WASA-at-COSY
<i>Parallel Sessions 1-5 - Monday, Sep. 10, 2007 14:30 - 16:10</i>		
<i>Session 1: <math>\pi N</math> Interaction I</i>		
<i>chair: B. Nefkens</i>		
T. D. Cohen	University of Maryland	Interplay of the Chiral and Large $N(c)$ Limits in $\pi N$ Scattering
T. Inoue	Dept. Phys. Sophia University, Tokyo	Pion-Nucleon $P_{33}$ and $P_{11}$ Scatterings in the Lippmann-Schwinger Approach
P. Metsd	University of Helsinki	Pion-Nucleon Partial Wave Analysis with Fixed- $t$ Analyticity Constraints
M.E. Sainio	Helsinki Institute of Physics	The GMO Sum Rule Revisited
J. He	CEA-Saclay	$\pi N$ to $\eta N$ Process in a Chiral Quark Model Approach
<i>Session 2 : Scalar Mesons I</i>		
<i>chair: E. van Beveren</i>		
J.R. Pelaez	University Complutense de Madrid	Scalar Mesons from Unitarized Chiral Perturbation Theory
J. Oller	Universidad de Murcia	Topics on Scalar Meson Dynamics
M. Bashkanov	Univ. Tuebingen	$\sigma$ -Channel Low-Mass Enhancement in Double-Pionic Fusion
A.V. Nefediev	ITEP	The Nature of the Light Scalar Mesons from their Radiative Decays
A. Fariborz	SUNY Institute of Technology	Scalar Mesons: A Chiral Lagrangian Study of their Mixing and Substructure

<i>Session 3: Meson Production I</i>		<i>chair: W. Briscoe</i>
K. Nakayama	University of Georgia	Meson Production in NN Collisions
H. Haberzettl	George Washington University	Photoproduction of Pseudoscalar Mesons
A. Dzyuba	FZ Juelich	Kaon-Pair Production in Hadron-Induced Reactions at ANKE
W.-C. Chang	Institute of Physics, Academia Sinica, Taiwan	Explore Pomeron Trajectory at Low Energies - Measurement of $\phi$ -Meson Photoproduction from Protons and Deuterons Near Threshold by LEPS/SPring-8 Experiment
<i>Session 4: Baryon Spectroscopy I</i>		<i>chair: E. Oset</i>
M. Doering	University of Valencia	The Nature of the $N^*(1535)$
T. Skorodko	Uni. Tuebingen	Excitation of the Roper Resonance in Single and Double-Pion Production
I. Zychor	IPJ Swierk	Studies of $\Lambda(1405)$ in pp Collisions with ANKE at COSY-Juelich
S. Takeuchi	Japan College of Social Work	$\Lambda(1405)$ as a Resonance in the Baryon-Meson Scattering Coupled to the $q^3$ State in a Quark Model
<i>Session 5: Electron Scattering</i>		<i>chair: A. Szczurek</i>
I. Lehmann	University of Glasgow	HERMES Results on Hard-Exclusive Processes
R. De Masi	IPN Orsay	Generalized parton distributions and deeply virtual Compton scattering at CLAS
W. Melnitchouk	Jefferson Lab	Quark Hadron Duality in Electron Scattering
P. Kravchenko	PNPI, S.Petersburg	Latest HERMES Results on Quark Helicity Distribution from Semi-Inclusive Deep-Inelastic Scattering
<i>Parallel Sessions 6-10 - Monday, Sep. 10, 2007 16:50 - 18:30</i>		
<i>Session 6: <math>\pi N</math> Interaction II</i>		<i>chair: H. Lenske</i>
A.Kudryavtsev (V. Baru)	Institute for Theoretical and Experimental Physics, Moscow, Russia	Pion-Deuteron Scattering Length in Chiral Perturbation Theory up to Order $\chi^3/2$
J. Stahov	University of Tuzla	Evaluation of the $\pi N$ sigma Term Using Dispersion Relations - Present Status
T. Strauch	FZ Juelich	Pionic Deuterium

V. Sumachev	Petersburg Nuclear Physics Institute	Parameters A and R Measurements in the Resonance Region of the Pion-Nucleon Elastic Scattering: Recent Results and Subsequent Investigations
K. Semenov	Ruhr Universitaet Bochum, St. Petersburg State University	Bootstrap for Physical Values of $\pi$ N Resonance Parameters
<b>Poster Session</b>		
<b>Session 7: Scalar Mesons II</b>		<i>chair: G. Krein</i>
E. van Beveren	Coimbra University	How We Discovered the Nonet of Light Scalar Mesons
S.A. Ivashyn	National Science Center "Kharkov Institute for Physics and Technology", Institute for Theoretical Physics, Ukraine	Light Scalar Meson Decays and Mixing in ChPT
M. Albaladejo	Universidad de Murcia	S-Wave Meson Scattering in Unitary Chiral Perturbation Theory
Yu.S. Surovtsev	Bogoliubov Laboratory of Theoretical Physics, Joint Institute for Nuclear Research	On the Nature of the $f_0$ - and $f_2$ -Mesons
X. Yuan	FZ Juelich	Measurement of the reaction $dd \rightarrow \alpha K^+ K^-$ with ANKE/COSY
<b>Poster Session</b>		
<b>Session 8: Meson Decays</b>		<i>chair: F. Harris</i>
B. Borasoy	Bonn University	Decays of Eta and Eta' Mesons
A. Kupsc	Department of Nuclear And Particle Physics, Uppsala University	Multiple Meson Production in pp Interactions as a Background for eta and eta' Decay Studies
A. Bizzeti	Universita' di Modena e Reggio Emilia and INFN Sezione di Firenze	Highlights on Radiative Kaon and Hyperon Decays from NA48/2
S. Prakhov	University California Los Angeles	New Results on Measurement of Rare Decay $\eta \rightarrow \pi^0 \gamma \gamma$
A. Roy	IIT Bombay	Branching Ratio for $\eta \rightarrow \pi^0 \gamma \gamma$ with CBELSA/TAPS
<b>Poster Session</b>		
<b>Session 9: Symmetries</b>		<i>chair: W. van Oers</i>
A. Magiera	Institute of Physics, Jagiellonian University	Studies of Charge Symmetry Breaking Reactions at COSY
B. Kubis	Helmholtz-Institut fuer Strahlen- und Kernphysik (Theorie), Universitaet Bonn	Isospin Violating Nucleon Form Factors

D.S. Armstrong	College of William and Mary	Strangeness Content of the Nucleon via Parity Violating Asymmetries in Polarized Electron Scattering
F. Maas	CNRS/IN2P3/IPN Orsay	Parity Violating Electron Scattering: The Role of Strange Quarks at Small Momentum Transfer
M. Behler	Mainz University	Symmetry Tests in NA48 with Kaons
<b>Poster Session</b>		
<b>Session 10: Instrumentation</b>		<i>chair: J. Niskanen</i>
K. Foehl	University of Edinburgh	The PANDA Detector at FAIR
A. Wronska	Jagiellonian University, Cracow	Simulation of the PANDA Experiment with PandaRoot
R. Schleichert	FZ Juelich	Silicon Detectors for Internal Target Experiments
L. Barion	University of Ferrara and INFN / FZ Juelich	The PAX Experiment at FAIR
A. Lehrach	FZ Juelich	High-Energy Storage Ring (HESR)
<b>Poster Session</b>		
Welcome Dinner Seekasino		
<b>Plenary Session Tuesday, Sep. 11, 2007 8:30 - 12:30</b>		
<i>chair: A. Schaefer</i>		
C. Bini	Sapienza Universita' di Roma and INFN Roma	KLOE Results on Hadron Physics
M.R. Pennington	IPPP, Durham University	Structure of Light Scalar Mesons
J. Schechter	Physics Department, Syracuse University	Scalar Mesons from an Effective Lagrangian Approach
K.-T. Brinkmann	IKTP, TU Dresden	Physics Program at COSY
<i>chair: H. Gao</i>		
S. Beane	University of New Hampshire	Hadron, Hadron-Hadron and Hadron-Hadron Properties from Lattice QCD
U.-J. Wiese	Institute for Theoretical Physics, Bern University	Chiral Symmetry on the Lattice
A. Schaefer	University of Regensburg	Hadron Structure from Lattice QCD
<b>Parallel Sessions 11-15 - Tuesday, Sep. 11, 2007 14:30 - 16:10</b>		
<b>Session 11: Spin Physics</b>		<i>chair: W. Melnitchouk</i>
R. Fersch	College of William and Mary	Spin Physics with CLAS
St. Platchkov	CEA Saclay	The COMPASS Experiment at CERN: New Results and Forthcoming Studies
A. Fabbri	DESY-ZEUTHEN	Latest HERMES Results on Transverse Spin in Hadron Structure and Formation

F. Rathmann (A. Kacharava)	Erlangen University	Spin Physics from COSY to FAIR
A. Drago	University of Ferrara	Spin Physics with Antiprotons
<i>Session 12: Scalar Mesons III</i>		<i>chair: J. Schechter</i>
T. Lahde	Department of Physics, University of Washington, Seattle, WA	Scalar Pion Form Factor from J/psi Decays
D. Rodriguez Entem	University of Salamanca and IUFFyM	Chiral Symmetry Restoration in Excited Mesons
G. Ganbold	Joint Institute for Nuclear Research, Dubna and Institute of Physics and Technology, Ulaanbaatar	Mesons and Glueballs: A Quantum Field Approach
A. Khrykin	JINR	On a Possible Origin of a Resonance-Like Structure in the Two-Photon Invariant Mass Spectrum of the Reaction $pp \rightarrow pp \gamma \gamma$
<i>Session 13: Meson Production II</i>		<i>chair: H. Clement</i>
J. Pietraszko (I. Froehlich)	GSI Darmstadt	PP Collisions with HADES
W. Ullrich	TU Dresden	Reaction Dynamics of omega Meson Production in $\vec{p}p$ Collisions
K. Schoenning	Uppsala University, Sweden	Production of omega in $pd$ to $3He$ omega with CELSIUS/WASA
O. Khakimova	Univ. Tuebingen	Measurement of the ABC-Effect in the Most Basic Double-Pionic Fusion Process
G. Vankova	University of Sofia	Study of eta-Meson Production in the $\vec{d}d$ to $\alpha$ eta Reaction
<i>Session 14: Baryon Spectroscopy II</i>		<i>chair: B. Metsch</i>
B. McKinnon	University of Glasgow	Baryon Spectroscopy at CLAS (Pentaquark Review)
M. Nanova	University of Giessen	$\gamma p \rightarrow p \pi^0 \eta$ and Related Reactions Studied with CBELSA/TAPS
V. Shklyar	Inst. fuer Theor. Physik I, Universitaet Giessen	eta-Photoproduction on the Nucleon in the Resonance Energy Region
D.I. Glazier	University of Edinburgh	Recoil Polarisation Observables in pion and eta Photoproduction with the CB@MAMI

H. Hassanabadi	Shahrood University of Technology	Determination of the potential coefficients of the Baryons & the effect of spin & isospin potential on their energy
<i>Session 15: Hadrons in Medium I</i> <i>Magiera</i>		<i>chair: A.</i>
B.K. Jain	Mumbai University	Study of the p 6Li to eta 7Be reaction
V. Jha	Nuclear Physics Division, BARC, Mumbai	Search for eta-Nucleus Bound States
M. Papenbrock	IKP, Universitaet Muenster	Investigation of the dp to 3HeX (X=eta,pi0,pipi) Reactions at ANKE
A. Galoyan	LPP JINR	Monte Carlo Simulation of Meson-Nucleon and Meson-Nucleus Interactions at High Energies
<i>Parallel Sessions 16-20 - Tuesday, Sep. 11, 2007 16:50 - 18:30</i>		
<i>Session 16: KN Interaction</i>		<i>chair: A. Gardestig</i>
A. Rusetsky	HISKP, University of Bonn	Kaon-Nucleon Scattering Lengths from Experiment on Kaonic Deuterium
F. Huang	China Center of Advanced Science and Technology	Kaon Nucleon and Anti-Kaon Nucleon Interactions in a Chiral Constituent Quark Model
A. Cieply	Institute of Nuclear Physics, Rez near Prague, Czechia	Multichannel Chiral Approach for Kaonic Hydrogen
T. Ishiwatari	Stefan Meyer Institut fuer subatomare Physik	Precise Determination of Kaonic 4He X-ray Energy
<i>Session 17: Meson Production III</i>		<i>chair: H. Haberzettl</i>
M. Dugger	Arizona State University	Photoproduction of Eta and Eta' Mesons from the Proton
P. Klaja	FZ Juelich	Comparative Study of proton-eta and proton-eta' Interaction via pp and p-meson Invariant Mass Distributions
J. Przerwa	FZ Juelich	Isospin Dependence of the Eta' Meson Production in Nucleon-Nucleon Collisions
H. Pettersson	IKP, Uppsala University	High Statistics Measurements of eta-Production in Proton-Proton Collisions
C. Pauly	FZ Juelich	3pi0 Final States with WASA at CELSIUS and COSY
<i>Session 18: High Energy Processes I</i>		<i>chair: A. Drago</i>
R. Bijker	Instituto de Ciencias Nucleares	The Gottfried Sum Rule in an Unquenched Quark Model

Ch. Fischer	Institut fuer Kernphysik, TU Darmstadt	Meson Properties from Non-perturbative Quark-Gluon Dynamics
R. Kuhn	Technische Universitaet Muenchen, Department Physik	Measurements of the Gluon Polarization in the Nucleon
P. Fedorets	ITEP Moscow	A Frozen Pellet Target for PANDA
<i>Session 19: Heavy Mesons I</i>		<i>chair: H.-W. Hammer</i>
R.P. Springer	Duke University	Positive and Negative Parity Charmed Mesons in Heavy Quark Effective Field Theory
F.A. Harris	University Hawaii	Recent BES Results and the BESIII Upgrade
B. El-Bennich	LPNHE Univ. Pierre et Marie Curie, Paris	B Meson Decays into Pion Pion and Kaon: CP Violation and Pseudoscalar Meson Interactions
G. Krein	Instituto de Fisica Teorica	Dbar -Nucleon Interaction from Meson-Exchange and Quark-Gluon Dynamics
<i>Session 20: Baryon Spectroscopy III</i>		<i>chair: F. Stancu</i>
L.Ya.Glozman	University of Graz	QCD Symmetries in Excited Hadrons
M. Sumihama	Osaka University, RCNP	K+ Photoproduction by Linearly Polarized Photons at SPring-8/LEPS
R. Bradford	University of Rochester	Studies of Kaon Photoproduction from the Proton Using CLAS at Jefferson Lab
T. Hyodo	Yukawa Institute for Theoretical Physics, Kyoto	Exotic Hadrons in s-Wave Chiral Dynamics
A. Martinez Torres	IFIC-Universidad de Valencia	Dynamically Generated Resonances in the Two Mesons - One Baryon Systems
<i>Plenary Session Wednesday, Sep. 12, 2007 8:30 - 12:30</i>		
<i>chair: H. Stroeher</i>		
M. Lutz	GSI Darmstadt	Structure of Baryons
P. Achenbach	Institut fuer Kernphysik, Johannes Gutenberg-Universitaet Mainz	Physics Program at MAMI-C
U. Thoma	Bonn University	Baryon Spectroscopy - Recent results from the Crystal Barrel Experiment at ELSA -
B.S. Zou	IHEP Beijing	Baryon Resonances Observed at BES
<i>chair: J. Gasser</i>		
T. Nakano	RCNP, Osaka University	Evidence for Theta+ Photo-Production at LEPS

A. Starostin	University of California Los Angeles	Baryon Spectroscopy with Inelastic Channels: Crystal Ball Experience
H. Gao	Duke University and TUNL	Scaling in Charged Pion Photoproduction From Nucleon
<i>Parallel Sessions 21-25 - Wednesday, Sep. 12, 2007 14:30 - 16:10</i>		
<i>Session 21: Exotics</i>		<i>chair: R. Bijker</i>
E. Santopinto	INFN	Tetraquark Spectroscopy
F. Wang	Nanjing University	Systematic Study of Multi Quark States
H. Weigel	Fachbereich Physik, Siegen University	Soliton Model Approach to Kaon Nucleon Scattering in the Pentaquark Channel
Y. Azimov	Petersburg Nucl. Phys. Inst.	How Is Exotics Produced? Where to Search for It?
F. Taghavi Shahri	IUST	The Rule of Orbital Angular Momentum and Polarized Valon Model
<i>Session 22: NN Interaction</i>		<i>chair: J.-P. Didelez</i>
E. Ruiz Arriola	Universidad de Granada	Renormalizing the Schroedinger Equation for NN Scattering
A.E. Gardestig	University of South Carolina	Extraction of the neutron-neutron scattering length from $\pi^-d \rightarrow nn\gamma$ using $\chi$ PT
V. Lensky	FZ Juelich	Neutron-neutron scattering length from the reaction $\gamma d \rightarrow \pi^+ nn$
D. Chiladze	FZ Juelich	np-Amplitude Studies at ANKE
S. Kvinikhidze	Razmadze Mathematical Institute, Tbilisi	A Possible Renormalization Group Approach to Nuclear Current Operators
<i>Session 23: Baryon Spectroscopy IV</i>		<i>chair: U. Thoma</i>
B. Metsch	Bonn University	The Relativistic Quark Model
F. Stancu	University of Liege	Quark Models: Recent Results
A. Svarc	Rudjer Bojskovic Institute	On Ambiguities and Uncertainties in PWA
A. Sibirtsev	HISKP, Universitaet Bonn	High Mass Baryons in Single Pion Photoproduction
N. Suzuki	Department of Physics, Osaka University	Resonance Pole by Speed Plot and Time Delay
<i>Session 24: Hadrons in Medium II</i>		<i>chair: B.K. Jain</i>
E. Oset	University of Valencia	Photoproduction of Omega and Omega in the Nuclear Medium
F. Dohrmann	FZ Dresden-Rossendorf	Inclusive dielectron production in C+C collisions with HADES

S. Eliseev	Bogoliubov Laboratory of Theoretical Physics, Joint Institute for Nuclear Research, Dubna	In Pursuit of New Physics with $K^+$ Scattering on Nuclei at Intermediate Energy
D. Gazda	Institute of Nuclear Physics, Rez near Prague	Dynamics of $K$ bar Nuclear States
<b>Session 25: Meson Production IV</b>		<i>chair: M. Sadler</i>
V. Baru	<i>Institute for Theoretical and Experimental Physics, Moscow, Russia</i>	<i>Progress in <math>NN \rightarrow NN \pi</math></i>
F. Myhrer	<i>University of South Carolina</i>	<i>Two Pion Exchange Effects in <math>pp</math> to <math>pp \pi^0</math></i>
A. Machavariani	<i>JINR Dubna, HEPI Tbilisi</i>	<i>Screening in the Bremsstrahlung Reactions and Magnetic Moment of the Delta Resonance</i>
D.G. Richards	<i>Jefferson Laboratory</i>	<i>Excited States of Charmonium from Lattice QCD</i>
<b>Guided Tour COSY</b>		
<b>Guided Tour Aachen</b>		
<b>Plenary Session Thursday, Sep. 13, 2007 8:30 - 12:30</b>		
<i>chair: B.S. Zou</i>		
M.B. Voloshin	FTPI, University of Minnesota	Decay of Open Charm Hadrons
R. Chistov	ITEP Moscow	Charmed Hadrons from B-Decay
W. Toki	Colorado State University	Hadronic B-Decays
I. Bigi	University of Notre Dame	On the Brink of Major Discoveries in Weak Charm Decays - a Bismarckian Chance to Make History
<i>chair: T. Nakano</i>		
S. Kistryn	Jagiellonian University, Krakow	Three-Nucleon System Dynamics Studied via d-p Breakup
K. Sekiguchi	RIKEN	Three Nucleon Scattering Experiments from RIKEN
D.R. Phillips	Ohio University	Chiral Effective Theory Calculations of Electron and Photon Scattering from Light Nuclei
<b>Parallel Sessions 26-30 - Thursday, Sep. 13, 2007 14:30 - 16:10</b>		
<b>Session 26: Strange Few Nucleon Systems</b>		<i>chair: E. Widmann</i>
H. Ohnishi	RIKEN	Search for Deeply Bound Kaonic State
P. Bicudo	IST, Lisboa	The Hexaquark-Flavoured AntiK-N-N state Computed Microscopically with a Clusterized Octoquark

Y. Ikeda	Department of Physics, Osaka University	Three-Body Resonance Pole of Strange Dibaryon in the $K\bar{N}N - \pi YN$ Coupled System
T. Suzuki	RIKEN	An Experimental Search for Strange Multi-Baryonic Systems in $^4\text{He}(\text{stopped } K^-, YN)$ Reaction
T. Nishikawa	Tokyo Institute of Technology	Bound Kaon Approach for the $ppK^+$ System in the Skyrme Model
<i>Session 27: Few Body I</i>		<i>chair: H. Griesshammer</i>
J. Blomgren	Uppsala University, Dept of Neutron Research	Three Body Force Effects in Neutron-Deuteron Scattering at 95 MeV
E. Epelbaum	FZ Juelich, Universitaet Bonn	Delta-Resonance Contributions to the Nuclear Force
A. Fonseca	Centro Fmsica Nuclear da Universidade Lisboa	Coulomb Effects in Few Nucleon Systems <a href="#">abstract</a> <a href="#">talk</a>
D. Kiselev	Paul Scherrer Institut	Vector and Tensor Analyzing Power of the $H(\vec{d}, \gamma)^3\text{He}$ Capture Reaction
S. Nakamura	TRIUMF	Bridging over $\pi$ -Production and Weak Processes in Few-Nucleon Systems with Chiral Perturbation Theory
<i>Session 28: Form Factors</i>		<i>chair: C. Roberts</i>
V. Pascalutsa	ECT* Trento, Italy	Delta-N Transition Form Factors
F.J. Llanes Estrada	Depto. Fisica Teorica I, Universidad Complutense Madrid	The $1/x$ Form Factor of the Nucleon
M. Ungaro	Jefferson Lab	Baryon Resonance Form Factor at CLAS
M. Colantoni	Universita' del Piemonte Orientale e INFN-Torino	First Results on Pion Polarizabilities @ COMPASS
M. Bychkov	University of Virginia	High Precision Measurement of the Pion Form Factors via Radiative Pion Decay $\pi \rightarrow e \nu \gamma$
<i>Session 29: Baryon Spectroscopy V</i> <i>Shimizu</i>		<i>chair: K.</i>
I. Strakovsky	The George Washington University	Partial-Wave Analysis and Spectroscopy. From Pion-Nucleon Scattering to Pion Electroproduction up to $W = 2.5$ GeV

B. Julia-Diaz	University of Barcelona	Dynamical Coupled-Channel Model Analysis of pi-N Scattering and Electromagnetic Pion Production Reactions
V. Nikonov	HISKP Bonn, PNPI Gatchina	First Results from Analysis of pp->p K Lambda Reaction
M. Paris	EBAC @ Jefferson Lab	Dynamical Coupled-Channel Approach to omega-Meson Production with Pions and Photons
E. Prencipe	University of Ferrara and INFN	Charm and Charmonium Spectroscopy at BaBar
<i>Session 30: Hadrons in Medium III</i>		<i>chair: F. Myhrer</i>
A.M. Gueler	Middle East Technical University	Measurement of Charged-Particle Multiplets in (Anti-)Neutrino-Nucleus Interactions
D.D. van Niekerk	Stellenbosch University	Neutrino-induced Kaon Production
<i>Parallel Sessions 31-35 - Thursday, Sep. 13, 2007 16:50 - 18:30</i>		
<i>Session 31: Lattice Calculations</i>		<i>chair: R. Springer</i>
C. McNeile	University of Glasgow	Lattice Approach to Light Scalars
G. Bali	Universitaet Regensburg	Lattice Approach to Charmed States
A. Tsapalis	University of Athens, Institute of Accelerating Systems and Applications	Nucleon and pion-nucleon form factors from Lattice QCD
T.T. Takahashi	Yukawa Institute for Theoretical Physics, Kyoto University	Lattice QCD Study of $g_A^{N^*N^*}$ with Two-Flavors of Dynamical Quarks
J. Hu	Duke University	Pion Physics from Lattice QCD
<i>Session 32: Few Body II</i>		<i>chair: A. Fonseca</i>
H. Griesshammer	Center for Nuclear Studies, The George Washington University	Compton Scattering off the Deuteron and the Nucleon Polarizabilities
A. Rouba	Research Institute for Nuclear Problems, Minsk	Deuteron Spin Dichroism in Carbon Target
Y. Uzikov (V. Serdyuk)	JINR Dubna	Scaling Behavior of the Reactions dd to p3H and pd to pd in the GeV Region
V.V. Kulikov	ITEP, Moscow	Quasielastic Deuteron and Triton Knockout from Light Nuclei by Intermediate Energy Pions

<b>Session 33: High Energy Processes II</b>			<i>chair: W. Toki</i>
A. Szczurek	Institute of Physics and University of Rzeszow	Exclusive Production of Quarkonia in pp and p $\bar{p}$ Collisions Far from the Threshold	
D. Nickel	Technische Universitaet Darmstadt	Studying Unquenching Effects in the Quark Propagator	
S. Atashbar Tehrani	Persian Gulf University	QCD analysis for nuclear parton distributions at next to leading order	
M. Nekipelov	FZ Juelich	Present Understanding of Spin-Filtering Experiments	
<b>Session 34: Heavy Mesons II</b>			<i>chair: I. Bigi</i>
V. Lyubovitskij	Institute of Theoretical Physics, University of Tuebingen	Strong and Radiative Decays of New Heavy Mesons Containing Strange Quarks and Hadronic Molecules	
V. Ziegler	SLAC	Cascade Resonance Properties from Charm Baryon Decays at BaBar	
S. Pacetti	LNF-INFN Frascati / Centro Studi e Ricerche Enrico Fermi, Roma	Extraction of Form Factors in ISR Processes at BaBar	
M. Pelliccioni	Universita' degli Studi di Torino, INFN	Charm Dalitz Analysis at BaBar	
Q. Zhao	Institute of High Energie Physics, Chinese Academy of Sciences	The Role of Electromagnetic Transitions in V to VP	
<b>Session 35: Hadrons in Medium IV</b>			<i>chair: M.B. Voloshin</i>
L. Tolos	FIAS. University of Frankfurt	Open-charm mesons in hot and dense nuclear matter	
S.S. Afonin	St. Petersburg State University	Spontaneous P-parity Violation in Dense Baryon Matter	
M. Takizawa	Showa Pharmaceutical University	Restoration of U <sub>A</sub> (1) Symmetry and eta' Meson at Finite Density	
S. Tamenaga	RCNP Osaka University	The Massless Linear Sigma Model for Finite Nuclei and at Finite Temperature	
<b>Conference Dinner Burg Baesweiler, Dinner Talk by D.Habs (LMU München)</b>			
<b>Plenary Session Friday, Sep. 14, 2007 8:30 - 12:30</b>			
<i>chair: A. Thomas</i>			
N. Saito	KEK	The Japanese Proton Accelerator Facility	
B. Krusche (cancelled)	Basel University	Photoproduction of Eta-Mesons off Nuclei	

U. Mosel	University of Giessen	Hadrons in Medium - Theory Meets Experiment
P. Lenisa	Universita' di Ferrara and INFN - Ferrara	Towards Polarized Antiprotons at FAIR
<i>chair: U. Mosel</i>		
J.G. Messchedorp	KVI/RuG	Hadron Physics with Anti-Protons
G. Rosner	University of Glasgow	Overview of CLAS Physics
A.W. Thomas	Jefferson Lab	Future Scientific Opportunities at Jefferson Lab
<i>chair: R. Maier</i>		
C. Roberts	Argonne National Lab	Dynamics, Symmetries and Hadron Properties
M. Anselmino	University and INFN, Torino	The Transverse Partonic Structure of the Proton
B.M.K. Nefkens	UCLA	Concluding Remarks
<a href="#">Tour COSY</a> , Farewell Coffee		

	<b>Poster</b>	
A.V.Glushkov	Odessa University	EPPP and Resonance Phenomena in Heavy Nuclei Collisions and Structurization of the Positron Spectrum. Compound Nucleus in Extreme External Electric Field
A.V.Glushkov	Odessa University	A Discharge of Meta-Stable Nuclei During Negative Muon Capture: Energy Approach
O. Khetselius	Nucl.Spectr.Lab., Odessa University	Nuclear Electric Quadrupole Moments and HFS Parameters for Heavy Isotopes: Nuclear Effects Contributions
O. Khetselius	Nucl.Spectr.Lab., Odessa University	Generalized Multi-Configuration Model of Decay of the Multipole Giant Resonances Applied to Aanalysis of Reaction mu-n on the Nucleus 40Ca
A. Machavariani	JINR Dubna, HEPI Tbilisi	Field-Theoretical Two-Body and Three-Body Equations for the Multichannel Reactions with the Intermediate Delta-Resonance and Quark-Gluon Degrees of Freedom
A. Machavariani	JINR Dubna, HEPI Tbilisi	Experimental test of the proton a structure effects in the polarized pp or pd elastic scattering experiments
H.P. Morsch	Soltan Institute for Nuclear Studies, Warsaw	Relation of nucleon resonances to the gluon structure of QCD
S. Nakamura	TRIUMF	Renormalization Group Analysis of the Chiral NLO Pion Production Operator
M. Mikirtychians	PNPI Gatchina	The Polarized Internal Target at ANKE
Y. Surovtsev	Bogoliubov Laboratory of Theoretical Physics, Joint Institute for Nuclear Research	Rho-like-meson family in the pion-pion scattering
F.J. Llanes Estrada	Depto. Fisica Teorica I, Universidad Complutense Madrid	The J=0 Fixed Pole in Deeply Virtual Compton Scattering - New Perspectives
F. Taghavi Shahri	IUST	Q <sup>2</sup> -Dependence of Polarized Parton Distribution Functions in the Valon Model
H. Alharbi	National Center for Mathematics and Physics at KACST	Poincaré Invariant Coupled Channel model for the Pion-Nucleon System: Instant Form Model
U. Badarch	University Giessen	In-Medium Nucleon-Nucleon Interaction Nuclear EOS

A. Galoyan	LPP JINR	Multiplicity Fluctuations in Interactions of Light Nucleus with Carbon Nuclei at Momentum of 4.2 GeV/c/nucleon and their Theoretical Interpretation
W.J. Briscoe	The George Washington University	Near Threshold Pion Production at MAXLAB
J. Stepaniak	Institute for Nuclear Studies, Warsaw	New eta Rare Decay Results from CELSIUS/WASA Experiment
M. Sadler	Abilene Christian University	Pion-Nucleon Scattering in the N*(1440) Resonance Region
S. Ivashyn	National Science Center "Kharkov Institute for Physics and Technology", Institute for Theoretical Physics, Ukraine	Application of chiPT with Vector Mesons: Kaon Electromagnetic Form Factors and KbarK Contribution to Muon Anomalous Magnetic Moment
W. Schroeder	University of Erlangen-Nuremberg	Improved Study of Possible Theta+ Production in the pp to pK0 Sigma+ Reaction with the COSY-TOF Experiment
W. Schroeder	University of Erlangen-Nuremberg	Hyperon Production in the Channel pp to K+ Lambda p at COSY-TOF
C. Pauly	FZ Juelich	WASA-at-COSY
B. Taddesse	Jacobs University Bremen	
D. Duniec	Dept. of Nuclear and Particle Physics, Uppsala University	eta' Decays with WASA-at-COSY
B.R. Jany	Nuclear Physics Department Jagiellonian University / FZ Juelich	
C.F. Redmer	FZ Juelich	In Search of the Box Anomaly with the WASA-at-COSY Facility
M. Janusz	FZ Juelich and Jagiellonian University, Krakow	From Charged Tracks to ChPT Anomalies (WASA-at-COSY)
L. Yurev	FZ Juelich	
T. Tolba	FZ Juelich	A Pellet Tracking System for WASA-at-COSY
T. Stockmanns	FZ Juelich	A High Rate and High Resolution Micro-Vertex-Detector for the PANDA-Experiment at FAIR

M. Mertens	FZ Juelich	<a href="#">Development of a Versatile Readout System for High Rate Detector Electronics</a>
P. Klaja	Jagellonian University and FZ Juelich	<a href="#">Proton-Proton Correlation Function for the pp to pp eta Reaction Measured with COSY-11</a>
P. Moskal		
R. Czyzykiewicz	Jagellonian University and FZ Juelich	<a href="#">Studies of the eta Meson Production with a Polarized Proton beam at COSY-11</a>
P. Moskal		

## Author Index

- Švarc, A., 663
- Achenbach, P., 111  
Ahn, J.K., 134  
Akimune, H., 134  
Arndt, R., 659  
Asano, Y., 134  
Author, N., 166
- Bargholtz C., 307  
Baru, V. , 286, 297  
Bashkanov M., 307  
Bazzi. M., 12  
Beane, S. R., 88  
Beer, G., 12  
Bergenwall, B., 332  
Beveren, E.van, 317  
Bicudo, P., 328  
Bigi, I., 177  
Bijnens, J., 33  
Bini, C., 44  
Blomgren, J., 332  
Bogoslowsky D., 307  
Bombelli, L., 12  
Borasoy, B., 348, 627  
Bragadireanu, A. M., 12  
Brinkmann, K.-Th., 76  
Briscoe, W., 659  
Brodsky, S.J., 502
- Calen H., 307  
Calle Cordón, A., 617  
Cappellaro F., 307  
Carasco, C., 466  
Cargnelli, M., 12  
Catitti, M., 12  
Ceci, S., 663  
Chang, W. C. , 134  
Clement H., 307
- Cloët, I. C., 262  
Curceanu, C., 12
- Döring, M., 363  
Daté, S., 134  
De Masi, R., 358  
Demiroers L., 307  
Doroshkevich E., 307  
Dugger, M., 373  
Duniec D., 307
- Ejiri, H., 134  
Ekström C., 307  
Epelbaum, E., 383
- Fariborz, A.H., 66  
Fiorini, C., 12  
Franssen K., 307  
Frizzi, T., 12  
Fujimura, H., 134  
Fujiwara, M., 134
- Galatà, G., 631  
Gao, H., 155  
Gasser, J., 2  
Geren L., 307  
Ghio, F., 12  
Girolami, B., 12  
Glozman, L. Ya., 414  
Goussev, I., 466  
Grießhammer, H. W., 424  
Guaraldo, C., 12  
Gustafsson L., 307  
Gårdestig, A., 403
- Höistad B., 307  
Haberzettl, H., 550  
Hanhart, C., 286, 297  
Harris, F. A., 435

Hauger, M., 466  
 Hayano, R., 12  
 Heisenbauer, J., 286, 297  
 Hernandez, E., 573  
 Hicks, K., 134  
 Hirenzaki, S., 573  
 Hotta, H., 134  
 Huang, F., 445  
  
 Iliescu, I., 12  
 Imai, K., 134  
 Ishikawa, Z., 134  
 Ishiwatari, T., 12  
 Ivanov G., 307  
 Iwasaki, M., 12  
 Iwata, T., 134  
  
 Jacewicz M., 307  
 Jido, D., 363  
 Jiganov E., 307  
 Johansson T., 307  
 Johansson, C., 332  
 Jonsson, O., 332  
 Jora, R., 66  
 Jourdan, J., 466  
 Julia-Diaz, B., 455  
  
 Kalantar-Nayestanaki, N., 190  
 Kaskulov M., 307  
 Kaskulov, M., 573  
 Kawai, H., 134  
 Keleta S., 307  
 Khakimova O., 307  
 Kienle, P., 12  
 Kino, K., 134  
 Kiselev, D., 466  
 Kistryn, St., 190  
 Klechneva, T., 466  
 Klug, J., 332  
 Koch I., 307  
 Kohri, H., 134  
 Krassnigg, A., 262  
  
 Kren F., 307  
 Krusche, B., 466  
 Kubis, B., 478  
 Kudryavtsev, A., 286, 297  
 Kullander S., 307  
 Kumagai, N., 134  
 Kupść A., 307  
 Kuznetsov A., 307  
  
 Lähde, T.A., 483  
 Lechner, P., 12  
 Lehmann, I., 493  
 Lenisa, P., 231  
 Lensky, V., 286, 297  
 Levi Sandri, P., 12  
 Lindberg K., 307  
 Llanes-Estrada, F.J., 502  
 Longoni, A., 12  
 Lucherini, V., 12  
  
 Mühry, H., 466  
 Maeda, Y., 332  
 Magiera, A., 513  
 Makino, S., 134  
 Marciniewski P., 307  
 Marton, J., 12  
 Matsumura, T., 134  
 Matsuoka, N., 134  
 McNeile, C., 523  
 Meier R., 307  
 Meißner, U., 286, 297  
 Meißner, U.-G., 627  
 Melnitchouk, W., 533  
 Mermod, P., 332  
 Messchendorp, J.G., 241  
 Mibe, T., 134  
 Miyabe, M., 134  
 Morita. M., 134  
 Morosov B., 307  
 Mosel, U., 221  
 Muramatsu, N., 134

Myhrer, F, 542  
 Nadel-Turonski, P., 332  
 Nagahiro, H., 573  
 Nakano, T. , 134  
 Nakayama, K., 550  
 Nefediev, A., 558  
 Nefkens, B., 273  
 Niiyama, M. , 134  
 Nilsson, L., 332  
 Nißler, R., 627  
 Nomachi, M. , 134  
 Normand, Ch., 466  
  
 Oehr, A., 332  
 Oesterlund, M., 332  
 Oh, Y., 550  
 Ohashi, Y., 134  
 Ohkuma, H., 134  
 Oller, J. A., 563  
 Olsson, N., 332  
 Ooba, T., 134  
 Oset, E., 363, 573  
 Oshuev, D. S. , 134  
  
 Pauly C., 307  
 Pavón, M., 617  
 Peláez, J.R., 583  
 Pennington, M. R., 54  
 Petterson H., 307  
 Petukhov Y., 307  
 Phillips, D. R., 210  
 Phillips, D.R., 403  
 Pietreanu, D., 12  
 Platchkov, S., 593  
 Pomp, S., 332  
 Ponta, T., 12  
 Povtorejko A., 307  
 Prakhov, S., 144, 598  
 Pricking A., 307  
 Prok, Y., 609  
 Prokofiev, A., 332  
  
 Ríos, G., 583  
 Raha, U., 627  
 Rangachary, C., 134  
 Rathmann, F., 231  
 Renberg, P.-U., 332  
 Roberts, C. D., 262  
 Roca, L., 563  
 Ruiz Arriola, E., 617  
 Rupp, G., 317  
 Rusetsky, A., 627  
  
 Sakaguchi, A., 134  
 Sakai, H., 332  
 Santopinto, E., 631  
 Sato, T., 134  
 Schönning K., 307  
 Schäfer, A., 98  
 Schat, C., 563  
 Schechter, J., 66  
 Scobel W., 307  
 Sekiguchi, K., 200  
 Seliverstov, D., 466  
 Shagin, P. M., 134  
 Shiino, Y., 134  
 Shimizu, H., 134  
 Shwartz B., 307  
 Sick, I., 466  
 Sirghi, D. L., 12  
 Sirghi, F., 12  
 Skorodko T., 307  
 Soltau, H., 12  
 Sopov V., 307  
 Springer, R. P., 641  
 Stancu, Fl., 649  
 Starostin, A., 144, 273  
 Stepeniak J., 307  
 Stephan, E., 190  
 Strakovsky, I., 659  
 Struder, L., 12  
 Sugaya, Y. , 134  
 Sumihama, M., 134

Szczepaniak, A.P., 502

Tamii, A., 332

Tatsuno, T., 12

Tegner P., 307

Thörngren-Engblom P., 307

Thomas, A. W., 251

Tikhomirov V., 307

Tippawan, U., 332

Toki, W., 166

Toyokawa, H., 134

Tsapalis A., 673

Vazquez Doce, O., 12

Wöhrle, H., 466

Wagner G.J., 307

Wang, C. W. , 134

Wang, S. C. , 134

Wang, W.L., 445

Wanke, R., 22

Warren, G., 466

Widmann, E., 12

Wolke M., 307

Workman, R., 659

Yamamoto A., 307

Yonehara, K. , 134

Yorita. T. , 134

Yosoi, M., 134

Zabierowski J., 307

Zartova I., 307

Zauner, B., 663

Zegers, R. G. T., 134

Zeier, M., 466

Zhang, Z.Y., 445

Zmeskal, J., 12

Zou, B. S., 121

Złomanczuk J., 307